

Université de Montréal

Conception, étude et applications de photocatalyseurs à base de cuivre et développement de diynes-1,3 tendus pour la bioconjugaison.

Par

Corentin Cruché

Université de Montréal, Département de Chimie

Faculté des Arts et des Sciences

Thèse présentée

à la Faculté des études supérieures et postdoctorales en vue de l'obtention en vue de l'obtention du grade de philosophiæ docteur (Ph.D), en chimie

Septembre 2023

© Corentin Cruché, 2023

Université de Montréal

Département de chimie, Faculté des arts et des sciences

Cette thèse intitulée

Conception, étude et applications de photocatalyseurs à base de cuivre et développement de diynes-1,3 tendus pour la bioconjugaison.

Présenté par

Corentin Cruché

A été évalué(e) par un jury composé des personnes suivantes

Hélène Lebel

Président-rapporteur

Shawn K. Collins

Directeur de recherche

Richard Giasson

Membre du jury

André Beauchemin

Examineur externe

Résumé

Cette thèse s'articule autour de deux grands axes indépendants. Le premier s'aligne sur les intérêts du groupe Collins pour la photocatalyse avec des complexes à base de cuivre. La photocatalyse apparaît comme une branche de la chimie permettant de débloquent des réactivités difficilement accessibles par la chimie thermique. Si la majorité des réactions photocatalysées utilise des catalyseurs à base de ruthénium ou d'iridium, les complexes de cuivre(I) sont une alternative digne d'intérêt. Cependant, une connaissance plus profonde de la relation structure/activité de ces complexes est encore nécessaire. Cette thèse tentera donc d'apporter des éléments de réponse à cette problématique, en particulier pour les complexes de cuivre(I) hétéroleptiques, possédant un ligand diimine et un ligand diphosphine.

Le premier chapitre présente le concept de la photocatalyse et les caractéristiques des photocatalyseurs de cuivre. Une sélection d'exemples de réactions photocatalysées par des complexes de cuivre permet d'établir l'état de l'art pour différents types de mécanismes.

Le chapitre 2 présente l'étude de ligands diimine possédant un système π -étendu dans des complexes. Les complexes correspondants ont été étudiés dans trois réactions passant par des voies mécanistiques différentes. Si les complexes sont actifs pour les réactions de transfert d'électrons et d'énergie, ils ne possèdent pas une efficacité supérieure aux complexes précédemment reportés.

Le chapitre 3 est une extension du chapitre 2. En effet, les ligands possédant un système π -étendu précédemment reportés ont été modifiés pour pouvoir former des complexes de cuivre avec la diphosphine BINAP. Les nouveaux complexes ont de nouveau été étudiés dans les trois réactions différentes, mais leur activité est semblable à celle des complexes reportés dans le chapitre 2. Les complexes ont aussi été étudiés pour leur activité anticancéreuse, et des résultats prometteurs ont été découverts.

Le chapitre 4 résume l'étude d'une bibliothèque étendue de complexes de cuivre(I) pour l'isomérisation d'alcènes E \rightarrow Z. L'efficacité des complexes dans la réaction est reliée à leurs

propriétés photophysiques. Un complexe optimal a été trouvé, et utilisé pour isomériser une série de 25 alcènes différents. L'utilisation de la chimie en flux continu a aussi permis la mise en échelle de la réaction. Enfin un procédé séquentiel ATRA/PI a permis la formation d'alcènes tri- et tétra-substitués à partir d'alcynes et de chlorures de sulfonyles.

Le deuxième axe de cette thèse se base sur le développement de diynes-1,3 pour leur utilisation dans les réactions de « click » promues par la tension. Le chapitre 6 introduit les concepts de chimie « click » et de cycloaddition alcyne-azoture promue par la tension (SPAAC), et l'état de l'art des diynes-1,3 et des alcynes tendus.

Le chapitre 7 présente donc le développement d'une nouvelle classe de diynes-1,3 tendus pour la réaction de SPAAC. La vitesse de la réaction est étudiée et des calculs computationnels viennent corroborer la réactivité observée. Un diyne-1,3, **3,5-TPDY**, a été utilisé dans une application de bioligation, et son utilisation dans une réaction de « click » avec une hydrazine a été montrée.

Mots-clés :

Photocatalyse, cuivre, relation structure/activité, isomérisation d'alcène, diynes-1,3, SPAAC, bioligation

Abstract

The thesis is structured around two independent themes. The first concerns the Collins Group's interest in copper-based complexes for photocatalysis. Photocatalysis is a branch of chemistry that aims to unlock reactivities that are difficult to access through thermally-promoted chemistry. While the majority of photocatalytic reactions use ruthenium- or iridium-based catalysts, copper(I) complexes are a valuable alternative, but a deeper understanding of the structure/activity relationship of the complexes is still required. The thesis will describe work to gain a better understanding of the reactivities and behavior of heteroleptic copper(I) complexes possessing a diimine ligand and a diphosphine ligand.

The first chapter introduces the concept of photocatalysis and the characteristics of copper-based photocatalysts. A selection of examples of reactions photocatalyzed by copper complexes establishes the state of the art for different types of mechanisms.

Chapter 2 presents the study of diimine ligands possessing a π -extended system in copper-based complexes. The corresponding complexes have been studied in 3 different photochemical reactions proceeding through different mechanistic pathways. While the complexes are active in electron and energy transfer reactions, they are not more efficient than previously reported complexes.

Chapter 3 is an extension of Chapter 2, in which the π -extended ligands previously reported are modified to form copper complexes with the diphosphine, BINAP. The new complexes are again studied in the 3 different reactions, but their activity is similar to that of the complexes reported in chapter 2. The complexes are also being studied for their anticancer activity, and promising results have been uncovered.

Chapter 4 summarizes the study of an extensive library of copper(I)-based complexes for the E \rightarrow Z isomerization of alkenes. The efficiency of the complexes in the reaction is compared with their photophysical data. An optimal complex is found and used to isomerize a series of 25 different alkenes. The use of continuous flow chemistry also enabled the reactions to be scaled up. Finally,

a sequential ATRA/PI process enabled the formation of tri- and tetra-substituted alkenes from alkynes and sulfonyl chlorides.

The second theme of the thesis is based on the development of 1,3-diynes for use in strain-promoted "click" reactions. Chapter 6 introduces the concepts of click chemistry and SPAAC, and the state of the art of 1,3-diynes and strained alkynes.

Chapter 7 presents the development of a new class of strained 1,3-diynes for the SPAAC reaction called TPDYs. The reaction rates are studied and computational calculations corroborate the observed reactivity. A 1,3-diyne, **3,5-TPDY**, is applied to a bioligation process, and its use in a potential new "click" reaction with a hydrazine is shown.

Keywords :

Photocatalysis, copper, structure/activity relationship, alkene isomerization, 1,3-diynes, SPAAC, bioligation

Table des matières

Résumé	3
Abstract.....	5
Table des matières.....	7
Liste des sigles et abréviations	24
Remerciements.....	29
Chapitre 1 L'utilisation de complexes de cuivre pour la photocatalyse	31
1.1 Généralités	31
1.1.1 Introduction à la photocatalyse	31
1.1.2 Le cuivre	34
1.2 Complexes homoleptiques de cuivre(I).....	35
1.2.1 Caractéristiques électroniques des complexes homoleptiques de cuivre(I)	35
1.2.2 Propriétés photophysiques des complexes homoleptiques de cuivre(I).....	36
1.2.3 Propriétés électrochimiques des complexes homoleptiques de cuivre(I).....	40
1.2.4 Synthèse des complexes homoleptiques de cuivre(I).....	42
1.3 Complexes hétéroleptiques de cuivre.....	42
1.3.1 Synthèse des complexes hétéroleptiques de cuivre(I)	42
1.3.2 Propriétés photophysiques des complexes hétéroleptiques de cuivre(I)	44
1.3.3 Propriétés électrochimiques des complexes hétéroleptiques de cuivre(I)	45
1.4 L'utilisation de complexe de cuivre pour la catalyse photorédox	46
1.4.1 Principe de la catalyse photorédox : Transfert d'électron simple	46
1.4.2 Transfert d'électron simple	47
1.4.3 Transfert d'atome radicalaire (ATRA)	52
1.4.4 Transfert d'électron et de proton simultané (PCET).....	54

1.5	<i>L'utilisation de complexe de cuivre pour la catalyse par transfert d'énergie</i>	59
1.5.1	Principe de la catalyse par transfert d'énergie	59
1.5.2	Réactions photosensibilisées par le cuivre	62
1.5.3	Principe de l'isomérisation d'alcène photocatalysée	63
1.6	<i>Conclusion</i>	66
1.7	<i>Références bibliographiques</i>	67
 Chapitre 2 Evaluating heteroleptic copper(I)-based complexes bearing π-extended diimines in different photocatalytic processes.....		71
2.1	<i>Abstract</i>	71
2.2	<i>Introduction</i>	72
2.3	<i>Results and discussions</i>	73
2.4	<i>Conclusions</i>	80
2.5	<i>References</i>	82
 Chapitre 3 Heteroleptic Copper(I)-Based Complexes Incorporating BINAP and π-Extended Diimines: Synthesis, Catalysis and Biological Applications.		85
3.1	<i>Abstract</i>	85
3.2	<i>Introduction</i>	86
3.3	<i>Results and discussions</i>	87
3.4	<i>Conclusions</i>	94
3.5	<i>References</i>	96
 Chapitre 4 Heteroleptic Copper-Based Complexes for Energy Transfer Processes: E\rightarrowZ Isomerization and Tandem Photocatalytic Sequences		98
4.1	<i>Abstract</i>	98
4.2	<i>Introduction</i>	99

4.3	<i>Results and discussions</i>	101
4.4	<i>Conclusions</i>	110
4.5	<i>References</i>	111
Chapitre 5 Conclusions et perspectives de la photocatalyse avec des complexes de cuivre.		115
5.1	<i>Conclusion sur la photocatalyse avec des complexes de cuivre</i>	115
5.1.1	Conclusion des chapitres 2, 3 et 4	115
5.1.2	Conclusion générale	118
5.2	<i>Perspectives</i>	119
5.2.1	Nouveaux complexes	119
5.2.2	Perspectives sur la relation structure activité dans les réactions photorédox	120
5.2.3	Perspective sur le développement de nouvelles réactions photoredox	121
5.2.4	Perspectives sur les réactions de transfert d'énergie	122
5.3	<i>Références</i>	124
Chapitre 6 Introduction de la stratégie de cycloaddition alcyne-azoture promues par la tension.		125
6.1	<i>Généralités</i>	125
6.1.1	La chimie « click »	125
6.1.2	La réaction de cycloaddition alcyne-azoture catalysée au cuivre (CuAAC)	126
6.2	<i>Développement de la stratégie de cycloaddition alcyne-azide promue par la tension</i> ...	128
6.2.1	Principe	128
6.2.2	Développement d'alcynes tendus	129
6.2.3	Réactivité et stabilité des alcynes tendus	131
6.3	<i>Les diynes-1,3</i>	134
6.3.1	Réactivité et fonctionnalisation des diynes-1,3	134
6.3.2	Synthèse de diynes-1,3 cycliques	137
6.4	<i>Conclusion</i>	139

6.5	<i>Références bibliographiques</i>	141
Chapitre 7	TPDYs: Strained Macrocyclic Diynes for Bioconjugation Processes.	145
7.1	<i>Abstract</i>	145
7.2	<i>Introduction</i>	146
7.3	<i>Results and discussion</i>	147
7.4	<i>Conclusions</i>	155
7.5	<i>References</i>	156
Chapitre 8	Conclusions et Perspectives pour le développement de diynes-1,3 tendus pour la bioconjugaison	159
8.1	<i>Conclusions</i>	159
8.2	<i>Perspectives</i>	160
8.2.1	Nouvelle génération de diynes tendus	160
8.2.2	Développement de la SPDHH	161
8.2.3	Références bibliographiques	162
Annexe 1	– Supporting information of Chapter 2	164
Annexe 2	– Supporting information of Chapter 3	212
Annexe 3	– Supporting information of Chapter 4	241
Annexe 4	– Decomposition of Lignin Models Enabled by Copper-Based Photocatalysis Under Biphasic Conditions	373
Annexe 5	– Supporting information of Annexe 4	388
Annexe 6	– Supporting information of Chapter 7	436

Liste des tableaux

Table 2.1 Synthesis of of Cu(I)-Based Photocatalysts and Photophysical Properties.....	75
Table 2.2 Yield of 2.2 (%).....	77
Table 2.3 Yield of 2.4 (%).....	78
Table 2.4 Yield of 2.6 (%).....	80
Table 3.1 Synthesis and Properties of Cu(I)-Based Photocatalysts of the Type Cu(NN)(BINAP)BF ₄	89
Table 4.1 Evaluation of Cu(I)-Based Photocatalysts in E↔Z Isomerization Processes ^a	106
Table 4.2 Sequential ATRA/photoisomerization processes employing the Cu(bphen)(XantPhos)BF ₄ catalyst	109
Table A2 - 1 Tabular data for the maximum of absorbance and emission of copper complexes	220
Table A2 - 2 Tabular data for the excited state lifetime of copper complexes.....	223
Table A2 - 3 Tabular data for the redox potentials of copper complexes	225
Table A3 - 1 Evaluation of Cu(dmp)(PP)BF ₄ -Based Photocatalysts in a Model E↔Z Isomerization Process	263
Table A3 - 2 Evaluation of Cu(NN)(XantPhos)BF ₄ -Based Photocatalysts in a Model E↔Z Isomerization Process	265
Table A3 - 3 Ratio of <i>E</i> - and <i>Z</i> -isomers during a 1-hour irradiation time at 400 nm.....	277
Table A3 - 4 Percentage of isomerisation and yield of the scale-up reactions using the flow setup	278
Table A3 - 5 Tabular data for the maximum of absorbance of copper complexes	286
Table A3 - 6 Tabular data for the maximum of emission of copper complexes	289
Table A3 - 7 Tabular data for the excited state life time of copper complexes.....	299
Table A3 - 8 Tabular data for the photostability studies	308

Table A3 - 9 Crystal data and structure refinement for Cu(Bphen)(Xantphos)BF ₄	356
Table A3 - 10 Atomic coordinates and U_{eq} [Å ²] for Cu(bphen)(XantPhos)BF ₄	357
Table A3 - 11 Bond lengths and angles for Cu(Bphen)(Xantphos)BF ₄	362
Table A3 - 13 Torsion angles for Cu(Bphen)(Xantphos)BF ₄	367
Table A4 - 1 Optimization of Biphasic Conditions.....	378
Table A4 - 2 Activity of Various Catalysts under Biphasic Conditions.....	379
Table A4 - 3 Decomposition of Lignin Models.....	382
Table A5 - 1 Data used to build the 1-(3,4-dimethoxyphenyl)ethan-1-one calibration curve	401
Table A5 - 2 Evaluation of Cu(quintri)(PP)BF ₄ -Based Photocatalysts in a Model Lignin Decomposition Process.....	402
Table A5 - 3 Evaluation of Cu(NN)(XantPhos)BF ₄ -Based Photocatalysts in a Model Lignin Decomposition Process.....	402
Table A5 - 4 Excited State Lifetime Quenching with NABnH.....	410
Table A5 - 5 Excited State Lifetime Quenching with 1-(3,4-dimethoxyphenyl)-2-(2- methoxyphenoxy)ethan-1-one (1).....	412
Table A5 - 6 Excited State Lifetime Quenching with NaHCO ₃ and Na ₂ S ₂ O ₄	413
Table A5 - 7 Bimolecular quenching constant k_q	414
Table A6 - 1 Crystal data and structure refinement for 3,5-TPDY.....	505
Table A6 - 2 Atomic coordinates and U_{eq} [Å ²] for 3,5-TPDY.....	506
Table A6 - 3 Bond lengths and angles for 3,5-TPDY.....	507
Table A6 - 4 Torsion angles for 3,5-TPDY.....	508
Table A6 - 5 Crystal data and structure refinement for 3,5-Triazole-Reg2.....	510
Table A6 - 6 Atomic coordinates and U_{eq} [Å ²] for 3,5-Triazole-Reg2.....	511
Table A6 - 7 Anisotropic displacement parameters (Å ²) for 3,5-Triazole-Reg2.....	513
Table A6 - 8 Bond lengths and angles for 3,5-Triazole-Reg2.....	514

Table A6 - 9 Torsion angles for 3,5-Triazole-Reg2	517
Table A6 - 10 Hydrogen bonds for 3,5-Triazole-Reg2	519
Table A6 - 11 Crystal data and structure refinement for 2,6-Triazole-Reg2.....	520
Table A6 - 12 Atomic coordinates and U_{eq} [\AA^2] for 2,6-Triazole-Reg2.....	521
Table A6 - 13 Anisotropic displacement parameters (\AA^2) for 2,6-Triazole-Reg2.....	523
Table A6 - 14 Bond lengths and angles for 2,6-Triazole-Reg2	524
Table A6 - 15 Torsion angles for 2,6-Triazole-Reg2	525
Table A6 - 16 Crystal data and structure refinement for 3,5-Pyrazole.....	528
Table A6 - 17 Atomic coordinates and U_{eq} [\AA^2] for 3,5-Pyrazole.....	529
Table A6 - 18 Bond lengths and angles for 3,5-Pyrazole.....	532
Table A6 - 19 Torsion angles for 3,5-Pyrazole.....	534

Liste des figures

Figure 1.1 Spectre électromagnétique.....	32
Figure 1.2 Diagramme de Jablonski	33
Figure 1.3 Abondance (en fraction atomique) d'éléments chimiques dans la croûte terrestre supérieure en fonction de leur numéro atomique	35
Figure 1.4 Structure par rayons X montrant la configuration tétraédrique du complexe de cuivre(I) $\text{Cu(dmp)}_2\text{N(CN)}_2$	36
Figure 1.5 Représentation des transitions électroniques et des orbitales correspondantes dans les complexes de cuivre(I)	37
Figure 1.6 Diagramme d'énergie des différents états excités des complexes de cuivre(I)	38
Figure 1.7 Effet pseudo Jahn-Teller et mécanisme de désactivation de l'état excité de complexes de cuivre(I).....	38
Figure 1.8 Influence des substituants des ligands phénanthroliques sur le temps de vie de l'état excité du complexe	39

Figure 1.9 Différence de potentiels redox entre l'état fondamental et l'état excité de $\text{Cu}(\text{dmp})_2\text{BF}_4$	41
Figure 1.10 Influence des ligands sur les potentiels rédox des complexes de cuivre(I) homoleptiques	41
Figure 1.11 Synthèse de $\text{Cu}(\text{dmp})_2\text{BF}_4$ et couleurs de différents complexes homoleptiques sous forme solide	42
Figure 1.12 Équilibre entre le complexe hétéroleptique et les complexes homoleptiques correspondants	44
Figure 1.13 Comparaison des propriétés photophysiques de $\text{Cu}(\text{dmp})_2\text{BF}_4$ et $\text{Cu}(\text{dmp})(\text{DPEphos})\text{BF}_4$	45
Figure 1.14 Cycles de désexcitation réductrice et oxydante du $\text{Cu}(\text{dmp})(\text{DPEPhos})\text{BF}_4$	47
Figure 1.15. Liste des ligands utilisé pour la construction de la bibliothèque de complexes de cuivre(I)	50
Figure 1.16 Représentation des mécanismes de PCET oxydatif et réductif	55
Figure 1.17 Représentation du transfert d'énergie	60
Figure 1.18 Mécanismes de transfert d'énergie de Förster et Dexter	61
Figure 1.19 Représentation des niveaux d'énergie du donneur et de l'accepteur dans un transfert d'énergie	61
Figure 1.20 Différents photocatalyseurs et leur énergie triplet correspondante	62
Figure 1.21 Principe de la photoisomérisation $\text{E} \rightarrow \text{Z}$ d'alcènes	64
Figure 2.1 Copper-based complexes for photocatalysis.	72
Figure 2.2 Synthesis of of Cu(I)-Based Photocatalysts	75
Figure 2.3 Evaluation of the π -extended copper-based photocatalysts in a photochemical Appel-type process	76
Figure 2.4 Evaluation of the π -extended copper-based photocatalysts in a PCET process	78
Figure 2.5 Evaluation of the π -extended copper-based photocatalysts in an energy transfer process	79
Figure 3.1 Small bite-angle bisphosphine for heteroleptic copper-based complexes.	86
Figure 3.2 Synthesis of heteroleptic copper-based complexes using BINAP	88

Figure 3.3 Comparison of the BINAP-containing copper complexes bearing π -extended ligands in a photochemical Appel-type process.....	90
Figure 3.4 Effects of the diamine ligand of heteroleptic copper complexes in a photochemical Appel-type process.....	91
Figure 3.5 Comparison of the BINAP-containing copper complexes bearing π -extended ligands in a photochemical PCET process.....	92
Figure 3.6 Comparison of the BINAP-containing copper complexes bearing π -extended ligands in an energy transfer process.....	92
Figure 3.7 Ligand effects in heteroleptic copper complexes in an energy transfer process.	93
Figure 3.8 Viability of MDA-MB-231 cells at 5 μ M.....	94
Figure 4.1 Photocatalysis using Cu(NN)(PP)X complexes and possible application to E \leftrightarrow Z isomerization.	100
Figure 4.2 Evaluation of Cu-Based Sensitizers in a Model E \leftrightarrow Z Isomerization Process	102
Figure 4.3 X-crystallographic analysis of Cu(bphen)(XantPhos)BF ₄	104
Figure 4.4 Scale-up of the photochemical E \leftrightarrow Z isomerization using continuous flow methods.	104
Figure 5.1 Ligands π -étendus utilisés dans le chapitre 2	116
Figure 5.2 Utilisation de ligands diimines non-substitués en position 2 et 9 en combinaison avec une diphosphine possédant un petit angle de morsure	117
Figure 5.3 Photoisomérisation d'alcènes catalysée par Cu(bphen)(Xanphos)BF ₄	118
Figure 5.4 Augmentation de la taille de la sphère de coordination des ligands diimines	120
Figure 5.5 Cycles catalytiques du cuivre à explorer	121
Figure 5.6 Perspectives de projets pour la photocatalyse au cuivre passant par un transfert d'énergie.....	123
Figure 6.1 Réaction de cycloaddition 1,3 dipolaire et exemples de dipôle 1,3	126
Figure 6.2 CuAAC et mécanisme proposé	128
Figure 6.3 Schéma représentatif d'une réaction SPAAC.....	129
Figure 6.4 a. Synthèse d'alcynes cycliques reporté par Blomquist b. Synthèse de cyclooctyne développé par Verkruijsse.....	130

Figure 6.5 Première synthèse d'un alcyne tendu pour la bioconjugaison reportée par Bertozzi	131
Figure 6.6 Influence de l'énergie de tension de cycle (RSE) sur la stabilité de cycloalcynes.....	132
Figure 6.7 Constantes de vitesse de différents alcynes cycliques pour la cycloaddition avec l'azoture de benzyle.	132
Figure 6.8 Influence des substituants accepteurs σ d'un cycloalcyne sur la stabilisation de la distorsion et l'assistance à la formation de liens C-N	133
Figure 6.9 Représentation de la stabilisation du TS par activation à distance.	134
Figure 6.10 Réactions de formation de diynes 1,3 symétriques et non-symétriques.....	135
Figure 6.11 Fonctionnalisation de diynes 1,3.....	136
Figure 6.12 Réaction entre une hydrazine et un diyne 1,3 pour la formation d'un pyrazole reportée par Verniest et mécanisme proposé.	137
Figure 6.13 Diynes 1,3 cycliques et l'angle de la liaison Csp-Csp.....	138
Figure 6.14 a. Découverte de la synthèse de diyne 1,3 terphényle b. Structure cristallographique et angle du diyne 6.32.....	139
Figure 7.1 <i>top</i> : Comparison of cycloalkynes for SPAAC processes and analogous unexplored macrocyclic diynes. <i>middle</i> : Synthesis of three TPDY macrocycles as candidates for SPAAC. ^a B ₂ (pin) ₂ (3 equiv.). <i>bottom</i> : Structures of TPDYs and calculated ring strain energy (RSE).	148
Figure 7.2 <i>top</i> : Yields for SPAACs with various TPDYs determined for reactions performed in CH ₂ Cl ₂ with subsequent chromatography. <i>bottom</i> : Computed Gibbs energy profile (G at 298.15 K) of the cycloadditions between BnN ₃ and TPDYs	150
Figure 7.3 Calculated (B3LYP-D3/6-31+g(d,p)/SMD(CH ₂ Cl ₂) NBO ³⁵ analysis of orbital interactions for 3,5-TPDY and the SPAAC transition state of 3,5-TPDY and BnN ₃	151
Figure 7.4 <i>top</i> : Synthesis of a PEGylated 3,5-TPDY. <i>bottom</i> : MTG-mediated conjugation of human crystallizable fragment of IgG1 antibody (hFc)	152
Figure 7.5 Strain promoted diyne hydrazine hydroamination.....	154
Figure 8.1 Réaction de SPAAC entre le TPDY et l'azoture de benzyle (gauche) et réaction de SPDHC entre le TPDY et l'hydrazine de benzyle (droite).	160
Figure 8.2 Nouvelles générations de TPDY possibles.....	161

Figure 8.3 Perspectives de modifications de la structure de l'hydrazine et du TPDY pour améliorer la SPDHH.....	162
Figure A1 - 1 Absorption spectra of $\text{Cu}(\text{N}^{\wedge}\text{N})_2\text{BF}_4$	178
Figure A1 - 2 Absorption spectra of $\text{Cu}(\text{N}^{\wedge}\text{N})(\text{DPEPhos})\text{BF}_4$	178
Figure A1 - 3 Absorption spectra of $\text{Cu}(\text{N}^{\wedge}\text{N})(\text{XantPhos})\text{BF}_4$	178
Figure A1 - 4 Absorption spectra of $\text{Cu}(\text{N}^{\wedge}\text{N})(\text{dppf})\text{BF}_4$	179
Figure A1 - 5 Excitation (red curve) and emission (blue curve) spectrum of $\text{Cu}(\text{ddpq})_2\text{BF}_4$ excited at 450 nm, recorded at ambient temperature in CH_2Cl_2 ($5 \cdot 10^{-4}$ M).....	179
Figure A1 - 6 Excitation (red curve) and emission (blue curve) spectrum of $\text{Cu}(\text{ddpq})(\text{DPEPhos})\text{BF}_4$ excited at 395 nm, recorded at ambient temperature in CH_2Cl_2 ($1.25 \cdot 10^{-5}$ M).....	180
Figure A1 - 7 Excitation (red curve) and emission (blue curve) spectrum of $\text{Cu}(\text{ddpq})(\text{XantPhos})\text{BF}_4$ excited at 450 nm, recorded at ambient temperature in CH_2Cl_2 ($1.25 \cdot 10^{-5}$ M).....	180
Figure A1 - 8 Excitation (red curve) and emission (blue curve) spectrum of $\text{Cu}(\text{ddpq})(\text{dppf})\text{BF}_4$	181
Figure A1 - 9 Excitation (red curve) and emission (blue curve) spectrum of $\text{Cu}(\text{ddppz})_2\text{BF}_4$	181
Figure A1 - 10 Excitation (red curve) and emission (blue curve) spectrum of $\text{Cu}(\text{ddppz})(\text{DPEPhos})\text{BF}_4$	182
Figure A1 - 11 Excitation (red curve) and emission (blue curve) spectrum of $\text{Cu}(\text{ddppz})(\text{XantPhos})\text{BF}_4$ excited at 450 nm, recorded at ambient temperature in CH_2Cl_2 ($1.25 \cdot 10^{-5}$ M).....	182
Figure A1 - 12 Excitation (red curve) and emission (blue curve) spectrum of $\text{Cu}(\text{ddppz})(\text{dppf})\text{BF}_4$	183
Figure A1 - 13 Excitation (red curve) and emission (blue curve) spectrum of $\text{Cu}(\text{dbdppz})_2\text{BF}_4$..	183
Figure A1 - 14 Excitation (red curve) and emission (blue curve) spectrum of $\text{Cu}(\text{dbdppz})(\text{DPEPhos})\text{BF}_4$	184
Figure A1 - 15 Excitation (red curve) and emission (blue curve) spectrum of $\text{Cu}(\text{dbdppz})(\text{XantPhos})\text{BF}_4$	184
Figure A1 - 16 Excitation (red curve) and emission (blue curve) spectrum of $\text{Cu}(\text{dbdppz})(\text{dppf})\text{BF}_4$	185

Figure A1 - 17 Excitation (red curve) and emission (blue curve) spectrum of Cu(dmp)(Xantphos)]BF ₄	185
Figure A1 - 18 Lifetime spectrum of Cu(ddpq) ₂ BF ₄	186
Figure A1 - 19 Lifetime spectrum of Cu(ddpq)(DPEPhos)BF ₄	186
Figure A1 - 20 Lifetime spectrum of Cu(ddpq)(XantPhos)BF ₄	187
Figure A1 - 21 Lifetime spectrum of Cu(ddpq)(dppf)BF ₄	187
Figure A1 - 22 Lifetime spectrum of Cu(ddppz) ₂ BF ₄	188
Figure A1 - 23 Lifetime spectrum of Cu(ddppz)(DPEPhos)BF ₄	188
Figure A1 - 24 Lifetime spectrum of Cu(ddppz)(XantPhos)BF ₄	189
Figure A1 - 25 Lifetime spectrum of Cu(ddppz)(dppf)BF ₄	189
Figure A1 - 26 Lifetime spectrum of Cu(dbdppz) ₂ BF ₄	190
Figure A1 - 27 Lifetime spectrum of Cu(dbdppz)(DPEPhos)BF ₄	190
Figure A1 - 28 Lifetime spectrum of Cu(dbdppz)(XantPhos)BF ₄	191
Figure A1 - 29 Lifetime spectrum of Cu(dbdppz)(dppf)BF ₄	191
Figure A1 - 30 Lifetime spectrum of Cu(dmp)(Xantphos)BF ₄	192
Figure A1 - 31 Lifetime spectrum of Cu(dmp)(dppf)BF ₄	192
Figure A1 - 32 Cyclic voltammogram of Cu(ddpq) ₂ BF ₄	193
Figure A1 - 33 Cyclic voltammogram of Cu(ddpq)(DPEPhos)BF ₄	193
Figure A1 - 34 Cyclic voltammogram of Cu(ddpq)(Xantphos)BF ₄	194
Figure A1 - 35 Cyclic voltammogram of Cu(ddpq)(dppf)BF ₄	194
Figure A1 - 36 Cyclic voltammogram of Cu(ddppz) ₂ BF ₄	195
Figure A1 - 37 Cyclic voltammogram of Cu(ddppz)(DPEPhos)BF ₄	195
Figure A1 - 38 Cyclic voltammogram of Cu(ddppz)(Xantphos)BF ₄	196
Figure A1 - 39 Cyclic voltammogram of Cu(ddppz)(dppf)BF ₄	196
Figure A1 - 40 Cyclic voltammogram of Cu(dbddppz) ₂ BF ₄	197
Figure A1 - 41 Cyclic voltammogram of Cu(dbdppz)(DPEPhos)BF ₄	197
Figure A1 - 42 Cyclic voltammogram of Cu(dbdppz)(Xantphos)BF ₄	198
Figure A1 - 43 Cyclic voltammogram of Cu(dbdppz)(dppf)BF ₄	198
Figure A1 - 44 Cyclic voltammogram of Cu(dmp) ₂ BF ₄	199

Figure A1 - 45 Cyclic voltammogram of Cu(dmp)(DPEPhos)BF ₄	199
Figure A1 - 46 Cyclic voltammogram of Cu(dmp)(Xantphos)BF ₄	200
Figure A1 - 47 Cyclic voltammogram of Cu(dmp)(dppf)BF ₄	200
Figure A2 - 1 UV-visible absorption spectrum of new Cu(NN)(BINAP)BF ₄ complexes	221
Figure A2 - 2 Excitation (blue curve) and emission (orange curve) spectrum of Cu(dpq)(BINAP)BF ₄	221
Figure A2 - 3 Excitation (blue curve) and emission (orange curve) spectrum of Cu(dppz)(BINAP)BF ₄	222
Figure A2 - 4 Excitation (blue curve) and emission (orange curve) spectrum of Cu(bdppz)(BINAP)BF ₄	222
Figure A2 - 5 Lifetime spectrum of Cu(dpq)(BINAP)BF ₄	223
Figure A2 - 6 Lifetime spectrum of Cu(dppz)(BINAP)BF ₄	224
Figure A2 - 7 Lifetime spectrum of Cu(bdppz)(BINAP)BF ₄	224
Figure A2 - 8 OSWVs of Cu(NN)(BINAP)BF ₄	225
Figure A2 - 9 OSWVs of Cu(NN)(BINAP)BF ₄	226
Figure A3 - 1 Homemade photoreactor used for the photochemical isomerizations	262
Figure A3 - 2 Correlation between Cu(dmp)(PP)BF ₄ photocatalysts triplet energy and formation of the Z-isomer	264
Figure A3 - 3 Correlation between Cu(NN)(XantPhos)BF ₄ photocatalysts triplet energy and formation of the Z-isomer	266
Figure A3 - 4 Continuous flow reactor set-up used for the scale-up reactions	278
Figure A3 - 5 Experimental set-up for the ATRA reactions.	284
Figure A3 - 6 UV-visible absorption spectrum of new Cu(NN)(XantPhos) BF ₄ complexes	287
Figure A3 - 7 UV-visible absorption spectrum of new Cu(dmp)(PP)BF ₄ complexes	288
Figure A3 - 8 Emission spectrum of Cu(dmp)(XantPhos) BF ₄	289
Figure A3 - 9 Emission spectrum of Cu(dmp)(Phanephos) BF ₄	290
Figure A3 - 10 Emission spectrum of Cu(dmp)(Xantphos) BF ₄	290

Figure A3 - 11 Emission spectrum of Cu(dmp)(dppf)BF ₄	291
Figure A3 - 12 Emission spectrum of Cu(dmp)(dppn)BF ₄	291
Figure A3 - 13 Emission spectrum of Cu(dmp)(BINAP)BF ₄	292
Figure A3 - 14 Emission spectrum of Cu(dmp)(SEGPHOS) BF ₄	292
Figure A3 - 15 Emission spectrum of Cu(dpa)(Xantphos)BF ₄	293
Figure A3 - 16 Emission spectrum of Cu(quintri)(Xantphos)BF ₄	293
Figure A3 - 17 Emission spectrum of Cu(bathocup)(Xantphos) BF ₄	294
Figure A3 - 18 Emission spectrum of Cu(batho)(Xantphos) BF ₄	294
Figure A3 - 19 Emission spectrum of Cu(BPhen)(Xantphos) BF ₄	295
Figure A3 - 20 Emission spectrum of Cu(dmop)(Xantphos) BF ₄	295
Figure A3 - 21 Emission spectrum of Cu(phen)(Xantphos) BF ₄	296
Figure A3 - 22 Emission spectrum of Cu(dmbp)(Xantphos)BF ₄	296
Figure A3 - 23 Emission spectrum of Cu(dtbbp)(Xantphos)BF ₄	297
Figure A3 - 24 Emission spectrum of Cu(iquintri)(Xantphos)BF ₄	297
Figure A3 - 25 Emission spectrum of Cu(pytri)(Xantphos)BF ₄	298
Figure A3 - 26 Emission spectrum of Cu(tmp)(Xantphos)BF ₄	298
Figure A3 - 27 Lifetime spectrum of Cu(dmp)(NXantphos)BF ₄	300
Figure A3 - 28 Lifetime spectrum of Cu(dmp)(Xantphos)BF ₄	300
Figure A3 - 29 Lifetime spectrum of Cu(dmp)(Phanephos)BF ₄	301
Figure A3 - 30 Lifetime spectrum of Cu(dmp)(dppf)BF ₄	301
Figure A3 - 31 Lifetime spectrum of Cu(dmp)(dppn)BF ₄	302
Figure A3 - 32 Lifetime spectrum of Cu(dmp)(SEGphos)BF ₄	302
Figure A3 - 33 Lifetime spectrum of Cu(dpa)(Xantphos)BF ₄	303
Figure A3 - 34 Lifetime spectrum of Cu(quintri)(Xantphos)BF ₄	303
Figure A3 - 35 Lifetime spectrum of Cu(bphen)(Xantphos)BF ₄	304
Figure A3 - 36 Lifetime spectrum of Cu(iquintri)(Xantphos)BF ₄	304
Figure A3 - 37 Lifetime spectrum of Cu(dmop)(Xantphos)BF ₄	305
Figure A3 - 38 Lifetime spectrum of Cu(phen)(Xantphos)BF ₄	305
Figure A3 - 39 Lifetime spectrum of Cu(pytri)(Xantphos)BF ₄	306

Figure A3 - 40 Lifetime spectrum of Cu(tmp)(Xantphos)BF ₄	306
Figure A3 - 41 Lifetime spectrum of Cu(dtbbp)(Xantphos)BF ₄	307
Figure A3 - 42 Lifetime spectrum of Cu(dmbp)(Xantphos)BF ₄	307
Figure A3 - 43 Setup for the photostability of copper complexes	308
Figure A4 - 1 Decomposition of Lignin Models	375
Figure A4 - 2 Evaluation of Cu(I)-Based Photocatalysts in the Cleavage of a Lignin Model.	377
Figure A4 - 3 Mechanistic Proposal for the Cleavage of the Lignin Models	380
Figure A5 - 1 Calibration curve of 1-(3,4-dimethoxyphenyl)ethan-1-one	401
Figure A5 - 2 Continuous flow reactor set-up used for the scale-up reactions.	408
Figure A5 - 3 Synthesis of the model polymer	409
Figure A5 - 4 Life-time spectra of Cu(bathocup)(Xantphos)BF ₄ with various concentrations of NABnH	411
Figure A5 - 5 Stern-Volmer plot of Cu(bathocup)(Xantphos)BF ₄ with NABnH	411
Figure A5 - 6 Life-time spectra of Cu(bathocup)(Xantphos)BF ₄ with various concentrations of 1	412
Figure A5 - 7 Stern-Volmer plot of Cu(Bathocup)(Xantphos)BF ₄ with 1	413
Figure A5 - 8 Life-time spectra of Cu(bathocup)(Xantphos)BF ₄ with various concentrations of NaHCO ₃ and Na ₂ S ₂ O ₄	414
Figure A5 - 9 Stern-Volmer plot of Cu(bathocup)(Xantphos)BF ₄ with NaHCO ₃ and Na ₂ S ₂ O ₄	414
Figure A5 - 10 NMR Spectra for the deuteration experiment	415
Figure A6 - 1 HPLC chromatogram of 3,5-TPDY-PEG-NH ₃ Cl.....	444
Figure A6 - 2 ¹ H NMR peaks of the 3,5-triazole products and the internal standard	451
Figure A6 - 3 Plot of $1(a - b) \times \ln b(a - x)a(b - x)$ versus the reaction time for 3,5-TPDY Run 1.....	453
Figure A6 - 4 Plot of $1(a - b) \times \ln b(a - x)a(b - x)$ versus the reaction time for 3,5-TPDY Run 2	453

Figure A6 - 5 Plot of $1(a - b) \times \ln b(a - x)a(b - x)$ versus the reaction time for 3,5-TPDY Run 3	454
Figure A6 - 6 ^1H NMR peaks of the 2,6-triazole products and the internal standard.....	455
Figure A6 - 7 Plot of $1(a - b) \times \ln b(a - x)a(b - x)$ versus the reaction time for 2,6-TPDY Run 1	456
Figure A6 - 8 Plot of $1(a - b) \times \ln b(a - x)a(b - x)$ versus the reaction time for 2,6-TPDY Run 2	457
Figure A6 - 9 Plot of $1(a - b) \times \ln b(a - x)a(b - x)$ versus the reaction time for 2,6-TPDY Run 3	457
Figure A6 - 10 ^1H NMR peaks of the 2,4-triazole products and the internal standard.....	458
Figure A6 - 11 Plot of $1(a - b) \times \ln b(a - x)a(b - x)$ versus the reaction time for 2,4-TPDY Run 1	459
Figure A6 - 12 Plot of $1(a - b) \times \ln b(a - x)a(b - x)$ versus the reaction time for 2,4-TPDY Run 2	459
Figure A6 - 13 Plot of $1(a - b) \times \ln b(a - x)a(b - x)$ versus the reaction time for 2,4-TPDY Run 3	460
Figure A6 - 14 MTG-mediated conjugation of B domain of protein G (Gb1).....	465

Liste des schémas

Schéma 1.1 Synthèse du complexe hétéroleptique $\text{Cu}(\text{dcbqH}_2)(\text{dmesp})\text{PF}_6$	43
Schéma 1.2 Couplage C-C du bromure de para-nitrobenzyle photocatalysé par $\text{Cu}(\text{dap})_2\text{Cl}$ et mécanisme proposé	48
Schéma 1.3 Synthèse de [5]héliène photocatalysée par $\text{Cu}(\text{dmp})(\text{Xantphos})\text{BF}_4$ et mécanisme proposé.....	49
Schéma 1.4 Fragmentation décarboxylative de N-(acyloxy)phtalimide photocatalysée par $\text{Cu}(\text{dq})(\text{BINAP})\text{BF}_4$ et mécanisme proposé	51
Schéma 1.5 Réaction d'Appel catalysée par $\text{Cu}(\text{tmp})(\text{BINAP})\text{BF}_4$ et un mécanisme possible	52

Schéma 1.6 Trifluorométhylchlorosulfonylation d'alcène catalysée par Cu(dap) ₂ Cl et le mécanisme proposé	54
Schéma 1.7 Réaction de PCET catalysée par Cu(quintri)(Xantphos)BF ₄ et mécanisme proposé. .	56
Schéma 1.8 Dimérisation de carbonyle catalysée par Cu(ppyzs)(BINAP)BF ₄ et mécanisme proposé.....	57
Schéma 1.9 Représentation de la structure de la lignine et décomposition de modèles de lignine photocatalysée.....	59
Schéma 1.10 Décomposition d'azoture catalysée par Cu(dmp)(BINAP)BF ₄ pour la synthèse de pyrrole et mécanisme proposé	63
Schéma 1.11 a. Influence de l'énergie triplet du photocatalyseur sur le ratio E:Z de l'isomérisation b. Exemples de photoisomérisations d'alcènes.	65
Schéma 4.1 Diversification of haloalkenes	110
Schéma 6.1 Réaction de cycloaddition azoture-alcyne et structures des molécules proposées par Michael.....	127

Liste des sigles et abréviations

β	Bêta
τ	Temps de vie de l'état excité
ΔG	Énergie libre de Gibbs
δ	Déplacement chimique
ϵ	Coefficient d'absorption molaire
λ_{\max}	Longueur d'onde d'absorbance maximale
λ_{em}	Longueur d'onde d'émission maximale
μs	Microseconde
μL	Microlitre
ν	Fréquence
π	Pi
Å	Angström
A	Absorption/Absorbance
acac	Acétylacétone
atm	Atmosphère (pression)
ATRA	Transfert d'atome radicalaire
bpy	2,2'-Bipyridine
Boc	<i>tert</i> -Butoxycarbone
br	Large
Bu	Butyle
°C	Degré celsius
CI	Conversion interne
CIS	Croisement intersystème
CISI	Croisement intersystème inverse
cm	Centimètre
CuAAC	Cycloaddition azoture alcyne catalysée par le cuivre
d	Doublet
DCM	Dichlorométhane
DEL/LED	Diode Électroluminescente
DFT	Théorie de la densité fonctionnelle
DIPEA	<i>N,N</i> -Diisopropyléthylamine
DME	1,2-Diméthoxyétane
DMF	<i>N,N</i> -Diméthylformamide
DMSO	Diméthylsulfoxyde
dppa	Acide diphényle phosphorique

dtbbpy	4,4'-Di- <i>tert</i> -butyl-2,2'-dipyridyle
E	Énergie
E _{ox}	Potentiel d'oxydation
E _{red}	Potentiel de réduction
<i>E</i>	Entgegen (opposé)
ET	Transfert d'électron
E _T	Énergie Triplet
Et	Éthyle
Équiv.	Équivalent
eV	Électron Volt
ESI	Spectrométrie de masse par électronébulisation
<i>fac</i>	Facial
FL	Fluorescence
g	Gramme
GC-MS	Chromatographie en phase gazeuse couplée à la spectrométrie de masse
h	Heure
<i>h</i>	Constante de Planck
HEH	Diéthyl 1,4-dihydro-2,6-diméthyl-3,5-pyridinedicarboxylate
HOMO	Plus haute orbitale moléculaire occupée
HPLC	Chromatographie liquide à haute pression
HRMS	Spectrométrie de masse haute résolution
Hz	Hertz
<i>i</i> -Pr	Isopropyle
<i>J</i>	Constante de couplage
J.C.	Jésus Christ
k	Constante de vitesse
K	Constante d'équilibre
L	Litre
LC	Centré sur le ligand
LDA	Diisopropylamidure de lithium
LUMO	Plus basse orbitale moléculaire vacante
m/z	Masse sur charge
m	Multiplet
m	Mètre
M	Molaire
Me	Méthyle
mg	Milligramme
MHz	Mégahertz

min	Minute
mL	Millilitre
MLCT	Transfert de Charge Métal-Ligand
mm	Millimètre
mM	Millimolaire
mmol	Millimole
mol	Mole
MS	Spectrométrie de masse
MTT	Bromure de 3-(4,5-diméthylthiazol-2-yl)-2,5-diphényltetrazolium
<i>n</i>	Normal
ns	Nanoseconde
nm	Nanomètre
<i>o</i>	Ortho
<i>p</i>	Para
PH	Phosphorescence
PC	Photocatalyseur
PC*	Photocatalyseur dans son état excité
PCET	Transfert couplé électron-proton
Ph	Phényle
Phen	Phénanthroline
PI	Photoisomérisation
PJT	Pseudo Jahn-Teller
PJTI	Pseudo Jahn-Teller inverse
PMDTA	Pentaméthyl-diéthylène-triamine
PPC	Pseudo plan-carré
Ppm	Partie par million
ppy	Phénylpyridine
PT	Pseudo-tétrahédral
q	Quadruplet
RMN	Résonance Magnétique Nucléaire
RSE	Énergie de tension de cycle
r. t.	Température ambiante (<i>room temperature</i>)
s	Singulet
s	Seconde
S ₀	État fondamental singulet
S ₁	État excité singulet
SCE	Électrode de calomel saturée
SET	Transfert d'électron simple

S_N2	Substitution Nucléophile bimoléculaire
SOMO	Plus haute orbitale individuellement occupée
SPAAC	Cycoaddition azoture alcyne promue par la tension
SPDHH	Hydroamination diyne hydrazine promue par la tension
<i>t</i>	<i>tert</i>
t	Triplet
T_1	État excité triplet
TBAF	Fluorure de tétra- <i>n</i> -butylammonium
<i>t</i> -Bu	<i>tert</i> -Butyle
TEMPO	(2,2,6,6-Tetraméthylpiperidin-1-yl)oxyl
t.p.	Température pièce
TP	Transfert de proton
TMS	Triméthylsilyle
THF	Tétrahydrofurane
TLC	Chromatographie sur couche mince
TS	État de transition
TSCI	Chlorure de 4-toluènesulfonyle
UICPA	Union Internationale de Chimie Pure et Appliquée
UV	Ultraviolet
V	Volt
Vis	Visible
<i>vs</i>	<i>versus</i>
W	Watt
Z	Zusammen (ensemble)

“Non, mais je crois qu’il faut que vous arrêtez d’essayer de dire des trucs. Ça vous fatigue, déjà, et pour les autres, vous vous rendez pas compte de ce que c’est ...” - Arthur Pendragon

Remerciements

Je remercie tout d'abord mon comité de thèse, Pr. A. Beauchemin, Pr. H. Lebel et Pr. R. Giasson d'avoir pris le temps de corriger cette thèse.

Je tiens ensuite à remercier mon professeur Shawn Collins pour l'opportunité d'avoir pu travailler au sein du groupe Collins. Merci pour le soutien et les encouragements qui m'ont permis de rester motivé pendant ces 5 ans. Merci d'avoir été aussi disponible à tout moment pour répondre à mes (nombreuses?) questions.

Je remercie mes collègues de travail avec qui j'ai pu travailler tout au long de ces années. Tout d'abord mes deux tuteurs de stage, Jeffrey Santandrea et Shawn Parisien-Collette, qui m'ont donné goût à la recherche et m'ont formé tout au long de mon année de stage; c'est sans doute grâce à vous que j'écris cette thèse aujourd'hui. Merci aussi aux « anciens » du groupe, Éric Godin, Émilie Morin et Antoine Caron, pour leur patience et leur aide durant mon début de doctorat. Merci à Clémentine Minozzi, avec qui j'ai pu passer l'entièreté de mon doctorat, d'avoir été là tous les jours pour râler sur nos projets qui ne marchaient pas, merci pour ton amitié et pour toute l'aide au labo que tu as pu m'apporter. Merci à Javier Guerrero, pour les bons moments au labo et dans la drinking room... je te passe le flambeau de doyen du groupe! Merci à Oliver Bleton pour les discussions pendant les flashes, la bonne musique, les radios GTA. Merci au reste du groupe, Noémie Beaucage, Nicolas Dowe, Guillaume Roland, Jérémie Bourdon pour la bonne ambiance au labo, les durs matins de group meeting et les McCarold!. Je tiens aussi à remercier particulièrement mes trois stagiaires, William Neiderer, Laurence Pelletier et Bernard D'Onofrio pour leur travail sous ma supervision, ça a été un plaisir d'avoir pu être votre tuteur.

Merci au reste du département pour les soirées et les discussions scientifiques. En premier évidemment Johann Sosoe, mon frère chimique, un énorme merci pour tout, les séances de whiskeymistry du vendredi soir, les posher, les al-amines, les séances de révisions du S-320... Merci à Gary Mathieu pour ces durs moments de prédoc passés ensemble à la bibliothèque et pour l'aide tout au long du doc. Merci au groupe Schmitzer de m'avoir accepté comme +1 pour toutes vos soirées.

Je remercie aussi les différentes plateformes de l'UdeM, Merci à Cedric pour l'aide durant les études cinétiques, merci à Karine et Louiza pour toute l'assistance avec les appareils de masse. Un grand merci aussi au Pr. Radu Iftimie pour avoir eu la patience de me former à la DFT, durant de nombreuses fins de journées.

Je remercie évidemment toute ma famille pour leur soutien malgré la distance, pour m'avoir toujours poussé pour réaliser le meilleur de moi-même c'est au tour de mon petit frère de se lancer à l'étranger, pour un futur doctorat?

Merci à mes amis du Québec, Max, Gab, Jordan pour toutes les soirées, toutes les sorties, les campings... tous ces moments qui permettent d'oublier qu'on est loin de chez soi.

Merci à mes amis de France, pour être toujours là malgré la distance, Stéphane, Kévin, Nico, et tout le groupe de conscrits.

Et enfin merci à toi Julie, sans qui tout ça aurait été beaucoup plus difficile... merci pour tout.

Chapitre 1 L'utilisation de complexes de cuivre pour la photocatalyse

1.1 Généralités

1.1.1 Introduction à la photocatalyse

Depuis le début du 19^{ième} siècle et les premiers travaux des photochimistes italiens (Ciamician, Paterno),¹⁻² la photochimie a été développée pour devenir un outil synthétique puissant. La photochimie peut être décrite comme l'utilisation de la lumière pour promouvoir des transformations chimiques.³ Accéder à des états excités (singulet ou triplet) par voie thermique est très difficile voire impossible; de nouvelles voies mécanistiques peuvent alors être permises grâce à la photochimie, augmentant le répertoire des réactions à la disposition du chimiste de synthétique.⁴⁻⁵

Bien que la photochimie soit étudiée depuis pratiquement 130 ans, son développement a connu un essor beaucoup plus lent que la chimie thermique. En effet pendant des décennies, la photochimie a été considérée comme difficilement maîtrisable, réservée à une poignée d'experts et donc cantonnée à des études physiques et théoriques.⁶ La condition *sine qua non* d'une réaction photochimique est l'absorption du photon par un réactif; or la majorité des molécules organiques utilisées en chimie organique absorbent dans le domaine de l'ultraviolet. L'excitation directe des substrats nécessite donc souvent une irradiation hautement énergétique, dans le domaine de l'UV C ou B (entre 100 et 315 nm) (**Figure 1.1**). Les premières réactions photochimiques ont utilisé la lumière directe du soleil, cependant le manque de reproductibilité dû à la météo variable a poussé les chimistes à utiliser des sources lumineuses comme les lampes à mercure à large spectre.⁷ Une verrerie spéciale en quartz est souvent requise, le verre en borosilicate absorbant dans l'UV. Enfin, l'excitation directe génère des espèces très réactives non sélectives, entraînant des réactions secondaires difficilement contrôlables.⁸⁻⁹

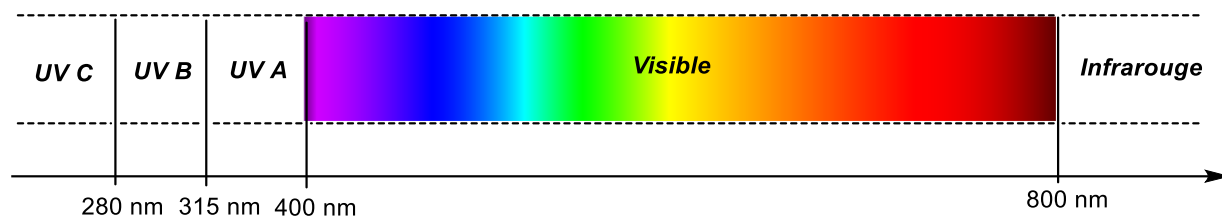


Figure 1.1 Spectre électromagnétique

La photocatalyse est définie par la UICPA comme: *"Change in the rate of a chemical reaction or its initiation under the action of ultraviolet, visible or infrared radiation in the presence of a substance—the photocatalyst—that absorbs light and is involved in the chemical transformation of the reaction partners."* La photocatalyse peut être séparée en deux grands groupes, la photocatalyse hétérogène et homogène. De multiples applications à la photocatalyse hétérogène (du traitement de l'eau¹⁰ à la production d'énergie¹¹) en font le groupe prédominant. La photocatalyse homogène correspond à la présence en solution du photocatalyseur, plus appliquée à la chimie synthétique. Cette thèse se concentrera sur cette dernière.

La photocatalyse utilise donc des chromophores, appelés *photocatalyseurs* de façon générale, ou parfois *photosensibilisateurs* dans le cadre d'un transfert d'énergie, qui agissent comme « relais » entre la source d'énergie (les photons) et les substrats. Un photocatalyseur, dans son état fondamental S_0 , absorbe un photon d'énergie $h\nu$, pour accéder à un état excité S_n (**Figure 1.2**). Une relaxation rapide par conversion interne (CI) ramène le photocatalyseur à l'état excité de plus basse énergie S_1 . Cet état excité, appelé état singulet, possède deux électrons non-pairés de spin différent; et l'orbitale de plus haute énergie est appelée la SOMO (pour *Single-Occupied Molecular Orbital*).¹²⁻¹³

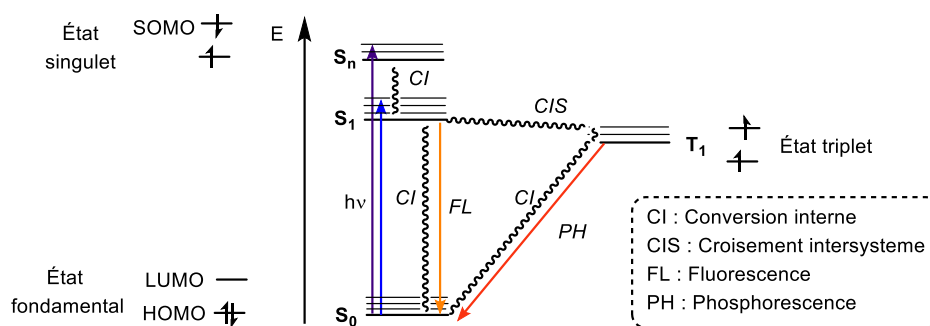


Figure 1.2 Diagramme de Jablonski

Depuis cet état singulet, le photocatalyseur peut alors se relaxer, soit par relaxation non-radiative, soit par l'émission d'un photon d'énergie correspondant à la différence d'énergie en S_1 et S_0 selon le processus de fluorescence. Cependant, dans la majorité des photocatalyseurs, un croisement intersystème est observé vers l'état triplet T_1 de plus basse énergie, correspondant à un changement de spin pour l'électron situé sur la SOMO.¹⁴ Ce dernier va alors se relaxer de façon non-radiative ou par l'émission d'un photon, selon le processus de phosphorescence. L'état triplet a généralement un temps de vie plus long que l'état singulet, car une conversion de spin est de nouveau nécessaire. Dans le cas où le photocatalyseur dans son état excité est en présence d'autres molécules, des réactions intermoléculaires peuvent avoir lieu, selon plusieurs mécanismes discutés ultérieurement dans ce chapitre. L'intérêt de cette stratégie est donc d'utiliser une longueur d'onde d'irradiation beaucoup moins énergétique, absorbée uniquement par le photocatalyseur, limitant les réactions secondaires indésirées. De plus, la réaction peut être contrôlée dans le sens désiré avec un choix judicieux du photocatalyseur et de ses propriétés photophysiques (potentiel rédox ou énergie triplet).

Pour être performant, un photocatalyseur doit posséder les propriétés suivantes:¹⁵

- Absorber fortement dans le domaine du visible (entre 400 et 800 nm)
- Avoir un état excité avec un temps de vie suffisamment long pour pouvoir réagir avec les réactifs
- Être stable durant les nombreux cycles d'excitation/relaxation

Les premiers exemples de photocatalyse remontent au début du siècle dernier en 1911, alors que le professeur Eibner rapporte le blanchissement du bleu de Prusse par illumination d'oxyde de zinc.¹⁶ Plusieurs autres exemples de photocatalyse hétérogène ont continué d'apparaître, comme l'utilisation de sels d'uranyles pour la dégradation d'acide oxalyles en 1911 par Bruner.¹⁷ En photocatalyse homogène, la majorité des travaux utilisent des complexes de ruthénium¹⁸ ou d'iridium.¹⁹ En effet, ces complexes possèdent une grande absorption dans le visible, un long temps de vie de l'état excité et une excellente photostabilité. Leur potentiel rédox et leur énergie triplet les rendent extrêmement versatiles pour diverses réactions. Cependant ces métaux nobles sont rares, et leur utilisation grandissante pose des problèmes d'approvisionnement. De plus, la synthèse non triviale de ses complexes limite la facilité d'optimisation de ces derniers. Un grand intérêt a été développé pour les photocatalyseurs organiques, comme les dérivés de porphyrine pour la génération d'oxygène singulet,²⁰ mais ces derniers souffrent de faible photostabilité et la modification de leur structure nécessite souvent une nouvelle synthèse complète. Il est donc important de s'intéresser à d'autres complexes organométalliques, se basant sur des métaux plus communs.

1.1.2 Le cuivre

Le cuivre est l'un des premiers métaux travaillé par l'homme, avec des bijoux en cuivre trouvés dans le nord de l'Irak datant de 8700 avant J.C. Vers 3000 ans avant J.C., les Égyptiens notent que l'addition d'étain au cuivre le rend plus malléable, permettant alors le développement de l'âge du bronze. Durant l'empire romain, le cuivre, métal prédominant alors, est appelé *aes Cyprium*, puisque la majorité de la production provenait de l'île de Chypre. Son nom se transforme peu à peu en *Cuprum* (donnant le signe chimique Cu), qui se francisera en cuivre.²¹

Le cuivre représente 0,006% de la croûte terrestre, ce qui en fait l'un des métaux les plus abondant sur la Terre (ruthénium, iridium : 0,000007%) (**Figure 1.3**). Le cuivre est un métal malléable, bon conducteur d'électricité et bon conducteur thermique, en plus de posséder une grande résistance à la corrosion. C'est pourquoi il est aujourd'hui le troisième métal le plus utilisé dans le monde, avec une production annuelle de 25,3 millions de tonnes en 2021.²²

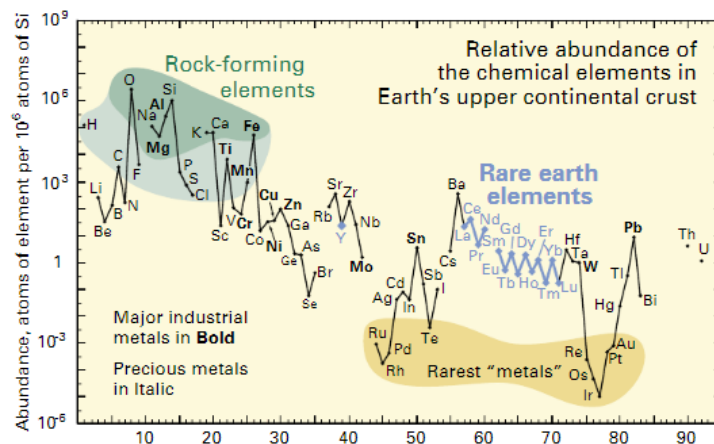


Figure 1.3 Abondance (en fraction atomique) d'éléments chimiques dans la croûte terrestre supérieure en fonction de leur numéro atomique. Image tirée de: Haxel, Gordon & Hedrick, James & Orris, Greta. (2002). Rare Earth Element Resources: A Basis for High Technology

1.2 Complexes homoleptiques de cuivre(I)

1.2.1 Caractéristiques électroniques des complexes homoleptiques de cuivre(I)

Le cuivre est le premier élément de la colonne 11 du tableau périodique avec l'argent et l'or. Il possède une configuration électronique de type : $[Ar] 3d^{10} 4s^1$. Le cuivre possède 4 états d'oxydation connus; 0, +1, +2 et +3. En solution, les états d'oxydation prévalents sont le cuivre(I) et (II); cependant la très grande majorité des photocatalyseurs de cuivre rapportés dans la littérature et dans cette thèse sont des complexes cationiques de cuivre(I) pour des raisons expliquées par la suite.

Les premiers complexes de cuivre reportés exhibant des propriétés photophysiques sont des complexes homoleptiques de type $Cu(N^{\wedge}N)_2X$, où $N^{\wedge}N$ représente un ligand bidentate diimine (souvent dérivé de la phénanthroline) et X représente le contre-ion. La configuration électronique de type d^{10} donne une symétrisation de la charge autour du métal, favorisant l'adoption d'une conformation pseudo-tétraédrique pour minimiser la répulsion électronique (**Figure 1.4**). La sous-couche électronique d remplie ne permet pas de réaliser des transitions d-d centrées sur le métal pour le cuivre(I). Dans le cas du cuivre(II) de configuration d^9 cependant, ces transitions entraînent

une relaxation non radiative très rapide, diminuant donc l'intérêt du cuivre(II) pour la photocatalyse.

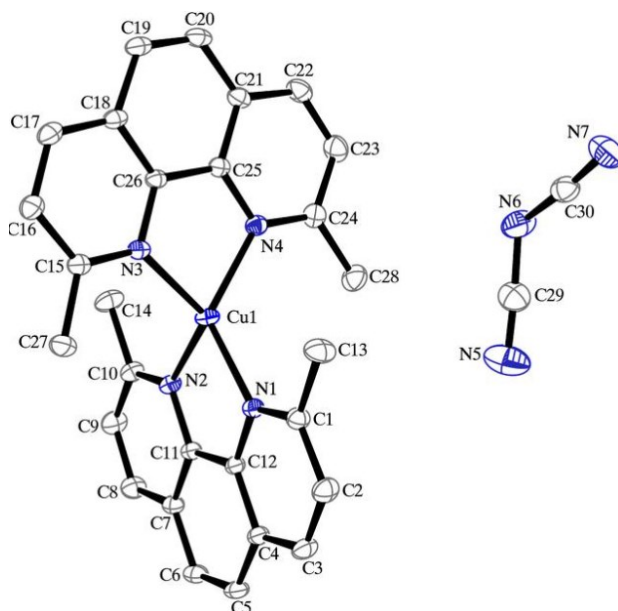


Figure 1.4 Structure par rayons X montrant la configuration tétraédrique du complexe de cuivre(I) $\text{Cu}(\text{dmp})_2\text{N}(\text{CN})_2$. Image tirée de : King et al. (2005). *Acta Cryst.* C61, 329-332, <https://doi.org/10.1107/S0108270105010760> et reproduite avec la permission de *International Union of Crystallography*

1.2.2 Propriétés photophysiques des complexes homoleptiques de cuivre(I)

Les complexes de cuivre(I) possèdent une importante bande d'absorption dans l'UV, correspondant aux transitions $\pi-\pi^*$ centrées sur les ligands (LC) conjugués diimines (**Figure 1.5**). La deuxième bande d'absorbance, située dans la zone du visible (entre 400 et 600 nm), est caractéristique d'une transition de transfert de charge métal à ligand (MLCT), entre l'orbitale d du cuivre et l'antiliante π^* du ligand diimine.²³ Cette transition, facilitée par le bas degré d'oxydation du cuivre, est aussi retrouvée dans les complexes de métaux d^6 comme le ruthénium et l'iridium.²⁴

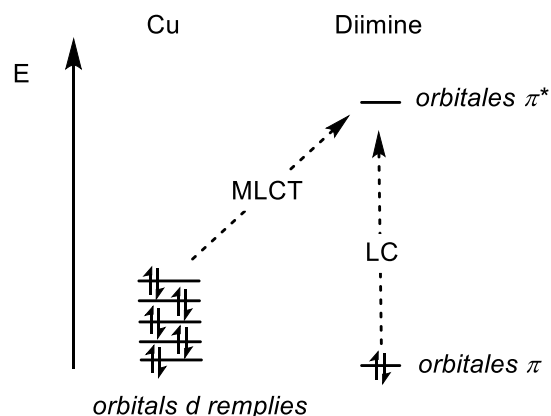


Figure 1.5 Représentation des transitions électroniques et des orbitales correspondantes dans les complexes de cuivre(I)

Après absorption d'un photon et MLCT, l'atome de cuivre passe donc dans un état d'oxydation (II), tandis qu'un des ligands est réduit, pour atteindre l'état singulet de configuration pseudo tétraédrique ${}^{\text{PT}}\text{S}_1$ (**Figure 1.6**). Dû à la présence du lourd atome de cuivre, un grand couplage spin-orbite est observé pour ces complexes, ce qui entraîne un croisement intersystème rapide vers l'état triplet ${}^{\text{PT}}\text{T}_1$. La configuration électronique d^9 du cuivre(II) entraîne une distorsion de la géométrie du complexe par effet pseudo Jahn-Teller (PJT)²⁵ pour adopter une conformation pseudo plan-carré (PPC). La distorsion de géométrie et le croisement intersystème se produisant à l'échelle de la picoseconde, la distorsion peut avoir lieu avant le CIS, pour atteindre l'état ${}^{\text{PPC}}\text{S}_1$, ou l'inverse, pour atteindre l'état ${}^{\text{PT}}\text{T}_1$. Les deux routes mènent cependant au même état triplet de plus basse énergie ${}^{\text{PPC}}\text{T}_1$. Ce dernier va alors se relaxer de façon non-radiative ou par l'émission d'un photon, selon le processus de phosphorescence **PH**. Dans le cas où les niveaux S_1 et T_1 sont proches en énergie, avec un ΔE inférieur à 0.3 eV, le complexe peut revenir à l'état singulet depuis l'état triplet par croisement intersystème inverse (CISI) et par effet pseudo Jahn-Teller inverse (PJT_I). L'émission d'un photon depuis le S_1 peut alors se produire, selon le principe de fluorescence retardée assistée par la température (*Thermally-Assisted Delayed Fluorescence* TADF).²⁶

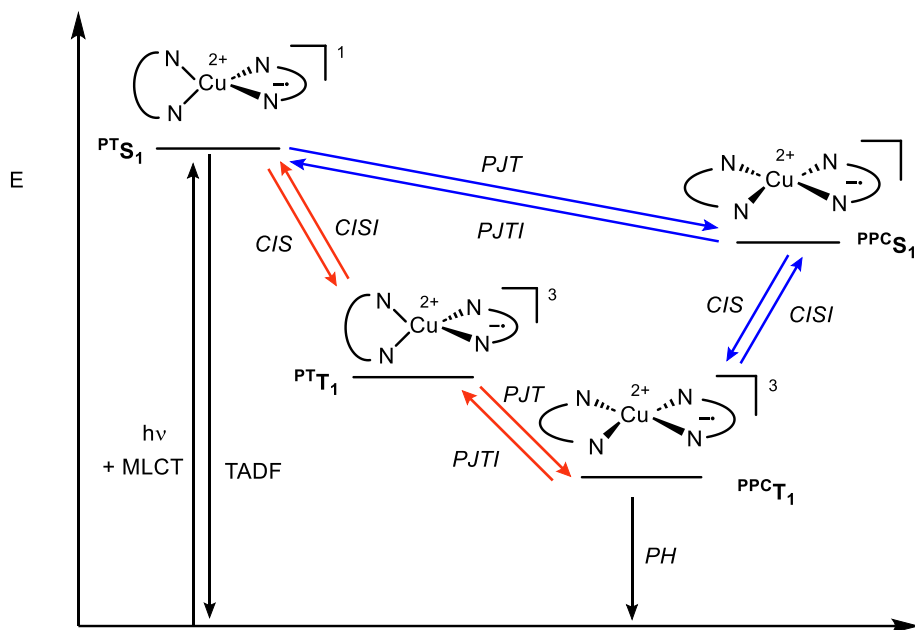


Figure 1.6 Diagramme d'énergie des différents états excités des complexes de cuivre(I)

Lors de l'excitation du complexe de cuivre, ce dernier subit donc un aplatissement de sa structure vers une configuration pseudo plan-carré (**Figure 1.7**). Cet aplatissement rend disponible un site de coordination sur l'atome de cuivre, permettant l'attaque de nucléophiles en solution, tels que des molécules de solvant coordinantes comme l'acétonitrile.²⁷ Le complexe résultant, appelé « exciplexe pentacoordiné », se relaxe de façon non-radiative. Ce processus a été étudié par McMillin en 1989, qui montre la dépendance du temps de vie de complexes de cuivre bisphénanthroliques en fonction de la nucléophilie du contre ion.²⁸

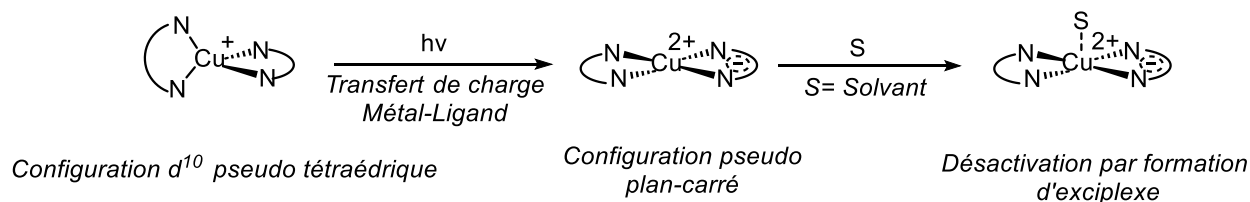


Figure 1.7 Effet pseudo Jahn-Teller et mécanisme de désactivation de l'état excité de complexes de cuivre(I)

Dans le but de maintenir un long temps de vie excité, il est nécessaire de limiter cet aplanissement, par l'utilisation de ligands encombrés. C'est pourquoi le premier complexe homoleptique de cuivre étudié pour ses propriétés photophysiques est le $\text{Cu}(\text{dmp})_2\text{BF}_4$ **1.2** par McMillin en 1977.²⁹ Il montre alors une absorption dans le visible, avec un maximum à 454 nm, et une émission à 750 nm, dans le CH_2Cl_2 . Les deux substituants méthyles en position 2 et 9 des phénanthrolines jouent donc le rôle de rigidificateurs de la structure du complexe en le bloquant dans une configuration pseudo-tétraédrique dans son état excité. En effet, l'analogue non-substitué $\text{Cu}(\text{phen})_2\text{BF}_4$ **1.1** ne montre aucune émission en solution.³⁰ Au contraire, l'utilisation de substituants plus encombrants permet d'augmenter le temps de vie de l'état excité du complexe, passant de 90 ns pour des substituants méthyles à 150 ns pour des substituants butyles, et à 365 ns pour des substituants isopropyles (**Figure 1.8**).

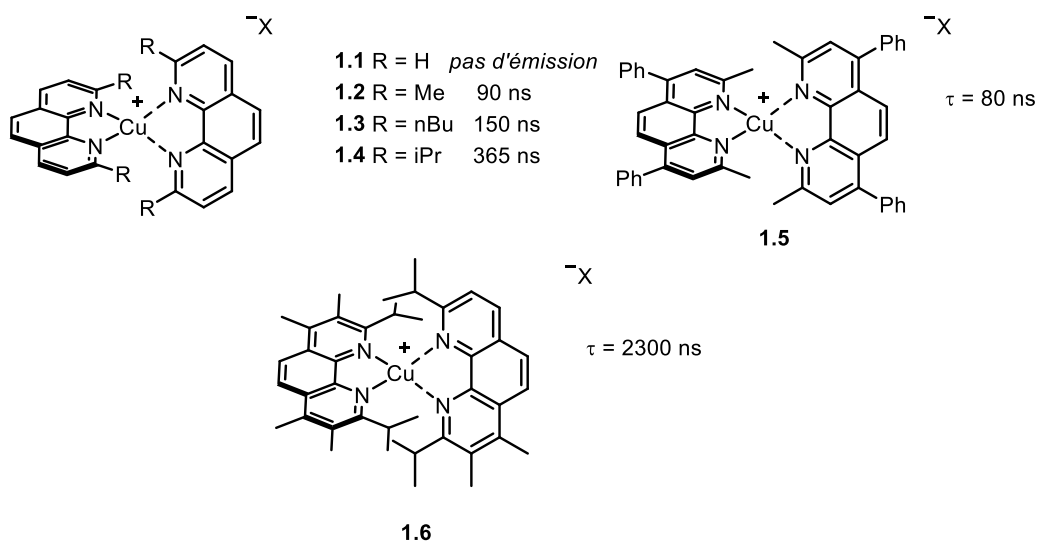


Figure 1.8 Influence des substituants des ligands phénanthroliques sur le temps de vie de l'état excité du complexe

L'influence des substituants sur le temps de vie de l'état excité relève plus de l'influence stérique qu'électronique, comme le montre le temps de vie du $\text{Cu}(\text{bathocup})_2\text{BF}_4$ **1.5** similaire à celui du $\text{Cu}(\text{dmp})_2\text{BF}_4$ **1.2**. La substitution des autres positions de la phénanthroline peut aussi avoir un effet sur le temps de vie, comme pour le complexe $\text{Cu}(\text{diptmp})_2\text{PF}_6$ **1.6** qui montre un temps de vie supérieur à 2 ms.³¹ L'utilisation de diimines très encombrées peut cependant devenir

problématique, car la formation du complexe devient thermodynamiquement défavorisée, et une dissociation rapide d'un ligand peut alors avoir lieu.³²

1.2.3 Propriétés électrochimiques des complexes homoleptiques de cuivre(I)

Les photocatalyseurs de cuivre sont majoritairement utilisés en photocatalyse photorédox. Dans ce domaine, les catalyseurs dans leur états excités permettent de promouvoir des réactions rédox qui seraient thermodynamiquement impossibles à réaliser à l'état fondamental. Les potentiels de l'état excité des complexes de cuivre peuvent être estimés selon les équations suivantes:³³

$$E(A^+/A^*) = E(A^+/A) + E^{00}$$

$$E(A^*/A^-) = E(A/A^-) - E^{00}$$

$E(A^+/A^*)$ et $E(A^*/A^-)$ représentent les potentiels des couples $Cu(II)/Cu(I)^*$ et $Cu(I)^*/Cu(0)$, $E(A^+/A)$ et $E(A/A^-)$ représentent les potentiels des couples $Cu(II)/Cu(I)$ et $Cu(I)/Cu(0)$, et E^{00} représente la différence d'énergie entre le niveau excité de plus basse énergie et le niveau fondamental. $E(A^+/A)$ et $E(A/A^-)$ peuvent être mesurés par des expériences de voltampérométrie, tandis que E^{00} peut être estimé en utilisant le maximum d'émission du complexe.

Dans leur état fondamental, les complexes de cuivre(I) $Cu(N^N)_2X$ possèdent un potentiel d'oxydation entre +0,5 V et +1 V et un potentiel de réduction entre -1,40 V et -1,80 V, ce qui en font de meilleurs réducteurs que oxydants. Dans leur état excité, les complexes de cuivre deviennent à la fois de meilleurs oxydants et de meilleurs réducteurs. Ceci est dû au transfert de charge qui induit la formation d'un centre métallique de cuivre(II), et la réduction d'un ligand diimine (**Figure 1.9**). Le potentiel d'oxydation de ces complexes à l'état excité est entre -0,5 V et -1 V, tandis que leur potentiel de réduction est entre -0,2 V et + 0,5 V.³⁴

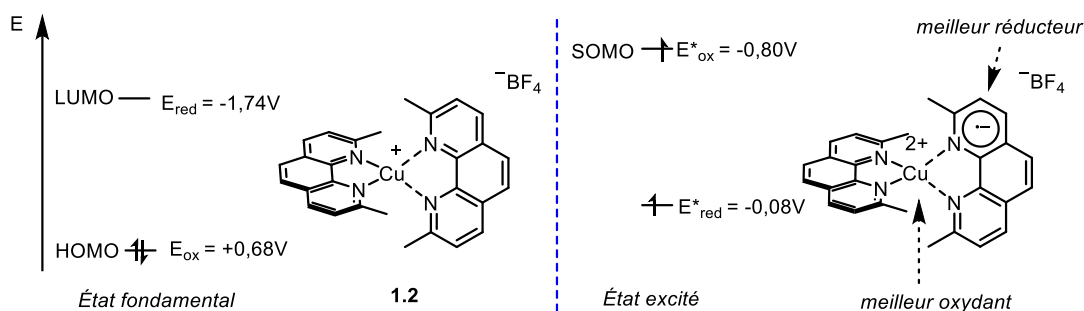


Figure 1.9 Différence de potentiels redox entre l'état fondamental et l'état excité de $\text{Cu}(\text{dmp})_2\text{BF}_4$

En raison de leur faible potentiel d'oxydation, les complexes homoleptiques de cuivre(I) sont majoritairement utilisés comme donneurs d'électrons. Dans l'état excité, l'électron de plus haute énergie est situé sur le ligand diimine. Il est donc possible de modifier ces substituants afin d'augmenter la densité électronique, résultant alors en une diminution du potentiel d'oxydation. Cette influence est montrée à la **Figure 1.10**, avec l'utilisation de substituants *p*-anisole (dap) diminuant le potentiel d'oxydation de l'état excité de **1.7** à -1,13 V (contre -0,8 V pour **1.2**).³⁵ À l'inverse, le ligand électrodéficient (bfp) entraîne un potentiel plus élevé à -0,31 V pour le complexe **1.8**. Le potentiel de réduction de l'état excité est aussi influencé par la nature des ligands; des ligands électroattracteurs stabilisent la réduction du cuivre en Cu(0) comme le ligand (bfp) qui possède un potentiel du couple Cu(I)* / Cu(0) extrêmement élevé pour un complexe homoleptique de cuivre à +0,64 V. Cependant le processus de réduction se déroulant au niveau de l'atome de cuivre, une réorganisation de la géométrie du complexe est nécessaire; limitant la cinétique de transfert d'électron.³⁶

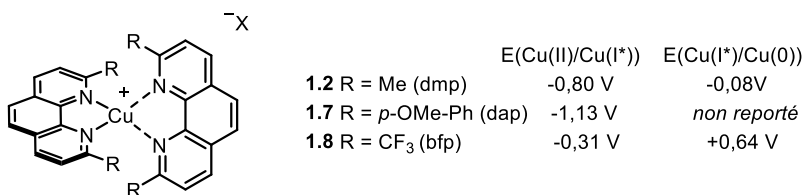


Figure 1.10 Influence des ligands sur les potentiels rédox des complexes de cuivre(I) homoleptiques

1.2.4 Synthèse des complexes homoleptiques de cuivre(I)

L'un des principaux avantages des complexes de cuivre est leur facilité de synthèse (**Figure 1.11**). En effet une source de cuivre(I) est mélangée à deux équivalents de ligand. Après agitation à température ambiante, le complexe peut souvent être précipité dans un solvant apolaire comme l'éther diéthylique pour obtenir le catalyseur pur sous la forme d'une poudre jaune à rouge, dépendamment de la diimine utilisée. Une librairie de complexes portant différents substituants peut donc rapidement être construite, facilitant le criblage pour l'optimisation d'une réaction.

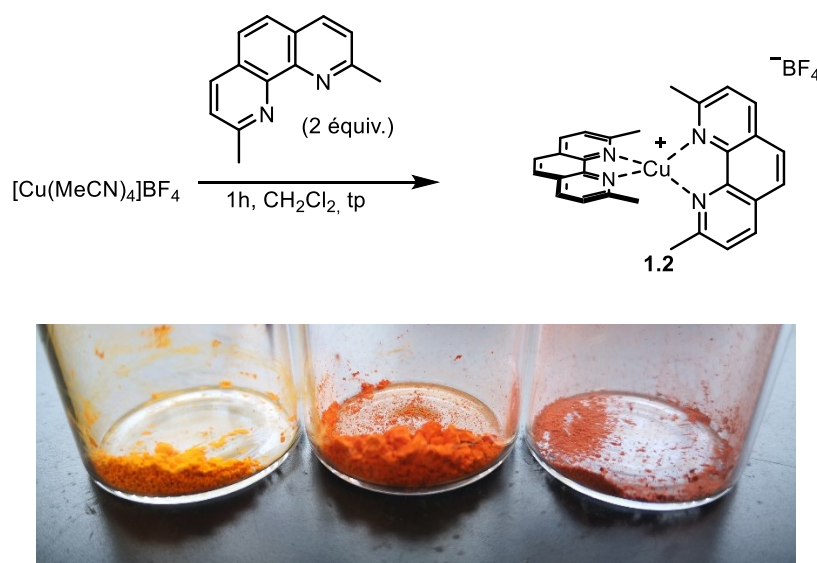


Figure 1.11 Synthèse de $\text{Cu}(\text{dmp})_2\text{BF}_4$ et couleurs de différents complexes homoleptiques sous forme solide

1.3 Complexes hétéroleptiques de cuivre

1.3.1 Synthèse des complexes hétéroleptiques de cuivre(I)

Les complexes homoleptiques sont limités dans leurs propriétés photophysiques par l'utilisation de deux ligands identiques. Le développement de complexes hétéroleptiques bisdiimines de cuivre(I), appelé stratégie HETPHEN (pour *HETeroleptic bis-PHENanthroline metal complexes*),³⁷ repose sur l'utilisation d'une diimine très encombrée avec une diimine plus petite

pour permettre la formation d'un complexe hétéroleptique. Cette stratégie est utile pour le développement d'appareils électroluminescents ou de cellules photovoltaïques, permettant une optimisation minutieuse des différents procédés photoinduits, comme pour le photocatalyseur développé par Odobel en 2013 (**Schéma 1.1**).³⁸ Dans le complexe synthétisé **1.11**, le ligand **dmesp 1.9** agit comme donneur d'électron, tandis que le ligand **dcbqH₂ 1.10** permet de lier le complexe à des nanoparticules de TiO₂. L'utilisation du ligand phénanthroline avec des substituants mésityles empêche la formation du complexe homoleptique Cu(dmesp)₂PF₆, et permet la coordination du deuxième ligand, moins encombré stériquement.

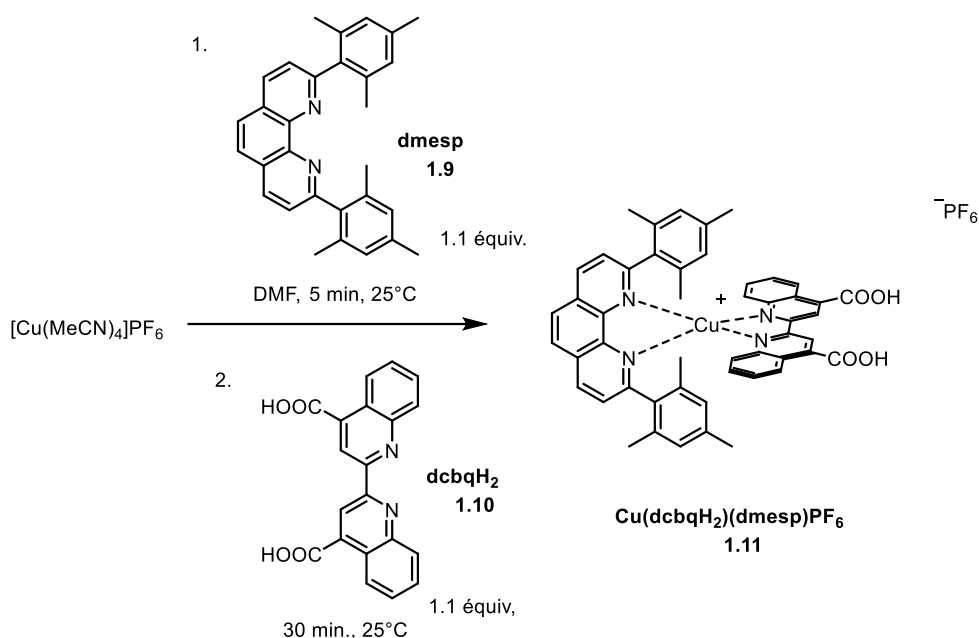


Schéma 1.1 Synthèse du complexe hétéroleptique Cu(dcbqH₂)(dmesp)PF₆

Si les complexes hétéroleptiques de type Cu(N[^]N)(N[^]N)X permettent de diversifier les champs de propriétés photophysiques disponibles, ils sont limités à l'utilisation d'une combinaison de deux diimines stériquement complémentaires. Les chimistes se sont aussi intéressés aux complexes hétéroleptiques de type Cu(N[^]N)(P[^]P)X possédant un ligand diimine et un ligand bidentate diphosphine. Les complexes Cu(N[^]N)(P[^]P)X peuvent être synthétisés de la même manière que les complexes hétéroleptiques bisdiimine. La source de cuivre, souvent le

cuivre tétrakis-acétonitrile, est mélangé à la diphosphine. Après 1h, la diimine est ajoutée, et la solution est agitée pendant une heure supplémentaire. Enfin, la précipitation du complexe dans un solvant apolaire donne le complexe pur. La formation de ces complexes nécessite cependant une bonne combinaison des deux ligands, car l'utilisation de diimines trop encombrées ou de diphosphines avec un angle de morsure trop faible peut entraîner un équilibre en solution entre le complexe hétéroleptique et les complexes homoleptiques (**Figure 1.13**). La reste de cette thèse se concentrera sur les complexes hétéroleptiques de type $\text{Cu}(\text{N}^{\wedge}\text{N})(\text{P}^{\wedge}\text{P})\text{X}$.

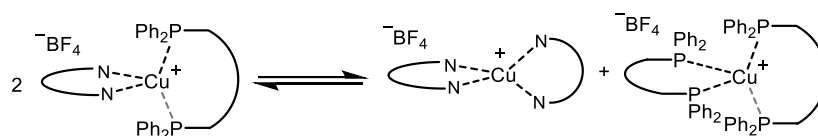


Figure 1.12 Équilibre entre le complexe hétéroleptique et les complexes homoleptiques correspondants

1.3.2 Propriétés photophysiques des complexes hétéroleptiques de cuivre(I)

Les complexes hétéroleptiques de type $\text{Cu}(\text{N}^{\wedge}\text{N})(\text{P}^{\wedge}\text{P})\text{X}$ possèdent une bande d'absorption dans l'UV correspondant à la transition $\pi\text{-}\pi^*$ centrée sur la diimine, similaire à celle observée avec les complexes homoleptiques. La donation du cuivre vers la diimine est cependant moins favorisée en raison du caractère électroattracteur des phosphines. Il en résulte une transition MLCT absorbant dans le proche UV, et un déplacement hypsochromique du maximum d'émission entre 450 et 600 nm (contre 550-700 nm pour les complexes homoleptiques). De plus, la perte d'un ligand diimine réduit le coefficient d'absorption molaire de ces complexes.

Les ligands diphosphines exercent une influence électronique différente de celle des ligands diimines, mais possèdent aussi une structure moins planaire. Les premiers complexes hétéroleptiques proviennent des travaux de McMillin dans les années 70, avec la synthèse du complexe $\text{Cu}(\text{dmp})(\text{PPh}_3)_2\text{BF}_4$.³⁹ Si ce complexe présente une émission à 600 nm, il possède un temps de vie de l'état excité inférieur à la nanoseconde, le rendant peu utile en photocatalyse. Au début des années 2000, McMillin a rapporté l'utilisation de la diphosphine DPEPhos pour la formation du complexe $\text{Cu}(\text{dmp})(\text{DPEPhos})\text{BF}_4$ **1.12**.⁴⁰ Ce dernier possède une émission à 565 nm

et un temps de vie de l'état excité extrêmement long de 14,3 μs (**Figure 1.14**), indiquant l'intérêt d'utiliser des ligands rigides bidentates, protégeant le centre métallique lors de l'aplanissement du complexe. Ces complexes sont cependant très sensibles à l'oxygène, comme le montre la différence de temps de vie de l'état excité pour le complexe $\text{Cu}(\text{dpp})(\text{DPEphos})\text{PF}_6$ **1.13** en milieu aéré (250 ns) et dans des conditions inertes (17600 ns).⁴¹

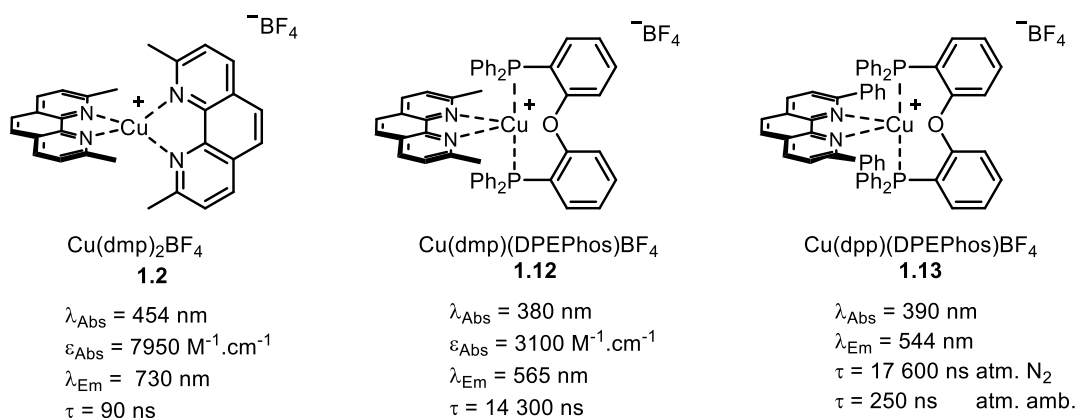


Figure 1.13 Comparaison des propriétés photophysiques de $\text{Cu}(\text{dmp})_2\text{BF}_4$ et $\text{Cu}(\text{dmp})(\text{DPEphos})\text{BF}_4$

1.3.3 Propriétés électrochimiques des complexes hétéroleptiques de cuivre(I)

Le potentiel d'oxydation à l'état excité du couple $\text{Cu}(\text{II})/\text{Cu}(\text{I})^*$ des complexes hétéroleptiques $\text{Cu}(\text{N}^{\wedge}\text{N})(\text{P}^{\wedge}\text{P})^+$ est similaire à celui des complexes homoleptiques car l'oxydation se fait sur le ligand diimine réduit ($\text{Cu}(\text{dmp})_2\text{BF}_4$ $E^*_{\text{ox}} = -0.80 \text{ V}$, $\text{Cu}(\text{dmp})(\text{DPEphos})\text{BF}_4$ $E^*_{\text{ox}} = -0.92 \text{ V}$). Au contraire, le potentiel de réduction à l'état excité est grandement augmenté ($\text{Cu}(\text{dmp})_2\text{BF}_4$ $E^*_{\text{red}} = -0.80 \text{ V}$, $\text{Cu}(\text{dmp})(\text{DPEphos})\text{BF}_4$ $E^*_{\text{ox}} = +0.53 \text{ V}$), dû à la rétrodonation π des phosphines. La HOMO qui était concentrée sur le centre métallique dans les complexes homoleptiques est maintenant répartie entre le cuivre et la diphosphine. Cela entraîne un abaissement de son énergie et donc favorise la réduction du centre métallique $\text{Cu}(\text{II})$. Un effet stérique entre aussi en jeu, puisque le grand angle de morsure de la diphosphine empêche la formation de la géométrie plan carré favorisé par le cuivre(II).

1.4 L'utilisation de complexe de cuivre pour la catalyse photorédox

1.4.1 Principe de la catalyse photorédox : Transfert d'électron simple

Le transfert d'électron simple (*Single Electron Transfer*, SET) est le transfert d'un électron d'un donneur d'électron (D) à un accepteur d'électron (A). Comme mentionné dans la section 1.2.3, les photocatalyseurs de cuivre dans leur état excité peuvent agir à la fois comme donneurs et accepteurs d'électron, dû à la présence à la fois d'un trou électronique et d'un électron de haute énergie après le MLCT (**Figure 1.15**). Le complexe passe alors d'une configuration électronique $d^{10}-L^0$ à d^9-L^{-1} . Le complexe dans son état triplet peut se relaxer par l'émission d'un photon ou par voie non-radiative. En présence d'un donneur d'électron **D**, le complexe se réduit pour atteindre l'état fondamental de configuration $d^{10}-L^{-1}$, soit un degré d'oxydation formel Cu(0). Par la suite, un accepteur d'électron **A** vient régénérer le catalyseur pour clore le cycle. Cette voie est appelée désexcitation réductrice et est souvent la voie majoritaire en présence de bons donneurs d'électrons comme des amines tertiaires (telles que Et₃N ou DIPEA). L'autre cycle, appelé désexcitation oxydante, fait d'abord réagir le complexe excité avec un accepteur d'électron, pour atteindre un degré d'oxydation formel Cu(II), avec une configuration électronique d^9-L^0 . Pour clore le cycle, une étape de réduction du cuivre à lieu, en présence d'un donneur d'électron. En absence d'un donneur sacrificiel d'électron, ce sera souvent la voie favorisée.⁴²

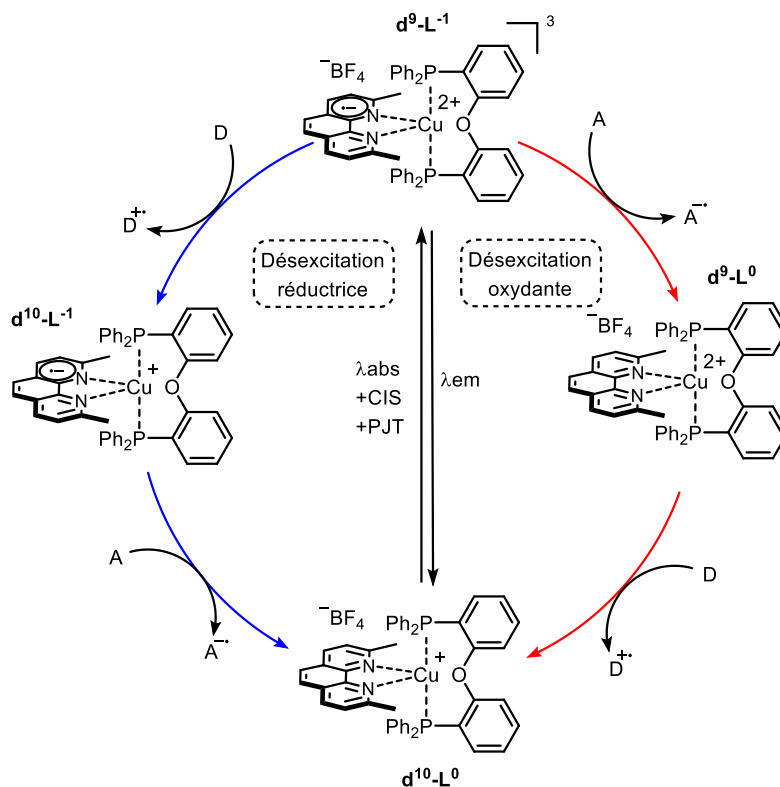


Figure 1.14 Cycles de désexcitation réductrice et oxydante du $\text{Cu}(\text{dmp})(\text{DPEPhos})\text{BF}_4$

1.4.2 Transfert d'électron simple

Un des premiers exemples de réaction rédox photocatalysée par un complexe de cuivre a été rapporté en 1987 avec les travaux de Sauvage.³⁵ Les auteurs ont montré l'efficacité du $\text{Cu}(\text{dap})_2\text{Cl}$ **1.7** pour la dimérisation du *p*-nitrobenzyle **1.14** (Schéma 1.2.). Le produit a été obtenu avec 47% de rendement, après 25h d'irradiation. Le mécanisme proposé, appuyé par des expériences de Stern-Volmer⁴³ passe par un cycle de désexcitation oxydante. Après excitation par un photon, le complexe de cuivre réduit **1.14** ($E_{\text{ox}}^*(\text{Cu}(\text{dap})_2\text{Cl}) = -1.13 \text{ V}$; $E_{\text{red}}(\text{1.11}) = -0.86 \text{ V}$) pour former le radical benzylique **1.16**. Ce dernier peut alors se recombinaison avec lui-même pour former **1.15** (voie 1). Une seconde réduction par le catalyseur, de **1.16** à **1.17** est aussi possible, facilitée par le groupe aryle électrodéficient (voie 2). Une substitution de type $\text{S}_{\text{N}}2$ sur **1.14** permet alors d'obtenir le produit **1.15**. Il est intéressant de noter que $\text{Cu}(\text{dmp})_2\text{BF}_4$ ($E_{\text{ox}} = -0.8 \text{ V}$) ne donne aucune réaction.

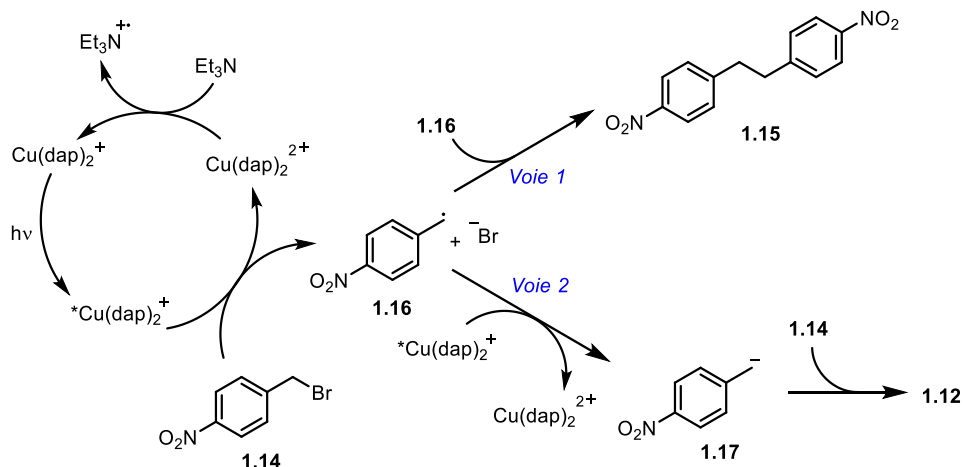
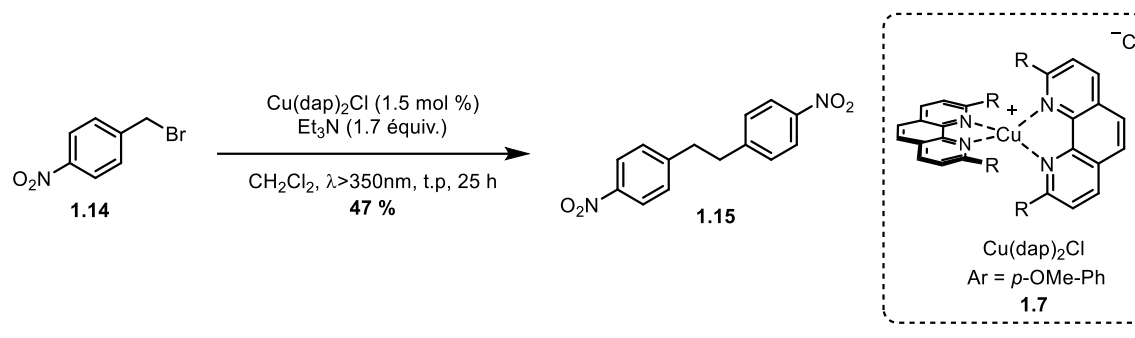


Schéma 1.2 Couplage C-C du bromure de para-nitrobenzyle photocatalysé par $\text{Cu(dap)}_2\text{Cl}$ et mécanisme proposé

Le premier exemple d'utilisation de complexes hétéroleptiques $\text{Cu(N}^{\wedge}\text{N)}(\text{P}^{\wedge}\text{P})\text{X}$ en photocatalyse rédox a été rapporté par Collins *et al.* pour la synthèse de [5]héliènes (**Schéma 1.3**).⁴⁴ Le photocatalyseur utilisé, $\text{Cu(dmp)(Xantphos)BF}_4$ **1.18** a été formé *in-situ* en prémélangeant les ligands et la source de cuivre. Les conditions optimales permettent de former **1.20** avec un rendement de 50% après 5 jours d'irradiation. Le mécanisme proposé passe par un cycle de désexcitation oxydante, avec le cuivre venant décomposer I_2 en I^- et I^\cdot . Ce dernier peut alors oxyder l'alcène **1.19**, qui par cyclisation forme l'intermédiaire **1.21**. Une première déprotonation par un iodure est proposée pour former **1.22**, puis un transfert d'un électron avec le cuivre(II) suivi d'une seconde déprotonation va former le [5]héliène **1.20**. L'oxyde de propylène présent en excès joue le rôle de piègeur de HI, qui pourrait détruire le catalyseur. Le catalyseur **1.18** s'est révélé être le plus efficace pour cette réaction, les catalyseurs de ruthénium et d'iridium testés ne donnant que des traces du produit.

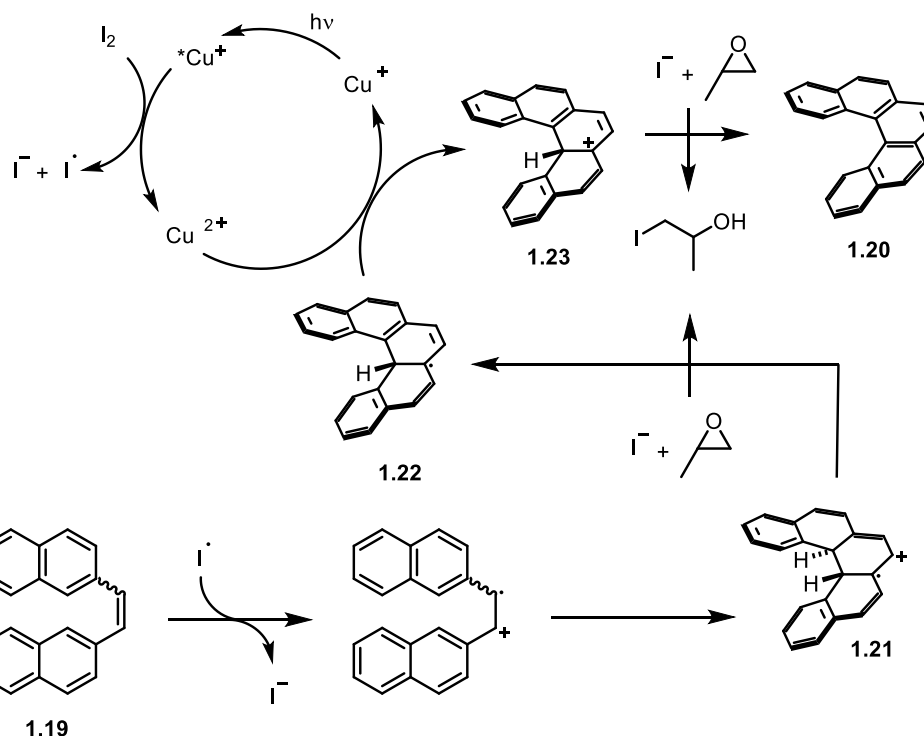
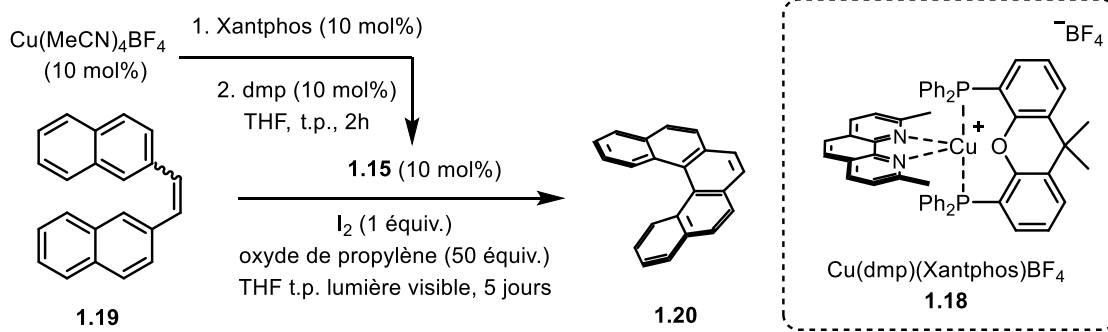


Schéma 1.3 Synthèse de [5]hélécène photocatalysée par $\text{Cu}(\text{dmp})(\text{Xantphos})\text{BF}_4$ et mécanisme proposé

Un grand intérêt s'est alors développé pour ces complexes, dont la facilité de synthèse permet une rapide modification de la structure. En 2018, notre groupe a développé une librairie de 40 complexes hétéroleptiques, se basant sur 4 diphosphines et 10 diimines.⁴⁵ Les diphosphines sont commercialement disponibles et ont été sélectionnées pour leurs différents angles de morsure. Les diimines se basent sur des motifs de type phénanthroline, bipyridine, et de nouveaux ligands non-symétriques portant une fonction triazole (**Figure 1.15**)

40 complexes hétéroleptiques synthétisés

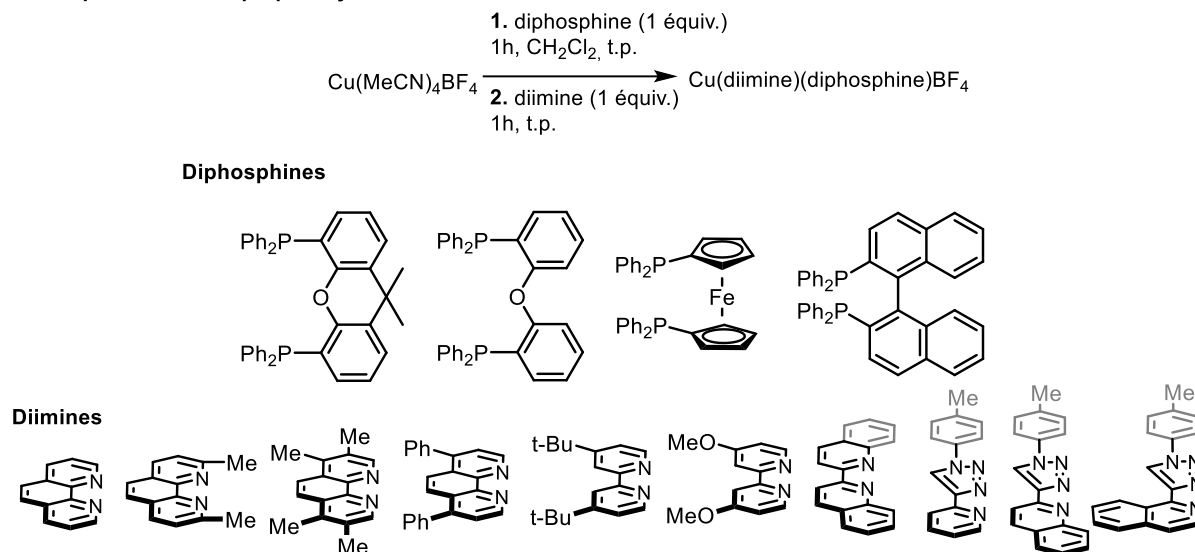


Figure 1.15 Liste des ligands utilisé pour la construction de la bibliothèque de complexes de cuivre(I)

Ces complexes ont alors pu être testés sur différentes réactions; la première étant la réduction d'un N-(acyloxy)phtalimide **1.24** (Schéma 1.4). Un catalyseur optimal, $\text{Cu}(\text{dq})(\text{BINAP})\text{BF}_4$ **1.25** a été trouvé, permettant le couplage $\text{C}_{\text{sp}}-\text{C}_{\text{sp}^3}$ avec le bromure d'alcyne **1.26** à 87% après 24h d'irradiation à 450 nm. Le mécanisme proposé se base sur les travaux de Chen qui utilise des conditions similaires avec un catalyseur de ruthénium.⁴⁶ Il passe par un cycle de désexcitation réductif, avec la réduction du complexe excité par la DIPEA ou l'ester de Hantzsch (HEH). Le complexe $\text{Cu}(0)$ transfère un électron au motif phtalimide, entraînant la décomposition de **1.24** pour former le radical cyclohexyle. Ce dernier attaque alors **1.26**, formant l'intermédiaire **1.27**, puis le produit **1.28** après élimination de l'halogénure.

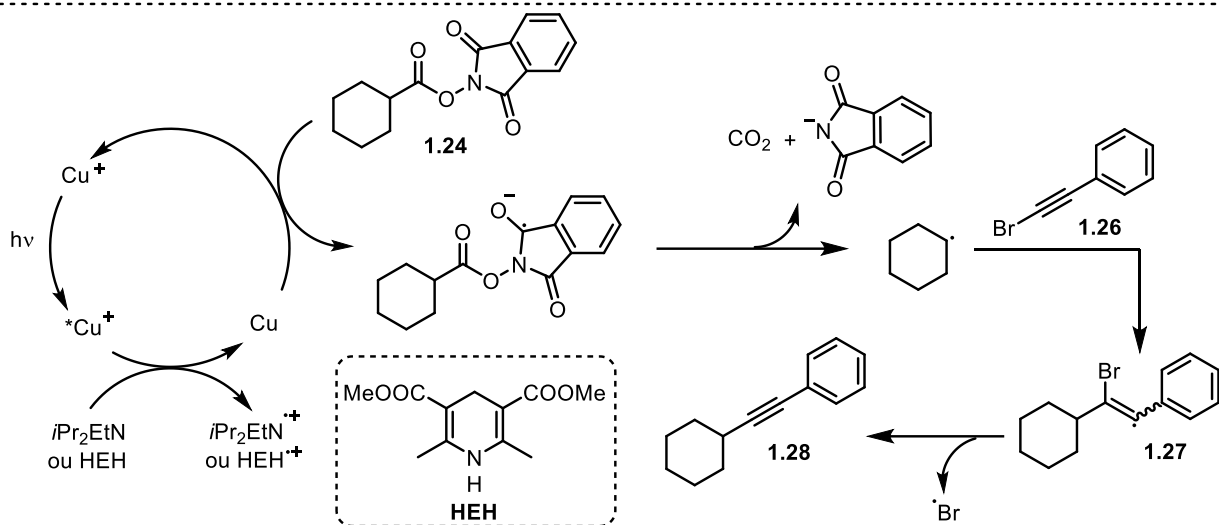
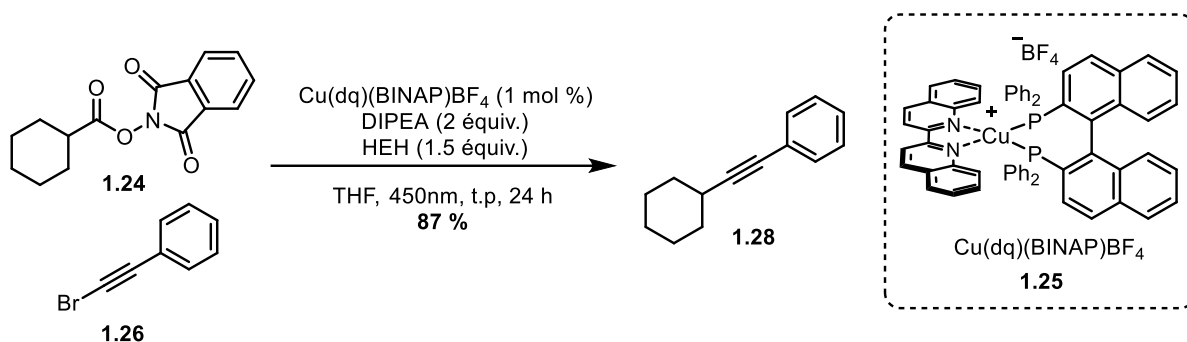


Schéma 1.4 Fragmentation décarboxylative de N-(acyloxy)phthalimide photocatalysée par Cu(dq)(BINAP)BF_4 et mécanisme proposé

Notre librairie de complexes a également été étudiée dans une réaction photocatalytique d'Appel, précédemment rapportée par Stephenson avec un catalyseur de ruthénium.⁴⁷ Un catalyseur optimal fut trouvé, $\text{Cu(tmp)(BINAP)BF}_4$ **1.29**, permettant la transformation de l'alcool **1.30** en halogénure correspondant **1.31** avec un rendement quantitatif en 24h d'irradiation à 400 nm (Schéma 1.5).⁴⁸ Le mécanisme proposé passe par un cycle de désexcitation oxydatif entre le cuivre(I) dans son état excité ($E^*_{\text{ox}} = -1,93$ V) et le tetrabromocarbène ($E_{\text{red}} = 0,30$ V). Le radical tribromométhyle réagit avec le DMF présent comme solvant pour former **1.32**, qui peut alors réagir avec le cuivre(II) pour former l'iminium **1.33**. Deux voies sont alors possibles, une réaction d'addition/élimination avec un bromure peut venir former le réactif de Vilsmeier–Haack **1.34** correspondant (Voie 1). Ce dernier peut alors réagir avec l'alcool **1.30** pour former l'intermédiaire

1.35. L'iminium **1.33** peut aussi directement réagir avec **1.30** pour former **1.35** (Voie 2). Une substitution de l'alcool activé **1.35** forme le produit bromé **1.31**. Il est intéressant de noter que les complexes homoleptiques testés sont inefficaces pour cette réaction.

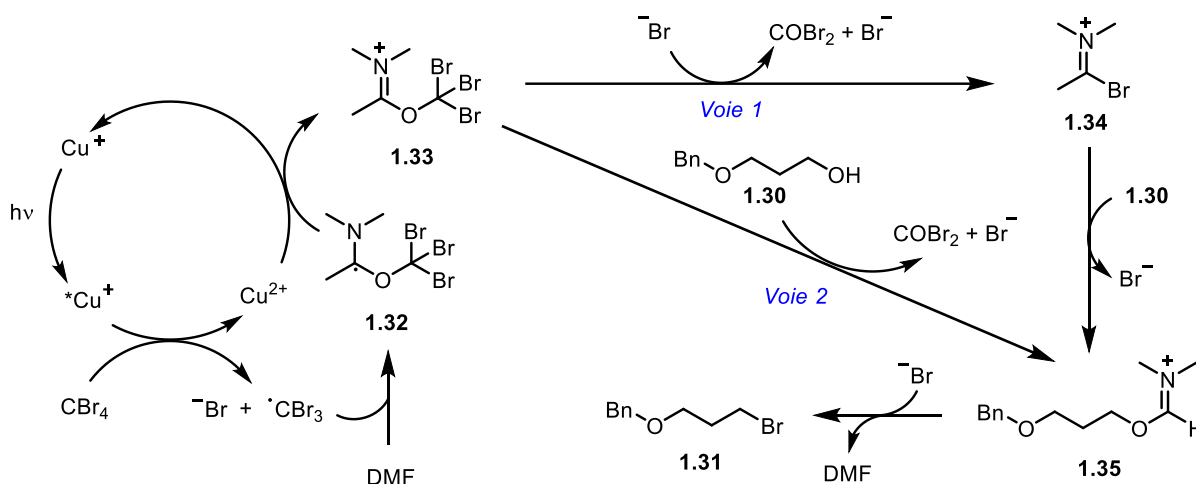
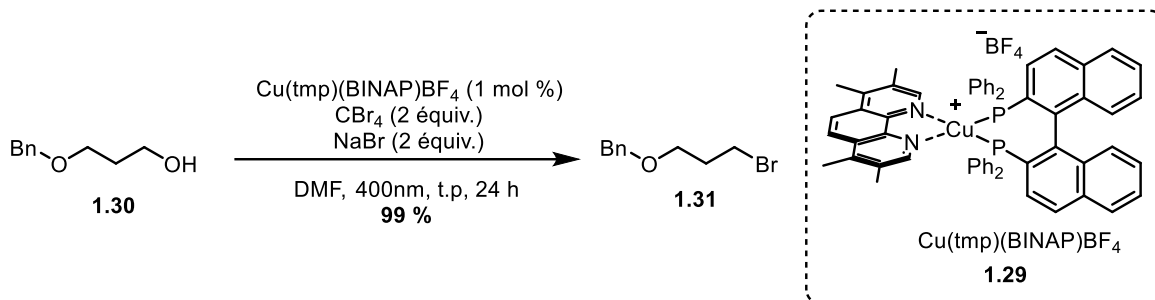


Schéma 1.5 Réaction d'Appel catalysée par $\text{Cu}(\text{tmp})(\text{BINAP})\text{BF}_4$ et un mécanisme possible

1.4.3 Transfert d'atome radicalaire (ATRA)

Les complexes de cuivre(I) ont aussi été très étudiés pour leur efficacité dans des réactions de transfert d'atome radicalaire (*Atom-Transfer Radical Addition*, ATRA), particulièrement par le groupe du Pr. Reiser.⁴⁹⁻⁵¹ Formellement, une réaction de transfert d'atome radicalaire correspond au bris homolytique d'un lien σ ; les deux radicaux résultants s'additionnant de chaque côté d'une liaison π , formant donc deux nouvelles liaisons σ .⁵² Ce processus a été développé bien avant l'arrivée de la photocatalyse, mais nécessitait des initiateurs radicalaires hautement réactifs menant à des réactions secondaires de polymérisation.⁵³⁻⁵⁴ En 2015, Reiser *et al.* rapportent

l'utilisation de $\text{Cu}(\text{dap})_2\text{Cl}$ **1.7** pour l'addition de trifluorométhylchlorosulfonate sur des alcènes (**Schéma 1.6**).⁵⁰ Cette réaction montre une caractéristique inhérente aux complexes de cuivre : la possibilité d'un mécanisme passant par la sphère intérieure du complexe. En effet, les ligands diimines labiles des complexes de cuivre et l'adoption d'une géométrie plan carré lors de l'excitation du complexe permettent la coordination de molécules au cuivre. C'est le mécanisme proposé ici, où la réduction du chlorure de triflate **1.37** entraîne la coordination du motif ClSO_2^- au cuivre pour former le complexe **1.39**. Le radical trifluorométhyle libre peut alors attaquer l'alcène **1.36**, formant l'intermédiaire **1.40**. Une recombinaison du radical alkyle avec le complexe de cuivre forme alors le produit désiré **1.38**. Ce mécanisme passant par la sphère intérieure du complexe est essentiel à la formation du produit désiré : quand $\text{Ru}(\text{bpy})_3\text{Cl}_2$ est utilisé comme catalyseur, le produit de trifluorométhylchlorination **1.41** est formé. En effet, le radical chlorosulfonyle ne pouvant pas se coordonner au ruthénium, il se décompose alors pour former le radical chlorure, qui se recombine avec le radical alkyle.

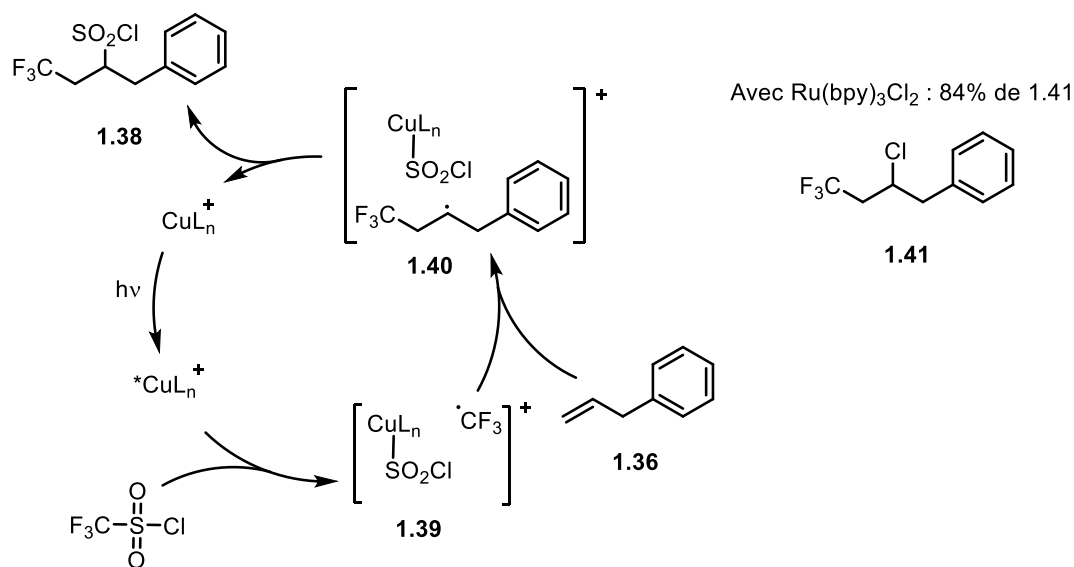
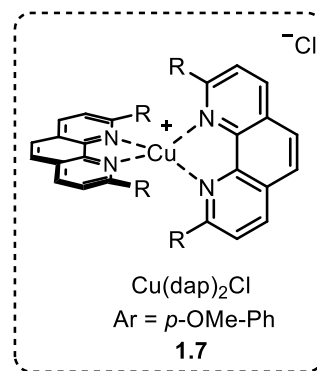
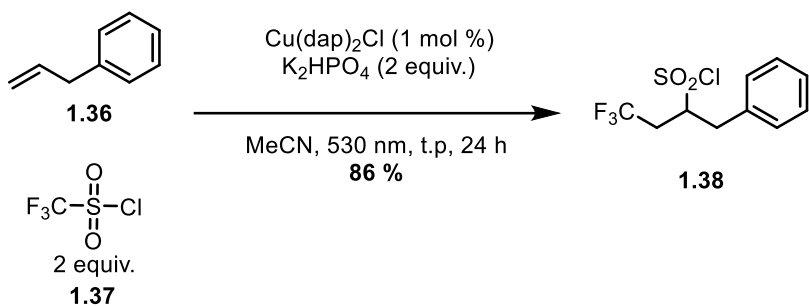


Schéma 1.6 Trifluorométhylchlorosulfonylation d'alcène catalysée par $\text{Cu}(\text{dap})_2\text{Cl}$ et le mécanisme proposé

1.4.4 Transfert d'électron et de proton simultané (PCET)

1.4.4.1 Principe du PCET

Le transfert d'électron et de proton simultané (*Proton Coupled Electron Transfer*, PCET) est un processus couramment observé dans des procédés biologiques connus comme l'oxydation C-H enzymatique,⁵⁵ la réduction de ribonucléotides⁵⁶ ou encore la photosynthèse.⁵⁷ Dans ce processus, les deux étapes de transfert d'électrons (ET) et de transfert de proton (TP) se font de manière concertée; il en résulte un abaissement de l'enthalpie de la réaction, comparé aux deux

étapes successives. Le PCET peut être oxydatif, en présence d'une base et d'un oxydant, ou réductif, présence d'un réducteur et d'un acide (**Figure 1.16**).

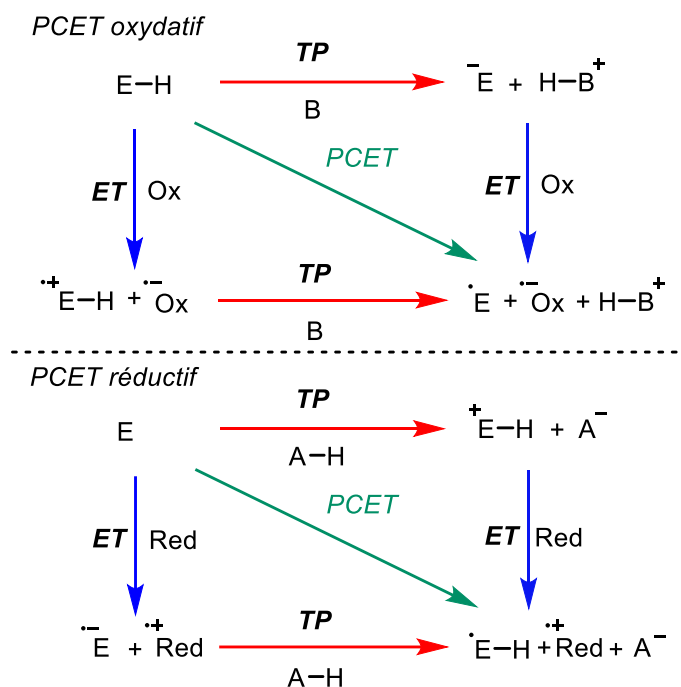


Figure 1.16 Représentation des mécanismes de PCET oxydatif et réductif

1.4.4.2 Réaction de PCET catalysée au cuivre

Les complexes de cuivre étant de meilleurs réducteurs qu'oxydants, les réactions de PCET catalysées au cuivre passent principalement par un mécanisme de PCET réductif. Se basant sur les travaux de Knowles,⁵⁸ notre groupe rapporte l'utilisation du complexe Cu(quintri)(Xantphos)BF₄ **1.42** pour la formation du bicycle **1.44** avec 79% de rendement (**Schéma 1.7**).⁴⁵ Le transfert de proton est ici assuré par l'utilisation en quantité catalytique d'acide diphenyle phosphorique (dppa). Après réduction du cuivre(I) par l'ester de Hantzsch (HEH), un PCET avec **1.43** en présence de dppa forme le radical cétylique **1.45**. Une cyclisation intramoléculaire forme alors le composé cyclique **1.46**, qui va alors pouvoir réagir par transfert

d'hydrogène avec le HEH oxydé pour former **1.47**. Finalement une lactonisation produit le second cycle pour obtenir **1.44**.

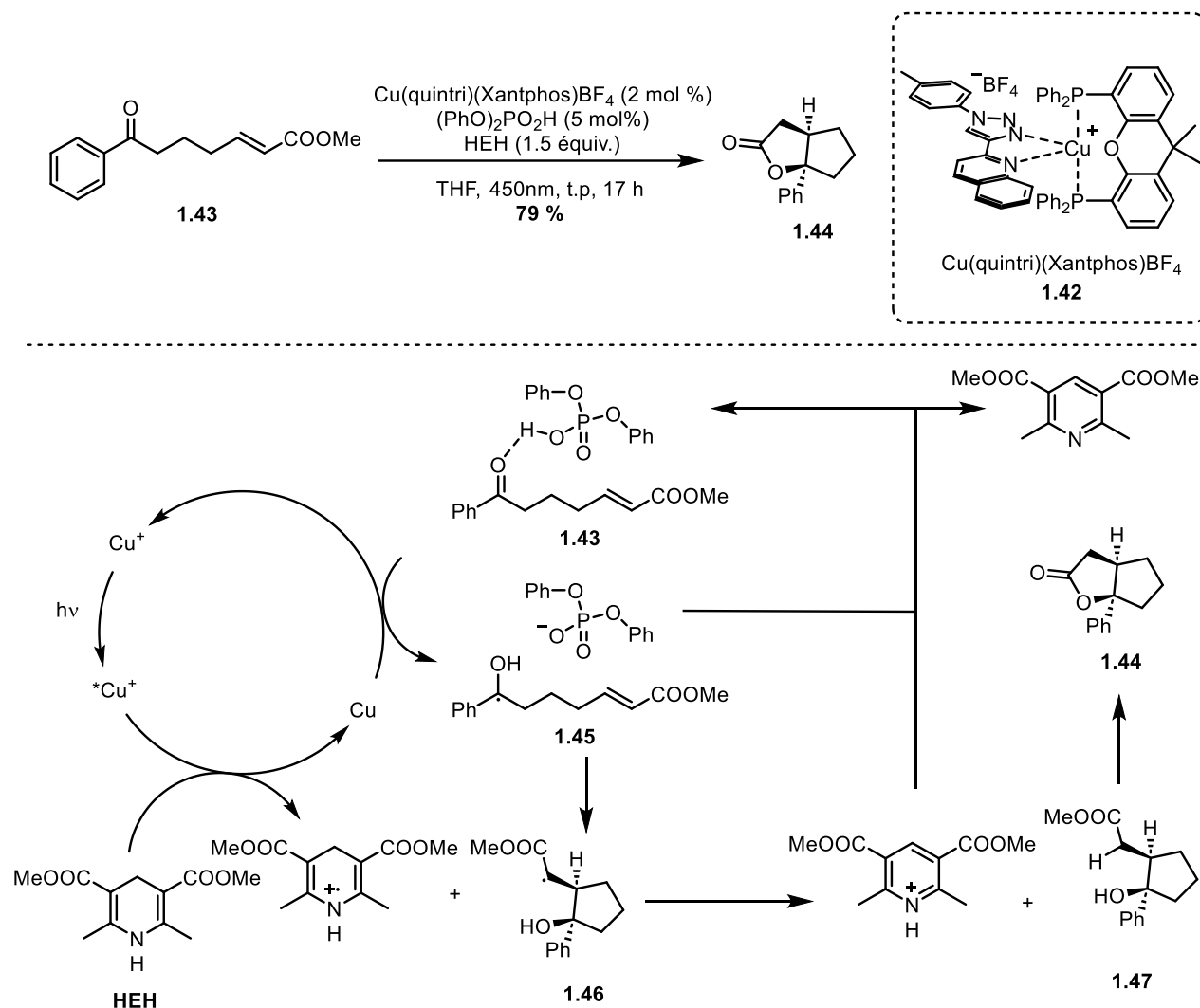


Schéma 1.7 Réaction de PCET catalysée par $\text{Cu}(\text{quintri})(\text{Xantphos})\text{BF}_4$ et mécanisme proposé.

En 2019, notre groupe rapporte l'utilisation d'un complexe hétéroleptique de cuivre(I) bifonctionnel $\text{Cu}(\text{pypzs})(\text{BINAP})\text{BF}_4$ **1.47**, pour la dimérisation de cétones et aldéhydes aromatiques (**Schéma 1.8**).⁵⁹ Le ligand possède en effet deux liaisons N-H qui jouent le rôle de donneur de proton. Après absorption d'un photon, le catalyseur est réduit par HEH. Avec l'assistance des liaisons hydrogènes entre le ligand diimine et le carbonyle, représentés sur l'intermédiaire **1.50**, une PCET est alors possible, formant le radical centré sur le carbone. Ce

dernier peut alors réagir avec une autre molécule de **1.48** pour former l'intermédiaire radicalaire **1.51**. Ce dernier prend un hydrogène du HEH oxydé pour former le composé diol **1.49** avec un rendement de 99%. L'interaction non-covalente entre le complexe et le carbonyle a pu être observée par spectroscopie RMN, et l'utilisation d'un ligand ne possédant pas de liens N-H entraîne aucune réactivité.

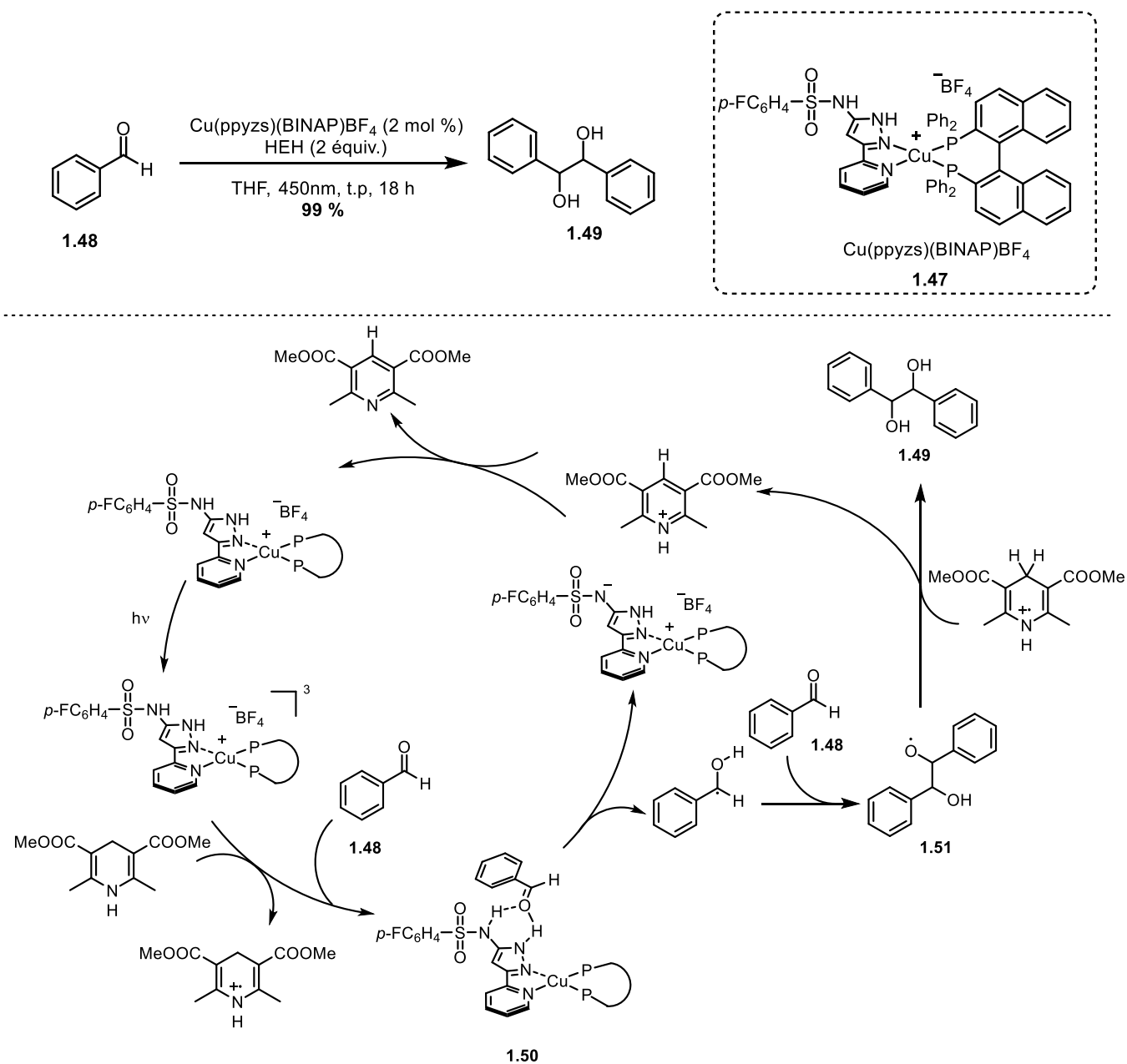
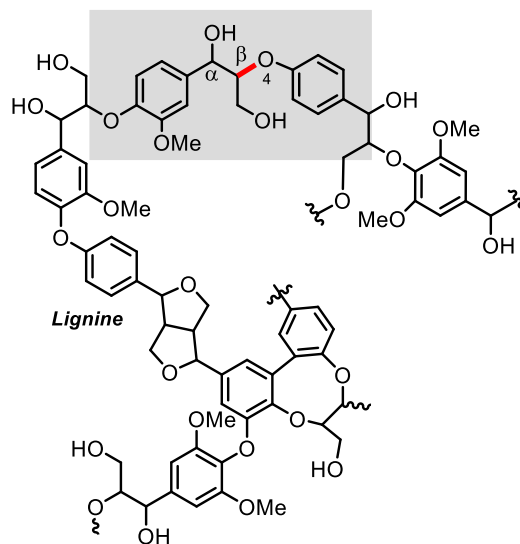


Schéma 1.8 Dimérisation de carbonyle catalysée par $\text{Cu}(\text{ppyzs})(\text{BINAP})\text{BF}_4$ et mécanisme proposé

1.4.4.3 Décomposition photocatalytique de modèles de lignine par PCET

La lignine est un polymère naturel présent dans les arbres et représente 20% en masse de ces derniers. Elle est aujourd’hui le premier déchet de l’industrie du papier et présente une grande opportunité dans le contexte de valorisation de la biomasse car sa structure est constituée de cycles aromatiques hautement oxygénés (**Schéma 1.9.a**).⁶⁰ La stratégie principalement utilisée pour sa dépolymérisation est le bris du lien β -O, du à son abondance (45-60%).⁶¹ En 2019 Stephenson rapporte l’utilisation de la photocatalyse pour la décomposition de modèles de lignine en présence de catalyseur d’iridium (**Schéma 1.9.b**).⁶² La réaction passe par un PCET similaire à celui reporté à la Figure 1.18 avec l’acide formique jouant le rôle de donneur de proton.

a.



b.

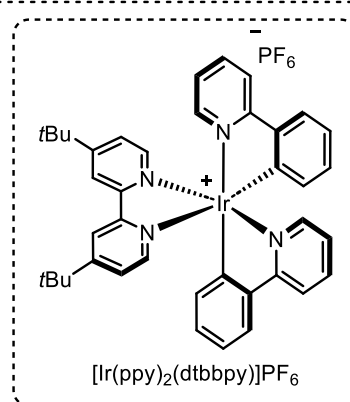
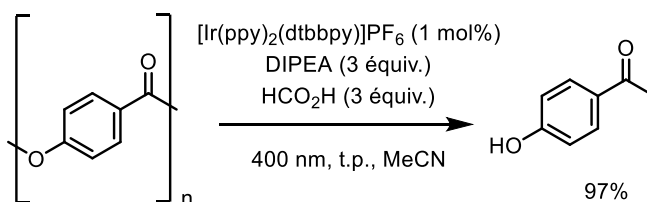


Schéma 1.9 Représentation de la structure de la lignine et décomposition de modèles de lignine photocatalysée.

1.5 L'utilisation de complexe de cuivre pour la catalyse par transfert d'énergie

1.5.1 Principe de la catalyse par transfert d'énergie

Un autre domaine de la photocatalyse dont nous n'avons pas encore parlé dans cette thèse est le transfert d'énergie. Comme son nom l'indique, un transfert d'énergie correspond à la réaction entre un donneur D^* dans son état excité (singulet ou triplet) et un accepteur A dans son état fondamental (**Figure 1.17**).³ Après le transfert d'énergie, le donneur est donc revenu à

son état fondamental **D**, et l'accepteur est maintenant dans un état excité **A*** (singulet ou triplet). Il est important de noter que ce transfert ne change pas les degrés d'oxydations du donneur et de l'accepteur; le transfert d'énergie ne nécessite donc pas de donneur ou d'accepteur sacrificiel d'électron pour régénérer le photocatalyseur. Cette catalyse est très intéressante car l'excitation directe de molécules est difficile sans l'utilisation d'une irradiation UV; et l'état triplet est souvent inatteignable car peu de molécules ont un croisement intersystème efficace.

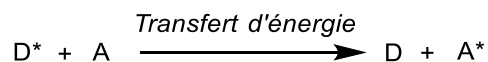


Figure 1.17 Représentation du transfert d'énergie

L'accepteur ne possédant pas une absorption dans le visible, le transfert d'énergie nécessite un mécanisme non-radiatif. Deux mécanismes sont connus, le mécanisme de Förster⁶³ et le mécanisme de Dexter (**Figure 1.18**).⁶⁴ Le mécanisme de Förster, aussi appelé FRET (*Forster resonance energy transfer*) correspond à une interaction dipôle-dipôle entre le donneur et l'accepteur. L'oscillation électronique du donneur dans son état excité induit par répulsion de charge une oscillation chez l'accepteur, entraînant une relaxation du donneur et une excitation de l'accepteur simultanées. Si ce mécanisme est souvent observé dans les milieux biologiques, il est incompatible avec l'utilisation de photocatalyseur possédant un état excité triplet. En effet cela nécessiterait une excitation du substrat de l'état singulet à l'état triplet, ce qui est interdit selon la loi de conservation de spin. L'autre mécanisme possible est le mécanisme de Dexter, qui correspond à un échange simultané d'électrons entre le donneur et l'accepteur. Dans ce cas, les électrons échangés ne changent pas de spin, ce qui permet donc de promouvoir l'accepteur dans son état triplet, et le photocatalyseur dans son état fondamental. Ce sera donc le mécanisme favorisé pour les réactions photocatalysées au cuivre.

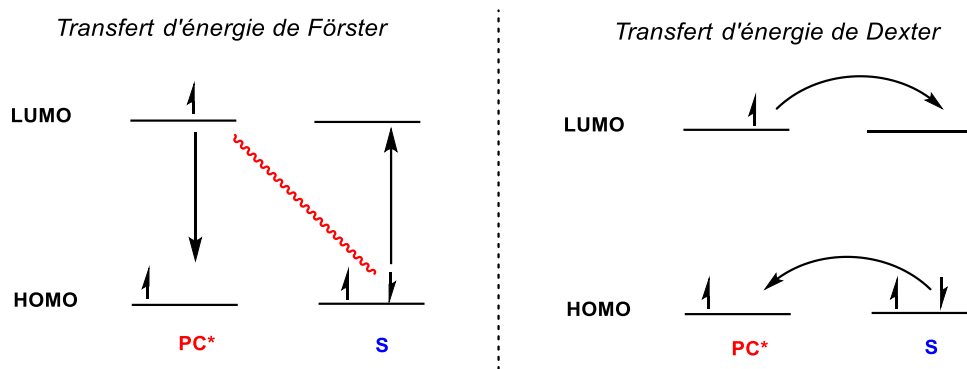


Figure 1.18 Mécanismes de transfert d'énergie de Förster et Dexter

La vitesse d'un transfert d'énergie de Dexter peut être estimée selon l'équation suivante:⁶⁴

$$k_{EnT} = K.J.e^{-\frac{2R_{DA}}{L}}$$

K représente les interactions orbitales entre le donneur D et l'accepteur A, qui dépendent de la répulsion stérique entre les deux espèces. Cela a été démontré par les travaux de Weaver en 2016 qui montre une diminution de l'efficacité du transfert d'énergie en fonction de la taille du complexe d'iridium utilisé.⁶⁵ J représente l'intégrale de recouvrement spectral, qui correspond à la différence d'énergie ΔE entre les niveaux T_1-S_0 (aussi appelé énergie triplet E_T) du donneur et les niveaux T_1-S_0 de l'accepteur (**Figure 1.19**). Pour un transfert d'énergie efficace, il faut donc que le T_1 du photocatalyseur soit de plus haute énergie que le T_1 du substrat. Enfin, $e^{-\frac{2R_{DA}}{L}}$ représente la distance entre le donneur et l'accepteur. Logiquement, pour un transfert simultané d'électrons, les deux espèces ont besoin d'être au contact l'une de l'autre; l'éloignement diminue de façon exponentielle la vitesse du transfert d'énergie.

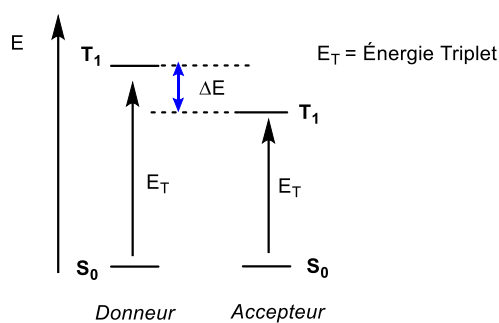


Figure 1.19 Représentation des niveaux d'énergie du donneur et de l'accepteur dans un transfert d'énergie

1.5.2 Réactions photosensibilisées par le cuivre

Bien que les complexes de cuivre soient utilisés comme photocatalyseurs dans de nombreuses réactions photorédox, leur utilisation dans des réactions de transfert d'énergie est beaucoup plus rare. Cela est surprenant car les complexes de cuivre, en particulier les complexes de cuivre hétéroleptiques $\text{Cu}(\text{N}^{\wedge}\text{N})(\text{P}^{\wedge}\text{P})\text{X}$ possèdent des énergies triplet proches des photosensibilisateurs couramment utilisés (**Figure 1.20**). $\text{Cu}(\text{dmp})_2\text{BF}_4$ possède une énergie triplet de seulement 1,65 eV, mais son équivalent hétéroleptique $\text{Cu}(\text{dmp})(\text{Xantphos})\text{BF}_4$ possèdent une énergie de 2,21 eV entre celle du $\text{Ru}(\text{bpy})_3\text{Cl}_2$ ($E_T = 2,12$ eV) et du *fac*- $[\text{Ir}(\text{ppy})_3]\text{PF}_6$ ($E_T = 2,51$ eV).

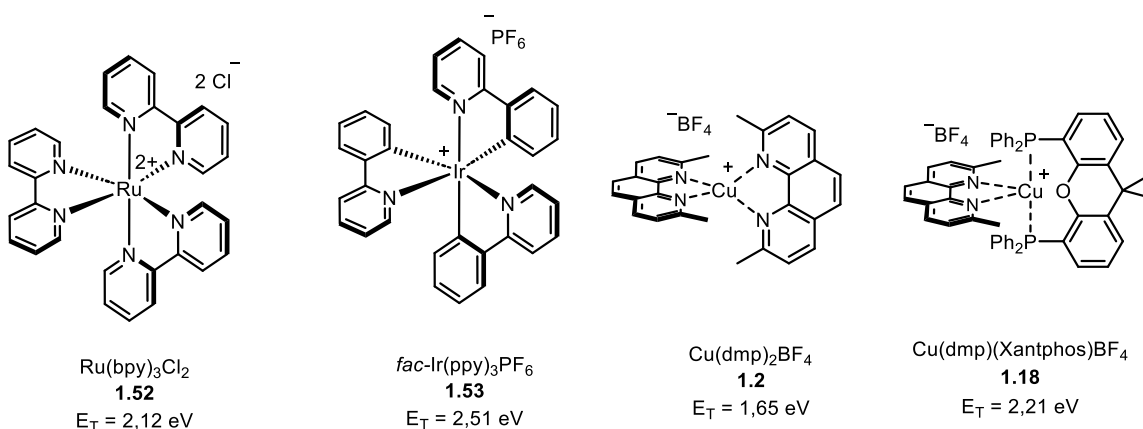


Figure 1.20 Différents photocatalyseurs et leur énergie triplet correspondante

Avant le début de mes travaux sur l'isomérisation d'alcène (**Chapitre 4**), la seule étude des complexes de cuivre pour une réaction de transfert d'énergie provenait de notre groupe, qui a étudié la librairie de complexe développée dans la réaction de décomposition d'azoture pour la formation de pyrrole (**Schéma 1.10**).⁴⁵ Un catalyseur optimal, $\text{Cu}(\text{dmp})(\text{BINAP})\text{BF}_4$ **1.56** a été trouvé, formant le pyrrole **1.55** à partir de l'azoture **1.54** avec un rendement de 99% après 3h d'irradiation à 450 nm. Après excitation de **1.56** par un photon, un transfert d'énergie se fait avec **1.54** ($E_T(1.56) = 2,0$ eV, $E_T(1.54) = 1,96$ eV). L'excitation de **1.54** à son état triplet entraîne la décomposition de l'azoture pour former l'intermédiaire nitrène avec libération de N_2 . Le nitrène réagit alors avec l'alcène adjacent pour former l'intermédiaire aziridine **1.57**, qui se réarrange

pour former le pyrrole **1.55**. En accord avec les énergies triplet, aucune réactivité n'est observée lors de l'utilisation du complexe homoleptique $\text{Cu}(\text{dmp})_2\text{BF}_4$ ($E_T = 1,65 \text{ eV}$).

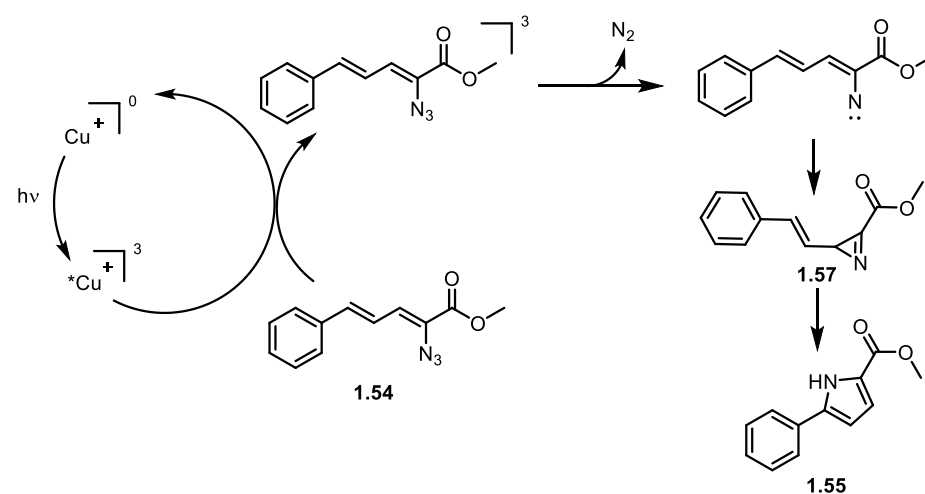
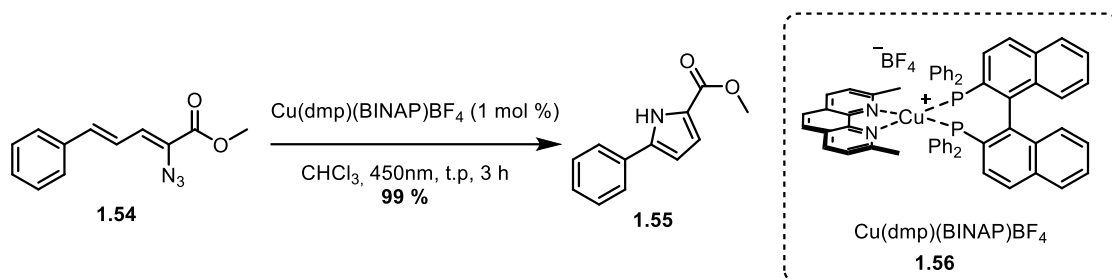


Schéma 1.10 Décomposition d'azoture catalysée par $\text{Cu}(\text{dmp})(\text{BINAP})\text{BF}_4$ pour la synthèse de pyrrole et mécanisme proposé

1.5.3 Principe de l'isomérisation d'alcène photocatalysée

Une autre réaction passant par un transfert d'énergie ayant reçu beaucoup d'attention au cours de la dernière décennie est la photoisomérisation $E \rightarrow Z$ d'alcène.⁶⁶⁻⁶⁹ En effet, la géométrie d'un alcène peut grandement influencer les propriétés d'une molécule,⁷⁰⁻⁷¹ c'est pourquoi beaucoup d'efforts ont été déployés pour développer des réactions d'oléfination stéréosélectives.⁷² Si l'isomère E, thermodynamiquement plus stable, est relativement facile à obtenir, l'alcène Z présente plus de défis.⁷³ Les méthodes de formation sélective d'alcène Z sont plus rares; on peut penser à la modification de Still-Gennari pour l'oléfination de Horner-

Emmons,⁷⁴ l'hydrogénation d'alcynes ou encore l'utilisation de catalyseur spécifiques pour la métathèse d'alcènes.⁷⁵⁻⁷⁶ Une autre stratégie repose sur la conversion d'alcène E (ou d'un mélange E/Z), en un mélange enrichi en isomère Z, grâce à la photocatalyse. Un schéma du mécanisme est représenté à la **Figure 1.21**. L'alcène E **1.58** peut réagir avec un photocatalyseur PC par transfert d'énergie pour accéder à son état triplet **1.59**. Une répulsion électronique des deux électrons non-pairés entraîne une rotation de la liaison C-C d'environ 90°, pour atteindre l'intermédiaire de plus basse énergie **1.60**. Ce dernier va alors se relaxer à l'état fondamental pour former soit l'alcène E, soit l'alcène Z. Chaque isomère peut alors de nouveau se faire exciter, entraînant la même série de réactions. Cependant dans le cas de l'alcène Z **1.61**, en présence d'un substituant aryle, la torsion 1,3-allylique induit une distorsion du système π -conjugué. Cela entraîne une augmentation de l'énergie triplet nécessaire pour l'exciter dans son état triplet **1.62**, comparé à son analogue E, avec une constante d'équilibre K_4 inférieure à K_3 . Cela aura donc pour conséquence de déplacer le mélange E/Z jusqu'à l'obtention d'un état photostationnaire enrichi en isomère Z.

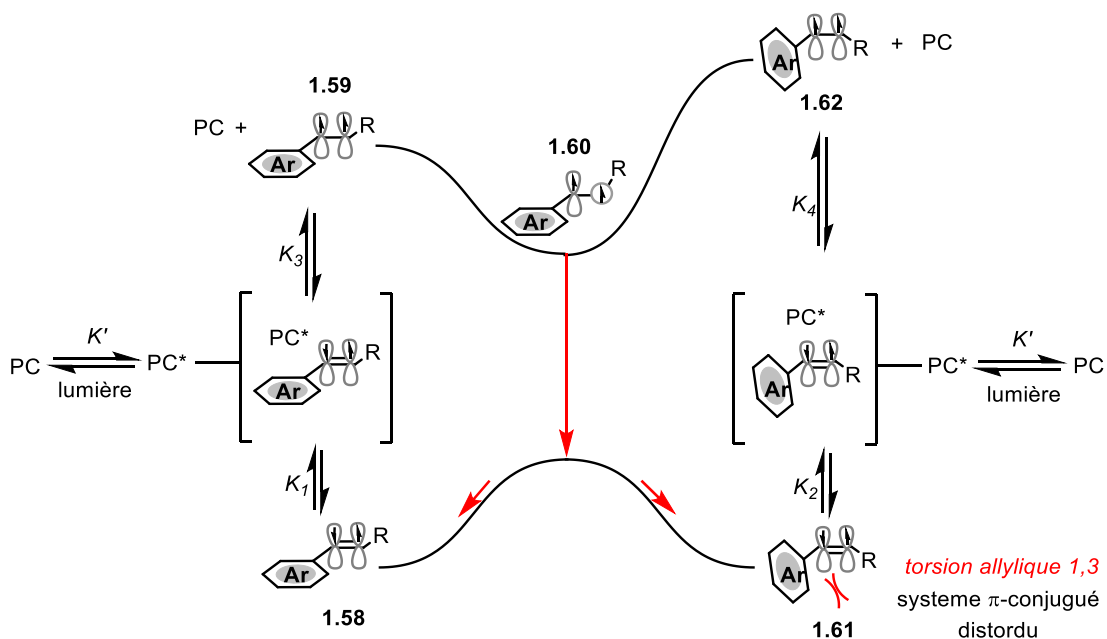


Figure 1.21 Principe de la photoisomérisation E → Z d'alcènes

Dans les années 60, Hammond rapporte l'influence de différents photocatalyseurs pour l'isomérisation du stilbène (**Schéma 1.11.a**)⁷⁷. Lorsque le pyrène ($E_T = 2,09$ V) est utilisé, le

transfert d'énergie est efficace avec le *trans*-stilbène ($E_T = 2,14$ eV), mais beaucoup moins avec le *cis*-stilbène ($E_T = 2,35$ eV). Il en résulte un ratio E:Z hautement enrichi en Z (9:91). L'utilisation de thioxanthone, avec une énergie triplet beaucoup plus élevée ($E_T = 2,75$ eV), résulte en une excitation non sélective des deux isomères, entraînant un ratio E:Z de 39:61. La réaction est revisitée en 2014 par Weaver pour l'isomérisation d'amines allyliques avec un catalyseur d'iridium (**Schéma 1.11.b**)⁷⁸. Par la suite, le groupe de Gilmour a étudié l'étendue de substrats possibles, avec par exemple l'isomérisation de dérivés de cinnamates par la (-)-riboflavine en 2015⁶⁷, ou encore l'isomérisation de composés borés en présence de thioxanthone en 2020 avec un excellent ratio E:Z (1:99)⁶⁸. Il est intéressant de noter dans ce cas-ci l'absence de substituant aryle, l'orbitale vide du bore jouant le rôle de système π -conjugué avec l'alcène adjacent.

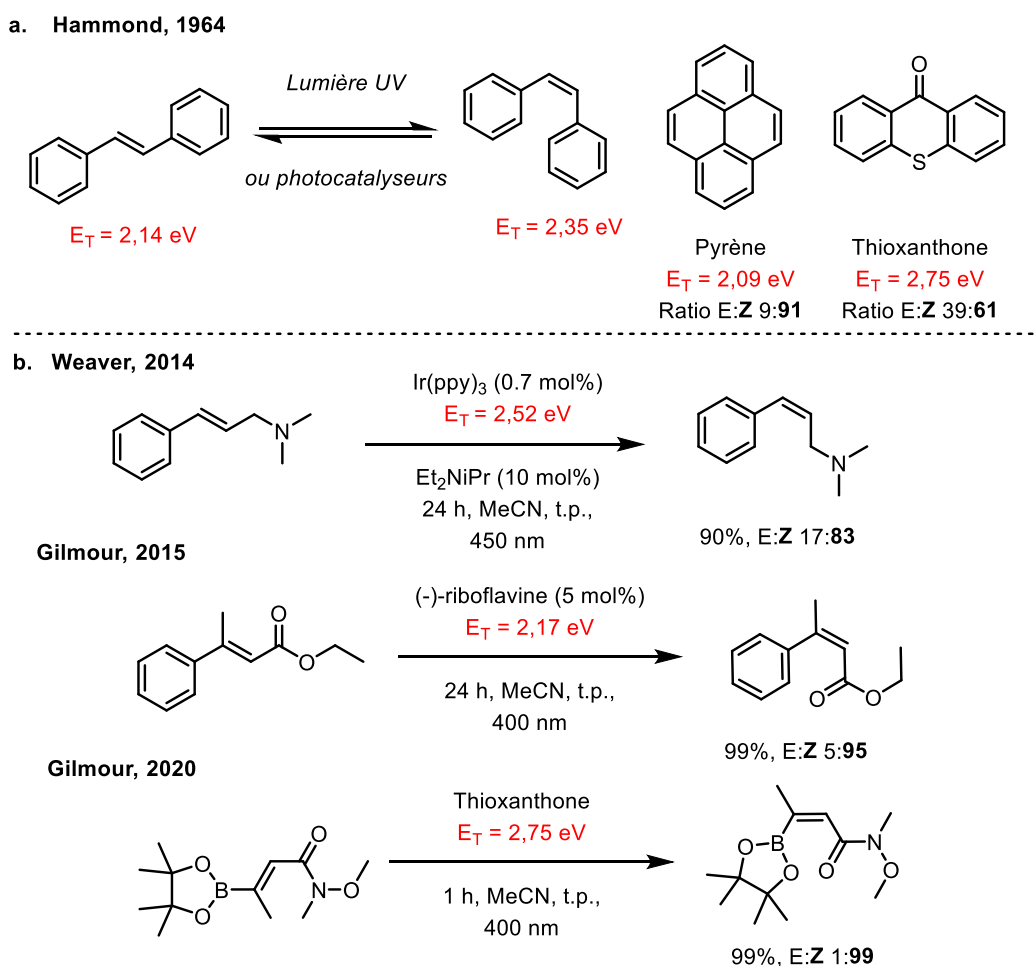


Schéma 1.11 a. Influence de l'énergie triplet du photocatalyseur sur le ratio E:Z de l'isomérisation b. Exemples de photoisomérisations d'alcènes.

1.6 Conclusion

Les complexes de cuivre(I) de type $\text{Cu}(\text{N}^{\wedge}\text{N})_2\text{X}$ et $\text{Cu}(\text{N}^{\wedge}\text{N})(\text{P}^{\wedge}\text{P})\text{X}$ possèdent les caractéristiques nécessaires pour leur utilisation en photocatalyse homogène. Ils possèdent une absorption dans le visible grâce à leurs transitions MLCT, et un temps de vie de l'état excité suffisamment long pour promouvoir des réactions intermoléculaires. Ils possèdent une fenêtre de potentiel rédox suffisante et une énergie triplet élevée, permettant donc de catalyser des réactions de photorédox et de transfert d'énergie. Enfin, la labilité de leurs ligands peut entraîner des mécanismes de sphère intérieure, débloquant des réactivités différentes des autres photocatalyseurs.

Cependant, l'utilisation de complexes de cuivre en photocatalyse homogène est encore limitée. La labilité des ligands est aussi une faiblesse, rendant ces complexes sensibles à la photodécomposition. De plus, si les complexes de cuivre sont de bons réducteurs, leur faible potentiel de réduction en fait de mauvais oxydants, pouvant limiter la portée de réactions réalisables. Enfin il est encore difficile de prédire la relation structure/activité de ces complexes; un criblage des photocatalyseurs pour chaque nouvelle réaction est nécessaire. C'est pourquoi dans les prochains chapitres 2,3 et 4, mes travaux essayeront de résoudre cette problématique en étudiant l'efficacité d'une librairie de complexes sur différentes réactions, passant par des mécanismes de SET, PCET et EnT et en reliant ces résultats aux données photophysiques de chacun des complexes. Les travaux du groupe sur la décomposition de modèles de lignine par PCET peuvent aussi être trouvés en Annexe 4 .

1.7 Références bibliographiques

1. Ciamician, G., *Science* **1912**, 36 (926), 385-394.
2. Büchi, G.; Inman, C. G.; Lipinsky, E. S., *J. Am. Chem. Soc.* **1954**, 76 (17), 4327-4331.
3. Verhoeven, J. W., *Pure Appl. Chem.* **1996**, 68 (12), 2223-2286.
4. Lima, C. G. S.; de M. Lima, T.; Duarte, M.; Jurberg, I. D.; Paixão, M. W., *ACS Catal.* **2016**, 6 (3), 1389-1407.
5. Rackl, D.; Kreitmeier, P.; Reiser, O., *Green Chem.* **2016**, 18 (1), 214-219.
6. Ciana, C.-L.; Bochet, C. G., *CHIMIA* **2007**, 61 (10), 650.
7. Círka, V.; Vlková, L.; Relich, S.; Hájek, M., *J. Photochem. Photobiol. A Chem.* **2006**, 179 (1), 229-233.
8. Bally, T., *CHIMIA* **2007**, 61 (10), 645.
9. Blanc, A.; Bochet, C. G., *J. Am. Chem. Soc.* **2004**, 126 (23), 7174-7175.
10. Zhang, T., Heterogeneous Catalytic Process for Wastewater Treatment. 2020.
11. Hu, X.; Yip, A. C. K., *Frontiers in Catalysis* **2021**, 1.
12. Jablonski, A., *Nature* **1933**, 131 (3319), 839-840.
13. Damrauer, N. H.; Cerullo, G.; Yeh, A.; Boussie, T. R.; Shank, C. V.; McCusker, J. K., *Science* **1997**, 275 (5296), 54-57.
14. Juris, A.; Balzani, V.; Barigelletti, F.; Campagna, S.; Belser, P.; von Zelewsky, A., *Coord. Chem. Rev.* **1988**, 84, 85-277.
15. Arias-Rotondo, D. M.; McCusker, J. K., *Chem. Soc. Rev.* **2016**, 45 (21), 5803-5820.
16. Eibner, A., *Chem.-Ztg* **1911**, 35, 753-755.
17. Bruner, L.; Kozak, J., *Z. Elektrochem. Angew. Phys. Chem* **1911**, 17 (9), 354-360.
18. Polo, A. S.; Itokazu, M. K.; Murakami Iha, N. Y., *Coord. Chem. Rev.* **2004**, 248 (13), 1343-1361.
19. Teegardin, K.; Day, J. I.; Chan, J.; Weaver, J., *Org. Process Res. Dev.* **2016**, 20 (7), 1156-1163.
20. Jeong, H.-G.; Choi, M.-S., *Isr. J. Chem.* **2016**, 56 (2-3), 110-118.
21. Radetzki, M., *Resources Policy* **2009**, 34 (4), 176-184.
22. *Mineral commodity summaries; 2023*; p 210.

23. Felder, D.; Nierengarten, J.-F.; Barigelletti, F.; Ventura, B.; Armaroli, N., *J. Am. Chem. Soc.* **2001**, *123* (26), 6291-6299.
24. Lowry, M. S.; Bernhard, S., *Chem. - Eur. J.* **2006**, *12* (31), 7970-7977.
25. Öpik, U.; Pryce, M. H. L., *Proceedings of the Royal Society of London. Series A. Mathematical and Physical Sciences* **1957**, *238* (1215), 425-447.
26. Shi, Y.-Z.; Wu, H.; Wang, K.; Yu, J.; Ou, X.-M.; Zhang, X.-H., *Chem. Sci.* **2022**, *13* (13), 3625-3651.
27. Dietrich-Buchecker, C. O.; Marnot, P. A.; Sauvage, J.-P.; Kirchhoff, J. R.; McMillin, D. R., *J. Chem. Soc., Chem. Commun.* **1983**, (9), 513-515.
28. Everly, R. M.; McMillin, D. R., *Photochem. Photobiol.* **1989**, *50* (6), 711-716.
29. Ahn, B.-T.; McMillin, D. R., *Inorg. Chem.* **1978**, *17* (8), 2253-2258.
30. Ichinaga, A. K.; Kirchhoff, J. R.; McMillin, D. R.; Dietrich-Buchecker, C. O.; Marnot, P. A.; Sauvage, J. P., *Inorg. Chem.* **1987**, *26* (25), 4290-4292.
31. Garakyaraghi, S.; Crapps, P. D.; McCusker, C. E.; Castellano, F. N., *Inorg. Chem.* **2016**, *55* (20), 10628-10636.
32. Green, O.; Gandhi, B. A.; Burstyn, J. N., *Inorg. Chem.* **2009**, *48* (13), 5704-5714.
33. Rehm, D.; Weller, A., *Isr. J. Chem.* **1970**, *8* (2), 259-271.
34. Beaudelot, J.; Oger, S.; Peruško, S.; Phan, T.-A.; Teunens, T.; Moucheron, C.; Evano, G., *Chem. Rev.* **2022**, *122* (22), 16365-16609.
35. Kern, J.-M.; Sauvage, J.-P., *J. Chem. Soc., Chem. Commun.* **1987**, (8), 546-548.
36. Miller, M. T.; Gantzel, P. K.; Karpishin, T. B., *Angew. Chem., Int. Ed.* **1998**, *37* (11), 1556-1558.
37. Saha, M. L.; Neogi, S.; Schmittel, M., *Dalton Trans.* **2014**, *43* (10), 3815-3834.
38. Sandroni, M.; Kayanuma, M.; Planchat, A.; Szuwarski, N.; Blart, E.; Pellegrin, Y.; Daniel, C.; Boujtita, M.; Odobel, F., *Dalton Trans.* **2013**, *42* (30), 10818-10827.
39. Buckner, M. T.; McMillin, D. R., *J. Chem. Soc., Chem. Commun.* **1978**, (17), 759-761.
40. Cuttell, D. G.; Kuang, S.-M.; Fanwick, P. E.; McMillin, D. R.; Walton, R. A., *J. Am. Chem. Soc.* **2002**, *124* (1), 6-7.

41. Armaroli, N.; Accorsi, G.; Holler, M.; Moudam, O.; Nierengarten, J. F.; Zhou, Z.; Wegh, R. T.; Welter, R., *Adv. Mater.* **2006**, *18* (10), 1313-1316.
42. Sandoval-Pauker, C.; Molina-Aguirre, G.; Pinter, B., *Polyhedron* **2021**, *199*, 115105.
43. Buzzetti, L.; Crisenza, G. E. M.; Melchiorre, P., *Angew. Chem., Int. Ed.* **2019**, *58* (12), 3730-3747.
44. Hernandez-Perez, A. C.; Vlassova, A.; Collins, S. K., *Org. Lett.* **2012**, *14* (12), 2988-2991.
45. Minozzi, C.; Caron, A.; Grenier-Petel, J. C.; Santandrea, J.; Collins, S. K., *Angew. Chem., Int. Ed.* **2018**, *57* (19), 5477-5481.
46. Yang, J.; Zhang, J.; Qi, L.; Hu, C.; Chen, Y., **2015**, *51* (25), 5275-5278.
47. Dai, C.; Narayanam, J. M.; Stephenson, C. R., *Nat. Chem.* **2011**, *3* (2), 140-145.
48. Minozzi, C.; Grenier-Petel, J.-C.; Parisien-Collette, S.; Collins, S. K., *Beilstein J. Org. Chem.* **2018**, *14*, 2730-2736.
49. Hossain, A.; Engl, S.; Lutsker, E.; Reiser, O., *ACS Catal.* **2019**, *9* (2), 1103-1109.
50. Bagal, D. B.; Kachkovskiy, G.; Knorn, M.; Rawner, T.; Bhanage, B. M.; Reiser, O., *Angew. Chem., Int. Ed.* **2015**, *54* (24), 6999-7002.
51. Henriquez, M. A.; Engl, S.; Jaque, P.; Gonzalez, I. A.; Natali, M.; Reiser, O.; Cabrera, A. R., *Eur. J. Inorg. Chem.* **2021**, *2021* (38), 4020-4029.
52. Engl, S.; Reiser, O., *Chem. Soc. Rev.* **2022**, *51* (13), 5287-5299.
53. Kharasch, M. S.; Skell, P. S.; Fisher, P., *J. Am. Chem. Soc.* **1948**, *70* (3), 1055-1059.
54. Curran, D. P.; Chen, M. H.; Spletzer, E.; Seong, C. M.; Chang, C. T., *J. Am. Chem. Soc.* **1989**, *111* (24), 8872-8878.
55. Yosca, T. H.; Rittle, J.; Krest, C. M.; Onderko, E. L.; Silakov, A.; Calixto, J. C.; Behan, R. K.; Green, M. T., *Science* **2013**, *342* (6160), 825-829.
56. Minnihan, E. C.; Nocera, D. G.; Stubbe, J., *Acc. Chem. Res.* **2013**, *46* (11), 2524-2535.
57. Hammarström, L.; Styring, S., *Energy Environ. Sci.* **2011**, *4* (7), 2379-2388.
58. Tarantino, K. T.; Liu, P.; Knowles, R. R., *J. Am. Chem. Soc.* **2013**, *135* (27), 10022-10025.
59. Caron, A.; Morin, É.; Collins, S. K., *ACS Catal.* **2019**, *9* (10), 9458-9464.
60. Tuck, C. O.; Pérez, E.; Horváth, I. T.; Sheldon, R. A.; Poliakov, M., *Science* **2012**, *337* (6095), 695-9.

61. Rinaldi, R.; Jastrzebski, R.; Clough, M. T.; Ralph, J.; Kennema, M.; Bruijninx, P. C. A.; Weckhuysen, B. M., *Angew. Chem., Int. Ed.* **2016**, *55* (29), 8164-8215.
62. Magallanes, G.; Kärkäs, M. D.; Bosque, I.; Lee, S.; Maldonado, S.; Stephenson, C. R. J., *ACS Catal.* **2019**, *9* (3), 2252-2260.
63. Förster, T., *Ann. Phys.* **1948**, *437* (1-2), 55-75.
64. Dexter, D. L., *J. Chem. Phys.* **1953**, *21* (5), 836-850.
65. Singh, A.; Fennell, C. J.; Weaver, J. D., *Chem. Sci.* **2016**, *7* (11), 6796-6802.
66. Neveselý, T.; Wienhold, M.; Molloy, J. J.; Gilmour, R., *Chem. Rev.* **2022**, *122* (2), 2650-2694.
67. Metternich, J. B.; Gilmour, R., *J. Am. Chem. Soc.* **2015**, *137* (35), 11254-11257.
68. Molloy, J. J.; Schaefer, M.; Wienhold, M.; Morack, T.; Daniliuc, C. G.; Gilmour, R., *Science* **2020**, *369*, 302.
69. Gilmour, R.; Metternich, J., *Synlett* **2016**, *27* (18), 2541-2552.
70. Liu, Z.; Yu, L.; Zhou, L.; Zhou, Z., *Appl. Environ. Microbiol.* **2019**, *85* (19), e01327-19.
71. Alder, A.; Jamil, M.; Marzorati, M.; Bruno, M.; Vermathen, M.; Bigler, P.; Ghisla, S.; Bouwmeester, H.; Beyer, P.; Al-Babili, S., *Science* **2012**, *335* (6074), 1348-1351.
72. Takeda, T., *Modern Carbonyl Olefination: Methods and Applications.* **2004**.
73. Siau, W.-Y.; Zhang, Y.; Zhao, Y., *Stereoselective Synthesis of Z-Alkenes.* Springer Berlin Heidelberg: **2012**; pp 33-58.
74. Still, W. C.; Gennari, C., *Tetrahedron Lett.* **1983**, *24*, 4405.
75. Montgomery, T. P.; Johns, A. M.; Grubbs, R. H., *Catalysts* **2017**, *7*, 87.
76. Ogba, O. M.; Warner, N. C.; O'Leary, D. J.; Grubbs, R. H., *Chem. Soc. Rev.* **2018**, *47* (12), 4510-4544.
77. Hammond, G. S.; Saltiel, J.; Lamola, A. A.; Turro, N. J.; Bradshaw, J. S.; Cowan, D. O.; Counsell, R. C.; Vogt, V.; Dalton, C., *J. Am. Chem. Soc.* **1964**, *86* (16), 3197-3217.
78. Singh, K.; Staig, S.; Weaver, J. D., *J. Am. Chem. Soc.* **2014**, *136*, 5275.

Chapitre 2 Evaluating heteroleptic copper(I)-based complexes bearing π -extended diimines in different photocatalytic processes

Johann Sosoe, Corentin Cruché, Émilie Morin, and Shawn K. Collins*

Département de Chimie, Centre for Green Chemistry and Catalysis, Université de Montréal, Montréal, QC H3C 3J7, Canada.

Canadian Journal of Chemistry **2020**, 98 (9), 461-465. <https://doi.org/10.1139/cjc-2020-0014>

Contributions :

- Johann Sosoe a réalisé la synthèse des ligands et des complexes, et a participé au criblage des catalyseurs pour les réactions de transfert d'énergie et de PCET. Il a aussi participé à l'obtention des données photophysiques et à la rédaction de la partie expérimentale et du manuscrit.
- Corentin Cruché a participé au criblage des catalyseurs pour les réactions de transfert d'énergie, et d'Appel. Il a aussi participé à l'obtention des données photophysiques et à la rédaction de la partie expérimentale et du manuscrit.
- Émilie Morin a participé à l'obtention des données photophysiques
- Shawn K. Collins a participé à la mise en œuvre des expériences chimiques et à la rédaction du manuscrit.

2.1 Abstract

A series of 12 new copper-based photocatalysts of the type $\text{Cu}(\text{N}^{\wedge}\text{N})(\text{P}^{\wedge}\text{P})\text{BF}_4$ were synthesized bearing π -extended diimine ligands. The complexes have red shifted absorptions and larger extinction coefficients than complexes prepared with a parent diimine, dmp. The complexes

were evaluated for their ability to promote three different photochemical transformations. While the complexes were inactive in a reductive PCET process, the complexes afforded good yields in both SET and ET processes. Interestingly, homoleptic copper-complexes derived from the π -extended diimines were significantly more active in SET processes than analogous complexes with simpler diimines.

2.2 Introduction

Photocatalysis using precious metal complexes have had a significant impact in photochemical synthesis.¹⁻³ As issues of sustainability become increasingly important,⁴⁻⁵ research into photoactive base metal complexes has widened, involving a diverse range of elements demonstrating reactivity in a wide range of chemical transformations.⁶ Copper-based complexes have a rich history in UV-based photochemistry,⁷⁻⁸ with recent investigations involving their use in solar energy sciences,⁹ photocatalytic water-splitting,¹⁰ and organic light emitting diodes.¹¹ Synthetic photocatalysis has also made use of copper-based complexes¹² when using irradiation in the UV¹³⁻¹⁵ and visible ranges.¹⁶⁻¹⁸ The use of homoleptic polypyridyl-type complexes of copper in particular have re-emerged¹⁹ as photocatalysts of interest for photoredox-type reactions.²⁰

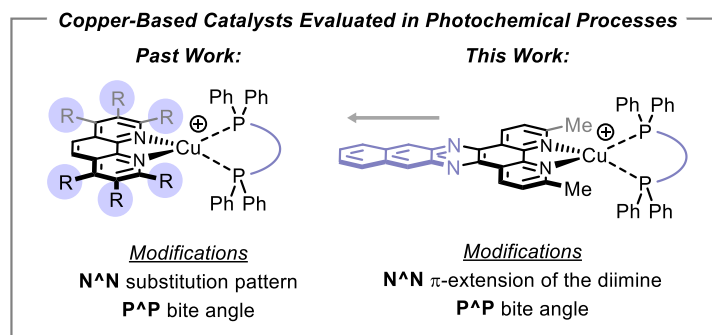


Figure 2.1 Copper-based complexes for photocatalysis.

Heteroleptic copper-based complexes of the type $\text{Cu}(\text{N}^{\wedge}\text{N})(\text{P}^{\wedge}\text{P})\text{X}$ were first reported by McMillin and co-workers²¹ and highlighted for their long excited state lifetimes when bearing the bisphosphine ($\text{P}^{\wedge}\text{P}$) DPEPhos. Our group first applied these catalysts to synthetic photocatalysis

for the synthesis of helical hydrocarbons and heterocycle synthesis.²² While the catalysts have now been explored by many more groups,²³⁻²⁴ our group has focused on trying to elucidate important structure/activity relationships that optimize the catalysts for applications in single electron transfer (SET),²⁵⁻²⁶ energy transfer (ET),²⁷ and proton-coupled electron transfer (PCET) reactions.²⁸ Our group previously reported a library of 50 copper complexes that were evaluated in three different bond-forming transformations. The library consisted of four different bisphosphine ligands (**P^P**) and a series of diimines (**N^N**) which were mainly phenanthroline-type ligands with different substituents at the 2-, 3- and 4-positions.²⁹ One aspect of diimine structure that was not examined was the impact of the π -surface on photocatalysis. The study of extended aromatic ligands on photoactive ruthenium(II) polypyridyl complexes has already been of interest. Representative complexes have been studied for their cytotoxic activity involving both modification of cell membrane function as well as DNA-intercalation.³⁰ The effects of π -extended diimines on heteroleptic copper(I)-photosensitizers has also been studied with regards to proton reduction experiments. Using XantPhos as the bisphosphine, the investigation of photophysical properties of the four complexes revealed large shifts in the cyclic voltamperograms and reduction potential, but relatively unchanged absorption spectra and weak emission spectra.³¹ However, a comparative assessment of the impact of the π -extended ligands on synthetic transformations has not appeared. Our previous studies have shown that even with suitable photophysical data, it is difficult to predict *a priori* which photocatalyst will be optimal, or not, for a given transformation. The efficiency of a synthetic process can be influenced by factors such as photostability,³² and resisting attack from reactive radicals in solution upon the catalyst framework.³³ Herein we describe the synthesis of 12 copper-based complexes of the type $\text{Cu}(\text{N}^{\wedge}\text{N})(\text{P}^{\wedge}\text{P})\text{BF}_4$ and evaluation in three photochemical processes. The photophysical properties and yields are compared with a parent complex, $\text{Cu}(\text{dmp})(\text{P}^{\wedge}\text{P})\text{BF}_4$.

2.3 Results and discussions

Synthesis of a series of heteroleptic Cu(I)-based photocatalysts using the known ligands^{30, 34} **ddpq**, **ddppz** and **dbdppz** were attempted with four bisphosphines: **DPEPhos**, **XantPhos**, **dppf** and **BINAP**. Commercially available $\text{Cu}(\text{MeCN})_4\text{BF}_4$ is placed in solution and the corresponding

bisphosphine ligand is added. Following subsequent diimine addition into the same reaction vessel, the desired heteroleptic complex is typically isolated by precipitation (**Table 2.1; Figure 2.2**). While **DPEPhos**, **XantPhos** and **dppf** formed good yields of the desired complexes, the bisphosphine **BINAP** was problematic. Analysis of the precipitates by ^1H NMR and mass spectrometry showed that mixtures of the corresponding hetero- and homoleptic complexes were formed. As such, complexes derived from **BINAP** were excluded from the present study. In addition, synthesis of the corresponding homoleptic complexes was also performed. When examining the photophysical data, the UV-vis absorption characteristics of the photocatalysts tend to vary very little with respect to either the diimine or bisphosphine, with absorption maxima all within the 380-410 nm range, with the exception of the homoleptic complexes which are farther red shifted. Extinction coefficients tend to grow with increasing size of the diimine ligand, although differences do occur with respect to the bisphosphine. Similar trends are observed with the excited state lifetimes, although again the differences vary only by a factor of ten and the lifetimes remain in the 3-80 ns range. However, interestingly the π -extended ligands significantly decrease the excited state lifetime which regards to the parent complex with the dmp ligand $\text{Cu}(\text{dmp})(\text{XantPhos})\text{BF}_4$ $\tau = 14300$ ns vs. $\text{Cu}(\text{ddpq})(\text{XantPhos})\text{BF}_4$ $\tau = 3$ ns. It was similarly difficult to discern general trends in excited state reduction potentials. For example, when complexes bore the **XantPhos** or **dppf** bisphosphine ligands, the potentials tended to decrease with increasing π -extension (for $\text{Cu}(\text{N}^{\wedge}\text{N})(\text{XantPhos})\text{BF}_4$: **ddpq** = -1.72 V; **ddppz** = -0.82 V; **dbdppz** = -1.29 V), however with the **DPEPhos**, which bears a striking resemblance to **Xantphos**, the trend is reversed and the excited state reduction potential increases with π -extension of the diimine ligand (for $\text{Cu}(\text{N}^{\wedge}\text{N})(\text{DPEPhos})\text{BF}_4$: **ddpq** = -1.26 V; **ddppz** = -1.12 V; **dbdppz** = -1.82 V).

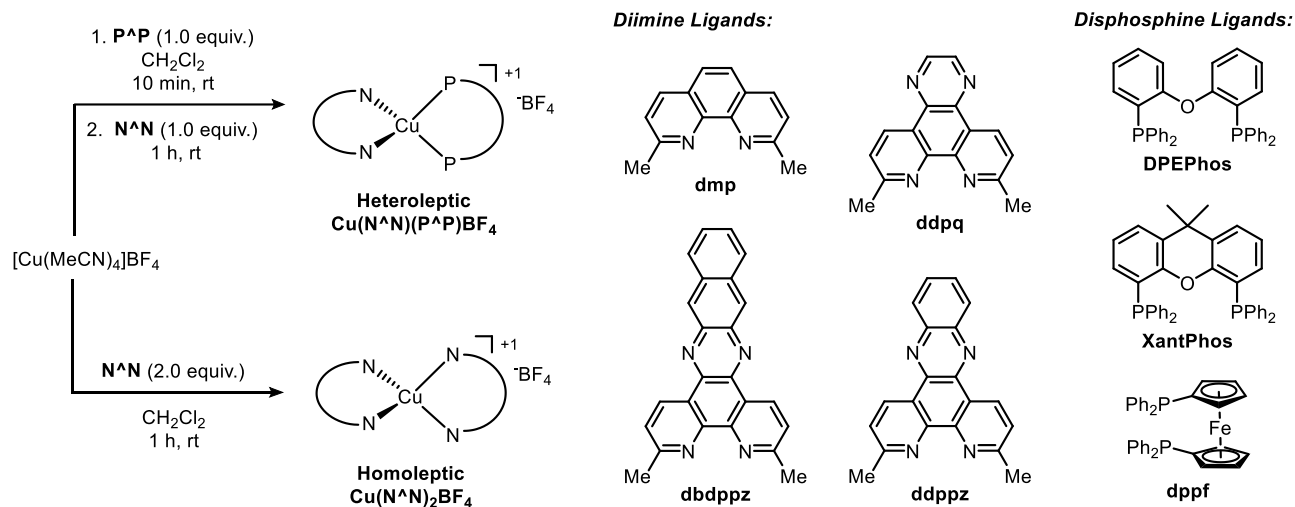


Figure 2.2 Synthesis of of Cu(I)-Based Photocatalysts

Table 2.1 Synthesis of of Cu(I)-Based Photocatalysts and Photophysical Properties.

Entry	$\text{N}^{\wedge}\text{N}$	$\text{P}^{\wedge}\text{P}$	Yield (%) ^a	λ_{max} (nm)	ϵ (L/mol·cm)	τ (ns)	λ_{em} (nm)	E_{T} (eV)	E (*Cu ^I /Cu ^{II})
1	dmp	None	97	463	17200	90	750	1.65	-1.12
2		DPEPhos	98	383	1580	14300	570	2.17	-1.68
3		XantPhos	46	380	3960	1133	560	2.21	-1.76
4		dppf	81	379	2890	1060	570	2.17	-1.56
5	ddpq	None	78	458	6760	3	680	1.82	-1.36
6		DPEPhos	84	382	4485	5	565	2.19	-1.26
7		XantPhos	85	386	3444	3	560	2.21	-1.72
8		dppf	91	380	3346	73	530	2.34	-1.15
9	ddppz	None	99	453	14428	4	762	1.63	-0.90
10		DPEPhos	78	380	17508	44	664	1.87	-1.12
11		XantPhos	91	380	12489	71	634	1.95	-0.82
12		dppf	79	380	17508	61	510	2.43	-1.59
13	dbdppz	None	82	412	25891	78	567	2.19	-1.34

14	DPEPhos	77	409	16663	69	489	2.53	-1.82
15	XantPhos	50	408	13754	75	565	2.19	-1.29
16	dppf	79 ^b	413	11711	69	597	2.08	-0.80

^a Isolated yields following precipitation with Et₂O. ^b in 1 :1 CH₂Cl₂:MeCN [5 mM]

With the library of copper-based complexes in hand, their evaluation in three mechanistically distinct photocatalytic transformations was pursued. Given the interesting changes in reduction potential with regards to diimine and bisphosphines, evaluation of the catalyst in a single electron transfer process was pursued first. The catalysts were investigated in a visible-light mediated conversion of an alcohol to a halide via a catalytic Appel-type reaction (**Figure 2.3; Table 2.2**).³⁵ Stephenson and co-workers had previously reported the use of Ru(bpy)₃Cl₂ to transform alcohols to halides, and our group also investigated copper-based complexes for the transformation in continuous flow.³⁶ The 12 copper-based catalysts with π -extended ligands were evaluated and compared with the parent catalysts having the **dmp** diimine.

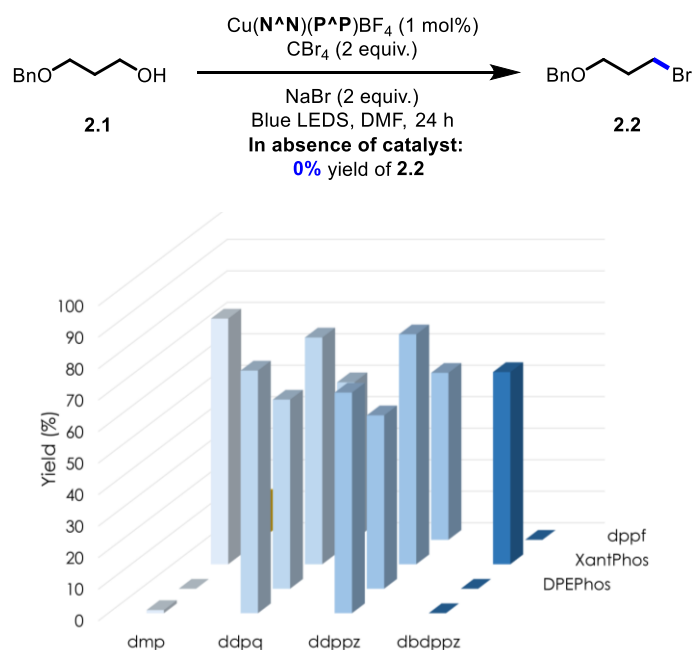


Figure 2.3 Evaluation of the π -extended copper-based photocatalysts in a photochemical Appel-type process. Column color darkens with increasing size of diimine ligand. Front entries without

an indicated phosphine ligand pertain to homoleptic complexes of the form $\text{Cu}(\text{N}^{\wedge}\text{N})_2\text{BF}_4$. No reaction is observed in the absence of light.

Table 2.2 Yield of **2.2** (%)

	none	DPEPhos	XantPhos	Dppf
dmp	1	0	78	13
ddpq	77	60	72	50
ddppz	70	55	73	53
dbdppz	78	72	61	53

Control reactions performed in the absence of light or in the absence of catalyst at 450 nm revealed no conversion to the alkyl bromide **2.2**, whereas most of the catalysts provide modest to good yields of **2.2** under irradiation. In general, the **DPEPhos** and **Xantphos** ligands were superior to the **dppf** bisphosphine ligand. While the homoleptic complex $\text{Cu}(\text{dmp})_2\text{BF}_4$ was essentially inactive, increasing the π -extended provided homoleptic complexes that afforded good yields of product.³⁷ The results would have been difficult to rationalize when examining the excited state reduction potentials and excited state lifetimes ($\text{Cu}(\text{dmp})_2\text{BF}_4$ $E = -1.12$ V; $\text{Cu}(\text{ddpq})_2\text{BF}_4$ $E = -1.36$ V; $\text{Cu}(\text{ddppz})_2\text{BF}_4$ $E = -0.90$ V; $\text{Cu}(\text{dbdppz})_2\text{BF}_4$ $E = -1.34$ V). All of the above catalysts possess excited state reduction potentials that should promote SET to CBr_4 ($E_{1/2} = 0.30$ V vs. SCE).³⁸ Apart from the homoleptic complex $\text{Cu}(\text{dbdppz})_2\text{BF}_4$ (78 % **2.2**), the best heteroleptic complexes were $\text{Cu}(\text{dmp})(\text{Xantphos})\text{BF}_4$ (78 % **2.2**) and $\text{Cu}(\text{dbdppz})(\text{DPEPhos})\text{BF}_4$ (72 % **2.2**).

The catalysts were then evaluated in a reductive proton-coupled electron transfer (PCET) reaction. Such redox processes have surged in interest amongst synthetic chemists for their ability to decrease the energy barrier to activating strong bonds. Our group has previously used the homolytic activation of ketones to evaluate copper-based catalysts for PCET processes (**Figure 2.4**; **Table 2.3**).³⁹

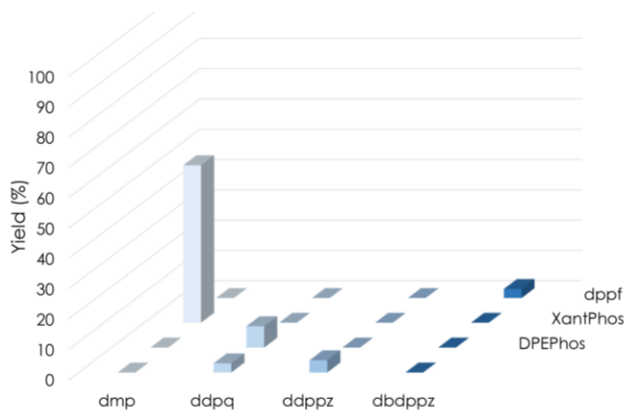
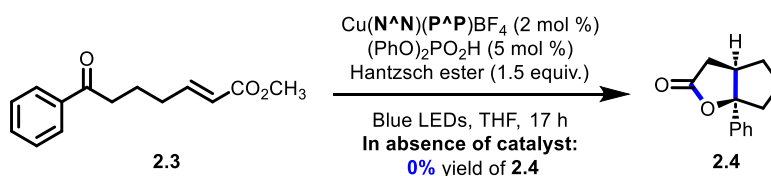


Figure 2.4 Evaluation of the π -extended copper-based photocatalysts in a PCET process. Column color darkens with increasing size of diimine ligand. Front entries without an indicated phosphine ligand pertain to homoleptic complexes of the form $\text{Cu}(\text{N}^{\wedge}\text{N})_2\text{BF}_4$. No reaction is observed in the absence of light.

Table 2.3 Yield of **2.4** (%).

	none	DPEPhos	XantPhos	dppf
dmp	0	0	52	0
ddpq	3	7	18	0
ddppz	4	0	0	0
dbdppz	0	20	0	3

Control reactions for the PCET process (**2.3**→**2.4**) showed no reaction in the absence of light and or catalyst. In examining the results from the screening in the PCET process, the Cu-based complexes bearing π -extended ligands were very poor catalysts, with only two catalysts ($\text{Cu}(\text{ddpq})(\text{XantPhos})\text{BF}_4$ and $\text{Cu}(\text{dbdppz})(\text{DPEPhos})\text{BF}_4$) providing appreciable yields of bicycle **2.4**. Knowles and co-workers had previously shown that a Ru-based intermediate ($\text{Ru}^{\text{I}}(\text{bpy})_3$ ($E_{1/2}^{\text{ox}} = -1.35$ V vs. SCE))⁴⁰ possessed a redox potential high enough to promote the PCET process.

Almost all of the catalysts bearing π -extended ligands surveyed possess an excited state redox potential capable of promoting the PCET process, but do not afford useful yields of the bicyclic product **2.4**. The inability of the π -extended ligand complexes to promote the PCET process could be due to the quenching mechanism of the photochemical transformation. Recent work with Cu-based photocatalysts has shown that a combination of particular diimine and suitable electron donor (such as Hantzsch esters), can allow Cu-based complexes to undergo reductive quenching from their excited state.⁴¹⁻⁴² If single electron reduction is unfavorable with the extended diimines, it would explain why the PCET processes are challenging.

Lastly, the new family of Cu-based photocatalysts were evaluated in a visible light sensitization of vinyl azides as a representative energy transfer process (**Figure 2.5; Table 2.4**).⁴³ Both Ru- and Cu-based catalysts have been shown to promote the decomposition of the azide to corresponding azirine, and eventual pyrrole. In examining the conversion of **2.5**→**2.6** with the π -extended copper-based photocatalysts (**Figure 2.5**), controls showed a slight background reaction in the absence of any catalyst at 450 nm (19 % of **2.6**).

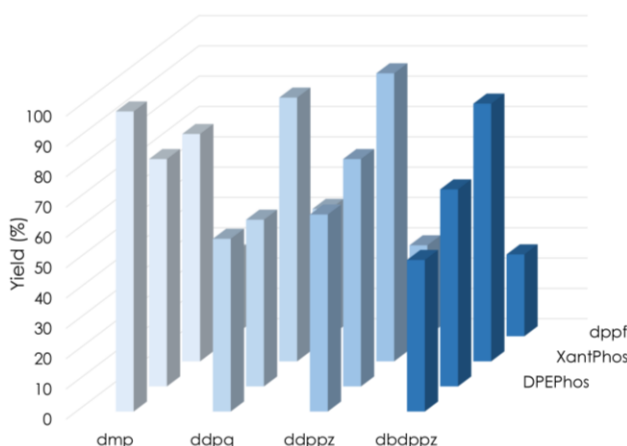
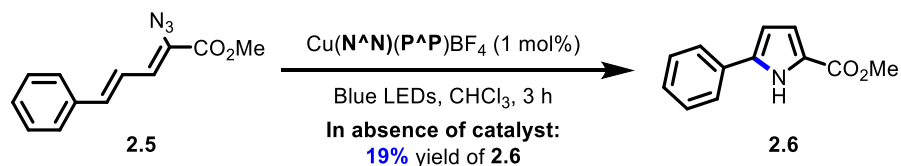


Figure 2.5 Evaluation of the π -extended copper-based photocatalysts in an energy transfer process. Column color darkens with increasing size of diimine ligand. Front entries without an indicated phosphine ligand pertain to homoleptic complexes of the form $\text{Cu}(\text{N}^{\text{A}}\text{N})_2\text{BF}_4$. No reaction is observed in the absence of light.

Table 2.4 Yield of **2.6** (%)

	none	DPEPhos	XantPhos	dppf
dmp	99	75	75	27
ddpq	57	55	87	42
ddppz	65	75	99	30
dbdppz	50	65	85	27

From the results, all complexes provide good to excellent yields of the desired pyrrole **2.6**. The heteroleptic complexes formed from the bisphosphine ligand **Xantphos** tend to display the highest yields regardless of diimine ligand, with Cu(**ddppz**)(**XantPhos**)BF₄ providing quantitative yields of **2.6**. The homoleptic complex Cu(**dmp**)₂BF₄ also provided a quantitative yield of the pyrrole **2.6**. Previous analyses of the energy transfer process showed that if the catalysts possess a suitable triplet state energy (E_T), the length of the excited state lifetime becomes the most important parameter in improving energy transfer processes. The excited state lifetimes of copper(I) complexes are lengthened through substitution on the ligands that enforce a tetrahedral geometry about the Cu center.²⁰ Wide bite-angle phosphines such as **XantPhos** complexes are known to extend excited state lifetimes,²⁰ so it is not surprising to see the catalyst Cu(**dbdppz**)(**XantPhos**)BF₄ with the best yield. All **XantPhos** catalysts possess a triplet energy that is sufficient to promote the reaction of dienyl azide **2.5** (estimated to have a triplet energy of approximately 1.9 eV).⁴⁴ However, the **Xantphos**-containing copper complexes have widely different excited state lifetimes (14330, 3, 71 and 69 ns **Table 2.1**). As such, predicting the “optimal” catalyst strictly from the photophysical properties would have been challenging.

2.4 Conclusions

In summary, a series of copper-based photocatalysts of the type Cu(**N^N**)(**P^P**)BF₄ were synthesized bearing π -extended diimine ligands. Their behavior in several photocatalytic processes were evaluated and revealed the following:

- 1) Copper-based complexes having π -extended diimine ligands have absorptions that are red-shifted and larger extinction coefficients than complexes prepared with smaller diimine ligands such as **dmp**.
- 2) The π -extended diimine ligands afford photocatalysts that can participate in oxidative quenching SET processes. However, the heteroleptic complexes bearing the **ddpq**, **ddppz** or **dbdppz** ligands are not particularly more active than the complexes having the parent **dmp** ligand. Interestingly, the π -extended diimine ligands do produce homoleptic complexes which were much more active in the visible-light mediated Appel process than the $\text{Cu}(\text{dmp})_2\text{BF}_4$ catalyst.
- 3) The new complexes did not seem to participate in PCET processes that likely pass through reductive quenching, suggesting that any further development of photocatalysis via reductive quenching should avoid using such diimine ligands.
- 4) Almost all complexes have similar excited state lifetimes and triplet state energies. While the complexes possessed characteristics suitable for the azide decomposition reaction described herein, the use of the π -extended ligands do not extend excited lifetimes or afford advantages for tuning properties for energy transfer processes.

2.5 References

1. Albin, A.; Fagnoni, M., *Handbook of synthetic photochemistry*. John Wiley & Sons: 2010.
2. Tepy, F., *Chem. Photocatal.* **2013**, 111.
3. For some early examples of iridium in photoredox catalysis see: Nagib, D. A.; Scott, M. E.; MacMillan, D. W., *J. Am. Chem. Soc.* **2009**, 131 (31), 10875-7.
4. Protti, S. F., M.; Albin, A. In Zhang, W.; Cue, B. W., Jr., Eds., *Green Techniques for Organic Synthesis and Medicinal Chemistry*. John Wiley & Sons Ltd: Chichester, UK, **2012**; p 363.
5. Rackl, D.; Kreitmeier, P.; Reiser, O., *Green Chem.* **2016**, 18 (1), 214-219.
6. Reiser, O. K., G.; Kais, V.; Kohls, P.; Paria, S.; Pirtsch, M.; Rackl, D.; Seo, H., *Chemical Photocatalysis*. De Gruyter: **2013**; p 139. doi:10.1515/9783110269246.
7. Horváth, O., *Coord. Chem. Rev.* **1994**, 135, 303-324.
8. McMillin, D. R.; Kirchhoff, J. R.; Goodwin, K. V., *Coord. Chem. Rev.* **1985**, 64, 83-92.
9. Sandroni, M.; Pellegrin, Y.; Odobel, F., *C. R. Chim.* **2016**, 19 (1-2), 79-93.
10. Luo, S. P.; Mejía, E.; Friedrich, A.; Pazidis, A.; Junge, H.; Surkus, A. E.; Jackstell, R.; Denurra, S.; Gladiali, S.; Lochbrunner, S.; Beller, M., *Angew. Chem. Int. Ed. Engl.* **2013**, 52 (1), 419-23.
11. Armaroli, N.; Accorsi, G.; Holler, M.; Moudam, O.; Nierengarten, J. F.; Zhou, Z.; Wegh, R. T.; Welter, R., *Adv. Mater.* **2006**, 18 (10), 1313-1316.
12. Hossain, A.; Bhattacharyya, A.; Reiser, O., *Science* **2019**, 364 (6439).
13. Schwendiman, D. P.; Kutal, C., *J. Am. Chem. Soc.* **1977**, 99 (17), 5677-5682.
14. Hertel, R.; Mattay, J.; Runsink, J., *J. Am. Chem. Soc.* **1991**, 113 (2), 657-665.
15. Mitani, M.; Nakayama, M.; Koyama, K., *Tetrahedron Lett.* **1980**, 21 (46), 4457-4460.
16. Do, H.-Q.; Bachman, S.; Bissember, A. C.; Peters, J. C.; Fu, G. C., *J. Am. Chem. Soc.* **2014**, 136 (5), 2162-2167.
17. Ziegler, D. T.; Choi, J.; Muñoz-Molina, J. M.; Bissember, A. C.; Peters, J. C.; Fu, G. C., *J. Am. Chem. Soc.* **2013**, 135 (35), 13107-13112.
18. Paria, S.; Reiser, O., *ChemCatChem* **2014**, 6 (9), 2477-2483.
19. Kern, J.-M.; Sauvage, J.-P., *J. Chem. Soc., Chem. Commun.* **1987**, (8), 546-548.
20. Pirtsch, M.; Paria, S.; Matsuno, T.; Isobe, H.; Reiser, O., *Chem. - Eur. J.* **2012**, 18 (24), 7336-7340.

21. Cuttell, D. G.; Kuang, S.-M.; Fanwick, P. E.; McMillin, D. R.; Walton, R. A., *J. Am. Chem. Soc.* **2002**, *124* (1), 6-7.
22. Hernandez-Perez, A. C.; Collins, S. K., *Angew. Chem., Int. Ed.* **2013**, *52* (48), 12696-12700.
23. Knorn, M.; Rawner, T.; Czerwieniec, R.; Reiser, O., *ACS Catal.* **2015**, *5* (9), 5186-5193.
24. Hernandez-Perez, A. C.; Collins, S. K., *Acc. Chem. Res.* **2016**, *49* (8), 1557-1565.
25. Beatty, J. W.; Stephenson, C. R., *Acc. Chem. Res.* **2015**, *48* (5), 1474-1484.
26. Prier, C. K.; Rankic, D. A.; MacMillan, D. W., *Chem. Rev.* **2013**, *113* (7), 5322-5363.
27. Arias-Rotondo, D. M.; McCusker, J. K., *Chem. Soc. Rev.* **2016**, *45* (21), 5803-5820.
28. Gentry, E. C.; Knowles, R. R., *Acc. Chem. Res.* **2016**, *49* (8), 1546-1556.
29. Minozzi, C.; Grenier-Petel, J.-C.; Parisien-Collette, S.; Collins, S. K., *Beilstein J. Org. Chem.* **2018**, *14* (1), 2730-2736.
30. Schatzschneider, U.; Niesel, J.; Ott, I.; Gust, R.; Alborzina, H.; Wölfel, S., *ChemMedChem: Chemistry Enabling Drug Discovery* **2008**, *3* (7), 1104-1109.
31. Heberle, M.; Tschierlei, S.; Rockstroh, N.; Ringenberg, M.; Frey, W.; Junge, H.; Beller, M.; Lochbrunner, S.; Karnahl, M., *Chem. - Eur. J.* **2017**, *23* (2), 312-319.
32. Deldaele, C.; Michelet, B.; Baguia, H.; Kajouj, S.; Romero, E.; Moucheron, C.; Evano, G., *CHIMIA* **2018**, *72* (9), 621.
33. Devery III, J. J.; Douglas, J. J.; Nguyen, J. D.; Cole, K. P.; Flowers II, R. A.; Stephenson, C. R., *Chem. Sci.* **2015**, *6* (1), 537-541.
34. Guo, W.; Engelman, B. J.; Haywood, T. L.; Blok, N. B.; Beaudoin, D. S.; Obare, S. O., *Talanta* **2011**, *87*, 276-283.
35. Dai, C.; Narayanam, J. M.; Stephenson, C. R., *Nat. Chem.* **2011**, *3* (2), 140-145.
36. Minozzi, C.; Caron, A.; Grenier-Petel, J. C.; Santandrea, J.; Collins, S. K., *Angew. Chem., Int. Ed.* **2018**, *57* (19), 5477-5481.
37. Engl, S.; Reiser, O., *European J. Org. Chem.* **2019**.
38. Kenichi, F.; Keiji, M.; Hiroshi, K.; Teijiro, Y., *Bull. Chem. Soc. Jpn.* **1963**, *36* (2), 217-222.
39. Tarantino, K. T.; Liu, P.; Knowles, R. R., *J. Am. Chem. Soc.* **2013**, *135* (27), 10022-10025.
40. Juris, A.; Balzani, V.; Belser, P.; von Zelewsky, A., *Helv. Chim. Acta* **1981**, *64* (7), 2175-2182.
41. Caron, A.; Morin, É.; Collins, S. K., *ACS Catal.* **2019**, *9*, 9458.

42. Michelet, B.; Deldaele, C.; Kajouj, S.; Moucheron, C.; Evano, G., *Org. Lett.* **2017**, *19* (13), 3576-3579.
43. Farney, E. P.; Chapman, S. J.; Swords, W. B.; Torelli, M. D.; Hamers, R. J.; Yoon, T. P., *J. Am. Chem. Soc.* **2019**, *141* (15), 6385-6391.
44. Farney et al. have reported the methyl dienyl azide as having a calculated value of approximately 45.4 kcal/mol. Given that 5 used in the study possesses additional conjugation, the triplet value may be slightly lower, but using the 45.4 kcal value provides a good standard for comparison (1.96 eV).

Chapitre 3 Heteroleptic Copper(I)-Based Complexes Incorporating BINAP and π -Extended Diimines: Synthesis, Catalysis and Biological Applications.

Corentin Cruché, Sayak Gupta,[†] Jeremy Kodanko^{*†} and Shawn K. Collins*

Département de Chimie, Centre for Green Chemistry and Catalysis, Université de Montréal, 1375 Avenue Thérèse-Lavoie-Roux, Montréal, QC H2V 0B3 CANADA. [†] Department of Chemistry, Wayne State University, 5101 Cass Ave, Detroit, MI 48202, USA.

Molecules **2022**, *27*, 3745. <https://doi.org/10.3390/molecules27123745>

Contributions:

- Corentin Cruché a réalisé la synthèse des ligands et des complexes, et le criblage des photocatalyseurs sur les différentes réactions, a participé à la rédaction de l'article, et a rédigé une partie de la partie expérimentale.
- Sayak Gupta a réalisé les tests de toxicité des catalyseurs sur les cellules cancéreuses, et a rédigé une partie de la partie expérimentale.
- Jeremy Kodanko a participé à la mise en œuvre des expériences biologiques et à la rédaction du manuscrit.
- Shawn K. Collins a participé à la mise en œuvre des expériences chimiques et à la rédaction du manuscrit.

3.1 Abstract

A series of copper-based photocatalysts of the type Cu(**NN**)(**BINAP**)BF₄ were synthesized bearing π -extended diimine ligands. Their behavior in several photocatalytic processes were evaluated and revealed acceptable levels of activity in an SET process, but negligible activity in PCET or ET processes. Suitable activity in ET processes could be restored through modification on

the ligand. The BINAP-derived complexes were then evaluated for activity against triple negative breast cancer cell lines. Controls indicated that copper complexes, and not their ligands, were responsible for activity. Encouraging activity was displayed by a homoleptic complex $\text{Cu}(\text{dppz})_2\text{BF}_4$.

3.2 Introduction

Copper-based complexes have demonstrated their potential across photocatalysis.¹ As an alternative to precious metal complexes,²⁻⁴ discreet copper-based complexes can be exploited as photocatalysts under UV⁵⁻⁷ and visible light irradiation.⁸⁻¹² In turn, a number of copper complexes can be formed in-situ and used in metallaphotoredox processes, which are particularly advantageous for asymmetric photocatalysis.¹³ In addition to synthetic applications, copper-based complexes have found interest in solar energy sciences,¹⁴ photocatalytic water-splitting,¹⁵ and organic light emitting diodes.¹⁶

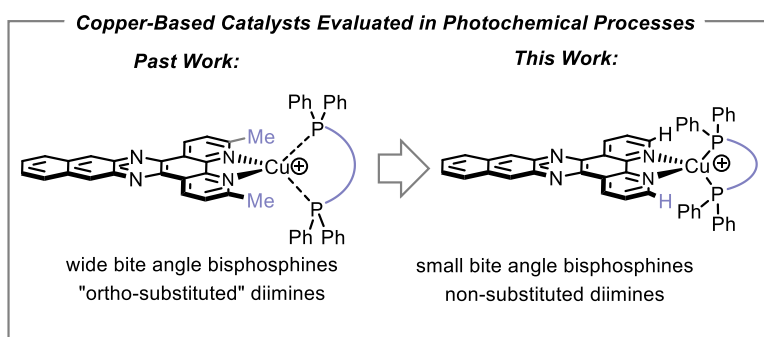


Figure 3.1 Small bite-angle bisphosphine for heteroleptic copper-based complexes.

McMillin and co-workers first reported that heteroleptic copper-based complexes ($\text{Cu}(\text{NN})(\text{PP})\text{X}$) bearing the wide bite angle bisphosphine **DPEPhos** possessed unusually long excited state lifetimes.¹⁷ Following our initial discovery that such complexes exhibited significant potential for synthetic photocatalysis,¹⁸ we reported a structure/activity study library of 50 copper complexes that were evaluated in single electron transfer (SET),¹⁹⁻²⁰ energy transfer (ET),²¹

and proton-coupled electron transfer (PCET) reactions.²² Although most photocatalysis using heteroleptic complexes continue to employ wide bite-angle bisphosphines,²³⁻²⁴ the aforementioned library study revealed that the small bite angle bisphosphine **BINAP** could form copper complexes that afforded high yields in all three of the mechanistic processes evaluated. Our bank of available diimines and bisphosphines has since expanded to allow for development of improved complexes for energy transfer processes.²⁵ Among the diimine structures evaluated were those that possessed extended π -surfaces, which unfortunately did not afford heteroleptic complexes with remarkable activities in photocatalysis.²⁶ However, previous studies were limited to wide bite-angle bisphosphines, as the preparation of the corresponding complexes with BINAP was problematic (**Figure 3.1**). Herein we describe the synthesis of the “missing” copper-based complexes of the type $\text{Cu}(\text{NN})(\text{BINAP})\text{BF}_4$, their evaluation in photochemical processes and preliminary biological testing against triple-negative breast cancer cell lines.

3.3 Results and discussions

Heteroleptic complexes are typically formed by sequential addition of the diimine and bisphosphine ligands to a copper salt in a solvent, followed by precipitation. When the synthesis of heteroleptic Cu(I)-based photocatalysts using **BINAP** and the ligands **ddpq**, **ddppz** or **dbdppz**²⁷ was attempted, the resulting solids were mixtures of the corresponding hetero- and homoleptic complexes (¹H NMR and mass spectrometry) (**Figure 3.2**). Our hypothesis was that the small bite-angle oriented the phenyl groups of the phosphine over the copper center, which is already encumbered by the methyl groups found on the diimine ligands. Attempts at conducting the synthesis in other solvents (Toluene, THF and mixtures thereof with CH_2Cl_2) did not result in a

shift of the equilibrium between heteroleptic and homoleptic complexes. Experiments involving lower temperatures and/or slow addition of the bisphosphine were also non-productive. Repeated crystallization of crude reaction mixtures did improve the ratio of heteroleptic versus homoleptic complexes, but did not approach selectivities or yields that were synthetically useful.

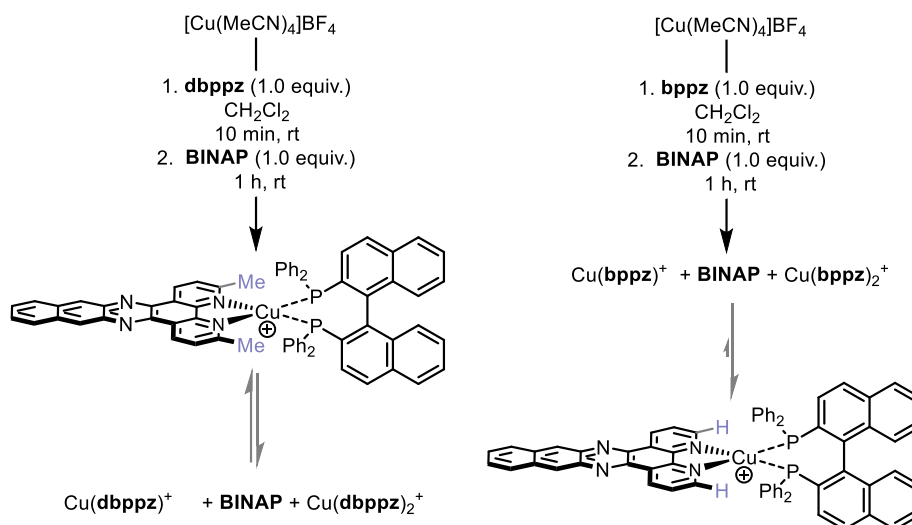
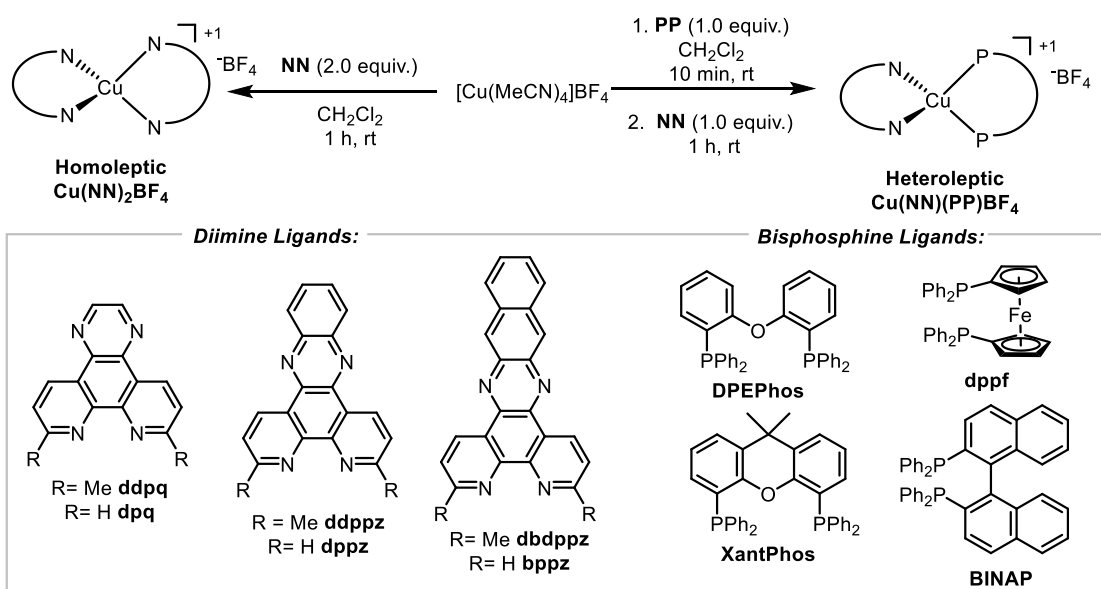


Figure 3.2 Synthesis of heteroleptic copper-based complexes using BINAP.

Consequently, the **BINAP**-containing complexes were prepared with the analogous diimines **dpq**, **dppz** and **bdppz** (Table 3.1). Gratifyingly, all three complexes were isolated in good yields (53-77%). When examining the photophysical data, the UV-vis absorption characteristics of the **BINAP**-containing photocatalysts do not change significantly with respect to the diimine. The absorption maxima are all within a narrow window (424-462 nm), although the emission maxima are more spread out (560-625 nm) with lower wavelength emissions observed for the larger diimine ligands. Extinction coefficients and excited state lifetimes are again all relatively similar across the series. The short excited state lifetimes are to be expected, as the absence of both *ortho*-substitution on the diimines and the small bite angle of the bisphosphine will not stabilize

the geometry of the excited state. Excited state reduction potentials all were in the range of -1.0 eV which corresponds to what was observed with the complexes derived from ortho-substituted analogues having **ddpq**, **ddppz** and **dbdppz** ligands.

Table 3.1 Synthesis and Properties of Cu(I)-Based Photocatalysts of the Type Cu(NN)(BINAP)BF₄.



Entry	NN	PP	Yield (%) ^a	λ_{\max} (nm)	ϵ (L/mol·cm)	τ (ns)	λ_{em} (nm)	E_T (eV)	E (*Cu ^I /Cu ^{II})
1	ddpq		78	458	6760	3	680	1.82	-1.36
2	ddpq	DPEPhos	84	382	4485	5	565	2.19	-1.26
3	ddpq	XantPhos	85	386	3444	3	560	2.21	-1.72
4	ddpq	dppf	91	380	3346	73	530	2.34	-1.15
5	dpq	BINAP	75	424	5752	1.4	625	2.38	-1.02
6	ddppz		99	453	14428	4	762	1.63	-0.90
7	ddppz	DPEPhos	78	380	17508	44	664	1.87	-1.12
8	ddppz	XantPhos	91	380	12489	71	634	1.95	-0.82
9	ddppz	dppf	79	380	17508	61	510	2.43	-1.59
10	dppz	BINAP	77	433	6759	1.8	545	2.27	-1.26
11	dbdppz		82	412	25891	78	567	2.19	-1.34
12	dbdppz	DPEPhos	77	409	16663	69	489	2.53	-1.82
13	dbdppz	XantPhos	50	408	13754	75	565	2.19	-1.29
14	dbdppz	dppf	79 ^b	413	11711	69	597	2.08	-0.80
15	bdppz	BINAP	53	462	5930	2.3	560	2.21	-1.20

^a Isolated yields following precipitation with Et₂O.

With the new **BINAP**-containing copper-based complexes, their evaluation in photocatalysis was performed and compared to analogous catalysts. Three mechanistically distinct photocatalytic transformations were pursued. In a visible-light Appel-type reaction (**Figure 3.3**)²⁸⁻²⁹ the new **BINAP**-containing copper-based catalyst Cu(**dpq**)(**BINAP**)BF₄ provided similar yields to other complexes having large bite angle bisphosphines. Note that control reactions performed in the absence of light or in the absence of catalyst at 450 nm did not afford any significant conversion to the alkyl bromide **3.2**. However as the π-surface of the ligands grew, the **BINAP**-containing complexes of **dppz** and **bdppz** were all inferior to analogous complexes having wide bite angles bisphosphines. Although the complexes of **dppz** and **bdppz** had larger excited state reduction potentials, it is possible that the complexes with ligands with larger π-surfaces could be more unstable in solution. The stability of various copper complexes with diimines having large π-surfaces was previously shown to decrease with the size of ligand in other photocatalytic processes. However, it should be noted that amongst other **BINAP**-derived complexes, the Cu(**dpq**)(**BINAP**)BF₄ (66% of **3.2**) was superior in the Appel-type reaction to other structurally similar complexes such as Cu(**dmp**)(**BINAP**)BF₄ (18% of **3.2**) and Cu(**phen**)(**BINAP**)BF₄ (45% of **3.2**), suggesting that the **dpq** offered some beneficial reactivity (**Figure 3.4**).

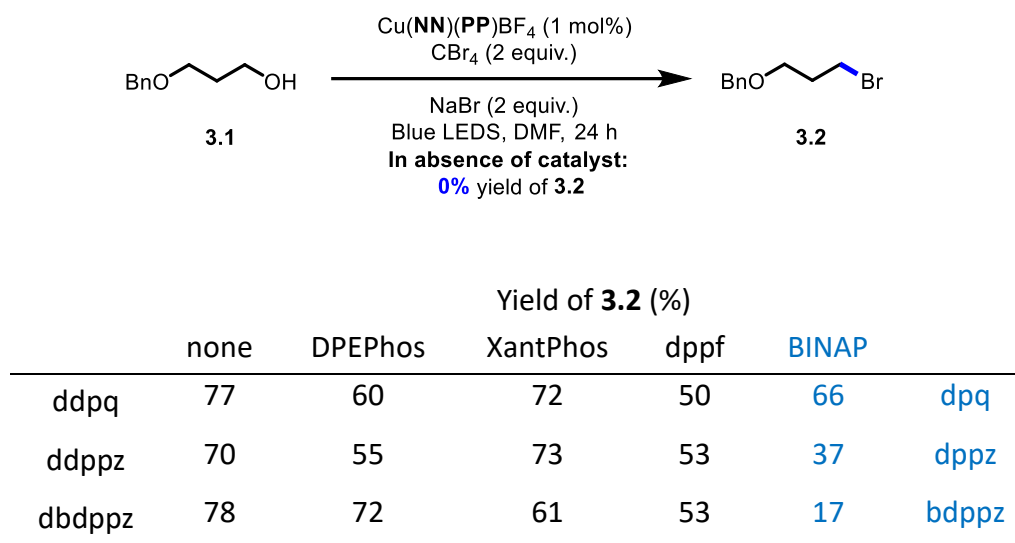


Figure 3.3 Comparison of the **BINAP**-containing copper complexes bearing π-extended ligands in a photochemical Appel-type process.

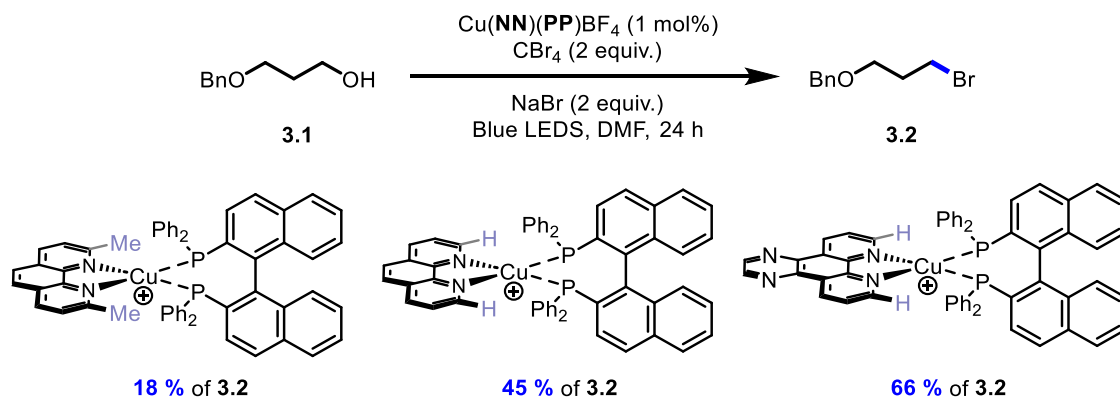
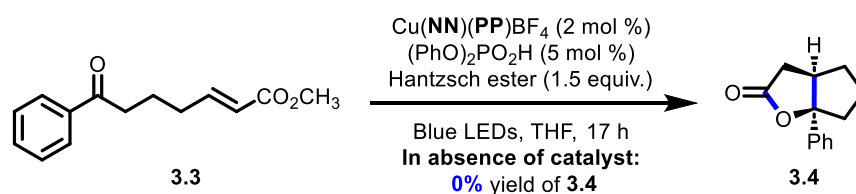


Figure 3.4 Effects of the diamine ligand of heteroleptic copper complexes in a photochemical Appel-type process.

The **BINAP**-containing catalysts were then compared to the previous series being the ortho-substituted diimines in a reductive proton-coupled electron transfer (PCET) reaction. Our group has previously used the homolytic activation of ketones to benchmark complexes for their efficiency in a PCET process (**Figure 3.5**).³⁰ Previous evaluation with the ortho-substituted series revealed very poor reactivity and low yields (0-20% yield). Unfortunately, the screening with the new **BINAP**-containing complexes was equally disappointing. Recent work suggests that the process is in fact a reductive quenching of the Cu-based photocatalysts in the excited state.³¹⁻³² The electron-rich π -extended ligands would not be favorable in such a mechanism. Furthermore, given the results from the oxidative quenching in the Appel process, it is clear that the bisphosphine is not playing a significant role in altering the excited state redox potentials of the resulting complexes.

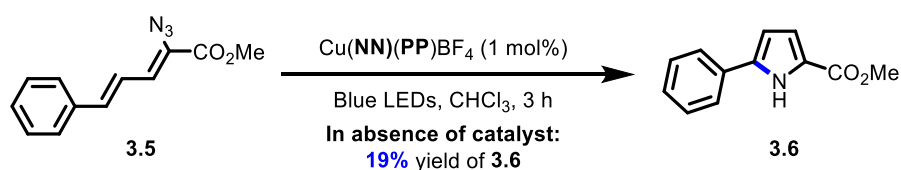


Yield of **3.4** (%)

	none	DPEPhos	XantPhos	dppf	BINAP	
ddpq	3	7	18	0	2	dpq
ddppz	4	0	0	0	0	dppz
dbdppz	0	20	0	3	0	bdppz

Figure 3.5 Comparison of the BINAP-containing copper complexes bearing π -extended ligands in a photochemical PCET process.

The last evaluation of the new **BINAP**-containing Cu-based photocatalysts was via energy transfer for the transformation of vinyl azides to the corresponding pyrrole (**Figure 3.6**).³³ Given that the new complexes had neither wide bite angle phosphines or ortho-substituted diimines to stabilize the excited state, the yields of the pyrrole were expected to drop. Note that the excited state lifetimes of the new **BINAP**-containing complexes were all approximately an order of magnitude less than analogous complexes (eg: Cu(**bdppz**)(**XantPhos**)BF₄ τ =71 ns; Cu(**dppz**)(**BINAP**)BF₄ τ =1.8 ns). Indeed, the yields of the pyrrole **3.6** with the **BINAP**-containing complexes (21-23% of **3.6**) were barely above the observed background reaction in the absence of any catalyst at 450 nm (19 % of **3.6**). A further comparison of Cu(**phen**)(**BINAP**)BF₄ (38% of **3.6**) and Cu(**dpq**)(**BINAP**)BF₄ (21% of **3.6**) showed that the **dpq** ligand had a deleterious effect on the energy transfer process. It should be noted that good yields of the pyrrole are possible when switching to any ligand known to extend the excited state lifetimes (**Figure 3.7**). For example, using an ortho-substituted diimine ligand in a complex with **BINAP** affords quantitative yields of the product (Cu(**dmp**)(**BINAP**)BF₄, 99% of **3.6**). In addition, using a wide bite angle bisphosphine also affords a quantitative yield of **3.6** (Cu(**dppz**)(**XantPhos**)BF₄, 99% of **3.6**).



	none	DPEPhos	XantPhos	dppf	BINAP	
ddpq	57	55	87	42	21	dpq
ddppz	65	75	99	30	23	dppz
dbdppz	50	65	85	27	23	bdppz

Figure 3.6 Comparison of the **BINAP**-containing copper complexes bearing π -extended ligands in an energy transfer process.

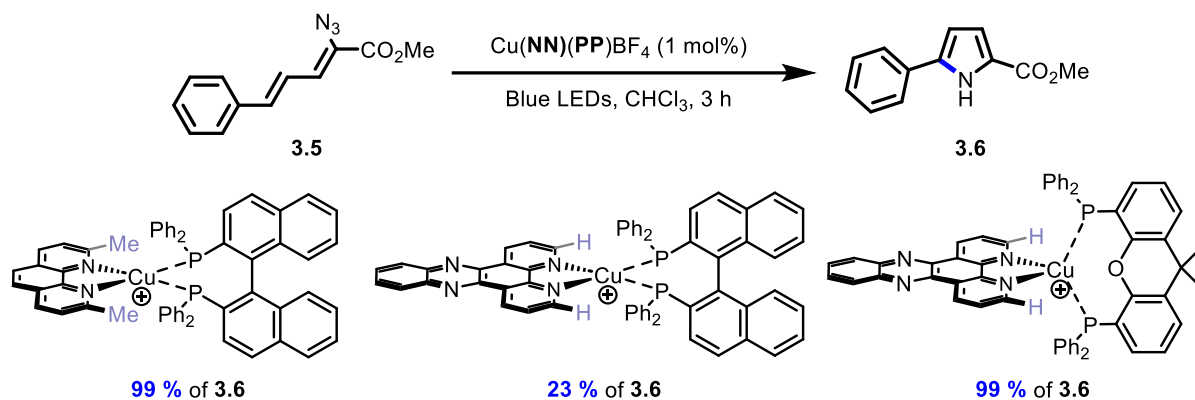


Figure 3.7 Ligand effects in heteroleptic copper complexes in an energy transfer process.

Given the recent interest in copper-containing complexes for medicinal chemistry,³⁴⁻³⁶ it was decided to test the most soluble of new **BINAP**-containing complexes against triple negative breast cancer cell lines (MBA-MB-231) (**Figure 3.8**). The viability of the cell lines was evaluated with the $\text{Cu}(\text{dppq})(\text{BINAP})\text{BF}_4$ and $\text{Cu}(\text{dppz})(\text{BINAP})\text{BF}_4$ complexes (entries 1 and 2 respectively) and both displayed approximately 25-35% viability. Controls performed from the **dppq**, **dppz** and **BINAP** ligands (entries 10-12) demonstrated that biological activity was originating from the metal-complexes themselves. While a homoleptic complex $\text{Cu}(\text{BINAP})_2\text{BF}_4$ was poorly active, the homoleptic complexes derived from the diimines showed low cell viabilities, with $\text{Cu}(\text{dppz})_2\text{BF}_4$ being the most active of all complexes tested. Finally, given that the **BINAP** used in the above photocatalysis and biological evaluations was racemic, we prepared and evaluated the enantiomer variants of the **dppq** and **dppz**-containing complexes. Interestingly, for the **dppq**-complexes, the (*S*)-**BINAP** containing complex $\text{Cu}(\text{dppq})((S)\text{-BINAP})\text{BF}_4$ was approximately twice as active as the analogous (*R*)-**BINAP** complex. The copper complexes of **dppz** bearing either (*S*)- or (*R*)-**BINAP** did not show any difference in activity. The complex $[\text{Cu}(\text{MeCN})_4]\text{BF}_4$ (10 μM) had

negligible effects on cell viability > 75%, indicating that the complexes, rather than free copper, were responsible for biological activity.

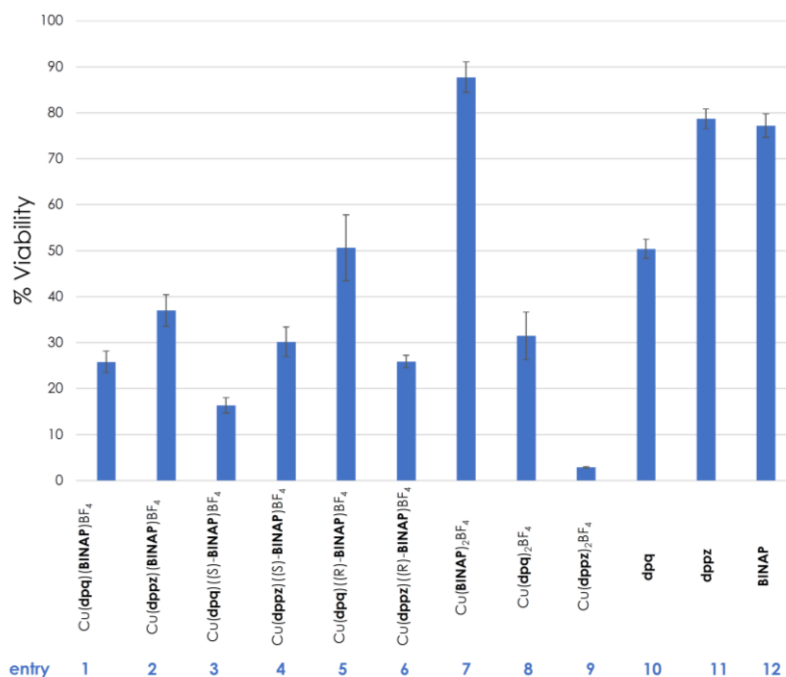


Figure 3.8 Viability of MDA-MB-231 cells at 5 μ M. MDA-MB-231 cells were seeded at the density of 7,000 cells per well in 96 well plates, plates were incubated overnight. The cells were then treated with growth media containing 5 μ M of the copper complexes (entries 1 - 9) or controls (entries 10 – 12) and allowed to incubate at 37 $^{\circ}$ C for 72 hrs. The viabilities of cells were finally determined by MTT assay and converted to percentages. Data are an average of three different experiments.

3.4 Conclusions

In summary, a series of copper-based photocatalysts of the type Cu(NN)(BINAP)BF₄ were synthesized bearing π -extended diimine ligands. Their behavior in several photocatalytic processes were evaluated and revealed the following:

1) Copper-based complexes derived from **BINAP** with π -extended diimine ligands without ortho-substitution do not show significant different photophysical properties when compared to analogous complexes with the exception of the excited state lifetime, which decreased by approximately an order of magnitude.

2) The new **BINAP**-containing complexes were active in the visible-light Appel-type process, with the $\text{Cu}(\text{dpq})(\text{BINAP})\text{BF}_4$ complex having slightly better activity than analogous complexes derived from **phen** or **dmp** ligands.

3) The new **BINAP**-derived did not afford complexes active for a PCET process.

4) In an energy transfer process, high yields of the desired product could be obtained with either **BINAP** or the **dpq**, **dppz** and **ddppz** diimines through judicious choice of the accompanying ligand. For example, $\text{Cu}(\text{dmp})(\text{BINAP})\text{BF}_4$ and $\text{Cu}(\text{dppz})(\text{XantPhos})\text{BF}_4$ afforded quantitative yields of product.

In addition to the photocatalysis, the copper complexes were evaluated for the first time in a medicinal chemistry context against triple negative breast cancer cell lines. Controls indicated that copper complexes, and not their ligands, were responsible for activity. Encouraging activity was displayed by a homoleptic complex $\text{Cu}(\text{dppz})_2\text{BF}_4$.

3.5 References

1. Hossain, A.; Bhattacharyya, A.; Reiser, O., *Science* **2019**, *364* (6439).
2. Albini, A.; Fagnoni, M., *Handbook of synthetic photochemistry*. John Wiley & Sons: 2010.
3. Tepy, F., *Chem. Photocatal.* **2013**, 111.
4. For some early examples of iridium in photoredox catalysis see: Nagib, D. A.; Scott, M. E.; MacMillan, D. W., *J. Am. Chem. Soc.* **2009**, *131* (31), 10875-7.
5. Schwendiman, D. P.; Kutal, C., *J. Am. Chem. Soc.* **1977**, *99* (17), 5677-5682.
6. Hertel, R.; Mattay, J.; Runsink, J., *J. Am. Chem. Soc.* **1991**, *113* (2), 657-665.
7. Mitani, M.; Nakayama, M.; Koyama, K., *Tetrahedron Lett.* **1980**, *21* (46), 4457-4460.
8. Do, H.-Q.; Bachman, S.; Bissember, A. C.; Peters, J. C.; Fu, G. C., *J. Am. Chem. Soc.* **2014**, *136* (5), 2162-2167.
9. Ziegler, D. T.; Choi, J.; Muñoz-Molina, J. M.; Bissember, A. C.; Peters, J. C.; Fu, G. C., *J. Am. Chem. Soc.* **2013**, *135* (35), 13107-13112.
10. Paria, S.; Reiser, O., *ChemCatChem* **2014**, *6* (9), 2477-2483.
11. Kern, J.-M.; Sauvage, J.-P., *J. Chem. Soc., Chem. Commun.* **1987**, (8), 546-548.
12. Pirtsch, M.; Paria, S.; Matsuno, T.; Isobe, H.; Reiser, O., *Chem. - Eur. J.* **2012**, *18* (24), 7336-7340.
13. Prentice, C.; Morrisson, J.; Smith, A. D.; Zysman-Colman, E., *Beilstein J. Org. Chem.* **2020**, *16* (1), 2363-2441.
14. Sandroni, M.; Kayanuma, M.; Planchat, A.; Szuwarski, N.; Blart, E.; Pellegrin, Y.; Daniel, C.; Boujtita, M.; Odobel, F., *Dalton Trans.* **2013**, *42* (30), 10818-10827.
15. Luo, S. P.; Mejía, E.; Friedrich, A.; Pazidis, A.; Junge, H.; Surkus, A. E.; Jackstell, R.; Denurra, S.; Gladiali, S.; Lochbrunner, S., *Angew. Chem.* **2013**, *125* (1), 437-441.
16. Armaroli, N.; Accorsi, G.; Holler, M.; Moudam, O.; Nierengarten, J. F.; Zhou, Z.; Wegh, R. T.; Welter, R., *Adv. Mater.* **2006**, *18* (10), 1313-1316.
17. Cuttell, D. G.; Kuang, S.-M.; Fanwick, P. E.; McMillin, D. R.; Walton, R. A., *J. Am. Chem. Soc.* **2002**, *124* (1), 6-7.
18. Hernandez-Perez, A. C.; Collins, S. K., *Angew. Chem., Int. Ed.* **2013**, *52* (48), 12696-12700.
19. Beatty, J. W.; Stephenson, C. R., *Acc. Chem. Res.* **2015**, *48* (5), 1474-1484.

20. Prier, C. K.; Rankic, D. A.; MacMillan, D. W., *Chem. Rev.* **2013**, *113* (7), 5322-5363.
21. Arias-Rotondo, D. M.; McCusker, J. K., *Chem. Soc. Rev.* **2016**, *45* (21), 5803-5820.
22. Gentry, E. C.; Knowles, R. R., *Acc. Chem. Res.* **2016**, *49* (8), 1546-1556.
23. Hernandez-Perez, A. C.; Collins, S. K., *Acc. Chem. Res.* **2016**, *49*, 1557.
24. Knorn, M.; Rawner, T.; Czerwieniec, R.; Reiser, O., *ACS Catal.* **2015**, *5* (9), 5186-5193.
25. Cruche, C.; Neiderer, W.; Collins, S. K., *ACS Catal.* **2021**, *11* (14), 8829-8836.
26. Sosoe, J.; Cruché, C.; Morin, É.; Collins, S. K., *Can. J. Chem.* **2020**, *98* (9), 461-465.
27. Guo, W.; Engelman, B. J.; Haywood, T. L.; Blok, N. B.; Beaudoin, D. S.; Obare, S. O., *Talanta* **2011**, *87*, 276-283.
28. Dai, C.; Narayanam, J. M.; Stephenson, C. R., *Nat. Chem.* **2011**, *3* (2), 140-145.
29. Minozzi, C.; Grenier-Petel, J.-C.; Parisien-Collette, S.; Collins, S. K., *Beilstein J. Org. Chem.* **2018**, *14*, 2730-2736.
30. Tarantino, K. T.; Liu, P.; Knowles, R. R., *J. Am. Chem. Soc.* **2013**, *135* (27), 10022-10025.
31. Caron, A.; Morin, E.; Collins, S. K., *ACS Catal.* **2019**, *9* (10), 9458-9464.
32. Michelet, B.; Deldaele, C.; Kajouj, S.; Moucheron, C.; Evano, G., *Org. Lett.* **2017**, *19* (13), 3576-3579.
33. Farney, E. P.; Yoon, T. P., *Angew. Chem., Int. Ed.* **2014**, *53* (3), 793-797.
34. Smith, C. B.; Days, L. C.; Alajroush, D. R.; Faye, K.; Khodour, Y.; Beebe, S. J.; Holder, A. A., *Photochem. Photobiol.* **2022**, *98* (1), 17-41.
35. Ruan, Y.; Jia, X.; Wang, C.; Zhen, W.; Jiang, X., *ACS Biomater. Sci. Eng.* **2019**, *5* (2), 1016-1022.
36. Devi, L. R.; Raza, M. K.; Musib, D.; Roy, M., *Anticancer Agents Med. Chem.* **2021**, *21* (1), 33-41.

Chapitre 4 Heteroleptic Copper-Based Complexes for Energy Transfer Processes: E→Z Isomerization and Tandem Photocatalytic Sequences

Corentin Cruché, William Neiderer, Shawn K. Collins*

Département de Chimie, Centre for Green Chemistry and Catalysis, Université de Montréal, 1375 Avenue Thérèse-Lavoie-Roux, Montréal, QC H2V 0B3 CANADA.

ACS Catal. **2021**, *11*, *14*, 8829–8836 <https://doi.org/10.1021/acscatal.1c01983>

Contributions:

- Corentin Cruché a réalisé la synthèse des ligands et des complexes, le criblage des photocatalyseurs, l'étendue de la réaction, la mise en échelle en débit continu et les mesures spectrométriques. Il a aussi participé à la rédaction de l'article, et a rédigé une partie de la partie expérimentale.
- William Neiderer a participé aux criblages des photocatalyseurs.
- Shawn K. Collins a participé à la mise en œuvre des expériences chimiques et à la rédaction du manuscrit.

4.1 Abstract

Energy transfer processes involving copper complexes are rare. Using an optimized heteroleptic copper complex, Cu(bphen)(XantPhos)BF₄, photosensitized E→Z isomerization of olefins is demonstrated. The XantPhos ligand afforded sensitizers with improved catalyst stability, while the bphen ligand lengthened the excited state lifetime. A series of 25 di- and tri-substituted alkenes underwent photoisomerization, including macrocycles and 1,3-enynes. Cu(bphen)(XantPhos)BF₄ could also be employed in a tandem ATRA/photoisomerization process

employing arylsulfonyl chlorides, an example of photoisomerization with halide-substituted olefins.

4.2 Introduction

Heteroleptic copper-based complexes possessing one diimine ligand (**NN**) and bisphosphine (**PP**) have exhibited considerable potential in photocatalysis.¹⁻⁵ The potential for broad tuning of photophysical properties has been exploited for a variety of photoredox processes.⁶⁻¹⁴ Recently, our group has demonstrated that control of the ligand framework can also fine tune complexes for other photocatalytic processes (**Figure 4.1**).¹⁵ For example, judicious choice of ligands resulted in the first proton-coupled electron transfer (PCET) reactions catalyzed by Cu(**NN**)(**PP**)X complexes.¹⁵⁻¹⁶ The use of copper-based catalysts for energy transfer processes are rare. A recent example was reported by Poisson and co-workers, where a Cu(OAc)₂/**BINAP** system was exploited for photoisomerization of polarized alkenes.¹⁷ Surprisingly, only a single report of Cu(**NN**)(**PP**)X complexes for synthetic energy transfer (ET) processes has been reported, where a screening afforded a Cu(**dmp**)(**BINAP**)BF₄ complex as optimum for vinyl azide sensitization.¹⁵ In 2002, McMillin and co-workers reported that complexes of the type Cu(**NN**)(**PP**)X can have excited state lifetimes as high as ~16 μs,¹⁸ which would be beneficial for transformations occurring via ET.¹⁹ In addition, optimizing the diimine or the bisphosphine ligand could fine tune important photophysical parameters such as triplet energies and excited state lifetimes. As mentioned above, an emerging ET process in organic synthesis is photocatalytic *E*↔*Z* isomerization. Control of alkene geometry is known to be critical to biological function,²⁰⁻²³ but it is equally important in the context of organic synthesis. Alkenes remain one of the most utilized building blocks, and olefination methods such as phosphorous ylide chemistry²⁴⁻²⁷ and catalytic olefin cross metathesis²⁸⁻³¹ have identified control of the resulting olefin geometry as a key goal. In 1964, Hammond and co-workers reported the *E*↔*Z* isomerization of stilbenes through sensitized excitation,³²⁻³⁴ where the extended conjugation of the arene and alkene π-systems in the *E*-isomer can be preferentially excited over the *Z*-isomer. The resulting *Z*-isomer is relatively deconjugated through twisting of the arene due to allylic strain. The strategy proposed by Hammond represents an interested shift in thinking on how to control olefin geometry in synthesis, as the *Z*-isomer could become accessible from any *E*:*Z* mixture through

photochemistry. Not surprisingly, the interest in visible-light mediated photocatalysis has helped advance the field considerably.³⁵⁻³⁶ Weaver and co-workers have studied the use of Ir(ppy)₃ for the isomerization of allylic amines,³⁷⁻⁴⁰ while Gilmour and co-workers have exploited (-)-riboflavin for a host of isomerization processes.⁴¹⁻⁴⁵

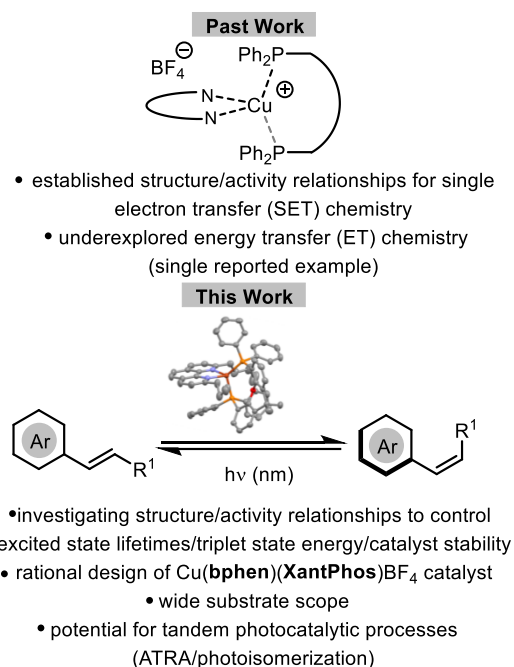
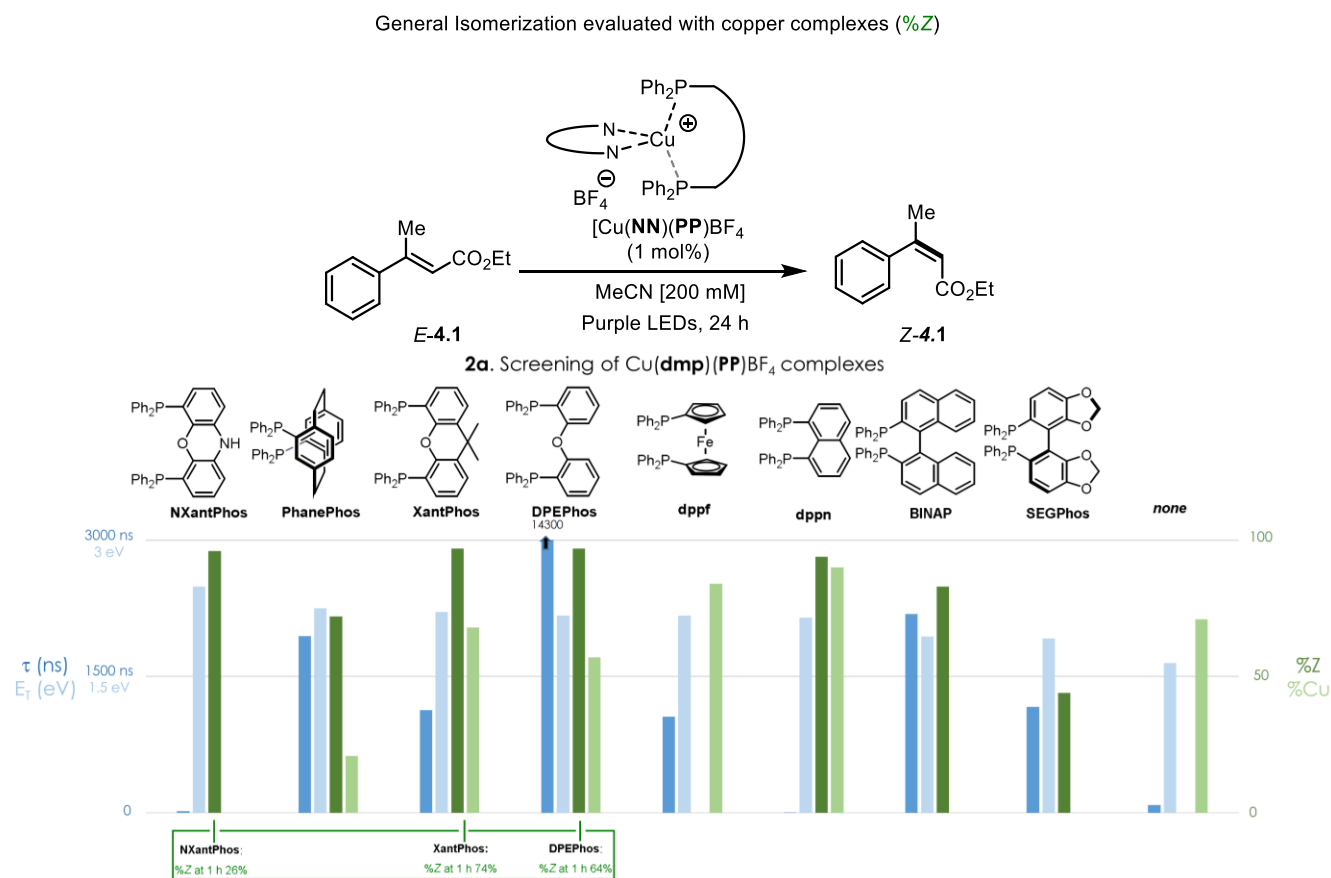


Figure 4.1 Photocatalysis using Cu(NN)(PP)X complexes and possible application to $E \leftrightarrow Z$ isomerization.

The value of isomerization can be illustrated by tandem processes utilizing the Z-isomer, which consist of isomerization followed by C-C cross-coupling⁴⁶⁻⁴⁷ C-O cross-coupling,⁴⁸ selective reduction,⁴⁹⁻⁵⁰ condensation/cyclization,⁵¹ and photochemical [2+2] cycloaddition.⁵² Herein, we report on the design of a heteroleptic copper-based photosensitizer for $E \leftrightarrow Z$ isomerization via energy transfer. In addition, the first isomerization of 1,3-enynes and macrocyclic alkenes, a new tandem ATRA/photoisomerization process employing arylsulfonyl chlorides, and a rare example of photoisomerization with halide-substituted olefins are reported.

4.3 Results and discussions

Optimization of Catalyst Structure. As previous work has shown that the diimine **dmp** affords complexes with higher excited state lifetimes¹⁸ which would have the potential as energy transfer catalysts,^{42-43, 45, 53-55} initial investigations involved screening Cu-based complexes bearing **dmp** and 8 other bisphosphines. Efficiency was judged against four criteria (**Figure 4.2a**).



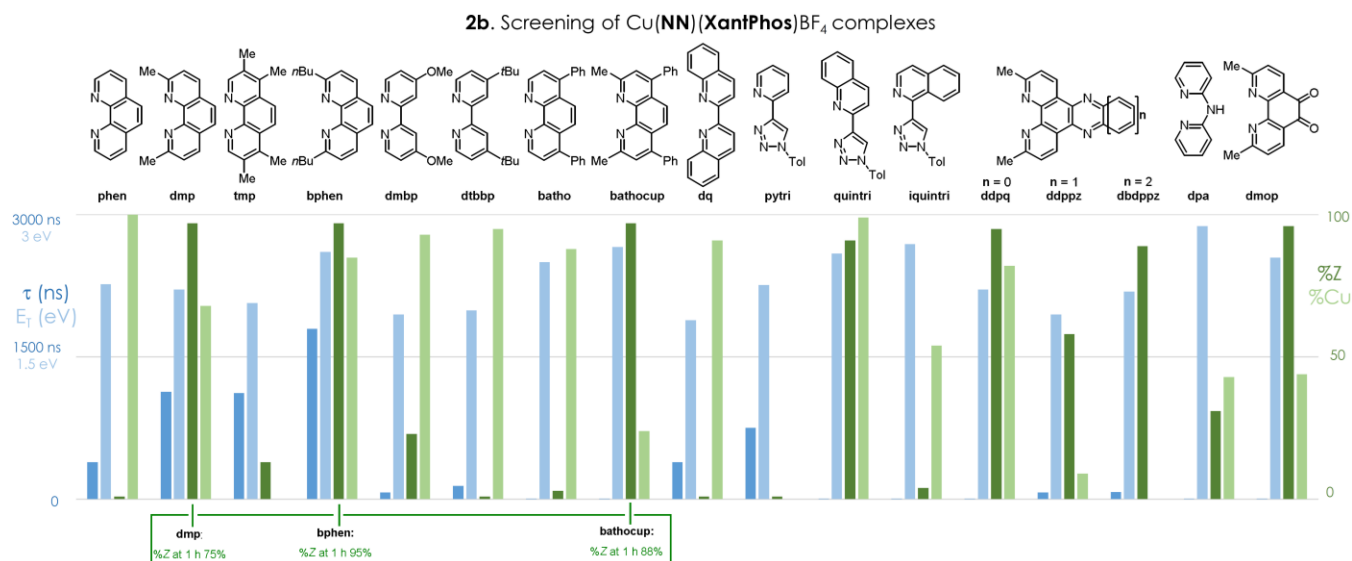


Figure 4.2 Evaluation of Cu-Based Sensitizers in a Model $E \leftrightarrow Z$ Isomerization Process^a. ^aTabular data found in Supporting Information. For details on obtaining τ and E_T , please see the Supporting Information. The %Z is derived from the $Z:E$ ratios determined by crude ¹H NMR for the photochemical $E \leftrightarrow Z$ isomerization of alkenyl ester **E-4.1** (MeCN, Purple LEDs, 400 nm, shown as dark green bars). Note that the $E:Z$ ratio remains identical following chromatography. The %Cu represent complex photostability: solutions of the complexes were irradiated for 24 h and the %catalyst remaining was calculated by ¹H NMR.

The first and second criteria included photophysical properties such as triplet state energy (E_T , shown as light blue bars) and excited state lifetime (shown as dark blue bars). The third criterion was the efficiency to promote the photochemical $E \leftrightarrow Z$ isomerization of alkenyl ester **E-4.1** (MeCN, Purple LEDs, 400 nm, shown as dark green bars). Lastly, an attempt was made to evaluate the photostability of the complexes. Solutions of the complexes were irradiated for 24 h and the %catalyst remaining was calculated by ¹H NMR⁵⁶⁻⁵⁷⁻⁵⁸ (indicated as %Cu in light green bars, **Figure 4.2.a**). Successful $E \leftrightarrow Z$ photoisomerization relies on selectively activating one geometric isomer over the other. Three complexes were shown to promote >96% $E \rightarrow Z$ isomerization.⁵⁹ Although the Cu(**dmp**)(**BINAP**)BF₄ complex possessed promising photophysical properties and promoted isomerization (83%Z), stability studies showed that the complex had completely degraded in solution during the time of irradiation (indicated as %Cu in light green bars in **Figure 4.2.a**) and other complexes displaying greater stability were prioritized. Neither the corresponding homoleptic complex (Cu(**dmp**)₂BF₄) or the Cu(**dmp**)(**dppf**)BF₄ complex resulted in any conversion of E - to Z -**4.1** (**Figure 4.2**). Note that complexes containing the **dppf** ligand have

been reported to possess competing photoinduced energy transfer from the Cu(I) complex to the ferrocene moiety with little observable emission at room temperature.⁵⁸ When evaluating the four criteria (E_T , τ , %Z and %Cu), both the Cu(**dmp**)(**XantPhos**)BF₄ and Cu(**dmp**)(**DPEPhos**)BF₄ complexes were identified as most promising since it ranked consistently high in τ , %Z and %Cu. To distinguish between the complexes, the isomerization processes were evaluated at only 1 h of reaction time (see insert in **Figure 4.2.a**). The %Z for copper complex based on **DPEPhos** dropped to 64%, while the %Z for the **XantPhos** complex decreased to only 74%. As such, a slight edge was given to the Cu-based complex bearing **XantPhos**, and further optimization was conducted to investigate the effect of the diimine. Given the promising results with Cu-based complexes bearing **XantPhos** as a bisphosphine, another screening was performed using 17 different diimines with **XantPhos** as the bisphosphine (**Figure 4.2b**). Diimines included phenanthroline- and bipyridine-based scaffolds, and possessed different degrees of substitution that influenced both steric and electronic properties. Once again, all complexes were evaluated against four criteria (E_T , τ , %Z and %Cu). A total of 6 sensitizers demonstrated >90 % *E*→*Z* isomerization (**Figure 4.2b**, dark green bars). The three complexes showing the largest %Z were based on the ligands **dmp**, **bphen** and **bathocup**. The **bathocup**-containing complex had a low stability (24 %Cu), so all three complexes were evaluated in the same model photoisomerization but for only 1 h of irradiation time. Indeed, the Cu(**bphen**)(**XantPhos**)BF₄ complex was the only candidate to maintain the high %Z. As such, when considering *both* high %Z and high %Cu, two complexes displayed excellent photoisomerization and stability: Cu(**bphen**)(**XantPhos**)BF₄ and Cu(**quintri**)(**XantPhos**)BF₄. The former was selected for further study, given the **bphen** diimine afforded a longer τ (1798 ns) than the **quintri** complex. The analogous triazole-based ligand complexes underwent significant degradation in solution during irradiation (Cu(**pytri**)(**XantPhos**)BF₄: 0%Cu; Cu(**iquintri**)(**XantPhos**)BF₄: 54%Cu). However, further study is warranted to understand the structure/activity relationships in complexes bearing the triazole-based ligands.

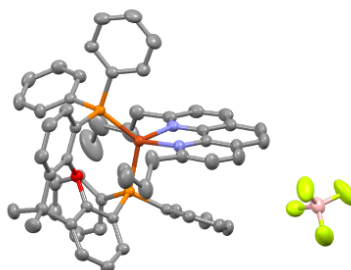


Figure 4.3 X-ray crystallographic analysis of Cu(bphen)(XantPhos)BF₄. Atoms represented as ellipsoids. Hydrogens omitted for clarity. Carbon = grey. Phosphorus = orange. Oxygen = red. Copper = bronze. Nitrogen = purple. Boron = pink. Fluorine = bright green.

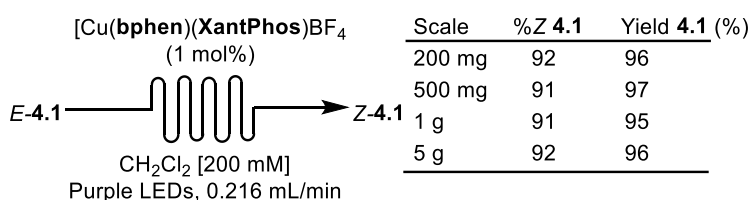


Figure 4.4 Scale-up of the photochemical E \leftrightarrow Z isomerization using continuous flow methods.

The complex Cu(bphen)(XantPhos)BF₄ was crystallized via vapor diffusion of Et₂O into a CH₂Cl₂ solution. X-ray crystallographic analysis (Figure 4.3) confirmed the tetrahedral geometry about the copper center in the ground state. The shielding provided by the *n*-Bu groups (proposed to extend the excited lifetime through restricting relaxation via isomerization to a square planar geometry) is also visible. The photoisomerization was also evaluated for possible scale up. As such, the reaction mixture was injected into a continuous flow apparatus.⁶⁰ The process was performed at scales of 200 mg, 500 mg, 1 g and 5 g and all provided the desired product *Z*-4.1 in reproducible %Z (91-92) and yield (95-97 %) (Figure 4.4). Further investigation of the Cu(bphen)(XantPhos)BF₄ sensitizer showed that the efficiency of the isomerization of *E*-4.1

decreased when carried out in the presence of ambient air (97→70 %Z), or TEMPO (1 equiv, 97→44 %Z), suggesting a mechanism for photoisomerization involving energy transfer⁶¹ and formation of a diradical intermediate.¹⁹ When the isomerization of *E*-**4.1** was performed with Cu(**bphen**)(**XantPhos**)BF₄ under blue LEDs, the %Z decreased to 91%, however performing the reaction with 5 mol % of complex restored the %Z to 97 %. The isomerization process was equally efficient in dichloromethane with 1 h reaction time (97 %Z-**4.1**). Note that no significant isomerization of *E*-**4.1** (<3 %) was observed when irradiation occurred with the ligands **bphen** or **XantPhos** alone, neither when in the presence of the homoleptic complex Cu(**bphen**)₂BF₄.⁶²

Table 4.1 Evaluation of Cu(I)-Based Photocatalysts in E↔Z Isomerization Processes^a

 4.2	 4.3	 4.4	 4.5	 4.6
Cu 89 % (1 h) 40:60 Z:E	Cu 70 % (1 h) 75:25 Z:E	Cu 94 % (in CH ₂ Cl ₂) 73:27 Z:E	Cu 79 % ^[b]	Cu 78 % 74:26 Z:E
 4.7	 4.1	 4.8	 4.9	 4.10
Cu 86 % ^[c] 77:23 Z:E	Cu 98 % (1 h) 95:5 Z:E	Cu 99 % 94:6 Z:E	Cu 98 %, 95:5 Z:E	Cu 80 % 99:1 Z:E
 4.11	 4.12	 4.13	 4.14	 4.15
Cu 85 % 56:44 Z:E	Cu 96 % 98:2 Z:E	Cu 97 % 97:3 Z:E	Cu 90 % 94:6 Z:E	Cu (CH ₂ Cl ₂) 90% 94:06 Z:E
 4.16	 4.17	 4.18	 4.19	 4.20
Cu (CH ₂ Cl ₂) 92 % 97:3 Z:E	Cu (5 mol%) 93 % 92:8 Z:E	Cu (5 mol%) 94 % 90:10 Z:E	Cu (5 mol%) 91 % ^[d] 90:10 Z:E	Cu 94 % 92:8 Z:E
 4.21	 4.22	 4.23	 4.24	 4.25
Cu 89 % 84:16 Z:E	Cu 93 % 9:91 Z:E	Cu 97 % 96:4 Z:E	Cu 92 % 47:53 Z:E	Cu 97 % 50:50 Z:E

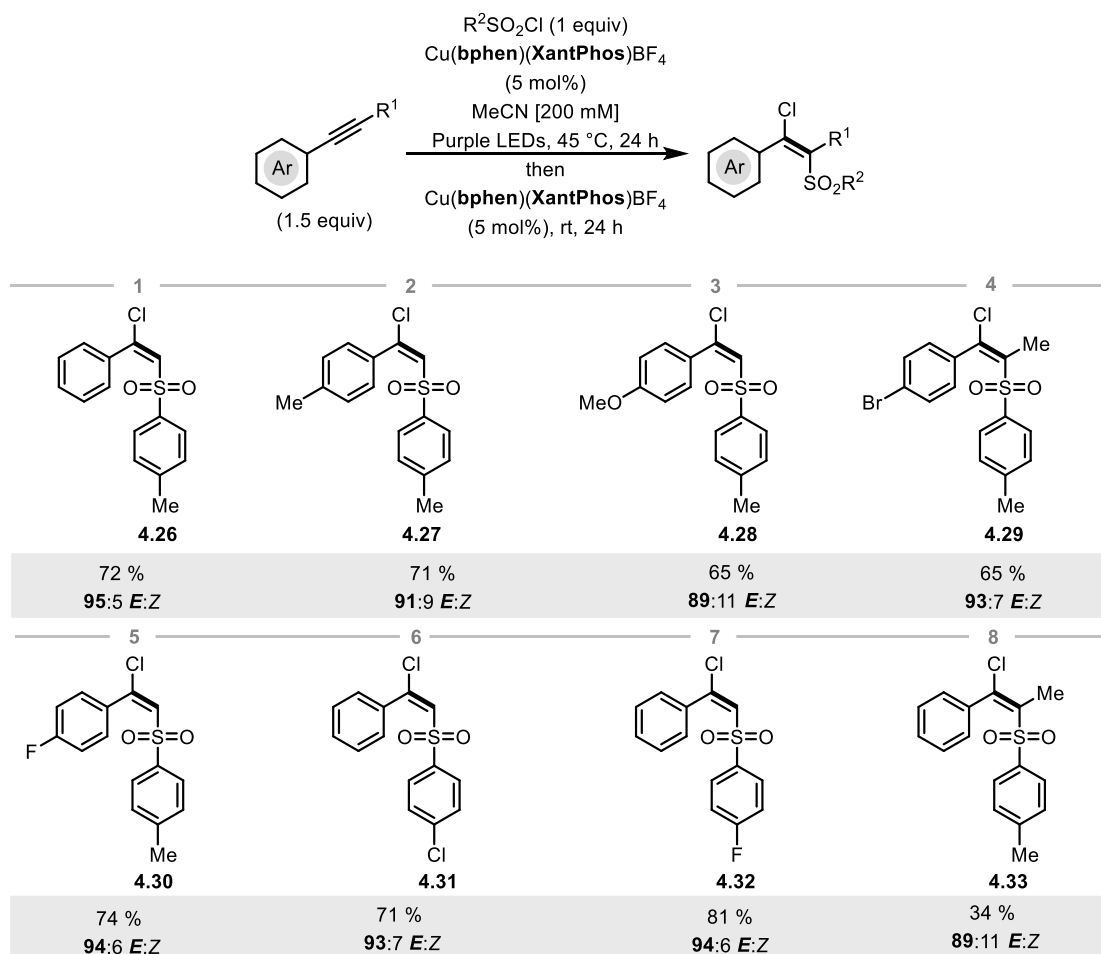
^a Yields following chromatography (single experiment). All isomerizations used pure *E*-isomers as starting materials unless otherwise noted. *Z:E* ratios determined by crude ¹H NMR. ^b Starting from ethyl (*E*)-3-(2-hydroxyphenyl)acrylate. ^c Starting material was a 80:20 *E:Z* mixture. ^d Yield determined by ¹H NMR.

Evaluation of Scope. Following identification of the heteroleptic Cu(**bphen**)(**XantPhos**)BF₄ complex, it was evaluated in the isomerization of various olefins (**Table 4.1**). In addition to the optimized conditions (MeCN, Purple LEDs), substrates with problematic solubility could undergo photoisomerization in CH₂Cl₂ (Blue LEDs). First, the photoisomerization of various di-substituted olefins such as cinnamates **4.3** and **4.5**,⁶³ allylic alcohol **4.4** and the stilbenes⁶⁴ **4.6** and **4.7**, were studied and afforded good selectivities (73-77%Z, entries 1→5). Next tri-substituted cinnamates and allylic alcohols were investigated (entries 6→22). When the ester **4.1** was irradiated for only 1 h, a 95:5 Z:E ratio was obtained, while 24 h irradiation was reported for riboflavin to achieve the same selectivities.⁴¹ Various other cinnamates possessing heterocycles (**4.12**), electron-withdrawing groups (**4.13**) or olefin substituents (**4.14**) all generally provided high yields (>90%) and selectivities (>90%Z). Tri-substituted olefins appended to bicyclic systems were also isomerized with high selectivities. The cycloheptyl-derivative **4.9** provided the Z-isomer (95:5 Z:E) in 98 % yield following irradiation in the presence of Cu(**bphen**)(**XantPhos**)BF₄. In addition, the indalone-substituted olefin **4.10** underwent smooth isomerization (99% yield, 99:1 Z:E). In contrast, the indenyl-olefin **4.11** was only isolated in 56%Z, demonstrating the importance of the additional endocyclic carbonyl in **4.10** for achieving high selectivity in the isomerization. The ethyl- and methyl substituted allylic alcohols **4.15**⁴⁸ and **4.16**⁶⁵⁻⁶⁶ could be photoisomerized using the copper-based photocatalyst at 400 nm to afford the Z-isomer in 94 and 97 %Z respectively. Phosphonate ester **4.17** was isomerized to a 92:8 Z:E ratio using the optimized copper catalyst under blue LEDs (previously reported under UV-light conditions).⁴⁸ In addition, recent reports of using other copper-based systems (Cu(OAc)₂/**BINAP**, Blue LEDs) for photoisomerization reported only a 14:86 Z:E ratio.¹⁷ In addition, a *p*-MeO-substituted phosphonate ester **4.18** whose isomerization had previously been challenging under photocatalysis with anthracene at 365 nm (58:42 Z:E),⁴⁹ underwent isomerization in 94 % and 90:10 Z:E (at 450 nm). The boronate ester **4.20** and the tri-substituted olefinic nitrile **4.21** underwent photoisomerization efficiently. Previously reported isomerization of the diester **4.22** used riboflavin (5 mol %) as a photocatalyst,⁶⁷ and comparable results could be obtained with the optimized copper complex (1 mol %, 9:91 Z:E, 93 % yield **4.22**). A macrocyclic tri-substituted olefin **4.23** was also treated to the optimized conditions and could be converted to the Z-isomer in 97% yield (96:4 Z:E). The photoisomerization

of 1,3-enynes was also explored with the Cu(**bphen**)(**XantPhos**)BF₄ complex. The TMS-substituted enyne **4.24** afforded a good yield (92 %) but only a 47:53 *Z:E* ratio of stereoisomers. A tri-substituted enyne **4.25** was not more successful, and isomerization resulted in only 50% conversion to the corresponding *Z*-isomer under the optimized conditions.

While photoisomerization (PI) has been used in tandem with other thermally promoted transformations, sequential photocatalytic processes are rare.^{53, 68} As such, the Cu(**bphen**)(**XantPhos**)BF₄ complex was investigated for a tandem atom-transfer radical addition (ATRA)¹¹⁻¹⁴ of TsCl⁶⁹ across alkynes and subsequent photoisomerization. Photoisomerization of tri-substituted olefins bearing halogen substituents is rare,⁷⁰ but should prove useful given the precedent for cross-coupling. Gratifyingly, ATRA of TsCl across phenylacetylene under purple LED irradiation afforded a 55:45 *E:Z* ratio of **4.26** and upon addition of an additional portion of complex,⁷¹ subsequent isomerization afforded a 95:5 *E:Z* ratio of **4.26** in an overall yield of 83% for the two steps (Table 2). The tandem ATRA/PI process was applicable to other alkynes such as 4-Me, 4-MeO, 4-Br and 4-F-phenylacetylenes, which afforded the corresponding chloroalkenes in good yields and selectivities (**4.27**→**4.30**, 65-74 %, >90% *E:Z*). Different sulfonylchlorides could also be used, as the 4-chlorophenylsulfonylchloride and 4-fluorophenylsulfonylchloride provided the corresponding products **4.31** and **4.32** following ATRA/PI with phenylacetylene (71-81 %, 93-94 %*E*). Finally, although tetra-substituted alkenes are rare products for both ATRA and PI processes, submitting phenylpropyne to the optimized conditions afforded olefin **4.33** in good *E*-selectivity (34%, 89:11 *E:Z*).

Table 4.2 Sequential ATRA/photoisomerization processes employing the Cu(bphen)(XantPhos)BF₄ catalyst.^a



^a Yields represent the pure *E*-isomers following chromatography. Control reactions investigated during the synthesis of **4.26**: with no catalyst: 0 % **4.26** (ii) in the dark with catalyst: 19 % **4.26**, 58:42 *E:Z*

The chloroalkene **4.26** could be engaged in sequential functionalization reactions (**Scheme 4.1**). When subjected to standard palladium catalysis with phenylacetylene, the enyne **4.34** was isolated in 86% yield. Subsequent stereoinvertive cross-coupling via Ni catalysis afforded the trisubstituted alkene **4.35** in 71 % yield (unoptimized).

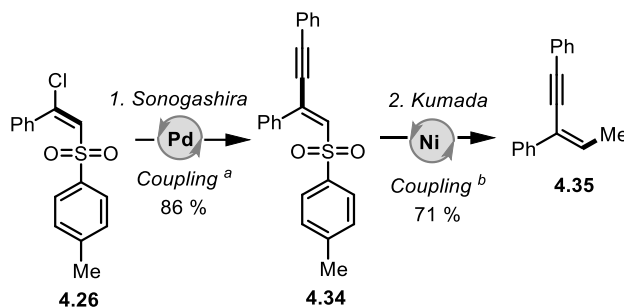


Schéma 4.1 Diversification of haloalkenes. a PhCCH (3 equiv), Pd(PPh₃)₂Cl₂ (10 mol %), CuI (15 mol%), DIPEA (4 equiv), CH₂Cl₂, 21 °C, 18 h. b MeMgBr (3 equiv), Ni(acac)₂ (10 mol%), THF, -78 °C to rt, 2 h.

4.4 Conclusions

In summary, photoisomerization of olefins has been demonstrated with heteroleptic copper complexes. Using Cu(**bphen**)(**XantPhos**)BF₄, 25 di- and tri-substituted alkenes underwent photoisomerization, including the first attempts at photoisomerization of macrocyclic alkenes and challenging 1,3-enynes. Cu(**NN**)(**PP**)X-type complexes bearing different bisphosphines and diimines afford sensitizers with a range of triplet energies and excited state lifetimes, that can theoretically allow optimization of a catalyst structure to selectively excite one geometric isomer of a compound over another, as well as be applicable to the design of other energy transfer processes. The optimization of the Cu(**bphen**)(**XantPhos**)BF₄ complex also highlighted the importance of photostability in photocatalysis using the complexes. Even if structure/activity relationships for photostability are still not clear, the above investigations highlight the need for further in-depth studies. The Cu(**bphen**)(**XantPhos**)BF₄ complex could also be employed in a new tandem ATRA/photoisomerization process employing arylsulfonyl chlorides. The above exemplifies the potential utility of the complexes for new energy transfer processes in synthetic photochemistry.⁷²

4.5 References

1. Lévêque, C.; Levernier, E.; Corcé, V.; Fensterbank, L.; Malacria, M.; Ollivier, C., Photoredox Catalysis, an Opportunity for Sustainable Radical Chemistry. In *Advanced Green Chemistry: Part 2: From Catalysis to Chemistry Frontiers*, World Scientific: **2020**; pp 49-121.
2. Traub, L.; Reiser, O., *Phys. Sci. Rev.* **2019**, *4*, 172.
3. Ehrnsberger, P.; Reiser, O.; König, B., *Science of Synthesis: Photocatalysis in Organic Synthesis*. **2019**; p 271.
4. Hossain, A.; Bhattacharyya, A.; Reiser, O., *Science* **2019**, *364* (6439).
5. Hockin, B.; Li, C.; Robertson, N.; Zysman-Colman, E., *Catal. Sci. Technol.* **2019**, *9*, 889.
6. Li, C.; Dickson, R.; Rockstroh, N.; Rabeah, J.; Cordes, D. B.; Slawin, A. M. Z.; Hünemörder, P.; Spannenberg, A.; Bühl, M.; Mejía, E.; Zysman-Colman, E.; Kamer, P. C. J., *Catal. Sci. Technol.* **2020**, *10* (22), 7745-7756.
7. Gracia, L. L.; Luci, L.; Bruschi, C.; Sambri, L.; Weis, P.; Fuhr, O.; Bizzarri, C., *Chem. - Eur. J.* **2020**, *26*, 9929.
8. Hunter, C. J.; Boyd, M. J.; May, G. D.; Fimognari, R., *J. Org. Chem.* **2020**, *85*, 8732.
9. Matsuo, K.; Yamaguchi, E.; Itoh, A., *Asian J. Org. Chem.* **2018**, *7*, 2435.
10. Mejía, E.; Luo, S. P.; Karnahl, M.; Friedrich, A.; Tschierlei, S.; Surkus, A. E.; Junge, H.; Gladiali, S.; Lochbrunner, S.; Beller, M., *Chem. - Eur. J.* **2013**, *19*, 15972.
11. Engl, S.; Reiser, O., *ACS Catal.* **2020**, *10*, 9899.
12. Hossain, A.; Engl, S.; Lutsker, E.; Reiser, O., *ACS Catal.* **2019**, *9* (2), 1103-1109.
13. Hossain, A.; Vidyasagar, A.; Eichinger, C.; Lankes, C.; Phan, J.; Rehbein, J.; Reiser, O., *Angew. Chem., Int. Ed.* **2018**, *57*, 8288.
14. Alkan-Zambada, M.; Hu, X., *Organometallics* **2018**, *37*, 3928.
15. Minozzi, C.; Caron, A.; Grenier-Petel, J. C.; Santandrea, J.; Collins, S. K., *Angew. Chem., Int. Ed.* **2018**, *57* (19), 5477-5481.
16. Caron, A.; Morin, E.; Collins, S. K., *ACS Catal.* **2019**, *9* (10), 9458-9464.
17. Brégent, T.; Bouillon, J.-P.; Poisson, T., *Org. Lett.* **2020**, *22* (19), 7688-7693.
18. Cuttell, D. G.; Kuang, S.-M.; Fanwick, P. E.; McMillin, D. R.; Walton, R. A., *J. Am. Chem. Soc.* **2002**, *124* (1), 6-7.

19. Zhou, Q.-Q.; Zou, Y.-Q.; Lu, L.-Q.; Xiao, W.-J., *Angew. Chem., Int. Ed.* **2019**, *58* (6), 1586-1604.
20. Fisch, F.; Fleites, C. M.; Delenne, M.; Baudendistel, N.; Hauer, B.; Turkenburg, J. P.; Hart, S.; Bruce, N. C.; Grogan, G., *J. Am. Chem. Soc.* **2010**, *132* (33), 11455-11457.
21. Alder, A.; Jamil, M.; Marzorati, M.; Bruno, M.; Vermathen, M.; Bigler, P.; Ghisla, S.; Bouwmeester, H.; Beyer, P.; Al-Babili, S., *Science* **2012**, *335* (6074), 1348-1351.
22. Wald, G., *Nature* **1934**, *134*, 65.
23. Wald, G., *Science* **1968**, *162* (3850), 230-239.
24. Takeda, T., *Modern Carbonyl Olefination: Methods and Applications.* **2004**.
25. Maryanoff, B. E.; Reitz, A. B., *Chem. Rev.* **1989**, *89*, 863.
26. Byrne, P. A.; Gilheany, D. G., *Chem. Soc. Rev.* **2013**, *42*, 6670.
27. Still, W. C.; Gennari, C., *Tetrahedron Lett.* **1983**, *24*, 4405.
28. Montgomery, T. P.; Johns, A. M.; Grubbs, R. H., *Catalysts* **2017**, *7*, 87.
29. Liu, Z.; Xu, C.; del Pozo, J.; Torker, S.; Hoveyda, A. H., *J. Am. Chem. Soc.* **2019**, *141*, 7137.
30. Mu, Y.; Nguyen, T.; Koh, M. J.; Schrock, R. R.; Hoveyda, A. H., *Nat. Chem.* **2019**, *11*, 478.
31. Nguyen, T. T.; Koh, M. J.; Mann, T. J.; Schrock, R. R.; Hoveyda, A. H., *Nature* **2017**, *552*, 347.
32. Hammond, G. S.; Saltiel, J.; Lamola, A. A.; Turro, N. J.; Bradshaw, J. S.; Cowan, D. O.; Counsell, R. C.; Vogt, V.; Dalton, C., *J. Am. Chem. Soc.* **1964**, *86* (16), 3197-3217.
33. Hammond, G. S.; Turro, N. J.; Leermakers, P. A., *J. Phys. Chem. A* **1962**, *66*, 1144.
34. Saltiel, J., *J. Am. Chem. Soc.* **1967**, *89*, 1036.
35. Molloy, J. J.; Morack, T.; Gilmour, R., *Angew. Chem., Int. Ed.* **2019**, *58*, 13654.
36. Gilmour, R.; Metternich, J., *Synlett* **2016**, *27* (18), 2541-2552.
37. Day, J. I.; Singh, K.; Trinh, W.; Weaver, J. D., *J. Am. Chem. Soc.* **2018**, *140*, 9934.
38. Singh, K.; Trinh, W.; Weaver, J. D., *Org. Biomol. Chem.* **2019**, *17* (7), 1854-1861.
39. Singh, K.; Fennell, C. J.; Coutsiyas, E. A.; Latifi, R.; Hartson, S.; Weaver, J. D., *Chem* **2018**, *4*, 124.
40. Singh, K.; Staig, S. J.; Weaver, J. D., *J. Am. Chem. Soc.* **2014**, *136* (14), 5275-5278.
41. Metternich, J. B.; Gilmour, R., *J. Am. Chem. Soc.* **2016**, *138* (3), 1040-1045.
42. Metternich, J. B.; Gilmour, R., *J. Am. Chem. Soc.* **2015**, *137* (35), 11254-11257.

43. Metternich, J. B.; Sagebiel, S.; Lückener, A.; Lamping, S.; Ravoo, B. J.; Gilmour, R., *Chem. - Eur. J.* **2018**, *24* (17), 4228-4233.
44. Metternich, J. B.; Artiukhin, D. G.; Holland, M. C.; Von Bremen-Kühne, M.; Neugebauer, J.; Gilmour, R., *J. Org. Chem.* **2017**, *82* (19), 9955-9977.
45. Livingstone, K.; Tenberge, M.; Pape, F.; Daniliuc, C. G.; Jamieson, C.; Gilmour, R., *Org. Lett.* **2019**.
46. Faßbender, S. I.; Molloy, J. J.; Mack-Lichtenfeld, C.; Gilmour, R., *Angew. Chem., Int. Ed.* **2019**, *58*, 18619.
47. Molloy, J. J.; Metternich, J. B.; Daniliuc, C. G.; Watson, A. J. B.; Gilmour, R., *Angew. Chem., Int. Ed.* **2018**, *57*, 3168.
48. Faßbender, S. I.; Metternich, J. B.; Gilmour, R., *Org. Lett.* **2018**, *20* (3), 724-727.
49. Onneken, C.; Bussmann, K.; Gilmour, R., *Angew. Chem., Int. Ed.* **2020**, *59* (1), 330-334.
50. Hostmann, T.; Molloy, J. J.; Bussmann, K.; Gilmour, R., *Org. Lett.* **2019**, *21*, 10164.
51. Walker, J. C. L.; Werrel, S.; Donohoe, T. J., *Chem. - Eur. J.* **2019**, *25* (57), 13114-13118.
52. Neveselý, T.; Daniliuc, C. G.; Gilmour, R., *Org. Lett.* **2019**, *21*, 9724.
53. Metternich, J. B.; Gilmour, R., *J. Am. Chem. Soc.* **2016**, *138*, 1040.
54. Metternich, J. B.; Artiukhin, D. G.; Holland, M. C.; von Bremen-Kühne, M.; Neugebauer, J.; Gilmour, R., *J. Org. Chem.* **2017**, *82*, 9955.
55. Hernandez-Perez, A. C.; Collins, S. K., *Acc. Chem. Res.* **2016**, *49* (8), 1557-1565.
56. Heteroleptic copper complexes are known to engage in an equilibrium to form the corresponding homoleptic complex Cu(NN)2BF4
57. Leoni, E.; Mohanraj, J.; Holler, M.; Mohankumar, M.; Nierengarten, I.; Monti, F.; Sournia-Saquet, A.; Delavaux-Nicot, B.; Nierengarten, J.-F. i.; Armaroli, N., *Inorg. Chem.* **2018**, *57* (24), 15537-15549.
58. Armaroli, N.; Accorsi, G.; Bergamini, G.; Ceroni, P.; Holler, M.; Moudam, O.; Duhayon, C.; Delavaux-Nicot, B.; Nierengarten, J.-F., *Inorganica Chimica Acta* **2007**, *360* (3), 1032-1042.
59. Additional graphical correlations between ET and %Z can be found in the Supporting Information that suggest an optimal range of triplet energies for the isomerization of E-1. The values are very similar to an analogous cinnamate ester previously studied (reference (42)).

60. Parisien-Collette, S.; Cruché, C.; Abel-Snape, X.; Collins, S. K., *Green Chem.* **2017**, *19*, 4798.
61. In previous work (ref (17)), coordination of copper to substrates was proposed in the mechanism of energy transfer. Note that in the previous work, the substrates are designed to promote bidentate coordination to the copper atom. Most substrates in Table 1 do not possess the same ability. For the heteroleptic complexes to engage in coordination, ligand dissociation would likely be necessary. If one assumes that the %Cu value is indicative of the propensity for ligand dissociation, then complexes that readily undergo ligand dissociation do not tend to show better %Z, which would have been expected if coordination was an active mechanism.
62. Pallenberg, A. J.; Koenig, K. S.; Barnhart, D. M., *Inorg. Chem.* **1995**, *34*, 2833.
63. Zhan, K.; Li, Y., *Catalysts* **2017**, *7*, 337.
64. Saltiel, J.; Klima, R. F., *Photochem. Photobiol.* **2006**, *82*, 38.
65. Note that the Cu(dmp)(dppn)BF₄ catalyst that was also considered promising in the first screening only provided a 72:28 Z/E ratio of alcohol 16.
66. Li, H.; Chen, H.; Zhou, Y.; Huang, J.; Yi, J.; Zhao, H.; Wang, W.; Jing, L., *Chem. - Asian J.* **2020**, *15*, 555.
67. Litman, Z. C.; Wang, Y.; Zhao, H.; Hartwig, J. F., *Nature* **2018**, *560* (7718), 355-359.
68. Abramov, A.; Maiti, B.; Keridou, I.; Puiggali, J.; Reiser, O.; Díaz, D. D., *Macromol. Rapid Commun.* **2021**, *78*, 2100213.
69. Alkan-Zambada, M.; Hu, X., *J. Org. Chem.* **2019**, *84*, 4525.
70. Zhang, H.; Xu, Q.; Yu, L.; Yu, S., *Eur. J. Org. Chem.* **2020**, *2020*, 1472.
71. The sulfonyl chlorides tend to have traces of HCl which contribute to catalyst degradation. A second portion of catalyst was necessary to maintain the efficiency of the isomerization. It is possible with further optimization, purification of the sulfonyl chlorides or addition of bases, that the catalyst loading could be further reduced.
72. Other tandem processes involving cross couplings could be envisioned given recent advances in photoisomerization: Molloy, J. J.; Schaefer, M.; Wienhold, M.; Morack, T.; Daniliuc, C. G.; Gilmour, R., *Science* **2020**, *369*, 302.

Chapitre 5 Conclusions et perspectives de la photocatalyse avec des complexes de cuivre

Mes travaux sur la photocatalyse avec des complexes de cuivre se sont articulés autour de deux projets principaux. Le premier projet a porté sur la conception et l'étude de complexes de cuivre portant un système π -étendu dans différentes réactions photochimiques et a fait l'objet des chapitres 2 et 3. Le deuxième projet, discuté dans le chapitre 4, porte sur l'étude de complexes de cuivre pour une réaction passant par un transfert d'énergie. Enfin j'ai pu participer à un projet supplémentaire sur la photodégradation de modèles de lignine catalysée par un complexe de cuivre, qui se retrouve dans l'annexe 4.

5.1 Conclusion sur la photocatalyse avec des complexes de cuivre

5.1.1 Conclusion des chapitres 2, 3 et 4

Dans le Chapitre 2, trois ligands analogues du dmp, portant un système π -étendu ont été étudiés: **ddpq**, **ddppz** et **dbdppz (Figure 5.1)**.¹ Ces ligands ont alors été utilisés dans la synthèse de complexes de cuivre(I), formant 3 complexes homoleptiques et 9 complexes hétéroleptiques en combinaison avec 3 diphosphines : DPEPhos, Xantphos et dppf. Les propriétés photophysiques ont été mesurées et ont révélé une augmentation du coefficient d'absorption molaire et un déplacement bathochromique de la longueur d'onde d'absorbance en comparaison avec les complexes analogues portant le ligand dmp. Ils possèdent de façon générale un potentiel de réduction plus faible que ces derniers, dû à la stabilisation du radical diimine à l'état excité par le système π -étendu. Ces complexes ont ensuite été étudiés dans trois réactions passant par des mécanismes différents. Ils se sont révélés efficaces pour la réaction de transfert d'énergie et la réaction passant par un mécanisme de désactivation oxydante, mais très peu pour la réaction passant par un mécanisme de désactivation réductrice. L'extension du système π n'apporte pas d'avantages pour les complexes hétéroleptiques et la nature de la diphosphine ne semble pas

avoir un effet majeur sur ces derniers. Cependant les complexes homoleptiques formés se sont révélés bien plus efficaces que le complexe initial $\text{Cu}(\text{dmp})_2\text{BF}_4$.

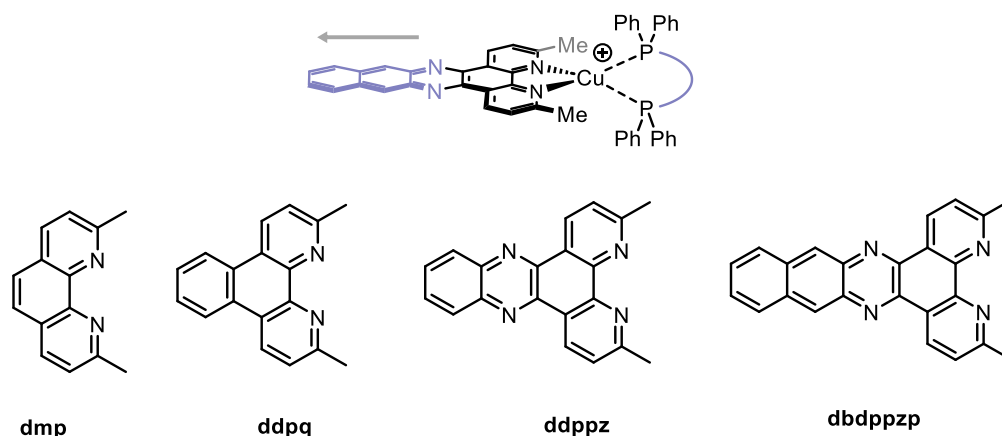


Figure 5.1 Ligands π -étendus utilisés dans le chapitre 2

Le chapitre 3 correspond à la suite du projet précédent. Au cours de ce dernier, la diphosphine BINAP avait été retirée de la liste de diphosphines étudiées, était observé une rapide dissociation des ligands en solution pour former les complexes homoleptiques, probablement à cause de l'encombrement stérique des substituants méthyles sur les diimines et du petit angle de morsure du BINAP. Pour contourner ce problème, des ligands portant un système π -étendu similaire à ceux du chapitre 2 mais sans substituants en position 2 et 9 ont été synthétisés (**Figure 5.2**)². En combinaison avec le BINAP, trois complexes hétéroleptiques ont été synthétisés et testés dans les mêmes réactions que pour le chapitre 2. Avec une tendance similaire, les nouveaux complexes se sont révélés faiblement efficaces dans la réaction d'Appel et complètement inefficaces pour la réaction de PCET. De plus, en raison de la diminution de la stabilisation de l'état excité, les complexes avec les ligands diimines non substitués ne sont pas actifs pour la réaction de transfert d'énergie en présence du BINAP. L'activité est cependant retrouvée lorsque le BINAP est substitué par une diphosphine avec un plus grand angle de morsure (Xantphos), montrant le bénéfice de ce type de phosphine pour les réactions de transfert d'énergie. Enfin, les complexes ont pu être testés sur des cellules cancéreuses, montrant une efficacité encourageante pour le complexe homoleptique $\text{Cu}(\text{dppz})_2\text{BF}_4$.

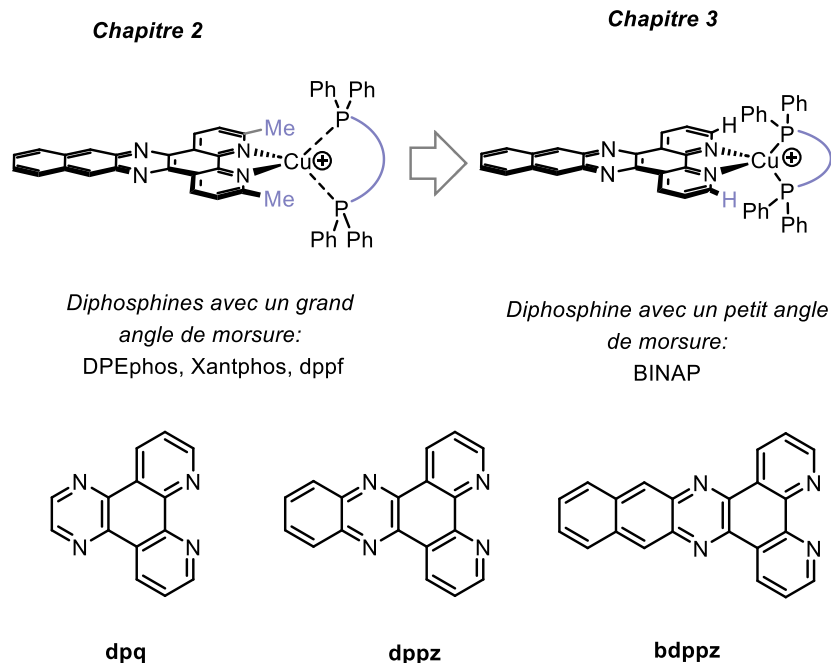


Figure 5.2 Utilisation de ligands diimines non-substitués en position 2 et 9 en combinaison avec une diphosphine possédant un petit angle de morsure

Enfin, le chapitre 4 résume mon étude des complexes de cuivre pour l'isomérisation photochimique d'alcènes, une réaction passant par un transfert d'énergie(**Figure 5.3**)³. Un balayage de 8 diphosphines et 18 diimines a permis de trouver un catalyseur optimal pour la réaction, Cu(bphen)(Xantphos)BF₄. Une étude de ses propriétés photophysiques montrent en effet qu'il possède trois caractéristiques essentielles pour être un bon photosensibilisateur: une haute énergie triplet, un long temps de vie de l'état excité, et une bonne stabilité à l'irradiation. Avec ce complexe, plusieurs alcènes *E* différents di et tri-substitués ont pu être isomérisés vers l'isomère *Z* et un montage en débit continu a permis la mise en échelle de la réaction sur plusieurs grammes. De plus, le catalyseur a été étudié pour un procédé séquentiel ATRA/isomérisation, montrant la versatilité de ce dernier.

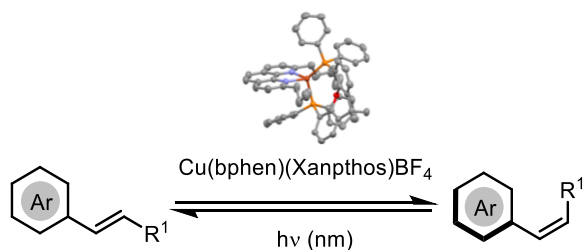


Figure 5.3 Photoisomérisation d'alcènes catalysée par $\text{Cu}(\text{bphen})(\text{Xantphos})\text{BF}_4$

5.1.2 Conclusion générale

Les complexes de cuivre sont une classe de photocatalyseurs extrêmement intéressante à étudier. Leur facilité de synthèse nous a permis de construire rapidement de grandes bibliothèques de complexes, possédant des caractéristiques très différentes. Le but premier de ces librairies est de définir des liens entre la structure de ces complexes, et donc la structure des ligands qui les composent, et leur activité dans des réactions photochimiques. Les travaux de cette thèse ont donc permis de tirer de nombreuses informations sur la relation structure activité des complexes hétéroleptiques de cuivre(I).

Premièrement, les chapitres 2 et 3 nous ont montré qu'augmenter le système π -étendu du ligand diimine vers l'extérieur du complexe n'améliore pas l'efficacité de ce dernier en photocatalyse. Le facteur le plus important semble être la protection du centre métallique contre les désactivateurs externes. La première stratégie est d'utiliser des ligands diphosphine avec un large angle de morsure, comme les ligand Xantphos ou DPEphos. L'intérêt de ces diphosphines est double, puisqu'ils sont suffisamment loin du centre métallique pour permettre la formation de complexes hétéroleptiques stables avec des diimines encombrées. La deuxième stratégie est d'insérer des substituants sur le ligand diimine afin de bloquer l'aplanissement du complexe dans l'état excité, comme le montre l'efficacité du complexe $\text{Cu}(\text{bphen})(\text{Xantphos})\text{BF}_4$ en transfert d'énergie, avec le ligand bphen possédant deux groupements *n*-butyles encombrants.

Il est cependant encore difficile de déterminer à l'avance quel catalyseur sera le plus efficace pour une réaction donnée, un balayage des ligands est donc toujours nécessaire. De plus, les propriétés photophysiques comme les potentiels redox ou l'énergie triplet ne suffisent pas à

expliquer la différence de réactivité de certains complexes. D'autres facteurs devraient être pris en compte, comme la stabilité du complexe durant la réaction ou encore la taille du complexe pour les transferts d'énergie.

5.2 Perspectives

5.2.1 Nouveaux complexes

Au cours de ma thèse, nous nous sommes limités à l'utilisation de complexes hétéroleptiques possédant un ligand diphosphine d'un côté et un ligand diimine de l'autre, principalement dérivé de la phénanthroline. Cependant, d'autres types de ligands pourraient permettre de débloquent des propriétés intéressantes en photocatalyse.

Une première perspective serait de sortir de la structure type des ligands diimines, avec une coordination formant des cycles à 5 chaînons avec le cuivre. En effet, l'efficacité des ligands diphosphines avec un grand angle de morsure montre l'intérêt potentiel d'augmenter la sphère de coordination des ligands (**Figure 5.4**). Un exemple concret est le ligand **dpa** synthétisé au cours du chapitre 4: bien que possédant un faible système conjugué, proche de la bipyridine, ce dernier possède la plus grande énergie triplet de notre bibliothèque et montre une certaine activité pour l'isomérisation d'alcène. Une nouvelle classe de ligands pourrait alors être dérivée de ce dernier.⁴⁻

⁵ Augmentant encore plus l'angle de morsure des ligands diimines, il serait intéressant de synthétiser des ligands possédant une géométrie proche des ligands DPEPhos ou Xantphos comme la diimine **5.1**. En effet, les ligands diphosphines sont difficilement synthétisables et peuvent souffrir d'oxydation durant les réactions. Les remplacer par des ligands diimines offrirait donc plus de flexibilité de conception et pourrait améliorer leur photostabilité.

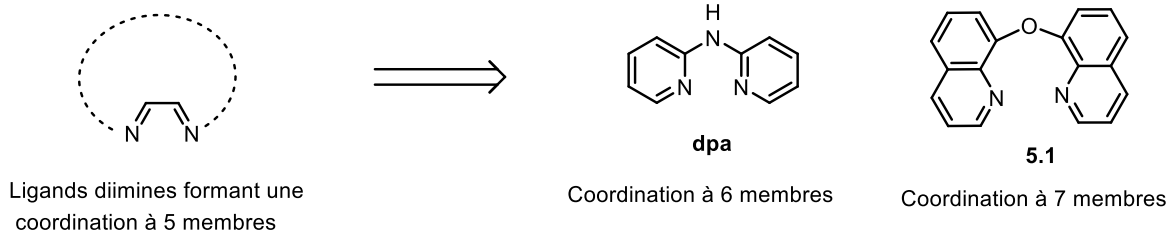


Figure 5.4 Augmentation de la taille de la sphère de coordination des ligands diimines

5.2.2 Perspectives sur la relation structure activité dans les réactions photorédox

L'une des principales difficultés lors de l'étude structure/activité des complexes de cuivre est de connaître le mécanisme d'action par lequel passe le complexe. En effet, si l'on compare les potentiels d'oxydation des complexes par exemple, il faut s'assurer que la réaction passe bien par un mécanisme de désactivation oxydante. En effet si le cycle Cu(I)/Cu(II) est le mécanisme principalement proposé, beaucoup de réactions semblent passer par une désactivation réductrice.⁶⁻⁸ Reprenant les cycles catalytiques de désexcitation du cuivre (**Figure 5.5**), il serait intéressant de trouver 4 réactions dont le substrat se trouverait être à chaque fois une espèce différente du cycle. Les deux premières réactions passeraient par une désexcitation réductrice: le substrat pourrait dans un cas jouer le rôle de l'accepteur, dans l'autre cas, le rôle du donneur. De même, les deux réactions suivantes passeraient par une désexcitation oxydante, le substrat jouant le rôle du donneur ou de l'accepteur. En balayant l'ensemble de notre bibliothèque de complexes pour ces 4 réactions de bases, il serait alors possible d'établir des tendances quant au choix des ligands selon le mécanisme de la réaction en jeu. A l'inverse, pour une réaction passant par un mécanisme inconnu, l'efficacité d'un certain type de ligands pourrait permettre de proposer un cycle de désexcitation.

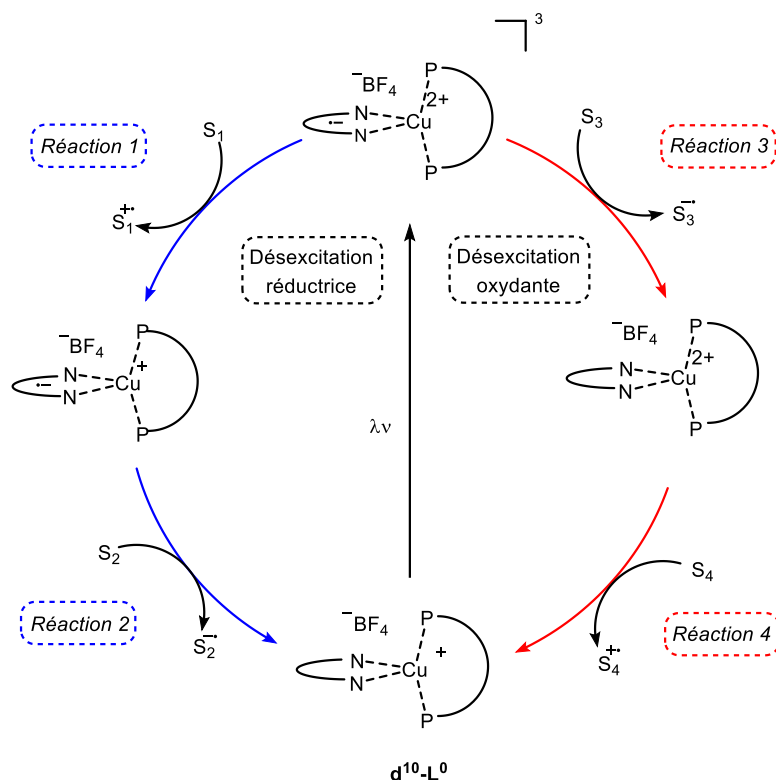


Figure 5.5 Cycles catalytiques du cuivre à explorer

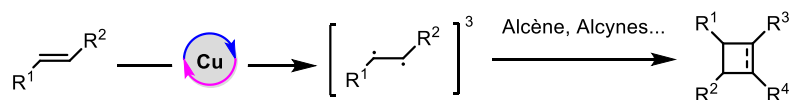
5.2.3 Perspective sur le développement de nouvelles réactions photoredox

Les complexes de cuivre se démarquent des autres photocatalyseurs organiques et organométalliques grâce à leur propension à passer par un mécanisme de sphère intérieure. Ce type de réaction a l'avantage de pouvoir accéder à des réactivités uniques au cuivre. Une perspective serait d'utiliser nos connaissances sur l'équilibre en solution entre les complexes homoleptiques et hétéroleptiques pour développer des réactions avec plusieurs cycles catalytiques.⁹ En particulier, un mécanisme de sphère intérieure pourrait permettre de profiter de l'environnement des ligands; l'utilisation de ligand chiraux pourrait donc développer des versions asymétriques de réactions connues. Un premier exemple de cette stratégie a été montrée par les travaux de Fu qui décrivent l'utilisation d'un ligand diimine chiral pour la formation de composé énanti enrichis.¹⁰

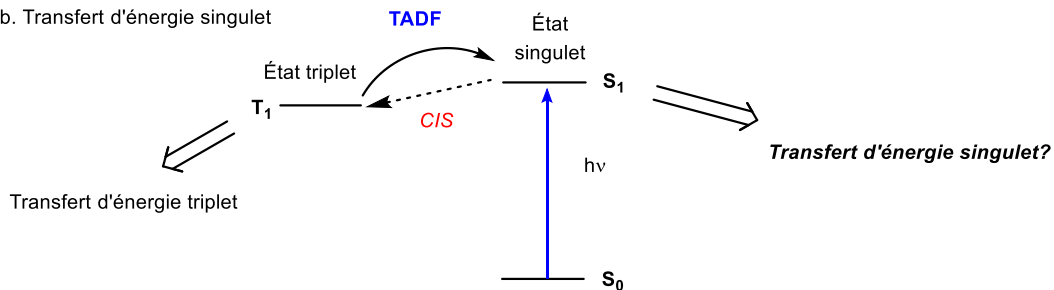
5.2.4 Perspectives sur les réactions de transfert d'énergie

Depuis nos travaux sur l'isomérisation d'alcènes en 2021, seule une publication rapporte l'utilisation de complexes de cuivre pour la dimérisation de chalcones par cycloaddition [2+2]. Cependant, l'étendue de la réaction de [2+2] photocatalysée au cuivre pourrait être grandement élargie au vu des énergies triplet des complexes de cuivre(I) hétéroleptiques pour accéder à différents types de cyclobutanes, cyclobutènes, ect. (**Figure 5.6.a**). Une deuxième perspective serait d'utiliser la propension de certains complexes de cuivre à revenir à leur état singulet par TADF (**Figure 5.6.b**).¹¹⁻¹² Cet état singulet de haute énergie pourrait être exploité pour réaliser des transferts d'énergie, permettant des réactions de réarrangement uniquement possibles dans l'état singulet et jusque-là nécessitant l'utilisation de lumière UV. Une troisième perspective serait d'étudier l'efficacité de ligands pouvant former des liaisons hydrogène avec les substrats, comme le ligands ppyzs développé en 2019 dans notre groupe (**Figure 5.6.c**).¹³ En effet, les travaux de Yoon ont montré l'utilisation d'acides de Lewis pour abaisser l'énergie triplet d'un substrat, stratégie appelée « LUMO-lowering ».¹⁴ L'utilisation de ligands possédant des hydrogènes acides pourrait avoir le même effet en plus de faciliter la rencontre entre le catalyseur et le substrat désiré.

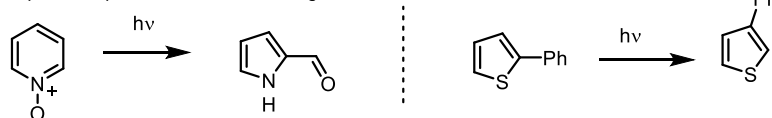
a. Cycloadditions [2+2]



b. Transfert d'énergie singulet



Réarrangements passant par un mécanisme singulet:



c. Utilisation de complexes bifonctionnels

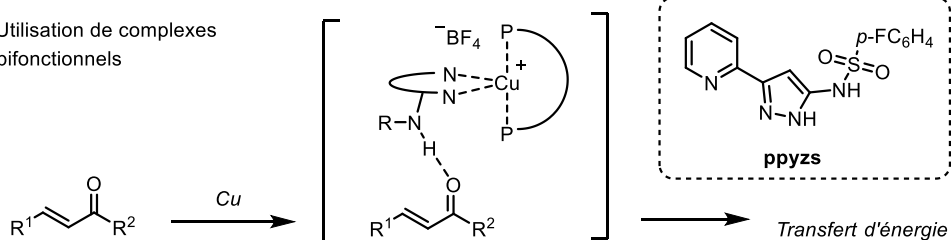


Figure 5.6 Perspectives de projets pour la photocatalyse au cuivre passant par un transfert d'énergie

En conclusion, les complexes de cuivre(I) sont des photocatalyseurs polyvalents qui sont l'objet de nombreuses études; une compréhension poussée de leurs propriétés est aujourd'hui la clé pour une plus grande adoption de ces complexes.

5.3 Références

1. Sosoe, J.; Cruché, C.; Morin, É.; Collins, S. K., *Can. J. Chem.* **2020**, *98* (9), 461-465.
2. Cruché, C.; Gupta, S.; Kodanko, J.; Collins, S. K., *Molecules* **2022**, *27* (12), 3745.
3. Cruché, C.; Neiderer, W.; Collins, S. K., *ACS Catal.* **2021**, *11* (14), 8829-8836.
4. Marion, R.; Sguerra, F.; Di Meo, F.; Sauvageot, E.; Lohier, J.-F.; Daniellou, R.; Renaud, J.-L.; Linares, M.; Hamel, M.; Gaillard, S., *Inorg. Chem.* **2014**, *53* (17), 9181-9191.
5. Henriquez, M. A.; Engl, S.; Jaque, P.; Gonzalez, I. A.; Natali, M.; Reiser, O.; Cabrera, A. R., *Eur. J. Inorg. Chem.* **2021**, *2021* (38), 4020-4029.
6. Michelet, B.; Deldaele, C.; Kajouj, S.; Moucheron, C.; Evano, G., *Org. Lett.* **2017**, *19* (13), 3576-3579.
7. Bertin, C.; Cruché, C.; Chacón-Huete, F.; Forgione, P.; Collins, S. K., *Green Chem.* **2022**, *24* (11), 4414-4419.
8. Caron, A.; Morin, E.; Collins, S. K., *ACS Catal.* **2019**, *9* (10), 9458-9464.
9. Corpas, J.; Gomez-Mendoza, M.; Ramírez-Cárdenas, J.; de la Peña O'Shea, V. A.; Mauleón, P.; Gómez Arrayás, R.; Carretero, J. C., *J. Am. Chem. Soc.* **2022**, *144* (28), 13006-13017.
10. Chen, C.; Peters, J. C.; Fu, G. C., *Nature* **2021**, *596* (7871), 250-256.
11. Czerwieniec, R.; Leitl, M. J.; Homeier, H. H. H.; Yersin, H., *Coord. Chem. Rev.* **2016**, *325*, 2-28.
12. Shi, Y.-Z.; Wu, H.; Wang, K.; Yu, J.; Ou, X.-M.; Zhang, X.-H., *Chem. Sci.* **2022**, *13* (13), 3625-3651.
13. Caron, A.; Morin, É.; Collins, S. K., *ACS Catal.* **2019**, *9*, 9458.
14. Daub, M. E.; Jung, H.; Lee, B. J.; Won, J.; Baik, M.-H.; Yoon, T. P., *J. Am. Chem. Soc.* **2019**, *141* (24), 9543-9547.

Chapitre 6 Introduction de la stratégie de cycloaddition alcyne-azoture promues par la tension

6.1 Généralités

6.1.1 La chimie « click »

Le principe de chimie « click », faisant l'analogie avec le son que produit une attache de sangle rapide, est introduit en 2001 par Sharpless¹. Il met alors en lumière le besoin des scientifiques de tous les domaines, d'assembler des molécules efficacement. En effet de nouvelles propriétés moléculaires peuvent être créées à partir de molécules simples. L'utilisation de réactions rapides et efficaces permettent de construire rapidement une grande librairie de molécules à partir d'une réserve de « blocs » de départ. Les travaux de Guida estiment environ à 10^{63} molécules possibles de moins de 30 atomes de composition H, C, N, O, P, S, F, Cl, et Br, montrant l'immensité des structures synthétisables.²

Sharpless assemble alors une série de critères pour une réaction « click » idéale: elle doit être modulaire, avoir une large étendue et donner des rendements élevés d'un seul produit. Elle doit également utiliser des réactifs facilement accessibles et être compatible à l'oxygène et à l'eau. Enfin elle doit former le moins de sous-produits toxiques possibles et la purification ne doit pas nécessiter de chromatographie. Pour répondre à ces critères, une réaction doit souvent avoir une force motrice élevée (supérieure à 20 kcal.mol^{-1}).³

Plusieurs réactions répondent à ses critères et peuvent être appelées des réactions « click »: les ouvertures de cycles tendus, comme les attaques nucléophiles d'époxydes ou d'aziridines⁴; les réactions d'addition d'hétéroatomes sur des carbonyles⁵ ou des liaisons C-C insaturées⁶; ou encore des réactions de cycloadditions.⁷ Les réactions « clicks » sont utilisées dans plusieurs domaines de la chimie: biotechnologie,⁸ chimie médicinale,³ chimie des polymères,⁹ chimie des matériaux¹⁰... Les réactions « clicks » sont particulièrement attrayantes pour les non-organiciens, car elles sont souvent faciles à réaliser et à purifier. L'importance de cette chimie a été reconnue avec le prix Nobel de 2022 remis à Carolyn Bertozzi, Morten Meldal et Barry

Sharpless pour leurs travaux sur le développement de la chimie « click » et la chimie bioorthogonale. La réaction « click » par excellence est la réaction de cycloaddition 1,3-dipolaire azoture-alcyne catalysée au cuivre (CuAAC), qui sera le sujet de la prochaine section.

6.1.2 La réaction de cycloaddition alcyne-azoture catalysée au cuivre (CuAAC)

La réaction de cycloaddition entre un azoture et un alcyne, aussi appelé réaction de Huisgen,¹¹ est une réaction de cycloaddition [3+2]. Ce type de cycloaddition formant un cycle à 5 chaînons non chargé n'est pas possible avec des réactifs sans charge formelle. Le dipôle 1,3 de structure x-y-z doit donc posséder un atome x avec une couche de valence incomplète (chargé positivement) et un atome possédant une paire d'électrons non liée (chargé négativement). (**Figure 6.1**). Ce dipôle peut alors réagir avec les deux atomes A et B d'une liaison insaturée pour former le cycle correspondant avec disparition des charges.

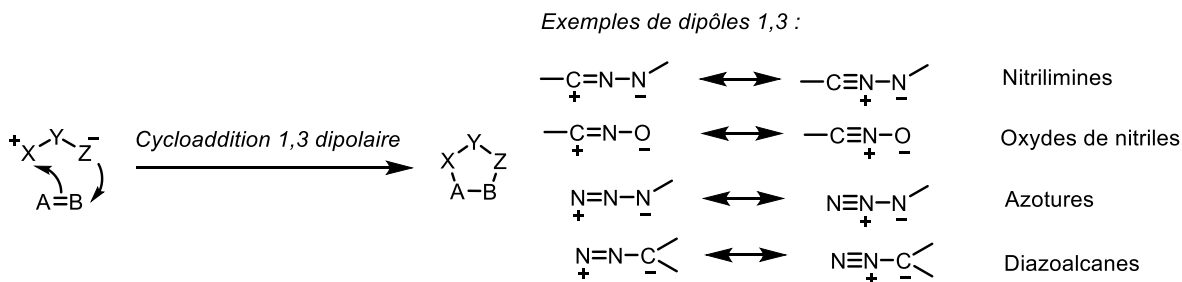


Figure 6.1 Réaction de cycloaddition 1,3 dipolaire et exemples de dipôle 1,3

Si la forme $^+\text{X—Y—Z}^-$ est la représentation la plus simple d'un dipôle 1,3, elle n'est toutefois pas la forme la plus stabilisée. En effet, sous cette forme, la charge positive n'est portée que par un atome X. La répartition de cette charge est alors assurée par résonance grâce au doublet non liant de l'atome Y, pouvant former un lien double entre X et Y. Plusieurs fonctions peuvent agir comme dipôles 1,3, comme les nitrilimines¹², les oxydes de nitriles¹³, les azotures¹⁴ et les diazoalcanes¹⁵.

Les azotures sont des dipôles particulièrement intéressants car ils sont stables et faciles à synthétiser (souvent par substitution d'un électrophile par le sel d'azoture NaN_3). La réaction de cycloaddition entre un azoture et un alcyne a été rapportée pour la première fois en 1893 par

Michael avec la réaction entre l'azoture de phényle et l'acétylène diméthylester à 100°C pour former le triazole correspondant (**Schéma 6.1**)¹⁶. Les structures proposées à l'époque de la publication pour l'azoture, l'alcyne et le triazole sont ainsi présentées dans ce schéma. L'utilisation de températures élevées est nécessaire pour induire la cycloaddition entre les deux molécules peu réactives, et mène à la formation d'un mélange de régioisomères 1,4 et 1,5¹⁷.

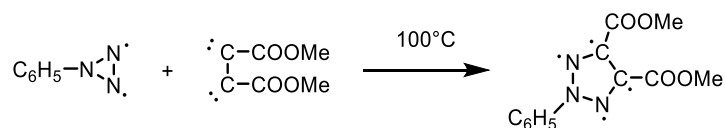


Schéma 6.1 Réaction de cycloaddition azoture-alcyne et structures des molécules proposées par Michael

Le développement de la chimie « click » a pris un essor considérable lorsque les groupes de Meldal¹⁸ et Sharpless¹⁹ ont reporté en 2002 indépendamment l'utilisation de sels de cuivre(I) comme catalyseur de la cycloaddition azoture-alcyne. Si la réaction techniquement ne se qualifie pas comme une réaction « click » (puisque l'on utilise un catalyseur externe), sa tolérance vis-à-vis des autres groupements fonctionnels, son efficacité à température ambiante et sa régiosélectivité en fait la réaction « click » phare encore aujourd'hui, jusqu'à accaparer le terme de « click ».²⁰⁻²² Le mécanisme de la réaction a reçu énormément d'intérêt et est encore discuté aujourd'hui. Le mécanisme proposé actuellement est rapporté à la **figure 6.2** et repose sur la collaboration de deux atomes de cuivre.²³⁻²⁴ La première étape est la formation de l'acétylure σ,π de bicuivre **6.1**. L'azoture se lie à un des deux cuivre pour former l'intermédiaire **6.2**. L'attaque d'un cuivre sur l'alcyne entraîne la formation du premier lien C-N avec oxydation du cuivre(I) en cuivre(III) pour former le métallocycle à 6 chaînons **6.3**. La contraction de cycle réductrice forme le second lien C-N pour produire le complexe triazolide de cuivre **6.4**. La déprotonation d'un alcyne libère alors le triazole pour obtenir **6.1**. Le mécanisme ne permet donc que la formation exclusive du régioisomère 1,4.

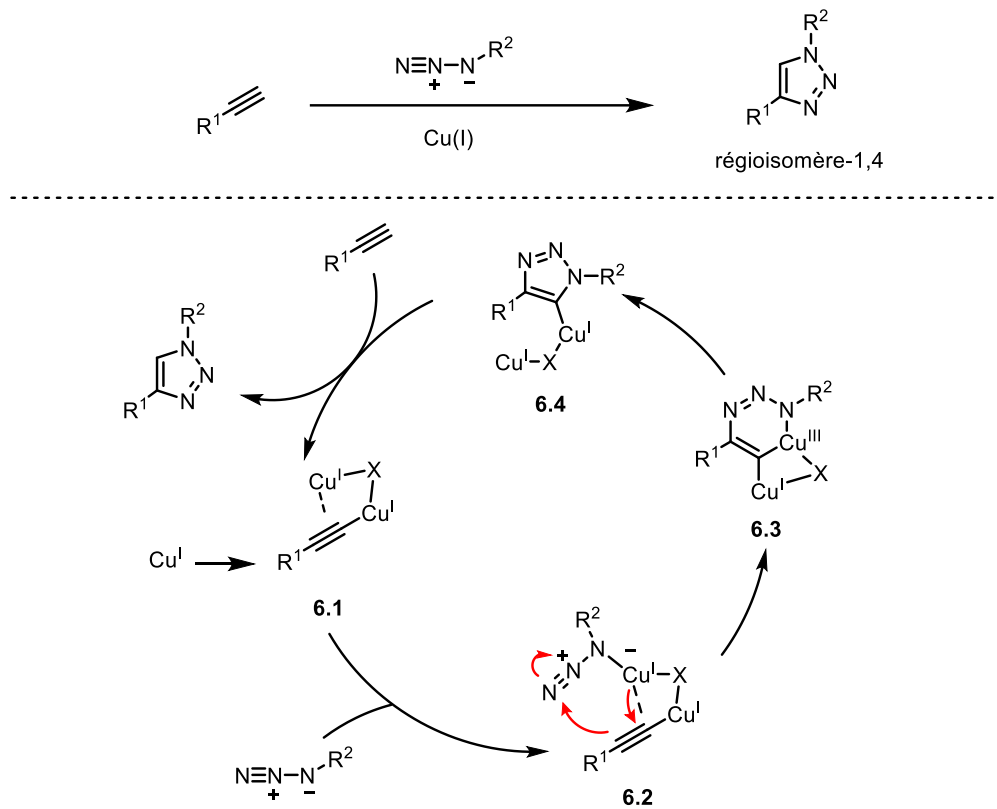


Figure 6.2 CuAAC et mécanisme proposé

6.2 Développement de la stratégie de cycloaddition alcyne-azide promue par la tension

6.2.1 Principe

Les travaux de Bertozzi se sont concentrés sur le développement d'une sous-classe de réaction « click », appelées réactions bioorthogonales, qui regroupent les réactions dont les composants sont inertes aux environnements biologiques, c'est-à-dire qu'ils ne perturbent pas l'activité biologique d'un milieu²⁵⁻²⁶. La réaction de CuAAC ne peut pas être considérée comme bioorthogonale, car les catalyseurs de cuivre possèdent une cytotoxicité non négligeable²⁷. De plus, l'oxygène présent peut venir oxyder le cuivre en cuivre(II), stoppant la réaction et favorisant la réaction de dimérisation de l'alcyne selon la réaction de Glaser²⁸. Cependant les fonctions azoture et alcyne sont particulièrement intéressantes dans un cadre biologique car elles sont insensibles à l'eau et à l'air, résistent aux conditions réductrices du cytosol et réagissent peu avec

les différents composants d'une cellule. L'utilisation d'alcynes tendus comme réactif dans les cycloadditions alcyne-azote promues par la tension (SPAAC) a émergé comme une stratégie prometteuse pour l'assemblage moléculaire en milieu biologique. La tension du cycle de l'alcyne va en effet entraîner une cycloaddition avec un azoture à la température de la pièce sans aucun catalyseur externe (**Figure 6.3**). La réaction ne génère aucun sous-produit, avantage non négligeable lors de son utilisation en conditions biologiques. Les inconvénients notables de la SPAAC proviennent de l'alcyne tendu, généralement peu stable et peu soluble dans l'eau. Dans le cas où l'alcyne est non-symétrique, la réaction va former les deux régioisomères correspondants. Néanmoins, les réactions de SPAAC sont maintenant utilisées dans de nombreux domaines, en biologie pour la ligation de sondes aux protéines d'intérêt⁸, ou dans la chimie des matériaux pour la formation de dendrimères²⁹ ou pour la fonctionnalisation de surfaces³⁰

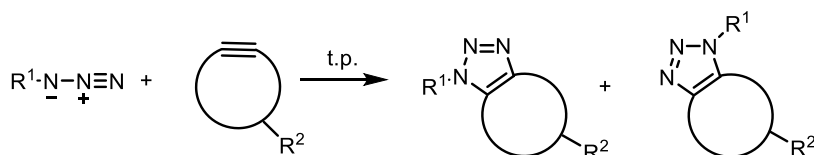


Figure 6.3 Schéma représentatif d'une réaction SPAAC

6.2.2 Développement d'alcynes tendus

Depuis les années 50, les chimistes se sont intéressés à la formation d'alcynes cycliques, en particulier avec les travaux de Blomquist, qui rapportent la formation de cyclooctyne³¹, cyclononyne et cyclodécyne³² par décomposition oxydante de 1,2-cycloalkadiones dihydrazones en présence d'oxyde de mercure (**Figure 6.4.a**). Si la synthèse de cycloheptyne³³, cyclohexyne et de benzyne³⁴ a été par la suite rapportée, ces derniers sont trop instables pour être isolés et nécessitent d'être piégés *in-situ*. D'autres méthodes de formation d'alcynes cycliques ont été rapportées, la plus utilisée est la synthèse développée par Verkrujse en 1978 (**Figure 6.4.b**)³⁵. Partant de l'alcène **6.5** correspondant, une double bromination suivi d'une élimination E2 forme le bromoalcène **6.6**. Une deuxième élimination avec une base forte donne le cyclooctyne **6.7** correspondant.

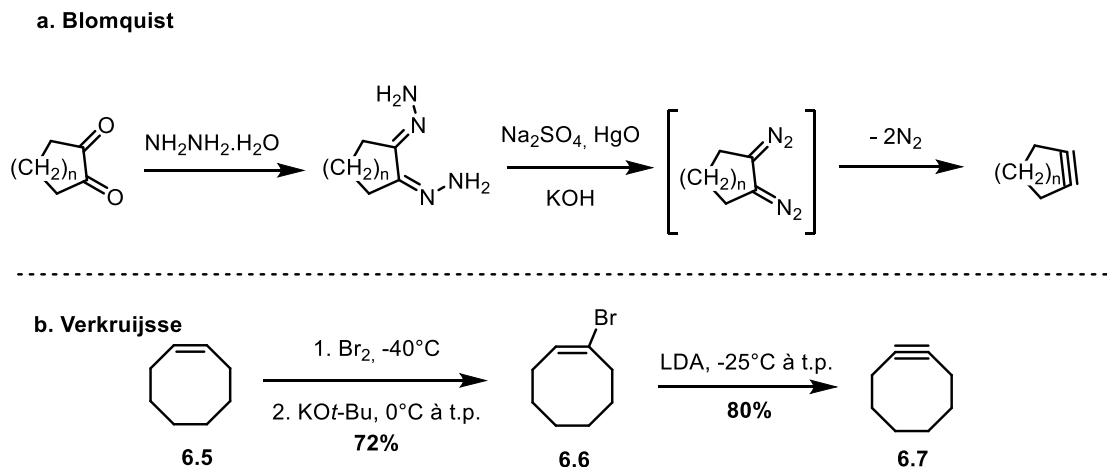


Figure 6.4 a. Synthèse d'alcynes cycliques reporté par Blomquist b. Synthèse de cyclooctyne développé par Verkruisje

Le cyclooctyne est le plus petit cycloalcyne isolé par Blomquist en 1953. Ce dernier montre alors que l'addition d'azote de phényle sur le cyclooctyne résulte en une réaction « explosive » : c'est le premier rapport de cycloaddition alcyne-azote promue par la tension. Si le cyclooctyne est isolable, il se décompose rapidement à l'air libre; sa réactivité est alors cantonnée à une curiosité scientifique pendant 50 ans. En 2004, Bertozzi redécouvre cette réaction et montre son application en milieu cellulaire avec l'utilisation de **6.11** (**Figure 6.5**).³⁶ L'ouverture électrocyclique de **6.8** par le perchlorate d'argent avec piégeage *in-situ* du cation allylique par l'alcool benzylique forme le bromoalcène **6.9**. L'élimination E₂ avec le méthoxyde de sodium donne l'alcyne, et l'ester est par la suite saponifié pour former **6.10**. Finalement, la formation de l'ester activé et la réaction avec un dérivé de la biotine forme le composé **6.11**. La réaction de ce dernier avec différents azotures montre une conversion complète pour la formation des deux régioisomères triazoles. La constante de vitesse de la réaction entre **6.11** et l'azoture de benzyle a été calculé à $2,4 \times (10^{-3}) \text{ M}^{-1} \cdot \text{s}^{-1}$ dans l'acétonitrile deutéré.

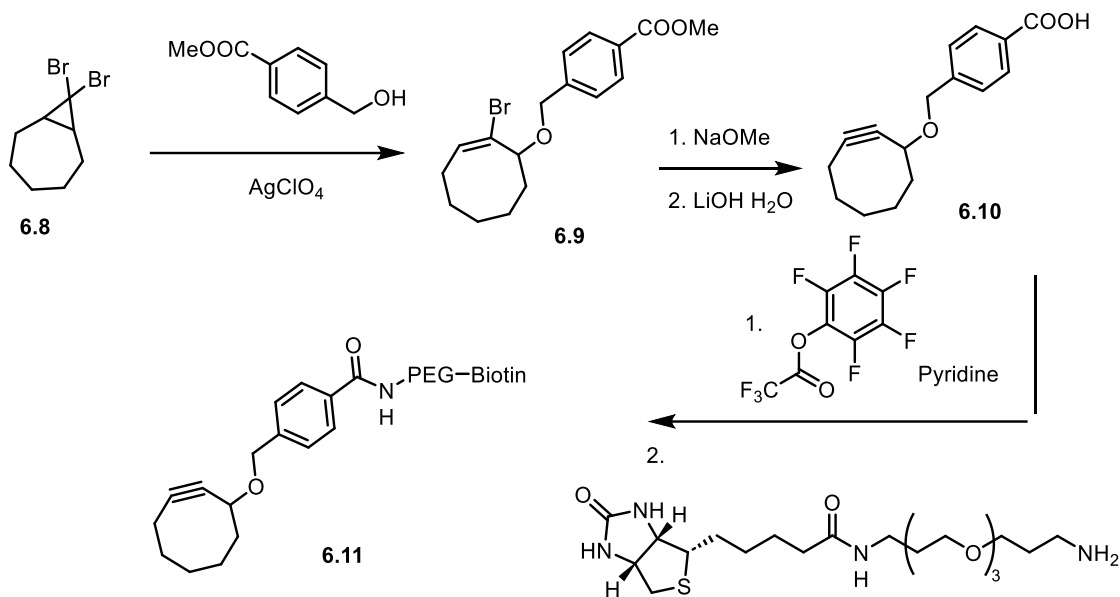


Figure 6.5 Première synthèse d'un alcyne tendu pour la bioconjugaison rapportée par Bertozzi

6.2.3 Réactivité et stabilité des alcynes tendus

La réactivité des alcynes tendus dans la réaction de SPAAC provient de la tension inhérente au cycle. En effet dans le cyclooctyne, les carbones C_{sp} de l'alcyne doivent adopter un angle de 163° , (contre 180° dans un alcyne acyclique). La tension de cycle (RSE) est la première caractéristique permettant de prédire la réactivité d'un alcyne; sa géométrie distordue se rapproche de la géométrie que doit adopter l'alcyne à l'état de transition, diminuant donc la pénalité d'énergie de distorsion et donc abaissant la barrière énergétique. Utilisant la théorie de densité fonctionnelle (DFT), Houk a montré que l'énergie d'activation pour la cycloaddition du cyclooctyne ($\Delta E^\ddagger = 8,0 \text{ kcal/mol}$) est bien plus basse celle de l'alcyne linéaire ($\Delta E^\ddagger = 16,2 \text{ kcal/mol}$)³⁷. Cependant, une grande tension de cycle augmente la réactivité de l'alcyne, au détriment de sa stabilité. Les cycles à 7 chaînons ou moins ($\text{RSE} < 25 \text{ kcal/mol}$) ne sont pas isolables, tandis que le cyclooctyne possède une stabilité relative. Les cycles plus grands sont stables, mais leur réactivité se rapproche de celle des alcynes linéaires.

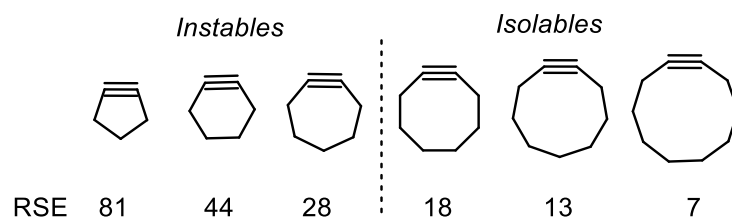


Figure 6.6 Influence de l'énergie de tension de cycle (RSE) sur la stabilité de cycloalcyne

Les chimistes ont alors tenté d'augmenter la tension de cycle par d'autres moyens que la taille du cycle. Une stratégie rapidement découverte est l'ajout dans le cycle d'unités hybridées sp^2 , qui viennent rigidifier la structure et bloquer l'alcyne dans une conformation élevée en énergie. En 2008, Ning rapporte l'incorporation de deux groupements aryles dans le cycle, formant le composé **DIBO**³⁸ avec une constante de vitesse de SPAAC presque 100 fois supérieure ($k = 170 \cdot 10^{-3} \text{ M}^{-1} \cdot \text{s}^{-1}$) au simple cyclooctyne **OCT** ($k = 2,4 \cdot 10^{-3} \text{ M}^{-1} \cdot \text{s}^{-1}$). L'ajout d'une fonction amide dans le composé **BARAC** ajoute encore plus de tension dans le cycle, permettant une vitesse de cycloaddition proche de $1 \text{ M}^{-1} \cdot \text{s}^{-1}$; le composé est cependant trop instable pour être isolé³⁹. Si ces composés dibenzoannulés possèdent une excellente réactivité, leur lipophilie peut être problématique pour des applications biologiques. La présence d'un cyclopropane dans le **BCN** vient ajouter un caractère sp^2 aux carbones et donne un composé plus soluble dans l'eau.⁴⁰

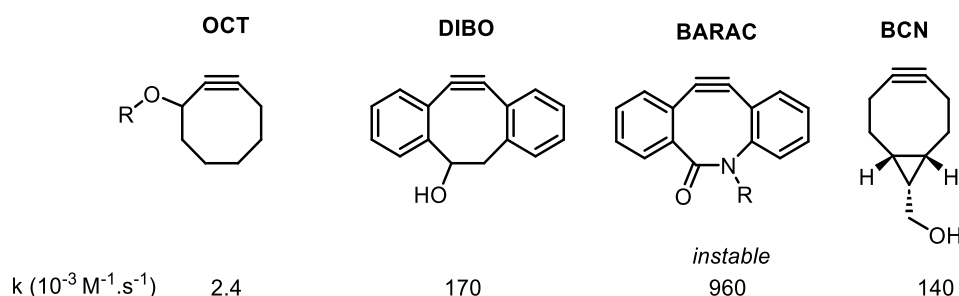


Figure 6.7 Constantes de vitesse de différents alcyne cycliques pour la cycloaddition avec l'azoture de benzyle.

Les effets électroniques des substituants d'un cycloalcyne exercent aussi une influence sur la réactivité des alcyne tendus. Dans le composé **DIFO**, l'ajout d'un groupement CF_2 adjacents à

l'alcyne augmente la réactivité ($k = 76 \cdot 10^{-3} \text{ M}^{-1} \cdot \text{s}^{-1}$) comparé à l'analogue cyclooctyne⁴¹. Plusieurs explications sont proposées notamment l'assistance à la distorsion (**Figure 6.8**). En effet le caractère π -donneur de l'alcyne augmente avec sa distorsion; la présence de l'orbitale σ^* du lien C-F vient par hyperconjugaison⁴² stabiliser la torsion de l'alcyne et par conséquent abaisser la pénalité de distorsion. Le second effet observé est l'assistance à la formation du lien C-N. En effet dans l'état de transition, on observe un recouvrement de la HOMO de l'azoture et de la LUMO de l'alcyne. Il en résulte une augmentation de la densité électronique dans la π^* de l'alcyne. La présence d'un groupement accepteur σ adjacent à l'alcyne permet alors de délocaliser cette densité et donc d'abaisser l'énergie de formation du lien C-N. Un autre exemple de ces effets électroniques est le composé **6.12**, qui possède un oxygène et un azote endocyclique⁴³. La présence de des deux hétéroatomes permet au cycle à 9 chaînons de posséder une bonne réactivité pour la cycloaddition avec l'azoture de benzyle ($k = 19 \cdot 10^{-3} \text{ M}^{-1} \text{ s}^{-1}$).

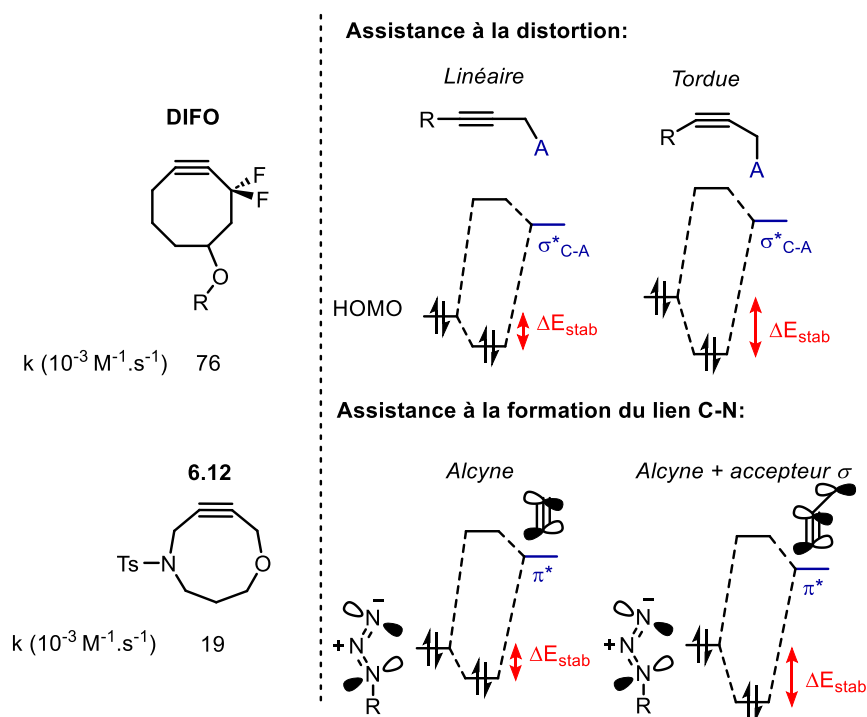


Figure 6.8 Influence des substituants accepteurs σ d'un cycloalcyne sur la stabilisation de la distorsion et l'assistance à la formation de liens C-N

Si la stratégie repose sur l'utilisation d'hétéroatomes comme accepteur σ , ces derniers peuvent aussi être donneurs grâce à leur paire d'électrons non liante n . La stratégie d'activation

à distance joue sur l'utilisation de systèmes π loin de l'alcyne pour favoriser l'assistance de l'hétéroatome dans l'état de transition (TS). C'est la stratégie utilisée dans le cas du **BINOC** ou la présence de groupements aryles stabilise l'état de transition en permettant la délocalisation de l'orbitale n de l'hétéroatome avec le cycle aromatique (**Figure 6.9**)⁴⁴. Il en résulte un composé **BINOC** réactif pour la SPAAC ($k = 0,62 \cdot 10^{-3} \text{ M}^{-1} \text{ s}^{-1}$) malgré un grand cycle à 10 chaînons.

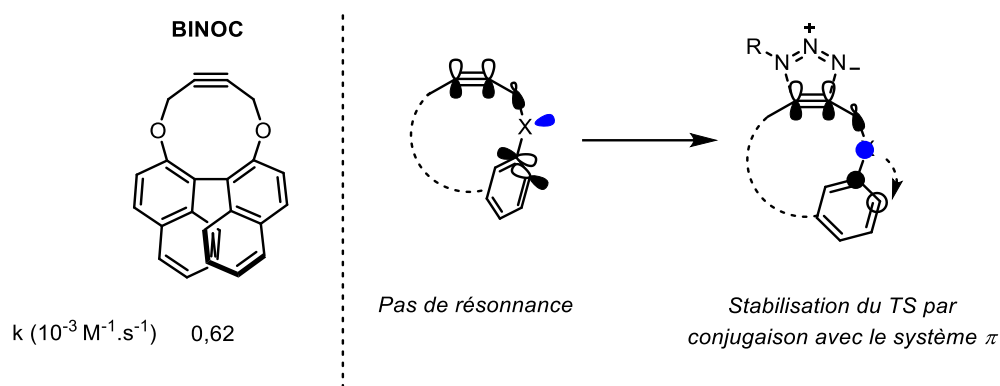


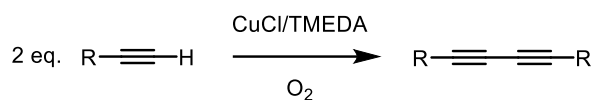
Figure 6.9 Représentation de la stabilisation du TS par activation à distance.

6.3 Les diynes-1,3

6.3.1 Réactivité et fonctionnalisation des diynes-1,3

Le diyne-1,3 est une fonction constituée de deux alcynes liées par une liaison σ . La présence de 4 liaisons π en fait un groupement fonctionnalisable, largement utilisé comme précurseur de molécules complexes⁴⁵⁻⁴⁶, en chimie des matériaux⁴⁷ ou en chimie des polymères⁴⁸. Deux méthodes sont majoritairement utilisées pour la synthèse de diynes-1,3 (**Figure 6.10**). Pour la formation de diynes-1,3 symétriques, la réaction de Glaser-Hay permet la dimérisation d'un alcyne terminal en présence de sels de cuivre(I) et d'oxygène⁴⁹. Dans le cas de diynes-1,3 non-symétriques, il peut y avoir des problèmes de sélectivité et de formation de produits d'homocouplage avec la réaction de Glaser-Hay; la réaction de Cadiot-Chodkiewicz permet le couplage entre un bromoalcyne et un alcyne terminal catalysé par du cuivre(I)⁵⁰. Dans les deux cas, la présence d'amine comme additif ou comme solvant est nécessaire pour accélérer la réaction.

Homocouplage de Glaser-Hay



Hétérocouplage de Cadiot-Chodkiewicz

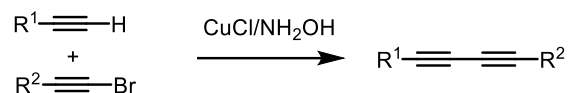


Figure 6.10 Réactions de formation de diyne-1,3 symétriques et non-symétriques.

Comme mentionné précédemment, les diyne-1,3 sont de bons précurseurs pour la formation de molécules complexes. Les diyne-1,3 peuvent être par exemple utilisés dans la réaction de CuAAC comme reporté en 2009 par Capuzzolo (**Figure 6.11.a**)⁵¹. Une première cycloaddition sélective de l'alcyne terminal sur le diyne **6.13** avec l'azote benzylique forme le triazole **6.14** avec un rendement de 77%. Une deuxième cycloaddition sur le second alcyne est alors possible grâce à une déprotection *in-situ* du groupement TMS avec le fluorure de tetra-*n*-butylammonium pour former le bis-triazole **6.15** avec un rendement de 64%. Les deux alcynes d'un diyne-1,3 peuvent aussi réagir pour former, en présence de nucléophiles, différents hétérocycles. Zhang a montré en 2014 la formation du furane **6.17** avec un rendement de 92% lorsque le diyne **6.16** est chauffé à 80 °C en présence d'eau et d'une quantité catalytique de KOH (**Figure 6.11.b**)⁵². D'autres hétéroatomes peuvent être incorporés, augmentant la généralité de la réaction à la formation de pyroles (**6.18**) et de thiophènes (**6.19**) avec d'excellents rendements (84 et 97%, respectivement).

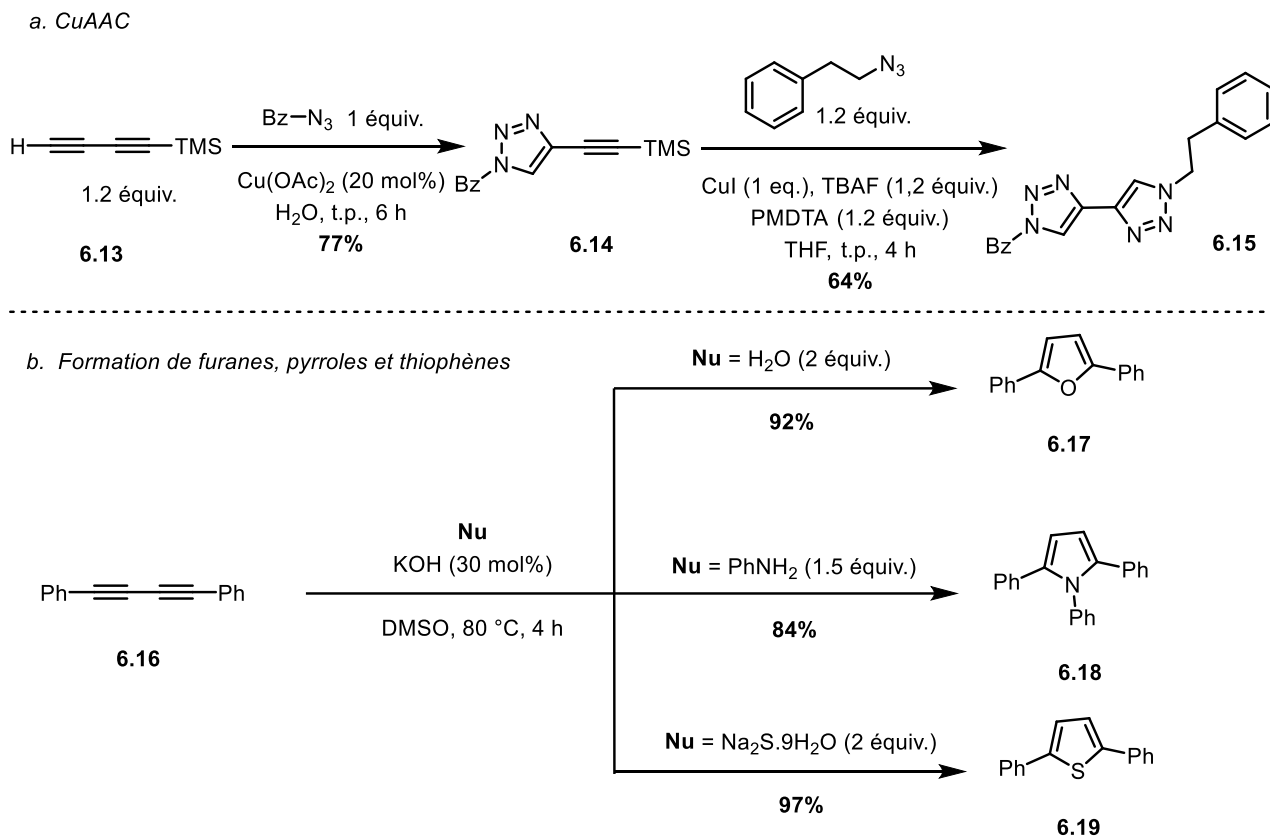


Figure 6.11 Fonctionnalisation de diynes-1,3 par **a.** Cycloadditions alcyne-azoture catalys\u00e9es par le cuivre. **b.** Attaque nucl\u00e9ophile pour la formation d'h\u00e9t\u00e9rocycles.

En 2016, Verniest a rapport\u00e9 l'utilisation d'hydrazine comme bisnucl\u00e9ophile-1,2 pour la formation de pyrazole (**Figure 6.12**)⁵³. Le diyne macrocyclique **6.20** est chauff\u00e9 \u00e0 60\u00b0C en pr\u00e9sence de m\u00e9thyle hydrazine dans le DMSO. Apr\u00e8s 48 h, 39% d'un m\u00e9lange du pyrazole **6.21** et de son r\u00e9gioisom\u00e8re a \u00e9t\u00e9 obtenu. Le m\u00e9canisme propos\u00e9 est bas\u00e9 sur les travaux pr\u00e9c\u00e9dents de Bao avec l'hydrazine non substitu\u00e9e⁵⁴. Une hydroamination de type Cope⁵⁵ entre l'hydrazine et un des alcynes va former l'ylure **6.22**, suivi d'un transfert de proton qui donne l'\u00e8nyne **6.23**. Une isom\u00e9risation du compos\u00e9 peut alors former l'all\u00e8ne **6.24** et une addition \u00e9lectrophile du second azote forme le cycle \u00e0 5 cha\u00eenons **6.25** correspondant. Une r\u00e9activit\u00e9 similaire est observ\u00e9e avec les hydroxylamines, formant les isoxazoles correspondants⁵⁶. Finalement, des fonctionnalisations de diynes-1,3 catalys\u00e9es par des m\u00e9taux sont possibles, pour la formation de motifs aryles par

[2+2+2]⁴⁵, ou pour la formation d'hétérocycles contenant des atomes de silicium⁵⁷, sélénium⁵⁸, ou germanium⁵⁹.

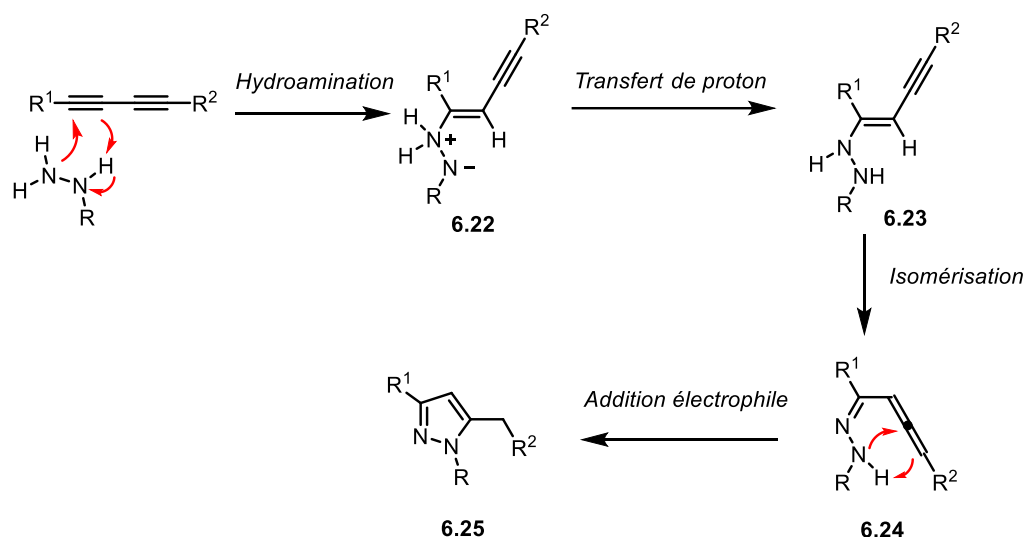
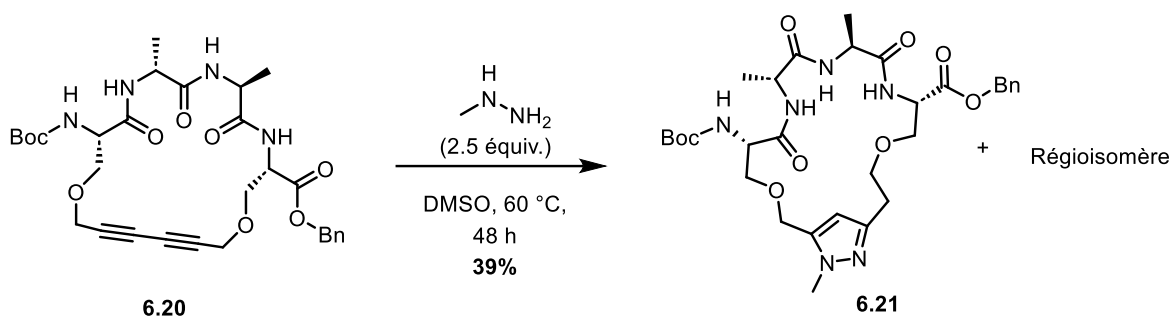


Figure 6.12 Réaction entre une hydrazine et un diyne 1,3 pour la formation d'un pyrazole reportée par Verniest et mécanisme proposé.

6.3.2 Synthèse de diynes-1,3 cycliques

Les diynes-1,3 cycliques sont une classe de macrocycles qui ont été beaucoup étudiés pour leur géométrie supramoléculaire⁶⁰, et leur applications potentielles comme substrat de polymères insaturés⁶¹ et de fullerènes⁶². Vollhardt en 1995 a rapporté la synthèse du diyne **6.26** possédant une fonction diyne avec un angle non-linéaire (168,8°) malgré un cycle à 14 chaînons (**Figure 6.13**).⁶³ De Meijere a rapporté en 1994 le composé à 14 chaînons **6.27** possédant des

cyclopropanes exocycliques⁶⁴. Enfin en 2000, le groupe de Tykwinski a montré la formation du composé **6.28** à 12 chaînons avec un angle du diyne de 160,3°, plus tendu que l'angle du cyclooctyne (163°)⁶⁵.

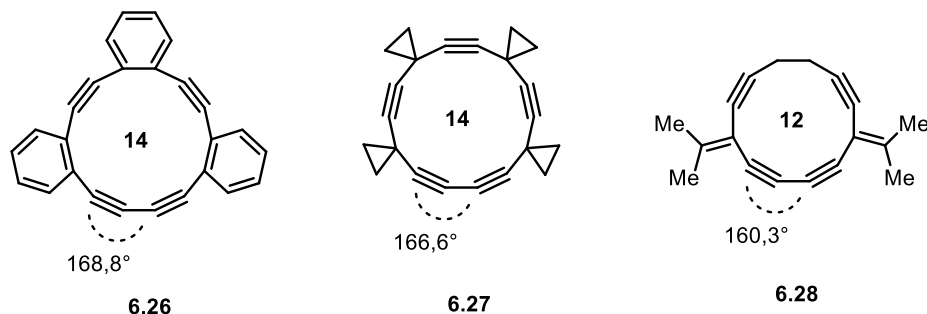


Figure 6.13 Diynes-1,3 cycliques et l'angle de la liaison Csp-Csp. Les nombres en gras représentent la taille des cycles

En 2002, le groupe de Fallis a rapporté la découverte inattendue du diyne **6.29** (Figure 6.14.a). En effet, le groupe s'intéresse alors à la formation de cages acétyléniques et a proposé la formation de **6.30** par couplage de Glaser-Hay avec le monomère **6.31**.⁶⁶ Cependant le seul produit formé est le diyne **6.29**, avec un rendement de 62%. Le composé est peu stable, mais son analogue bromé **6.32** est alors isolé et l'élucidation de la structure par rayons X montre alors la formation d'un cycle à 11 chaînons avec un angle diyne C(14)-C(15)-C(16) de 153,4 ° (Figure 6.14.b). Si cette molécule a été étudiée dans une réaction de Diels-Alder avec du cyclopentadiène à 120 °C, sa découverte relève alors plus de la curiosité scientifique que d'un vrai intérêt pour cette molécule réactive. En effet en 2002 la SPAAC était encore très peu développée. A ce jour, aucun diyne 1,3 cyclique n'a été étudié pour des réactions promues par la tension.

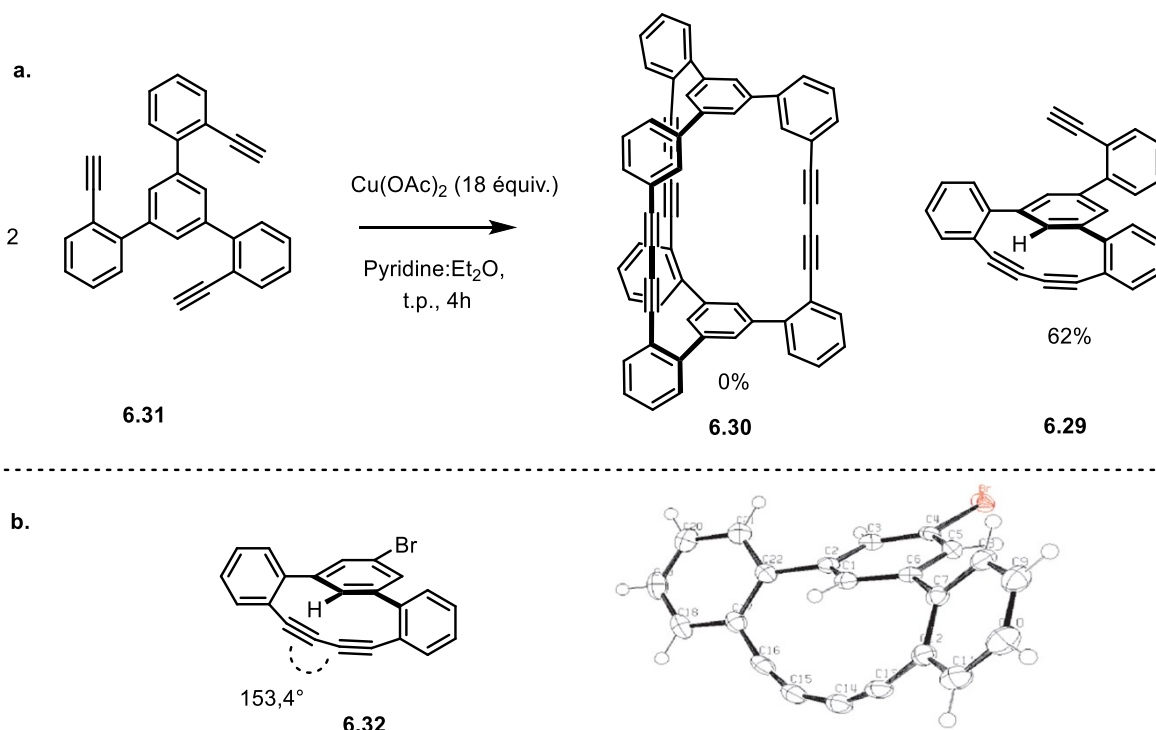


Figure 6.14 a. Découverte de la synthèse de diyne 1,3 terphényle b. Structure cristallographique et angle du diyne **6.32**

6.4 Conclusion

La chimie « click » se définit comme l'ensemble des réactions permettant un assemblage rapide de molécules simples, facile à utiliser et avec une grande économie d'atomes. Son intérêt a gagné tout les domaines de la chimie, en particulier celui de la biologie, où le sous-domaine des réactions bioorthogonales permet l'association de molécules en milieu biologique complexe. Parmi les réactions bioorthogonales, la SPAAC s'est développée pour devenir une réaction de choix, grâce à l'utilisation d'alcynes tendus qui réagissent spécifiquement avec des azotures. De nombreuses classes d'alcynes tendus sont alors apparues: commençant par des cycloalcynes simples, les chimistes ont alors modifié leur structure, pour augmenter leur réactivité, tout en gardant des molécules stables et isolables. L'ajout de carbones C_{sp}^2 dans le cycle permet d'augmenter la tension et l'ajout d'hétéroatomes permet de stabiliser l'état de transition de la cycloaddition. Ces modifications ont donné lieu à des cycles à 8, 9 et 10 chaînons possédant un

alcyne tendu. Cependant une classe d'alcyne inexplorée est la classe des diyne-1,3 cycliques. Cela est surprenant car ces derniers possèdent plusieurs avantages qui pourraient en faire de bons candidats en SPAAC : elles possèdent des fonctions alcynes extrêmement tendues, sans pour autant être très instables. De plus, leur synthèse par couplage de Glaser est beaucoup plus simple d'opération que les synthèses traditionnelles de cycloalcynes. Enfin, la présence d'une fonction dyine tendue pourrait débloquent de nouvelles réactivités en chimie click, par exemple avec l'utilisation de bis-nucléophiles 1,2 comme les hydrazines.

6.5 Références bibliographiques

1. Kolb, H. C.; Finn, M. G.; Sharpless, K. B., *Angew. Chem., Int. Ed.* **2001**, *40* (11), 2004-2021.
2. Bohacek, R. S.; McMartin, C.; Guida, W. C., *Med. Res. Rev.* **1996**, *16* (1), 3-50.
3. Hein, C. D.; Liu, X.-M.; Wang, D., *Pharm. Res.* **2008**, *25* (10), 2216-2230.
4. Sabir, S.; Kumar, G.; Verma, V. P.; Jat, J. L., *ChemistrySelect* **2018**, *3* (13), 3702-3711.
5. Song, H.-X.; Han, Z.-Z.; Zhang, C.-P., *Chem. - Eur. J.* **2019**, *25* (46), 10907-10912.
6. Northrop, B. H.; Coffey, R. N., *J. Am. Chem. Soc.* **2012**, *134* (33), 13804-13817.
7. Blackman, M. L.; Royzen, M.; Fox, J. M., *J. Am. Chem. Soc.* **2008**, *130* (41), 13518-13519.
8. Jewett, J. C.; Bertozzi, C. R., *Chem. Soc. Rev.* **2010**, *39* (4), 1272-1279.
9. Geng, Z.; Shin, J. J.; Xi, Y.; Hawker, C. J., *J. Polym. Sci.* **2021**, *59* (11), 963-1042.
10. Xi, W.; Scott, T. F.; Kloxin, C. J.; Bowman, C. N., *Adv. Funct. Mater.* **2014**, *24* (18), 2572-2590.
11. Huisgen, R.; Szeimies, G.; Möbius, L., *Chem. Ber.* **1967**, *100* (8), 2494-2507.
12. Huisgen, R.; Seidel, M.; Wallbillich, G.; Knupfer, H., *Tetrahedron* **1962**, *17* (1), 3-29.
13. Katritzky, A. R.; Button, M. A. C.; Denisenko, S. N., *J. Heterocycl. Chem.* **2000**, *37* (6), 1505-1510.
14. Huisgen, R., *Angew. Chem. Int. Ed. Engl.* **1963**, *2* (10), 565-598.
15. Kadaba, P. K.; Edwards, J. O., *J. Org. Chem.* **1961**, *26* (7), 2331-2335.
16. Michael, A., *J. Prakt. Chem.* **1893**, *48* (1), 94-95.
17. Breugst, M.; Reissig, H. U., *Angew. Chem. Int. Ed. Engl.* **2020**, *59* (30), 12293-12307.
18. Tornøe, C. W.; Christensen, C.; Meldal, M., *J. Org. Chem.* **2002**, *67* (9), 3057-3064.
19. Rostovtsev, V. V.; Green, L. G.; Fokin, V. V.; Sharpless, K. B., *Angew. Chem., Int. Ed.* **2002**, *41* (14), 2596-2599.
20. Meldal, M.; Tornøe, C. W., *Chem. Rev.* **2008**, *108* (8), 2952-3015.
21. Haldón, E.; Nicasio, M. C.; Pérez, P. J., *Org. Biomol. Chem.* **2015**, *13* (37), 9528-9550.
22. Tiwari, V. K.; Mishra, B. B.; Mishra, K. B.; Mishra, N.; Singh, A. S.; Chen, X., *Chem. Rev.* **2016**, *116* (5), 3086-3240.
23. Worrell, B. T.; Malik, J. A.; Fokin, V. V., *Science* **2013**, *340* (6131), 457-460.

24. Presolski, S. I.; Hong, V.; Cho, S.-H.; Finn, M. G., *J. Am. Chem. Soc.* **2010**, *132* (41), 14570-14576.
25. Sletten, E. M.; Bertozzi, C. R., *Acc. Chem. Res.* **2011**, *44* (9), 666-676.
26. Bird, R. E.; Lemmel, S. A.; Yu, X.; Zhou, Q. A., *Bioconjug. Chem.* **2021**, *32* (12), 2457-2479.
27. Gaetke, L. M.; Chow, C. K., *Toxicology* **2003**, *189* (1-2), 147-63.
28. Siemsen, P.; Livingston, R. C.; Diederich, F., *Angew. Chem. Int. Ed. Engl.* **2000**, *39* (15), 2632-2657.
29. Ornelas, C.; Broichhagen, J.; Weck, M., *J. Am. Chem. Soc.* **2010**, *132* (11), 3923-3931.
30. Orski, S. V.; Poloukhine, A. A.; Arumugam, S.; Mao, L.; Popik, V. V.; Locklin, J., *J. Am. Chem. Soc.* **2010**, *132* (32), 11024-11026.
31. Blomquist, A. T.; Liu, L. H., *J. Am. Chem. Soc.* **1953**, *75* (9), 2153-2154.
32. Blomquist, A. T.; Burge, R. E., Jr.; Liu, L. H.; Bohrer, J. C.; Sucsy, A. C.; Kleis, J., *J. Am. Chem. Soc.* **1951**, *73* (11), 5510-5511.
33. Wittig, G.; Krebs, A., *Chem. Ber.* **1961**, *94* (12), 3260-3275.
34. Shi, J.; Li, L.; Li, Y., *Chem. Rev.* **2021**, *121* (7), 3892-4044.
35. Brandsma, L.; Verkruijsse, H. D., *Synthesis* **1978**, *1978* (04), 290-290.
36. Agard, N. J.; Prescher, J. A.; Bertozzi, C. R., *J. Am. Chem. Soc.* **2004**, *126* (46), 15046-15047.
37. Ess, D. H.; Jones, G. O.; Houk, K. N., *Org. Lett.* **2008**, *10* (8), 1633-1636.
38. Ning, X.; Guo, J.; Wolfert, M. A.; Boons, G. J., *Angew. Chem. Int. Ed. Engl.* **2008**, *47* (12), 2253-5.
39. Jewett, J. C.; Sletten, E. M.; Bertozzi, C. R., *J. Am. Chem. Soc.* **2010**, *132* (11), 3688-3690.
40. Dommerholt, J.; Schmidt, S.; Temming, R.; Hendriks, L. J. A.; Rutjes, F. P. J. T.; van Hest, J. C. M.; Lefeber, D. J.; Friedl, P.; van Delft, F. L., *Angew. Chem., Int. Ed.* **2010**, *49* (49), 9422-9425.
41. Baskin, J. M.; Prescher, J. A.; Laughlin, S. T.; Agard, N. J.; Chang, P. V.; Miller, I. A.; Lo, A.; Codelli, J. A.; Bertozzi, C. R., *Proc. Natl. Acad. Sci.* **2007**, *104* (43), 16793-16797.
42. Gold, B.; Dudley, G. B.; Alabugin, I. V., *J. Am. Chem. Soc.* **2013**, *135* (4), 1558-1569.
43. Ni, R.; Mitsuda, N.; Kashiwagi, T.; Igawa, K.; Tomooka, K., *Angew. Chem., Int. Ed.* **2015**, *54* (4), 1190-1194.

44. Harris, T.; Gomes, G. d. P.; Ayad, S.; Clark, R. J.; Lobodin, V. V.; Tuscan, M.; Hanson, K.; Alabugin, I. V., *Chem* **2017**, *3* (4), 629-640.
45. Doherty, S.; Knight, J. G.; Smyth, C. H.; Harrington, R. W.; Clegg, W., *Org Lett* **2007**, *9* (23), 4925-8.
46. Holden, C.; Greaney, M. F., *Angew. Chem., Int. Ed.* **2014**, *53* (23), 5746-5749.
47. Stiegman, A. E.; Graham, E.; Perry, K. J.; Khundkar, L. R.; Cheng, L. T.; Perry, J. W., *J. Am. Chem. Soc.* **1991**, *113* (20), 7658-7666.
48. Babudri, F.; Colangiuli, D.; Di Lorenzo, P. A.; Farinola, G. M.; Omar, O. H.; Naso, F., *Chem. Commun.* **2003**, (1), 130-131.
49. Akhtar, R.; Zahoor, A. F., *Synth. Commun.* **2020**, *50* (22), 3337-3368.
50. Sindhu, K. S.; Thankachan, A. P.; Sajitha, P. S.; Anilkumar, G., *Org. Biomol. Chem.* **2015**, *13* (25), 6891-6905.
51. Fiandanese, V.; Bottalico, D.; Marchese, G.; Punzi, A.; Capuzzolo, F., *Tetrahedron* **2009**, *65* (51), 10573-10580.
52. Zheng, Q.; Hua, R.; Jiang, J.; Zhang, L., *Tetrahedron* **2014**, *70* (44), 8252-8256.
53. Verlinden, S.; Ballet, S.; Verniest, G., *European J. Org. Chem.* **2016**, *2016* (35), 5807-5812.
54. Wang, L.; Yu, X.; Feng, X.; Bao, M., *J. Org. Chem.* **2013**, *78* (4), 1693-1698.
55. Moran, J.; Gorelsky, S. I.; Dimitrijevic, E.; Lebrun, M.-E.; Bédard, A.-C.; Séguin, C.; Beauchemin, A. M., *J. Am. Chem. Soc.* **2008**, *130* (52), 17893-17906. Loiseau, F.; Clavette, C.; Raymond, M.; Roveda, J.-G.; Burrell, A.; Beauchemin, A. M., *Chem. Commun.* **2011**, *47* (1), 562-564.
56. Wang, L.; Yu, X.; Feng, X.; Bao, M., *Org. Lett.* **2012**, *14* (9), 2418-2421.
57. Matsuda, T.; Kadowaki, S.; Murakami, M., *Chem. Commun.* **2007**, (25), 2627-2629.
58. Alves, D.; Luchese, C.; Nogueira, C. W.; Zeni, G., *J. Org. Chem.* **2007**, *72* (18), 6726-6734.
59. Matsuda, T.; Kadowaki, S.; Yamaguchi, Y.; Murakami, M., *Org. Lett.* **2010**, *12* (5), 1056-1058.
60. Seel, C.; Vögtle, F., *Angew. Chem. Int. Ed. Engl.* **1992**, *31* (5), 528-549.
61. Chauvin, R., *Tetrahedron Lett.* **1995**, *36* (3), 397-400.
62. H. F. Bunz, U.; Rubin, Y.; Tobe, Y., *Chem. Soc. Rev.* **1999**, *28* (2), 107-119.

63. Boese, R.; Matzger, A. J.; Vollhardt, K. P. C., *J. Am. Chem. Soc.* **1997**, *119* (8), 2052-2053.
64. Scott, L. T.; Cooney, M. J.; Otte, C.; Puls, C.; Haumann, T.; Boese, R.; Smith, A. B., III; Carroll, P. J.; de Meijere, A., *J. Am. Chem. Soc.* **1994**, *116* (22), 10275-10283.
65. Eisler, S.; McDonald, R.; Loppnow, G. R.; Tykwinski, R. R., *J. Am. Chem. Soc.* **2000**, *122* (29), 6917-6928.
66. Collins, S. K.; Yap, G. P. A.; Fallis, A. G., *Org. Lett.* **2002**, *4* (1), 11-14.

Chapitre 7 TPDYs: Strained Macrocyclic Diynes for Bioconjugation Processes.

Corentin Cruché, Adem Hadjabdelhafid-Parisien, Bernard D’Onofrio, Joelle N. Pelletier, Radu Iftimie, and Shawn K. Collins (Soumis)

Département de Chimie, Centre for Green Chemistry and Catalysis, Université de Montréal, 1375 Avenue Thérèse-Lavoie-Roux, Montréal, QC H2V 0B3

Contributions:

- Corentin Cruché a réalisé la synthèse des molécules, les mesures de constantes de vitesse, et les calculs computationnels. Il a aussi rédigé une partie de la partie expérimentale et participé à la rédaction du manuscrit.
- Adem Hadjabdelhafid-Parisien a réalisé les expériences biologiques. Il a aussi rédigé une partie de la partie expérimentale et participé à la rédaction du manuscrit.
- Bernard D’Onofrio a participé à la synthèse des molécules.
- Joelle N. Pelletier a participé à la mise en œuvre des expériences biologiques et à la rédaction du manuscrit.
- Radu Iftimie a participé à la mise en œuvre des expériences computationnelles et à la rédaction du manuscrit.
- Shawn K. Collins a participé à la mise en œuvre des expériences chimiques et à la rédaction du manuscrit.

7.1 Abstract

Terphenyl diyne (TPDY) macrocycles have been developed for bioligation. The reagents incorporate highly bent 1,3-diynes that are active in SPAAC processes affording atropisomeric triazole products. In particular, the 3,5-TPDY derivative was found to be bench stable and easily accessible via a streamlined two-pot synthesis. Experimental evidence and computation support SPAAC rates that rival typical cyclooctyne reagents. TPDYs can also exploit the 1,3-diyne in a strain-promoted diyne/hydrazine hydroamination. The cycloadduct obtained exhibited a novel

fused hexacyclic pyrazole. A pendant amine allowed bioconjugation of TPDY to two proteins in a microbial transglutaminase-catalyzed reaction. The resulting TPDY-conjugated crystallizable fragment of IgG1 antibody (hFc) and B domain of protein G (GB1) were subsequently labelled with a fluorophore via SPAAC.

7.2 Introduction

Bioorthogonal bioconjugation¹ is a valuable tool in chemical biology. The development of cyclooctyne reagents for strain-promoted azide-alkyne cycloaddition (SPAAC)²⁻⁴ exemplifies the strategy of using non-native functional groups in a non-catalyzed, “waste-free” process for imaging, identifying, and characterizing biomolecules with broad application.⁵⁻⁸ Given the widespread adoption of the technology, it is no surprise that there is significant interest in the discovery of new cyclic strained alkynes. In general, SPAAC reagent design consists of two general paradigms.^{2, 9-11} The first incorporates the alkyne into medium-sized rings, and additional annulation increases bending thereof. The bond angles in a strained cycloalkyne are believed to mimic the geometry of the transition state (TS) of the azide-alkyne cycloaddition. Secondly, the aforementioned TS can also be stabilized through stereoelectronic effects with neighboring antibonding orbitals (most often $\pi \rightarrow \sigma^*$). While much effort is devoted to improving both the rate of SPAAC, and the stability of the reagent itself, it is equally important to consider the synthetic accessibility,¹² the selectivity of the reagent for one specific transformation,¹³ or its ability to participate in multiple different conjugations.¹⁴ Given the need for new active, yet stable and readily accessible cycloalkynes, it is surprising that strained diynes have not received further attention.¹⁵⁻¹⁷ The electronic and structural characteristics of distorted, highly conjugated acetylenic systems have long been exploited for materials applications,¹⁸ including assembling carbon nanostructures¹⁹⁻²¹ and synthetic endeavors toward fullerenes.²² Strained cyclic diynes may also possess other advantages for application as SPAAC reagents: 1) their synthesis is relatively straightforward via Glaser-type couplings,²³⁻²⁶ and 2) the diyne could possibly be exploited for the development of new “Click” processes. In 2002, Fallis reported the serendipitous synthesis of a strained undecadiyne macrocycle (**Figure 7.1**).²⁷ The X-ray crystal analysis of the 1,1':3',1''-terphenyl skeleton revealed bent diyne bond angles 159.4° and 156.2°, which are in line with bond angles observed in analogous cyclooctyne SPAAC reagents.²⁸ Herein, the synthesis and

reactivity of various terphenyl diyne (TPDY) macrocycles for SPAAC is reported. Computational and experimental studies elucidate the electronic effects of the diyne upon reactivity. The applicability of an aminated 3,5-TPDY derivative for *in vitro* bioconjugation was exemplified via microbial transglutaminase (mTG)-mediated conjugation to either of two target proteins and subsequent labelling with sulfo-cyanine 5-azide via SPAAC. In addition, a new potential bioconjugation involving formal cycloaddition of hydrazines to the strained 1,3-diyne is reported.

7.3 Results and discussion

Reactivity of TPDYs in SPAAC: Cycloalkyne SPAAC reagents are typically prepared using one of two key steps to insert the bent alkyne. The corresponding cycloalkene can undergo a bromination/elimination sequence, or the cyclic compounds insert the alkyne via Sonogashira coupling/Nicholas reaction, the latter requires the use of stoichiometric dicobalt carbonyl complexes of the alkyne. The original synthesis of the TPDY skeleton took place in five steps involving Negishi cross-coupling to assemble the terphenyl skeleton.²⁷ In designing a TPDY SPAAC reagent, functionality was needed to append any possible tag such as a fluorophore. Consequently, three TPDY derivatives were selected for study: 3,5-TPDY **7.5c**, 2,4-TPDY **7.5a** and 2,6-TPDY **7.5b**. Each derivative places a pendant ester at a different position (R^1 , R^2 and R^3 , **Figure 7.1**) of the central aromatic ring. Starting from the commercially available methyl esters, Miyaura borylation afforded the pinacol borane derivatives **7.2a**, **7.2b** and **7.2c** in good yields (57-92%), albeit derivative **7.2b** likely suffers from steric hindrance. Subsequent Suzuki cross-coupling with commercially available alkyne **7.3** and one-pot desilylation affords each of the terminal alkynes **7.4c** (71 %) and **7.4a** (63 %) in acceptable yields. Alkyne **7.4b** was again obtained in lower yield (34 %) due to steric congestion. Glaser coupling using established conditions afforded the desired macrocyclic diynes in 66-98 % yield. The 3,5-TPDY **7.5c** was isolated as a pale yellow solid that was stable on the benchtop for months. However, the analogous 2,6-TPDY **7.5b** (in which the ester is located in between the two flanking aryl units) and 2,4-TPDY **7.5a** (where the ester is ortho to one of aryl units) were not stable. Following isolation by chromatography, the two diynes afforded pale yellow solutions, however upon concentration, the solids turned black within minutes to an hour. Given the potential of 3,5-TPDY **7.5c**, a streamlined approach for gram scale synthesis was devised (grey insert, **Figure 7.1**). A one pot borylation/cross-coupling/desilylation sequence could

be performed to afford the diyne **7.4c** in 55 % yield. Subsequent Glaser coupling affords 3,5-TPDY **7.5c** in a two-step sequence from commercially available materials. X-Ray crystal analysis of 3,5-TPDY **7.5c** revealed a bond angle between the alkynes of 153.5°, which is reflected in the calculated ring strain energy (22 kcal/mol, calculated using the enthalpies of an isodesmic reaction, **Figure 7.1 bottom**).

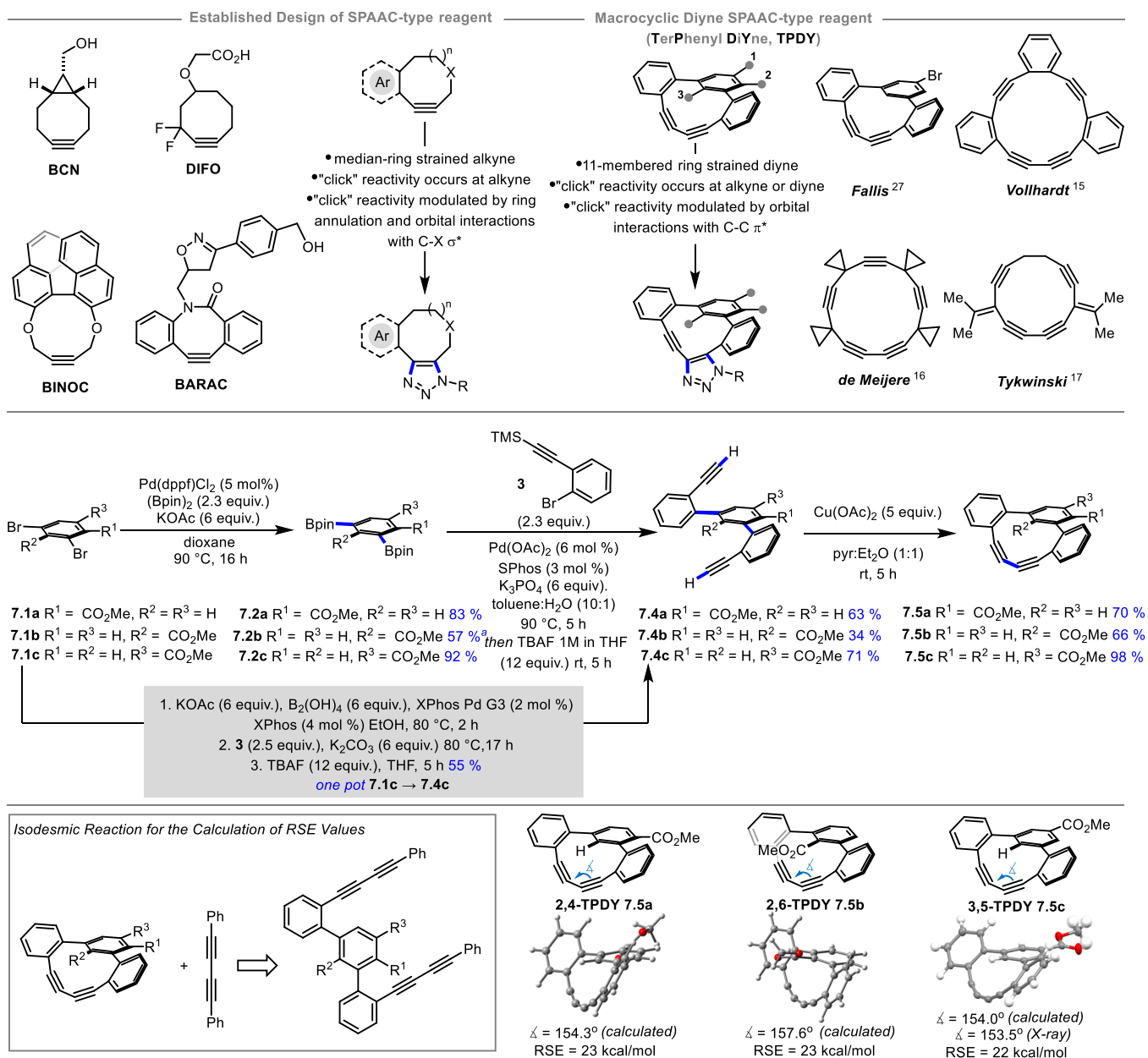


Figure 7.1 top: Comparison of cycloalkynes for SPAAC processes and analogous unexplored macrocyclic diynes. middle: Synthesis of three TPDY macrocycles as candidates for SPAAC.^a

$B_2(\text{pin})_2$ (3 equiv.). *bottom*: Structures of TPDYs and calculated ring strain energy (RSE) (B3LYP-D3/6-31+g(d,p)/SMD(CH_2Cl_2)).

Given the solid state instabilities of 2,4- and 2,6-TPDY, their ground state structures were calculated which suggested bond angles of 154.3° and 157.6° respectively (using a B3LYP-D3/6-31+g(d,p)/SMD (CH_2Cl_2) calculation).²⁹⁻³⁴ Calculation also provided RSE values (23 kcal/mol 2,4-TPDY and 23 kcal/mol 2,6-TPDY) higher than 3,5-TPDY. The RSEs are considerably higher than other heterocycloalkynes previously investigated.²⁸ Despite the differing stabilities, all three TPDY candidates had their reactivity for SPAAC studied via cycloaddition with benzyl azide in CDCl_3 (**Figure 7.2**).

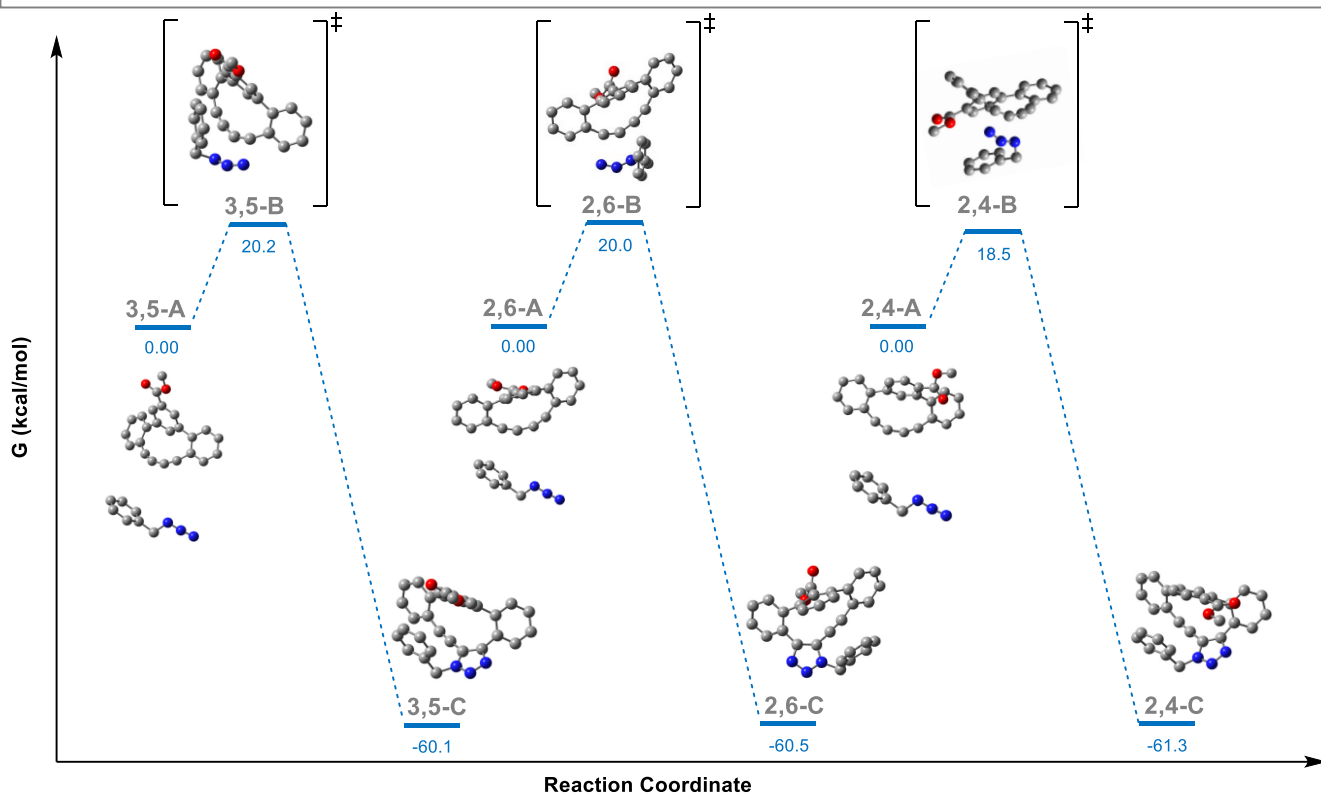
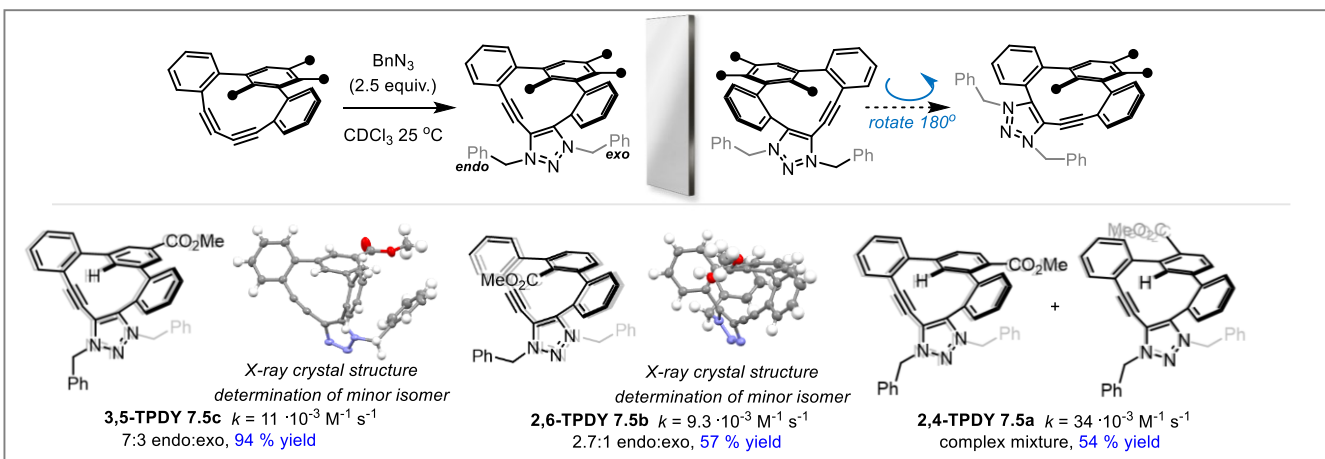


Figure 7.2 *top*: Yields for SPAACs with various TPDYs determined for reactions performed in CH_2Cl_2 with subsequent chromatography. *bottom*: Computed Gibbs energy profile (G at 298.15 K) of the cycloadditions between BnN_3 and TPDYs. Relative Gibbs energies are given in kcal mol^{-1} .

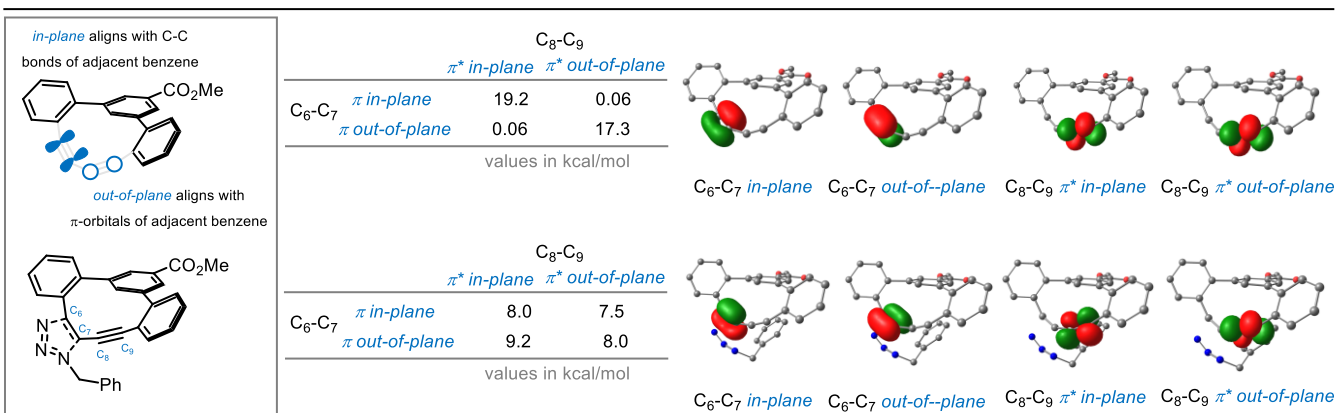


Figure 7.3 Calculated (B3LYP-D3/6-31+g(d,p)/SMD(CH₂Cl₂) NBO³⁵ analysis of orbital interactions for 3,5-TPDY and the SPAAC transition state of 3,5-TPDY and BnN₃.

First, 3,5-TPDY **7.5c** was evaluated and upon reaction with BnN₃, a 7:3 mixture of two regioisomeric triazoles (94 % total yield) were obtained, which differ in whether the benzyl unit is next to the aryl unit (exo) or to the remaining alkyne moiety, (endo). The triazoles could be separated and the minor exo-product was crystallized and had its connectivity confirmed by X-ray crystal analysis. Although 3,5-TPDY **7.5c** is symmetrical, the resulting triazoles are atropisomeric in nature (note **Figure 7.2** shows only one possible atropisomer for each product). A second-order rate constant of $11 \cdot 10^{-3} \text{ M}^{-1}\text{s}^{-1}$ was measured using ¹H NMR kinetic experiments, which is comparable with other cyclooctyne reagents and several orders of magnitude faster than twisted 10-membered cyclic alkyne, BINOC (**Figure 7.1**). The more unstable 2,6- and 2,4-TPDYs **7.5b** and **7.5a** were evaluated in SPAAC immediately following chromatography. As with 3,5-TPDY, the 2,6-TPDY **7.5b** is also symmetrical, and the extension of the CO₂Me unit out over the diyne moiety slightly reduced the diyne bond angle to 157.6°. Upon reaction with BnN₃, a 2.7:1 exo:endo mixture (59 % total yield) of the two regioisomeric triazoles were isolated. An X-ray crystal structure analysis confirmed the connectivity of the minor exo isomer. Unsurprisingly, the second-order rate constant for the SPAAC was measured at $9.3 \cdot 10^{-3} \text{ M}^{-1}\text{s}^{-1}$, again slightly less than 3,5-TPDY. Finally, the unsymmetrical 2,4-TPDY **7.5a** was investigated. Although 2,4-TPDY **7.5a** has a similar diyne bond angle as 3,5-TPDY (154.3° vs, 153.5°), its second-order rate constant for the SPAAC was three times as great ($34 \cdot 10^{-3} \text{ M}^{-1}\text{s}^{-1}$). A 54% yield of all four possible regioisomers was observed, without one particular regioisomer being favored.³⁶ The experimental trends were corroborated with computational analysis (**Figure 7.2, bottom**) of the SPAAC process using a

B3LYP-D3/6-31+g(d,p)/SMD (CH₂Cl₂) calculation similar to that used by others.²⁸ The free energy of the transition state (TS) **3,5-B** in the cycloaddition between 3,5-TPDY and BnN₃ is 20.2 kcal/mol, suggesting facile reaction at room temperature. The overall transformation to cycloadduct **3,5-C** is highly favorable (-60.1 kcal/mol). The second order rate constants for the SPAACs of 3,5-TPDY and 2,6-TPDY were similar and indeed, calculations support that the symmetrical 2,6-TPDY undergoes dipolar cycloaddition via TS **2,6-B** (20.0 kcal/mol) to afford cycloadduct **2,6-C** (-60.5 kcal/mol) with similar energies to those calculated for 3,5-TPDY. The SPAAC reaction with 2,4-TPDY **7.5a** was approximately three times faster than with 3,5-TPDY and 2,6-TPDY. Indeed, computation suggests a TS **2,4-B** that is slightly lower in energy than the other diynes (TS **2,4-B** = 18.5 kcal/mol vs. TS **3,5-B** = 20.2 kcal/mol). Note that the calculated energies of the various TSs correspond with those obtained experimentally from kinetic data (TS **3,5-B** 20.1 experimental, 20.2 calculated, **2,4-B** 19.4 experimental, 18.5 calculated; **2,6-B** 20.2 experimental, 20.0 calculated).

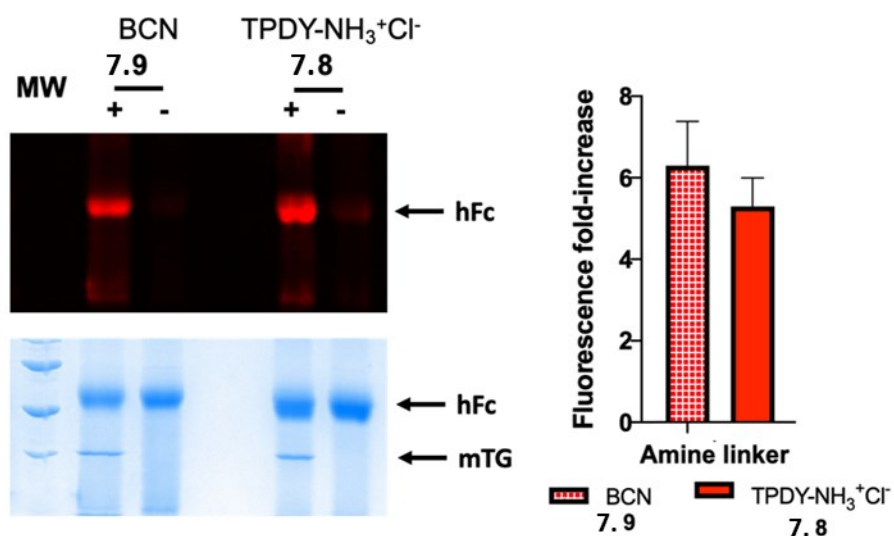
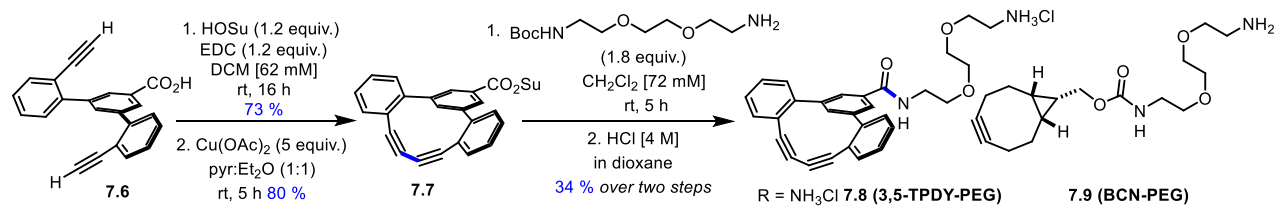


Figure 7.4 *top*: Synthesis of a PEGylated 3,5-TPDY. *bottom*: MTG-mediated conjugation of human crystallizable fragment of IgG1 antibody (hFc). Upper gel image: Fluorescence of sulfo-

Cy-5 (500 ms exposure) Lower gel image: Coomassie stained to confirm equal loading of the protein. MW: molecular weight marker. The presence/absence (+ or -) of mTG is indicated. The bar graph represents fluorescence-fold increase relative to background (no mTG) for each reaction.

The resonance stabilization energies were also calculated for 3,5-TPDY **7.5c** and its respective transition state during cycloaddition with BnN_3 (**Figure 7.3**). In many existing cycloalkyne SPAAC reagents, $\pi \rightarrow \sigma^*$ hyperconjugation of an in-plane π -orbital of the triple bond and σ^* -orbital of an adjacent C-heteroatom bond significantly stabilizes the ground state. In contrast, in the TPDYs, stabilization must occur via interactions of both alkyne units. Indeed, resonance stabilization energy analysis revealed that there is significant stabilization of 3,5-TPDY **7.5c** via both the in-plane and out-of-plane π -orbitals of the $\text{C}_6\text{-C}_7$ alkyne with the corresponding π^* -orbitals of the $\text{C}_8\text{-C}_9$ orbitals. In the SPAAC transition state, geometry distortion is stabilized by both the π out-of-plane and π^* in-plane orbitals, however the stabilization during cycloaddition is much less pronounced.

Applying 3,5-TPDY to protein bioconjugation: To demonstrate the applicability of 3,5-TPDY in protein bioconjugation, an amino derivative was synthesized (**Figure 7.4**). The amino group was inserted to serve as a reactive handle for the enzymatic conjugation to microbial transglutaminase (mTG). mTG can form an amide between an amine and the amide of a protein-bound glutamine sidechain.³⁷⁻³⁸ To ensure recognition of the TPDY-amine by mTG, a moderately hydrophilic PEG spacer was included. The combination of mTG-mediated conjugation and SPAAC represents a versatile platform for procuring labelled proteins.³⁹ Consequently, the water soluble 3,5-TPDY-PEG **7.8** as its ammonium salt was conjugated to the human crystallizable fragment of IgG1 antibody (hFc). The hFc was reacted simultaneously with 3,5-TPDY-PEG **7.8** and sulfo-Cy5-azide fluorophore (**Figure 7.4**). The ammonium salt of 3,5-TPDY-PEG **7.8** was approximately 5-fold more reactive than background. We were pleased that the reactivity of 3,5-TPDY-PEG **7.8** was on the same order of magnitude as the commonly employed bicyclononyne-PEG BCN **7.9** (in its free amine form), confirming the utility of both BCN and TPDY reagents in hFc labelling. Importantly, the mTG-mediated conjugation of hFc was previously demonstrated to be transposable to the full-length trastuzumab IgG1 antibody, promising application of 3,5-TPDY-PEG in antibody conjugation.⁴⁰ As a further demonstration of protein bioconjugation, the labelling reaction was also performed with

the small, well-behaved B domain of protein G (GB1). Once more, the reactivity was on the same order of magnitude as BCN **7.9**.⁴¹

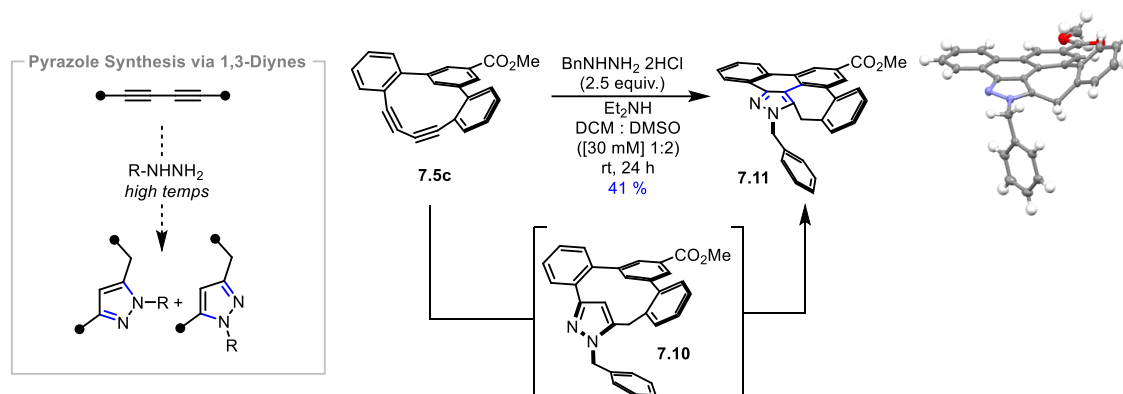


Figure 7.5 Strain promoted diyne hydrazine hydroamination.

Reactivity of TPDYs in Strain Promoted Diyne Hydrazine Hydroamination: The macrocyclic TPDYs offer new possibilities to develop bioconjugation processes in that they are not only strained cycloalkynes, but strained cyclo-1,3-diynes. Diyne building blocks⁴² are valuable synthons for the construction of heterocycles, offering routes to thiophenes,⁴³ furans,⁴⁴⁻⁴⁷ pyrroles,⁴⁸⁻⁴⁹ pyrazoles,⁵⁰⁻⁵¹ and isoxazoles.⁴⁴ Bao reported that heating of 1,3-diynes with NH_2NH_2 in DMSO afforded the corresponding pyrazole, and proposed a mechanism consisting of Cope-type amination and subsequent intramolecular electrophilic addition.⁵² Even if the inherent strain in the TPDY skeleton permitted room temperature reactivity, reaction with substituted hydrazines could produce regioisomeric products (**Figure 7.5**). When 3,5-TPDY **7.5c** was treated with the HCl salt of benzylhydrazine in basic solution, a total consumption of 3,5-TPDY **7.5c** is observed in under 5 minutes at room temperature. Interestingly, the expected pyrazole product **7.10** was observed in trace quantities only. Instead, a 41% yield of a cycloadduct **7.11** was isolated. The unique hexacyclic array appears to result from reaction from the pyrazole ring at the aromatic C-H bond of the central benzene ring of the TPDY skeleton. The rapid kinetics and unique heterocyclic product suggest further development of new opportunities are possible by exploiting the strained 1,3-diyne moiety in biorthogonal chemistries.

7.4 Conclusions

The synthesis of 3 terphenyl diyne (TPDY) macrocycles for SPAAC is reported. Each variant possesses a 1,1':3',1''-terphenyl skeleton with a methyl ester substituent at various positions along the central aromatic ring. 3,5-TPDY **7.5c** was found to be bench stable (months at room temperature, no precautions) despite possessing a highly strained 1,3-diyne motif. A streamlined two-pot synthesis was developed for facile access. Diyne bond angles in the TPDY series rival those observed in typical cyclooctyne reagents. SPAAC with benzylazide produces atropisomeric triazoles whose connectivity was confirmed by X-ray crystal analysis. Second order rate constants were on the order of $10 \cdot 10^{-3} \text{ M}^{-1}\text{s}^{-1}$ and were consistent with computational investigations. The applicability of the 3,5-TPDY derivative for in vitro bioconjugation was exemplified via a MTG mediated labelling to a target protein and subsequent SPAAC with Sulfo-Cy-5 azide. The modular nature and facile synthesis of the TPDY design suggests further applications in biorthogonal chemistries. A high degree of fine tuning is possible that could tailor a TPDY for a specific chemistry: the central aromatic ring could be decorated to improve solubility and/or add valuable tags, while substitution and/or the nature of the outer aromatic rings could affect bond angles, vary HOMO/LUMO levels or alter photophysical properties. In addition, preliminary results demonstrated that the strain energy in the TPDYs afforded a room temperature reaction with benzyldiazine. Interestingly, the cycloadduct obtained was a novel fused hexacyclic pyrazole. Such reactivity emphasizes the prospects for developing new biorthogonal processes that exploit the strained 1,3-diyne moiety.

7.5 References

1. Agard, N. J.; Prescher, J. A.; Bertozzi, C. R., *J. Am. Chem. Soc.* **2004**, *126* (46), 15046-15047.
2. Kolb, H. C.; Finn, M. G.; Sharpless, K. B., *Angew. Chem., Int. Ed.* **2001**, *40* (11), 2004-2021.
3. Li, K.; Fong, D.; Meichsner, E.; Adronov, A., *Chem. - Eur. J.* **2021**, *27* (16), 5057-5073.
4. Patterson, D. M.; Nazarova, L. A.; Prescher, J. A., *ACS Chem. Biol.* **2014**, *9* (3), 592-605.
5. Kim, E.; Koo, H., *Chem. Sci.* **2019**, *10* (34), 7835-7851.
6. Takayama, Y.; Kusamori, K.; Nishikawa, M., *Molecules* **2019**, *24* (1), 172.
7. Nguyen, S. S.; Prescher, J. A., *Nat. Rev. Chem.* **2020**, *4* (9), 476-489.
8. Row, R. D.; Prescher, J. A., *Acc. Chem. Res.* **2018**, *51* (5), 1073-1081.
9. Monzón, D. M.; Betancort, J. M.; Martín, T.; Ramírez, M. Á.; Martín, V. S.; Díaz Díaz, D., *Molecules* **2021**, *26* (6), 1629.
10. Ning, X.; Guo, J.; Wolfert, M. A.; Boons, G. J., *Angew. Chem. Int. Ed. Engl.* **2008**, *47* (12), 2253-5.
11. Jewett, J. C.; Sletten, E. M.; Bertozzi, C. R., *J. Am. Chem. Soc.* **2010**, *132* (11), 3688-3690.
12. Sletten, E. M.; Nakamura, H.; Jewett, J. C.; Bertozzi, C. R., *J. Am. Chem. Soc.* **2010**, *132* (33), 11799-11805.
13. Sletten, E. M.; Bertozzi, C. R., *Angew. Chem., Int. Ed.* **2009**, *48* (38), 6974-6998.
14. Scinto, S. L.; Bilodeau, D. A.; Hincapie, R.; Lee, W.; Nguyen, S. S.; Xu, M.; am Ende, C. W.; Finn, M. G.; Lang, K.; Lin, Q.; Pezacki, J. P.; Prescher, J. A.; Robillard, M. S.; Fox, J. M., *Nat. Rev. Methods Primers* **2021**, *1* (1), 30.
15. Baldwin, K. P.; Matzger, A. J.; Scheiman, D. A.; Tessier, C. A.; Vollhardt, K. P. C.; Youngs, W. J., *Synlett* **1995**, *1995* (12), 1215-1218.
16. Scott, L. T.; Cooney, M. J.; Otte, C.; Puls, C.; Haumann, T.; Boese, R.; Smith, A. B., III; Carroll, P. J.; de Meijere, A., *J. Am. Chem. Soc.* **1994**, *116* (22), 10275-10283.
17. Eisler, S.; McDonald, R.; Loppnow, G. R.; Tykwinski, R. R., *J. Am. Chem. Soc.* **2000**, *122* (29), 6917-6928.
18. Modern Acetylene Chemistry; Stang, P. J., Deiderich, F., Eds.; VCH: Weinheim, 1995.
19. Zhou, Q.; Carroll, P. J.; Swager, T. M., *J. Org. Chem.* **1994**, *59* (6), 1294-1301.

20. Boese, R.; Matzger, A. J.; Vollhardt, K. P. C., *J. Am. Chem. Soc.* **1997**, *119* (8), 2052-2053.
21. Dosa, P. I.; Erben, C.; Iyer, V. S.; Vollhardt, K. P. C.; Wasser, I. M., *J. Am. Chem. Soc.* **1999**, *121* (44), 10430-10431.
22. H. F. Bunz, U.; Rubin, Y.; Tobe, Y., *Chem. Soc. Rev.* **1999**, *28* (2), 107-119.
23. Akhtar, R.; Zahoor, A. F., *Synth. Commun.* **2020**, *50* (22), 3337-3368.
24. Sindhu, K. S.; Anilkumar, G., *RSC Adv.* **2014**, *4* (53), 27867-27887.
25. Hay, A., *J. Org. Chem.* **1960**, *25* (7), 1275-1276.
26. Hay, A. S., *J. Org. Chem.* **1962**, *27* (9), 3320-3321.
27. Collins, S. K.; Yap, G. P. A.; Fallis, A. G., *Org. Lett.* **2002**, *4* (1), 11-14.
28. Danilkina, N. A.; Govdi, A. I.; Khlebnikov, A. F.; Tikhomirov, A. O.; Sharoyko, V. V.; Shtyrov, A. A.; Ryazantsev, M. N.; Bräse, S.; Balova, I. A., *J. Am. Chem. Soc.* **2021**, *143* (40), 16519-16537.
29. Becke, A. D., *J. Chem. Phys.* **1993**, *98* (7), 5648-5652.
30. Becke, A. D., *Phys. Rev. A* **1988**, *38* (6), 3098-3100.
31. Lee, C.; Yang, W.; Parr, R. G., *Phys. Rev. B* **1988**, *37* (2), 785-789.
32. Grimme, S.; Antony, J.; Ehrlich, S.; Krieg, H., *J. Chem. Phys.* **2010**, *132* (15).
33. Grimme, S.; Ehrlich, S.; Goerigk, L., *J. Comput. Chem.* **2011**, *32* (7), 1456-1465.
34. Marenich, A. V.; Cramer, C. J.; Truhlar, D. G., *J. Phys. Chem. B* **2009**, *113* (18), 6378-6396.
35. Glendening, E. D.; Landis, C. R.; Weinhold, F., *J. Comput. Chem.* **2019**, *40* (25), 2234-2241.
36. See Supporting Information for details.
37. Gundersen, M. T.; Keillor, J. W.; Pelletier, J. N., *Appl. Microbiol. Biotechnol.* **2014**, *98* (1), 219-230.
38. Ando, H.; Adachi, M.; Umeda, K.; Matsuura, A.; Nonaka, M.; Uchio, R.; Tanaka, H.; Motoki, M., *Agric. Biol. Chem.* **1989**, *53* (10), 2613-2617.
39. Rachel, N. M.; Toulouse, J. L.; Pelletier, J. N., *Bioconjug. Chem.* **2017**, *28* (10), 2518-2523.
40. Hadjabdelhafid-Parisien, A.; Bitsch, S.; Macarrón Palacios, A.; Deweid, L.; Kolmar, H.; Pelletier, J. N., *RSC Adv.* **2022**, *12* (52), 33510-33515.
41. See Supporting Information for details.
42. Shi, W.; Lei, A., *Tetrahedron Lett.* **2014**, *55* (17), 2763-2772.
43. Kaikawa, T.; Takimiya, K.; Aso, Y.; Otsubo, T., *Org. Lett.* **2000**, *2* (26), 4197-4199.

44. Han, B.; Yang, X.-L.; Wang, C.; Bai, Y.-W.; Pan, T.-C.; Chen, X.; Yu, W., *J. Org. Chem.* **2012**, *77* (2), 1136-1142.
45. Zheng, Q.; Hua, R.; Jiang, J.; Zhang, L., *Tetrahedron* **2014**, *70* (44), 8252-8256.
46. Nun, P.; Dupuy, S.; Gaillard, S.; Poater, A.; Cavallo, L.; Nolan, S. P., *Catal. Sci. Technol.* **2011**, *1* (1), 58-61.
47. Kramer, S.; Madsen, J. L. H.; Rottländer, M.; Skrydstrup, T., *Org. Lett.* **2010**, *12* (12), 2758-2761.
48. Maeda, C.; Yoneda, T.; Aratani, N.; Yoon, M.-C.; Lim, J. M.; Kim, D.; Yoshioka, N.; Osuka, A., *Angew. Chem., Int. Ed.* **2011**, *50* (25), 5691-5694.
49. Lavallo, V.; Frey, G. D.; Donnadieu, B.; Soleilhavoup, M.; Bertrand, G., *Angew. Chem., Int. Ed.* **2008**, *47* (28), 5224-5228.
50. Bassaco, M. M.; Fortes, M. P.; Back, D. F.; Kaufman, T. S.; Silveira, C. C., *RSC Adv.* **2014**, *4* (105), 60785-60797.
51. Wang, L.; Yu, X.; Feng, X.; Bao, M., *Org. Lett.* **2012**, *14* (9), 2418-2421.
52. Wang, L.; Yu, X.; Feng, X.; Bao, M., *J. Org. Chem.* **2013**, *78* (4), 1693-1698.

Chapitre 8 Conclusions et perspectives pour le développement de diynes-1,3 tendus pour la bioconjugaison

8.1 Conclusions

Les réactions de cycloaddition alcyne-azoture promues par la tension (SPAAC) est un sujet en plein expansion. En effet, les chimistes de tous les domaines ont besoin d'avoir à disposition des réactions rapides et efficaces, connues sous le terme de réactions « clicks ». Des dizaines d'alcyne tendus ont vu le jour au cours des deux dernières décennies, constitués majoritairement de cyclooctyne ou d'alcyne cycliques benzoannulés. Le chapitre 7 résume brièvement le développement d'une nouvelle classe d'alcyne tendus pour la réaction de SPAAC, les diynes-1,3 (**Figure 8.1.a**). La molécule **TerPhenyl DiYne (TPDY) 8.1** a été synthétisé en 3 étapes à partir de produits commercialement disponibles. Le corps terphenyl du TPDY permet d'obtenir un cycle à 11 chaînons extrêmement tendu, qui permet de réaliser une cycloaddition avec un rendement élevé avec l'azoture de benzyle à température ambiante pour former les régioisomères du triazole correspondant **8.2**. Bien que très réactif, cette molécule possède aussi une excellente stabilité, ne se dégradant pas lorsque laissée à température ambiante et à l'air libre. Des calculs computationnels ont permis d'estimer l'énergie de l'état de transition pour la SPAAC ($\Delta G^\ddagger = 20,2$ kcal/mol), confirmant la possibilité d'une réaction à température ambiante, avec une constante de vitesse estimée proche de la valeur expérimentale ($k = 11 \cdot 10^{-3} \text{ M}^{-1} \cdot \text{s}^{-1}$). Deux autres régioisomères ont été synthétisés et malgré une efficacité comparable en SPAAC, ils ne sont pas intéressants, du fait de leur faible stabilité. Une version du TPDY possédant un bras aminé a été utilisée pour une application biologique, montrant une efficacité similaire à son analogue BCN, alcyne tendu commercialement disponible le plus utilisé en biologie. Enfin, profitant de la fonction diyne tendue, un couplage avec l'hydrazine benzyle a été effectué, qui a donné le composé hétérocyclique inattendu **8.3**, ce qui constitue une nouvelle réaction bioorthogonale potentielle (SPDH pour *Strain Promoted Diyne-Hydrazine Hydroamination*).

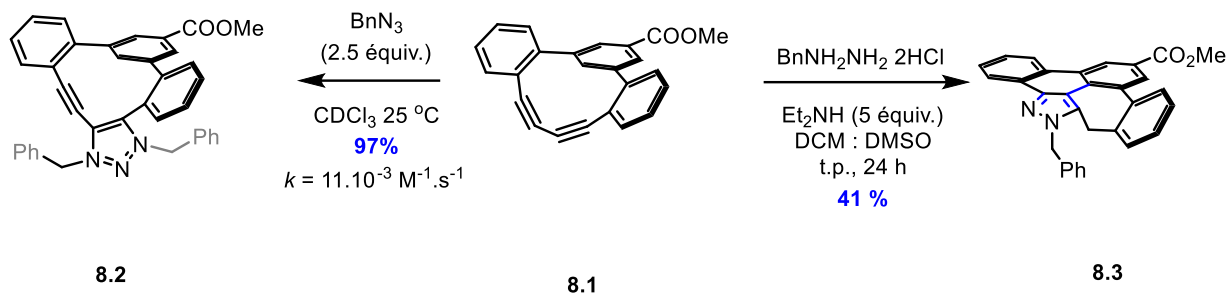


Figure 8.1 Réaction de SPAAC entre le TPDY et l'azoture de benzyle (gauche) et réaction de SPDHC entre le TPDY et l'hydrazine de benzyle (droite).

8.2 Perspectives

8.2.1 Nouvelle génération de diynes tendus

Le développement du 3,5-TPDY a montré l'utilité de ce type de molécules pour des réactions de « clicks » promues par la tension. Cependant, plusieurs points pourraient être améliorés en modifiant la structure du TPDY :

- La solubilité dans l'eau : une grande partie des applications de SPAAC sont dans le domaine de la biologie, donc en conditions aqueuses. Si l'installation d'un bras PEG est venu augmenter le caractère hydrosoluble du TPDY, il reste très limité. Il serait donc intéressant de rajouter des fonctionnalités venant augmenter cette solubilité, comme l'ajout de groupements méthoxyles sur les phényles (**8.4**),¹ ou l'utilisation d'une pyridine qui pourra être attachée à un espaceur pour former un sel pyridinium (**8.5**) (**Figure 8.2**).²
- La réactivité de la SPAAC : plusieurs travaux ont montré l'augmentation de la vitesse de cycloaddition par la présence d'hétérocycles adjacents à l'alcyne, par stabilisation de l'état de transition ou par effet directeur³. L'insertion d'une pyridine (**8.6**) à côté des deux alcynes pourrait venir augmenter la constante de vitesse de SPAAC pour se rapprocher des cyclooctynes les plus réactives (**Figure 8.2**).
- La fluorescence du TPDY : en effet, l'une des utilisations majeures de la SPAAC en biologie est de coupler une protéine d'intérêt à un fluorophore, application réalisée dans le

chapitre 7. Un avantage considérable serait que le triazole résultant de la SPAAC soit émissif, rendant obsolète l'utilisation d'un fluorophore externe. Au vu des nombreux aromatiques du TPDYs, on peut faire l'hypothèse que l'incorporation de groupements connus pour être émissifs, comme les thiophènes par exemple,⁴ pourrait donner des propriétés lumineuses intéressantes (**Figure 8.2**)

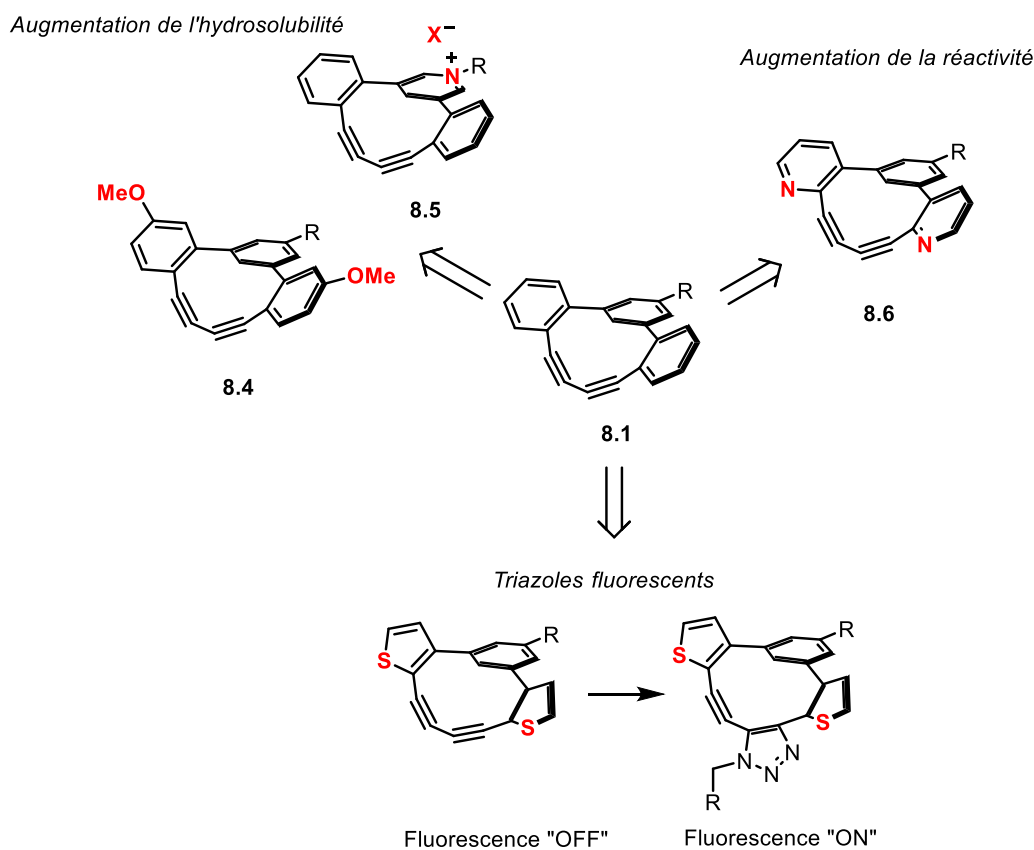


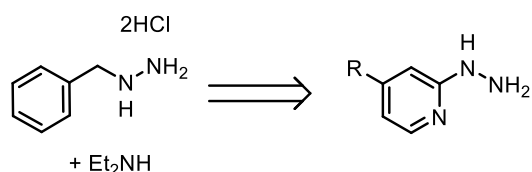
Figure 8.2 Nouvelles générations de TPDY possibles

8.2.2 Développement de la SPDHH

Des résultats prometteurs ont été obtenus pour la cycloaddition diyne-hydrazone promue par la tension. L'intérêt serait maintenant de développer une méthode plus efficace et plus générale, tout en étudiant son mécanisme de formation. En effet, si le TPDY est rapidement consommé, la vitesse de formation du pyrazole **8.3** semble plus lente et de nombreux autres sous-produits se forment, montrant plusieurs voies mécanistiques possibles. Des résultats

préliminaires montrent un potentiel intéressant pour la 2-pyridine hydrazine, qui serait un motif de base intéressant à explorer (**Figure 8.3.a**). Modifier la structure du TPDY pourrait aussi nous donner des informations sur cette réaction, en bloquant la position en para de l'ester méthylique, ou en le remplaçant par un groupement non-électroattracteur (**Figure 8.3.b**).

a) Modification de l'hydrazine



b) Modification du diyne

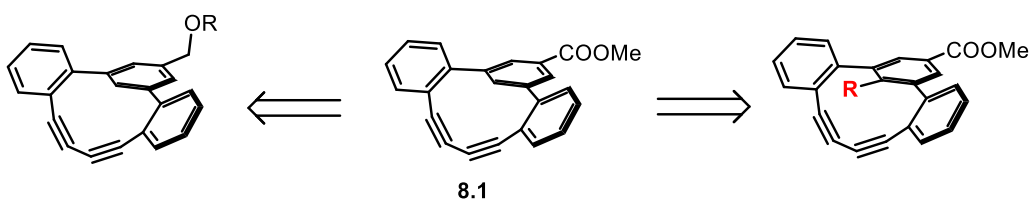


Figure 8.3 Perspectives de modifications de la structure de l'hydrazine et du TPDY pour améliorer la SPDHH

Les résultats prometteurs de la première génération de diyne tendus ouvrent maintenant la porte à une multitude de projets à fort potentiel pour des collaborations multidisciplinaires.

8.2.3 Références bibliographiques

1. Tummatorn, J.; Batsomboon, P.; Clark, R. J.; Alabugin, I. V.; Dudley, G. B., *J. Org. Chem.* **2012**, *77* (5), 2093-2097.
2. Marek, J.; Stodulka, P.; Cabal, J.; Soukup, O.; Pohanka, M.; Korabecny, J.; Musilek, K.; Kuca, K., *Molecules* **2010**, *15* (3), 1967-1972.
3. Danilkina, N. A.; Govdi, A. I.; Khlebnikov, A. F.; Tikhomirov, A. O.; Sharoyko, V. V.; Shtyrov, A. A.; Ryazantsev, M. N.; Bräse, S.; Balova, I. A., *J. Am. Chem. Soc.* **2021**, *143* (40), 16519-16537.

4. Rasmussen, S. C.; Evenson, S. J.; McCausland, C. B., *Chem. Commun.* **2015**, 51 (22), 4528-4543.

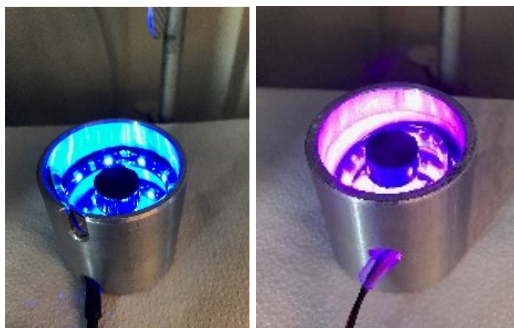
Annexe 1 – Supporting information of Chapter 2

A1.1 - General

All chemical products were obtained from *MiliporeSigma*, *Alfa Aesar* or *Oakwood Chemicals* and were reagent quality. For the bisphosphine ligands these include: bis[(2-diphenylphosphino)phenyl] ether (DPEPhos), 4,5-bis(diphenylphosphino)9,9-dimethylxanthene (XantPhos) and (±)-2,2'-bis(diphenylphosphino)-1,1'-binaphthalene (BINAP). The diimine ligands were derived from commercial sources of 2,9-dimethyl-1,10-phenanthroline (dmp) or its chlorhydric acid (HCl) and aqueous salts. Technical solvents were obtained from *Fisher Scientific* or *VWR International Co.* Anhydrous solvents (CH₂Cl₂, Et₂O, THF, DMF, toluene) were dried and deoxygenated using a *Seca* system from *GlassContour* on a alumina column under an argon atmosphere (Irvine, CA). All reactions that were carried out under anhydrous conditions were performed under an inert argon or nitrogen atmosphere in glassware that had previously been dried at least 15 h at 110-140 °C or had been flame dried and cooled under a stream of argon or nitrogen.

Photocatalysis

All the Appel-type and triplet energy transfer (TET) reactions were performed in 1 dram vials (5 dram for proton-coupled coupled electron transfer, PCET) that were placed in the center of an aluminum cylinder the interior of which was lined with a light-emitting diode (LED) strip connected to a power source. The reactions media were thoroughly purged under a nitrogen stream prior to irradiation. LED strips were purchased from *Creative Lightings* (<https://www.creativelightings.com/>). Reactions that ran under purple light were put under a motored fan cooling system.



Blue LED strips (up left): <https://www.creativelightings.com/LED-Ribbon-Flexible-Strips-12v-Blue-5M-Spool-p/cl-frs1210wp-5m-12v-bl.htm>; Purple LED strips (up right): <http://www.creativelightings.com/Purple-UV-LED-Flex-Strips-12vdc-WP-300-Meter-p/cl-frs5050wpdd-5m-12v-uv.htm>

Chromatography

Isolated yields reflect the mass obtained following flash column silica gel chromatography. Organic compounds were purified using the method reported by W. C. Still¹ and using silica gel obtained from *Silicycle Chemical Division* (40-63 nm; 230-240 mesh). Analytical thin-layer chromatography (TLC) was performed on glass-backed silica gel 60 coated with a fluorescence indicator (*Silicycle Chemical division*, 0.25 mm, F₂₅₄). Visualization of TLC plate was performed by UV (254 nm), KMnO_{4(aq)} or *p*-anisaldehyde stains. All mixed solvent eluents are reported as v/v solutions. Concentration refers to removal of volatiles at low pressure on a rotary evaporator. All reported compounds were homogeneous by thin layer chromatography (TLC).

Nuclear Magnetic Resonance Spectroscopy (NMR)

All ¹H NMR. NMR spectra were taken in deuterated CDCl₃ using Bruker AV-300 and AV-400 instruments unless otherwise noted. Signals due to the solvent served as the internal standard (CHCl₃: δ 7.27 for ¹H, δ 77.0 for ¹³C). The ¹H NMR chemical shifts (δ) and coupling constants (*J*) are given on parts per million (ppm) and hertz (Hz) respectively. They both were determined assuming first-order behavior. Multiplicity is indicated by one or more of the following: s (singlet), d (doublet), t (triplet), q (quartet), m (multiplet), br (broad); the list of couplings constants (*J*) corresponds to the order of the multiplicity assignment.

High Resolution Mass Spectroscopy (HRMS)

Every analysis were carried out by the *Centre régional de spectrométrie de masse* at the Département de Chimie, Université de Montréal from an *Agilent* LC-MSD TOF system using electron-spray mode of ionization (ESI) unless otherwise noted.

Absorbance and Fluorimetric data

Absorbance UV-Vis spectra were recorded with a *Varian Cary 5000* UV-Vis-NIR spectrophotometer in a quartz cuvette. Emission spectra were recorded with a *Varian Cary Eclipse* fluorescence spectrophotometer/fluorometer in a quartz cuvette.

Lifetime data

Lifetime measurements were done with an *Edinburgh Instruments FLS-920* fluorimeter with an EPL 375 laser (excitation wavelength = 375 nm).

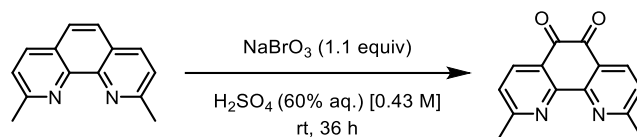
Electrochemistry

Cyclic voltammetry measurements were done in dry acetonitrile (MeCN) with tetra-*N*-butylammonium hexafluorophosphate (TBAPF₆) as the supporting electrolyte using a standard three-electrode cell consisting of a silver wire pseudo-reference electrode, a platinum wire counter electrode and a platinum working electrode with a *BioLogic SP-50* potentiostat. The solutions were degassed with a flow of argon for 5 minutes prior to the measurements, which was left over the surface of the solution during the measurements. All measurements were carried out at 22 °C. All potentials were reported to the mid-point potential of the ferrocene/ferrocenium (Fc/Fc⁺) redox couple which was determined in the aforementioned electrolyte.

A1.2 - Experimental Procedures and Characterization Data

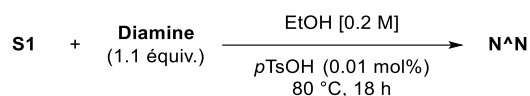
General Comments/Procedures for Ligands:

Procedure A

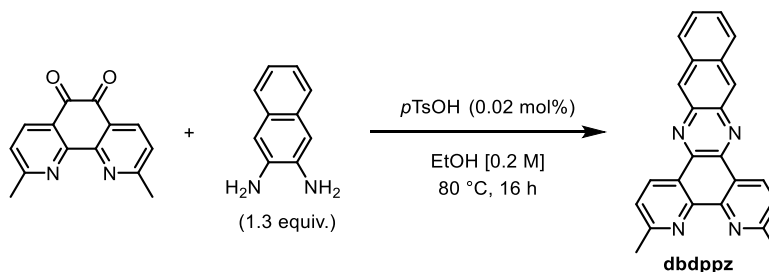


1,10-Phenanthroline-5,6-dione (S1): Following a slightly modified procedure² 2,9-dimethyl-1,10-phenanthroline (2.00 g, 9.6 mmol) was dissolved in H₂SO₄(60% aq.) (22.3 mL) at room temperature. NaBrO₃ (1.26 g, 10.6 mmol) was then added portion wise over 30 min. The orange solution was then stirred for 36 h. The mixture was then poured over ice and neutralized under intense stirring, using KHCO₃(sat). Spectroscopic data were consistent with what was previously reported.

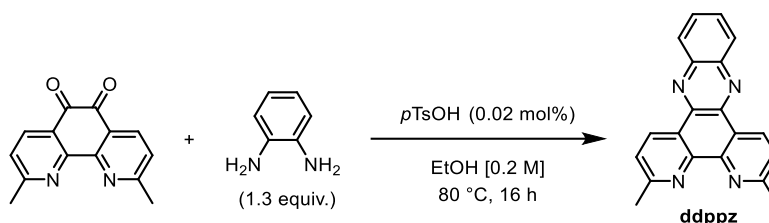
General Procedure For Preparing Ligands from Dione S1.



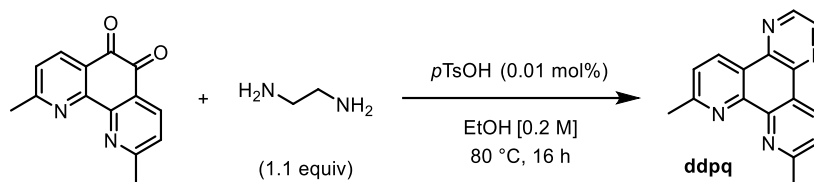
The compound **S1** (1.0 equiv), the diamine (1.1 equiv.) and *p*-toluenesulfonic acid (0.01 mol %) were all dissolved in EtOH (0.2 M). The solution was then refluxed. The conversion of the starting material was followed by TLC. Upon completion of the reaction, the solution was cooled to room temperature before being filtered. The desired product was washed with cold EtOH prior to be collected. Finally, recrystallisation in EtOH or column chromatography (using 15 to 30% EtOAc and *n*-hexanes) afforded the pure desired ligand. Spectroscopic data were in accordance with previously reported literature.³



3,6-Dimethylbenzo[*i*]dipyrido[3,2-*a*:2',3'-*c*]phenazine (dbdppz): Following the general procedure, the dione **S1** (400 mg, 1.0 equiv), 2,3-diaminonaphthalene (356 mg, 1.3 equiv.) and *p*-toluenesulfonic acid (5.78 mg, 0.02 mol%) were all dissolved in EtOH (8.4 mL, 0.2 M). The solution was then refluxed for 18 h. The conversion of the starting material was followed by TLC. The solution was cooled down to room temperature and then filtered and washed with cold EtOH. Recrystallisation in EtOH afforded the pure desired product as a dark brown crystalline solid (494 mg, 82 %). Spectroscopic data were in accordance with previously reported literature.²



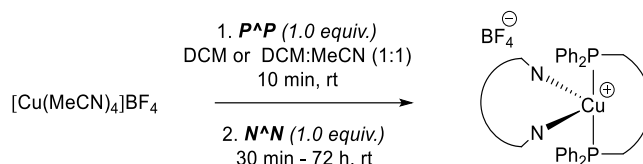
3,6-Dimethyldipyrido[3,2-*a*:2',3'-*c*]phenazine (ddppz): Following the general procedure, dione **S1** (1.05 g, 1.0 equiv), 1,2-phenylenediamine (533 mg, 1.1 equiv.) and *p*-toluenesulfonic acid (7.6 mg, 0.01 mol%) were dissolved in EtOH (22 mL, 0.2 M). The solution was then refluxed. After ~30 seconds, precipitation occurred. More EtOH (10 mL) was then added in order to allow stirring to continue for 48 h. The conversion of the starting material was followed by TLC. The solution was then cooled to room temperature and then filtered and washed with cold EtOH. Finally, recrystallization in EtOH afforded the pure desired product as a white solid (384 mg, 28 %). Spectroscopic data were in accordance with previously reported literature.⁴



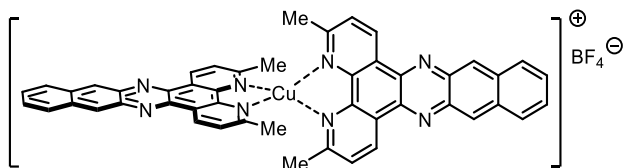
3,6-Dimethyl-dipyrido[3,2-*f*:2',3'-*h*]-quinoxaline (ddpq): Following the general procedure C, **2.1** (1.42 g, 1.0 equiv), ethylenediamine (598 μ L, 1.5 equiv.) and *p*-toluenesulfonic acid (10.2 mg, 0.01 mol%) were dissolved in EtOH (30 mL, 0.2 M). The solution was then refluxed, and conversion of

the starting material was followed by TLC. After 2 h, the solution was cooled to room temperature, filtered and the solid washed with cold EtOH. Recrystallisation in EtOH afforded the pure desired product as a white solid (1.55 g, 75 %). Spectroscopic data were in accordance with previously reported literature.⁴

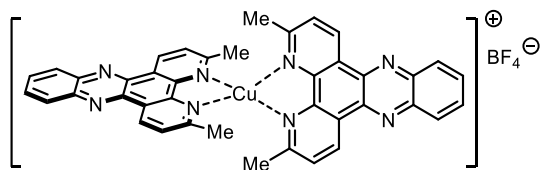
General Procedure for the Synthesis of Copper Complexes:



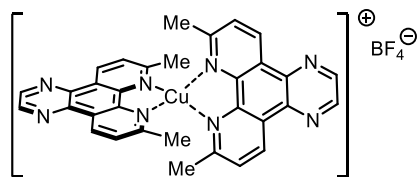
To a stirred solution of $\text{Cu}(\text{MeCN})_4\text{BF}_4$ (1.0 equiv.) in anhydrous and degassed CH_2Cl_2 (0.005 M) was added the corresponding bisphosphine (1.0 equiv.). The reaction was stirred at room temperature for 10 min. Then, to the reaction mixture was added the corresponding diimine (1.0 equiv.). The reaction mixture was stirred until complete dissolution of the diimine. The reaction mixture was concentrated under vacuum until a few mL of solution remains. Then, Et_2O was added in one portion to precipitate the product. Filtration afforded the desired complex as a coloured solid.



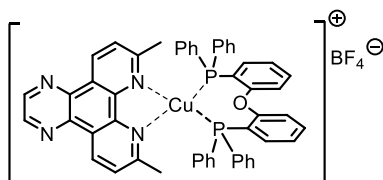
$\text{Cu}(\text{dbdppz})_2\text{BF}_4$: Following the general procedure, $\text{Cu}(\text{MeCN})_4\text{BF}_4$ (25 mg, 0.08 mmol, 1 equiv.) and **dbdppz** (57.6 mg, 0.16 mmol, 2.0 equiv.) were dissolved in anhydrous and degassed CH_2Cl_2 . After complete dissolution of the solids the reaction mixture was stirred for three hours prior to concentration. The desired product was obtained by filtration as a brown solid (57 mg, 82 %). **$^1\text{H NMR}$** (400 MHz, CDCl_3) δ = 9.79 (d, J = 8.1 Hz, 4H), 9.06 (s, 4H), 8.27 (m, 4H), 8.01 (d, J = 8.2 Hz, 4H), 7.70 (m, 4H), 2.61 (s, 12 H); **$^{13}\text{C NMR}$** (176 MHz, CDCl_3) δ = 160.0, 145.8, 140.8, 139.0, 135.2, 135.0, 128.7, 128.2, 127.6, 127.4, 127.0, 26.1 ; **HRMS** (ESI) m/z calculated for $\text{C}_{48}\text{H}_{32}\text{CuN}_8$ $[\text{M}]^+$ 783.2040 found 783.2038; **HRMS** (ESI) m/z calculated for BF_4 $[\text{M}]^-$ 87.0035 found 87.0041.



Cu(ddppz)₂BF₄: Following the general procedure, Cu(MeCN)₄BF₄ (25 mg, 0.08 mmol, 1 equiv.) and **ddppz** (52 mg, 0.16 mmol, 2.0 equiv.) were dissolved in anhydrous and degassed CH₂Cl₂. After complete dissolution of the solids the reaction mixture was stirred for one hour prior to concentration. The desired product was obtained by filtration as a dark orange solid (66 mg, 99 %). **¹H NMR** (700 MHz, CDCl₃) δ = 9.81 (d, *J* = 8.2 Hz, 2H), 8.47 (dd, *J* = 6.4, 3.4 Hz, 2H), 8.03 (m, 4H), 2.59 (s, 6H); **¹³C NMR** (176 MHz, CDCl₃) δ = 160.0, 145.3, 142.8, 139.9, 135.1, 131.5, 129.8, 127.0, 126.8, 26.1; **HRMS** (ESI) *m/z* calculated for C₄₀H₂₈CuN₈ [M]⁺ 683.1728 found 683.1741; **HRMS** (ESI) *m/z* calculated for BF₄ [M]⁻ 87.0035 found 87.0035.

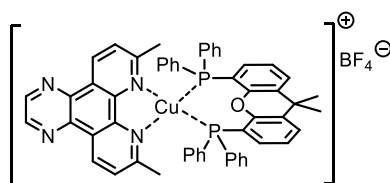


Cu(ddpq)₂BF₄: Following the general procedure, Cu(MeCN)₄BF₄ (25 mg, 0.08 mmol, 1 equiv.) and **ddpq** (42 mg, 0.16 mmol, 2.0 equiv.) were dissolved in anhydrous and degassed CH₂Cl₂. After complete dissolution of the solids the reaction mixture was stirred for one hour prior to concentration. The desired product was obtained by filtration as dark orange solid (42 mg, 78 %). **¹H NMR** (700 MHz, CDCl₃) δ = 9.65 (d, *J* = 8.2 Hz, 2H), 9.14 (s, 2H), 8.00 (d, *J* = 8.2 Hz, 2H), 2.56 (s, 6H); **¹³C NMR** (176 MHz, CDCl₃) δ = 159.9, 145.4, 144.3, 139.6, 134.6, 126.7, 126.5 26.1; **HRMS** (ESI) *m/z* calculated for C₃₂H₂₄CuN₈ [M]⁺ 583.1414 found 583.1422; **HRMS** (ESI) *m/z* calculated for BF₄ [M]⁻ 87.0035 found 87.0035.

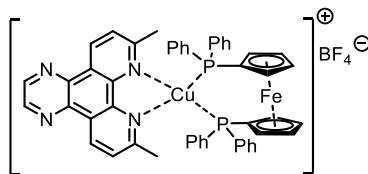


Cu(ddpq)(DPEPhos)BF₄ Following the general procedure, Cu(MeCN)₄BF₄ (25 mg, 0.08 mmol, 1 equiv.) and **DPEPhos** (45.2 mg, 0.08 mmol, 1.0 equiv.) were dissolved in anhydrous and

degassed CH_2Cl_2 . After complete dissolution of the solids, **ddpq** (21 mg, 0.08 mmol, 1.0 equiv.) was added. The reaction mixture was stirred for one hour prior to concentration. The desired product was obtained by filtration as a yellow solid (64 mg, 84 %). $^1\text{H NMR}$ (700 MHz, CDCl_3) δ = 9.52 (d, J = 8.3 Hz, 2H), 9.08 (s, 2H), 9.52 (d, J = 8.3 Hz, 2H), 7.81 (d, J = 8.3 Hz, 2H), 7.36 (m, 2H), 7.20 (m, 8H), 7.06 (t, J = 7.4 Hz, 8H), 6.99 (m, 10H), 2.53 (s, 6H); $^{13}\text{C NMR}$ (176 MHz, CDCl_3) δ = 161.2, 158.2, 145.5, 144.3, 139.0, 134.9, 133.8, 132.8 (t, J = 7.8 Hz), 132.4, 131.5 (t, J = 16.7 Hz), 130.0, 128.7 (t, J = 4.68 Hz) 126.7, 126.2, 125.4, 120.1, 27.2; **HRMS** (ESI) m/z calculated for $\text{C}_{52}\text{H}_{40}\text{CuN}_4\text{OP}_2$ $[\text{M}]^+$ 861.1968 found 861.1970; **HRMS** (ESI) m/z calculated for BF_4 $[\text{M}]^-$ 87.0035 found 87.0039.

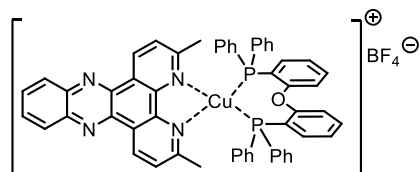


Cu(ddpq)(XantPhos)BF₄: Following the general procedure, $\text{Cu}(\text{MeCN})_4\text{BF}_4$ (25 mg, 0.08 mmol, 1 equiv.) and **XantPhos** (48.6 mg, 0.08 mmol, 1.0 equiv.) were dissolved in anhydrous and degassed CH_2Cl_2 . After complete dissolution of the solids, **ddpq** (21 mg, 0.08 mmol, 1.0 equiv.) was added. The reaction mixture was stirred for one hour prior to concentration. The desired product was obtained by filtration as a yellow solid (67 mg, 85 %). NMR data were in accordance with what was previously reported.^{3b} **HRMS** (ESI) m/z calculated for $\text{C}_{55}\text{H}_{44}\text{CuN}_4\text{OP}_2$ $[\text{M}]^+$ 901.2281 found 901.2286; **HRMS** (ESI) m/z calculated for BF_4 $[\text{M}]^-$ 87.0035 found 87.0036.

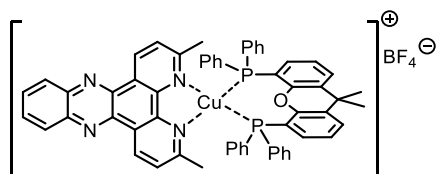


Cu(ddpq)(dppf)BF₄: Following the general procedure, $\text{Cu}(\text{MeCN})_4\text{BF}_4$ (25 mg, 0.08 mmol, 1 equiv.) and **dppf** (46.6 mg, 0.08 mmol, 1.0 equiv.) were dissolved in anhydrous and degassed CH_2Cl_2 (16 mL). After complete dissolution of the solids, **ddpq** (21 mg, 0.08 mmol, 1.0 equiv.) was added. The reaction mixture was stirred for one hour prior to concentration. The desired product was obtained by filtration as a yellow solid (70 mg, 91 %). $^1\text{H NMR}$ (700 MHz, CDCl_3) δ = 9.75 (d, J = 8.3

Hz, 2H), 9.25 (s, 2H), 7.86 (d, $J = 8.3$ Hz, 2H), 7.39 (m, 7H), 4.91 (s, 4H), 4.78 (s, 4H), 2.51 (s, 6H); ^{13}C NMR (176 MHz, CDCl_3) $\delta = 161.6, 145.7, 144.3, 139.3, 135.2, 133.7$ (t, $J = 15.2$ Hz), 132.2 (t, $J = 7.46$ Hz), 130.2, 128.8 (t, $J = 4.5$ Hz), 126.8, 126.7 (d, $J = 10.6$ Hz), 74.9 (t, $J = 5.4$ Hz), 72.9 (t, $J = 2.4$ Hz), 27.7; **HRMS** (ESI) m/z calculated for $\text{C}_{50}\text{H}_{40}\text{CuFeN}_4\text{P}_2$ $[\text{M}]^+$ 877.1368 found 877.1362; **HRMS** (ESI) m/z calculated for BF_4 $[\text{M}]^-$ 87.0035 found 87.0047.

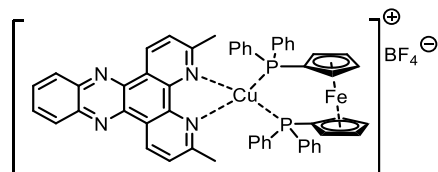


Cu(ddppz)(DPEPhos)BF₄: Following the general procedure, $\text{Cu}(\text{MeCN})_4\text{BF}_4$ (25 mg, 0.08 mmol, 1 equiv.) and **DPEPhos** (45.2 mg, 0.08 mmol, 1.0 equiv.) were dissolved in anhydrous and degassed CH_2Cl_2 . After complete dissolution of the solids, **ddppz** (26 mg, 0.08 mmol, 1.0 equiv.) was added. The reaction mixture was stirred for one hour prior to concentration. The desired product was obtained by filtration as a yellow solid (62 mg, 78 %). ^1H NMR (400 MHz, CDCl_3) $\delta = 9.67$ (d, $J = 8.3$ Hz, 2H), 8.40 (dd, $J = 6.2, 3.2$ Hz, 2H), 8.00 (m, 2H), 7.83 (d, $J = 8.2$ Hz, 2H), 7.37 (m, 2H), 7.21 (m, 7H), 7.08 (dd, $J = 7.4$ Hz, 8H), 7.01 (m, 10H), 2.53 (s, 6H); ^{13}C NMR (176 MHz, CDCl_3) $\delta = 161.3, 158.3$ (t, $J = 6.0$ Hz), 145.3, 142.8, 139.3, 135.4, 133.8, 132.8 (t, $J = 7.8$ Hz), 132.4, 131.6, 131.5 (t, $J = 8.0$ Hz), 130.0, 129.7, 128.7 (t, $J = 4.6$ Hz), 126.8, 126.7, 125.4, 120.2, 27.2; **HRMS** (ESI) m/z calculated for $\text{C}_{56}\text{H}_{42}\text{CuN}_4\text{OP}_2$ $[\text{M}]^+$ 911.2124 found 911.2114; **HRMS** (ESI) m/z calculated for BF_4 $[\text{M}]^-$ 87.0035 found 87.0044.

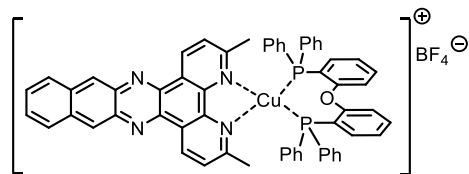


Cu(ddppz)(XantPhos)BF₄: Following the general procedure, $\text{Cu}(\text{MeCN})_4\text{BF}_4$ (50 mg, 0.16 mmol, 1 equiv.) and **XantPhos** (97.2 mg, 0.16 mmol, 1.0 equiv.) were dissolved in anhydrous and degassed CH_2Cl_2 . After complete dissolution of the solids, **ddppz** (52 mg, 0.16 mmol, 1.0 equiv.)

was added. The reaction mixture was stirred for one hour prior to concentration. The desired product was obtained by filtration as a bright yellow solid (152 mg, 91 %). NMR data was in accordance with what was previously reported.^{3b} **HRMS** (ESI) m/z calculated for $C_{59}H_{46}CuN_4OP_2$ $[M]^+$ 951.2413 found 951.2437; **HRMS** (ESI) m/z calculated for BF_4 $[M]^-$ 86.0075 found 86.0065.

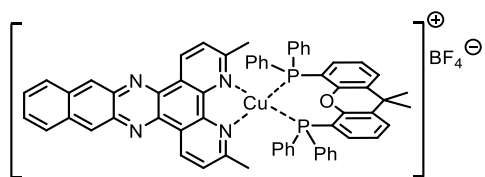


Cu(ddppz)(dppf)BF₄: Following the general procedure, $Cu(MeCN)_4BF_4$ (25 mg, 0.08 mmol, 1 equiv.) and **dppf** (46.6 mg, 0.08 mmol, 1.0 equiv.) were dissolved in anhydrous and degassed CH_2Cl_2 . After complete dissolution of the solids, **ddppz** (26 mg, 0.08 mmol, 1.0 equiv.) was added. The reaction mixture was stirred for one hour prior to concentration. The desired product was obtained by filtration as an orange solid (64 mg, 79%). **¹H NMR** (700 MHz, $CDCl_3$) δ = 9.80 (d, J = 8.3 Hz, 2H); 8.45 (dd, J = 6.5, 3.5 Hz, 2H), 8.03 (dd, J = 6.3, 3.3 Hz, 2H), 7.77 (d, J = 8.0 Hz, 2H), 7.32 (dd J = 7.0, 4H), 7.19 (m, 16H), 4.81 (s, 4H), 4.69 (s, 4H), 2.42 (s, 6H); **¹³C NMR** (176 MHz, $CDCl_3$) δ = 161.62, 145.25 (t, J = 2.0 Hz), 142.97, 139.52, 135.70, 133.76, 133.67, 133.59, 132.18 (t, J = 7.3 Hz), 131.65, 130.20, 129.75, 128.84 (t, J = 4.6 Hz), 127.22, 126.88, 74.91 (t, 5.9 Hz), 72.92 (t, 2.60 Hz), 27.69; **HRMS** (ESI) m/z calculated for $C_{54}H_{42}CuFeN_4P_2$ $[M]^+$ 927.1553 found 927.1550; **HRMS** (ESI) m/z calculated for BF_4 $[M]^-$ 87.0035 found 87.0047.

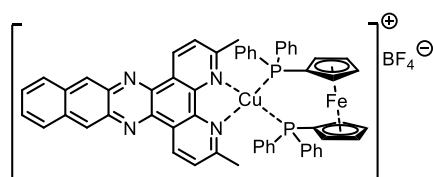


Cu(dbdppz)(DPEPhos)BF₄ Following the general procedure, $Cu(MeCN)_4BF_4$ (25 mg, 0.08 mmol, 1 equiv.) and **DPEPhos** (45.2 mg, 0.08 mmol, 1.0 equiv.) were dissolved in anhydrous and degassed CH_2Cl_2 . After complete dissolution of the solids, **dbdppz** (28.8 mg, 0.08 mmol, 1.0 equiv.) was added. The reaction mixture was stirred for three hours prior to concentration. The

desired product was obtained by filtration as a yellow solid (65 mg, 77 %). $^1\text{H NMR}$ (700 MHz, CDCl_3) δ = 9.66 (d, J = 7.9 Hz, 2H), 9.00 (s, 2H), 8.23 (s, 2H), 7.81 (d, J = 7.9 Hz, 2H), 7.66 (d, J = 3.8 Hz, 2H), 7.37 (dd, J = 7.1 Hz, 2H), 7.20 (m, 5H), 7.04 (m, 23H), 2.53 (s, 6H); $^{13}\text{C NMR}$ (176 MHz, CDCl_3) δ = 161.4, 158.3 (t, J = 6.0 Hz), 145.8, 140.2, 139.0, 135.5, 134.9, 133.8, 132.9 (t, J = 7.8 Hz), 132.4, 131.5 (t, J = 16 Hz), 130.1, 128.8 (t, J = 4.6 Hz), 128.7, 128.1, 127.6, 127.0 (d, J = 5.4 Hz), 125.4, 120.1, 27.2; **HRMS** (ESI) m/z calculated for $\text{C}_{60}\text{H}_{44}\text{CuN}_4\text{OP}_2$ $[\text{M}]^+$ 961.2281 found 961.2283; **HRMS** (ESI) m/z calculated for BF_4 $[\text{M}]^-$ 87.0035 found 87.0043.

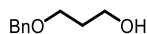


Cu(dbdppz)(XantPhos)BF₄ Following the general procedure, $\text{Cu}(\text{MeCN})_4\text{BF}_4$ (25 mg, 0.08 mmol, 1 equiv.) and **XantPhos** (48.6 mg, 0.08 mmol, 1.0 equiv.) were dissolved in anhydrous and degassed CH_2Cl_2 . After complete dissolution of the solids, **dbdppz** (28.8 mg, 0.08 mmol, 1.0 equiv.) was added. The reaction mixture was stirred for one hour prior to concentration. The desired product was then collected by filtration. It was then purified by liquid diffusion of Et_2O through a minimum amount of CH_2Cl_2 to afford as a brownish solid (44 mg, 50 %). $^1\text{H NMR}$ (700 MHz, CDCl_3) δ = 9.60 (d, J = 7.9 Hz, 2H), 9.00 (s, 2H), 8.24 (dd, J = 6.28, 3.1 Hz, 2H), 7.76 (d, J = 8.2 Hz, 2H), 7.68 (m, 4H), 7.23 (dd, J = 7.7 Hz, 2H), 7.17 (dd, J = 7.3 Hz, 4H), 7.11 (m, 8H), 7.06 (dd, J = 7.5, 7.5 Hz, 8H), 6.98 (m, 2H), 2.35 (s, 6H), 1.77 (s, 6H); $^{13}\text{C NMR}$ (176 MHz, CDCl_3) δ = 160.9, 155.1 (t, J = 6.7 Hz), 145.6, 140.4, 139.1, 135.6, 135.0, 133.9, 133.1 (t, J = 7.64 Hz), 131.4 (t, J = 16 Hz), 130.5, 130.2, 129.0 (t, J = 4.6 Hz), 128.8, 128.3, 127.9, 127.8, 127.2, 126.8, 125.7, 121.4 (t, J = 13.7 Hz), 36.3, 28.8, 27.4; **HRMS** (ESI) m/z calculated for $\text{C}_{63}\text{H}_{48}\text{CuN}_4\text{OP}_2$ $[\text{M}]^+$ 1001.2594 found 1001.2566; **HRMS** (ESI) m/z calculated for BF_4 $[\text{M}]^-$ 87.0035 found 86.0063.



Cu(dbdppz)(dppf)]BF₄ Following the general procedure, Cu(MeCN)₄BF₄ (25 mg, 0.08 mmol, 1 equiv.) and **dppf** (46.6 mg, 0.08 mmol, 1.0 equiv.) were dissolved in anhydrous and degassed CH₂Cl₂. After complete dissolution of the solids, **dbdppz** (28.8 mg, 0.08 mmol, 1.0 equiv.) was added. The reaction mixture was stirred for one hour prior to concentration. The desired product was obtained by filtration as a dark yellow solid (67 mg, 79%). **¹H NMR** (700 MHz, CDCl₃) δ = 9.80 (d, *J* = 8.2 Hz, 2H), 9.07 (s, 2H), 8.27 (dd, *J* = 6.0, 3.1 Hz, 2H), 7.76 (d, *J* = 8.8 Hz, 2H), 7.69 (dd, *J* = 2.8, 6.5 Hz, 2H), 7.33 (dd, *J* = 6.9 Hz, 4H), 7.20 (m, 16 H), 4.81 (s, 4H), 4.69 (s, 4H), 2.41 (s, 6H); **¹³C NMR** (176 MHz, CDCl₃) δ = 161.75, 145.75 (t, *J* = 2.0 Hz), 140.46, 139.08, 135.84, 133.68 (t, *J* = 15 Hz), 132.20 (t, *J* = 7.3 Hz), 130.23, 128.68 (t, *J* = 4.4 Hz), 128.73, 128.19, 127.70, 127.54, 127.02, 74.92 (t, *J* = 5.4 Hz), 72.92 (t, *J* = 2.6 Hz), 27.66; **HRMS** (ESI) *m/z* calculated for C₅₈H₄₄CuFeN₄P₂ [M]⁺ 977.16811 found 977.16774; **HRMS** (ESI) *m/z* calculated for BF₄ [M]⁻ 87.00347 found 87.00387.

A1.3 - Visible-Light Mediated Conversion of an Alcohol to a Halide (Appel-type Reaction):

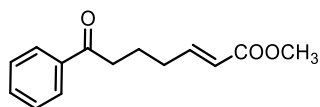


3-(Benzyloxy)propanol (1): The benzyl(Bn)-protected alcohol **1** was prepared using a procedure reported by Glimore *et al.*⁵ NMR data was in accordance with what was previously reported.

General Procedure for Appel Reaction: To an open oven-dried reaction vial charged with a stir bar was added copper catalyst (0.002 mmol, 0.01 equiv), the alcohol (33 mg, 0.20 mmol, 1.0 equiv), carbon tetrabromide (67 mg, 0.4 mmol, 2.0 equiv) and sodium bromide (41 mg, 0.40 mmol, 2.0 equiv). The flask vial was capped, purged with a stream of nitrogen and dry DMF (1.5 mL) was added via syringe. The reaction mixture was stirred under LEDs for 24 h. The mixture was poured into a separatory funnel containing Et₂O (10 mL) and H₂O (10 mL). The layers were separated and the aqueous layer was extracted with Et₂O (2 × 10 mL). The combined organic layers were washed with sat. Na₂S₂O₃ solution, brine, dried over Na₂SO₄ and concentrated *in*

vacuo. The residue was purified by chromatography (100 % Hexanes) to afford the desired product as a colorless oil. NMR data was in accordance with what was previously reported.⁶

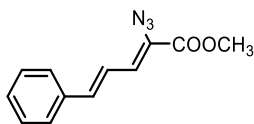
A1.4 - Visible-Light Homolytic Activation of Ketones (PCET):



Methyl (*E*)-7-oxo-7-phenylhept-2-enoate (3) The ketone **3** was prepared using a modified procedure reported by Knowles. Spectroscopic data was in accordance with what was previously reported.⁷

General Procedure for PCET Reaction: (3a*S*,6a*S*)-6a-Phenylhexahydro-2H-cyclopenta[*b*]furan-2-one (4): To an oven dried reaction vial charged with a stir bar is added (35.6 mg, 0.16 mmol, 1 eq.), the copper catalyst (0.00314 mmol, 5 mol %), Hantzsch ester (55.34 mg, 0.24 mmol 1.5 eq.), diphenylphosphoric acid (2 mg, 0.00785 mmol 5 mol %), and THF (3.14 ml 0.05M). The mixture is then degassed for 5 minutes with a nitrogen stream and irradiated over night. The reaction mixture is then directly purified by flash chromatography (100 % →10%, *n*-hexanes:EtOAc). The yield of the desired bicyclic lactone is calculated by NMR. Spectroscopic data was in accordance with what was previously reported.⁸

A1.5 - Visible-Light Sensitization of Vinyl Azides:



Methyl (2*Z*,4*E*)-2-azido-5-phenylpenta-2,4-dienoate (5): To a cooled (−22 °C) solution of NaOMe (2.67 mL, 9.93 mmol, 2.5 equiv.) in MeOH (2 mL) was added a solution of cinnamaldehyde (0.50 mL, 3.97 mmol, 1 equiv.) and methyl azidoacetate (9.93 mmol, 0.97 mL, 2.5 equiv.) dropwise over 20 min. The resulting reaction mixture was warmed to -10 °C. After four hours, the heterogeneous

mixture was diluted with water (10 mL) and EtOAc (10 mL). The phases were separated, and the resulting aqueous phase was extracted with additional EtOAc (2 × 10 mL). The combined organic phases were washed with distilled water (2 × 10 mL) and brine (10 mL). The combined organic phases were dried over Na₂SO₄, filtered and the filtrate was concentrated *in vacuo*. The crude residue was purified by flash column chromatography (0:100 – 5:95 EtOAc:*n*-hexanes) to afford the product as a colorless oil. NMR data was in accordance with what was previously reported.⁹

General Procedure for the Visible Light Sensitization of Vinyl Azides: Methyl 5-phenyl-1H-pyrrole-2-carboxylate (6): To an oven-dried 4 mL vial with a stir bar were added the azide (46 mg, 0.20 mmol, 1 equiv.), the copper catalyst (0.002 mmol, 0.01 equiv.) and dry and degassed CHCl₃ (2 mL, 0.1 M). The solution was purged with N₂ and irradiated at room temperature with a 1W blue light-emitting diode (LED) strip for 3 hours. The mixture was concentrated *in vacuo*, and the crude residue was purified by silica gel flash column chromatography (100% CH₂Cl₂) to afford the desired pyrrole as a white solid. NMR data was in accordance with what was previously reported.⁸

A1.6 - Photophysical data

Absorbance Data

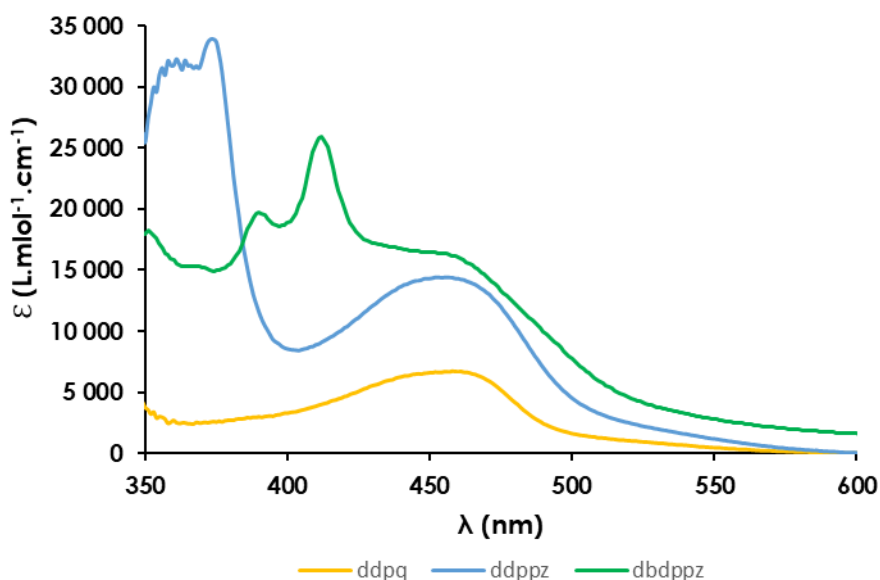


Figure A1 - 1 Absorption spectra of $\text{Cu}(\text{N}^{\wedge}\text{N})_2\text{BF}_4$ recorded at ambient temperature in CH_2Cl_2 ($5.0 \cdot 10^{-5}$ M).

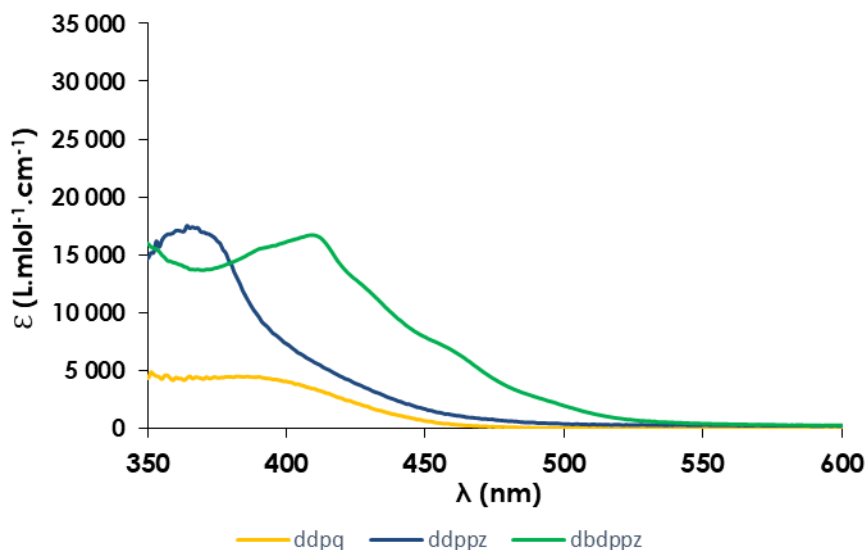


Figure A1 - 2 Absorption spectra of $\text{Cu}(\text{N}^{\wedge}\text{N})(\text{DPEPhos})\text{BF}_4$ recorded at ambient temperature in CH_2Cl_2 ($5.0 \cdot 10^{-5}$ M).

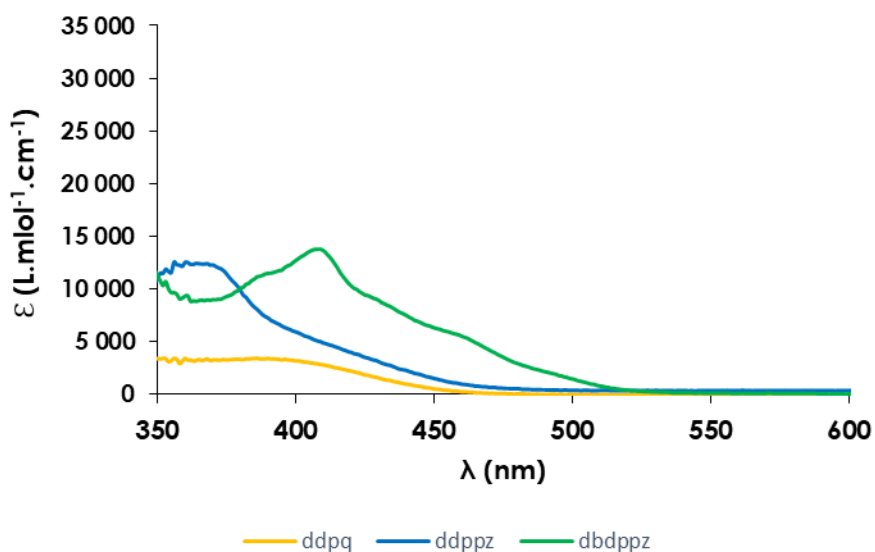


Figure A1 - 3 Absorption spectra of $\text{Cu}(\text{N}^{\wedge}\text{N})(\text{XantPhos})\text{BF}_4$ recorded at ambient temperature in CH_2Cl_2 ($5.0 \cdot 10^{-5}$ M).

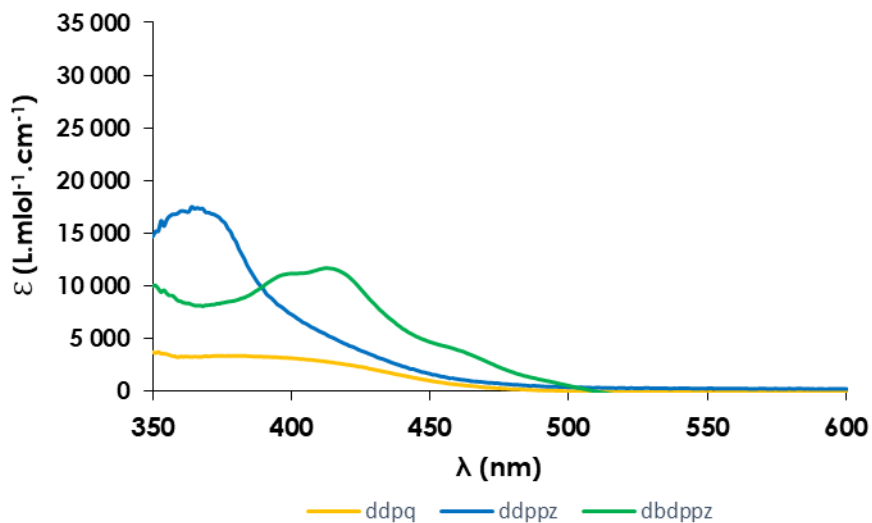


Figure A1 - 4 Absorption spectra of Cu(N^N)(dppf)BF₄ recorded at ambient temperature in CH₂Cl₂ (5.0·10⁻⁵ M).

Emission/Excitation Data

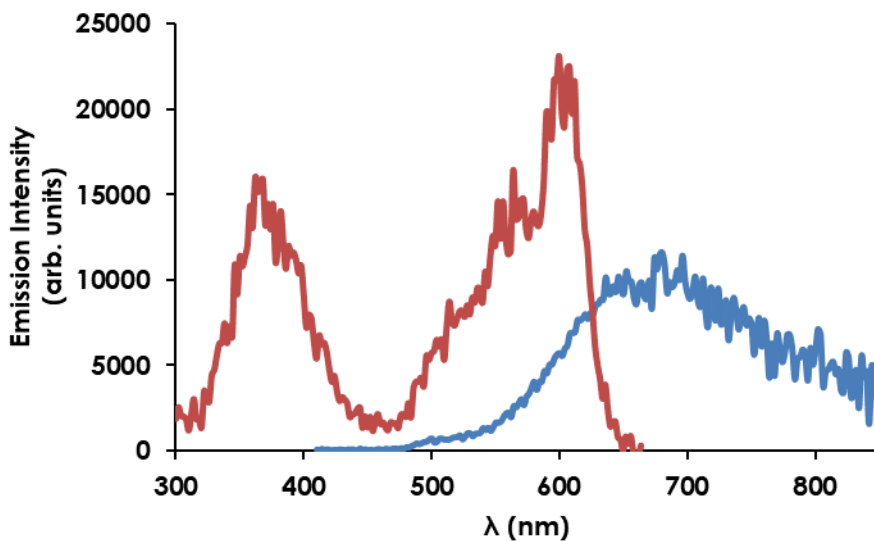


Figure A1 - 5 Excitation (red curve) and emission (blue curve) spectrum of Cu(ddpq)₂BF₄ excited at 450 nm, recorded at ambient temperature in CH₂Cl₂ (5·10⁻⁴ M).

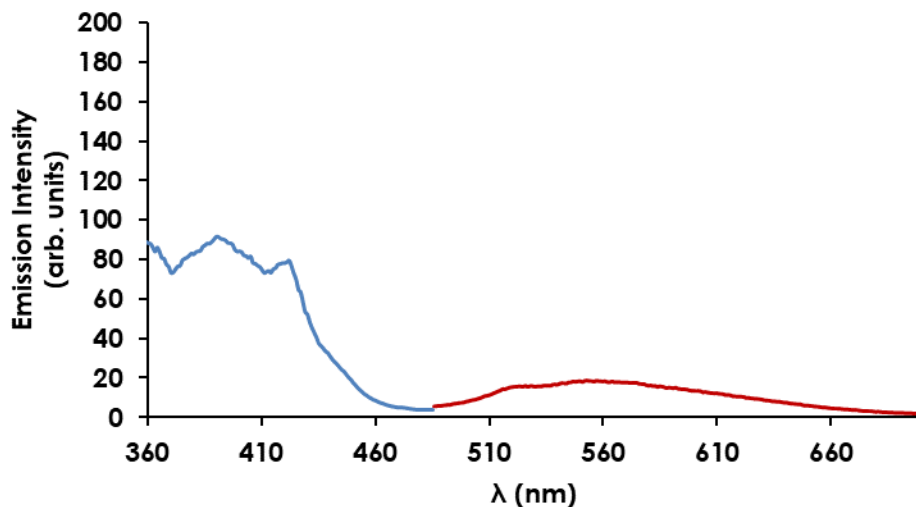


Figure A1 - 6 Excitation (red curve) and emission (blue curve) spectrum of $\text{Cu}(\text{ddpq})(\text{DPEPhos})\text{BF}_4$ excited at 395 nm, recorded at ambient temperature in CH_2Cl_2 ($1.25 \cdot 10^{-5}$ M).

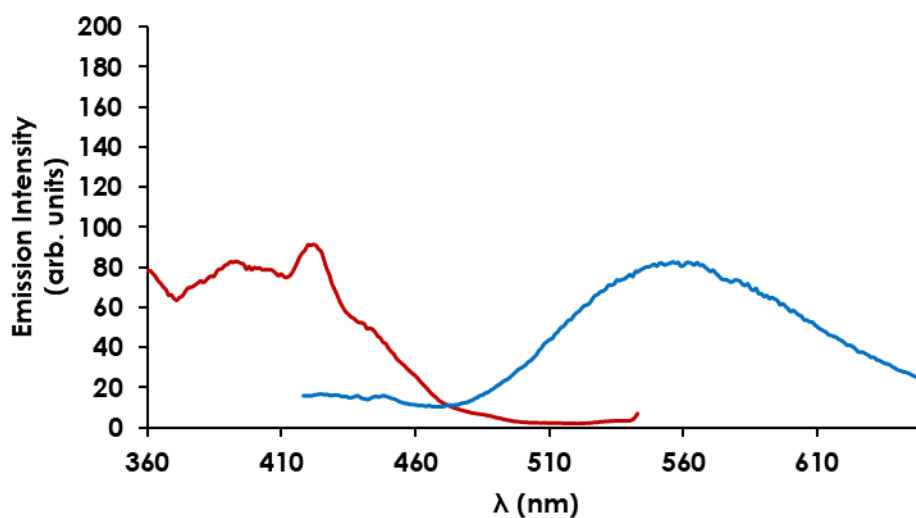


Figure A1 - 7 Excitation (red curve) and emission (blue curve) spectrum of $\text{Cu}(\text{ddpq})(\text{XantPhos})\text{BF}_4$ excited at 450 nm, recorded at ambient temperature in CH_2Cl_2 ($1.25 \cdot 10^{-5}$ M).

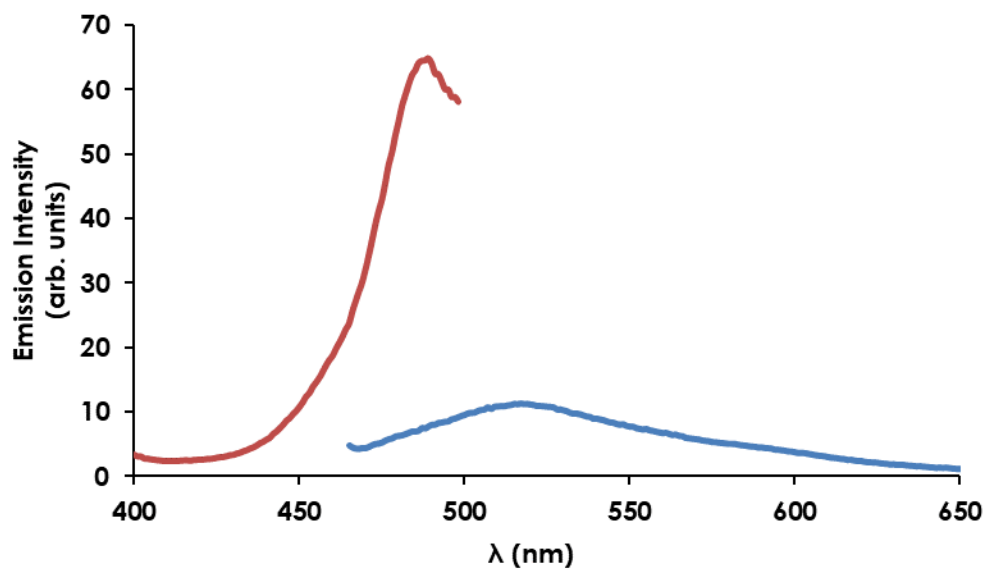


Figure A1 - 8 Excitation (red curve) and emission (blue curve) spectrum of $\text{Cu(dddq)(dppf)BF}_4$ excited at 450 nm, recorded at ambient temperature in CH_2Cl_2 ($5 \cdot 10^{-4}$ M).

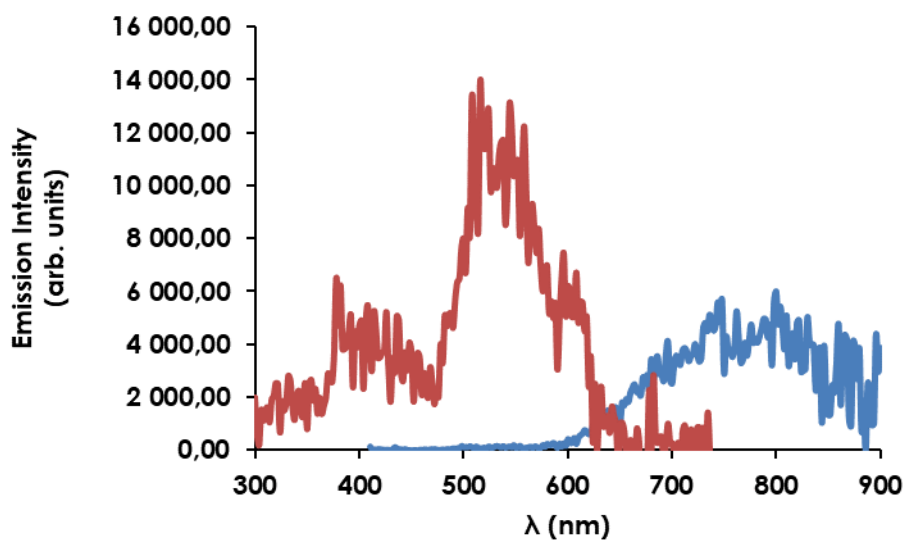


Figure A1 - 9 Excitation (red curve) and emission (blue curve) spectrum of $\text{Cu(dddppz)}_2\text{BF}_4$ excited at 450 nm, recorded at ambient temperature in CH_2Cl_2 ($1.25 \cdot 10^{-5}$ M).

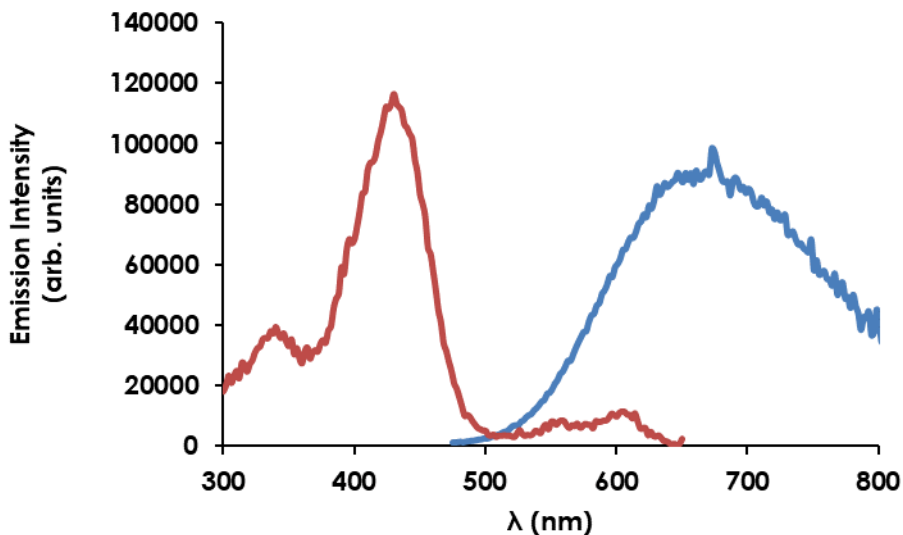


Figure A1 - 10 Excitation (red curve) and emission (blue curve) spectrum of Cu(ddppz)(DPEPhos)BF₄ excited at 450 nm, recorded at ambient temperature in CH₂Cl₂ (1.25·10⁻⁵ M).

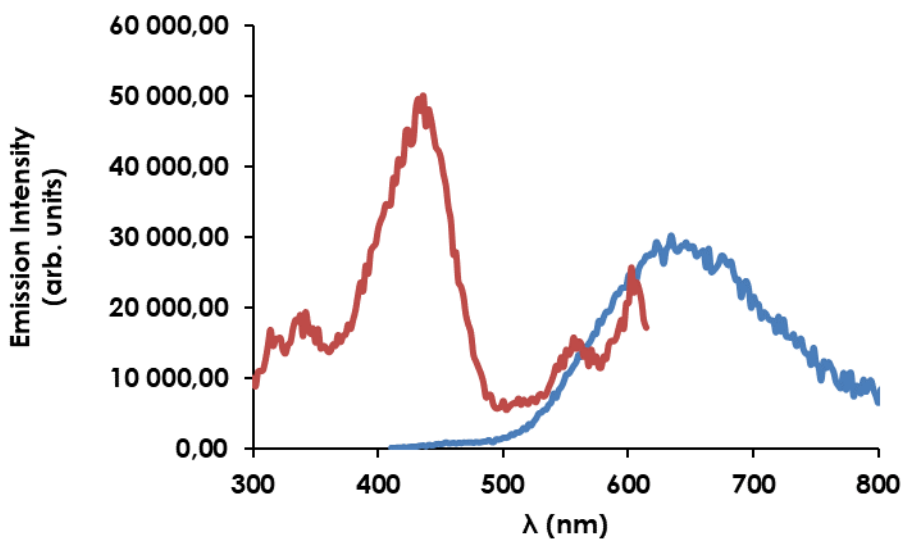


Figure A1 - 11 Excitation (red curve) and emission (blue curve) spectrum of Cu(ddppz)(XantPhos)BF₄ excited at 450 nm, recorded at ambient temperature in CH₂Cl₂ (1.25·10⁻⁵ M).

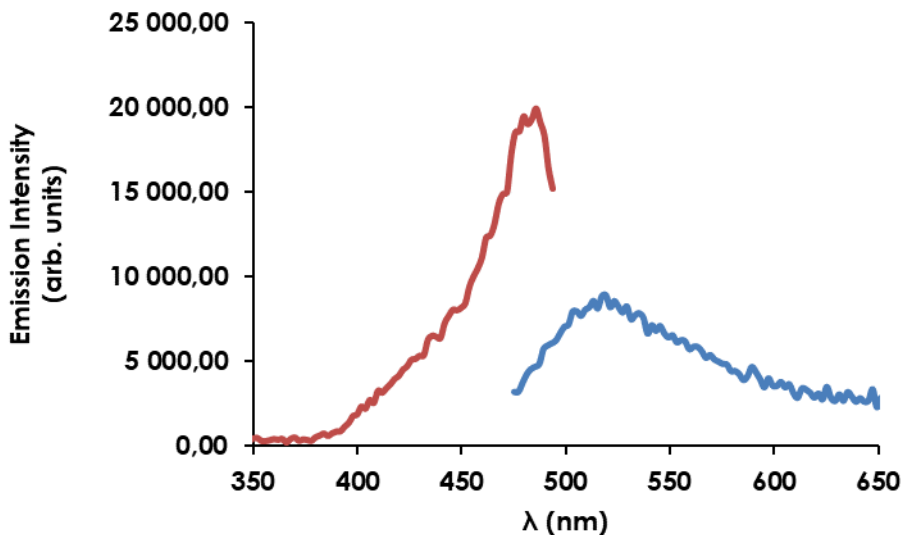


Figure A1 - 12 Excitation (red curve) and emission (blue curve) spectrum of $\text{Cu}(\text{ddppz})(\text{dppf})\text{BF}_4$ excited at 450 nm, recorded at ambient temperature in CH_2Cl_2 ($1.25 \cdot 10^{-5}$ M).

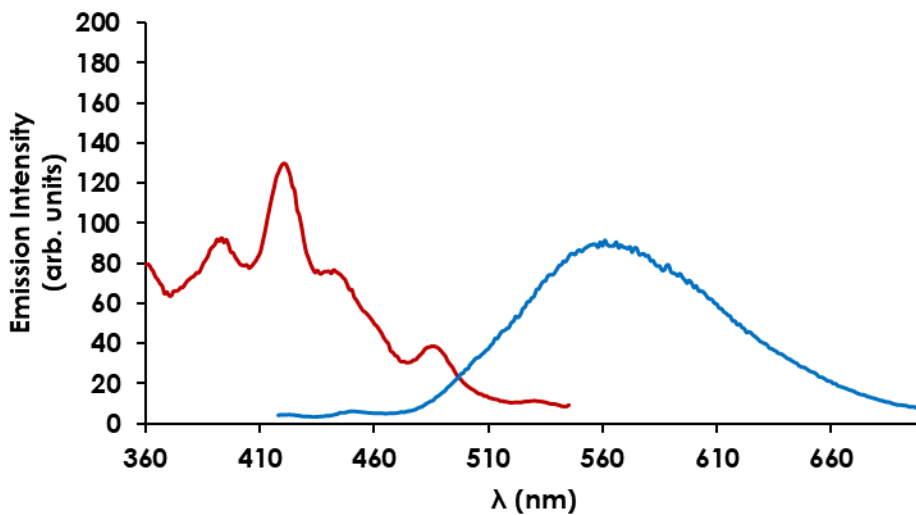


Figure A1 - 13 Excitation (red curve) and emission (blue curve) spectrum of $\text{Cu}(\text{dbdppz})_2\text{BF}_4$ excited at 395 nm, recorded at ambient temperature in CH_2Cl_2 ($1.25 \cdot 10^{-5}$ M).

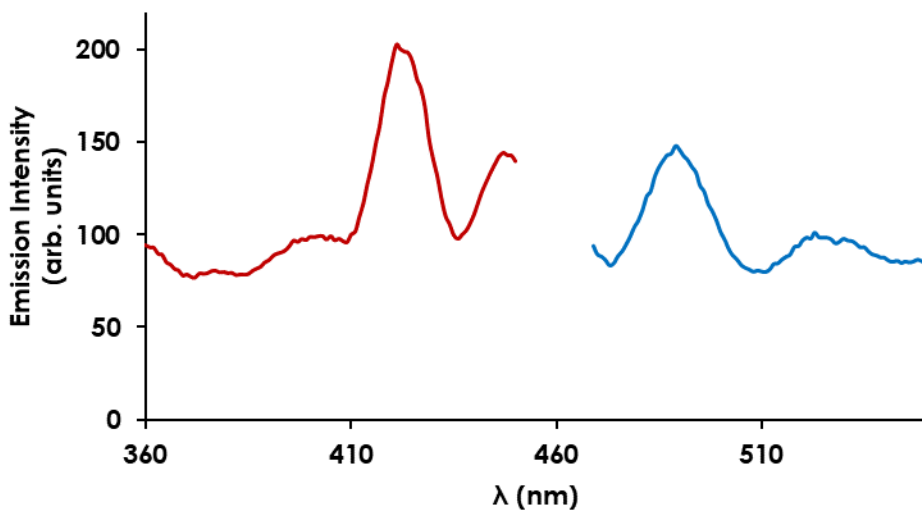


Figure A1 - 14 Excitation (red curve) and emission (blue curve) spectrum of $\text{Cu}(\text{dbdppz})(\text{DPEPhos})\text{BF}_4$ excited at 450 nm, recorded at ambient temperature in CH_2Cl_2 ($1.25 \cdot 10^{-5}$ M).

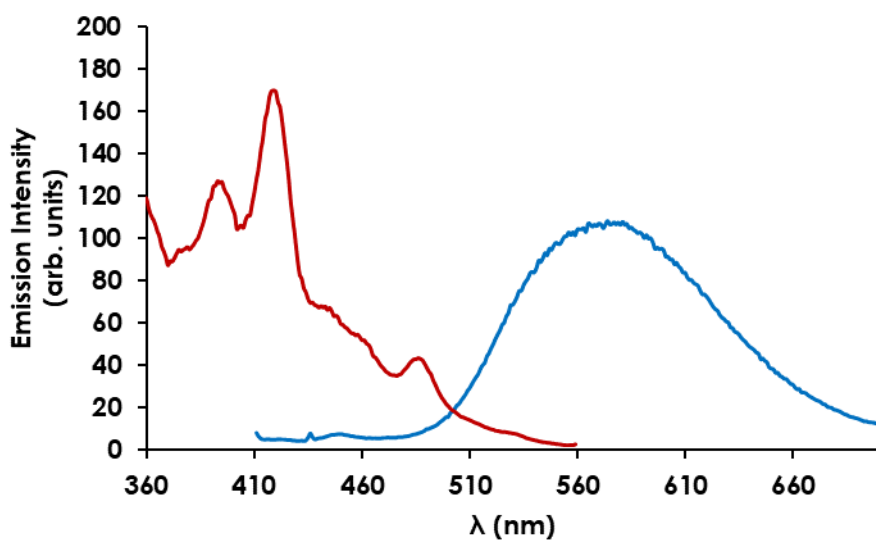


Figure A1 - 15 Excitation (red curve) and emission (blue curve) spectrum of $\text{Cu}(\text{dbdppz})(\text{XantPhos})\text{BF}_4$ excited at 395 nm, recorded at ambient temperature in CH_2Cl_2 ($1.25 \cdot 10^{-5}$ M).

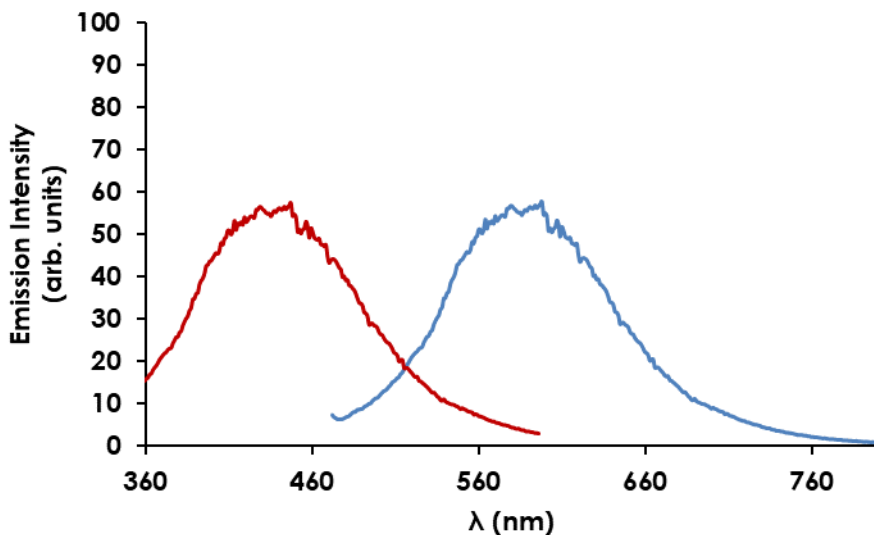


Figure A1 - 16 Excitation (red curve) and emission (blue curve) spectrum of Cu(dbdppz)(dppf)BF₄ excited at 450 nm, recorded at ambient temperature in CH₂Cl₂ ($1.25 \cdot 10^{-5}$ M).

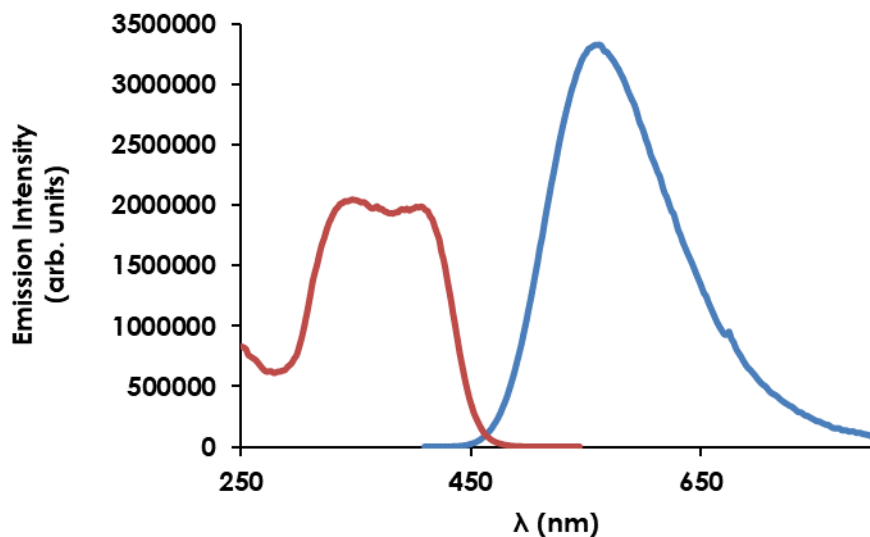


Figure A1 - 17 Excitation (red curve) and emission (blue curve) spectrum of Cu(dmp)(Xantphos)BF₄ excited at 395 nm, recorded at ambient temperature in CH₂Cl₂ ($5 \cdot 10^{-4}$ M).

Excited State Lifetime Data

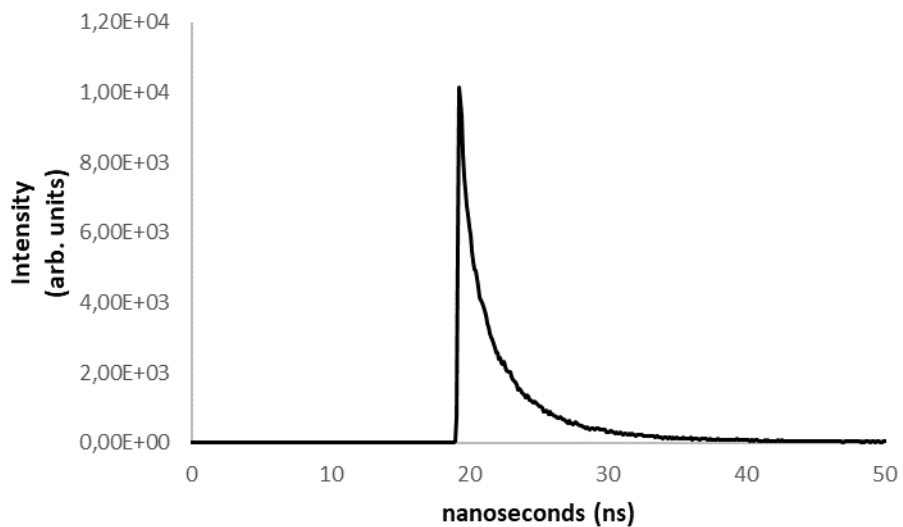


Figure A1 - 18 Lifetime spectrum of Cu(ddpq)₂BF₄ excited at 375 nm, recorded at ambient temperature in CH₂Cl₂ (5·10⁻⁵ M).

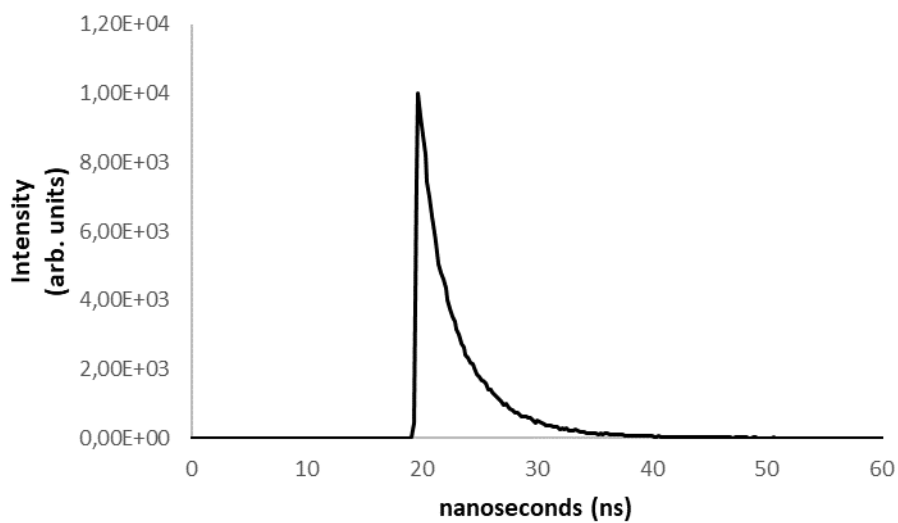


Figure A1 - 19 Lifetime spectrum of Cu(ddpq)(DPEPhos)BF₄ excited at 375 nm, recorded at ambient temperature in CH₂Cl₂ (5·10⁻⁵ M).

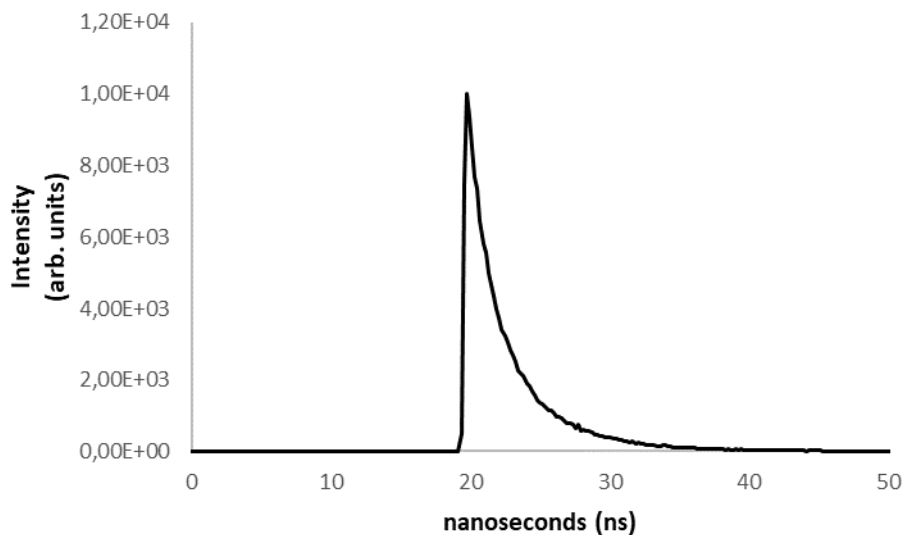


Figure A1 - 20 Lifetime spectrum of Cu(dddpq)(XantPhos)BF₄ excited at 375 nm, recorded at ambient temperature in CH₂Cl₂ (5·10⁻⁵ M).

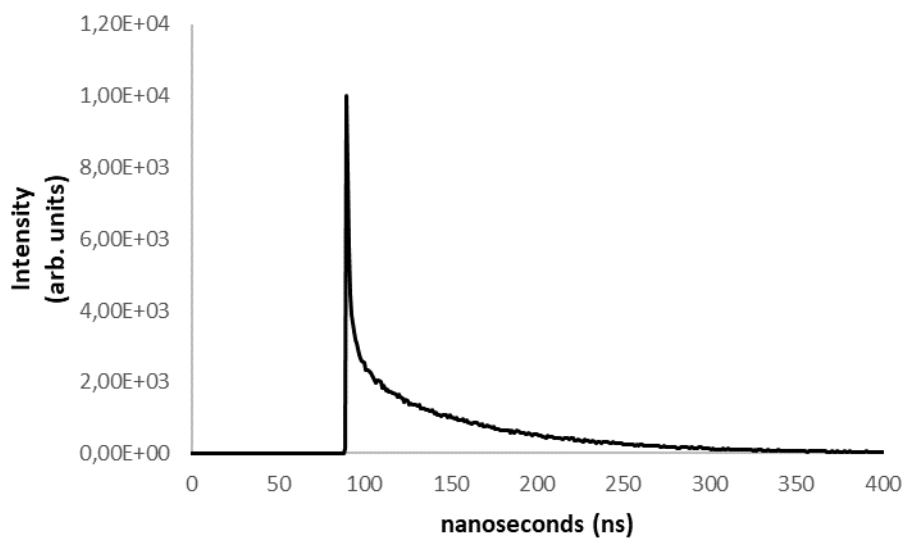


Figure A1 - 21 Lifetime spectrum of Cu(dddpq)(dppf)BF₄ excited at 375 nm, recorded at ambient temperature in CH₂Cl₂ (5·10⁻⁵ M).

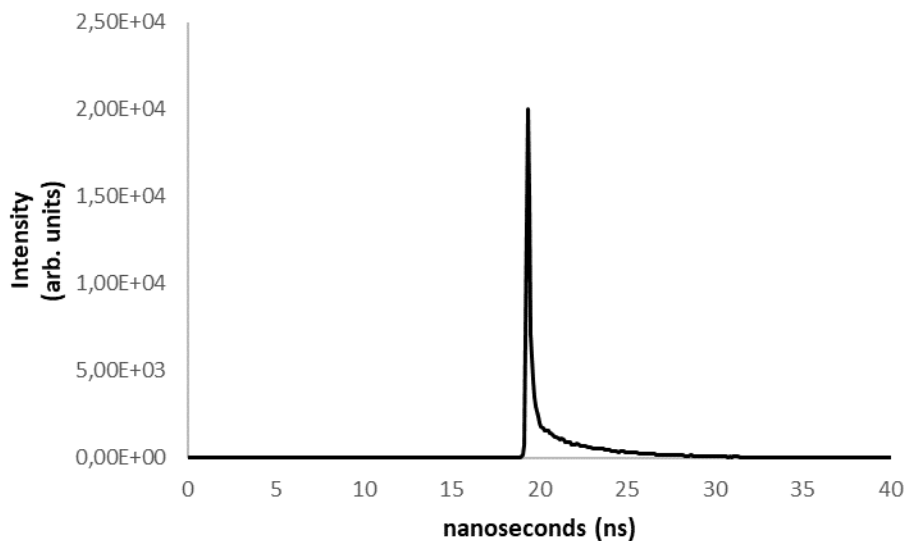


Figure A1 - 22 Lifetime spectrum of Cu(ddppz)₂BF₄ excited at 375 nm, recorded at ambient temperature in CH₂Cl₂ (5·10⁻⁵ M).

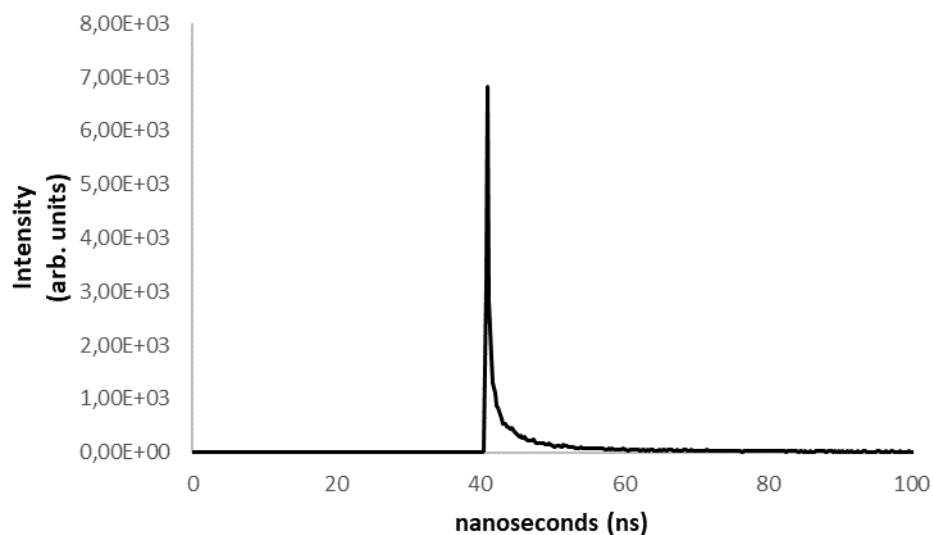


Figure A1 - 23 Lifetime spectrum of Cu(ddppz)(DPEPhos)BF₄ excited at 375 nm, recorded at ambient temperature in CH₂Cl₂ (5·10⁻⁵ M).

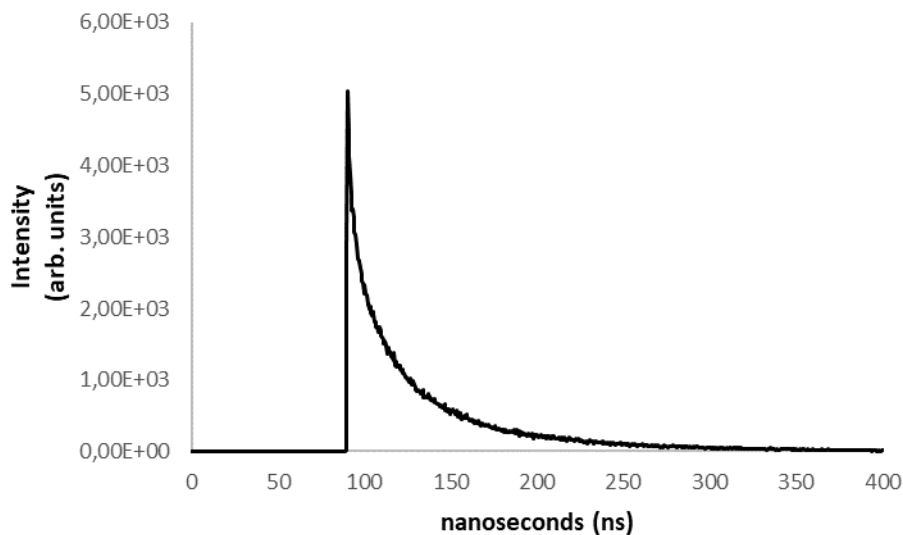


Figure A1 - 24 Lifetime spectrum of Cu(ddppz)(XantPhos)BF₄ excited at 375 nm, recorded at ambient temperature in CH₂Cl₂ ($5 \cdot 10^{-5}$ M).

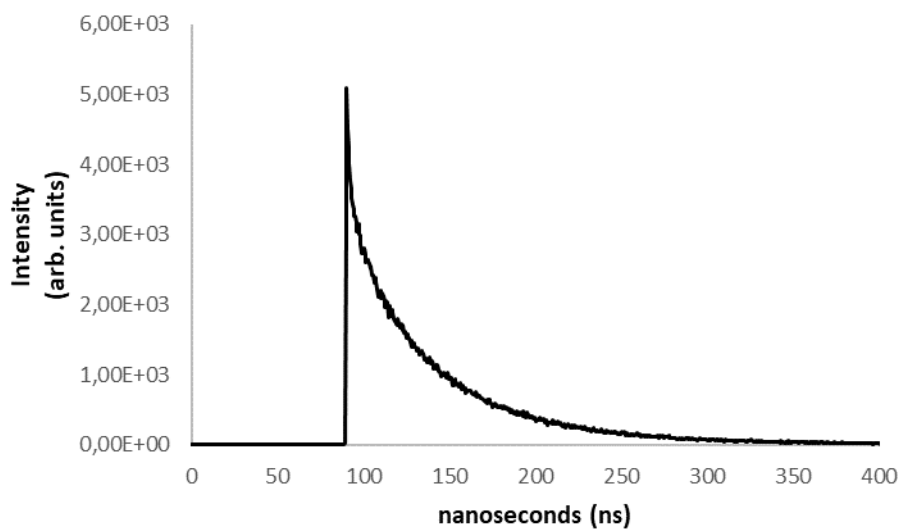


Figure A1 - 25 Lifetime spectrum of Cu(ddppz)(dppf)BF₄ excited at 375 nm, recorded at ambient temperature in CH₂Cl₂ ($5 \cdot 10^{-5}$ M).

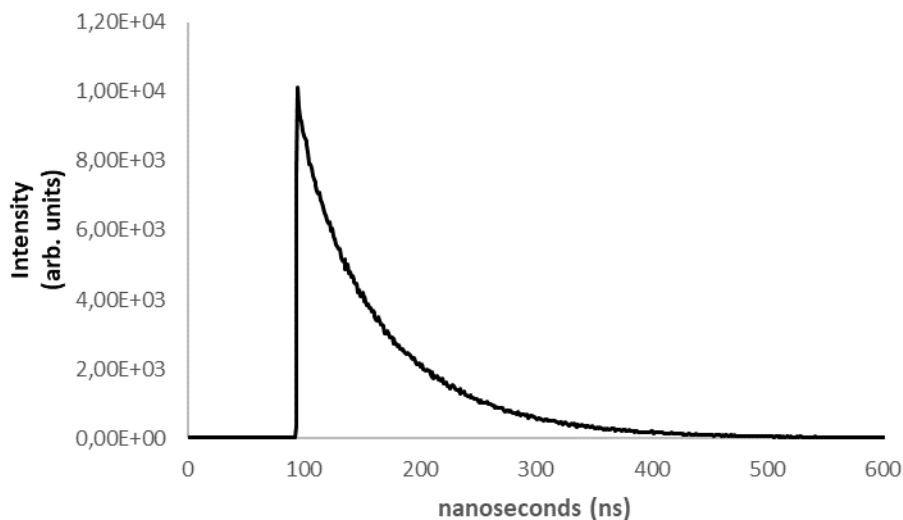


Figure A1 - 26 Lifetime spectrum of Cu(dbdppz)₂BF₄ excited at 375 nm, recorded at ambient temperature in CH₂Cl₂ (5·10⁻⁵ M).

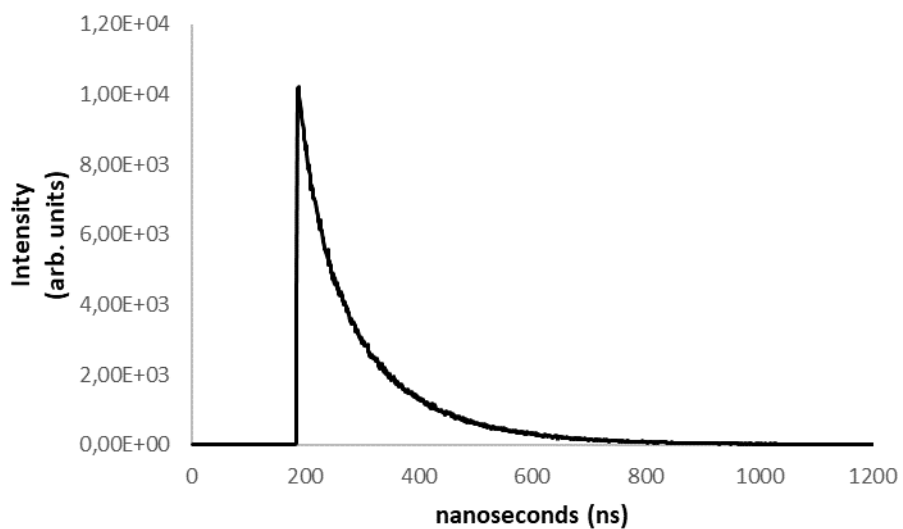


Figure A1 - 27 Lifetime spectrum of Cu(dbdppz)(DPEPhos)BF₄ excited at 375 nm, recorded at ambient temperature in CH₂Cl₂ (5·10⁻⁵ M).

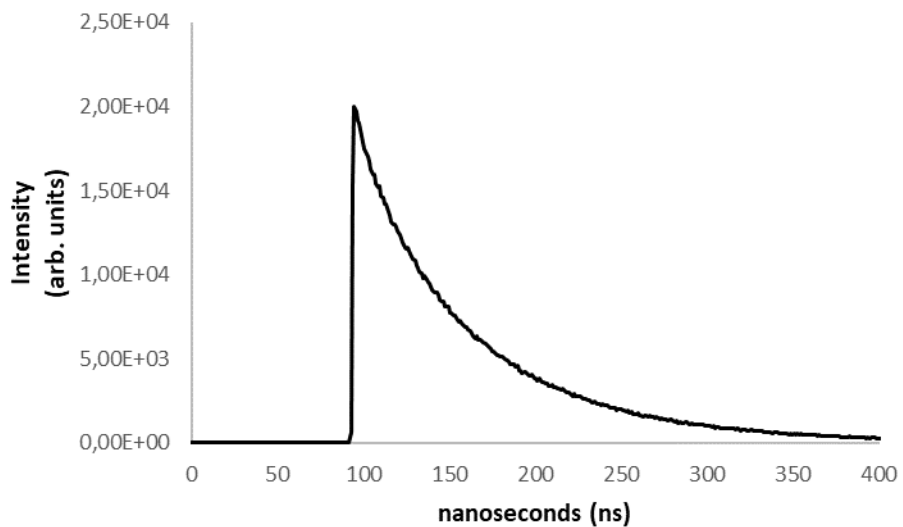


Figure A1 - 28 Lifetime spectrum of Cu(dbdppz)(XantPhos)BF₄ excited at 375 nm, recorded at ambient temperature in CH₂Cl₂ (5·10⁻⁵ M).

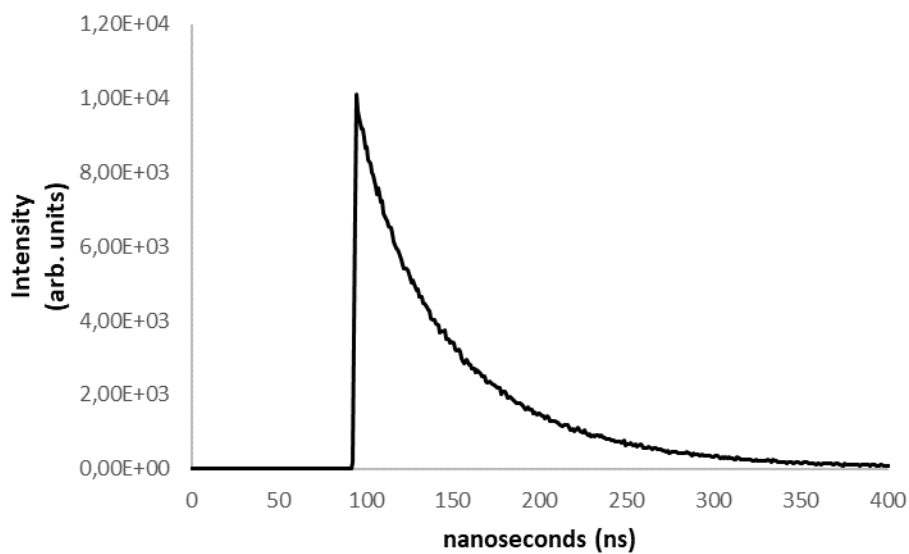


Figure A1 - 29 Lifetime spectrum of Cu(dbdppz)(dppf)BF₄ excited at 375 nm, recorded at ambient temperature in CH₂Cl₂ (5·10⁻⁵ M).

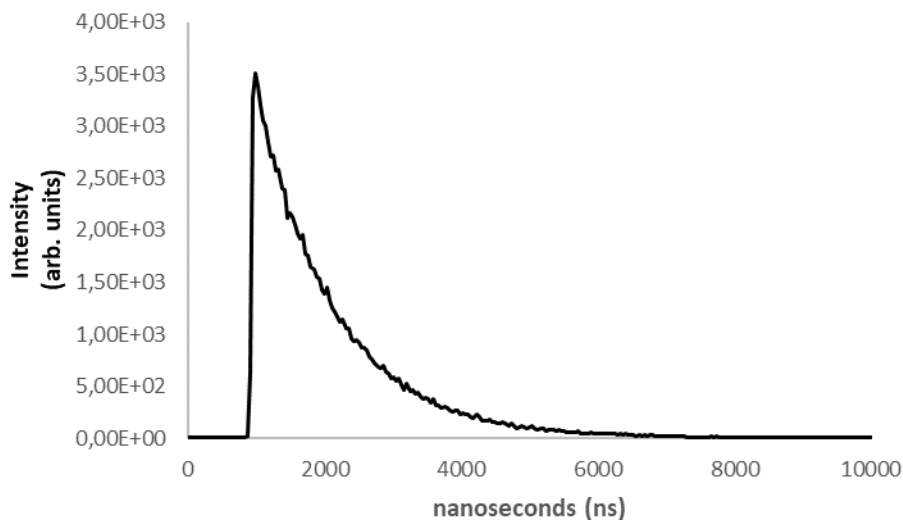


Figure A1 - 30 Lifetime spectrum of Cu(dmp)(Xantphos)BF₄ excited at 375 nm, recorded at ambient temperature in CH₂Cl₂ (5·10⁻⁴ M).

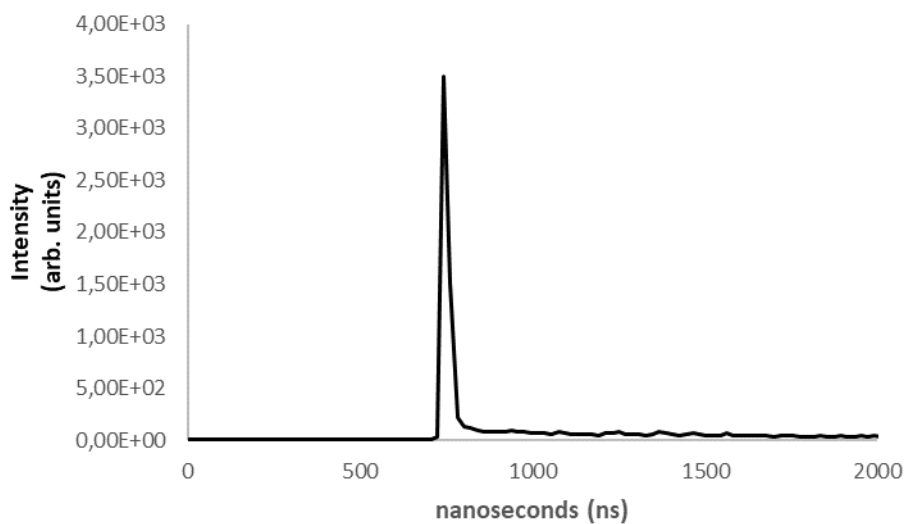


Figure A1 - 31 Lifetime spectrum of Cu(dmp)(dppf)BF₄ excited at 375 nm, recorded at ambient temperature in CH₂Cl₂ (5·10⁻⁴ M).

A1.7 - Electrochemical data

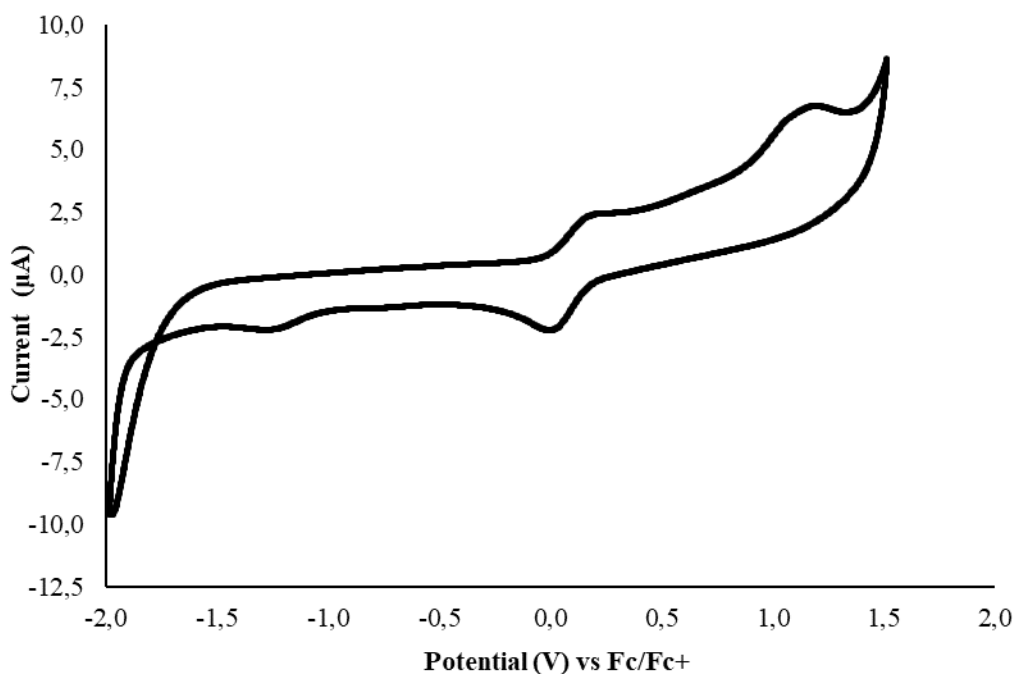


Figure A1 - 32 Cyclic voltammogram of $\text{Cu}(\text{dddpq})_2\text{BF}_4$ in MeCN (1 mM) using TBAPF_6 (100 mM) as supporting electrolyte at a scan rate of $50 \text{ mV}\cdot\text{s}^{-1}$

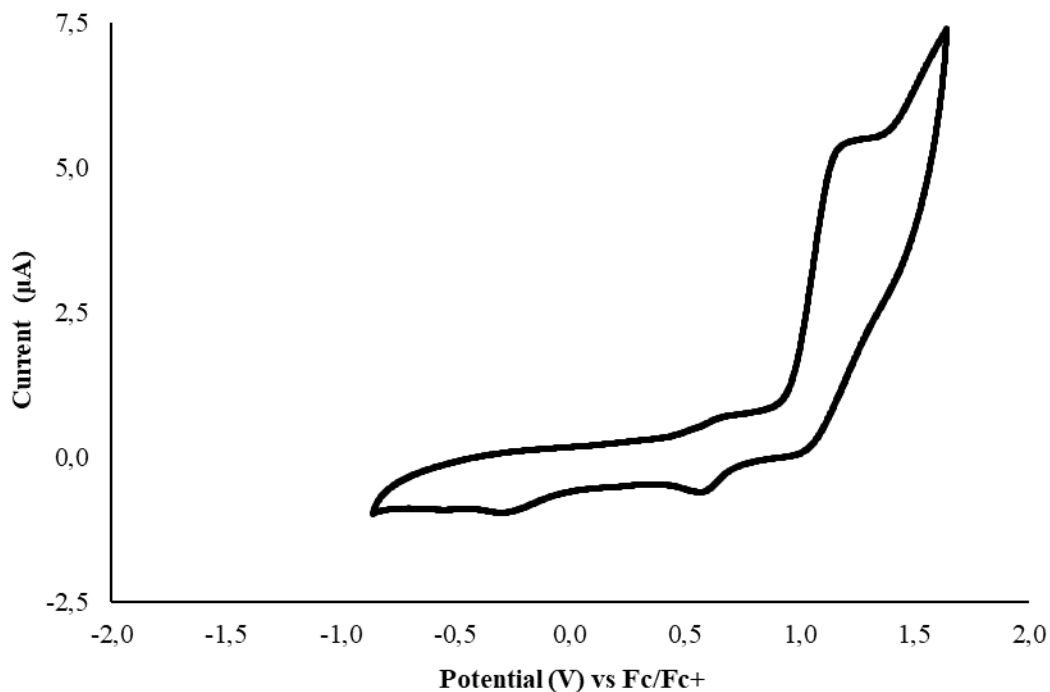


Figure A1 - 33 Cyclic voltammogram of $\text{Cu}(\text{dddpq})(\text{DPEPhos})\text{BF}_4$ in MeCN (1 mM) using TBAPF_6 (100 mM) as supporting electrolyte at a scan rate of $50 \text{ mV}\cdot\text{s}^{-1}$

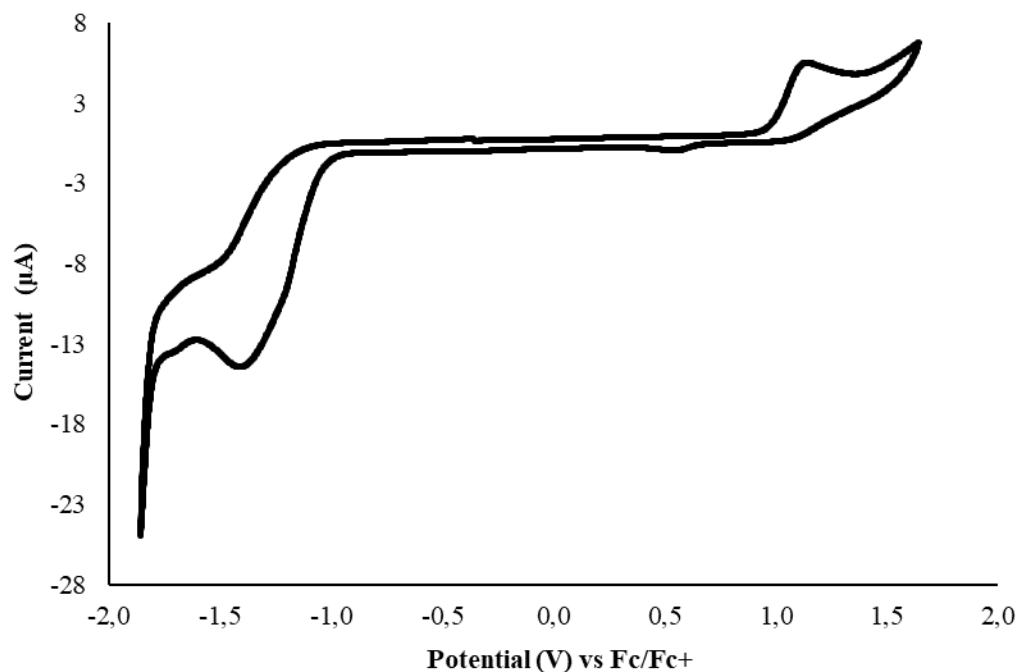


Figure A1 - 34 Cyclic voltammogram of $\text{Cu}(\text{ddpq})(\text{Xantphos})\text{BF}_4$ in MeCN (1 mM) using TBAPF_6 (100 mM) as supporting electrolyte at a scan rate of $50 \text{ mV}\cdot\text{s}^{-1}$.

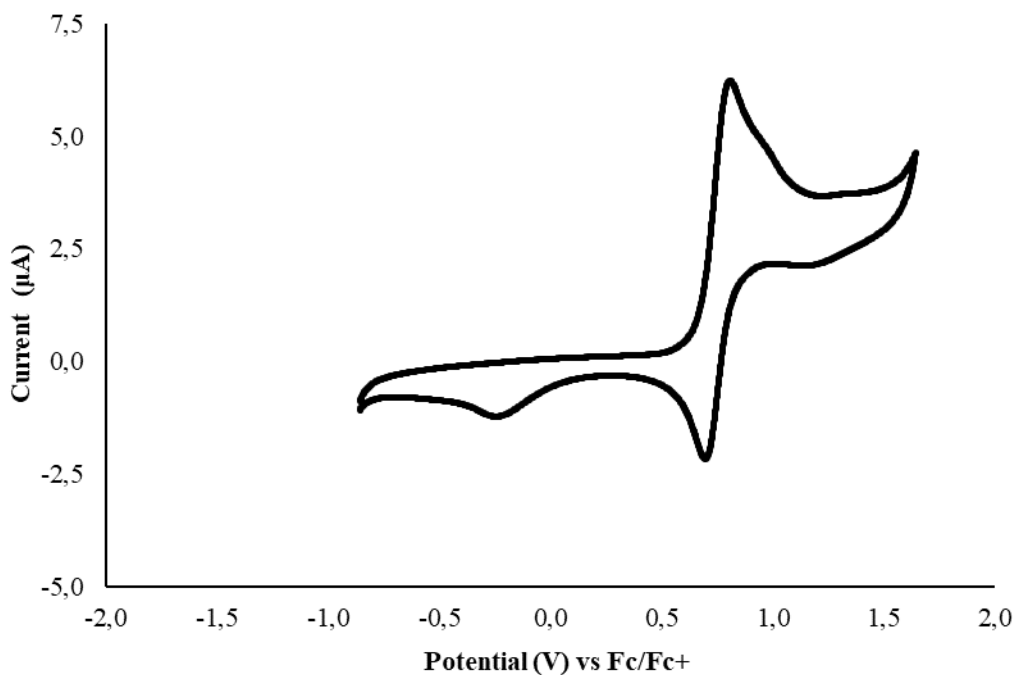


Figure A1 - 35 Cyclic voltammogram of $\text{Cu}(\text{ddpq})(\text{dppf})\text{BF}_4$ in MeCN (1 mM) using TBAPF_6 (100 mM) as supporting electrolyte at a scan rate of $50 \text{ mV}\cdot\text{s}^{-1}$.

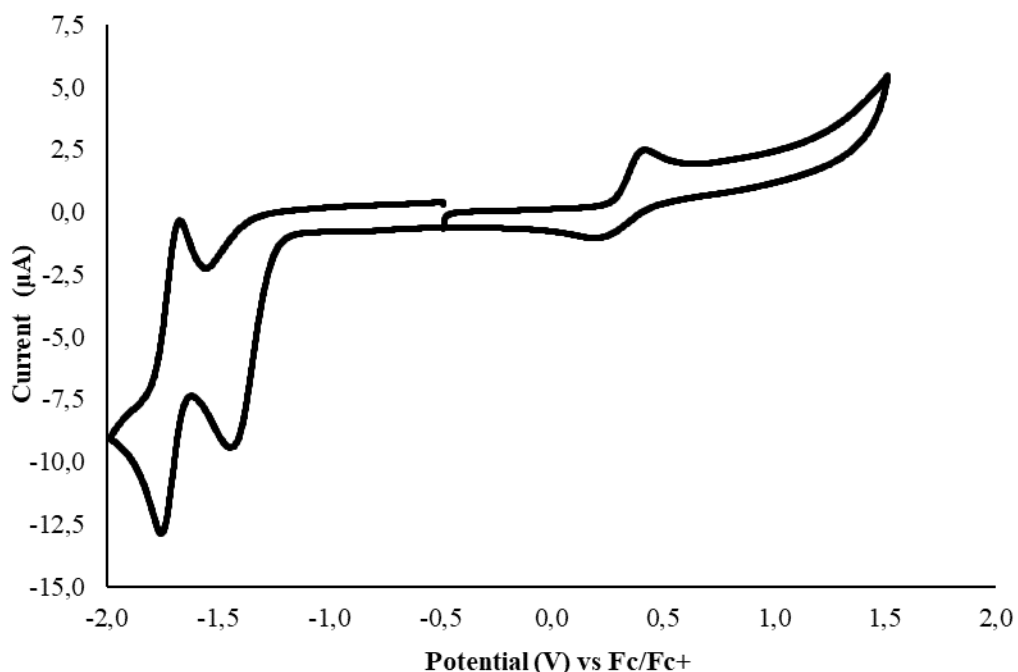


Figure A1 - 36 Cyclic voltammogram of $\text{Cu}(\text{ddppz})_2\text{BF}_4$ in MeCN (1 mM) using TBAPF_6 (100 mM) as supporting electrolyte at a scan rate of $50 \text{ mV}\cdot\text{s}^{-1}$.

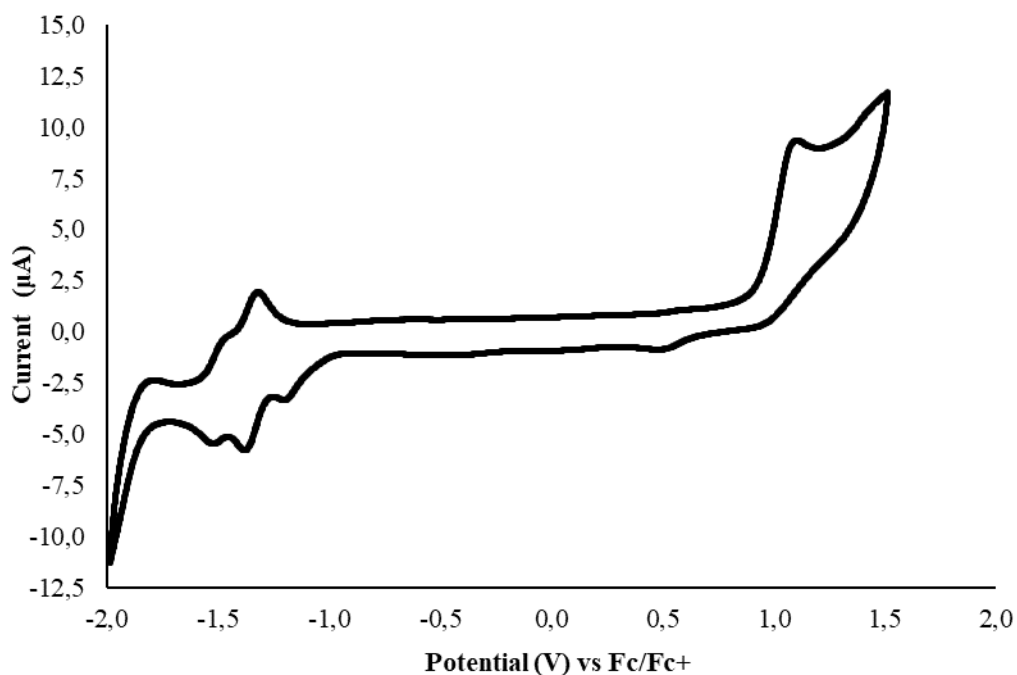


Figure A1 - 37 Cyclic voltammogram of $\text{Cu}(\text{ddppz})(\text{DPEPhos})\text{BF}_4$ in MeCN (1 mM) using TBAPF_6 (100 mM) as supporting electrolyte at a scan rate of $50 \text{ mV}\cdot\text{s}^{-1}$.

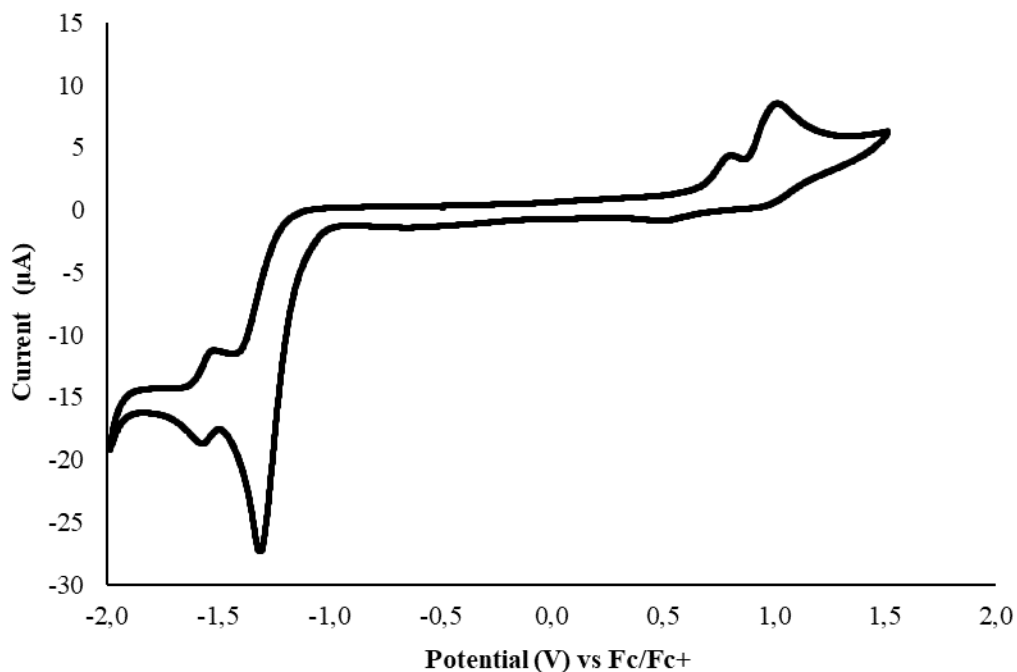


Figure A1 - 38 Cyclic voltammogram of Cu(**ddppz**)(**Xantphos**)BF₄ in MeCN (1 mM) using TBAPF₆ (100 mM) as supporting electrolyte at a scan rate of 50 mV·s⁻¹

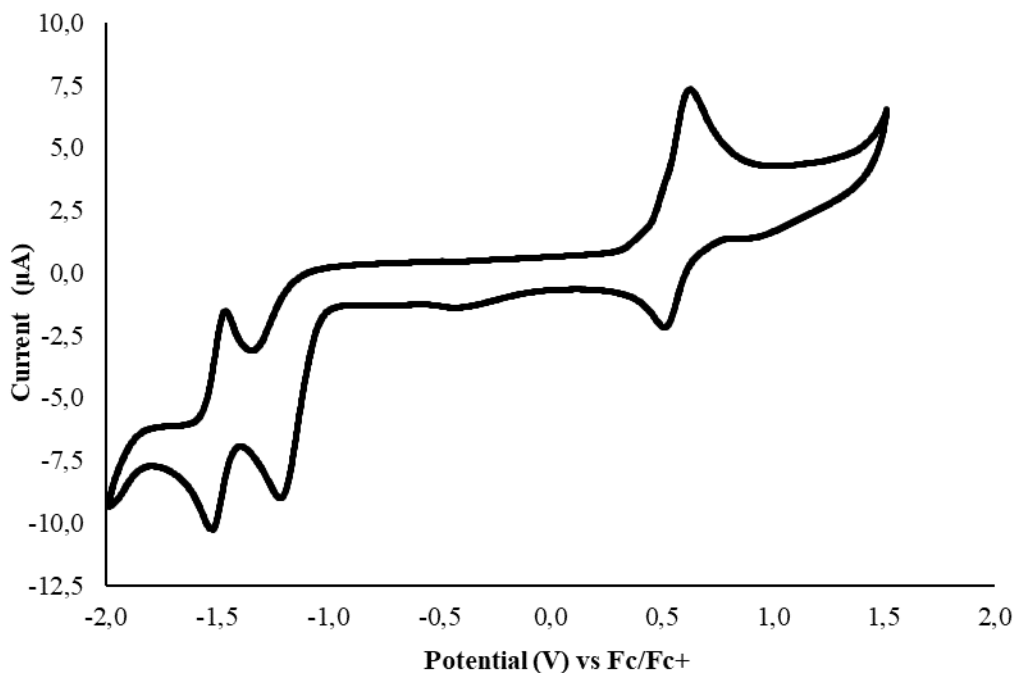


Figure A1 - 39 Cyclic voltammogram of Cu(**ddppz**)(**dppf**)BF₄ in MeCN (1 mM) using TBAPF₆ (100 mM) as supporting electrolyte at a scan rate of 50 mV·s⁻¹.

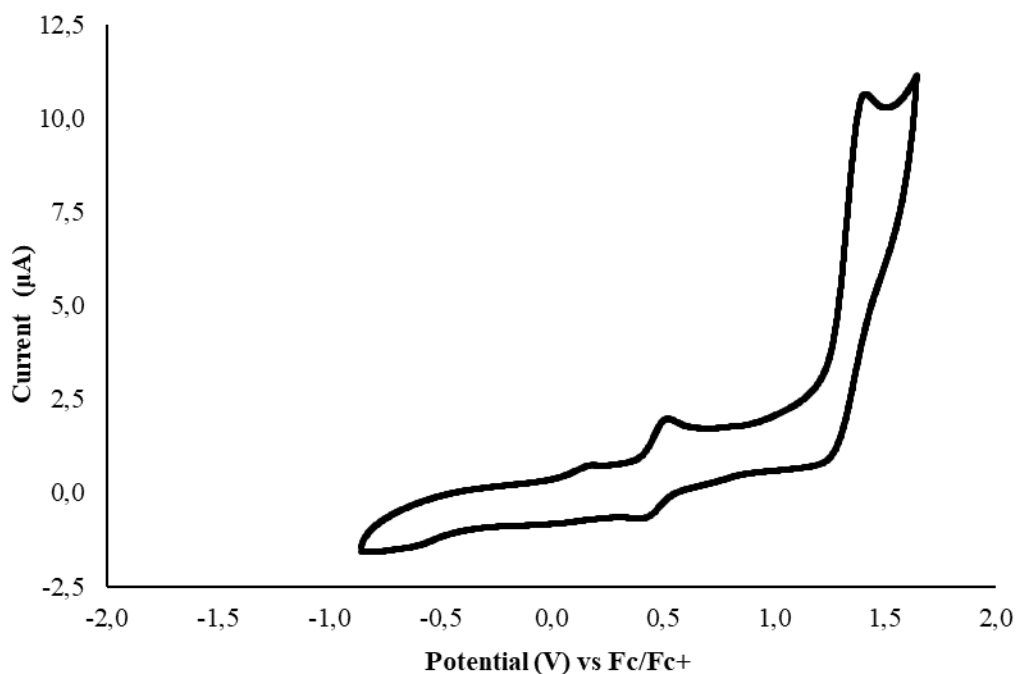


Figure A1 - 40 Cyclic voltammogram of Cu(**dbddppz**)₂BF₄ in MeCN (1 mM) using TBAPF₆ (100 mM) as supporting electrolyte at a scan rate of 50 mV·s⁻¹.

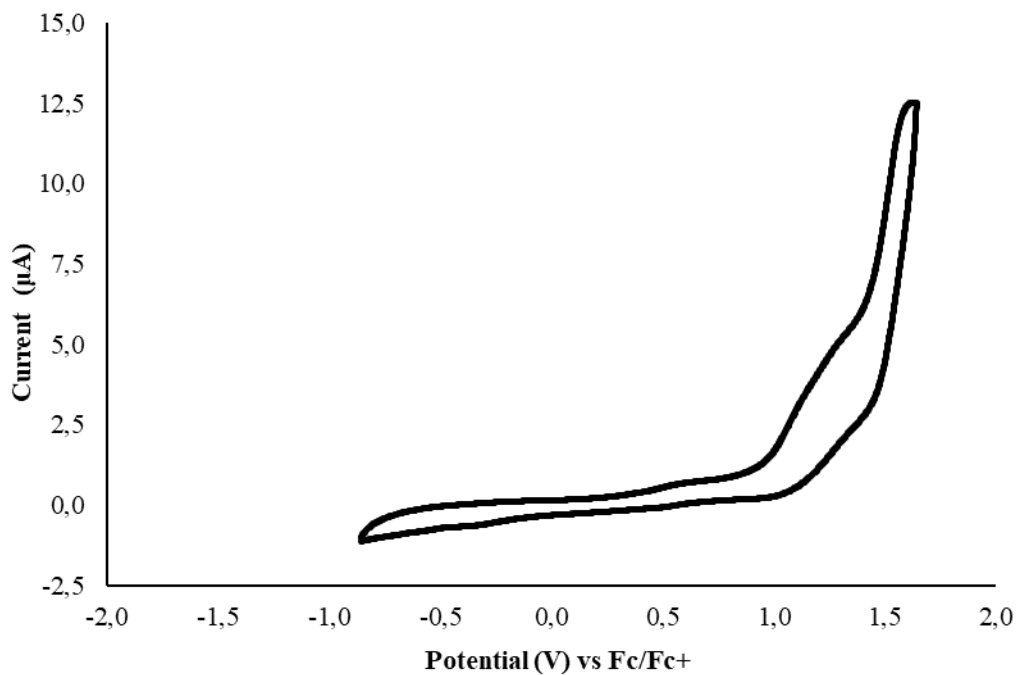


Figure A1 - 41 Cyclic voltammogram of Cu(**dbdppz**)(**DPEPhos**)BF₄ in MeCN (1 mM) using TBAPF₆ (100 mM) as supporting electrolyte at a scan rate of 50 mV·s⁻¹.

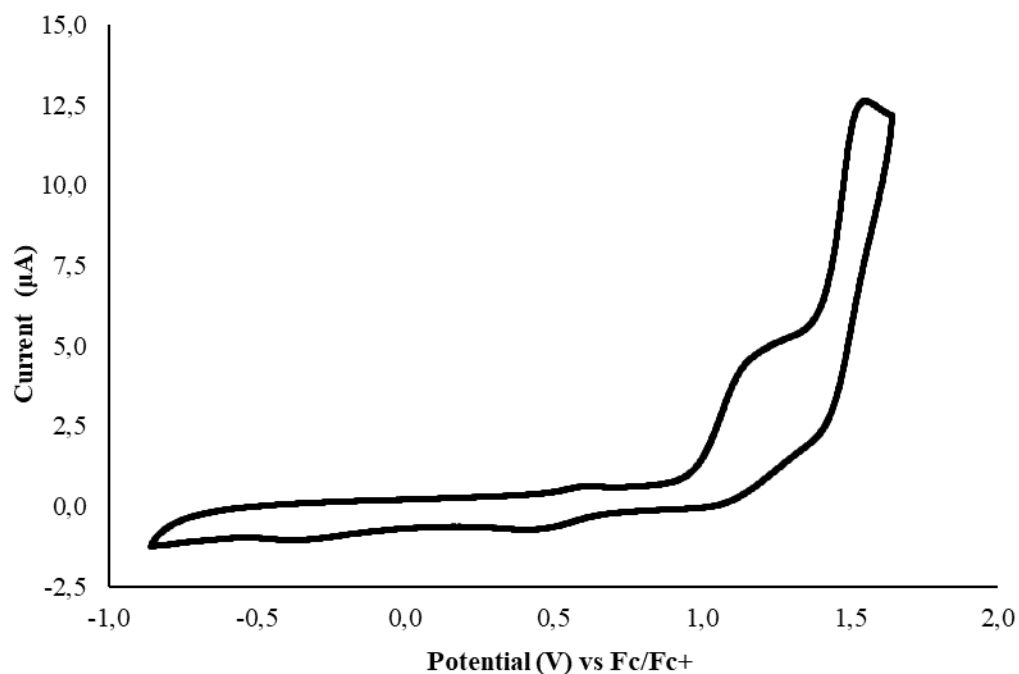


Figure A1 - 42 Cyclic voltammogram of Cu(**dbdppz**)(**Xantphos**)BF₄ in MeCN (1 mM) using TBAPF₆ (100 mM) as supporting electrolyte at a scan rate of 50 mV·s⁻¹.

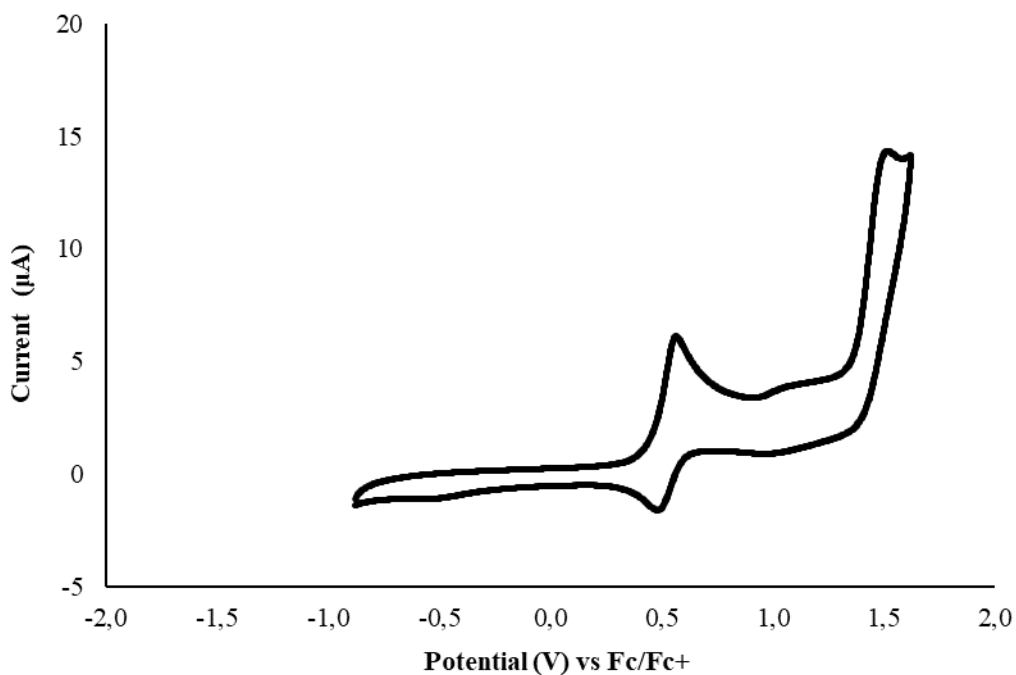


Figure A1 - 43 Cyclic voltammogram of Cu(**dbdppz**)(**dppf**)BF₄ in MeCN (1 mM) using TBAPF₆ (100 mM) as supporting electrolyte at a scan rate of 50 mV·s⁻¹.

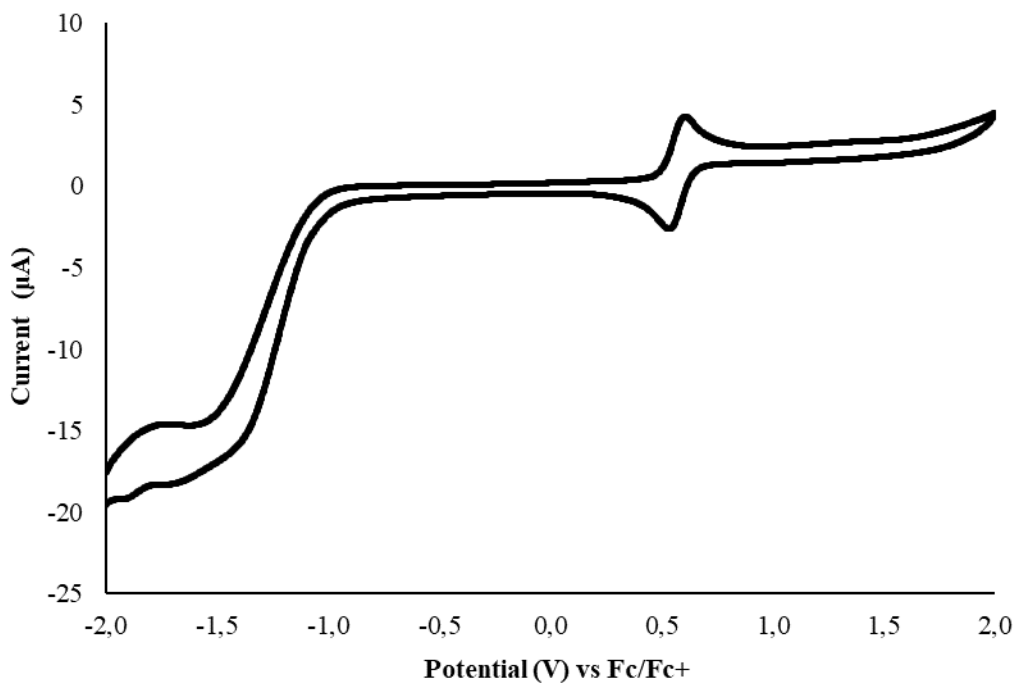


Figure A1 - 44 Cyclic voltammogram of Cu(**dmp**)₂BF₄ in MeCN (1 mM) using TBAPF₆ (100 mM) as supporting electrolyte at a scan rate of 50 mV·s⁻¹.

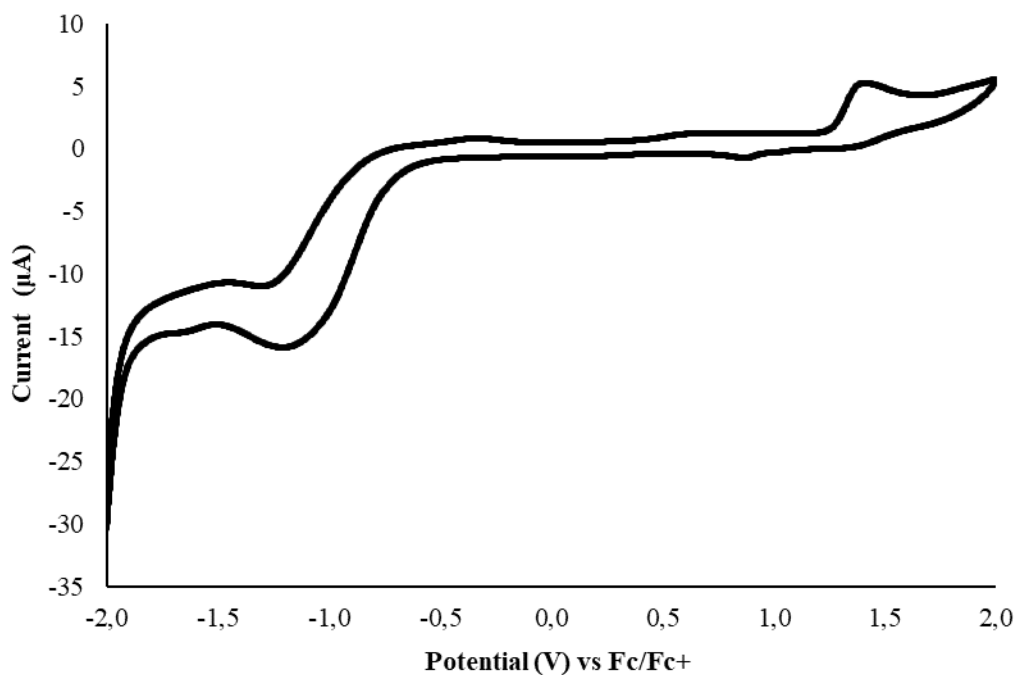


Figure A1 - 45 Cyclic voltammogram of Cu(**dmp**)(**DPEPhos**)BF₄ in MeCN (1 mM) using TBAPF₆ (100 mM) as supporting electrolyte at a scan rate of 50 mV·s⁻¹.

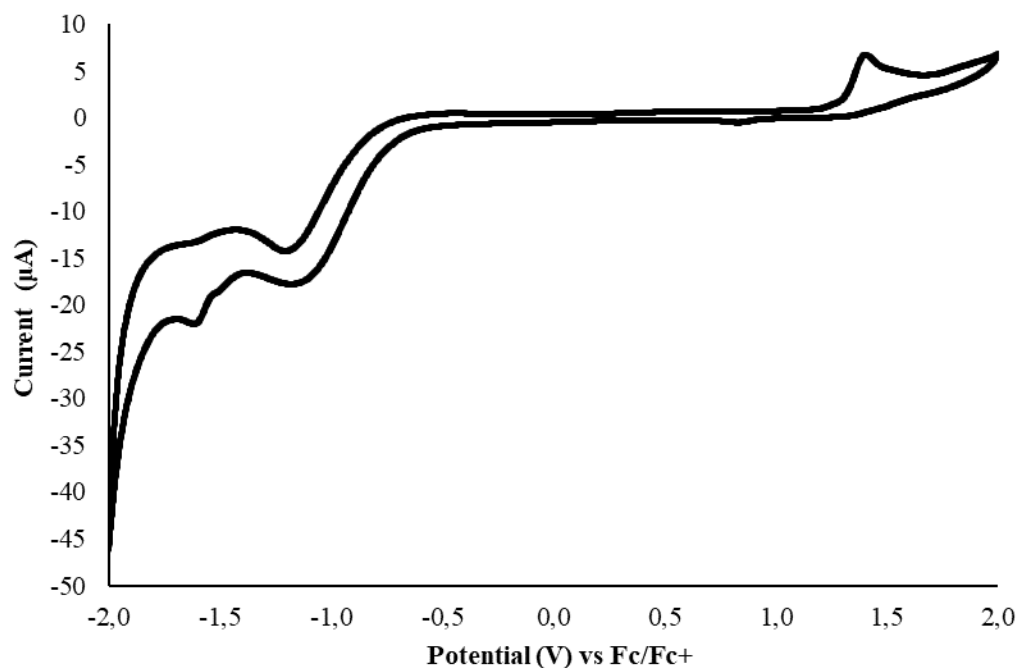


Figure A1 - 46 Cyclic voltammogram of Cu(**dmp**)(**Xantphos**)BF₄ in MeCN (1 mM) using TBAPF₆ (100 mM) as supporting electrolyte at a scan rate of 50 mV·s⁻¹

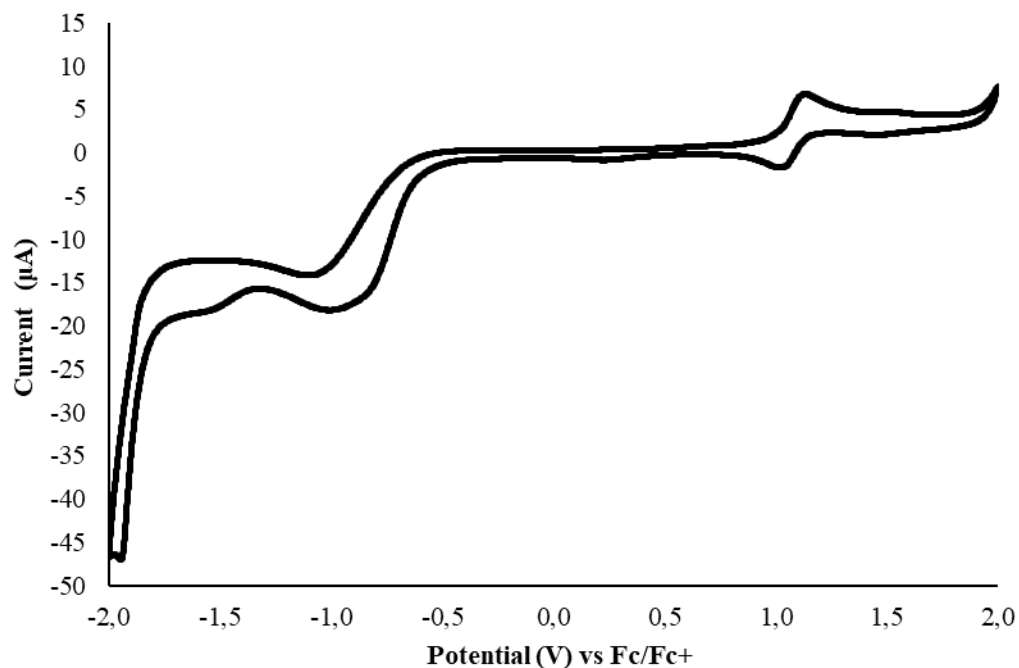
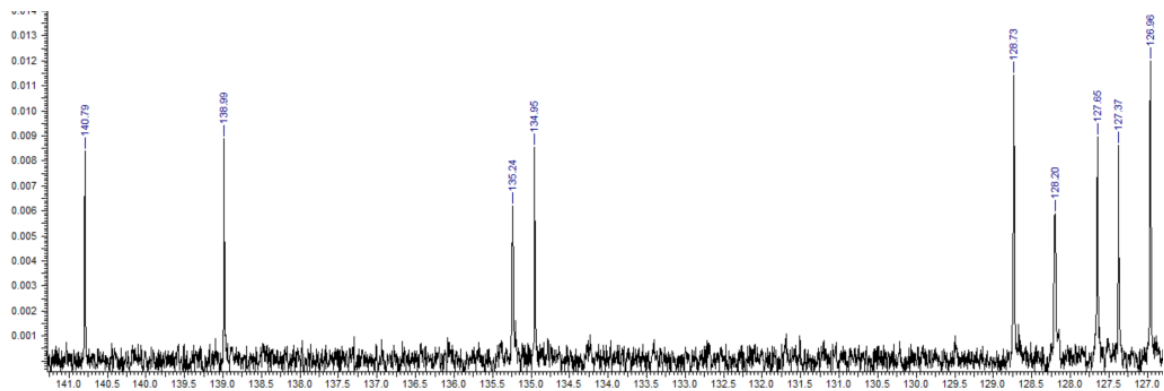
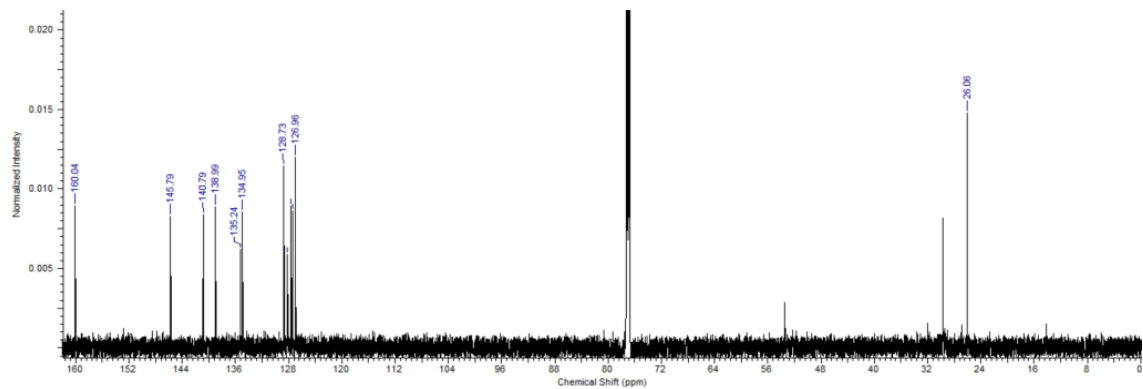
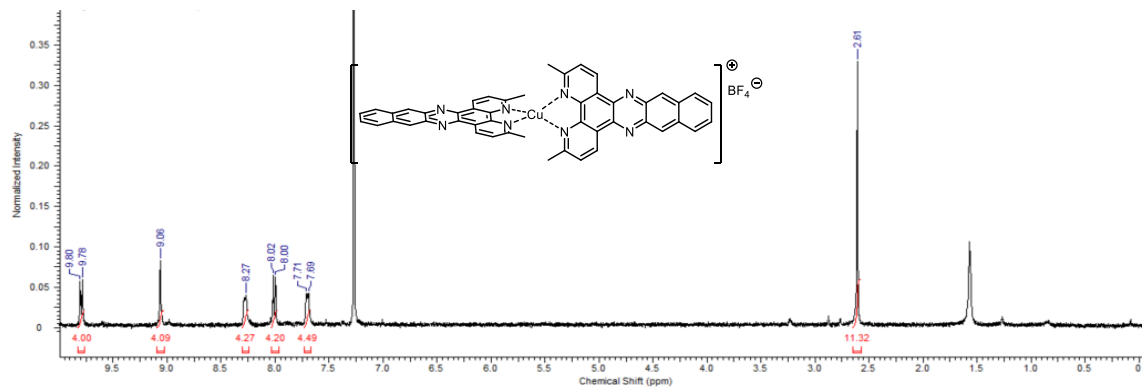
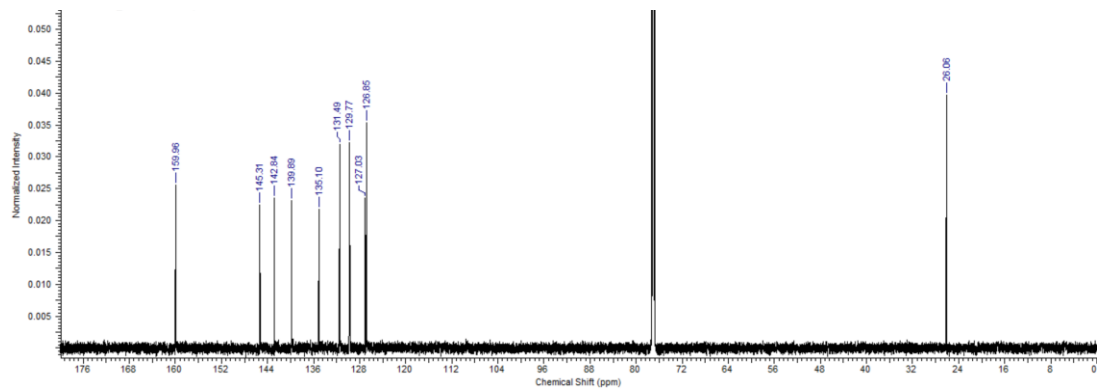
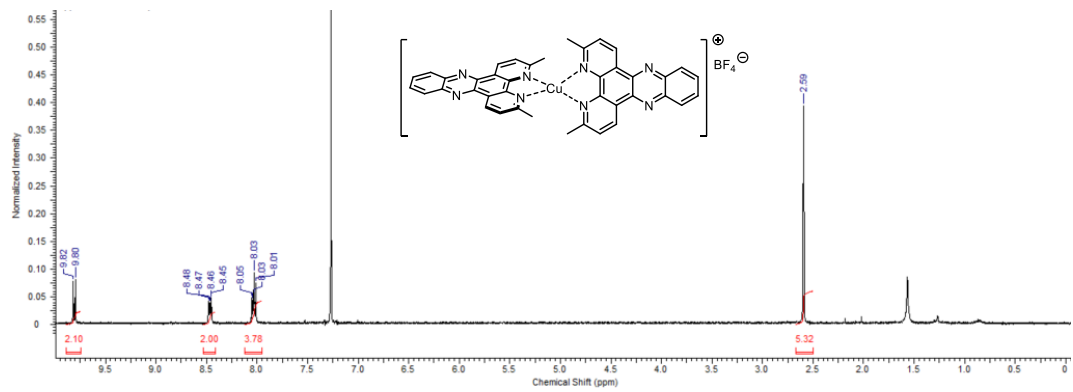
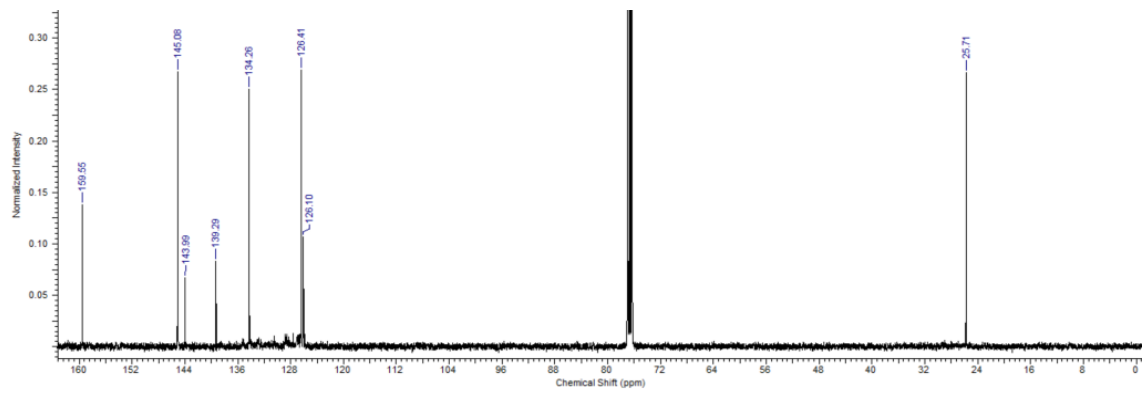
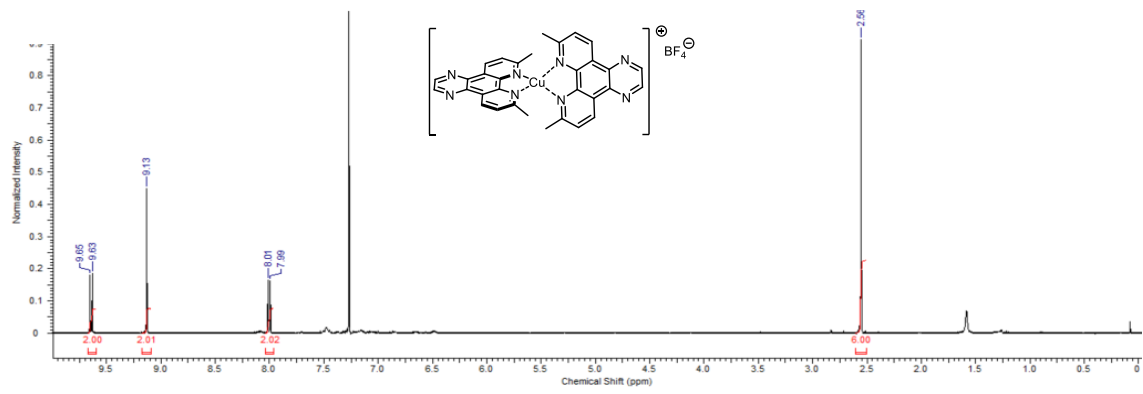


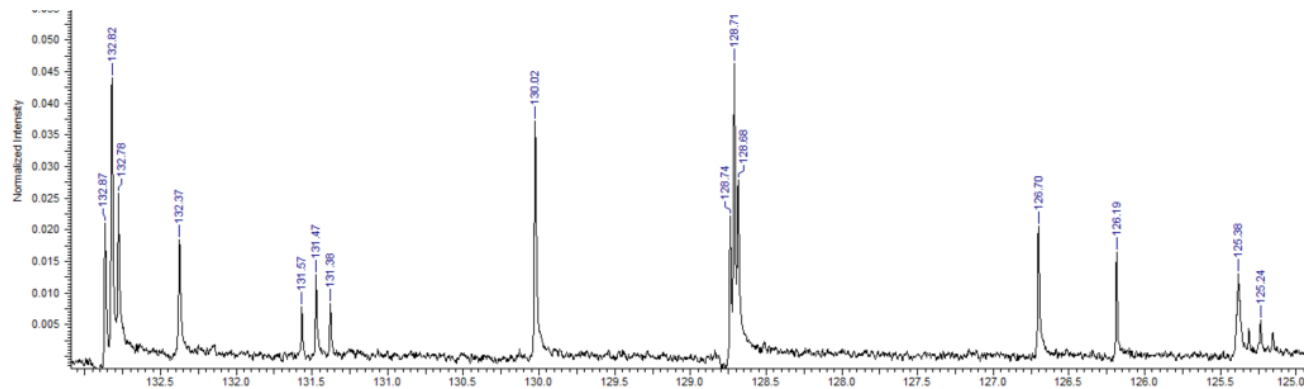
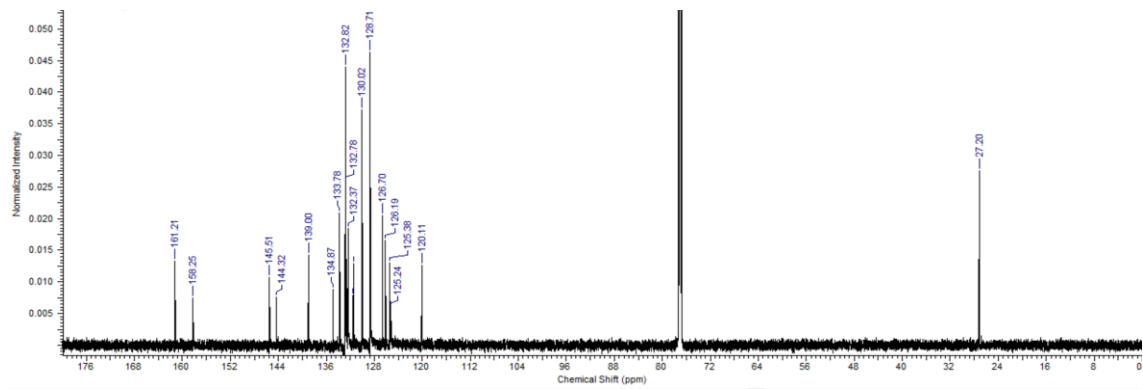
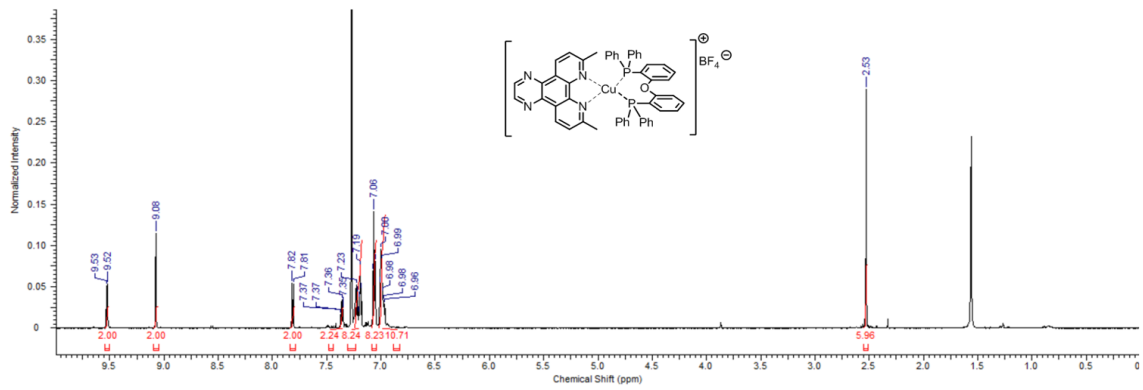
Figure A1 - 47 Cyclic voltammogram of Cu(**dmp**)(**dppf**)BF₄ in MeCN (1 mM) using TBAPF₆ (100 mM) as supporting electrolyte at a scan rate of 50 mV·s⁻¹

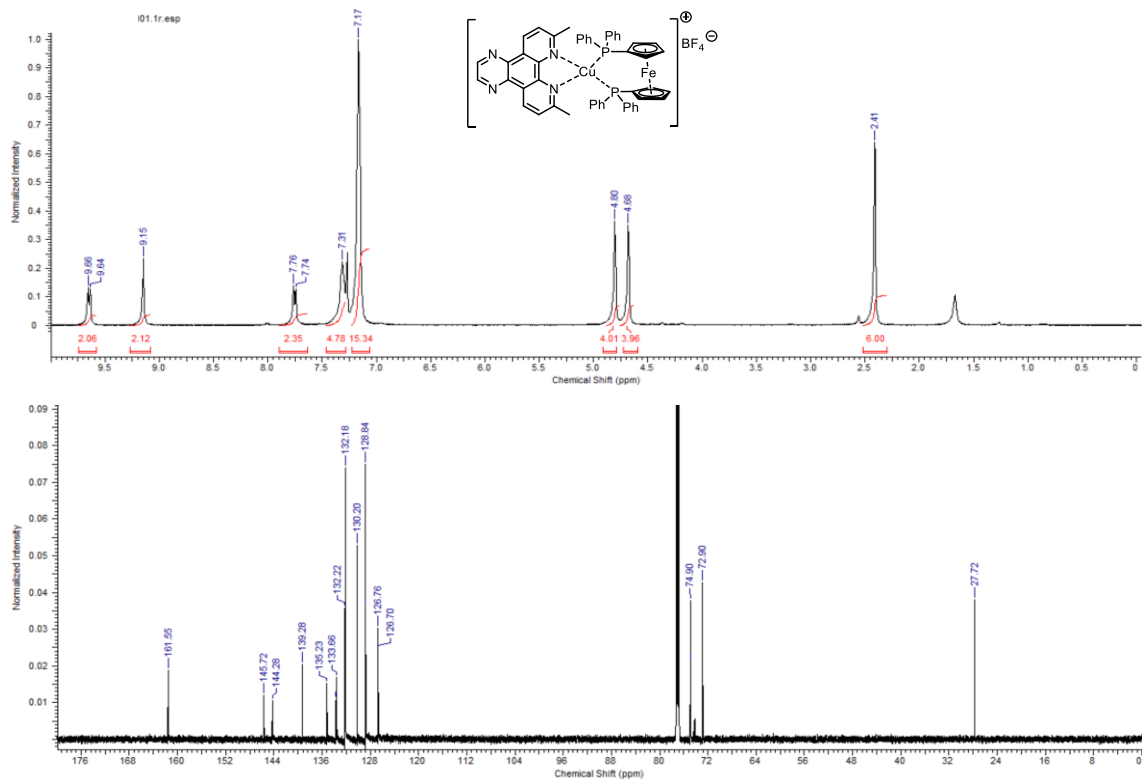
A1.8 - NMR Spectra

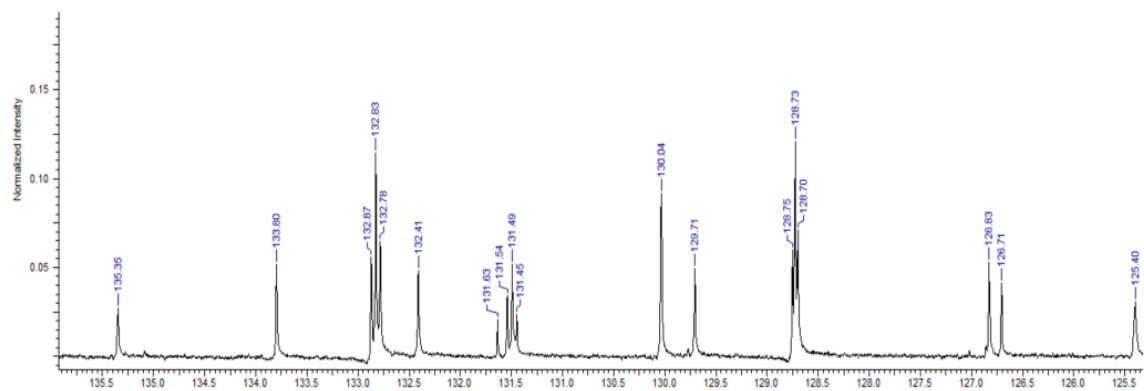
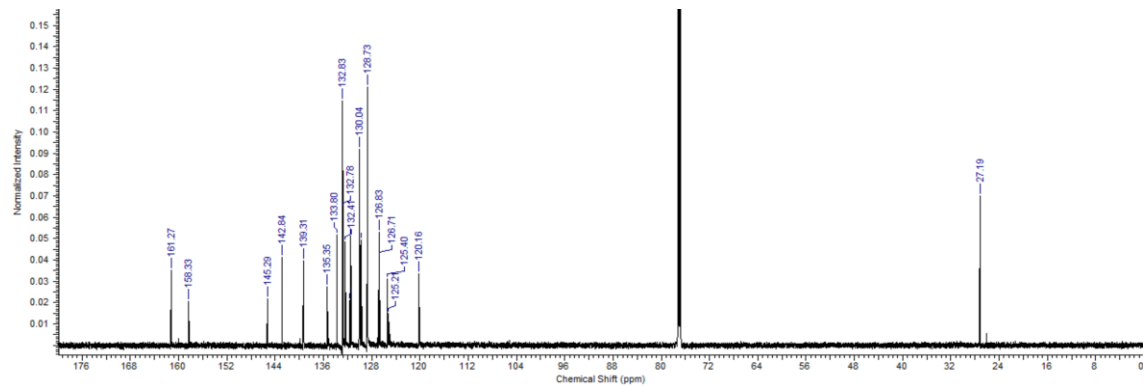
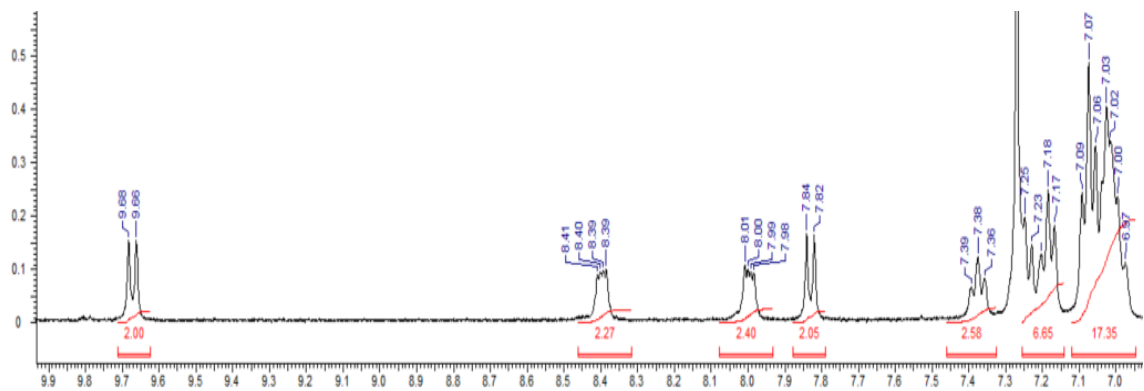
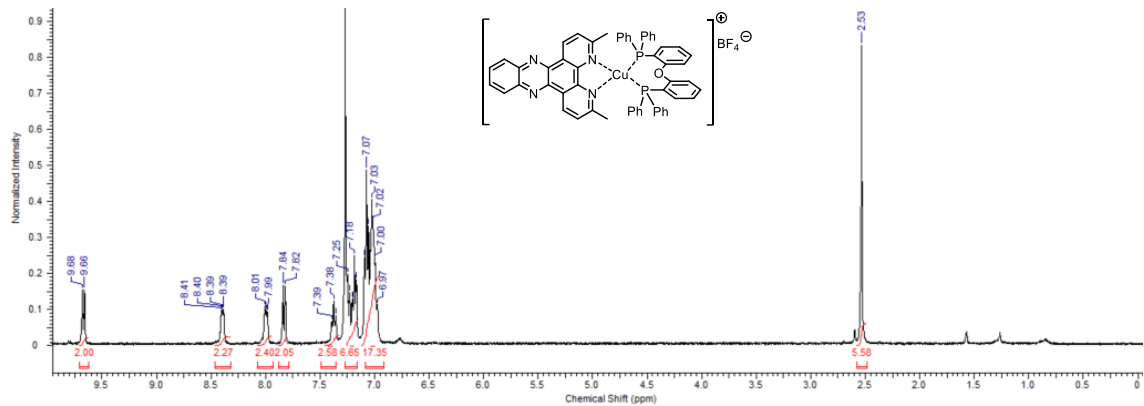


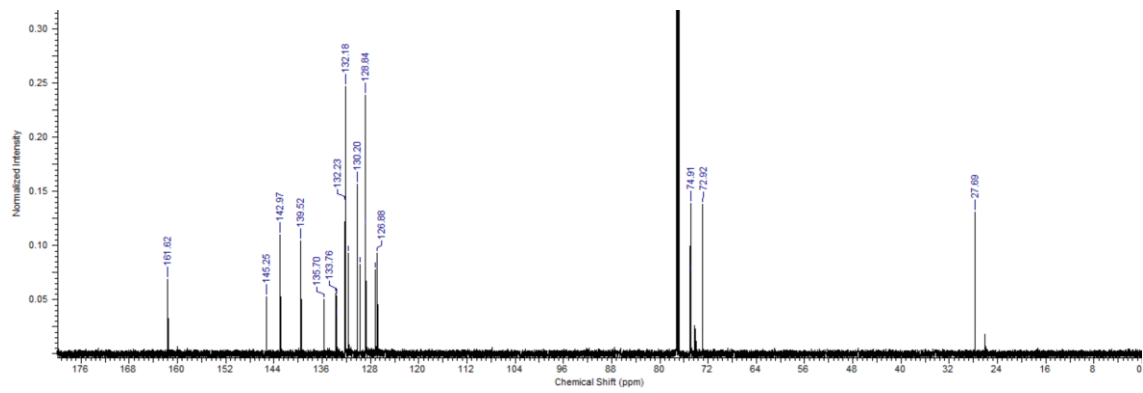
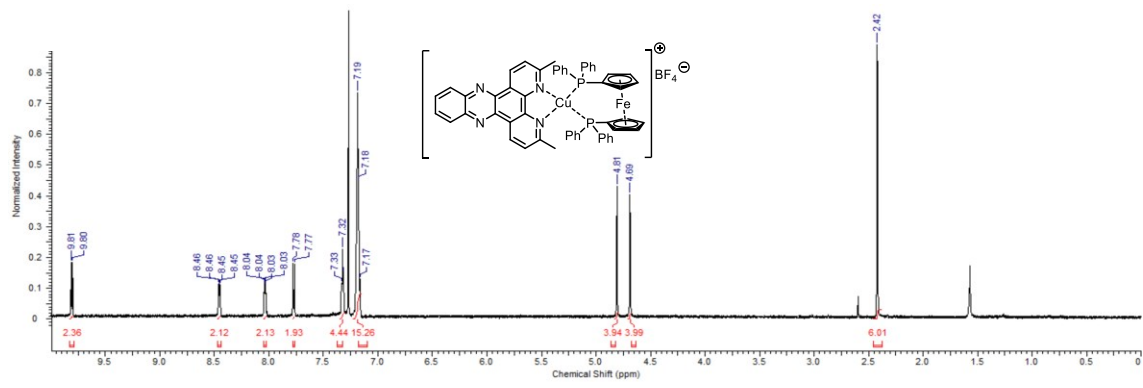


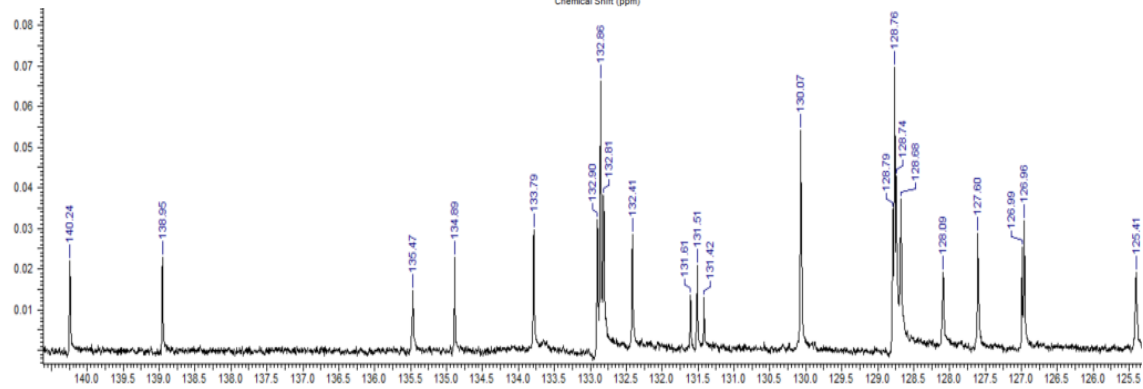
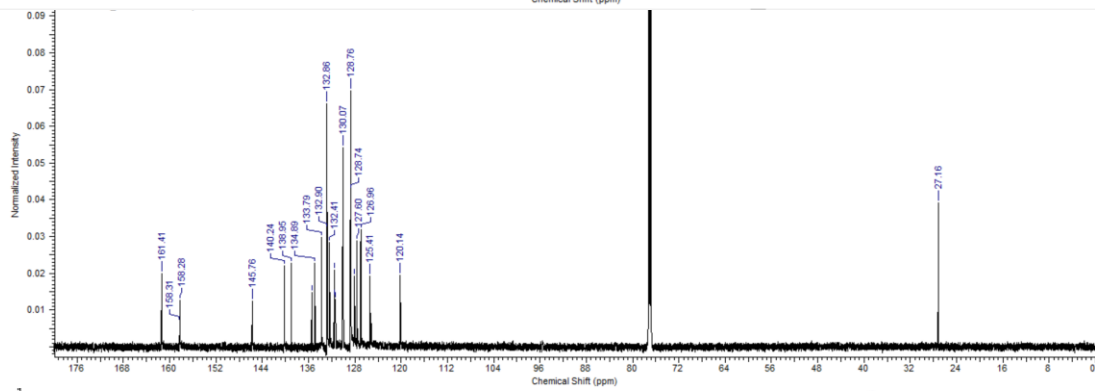
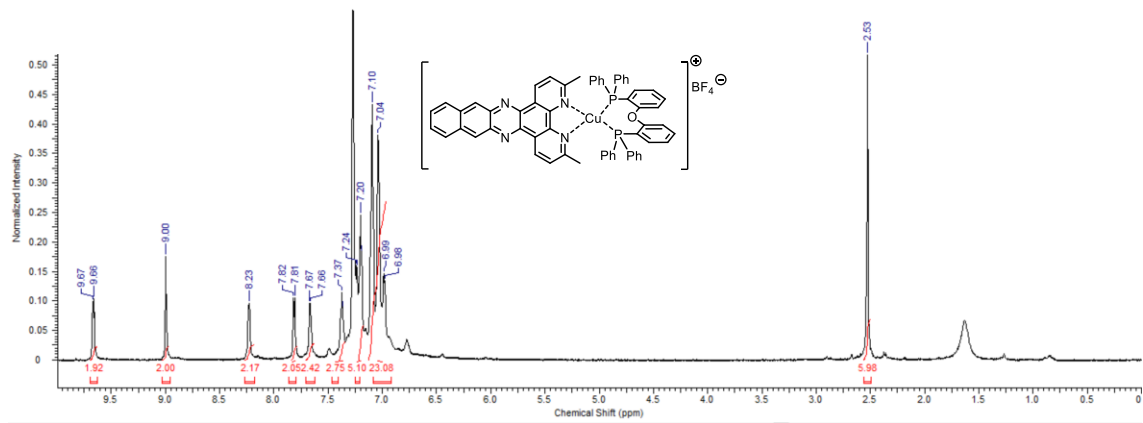


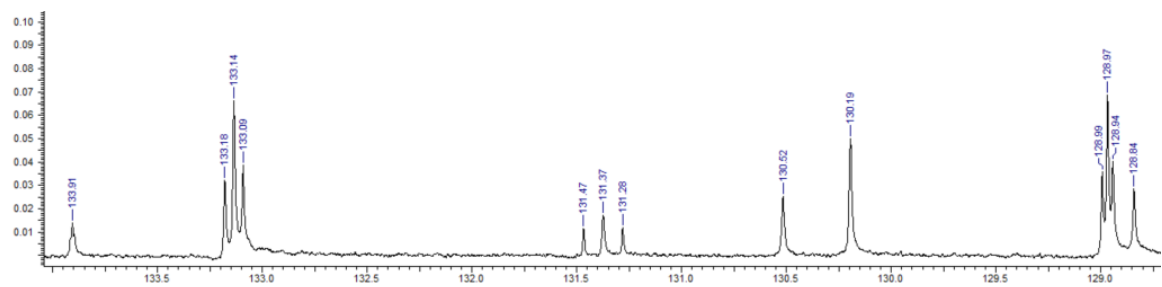
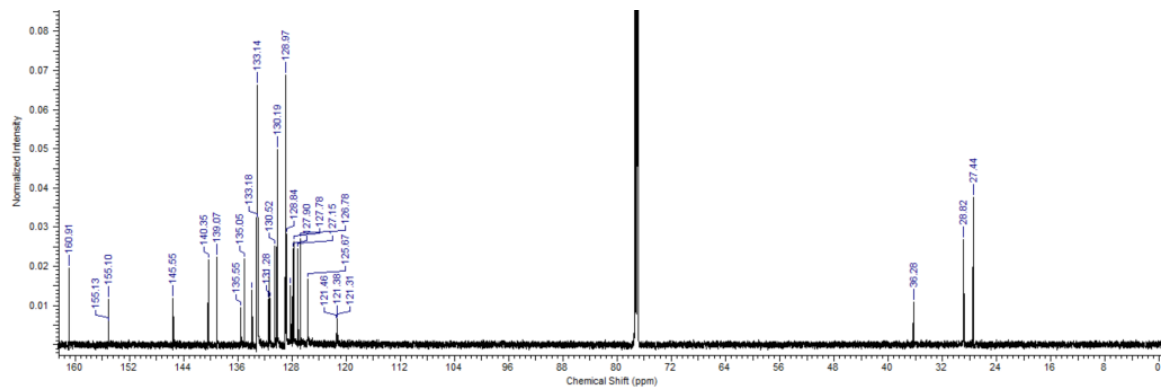
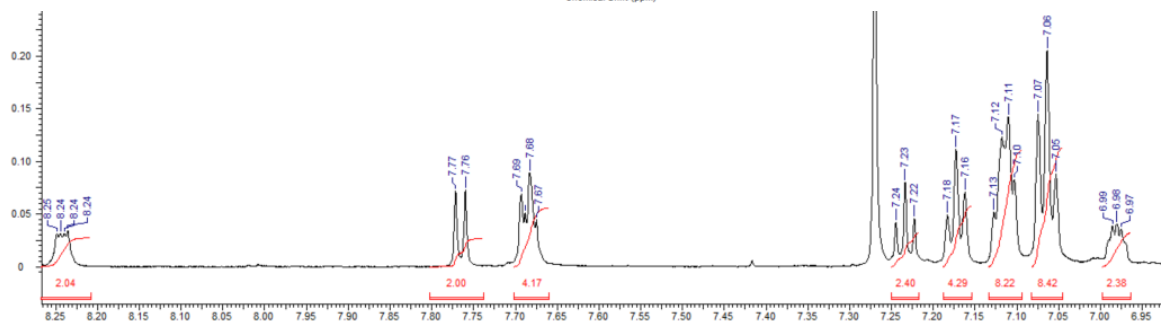
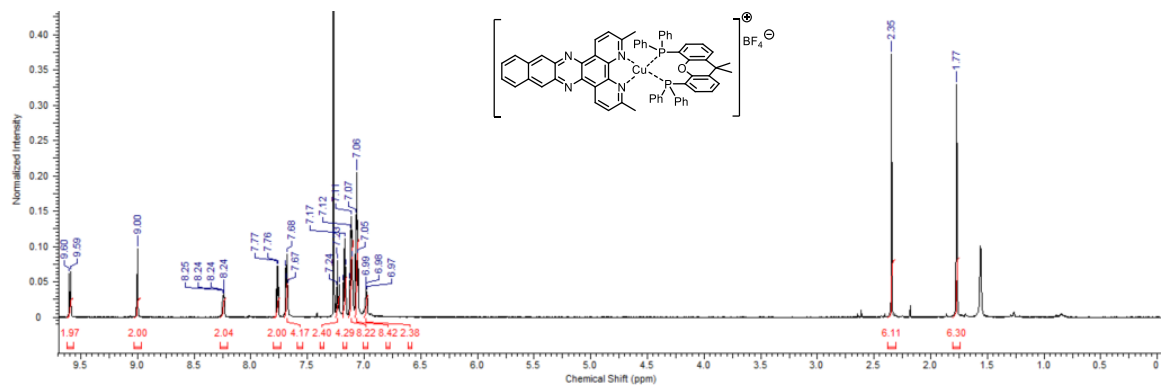


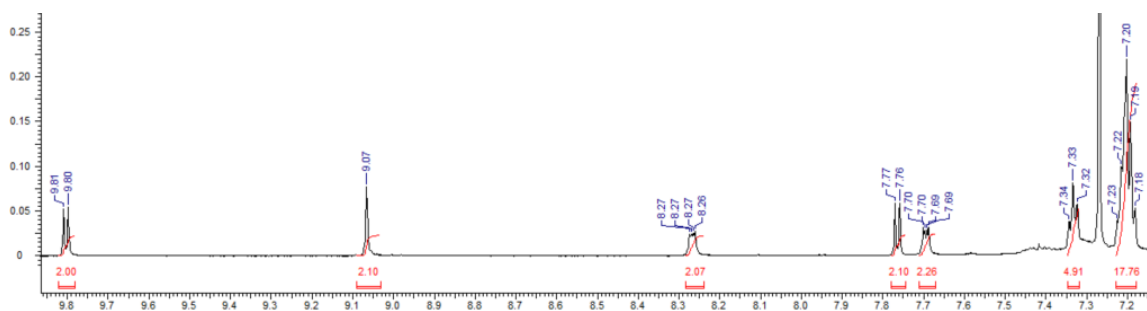
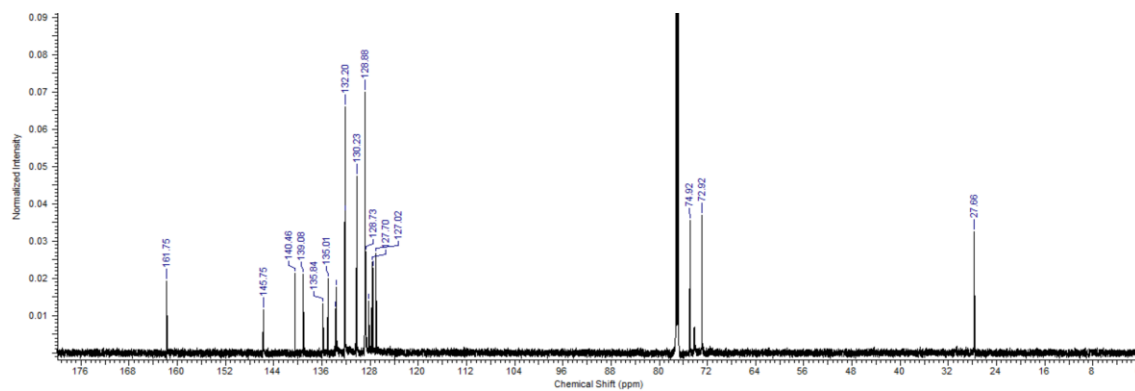
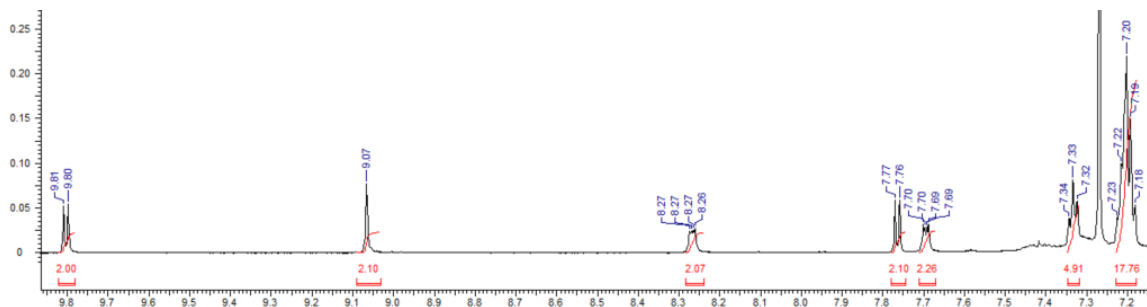
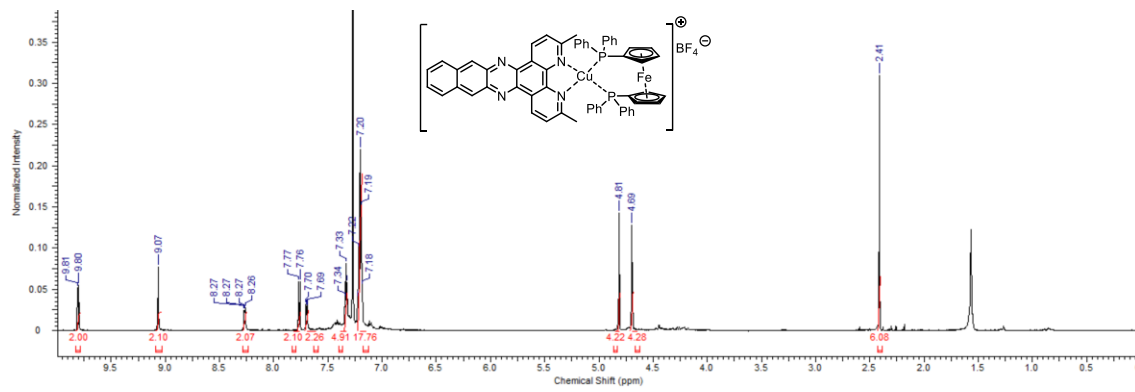












A1.9 - References

1. Still, W. C.; Kahn, M.; Mitra, A., *J. Org. Chem.* **1978**, *43* (14), 2923-2925.
2. Zheng, R. H.; Guo, H. C.; Jiang, H. J.; Xu, K. H.; Liu, B. B.; Sun, W. L.; Shen, Z. Q., *Chin. Chem. Lett.* **2010**, *21* (11), 1270-1272.

3. Guo, W.; Engelman, B. J.; Haywood, T. L.; Blok, N. B.; Beaudoin, D. S.; Obare, S. O., *Talanta* **2011**, *87*, 276-283.
4. Heberle, M.; Tschierlei, S.; Rockstroh, N.; Ringenberg, M.; Frey, W.; Junge, H.; Beller, M.; Lochbrunner, S.; Karnahl, M., *Chem. - Eur. J.* **2017**, *23* (2), 312-319.
5. Plutschack, M. B.; Seeberger, P. H.; Gilmore, K., *Org. Lett.* **2017**, *19* (1), 30-33.
6. Minozzi, C.; Grenier-Petel, J.-C.; Parisien-Collette, S.; Collins, S. K., *Beilstein J. Org. Chem.* **2018**, *14*, 2730-2736.
7. Tarantino, K. T.; Liu, P.; Knowles, R. R., *J. Am. Chem. Soc.* **2013**, *135* (27), 10022-10025.
8. Minozzi, C.; Caron, A.; Grenier-Petel, J. C.; Santandrea, J.; Collins, S. K., *Angew. Chem., Int. Ed.* **2018**, *57* (19), 5477-5481.
9. Farney, E. P.; Yoon, T. P., *Angew. Chem., Int. Ed.* **2014**, *53* (3), 793-797.

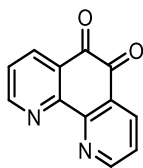
Annexe 2 – Supporting information of Chapter3

A2.1 General

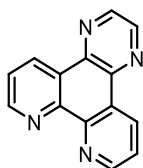
All reactions that were carried out under anhydrous conditions were performed under an inert argon or nitrogen atmosphere in glassware that had previously been dried overnight at 120 °C or had been flame dried and cooled under a stream of argon or nitrogen. All chemical products were obtained from Sigma-Aldrich Chemical Company, Oakwood Chemical or Alfa Aesar and were reagent quality. Technical solvents were obtained from VWR International Co. Anhydrous solvents (CH₂Cl₂, Et₂O, THF, DMF, toluene, and *n*-hexane) were dried and deoxygenated using a GlassContour system (Irvine, CA). Isolated yields reflect the mass obtained following flash column silica gel chromatography. Organic compounds were purified using silica gel obtained from Silicycle Chemical division (40-63 nm; 230-240 mesh). Analytical thin-layer chromatography (TLC) was performed on glass-backed silica gel 60 coated with a fluorescence indicator (Silicycle Chemical division, 0.25 mm, F254.). Visualization of TLC plate was performed by UV (254 nm), KMnO₄ or *p*-anisaldehyde stains. All mixed solvent eluents are reported as v/v solutions. Concentration refers to removal of volatiles at low pressure on a rotary evaporator. All reported compounds were homogeneous by thin layer chromatography (TLC) and by ¹H NMR. NMR spectra were taken in deuterated CDCl₃ using Bruker AV-300 and AV-400 instruments unless otherwise noted. Signals due to the solvent served as the internal standard (CHCl₃: δ 7.27 for 1H, δ 77.0 for 13C). The acquisition parameters are shown on all spectra. The ¹H NMR chemical shifts and coupling constants were determined assuming first-order behavior. Multiplicity is indicated by one or more of the following: s (singlet), d (doublet), t (triplet), q (quartet), m (multiplet), br (broad); the list of couplings constants (*J*) corresponds to the order of the multiplicity assignment. High resolution mass spectroscopy (HRMS) was done by the Centre régional de spectrométrie de masse at the Département de Chimie, Université de Montréal from an Agilent LC-MSD TOF system using ESI mode of ionization unless otherwise noted.

A2.2 Synthesis of ligands and catalysts

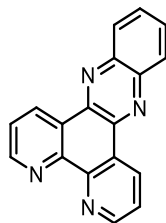
General Comments/Procedures for Ligands:



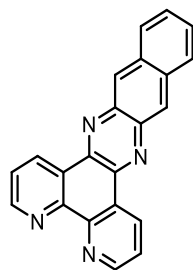
1,10-Phenanthroline-5,6-dione: 1,10-Phenanthroline (3.00 g, 16.6 mmol) was dissolved in concentrated H₂SO₄ (20 mL) and H₂O (10 mL) at 0°C. NaBrO₃ (2.76 g, 18.3 mmol, 1.1 eq.) in H₂O (10 mL) was then added dropwise. The yellow solution was then stirred for 36 h. The mixture was then neutralized under intense stirring, using a saturated solution of K₂CO₃. The mixture was extracted with CH₂Cl₂ three times, and the organic phase dried with MgSO₄. The solution was concentrated *in vacuo*. Purification by flash column chromatography (100% CH₂Cl₂ → 95:5 CH₂Cl₂:MeOH) afforded the pure product as a yellow powder (1.89 g, 54%). Spectral data were in accordance with previous reports.¹ **¹H NMR (500 MHz, CDCl₃):** δ 9.12 (dd, *J* = 4.7, 1.9 Hz, 2H), 8.51 (dd, *J* = 7.9, 1.8 Hz, 2H), 7.59 (dd, *J* = 7.9, 4.7 Hz, 2H).



Pyrazino[2,3-f][1,10]phenanthroline (dpq): 1,10-Phenanthroline-5,6-dione (400 mg, 1.9 mmol, 1.0 equiv), ethylenediamine (152 μL, 2.28 mmol, 1.2 equiv.) and *p*-toluenesulfonic acid (5.78 mg, 0.02 eq.) were all dissolved in EtOH (10 mL, 0.19 M). The solution was then refluxed for 18 h in a sealed tube. The solution was cooled down to room temperature and water was added. The mixture was extracted with CH₂Cl₂ three times, and the organic phase dried with MgSO₄. The solution was concentrated *in vacuo*. Purification by flash column chromatography (100% CH₂Cl₂ → 95:5 CH₂Cl₂:MeOH) afforded the pure product as a pale orange solid (365 mg, 83 %). Spectral data were in accordance with previous reports.² **¹H NMR (500 MHz, CDCl₃):** δ 9.52 (dd, *J* = 8.1, 1.8 Hz, 2H), 9.32 (dd, *J* = 4.4, 1.8 Hz, 1H), 9.00 (s, 2H), 7.82 (dd, *J* = 8.1, 4.4 Hz, 2H).



Dipyrido[3,2-a:2',3'-c]phenazine (dppz): 1,10-Phenanthroline-5,6-dione (500 mg, 2.38 mmol, 1.0 eq.), 1,2-phenylenediamine (289mg, 2.62 mmol, 1.1 eq.) and *p*-toluenesulfonic acid (4.52 mg, 28.8 μ mol, 0.01 eq.) were all dissolved in EtOH (10 mL, 0.19 M). The solution was then refluxed for 18 h in a sealed tube. The solution was cooled down to room temperature and water was added. The mixture was extracted with CH₂Cl₂ three times, and the organic phase dried with MgSO₄. The solution was concentrated *in vacuo*. Purification by flash column chromatography (100% CH₂Cl₂ \rightarrow 95:5 CH₂Cl₂:MeOH) afforded the pure product as an orange solid (432 mg, 64 %). Spectral data were in accordance with previous reports.³ **¹H NMR (500 MHz, CDCl₃):** δ 9.67 (dd, *J* = 8.2, 2.0 Hz, 2H), 9.32 (s, 2H), 8.39 – 8.32 (m, 2H), 7.97 – 7.90 (m, 1H), 7.87 – 7.80 (m, 2H).



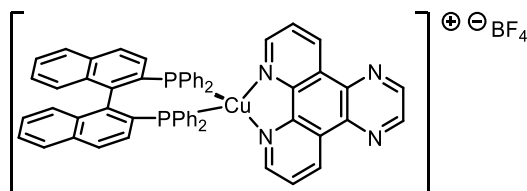
Benzo[i]dipyrido[3,2-a:2',3'-c]phenazine (bdppz): 1,10-Phenanthroline-5,6-dione (200 mg, 0.95 mmol, 1 eq.), 2,3-Diaminonaphthalene (166 mg, 1.05 mmol, 1.1 eq.) and *p*-toluenesulfonic acid (1.81 mg, 9.52 μ mol, 0.01 eq.) were all dissolved in EtOH (10 mL, 0.19 M). The solution was then refluxed in a sealed tube for 30 min until a precipitate formed. The mixture was cooled down to room temperature, the solid was filtered and washed with a minimum of acetone to give the pure product as a dark orange solid (134 mg, 42 %). Spectral data were in accordance with previous reports.³ **¹H NMR (500 MHz, CDCl₃):** δ 9.70 (d, *J* = 8.1 Hz, 2H), 9.41 – 9.25 (m, 2H), 8.96 (s, 2H), 8.21 (dd, *J* = 6.4, 3.3 Hz, 2H), 7.93 – 7.78 (m, 2H), 7.65 (dd, *J* = 6.6, 3.1 Hz, 2H).

Synthesis of Copper Complexes

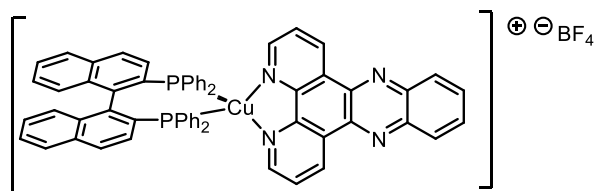
General Procedure for the Synthesis of Heteroleptic Complexes:

To a stirred solution of $[\text{Cu}(\text{MeCN})_4]\text{BF}_4$ (1.0 equiv.) in anhydrous CH_2Cl_2 (0.032 M) was added the corresponding phosphine (1.05 equiv.). The reaction was stirred at room temperature for one hour. Then, to the reaction mixture was added the corresponding diimine (1.05 equiv.). The reaction mixture was stirred for an additional hour. The reaction mixture was concentrated to approximately a fifth of the original volume and Et_2O was added dropwise to precipitate the product. Filtration afforded the desired complex as a coloured solid.

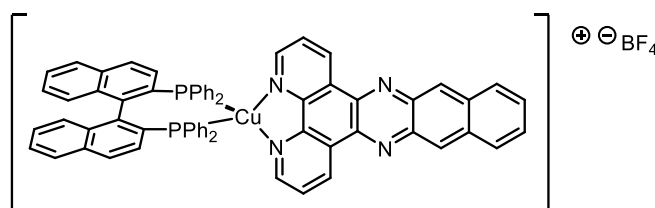
Note: Complexes bearing S- or R-BINAP were synthesized according to the same procedure and the corresponding ^1H NMR were in accordance with the racemic analogs.



[Cu(dpq)(BINAP)]BF₄ : Following the general procedure, $[\text{Cu}(\text{MeCN})_4]\text{BF}_4$ (50.0 mg, 0.16 mmol, 1 equiv.) and (rac)-2,2-bis(diphenylphosphino)-1,1-binaphthyl (99.2 mg, 0.16 mmol, 1 eq.) were dissolved in anhydrous dichloromethane (25 mL). After one hour of mixing, dpq (37.0 mg, 0.16 mmol, 1 eq.) was added. The reaction mixture was stirred for another hour. The solution was concentrated *in vacuo*, and 30 mL of diethyl ether was added to the solution. The desired product was obtained by filtration as a yellow solid (120 mg, 75%). **^1H NMR (700 MHz, Acetone- d_6):** δ 9.83 (dd, $J = 8.2, 1.5$ Hz, 2H), 9.38 – 9.35 (m, 2H), 9.31 (s, 2H), 8.31 (dd, $J = 8.1, 4.8$ Hz, 2H), 7.93 (d, $J = 8.6$ Hz, 2H), 7.80 (d, $J = 1.2$ Hz, 1H), 7.79 (s, 1H), 7.53 – 7.44 (m, 8H), 7.43 (s, 1H), 7.36 – 7.32 (m, 2H), 7.33 – 7.27 (m, 4H), 7.27 – 7.22 (m, 6H), 7.22 (s, 2H), 6.97 (d, $J = 8.6$ Hz, 2H), 6.89 – 6.85 (m, 2H), 6.74 – 6.70 (m, 4H). **^{13}C NMR (176 MHz, Acetone- d_6):** δ 153.3, 147.3, 145.8, 140.7, 140.3, 135.7, 135.2, 134.7, 134.3, 134.0, 133.5, 132.3, 131.5, 130.3, 130.3, 130.0, 130.0, 130.0, 129.0, 128.5, 128.3, 128.2, 127.8, 127.5, 127.4. **HRMS (ESI)** m/z calculated for $\text{C}_{58}\text{H}_{40}\text{CuN}_4\text{P}_2$ $[\text{M}]^+$ 917.2019; found 917.2006; **HRMS (ESI)** m/z calculated for $[\text{BF}_4]^-$ 87.0029; found 87.0048.

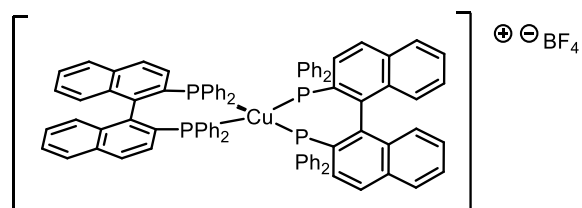


[Cu(dppz)(BINAP)]BF₄ : Following the general procedure, [Cu(MeCN)₄]BF₄ (50.0 mg, 0.16 mmol, 1 equiv.) and (rac)-2,2-bis(diphenylphosphino)-1,1-binaphthyl (99.2 mg, 0.16 mmol, 1 eq.) were dissolved in anhydrous dichloromethane (25 mL). After one hour of mixing, dppz (45.0 mg, 0.16 mmol, 1 eq.) was added. The reaction mixture was stirred for another hour. The solution was concentrated *in vacuo*, and 30 mL of diethyl ether was added to the solution. The desired product was obtained by filtration as a brown solid (132 mg, 77%). **¹H NMR (700 MHz, Acetone-d₆)**: δ 9.93 (dd, *J* = 8.0, 1.5 Hz, 2H), 9.34 (dd, *J* = 4.9, 1.4 Hz, 2H), 8.49 (dd, *J* = 6.4, 3.4 Hz, 2H), 8.31 (dd, *J* = 8.0, 4.8 Hz, 2H), 8.20 – 8.14 (m, 2H), 7.94 (d, *J* = 8.6 Hz, 2H), 7.81 (dd, *J* = 8.3, 1.3 Hz, 2H), 7.56 – 7.51 (m, 4H), 7.53 – 7.44 (m, 4H), 7.38 – 7.31 (m, 4H), 7.34 – 7.30 (m, 2H), 7.30 – 7.23 (m, 6H), 6.98 (dd, *J* = 8.6, 1.1 Hz, 2H), 6.91 – 6.85 (m, 2H), 6.74 (dd, *J* = 7.4 Hz, 4H). **¹³C NMR (176 MHz, Acetone-d₆)**: δ 153.4, 146.8, 143.6, 141.2, 140.4, 136.1, 135.2, 134.8, 134.3, 134.0, 133.5, 133.0, 132.3, 131.5, 130.5, 130.5, 130.4, 130.3, 130.1, 130.0, 129.0, 128.5, 128.3, 128.2, 127.9, 127.6, 127.6; **HRMS (ESI)** *m/z* calculated for C₆₂H₄₂CuN₄P₂ [M]⁺ 967.2175; found 967.2176; **HRMS (ESI)** *m/z* calculated for [¹¹B]F₄ [M]⁻ 87.0029; found 87.0050.

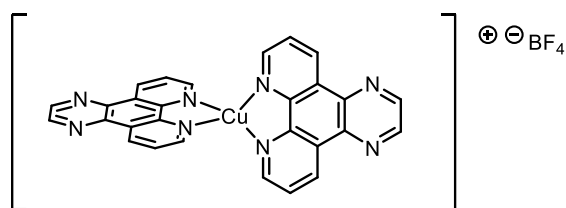


[Cu(bdppz)(BINAP)]BF₄ : Following the general procedure, [Cu(MeCN)₄]BF₄ (50.0 mg, 0.16 mmol, 1 equiv.) and (rac)-2,2-bis(diphenylphosphino)-1,1-binaphthyl (99.2 mg, 0.16 mmol, 1 eq.) were dissolved in anhydrous dichloromethane (25 mL). After one hour of mixing, bdppz (52.9 mg, 0.16 mmol, 1 eq.) was added. The reaction mixture was stirred for another hour. The solution was concentrated *in vacuo*, and 30 mL of diethyl ether was added to the solution. The desired product was obtained by filtration as a brown solid (93 mg, 53%). **¹H NMR (700 MHz, Acetone-d₆)**: δ 9.84 (d, *J* = 7.9 Hz, 2H), 9.32 (d, *J* = 4.7 Hz, 2H), 9.05 (s, 2H), 8.31 – 8.25 (m, 4H), 7.94 (d, *J* = 8.5 Hz, 2H),

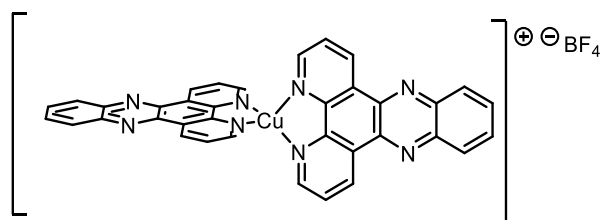
7.81 (d, $J = 8.3$ Hz, 2H), 7.65 (d, $J = 7.3$ Hz, 2H), 7.56 (q, $J = 6.1$ Hz, 4H), 7.48 (dd, $J = 7.4$ Hz, 5H), 7.34 (td, $J = 16.8, 15.1, 8.8$ Hz, 8H), 7.31 – 7.25 (m, 4H), 7.24 (d, $J = 7.4$ Hz, 2H), 6.98 (d, $J = 8.5$ Hz, 2H), 6.89 (dd, $J = 7.4$ Hz, 2H), 6.75 (dd, $J = 7.5$ Hz, 4H). **^{13}C NMR (176 MHz, Acetone- d_6):** δ 153.50, 147.27, 142.06, 140.35, 139.47, 136.12, 135.80, 135.27, 134.75, 134.33, 133.99, 133.50, 132.29, 131.51, 130.78, 130.39, 130.27, 130.09, 130.07, 129.42, 129.04, 128.93, 128.67, 128.53, 128.34, 128.15, 127.86, 127.76, 127.55. **HRMS (ESI)** m/z calculated for $\text{C}_{66}\text{H}_{44}\text{CuN}_4\text{P}_2$ $[\text{M}]^+$ 1017.23317; found 1017.23595; **HRMS (ESI)** m/z calculated for $[\text{B}^{11}\text{F}_4]^-$ 87.0035; found 87.0047.



$[\text{Cu}(\text{BINAP})_2]\text{BF}_4$: $[\text{Cu}(\text{MeCN})_4]\text{BF}_4$ (50.0 mg, 0.16 mmol, 1 equiv.) and (rac)-2,2-Bis(diphenylphosphino)-1,1-binaphthyl (198 mg, 0.32 mmol, 2 eq.) were dissolved in anhydrous dichloromethane (5 mL) in a sealed tube. The solution was sparged with N_2 for 5 min, and the reaction was mixed at 90°C for 16h. The reaction was cooled down, and 40 mL of deoxygenated Et_2O was added. The desired product was obtained by filtration as a white powder (183 mg, 82%). **^1H NMR (500 MHz, Acetone- d_6):** δ 8.02 (d, $J = 6.9$ Hz, 8H), 7.95 (d, $J = 8.8$ Hz, 4H), 7.74 – 7.70 (m, 4H), 7.68 – 7.63 (m, 9H), 7.53 (dd, $J = 7.6$ Hz, 8H), 7.46 (ddd, $J = 8.0, 6.8, 1.1$ Hz, 4H), 7.27 – 7.21 (m, 12H), 7.06 (dd, $J = 8.7, 1.0$ Hz, 4H), 6.47 (dd, $J = 7.4$ Hz, 4H), 5.96 (dd, $J = 7.6$ Hz, 8H). **^{13}C NMR (176 MHz, Acetone- d_6):** δ 140.74, 137.86, 134.83, 134.31, 134.11, 132.91, 132.44, 132.03, 129.76, 129.68, 129.61, 129.36, 129.01, 128.09, 127.80, 127.53, 127.32. **HRMS (ESI)** m/z calculated for $\text{C}_{88}\text{H}_{64}\text{CuP}_4$ $[\text{M}]^+$ 1307.32490; found 1307.33098; **HRMS (ESI)** m/z calculated for $[\text{B}^{11}\text{F}_4]^-$ 87.0035; found 87.0042.

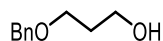


[Cu(dpq)₂]BF₄ : Following the general procedure, [Cu(MeCN)₄]BF₄ (50.0 mg, 0.16 mmol, 1 equiv.) and dpq (74 mg, 0.38 mmol, 2 eq.) were dissolved in anhydrous dichloromethane (25 mL). After one hour of mixing, the solution was concentrated *in vacuo*, and 30 mL of diethyl ether was added to the solution. The desired product was obtained by filtration as a brown solid (74.2 mg, 76%). Note that we observed broad peaks in the NMR spectra as reported by others who prepared the complex through a different route. ⁴¹H NMR (500 MHz, DMSO-d₆): δ 9.81 – 9.55 (m, 1H), 9.43 – 9.27 (m, 1H), 9.26 – 9.08 (m, 1H), 8.40 – 8.09 (m, 1H). HRMS (ESI) m/z calculated for C₂₈H₁₆CuN₈ [M]⁺ 527.0788; found 527.0798; HRMS (ESI) m/z calculated for [¹¹B]F₄ [M]⁻ 87.0035; found 87.0041.



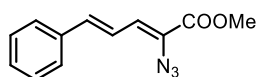
[Cu(dppz)₂]BF₄ : : Following the general procedure, [Cu(MeCN)₄]BF₄ (50.0 mg, 0.16 mmol, 1 equiv.) and dpq (89 mg, 0.38 mmol, 2 eq.) were dissolved in anhydrous dichloromethane (25 mL). After one hour of mixing, the solution was concentrated *in vacuo*, and 30 mL of diethyl ether was added to the solution. The desired product was obtained by filtration as a brown solid (83.9 mg, 74%). Note: Similar NMR spectra as [Cu(dpq)₂]BF₄ was observed. ¹H NMR (500 MHz, DMSO) δ 9.92 – 9.68 (m, 1H), 9.30 – 9.13 (m, 1H), 8.62 – 8.42 (m, 1H), 8.36 – 8.09 (m, 2H). HRMS (ESI) m/z calculated for C₃₆H₂₀CuN₈ [M]⁺ 627.1101; found 627.1114; HRMS (ESI) m/z calculated for [¹¹B]F₄ [M]⁻ 87.0051; found 87.0035.

A2.3 Substrat synthesis



3-(Benzyloxy)propanol : The benzyl(Bn)-protected alcohol was prepared using a procedure reported by Gilmore et al.⁵ NMR data was in accordance with what was previously reported.

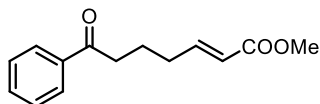
General Procedure for the Appel Reaction: To an open oven-dried reaction vial charged with a stir bar was added the copper catalyst (0.002 mmol, 0.01 equiv), the alcohol (33 mg, 0.20 mmol, 1.0 equiv), carbon tetrabromide (67 mg, 0.4 mmol, 2.0 equiv) and sodium bromide (41 mg, 0.40 mmol, 2.0 equiv). The flask vial was capped, purged with a stream of nitrogen and dry DMF (1.5 mL) was added via syringe. The reaction mixture was stirred under 400 nm irradiation for 24 h. The mixture was poured into a separatory funnel containing Et₂O (10 mL) and H₂O (10 mL). The layers were separated, and the aqueous layer was extracted with Et₂O (2 × 10 mL). The combined organic layers were washed with sat. Na₂S₂O₃ solution, brine, dried over Na₂SO₄ and concentrated *in vacuo*. The residue was purified by chromatography (100 % Hexanes) to afford the desired product as a colorless oil. NMR data was in accordance with what was previously reported.⁶



Methyl (2Z,4E)-2-azido-5-phenylpenta-2,4-dienoate: To a cooled (−22 °C) solution of NaOMe (2.67 mL, 9.93 mmol, 2.5 equiv.) in MeOH (2 mL) was added a solution of cinnamaldehyde (0.50 mL, 3.97 mmol, 1 equiv.) and methyl azidoacetate (9.93 mmol, 0.97 mL, 2.5 equiv.) dropwise over 20 min. The resulting reaction mixture was warmed to 10 °C. After four hours, the heterogeneous mixture was diluted with water (10 mL) and EtOAc (10 mL). The phases were separated, and the resulting aqueous phase was extracted with additional EtOAc (2 × 10 mL). The combined organic phases were washed with distilled water (2 × 10 mL) and brine (10 mL). The combined organic phases were dried over Na₂SO₄, filtered and the filtrate was concentrated *in vacuo*. The crude residue was purified by flash column chromatography (0:100 – 5:95 EtOAc:hexanes) to afford the product as a colorless oil (628 mg, 69 %). NMR data was in accordance with what was previously reported.⁷

General Procedure for the Sensitization of Vinyl Azides: To an oven-dried 4 mL vial with a stir bar were added the azide (46 mg, 0.20 mmol, 1 equiv.), the copper catalyst (0.002 mmol, 0.01 equiv.) and dry and degassed CHCl₃ (2 mL, 0.1 M). The solution was purged with N₂ and irradiated at room temperature with a 1W blue light-emitting diode (LED) strip for 3 hours. The mixture was concentrated *in vacuo*, and the crude residue was purified by silica gel flash column

chromatography (100% CH₂Cl₂) to afford the desired pyrrole as a white solid. NMR data was in accordance with what was previously reported.⁶



Methyl (E)-7-oxo-7-phenylhept-2-enoate: The ketone was prepared using a modified procedure reported by Knowles. Spectroscopic data was in accordance with what was previously reported.⁸

General Procedure for the PCET Reaction: To an oven dried reaction vial charged with a stir bar is added (35.6 mg, 0.16 mmol, 1 eq.), the copper catalyst (0.00314 mmol, 5 mol %), Hantzsch ester (55.34mg, 0.24 mmol 1.5 eq.), diphenylphosphoric acid (2mg, 0.00785 mmol 5 mol %), and THF (3.14 ml 0.05M). The mixture is then degassed for 5 minutes with a nitrogen stream and irradiated over night. The reaction mixture is then directly purified by flash chromatography (100 % →10%, *n*-hexanes:EtOAc). The yield of the desired bicyclic lactone is calculated by NMR. Spectroscopic data was in accordance with what was previously reported.⁶

A2.4 Photophysical data

Table A2 - 1 Tabular data for the maximum of absorbance and emission of copper complexes

Cu(NN)(BINAP)BF ₄	λ_{abs} (nm)	E (L/mol cm)	λ_{em} (nm)	E _T (eV)
DPQ	424	5752	521	2.38
DPPZ	433	6759	545	2.27
BDPPZ	462	5930	560	2.21

Absorbance Spectra

Absorbance UV-Vis spectra were recorded with Varian Cary 5000 UV-Vis-NIR spectrophotometer in a quartz cuvette.

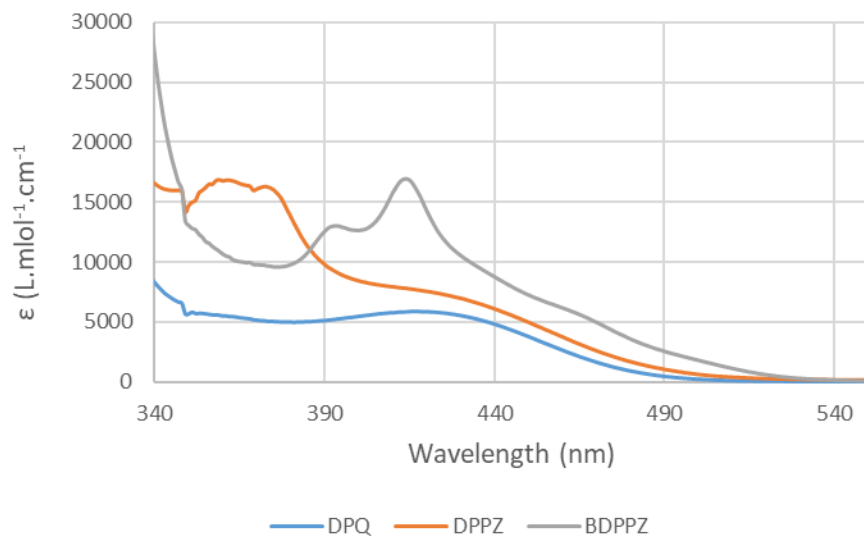


Figure A2 - 1 UV-visible absorption spectrum of new Cu(NN)(BINAP)BF₄ complexes recorded at ambient temperature in CH₂Cl₂ (1.0·10⁻⁴M)

Emission Spectra

Emission spectra were recorded with the Varian Cary Eclipse Fluorescence Spectrophotometer/Fluorometer in a quartz cuvette.

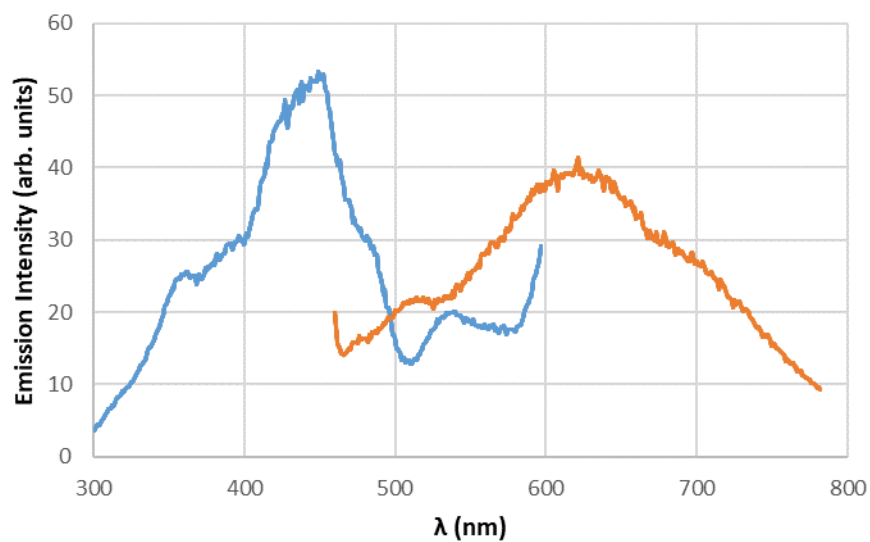


Figure A2 - 2 Excitation (blue curve) and emission (orange curve) spectrum of Cu(dpq)(BINAP)BF₄ excited at 450 nm, recorded at ambient temperature in CH₂Cl₂

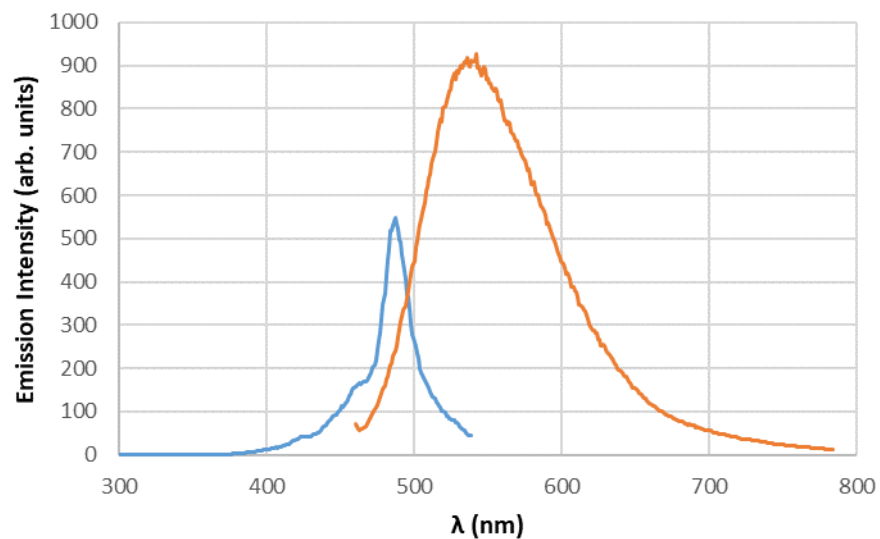


Figure A2 - 3 Excitation (blue curve) and emission (orange curve) spectrum of $\text{Cu(dppz)(BINAP)BF}_4$ excited at 450 nm, recorded at ambient temperature in CH_2Cl_2 ($5.0 \cdot 10^{-4}\text{M}$).

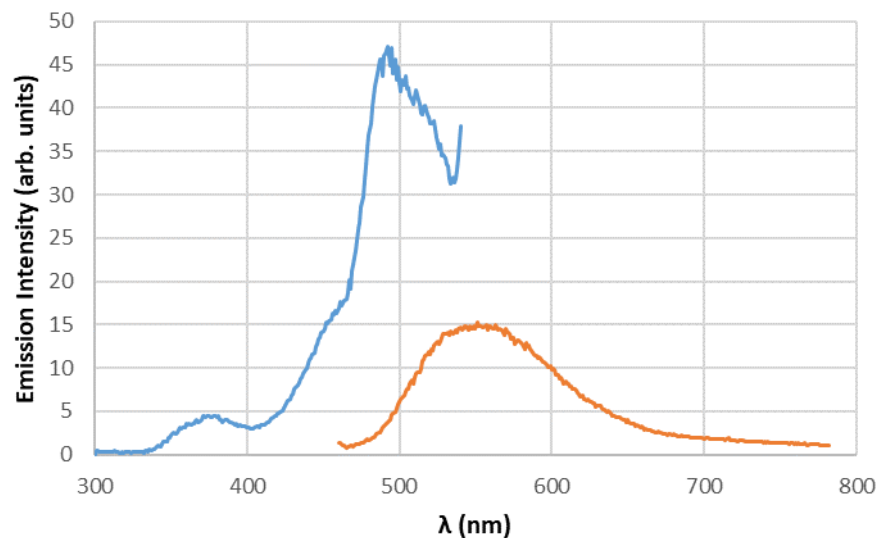


Figure A2 - 4 Excitation (blue curve) and emission (orange curve) spectrum of $\text{Cu(bdppz)(BINAP)BF}_4$ excited at 450 nm, recorded at ambient temperature in CH_2Cl_2 ($5.0 \cdot 10^{-4}\text{M}$).

Excited-state lifetime data

Lifetime measurements were done with an Edinburgh Instruments Mini Tau Lifetime Fluorimeter with an EPL 405 laser (exciting at 405 nm) with a standard deviation of 1-2%.

Table A2 - 2 Tabular data for the excited state lifetime of copper complexes

Cu(NN)(BINAP)BF ₄	τ (ns)
dpq	1.4
dppz	1.8
bdppz	2.3

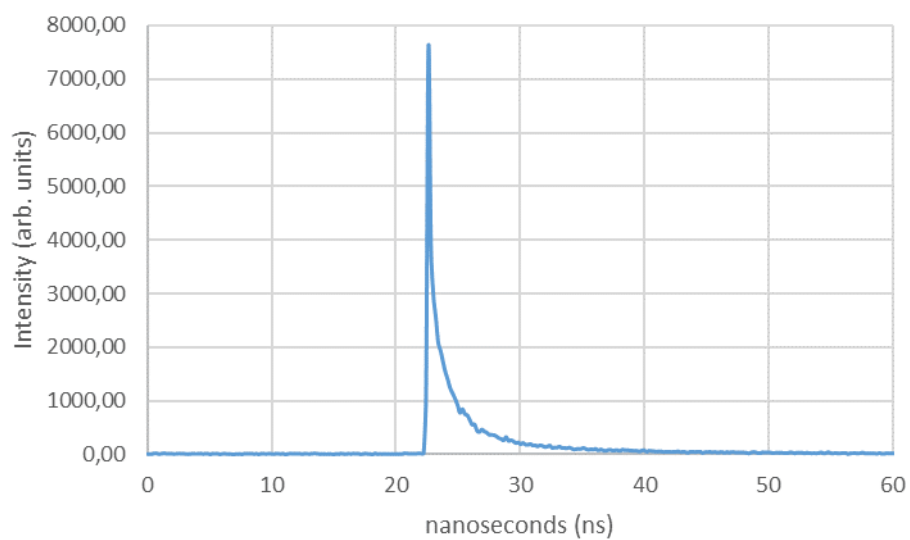


Figure A2 - 5 Lifetime spectrum of Cu(dpq)(BINAP)BF₄ excited at 405 nm, recorded at ambient temperature in degassed CH₂Cl₂ (1.25 · 10⁻⁴ M).

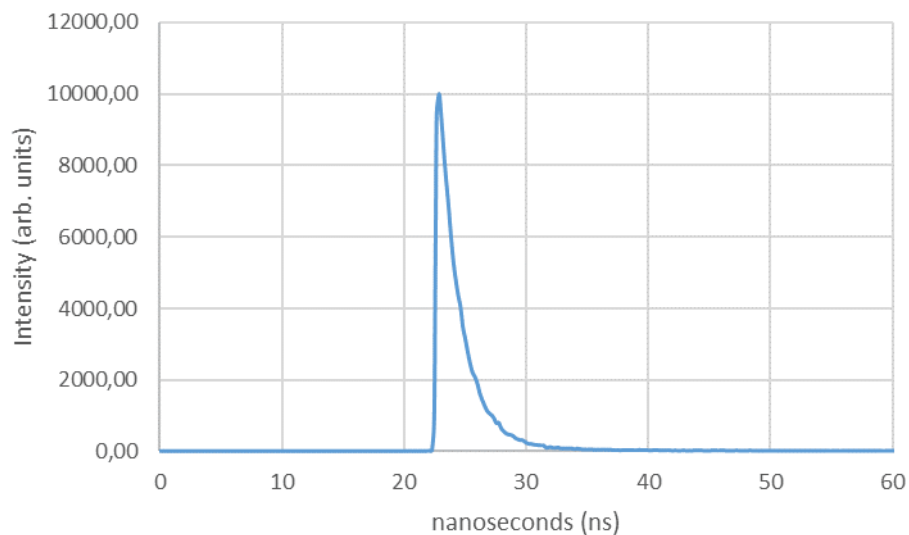


Figure A2 - 6 Lifetime spectrum of Cu(dppz)(BINAP)BF₄ excited at 405 nm, recorded at ambient temperature in degassed CH₂Cl₂ (1.25 · 10⁻⁴ M).

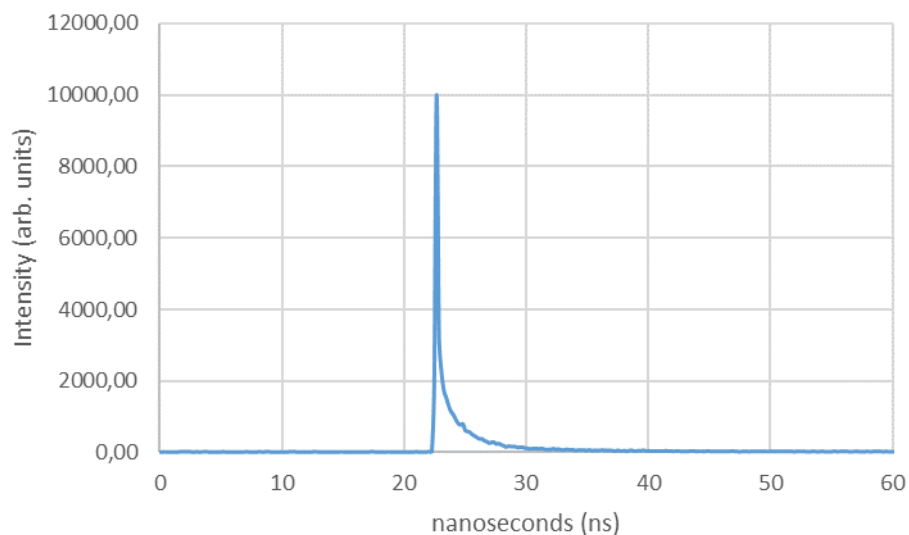


Figure A2 - 7 Lifetime spectrum of Cu(bdppz)(BINAP)BF₄ excited at 405 nm, recorded at ambient temperature in degassed CH₂Cl₂ (1.25 · 10⁻⁴ M).

A2.5 Electrochemical data

Osteryoung Square Wave Voltammetry (OSWV) measurements were done in dry acetonitrile (MeCN) with tetra-*N*-butylammonium hexafluorophosphate (TBAPF₆) as the supporting electrolyte using a standard three-electrode cell consisting of a silver wire pseudo-reference

electrode, a platinum wire counter electrode and a platinum working electrode with a BioLogic SP-50 potentiostat. The solutions were degassed with a flow of argon for 5 minutes prior to the measurements, which was left over the surface of the solution during the measurements. All measurements were carried out at 22 °C. All potentials were reported to the potential of the ferrocene/ferrocenium (Fc/Fc+) redox couple which was determined in the aforementioned electrolyte.

Table A2 - 3 Tabular data for the redox potentials of copper complexes

Cu(NN)(BINAP)BF ₄	E _{ox} (V)	E _{red} (V)	ΔE (V)
dpq	0.98	-1.14	2.12
dppz	1.01	-0.95	1.96
bdppz	1.01	-0.89	1.90

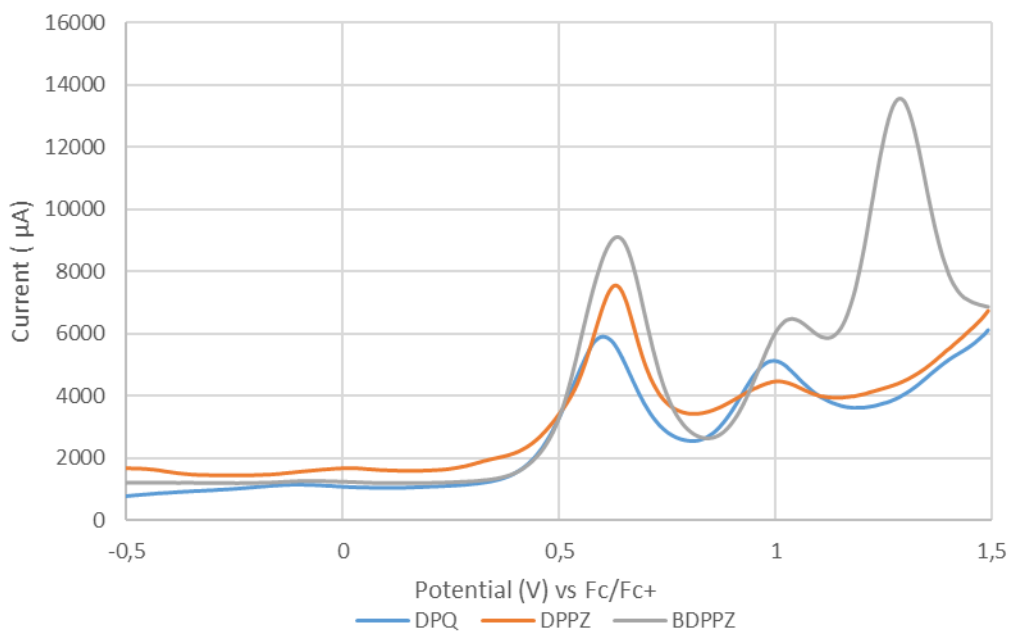


Figure A2 - 8 OSWVs of Cu(**NN**)(BINAP)BF₄ in MeCN (1 mM) using TBAPF₆ (100 mM) as supporting electrolyte (Anodic scan, frequency 20 Hz, amplitude 20 mV, step potential 5 mV).

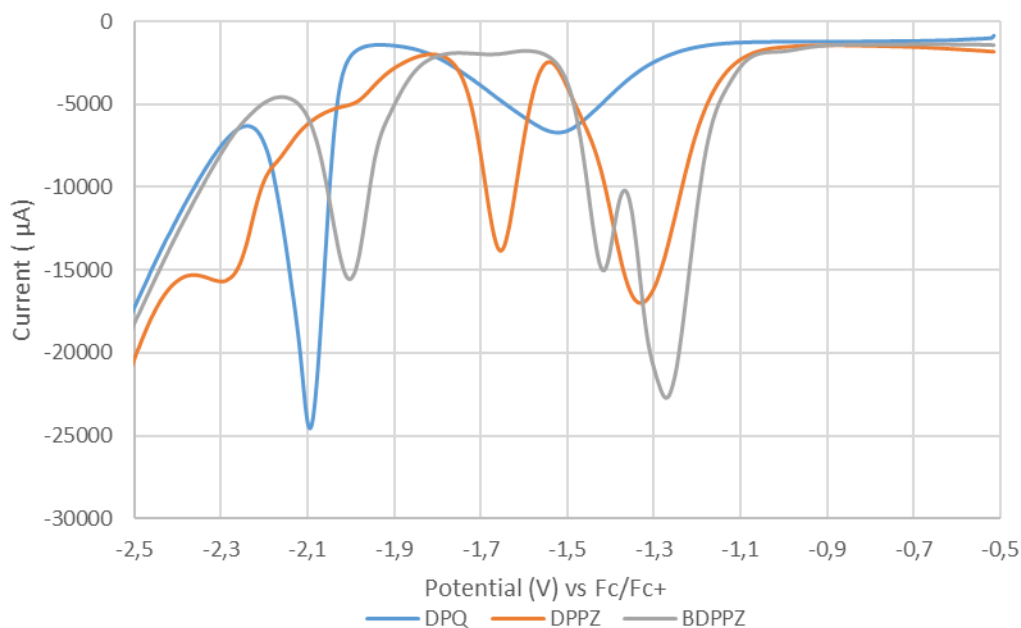


Figure A2 - 9 OSWVs of Cu(NN)(BINAP)BF₄ in MeCN (1 mM) using TBAPF₆ (100 mM) as supporting electrolyte (Cathodic scan, frequency 20 Hz, amplitude 20 mV, step potential 5 mV).

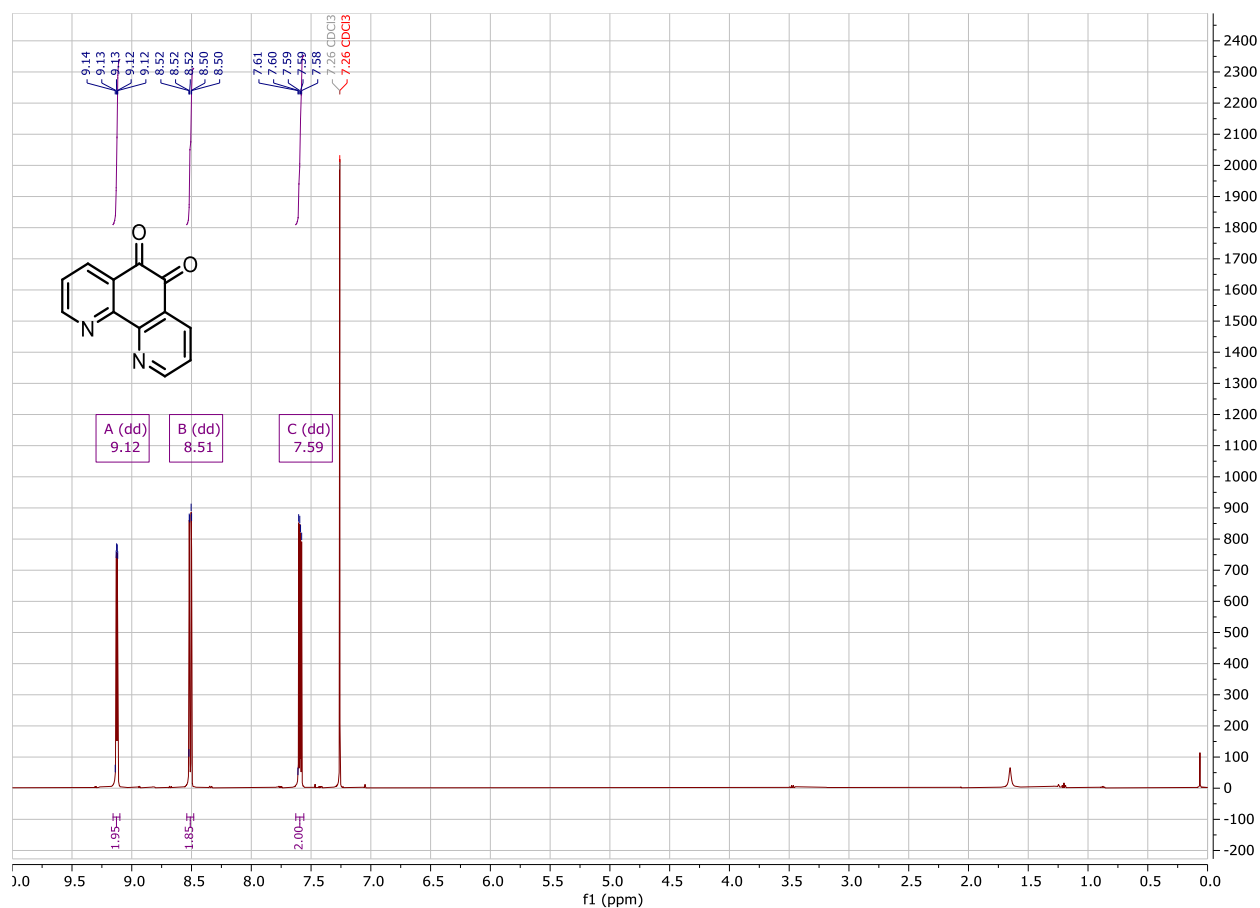
A2.6 Experimental Procedure for Biological Testing

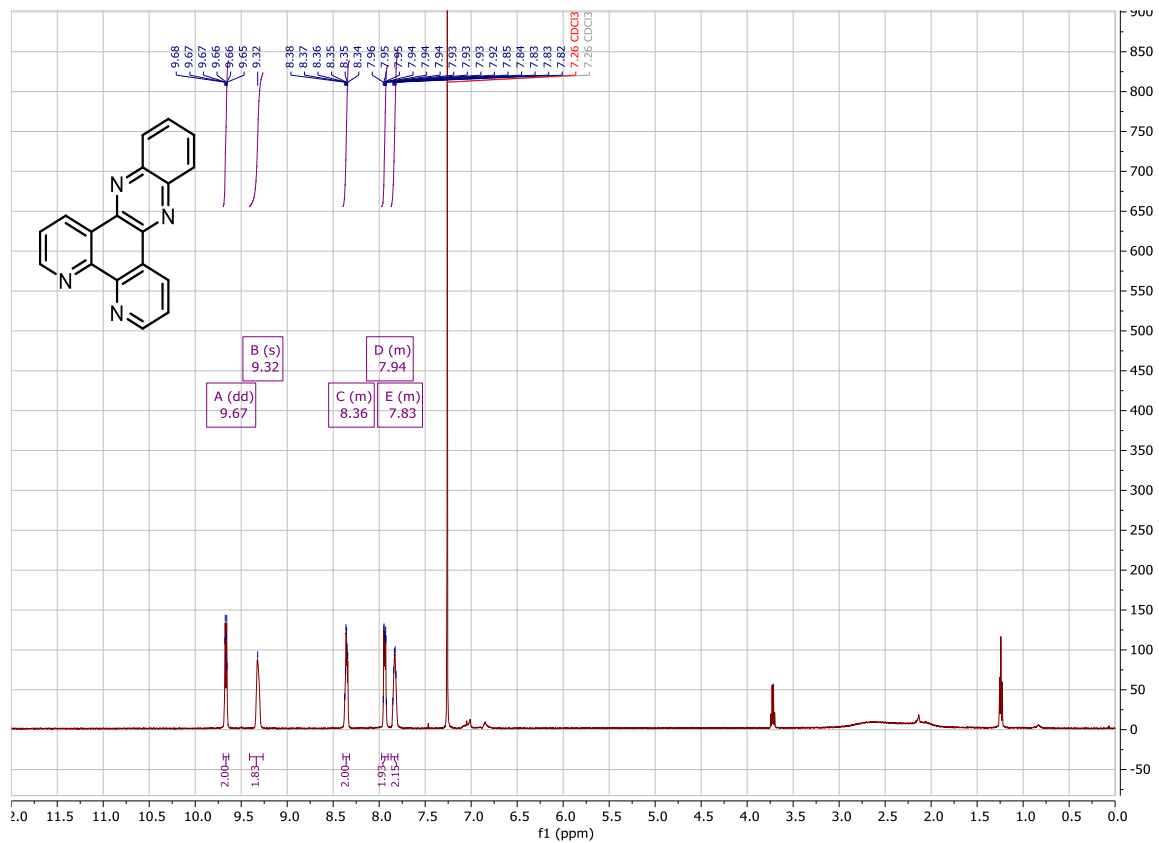
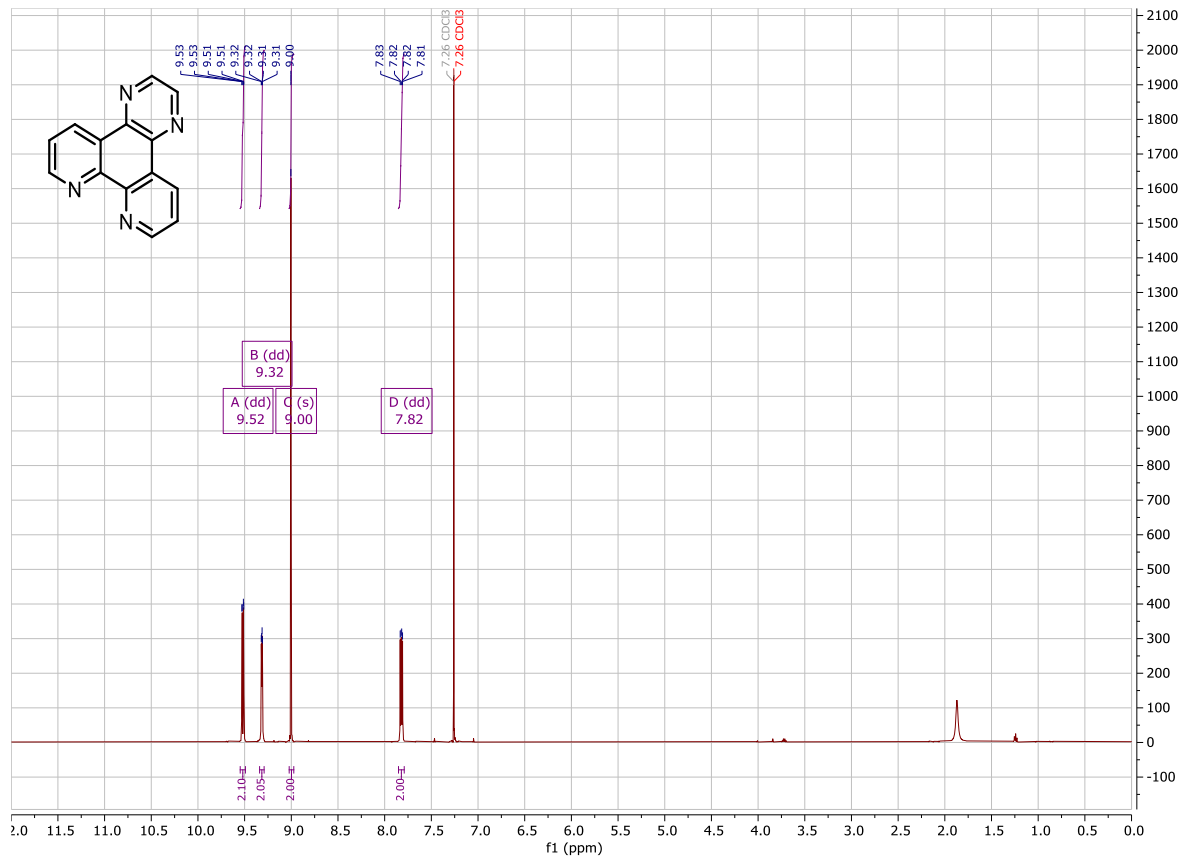
The biological activity of all the synthesized complexes **1-9** and controls **10-12** were determined by plating MDA-MB-231 in a 96 well plate at a density of 7,000 cells per well in MDA-MB-231 cell growth medium (Dulbecco's Modified Eagle's Medium (DMEM) supplemented with 10% FBS and 1,000 units/mL penicillin/streptomycin). The plates were incubated overnight in a 37°C humidified incubator ventilated with 5% CO₂. The growth media was aspirated off and then quadruplicate wells were treated with growth media containing 5 µM of the synthesized complexes or controls in 1% DMSO. The plate also contained wells with no cells which were designated as blank wells whereas wells with cells that were not treated with the compound but only with growth media containing 1% DMSO (vehicle) were designated as control wells. Following the addition of 5 µM of the synthesized complexes or controls, the plates were incubated in a 37°C humidified incubator ventilated with 5% CO₂ for 72 h. After incubation, 10 µL of 3-(4,5-dimethylthiazol-2-yl)-2,5-diphenyl tetrazolium bromide (MTT) reagent (5 mg/mL in PBS) was added to each well of the 96 well plate and incubated in a 37°C humidified incubator ventilated with 5% CO₂ for 2 h. After 2 h the media was aspirated off and 100 µL of DMSO was added. The plates were then shaken for 20 min to ensure complete dissolution of the purple

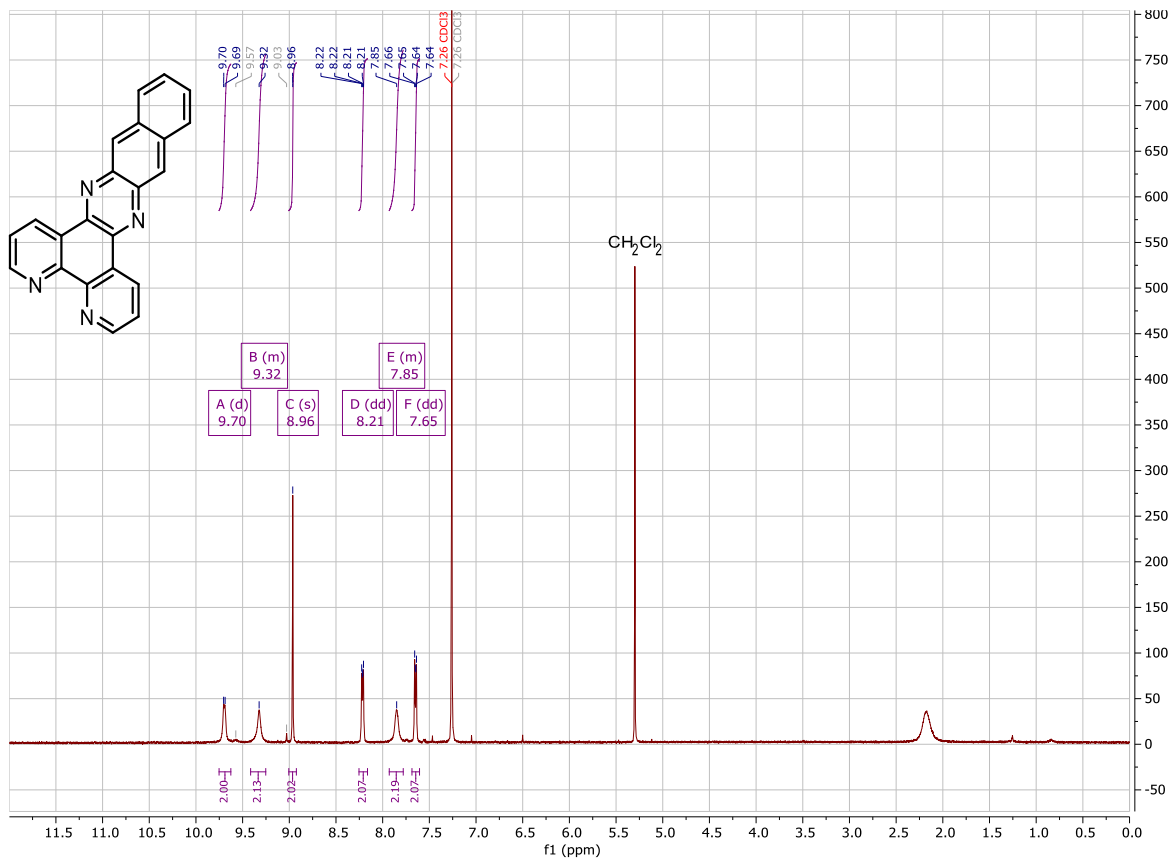
formazan crystals formed. Absorbance of each well was then measured at 570 nm. The mean absorbance values of the blank wells were calculated and subtracted from absorbance values for each well treated with 5 μ M of the synthesized complex or controls. The absorbance of the control wells was also taken and subtracted with the average of the blank wells. The mean of these corrected control absorbances were then calculated. Viability of the cells was finally determined by dividing the corrected absorbance of the wells containing 5 μ M of the synthesized complexes or controls by the mean corrected absorbance of the control wells and expressing the mean of the ratio as a percentage value.

A2.7 NMR and Mass Spectra

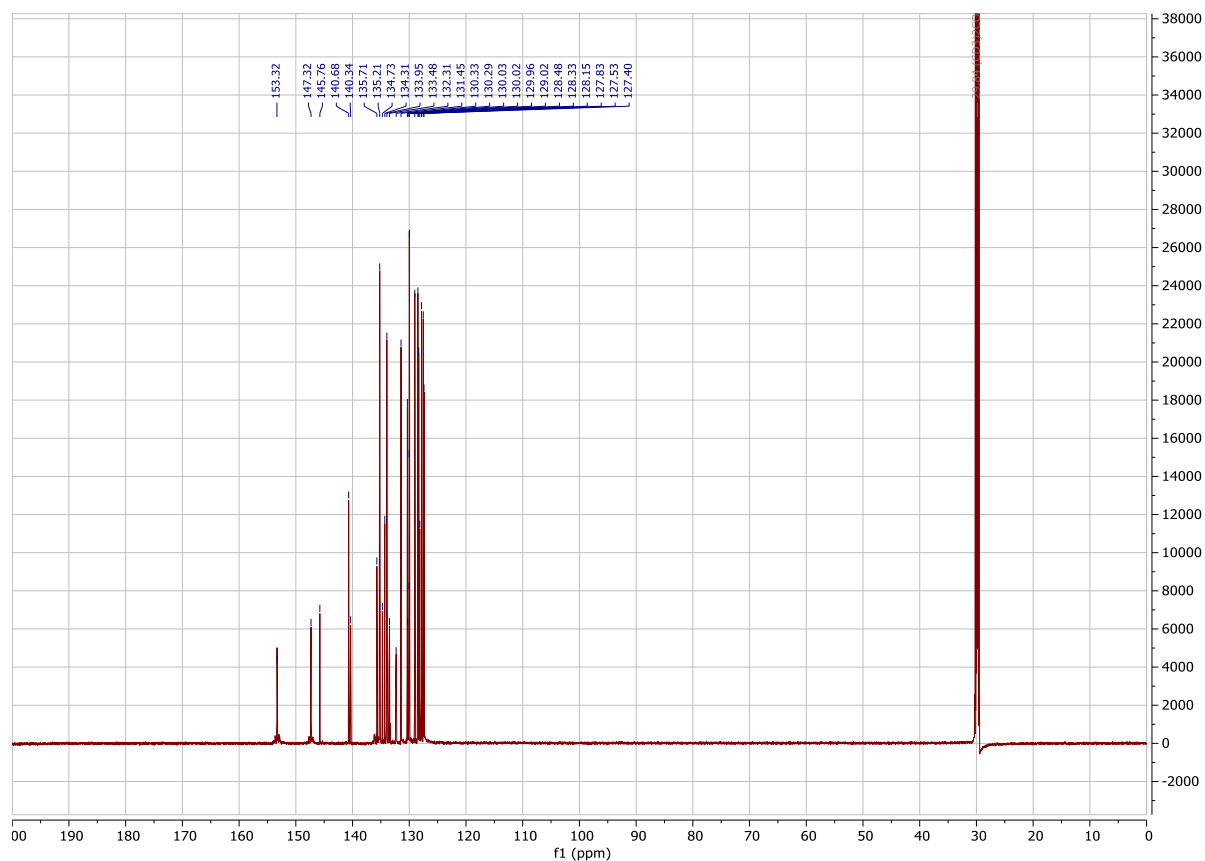
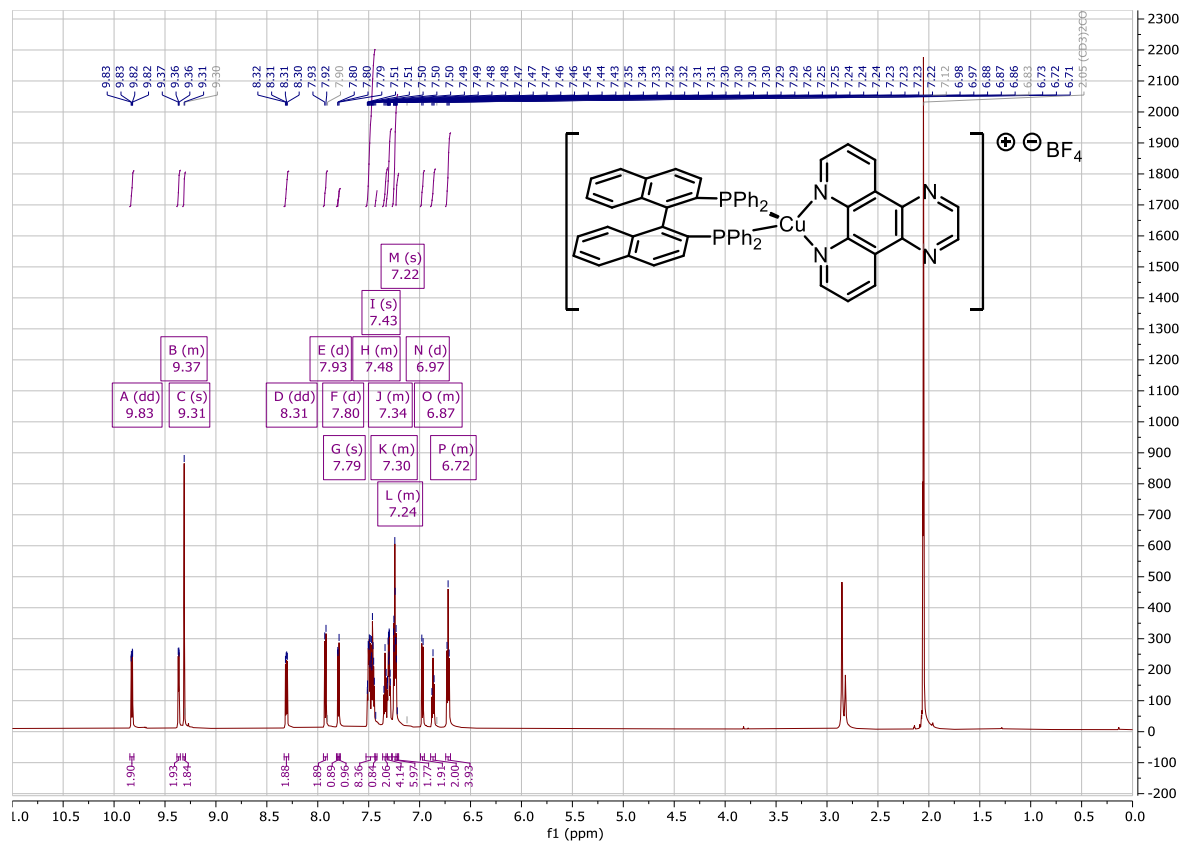
Ligands



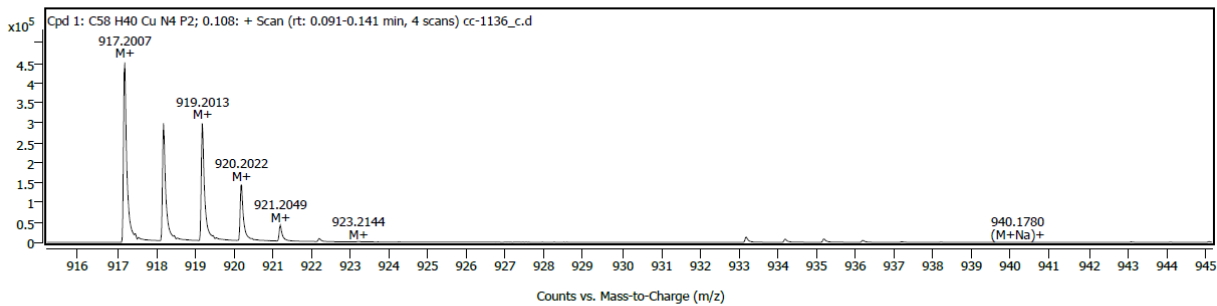
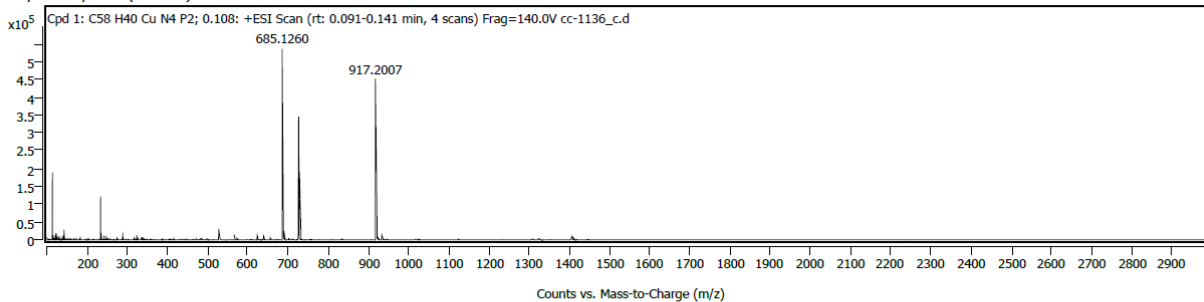




Copper Complexes

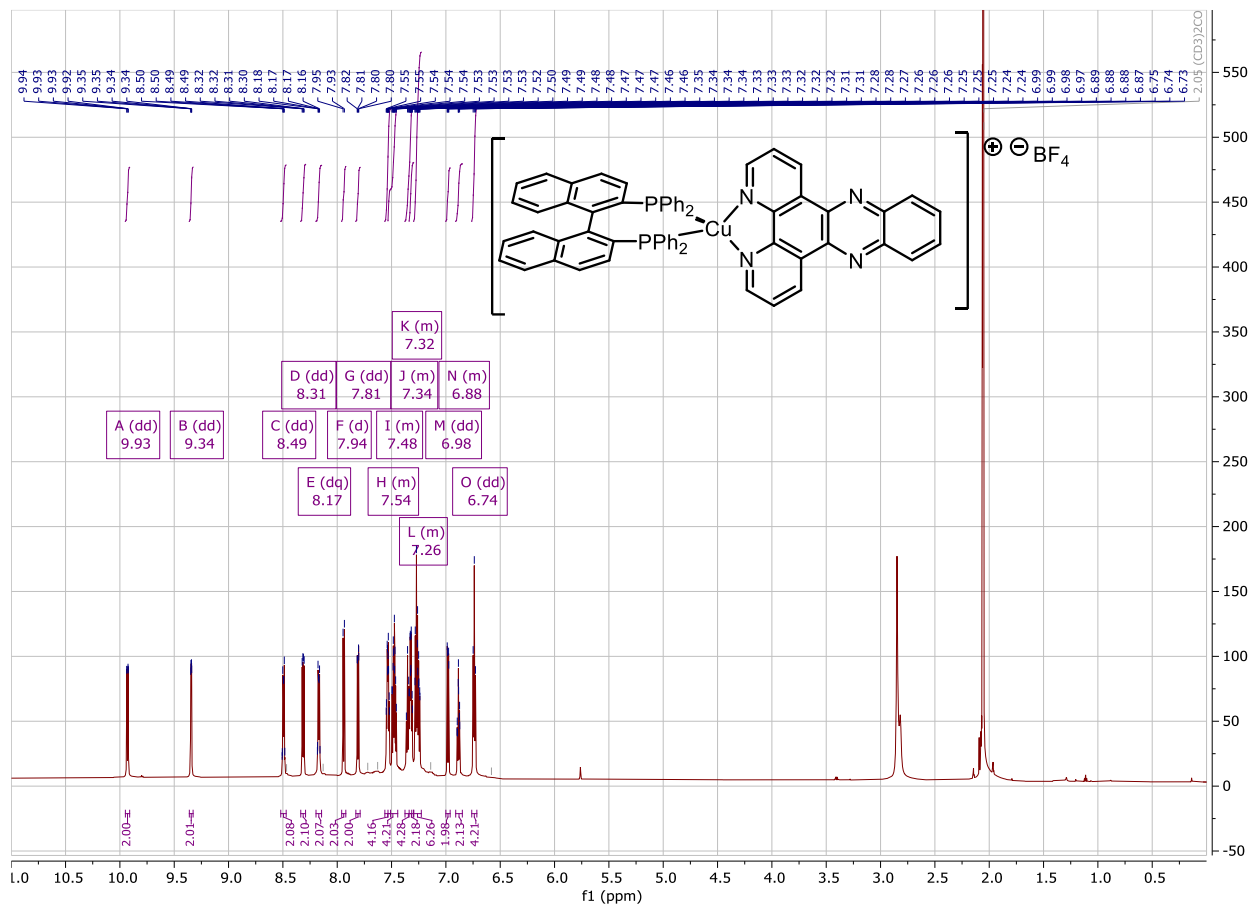


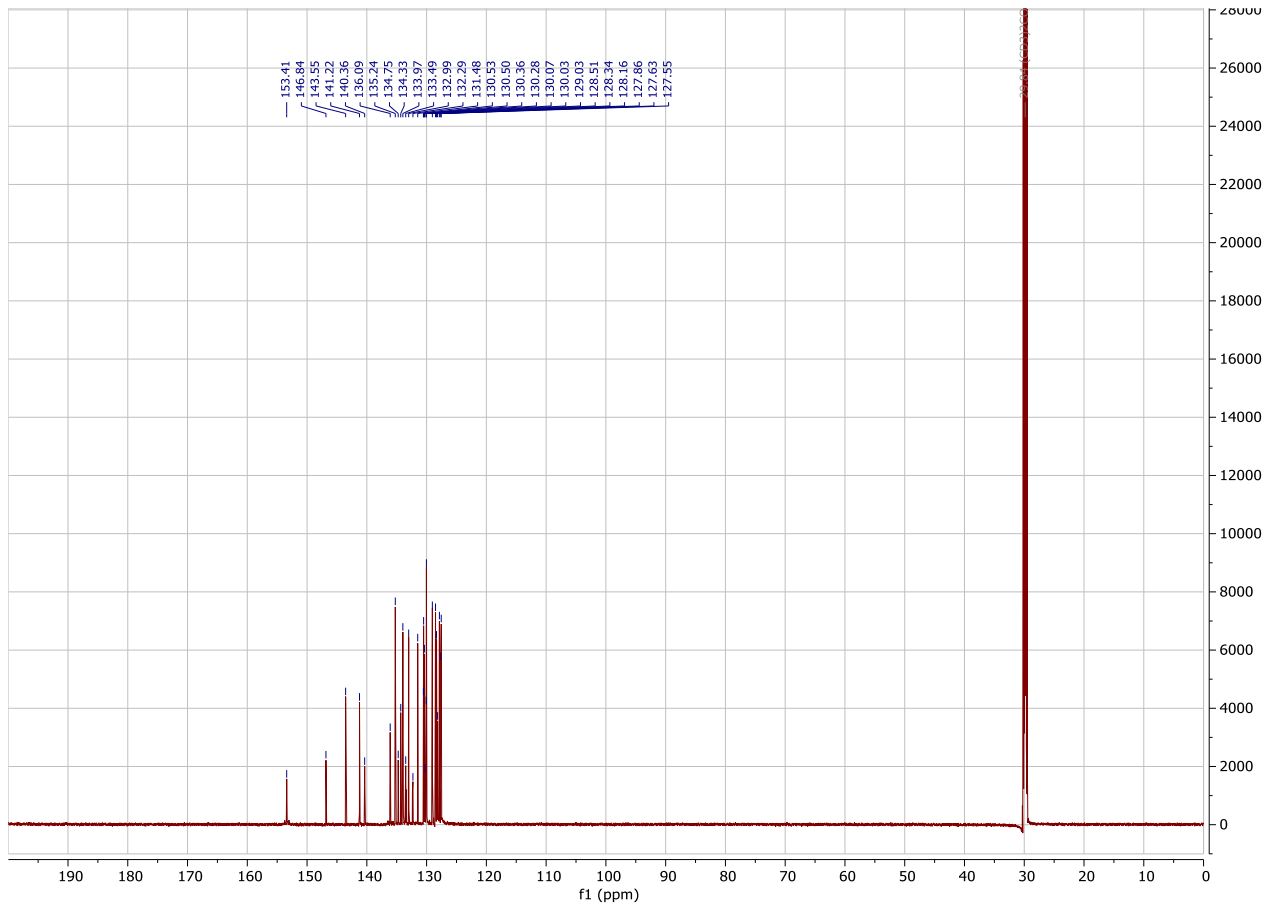
Compound Spectra (overlaid)



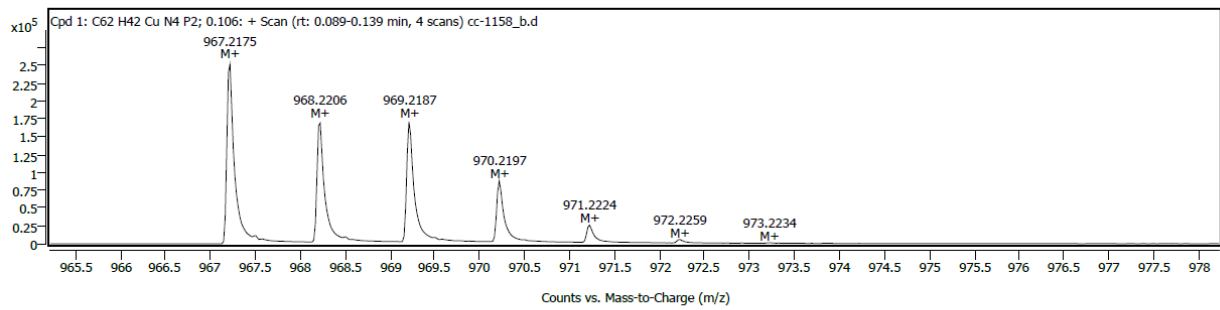
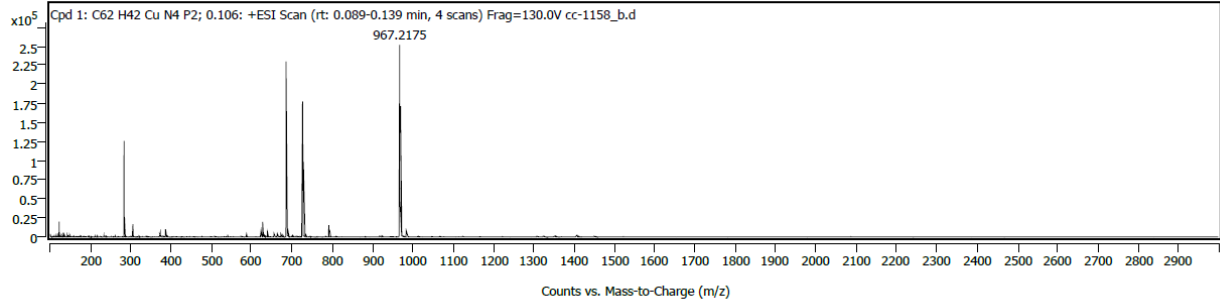
Spectrum Peaks (Max. 1)

Ion Species	Formula	Abund	m/z	m/z (Calc)	Diff (ppm)
M+	C58H40CuN4P2	456578	917.20065	917.20187	-1.33





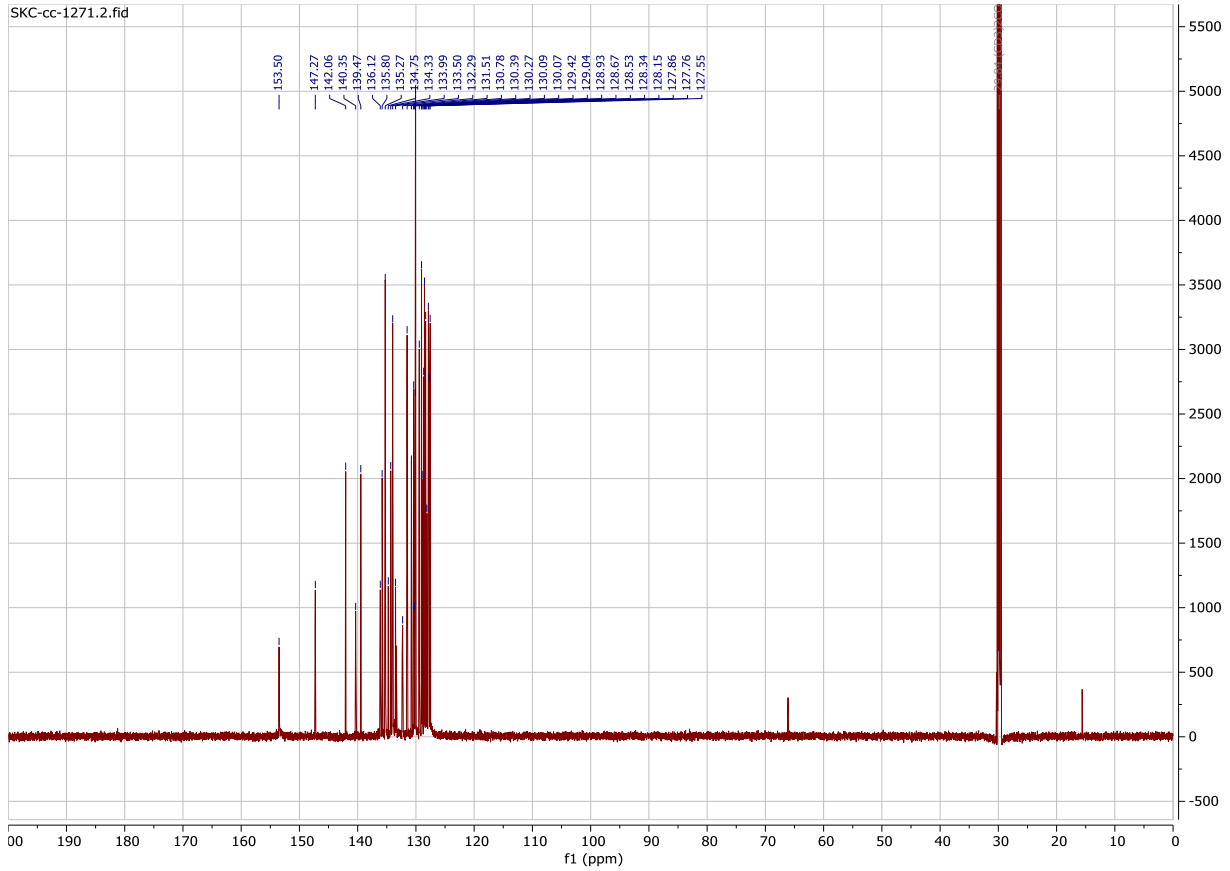
Compound Spectra (overlaid)



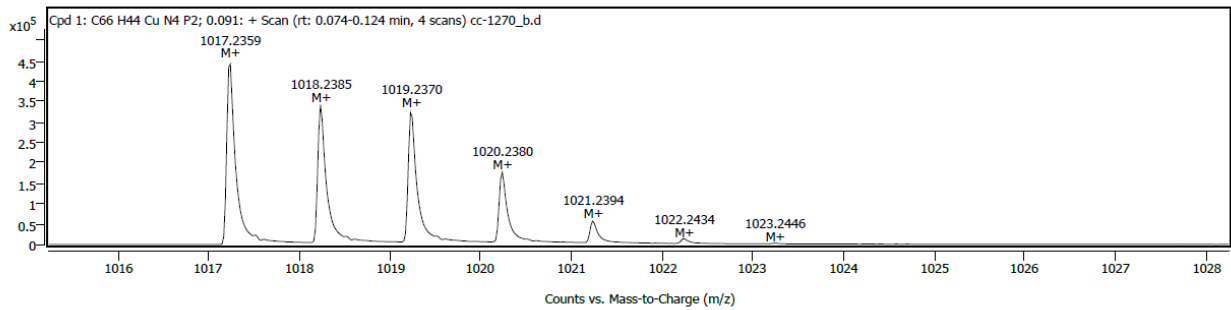
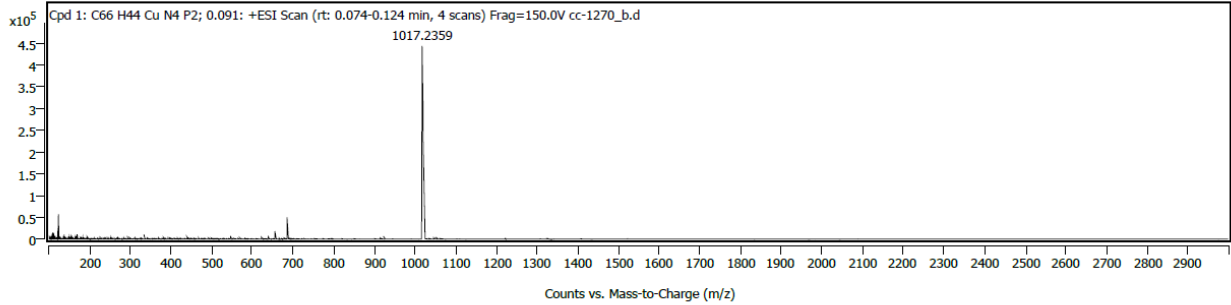
Spectrum Peaks (Max. 1)

Ion Species	Formula	Abund	m/z	m/z (Calc)	Diff (ppm)
M+	C62H42CuN4P2	255520	967.2175	967.21752	0.02



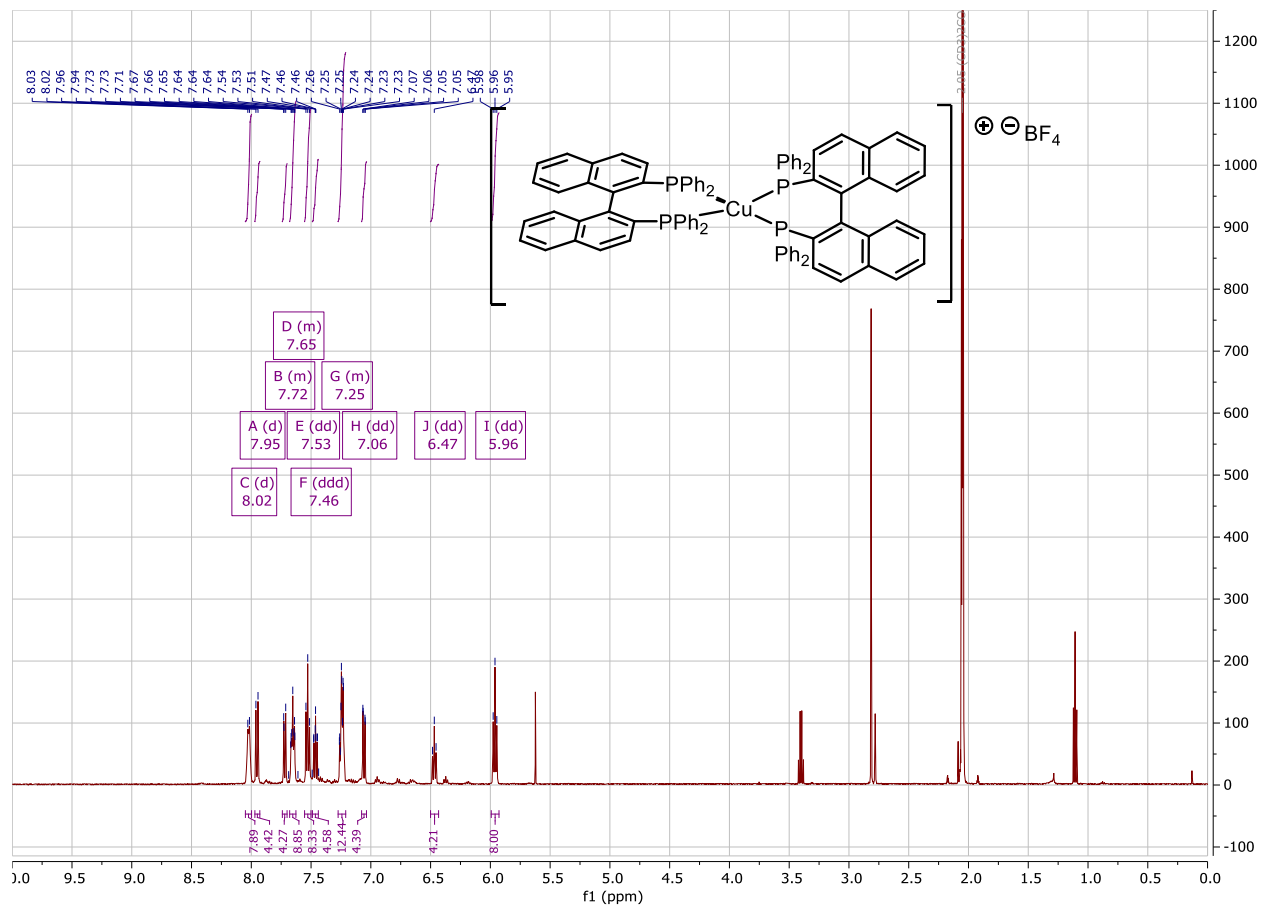


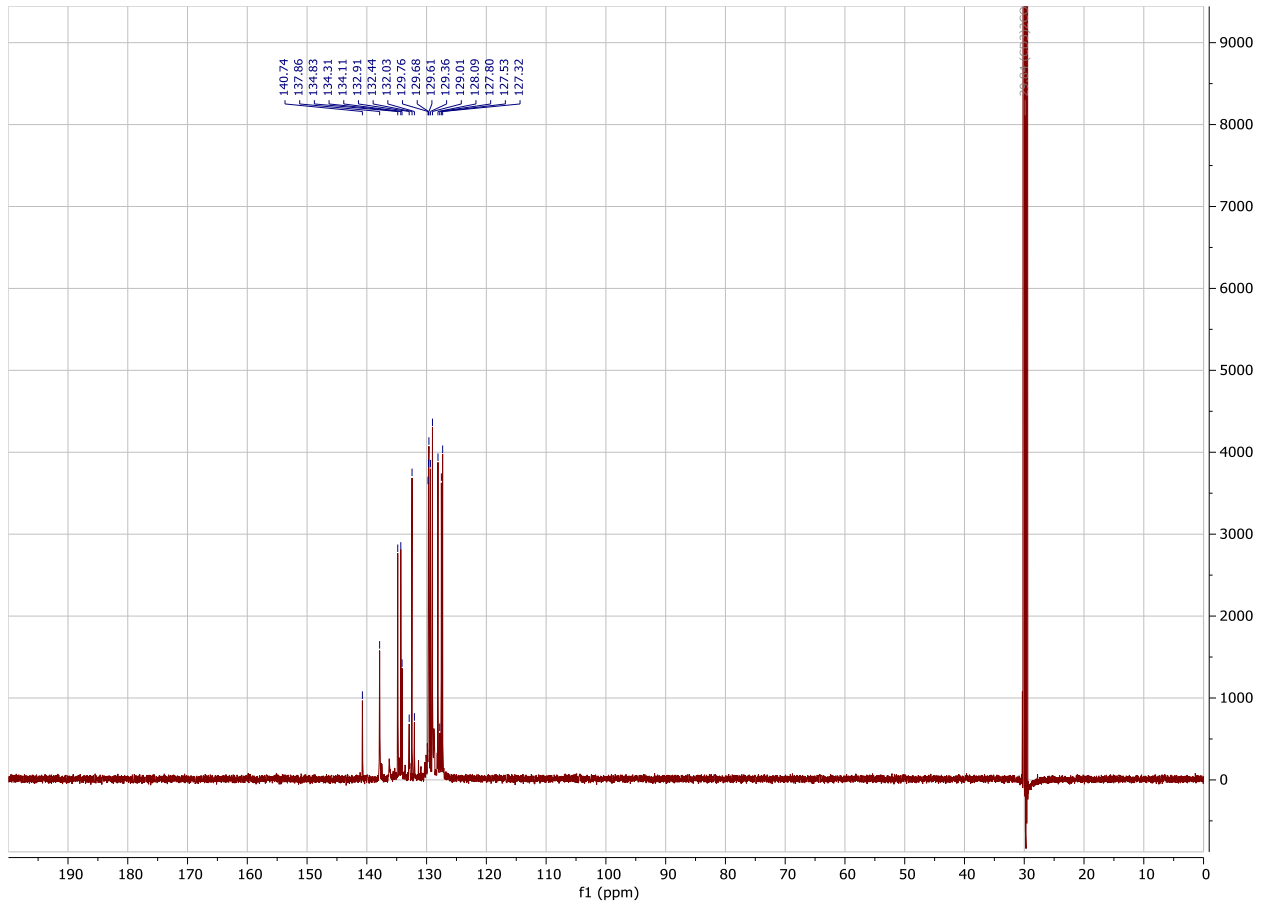
Compound Spectra (overlaid)



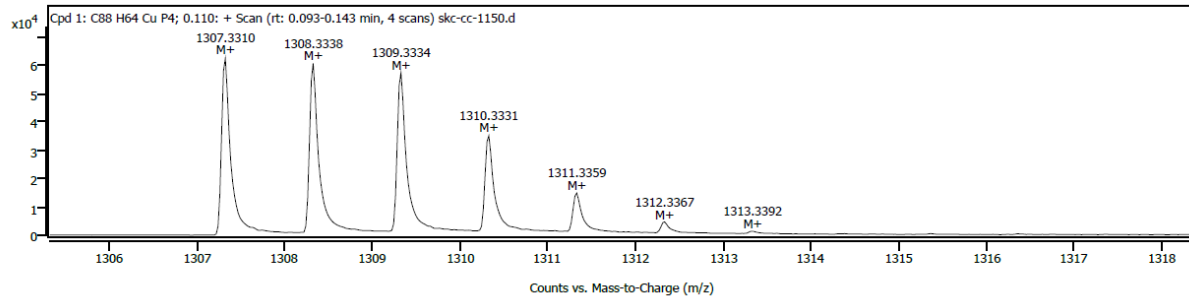
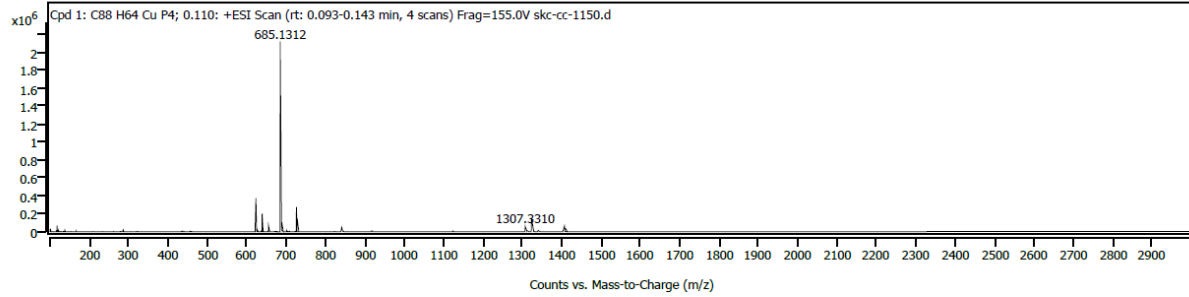
Spectrum Peaks (Max. 1)

Ion Species	Formula	Abund	m/z	m/z (Calc)	Diff (ppm)
M+	C66H44CuN4P2	450761	1017.23595	1017.23317	2.73



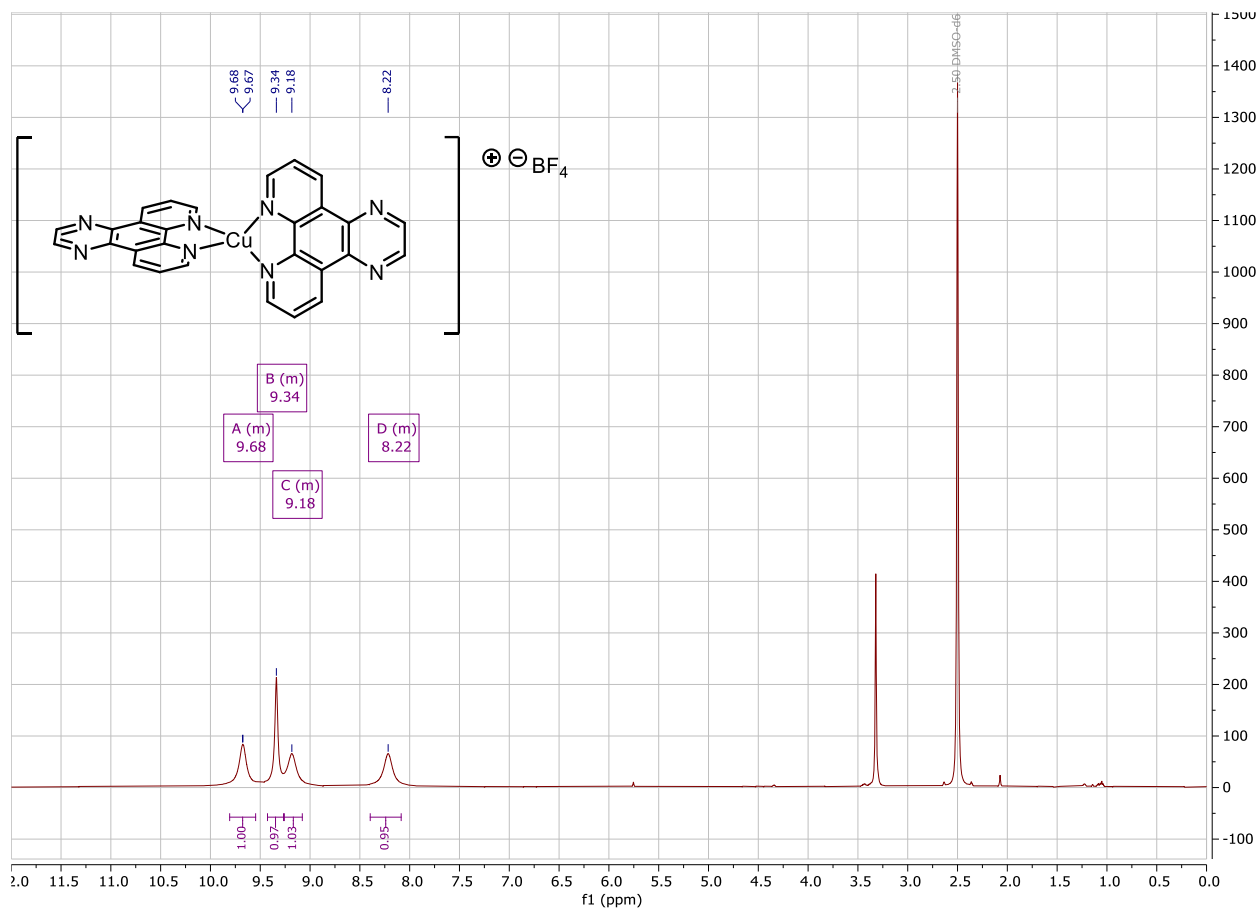


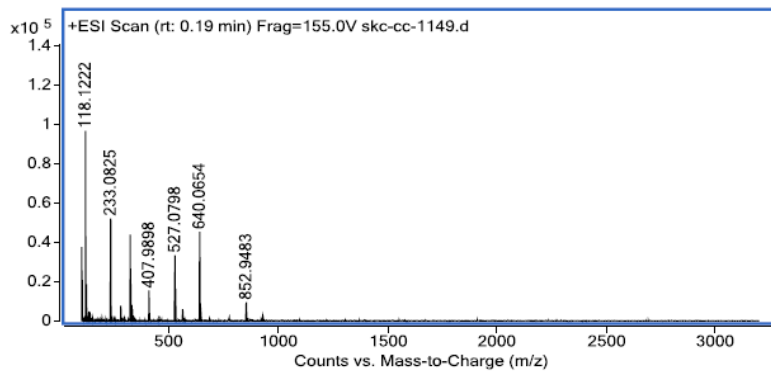
Compound Spectra (overlaid)



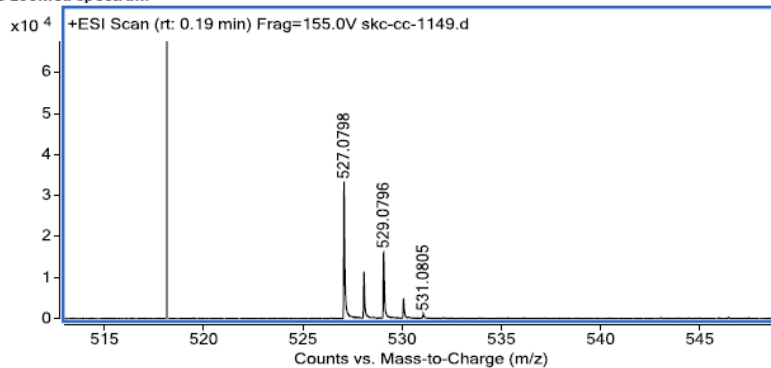
Spectrum Peaks (Max. 1)

Ion Species	Formula	Abund	m/z	m/z (Calc)	Diff (ppm)
M+	C88H64CuP4	62925	1307.33098	1307.32490	4.65

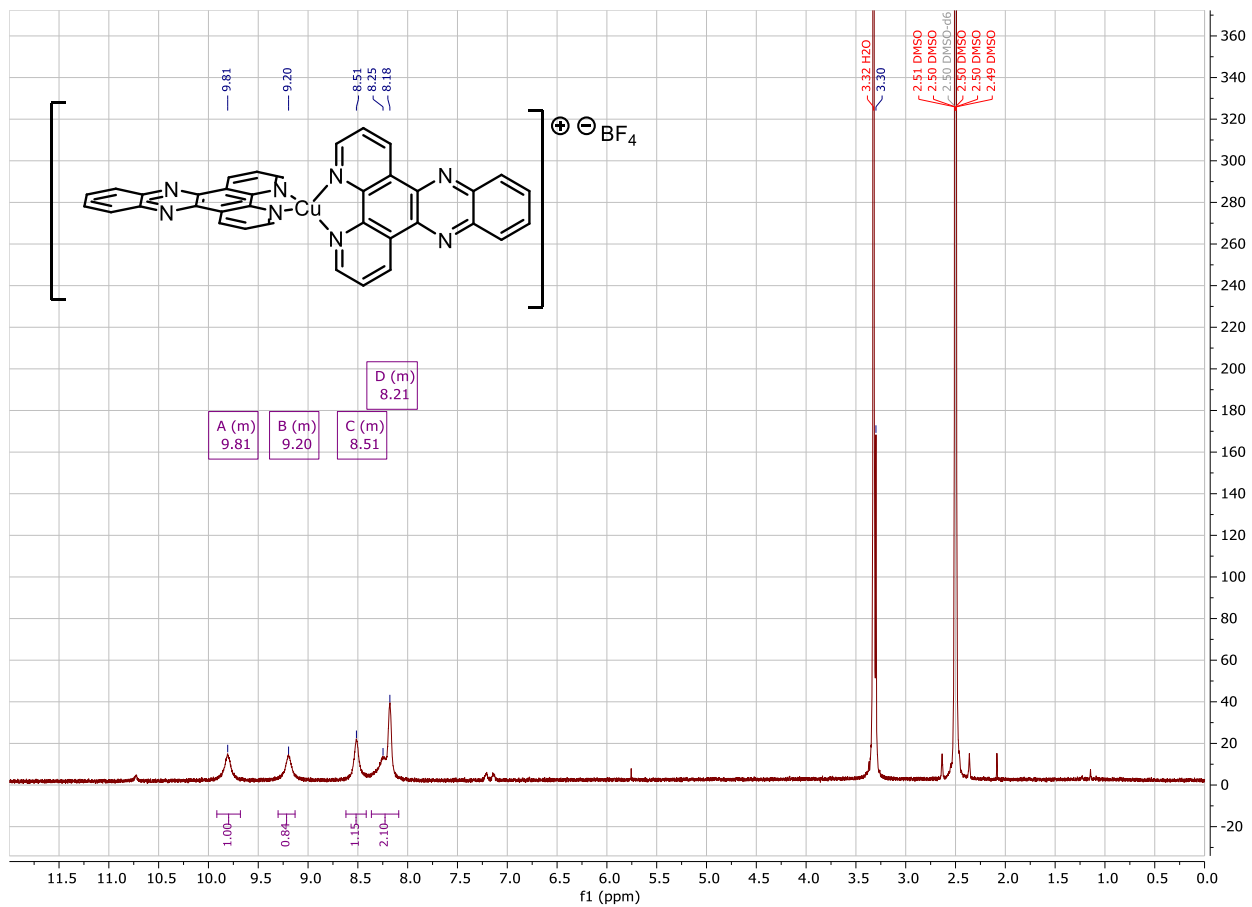




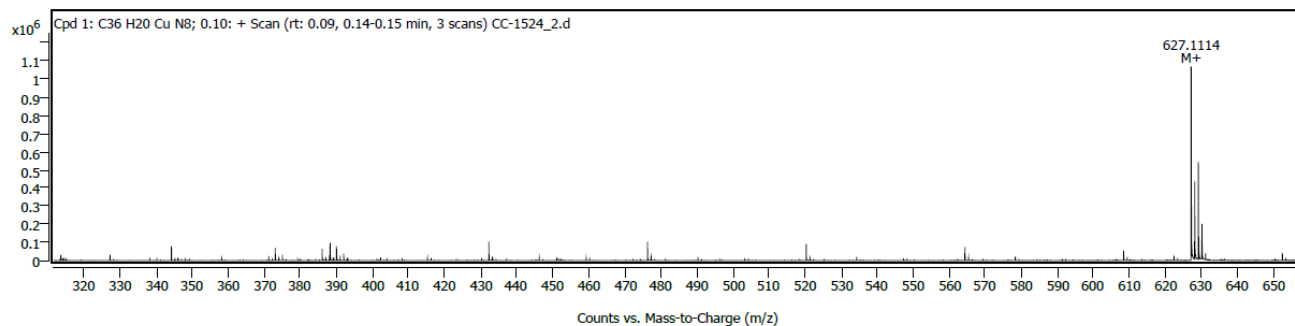
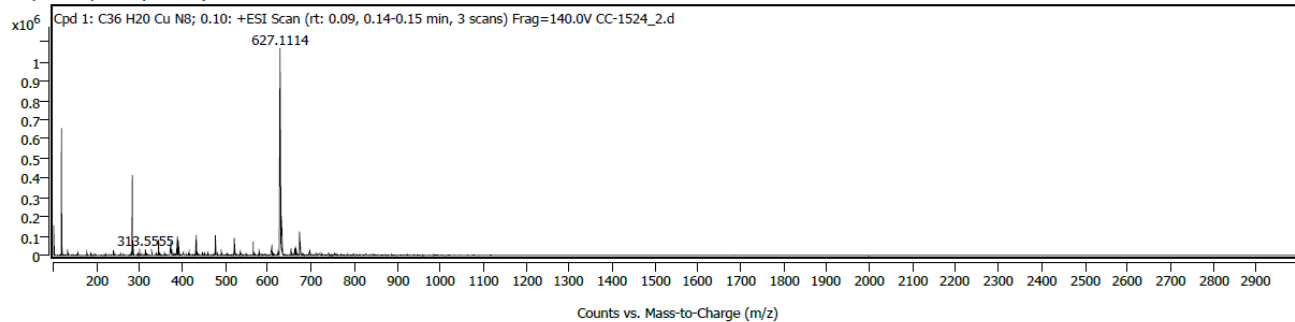
MS zoomed spectrum



Ion	Formula	Expe. m/z	Calc. m/z	Diff (ppm)
M+	C ₂₈ H ₁₆ CuN ₈ ⁺	527.0798	527.0788	1.81



Compound Spectra (overlaid)



A2.8 References

1. Wu, W.; Ji, S.; Wu, W.; Shao, J.; Guo, H.; James, T. D.; Zhao, J., *Chem. - Eur. J.* **2012**, *18* (16), 4953-4964.
2. Kitagawa, Y.; Kumagai, M.; Nakanishi, T.; Fushimi, K.; Hasegawa, Y., *Dalton Trans.* **2020**, *49* (8), 2431-2436.
3. Roy, N.; Sen, U.; Ray Chaudhuri, S.; Muthukumar, V.; Moharana, P.; Paira, P.; Bose, B.; Gauthaman, A.; Moorthy, A., *Dalton Trans.* **2021**, *50* (6), 2268-2283.
4. Barrientos, L.; Araneda, C.; Loeb, B.; Crivelli, I. G., *Polyhedron* **2008**, *27* (4), 1287-1295.
5. Plutschack, M. B.; Seeberger, P. H.; Gilmore, K., *Org. Lett.* **2017**, *19* (1), 30-33.
6. Sosoe, J.; Cruché, C.; Morin, É.; Collins, S. K., *Can. J. Chem.* **2020**, *98* (9), 461-465.
7. Farney, E. P.; Yoon, T. P., *Angew. Chem., Int. Ed.* **2014**, *53* (3), 793-797.
8. Tarantino, K. T.; Liu, P.; Knowles, R. R., *J. Am. Chem. Soc.* **2013**, *135* (27), 10022-10025.

Annexe 3 – Supporting information of Chapter 4

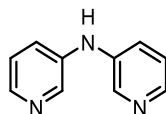
A3.1 General

All reactions that were carried out under anhydrous conditions were performed under an inert argon or nitrogen atmosphere in glassware that had previously been dried overnight at 120 °C or had been flame dried and cooled under a stream of argon or nitrogen. All chemical products were obtained from Sigma-Aldrich Chemical Company, Oakwood Chemical or Alfa Aesar and were reagent quality. Technical solvents were obtained from VWR International Co. Anhydrous solvents (CH₂Cl₂, Et₂O, THF, DMF, toluene, and *n*-hexane) were dried and deoxygenated using a GlassContour system (Irvine, CA). Isolated yields reflect the mass obtained following flash column silica gel chromatography. Organic compounds were purified using silica gel obtained from Silicycle Chemical division (40-63 nm; 230-240 mesh). Analytical thin-layer chromatography (TLC) was performed on glass-backed silica gel 60 coated with a fluorescence indicator (Silicycle Chemical division, 0.25 mm, F254.). Visualization of TLC plate was performed by UV (254 nm), KMnO₄ or *p*-anisaldehyde stains. All mixed solvent eluents are reported as v/v solutions. Concentration refers to removal of volatiles at low pressure on a rotary evaporator. All reported compounds were homogeneous by thin layer chromatography (TLC) and by ¹H NMR. NMR spectra were taken in deuterated CDCl₃ using Bruker AV-300 and AV-400 instruments unless otherwise noted. Signals due to the solvent served as the internal standard (CHCl₃: δ 7.27 for 1H, δ 77.0 for 13C). The acquisition parameters are shown on all spectra. The ¹H NMR chemical shifts and coupling constants were determined assuming first-order behavior. Multiplicity is indicated by one or more of the following: s (singlet), d (doublet), t (triplet), q (quartet), m (multiplet), br (broad); the list of couplings constants (*J*) corresponds to the order of the multiplicity assignment. High resolution mass spectroscopy (HRMS) was done by the Centre régional de spectrométrie de masse at the Département de Chimie, Université de Montréal from an Agilent LC-MSD TOF system using ESI mode of ionization unless otherwise noted.

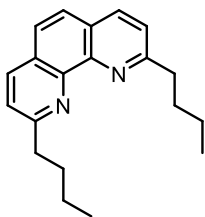
A3.2 Synthesis of ligands and catalysts

General Comments/Procedures for Ligands:

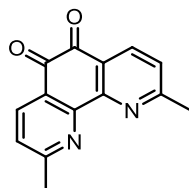
Commercially available diimines include: 1,10-phenanthroline (**phen**), 2,9-dimethyl-1,10-phenanthroline (**dmp**), 3,4,7,8-tetramethyl-1,10-phenanthroline (**tmp**), 4,4'-dimethoxy-2,2'-bipyridine (**dmbp**), 4,4'-di-*tert*-butyl-2,2'-dipyridyl (**dtbbp**), 4,4'-di-*tert*-butyl-2,2'-dipyridyl (**batho**), 2,9-dimethyl-4,7-diphenyl-1,10-phenanthroline (**bathocup**), 2,2'-biquinoline (**dq**). Previously synthesized diimines¹⁻³ include: 2-(1-(*p*-tolyl)-1H-1,2,3-triazol-4-yl)pyridine (**pytri**), 2-(1-(*p*-tolyl)-1H-1,2,3-triazol-4-yl)quinoline (**quintri**), 1-(1-(*p*-tolyl)-1H-1,2,3-triazol-4-yl)isoquinoline (**iquintri**), 3,6-dimethyl-dipyrido[3,2-*f*:2',3'-*h*]-quinoxaline (**ddpq**), 3,6-dimethyldipyrido[3,2-*a*:2',3'-*c*]phenazine (**ddppz**), 3,6-dimethylbenzo[*i*]dipyrido[3,2-*a*:2',3'-*c*]phenazine (**dbdppz**), 4-fluoro-N-(3-(pyridin-2-yl)-1H-pyrazol-5-yl)benzenesulfonamide (**pypzs**). Three other ligands were synthesized as described below:



Di(pyridin-3-yl)amine (dpa) : 2-Bromopyridine (2 mmol, 191 μ L), 2-aminopyridine (2.4 mmol, 258 μ L, 1.2 equiv.), Pd₂(dba)₃, (0.04 mmol, 37 mg, 0.02 equiv.), 1,3-bis(diphenylphosphino)propane (0.08 mmol, 33 mg, 0.04 equiv.), NaOtBu (2.8 mmol, 269 mg, 1.4 equiv.), and toluene (0.11 M) were added to an oven-dried flask and purged with nitrogen for approximately 10 minutes. The reaction mixture was then heated to 70 °C under nitrogen for 24 h. The reaction mixture was then allowed to cool to room temperature, diluted with diethyl ether, washed with water and saturated brine, dried over Na₂SO₄, and concentrated *in vacuo*. Purification by flash column chromatography (0→5% MeOH in CH₂Cl₂) afforded the pure product as a white powder (330 mg). Spectral data were in accordance with previous reports.⁴ **¹H NMR (400 MHz, CDCl₃):** δ 8.30 – 8.23 (m, 2H), 7.65 – 7.51 (m, 4H), 7.39 (br, 1H), 6.85 (m, 2H).



2,9-Dibutyl-1,10-phenanthroline (bphen): 1,10-Phenanthroline (2.00 g, 11.1 mmol) was added to dry THF (110 mL, 0.1M). The reaction mixture was cooled to $-78\text{ }^{\circ}\text{C}$ and purged with nitrogen for approximately 10 minutes. *n*-Butyllithium (30 mL, 1.90M in Hexanes, 57 mmol, 5 equiv.) was added dropwise and the mixture was stirred for 18 h and then allowed to gradually warm up to room temperature. The reaction was quenched by addition of water at $0\text{ }^{\circ}\text{C}$, and the aqueous phase was extracted with CH_2Cl_2 . The organic phase was dried over Na_2SO_4 and concentrated to around 50 mL. Manganese oxide (7.72 g, 89 mmol, 8 equiv.) was added and the mixture was stirred at room temperature for 1 h. Excess Na_2SO_4 was then added and the mixture was stirred for another hour. The resulting mixture was filtered and concentrated *in vacuo*. Purification by flash column chromatography (100% CH_2Cl_2) afforded the pure product as a pale orange crystalline product (2.05 mg). Spectral data were in accordance with previous reports.⁵ **$^1\text{H NMR}$ (400 MHz, CDCl_3):** δ 8.13 (d, $J = 8.2$ Hz, 2H), 7.69 (s, 2H), 7.51 (d, $J = 8.2$ Hz, 2H), 3.26 – 3.17 (m, 4H), 1.98 – 1.85 (m, 4H), 1.62 – 1.46 (m, 4H), 1.01 (t, $J = 7.4$ Hz, 6H).



1,10-Phenanthroline-5,6-dione (dmop): 2,9-Dimethyl-1,10-phenanthroline (996 mg, 4.76 mmol) was dissolved in H_2SO_4 (5.0 mL, 60% aq, 430mM) at room temperature. NaBrO_3 (794 mg, 5.26 mmol, 1.1 equiv.) was then added portion wise over 30 min and the orange solution stirred for 36 h. The mixture was then poured over water and neutralized with intense stirring, using saturated KHCO_3 . The precipitate was filtered and washed with *n*-hexane. Resolubilisation in a minimum of CH_2Cl_2 followed by a precipitation using *n*-hexane gave, after filtration, the pure product as a bright yellow powder (732 mg). Spectral data were in accordance with previous reports.² **$^1\text{H NMR}$ (400 MHz, CDCl_3):** δ 8.38 (d, $J = 8.0$ Hz, 2H), 7.42 (d, $J = 8.0$ Hz, 2H), 2.86 (s, 6H).

Synthesis of Copper Complexes

Some complexes were already synthesized from previous studies in our group. This include:

[Cu(dmp)(Xantphos)]BF₄, [Cu(dmp)(DPEPhos)]BF₄, [Cu(dmp)(BINAP)]BF₄,
[Cu(quintri)(Xantphos)]BF₄, [Cu(pytri)(Xantphos)]BF₄, [Cu(iquintri)(Xantphos)]BF₄,
[Cu(ddpq)(Xantphos)]BF₄, [Cu(ddppz)(Xantphos)]BF₄, [Cu(dbdppz)(Xantphos)]BF₄,
[Cu(dmp)₂]BF₄.^{1, 3} The other complexes were synthesized according to the general procedure described below.

General Procedure for the Synthesis of Heteroleptic Complexes:

To a stirred solution of [Cu(MeCN)₄]BF₄ (1.0 equiv.) in anhydrous CH₂Cl₂ (0.032 M) was added the corresponding phosphine (1.05 equiv.). The reaction was stirred at room temperature for one hour. Then, to the reaction mixture was added the corresponding diimine (1.05 equiv.). The reaction mixture was stirred for an additional hour. The reaction mixture was concentrated to approximately a fifth of the original volume and Et₂O was added dropwise to precipitate the product. Filtration afforded the desired complex as a coloured solid.

[Cu(dmp)(NXantPhos)]BF₄ : Following the general procedure, [Cu(MeCN)₄]BF₄ (50 mg, 0.16 mmol, 1 equiv.) and NXantphos (92 mg, 0.17 mmol, 1.05 equiv.) were dissolved in anhydrous dichloromethane (5 mL). After one hour, dmp (35 mg, 0.17 mmol, 1.05 equiv.) was added. The reaction mixture was stirred for one hour. The desired product was obtained by filtration as a yellow solid (130 mg, 90%). **¹H NMR (500 MHz, CDCl₃):** δ 8.24 (d, *J* = 8.2 Hz, 2H), 7.75 (s, 2H), 7.52 (d, *J* = 8.2 Hz, 2H), 7.35 (s, 1H), 7.19 (dd, *J* = 7.3, 7.3 Hz, 4H), 7.15 (dd, *J* = 7.8, 1.4 Hz, 2H), 7.06 – 6.96 (m, 16H), 6.86 (dd, *J* = 7.8, 7.8 Hz, 2H), 6.41 – 6.34 (m, 2H), 2.51 (s, 6H); **¹³C NMR (126 MHz, CDCl₃):** δ 158.9, 137.5, 133.1 (t, *J* = 7.7 Hz), 131.6, 129.9, 128.6, 127.6, 125.9, 125.8, 125.3, 123.2, 117.8, 27.7; **HRMS (ESI)** *m/z* calculated for C₅₀H₃₉CuN₃OP₂ [M]⁺ 822.1836; found 822.1859; **HRMS (ESI)** *m/z* calculated for [¹¹B]F₄ [M]⁻ 87.0038; found 87.0035.

[Cu(dmp)(PhanePhos)]BF₄ : Following the general procedure, [Cu(MeCN)₄]BF₄ (50 mg, 0.16 mmol, 1 equiv.) and PhanePhos (97 mg, 0.17 mmol, 1.05 equiv.) were dissolved in anhydrous

dichloromethane (5 mL). After one hour, dmp (35 mg, 0.17 mmol, 1.05 equiv.) was added. The reaction mixture was stirred for one hour. The desired product was obtained by filtration as a bright orange solid (141 mg, 95%). **¹H NMR (500 MHz, CDCl₃):** δ 8.70 (d, *J* = 8.3 Hz, 2H), 8.22 (s, 2H), 7.78 (d, *J* = 8.3 Hz, 2H), 7.56 (dd, *J* = 9.3, 9.3 Hz, 2H), 7.38 – 7.32 (m, 4H), 7.29 (d, *J* = 7.2 Hz, 2H), 7.16 (dd, *J* = 7.6 Hz, 4H), 7.09 (dd, *J* = 7.4, 7.4 Hz, 2H), 6.87 (d, *J* = 8.1 Hz, 2H), 6.81 (dd, *J* = 7.4, 7.4 Hz, 6H), 6.42 (m, 4H), 3.12 (m, 2H), 2.83 (m, 2H), 2.71 (m, 2H), 2.55 (s, 6H), 2.26 (m, 2H). **¹³C NMR (176 MHz, CDCl₃):** δ 159.8, 143.5, 143.2, 139.2, 138.8, 135.9, 135.6, 135.1, 133.2, 130.9, 130.6, 129.1, 128.7, 128.6, 127.2, 126.4, 36.2, 36.0, 28.2. *Note: Due to slow equilibria in solution, peaks of the homoleptic complexes appear in the ¹³C spectra.* **HRMS (ESI) m/z** calculated for C₅₄H₄₆CuN₂P₂ [M]⁺ 847.2427 found 847.2423; **HRMS (ESI) m/z** calculated for BF₄ [M]⁻ 86.0060; found 86.0069.

[Cu(dmp)(dppn)]BF₄ : Following the general procedure, [Cu(MeCN)₄]BF₄ (50 mg, 0.16 mmol, 1 equiv.) and dppn (90 mg, 0.17 mmol, 1.05 equiv.) were dissolved in anhydrous dichloromethane (5 mL). After one hour, dmp (35 mg, 0.17 mmol, 1.05 equiv.) was added. The reaction mixture was stirred for one hour. The desired product was obtained by filtration as an orange solid (121 mg, 89 %). **¹H NMR (500 MHz, CDCl₃):** δ 8.50 (d, *J* = 8.2 Hz, 2H), 8.25 (d, *J* = 8.0 Hz, 2H), 8.03 (s, 2H), 7.79 (d, *J* = 8.2 Hz, 2H), 7.55 (dd, *J* = 7.6, 7.6 Hz, 2H), 7.49 (s, 2H), 7.28 – 7.24 (m, 5H), 7.11 (dd, *J* = 7.3, 7.3 Hz, 4H), 6.77 (d, *J* = 8.0 Hz, 7H), 6.56 (s, 3H), 2.44 (s, 6H); **¹³C NMR (126 MHz, CDCl₃):** δ 157.9, 143.2, 137.5, 134.4, 133.3, 130.2, 128.8, 127.8, 126.3, 125.8, 125.8, 26.0; **HRMS (ESI) m/z** calculated for C₄₈H₃₈CuN₂P₂ [M]⁺ 767.1798 found 767.1801; **HRMS (ESI) m/z** calculated for [¹¹B]F₄ [M]⁻ 87.0040; found 87.0035.

[Cu(dmp)((S)-Segphos)]BF₄ : Following the general procedure, [Cu(MeCN)₄]BF₄ (50 mg, 0.16 mmol, 1 equiv.) and (S)-Segphos (108 mg, 0.17 mmol, 1.05 equiv.) were dissolved in anhydrous dichloromethane (5 mL). After one hour, dmp (35 mg, 0.17 mmol, 1.05 equiv.) was added. The reaction mixture was stirred for one hour. The desired product was obtained by filtration as an orange solid (128 mg, 83%). **¹H NMR (400 MHz, CDCl₃):** δ 8.69 (d, *J* = 8.3 Hz, 2H), 8.17 (s, 2H), 7.91

(d, $J = 8.3$ Hz, 2H), 7.29 – 7.24 (m, 5H), 7.21 – 7.13 (m, 6H), 7.02 – 6.90 (m, 8H), 6.59 (d, $J = 8.1$ Hz, 3H), 6.53 – 6.44 (m, 2H), 6.11 (d, $J = 1.4$ Hz, 2H), 5.94 (d, $J = 1.4$ Hz, 2H), 2.62 (s, 6H). **^{13}C NMR (101 MHz, CDCl_3)**: δ 159.7, 149.0, 147.9, 143.3, 139.0, 134.6, 132.4, 130.9, 130.1, 129.0, 128.6, 128.2, 127.3, 127.0, 126.2, 108.6, 101.8, 29.5. **HRMS (ESI)** m/z calculated for $\text{C}_{52}\text{H}_{40}\text{CuN}_2\text{O}_4\text{P}_2$ $[\text{M}]^+$ 881.1748 found 881.1754; **HRMS (ESI)** m/z calculated for BF_4 $[\text{M}]^-$ 86.0060; found 86.0074.

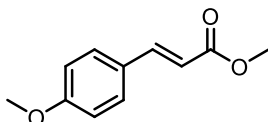
[Cu(dpa)(Xantphos)] BF_4 : Following the general procedure, $[\text{Cu}(\text{MeCN})_4]\text{BF}_4$ (50 mg, 0.16 mmol, 1 equiv.) and Xantphos (97 mg, 0.17 mmol, 1.05 equiv.) were dissolved in anhydrous dichloromethane (5 mL). After one hour, dpa (29 mg, 0.17 mmol, 1.05 equiv.) was added. The reaction mixture was stirred for one hour. The desired product was obtained by filtration as a white solid (104 mg, 73%). **^1H NMR (500 MHz, CDCl_3)**: δ 9.08 (s, 1H), 7.59 (dd, $J = 7.8, 1.4$ Hz, 2H), 7.47 (ddd, $J = 8.8, 7.1, 1.9$ Hz, 2H), 7.36 (d, $J = 8.5$ Hz, 2H), 7.33 – 7.27 (m, 6H), 7.17 (dd, $J = 7.6, 7.6$ Hz, 8H), 7.14 – 7.04 (m, 10H), 6.58 – 6.50 (m, 2H), 6.37 (ddd, $J = 6.9, 5.4, 1.1$ Hz, 2H), 1.75 (s, 6H). **^{13}C NMR (126 MHz, CDCl_3)**: δ 154.8, 153.8, 146.6, 139.1, 133.8, 133.2 (t, $J = 8.1$ Hz), 132.0 (t, $J = 16.2$ Hz), 131.2, 130.1, 128.9 (t, $J = 4.7$ Hz), 126.7, 125.3, 121.0, 116.9, 116.3, 36.2, 28.2. **HRMS (ESI)** m/z calculated for $\text{C}_{49}\text{H}_{41}\text{CuN}_3\text{OP}_2$ $[\text{M}]^+$ 812.2014 found 812.2015; **HRMS (ESI)** m/z calculated for $^{11}\text{B}\text{F}_4$ $[\text{M}]^-$ 87.0042; found 87.0035.

[Cu(bathocup)(Xantphos)] BF_4 : Following the general procedure, $[\text{Cu}(\text{MeCN})_4]\text{BF}_4$ (100 mg, 0.32 mmol, 1 equiv.) and Xantphos (193 mg, 0.34 mmol, 1.05 equiv.) were dissolved in anhydrous dichloromethane (10 mL). After one hour, bathocup (121 mg, 0.34 mmol, 1.05 equiv.) was added. The reaction mixture was stirred for one hour. The desired product was obtained by filtration as a yellow solid (304 mg, 88%). **^1H NMR (500 MHz, CDCl_3)**: δ 7.77 (s, 2H), 7.66 (d, $J = 7.8$ Hz, 2H), 7.63 – 7.50 (m, 7H), 7.49 – 7.43 (m, 6H), 7.30 – 7.24 (m, 4H), 7.21 (dd, $J = 7.8, 7.8$ Hz, 2H), 7.12 – 7.03 (m, 16H), 6.99 – 6.92 (m, 2H), 2.33 (s, 6H), 1.75 (s, 6H). **^{13}C NMR (126 MHz, CDCl_3)**: δ 157.9, 155.1, 150.3, 143.7, 136.4, 133.9, 133.1 (t, $J = 7.7$ Hz), 131.5 (t, $J = 16.3$ Hz), 130.5, 130.2, 129.5, 129.2, 128.8 (t, $J = 4.6$ Hz), 127.7, 125.8, 125.6, 123.7, 121.6, 36.3, 28.7, 27.5. **HRMS (ESI)** m/z calculated for $\text{C}_{65}\text{H}_{52}\text{CuN}_2\text{OP}_2$ $[\text{M}]^+$ 1001.2850 found 1001.2845; **HRMS (ESI)** m/z calculated for $^{11}\text{B}\text{F}_4$ $[\text{M}]^-$ 87.0034; found 87.0035.

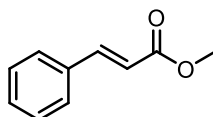
[Cu(bphen)(Xantphos)]BF₄: Following the general procedure, [Cu(MeCN)₄]BF₄ (50 mg, 0.16 mmol, 1 equiv.) and Xantphos (97 mg, 0.17 mmol, 1.05 equiv.) were dissolved in anhydrous dichloromethane (5 mL). After one hour, bphen (49 mg, 0.17 mmol, 1.05 equiv.) was added. The reaction mixture was stirred for one hour. The desired product was obtained by filtration as a bright yellow solid (106 mg, 65%). **¹H NMR (500 MHz, CDCl₃)**: δ 8.40 (d, *J* = 8.3 Hz, 2H), 7.84 (s, 2H), 7.61 (dd, *J* = 25.8, 8.1 Hz, 4H), 7.28 – 7.16 (m, 6H), 7.04 – 6.99 (m, 16H), 6.97 – 6.91 (m, 2H), 2.66 (t, *J* = 7.7 Hz, 4H), 1.72 (s, 6H), 1.19 – 1.09 (m, 4H), 0.59 – 0.55 (m, 10H). **¹³C NMR (126 MHz, CDCl₃)**: δ 162.1, 155.1, 155.1, 155.0, 142.9, 138.2, 134.1, 133.0 (t, *J* = 7.7 Hz), 131.3 (t, *J* = 16.0 Hz), 130.4, 130.1, 128.7 (t, *J* = 4.6 Hz), 128.2, 127.4, 126.3, 125.4, 123.2, 121.9 (t, *J* = 12.5 Hz), 41.0, 36.2, 30.6, 28.5, 21.9, 14.2. **HRMS (ESI)** *m/z* calculated for C₅₉H₅₆CuN₂OP₂ [M]⁺ 933.3164 found 933.3158; **HRMS (ESI)** *m/z* calculated for [¹¹B]F₄ [M]⁻ 87.0034; found 87.0036.

[Cu(dmop)(Xantphos)]BF₄: Following the general procedure, [Cu(MeCN)₄]BF₄ (50 mg, 0.16 mmol, 1 equiv.) and Xantphos (97 mg, 0.17 mmol, 1.05 equiv.) were dissolved in anhydrous dichloromethane (5 mL). After one hour, dmop (40 mg, 0.17 mmol, 1.05 equiv.) was added. The reaction mixture was stirred for one hour. The desired product was obtained by filtration as a brown solid (111 mg, 72%). **¹H NMR (500 MHz, CDCl₃)**: δ 8.38 (d, *J* = 8.0 Hz, 2H), 7.66 (d, *J* = 8.5 Hz, 2H), 7.55 (d, *J* = 8.0 Hz, 2H), 7.34 (dd, *J* = 7.4, 7.4 Hz, 4H), 7.22 (dd, *J* = 7.7, 7.7 Hz, 5H), 7.16 (m, 9H), 7.13 – 7.08 (m, 8H), 7.08 – 7.01 (m, 4H), 2.22 (s, 6H), 1.73 (s, 6H). **¹³C NMR (176 MHz, CDCl₃)**: δ 176.4, 164.8, 154.8, 149.8, 138.3, 133.7, 133.2 (t, *J* = 7.6 Hz), 130.9 (t, *J* = 16.8 Hz), 130.6, 130.5, 129.3 (t, *J* = 4.6 Hz), 128.1, 128.0, 126.9, 125.7, 120.8 (t, *J* = 13.5 Hz), 36.2, 29.0, 27.6. **HRMS (ESI)** *m/z* calculated for C₄₈H₃₆CuN₂OP₂ [M]⁺ 879.1961 found 879.1957; **HRMS (ESI)** *m/z* calculated for [¹¹B]F₄ [M]⁻ 87.0024; found 87.0039.

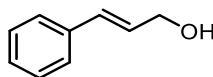
A3.3 Substrat synthesis



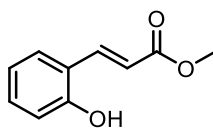
Methyl (E)-3-(4-methoxyphenyl)acrylate (E-2): 4-Methoxycinnamic acid (3.00 g, 16.5 mmol) was dissolved in MeOH (30 mL, 550 mM) in a sealed tube. H₂SO₄ (324 mg, 3.30 mmol, 0.2 eq.) was then added and the reaction mixture was stirred at 90 °C for 10 h. The mixture was cooled to room temperature, diluted in H₂O and extracted with AcOEt three times. The organic phases were combined, washed with brine, and dried with Na₂SO₄. The resulting mixture was filtered and concentrated *in vacuo*. Purification by flash column chromatography (10% AcOEt in hexanes) afforded the pure product as a white solid (3.07 g, 97 %). Spectral data were in accordance with previous report.⁶ **¹H NMR (300 MHz, CDCl₃):** δ 7.65 (d, *J* = 16.0 Hz, 1H), 7.51 – 7.44 (m, 2H), 6.95 – 6.86 (m, 2H), 6.31 (d, *J* = 15.9 Hz, 1H), 3.84 (s, 3H), 3.79 (s, 3H).



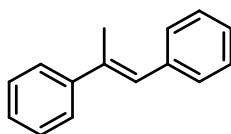
Methyl cinnamate (E-3): Cinnamic acid (1.05g, 7 mmol) was dissolved in MeOH (13 mL, 550 mM) in a sealed tube. H₂SO₄ (324 mg, 3.30 mmol, 0.2 eq.) was then added and the reaction mixture was stirred at 90°C for 16h. The mixture was cooled off to room temperature, diluted in H₂O and extracted with AcOEt three times. The organic phases were combined, washed with brine, and dried with Na₂SO₄. The resulting mixture was filtered and concentrated *in vacuo*. Purification by flash column chromatography (10% AcOEt in Hexanes) afforded the pure product as a white solid (1.12g, 98%). Spectral data were in accordance with previous report.⁶ **¹H NMR (300 MHz, CDCl₃):** δ 7.70 (d, *J* = 16.0 Hz, 1H), 7.58 – 7.48 (m, 2H), 7.44 – 7.34 (m, 3H), 6.45 (d, *J* = 16.0 Hz, 1H), 3.81 (s, 3H).



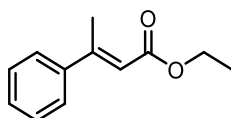
(E)-3-Phenylprop-2-en-1-ol (E-4): To a solution of methyl cinnamate (358 mg, 2.21 mmol, 1 eq.) in dry Et₂O (10 mL, 221 mM), was added DIBAL-H (11 mL, 11 mmol, 1.0 M in THF, 5 eq.) at -78 °C dropwise. The reaction mixture was stirred for 3 h at -78 °C and allowed to warm up gradually overnight. The reaction mixture was then cooled to 0 °C, and carefully quenched with 30 mL of a saturated solution of NH₄Cl. The reaction mixture was stirred at room temperature for 1 h, and the resulting white precipitate was filtered through a pad of Celite®. The filtrate was extracted three times with AcOEt, washed with brine, dried with Na₂SO₄, and concentrated *in vacuo*, giving the pure product as a colorless oil (287 mg, 97%). Spectral data were in accordance with previous report.⁷ **¹H NMR (400 MHz, CDCl₃):** δ 7.42 – 7.37 (m, 2H), 7.36 – 7.29 (m, 2H), 7.28 – 7.22 (m, 1H), 6.63 (dd, *J* = 15.9, 1.6 Hz, 1H), 6.38 (dt, *J* = 15.9, 5.7 Hz, 1H), 4.33 (dd, *J* = 5.8, 1.6 Hz, 2H), 1.49 (bs, 1H).



Methyl (E)-3-(2-hydroxyphenyl)acrylate (S1): 2-hydroxycinnamic acid (1.15 g, 7 mmol) was dissolved in MeOH (20 mL, 350 mM) in a sealed tube. H₂SO₄ (137 mg, 1.40 mmol, 0.2 eq.) was then added and the reaction mixture was stirred at 90 °C for 4 h. The mixture was cooled to room temperature, diluted in H₂O and extracted with AcOEt three times. The organic phases were combined, washed with brine, and dried with Na₂SO₄. The resulting mixture was filtered and concentrated *in vacuo*. Purification by flash column chromatography (20% AcOEt in hexanes) afforded the pure product as a white solid (1.03 g, 95 %). Spectral data were in accordance with previous report.⁸ **¹H NMR (400 MHz, CDCl₃):** δ 8.05 (d, *J* = 16.2 Hz, 1H), 7.47 (dd, *J* = 7.8, 1.6 Hz, 1H), 7.29 – 7.19 (m, 1H), 6.93 (td, *J* = 7.5, 1.1 Hz, 1H), 6.86 (dd, *J* = 8.1, 1.1 Hz, 1H), 6.65 (d, *J* = 16.2 Hz, 1H), 6.49 (s, 1H), 3.83 (s, 3H).

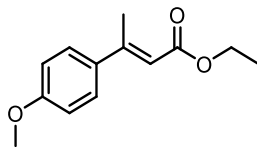


(E)-Prop-1-ene-1,2-diylidibenzene (E-7): To a solution of benzyltriphenylphosphonium bromide (2.14 g, 4.94 mmol, 1.2 eq.) in dry THF (5 mL, 824 mM), was added n-butyllithium (2.75 mL, 5.36 mmol, 1.95 mM in THF, 1.3 eq.) at 0°C dropwise. The reaction mixture was stirred for 30 min at 0°C and then acetophenone (0.485 mL, 4.12 mmol, 1 eq.) was added dropwise. The reaction mixture was warmed up to room temperature and stirred overnight. The reaction mixture was then quenched with 30 mL of a saturated solution of NH₄Cl. The solution was extracted three times with AcOEt, washed with brine, dried with Na₂SO₄, and concentrated *in vacuo*. Purification by flash column chromatography (100% Hexanes) afforded the product as a mixture of *E* and *Z* (53:47 *Z:E*) (465 mg, 58%). Further separation of the isomers by the chromatography afforded 60 mg of a mixture *E:Z* isomers (80:20) that was used in the isomerisation process. Spectral data were in accordance with previous report.⁹⁻¹⁰ **¹H NMR of the *E* isomer (400 MHz, CDCl₃):** δ 7.45 – 7.38 (m, 2H), 7.30 – 7.23 (m, 6H), 7.20 – 7.11 (m, 3H), 6.76 – 6.71 (m, 1H), 2.18 (d, *J* = 1.5 Hz, 3H).

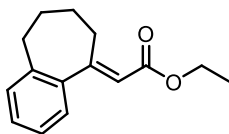


Ethyl (E)-3-phenylbut-2-enoate (E-1): NaH (60% in mineral oil) (1.40 g, 35 mmol, 2.2 eq.) was dissolved in dry THF (20 mL, 789 mM), and the mixture was cooled to 0 °C. Triethylphosphonoacetate (6.57 mL, 33.1 mmol, 2.1 eq.) was added dropwise to the solution and the resulting mixture was stirred for 2 hour at 0 °C. Acetophenone (1.84 mL, 15.8 mmol, 1 eq.) was added and the mixture was stirred for 1 hour at 0 °C. The mixture was then gradually warmed to room temperature and stirred for 48 h. The mixture was diluted in H₂O and extracted with Et₂O three times. The organic phases were combined, washed with brine, and dried with Na₂SO₄. The resulting mixture was filtered and concentrated *in vacuo*. Purification by flash column chromatography (0→2% AcOEt in Hexanes) afforded the pure product as a colorless oil (1.36 g, 45%). Spectral data were in accordance with a previous report.¹¹ **¹H NMR (300 MHz, CDCl₃):** δ

7.54 – 7.44 (m, 2H), 7.44 – 7.32 (m, 3H), 6.14 (q, $J = 1.3$ Hz, 1H), 4.22 (q, $J = 7.1$ Hz, 2H), 2.58 (d, $J = 1.3$ Hz, 3H), 1.32 (t, $J = 7.1$ Hz, 3H).

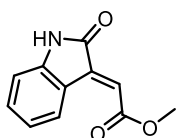


Ethyl (*E*)-3-(4-methoxyphenyl)but-2-enoate (*E*-9): NaH (60% in mineral oil) (120 mg, 5 mmol, 1.5 eq.) was dissolved in dry THF (15 mL, 222 mM), and the mixture was cooled to 0 °C. Triethylphosphonoacetate (2.92 mL, 1.15 mmol, 1.7 eq.) was added dropwise to the solution and the resulting mixture was stirred for 2 hours at 0 °C. 4-Methoxyacetophenone (1. , 15.8 mmol, 1 eq.) was added and the mixture was stirred for 1 hour at 0 °C. The mixture was then gradually warmed to room temperature and stirred for 72 h. The mixture was diluted in H₂O and extracted with Et₂O three times. The organic phases were combined, washed with brine, and dried with Na₂SO₄. The resulting mixture was filtered and concentrated *in vacuo*. Purification by flash column chromatography (0→2% AcOEt in Hexanes) afforded the pure product as a colorless oil (318 mg, 43%). Spectral data were in accordance with previous report.¹² **¹H NMR (500 MHz, CDCl₃):** δ 7.49 – 7.42 (m, 2H), 6.93 – 6.86 (m, 2H), 6.11 (q, $J = 1.3$ Hz, 1H), 4.21 (q, $J = 7.1$ Hz, 2H), 3.83 (s, 3H), 2.56 (d, $J = 1.3$ Hz, 3H), 1.31 (t, $J = 7.1$ Hz, 3H).

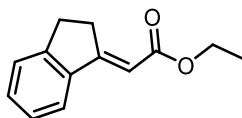


Ethyl (*E*)-2-(6,7,8,9-tetrahydro-5H-benzo[7]annulen-5-ylidene)acetate (*E*-10): NaH (60% in mineral oil) (120 mg, 5 mmol, 1.5 eq.) was dissolved in dry THF (15 mL, 222 mM), and the mixture was cooled to 0 °C. Triethylphosphonoacetate (2.92 mL, 1.15 mmol, 1.7 eq.) was added dropwise to the solution and the resulting mixture was stirred for 2 hour at 0 °C. 1-Benzosuberone (533 mg, 3.30 mmol, 1 eq.) was added and the mixture was stirred for 1 hour at 0 °C. The mixture was then gradually warmed to room temperature and stirred for 72 h. The mixture was diluted in H₂O and

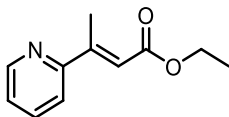
extracted with Et₂O three times. The organic phases were combined, washed with brine, and dried with Na₂SO₄. The resulting mixture was filtered and concentrated *in vacuo*. Purification by flash column chromatography (5% AcOEt in Hexanes) afforded the pure product as a colorless oil (99 mg, 13%). Spectral data were in accordance with previous report.¹³ **¹H NMR (500 MHz, CDCl₃):** δ 7.25 – 7.20 (m, 1H), 7.20 – 7.17 (m, 2H), 7.13 – 7.10 (m, 1H), 5.87 (t, *J* = 1.3 Hz, 1H), 4.21 (q, *J* = 7.1 Hz, 2H), 3.04 – 2.93 (m, 2H), 2.78 – 2.72 (m, 2H), 1.79 (tt, *J* = 8.8, 4.5 Hz, 4H), 1.32 (t, *J* = 7.1 Hz, 3H).



Methyl (*E*)-2-(2-oxoindolin-3-ylidene)acetate (*E*-11): NaH (60% in mineral oil) (1.39 g, 16.3 mmol, 2.4 eq.) was dissolved in dry THF (10 mL, 680 mM) , and the mixture was cooled to 0 °C. Triethylphosphonoacetate (1.62 mL, 8.16 mmol, 1.2 eq.) was added dropwise to the solution and the resulting mixture was stirred for 1 hour at 0 °C. Isatin (1.00 g, 6.80 mmol, 1 eq.) was added and the mixture was stirred for 1 hour at 0 °C. The mixture was then gradually warmed to room temperature and stirred for 48 h. The mixture was diluted in H₂O and extracted with Et₂O three times. The organic phases were combined, washed with brine, and dried with Na₂SO₄. The resulting mixture was filtered and concentrated *in vacuo*. Purification by flash column chromatography (2→10% AcOEt in Hexanes) afforded the pure product as an orange solid (680 mg, 46%). Spectral data were in accordance with previous report.¹⁴ **¹H NMR (400 MHz, CDCl₃):** δ 8.56 (d, *J* = 7.8 Hz, 1H), 7.72 (s, 1H), 7.32 (ddd, *J* = 7.7, 1.3 Hz, 1H), 7.06 (ddd, *J* = 7.7, 1.0 Hz, 1H), 6.88 (s, 1H), 6.84 (d, *J* = 7.8 Hz, 1H), 4.34 (q, *J* = 7.1 Hz, 2H), 1.37 (t, *J* = 7.1 Hz, 3H). **¹³C NMR (101 MHz, CDCl₃):** δ 169.4, 165.8, 143.5, 138.2, 132.7, 129.2, 123.0, 122.8, 120.6, 110.3, 61.4, 14.3. **Note:** The geometry of the *E* and *Z* isomers were confirmed by NOESY experiments.

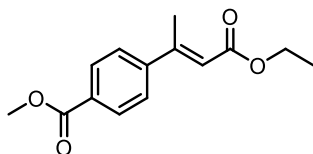


Ethyl (E)-2-(2,3-dihydro-1H-inden-1-ylidene)acetate (E-12): NaH (60% in mineral oil) (220 mg, 9.14 mmol, 3 eq.) was dissolved in dry THF (10 mL, 305 mM), and the mixture was cooled to 0 °C. Triethylphosphonoacetate (1.81 mL, 9.14 mmol, 3 eq.) was added dropwise to the solution and the resulting mixture was stirred for 1 hour at 0 °C. 1-Indanone (400 mg, 3.05 mmol, 1 eq.) was added and the mixture was stirred for 1 hour at 0 °C. The mixture was then gradually warmed to room temperature and stirred for 48 h. The mixture was diluted in H₂O and extracted with Et₂O three times. The organic phases were combined, washed with brine, and dried with Na₂SO₄. The resulting mixture was filtered and concentrated *in vacuo*. Purification by flash column chromatography (5% AcOEt in Hexanes) afforded the pure product as a colorless oil (64 mg, 10%). Spectral data were in accordance with previous report.¹³ **¹H NMR (400 MHz, CDCl₃):** δ 7.60 (d, *J* = 7.8 Hz, 1H), 7.39 – 7.33 (m, 2H), 7.30 – 7.22 (m, 1H), 6.31 (t, *J* = 2.6 Hz, 1H), 4.23 (q, *J* = 7.1 Hz, 2H), 3.36 – 3.26 (m, 2H), 3.14 – 3.03 (m, 2H), 1.33 (t, *J* = 7.1 Hz, 3H).

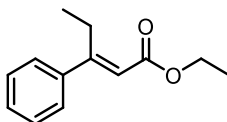


Ethyl (E)-3-(pyridin-2-yl)but-2-enoate (E-13): NaH (60% in mineral oil) (588 mg, 24.5 mmol, 3 eq.) was dissolved in dry THF (20 mL, 368 mM), and the mixture was cooled to 0 °C. Triethylphosphonoacetate (1.95 mL, 9.81 mmol, 1.2 eq.) was added dropwise to the solution and the resulting mixture was stirred for 1 hour at 0 °C. 2-Acetylpyridine (1.00 g, 8.17 mmol, 1 eq.) was added and the mixture was stirred for 1 hour at 0 °C. The mixture was then gradually warmed to room temperature and stirred for 48 h. The mixture was diluted in H₂O and extracted with Et₂O three times. The organic phases were combined, washed with brine, and dried with Na₂SO₄. The resulting mixture was filtered and concentrated *in vacuo*. Purification by flash column chromatography (2→10% AcOEt in Hexanes) afforded the pure product as colorless oil (404 mg, 26%). **¹H NMR (400 MHz, CDCl₃):** δ 8.71 – 8.61 (m, 1H), 7.77 – 7.68 (m, 1H), 7.55 (d, *J* = 8.0 Hz,

1H), 7.30 – 7.23 (m, 1H), 6.69 (q, $J = 1.5$ Hz, 1H), 4.24 (q, $J = 7.1$ Hz, 2H), 2.63 (d, $J = 1.4$ Hz, 3H), 1.32 (t, $J = 7.1$ Hz, 3H). ^{13}C NMR (101 MHz, CDCl_3): δ 167.1, 158.2, 153.1, 149.4, 136.8, 123.7, 121.1, 119.5, 77.5, 77.2, 76.8, 60.2, 16.2, 14.5. HRMS (ESI) m/z calculated for $\text{C}_{11}\text{H}_{13}\text{NO}_2$ $[\text{M}+\text{H}]^+$ 192.1019 found 192.1016.

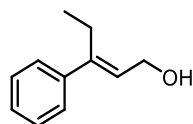


Methyl (E)-4-(4-ethoxy-4-oxobut-2-en-2-yl)benzoate (E-14): NaH (60% in mineral oil) (162 mg, 6.73 mmol, 1.2 eq.) was dissolved in dry THF (15 mL, 374 mM), and the mixture was cooled to 0 °C. Triethylphosphonoacetate (1.22 mL, 6.17 mmol, 1.1 eq.) was added dropwise to the solution and the resulting mixture was stirred for 1 hour at 0 °C. Methyl 4-acetylbenzoate (1.00 g, 5.61 mmol, 1 eq.) was added and the mixture was stirred for 1 hour at 0 °C. The mixture was then gradually warmed to room temperature and stirred for 24 h. The mixture was diluted with H_2O and extracted with Et_2O three times. The organic phases were combined, washed with brine, and dried with Na_2SO_4 . The resulting mixture was filtered and concentrated *in vacuo*. Purification by flash column chromatography (0→5% AcOEt in Hexanes) afforded the pure product as a white solid (550 mg, 39%). ^1H NMR (400 MHz, CDCl_3): δ 8.09 – 7.97 (m, 2H), 7.57 – 7.46 (m, 2H), 6.17 (q, $J = 1.4$ Hz, 1H), 4.23 (q, $J = 7.1$ Hz, 2H), 3.93 (s, 3H), 2.58 (d, $J = 1.4$ Hz, 3H), 1.32 (t, $J = 7.2$ Hz, 3H). ^{13}C NMR (101 MHz, CDCl_3): δ 166.8, 166.7, 154.3, 146.8, 130.5, 129.9, 126.5, 118.9, 60.2, 52.4, 18.0, 14.5. HRMS (ESI) m/z calculated for $\text{C}_{14}\text{H}_{16}\text{O}_4$ $[\text{M}+\text{H}]^+$ 249.1121 found ; 49.1133.

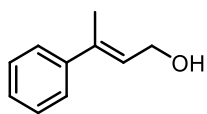


Ethyl (E)-3-phenylpent-2-enoate (E-15): NaH (60% in mineral oil) (3.15 g, 79.0 mmol, 5 eq.) was dissolved in dry THF (60 mL, 259 mM), and the mixture was cooled to 0 °C. Triethylphosphonoacetate (6.26 mL, 31.5 mmol, 2 eq.) was added dropwise to the solution and

the resulting mixture was stirred for 2 hours at 0 °C. Propiophenone (2.10 mL, 15.8 mmol, 1 eq.) was added and the mixture was stirred for 1 hour at 0 °C. The mixture was then gradually warmed to room temperature and stirred for 24 h. The mixture was diluted in H₂O and extracted with Et₂O three times. The organic phases were combined, washed with brine, and dried with Na₂SO₄. The resulting mixture was filtered and concentrated *in vacuo*. Purification by flash column chromatography (0→2% AcOEt in Hexanes) afforded the pure product as a yellow oil (1.05 g, 33%). Spectral data were in accordance with previous report.¹¹ **¹H NMR (400 MHz, CDCl₃):** δ 7.48 – 7.31 (m, 5H), 6.01 (s, 1H), 4.21 (q, *J* = 7.1 Hz, 2H), 3.11 (q, *J* = 7.5 Hz, 2H), 1.32 (t, *J* = 7.1 Hz, 3H), 1.08 (t, *J* = 7.5 Hz, 3H).

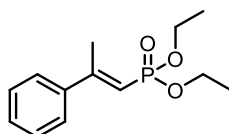


(E)-3-phenylpent-2-en-1-ol (E-16): To a solution of ethyl (E)-3-phenylpent-2-enoate (250 mg, 1.22 mmol, 1 eq.) in dry Et₂O (10 mL, 131mM), was added DIBAL-H (6.12 mL, 6.12 mmol, 1.0 M in THF, 5 eq.) at -78°C dropwise. The reaction mixture was stirred for 3 h at -78 °C and allowed to warm up gradually overnight. The reaction mixture was then cooled to 0°C, and carefully quenched with 30 mL of a saturated solution of NH₄Cl. The reaction mixture was stirred at room temperature for 1 h, and the resulting white precipitate was filtered through a pad of Celite®. The filtrate was extracted three times with AcOEt, washed with brine, dried with Na₂SO₄, and concentrated *in vacuo*, giving the pure product as a colorless oil (186 mg, 94%). Spectral data were in accordance with previous report.¹⁵ **¹H NMR (400 MHz, CDCl₃):** δ 7.44 – 7.25 (m, 5H), 5.87 (t, *J* = 6.8 Hz, 1H), 4.39 (d, *J* = 6.8 Hz, 2H), 2.58 (q, *J* = 7.5 Hz, 2H), 1.47 (br s, 1H), 1.03 (t, *J* = 7.5 Hz, 3H).

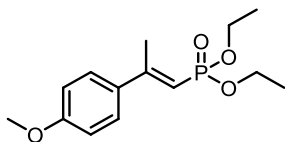


(E)-3-phenylbut-2-en-1-ol (E-17): To a solution of ethyl (E)-3-phenylbut-2-enoate (380 mg, 2.00 mmol, 1 eq.) in dry Et₂O (15 mL, 133 mM), was added DIBAL-H (10 mL, 10 mmol, 1.0 M in THF, 5

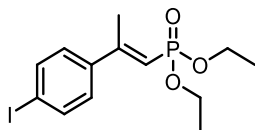
eq.) at -78°C dropwise. The reaction mixture was stirred for 3 h at -78 °C and allowed to warm up gradually overnight. The reaction mixture was then cooled to 0°C, and carefully quenched with 30 mL of a saturated solution of NH₄Cl. The reaction mixture was stirred at room temperature for 1 h, and the resulting white precipitate was filtered through a pad of Celite®. The filtrate was extracted three times with AcOEt, washed with brine, dried with Na₂SO₄, and concentrated *in vacuo*, giving the pure product as a colorless oil (296 mg, 90%). Spectral data were in accordance with previous report.¹⁶ **¹H NMR (500 MHz, CDCl₃):** δ 7.44 – 7.39 (m, 2H), 7.38 – 7.28 (m, 2H), 7.30 – 7.23 (m, 1H), 5.98 (tq, *J* = 6.7, 1.4 Hz, 1H), 4.37 (t, *J* = 5.9 Hz, 2H), 2.09 (dt, *J* = 1.5, 0.8 Hz, 3H), 1.55 (br s, 1H).



Diethyl (*E*)-(2-phenylprop-1-en-1-yl)phosphonate (*E*-18): NaH (60% in mineral oil) (250 mg, 6.24 mmol, 1.5 eq.) was dissolved in dry THF (5 mL, 832 mM), and the mixture was cooled to 0 °C and purged with N₂. Tetraethyl methylenediphosphonate (1.56 g, 5.41 mmol, 1.3 eq.) was added dropwise and the solution was stirred at 0 °C for 1 h. Acetophenone (485 μL, 4.16 mmol, 1 eq.) was added dropwise and the reaction was stirred at 60 °C for 3 days. The reaction mixture was then cooled down to room temperature and 20 mL of water was added. The mixture was extracted with AcOEt three times, washed with brine and dried with Na₂SO₄. The solvent was removed *in vacuo*, and a purification by flash column chromatography (0→20% MeOH in CH₂Cl₂) afforded the pure product as a yellow oil (1.06 g, 33%). Spectral data were in accordance with previous report.¹⁷ **¹H NMR (500 MHz, CDCl₃):** δ 7.50 – 7.44 (m, 2H), 7.41 – 7.33 (m, 3H), 5.90 (dd, *J* = 16.6, 1.1 Hz, 1H), 4.13 (dq, *J* = 8.1, 7.1 Hz, 4H), 2.51 (dd, *J* = 3.3, 1.0 Hz, 3H), 1.36 (t, *J* = 7.1 Hz, 6H).

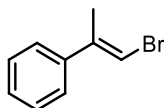


Diethyl (*E*)-(2-(4-methoxyphenyl)prop-1-en-1-yl)phosphonate (*E*-19): NaH (60% in mineral oil) (222 mg, 5.56 mmol, 1.67 eq.) was dissolved in dry THF (13.3 mL, 250 mM), and the mixture was cooled to 0 °C and purged with N₂. Tetraethylmethylenediphosphonate (1.25g, 4.33 mmol, 1.3eq.) was added dropwise and the solution was stirred at 0 °C for 1 h. 4'-Methoxyacetophenone (500 mg, 3.33 mmol, 1 eq.) was added dropwise and the reaction was stirred at 60 °C for 3 days. The reaction mixture was then cooled to room temperature and 20 mL of water was added. The mixture was extracted with AcOEt three times, washed with brine and dried with Na₂SO₄. The solvent was removed *in vacuo*, and a purification by flash column chromatography (50% AcOEt in Hexanes) afforded the pure product as a yellow oil (140 mg, 15%). Spectral data were in accordance with previous report.¹⁷ **¹H NMR (400 MHz, CDCl₃):** δ 7.48 – 7.42 (m, 2H), 6.91 – 6.86 (m, 2H), 5.85 (d, *J* = 16.4 Hz, 1H), 4.12 (dq, *J* = 7.2 Hz, 4H), 3.83 (s, 3H), 2.48 (d, *J* = 3.2 Hz, 3H), 1.35 (t, *J* = 7.1 Hz, 6H).

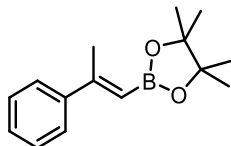


Diethyl (*E*)-(2-(4-iodophenyl)prop-1-en-1-yl)phosphonate (*E*-20): NaH (60% in mineral oil) (134 mg, 3.34 mmol, 1.67 eq.) was dissolved in dry THF (10 mL, 200 mM) and the mixture was cooled to 0 °C and purged with N₂. Tetraethyl methylenediphosphonate (749 mg, 2.60 mmol, 1.3 eq.) was added dropwise and the solution was stirred at 0 °C for 1 h. 4-Iodoacetophenone (500 mg, 2 mmol, 1 eq.) was added dropwise and the reaction was stirred at 60 °C for 3 days. The reaction mixture was then cooled to room temperature and 20 mL of water was added. The mixture was extracted with AcOEt three times, washed with brine and dried with Na₂SO₄. The solvent was removed *in vacuo*, and a purification by flash column chromatography (50% AcOEt in Hexanes) afforded the pure product as an orange oil (150 mg, 20%). Spectral data were in accordance with

previous report.¹⁸ **¹H NMR (400 MHz, CDCl₃):** δ 7.73 – 7.63 (m, 2H), 7.26 – 7.17 (m, 2H), 5.89 (dd, *J* = 15.9, 1.2 Hz, 1H), 4.13 (dq, *J* = 7.2 Hz, 4H), 2.47 (d, *J* = 3.0 Hz, 3H), 1.35 (t, *J* = 7.0 Hz, 6H).

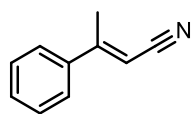


(E)-(1-Bromoprop-1-en-2-yl)benzene (S2): To a solution of dry CHCl₃ (25 mL, 0.66 mM) was added α-methylstyrene (2.20 mL, 17 mmol, 1 eq.). The solution was purged with N₂ and cooled to 0°C. Bromine (1.04 mL, 20.3 mmol, 1.2 eq.) was added dropwise and the reaction was stirred at room temperature for 2 h. Then, 50 mL of a saturated solution of sodium thiosulphate was added and the mixture was stirred for 5 minutes. The reaction mixture was extracted with AcOEt three times, washed with brine, and dried with Na₂SO₄. The solvent was removed *in vacuo* and the crude mixture was added to a sealed tube containing KOtBu (2.85 g, 25.4 mmol, 1.5 eq.) and tBuOH (85 mL, 0.2 mM). The vial was sealed, and the mixture was stirred at 95 °C for 1 h. After cooling to room temperature, 20 mL of water was added, and the reaction mixture was extracted with Et₂O three times. The organic phase was dried with Na₂SO₄ and concentrated *in vacuo*. Purification by flash column chromatography (100% Hexanes) afforded the pure product as a colorless oil (1.0 g, 30%). Spectral data were in accordance with previous report.¹⁹ **¹H NMR (400 MHz, CDCl₃):** δ 7.38 – 7.28 (m, 5H), 6.45 (q, *J* = 1.3 Hz, 1H), 2.23 (d, *J* = 1.3 Hz, 3H).

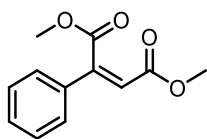


(E)-4,4,5,5-Tetramethyl-2-(2-phenylprop-1-en-1-yl)-1,3,2-dioxaborolane (E-21): To a solution of dry 1,4-dioxane (8 mL, 0.2 M) in a oven-dried flask was added (E)-(1-bromoprop-1-en-2-yl)benzene (300 mg, 1.52 mmol, 1 eq.), bis(pinacolato)diboron (467 mg, 1.67 mmol, 1.1 eq.), and KOAc (448 mg, 457 mmol, 3.0 eq.). The solution was purged with N₂, and Pd(dppf)Cl₂•DCM (62.2 mg, 76.1 mmol, 0.05 eq.) was added. The mixture was stirred at 90 °C for 24 h. The solvent was

removed under vacuo, and 30 mL of Et₂O was added. The crude mixture was filtered through a pad of Celite® and the pad washed with another 30 mL of Et₂O. Then, 30 mL of water was added to the filtrate, and the mixture was extracted three times with Et₂O. The organic phase was washed with brine, dried with Na₂SO₄, and concentrated *in vacuo*. Purification by flash column chromatography (0→10% Et₂O in Hexanes) afforded the pure product as a yellow oil (253 mg, 68%). Spectral data were in accordance with previous report.¹⁹ **¹H NMR (500 MHz, CDCl₃):** δ 7.53 – 7.47 (m, 2H), 7.36 – 7.25 (m, 3H), 5.75 (d, *J* = 1.2 Hz, 1H), 2.41 (d, *J* = 0.9 Hz, 3H), 1.32 (s, 12H).

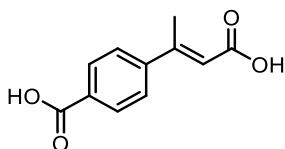


(E)-3-Phenylbut-2-enitrile (E-22): NaH (60% in mineral oil) (1.8 g, 75 mmol, 3 eq.) was dissolved in dry THF (70 mL, 832 mM) and the mixture was cooled to 0 °C and purged with N₂. Diethylcyanomethylphosphonate (6.78 g, 37.5 mmol, 1.5 eq.) was added dropwise and the solution was stirred at 0 °C for 1 h. Acetophenone (2.92 mL, 25 mmol, 1 eq.) was added dropwise and the reaction was stirred at room temperature for 48 h. Then, 20 mL of water was added, and the mixture was extracted with AcOEt three times, washed with brine and dried with Na₂SO₄. The solvent was removed *in vacuo*, and a purification by flash column chromatography (5% Et₂O in Hexanes) afforded the pure product as a colorless oil (2.96 g, 83%). Spectral data were in accordance with previous report.²⁰ **¹H NMR (400 MHz, CDCl₃):** δ 7.49 – 7.44 (m, 2H), 7.44 – 7.38 (m, 3H), 5.62 (s, 1H), 2.48 (s, 3H)

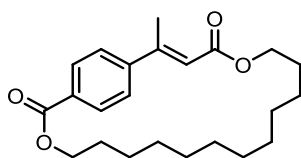


Dimethyl 2-phenylmaleate (Z-23): To an open sealed tube, methyl 2-oxo-2-phenylacetate (853 μL, 6.00 mmol, 1.00 eq.), methyl (triphenylphosphoranylidene)acetate (3.07 g, 9.00 mmol, 1.5 eq.), and 10 mL of toluene were added. The vial was sealed, and the reaction was heated at 130

°C for 4 h. The mixture was cooled down to room temperature and filtered through silica. The solid that remained on the silica was washed with ether. The filtrate was concentrated *in vacuo* and a purification by flash column chromatography (10% AcOEt in Hexanes) afforded the pure product as a colorless oil (250 mg, 19%). Spectral data were in accordance with previous report.²¹
¹H NMR (400 MHz, CDCl₃): δ 7.53 – 7.35 (m, 5H), 6.32 (s, 1H), 3.95 (s, 3H), 3.79 (s, 3H).

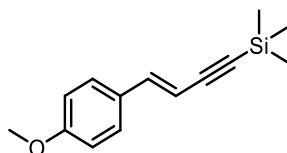


(E)-4-(1-Carboxyprop-1-en-2-yl)benzoic acid (S3): Methyl (*E*)-4-(4-ethoxy-4-oxobut-2-en-2-yl)benzoate (1.50 g, 6.04 mmol, 1 eq.) and LiOH (1.45 g, 60.4 mmol, 10 eq.) was added to a 1:1 MeCN:H₂O solution (60 mL, 101 mM). The solution was then stirred at room temperature for 48 h. A solution of HCl 1M was then slowly added until the apparition of a white solid. The solid was then filtered, washed with water, then Et₂O, and dried to give the pure compound as a white powder (1.10 g, 88 %). **¹H NMR (400 MHz, DMSO):** δ 12.96 – 12.34 (m, 2H), 7.99 – 7.92 (m, 2H), 7.70 – 7.64 (m, 2H), 6.20 – 6.15 (m, 1H), 2.59 – 2.39 (m, 3H). **¹³C NMR (126 MHz, DMSO):** δ 167.4, 166.9, 152.5, 145.6, 131.0, 129.6, 126.5, 119.2, 17.2. **HRMS (ESI) m/z** calculated for C₁₁H₁₀O₄ [M-H]⁻ 205.0520 found 205.0516.

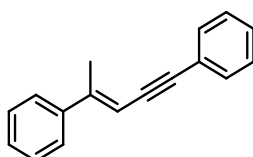


(E)-19-methyl-3,16-dioxa-1(1,4)-benzenacyclonadecaphan-18-ene-2,17-dione (E-24): In a oven-dried round-bottom flask was added (*E*)-4-(1-Carboxyprop-1-en-2-yl)benzoic acid (200 mg, 0.97 mmol, 1 eq.), *N,N'*-Dicyclohexylcarbodiimide (750 mg, 3.64 mmol, 3.75 eq.), *N,N*-Dimethylpyridin-4-amine (450 mg, 3.69 mmol, 3.8 eq.) and dodecane-1,12-diol (200 mg, 0.98 mmol, 1.01 eq.). Dry CH₂Cl₂ (50 mL, [19.4 mM]) was added and the heterogeneous reaction

mixture was stirred at room temperature for 48 h. The white solid was filtered, washed with Et₂O, and the filtrate was concentrated *in vacuo*. Purification by flash column chromatography (2% AcOEt in Hexanes) afforded the pure product as a white solid (35.2 mg, 10%). **¹H NMR (500 MHz, CDCl₃):** δ 8.06 – 8.00 (m, 2H), 7.51 – 7.45 (m, 2H), 5.91 (q, *J* = 1.3 Hz, 1H), 4.45 – 4.39 (m, 2H), 4.20 – 4.14 (m, 2H), 2.59 (d, *J* = 1.4 Hz, 3H), 1.76 – 1.63 (m, 4H), 1.46 – 1.30 (m, 6H), 1.23 – 1.14 (m, 4H), 1.12 – 1.01 (m, 4H), 1.01 – 0.92 (m, 2H). **¹³C NMR (126 MHz, CDCl₃):** δ 166.2, 165.9, 155.3, 147.7, 131.4, 130.0, 126.1, 121.7, 66.7, 65.8, 31.6, 31.5, 31.1, 31.0, 30.8, 28.5, 28.3, 27.9, 27.6, 16.6. **HRMS (ESI)** *m/z* calculated for C₂₃H₃₂O₄ [M+H]⁺ 373.2373 found 373.2360.



(E)-4-(4-Methoxyphenyl)but-3-en-1-yn-1-yl)trimethylsilane (E-25): To a 4 mL vial equipped with a stir bar was added 4-ethynylanisole (51.9 μL, 0.4 mmol, 1.0 eq.), 4CzIPN (2,4,5,6-tetra(9H-carbazol-9-yl)isophthalonitrile) (6.3 mg, 8 μmol, 2 mol%), dppp (9.9 mg, 24 μmol, 6 mol%) and Co(BF₄)₂·6H₂O (6.8 mg, 20 μmol, 5 mol%). The vial was capped with a rubber septum and sparged with N₂. Degassed MeCN (0.2 M) was added and the mixture was stirred under a N₂ atmosphere. Then, DIPEA (21 μL, 0.12 mmol, 30 mol%) and (trimethylsilyl)acetylene (139 μL, 1 mmol, 2.5 eq) were added and the septum was replaced with a screw cap. The reaction mixture was then stirred under irradiation from blue LEDs at ambient temperature for 24 hours. Concentration *in vacuo* and purification by flash column chromatography (100% Hexanes) afforded the pure product as a colorless oil (55 mg, 60%). Spectral data were in accordance with previous report.²² **¹H NMR (400 MHz, CDCl₃):** δ 7.35 – 7.27 (m, 2H), 6.96 (d, *J* = 16.3 Hz, 1H), 6.91 – 6.81 (m, 2H), 6.04 (d, *J* = 16.3 Hz, 1H), 3.81 (s, 3H), 0.23 (s, 9H).



(E)-Pent-3-en-1-yne-1,4-diyldibenzene (**E-26**): To an open sealed tube, (*E*)-(1-bromoprop-1-en-2-yl)benzene (78.8 mg, 0.4 mmol, 1 eq.), phenylacetylene (54.9 μ L, 0.5 mmol, 1.25 eq.), CuI (7.6 mg, 0.04 mmol, 10 mol%), K₃PO₄ (0.8 mmol), and DMSO (2 mL) were added, and the mixture was purged with N₂. The mixture was then heated at 130 °C for 24 h. Then, 10 mL of water was added and the mixture was extracted with AcOEt three times, washed with brine, and dried with Na₂SO₄. The solvent was removed *in vacuo*, and a purification by flash column chromatography (100% Hexanes) afforded the pure product as a colorless oil (20 mg, 23%). Spectral data were in accordance with previous report.²³ ¹H NMR (400 MHz, CDCl₃): δ 7.52 – 7.45 (m, 4H), 7.44 – 7.27 (m, 7H), 6.11 (s, 1H), 2.41 (s, 3H).

A3.4 Photochemical isomerization of alkenes

All photocatalysis reactions were performed in 5-dram vials that were placed in a homemade photoreactor. Each hole is aligned with a light-emitting diode (LED) strip connected to a power source. LED strips were purchased from Creative Lightings (<https://www.creativelightings.com/>). The vial bottoms were maintained at approximately 0.5 cm from the light source. An external fan was used to maintain an average temperature below 30 °C. No mixing was used as the volume of solvent was kept between 0.5 and 1 mL.

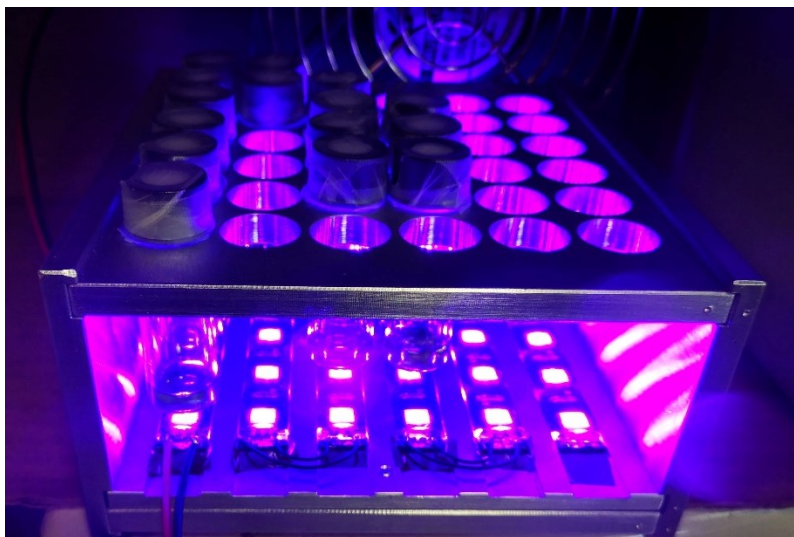


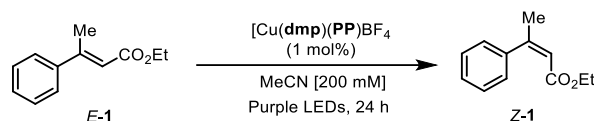
Figure A3 - 1 Homemade photoreactor used for the photochemical isomerizations.

General Procedure for the Photochemical Isomerisation of Alkenes:

In a 5-dram vial was added the copper complex (1 mol %, unless noted otherwise) and the alkene. Solvent (MeCN, unless noted otherwise) was added and the solution was purged with N₂ for 5 min in a sonicator bath. The vial was sealed and then put in the photoreactor and irradiated for 24 h under 400 nm wavelength (unless noted otherwise). The solvent was then removed under vacuum, and an ¹H NMR of the crude mixture was taken, to determine the *Z*:*E* ratio. Then, the NMR sample was recombined with the remaining reaction mixture and placed on a rotovap to remove all solvent *in vacuo*. The crude solid was dissolved in Et₂O and passed through a plug of silica to afford the pure mixture of *E* and *Z* isomers. If necessary, a purification by flash column chromatography was performed to separate the *E* and *Z* isomers.

Tabular data from screening

Table A3 - 1 Evaluation of Cu(dmp)(PP)BF₄-Based Photocatalysts in a Model *E*↔*Z* Isomerization Process



	PP	τ (ns)	E_T (eV)	% <i>Z</i> -1 ^a	%Cu
1	NXantPhos	19	2.49	96	0
2	NXantPhos(1 h)	19	2.49	26	-
3	PhanePhos	1948	2.25	72	21
4	XantPhos	1133	2.21	97	68
5	XantPhos(1 h)	1133	2.21	74	-
6	DPEPhos	14300	2.17	97	57
7	DPEPhos (1 h)	14300	2.17	64	-
8	dppf	1.5	2.17	0	84
9	dppn	1.43	2.15	94	90
10	BINAP	2188	1.94	83	0
11	SEGPhos	340	1.92	44	0
12	none	90	1.65	0	71

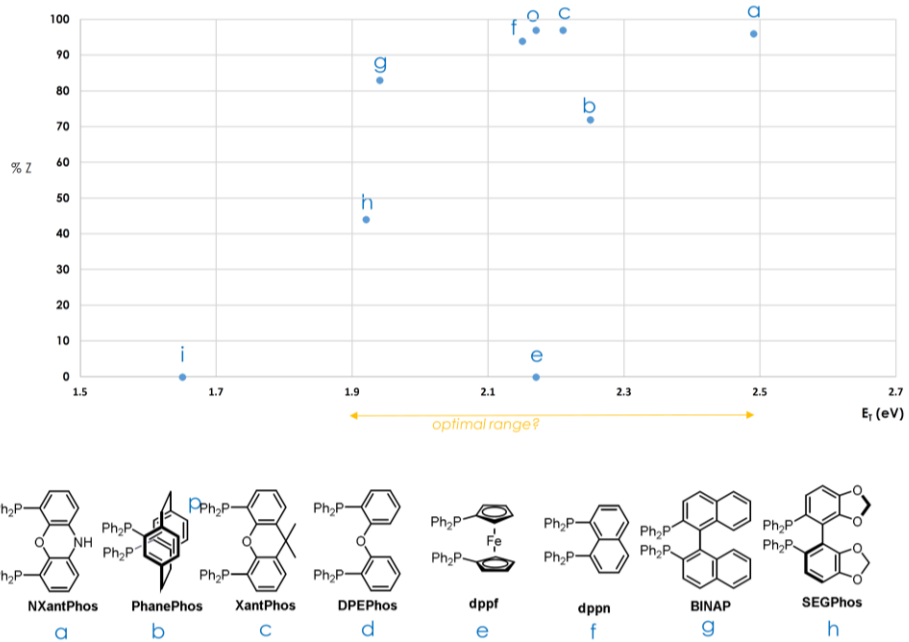
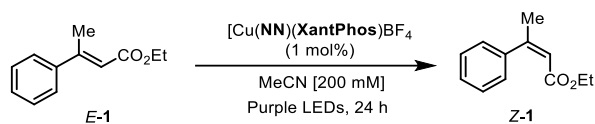


Figure A3 - 2 Correlation between Cu(dmp)(PP)BF₄ photocatalysts triplet energy and formation of the Z-isomer

Table A3 - 2 Evaluation of Cu(NN)(XantPhos)BF₄-Based Photocatalysts in a Model E↔Z Isomerization Process



	NN	τ (ns)	E_T (eV)	% Z	%Cu
1	phen	391	2.27	1	100
2	dmp	1133	2.21	97	68
3	tmp	1119	2.07	13	0
4	bphen	1798	2.61	95	85
5	dmbp	72	1.95	23	93
6	dtbbp	143	1.99	1	95
7	batho	3.2	2.50	3	88
8	bathocup	4	2.66	97	24
9	dq	393	1.89	1	91
10	pytri	752	2.26	1	0
11	quintri	3.6	2.59	91	99
12	iquintri	3.8	2.69	4	54
13	dpq	3	2.21	95	82
14	dppz	71	1.95	58	9
15	bdppz	75	2.19	89	0
16	dpa	3	2.88	31	43
17	dmop	4	2.55	96	44
18	bphen (Blue LEDs)	1798	2.61	91	-
19	bphen (Blue LEDs) ^a	1798	2.61	97	-
20	bphen (CH ₂ Cl ₂)	1798	2.61	97	-
21	bphen (1 h)	1798	2.61	95	-
22	bathocup (1 h)	4	2.66	88	-
23	dmp (1 h)	1133	2.21	75	-
24	Cu(bphen) ₂ BF ₄	na	na	0	-

^a 5 mol % of catalyst. na = not applicable.

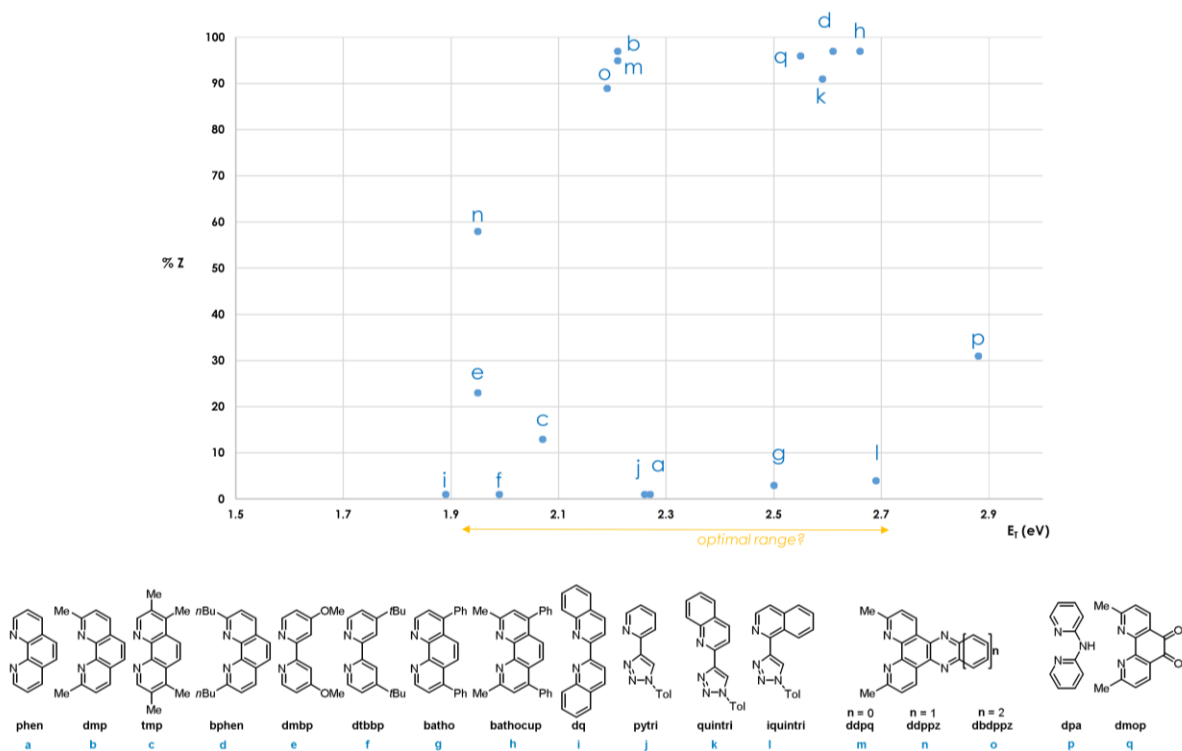
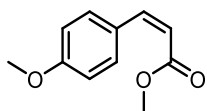
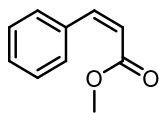


Figure A3 - 3 Correlation between $\text{Cu}(\text{NN})(\text{XantPhos})\text{BF}_4$ photocatalysts triplet energy and formation of the Z-isomer

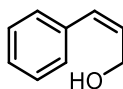
A3.5 Izomerized products



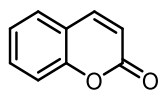
Methyl (Z)-3-(4-methoxyphenyl)acrylate (Z-2): According to the general procedure, methyl (*E*)-3-(4-methoxyphenyl)acrylate (19.2 mg, 0.1 mmol, 1 eq.) and $[\text{Cu}(\text{bphen})(\text{XantPhos})]\text{BF}_4$ (1.0 mg, 1 μmol , 1 mol%) in MeCN (0.5 mL, 200 mM) were irradiated at 400 nm for 1 hour to give a ratio of 40:60 (*Z*:*E*) (89%). Spectral data were in accordance with previous report.²⁴ **$^1\text{H NMR}$ (500 MHz, CDCl_3):** δ 7.74 – 7.66 (m, 2H), 6.90 – 6.83 (m, 3H), 5.83 (d, $J = 12.7$ Hz, 1H), 3.83 (s, 3H), 3.73 (s, 3H).



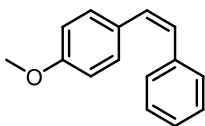
Methyl (Z)-3-phenylacrylate (Z-3): According to the general procedure, methylcinnamate (16.2 mg, 0.1 mmol, 1 eq.) and Cu(bphen)(XantPhos)BF₄ (1.0 mg, 1 μmol, 1 mol%) in MeCN (0.5 mL, 200 mM) were irradiated at 400 nm for 1 hour to give a ratio of 75:25 (Z:E) (70%). Spectral data were in accordance with previous report.²⁵ **¹H NMR (400 MHz, CDCl₃):** δ 7.64 – 7.56 (m, 2H), 7.44 – 7.35 (m, 3H), 6.96 (d, *J* = 12.7 Hz, 1H), 5.96 (d, *J* = 12.6 Hz, 1H), 3.71 (s, 3H).



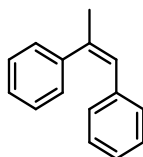
(Z)-3-Phenylprop-2-en-1-ol (Z-4): According to the general procedure, (*E*)-3-phenylprop-2-en-1-ol (26.8 mg, 0.2 mmol, 1 eq.) and Cu(bphen)(XantPhos)BF₄ (2.1 mg, 2 μmol, 1 mol%) in CH₂Cl₂ (1 mL, 200mM) were irradiated at 400 nm for 24 hours to give a ratio of 73:27 (Z:E) (94%). Spectral data were in accordance with previous report.²⁶ **¹H NMR (400 MHz, CDCl₃):** δ 7.41 – 7.19 (m, 5H), 6.58 (dt, *J* = 11.7, 1.9 Hz, 1H), 5.88 (dt, *J* = 11.7, 6.4 Hz, 1H), 4.44 (dd, *J* = 6.4, 1.7 Hz, 2H), 1.69 (bs, 1H).



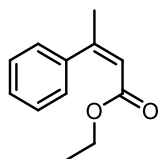
2H-Chromen-2-one (Z-5): According to the general procedure, methyl (*E*)-3-(2-hydroxyphenyl)acrylate (35.6 mg, 0.2 mmol, 1 eq.) and Cu(bphen)(XantPhos)BF₄ (2.1 mg, 2 μmol, 1 mol%) in MeCN (1 mL, 200 mM) were irradiated at 400 nm for 24 hours. The solvent was removed *in vacuo*, and a purification by flash column chromatography (100% Hexanes) afforded the pure product as a white solid (22.5 mg, 79%). Spectral data were in accordance with previous report.²⁷ **¹H NMR (400 MHz, CDCl₃):** δ 7.71 (d, *J* = 9.5 Hz, 1H), 7.54 (ddd, *J* = 8.6, 7.3, 1.6 Hz, 1H), 7.49 (dd, *J* = 7.7, 1.6 Hz, 1H), 7.38 – 7.24 (m, 2H), 6.43 (d, *J* = 9.5 Hz, 1H).



(Z)-1-Methoxy-4-styrylbenzene (Z-6): According to the general procedure, (*E*)-1-methoxy-4-styrylbenzene (42.1 mg, 0.2 mmol, 1 eq.) and Cu(bphen)(XantPhos)BF₄ (2.1 mg, 2 μmol, 1 mol%) in MeCN (1 mL, 200 mM) were irradiated at 400 nm for 24 hours to give a ratio of 76:24 (*Z*:*E*) (78%). Spectral data were in accordance with previous report.²⁷ **¹H NMR (400 MHz, CDCl₃):** δ 7.32 – 7.15 (m, 7H), 6.79 – 6.74 (m, 2H), 6.53 (d, *J* = 1.9 Hz, 2H), 3.79 (s, 3H).

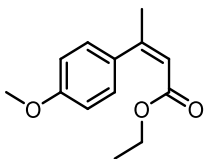


(Z)-prop-1-ene-1,2-diyl dibenzene (Z-7): According to the general procedure a mixture of (*E*)-prop-1-ene-1,2-diyl dibenzene and (*Z*)-prop-1-ene-1,2-diyl dibenzene (20:80 *Z*:*E*) (38.9 mg, 0.2 mmol, 1 eq.) and Cu(bphen)(XantPhos)BF₄ (2.1 mg, 2 μmol, 1 mol%) in MeCN (1 mL, 200 mM) were irradiated at 400 nm for 24 hours to give a ratio of 77:23 (*Z*:*E*) (86%). Spectral data were in accordance with previous report.¹⁰ **¹H NMR (400 MHz, CDCl₃):** δ 7.29 – 7.22 (m, 3H), 7.22 – 7.14 (m, 2H), 7.13 – 7.03 (m, 3H), 6.98 – 6.91 (m, 2H), 6.47 (d, *J* = 2.1 Hz, 1H), 2.21 (d, *J* = 1.6 Hz, 3H).

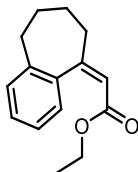


Ethyl (Z)-3-phenylbut-2-enoate (Z-8): According to the general procedure, ethyl (*E*)-3-phenylbut-2-enoate (19.0 mg, 0.1 mmol, 1 eq.) and Cu(bphen)(XantPhos)BF₄ (1.0 mg, 1 μmol, 1 mol%) in MeCN (0.5 mL, 200 mM) were irradiated at 400 nm for 1 hour to give a ratio of 95:5 (*Z*:*E*) (98%). Spectral data were in accordance with previous report.¹¹ **¹H NMR (400 MHz, CDCl₃):** δ 7.39 – 7.28

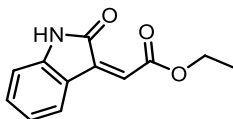
(m, 3H), 7.23 – 7.18 (m, 2H), 5.91 (q, $J = 1.5$ Hz, 1H), 4.00 (q, $J = 7.1$ Hz, 2H), 2.18 (d, $J = 1.5$ Hz, 3H), 1.08 (t, $J = 7.1$ Hz, 3H).



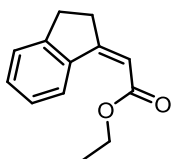
Ethyl (Z)-3-(4-methoxyphenyl)but-2-enoate (Z-9): According to the general procedure, ethyl (*E*)-3-(4-methoxyphenyl)but-2-enoate (44.1 mg, 0.2 mmol, 1 eq.) and Cu(bphen)(XantPhos)BF₄ (2.1 mg, 2 μmol, 1 mol%) in MeCN (1 mL, 200 mM) were irradiated at 400 nm for 24 hour to give a ratio of 94:6 (*Z*:*E*) (99%). Spectral data were in accordance with previous report.¹² **¹H NMR (400 MHz, CDCl₃):** δ 7.23 – 7.15 (m, 2H), 6.93 – 6.84 (m, 2H), 5.87 (s, 1H), 4.04 (q, $J = 7.1$ Hz, 2H), 3.81 (s, 3H), 2.17 (d, $J = 1.4$ Hz, 3H), 1.14 (t, $J = 7.1$ Hz, 3H).



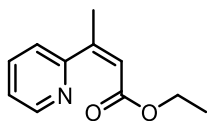
Ethyl (Z)-2-(6,7,8,9-tetrahydro-5H-benzo[7]annulen-5-ylidene)acetate (Z-10): According to the general procedure, ethyl (*E*)-2-(6,7,8,9-tetrahydro-5H-benzo[7]annulen-5-ylidene)acetate (46.1 mg, 0.2 mmol, 1 eq.) and Cu(bphen)(XantPhos)BF₄ (2.1 mg, 2 μmol, 1 mol%) in MeCN (1 mL, 200 mM) were irradiated at 400 nm for 24 hour to give a ratio of 95:5 (*Z*:*E*) (98%). Spectral data were in accordance with previous report.¹³ **¹H NMR (400 MHz, CDCl₃):** δ 7.27 – 7.18 (m, 1H), 7.22 – 7.13 (m, 2H), 7.12 – 7.05 (m, 1H), 5.99 (s, 1H), 4.02 (q, $J = 7.1$ Hz, 2H), 2.82 – 2.75 (m, 2H), 2.47 – 2.40 (m, 2H), 2.01 – 1.90 (m, 2H), 1.82 – 1.72 (m, 2H), 1.10 (t, $J = 7.1$ Hz, 3H).



Ethyl (Z)-2-(2-oxoindolin-3-ylidene)acetate (Z-11): According to the general procedure, ethyl (*E*)-2-(2-oxoindolin-3-ylidene)acetate (21.7 mg, 0.1 mmol, 1 eq.) and Cu(bphen)(XantPhos)BF₄ (1.0 mg, 1 μmol, 1 mol%) in MeCN (0.5 mL, 200 mM) were irradiated at 400 nm for 24 hours to give a ratio of 99:1 (*Z*:*E*) (80%). ¹H NMR (400 MHz, CDCl₃): δ 7.74 – 7.65 (m, 2H), 7.21 – 7.13 (m, 1H), 7.05 – 6.96 (m, 1H), 6.70 (d, *J* = 7.7 Hz, 1H), 4.53 (s, 1H), 4.02 – 3.90 (m, 1H), 3.85 (dq, *J* = 10.9, 7.2 Hz, 1H), 2.17 (s, 1H), 0.78 (t, *J* = 7.1 Hz, 3H). ¹³C NMR (101 MHz, CDCl₃): δ 174.4, 169.0, 140.7, 129.4, 128.6, 123.7, 121.4, 109.4, 61.1, 54.9, 43.0, 13.9. HRMS (ESI) *m/z* calculated for C₁₂H₁₁NO₃ [M+H]⁺ 218.0812 found 218.0808.

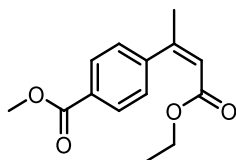


Ethyl (Z)-2-(2,3-dihydro-1H-inden-1-ylidene)acetate (Z-12): According to the general procedure, ethyl (*E*)-2-(2,3-dihydro-1H-inden-1-ylidene)acetate (21.8 mg, 0.1 mmol, 1 eq.) and Cu(bphen)(XantPhos)BF₄ (1 mg, 1 μmol, 1 mol%) in MeCN (0.5 mL, 200 mM) were irradiated at 400 nm for 24 hour to give a ratio of 56:44 (*Z*:*E*) (85%). Spectral data were in accordance with previous report.¹³ ¹H NMR (500 MHz, CDCl₃): δ 8.82 (d, *J* = 7.9 Hz, 1H), 7.39 – 7.24 (m, 3H), 5.97 (t, *J* = 2.0 Hz, 1H), 4.22 (q, *J* = 7.1 Hz, 2H), 3.03 – 2.96 (m, 2H), 2.95 – 2.89 (m, 2H), 1.32 (t, *J* = 7.1 Hz, 3H).

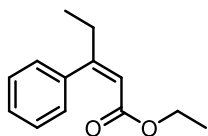


Ethyl (Z)-3-(pyridin-2-yl)but-2-enoate (Z-13): According to the general procedure, ethyl (*E*)-3-(pyridin-2-yl)but-2-enoate (18.9 mg, 0.1 mmol, 1 eq.) and Cu(bphen)(XantPhos)BF₄ (1.0 mg, 1 μmol, 1 mol%) in MeCN (0.5 mL, 200 mM) were irradiated at 400 nm for 24 hours to give a ratio of 98:2 (*Z*:*E*) (96%). ¹H NMR (500 MHz, CDCl₃): δ 8.59 (ddd, *J* = 5.0, 1.8, 1.0 Hz, 1H), 7.64 (ddd, *J* =

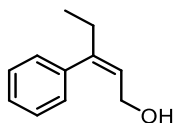
7.7, 1.8 Hz, 1H), 7.24 (dd, $J = 7.9, 1.1$ Hz, 1H), 7.19 (ddd, $J = 7.6, 4.9, 1.2$ Hz, 1H), 5.99 (q, $J = 1.6$ Hz, 1H), 4.00 (q, $J = 7.2$ Hz, 2H), 2.22 (d, $J = 1.6$ Hz, 3H), 1.08 (t, $J = 7.1$ Hz, 3H). $^{13}\text{C NMR}$ (126 MHz, CDCl_3): δ 165.9, 158.8, 153.5, 149.1, 135.8, 122.5, 122.5, 119.4, 60.0, 25.0, 14.1. HRMS (ESI) m/z calculated for $\text{C}_{11}\text{H}_{13}\text{NO}_2$ $[\text{M}+\text{H}]^+$ 192.1019 found 192.1017.



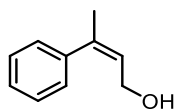
Methyl (Z)-4-(4-ethoxy-4-oxobut-2-en-2-yl)benzoate (Z-14): According to the general procedure, methyl (*E*)-4-(4-ethoxy-4-oxobut-2-en-2-yl)benzoate (49.7 mg, 0.2 mmol, 1 eq.) and $\text{Cu}(\text{bphen})(\text{XantPhos})\text{BF}_4$ (2.0 mg, 2 μmol , 1 mol%) in MeCN (1 mL, 200 mM) were irradiated at 400 nm for 24 hours to give a ratio of 97:3 (*Z:E*) (97%). $^1\text{H NMR}$ (400 MHz, CDCl_3): δ 8.05 – 7.98 (m, 2H), 7.25 (d, $J = 8.3$ Hz, 2H), 5.94 (q, $J = 1.6$ Hz, 1H), 3.98 (q, $J = 7.1$ Hz, 2H), 3.90 (s, 3H), 2.17 (d, $J = 1.5$ Hz, 3H), 1.06 (t, $J = 7.1$ Hz, 3H). $^{13}\text{C NMR}$ (101 MHz, CDCl_3): δ 166.9, 165.7, 154.5, 146.0, 129.4, 129.4, 127.0, 118.8, 77.5, 77.2, 76.8, 60.1, 52.2, 27.0, 14.1. HRMS (ESI) m/z calculated for $\text{C}_{14}\text{H}_{16}\text{O}_4$ $[\text{M}+\text{H}]^+$ 249.1121 found 249.1124.



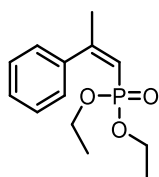
Ethyl (Z)-3-phenylpent-2-enoate (Z-15): According to the general procedure, ethyl (*E*)-3-phenylpent-2-enoate (20.6 mg, 0.1 mmol, 1 eq.) and $\text{Cu}(\text{bphen})(\text{XantPhos})\text{BF}_4$ (1.0 mg, 1 μmol , 1 mol%) in MeCN (0.5 mL, 200 mM) were irradiated at 400 nm for 1 hour to give a ratio of 94:6 (*Z:E*) (90%). Spectral data were in accordance with previous report.¹¹ $^1\text{H NMR}$ (400 MHz, CDCl_3): δ 7.39 – 7.26 (m, 3H), 7.19 – 7.12 (m, 2H), 5.87 (t, $J = 1.5$ Hz, 1H), 3.98 (q, $J = 7.1$ Hz, 2H), 2.46 (qd, $J = 7.4, 1.4$ Hz, 2H), 1.06 (td, $J = 7.3, 1.2$ Hz, 6H).



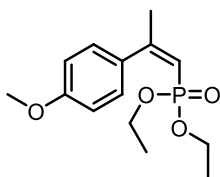
(Z)-3-Phenylpent-2-en-1-ol (Z-16): According to the general procedure, (*E*)-3-phenylpent-2-en-1-ol (16.2 mg, 0.1 mmol, 1 eq.) and Cu(bphen)(XantPhos)BF₄ (1.0 mg, 1 μmol, 1 mol%) in CH₂Cl₂ (0.5 mL, 200 mM) were irradiated at 400 nm for 24 hours to give a ratio of 98:2 (*Z*:*E*) (96%). Spectral data were in accordance with previous report.²⁸ **¹H NMR (400 MHz, CDCl₃):** δ 7.38 – 7.29 (m, 2H), 7.30 – 7.23 (m, 1H), 7.16 – 7.09 (m, 2H), 5.66 (tt, *J* = 7.0, 1.5 Hz, 1H), 4.03 (d, *J* = 6.9 Hz, 2H), 2.39 (q, *J* = 7.4 Hz, 2H), 1.46 (s, 1H), 0.99 (t, *J* = 7.4 Hz, 3H).



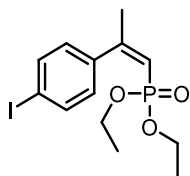
(Z)-3-Phenylbut-2-en-1-ol (Z-17): According to the general procedure, (*E*)-3-phenylbut-2-en-1-ol (14.8 mg, 0.1 mmol, 1 eq.) and Cu(bphen)(XantPhos)BF₄ (1.0 mg, 1 μmol, 1 mol%) in CH₂Cl₂ (0.5 mL, 200 mM) were irradiated at 400 nm for 24 hours to give a ratio of 97:3 (*Z*:*E*) (92%). Spectral data were in accordance with previous report.²⁹ **¹H NMR (400 MHz, CDCl₃):** δ 7.39 – 7.24 (m, 3H), 7.18 (dd, *J* = 6.9, 1.9 Hz, 2H), 5.76 – 5.68 (m, 1H), 4.08 (d, *J* = 7.0 Hz, 2H), 2.09 (s, 3H), 1.41 (bs, 1H).



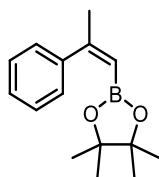
Diethyl (Z)-(2-phenylprop-1-en-1-yl)phosphonate (Z-18): According to the general procedure, diethyl (*E*)-(2-phenylprop-1-en-1-yl)phosphonate (25.4 mg, 0.1 mmol, 1 eq.) and Cu(bphen)(XantPhos)BF₄ (5.1 mg, 5 μmol, 5 mol%) in MeCN (0.5 mL, 200 mM) were irradiated at 450 nm for 24 hours to give a ratio of 92:8 (*Z*:*E*) (96%). Spectral data were in accordance with previous report.¹⁷ **¹H NMR (500 MHz, CDCl₃):** δ 7.41 – 7.25 (m, 5H), 5.72 (dq, *J* = 17.4, 1.5 Hz, 1H), 3.90 – 3.70 (m, 4H), 2.22 (dd, *J* = 1.3 Hz, 3H), 1.07 (t, *J* = 7.1, 0.6 Hz, 6H).



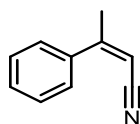
Diethyl (Z)-(2-(4-methoxyphenyl)prop-1-en-1-yl)phosphonate (Z-19): According to the general procedure, diethyl (*E*)-(2-(4-methoxyphenyl)prop-1-en-1-yl)phosphonate (56.9 mg, 0.2 mmol, 1 eq.) and Cu(bphen)(XantPhos)BF₄ (10.2 mg, 10 μmol, 5 mol%) in CH₂Cl₂ (1 mL, 200 mM) were irradiated at 450 nm for 24 hours to give a ratio of 90:10 (*Z*:*E*) (94%). Spectral data were in accordance with previous report.¹⁷ **¹H NMR (400 MHz, CDCl₃):** δ 7.38 (d, *J* = 8.7 Hz, 2H), 6.86 (d, *J* = 8.8 Hz, 2H), 5.64 (dt, *J* = 17.0, 1.5 Hz, 1H), 3.91 – 3.74 (m, 7H), 2.20 (d, *J* = 1.6 Hz, 3H), 1.09 (t, *J* = 7.1 Hz, 6H).



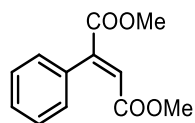
Diethyl (Z)-(2-(4-iodophenyl)prop-1-en-1-yl)phosphonate (Z-20): According to the general procedure, diethyl (*E*)-(2-(4-iodophenyl)prop-1-en-1-yl)phosphonate (76.0 mg, 0.2 mmol, 1 eq.) and Cu(bphen)(XantPhos)BF₄ (10.2 mg, 10 μmol, 5 mol%) in CH₂Cl₂ (1 mL, 200 mM) were irradiated at 450 nm for 24 hours to give a ratio of 90:10 (*Z*:*E*) (91%). **¹H NMR (400 MHz, CDCl₃):** δ 7.73 – 7.65 (m, 2H), 7.19 – 7.11 (m, 2H), 5.74 (dq, *J* = 16.8, 1.5 Hz, 1H), 3.94 – 3.76 (m, 4H), 2.20 (t, *J* = 1.3 Hz, 3H), 1.20 (s, 1H), 1.12 (t, *J* = 7.1 Hz, 6H). **¹³C NMR (126 MHz, CDCl₃):** δ 157.8 (d, *J* = 4.3 Hz), 140.1 (d, *J* = 7.5 Hz), 137.2, 129.4 (d, *J* = 1.8 Hz), 115.7 (d, *J* = 191.1 Hz), 94.3, 61.6 (d, *J* = 6.0 Hz), 28.3 (d, *J* = 22.8 Hz), 16.3 (d, *J* = 6.7 Hz). **HRMS (ESI)** *m/z* calculated for C₁₃H₁₈I₂O₃P [M+H]⁺ 381.0111 found 381.0113.



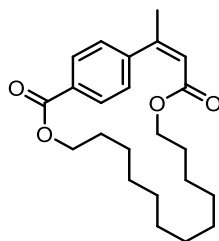
(Z)-4,4,5,5-Tetramethyl-2-(2-phenylprop-1-en-1-yl)-1,3,2-dioxaborolane (Z-21): According to the general procedure, (*E*)-4,4,5,5-tetramethyl-2-(2-phenylprop-1-en-1-yl)-1,3,2-dioxaborolane (24.4 mg, 0.1 mmol, 1 eq.) and Cu(bphen)(XantPhos)BF₄ (1.0 mg, 1 μmol, 1mol%) in MeCN (0.5 mL, 200mM) were irradiated at 400 nm for 24 hours to give a ratio of 92:8 (*Z*:*E*) (94%). Spectral data were in accordance with previous report.¹⁹ **¹H NMR (500 MHz, CDCl₃):** δ 7.33 – 7.22 (m, 5H), 5.47 (s, 1H), 2.21 (s, 3H), 1.14 (s, 12H).



(Z)-3-Phenylbut-2-enitrile (Z-22): According to the general procedure, (*E*)-3-phenylbut-2-enitrile (28.6 mg, 0.2 mmol, 1 eq.) and Cu(bphen)(XantPhos)BF₄ (2.0 mg, 2 μmol, 1mol%) in MeCN (1 mL, 200mM) were irradiated at 400 nm for 24 hours to give a ratio of 84:16 (*Z*:*E*) (89%). Spectral data were in accordance with previous report.²⁰ **¹H NMR (400 MHz, CDCl₃):** δ 7.58 – 7.51 (m, 2H), 7.48 – 7.38 (m, 4H), 5.40 (q, *J* = 1.6 Hz, 1H), 2.28 (d, *J* = 1.6 Hz, 3H).

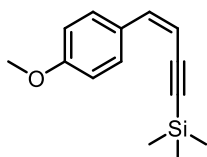


Dimethyl 2-phenylfumarate (E-23): According to the general procedure, dimethyl 2-phenylmaleate (44.0 mg, 0.2 mmol, 1 eq.) and Cu(bphen)(XantPhos)BF₄ (2.0 mg, 2 μmol, 1mol%) in MeCN (1 mL, 200mM) were irradiated at 400 nm for 24 hours to give a ratio of 89:11 (*E*:*Z*) (93%). Spectral data were in accordance with previous report.²¹ **¹H NMR (400 MHz, CDCl₃):** δ 7.42 – 7.32 (m, 3H), 7.27 – 7.19 (m, 2H), 7.02 (s, 1H), 3.81 (s, 3H), 3.61 (s, 3H).

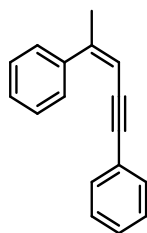


(Z)-19-methyl-3,16-dioxa-1(1,4)-benzenacyclononadecaphan-18-ene-2,17-dione (Z-24):

According to the general procedure, (E)-19-methyl-3,16-dioxa-1(1,4)-benzenacyclononadecaphan-18-ene-2,17-dione (37.2 mg, 0.1 mmol, 1 eq.) and Cu(bphen)(XantPhos)BF₄ (1.0 mg, 1 μmol, 1 mol%) in MeCN (0.5 mL, 200 mM) were irradiated at 400 nm for 24 hours to give a ratio of 96:4 (Z:E) (97%). ¹H NMR (500 MHz, CDCl₃): δ 8.04 – 7.98 (m, 2H), 7.27 – 7.21 (m, 2H), 5.93 (q, *J* = 1.5 Hz, 1H), 4.41 – 4.35 (m, 2H), 3.91 – 3.85 (m, 2H), 2.16 (d, *J* = 1.5 Hz, 3H), 1.82 – 1.74 (m, 2H), 1.51 (q, *J* = 7.3 Hz, 2H), 1.45 – 1.01 (m, 15H), 0.96 – 0.87 (m, 2H). ¹³C NMR (126 MHz, CDCl₃): δ 166.5, 166.5, 152.3, 146.3, 129.7, 129.3, 127.0, 119.8, 64.7, 64.2, 29.0, 28.7, 28.2, 28.1, 27.9, 27.5, 27.2, 26.8, 26.5, 25.4, 24.7. HRMS (ESI) *m/z* calculated for C₂₃H₃₂O₄ [M+H]⁺ 373.2373 found 373.2382.



(Z)-(4-(4-Methoxyphenyl)but-3-en-1-yn-1-yl)trimethylsilane (Z-25): According to the general procedure, (E)-(4-(4-methoxyphenyl)but-3-en-1-yn-1-yl)trimethylsilane (23.0 mg, 0.1 mmol, 1 eq.) and Cu(bphen)(XantPhos)BF₄ (1.0 mg, 1 μmol, 1 mol%) in MeCN (0.5 mL, 200mM) were irradiated at 400 nm for 24 hours to give a ratio of 47:53 (Z:E) (92%). Spectral data were in accordance with previous report.³⁰ ¹H NMR (500 MHz, CDCl₃): δ 7.92 – 7.85 (m, 2H), 6.90 – 6.86 (m, 2H), 6.59 (d, *J* = 12.0 Hz, 1H), 5.59 (d, *J* = 12.0 Hz, 1H), 3.84 (s, 3H), 0.26 (s, 9H).



(Z)-Pent-3-en-1-yne-1,4-diyl dibenzene (Z-26): According to the general procedure, (*E*)-pent-3-en-1-yne-1,4-diyl dibenzene (21.8 mg, 0.1 mmol, 1 eq.) and Cu(bphen)(XantPhos)BF₄ (1.0 mg, 1 μmol, 1 mol%) in MeCN (0.5 mL, 200mM) were irradiated at 400 nm for 24 hours to give a ratio of 50:50 (*Z*:*E*) (97%). **¹H NMR (500 MHz, CDCl₃):** δ 7.76 – 7.70 (m, 2H), 7.43 – 7.36 (m, 2H), 7.39 – 7.31 (m, 1H), 7.34 – 7.25 (m, 4H), 5.84 (q, *J* = 1.5 Hz, 1H), 2.25 (d, *J* = 1.5 Hz, 3H). **¹³C NMR (126 MHz, CDCl₃):** δ 148.3, 140.1, 131.4, 128.4, 128.2, 128.0, 128.0, 127.9, 124.0, 106.4, 91.6, 88.9, 24.4. **HRMS (ESI) *m/z*** calculated for C₁₇H₁₄ [M+H]⁺ 219.1168 found 219.1163.

A3.6 Kinetic Study of the Isomerisation of Ethyl (*E*)-3-phenylbut-2-enoate

Ethyl (*E*)-3-phenylbut-2-enoate (190 mg, 1 mmol, 1 eq.) and Cu(bphen)(XantPhos)BF₄ (10.2 mg, 10 μmol, 1 mol %) were added to MeCN (5 mL, 200 mM) that was previously purged with N₂. From the solution, 0.5 mL samples were injected in 8 vials which were then purged again for 5 min with N₂ in a sonicator bath. The vials were then placed in the photoreactor and irradiated at 400 nm for the required time. Solvent was removed and an NMR yield of the crude mixture, using triphenylmethane as internal standard, was calculated to give the *Z*:*E* ratio.

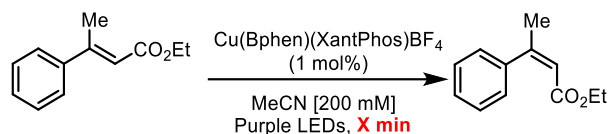
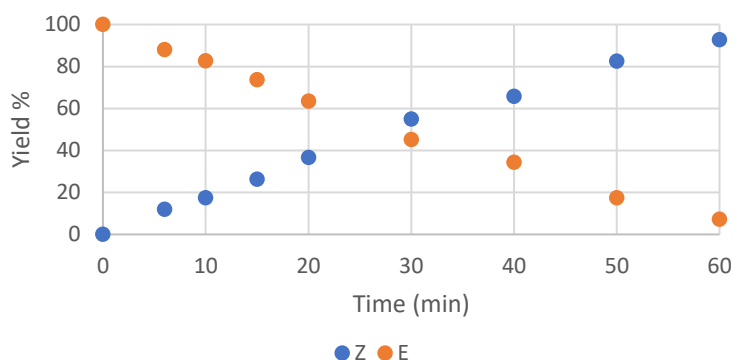


Table A3 - 3 Ratio of *E*- and *Z*-isomers during a 1-hour irradiation time at 400 nm.

TIME (MIN)	%Z	%E
0	0	100
6	12	88
10	17.4	82.6
15	26.3	73.7
20	36.6	63.4
30	54.9	45.1
40	65.7	34.3
50	82.5	17.5
60	92.8	7.2



A3.7 Reaction Scale-up using Flow Chemistry

Ethyl (*E*)-3-phenylbut-2-enoate (1 eq.) and Cu(bphen)(XantPhos)BF₄ (1 mol%) were added in N₂-purged CH₂Cl₂ [200mM]. The solution was purged again for 10 min with N₂ in a sonicator bath. The solution was then put in a 20 mL syringe. The syringe was then positioned onto a KD Scientific syringe pump. The pump was turned on at a flow rate of 0.216 mL/min. The reaction mixture was pumped through a 13 mL PFA-coiled reactor irradiated with 400 nm LEDs for a 1-hour residence time. Once the syringe was empty it was quickly replaced by a syringe of CH₂Cl₂ and pump was turned on again at the same flow rate. The collected solution was then concentrated *in vacuo* to provide a crude reaction mixture which was passed through a plug of silica with Et₂O to remove the copper complex. The *Z*:*E* ratio was measured by NMR yield.

Note: For reactions with more than 20 mL of solvent, several 20 mL syringes of the reaction mixture were quickly replaced one after the other.

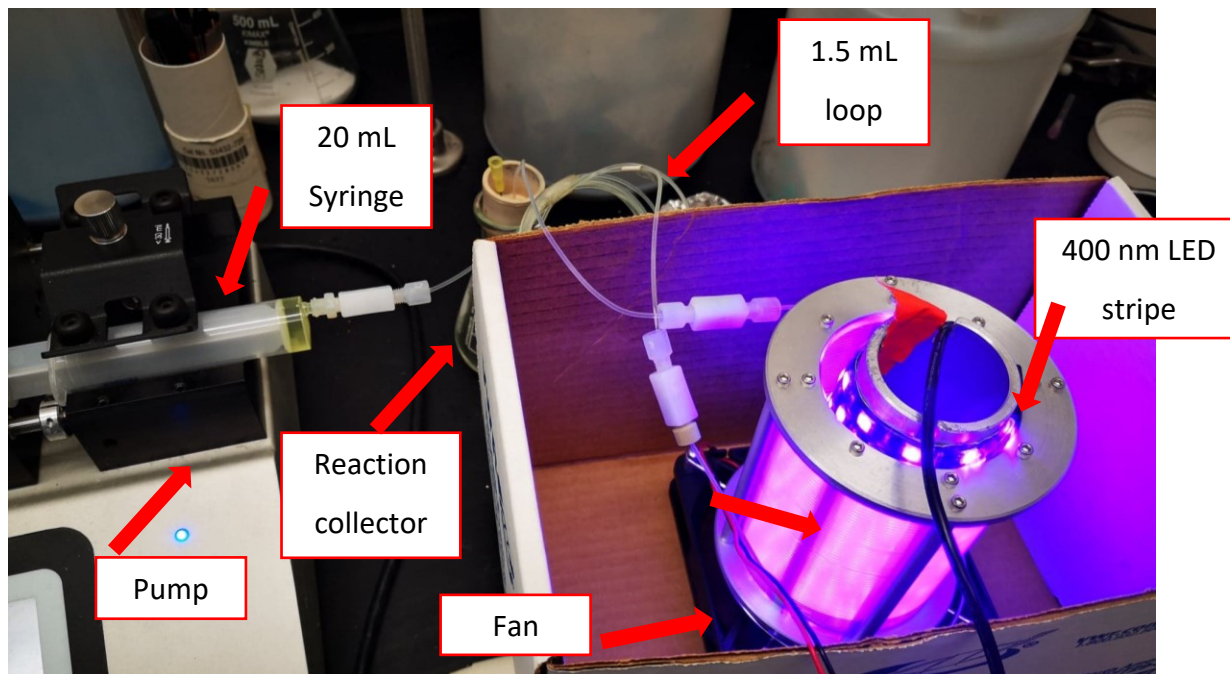
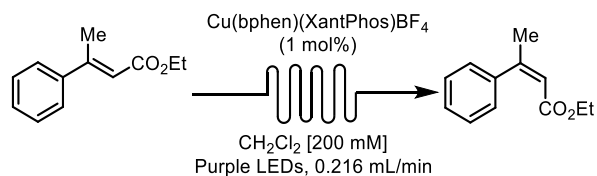


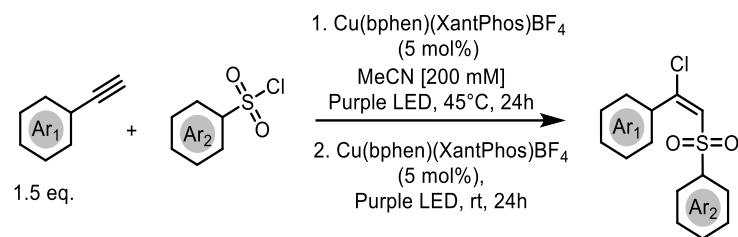
Figure A3 - 4 Continuous flow reactor set-up used for the scale-up reactions

Table A3 - 4 Percentage of isomerisation and yield of the scale-up reactions using the flow setup

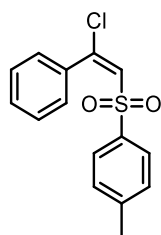


SCALE	%Z	YIELD (%)
200 MG	92	96
500 MG	91	97
1 G	91	95
5 G	92	96

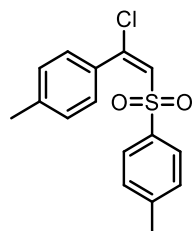
A3.8 Tandem Processes



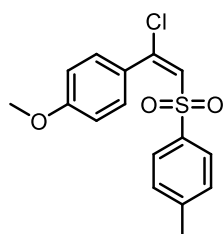
Note: As traces of HCl were deleterious to the catalyst, sulfonyl chlorides were purified by washing with 1M NaOH and extracted with Et₂O.



(E)-1-((2-Chloro-2-phenylvinyl)sulfonyl)-4-methylbenzene (26): In a 5-dram vial with a stirring bar was added tosyl chloride (38.1 mg, 0.2 mmol, 1 eq.) and [Cu(bphen)(XantPhos)]BF₄ (10.8 mg, 10 μmol, 5 mol%). MeCN (1 mL, 200mM) was added and the solution was purged with N₂ for 5 min in a sonicator bath. Phenylacetylene (32.9 μL, 0.3 mmol, 1.5 eq.) was added and the vial irradiated at 400 nm without any presence of a fan, allowing the reaction to heat up to 45°C. After 24h, another 5 mol% of [Cu(bphen)(XantPhos)]BF₄ was added under positive N₂ atmosphere and the solution was irradiated under fan cooling for 24h. The solvent was then removed in *vacuo*, and the crude passed through a plug of silica with Et₂O. ¹H NMR of the crude reaction gave the *E*:*Z* ratio (95:5 *E*:*Z*). Then, the NMR sample was recombined and a purification by flash column chromatography (1→5% AcOEt in Hexanes) afforded the pure *E* isomer as a white solid (42.8 mg, 72%). Spectral data were in accordance with previous report.³¹ **¹H NMR (400 MHz, CDCl₃):** δ 7.50 (d, *J* = 8.3 Hz, 2H), 7.47 – 7.39 (m, 1H), 7.42 – 7.31 (m, 4H), 7.20 (d, *J* = 8.0 Hz, 2H), 6.92 (s, 1H), 2.40 (s, 3H).

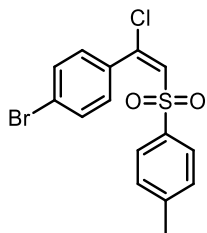


(E)-1-((2-Chloro-2-(p-tolyl)vinyl)sulfonyl)-4-methylbenzene (27): In a 5-dram vial with a stirring bar was added tosyl chloride (38.1 mg, 0.2 mmol, 1 eq.) and [Cu(bphen)(XantPhos)]BF₄ (10.8 mg, 10 μmol, 5 mol%). MeCN (1 mL, 200mM) was added and the solution was purged with N₂ for 5 min in a sonicator bath. 1-ethynyl-4-methylbenzene (38.0 μL, 0.3 mmol, 1.5 eq.) was added and the vial irradiated at 400 nm without any presence of a fan, allowing the reaction the heat up to 45°C. After 24h, another 5 mol% of [Cu(bphen)(XantPhos)]BF₄ was added under positive N₂ atmosphere and the solution was irradiated under fan cooling for 24h. The solvent was then removed in *vacuo*, and the crude passed through a plug of silica with Et₂O. ¹H NMR of the crude reaction gave the E:Z ratio (91:9 E:Z). Then, the NMR sample was recombined and a purification by flash column chromatography (1→5% AcOEt in Hexanes) afforded the pure *E* isomer as a white solid (44 mg, 71%). Spectral data were in accordance with previous report.³² **¹H NMR (500 MHz, CDCl₃):** δ 7.57 – 7.52 (m, 2H), 7.35 – 7.29 (m, 2H), 7.22 (d, *J* = 8.0 Hz, 2H), 7.17 (d, *J* = 7.9 Hz, 2H), 6.86 (s, 1H), 2.40 (s, 3H), 2.39 (s, 4H).

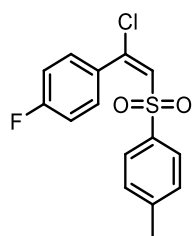


(E)-1-((2-Chloro-2-(4-methoxyphenyl)vinyl)sulfonyl)-4-methylbenzene (28): In a 5-dram vial with a stirring bar was added tosyl chloride (38.1 mg, 0.2 mmol, 1 eq.) and [Cu(bphen)(XantPhos)]BF₄ (10.8 mg, 10 μmol, 5 mol%). MeCN (1 mL, 200mM) was added and the solution was purged with N₂ for 5 min in a sonicator bath. 1-Ethynyl-4-methoxybenzene (39.6 mg, 0.3 mmol, 1.5 eq.) was added and the vial irradiated at 400 nm without any presence of a fan, allowing the reaction the heat up to 45°C. After 24h, another 5 mol% of [Cu(bphen)(XantPhos)]BF₄ was added under positive N₂ atmosphere and the solution was irradiated under fan cooling for 24h. The solvent was then removed in *vacuo*, and the crude passed through a plug of silica with Et₂O. ¹H NMR of the crude reaction gave the *E*:*Z* ratio (89:11 *E*:*Z*). Then, the NMR sample was recombined and a purification by flash column chromatography (2→5% AcOEt in Hexanes)

afforded the pure *E* isomer as a white solid (43 mg, 65%). Spectral data were in accordance with previous report³³. **¹H NMR (500 MHz, CDCl₃):** δ 7.58 – 7.53 (m, 2H), 7.45 – 7.38 (m, 2H), 7.22 (d, *J* = 8.0 Hz, 2H), 6.90 – 6.84 (m, 2H), 6.83 (s, 1H), 3.84 (s, 3H), 2.40 (s, 3H).

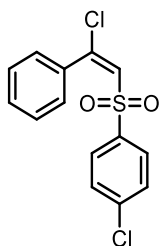


(*E*)-1-Bromo-4-(1-chloro-2-tosylvinyl)benzene (29): In a 5-dram vial with a stirring bar was added tosyl chloride (38.1 mg, 0.2 mmol, 1 eq.) and [Cu(bphen)(XantPhos)]BF₄ (10.8 mg, 10 μmol, 5 mol%). MeCN (1 mL, 200mM) was added and the solution was purged with N₂ for 5 min in a sonicator bath. 1-Bromo-4-ethynylbenzene (54.3 mg, 0.3 mmol, 1.5 eq.) was added and the vial irradiated at 400 nm without any presence of a fan, allowing the reaction the heat up to 45°C. After 24h, another 5 mol% of [Cu(bphen)(XantPhos)]BF₄ was added under positive N₂ atmosphere and the solution was irradiated under fan cooling for 24h. The solvent was then removed in *vacuo*, and the crude passed through a plug of silica with Et₂O. ¹H NMR of the crude reaction gave the *E*:*Z* ratio (93:7 *E*:*Z*). Then, the NMR sample was recombined and a purification by flash column chromatography (1→5% AcOEt in Hexanes) afforded the pure *E* isomer as a white solid (51 mg, 65%). Spectral data were in accordance with previous report.³³ **¹H NMR (500 MHz, CDCl₃):** δ 7.57 – 7.51 (m, 2H), 7.53 – 7.47 (m, 2H), 7.30 – 7.22 (m, 4H), 6.91 (s, 1H), 2.42 (s, 3H).

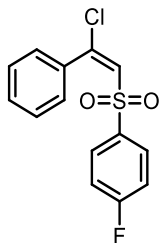


(*E*)-1-((2-Chloro-2-(4-fluorophenyl)vinyl)sulfonyl)-4-methylbenzene (30): In a 5-dram vial with a stirring bar was added tosyl chloride (38.1 mg, 0.2 mmol, 1 eq.) and [Cu(bphen)(XantPhos)]BF₄ (10.8 mg, 10 μmol, 5 mol%). MeCN (1 mL, 200mM) was added and the solution was purged with N₂ for 5 min in a sonicator bath. 1-Ethynyl-4-fluorobenzene (36.0 mg, 0.3 mmol, 1.5 eq.) was

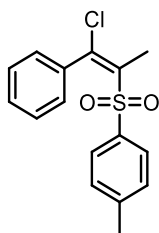
added and the vial irradiated at 400 nm without any presence of a fan, allowing the reaction the heat up to 45°C. After 24h, another 5 mol% of [Cu(bphen)(XantPhos)]BF₄ was added under positive N₂ atmosphere and the solution was irradiated under fan cooling for 24h. The solvent was then removed in *vacuo*, and the crude passed through a plug of silica with Et₂O. ¹H NMR of the crude reaction gave the *E*:*Z* ratio (94:6 *E*:*Z*). Then, the NMR sample was recombined and a purification by flash column chromatography (1→5% AcOEt in Hexanes) afforded the pure *E* isomer as a white solid (47 mg, 74%). Spectral data were in accordance with previous report³². **¹H NMR (500 MHz, CDCl₃):** δ 7.56 – 7.51 (m, 2H), 7.45 – 7.38 (m, 2H), 7.24 (d, *J* = 8.0 Hz, 2H), 7.09 – 7.01 (m, 2H), 6.91 (s, 1H), 2.41 (s, 3H).



(*E*)-1-Chloro-4-((2-chloro-2-phenylvinyl)sulfonyl)benzene (31): In a 5-dram vial with a stirring bar was added 4-chlorobenzenesulfonyl chloride (42.2 mg, 0.2 mmol, 1 eq.) and [Cu(bphen)(XantPhos)]BF₄ (10.8 mg, 10 μmol, 5 mol%). MeCN (1 mL, 200mM) was added and the solution was purged with N₂ for 5 min in a sonicator bath. Ethynylbenzene (32.9 μL, 0.3 mmol, 1.5 eq.) was added and the vial irradiated at 400 nm without any presence of a fan, allowing the reaction the heat up to 45°C. After 24h, another 5 mol% of [Cu(bphen)(XantPhos)]BF₄ was added under positive N₂ atmosphere and the solution was irradiated under fan cooling for 24h. The solvent was then removed in *vacuo*, and the crude passed through a plug of silica with Et₂O. ¹H NMR of the crude reaction gave the *E*:*Z* ratio (93:7 *E*:*Z*). Then, the NMR sample was recombined and a purification by flash column chromatography (1→5% AcOEt in Hexanes) afforded the pure *E* isomer as a white solid (46 mg, 71%). Spectral data were in accordance with previous report.³² **¹H NMR (500 MHz, CDCl₃):** δ 7.54 – 7.48 (m, 2H), 7.51 – 7.41 (m, 1H), 7.35 (dd, *J* = 5.9, 2.9 Hz, 6H), 6.94 (s, 1H).



(E)-1-((2-Chloro-2-phenylvinyl)sulfonyl)-4-fluorobenzene (32): In a 5-dram vial with a stirring bar was added 4-fluorobenzenesulfonyl chloride (38.9 mg, 0.2 mmol, 1 eq.) and [Cu(bphen)(XantPhos)]BF₄ (10.8 mg, 10 μmol, 5 mol%). MeCN (1 mL, 200mM) was added and the solution was purged with N₂ for 5 min in a sonicator bath. Ethynylbenzene (32.9 μL, 0.3 mmol, 1.5 eq.) was added and the vial irradiated at 400 nm without any presence of a fan, allowing the reaction the heat up to 45°C. After 24h, another 5 mol% of [Cu(bphen)(XantPhos)]BF₄ was added under positive N₂ atmosphere and the solution was irradiated under fan cooling for 24h. The solvent was then removed in *vacuo*, and the crude passed through a plug of silica with Et₂O. ¹H NMR of the crude reaction gave the *E*:*Z* ratio (94:6 *E*:*Z*). Then, the NMR sample was recombined and a purification by flash column chromatography (1→5% AcOEt in Hexanes) afforded the pure *E* isomer as a white solid (50 mg, 81%). Spectral data were in accordance with previous report.³⁴ **¹H NMR (500 MHz, CDCl₃):** δ 7.63 – 7.55 (m, 2H), 7.47 – 7.41 (m, 1H), 7.35 (d, *J* = 4.4 Hz, 4H), 7.09 – 7.01 (m, 2H), 6.95 (s, 1H).



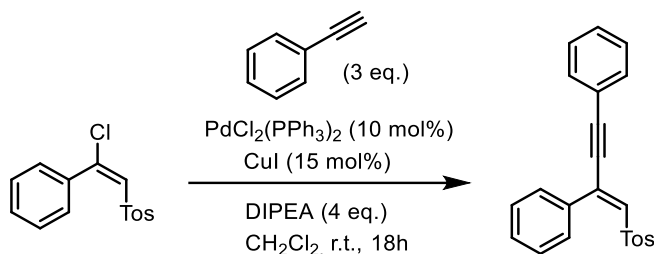
(E)-1-((1-Chloro-1-phenylprop-1-en-2-yl)sulfonyl)-4-methylbenzene (33): In a 5-dram vial with a stirring bar was added tosyl chloride (38.1 mg, 0.2 mmol, 1 eq.) and [Cu(bphen)(XantPhos)]BF₄ (10.8 mg, 10 μmol, 5 mol%). MeCN (1 mL, 200mM) was added and the solution was purged with N₂ for 5 min in a sonicator bath. Prop-1-yn-1-ylbenzene (37.6 μL, 0.3 mmol, 1.5 eq.) was added and the vial irradiated at 400 nm without any presence of a fan, allowing the reaction the heat up to 45°C. After 24h, another 5 mol% of [Cu(bphen)(XantPhos)]BF₄ was added under positive N₂

atmosphere and the solution was irradiated under fan cooling for 24h. The solvent was then removed in *vacuo*, and the crude passed through a plug of silica with Et₂O. ¹H NMR of the crude reaction gave the *E*:*Z* ratio (89:11 *E*:*Z*). Then, the NMR sample was recombined and a purification by flash column chromatography (1→5% AcOEt in Hexanes) afforded the pure *E* isomer as a white solid (20 mg, 34%). Spectral data were in accordance with previous report.³¹ **¹H NMR (500 MHz, CDCl₃):** δ 7.41 (d, *J* = 8.0 Hz, 2H), 7.39 – 7.33 (m, 1H), 7.32 – 7.27 (m, 2H), 7.24 – 7.19 (m, 2H), 7.17 (d, *J* = 8.0 Hz, 2H), 2.39 (s, 3H), 2.34 (s, 3H).



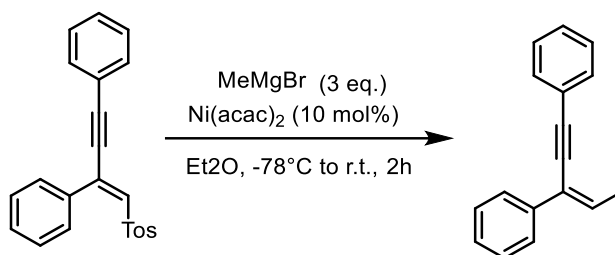
Figure A3 - 5 Experimental set-up for the ATRA reactions.

A3.9 Post-Functionalization Reactions



(E)-(4-Tosylbut-3-en-1-yne-1,3-diyl)dibenzene (S-2): A flame-dried round bottom flask under nitrogen was charged with Pd(PPh₃)₂Cl₂ (13 mg, 0.018 mmol, 10 mol%) and CuI (5 mg, 0.027 mmol, 0.15 eq.). Dry CH₂Cl₂ (3 mL, [60 mM]), DIPEA (0.126 mL, 0.725 mmol, 4 eq.), and (E)-1-((2-chloro-2-phenylvinyl)sulfonyl)-4-methylbenzene (53 mg, 0.181 mmol, 1 eq.) were then introduced sequentially. The solution was sparged for 5 minutes with N₂ before the addition of phenylacetylene (0.060 mL, 0.544 mmol, 3 eq.). The reaction was stirred for 18 h. The crude was

purified by flash column chromatography (1→5% AcOEt in Hexanes) affording the pure product as a yellow oil (56 mg, 86%). Spectral data were in accordance with previous report.³⁵ **¹H NMR (500 MHz, CDCl₃):** δ 7.57 – 7.50 (m, 2H), 7.50 – 7.44 (m, 2H), 7.44 – 7.28 (m, 9H), 7.23 – 7.17 (m, 2H), 6.94 (s, 1H), 2.39 (s, 3H).



(Z)-Pent-3-en-1-yne-1,3-diyl dibenzene (34) : A flame-dried round bottom flask under nitrogen was charged with (E)-(4-tosylbut-3-en-1-yne-1,3-diyl)dibenzene (71.1 mg, 0.198 mmol, 1 eq.) and Ni(acac)₂ (5 mg, 0.02 mmol, 10 mol%). Dry Et₂O (6 mL, [33 mM]) was added and the mixture was cooled down to -78°C. The mixture was sparged with N₂ for 5 minutes, and methylmagnesium bromide (0.2 mL, [3M] in Et₂O, 3 eq.) was added slowly, and the reaction was stirred at room temperature for 2 h. The crude was purified by flash column chromatography (0→2% AcOEt in Hexanes) affording the pure product as a transparent oil (31 mg, 71 %). Spectral data were in accordance with previous report.³⁶ **¹H NMR (500 MHz, CDCl₃):** δ 7.69 – 7.63 (m, 2H), 7.57 – 7.52 (m, 2H), 7.39 – 7.31 (m, 5H), 7.31 – 7.27 (m, 1H), 6.54 (q, *J* = 7.0 Hz, 1H), 2.16 (d, *J* = 7.1 Hz, 3H). **Note:** The geometry of the alkene was confirmed by a NOESY experiment.

A3.10 Photophysical data

Absorbance/Emission data

Absorbance UV-Vis spectra were recorded with Varian Cary 5000 UV-Vis-NIR spectrophotometer in a quartz cuvette.

Table A3 - 5 Tabular data for the maximum of absorbance of copper complexes

dmp/PP	λ_{max} (nm)	NN/ XantPhos	λ_{max} (nm)	NN/ XantPhos	λ_{max} (nm)
NXantPhos	387	phen	385	quintri	390
PhanePhos	381	dmp	380	iquintri	383
XantPhos	380	tmp	369	dpq	386
DPEPhos	380	bphen	385	dppz	380
dppf	379	dmbp	378	bdppz	408
dppn	381	dtbbp	366	dpa	<330
BINAP	387	batho	427	dmop	398
SEGPhos	401	bathocup	397		
None	460	dq	445		
		pytri	376		

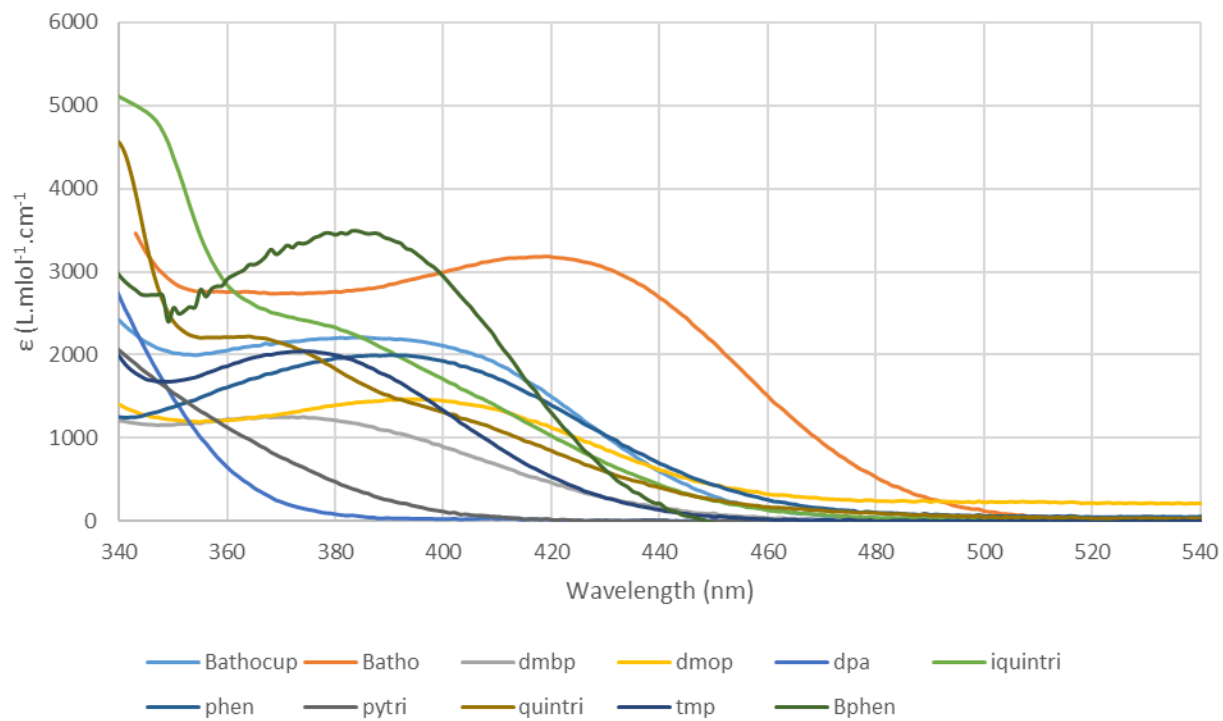


Figure A3 - 6 UV-visible absorption spectrum of new Cu(NN)(XantPhos) BF₄ complexes recorded at ambient temperature in CH₂Cl₂ (5.0·10⁻⁴M).

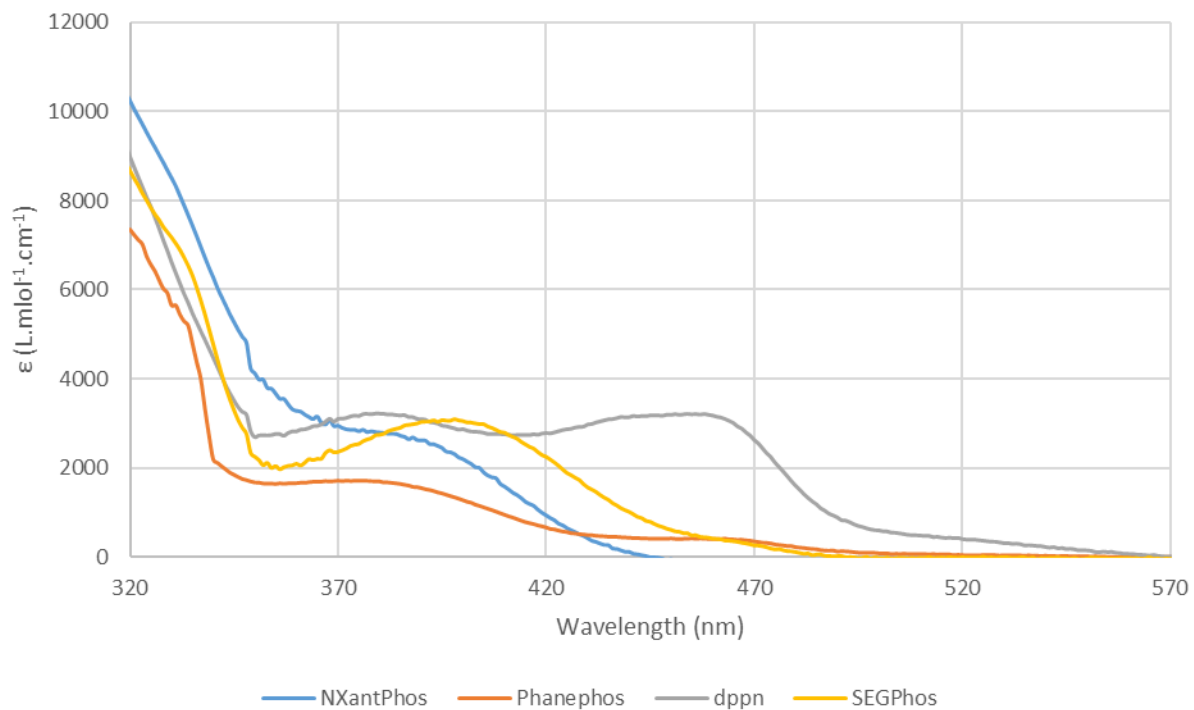


Figure A3 - 7 UV-visible absorption spectrum of new Cu(dmp)(PP)BF₄ complexes recorded at ambient temperature in CH₂Cl₂ (5.0·10⁻⁴M).

Emission spectra were recorded with the Varian Cary Eclipse Fluorescence Spectrophotometer/Fluorometer in a quartz cuvette.

Table A3 - 6 Tabular data for the maximum of emission of copper complexes

dmp/PP	λ_{max} (nm)	NN/ XantPhos	λ_{max} (nm)	NN/ XantPhos	λ_{max} (nm)
NXantPhos	493	phen	538	quintri	455
PhanePhos	546	tmp	596	iquintri	456
XantPhos	558	bphen	463	ddpq	560
dppf	572	dmbp	627	ddppz	634
dppn	569	dtbbp	616	dbdppz	565
BINAP	638	batho	491	dpa	428
SEGPhos	636	bathocup	441	dmop	482
None	750	dq	653		
		pytri	544		

For complexes of the type Cu(dmp)(PP)BF₄:

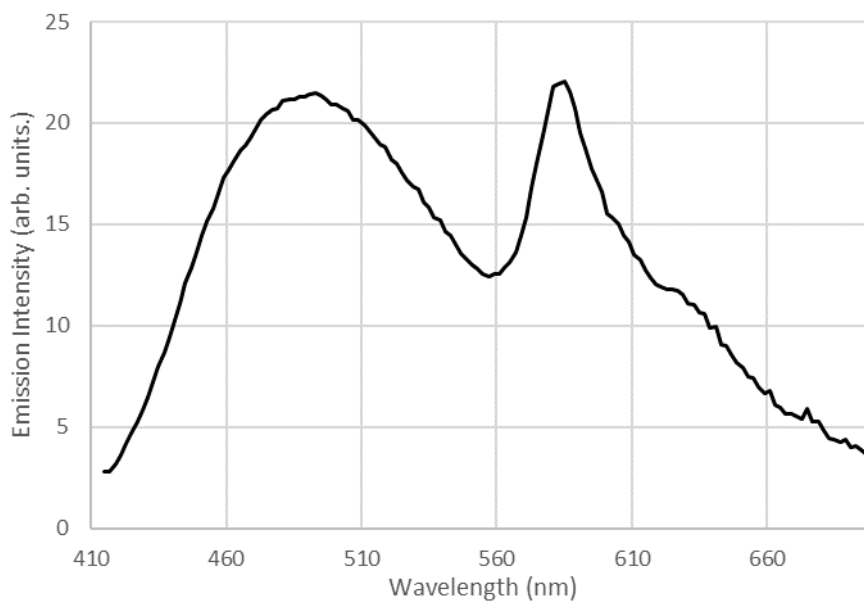


Figure A3 - 8 Emission spectrum of Cu(dmp)(XantPhos) BF₄ excited at 395 nm, recorded at ambient temperature in CH₂Cl₂ (5·10⁻⁴ M).

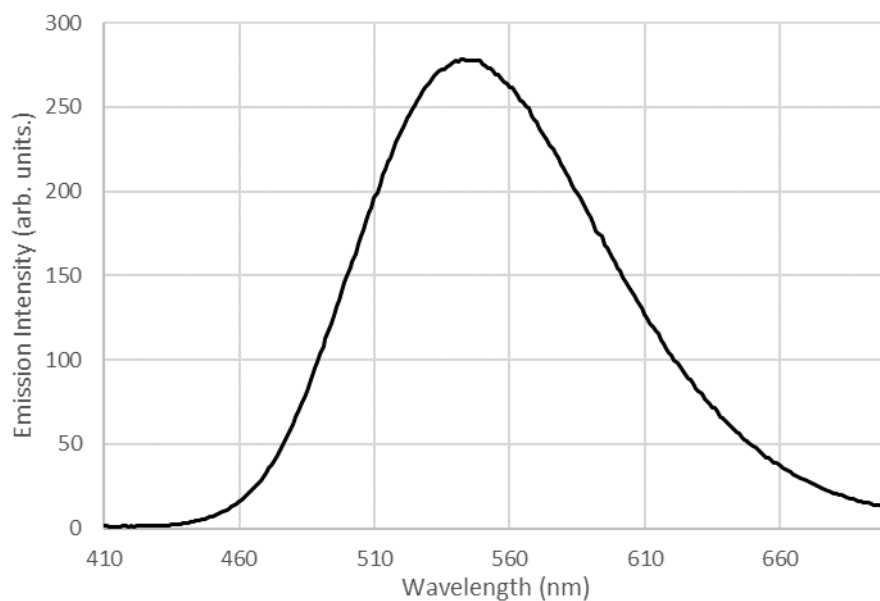


Figure A3 - 9 Emission spectrum of Cu(dmp)(Phanephos) BF₄ excited at 395 nm, recorded at ambient temperature in CH₂Cl₂ ($5 \cdot 10^{-4}$ M).

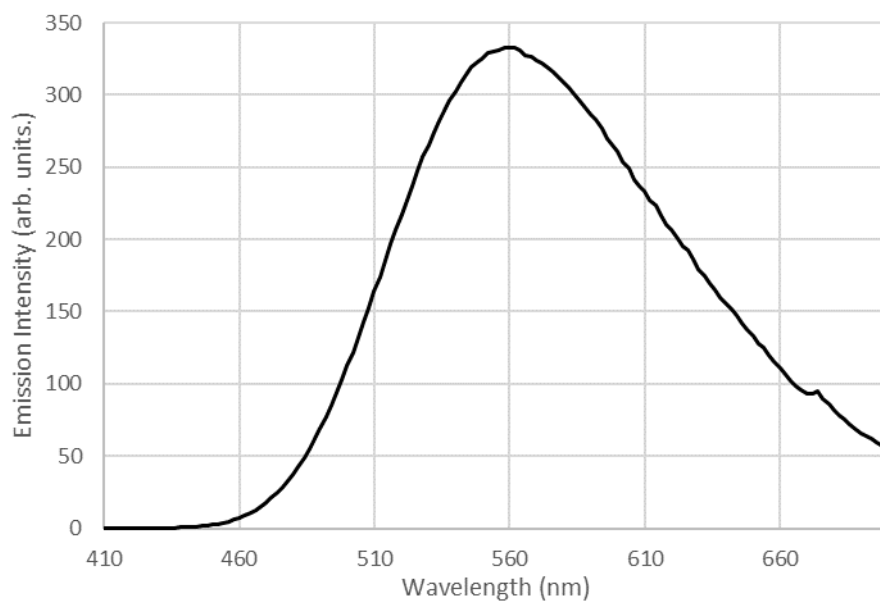


Figure A3 - 10 Emission spectrum of Cu(dmp)(Xantphos) BF₄ excited at 395 nm, recorded at ambient temperature in CH₂Cl₂ ($5 \cdot 10^{-4}$ M).

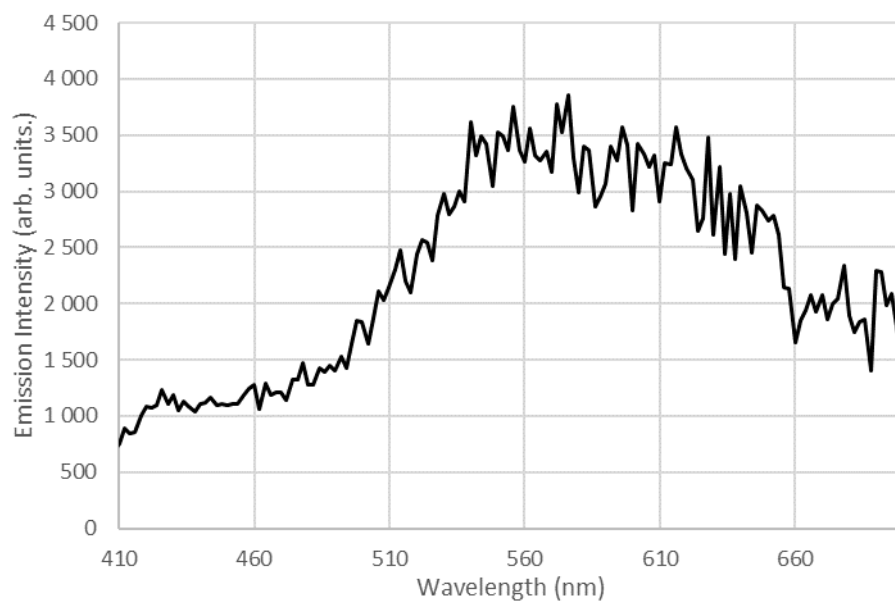


Figure A3 - 11 Emission spectrum of Cu(dmp)(dppf)BF₄ excited at 395 nm, recorded at ambient temperature in CH₂Cl₂ (5·10⁻⁴ M).

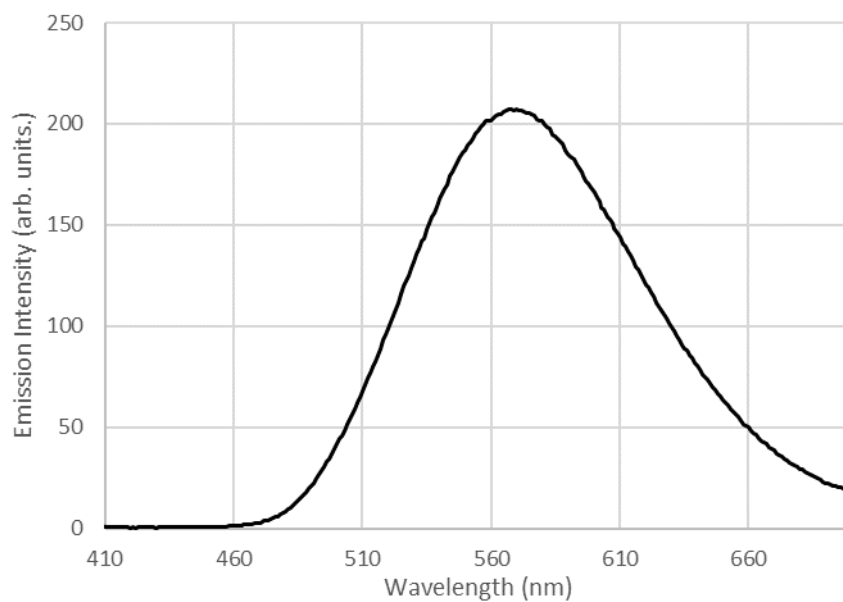


Figure A3 - 12 Emission spectrum of Cu(dmp)(dppn)BF₄ excited at 395 nm, recorded at ambient temperature in CH₂Cl₂ (5·10⁻⁴ M).

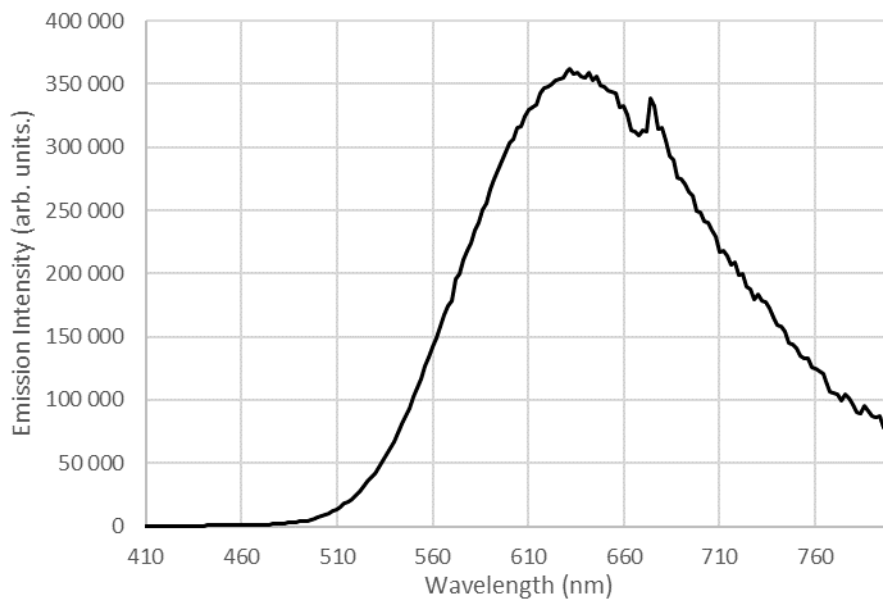


Figure A3 - 13 Emission spectrum of Cu(dmp)(BINAP)BF₄ excited at 395 nm, recorded at ambient temperature in CH₂Cl₂ (5·10⁻⁴ M).

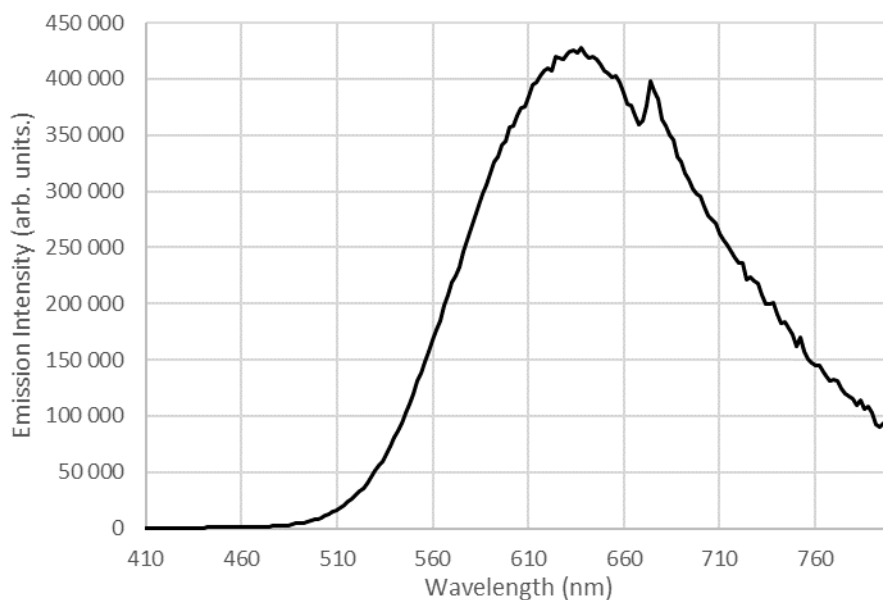


Figure A3 - 14 Emission spectrum of Cu(dmp)(SEGPPOS) BF₄ excited at 395 nm, recorded at ambient temperature in CH₂Cl₂ (5·10⁻⁴ M).

[Cu(NN)(Xantphos)]BF₄:

Emission datas for Cu(dq)(Xantphos)BF₄, Cu(ddpq)(Xantphos)BF₄, Cu(ddppz)(Xantphos)BF₄ and Cu(dbdppz)(Xantphos)BF₄ were previously reported¹⁻²

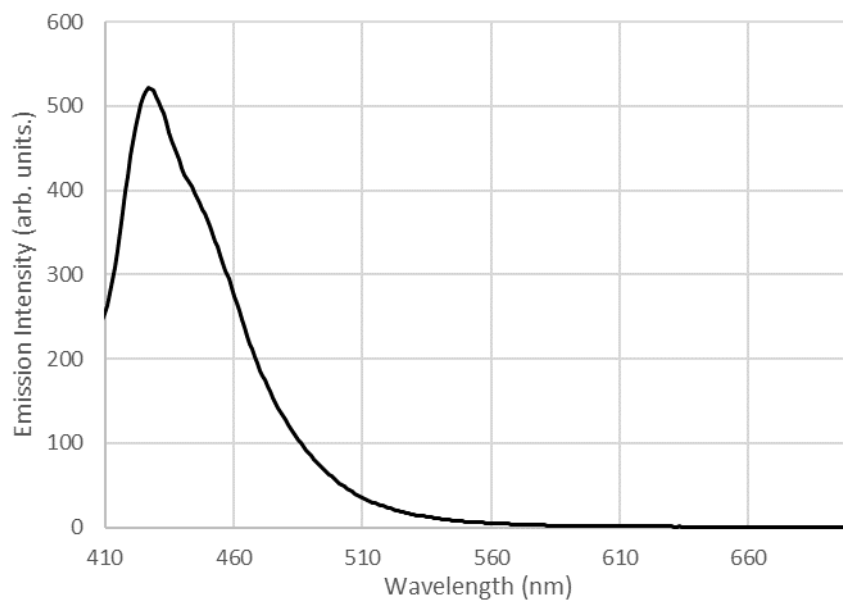


Figure A3 - 15 Emission spectrum of Cu(dpa)(Xantphos)BF₄ excited at 395 nm, recorded at ambient temperature in CH₂Cl₂ (5·10⁻⁴ M).

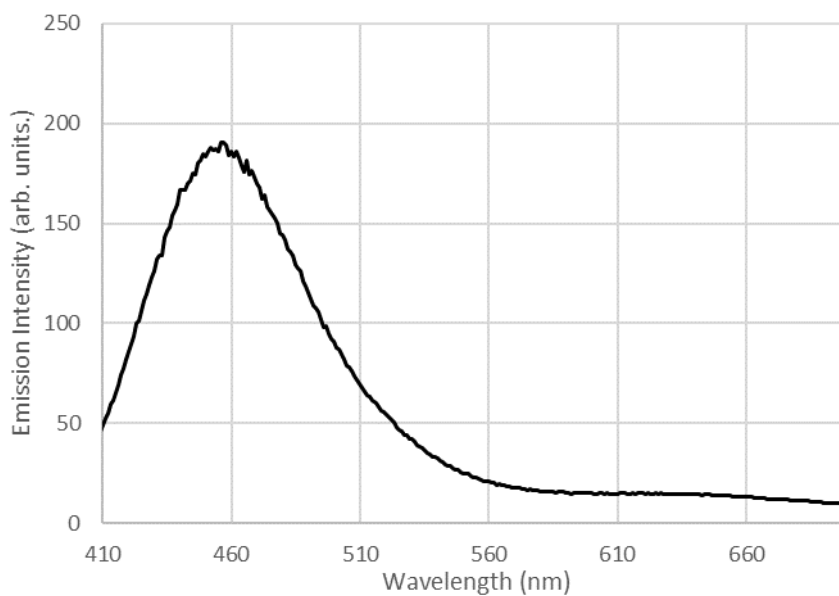


Figure A3 - 16 Emission spectrum of Cu(quintri)(Xantphos)BF₄ excited at 395 nm, recorded at ambient temperature in CH₂Cl₂ (5·10⁻⁴ M).

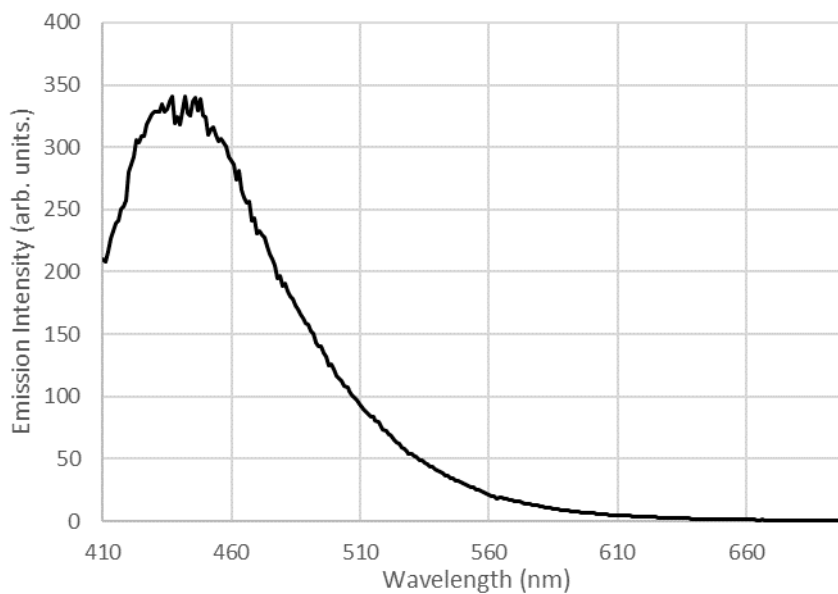


Figure A3 - 17 Emission spectrum of Cu(bathocup)(Xantphos) BF₄ excited at 395 nm, recorded at ambient temperature in CH₂Cl₂ (5·10⁻⁴ M).

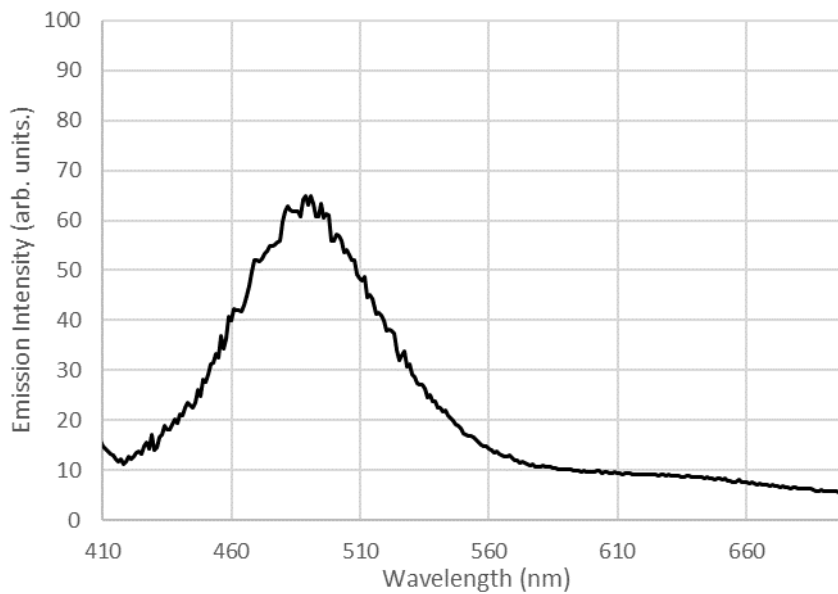


Figure A3 - 18 Emission spectrum of Cu(batho)(Xantphos) BF₄ excited at 395 nm, recorded at ambient temperature in CH₂Cl₂ (5·10⁻⁴ M).

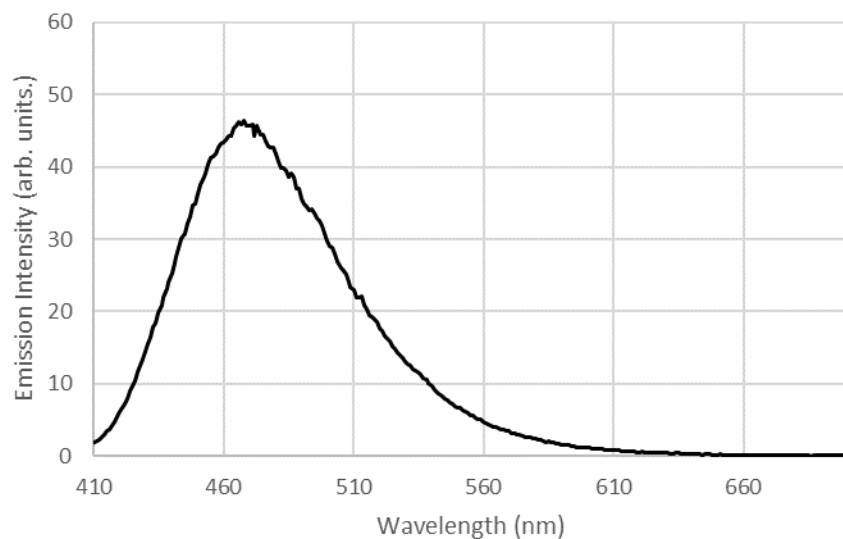


Figure A3 - 19 Emission spectrum of Cu(BPhen)(Xantphos) BF₄ excited at 395 nm, recorded at ambient temperature in CH₂Cl₂ (5·10⁻⁴ M).

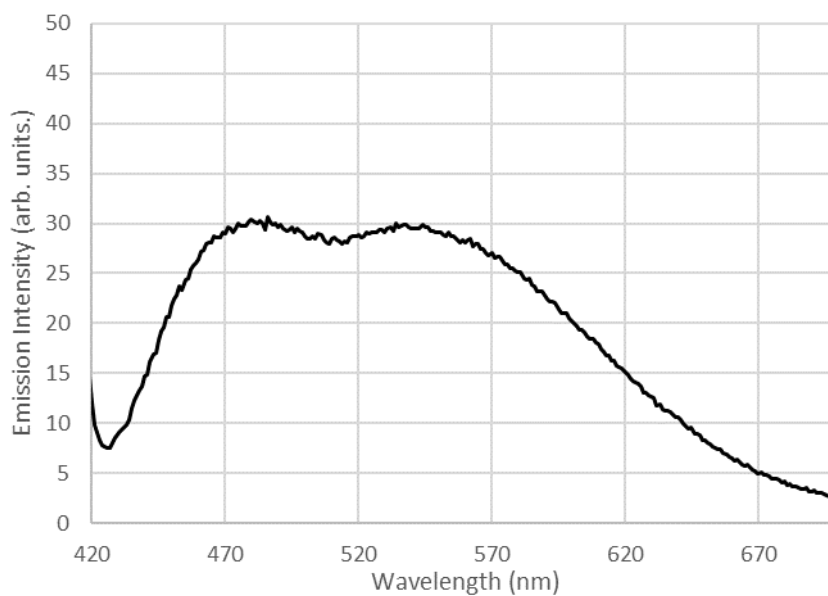


Figure A3 - 20 Emission spectrum of Cu(dmop)(Xantphos) BF₄ excited at 395 nm, recorded at ambient temperature in CH₂Cl₂ (5·10⁻⁴ M).

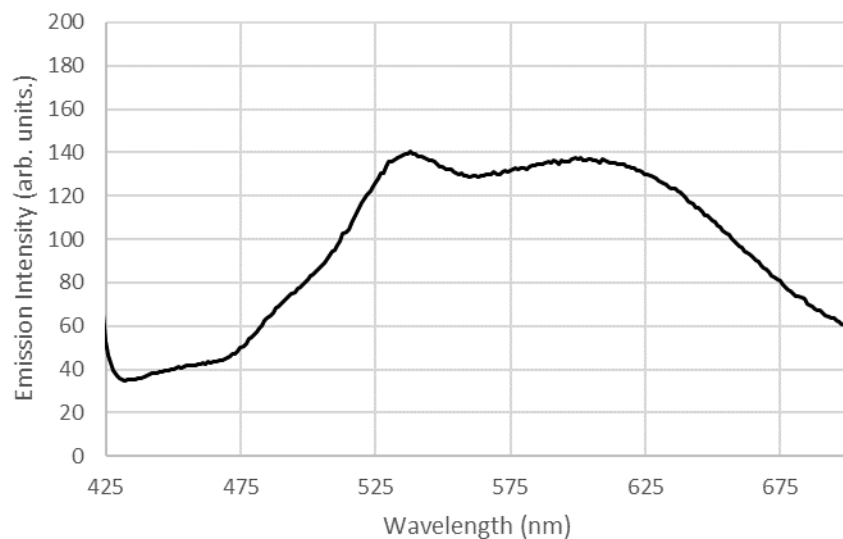


Figure A3 - 21 Emission spectrum of Cu(phen)(Xantphos) BF₄ excited at 395 nm, recorded at ambient temperature in CH₂Cl₂ (5·10⁻⁴ M).

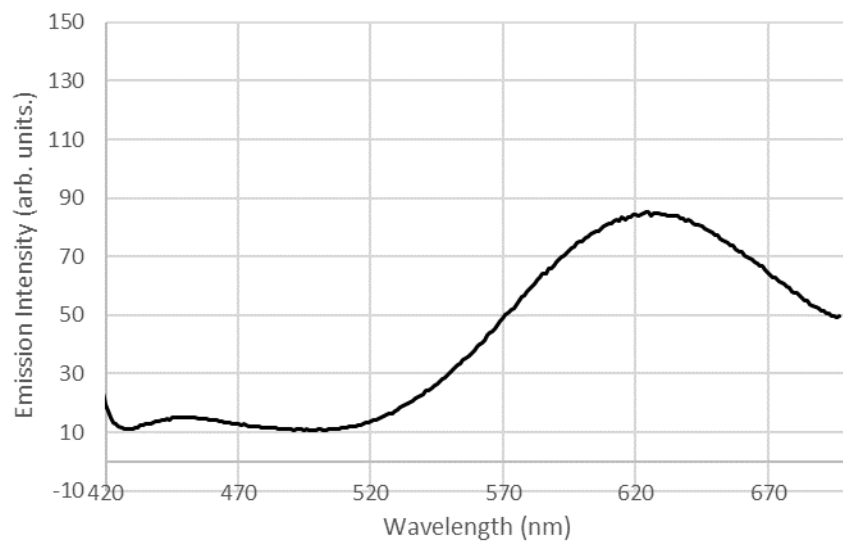


Figure A3 - 22 Emission spectrum of Cu(dmbp)(Xantphos)BF₄ excited at 395 nm, recorded at ambient temperature in CH₂Cl₂ (5·10⁻⁴ M).

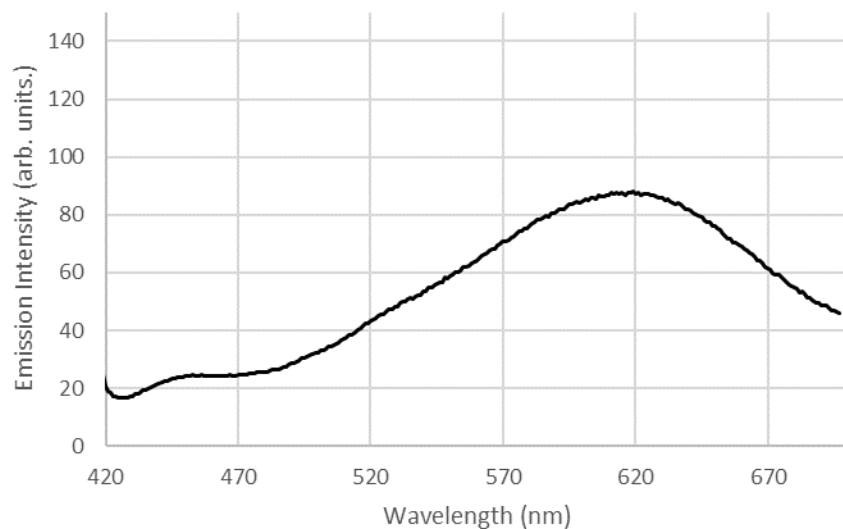


Figure A3 - 23 Emission spectrum of Cu(dtbbp)(Xantphos)BF₄ excited at 395 nm, recorded at ambient temperature in CH₂Cl₂ (5·10⁻⁴ M).

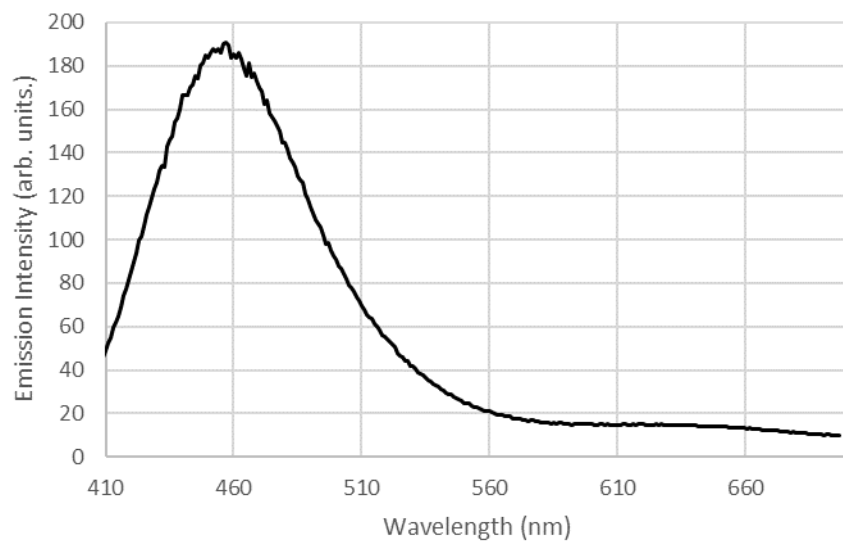


Figure A3 - 24 Emission spectrum of Cu(iquintri)(Xantphos)BF₄ excited at 395 nm, recorded at ambient temperature in CH₂Cl₂ (5·10⁻⁴ M).

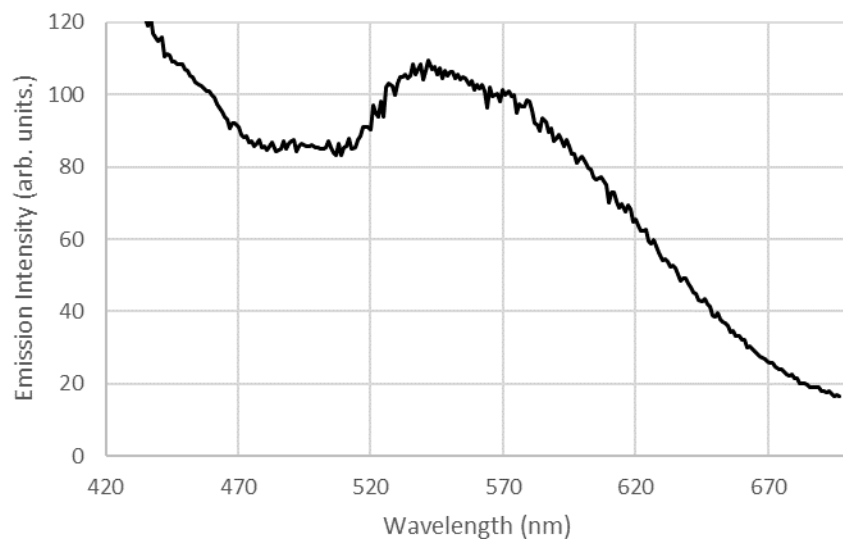


Figure A3 - 25 Emission spectrum of Cu(pytri)(Xantphos)BF₄ excited at 395 nm, recorded at ambient temperature in CH₂Cl₂ (5·10⁻⁴ M).

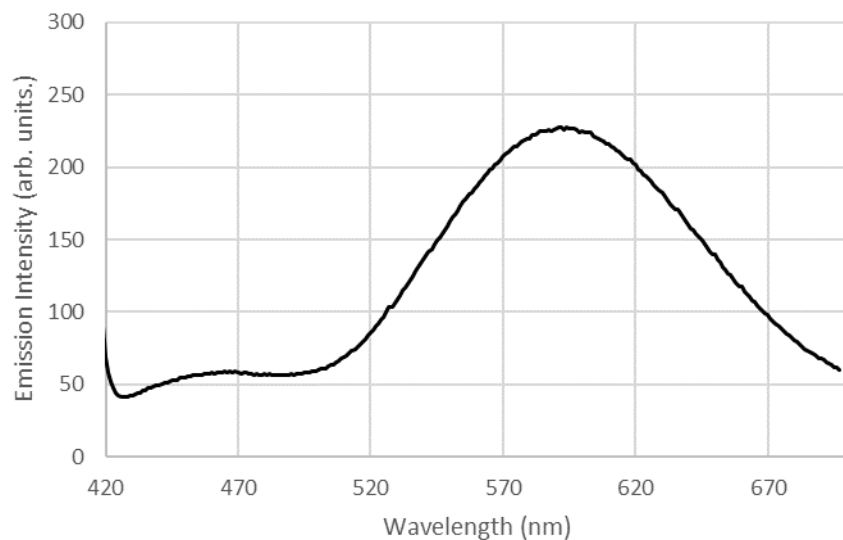


Figure A3 - 26 Emission spectrum of Cu(tmp)(Xantphos)BF₄ excited at 395 nm, recorded at ambient temperature in CH₂Cl₂ (5·10⁻⁴ M).

Excited state lifetime data

Lifetime data for Cu(dmp)(DPEPhos)BF₄, Cu(dmp)(BINAP)BF₄, Cu(dq)(Xantphos)BF₄, Cu(dpq)(Xantphos)BF₄, Cu(ddppz)(Xantphos)BF₄ and Cu(bdppz)(Xantphos)BF₄ were previously reported.^{2, 37} Lifetime measurements of new complexes were done with an Edinburgh

Instruments Mini Tau Lifetime Fluorimeter with an EPL 405 laser (exciting at 405 nm) with a standard deviation of 1-2%.

Table A3 - 7 Tabular data for the excited state life time of copper complexes

dmp/PP	τ (ns)	NN/ XantPhos	τ (ns)	NN/ XantPhos	τ (ns)
NXantPhos	19	phen	391	pytri	752
PhanePhos	1948	dmp	1133	quintri	3.6
XantPhos	1133	tmp	1119	iquintri	3.8
DPEPhos	14300	bphen	1798	dpq	3
dppf	1.5	dmbp	72	dppz	71
dppn	1.43	dtbbp	143	bdppz	75
BINAP	2188	batho	3.2	dpa	3
SEGPhos	340	bathocup	4		
none	90	dq	393		

Cu(dmp)(PP)BF₄:

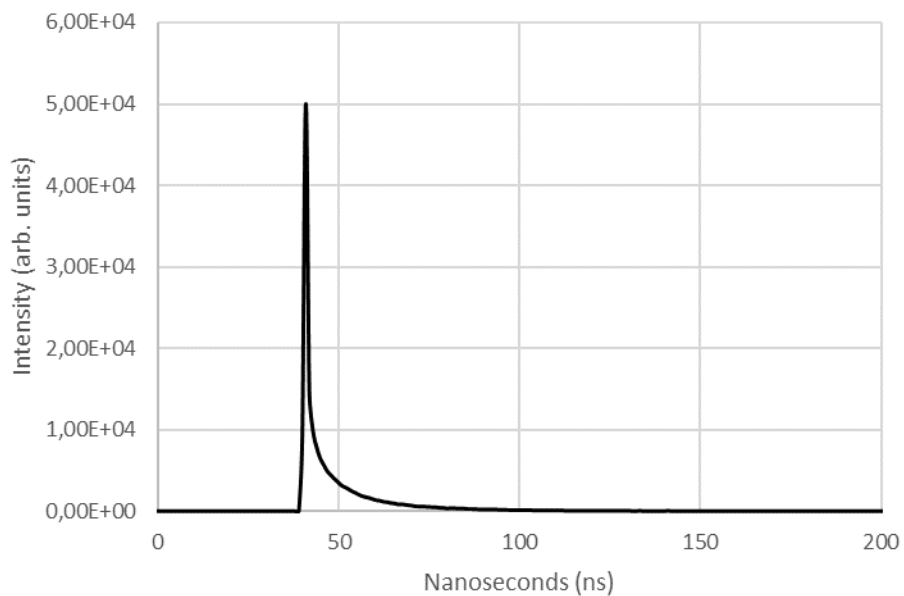


Figure A3 - 27 Lifetime spectrum of Cu(dmp)(NXantphos)BF₄ excited at 405 nm, recorded at ambient temperature in degassed CH₂Cl₂ (1.25 · 10⁻⁴ M).

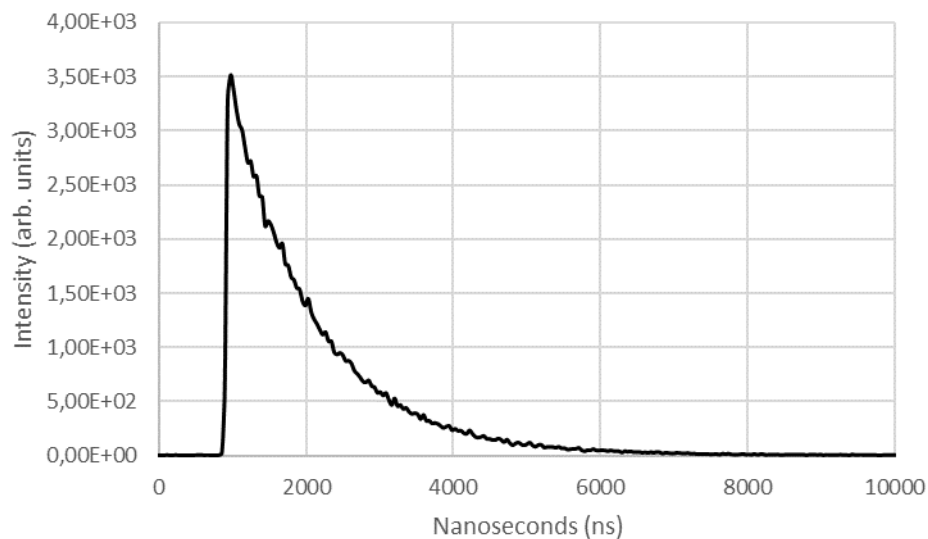


Figure A3 - 28 Lifetime spectrum of Cu(dmp)(Xantphos)BF₄ excited at 405 nm, recorded at ambient temperature in degassed CH₂Cl₂ (1.25 · 10⁻⁴ M).

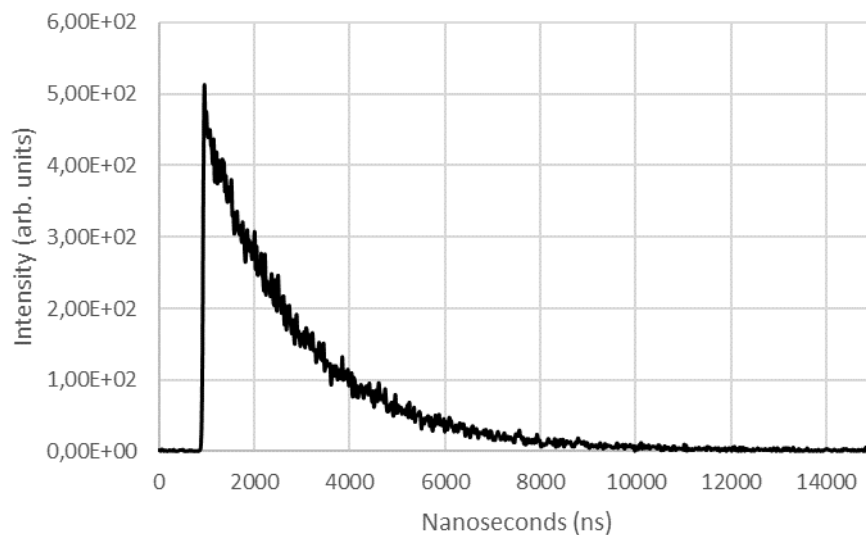


Figure A3 - 29 Lifetime spectrum of Cu(dmp)(Phanephos)BF₄ excited at 405 nm, recorded at ambient temperature in degassed CH₂Cl₂ (1.25 · 10⁻⁴ M).

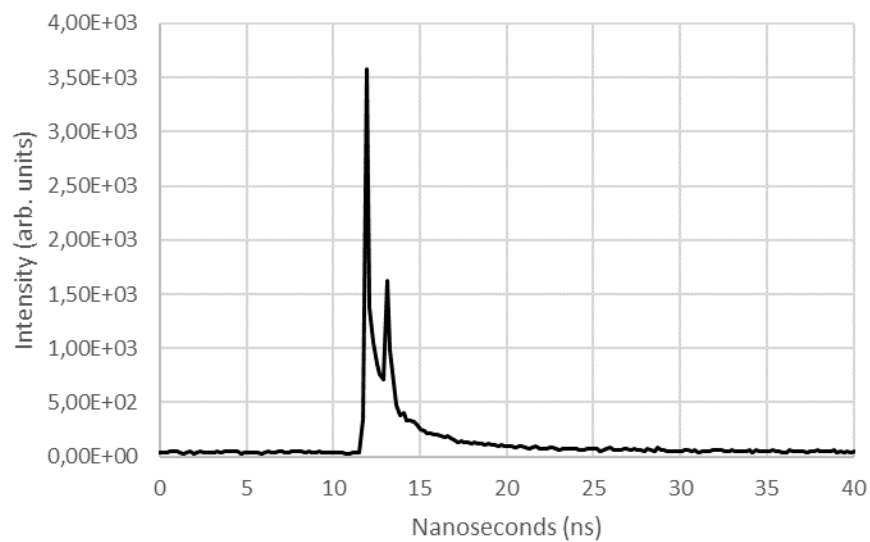


Figure A3 - 30 Lifetime spectrum of Cu(dmp)(dppf)BF₄ excited at 405 nm, recorded at ambient temperature in degassed CH₂Cl₂ (1.25 · 10⁻⁴ M).

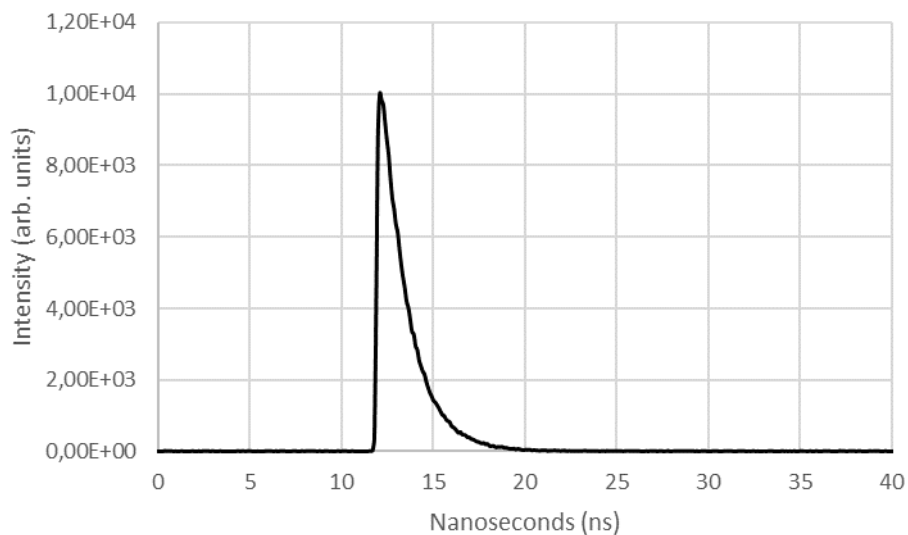


Figure A3 - 31 Lifetime spectrum of Cu(dmp)(dppn)BF₄ excited at 405 nm, recorded at ambient temperature in degassed CH₂Cl₂ (1.25 · 10⁻⁴ M).

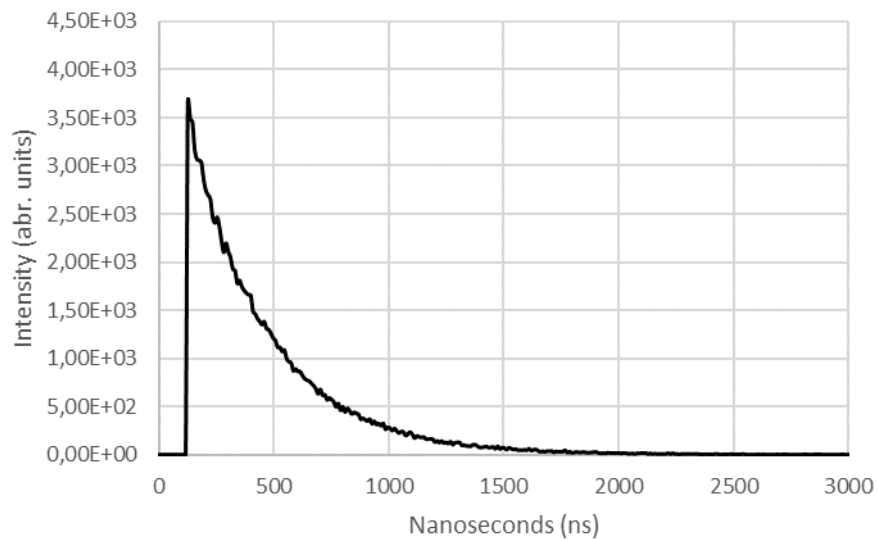


Figure A3 - 32 Lifetime spectrum of Cu(dmp)(SEGphos)BF₄ excited at 405 nm, recorded at ambient temperature in degassed CH₂Cl₂ (1.25 · 10⁻⁴ M).

Cu(NN)(Xantphos)BF₄:

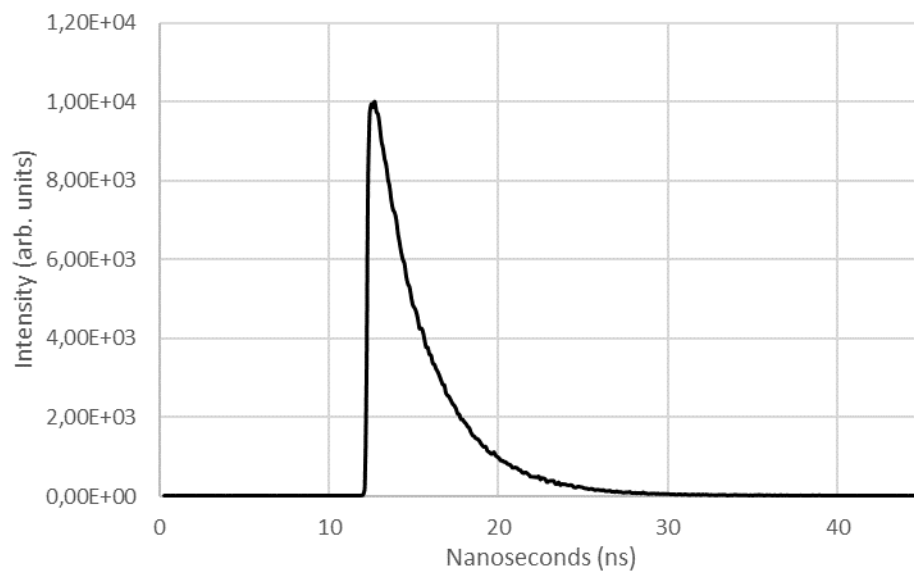


Figure A3 - 33 Lifetime spectrum of Cu(dpa)(Xantphos)BF₄ excited at 405 nm, recorded at ambient temperature in degassed CH₂Cl₂ (1.25 · 10⁻⁴ M).

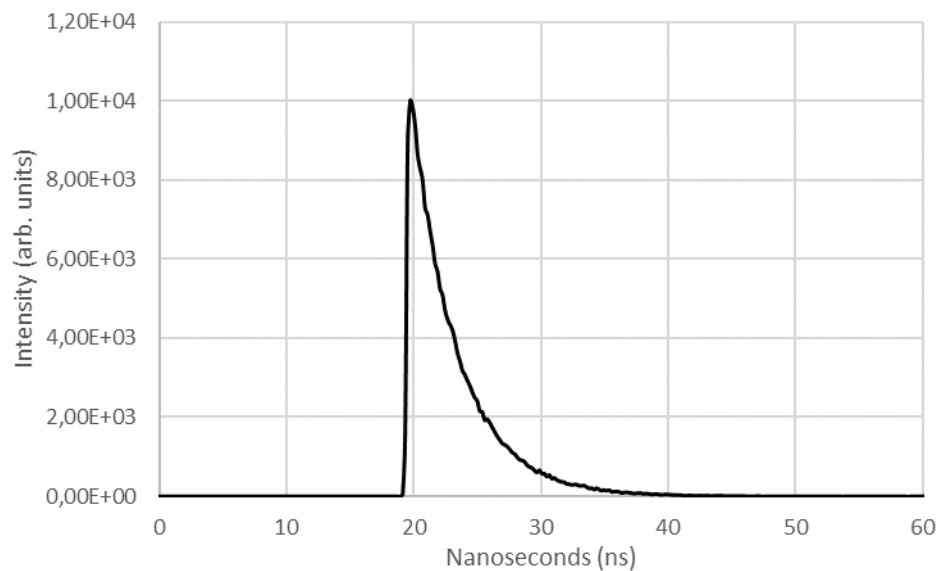


Figure A3 - 34 Lifetime spectrum of Cu(quintri)(Xantphos)BF₄ excited at 405 nm, recorded at ambient temperature in degassed CH₂Cl₂ (1.25 · 10⁻⁴ M).

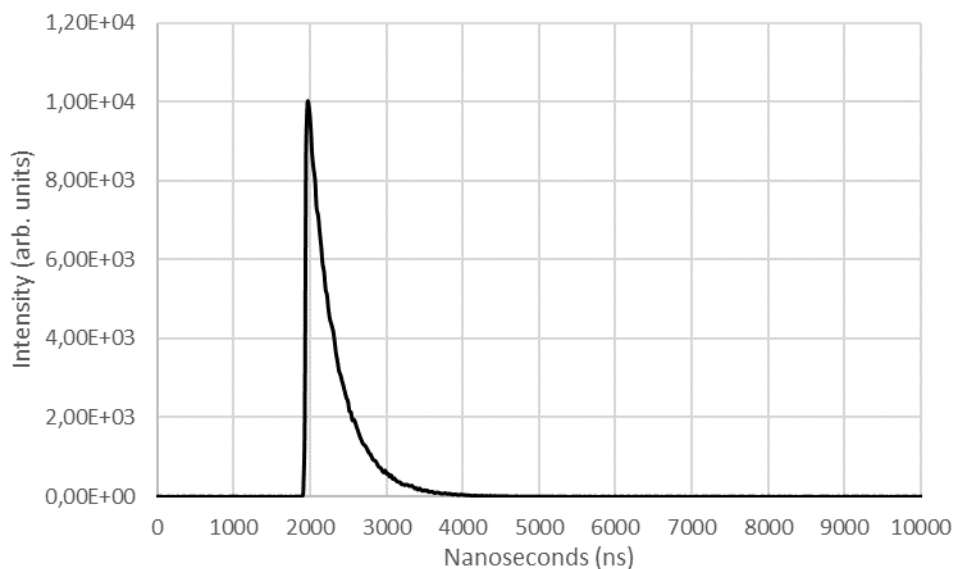


Figure A3 - 35 Lifetime spectrum of Cu(bphen)(Xantphos)BF₄ excited at 405 nm, recorded at ambient temperature in degassed CH₂Cl₂ (1.25 · 10⁻⁴ M).

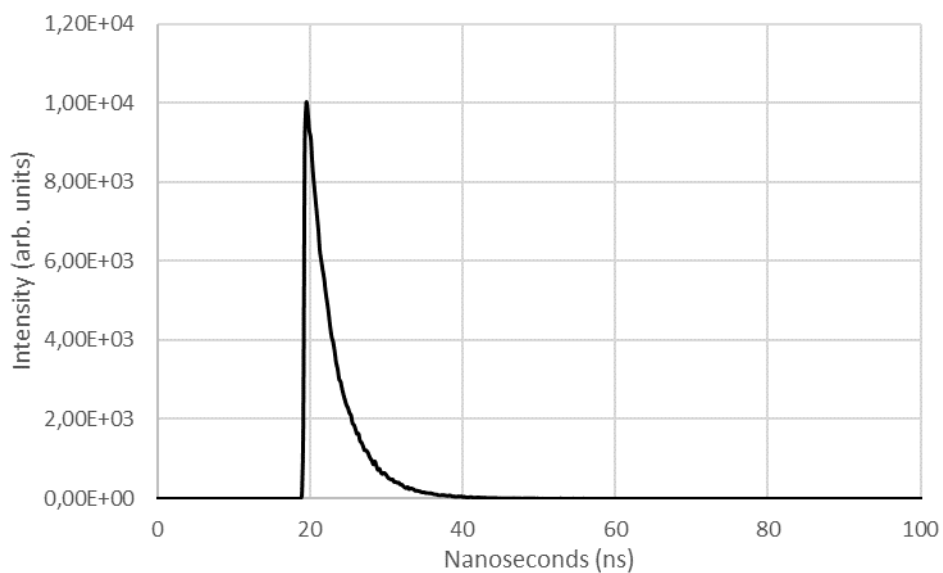


Figure A3 - 36 Lifetime spectrum of Cu(iquintri)(Xantphos)BF₄ excited at 405 nm, recorded at ambient temperature in degassed CH₂Cl₂ (1.25 · 10⁻⁴ M).

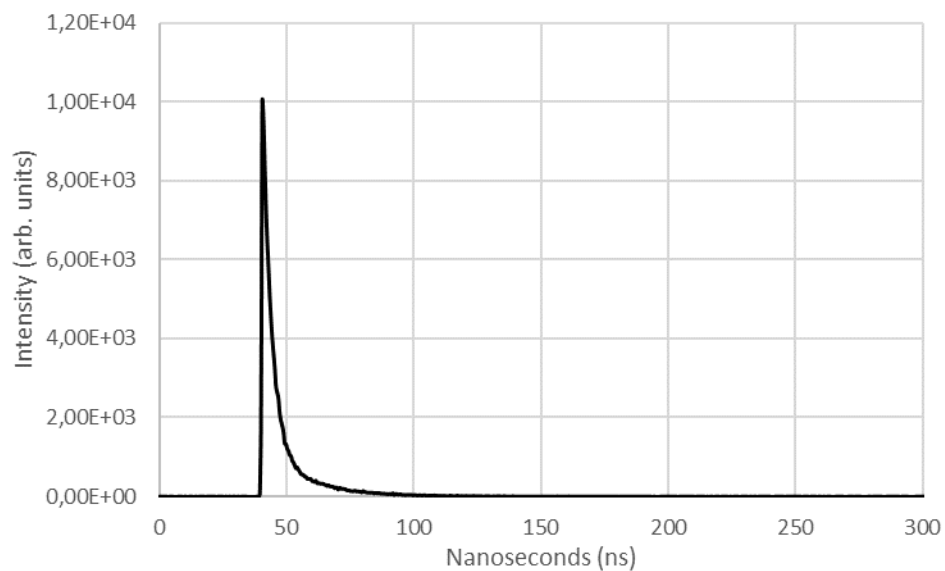


Figure A3 - 37 Lifetime spectrum of Cu(dmop)(Xantphos)BF₄ excited at 405 nm, recorded at ambient temperature in degassed CH₂Cl₂ (1.25 · 10⁻⁴ M).

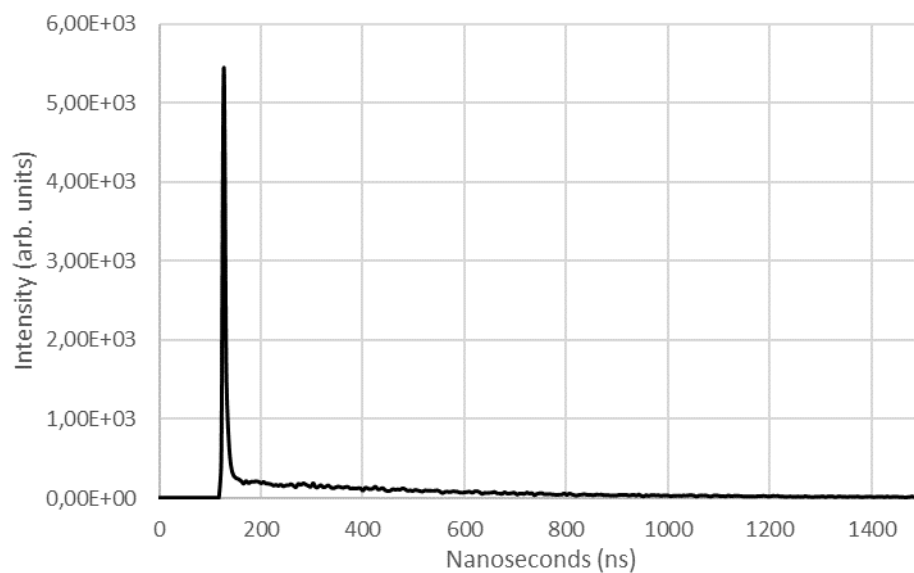


Figure A3 - 38 Lifetime spectrum of Cu(phen)(Xantphos)BF₄ excited at 405 nm, recorded at ambient temperature in degassed CH₂Cl₂ (1.25 · 10⁻⁴ M).

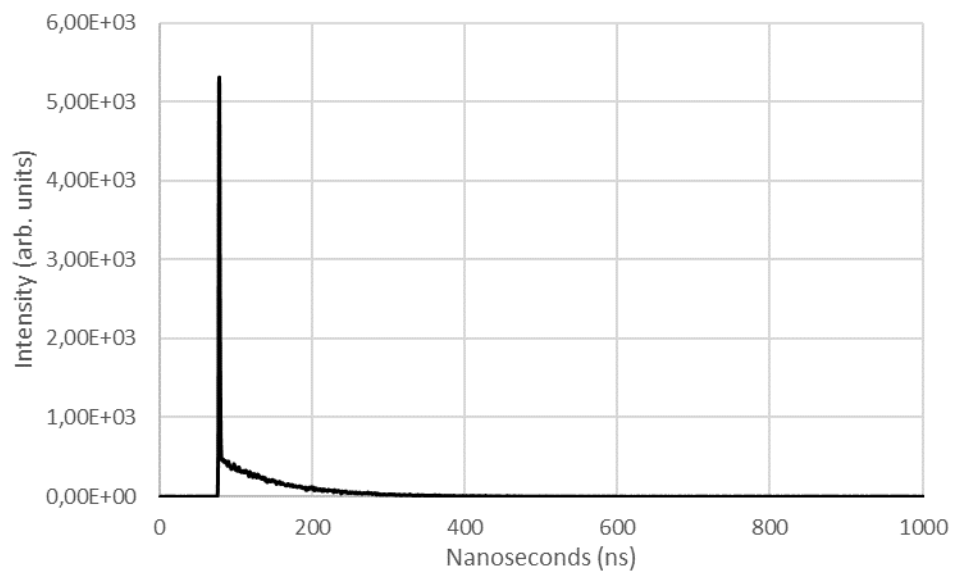


Figure A3 - 39 Lifetime spectrum of Cu(pytri)(Xantphos)BF₄ excited at 405 nm, recorded at ambient temperature in degassed CH₂Cl₂ (1.25 · 10⁻⁴ M).

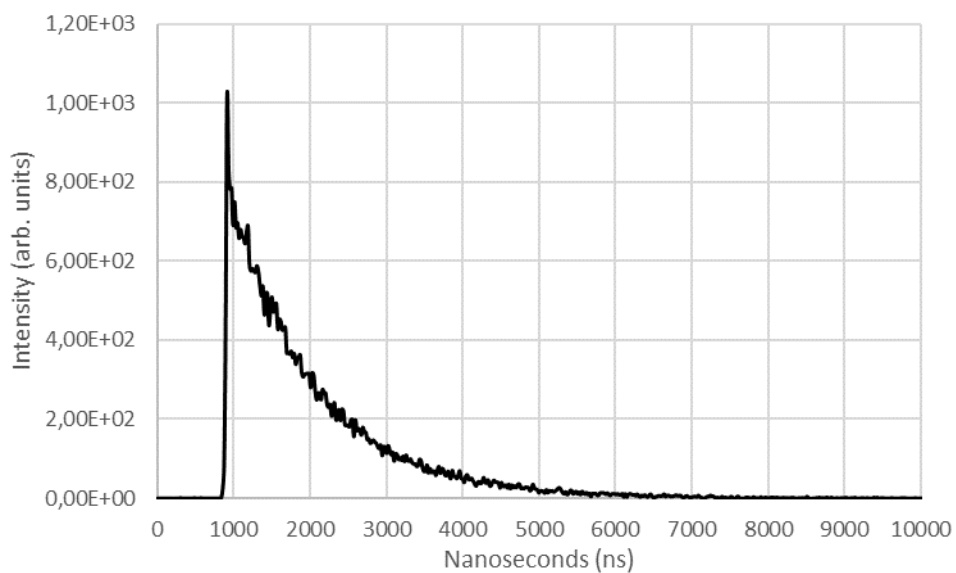


Figure A3 - 40 Lifetime spectrum of Cu(tmp)(Xantphos)BF₄ excited at 405 nm, recorded at ambient temperature in degassed CH₂Cl₂ (1.25 · 10⁻⁴ M).

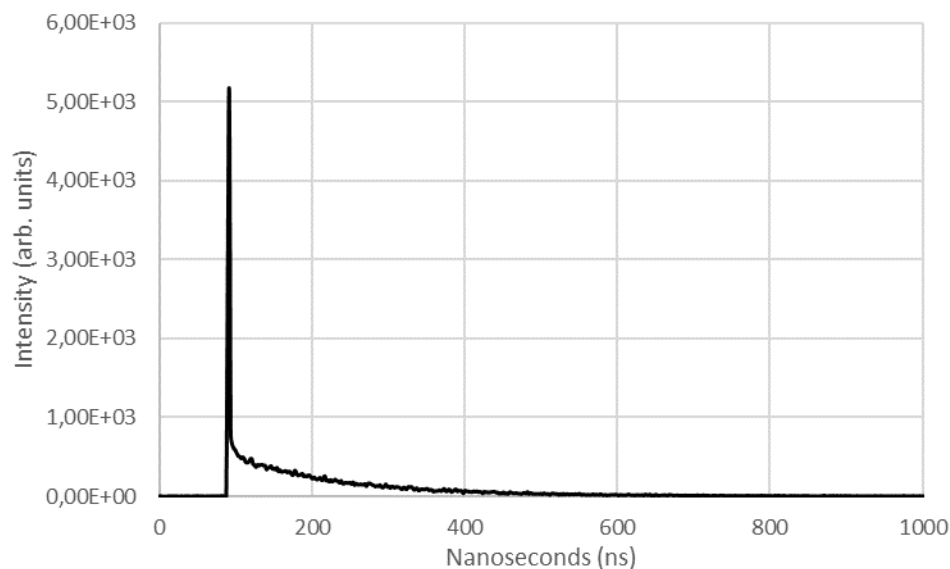


Figure A3 - 41 Lifetime spectrum of Cu(dtbbp)(Xantphos)BF₄ excited at 405 nm, recorded at ambient temperature in degassed CH₂Cl₂ (1.25 · 10⁻⁴ M).

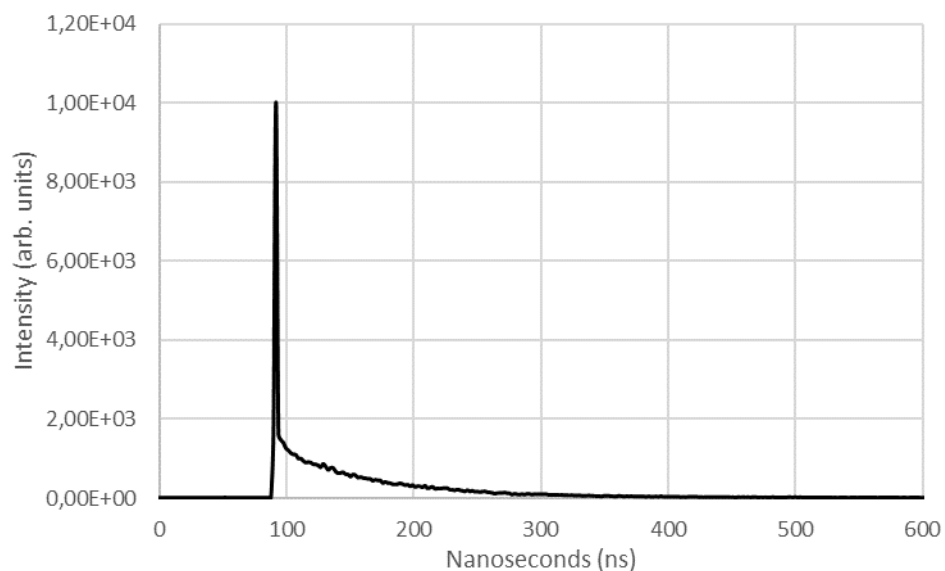


Figure A3 - 42 Lifetime spectrum of Cu(dmbp)(Xantphos)BF₄ excited at 405 nm, recorded at ambient temperature in degassed CH₂Cl₂ (1.25 · 10⁻⁴ M).

A3.11 Photostability studies

Each copper complex (10 mg) and triphenylmethane (10 mg) were precisely weighed in NMR tubes. CDCl₃ (0.6 mL) was added and the tubes were sealed with Parafilm® and Teflon®. Initial NMRs were recorded and the tubes were then irradiated for 24 h at 400 nm in the setup shown

below. NMR yields calculated using the triphenylmethane standard and the copper complexes afforded the remaining yield of the heteroleptic copper(I) complexes using the ratio:

$$\frac{\%Cu (t = 0h)}{\%Cu (t = 24h)} * 100$$



Figure A3 - 43 Setup for the photostability of copper complexes

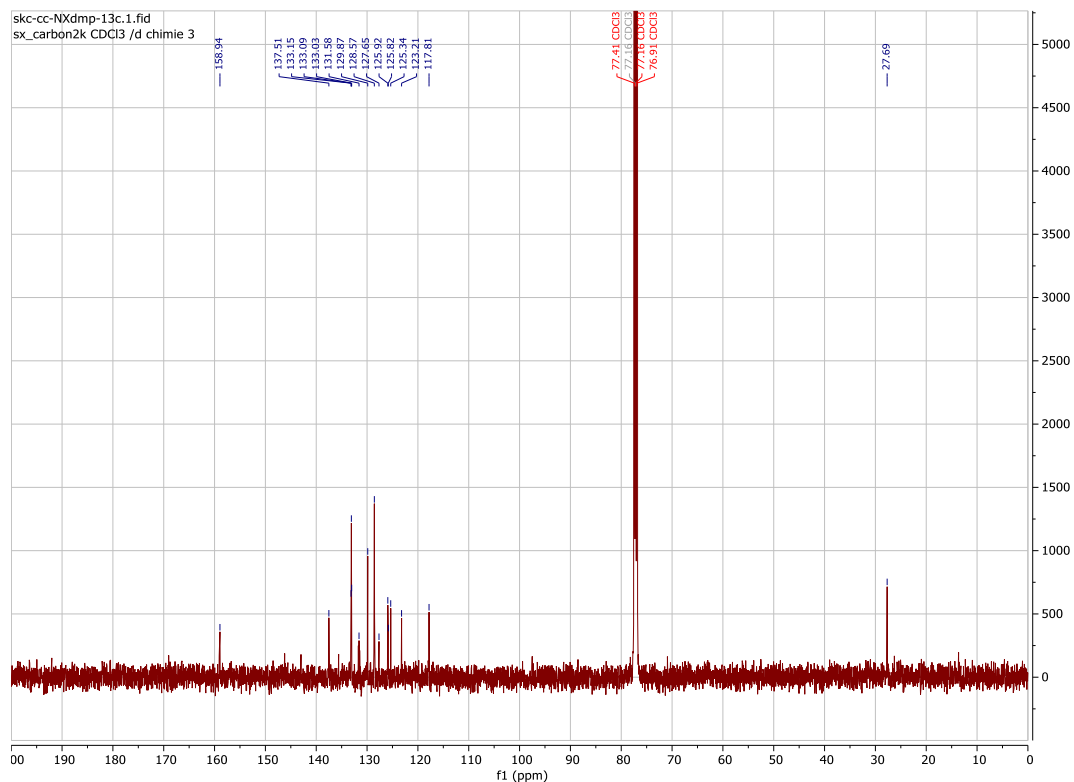
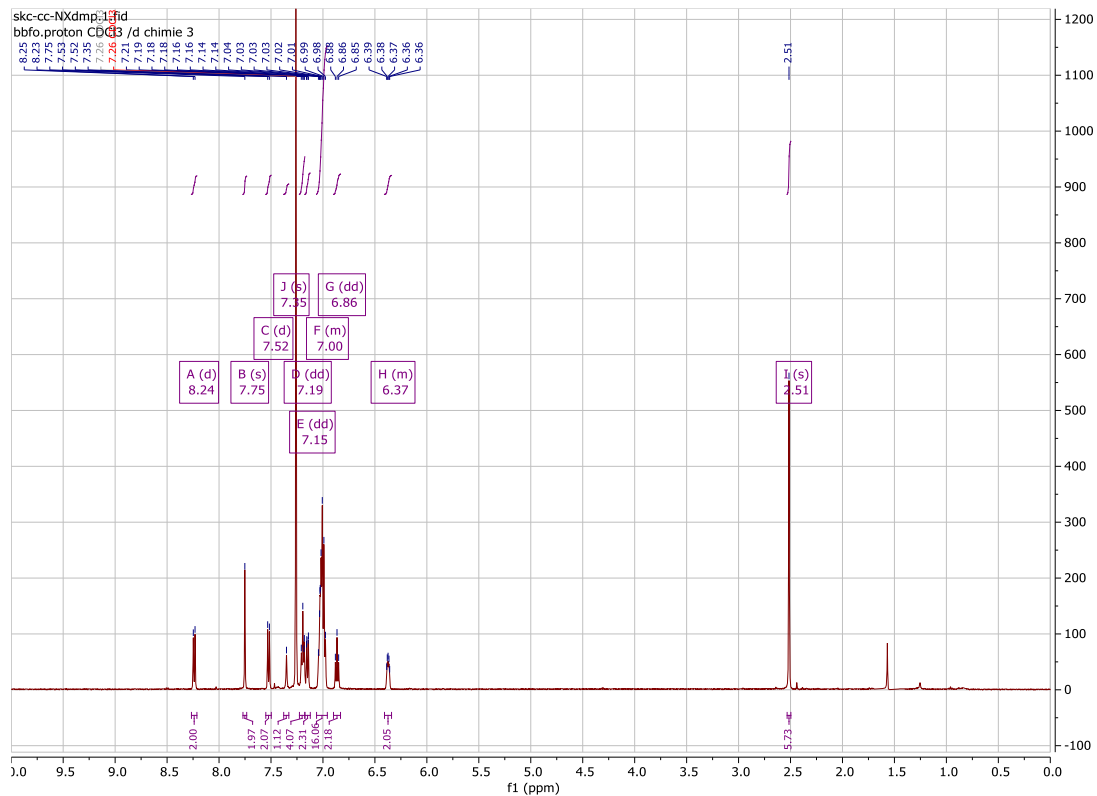
Table A3 - 8 Tabular data for the photostability studies

CU(PP)(DMP)	% CU	CU(XANTPHOS)(NN)	% CU
NXANTPHOS	0	PHEN	101
PHANEPHOS	21	TMP	0
XANTPHOS	68	BPHEN	85
DPEPHOS	57	DMBP	93
DPPF	84	DTTBP	95
DPPN	90	BATHO	88
BINAP	0	BATHOCUP	24
SEGPHOS	0	DQ	91
NONE	71	PYTRI	0
		QUINTRI	99

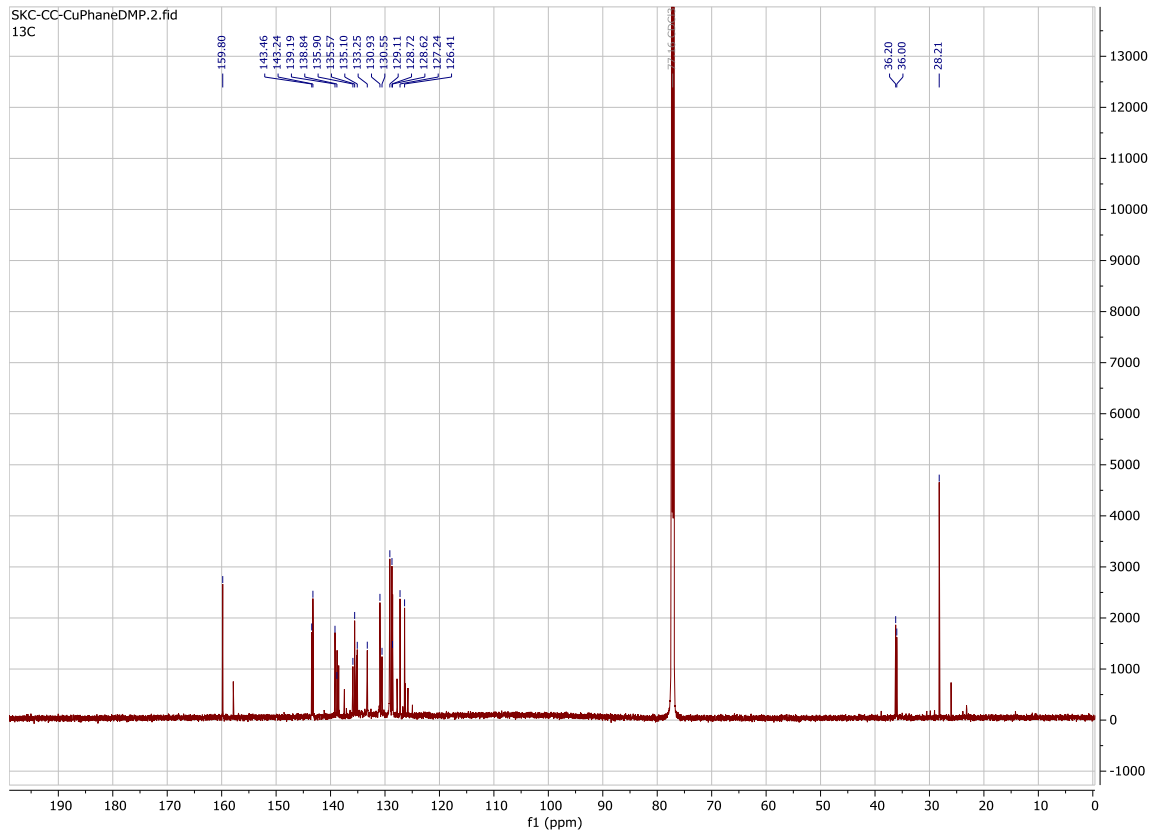
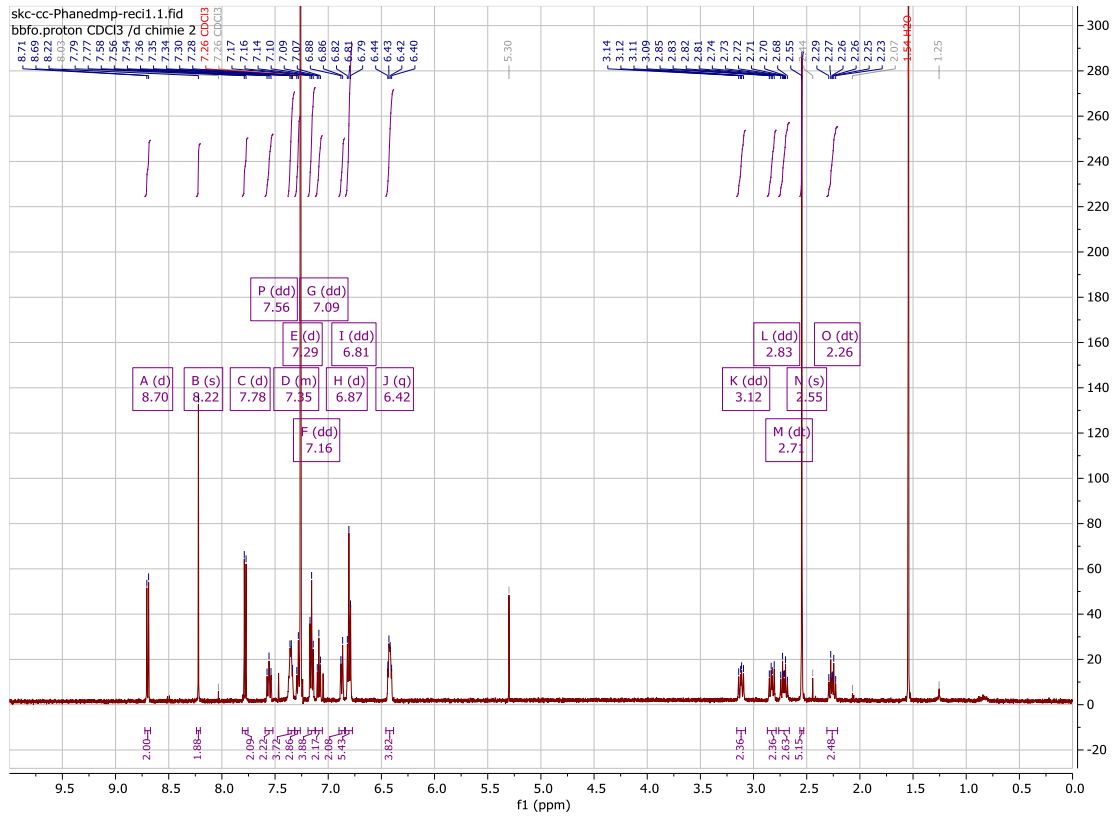
IQUINTRI	54
DDPQ	82
DDPPZ	9
DBDPPZ	0
DPA	43
DMOP	44

A3.12 NMR and Mass Spectra

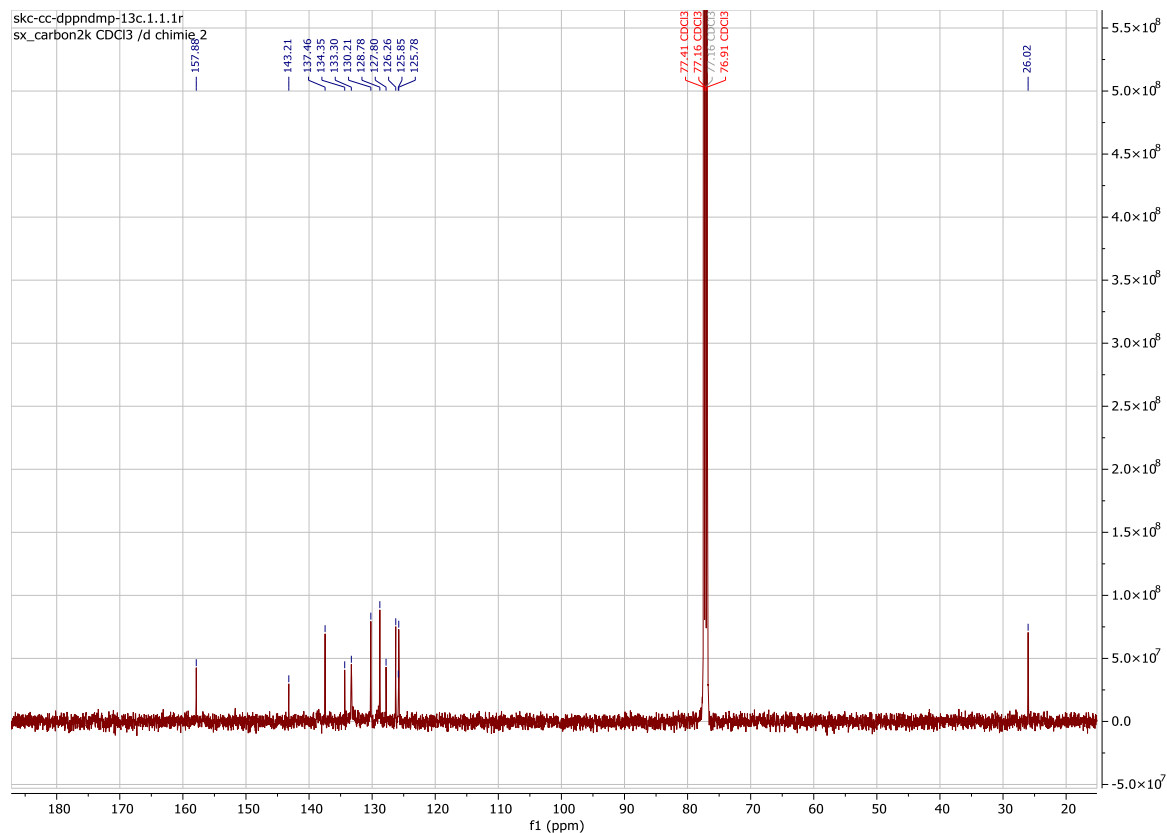
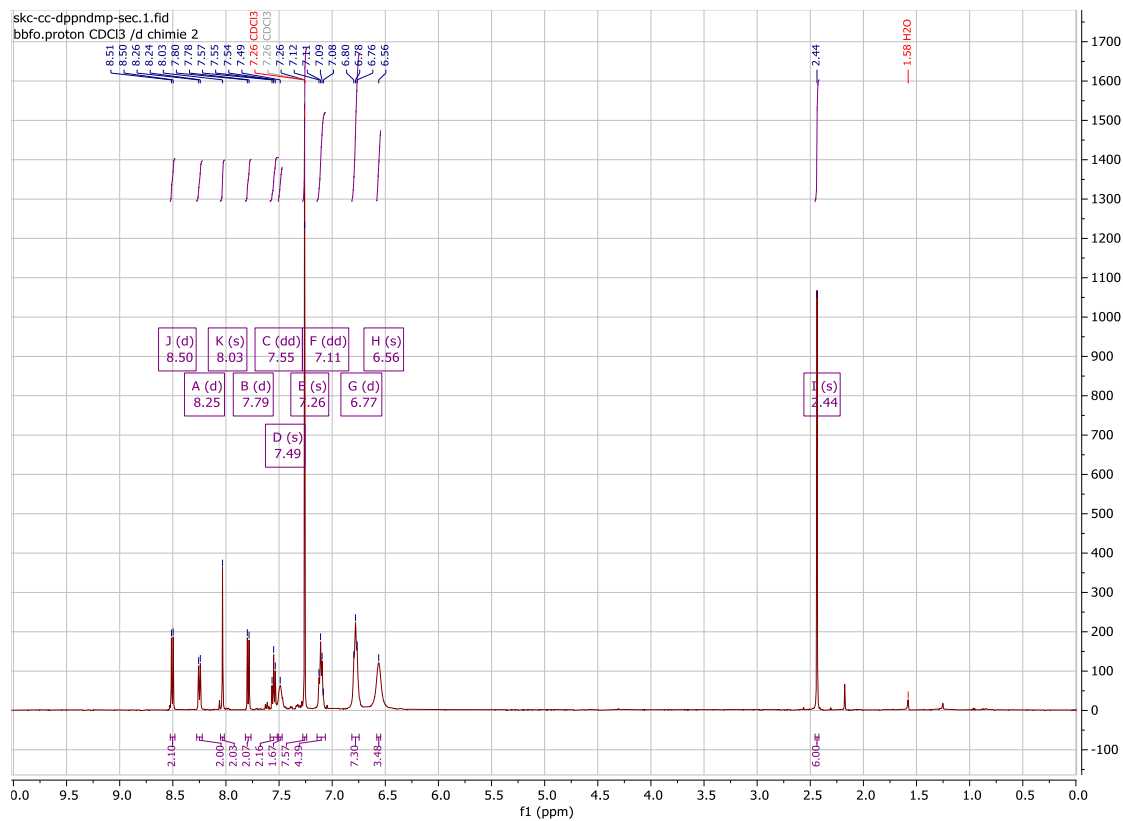
New Copper Complexes: Cu(dmp)(NXantphos)BF₄



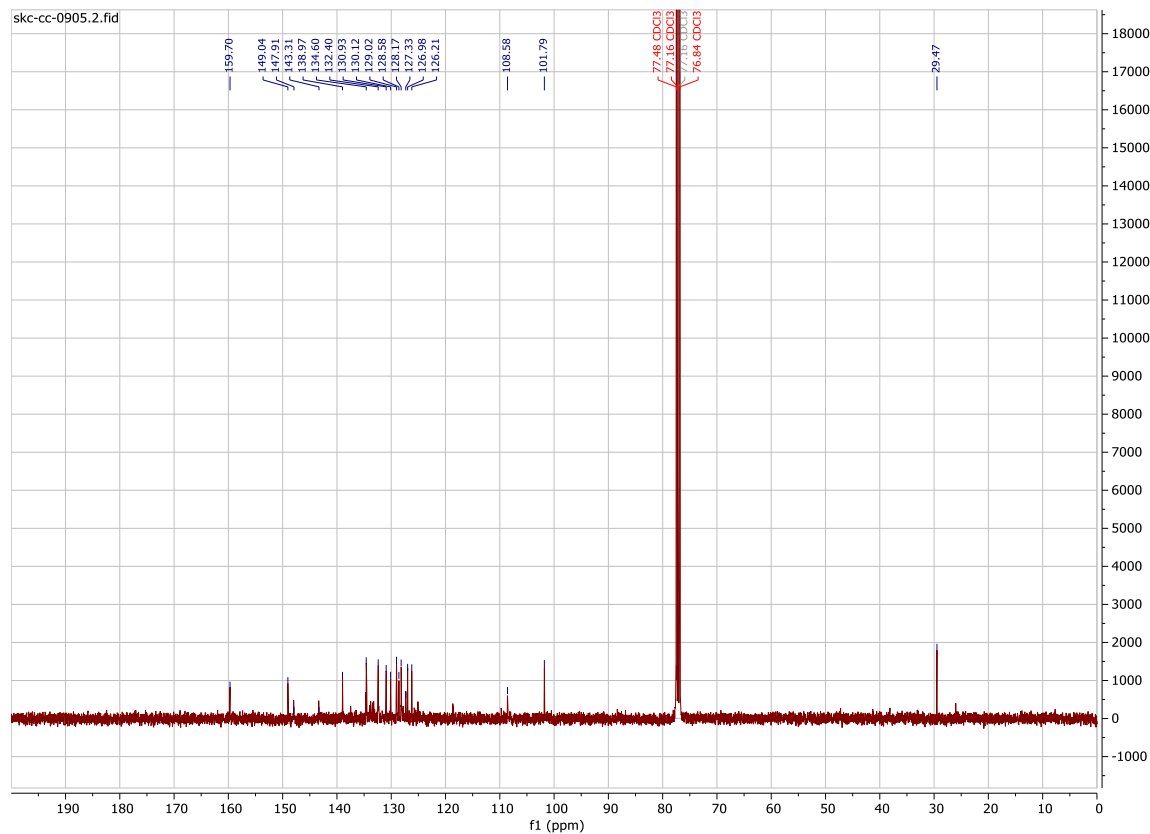
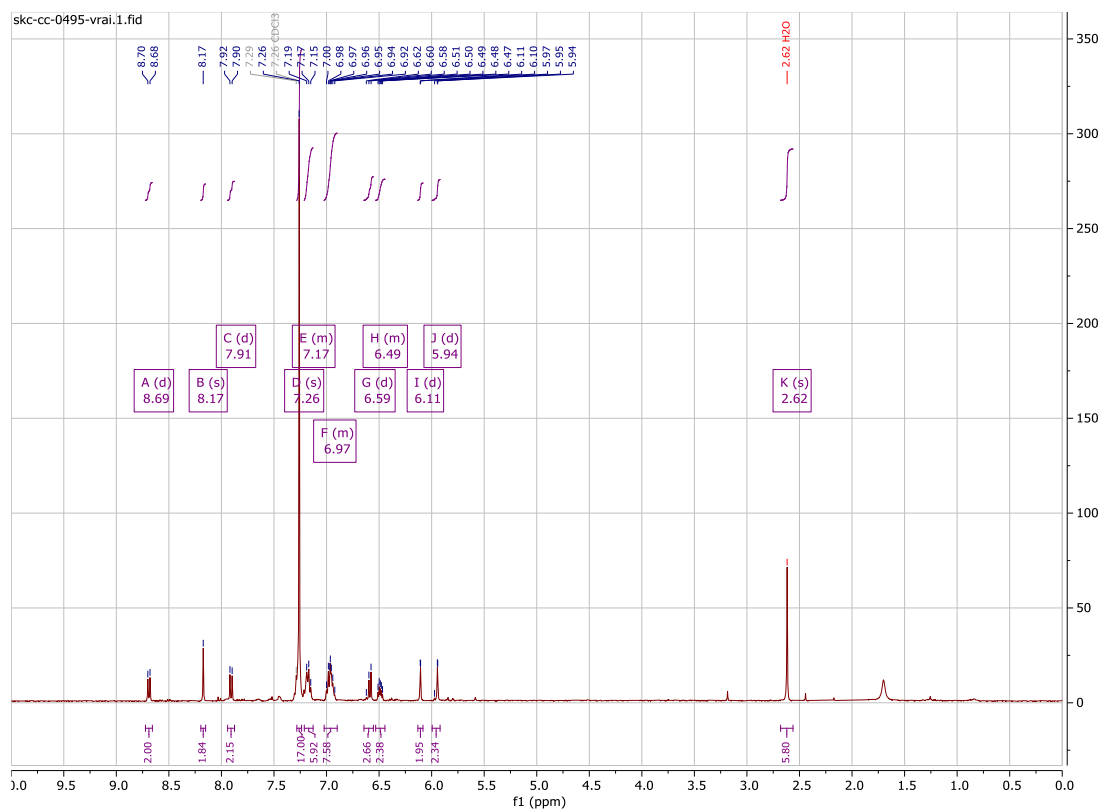
Cu(dmp)(Phanephos)BF₄



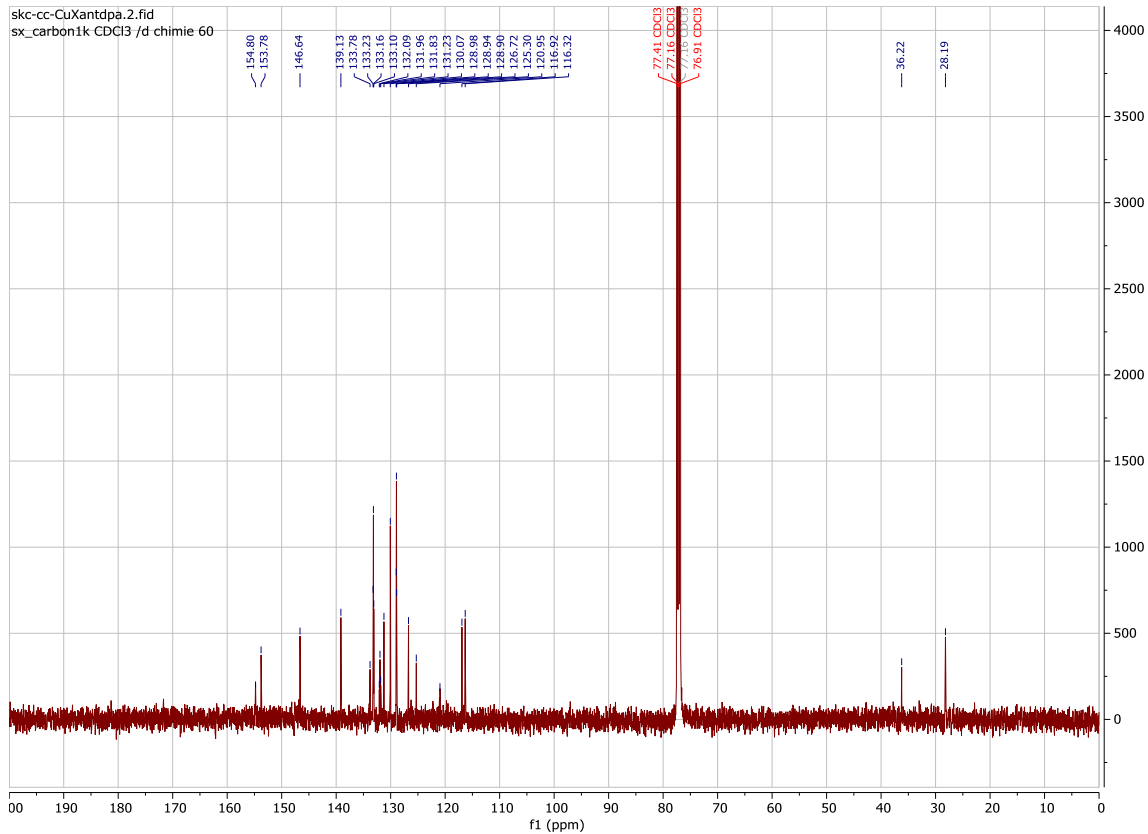
Cu(dmp)(dppn)BF₄



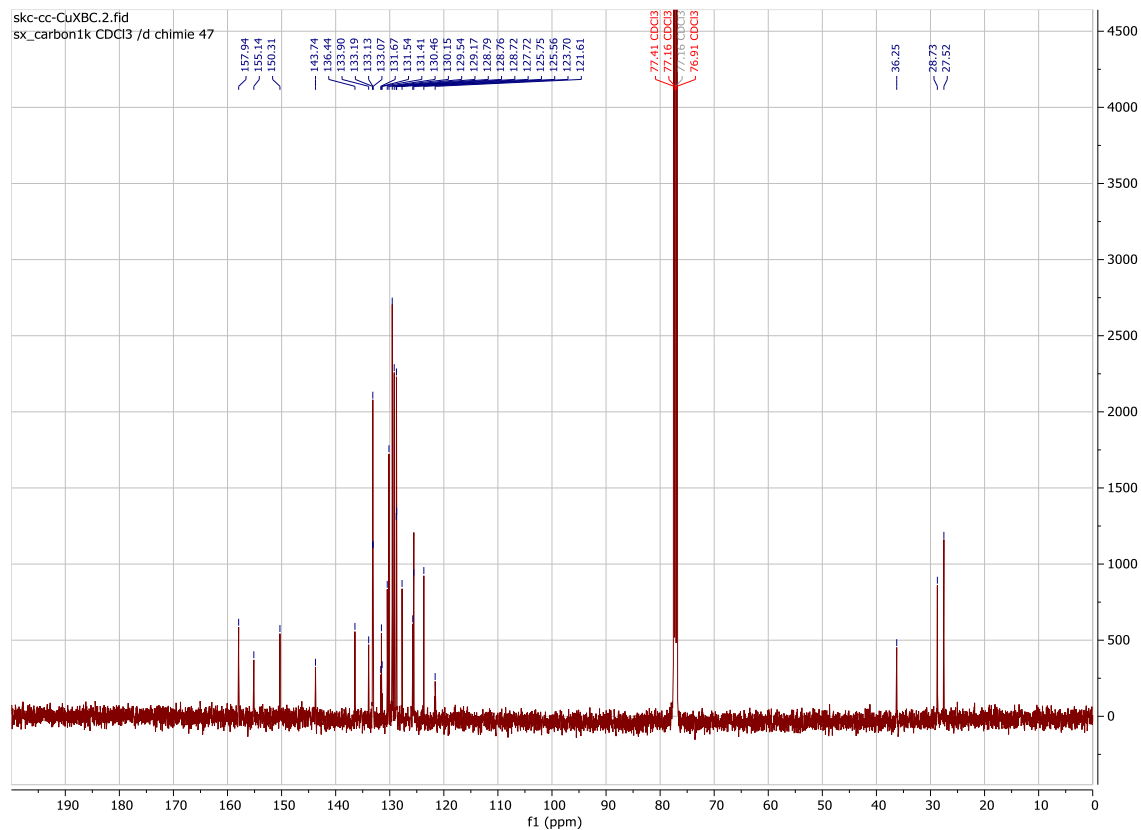
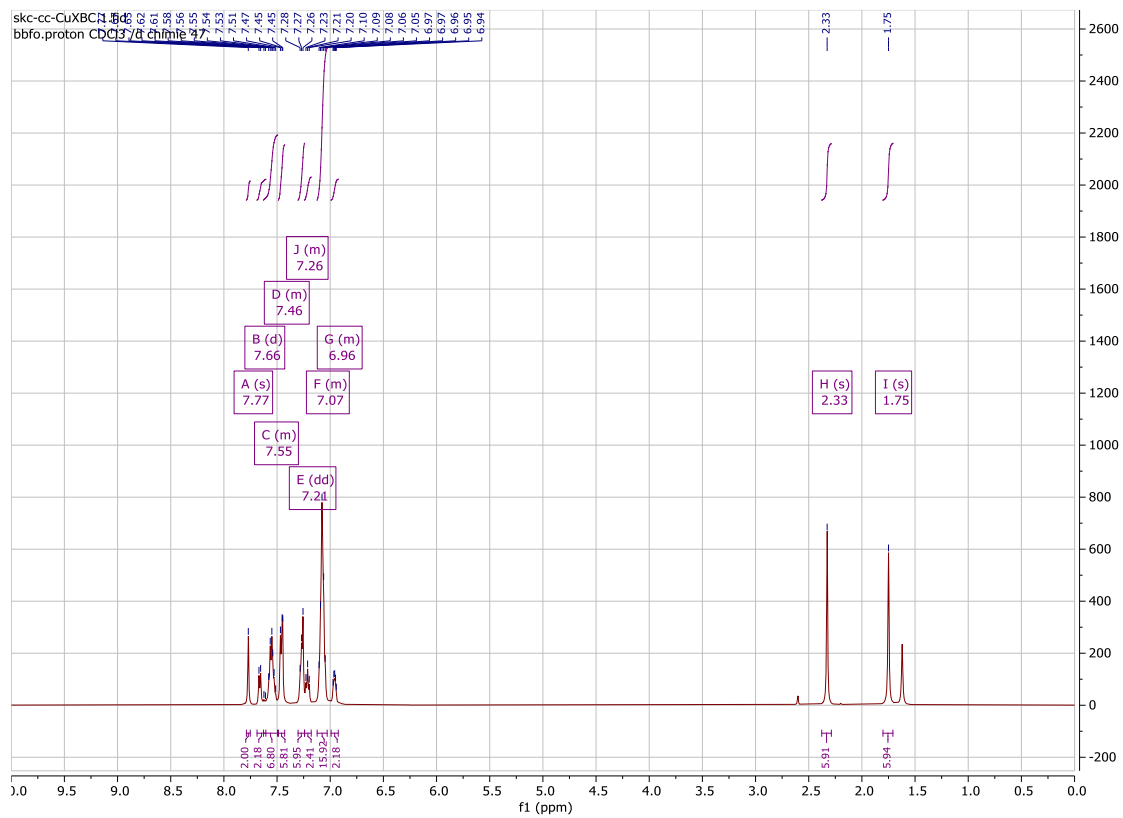
Cu(dmp)((S)-Segphos)BF₄



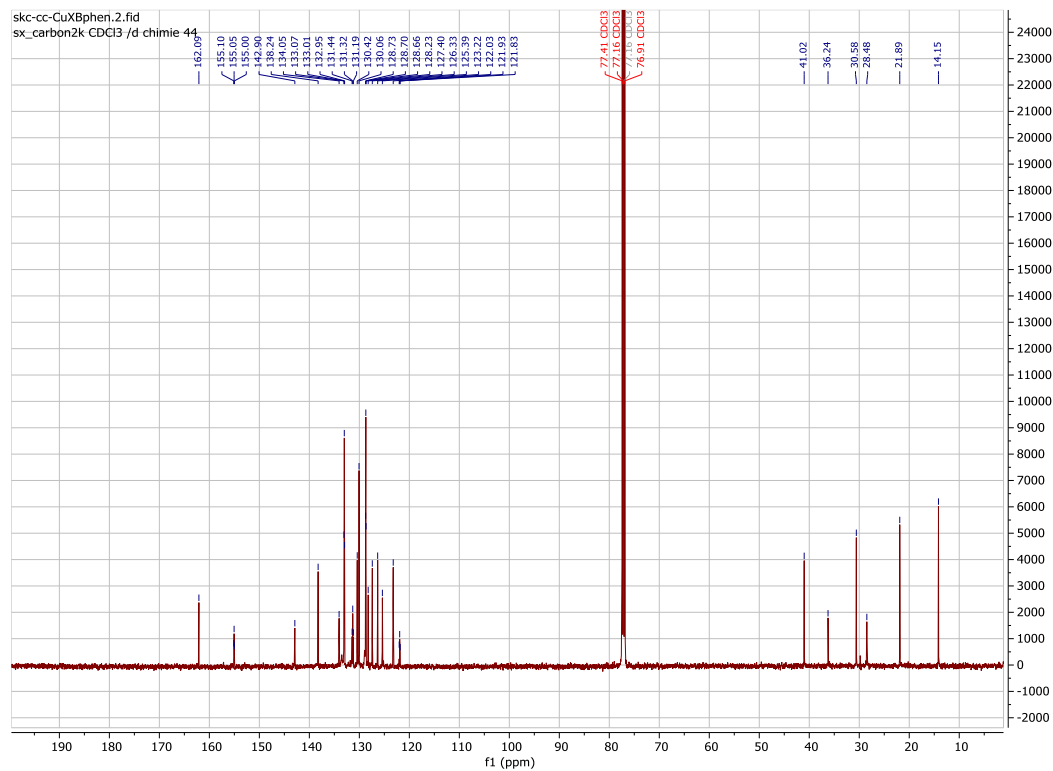
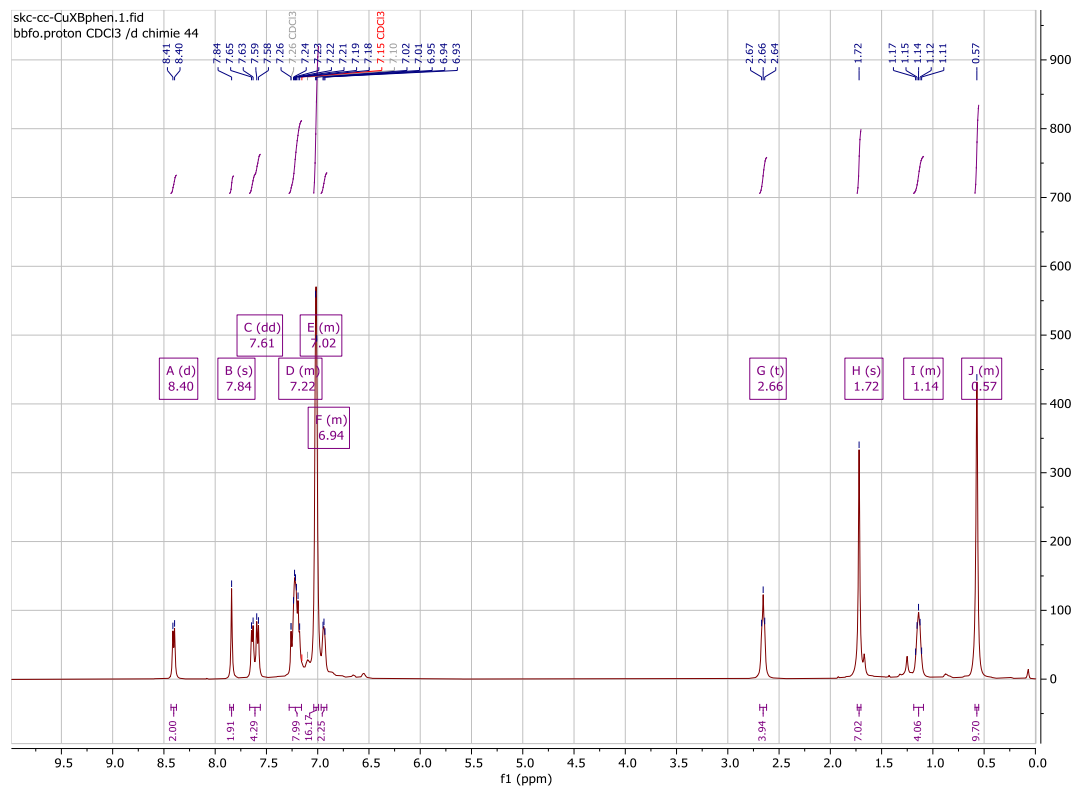
Cu(dpa)(Xantphos)BF₄



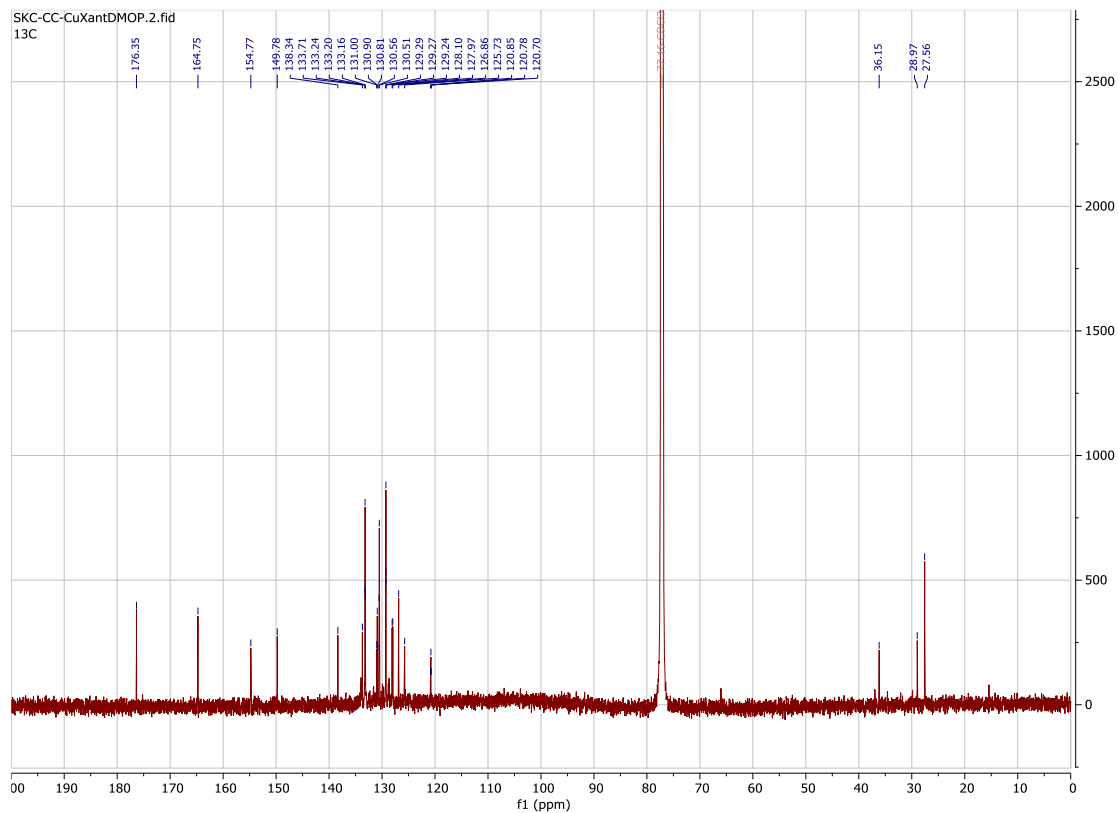
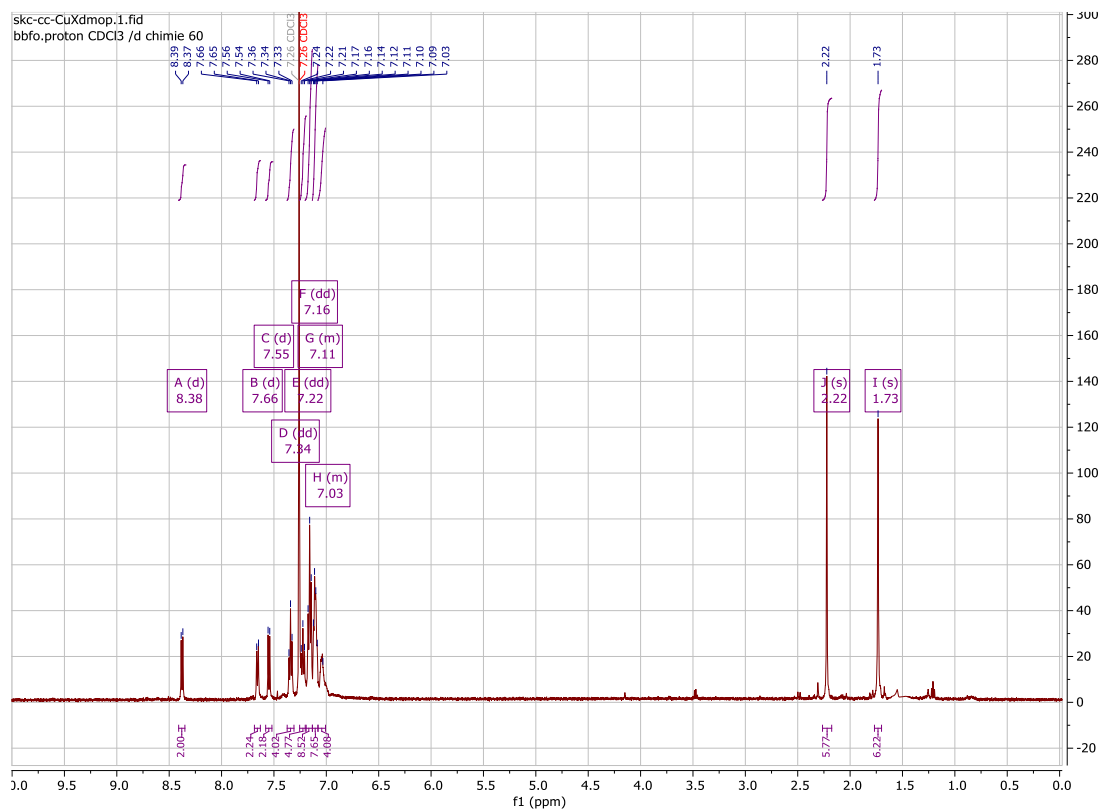
Cu(bathocup)(Xantphos)BF₄



Cu(bphen)(Xantphos)BF₄

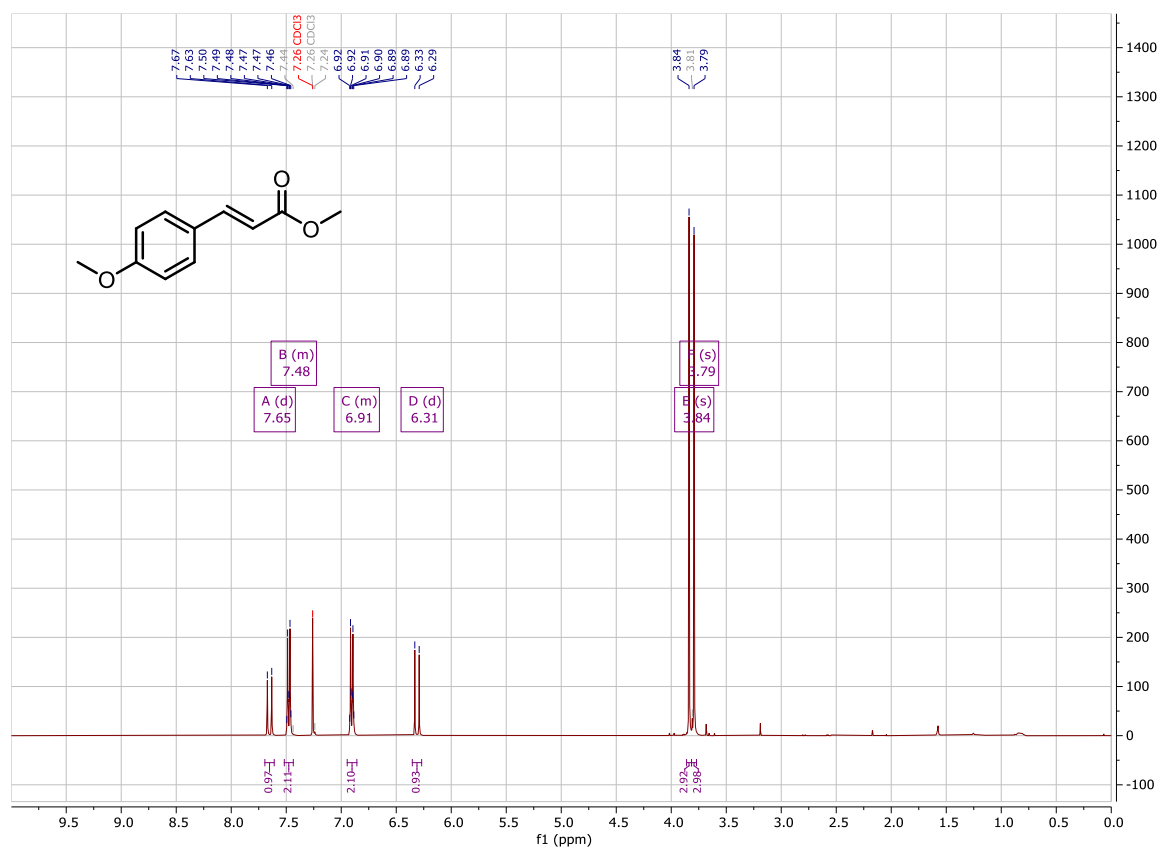


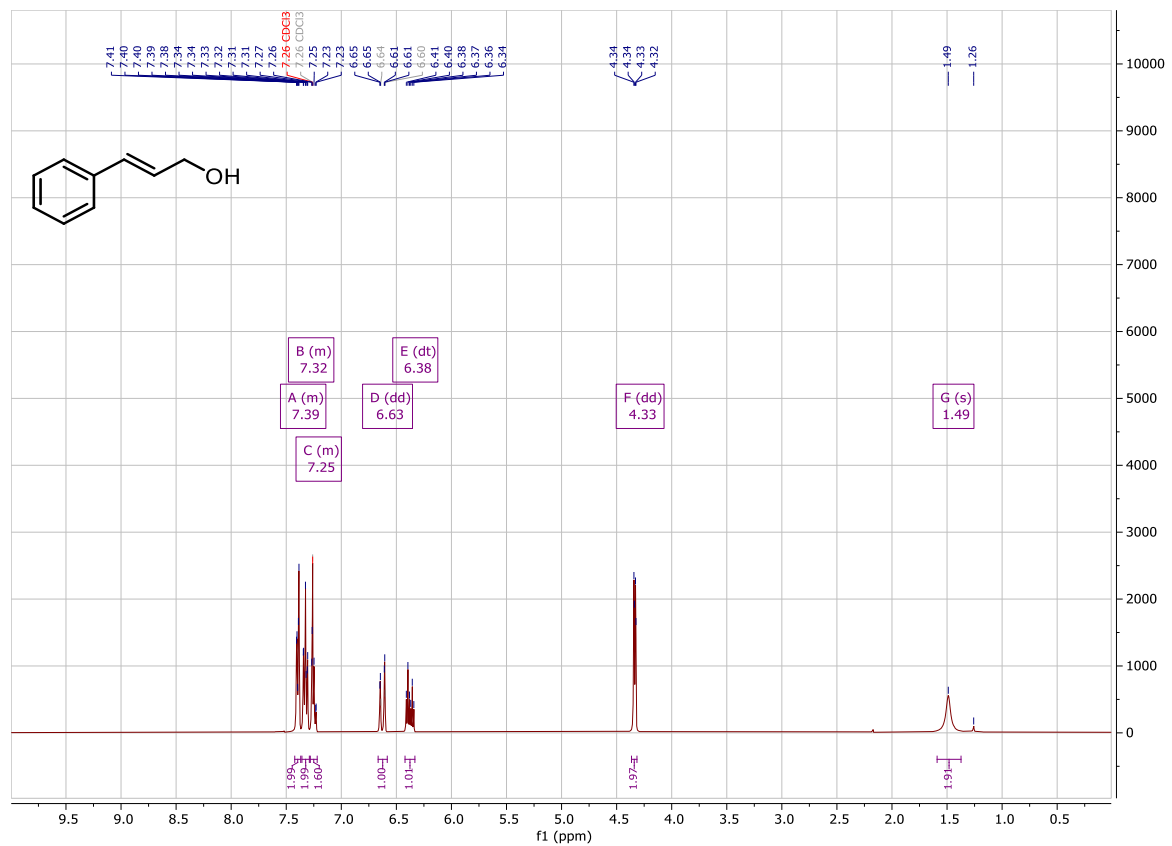
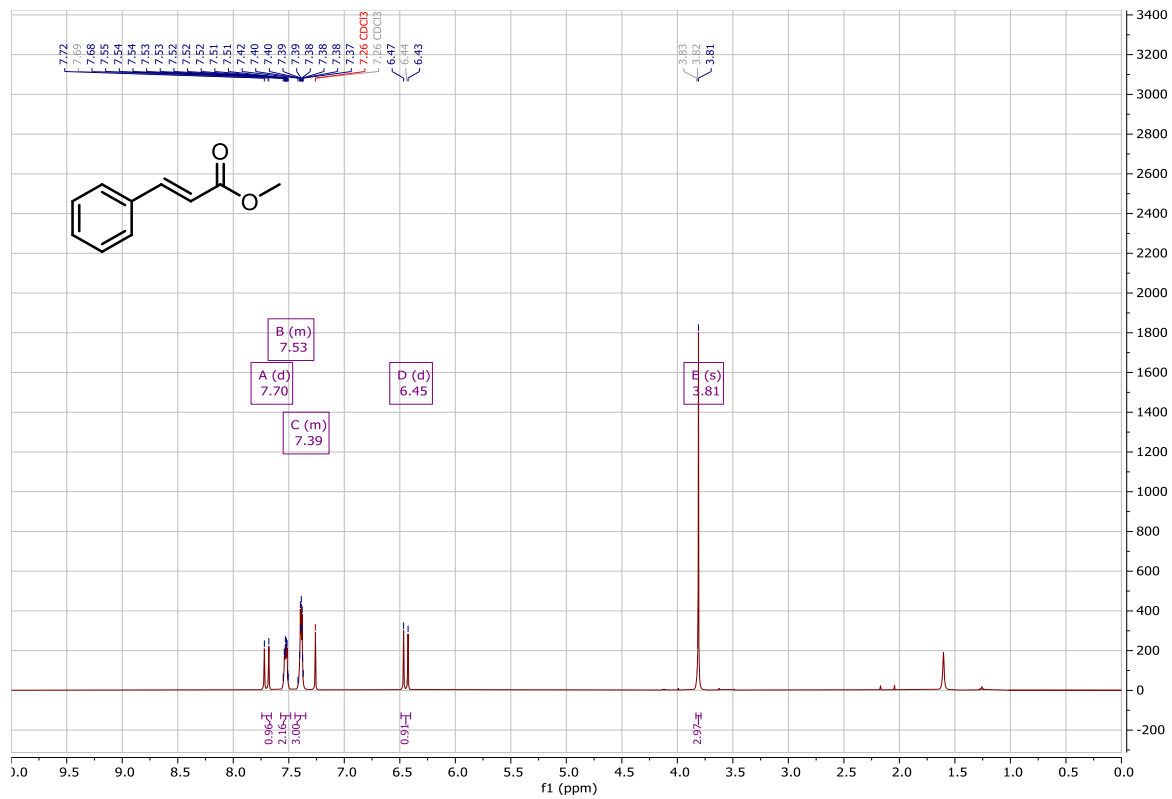
Cu(dmpo)(Xantphos)BF₄

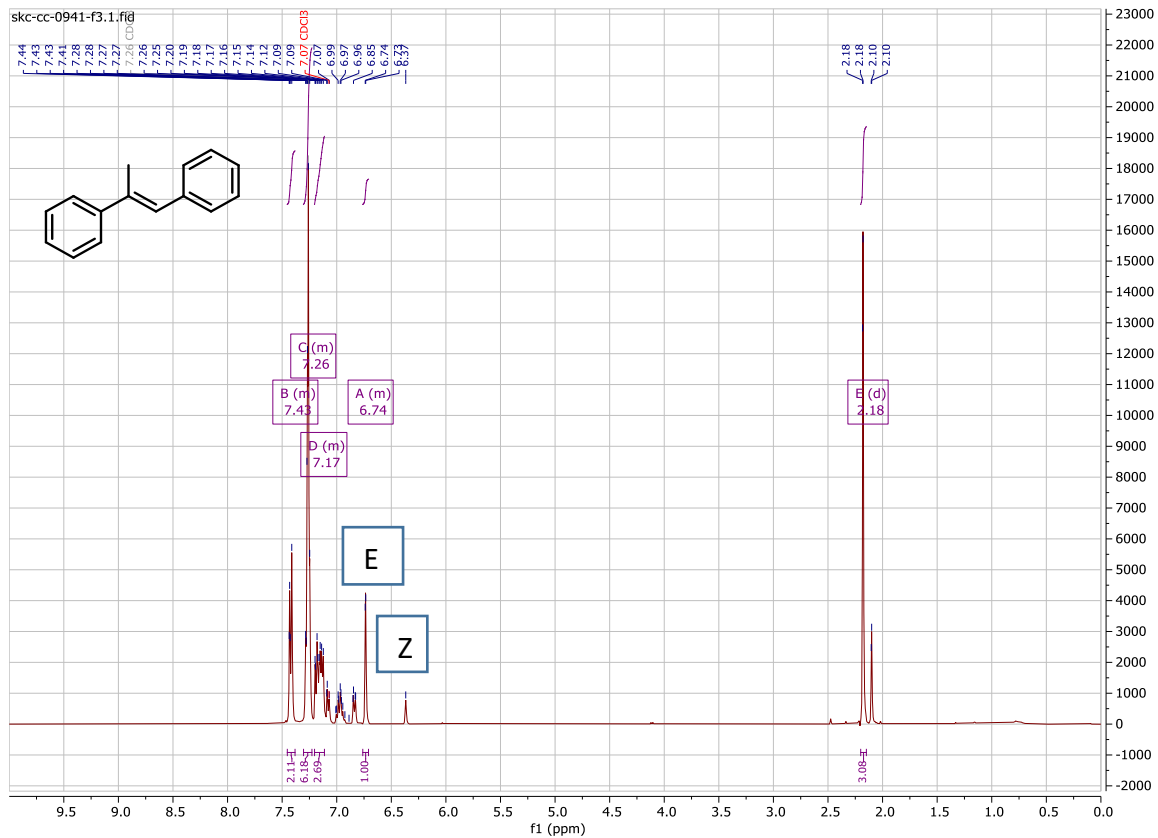
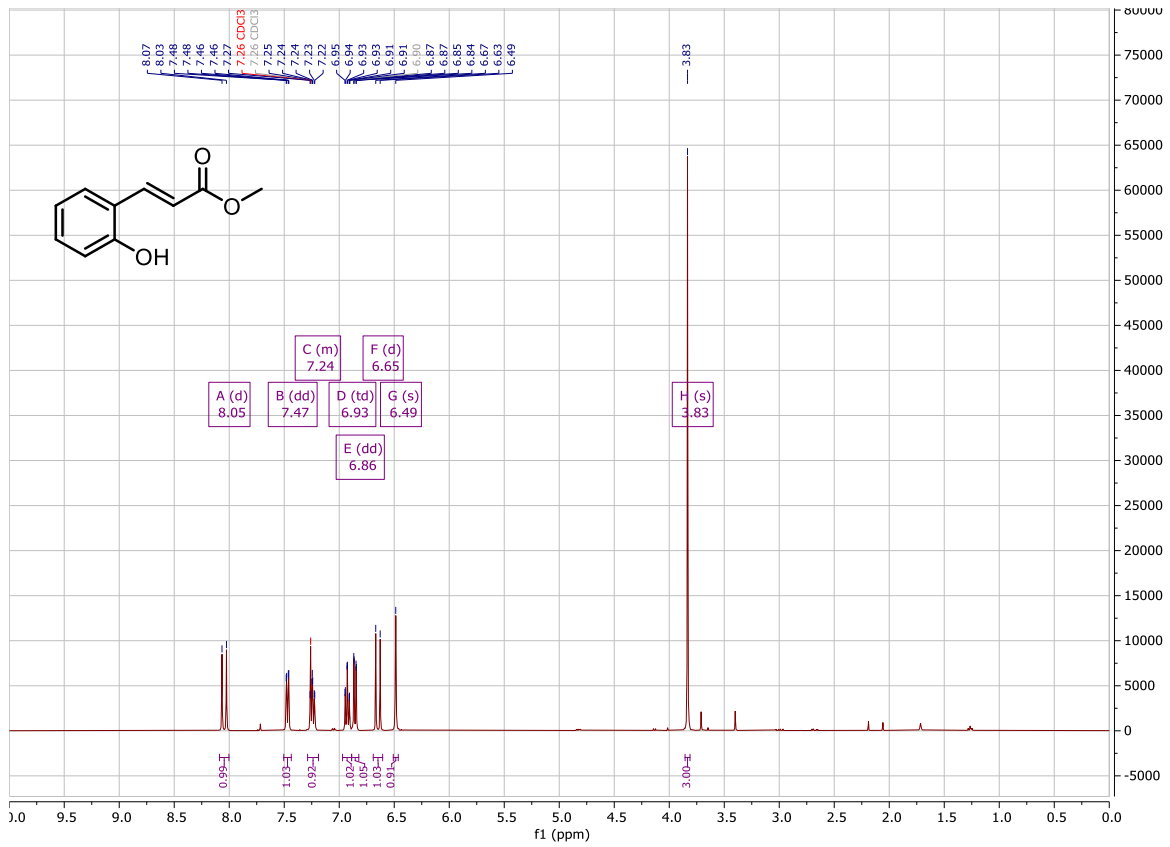


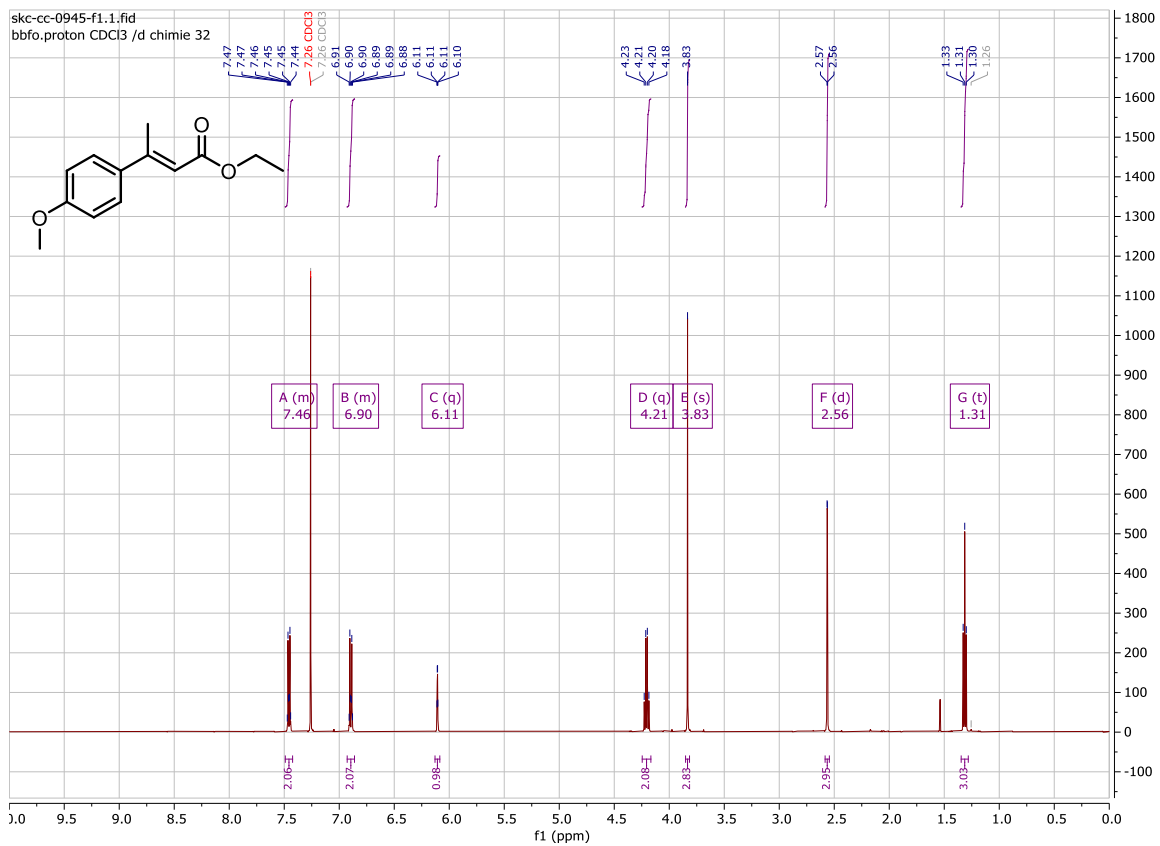
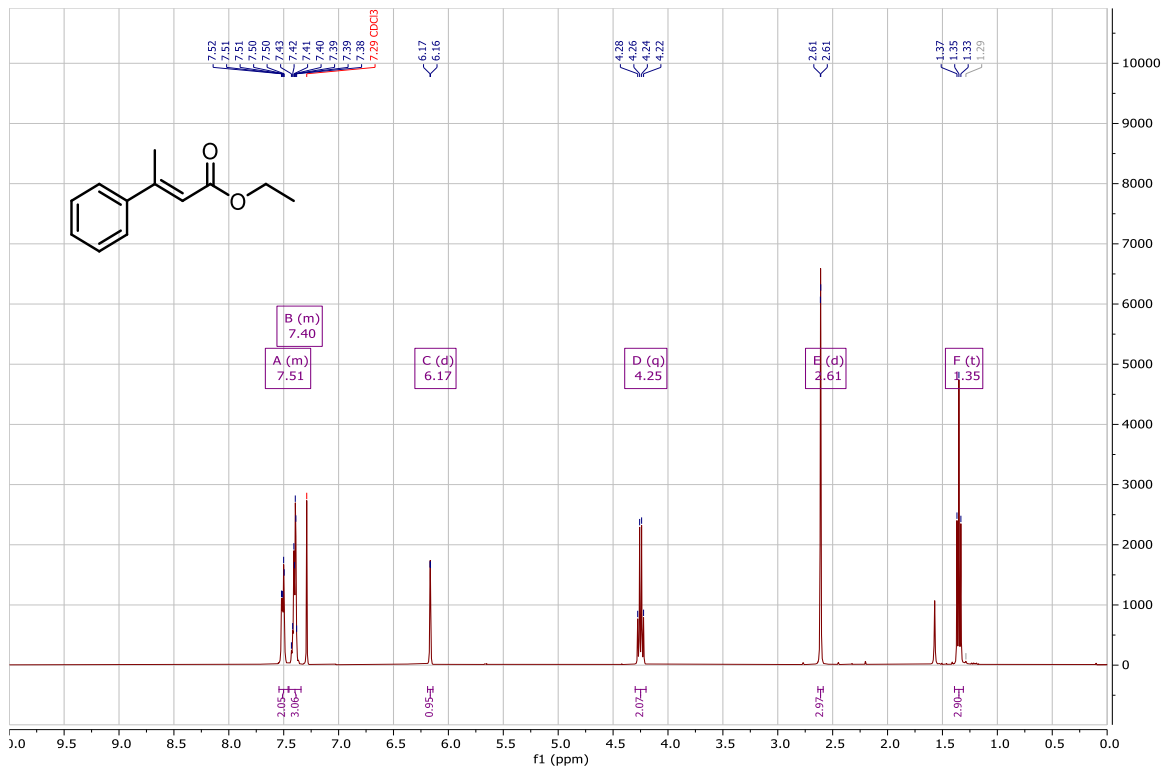
Alkenes Substrates

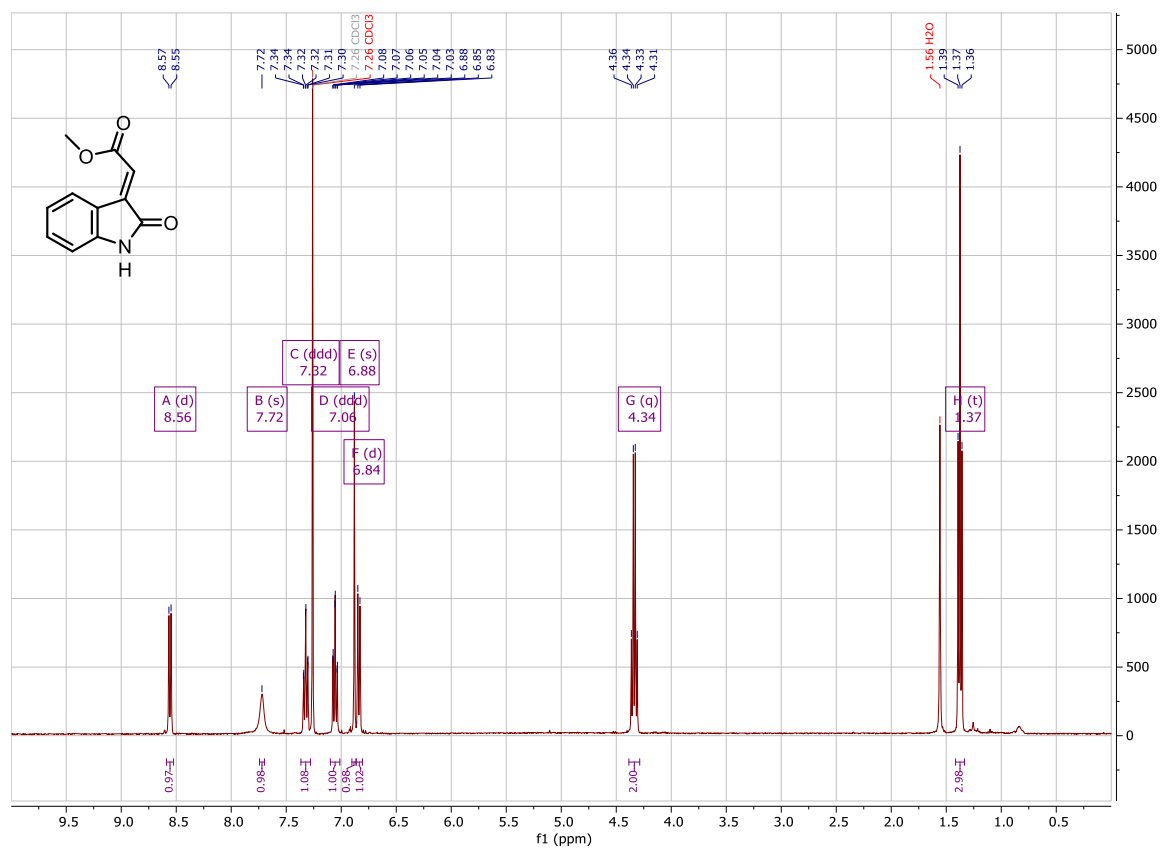
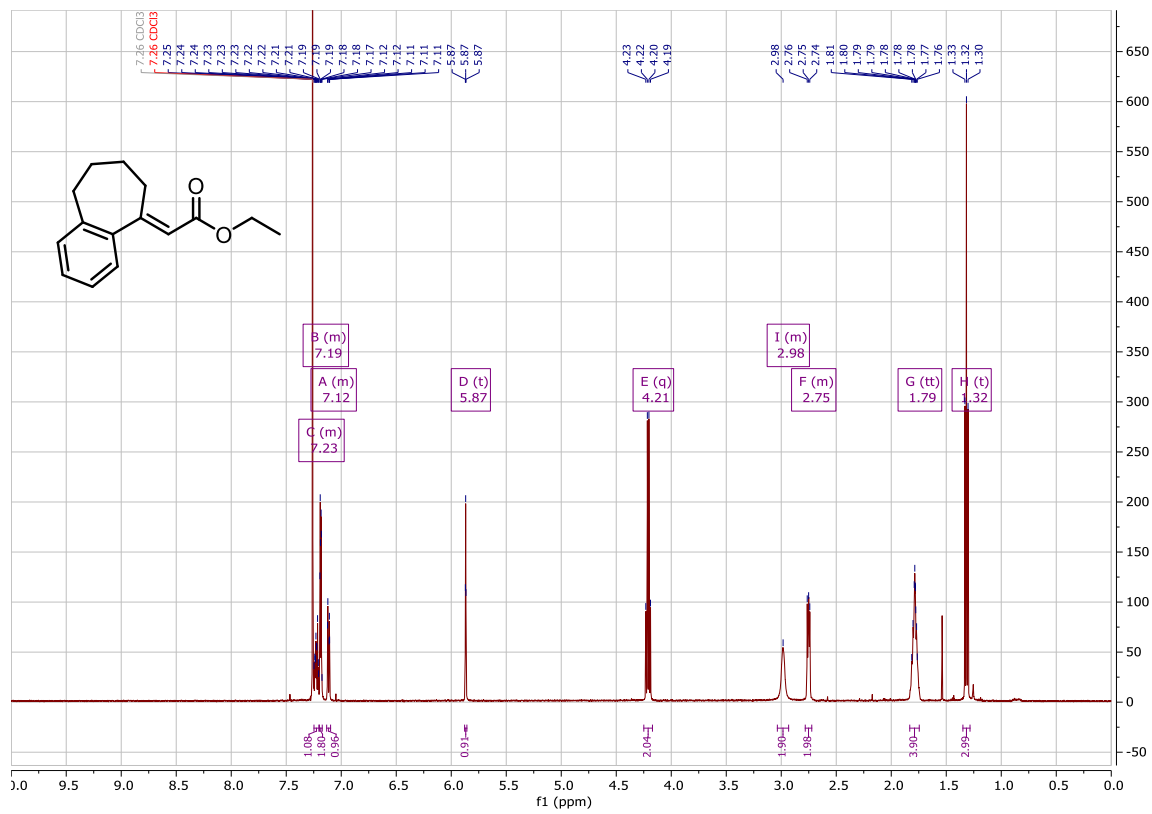
For previously reported compounds only the ^1H NMR is shown. For new compounds both the ^1H and ^{13}C NMR spectra are provided:

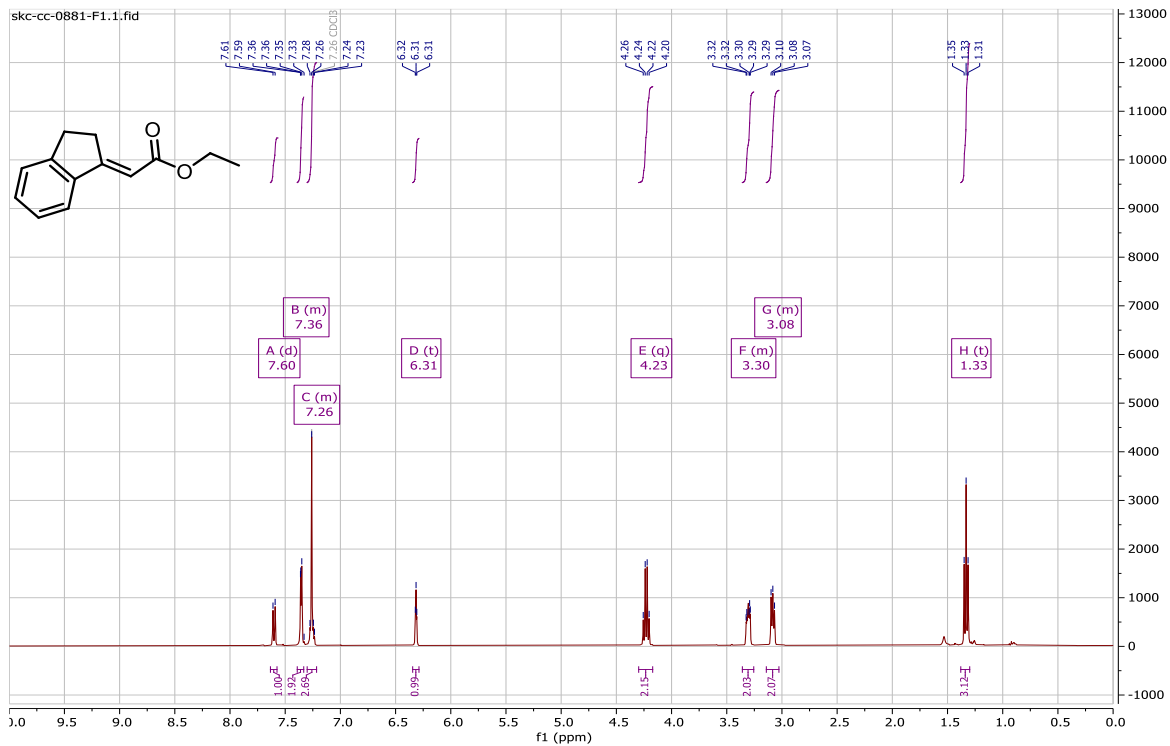
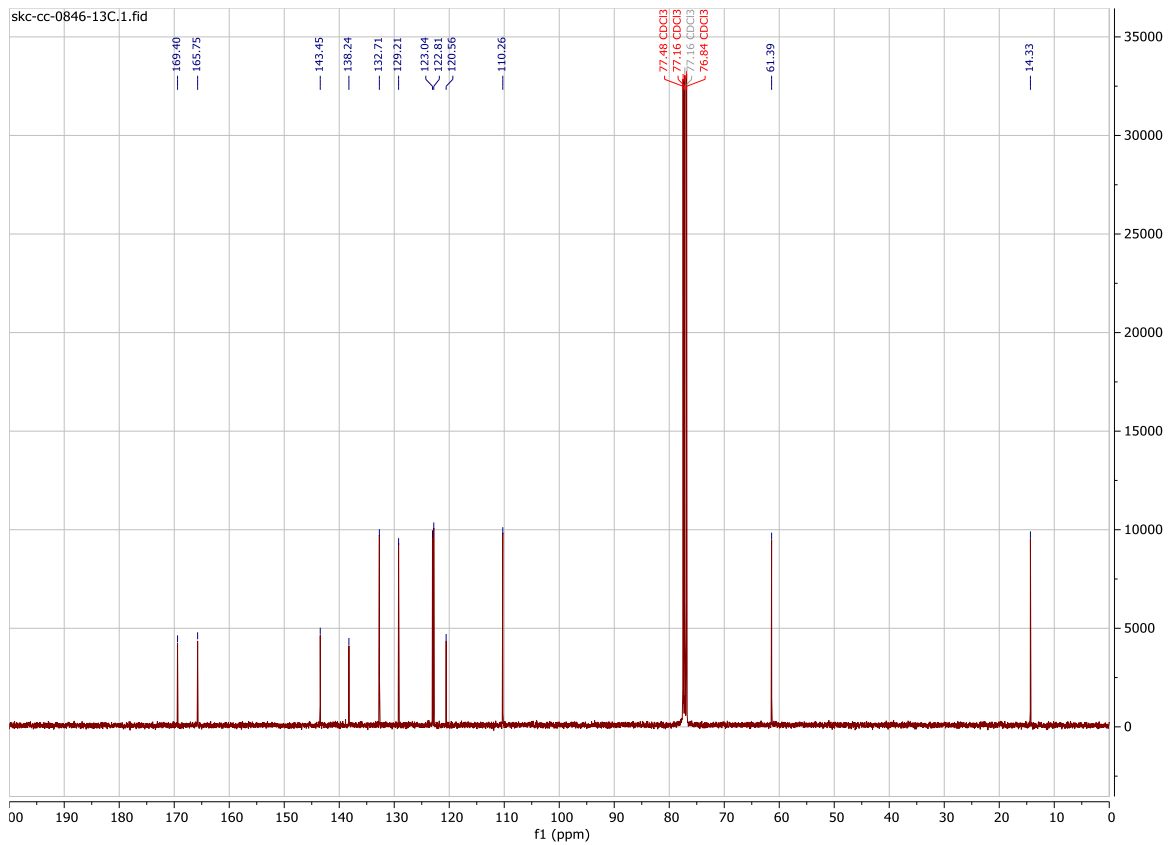


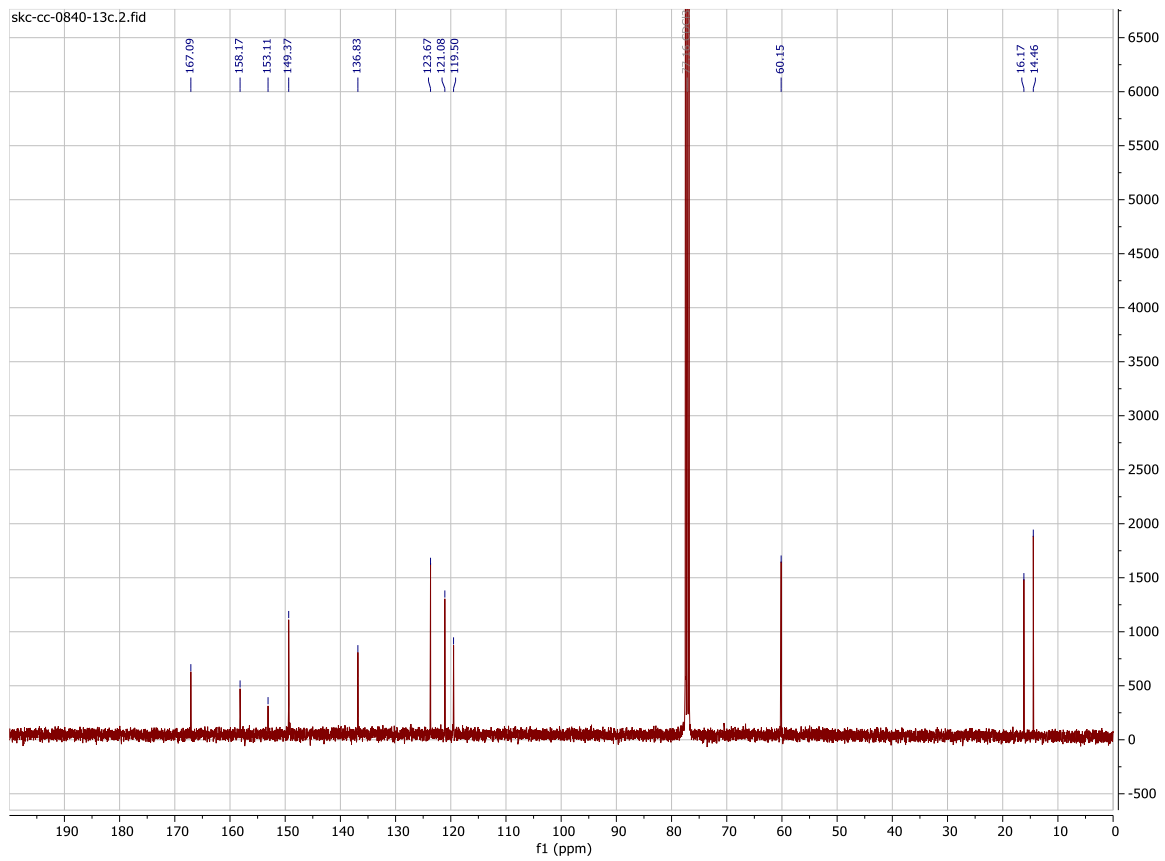
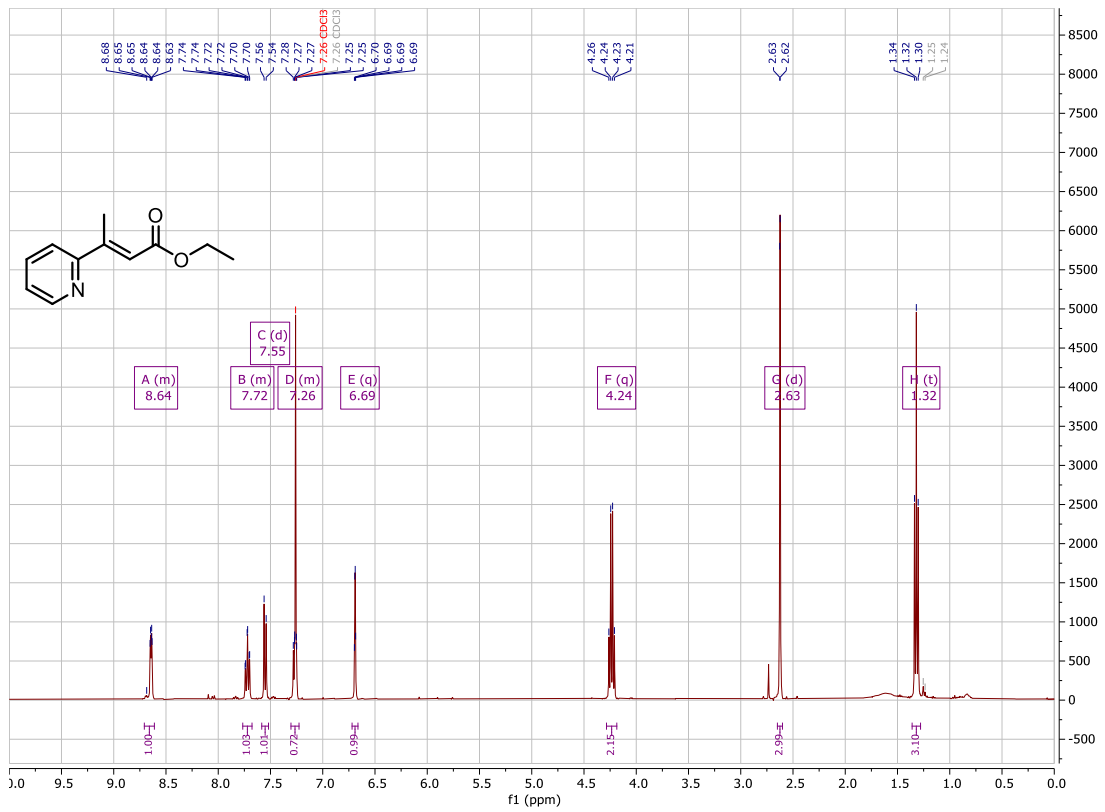


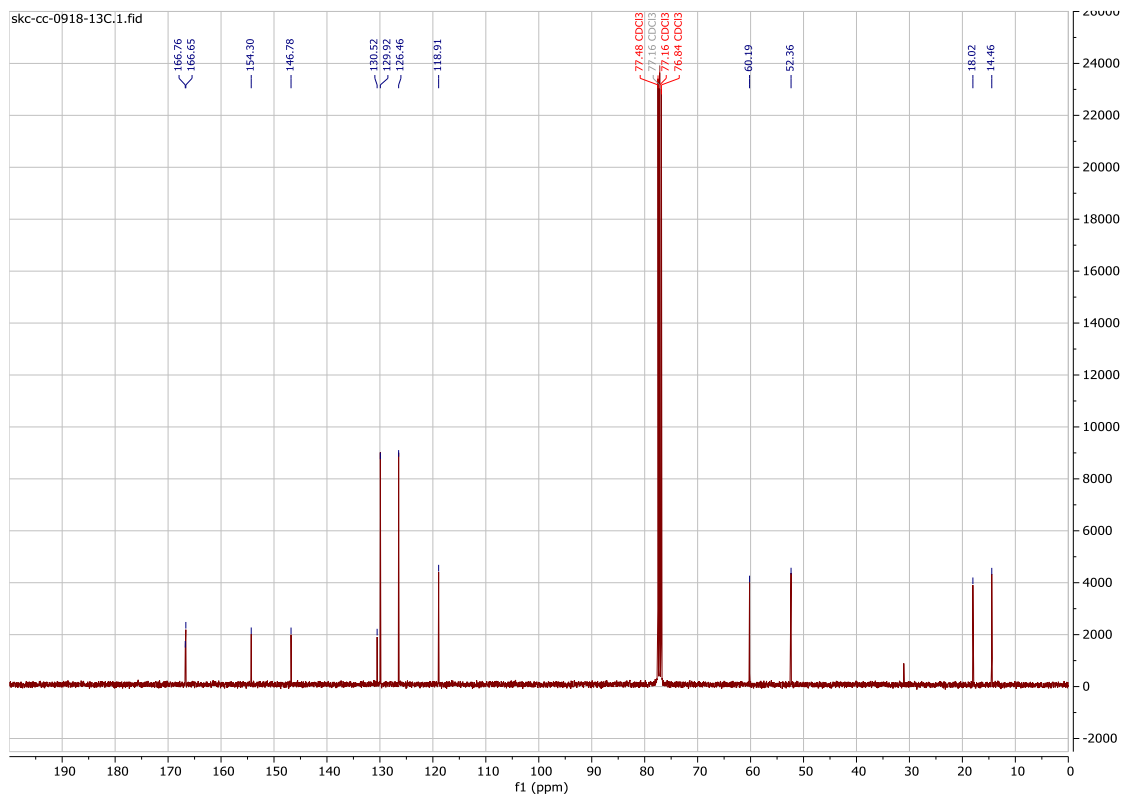
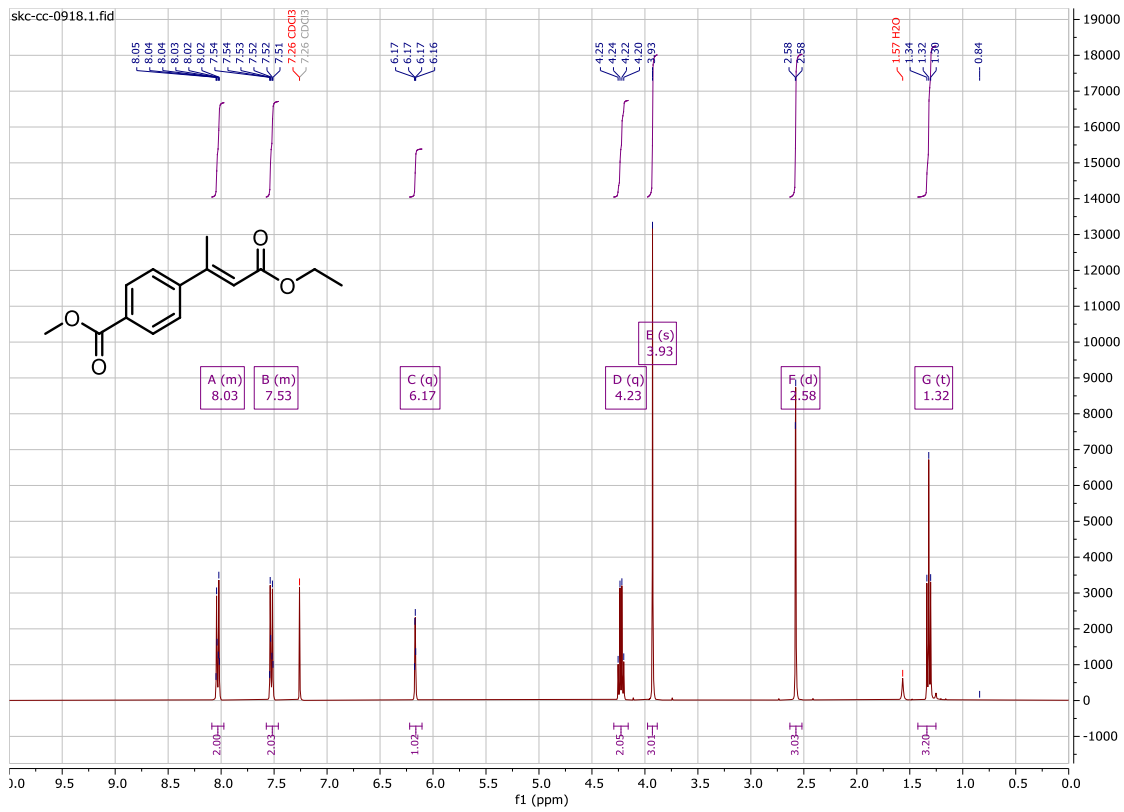


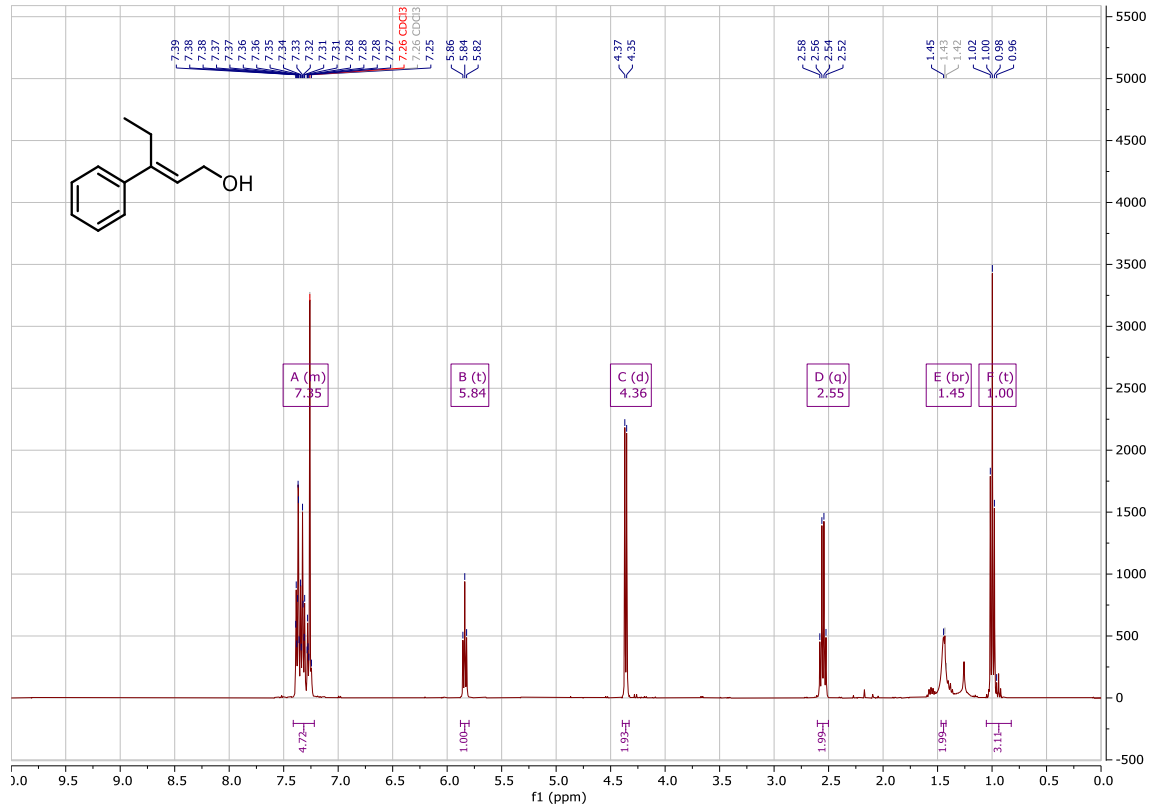
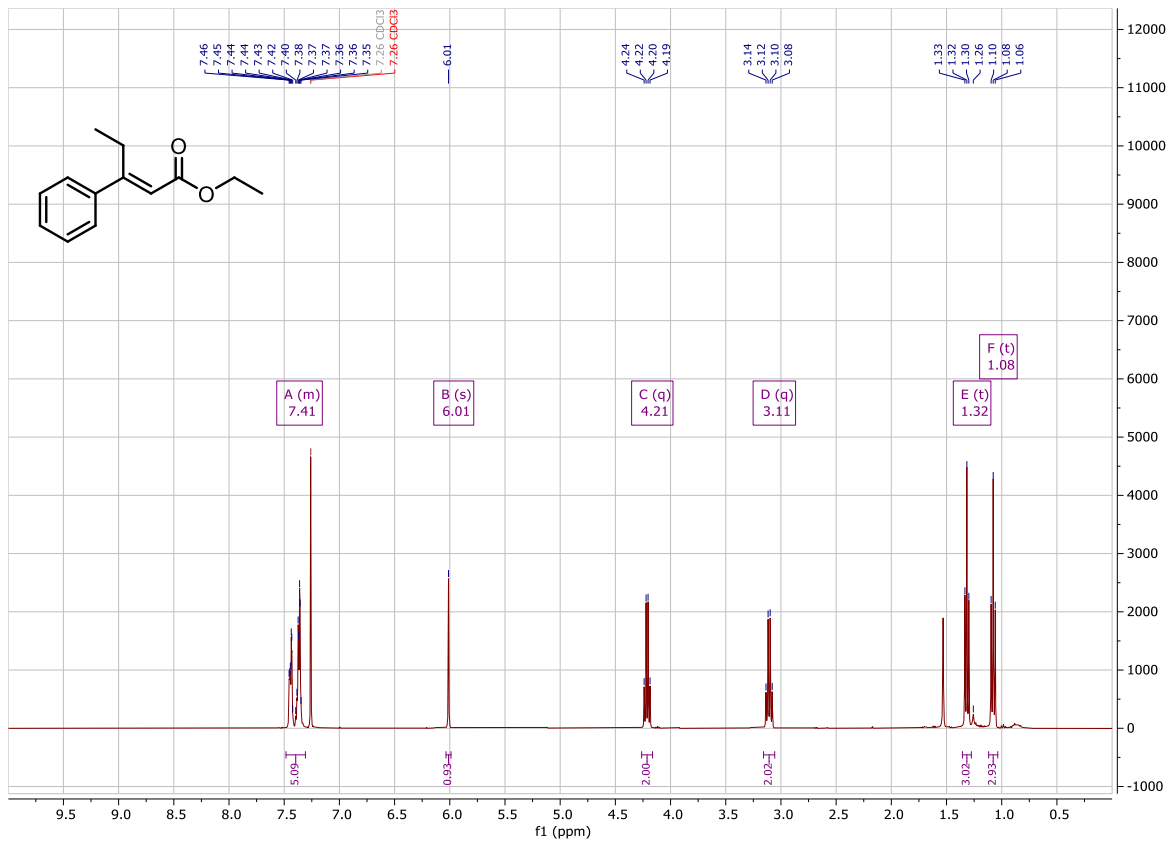


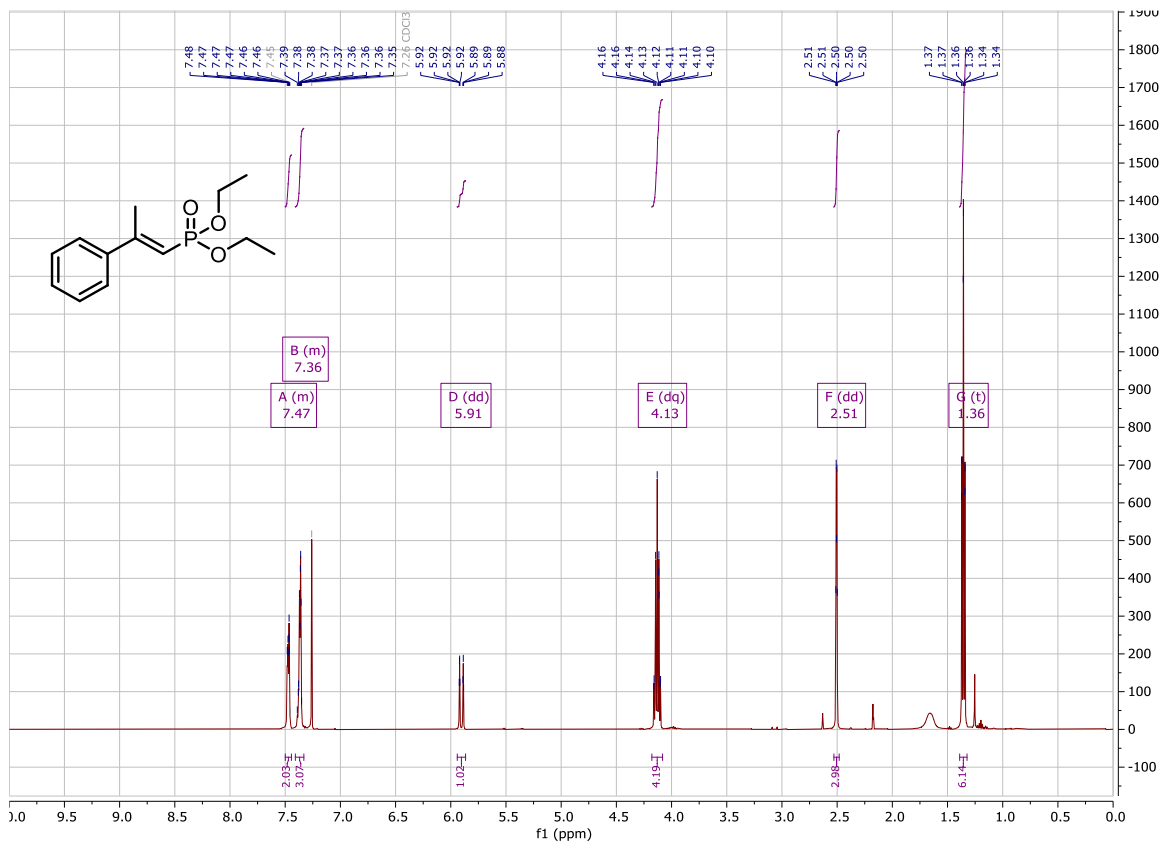
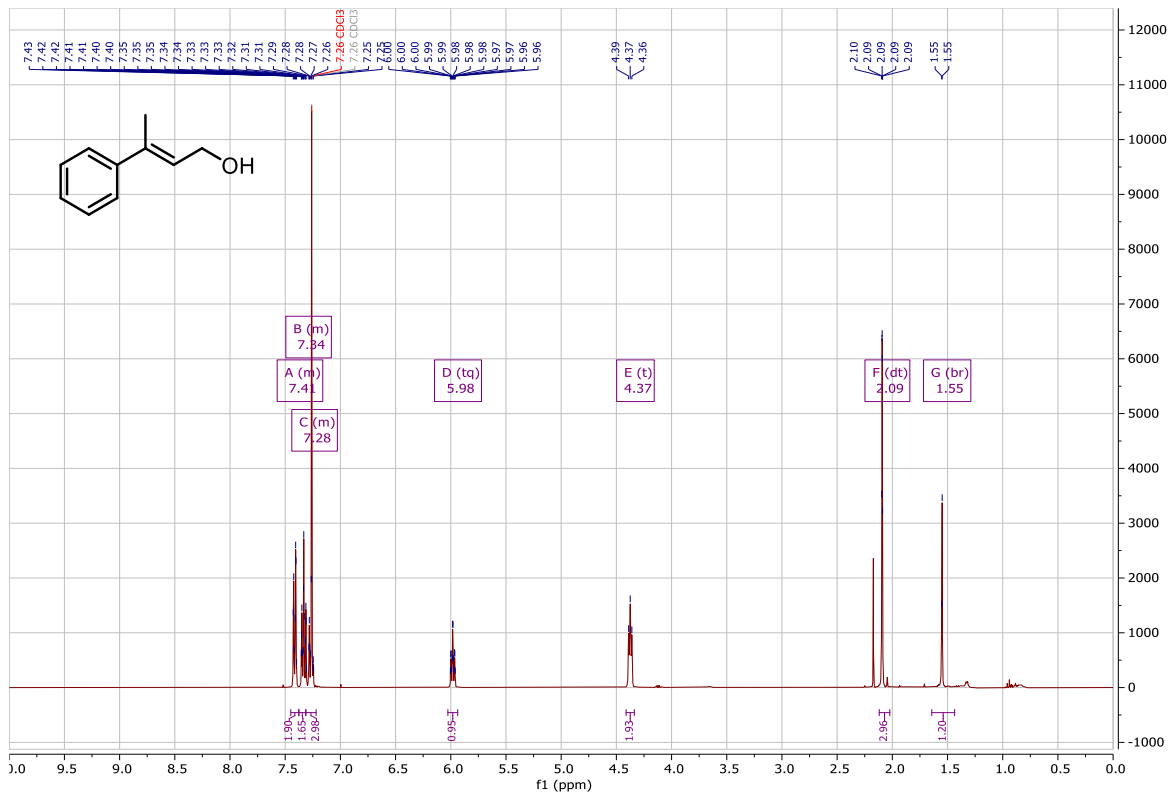


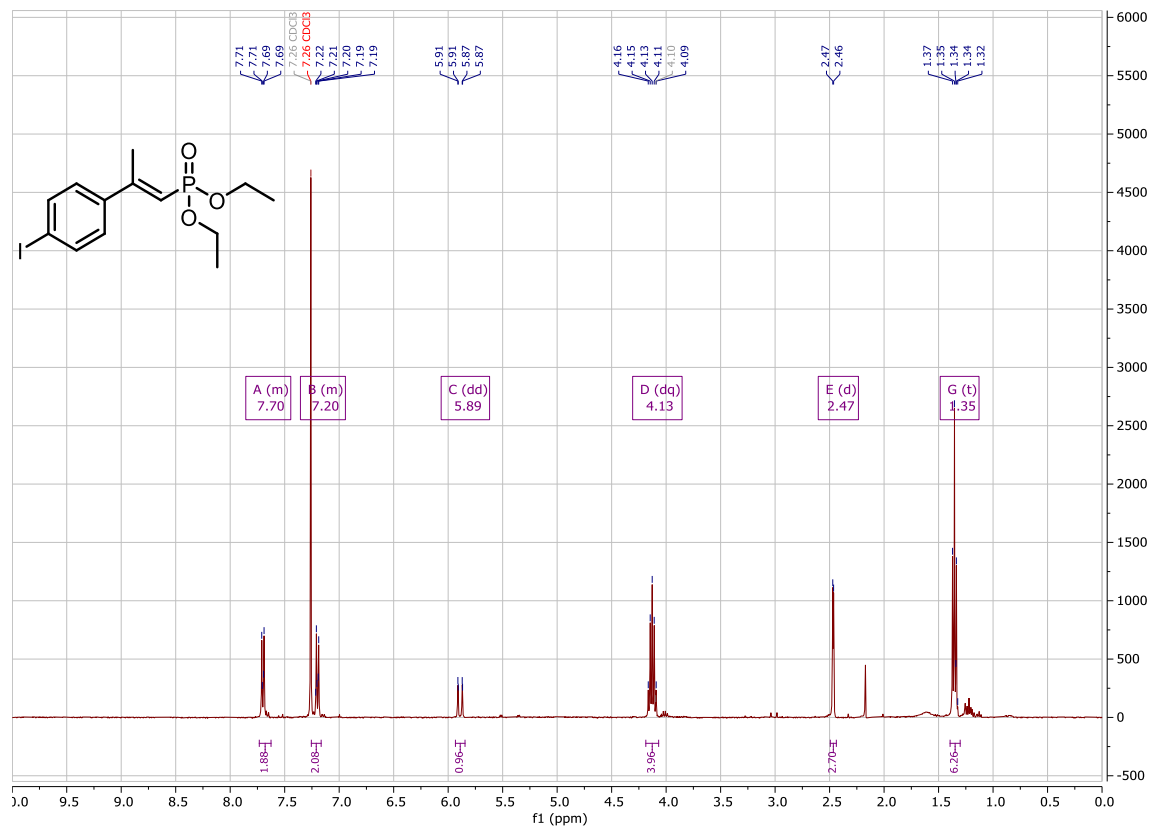
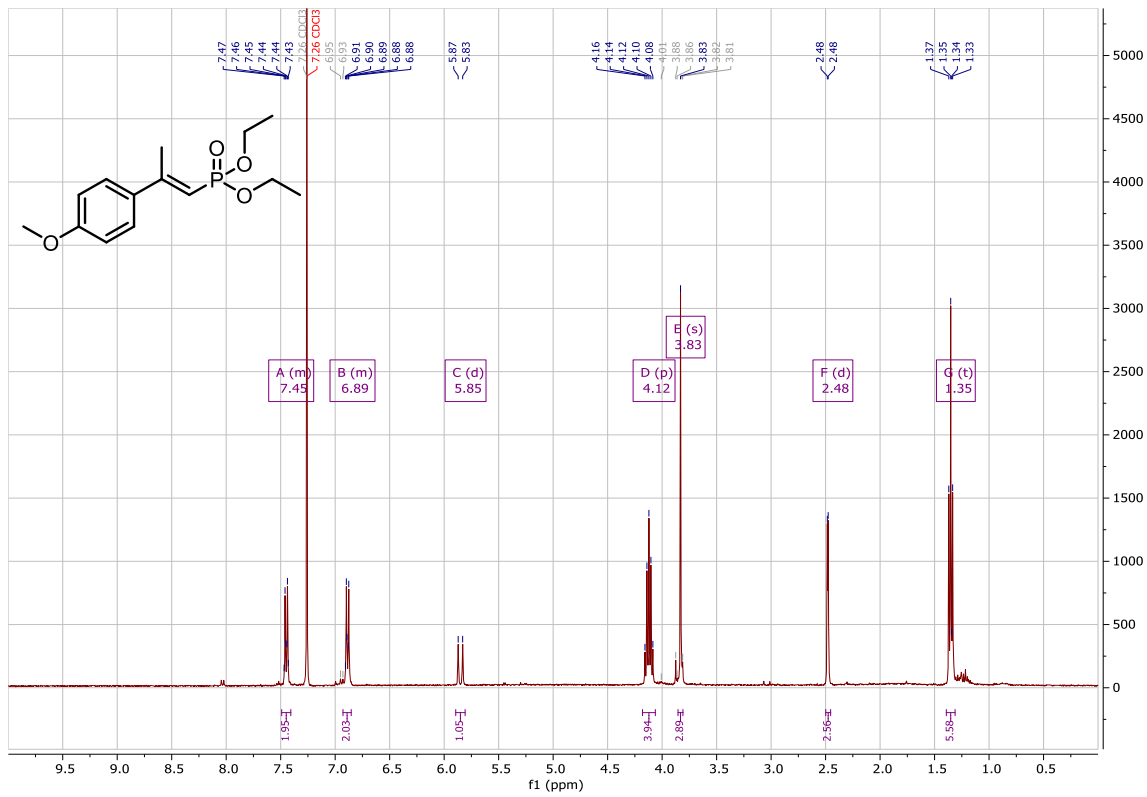


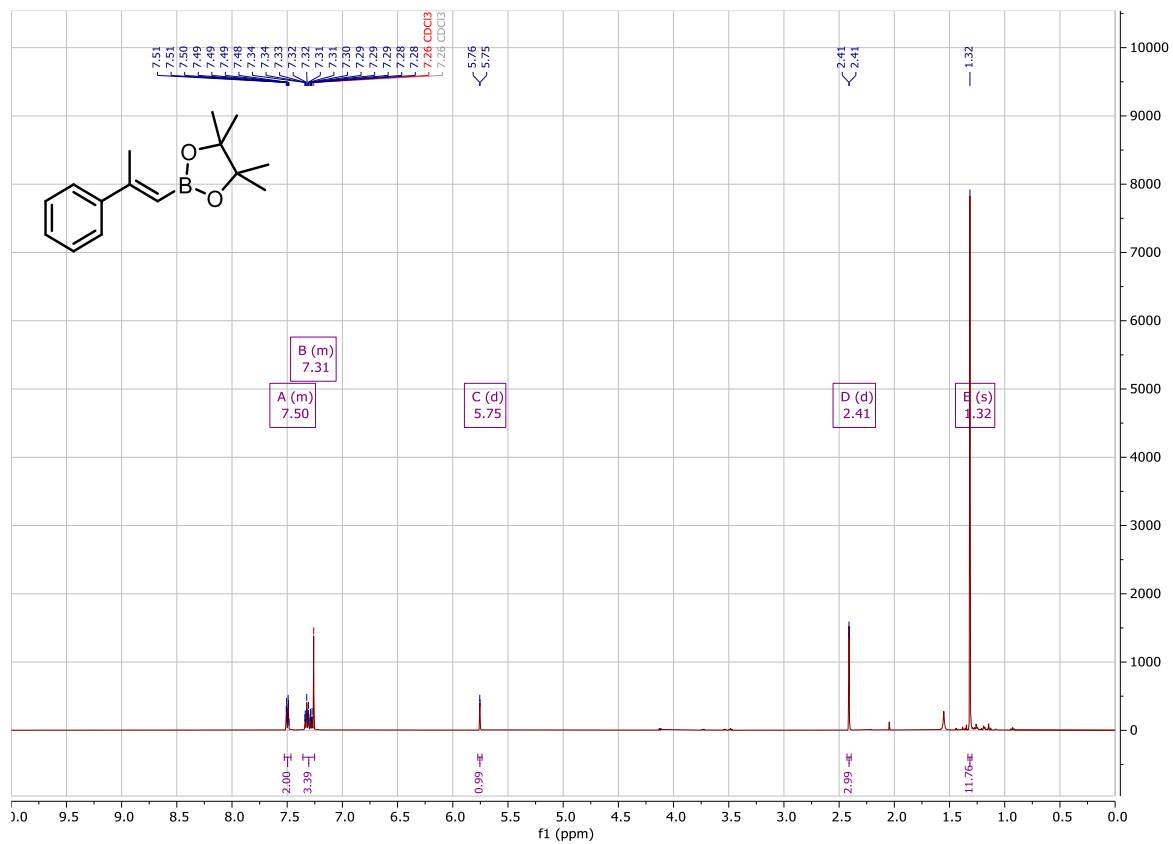
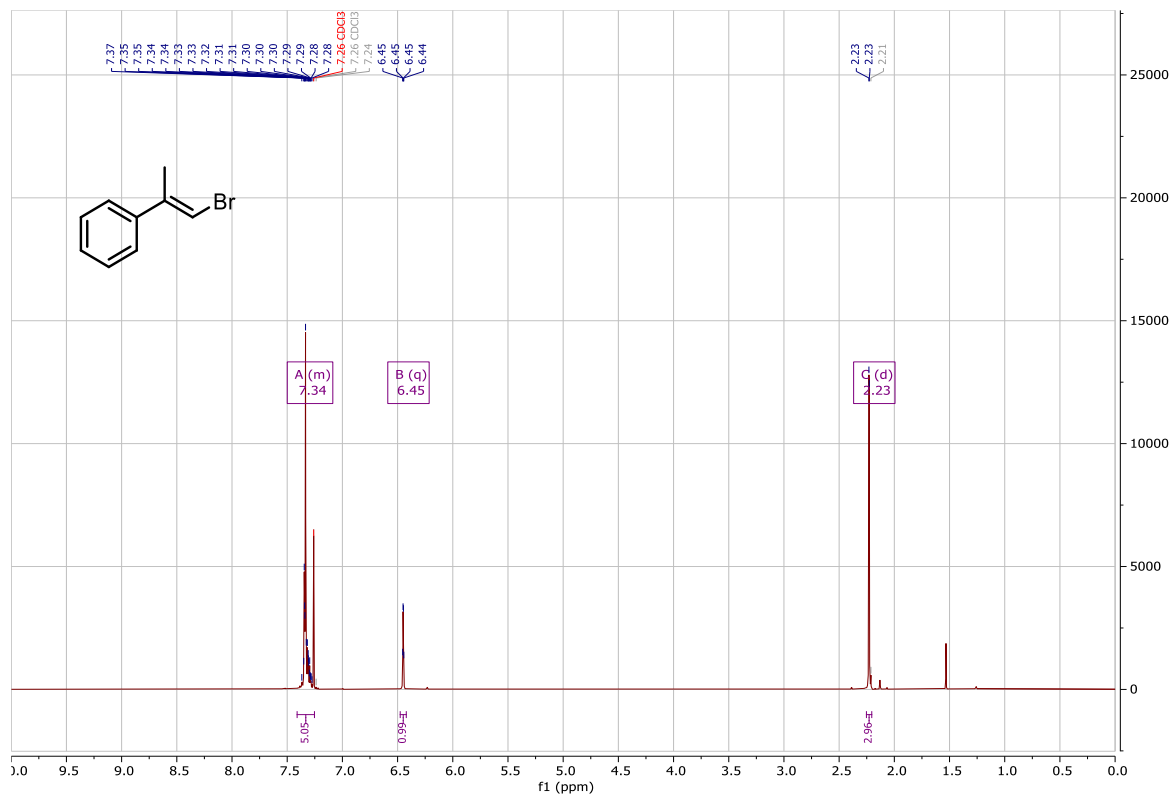


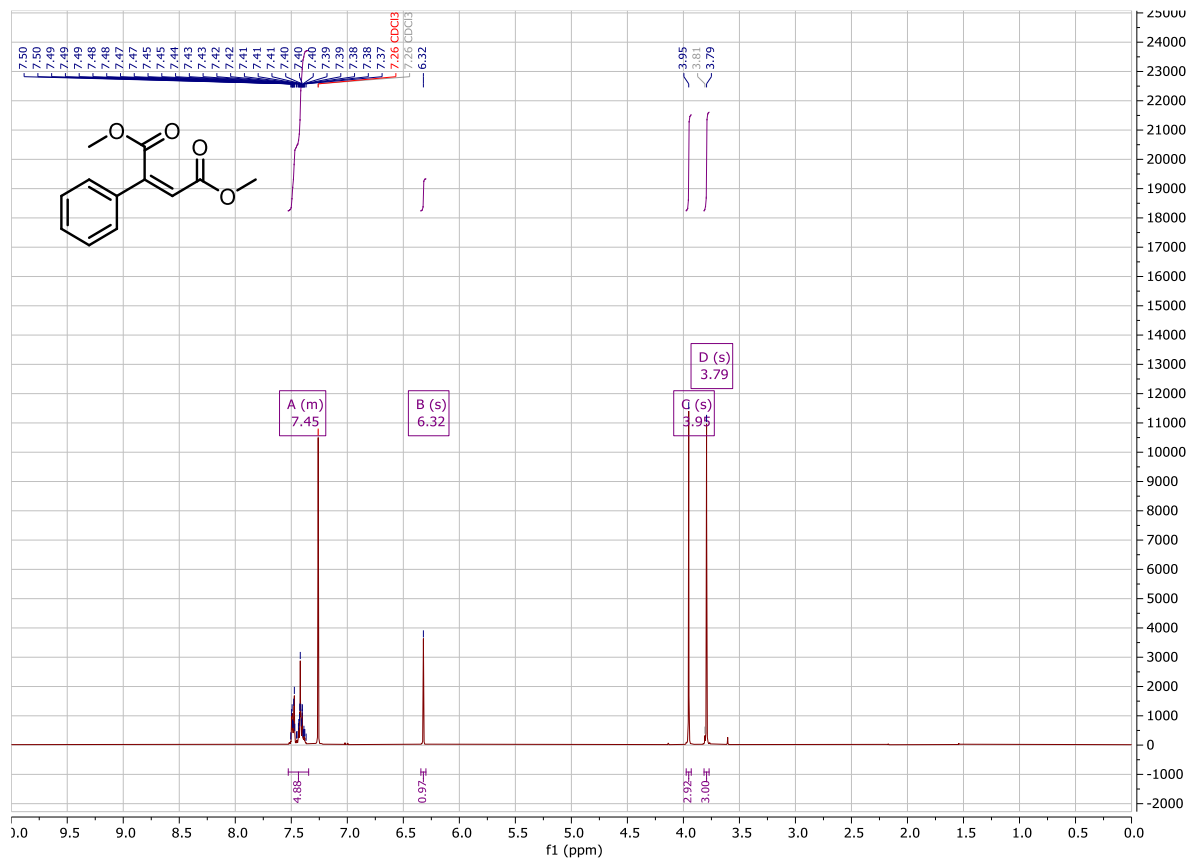
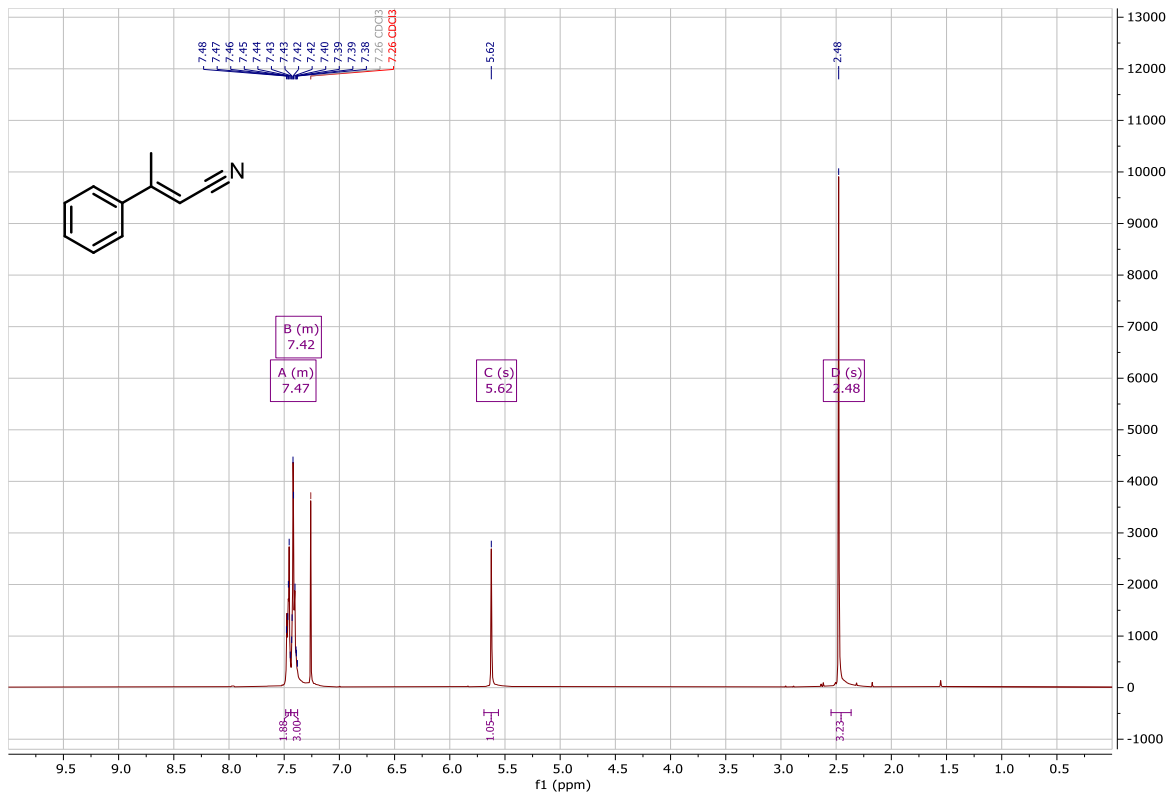


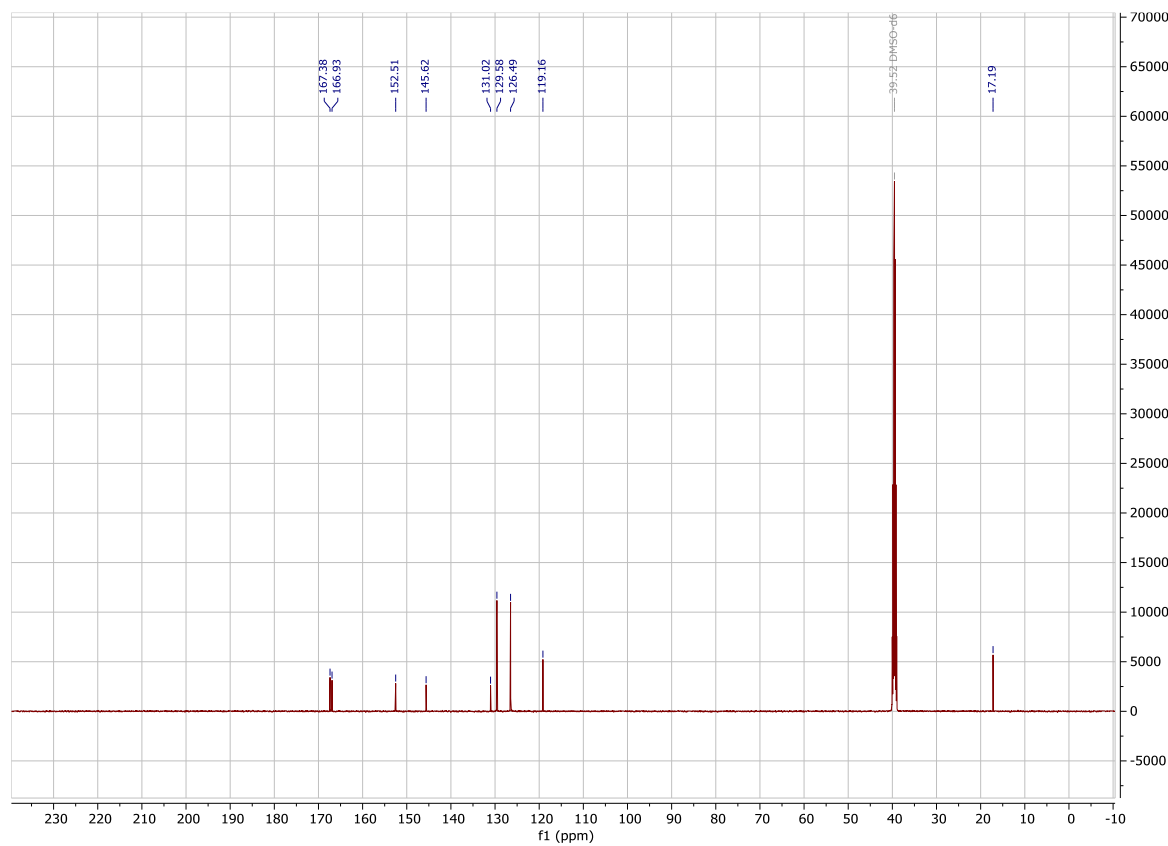
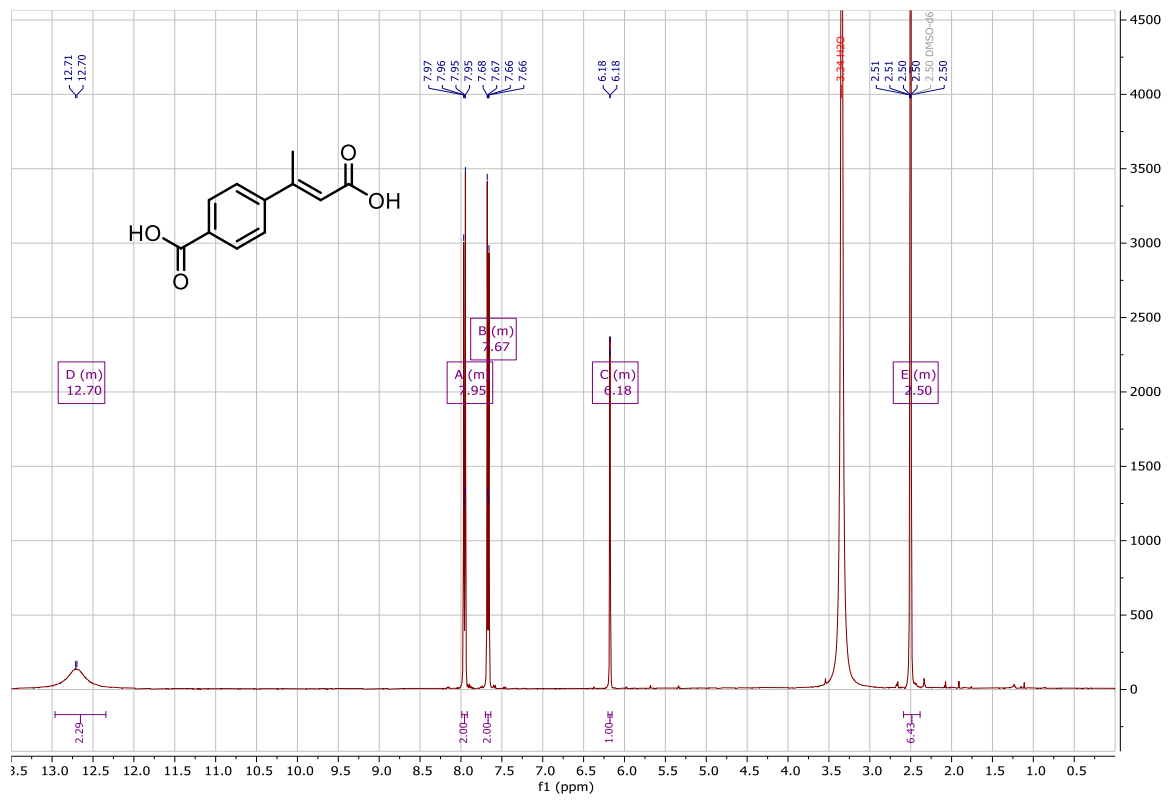


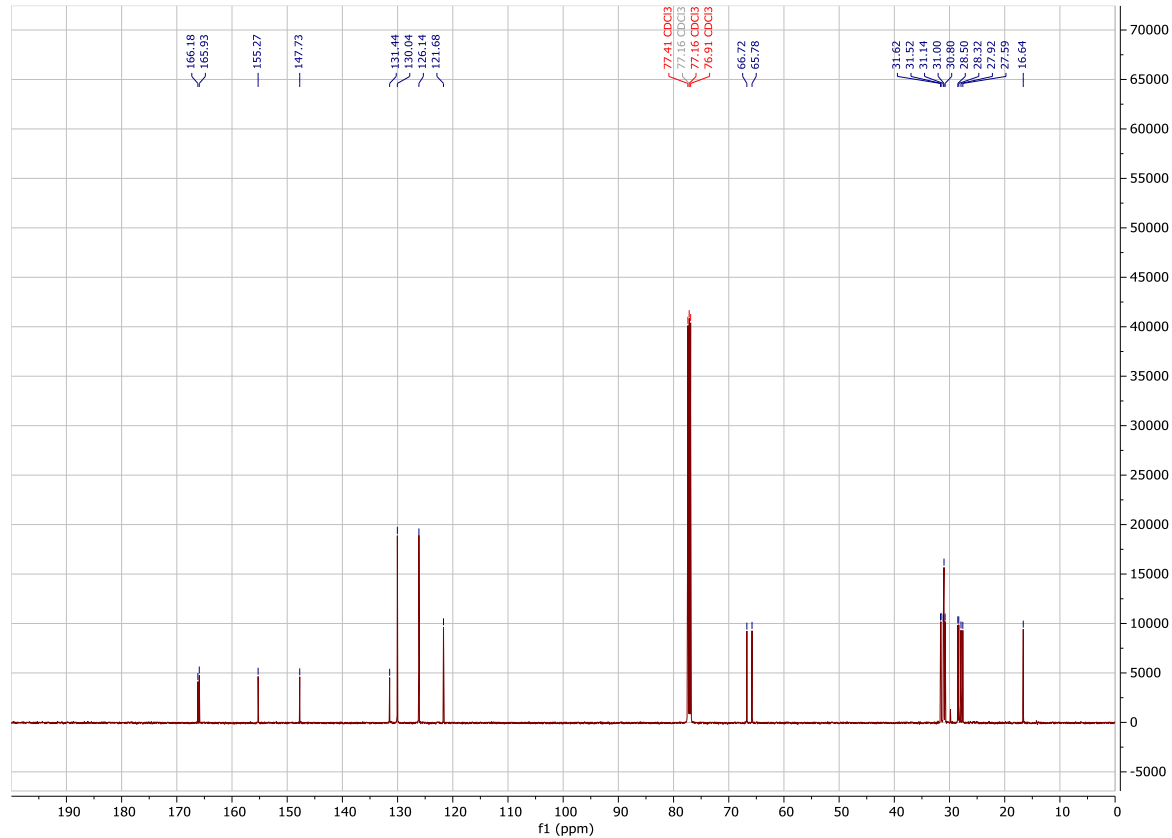
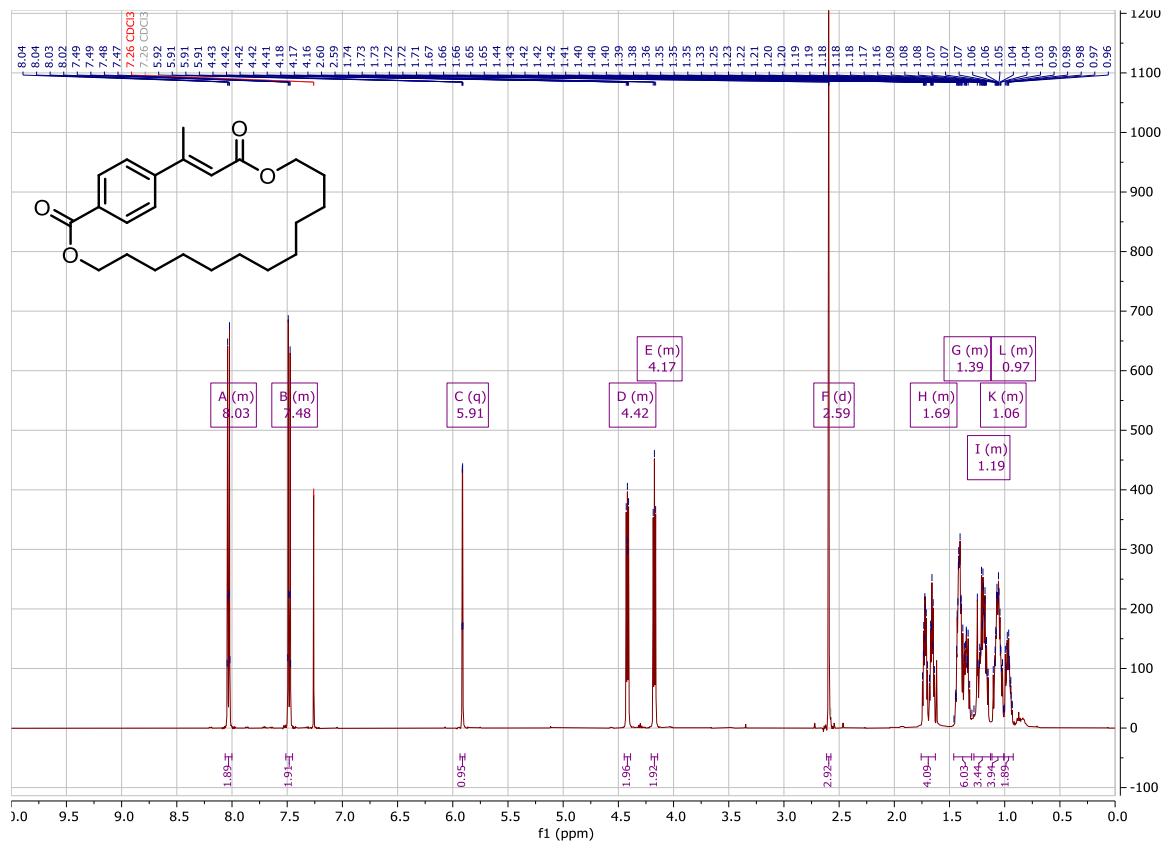


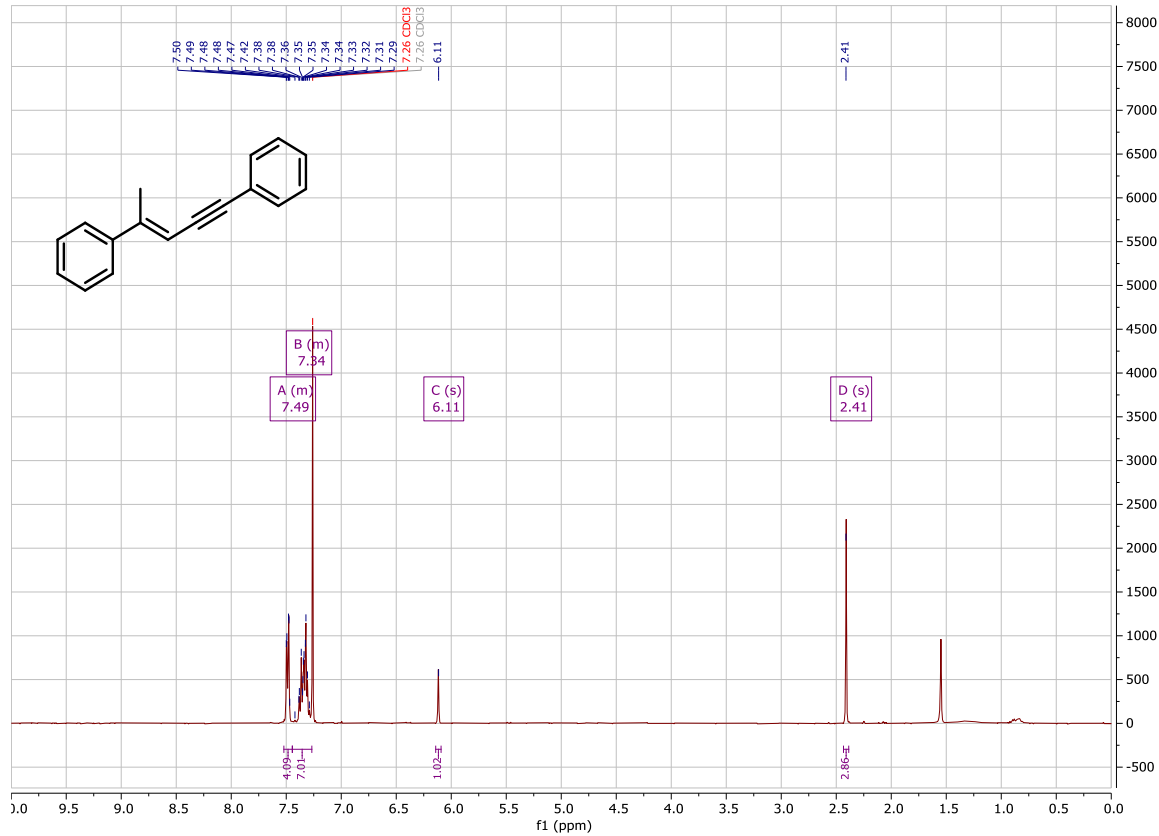
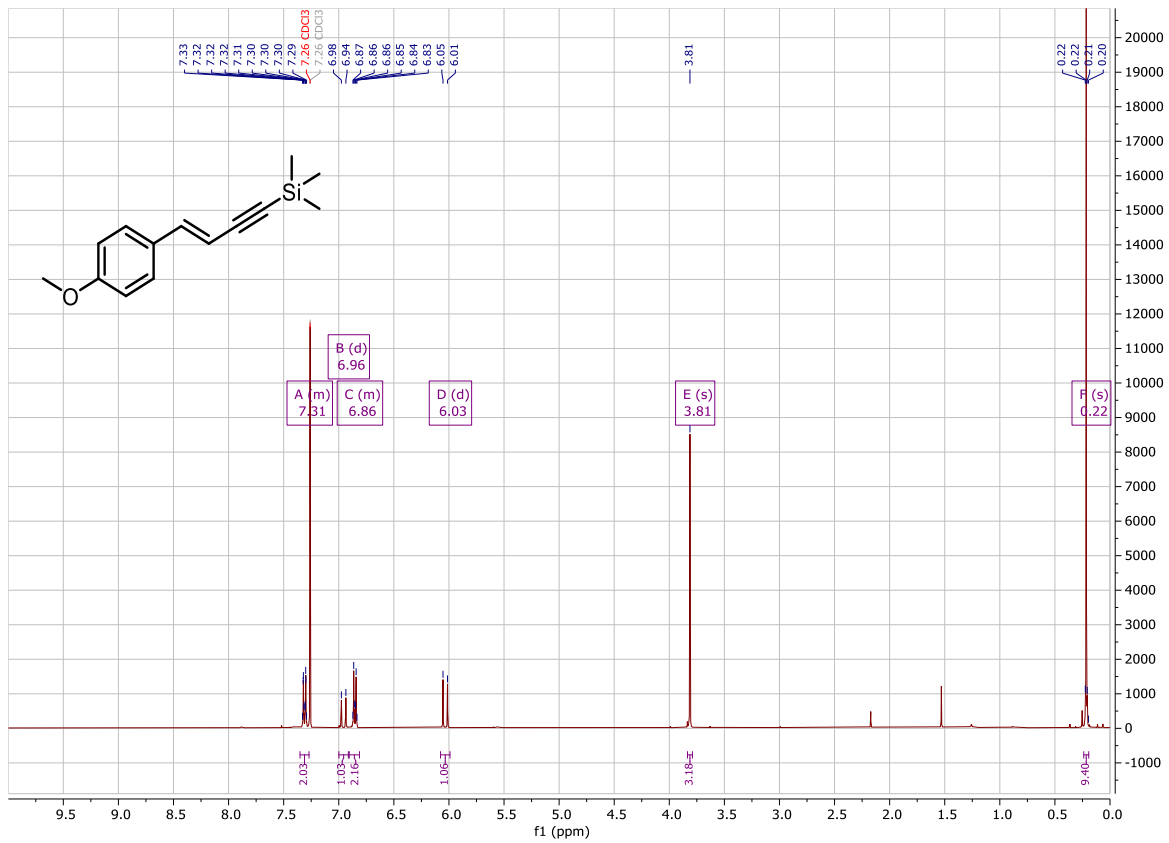








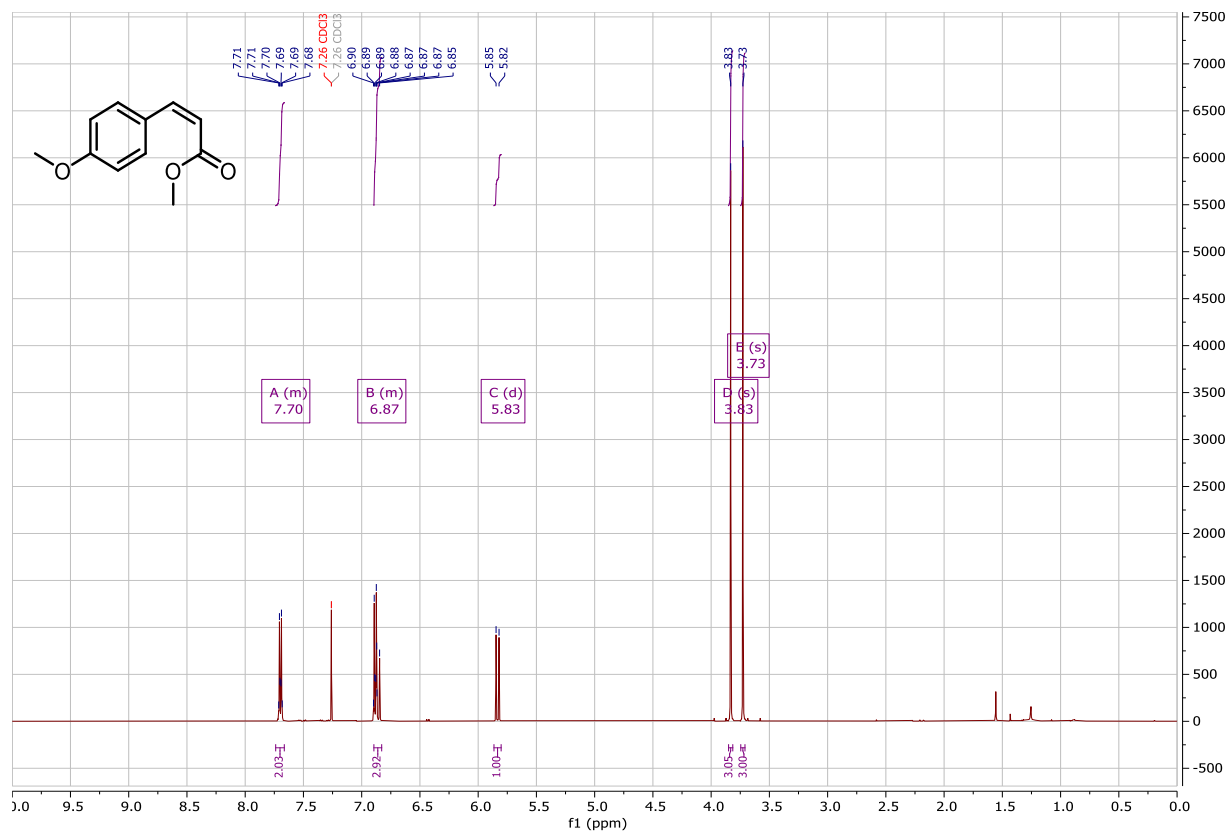


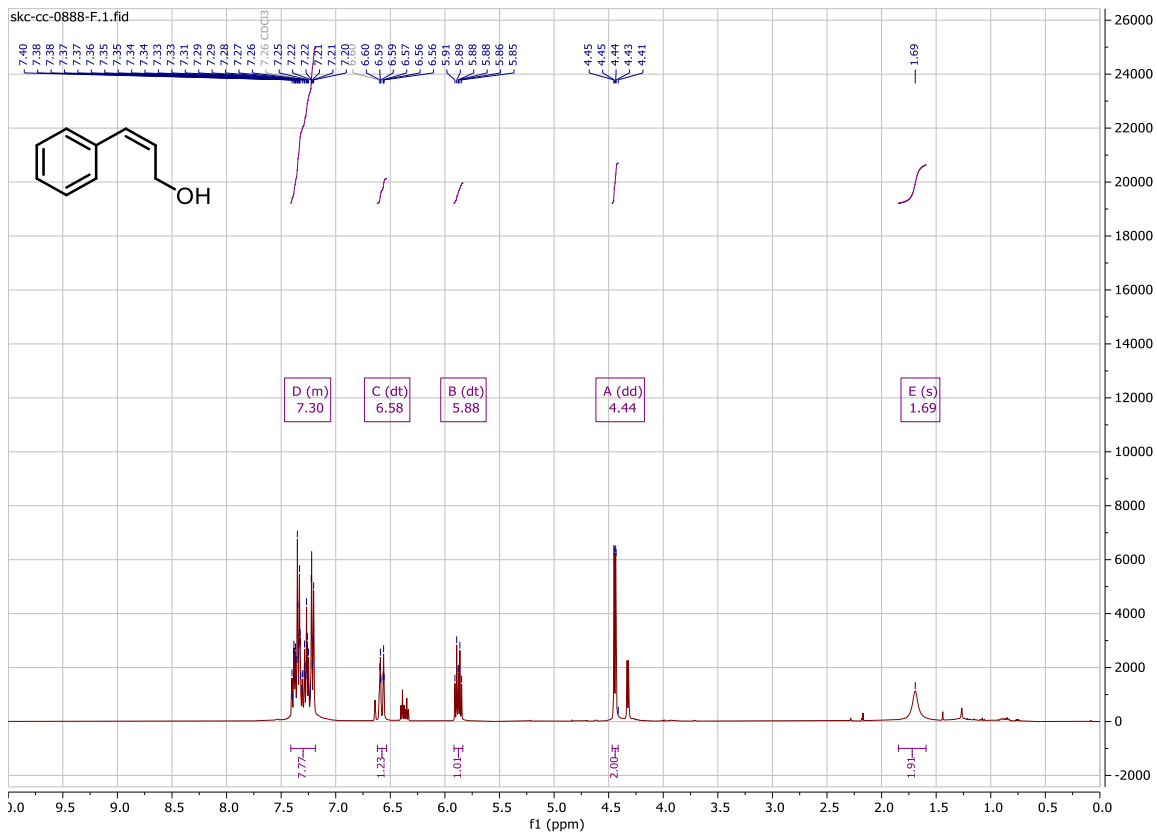
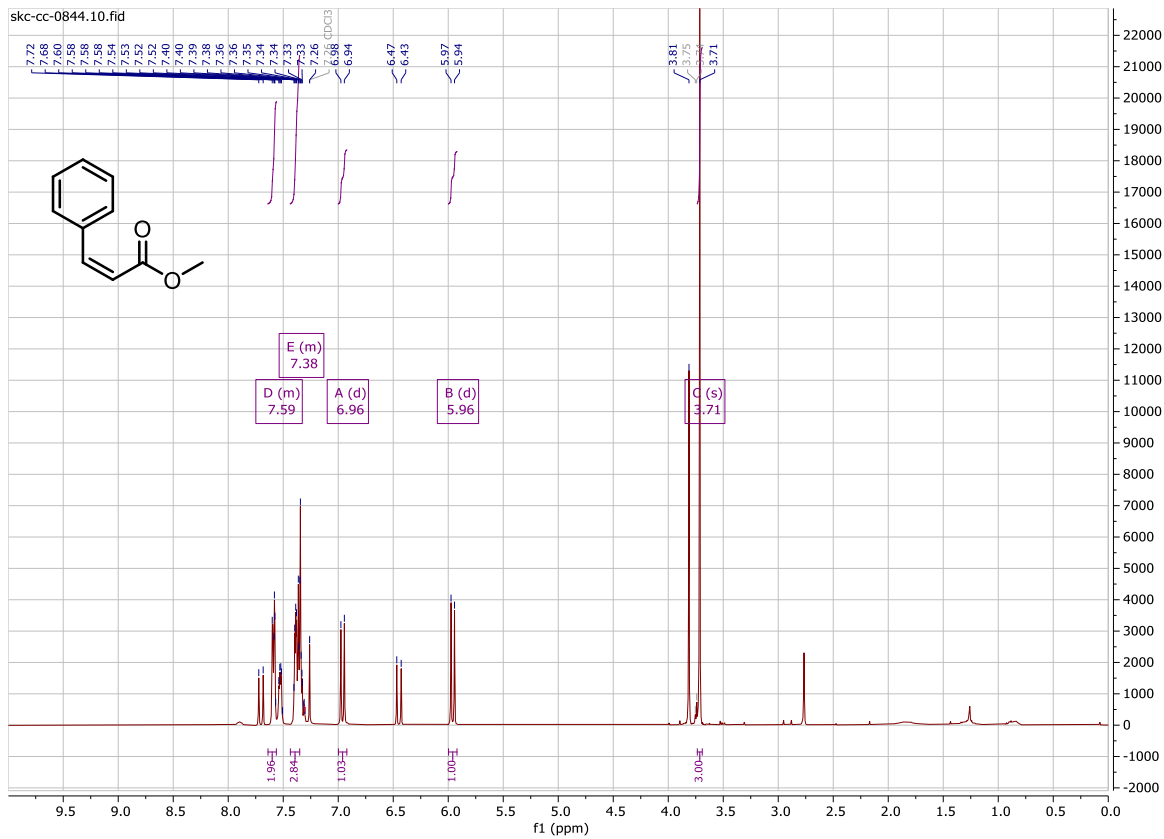


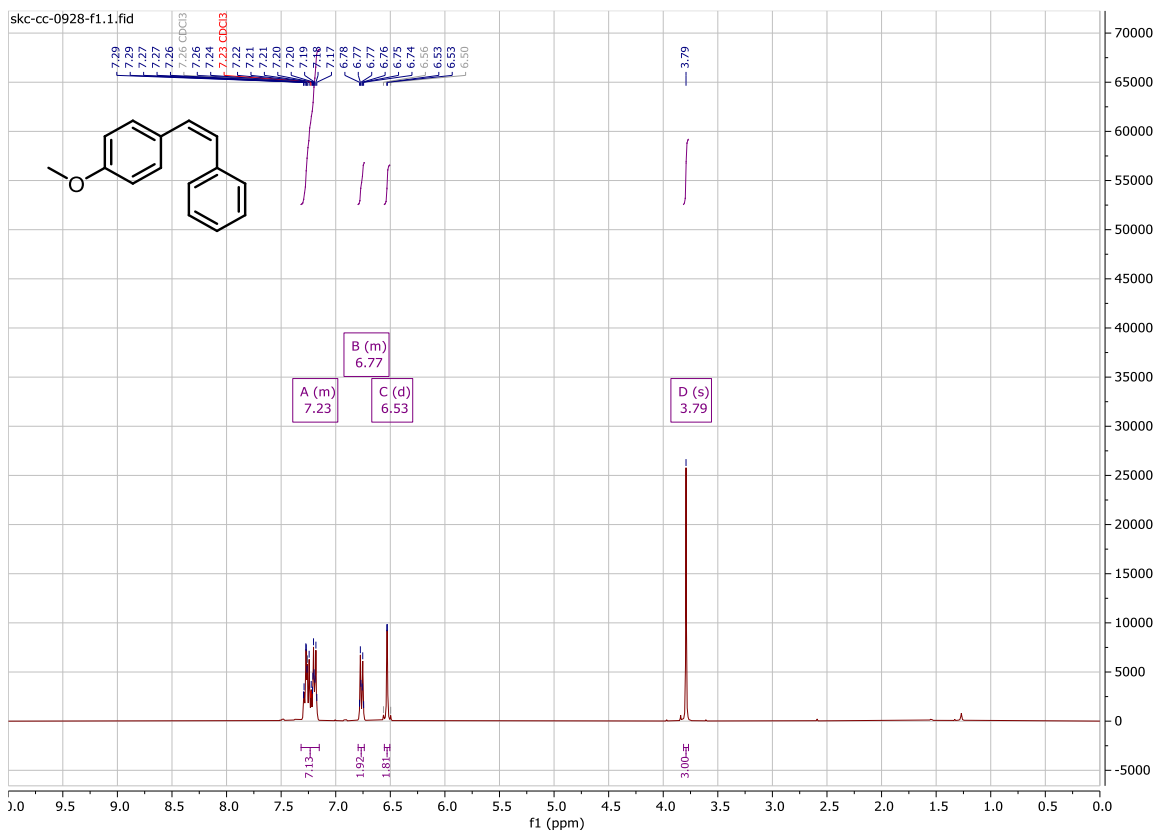
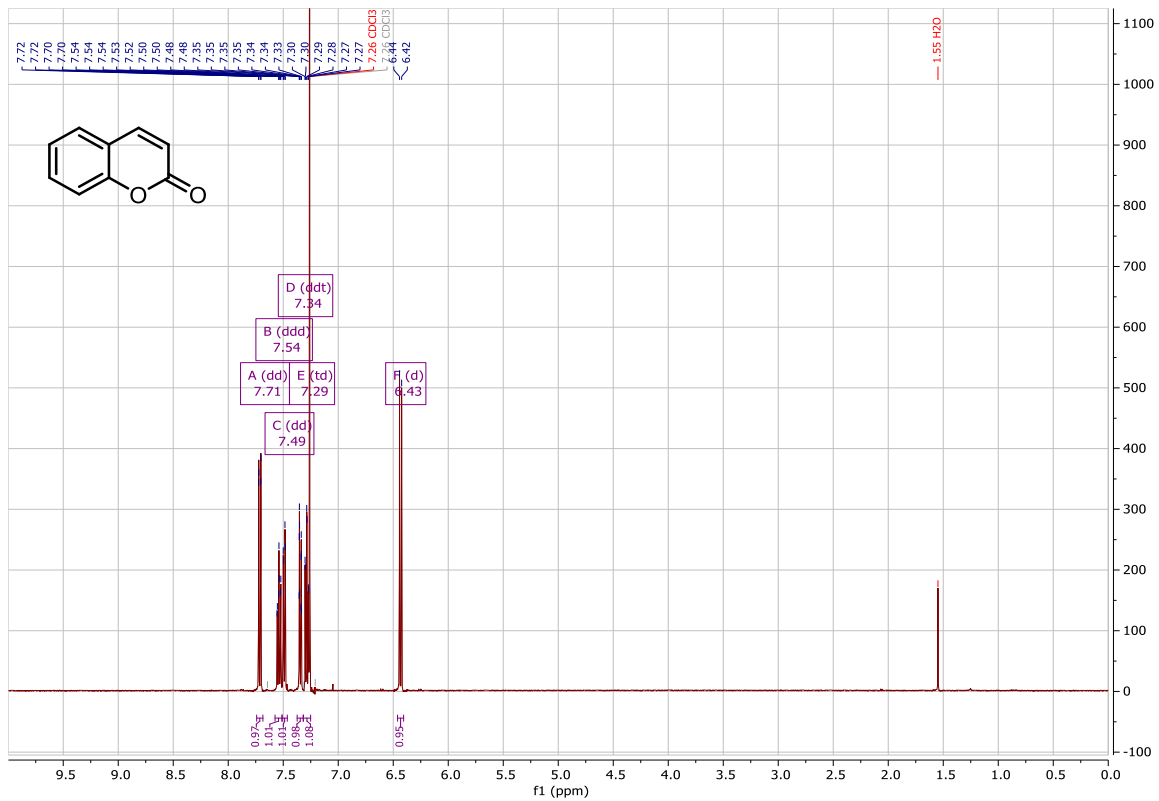
E/Z mixtures following isomerization.

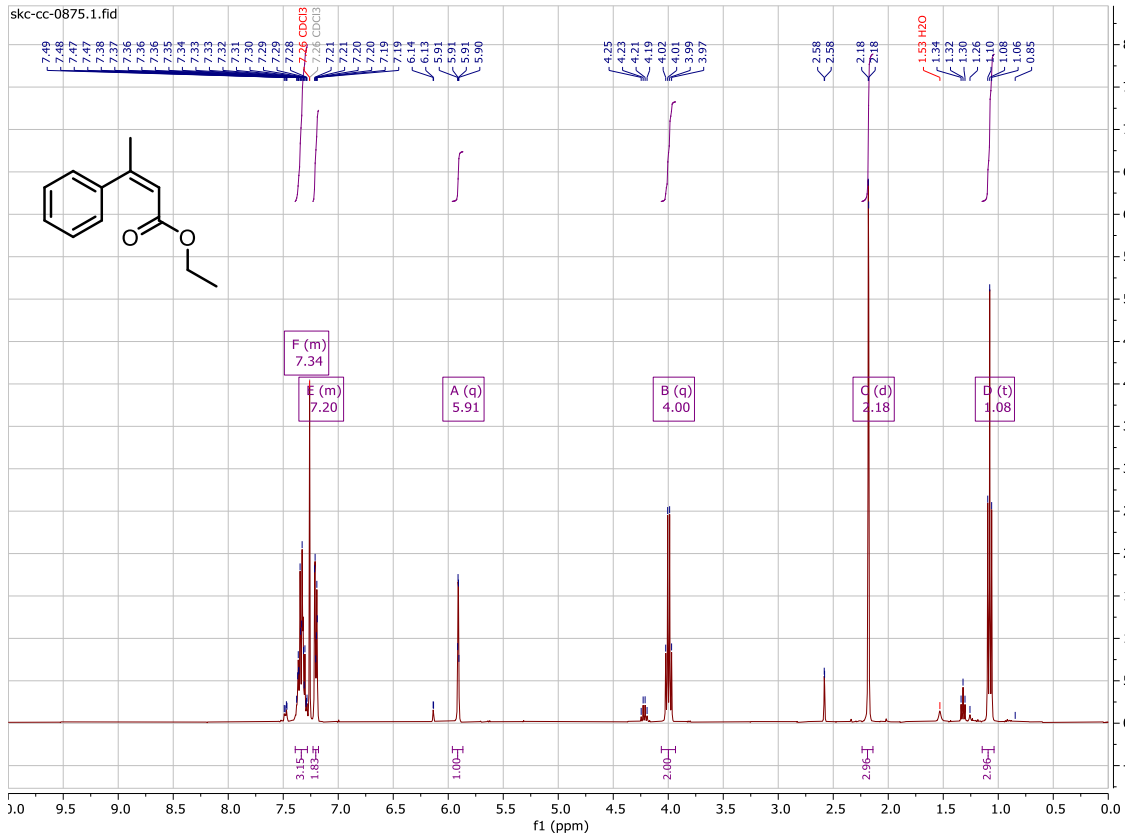
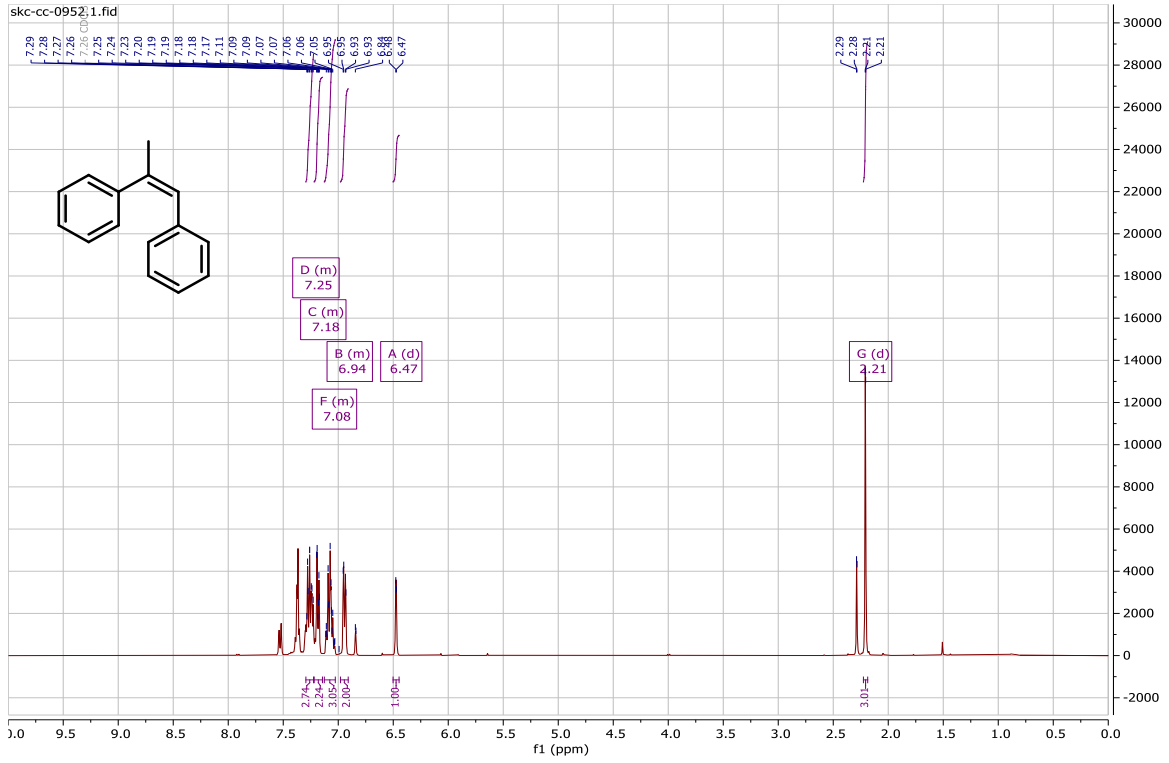
For previously reported compounds only the ^1H NMR is shown. For new compounds both the ^1H and ^{13}C NMR spectra are provided :

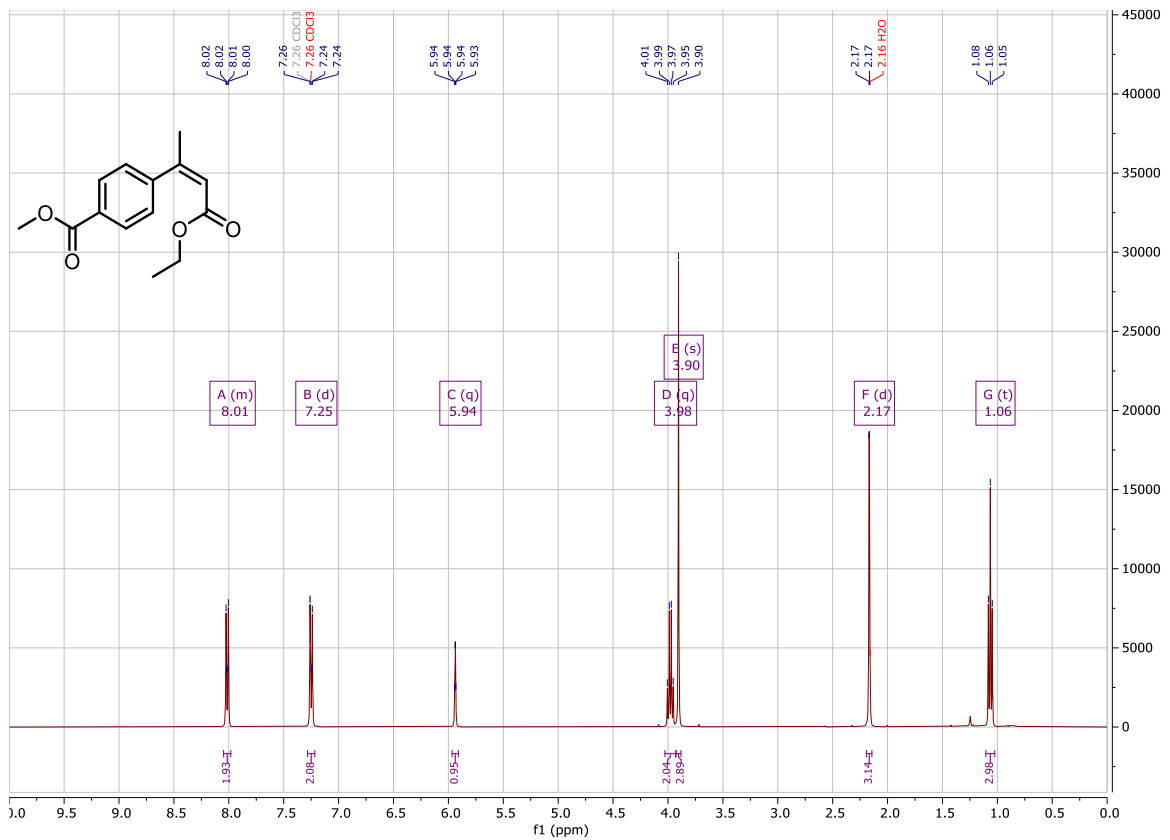
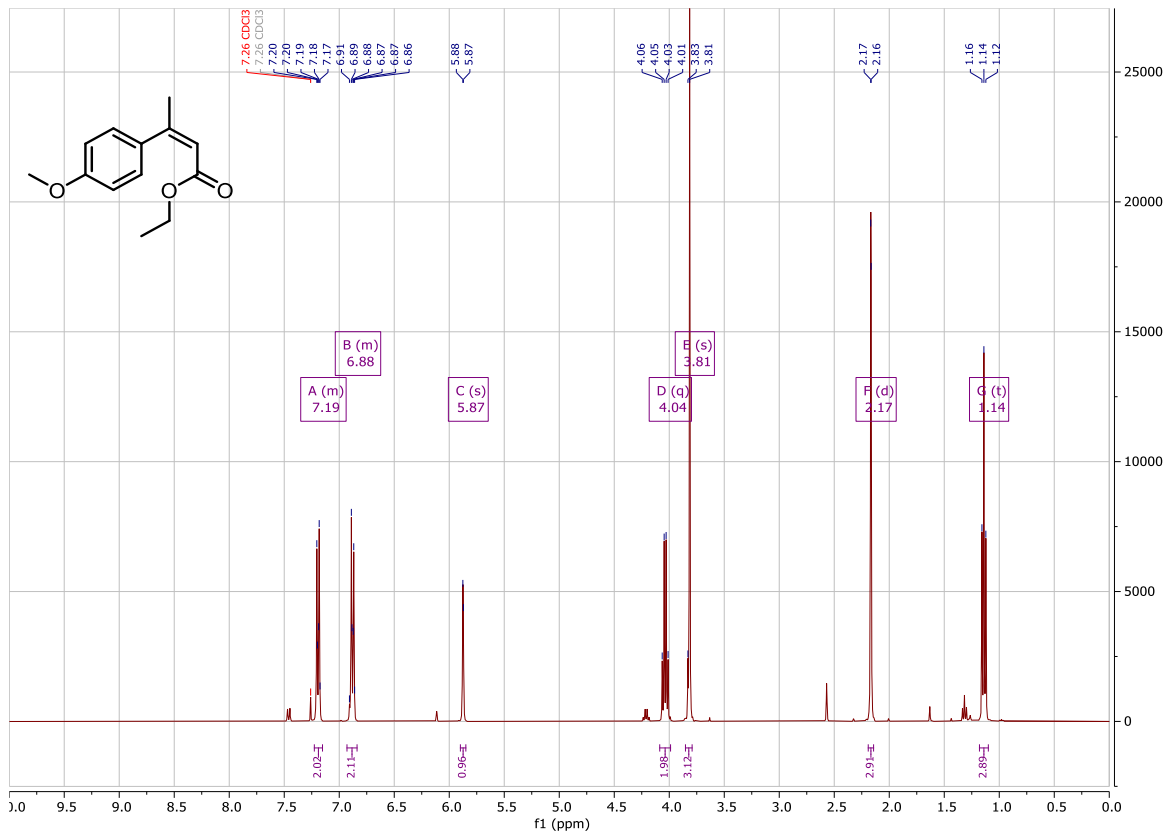
Methyl (*Z*)-3-(4-methoxyphenyl)acrylate:

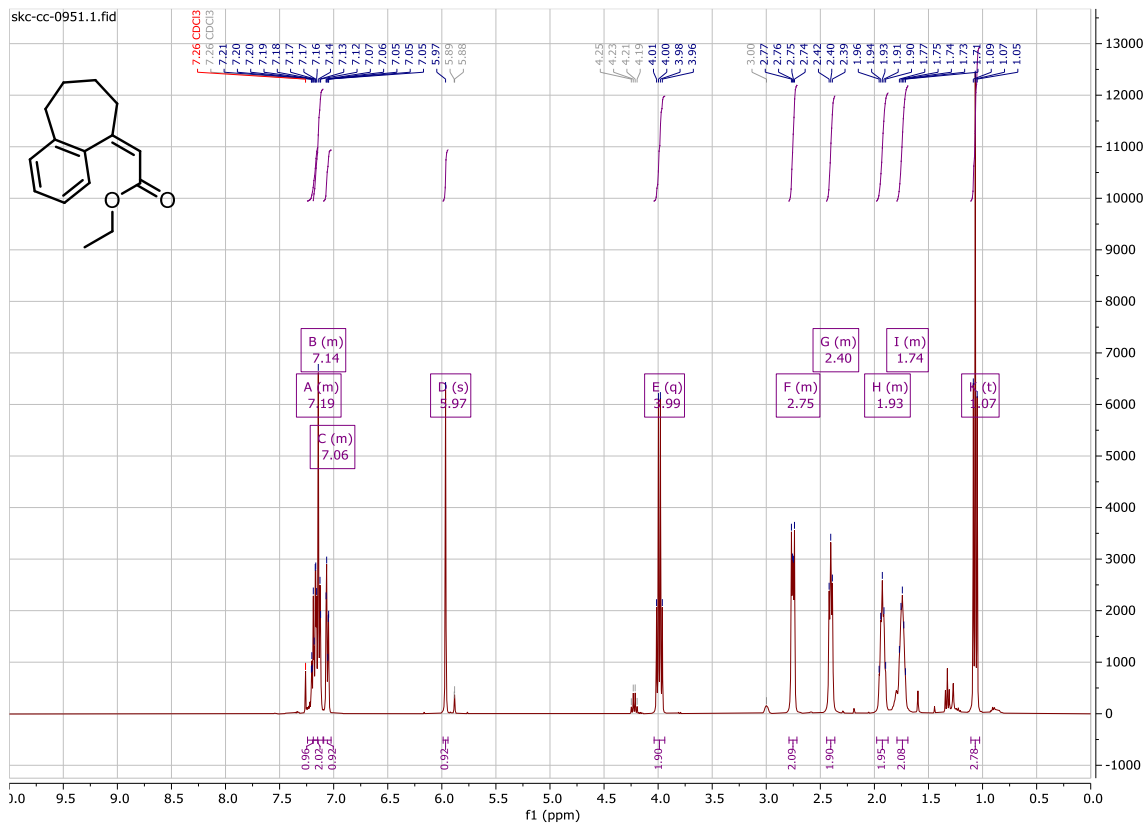
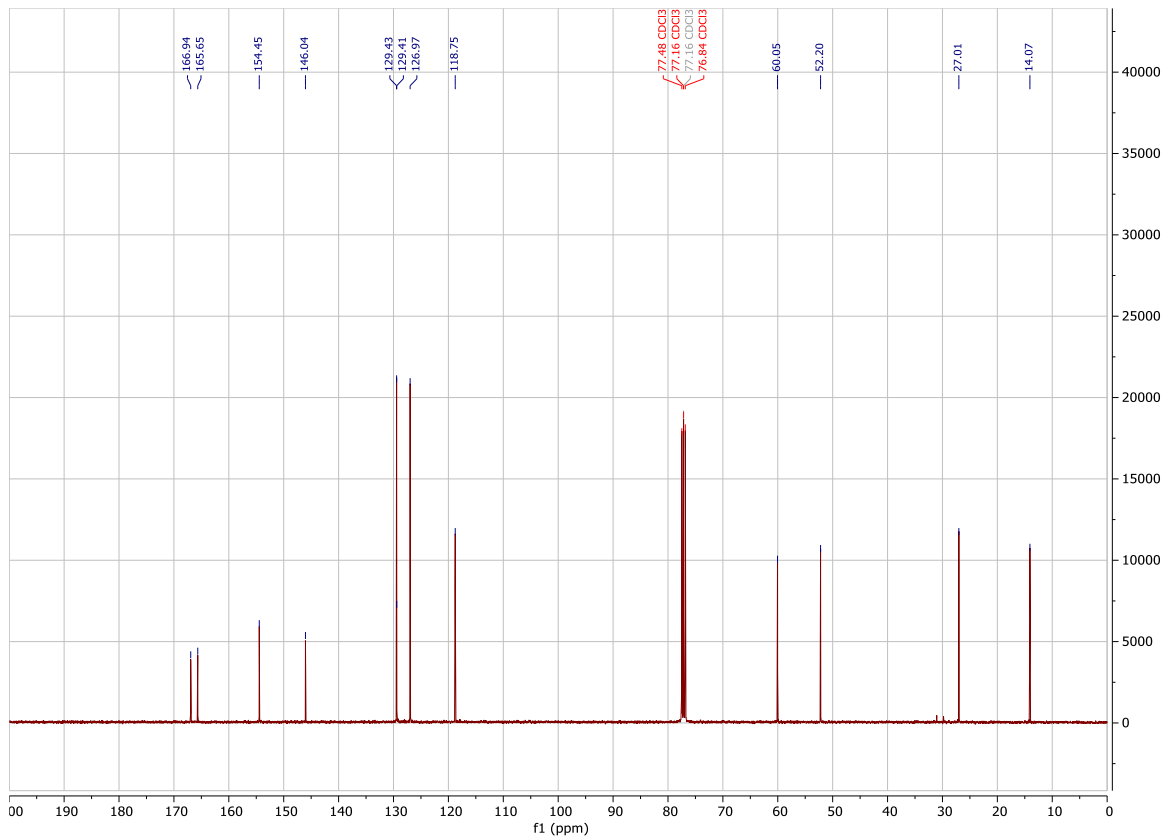


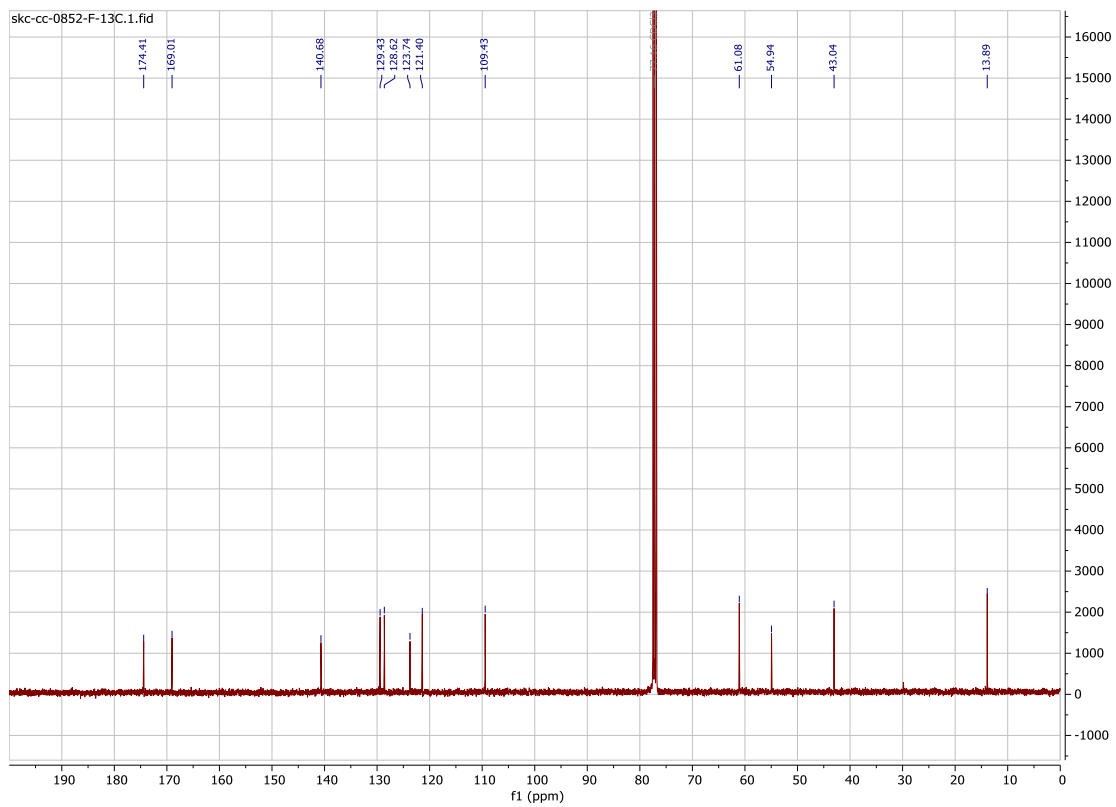
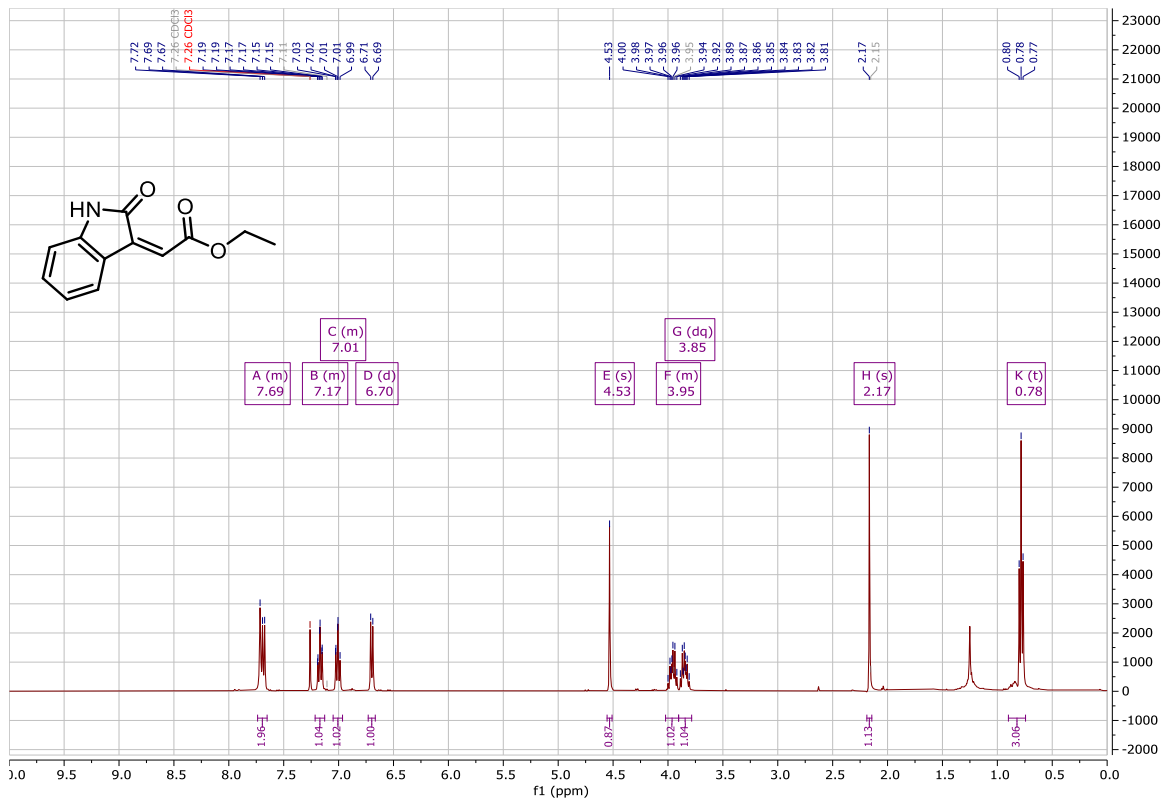


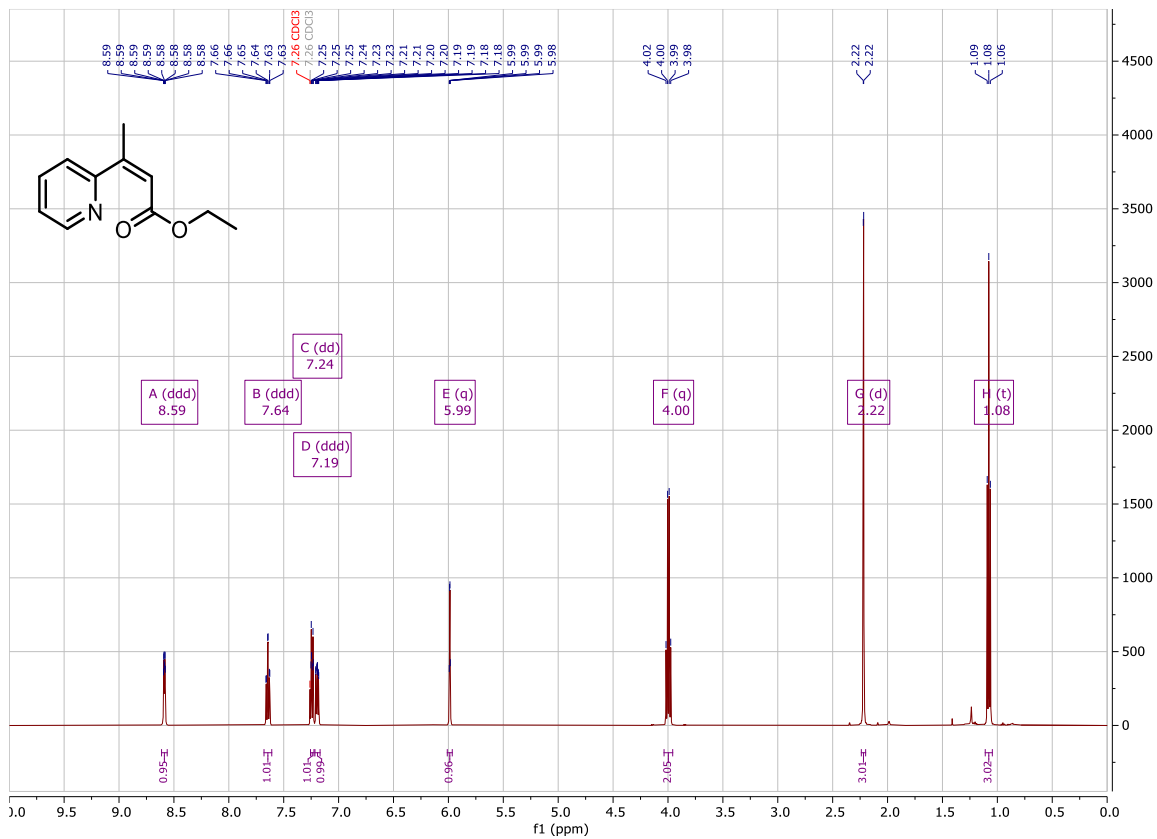
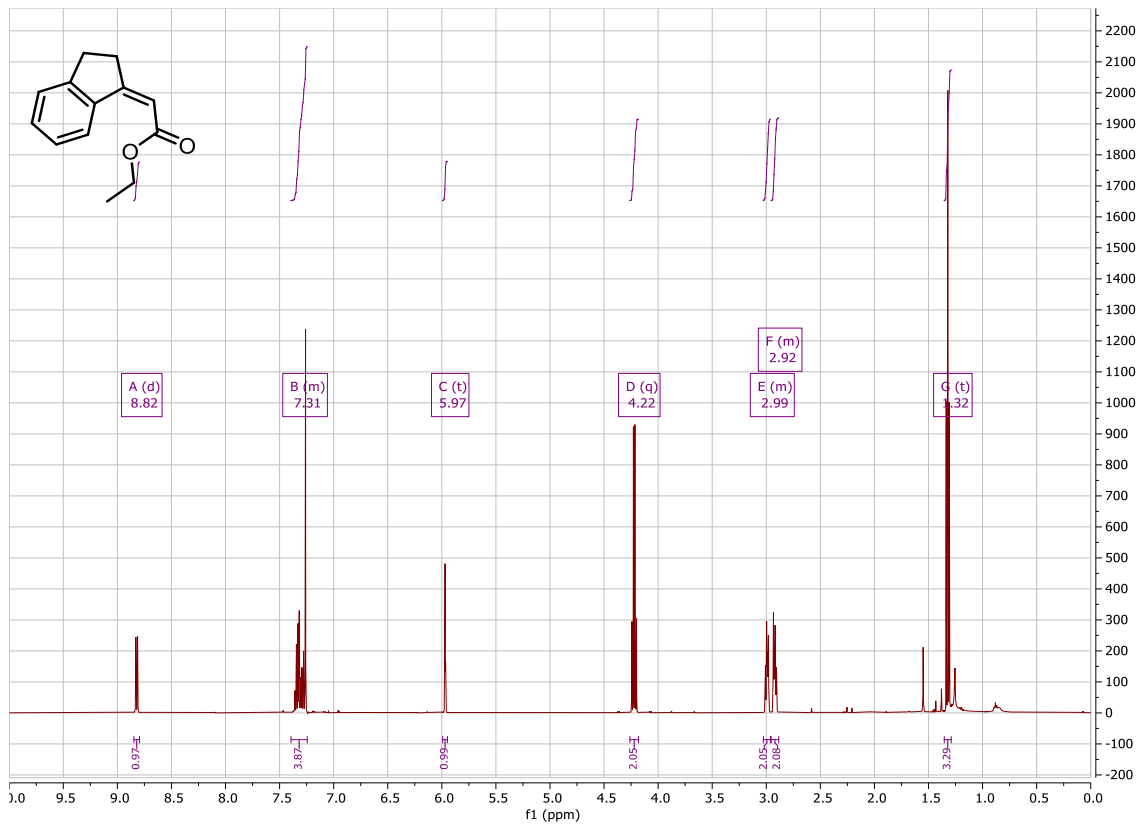


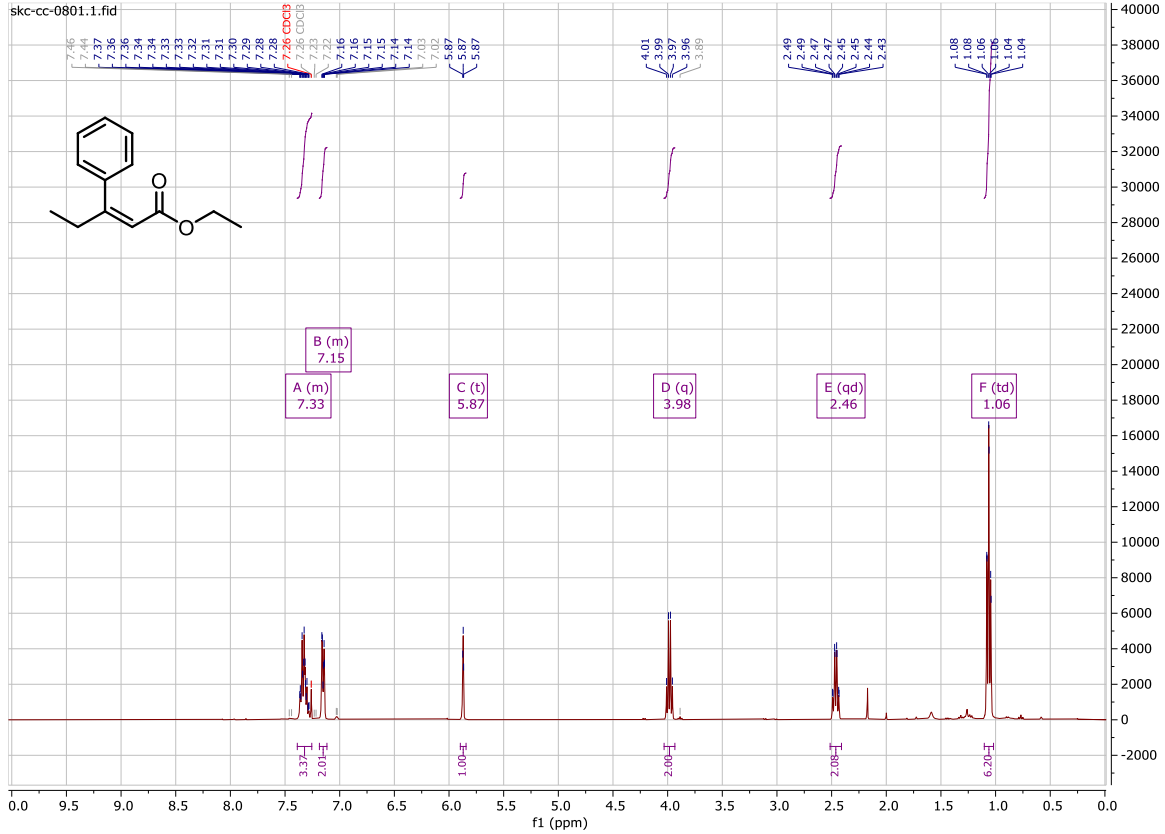
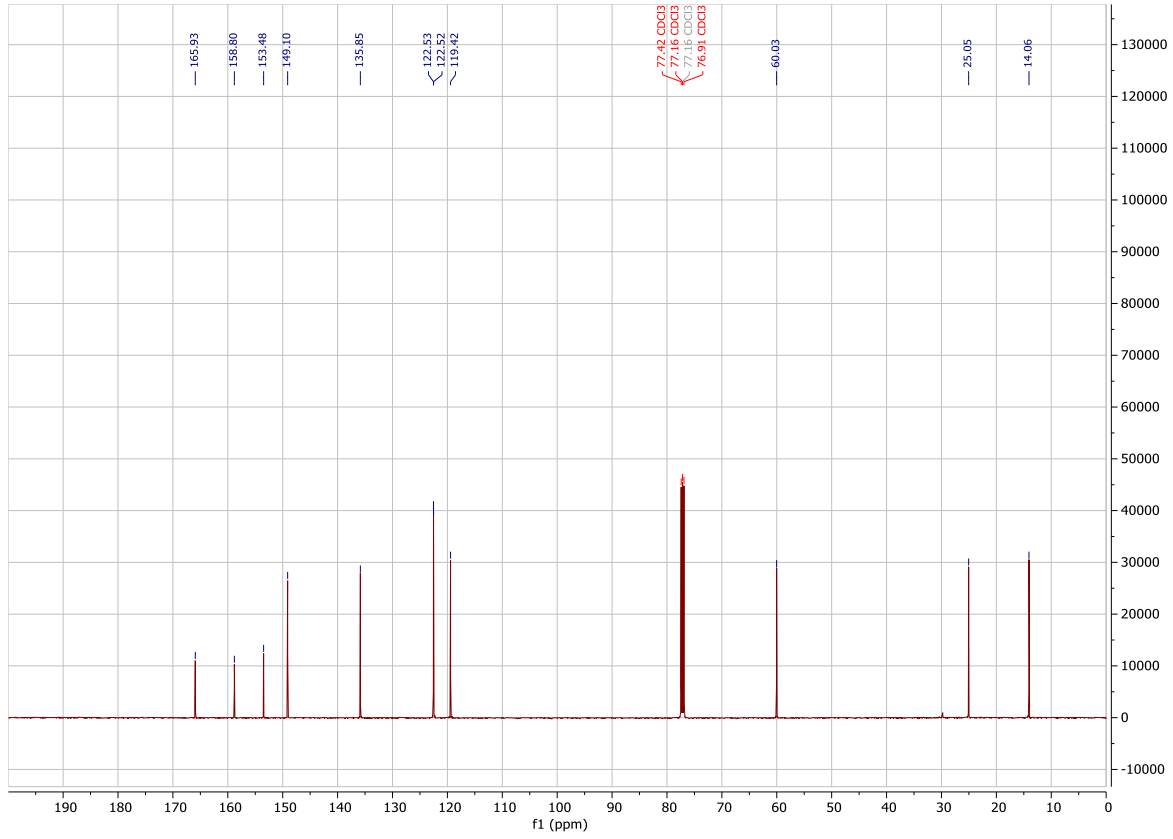


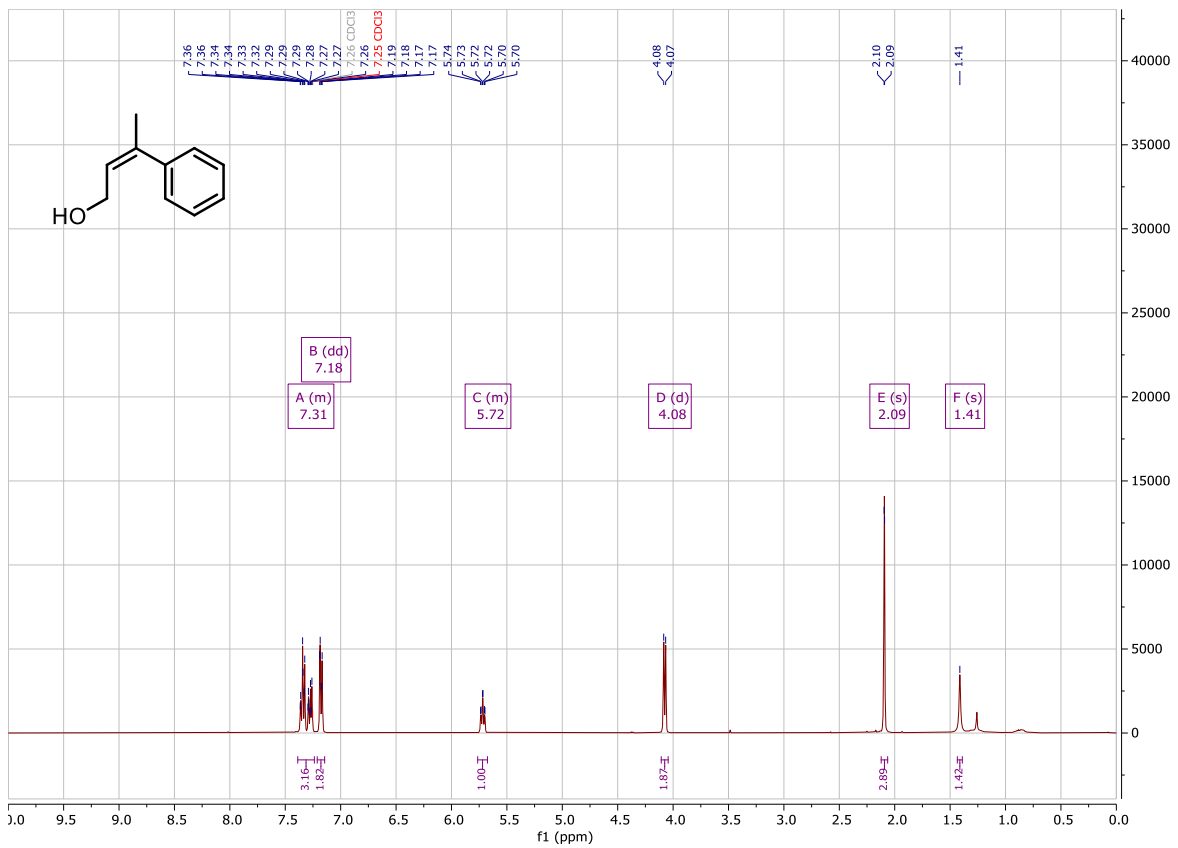
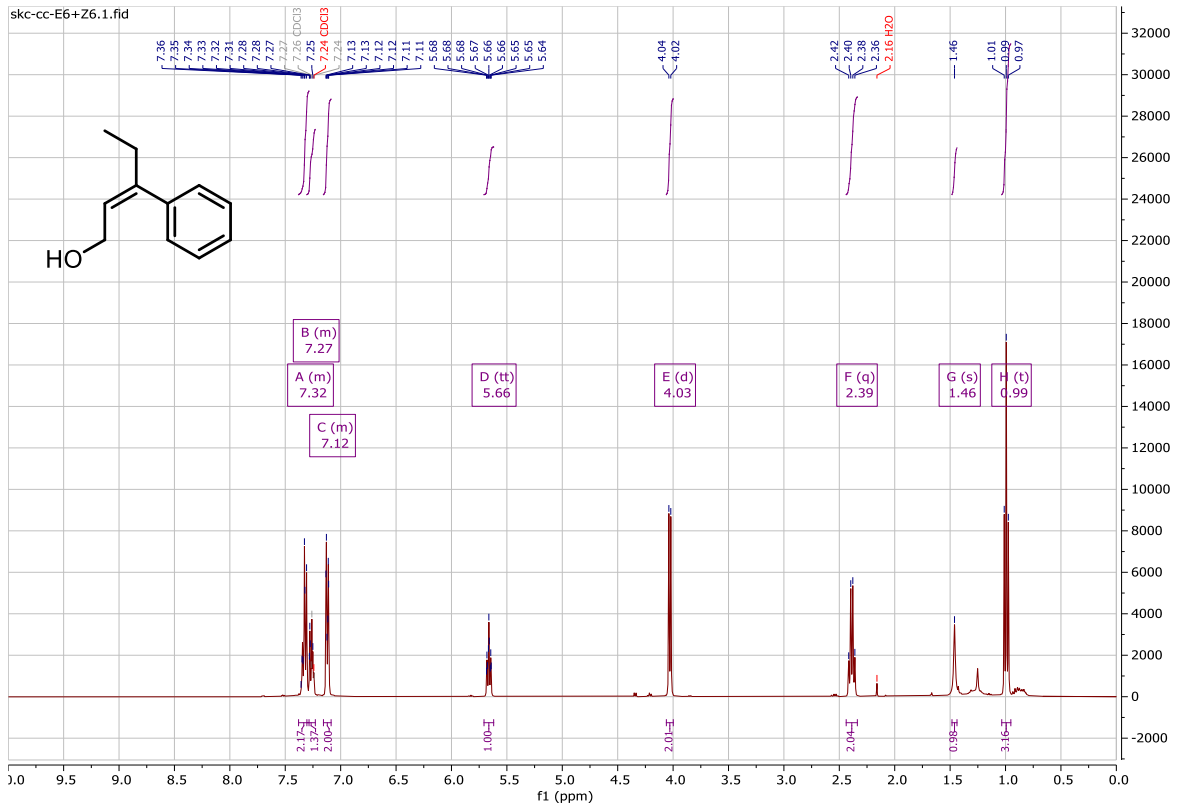


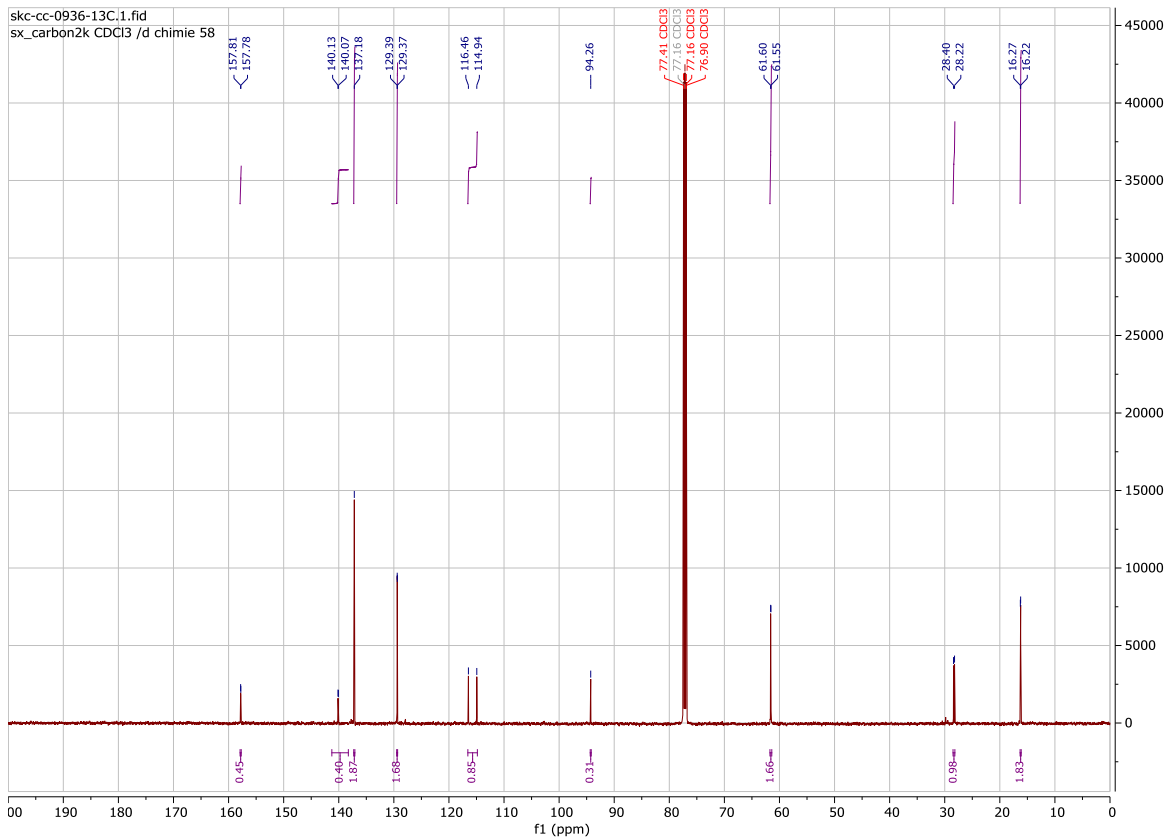
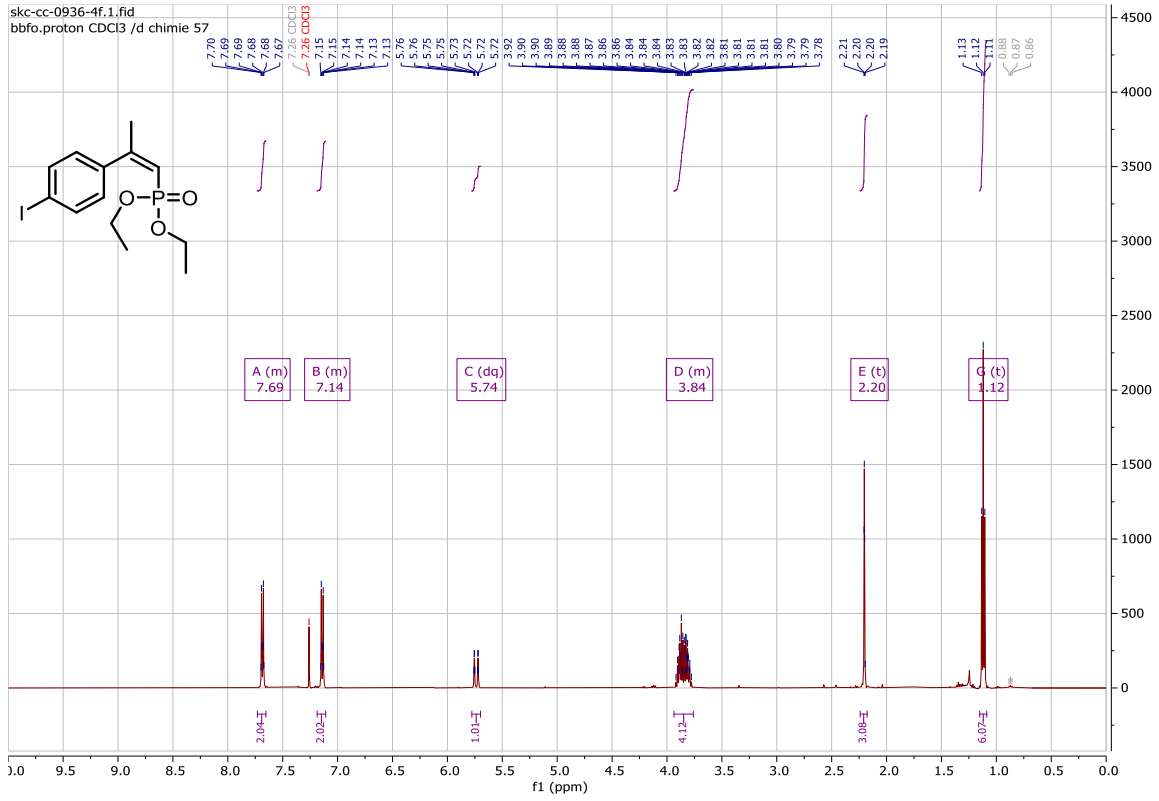


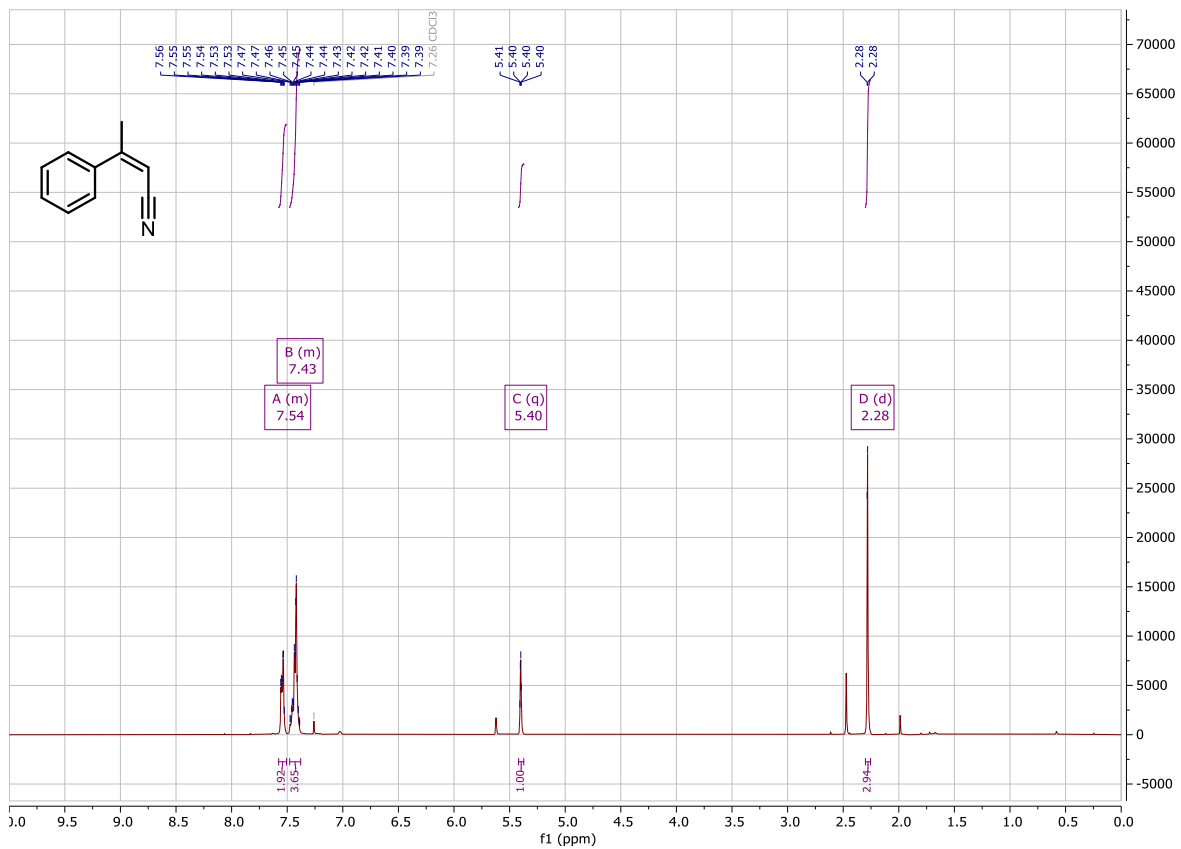
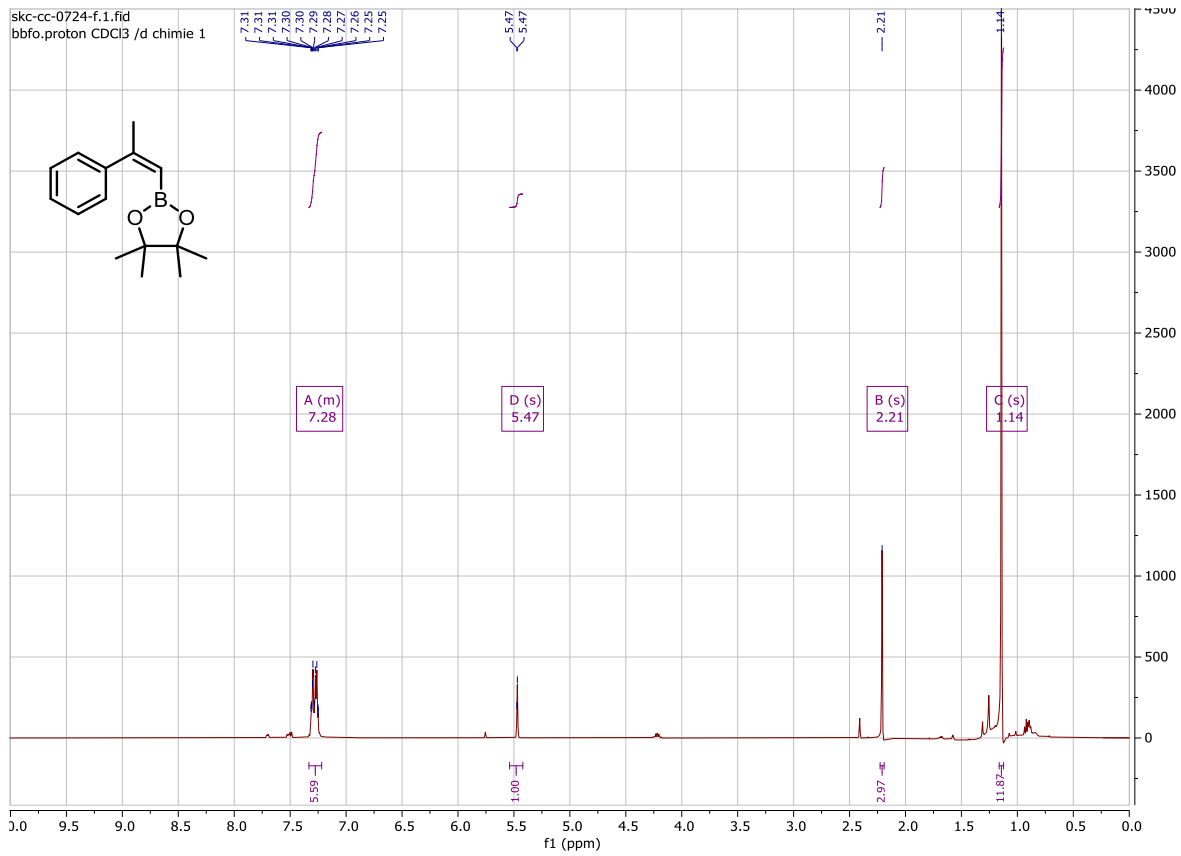


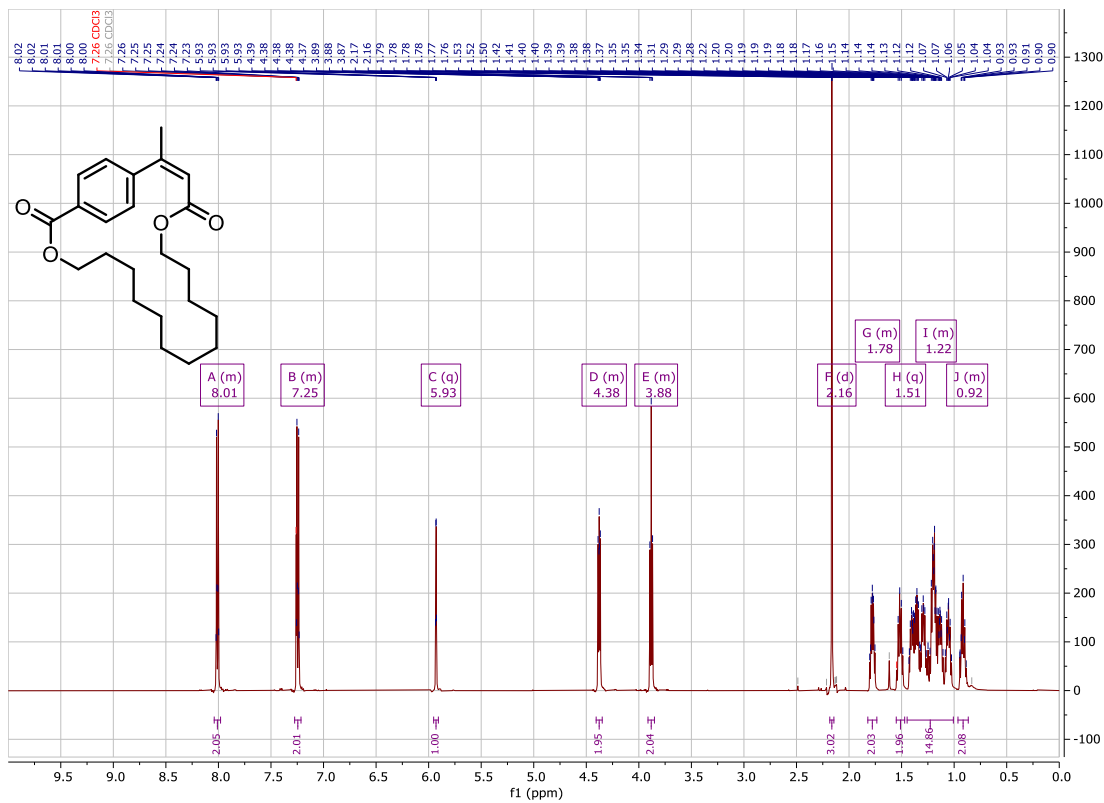
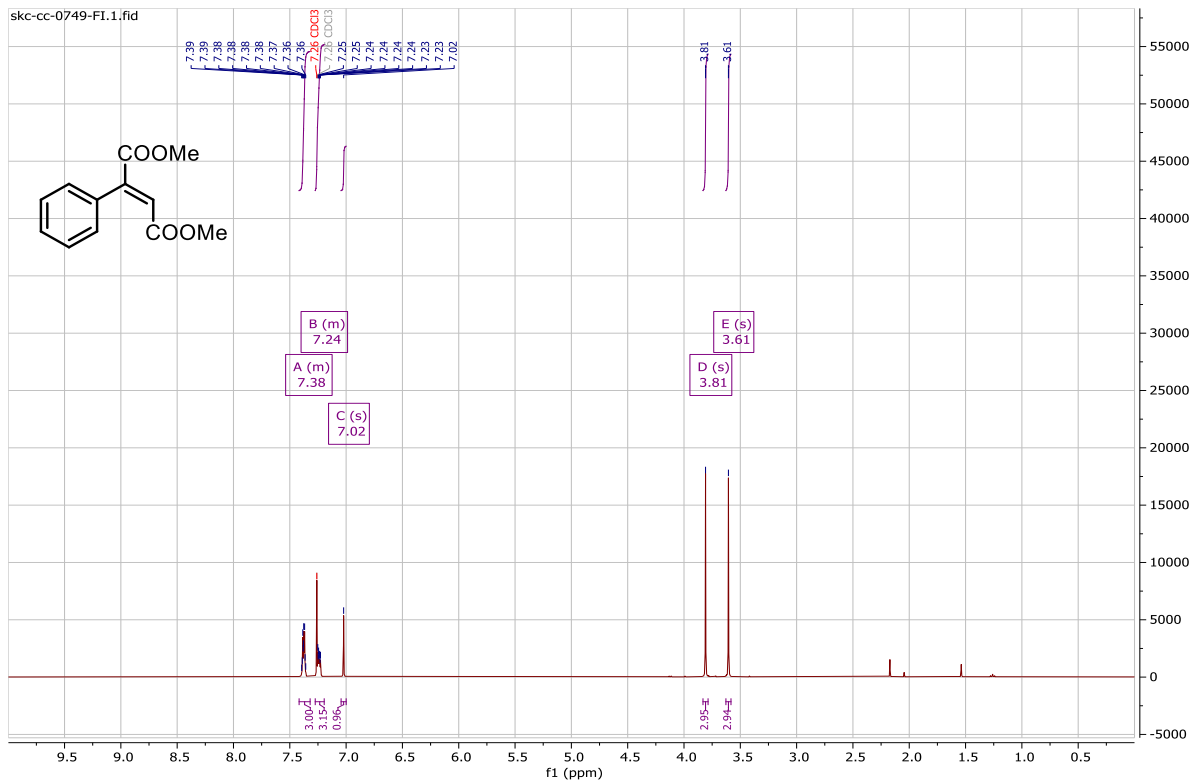


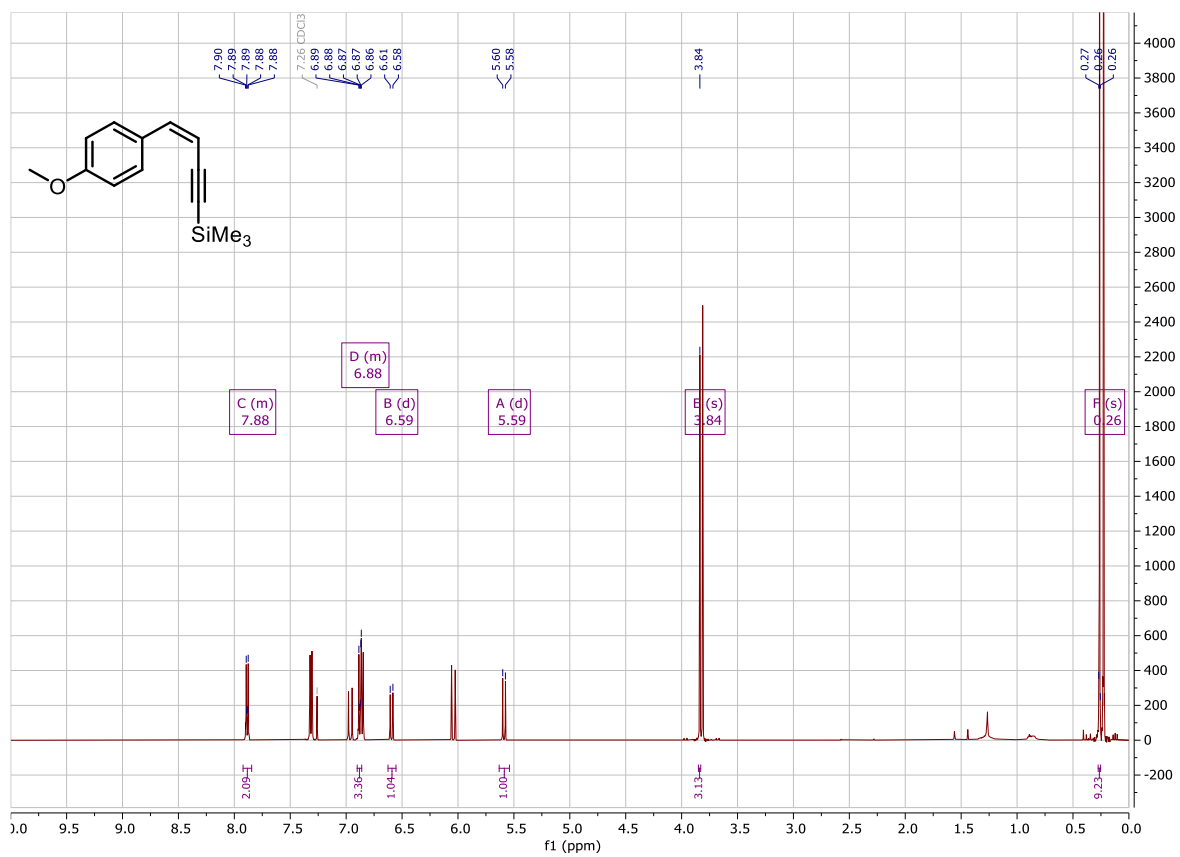
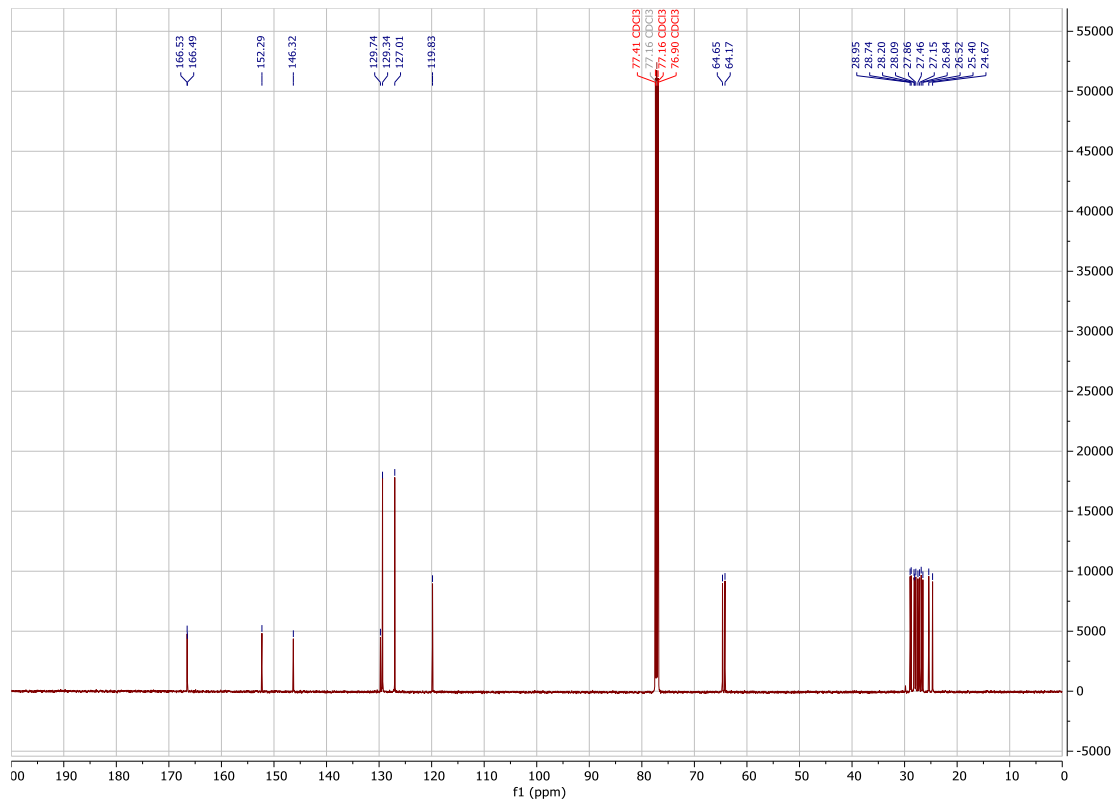


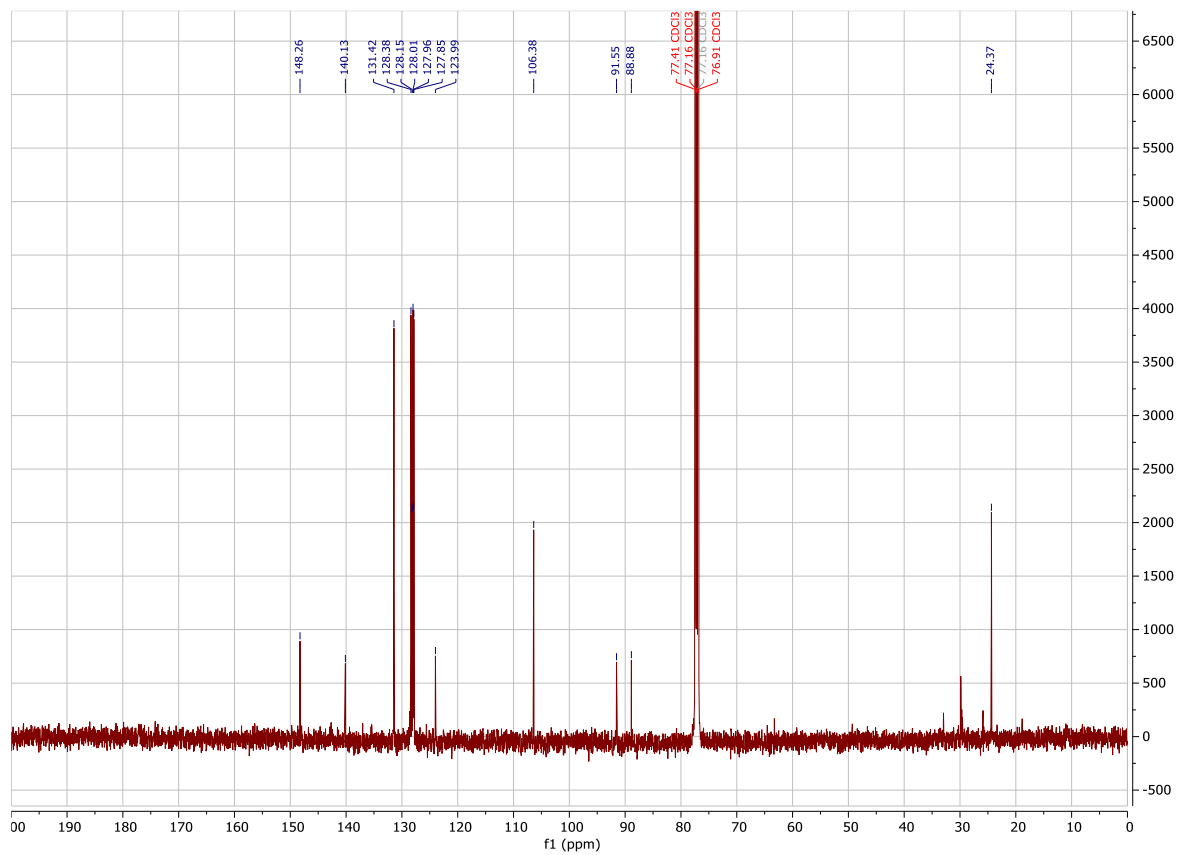
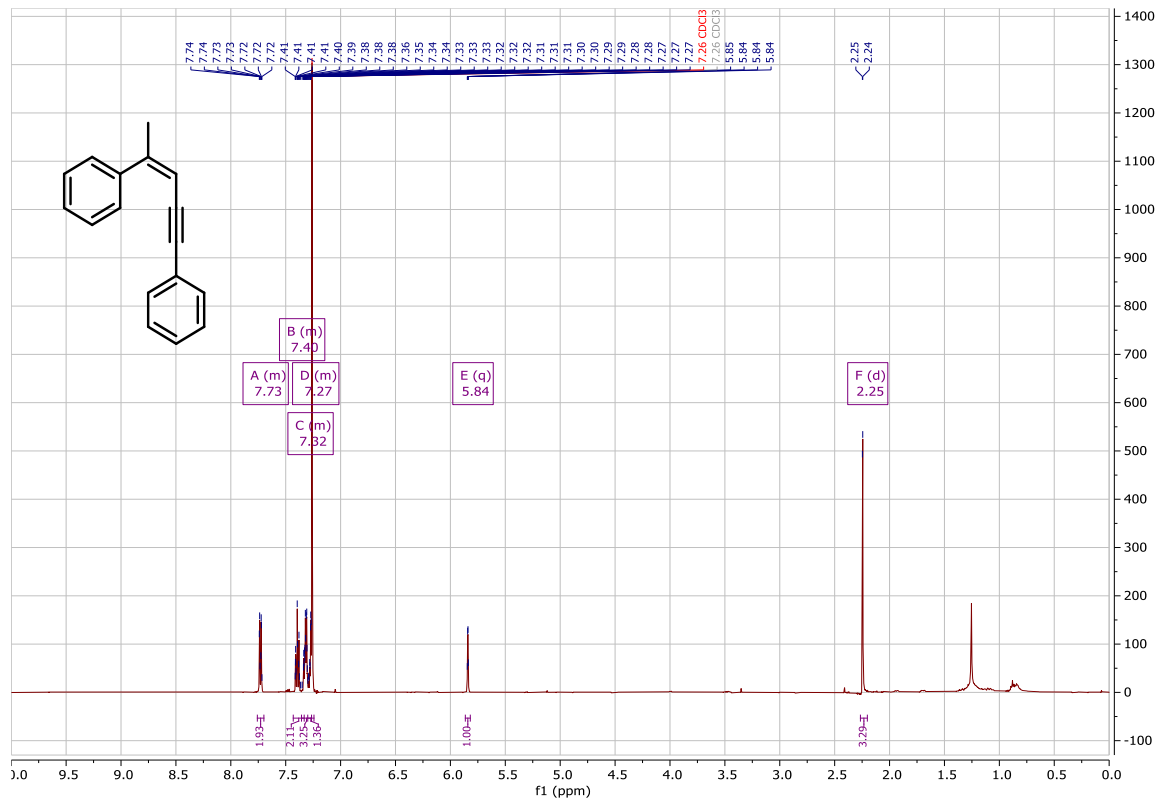


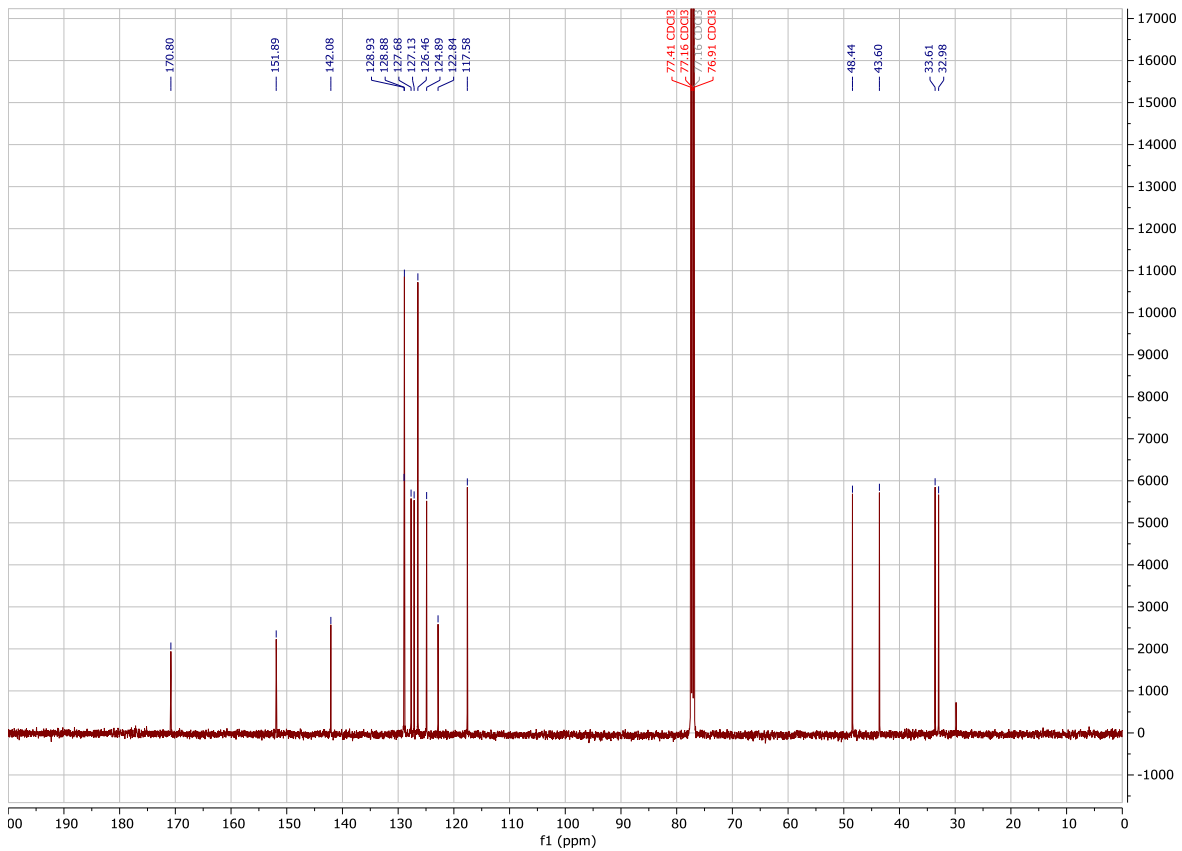
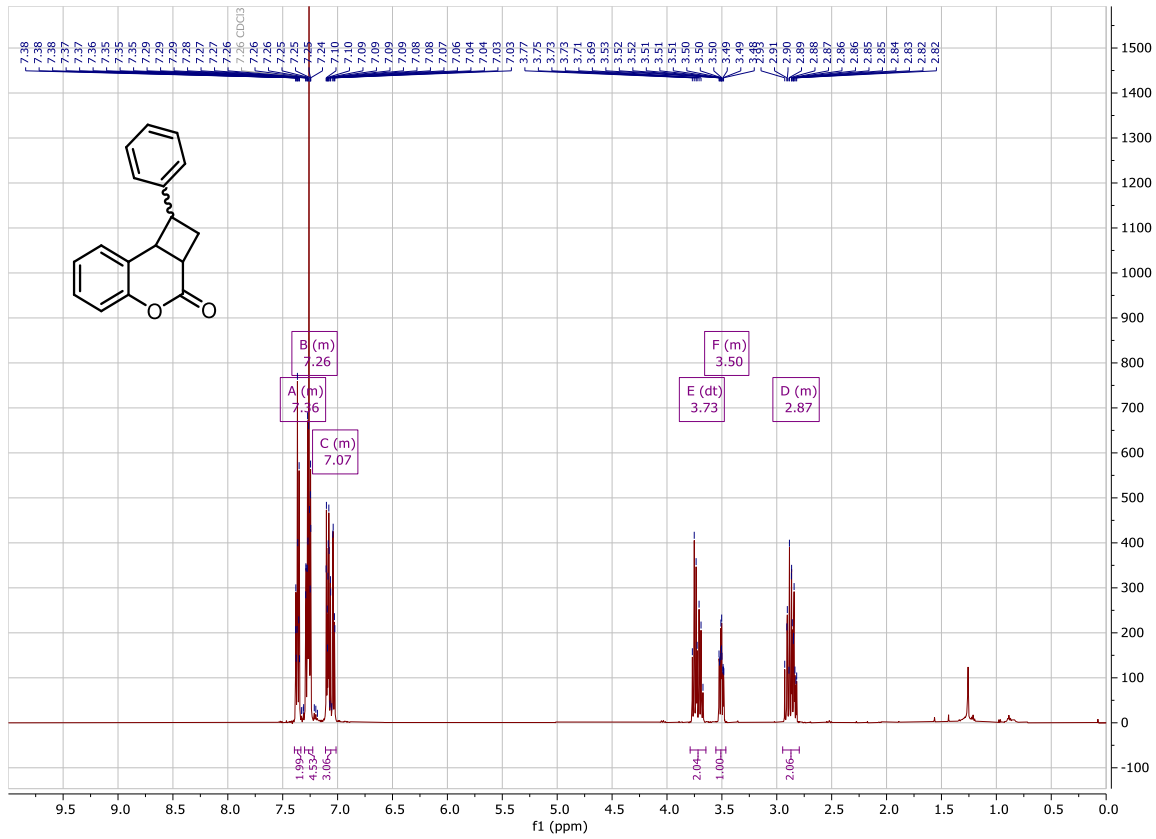


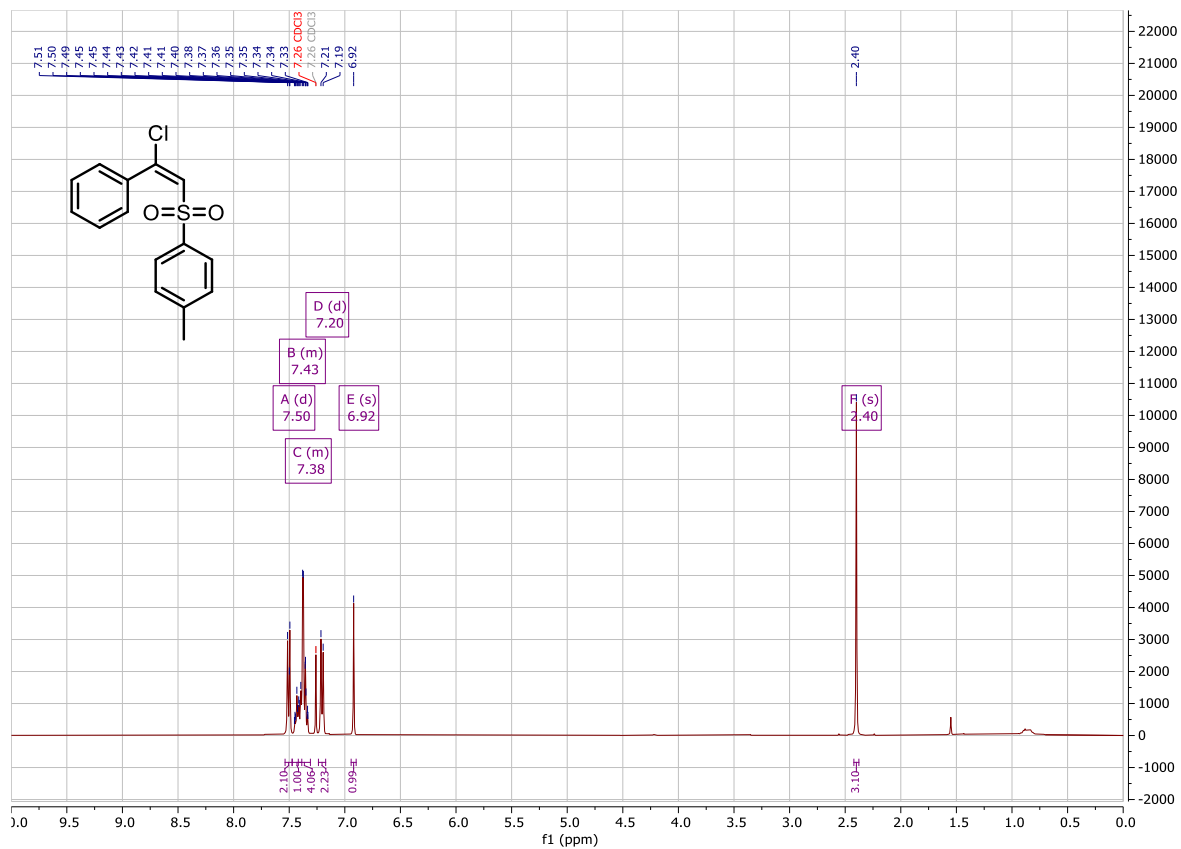


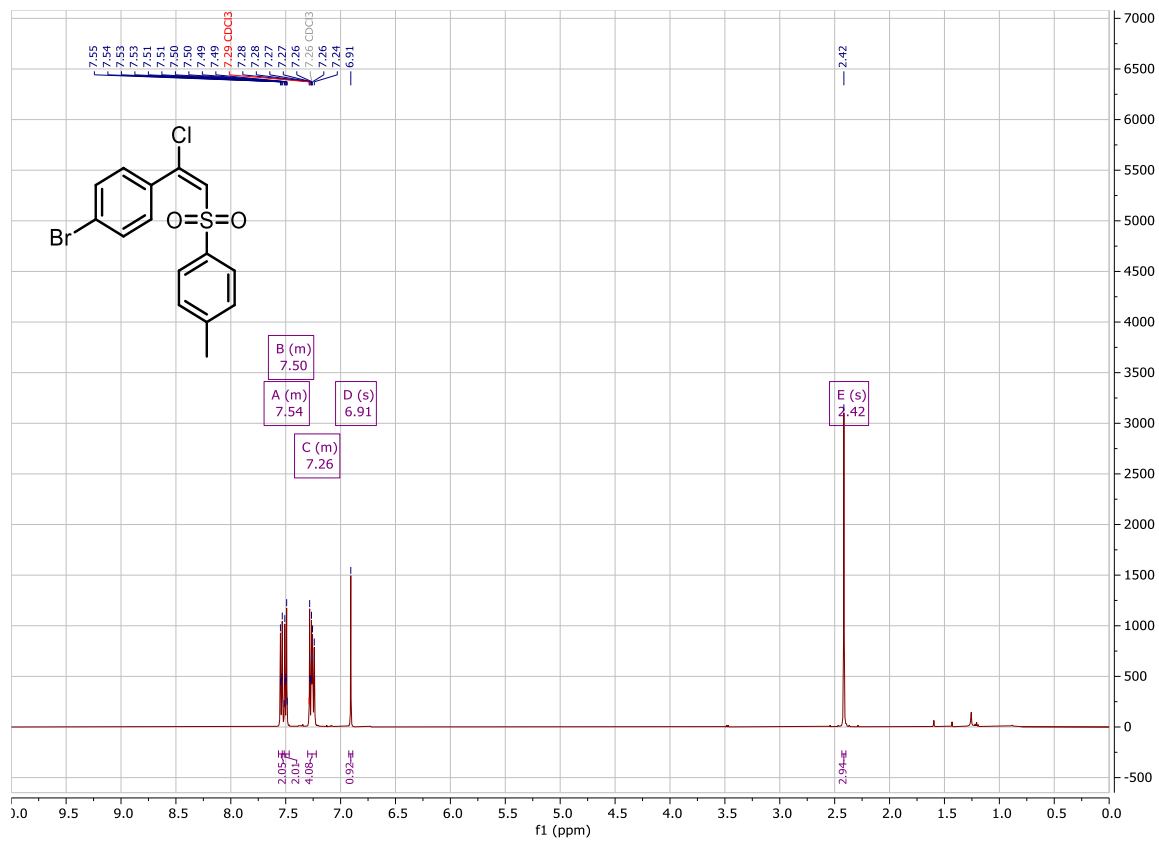
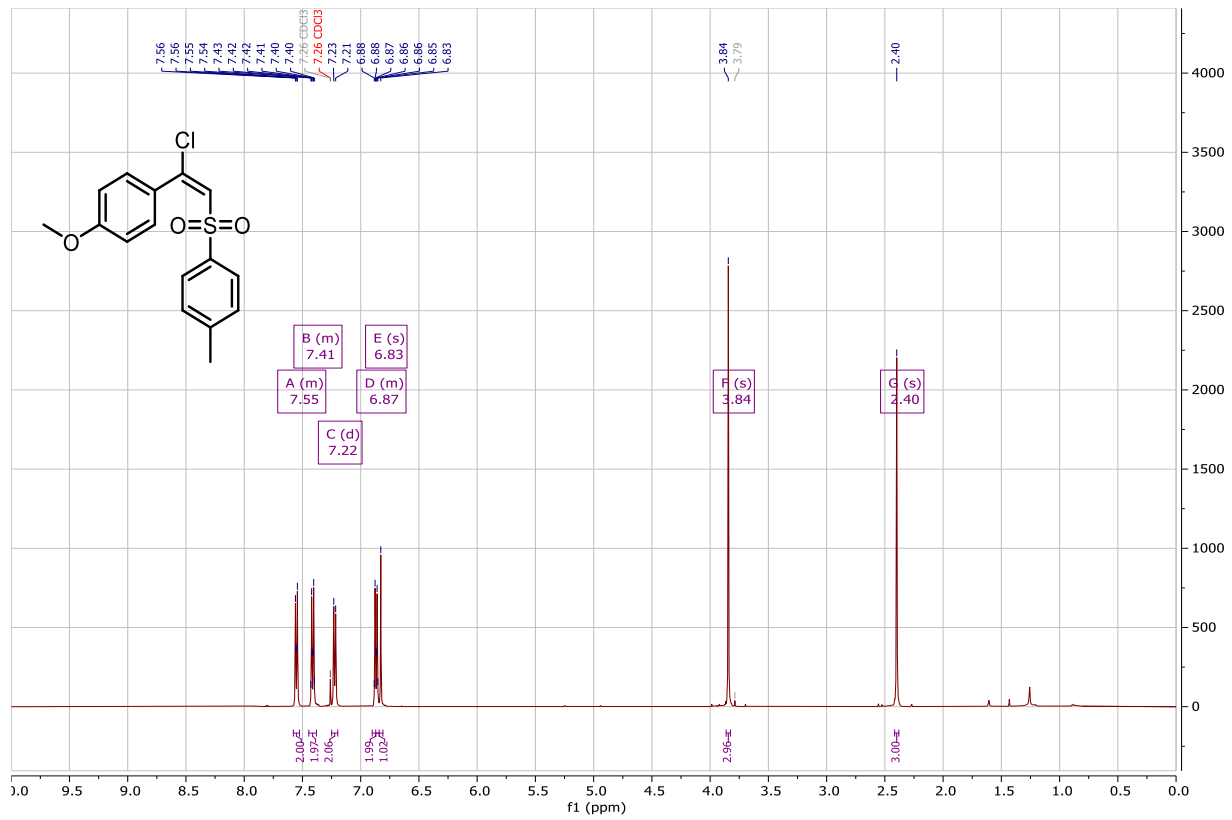


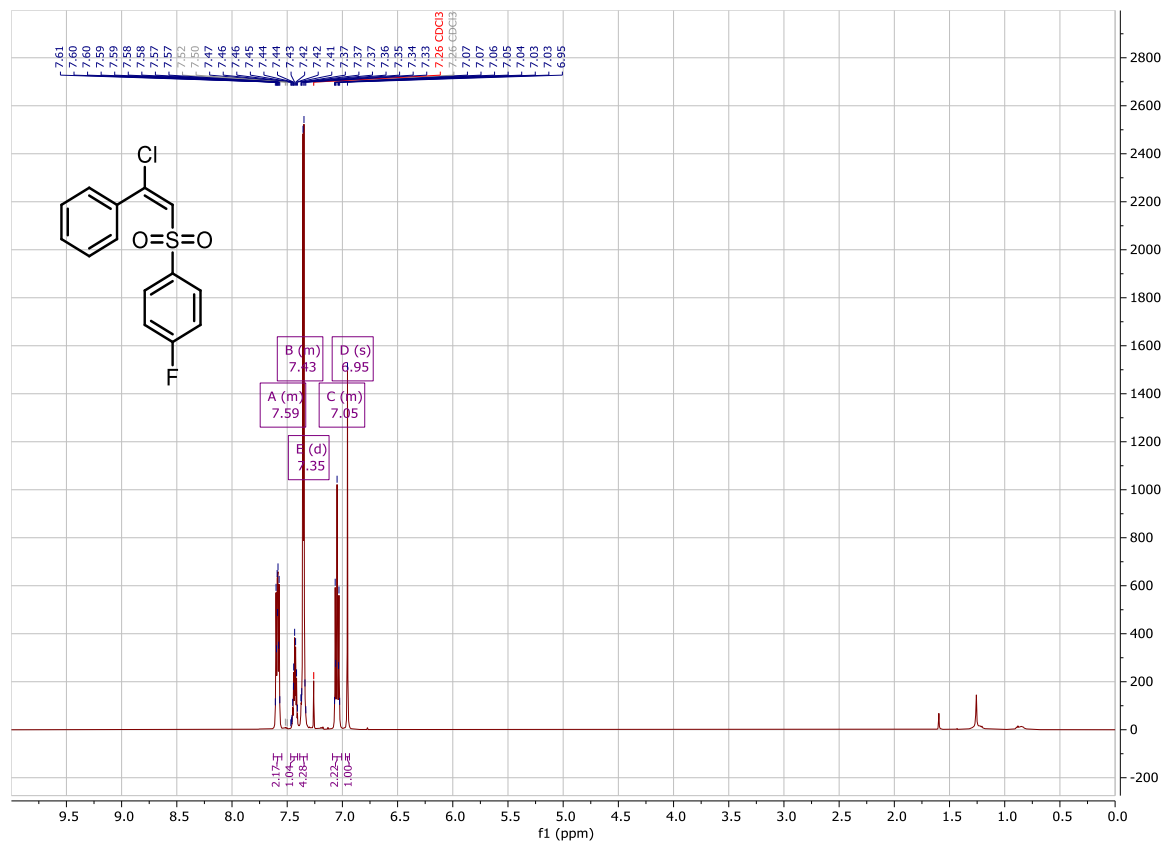
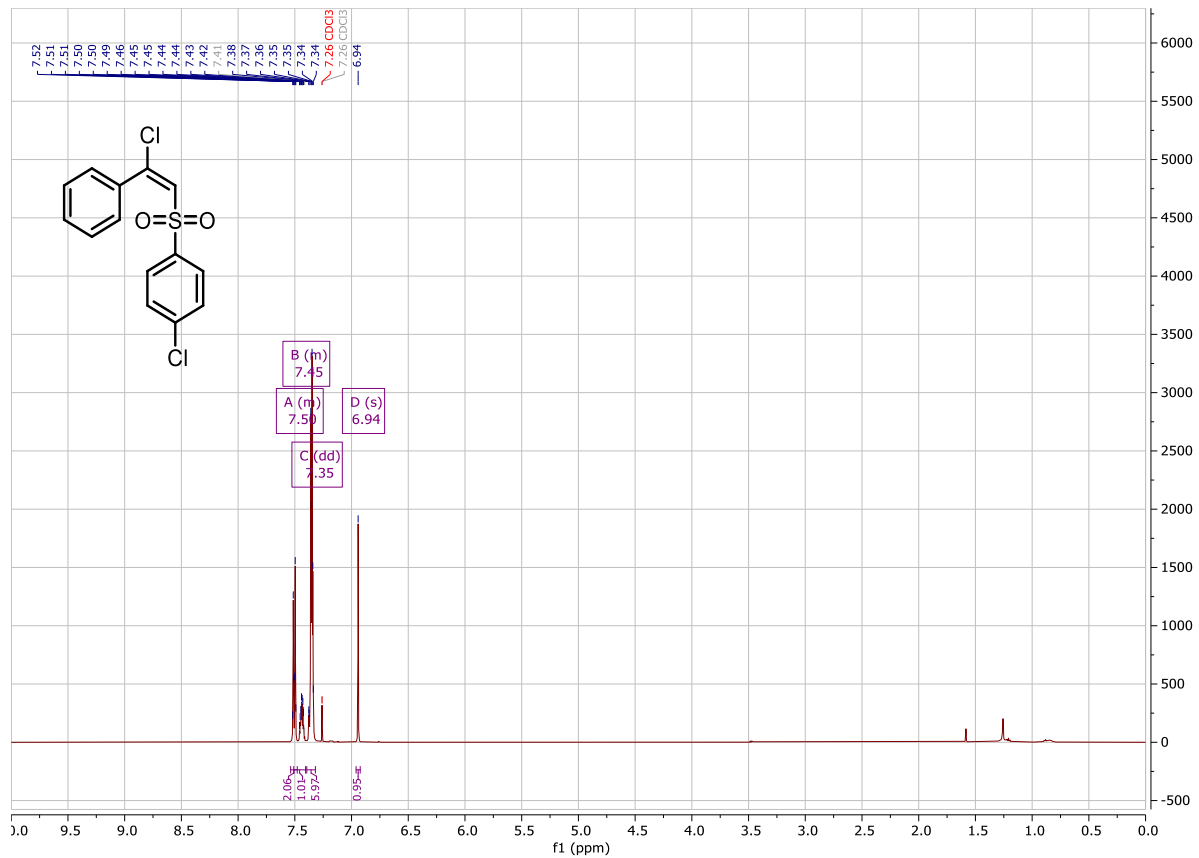


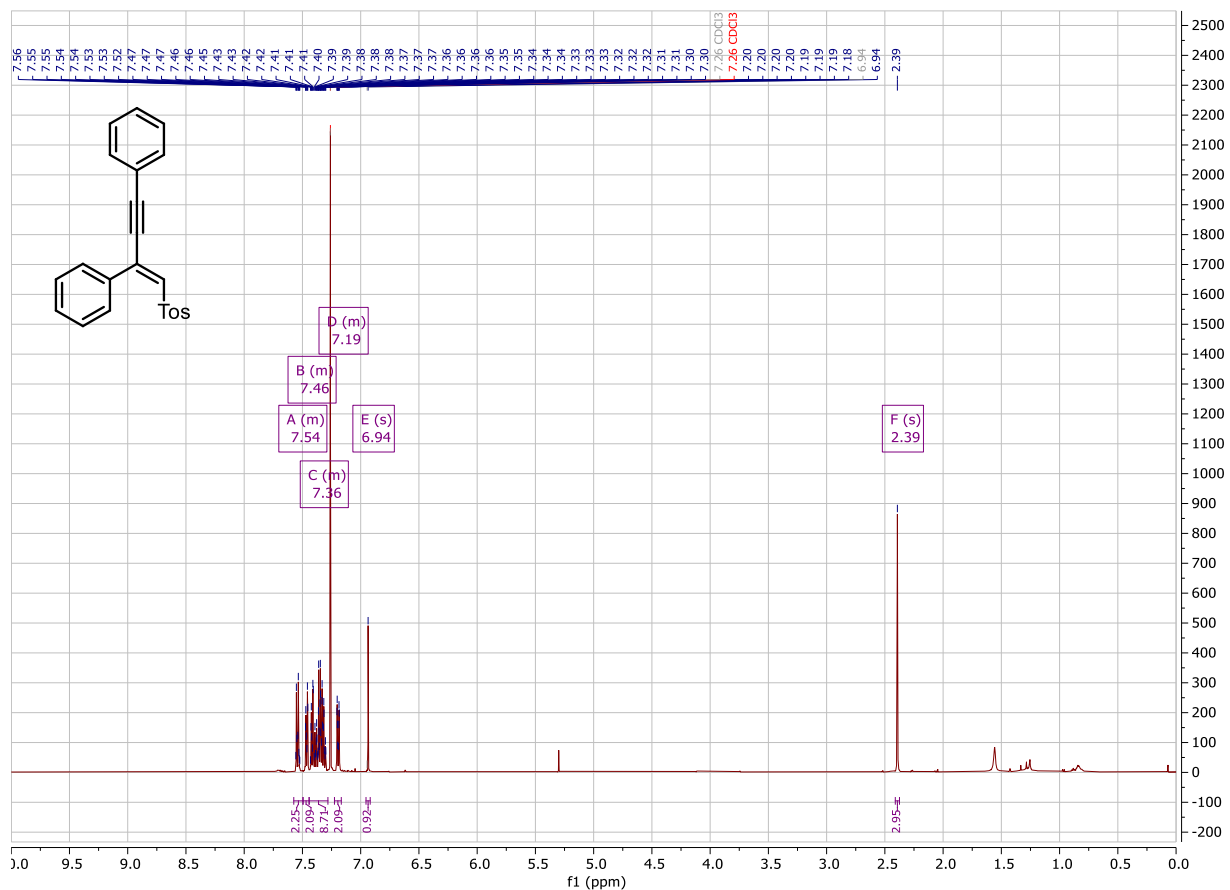
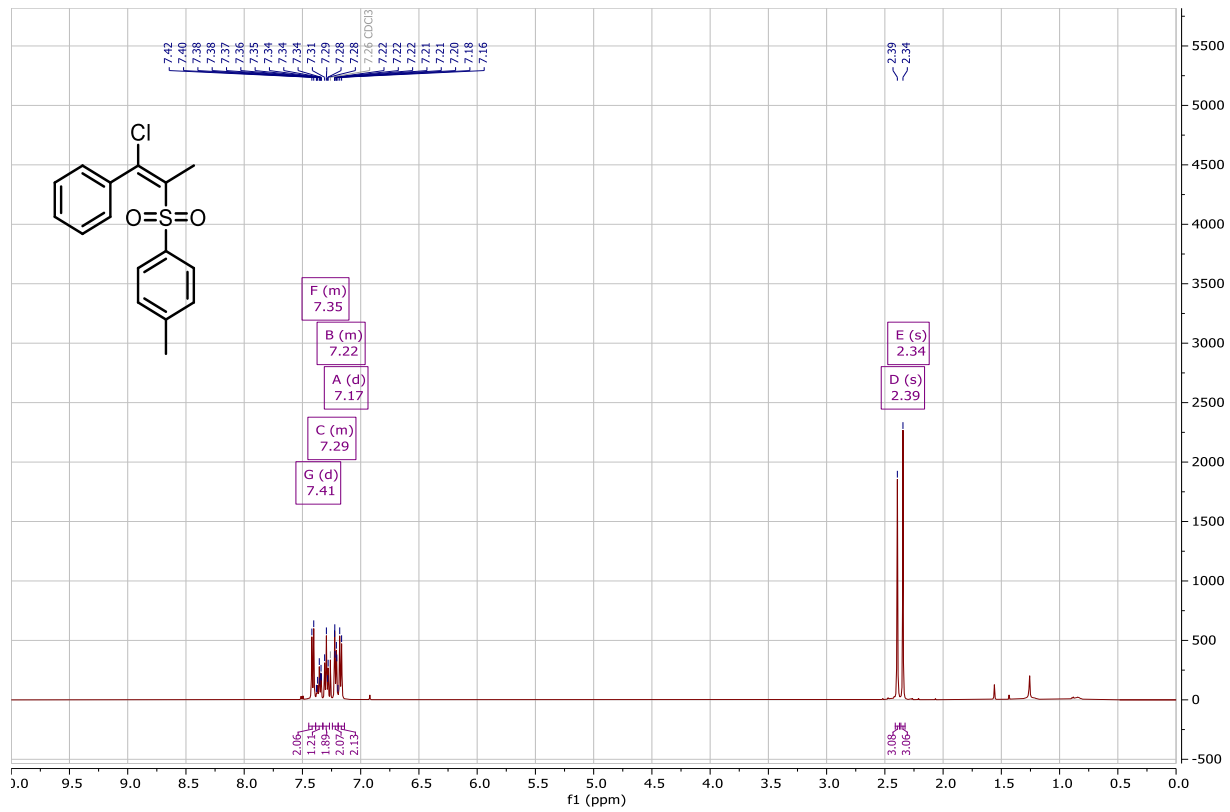


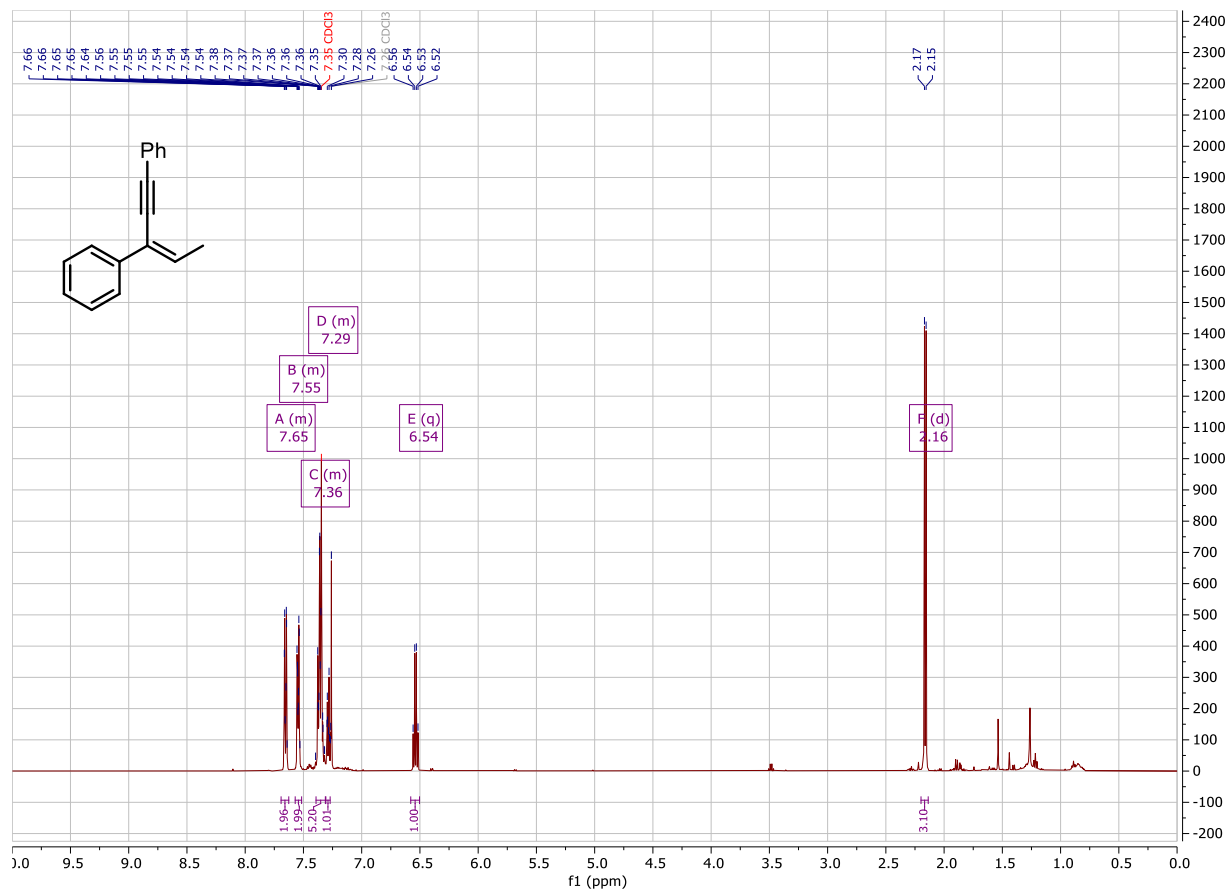




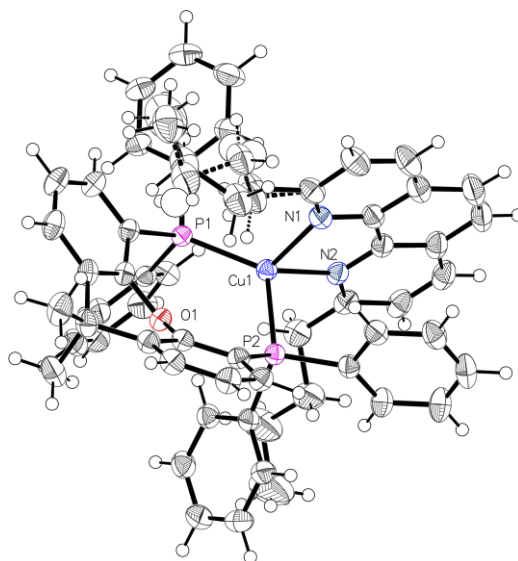








A3.13 X-ray Crystallography



The data for Cu(bphen)(XantPhos)BF₄ were collected from a shock-cooled single crystal at 150 K on a Bruker D8 VENTURE Metaljet four-circle diffractometer using mirror optics as monochromator and a Bruker PHOTON III detector. The diffractometer was equipped with an Oxford Cryostream 700 low temperature device and used GaK_α radiation ($\lambda = 1.34139 \text{ \AA}$). All data were integrated with SAINT and a multi-scan absorption correction using SADABS was applied.³⁸ The structure were solved by dual methods using SHELXT and refined by full-matrix least-squares methods against F^2 by SHELXL.³⁹⁻⁴⁰ All non-hydrogen atoms were refined with anisotropic displacement parameters. The hydrogen atoms were refined isotropically on calculated positions using a riding model with their U_{iso} values constrained to 1.5 times the U_{eq} of their pivot atoms for terminal sp³ carbon atoms and 1.2 times for all other carbon atoms. Disordered moieties were refined using bond lengths restraints and displacement parameter restraints. This report and the CIF file were generated using FinalCif⁴¹.

Table A3 - 9 Crystal data and structure refinement for Cu(Bphen)(Xantphos)BF₄

Empirical formula	C _{63.50} H ₆₇ BClCuF ₄ N ₂ O ₂ P ₂
Formula weight	1137.93
Temperature [K]	150
Crystal system	monoclinic
Space group (number)	$P2_1/c$ (14)
a [Å]	12.9884(3)
b [Å]	19.7561(4)
c [Å]	22.2957(5)
α [Å]	90
β [Å]	92.5410(10)
γ [Å]	90
Volume [Å ³]	5715.5(2)
Z	4
ρ_{calc} [g/cm ³]	1.322
μ [mm ⁻¹]	3.003
$F(000)$	2380
Crystal size [mm ³]	0.17×0.15×0.12
Crystal colour	clear light colourless

Crystal shape	block
Radiation	GaK α ($\lambda=1.34139 \text{ \AA}$)
2 θ range [°]	7.09 to 121.23 (0.77 \AA)
Index ranges	-16 $\leq h \leq$ 16 -25 $\leq k \leq$ 25 -28 $\leq l \leq$ 28
Reflections collected	104035
Independent reflections	13093 $R_{\text{int}} = 0.0415$ $R_{\text{sigma}} = 0.0245$
Completeness to $\theta = 53.594^\circ$	99.7 %
Data / Restraints / Parameters	13093/256/775
Goodness-of-fit on F^2	1.042
Final R indexes [$I \geq 2\sigma(I)$]	$R_1 = 0.0599$ $wR_2 = 0.1804$
Final R indexes [all data]	$R_1 = 0.0632$ $wR_2 = 0.1842$
Largest peak/hole [$e\text{\AA}^3$]	1.57/-1.06

Table A3 - 10 Atomic coordinates and U_{eq} [\AA^2] for Cu(bphen)(XantPhos)BF $_4$

Atom	x	y	z	U_{eq}
Cu1	0.25482(3)	0.50763(2)	0.75710(2)	0.02594(11)
P1	0.14618(4)	0.56303(3)	0.69288(3)	0.02493(14)
P2	0.36090(4)	0.42411(3)	0.72407(3)	0.02560(14)
O1	0.20097(13)	0.43599(8)	0.63206(8)	0.0275(3)
N1	0.19398(17)	0.46440(11)	0.83314(10)	0.0307(4)
N2	0.35132(16)	0.55441(11)	0.82335(10)	0.0297(4)
C1	0.1179(2)	0.42036(14)	0.83757(12)	0.0375(6)
C2	0.0935(3)	0.39052(17)	0.89257(14)	0.0473(7)
H2	0.037511	0.359703	0.894254	0.057
C3	0.1507(3)	0.40628(18)	0.94324(14)	0.0503(8)
H3	0.135966	0.385676	0.980390	0.060

C4	0.2317(3)	0.45303(16)	0.94045(13)	0.0421(6)
C5	0.2951(3)	0.47207(19)	0.99195(14)	0.0511(8)
H5	0.283409	0.452061	1.029793	0.061
C6	0.3707(3)	0.51772(18)	0.98745(14)	0.0481(7)
H6	0.410305	0.530747	1.022415	0.058
C7	0.3928(2)	0.54711(15)	0.93082(13)	0.0399(6)
C8	0.4741(2)	0.59280(16)	0.92367(14)	0.0442(7)
H8	0.515754	0.606756	0.957551	0.053
C9	0.4933(2)	0.61702(15)	0.86825(14)	0.0409(6)
H9	0.548926	0.647374	0.863192	0.049
C10	0.4300(2)	0.59692(13)	0.81801(13)	0.0345(5)
C11	0.3329(2)	0.52902(13)	0.87886(12)	0.0324(5)
C12	0.2502(2)	0.48124(13)	0.88399(12)	0.0328(5)
C13	0.4515(2)	0.62500(16)	0.75726(14)	0.0409(6)
H13A	0.439262	0.674455	0.757600	0.049
H13B	0.402268	0.604820	0.727191	0.049
C14	0.5615(3)	0.6119(2)	0.73766(17)	0.0572(9)
H14A	0.611167	0.627128	0.769825	0.069
H14B	0.571236	0.562629	0.732111	0.069
C15	0.5844(4)	0.6485(3)	0.6793(2)	0.0784(14)
H15A	0.579045	0.697968	0.685494	0.094
H15B	0.532294	0.635395	0.647644	0.094
C16	0.6922(4)	0.6315(4)	0.6582(3)	0.117(3)
H16A	0.705817	0.658091	0.622340	0.176
H16B	0.695856	0.583173	0.648759	0.176
H16C	0.743730	0.642454	0.690202	0.176
C21	0.0602(2)	0.51051(12)	0.64467(12)	0.0282(5)
C22	-0.0442(2)	0.52509(14)	0.63344(13)	0.0353(5)
H22	-0.072733	0.565152	0.649401	0.042
C23	-0.1066(2)	0.48129(16)	0.59901(15)	0.0416(6)
H23	-0.177433	0.491681	0.591765	0.050
C24	-0.0662(2)	0.42268(15)	0.57520(13)	0.0398(6)
H24	-0.109869	0.393195	0.552004	0.048
C25	0.0376(2)	0.40647(13)	0.58488(12)	0.0330(5)
C26	0.0895(2)	0.34389(14)	0.55980(12)	0.0363(6)
C27	0.1509(3)	0.36586(18)	0.50493(13)	0.0491(7)
H27A	0.103918	0.386598	0.474642	0.074
H27B	0.183793	0.326134	0.487689	0.074

H27C	0.203939	0.398727	0.517822	0.074
C28	0.0121(3)	0.28926(16)	0.54050(16)	0.0493(8)
H28A	-0.027567	0.275812	0.574950	0.074
H28B	0.048843	0.249857	0.525488	0.074
H28C	-0.034902	0.306970	0.508642	0.074
C29	0.1660(2)	0.31905(13)	0.60922(11)	0.0309(5)
C30	0.1877(2)	0.25171(13)	0.62207(13)	0.0354(5)
H30	0.151040	0.217100	0.600614	0.042
C31	0.2623(2)	0.23425(14)	0.66600(13)	0.0360(6)
H31	0.276211	0.187846	0.674091	0.043
C32	0.3169(2)	0.28375(13)	0.69821(12)	0.0330(5)
H32	0.368636	0.271178	0.727570	0.040
C33	0.29555(18)	0.35220(12)	0.68729(11)	0.0275(5)
C34	0.22071(19)	0.36774(12)	0.64276(11)	0.0274(5)
C35	0.09772(18)	0.45099(12)	0.61964(11)	0.0281(5)
C36	0.20839(18)	0.61784(12)	0.63943(11)	0.0273(5)
C37	0.2157(2)	0.60196(15)	0.57884(12)	0.0350(5)
H37	0.184591	0.561815	0.563112	0.042
C38	0.2683(2)	0.64479(17)	0.54145(13)	0.0427(6)
H38	0.273041	0.633630	0.500212	0.051
C39	0.3140(2)	0.70347(16)	0.56352(14)	0.0420(6)
H39	0.349679	0.732570	0.537605	0.050
C40	0.3074(2)	0.71950(15)	0.62373(15)	0.0415(6)
H40	0.338846	0.759669	0.639155	0.050
C41	0.2550(2)	0.67710(14)	0.66165(12)	0.0349(5)
H41	0.250773	0.688431	0.702877	0.042
C42	0.05692(19)	0.62108(13)	0.72755(12)	0.0302(5)
C43	0.0089(2)	0.67479(13)	0.69627(13)	0.0337(5)
H43	0.024068	0.683122	0.655640	0.040
C44	-0.0608(2)	0.71588(15)	0.72460(15)	0.0402(6)
H44	-0.093505	0.752140	0.703216	0.048
C45	-0.0829(2)	0.70418(17)	0.78386(16)	0.0480(7)
H45	-0.131343	0.732030	0.802924	0.058
C46	-0.0344(3)	0.65181(18)	0.81542(16)	0.0508(8)
H46	-0.048648	0.644399	0.856335	0.061
C47	0.0348(2)	0.61022(16)	0.78735(13)	0.0392(6)
H47	0.067322	0.574135	0.809041	0.047
C48	0.4328(2)	0.38881(13)	0.78868(11)	0.0299(5)

C49	0.3810(2)	0.35013(14)	0.83064(12)	0.0358(5)
H49	0.311601	0.336875	0.821931	0.043
C50	0.4296(3)	0.33095(15)	0.88473(13)	0.0426(6)
H50	0.393394	0.304959	0.912803	0.051
C51	0.5304(3)	0.34965(17)	0.89766(14)	0.0489(8)
H51	0.563869	0.336013	0.934444	0.059
C52	0.5832(3)	0.38837(17)	0.85708(14)	0.0481(7)
H52	0.652529	0.401400	0.866232	0.058
C53	0.5345(2)	0.40807(15)	0.80300(13)	0.0381(6)
H53	0.570767	0.434879	0.775548	0.046
C54	0.45583(19)	0.44157(13)	0.66794(11)	0.0295(5)
C55	0.4417(2)	0.49870(14)	0.63177(13)	0.0334(5)
H55	0.387685	0.529590	0.639157	0.040
C56	0.5065(2)	0.51055(16)	0.58496(14)	0.0415(6)
H56	0.495848	0.549029	0.559900	0.050
C57	0.5865(2)	0.4664(2)	0.57480(14)	0.0487(7)
H57	0.631290	0.474937	0.543100	0.058
C58	0.6015(3)	0.4099(2)	0.61064(15)	0.0526(8)
H58	0.656792	0.379888	0.603724	0.063
C59	0.5358(2)	0.39695(16)	0.65681(13)	0.0404(6)
H59	0.545391	0.357540	0.680823	0.048
C17A	0.0489(8)	0.4046(4)	0.7813(2)	0.0513(10)
H17A	0.083091	0.425221	0.746950	0.062
H17B	-0.016022	0.429977	0.785828	0.062
C18A	0.0178(5)	0.3324(4)	0.7618(3)	0.0561(9)
H18A	0.008743	0.302191	0.796634	0.067
H18B	0.067822	0.312104	0.734803	0.067
C19A	-0.0858(5)	0.3492(4)	0.7285(4)	0.0560(10)
H19A	-0.102238	0.396195	0.740180	0.067
H19B	-0.070675	0.350975	0.685382	0.067
C20A	-0.1878(7)	0.3097(5)	0.7315(5)	0.067(2)
H20A	-0.215255	0.300313	0.690665	0.101
H20B	-0.237739	0.336725	0.752852	0.101
H20C	-0.175282	0.266900	0.752806	0.101
C17B	0.0631(7)	0.4011(6)	0.7773(2)	0.0517(10)
H17C	0.111875	0.375585	0.753011	0.062
H17D	0.044289	0.443077	0.755231	0.062
C18B	-0.0348(5)	0.3581(4)	0.7839(3)	0.0533(9)

H18C	-0.090595	0.386673	0.799038	0.064
H18D	-0.020614	0.321146	0.813010	0.064
C19B	-0.0687(6)	0.3281(5)	0.7221(3)	0.0570(10)
H19C	-0.042030	0.353532	0.687820	0.068
H19D	-0.053334	0.279224	0.718463	0.068
C20B	-0.1830(7)	0.3428(8)	0.7328(8)	0.108(4)
H20D	-0.225178	0.330676	0.696884	0.161
H20E	-0.191668	0.391126	0.741368	0.161
H20F	-0.204924	0.316126	0.767026	0.161
F1	0.31772(15)	0.31202(10)	1.03375(10)	0.0552(5)
F2	0.2567(3)	0.22273(13)	1.08305(12)	0.0825(8)
F3	0.15182(18)	0.30809(18)	1.06100(11)	0.0859(9)
F4	0.2815(2)	0.32041(18)	1.13245(13)	0.0918(10)
B1	0.2521(3)	0.2928(2)	1.07810(16)	0.0444(8)
C11	-0.1365(2)	0.49821(12)	0.88094(11)	0.0766(7)
C12	-0.2154(2)	0.50137(13)	0.75777(13)	0.0774(6)
C17	-0.2230(6)	0.5355(4)	0.8301(4)	0.061(2)
H17E	-0.209120	0.584718	0.828560	0.073
H17F	-0.293708	0.529175	0.843919	0.073
C1C	0.0763(16)	0.8196(8)	0.9814(7)	0.167(4)
H1CA	0.013197	0.846515	0.976185	0.250
H1CB	0.080962	0.788042	0.947733	0.250
H1CC	0.136295	0.849685	0.982800	0.250
C2C	0.0739(12)	0.7805(6)	1.0390(5)	0.1632(13)
H2CA	0.101829	0.809950	1.071705	0.196
H2CB	0.000853	0.771348	1.047091	0.196
O3C	0.1261(8)	0.7201(6)	1.0424(4)	0.1647(10)
C4C	0.0894(10)	0.6580(5)	1.0229(5)	0.1648(12)
H4CA	0.013345	0.660717	1.018825	0.198
H4CB	0.106811	0.624256	1.054559	0.198
C5C	0.1278(9)	0.6318(6)	0.9648(5)	0.090(3)
H5CA	0.151264	0.584906	0.970249	0.135
H5CB	0.185371	0.659856	0.952493	0.135
H5CC	0.072005	0.633353	0.933830	0.135
C1D	0.0770(18)	0.8349(5)	1.0100(7)	0.167(4)
H1DA	0.106854	0.842552	0.971031	0.250
H1DB	0.115451	0.860987	1.040968	0.250
H1DC	0.004740	0.849419	1.008184	0.250

C2D	0.0828(16)	0.7611(6)	1.0253(5)	0.1627(12)
H2DA	0.141448	0.753905	1.054482	0.195
H2DB	0.019121	0.748146	1.045250	0.195
O3D	0.0946(8)	0.7184(4)	0.9768(4)	0.1647(10)
C4D	0.1493(6)	0.6585(6)	0.9801(7)	0.1636(13)
H4DA	0.180308	0.653864	1.021261	0.196
H4DB	0.206465	0.661374	0.952279	0.196
C5D	0.0879(8)	0.5961(4)	0.9654(5)	0.090(3)
H5DA	0.107622	0.578136	0.926592	0.135
H5DB	0.014291	0.607261	0.963369	0.135
H5DC	0.101512	0.561966	0.996677	0.135

U_{eq} is defined as 1/3 of the trace of the orthogonalized U_{ij} tensor.

Table A3 - 11 Bond lengths and angles for Cu(Bphen)(Xantphos)BF₄

Atom-Atom	Length [Å]	Atom-Atom	Length [Å]	Atom-Atom-Atom	Angle [°]
Cu1-P1	2.2494(7)	C48-C49	1.403(4)	C48-P2-C54	106.01(12)
Cu1-P2	2.2921(7)	C48-C53	1.398(4)	C54-P2-Cu1	121.16(9)
Cu1-N1	2.085(2)	C49-H49	0.9500	C54-P2-C33	98.82(11)
Cu1-N2	2.108(2)	C49-C50	1.389(4)	C35-O1-C34	114.20(18)
P1-C21	1.837(3)	C50-H50	0.9500	C1-N1-Cu1	129.88(18)
P1-C36	1.825(2)	C50-C51	1.379(5)	C1-N1-C12	118.2(2)
P1-C42	1.827(3)	C51-H51	0.9500	C12-N1-Cu1	111.59(17)
P2-C33	1.830(2)	C51-C52	1.389(5)	C10-N2-Cu1	130.42(19)
P2-C48	1.821(3)	C52-H52	0.9500	C10-N2-C11	118.6(2)
P2-C54	1.828(3)	C52-C53	1.392(4)	C11-N2-Cu1	110.57(17)
O1-C34	1.391(3)	C53-H53	0.9500	N1-C1-C2	122.5(3)
O1-C35	1.389(3)	C54-C55	1.395(4)	N1-C1-C17A	118.8(3)
N1-C1	1.324(4)	C54-C59	1.393(4)	N1-C1-C17B	114.5(3)
N1-C12	1.363(3)	C55-H55	0.9500	C2-C1-C17A	118.6(4)
N2-C10	1.332(4)	C55-C56	1.389(4)	C2-C1-C17B	122.8(3)
N2-C11	1.366(3)	C56-H56	0.9500	C1-C2-H2	120.3
C1-C2	1.410(4)	C56-C57	1.383(5)	C3-C2-C1	119.4(3)
C1-C17A	1.540(3)	C57-H57	0.9500	C3-C2-H2	120.3
C1-C17B	1.539(3)	C57-C58	1.381(5)	C2-C3-H3	120.1
C2-H2	0.9500	C58-H58	0.9500	C2-C3-C4	119.8(3)
C2-C3	1.361(5)	C58-C59	1.390(4)	C4-C3-H3	120.1
C3-H3	0.9500	C59-H59	0.9500	C3-C4-C5	122.8(3)
C3-C4	1.403(5)	C17A-H17A	0.9900	C3-C4-C12	117.3(3)
C4-C5	1.434(5)	C17A-H17B	0.9900	C12-C4-C5	119.8(3)

C4-C12	1.407(4)	C17A-C18A	1.541(3)	C4-C5-H5	119.5
C5-H5	0.9500	C18A-H18A	0.9900	C6-C5-C4	120.9(3)
C5-C6	1.341(6)	C18A-H18B	0.9900	C6-C5-H5	119.5
C6-H6	0.9500	C18A-C19A	1.545(3)	C5-C6-H6	119.5
C6-C7	1.430(5)	C19A-H19A	0.9900	C5-C6-C7	121.0(3)
C7-C8	1.404(5)	C19A-H19B	0.9900	C7-C6-H6	119.5
C7-C11	1.412(4)	C19A-C20A	1.542(3)	C8-C7-C6	122.8(3)
C8-H8	0.9500	C20A-H20A	0.9800	C8-C7-C11	117.3(3)
C8-C9	1.358(5)	C20A-H20B	0.9800	C11-C7-C6	119.8(3)
C9-H9	0.9500	C20A-H20C	0.9800	C7-C8-H8	120.0
C9-C10	1.416(4)	C17B-H17C	0.9900	C9-C8-C7	119.9(3)
C10-C13	1.501(4)	C17B-H17D	0.9900	C9-C8-H8	120.0
C11-C12	1.438(4)	C17B-C18B	1.540(3)	C8-C9-H9	120.1
C13-H13A	0.9900	C18B-H18C	0.9900	C8-C9-C10	119.9(3)
C13-H13B	0.9900	C18B-H18D	0.9900	C10-C9-H9	120.1
C13-C14	1.534(4)	C18B-C19B	1.546(3)	N2-C10-C9	121.8(3)
C14-H14A	0.9900	C19B-H19C	0.9900	N2-C10-C13	119.2(2)
C14-H14B	0.9900	C19B-H19D	0.9900	C9-C10-C13	119.0(3)
C14-C15	1.530(6)	C19B-C20B	1.542(3)	N2-C11-C7	122.5(3)
C15-H15A	0.9900	C20B-H20D	0.9800	N2-C11-C12	118.3(2)
C15-H15B	0.9900	C20B-H20E	0.9800	C7-C11-C12	119.1(3)
C15-C16	1.533(7)	C20B-H20F	0.9800	N1-C12-C4	122.7(3)
C16-H16A	0.9800	F1-B1	1.387(4)	N1-C12-C11	118.0(2)
C16-H16B	0.9800	F2-B1	1.390(5)	C4-C12-C11	119.3(3)
C16-H16C	0.9800	F3-B1	1.374(4)	C10-C13-H13A	108.7
C21-C22	1.397(4)	F4-B1	1.367(4)	C10-C13-H13B	108.7
C21-C35	1.399(4)	Cl1-C17	1.725(9)	C10-C13-C14	114.1(3)
C22-H22	0.9500	Cl2-C17	1.754(9)	H13A-C13-H13B	107.6
C22-C23	1.393(4)	C17-H17E	0.9900	C14-C13-H13A	108.7
C23-H23	0.9500	C17-H17F	0.9900	C14-C13-H13B	108.7
C23-C24	1.386(4)	C1C-H1CA	0.9800	C13-C14-H14A	109.1
C24-H24	0.9500	C1C-H1CB	0.9800	C13-C14-H14B	109.1
C24-C25	1.393(4)	C1C-H1CC	0.9800	H14A-C14-H14B	107.9
C25-C26	1.526(4)	C1C-C2C	1.4987(17)	C15-C14-C13	112.4(4)
C25-C35	1.389(3)	C2C-H2CA	0.9900	C15-C14-H14A	109.1
C26-C27	1.552(4)	C2C-H2CB	0.9900	C15-C14-H14B	109.1
C26-C28	1.524(4)	C2C-O3C	1.373(2)	C14-C15-H15A	109.3
C26-C29	1.532(4)	O3C-C4C	1.379(2)	C14-C15-H15B	109.3
C27-H27A	0.9800	C4C-H4CA	0.9900	C14-C15-C16	111.8(5)
C27-H27B	0.9800	C4C-H4CB	0.9900	H15A-C15-H15B	107.9

C27-H27C	0.9800	C4C-C5C	1.4996(17)	C16-C15-H15A	109.3
C28-H28A	0.9800	C5C-H5CA	0.9800	C16-C15-H15B	109.3
C28-H28B	0.9800	C5C-H5CB	0.9800	C15-C16-H16A	109.5
C28-H28C	0.9800	C5C-H5CC	0.9800	C15-C16-H16B	109.5
C29-C30	1.387(4)	C1D-H1DA	0.9800	C15-C16-H16C	109.5
C29-C34	1.394(3)	C1D-H1DB	0.9800	H16A-C16-H16B	109.5
C30-H30	0.9500	C1D-H1DC	0.9800	H16A-C16-H16C	109.5
C30-C31	1.391(4)	C1D-C2D	1.4987(17)	H16B-C16-H16C	109.5
C31-H31	0.9500	C2D-H2DA	0.9900	C22-C21-P1	123.3(2)
C31-C32	1.389(4)	C2D-H2DB	0.9900	C22-C21-C35	117.0(2)
C32-H32	0.9500	C2D-O3D	1.384(2)	C35-C21-P1	119.64(19)
C32-C33	1.400(3)	O3D-C4D	1.381(2)	C21-C22-H22	119.8
C33-C34	1.393(3)	C4D-H4DA	0.9900	C23-C22-C21	120.5(3)
C36-C37	1.394(4)	C4D-H4DB	0.9900	C23-C22-H22	119.8
C36-C41	1.398(4)	C4D-C5D	1.4978(17)	C22-C23-H23	119.7
C37-H37	0.9500	C5D-H5DA	0.9800	C24-C23-C22	120.6(3)
C37-C38	1.389(4)	C5D-H5DB	0.9800	C24-C23-H23	119.7
C38-H38	0.9500	C5D-H5DC	0.9800	C23-C24-H24	119.6
C38-C39	1.383(5)			C23-C24-C25	120.8(3)
C39-H39	0.9500	Atom-Atom-Atom	Angle [°]	C25-C24-H24	119.6
C39-C40	1.386(5)	P1-Cu1-P2	120.98(3)	C24-C25-C26	124.7(2)
C40-H40	0.9500	N1-Cu1-P1	117.86(6)	C35-C25-C24	117.2(3)
C40-C41	1.390(4)	N1-Cu1-P2	102.79(6)	C35-C25-C26	118.1(2)
C41-H41	0.9500	N1-Cu1-N2	81.07(9)	C25-C26-C27	108.2(2)
C42-C43	1.401(4)	N2-Cu1-P1	124.72(6)	C25-C26-C29	106.2(2)
C42-C47	1.393(4)	N2-Cu1-P2	101.16(6)	C28-C26-C25	112.4(3)
C43-H43	0.9500	C21-P1-Cu1	116.47(8)	C28-C26-C27	109.4(3)
C43-C44	1.389(4)	C36-P1-Cu1	114.89(8)	C28-C26-C29	112.0(2)
C44-H44	0.9500	C36-P1-C21	103.21(12)	C29-C26-C27	108.4(2)
C44-C45	1.384(5)	C36-P1-C42	102.21(12)	C26-C27-H27A	109.5
C45-H45	0.9500	C42-P1-Cu1	115.35(9)	C26-C27-H27B	109.5
C45-C46	1.387(5)	C42-P1-C21	102.79(12)	C26-C27-H27C	109.5
C46-H46	0.9500	C33-P2-Cu1	115.42(8)	H27A-C27-H27B	109.5
C46-C47	1.388(4)	C48-P2-Cu1	108.43(8)	H27A-C27-H27C	109.5
C47-H47	0.9500	C48-P2-C33	105.58(11)	H27B-C27-H27C	109.5
Atom-Atom-Atom	Angle [°]	Atom-Atom-Atom	Angle [°]		
C26-C28-H28A	109.5	C1-C17A-H17A	106.4		
C26-C28-H28B	109.5	C1-C17A-H17B	106.4		
C26-C28-H28C	109.5	C1-C17A-C18A	123.6(6)		

H28A-C28-H28B	109.5	H17A-C17A-H17B	106.5
H28A-C28-H28C	109.5	C18A-C17A-H17A	106.4
H28B-C28-H28C	109.5	C18A-C17A-H17B	106.4
C30-C29-C26	125.1(2)	C17A-C18A-H18A	112.1
C30-C29-C34	117.2(2)	C17A-C18A-H18B	112.1
C34-C29-C26	117.6(2)	C17A-C18A-C19A	98.5(6)
C29-C30-H30	119.6	H18A-C18A-H18B	109.7
C29-C30-C31	120.8(2)	C19A-C18A-H18A	112.1
C31-C30-H30	119.6	C19A-C18A-H18B	112.1
C30-C31-H31	119.6	C18A-C19A-H19A	105.6
C32-C31-C30	120.9(2)	C18A-C19A-H19B	105.6
C32-C31-H31	119.6	H19A-C19A-H19B	106.1
C31-C32-H32	120.1	C20A-C19A-C18A	127.0(7)
C31-C32-C33	119.8(2)	C20A-C19A-H19A	105.6
C33-C32-H32	120.1	C20A-C19A-H19B	105.6
C32-C33-P2	126.0(2)	C19A-C20A-H20A	109.5
C34-C33-P2	116.33(18)	C19A-C20A-H20B	109.5
C34-C33-C32	117.6(2)	C19A-C20A-H20C	109.5
O1-C34-C29	119.4(2)	H20A-C20A-H20B	109.5
O1-C34-C33	117.0(2)	H20A-C20A-H20C	109.5
C33-C34-C29	123.6(2)	H20B-C20A-H20C	109.5
O1-C35-C21	116.8(2)	C1-C17B-H17C	108.8
O1-C35-C25	119.3(2)	C1-C17B-H17D	108.8
C25-C35-C21	123.9(2)	C1-C17B-C18B	113.9(5)
C37-C36-P1	123.4(2)	H17C-C17B-H17D	107.7
C37-C36-C41	119.0(2)	C18B-C17B-H17C	108.8
C41-C36-P1	117.55(19)	C18B-C17B-H17D	108.8
C36-C37-H37	120.0	C17B-C18B-H18C	109.8
C38-C37-C36	120.1(3)	C17B-C18B-H18D	109.8
C38-C37-H37	120.0	C17B-C18B-C19B	109.4(5)
C37-C38-H38	119.6	H18C-C18B-H18D	108.2
C39-C38-C37	120.8(3)	C19B-C18B-H18C	109.8
C39-C38-H38	119.6	C19B-C18B-H18D	109.8
C38-C39-H39	120.3	C18B-C19B-H19C	113.4
C38-C39-C40	119.5(3)	C18B-C19B-H19D	113.4
C40-C39-H39	120.3	H19C-C19B-H19D	110.7
C39-C40-H40	119.8	C20B-C19B-C18B	91.6(8)
C39-C40-C41	120.3(3)	C20B-C19B-H19C	113.4

C41-C40-H40	119.8	C20B-C19B-H19D	113.4
C36-C41-H41	119.8	C19B-C20B-H20D	109.5
C40-C41-C36	120.3(3)	C19B-C20B-H20E	109.5
C40-C41-H41	119.8	C19B-C20B-H20F	109.5
C43-C42-P1	122.8(2)	H20D-C20B-H20E	109.5
C47-C42-P1	118.0(2)	H20D-C20B-H20F	109.5
C47-C42-C43	119.1(2)	H20E-C20B-H20F	109.5
C42-C43-H43	120.0	F1-B1-F2	107.7(3)
C44-C43-C42	120.1(3)	F3-B1-F1	110.3(3)
C44-C43-H43	120.0	F3-B1-F2	106.1(3)
C43-C44-H44	119.9	F4-B1-F1	111.5(3)
C45-C44-C43	120.2(3)	F4-B1-F2	108.5(3)
C45-C44-H44	119.9	F4-B1-F3	112.5(3)
C44-C45-H45	120.0	Cl1-C17-Cl2	112.3(4)
C44-C45-C46	120.0(3)	Cl1-C17-H17E	109.2
C46-C45-H45	120.0	Cl1-C17-H17F	109.2
C45-C46-H46	119.9	Cl2-C17-H17E	109.2
C45-C46-C47	120.1(3)	Cl2-C17-H17F	109.2
C47-C46-H46	119.9	H17E-C17-H17F	107.9
C42-C47-H47	119.8	H1CA-C1C-H1CB	109.5
C46-C47-C42	120.4(3)	H1CA-C1C-H1CC	109.5
C46-C47-H47	119.8	H1CB-C1C-H1CC	109.5
C49-C48-P2	119.4(2)	C2C-C1C-H1CA	109.5
C53-C48-P2	121.5(2)	C2C-C1C-H1CB	109.5
C53-C48-C49	118.2(2)	C2C-C1C-H1CC	109.5
C48-C49-H49	119.5	C1C-C2C-H2CA	107.9
C50-C49-C48	120.9(3)	C1C-C2C-H2CB	107.9
C50-C49-H49	119.5	H2CA-C2C-H2CB	107.2
C49-C50-H50	120.0	O3C-C2C-C1C	117.8(3)
C51-C50-C49	120.0(3)	O3C-C2C-H2CA	107.9
C51-C50-H50	120.0	O3C-C2C-H2CB	107.9
C50-C51-H51	119.9	C2C-O3C-C4C	126.4(3)
C50-C51-C52	120.2(3)	O3C-C4C-H4CA	108.0
C52-C51-H51	119.9	O3C-C4C-H4CB	108.0
C51-C52-H52	120.0	O3C-C4C-C5C	117.1(3)
C51-C52-C53	120.0(3)	H4CA-C4C-H4CB	107.3
C53-C52-H52	120.0	C5C-C4C-H4CA	108.0
C48-C53-H53	119.7	C5C-C4C-H4CB	108.0
C52-C53-C48	120.7(3)	C4C-C5C-H5CA	109.5
C52-C53-H53	119.7	C4C-C5C-H5CB	109.5

C55–C54–P2	118.2(2)	C4C–C5C–H5CC	109.5
C59–C54–P2	122.2(2)	H5CA–C5C–H5CB	109.5
C59–C54–C55	119.3(2)	H5CA–C5C–H5CC	109.5
C54–C55–H55	119.9	H5CB–C5C–H5CC	109.5
C56–C55–C54	120.2(3)	H1DA–C1D–H1DB	109.5
C56–C55–H55	119.9	H1DA–C1D–H1DC	109.5
C55–C56–H56	120.0	H1DB–C1D–H1DC	109.5
C57–C56–C55	120.1(3)	C2D–C1D–H1DA	109.5
C57–C56–H56	120.0	C2D–C1D–H1DB	109.5
C56–C57–H57	119.9	C2D–C1D–H1DC	109.5
C58–C57–C56	120.1(3)	C1D–C2D–H2DA	108.5
C58–C57–H57	119.9	C1D–C2D–H2DB	108.5
C57–C58–H58	119.9	H2DA–C2D–H2DB	107.5
C57–C58–C59	120.2(3)	O3D–C2D–C1D	114.9(3)
C59–C58–H58	119.9	O3D–C2D–H2DA	108.5
C54–C59–H59	119.9	O3D–C2D–H2DB	108.5
C58–C59–C54	120.1(3)	C4D–O3D–C2D	123.7(3)
C58–C59–H59	119.9	O3D–C4D–H4DA	108.5
		O3D–C4D–H4DB	108.5
		O3D–C4D–C5D	115.3(3)
		H4DA–C4D–H4DB	107.5
		C5D–C4D–H4DA	108.5
		C5D–C4D–H4DB	108.5
		C4D–C5D–H5DA	109.5
		C4D–C5D–H5DB	109.5
		C4D–C5D–H5DC	109.5
		H5DA–C5D–H5DB	109.5
		H5DA–C5D–H5DC	109.5
		H5DB–C5D–H5DC	109.5

Table A3 - 12 Torsion angles for Cu(Bphen)(Xantphos)BF₄

Atom–Atom–Atom–Atom	Torsion Angle [°]	Atom–Atom–Atom–Atom	Torsion Angle [°]
Cu1–P1–C21–C22	136.8(2)	C26–C29–C34–O1	2.7(3)
Cu1–P1–C21–C35	-40.0(2)	C26–C29–C34–C33	-177.3(2)
Cu1–P1–C36–C37	105.9(2)	C27–C26–C29–C30	-100.6(3)
Cu1–P1–C36–C41	-71.0(2)	C27–C26–C29–C34	77.3(3)

Cu1-P1-C42-C43	158.40(19)	C28-C26-C29-C30	20.2(4)
Cu1-P1-C42-C47	-22.8(2)	C28-C26-C29-C34	-161.9(3)
Cu1-P2-C33-C32	-133.7(2)	C29-C30-C31-C32	0.2(4)
Cu1-P2-C33-C34	49.0(2)	C30-C29-C34-O1	-179.3(2)
Cu1-P2-C48-C49	69.4(2)	C30-C29-C34-C33	0.8(4)
Cu1-P2-C48-C53	-100.0(2)	C30-C31-C32-C33	1.2(4)
Cu1-P2-C54-C55	-20.3(2)	C31-C32-C33-P2	-178.7(2)
Cu1-P2-C54-C59	165.4(2)	C31-C32-C33-C34	-1.5(4)
Cu1-N1-C1-C2	173.0(2)	C32-C33-C34-O1	-179.4(2)
Cu1-N1-C1-C17A	-11.1(6)	C32-C33-C34-C29	0.5(4)
Cu1-N1-C1-C17B	-3.3(7)	C33-P2-C48-C49	-54.9(2)
Cu1-N1-C12-C4	-173.3(2)	C33-P2-C48-C53	135.7(2)
Cu1-N1-C12-C11	5.6(3)	C33-P2-C54-C55	106.7(2)
Cu1-N2-C10-C9	-172.65(19)	C33-P2-C54-C59	-67.6(2)
Cu1-N2-C10-C13	8.1(4)	C34-O1-C35-C21	140.3(2)
Cu1-N2-C11-C7	174.4(2)	C34-O1-C35-C25	-38.3(3)
Cu1-N2-C11-C12	-4.6(3)	C34-C29-C30-C31	-1.1(4)
P1-C21-C22-C23	-176.6(2)	C35-O1-C34-C29	38.0(3)
P1-C21-C35-O1	-1.5(3)	C35-O1-C34-C33	-142.0(2)
P1-C21-C35-C25	177.0(2)	C35-C21-C22-C23	0.4(4)
P1-C36-C37-C38	-177.1(2)	C35-C25-C26-C27	-77.5(3)
P1-C36-C41-C40	177.3(2)	C35-C25-C26-C28	161.6(3)
P1-C42-C43-C44	177.9(2)	C35-C25-C26-C29	38.7(3)
P1-C42-C47-C46	-178.4(3)	C36-P1-C21-C22	-96.3(2)
P2-C33-C34-O1	-1.9(3)	C36-P1-C21-C35	86.8(2)

P2-C33-C34-C29	178.0(2)	C36-P1-C42-C43	33.0(2)
P2-C48-C49-C50	-170.3(2)	C36-P1-C42-C47	-148.2(2)
P2-C48-C53-C52	170.5(2)	C36-C37-C38-C39	0.0(5)
P2-C54-C55-C56	-174.1(2)	C37-C36-C41-C40	0.2(4)
P2-C54-C59-C58	175.2(3)	C37-C38-C39-C40	0.2(5)
N1-C1-C2-C3	-1.1(5)	C38-C39-C40-C41	-0.2(5)
N1-C1-C17A-C18A	134.2(7)	C39-C40-C41-C36	0.0(4)
N1-C1-C17B-C18B	-171.6(7)	C41-C36-C37-C38	-0.2(4)
N2-C10-C13-C14	-124.2(3)	C42-P1-C21-C22	9.7(3)
N2-C11-C12-N1	-0.6(4)	C42-P1-C21-C35	-167.2(2)
N2-C11-C12-C4	178.3(2)	C42-P1-C36-C37	-128.4(2)
C1-N1-C12-C4	1.0(4)	C42-P1-C36-C41	54.7(2)
C1-N1-C12-C11	179.9(2)	C42-C43-C44-C45	0.3(4)
C1-C2-C3-C4	1.5(5)	C43-C42-C47-C46	0.4(4)
C1-C17A-C18A-C19A	152.2(8)	C43-C44-C45-C46	0.8(5)
C1-C17B-C18B-C19B	-167.0(7)	C44-C45-C46-C47	-1.2(5)
C2-C1-C17A-C18A	-49.8(11)	C45-C46-C47-C42	0.6(5)
C2-C1-C17B-C18B	12.1(12)	C47-C42-C43-C44	-0.9(4)
C2-C3-C4-C5	180.0(3)	C48-P2-C33-C32	-14.0(3)
C2-C3-C4-C12	-0.6(5)	C48-P2-C33-C34	168.78(19)
C3-C4-C5-C6	-179.0(3)	C48-P2-C54-C55	-144.2(2)
C3-C4-C12-N1	-0.7(4)	C48-P2-C54-C59	41.5(3)
C3-C4-C12-C11	-179.5(3)	C48-C49-C50-C51	-0.3(4)
C4-C5-C6-C7	-2.2(5)	C49-C48-C53-C52	1.0(4)
C5-C4-C12-N1	178.8(3)	C49-C50-C51-C52	0.8(5)

C5-C4-C12-C11	-0.1(4)	C50-C51-C52-C53	-0.4(5)
C5-C6-C7-C8	-177.1(3)	C51-C52-C53-C48	-0.5(5)
C5-C6-C7-C11	1.3(5)	C53-C48-C49-C50	-0.6(4)
C6-C7-C8-C9	177.6(3)	C54-P2-C33-C32	95.5(2)
C6-C7-C11-N2	-178.8(3)	C54-P2-C33-C34	-81.8(2)
C6-C7-C11-C12	0.2(4)	C54-P2-C48-C49	-159.1(2)
C7-C8-C9-C10	1.0(4)	C54-P2-C48-C53	31.5(2)
C7-C11-C12-N1	-179.7(2)	C54-C55-C56-C57	-1.3(5)
C7-C11-C12-C4	-0.7(4)	C55-C54-C59-C58	0.9(5)
C8-C7-C11-N2	-0.3(4)	C55-C56-C57-C58	0.8(5)
C8-C7-C11-C12	178.7(2)	C56-C57-C58-C59	0.5(6)
C8-C9-C10-N2	0.0(4)	C57-C58-C59-C54	-1.3(5)
C8-C9-C10-C13	179.2(3)	C59-C54-C55-C56	0.4(4)
C9-C10-C13-C14	56.6(4)	C17A-C1-C2-C3	-177.0(6)
C10-N2-C11-C7	1.2(4)	C17A-C18A-C19A-C20A	-137.6(9)
C10-N2-C11-C12	-177.8(2)	C17B-C1-C2-C3	174.8(7)
C10-C13-C14-C15	-173.0(3)	C17B-C18B-C19B-C20B	-138.4(10)
C11-N2-C10-C9	-1.1(4)	C1C-C2C-O3C-C4C	-84.6(15)
C11-N2-C10-C13	179.7(2)	C2C-O3C-C4C-C5C	103.3(12)
C11-C7-C8-C9	-0.8(4)	C1D-C2D-O3D-C4D	147.1(14)
C12-N1-C1-C2	-0.1(4)	C2D-O3D-C4D-C5D	118.5(11)

A3.14 References

1. Minozzi, C.; Caron, A.; Grenier-Petel, J.-C.; Santandrea, J.; Collins, S. K., *Angew. Chem., Int. Ed.* **2018**, *57* (19), 5477-5481.
2. Sosoe, J.; Cruché, C.; Morin, É.; Collins, S. K., *Can. J. Chem.* **2020**, *98* (9), 461-465.
3. Caron, A.; Morin, É.; Collins, S. K., *ACS Catal.* **2019**, *9* (10), 9458-9464.
4. Qian, G.; Liu, B.; Tan, Q.; Zhang, S.; Xu, B., *European J. Org. Chem.* **2014**, *2014* (22), 4837-4843.
5. Yang, W.; Nakano, T., *Chem. Commun.* **2015**, *51* (97), 17269-17272.
6. She, Z.; Shi, Y.; Huang, Y.; Cheng, Y.; Song, F.; You, J., *Chem. Commun.* **2014**, *50* (90), 13914-13916.
7. Tomita, R.; Mantani, K.; Hamasaki, A.; Ishida, T.; Tokunaga, M., *Chem. - Eur. J.* **2014**, *20* (32), 9914-9917.
8. Rao, M. L. N.; Ramakrishna, B. S., *J. Org. Chem.* **2019**, *84* (9), 5677-5683.
9. Kindt, S.; Wicht, K.; Heinrich, M. R., *Angew. Chem., Int. Ed.* **2016**, *55* (30), 8744-8747.
10. Yang, Z.; Chen, X.; Kong, W.; Xia, S.; Zheng, R.; Luo, F.; Zhu, G., *Org. Biomol. Chem.* **2013**, *11* (13), 2175-2185.
11. Metternich, J. B.; Gilmour, R., *J. Am. Chem. Soc.* **2015**, *137* (35), 11254-11257.
12. Brégent, T.; Bouillon, J.-P.; Poisson, T., *Org. Lett.* **2020**, *22* (19), 7688-7693.
13. Nishikawa, K.; Fukuda, H.; Abe, M.; Nakanishi, K.; Tazawa, Y.; Yamaguchi, C.; Hiradate, S.; Fujii, Y.; Okuda, K.; Shindo, M., *Phytochemistry* **2013**, *96*, 223-234.
14. Satham, L.; Sankara, C. S.; Namboothiri, I. N. N., *European J. Org. Chem.* **2020**, *2020* (44), 6903-6908.
15. Nguyen, T. N. T.; Thiel, N. O.; Teichert, J. F., *Chem. Commun.* **2017**, *53* (85), 11686-11689.
16. Arai, N.; Sato, K.; Azuma, K.; Ohkuma, T., *Angew. Chem., Int. Ed.* **2013**, *52* (29), 7500-7504.
17. Onneken, C.; Bussmann, K.; Gilmour, R., *Angew. Chem., Int. Ed.* **2020**, *59* (1), 330-334.
18. Gui, Q.; Hu, L.; Chen, X.; Liu, J.; Tan, Z., *Chem. Commun.* **2015**, *51* (73), 13922-13924.
19. Molloy, J. J.; Metternich, J. B.; Daniliuc, C. G.; Watson, A. J. B.; Gilmour, R., *Angew. Chem., Int. Ed.* **2018**, *57* (12), 3168-3172.

20. Metternich, J. B.; Artiukhin, D. G.; Holland, M. C.; Von Bremen-Kühne, M.; Neugebauer, J.; Gilmour, R., *J. Org. Chem.* **2017**, *82* (19), 9955-9977.
21. Litman, Z. C.; Wang, Y.; Zhao, H.; Hartwig, J. F., *Nature* **2018**, *560* (7718), 355-359.
22. Grenier-Petel, J.-C.; Collins, S. K., *ACS Catal.* **2019**, 3213-3218.
23. Li, D.; Kim, Y. E.; Yun, J., *Org. Lett.* **2015**, *17* (4), 860-863.
24. Imashiro, R.; Seki, M., *J. Org. Chem.* **2004**, *69* (12), 4216-4226.
25. Byrne, P. A.; Gilheany, D. G., *J. Am. Chem. Soc.* **2012**, *134* (22), 9225-9239.
26. Tai, C.-C.; Yu, M.-S.; Chen, Y.-L.; Chuang, W.-H.; Lin, T.-H.; Yap, G. P. A.; Ong, T.-G., *Chem. Commun.* **2014**, *50* (33), 4344-4346.
27. Korytiaková, E.; Thiel, N. O.; Pape, F.; Teichert, J. F., *Chem. Commun.* **2017**, *53* (4), 732-735.
28. Faßbender, S. I.; Metternich, J. B.; Gilmour, R., *Org. Lett.* **2018**, *20* (3), 724-727.
29. Mantilli, L.; Gérard, D.; Torche, S.; Besnard, C.; Mazet, C., *Angew. Chem., Int. Ed.* **2009**, *48* (28), 5143-5147.
30. Rivada-Wheelaghan, O.; Chakraborty, S.; Shimon, L. J. W.; Ben-David, Y.; Milstein, D., *Angew. Chem., Int. Ed.* **2016**, *55* (24), 6942-6945.
31. Hossain, A.; Engl, S.; Lutsker, E.; Reiser, O., *ACS Catal.* **2019**, *9* (2), 1103-1109.
32. Zeng, K.; Chen, L.; Chen, Y.; Liu, Y.; Zhou, Y.; Au, C.-T.; Yin, S.-F., **2017**, *359* (5), 841-847.
33. Li, X.; Shi, X.; Fang, M.; Xu, X., *J. Org. Chem.* **2013**, *78* (18), 9499-9504.
34. Alkan-Zambada, M.; Hu, X., *J. Org. Chem.* **2019**, *84* (7), 4525-4533.
35. Sun, Y.; Abdukader, A.; Lu, D.; Zhang, H.; Liu, C., *Green Chem.* **2017**, *19* (5), 1255-1258.
36. Rao, W.; Chan, P. W. H., *Org. Biomol. Chem.* **2010**, *8* (17), 4016-4025.
37. Cuttell, D. G.; Kuang, S.-M.; Fanwick, P. E.; McMillin, D. R.; Walton, R. A., *J. Am. Chem. Soc.* **2002**, *124* (1), 6-7.
38. Bruker, S., 2016/2, Bruker AXS Inc., Madison, Wisconsin, USA.
39. Sheldrick, G., *Acta Crystallographica Section A* **2015**, *71* (1), 3-8.
40. Sheldrick, G., *Acta Crystallographica Section C* **2015**, *71* (1), 3-8.
41. D. Kratzert, F., V84, <https://www.xs3.uni-freiburg.de/research/finalcif>.

Annexe 4 – Decomposition of Lignin Models Enabled by Copper-Based Photocatalysis Under Biphasic Conditions

Cédric Bertin,^a Corentin Cruché,^a Franklin Chaçon-Huete,^{ab} Pat Forqione^{b*} and Shawn K. Collins^{a*}

a Département de Chimie, Centre for Green Chemistry and Catalysis, Université de Montréal, 1375 Avenue Thérèse-Lavoie-Roux, Montréal, QC H2V 0B3 CANADA b Department of Chemistry and Biochemistry, Concordia University, 7141 Sherbrooke St W., Montreal, QC H4B 1R6, CANADA

Green Chem., **2022**, 24, 4414-4419 <https://doi.org/10.1039/D2GC01116F>

A4.1 Abstract

A heteroleptic copper complex, Cu(bathocup)(XantPhos)BF₄ promotes the fragmentation of lignin models of the β-O-4 linkage under aqueous biphasic reaction conditions using catalytic amounts of NABnH, a hydrogen atom donor. The catalytic system as a whole represents a green shift from previous reaction conditions for analogous processes that either exploit expensive rare metals such as Ir for photocatalysis, employ stoichiometric amounts of proton- and/or hydrogen (H) atom donors and chlorinated solvents. The reaction conditions and catalyst system are amendable to flow chemistry set-ups for gram scale fragmentation of lignin polymer models.

A4.2 Introduction

The exploitation of biomass has received significant interest as a sustainable strategy toward abundant renewable sources of carbon.¹⁻³ In parallel with its current use as an energy source, lignin is a potential starting material towards low molecular weight⁴⁻⁵ aromatic commodity chemicals.⁶⁻⁷ A common strategy to depolymerize lignin is to target the β-O-4 linkage, since it is present in 45–60% of the bonds in lignin.⁸⁻⁹ Current technologies involve either a one- or two-step

fragmentation process that are generally classified as reductive,¹⁰⁻¹³ oxidative,¹⁴⁻²¹ or redox-neutral.²²⁻²⁹ Photochemical methods for lignin depolymerization are regarded as advantageous since they typically occur at room temperature, improving the selectivity of bond cleavage and consequently facilitating purification of the desired target compounds. Visible light photocatalysis, in particular, adheres to green chemistry principles employing low energy and readily abundant light sources.³⁰⁻³¹ Photochemical degradation of lignin can occur as a two-step process, in which oxidation of a benzylic secondary alcohol provides the corresponding ketone. Such oxidations can be promoted thermally, electrochemically or photochemically (**Figure A 4-1, A**). The resulting ketone is then a target for single electron transfer (SET) that can be catalyzed through heterogeneous catalysts,³² polymeric organic dyes³³ or discrete Ir-based complexes.³⁴⁻³⁷

Our group has reported two examples of reductive PCET using copper-based complexes (**Figure A 4-1, B**).³⁸⁻⁴² In one case, a diimine ligand (**NN**) was designed to function both as a ligand for the metal and proton-donor in photochemical pinacol reactions.⁴³ Additionally, we demonstrated that a Cu(**quintri**)(**XantPhos**)BF₄ catalyst was optimal for a PCET process that involved a reductive ketone/cyclization process⁴⁴ previously published by Knowles.⁴⁵

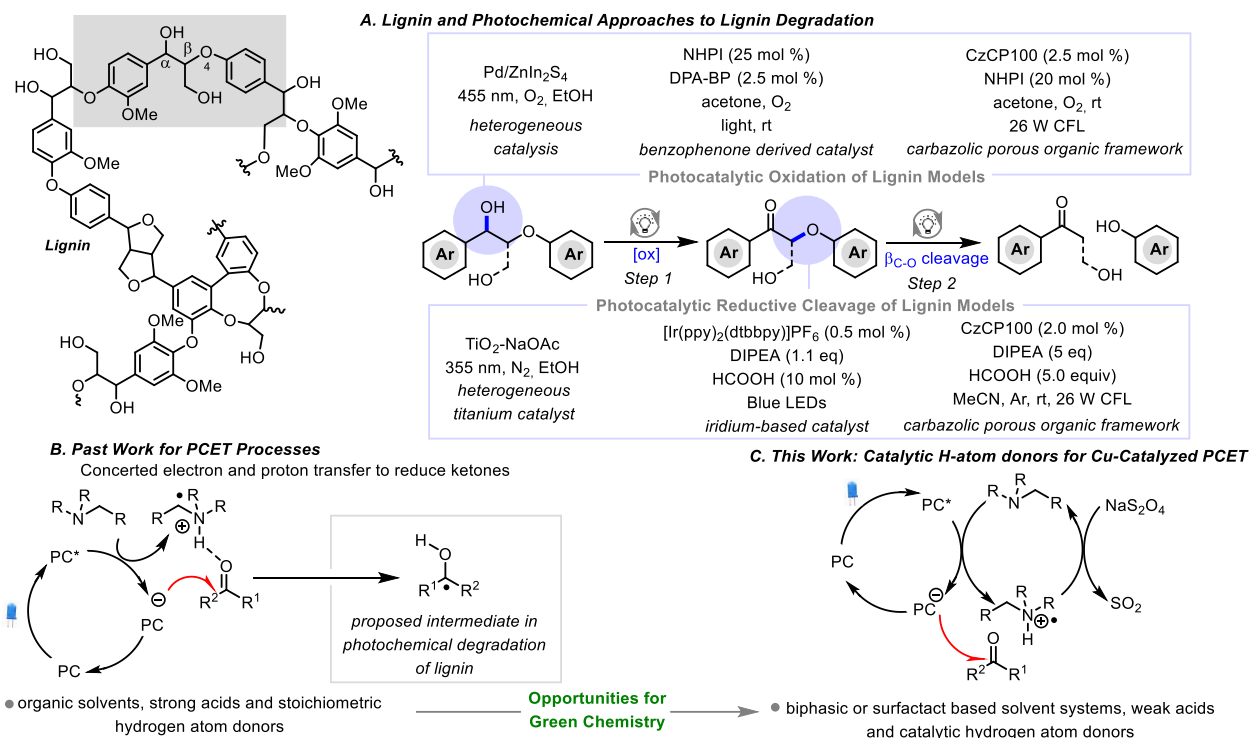


Figure A4 - 1 Decomposition of Lignin Models

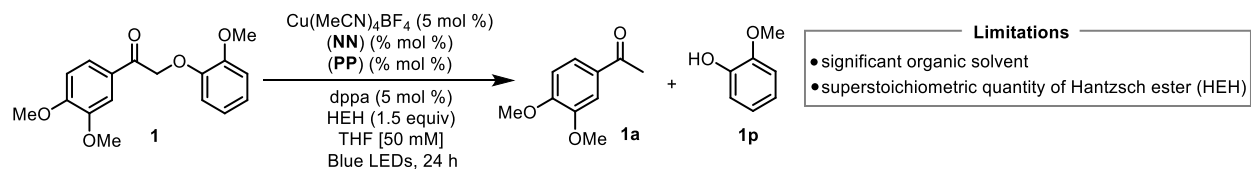
Given the mechanistic similarity between the aforementioned processes and photochemical lignin degradation, we envisioned optimizing a copper complex⁴⁶⁻⁵² for the degradation of lignin models of the β -O-4 linkage (**Figure A 4-1, C**). Previous methods for reductive PCET employed stoichiometric amounts of proton- and/or hydrogen (H) atom donors and chlorinated solvents that do not adhere to current green chemistry guidelines. To improve the process, catalytic H-atom donors and greener solvent systems were explored. Herein, we report the optimization of a heteroleptic copper-based photocatalyst for fragmentation of lignin models, development of aqueous biphasic reaction conditions that allow catalytic amounts of hydrogen atom donors, depolymerization of lignin models and scale-up via flow chemistry.

A4.3 Discussion

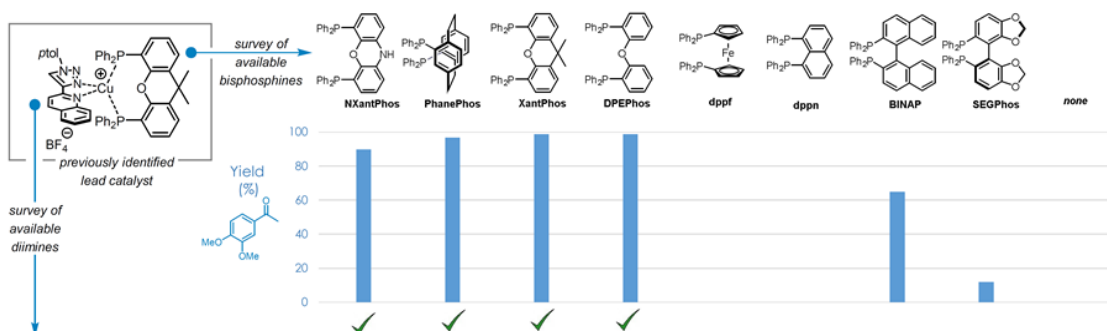
Optimization of Catalyst Structure.

Given the past success of the Cu(quintri)(XantPhos)BF₄ catalyst for a PCET process, the structure was chosen as a starting point for further optimization (**Figure A 4-2**). The photochemical cleavage

of the lignin model **1** to its corresponding acetophenone **1a** and phenol **1p**, was explored using previously reported conditions [catalyst (5 mol %), diphenylphosphoric acid (dppa, 5 mol %), Hantzsch ester (1.5 equiv), CH₂Cl₂, blue LEDs, 24 h]. First, a series of heteroleptic copper-based complexes possessing the **quintri** diimine ligand (**NN**) and various bisphosphines (**PP**) were evaluated (**Figure A 4-2, a**). Four of the eight ligands evaluated provided yields of the resulting acetophenone **1a** in >90 % yield (**XantPhos**, **DPEPhos**, **PhanePhos**, **NXantPhos**). In a second screening, the diimine ligand was varied and **XantPhos** was selected as the bisphosphine (**Figure A 4-2, b**). From the 17 diimines selected, four complexes were identified that provided the corresponding acetophenone **1a** in >90 % yield. The four complexes possessed the diimines **dmp**, **bphen**, **bathocup** and the original **quintri** ligand. Having identified seven complexes amongst the 25 screened, it was clear that heteroleptic copper complexes held substantial promise in reductive PCET processes to decompose lignin models. However, eliminating the need for the stoichiometric HEH additive would further align with green chemistry principles. Subsequently, reaction conditions were investigated employing catalytic H-atom donors and alternative solvents (**Table A 4-1**).



a. Screening of Cu(quintri)(PP)BF₄ complexes



b. Screening of Cu(NN)(XantPhos)BF₄ complexes

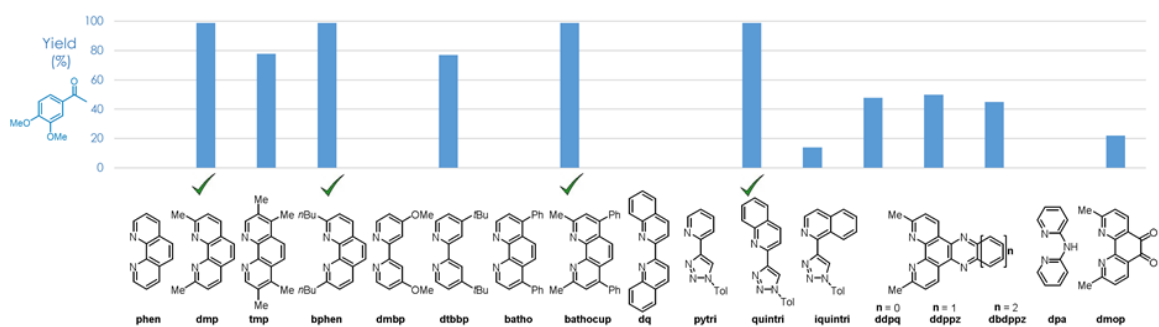
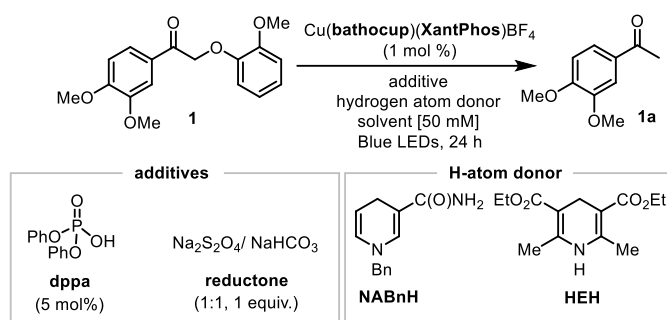


Figure A4 - 2 Evaluation of Cu(I)-Based Photocatalysts in the Cleavage of a Lignin Model. Reaction conditions for all reactions shown in top scheme. GC-MS yields of acetophenone 1a. See Supporting Information for details.

Table A4 - 1 Optimization of Biphasic Conditions



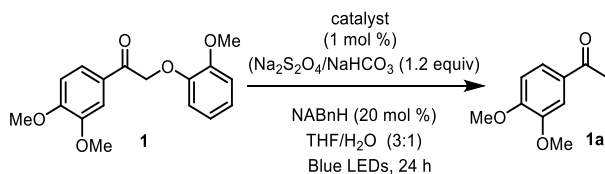
	additive	H- atom donor (equiv.)	solvent	yield 1a (%) ^a
1	dppa	HEH (1.5)	CH ₂ Cl ₂	99
2	dppa	HEH (1.5)	THF	62
3	dppa	NABnH (1.5)	THF	13
4	dppa, red	NABnH (0.2)	THF	9
5	dppa, red	NABnH (0.2)	THF/H ₂ O (1:1)	67
6	dppa, red	NABnH (0.2)	THF/H ₂ O (2:1)	78
7	dppa, red	NABnH (0.2)	THF/H ₂ O (3:1)	75
8	red	NABnH (0.2)	THF/H ₂ O (3:1)	78
9	red (1.2 equiv)	NABnH (0.2)	THF/H ₂ O (3:1) ^b	86
10	red (1.2 equiv)	NABnH (0.2)	H ₂ O	4 ^c

^a Yields following flash chromatography. ^b Less than 2% **1a** in the absence of light. ^c Yield determined by GC-MS.

The Cu(**bathocup**)(**XantPhos**)BF₄ was selected for the initial screening. An analogous catalyst (Cu(**bathocup**)(**DPEPhos**)BF₄) had been identified by Evano and co-workers as highly efficient at reductive quenching in the excited state.⁵³⁻⁵⁵ When the catalyst was used to

decompose the lignin model **1** under previously reported conditions in CH₂Cl₂, the yield of the acetophenone **1a** was quantitative, but dropped to 62 % when the solvent was changed to THF (**Table A 4-1**, entry 2). Replacing the HEH with NaBnH,⁵⁶ a bio-inspired analog of NADPH, further decreased the yield of **1a** to 13% (entry 3). In an effort to decrease the loading of NaBnH to 20 mol %, a mixture of Na₂S₂O₄/NaHCO₃ (“red”, 1 equiv) was added to facilitate the H-atom donor turnover. Disappointingly, no increase in the yield of **1a** was observed. Biphasic conditions were evaluated to improve the solubility of the reaction mixture. When a mixture of THF/H₂O (1:1) was used (entry 5), the yield improved to 67 % (**1a**). Subsequent optimization of the solvent ratio and additive quantities afforded reaction conditions that resulted in an 86 % yield of **1a** while also demonstrating that the dppa additive was no longer necessary (entry 9). With the optimized conditions in hand, the 6 other catalysts identified from the initial screening were re-evaluated (**Table A 4-2**).

Table A4 - 2 Activity of Various Catalysts under Biphasic Conditions



entry	catalyst	yield 1a (%) ^a
1	Cu(bathocup)(XantPhos)B F ₄	86
2	Cu(dmp)(XantPhos)BF ₄	70
3	Cu(bphen)(XantPhos)BF ₄	15
4	Cu(quintri)(XantPhos)BF ₄	12
5	Cu(quintri)(NXantPhos)BF ₄	12
6	Cu(quintri)(DPEPhos)BF ₄	18
7	Cu(quintri)(BINAP)BF ₄	10

^a Yields following flash chromatography

While the Cu(dmp)(XantPhos)BF₄ catalyst still afforded a good yield of **1a** (70 %, entry 2), all other complexes were ineffective under the new reaction conditions (entries 3-7). In analogy to previously reported PCET processes,⁴⁴ the Cu(bathocup)(XantPhos)BF₄ complex will undergo excitation when irradiated by the blue LEDs (**Figure A 4-3**). Stern-Volmer experiments confirmed that the excited state of the catalyst is quenched by the NABnH to afford the reduced ground state of the Cu(bathocup)(XantPhos)BF₄ complex, which would subsequently mediate single electron transfer (SET) to the lignin model. The subsequently formed radical anion undergoes hydrogen atom transfer providing NABn⁺ and promoting fragmentation to afford the corresponding products. The NABn⁺ is then regenerated via reduction with Na₂S₂O₈. When the decomposition of lignin model 6 to 6a was performed under the optimal conditions using 3:1 THF:D₂O, mono-deuterated acetophenone in the 2-position (**Figure A 4-3**) was observed (see Supporting Information for details.)

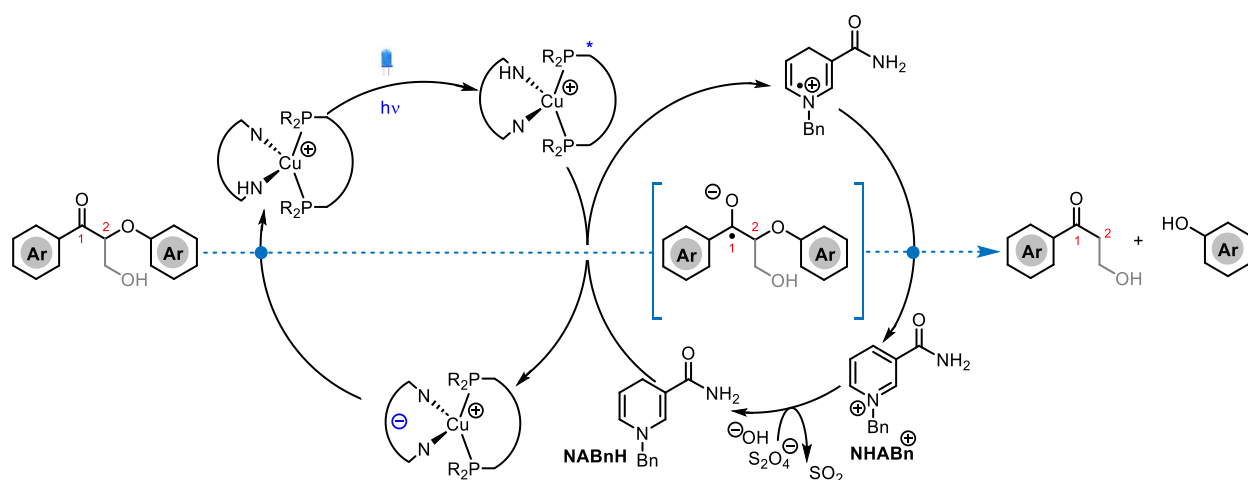


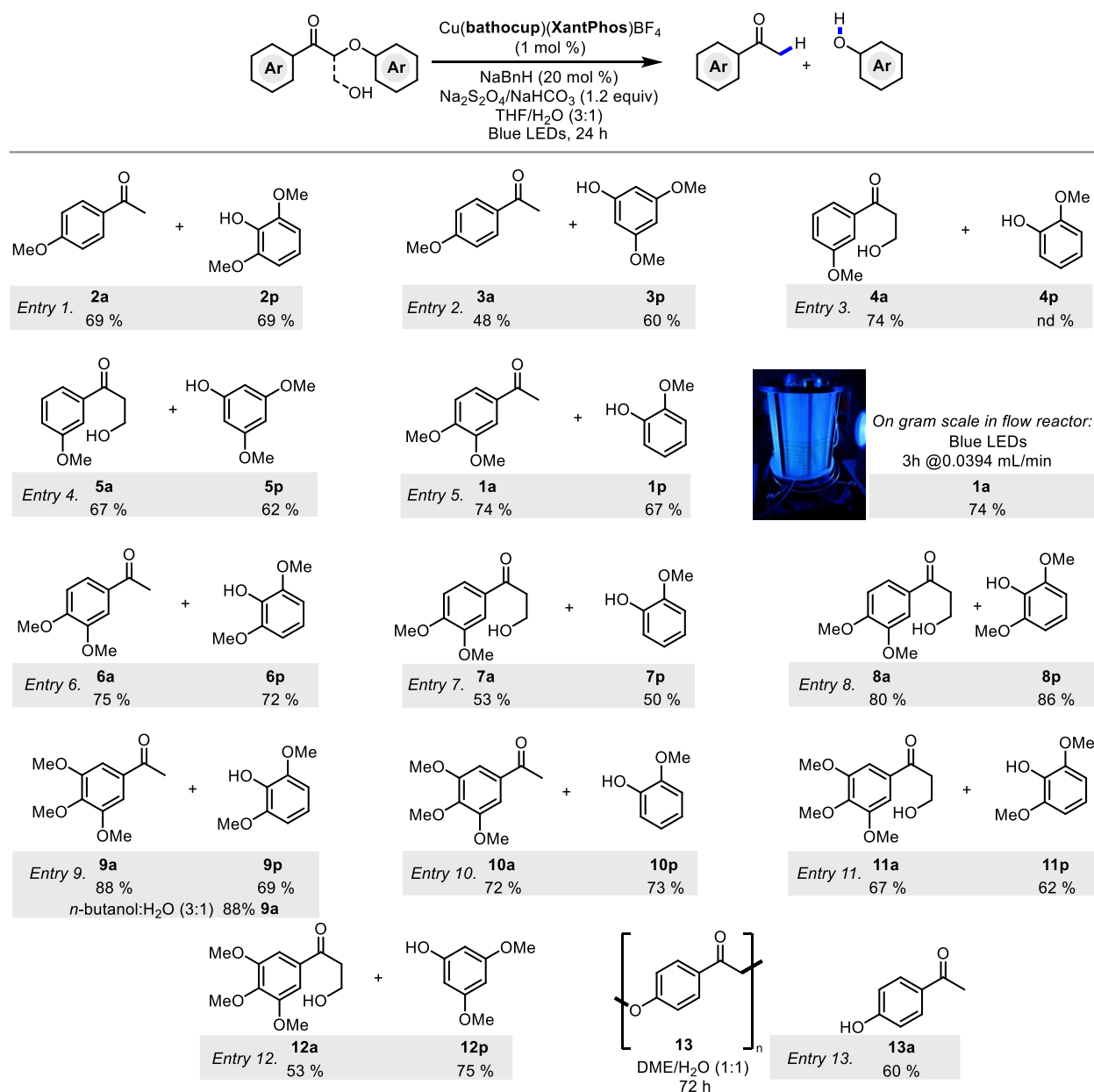
Figure A4 - 3 Mechanistic Proposal for the Cleavage of the Lignin Models

Evaluation of Scope.

With the optimized catalyst and reaction conditions in hand, several other lignin models were evaluated (**Table A 4-3**). Each decomposition was performed in triplicate and average yields following chromatography are reported. Lignin models possessing a single methoxy group on the “left” aryl group (or the aryl group which produces the target acetophenone) all underwent depolymerization in acceptable yields (48-74% yields including both acetophenone and phenol

products, entries 1-4, **Table A 4-3**). Yields were slightly higher when the model possessed the hydroxymethyl appendage on the β -carbon of the lignin model (entries 3-4). The fragmentation of the lignin models was efficient when the substrates had two methoxy groups on the “left” aryl group (50-86% for both the acetophenone and phenol products). No significant trends in yields were observed with respect to the number of methoxy groups on either aryl group, or the presence of the hydroxymethyl motif. In addition, four lignin models were evaluated that contained three methoxy groups on the “left” aryl group of the substrate. Again, efficient fragmentation to the corresponding acetophenones and phenols were observed (57-88% yields). Further improvement in the solvent profile could be achieved by replacing THF with n-butanol.⁵⁷⁻⁵⁸ During the fragmentation of lignin model **9**, identical yields of the acetophenone **9a** could be achieved with 3:1 THF:H₂O was replaced by 3:1 n-butanol:H₂O. A gram scale decomposition of lignin model **1** was attempted in continuous flow (entry 5).⁵⁹⁻⁶⁰ A revised solvent system that replaced THF for DME was selected to avoid precipitation of salts in the CFS tubing. Gratifyingly, a 70% yield of acetophenone **1a** was isolated in 3 h (74 % in batch, 24 h). The photocatalytic decomposition of lignin protocol was evaluated on a model polymer **13** (Entry 13). Although the polymer was initially poorly soluble under the biphasic reaction conditions, the reaction mixture became increasingly homogeneous as the conversion increased. After 72 h, a 60% conversion of the polymer to acetophenone **13a** was observed.

Table A4 - 3 Decomposition of Lignin Models



A4.4 Conclusions

In summary, the fragmentation of lignin models of the β -O-4 linkage has been demonstrated using a heteroleptic copper complex, Cu(bathocup)(XantPhos)BF₄. The reaction conditions involved the development of aqueous biphasic reaction conditions using catalytic amounts of NABnH, a hydrogen atom donor. The catalytic system as a whole represents a green

shift from previous reaction conditions for analogous processes that either exploit expensive rare metals such as Ir for photocatalysis, employ stoichiometric amounts of proton- and/or hydrogen (H) atom donors and chlorinated solvents. The reaction conditions and catalyst system are amendable to flow chemistry set-ups for gram scale processes and were able to promote fragmentation of oxidized model lignin polymers.

A4.5 References

1. Kugge, C.; Deuss, P. J., *Chem Catalysis* **2021**, *1* (1), 6-8.
2. Alonso, D. M.; Bond, J. Q.; Dumesic, J. A., *Green Chem.* **2010**, *12* (9), 1493-1513.
3. Löfstedt, J.; Dahlstrand, C.; Orebom, A.; Meuzelaar, G.; Sawadjoon, S.; Galkin, M. V.; Agback, P.; Wimby, M.; Corresa, E.; Mathieu, Y.; Sauvanaud, L.; Eriksson, S.; Corma, A.; Samec, J. S. M., *ChemSusChem* **2016**, *9* (12), 1392-1396.
4. Vennestrøm, P. N. R.; Osmundsen, C. M.; Christensen, C. H.; Taarning, E., *Angew. Chem., Int. Ed.* **2011**, *50* (45), 10502-10509.
5. Collinson, S. R.; Thielemans, W., *Coord. Chem. Rev.* **2010**, *254* (15), 1854-1870.
6. Kärkäs, M. D.; Matsuura, B. S.; Monos, T. M.; Magallanes, G.; Stephenson, C. R. J., *Org. Biomol. Chem.* **2016**, *14* (6), 1853-1914.
7. Deuss, P. J.; Barta, K., *Coord. Chem. Rev.* **2016**, *306*, 510-532.
8. Ralph, J.; Lundquist, K.; Brunow, G.; Lu, F.; Kim, H.; Schatz, P. F.; Marita, J. M.; Hatfield, R. D.; Ralph, S. A.; Christensen, J. H.; Boerjan, W., *Phytochemistry Reviews* **2004**, *3* (1), 29-60.
9. Vanholme, R.; Demedts, B.; Morreel, K.; Ralph, J.; Boerjan, W., *Plant Physiol.* **2010**, *153* (3), 895-905.
10. Zakzeski, J.; Jongorius, A. L.; Bruijnincx, P. C. A.; Weckhuysen, B. M., *ChemSusChem* **2012**, *5* (8), 1602-1609.
11. Samant, B. S.; Kabalka, G. W., *Chem. Commun.* **2012**, *48* (69), 8658-8660.
12. Zhang, J.; Teo, J.; Chen, X.; Asakura, H.; Tanaka, T.; Teramura, K.; Yan, N., *ACS Catal.* **2014**, *4* (5), 1574-1583.
13. Zhang, J.; Chen, Y.; Brook, M. A., *ACS Sustainable Chemistry & Engineering* **2014**, *2* (8), 1983-1991.
14. Zhang, G.; Scott, B. L.; Wu, R.; Silks, L. A. P.; Hanson, S. K., *Inorg. Chem.* **2012**, *51* (13), 7354-7361.
15. Biannic, B.; Bozell, J. J., *Org. Lett.* **2013**, *15* (11), 2730-2733.
16. Walsh, K.; Sneddon, H. F.; Moody, C. J., *Org. Lett.* **2014**, *16* (19), 5224-5227.
17. Dawange, M.; Galkin, M. V.; Samec, J. S. M., *ChemCatChem* **2015**, *7* (3), 401-404.

18. Zhu, C.; Ding, W.; Shen, T.; Tang, C.; Sun, C.; Xu, S.; Chen, Y.; Wu, J.; Ying, H., *ChemSusChem* **2015**, *8* (10), 1768-1778.
19. Mottweiler, J.; Puche, M.; Räuber, C.; Schmidt, T.; Concepción, P.; Corma, A.; Bolm, C., *ChemSusChem* **2015**, *8* (12), 2106-2113.
20. Patil, N. D.; Yao, S. G.; Meier, M. S.; Mobley, J. K.; Crocker, M., *Org. Biomol. Chem.* **2015**, *13* (11), 3243-3254.
21. Mottweiler, J.; Rinesch, T.; Besson, C.; Buendia, J.; Bolm, C., *Green Chem.* **2015**, *17* (11), 5001-5008.
22. Son, S.; Toste, F. D., *Angew. Chem., Int. Ed.* **2010**, *49* (22), 3791-3794.
23. Nichols, J. M.; Bishop, L. M.; Bergman, R. G.; Ellman, J. A., *J. Am. Chem. Soc.* **2010**, *132* (36), 12554-12555.
24. Magallanes, G.; Kärkäs, M. D.; Bosque, I.; Lee, S.; Maldonado, S.; Stephenson, C. R. J., *ACS Catal.* **2019**, *9* (3), 2252-2260.
25. vom Stein, T.; den Hartog, T.; Buendia, J.; Stoychev, S.; Mottweiler, J.; Bolm, C.; Klankermayer, J.; Leitner, W., *Angew. Chem., Int. Ed.* **2015**, *54* (20), 5859-5863.
26. Harms, R. G.; Markovits, I. I. E.; Drees, M.; Herrmann, h. c. m. W. A.; Cokoja, M.; Kühn, F. E., *ChemSusChem* **2014**, *7* (2), 429-434.
27. Galkin, M. V.; Dahlstrand, C.; Samec, J. S. M., *ChemSusChem* **2015**, *8* (13), 2187-2192.
28. vom Stein, T.; Weigand, T.; Merkens, C.; Klankermayer, J.; Leitner, W., *ChemCatChem* **2013**, *5* (2), 439-441.
29. Gazi, S.; Hung Ng, W. K.; Ganguly, R.; Putra Moeljadi, A. M.; Hirao, H.; Soo, H. S., *Chem. Sci.* **2015**, *6* (12), 7130-7142.
30. Das, A.; König, B., *Green Chem.* **2018**, *20* (21), 4844-4852.
31. Noël, T.; Zysman-Colman, E., *Chem Catalysis* **2022**, *2* (3), 468-476.
32. Luo, N.; Wang, M.; Li, H.; Zhang, J.; Liu, H.; Wang, F., *ACS Catal.* **2016**, *6* (11), 7716-7721.
33. Luo, J.-J.; Zhang, M.; Lin, J.-H.; Xiao, J.-C., *J. Org. Chem.* **2017**, *82* (20), 11206-11211.
34. Kärkäs, M. D.; Bosque, I.; Matsuura, B. S.; Stephenson, C. R. J., *Org. Lett.* **2016**, *18* (19), 5166-5169.

35. Bosque, I.; Magallanes, G.; Rigoulet, M.; Kärkäs, M. D.; Stephenson, C. R. J., *ACS Cent. Sci.* **2017**, *3* (6), 621-628.
36. Nguyen, S. T.; Murray, P. R. D.; Knowles, R. R., *ACS Catal.* **2020**, *10* (1), 800-805.
37. Zhu, Q.; Nocera, D. G., *ACS Catal.* **2021**, *11* (22), 14181-14187.
38. Lévêque, C.; Levernier, E.; Corcé, V.; Fensterbank, L.; Malacria, M.; Ollivier, C., Photoredox Catalysis, an Opportunity for Sustainable Radical Chemistry. In *Advanced Green Chemistry: Part 2: From Catalysis to Chemistry Frontiers*, World Scientific: **2020**; pp 49-121.
39. Traub, L.; Reiser, O., *Phys. Sci. Rev.* **2019**, *4*, 172.
40. Ehrnsberger, P.; Reiser, O.; König, B., *Science of Synthesis: Photocatalysis in Organic Synthesis*. 2019; p 271.
41. Hossain, A.; Bhattacharyya, A.; Reiser, O., *Science* **2019**, *364*, eaav9713.
42. Hockin, B.; Li, C.; Robertson, N.; Zysman-Colman, E., *Catal. Sci. Technol.* **2019**, *9*, 889.
43. Caron, A.; Morin, É.; Collins, S. K., *ACS Catal.* **2019**, *9* (10), 9458-9464.
44. Minozzi, C.; Caron, A.; Grenier-Petel, J. C.; Santandrea, J.; Collins, S. K., *Angew. Chem., Int. Ed.* **2018**, *57* (19), 5477-5481.
45. Tarantino, K. T.; Liu, P.; Knowles, R. R., *J. Am. Chem. Soc.* **2013**, *135* (27), 10022-10025.
46. Li, C.; Dickson, R.; Rockstroh, N.; Rabeah, J.; Cordes, D. B.; Slawin, A. M. Z.; Hünemörder, P.; Spannenberg, A.; Bühl, M.; Mejía, E.; Zysman-Colman, E.; Kamer, P. C. J., *Catal. Sci. Technol.* **2020**, *10* (22), 7745-7756.
47. Gracia, L.-L.; Luci, L.; Bruschi, C.; Sambri, L.; Weis, P.; Fuhr, O.; Bizzarri, C., *Chem. - Eur. J.* **2020**, *26* (44), 9929-9937.
48. Hunter, C. J.; Boyd, M. J.; May, G. D.; Fimognari, R., *J. Org. Chem.* **2020**, *85*, 8732.
49. Matsuo, K.; Yamaguchi, E.; Itoh, A., *Asian J. Org. Chem.* **2018**, *7*, 2435.
50. Mejía, E.; Luo, S. P.; Karnahl, M.; Friedrich, A.; Tschierlei, S.; Surkus, A. E.; Junge, H.; Gladiali, S.; Lochbrunner, S.; Beller, M., *Chem. - Eur. J.* **2013**, *19*, 15972.
51. Engl, S.; Reiser, O., *ACS Catal.* **2020**, *10*, 9899.
52. Alkan-Zambada, M.; Hu, X., *Organometallics* **2018**, *37*, 3928.

53. Jacob, C.; Baguia, H.; Dubart, A.; Oger, S.; Thilmany, P.; Beaudelot, J.; Deldaele, C.; Peruško, S.; Landrain, Y.; Michelet, B.; Neale, S.; Romero, E.; Moucheron, C.; Van Speybroeck, V.; Theunissen, C.; Evano, G., *Nature Communications* **2022**, *13* (1), 560.
54. Oger, S.; Baguia, H.; Phan, T.-A.; Teunens, T.; Beaudelot, J.; Moucheron, C.; Evano, G., *SynOpen* **2021**, *05* (02), 141-144.
55. Michelet, B.; Deldaele, C.; Kajouj, S.; Moucheron, C.; Evano, G., *Org. Lett.* **2017**, *19* (13), 3576-3579.
56. Nowak, C.; Pick, A.; Lommes, P.; Sieber, V., *ACS Catal.* **2017**, *7* (8), 5202-5208.
57. Alfonsi, K.; Colberg, J.; Dunn, P. J.; Fevig, T.; Jennings, S.; Johnson, T. A.; Kleine, H. P.; Knight, C.; Nagy, M. A.; Perry, D. A.; Stefaniak, M., *Green Chem.* **2008**, *10* (1), 31-36.
58. Prat, D.; Wells, A.; Hayler, J.; Sneddon, H.; McElroy, C. R.; Abou-Shehada, S.; Dunn, P. J., *Green Chem.* **2016**, *18* (1), 288-296.
59. Buglioni, L.; Raymenants, F.; Slattery, A.; Zondag, S. D. A.; Noël, T., *Chem. Rev.* **2022**, *122* (2), 2752-2906.
60. Donnelly, K.; Baumann, M., *J. Flow Chem.* **2021**, *11* (3), 223-241.

Annexe 5 – Supporting information of Annexe 4

A5.1 General

All reactions that were carried out under anhydrous conditions were performed under an inert argon or nitrogen atmosphere in glassware that had previously been dried overnight at 120 °C or had been flame dried and cooled under a stream of argon or nitrogen. All chemical products were obtained from Sigma-Aldrich Chemical Company, Oakwood Chemical or Alfa Aesar and were reagent quality. Technical solvents were obtained from VWR International Co. Anhydrous solvents (CH₂Cl₂, Et₂O, THF, DMF, toluene, and *n*-hexane) were dried and deoxygenated using a GlassContour system (Irvine, CA). Isolated yields reflect the mass obtained following flash column silica gel chromatography. Organic compounds were purified using silica gel obtained from Silicycle Chemical division (40-63 nm; 230-240 mesh). Analytical thin-layer chromatography (TLC) was performed on glass-backed silica gel 60 coated with a fluorescence indicator (Silicycle Chemical division, 0.25 mm, F254.). Visualization of TLC plate was performed by UV (254 nm), KMnO₄ or *p*-anisaldehyde stains. All mixed solvent eluents are reported as v/v solutions. Concentration refers to removal of volatiles at low pressure on a rotary evaporator. All reported compounds were homogeneous by thin layer chromatography (TLC) and by ¹H NMR. NMR spectra were taken in deuterated CDCl₃ using Bruker AV-300 and AV-400 instruments unless otherwise noted. Signals due to the solvent served as the internal standard (CHCl₃: δ 7.27 for 1H, δ 77.0 for 13C). The acquisition parameters are shown on all spectra. The ¹H NMR chemical shifts and coupling constants were determined assuming first-order behavior. Multiplicity is indicated by one or more of the following: s (singlet), d (doublet), t (triplet), q (quartet), m (multiplet), br (broad); the list of couplings constants (*J*) corresponds to the order of the multiplicity assignment. High resolution mass spectroscopy (HRMS) was done by the Centre régional de spectrométrie de masse at the Département de Chimie, Université de Montréal from an Agilent LC-MSD TOF system using ESI mode of ionization unless otherwise noted.

A5.2 Synthesis of ligands and catalysts

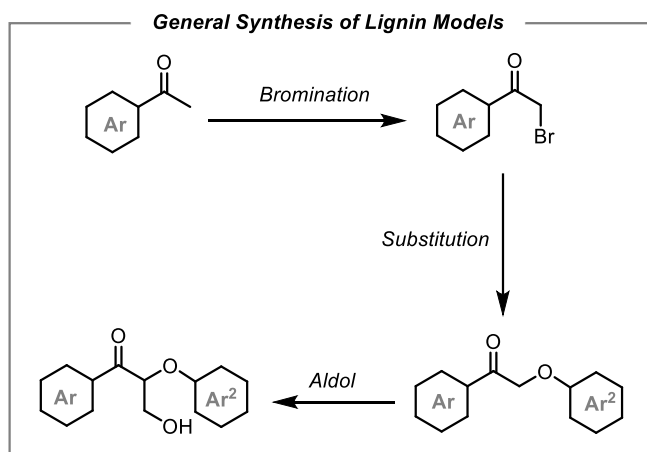
General Comments/Procedures for Ligands:

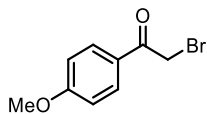
Commercially available diimines include: 1,10-phenanthroline (**phen**), 2,9-dimethyl-1,10-phenanthroline (**dmp**), 3,4,7,8-tetramethyl-1,10-phenanthroline (**tmp**), 4,4'-dimethoxy-2,2'-bipyridine (**dmbp**), 4,4'-di-*tert*-butyl-2,2'-dipyridyl (**dtbbp**), 4,4'-di-*tert*-butyl-2,2'-dipyridyl (**batho**), 2,9-dimethyl-4,7-diphenyl-1,10-phenanthroline (**bathocup**) 2,2'-biquinoline (**dq**). Previously synthesized diimines¹⁻⁴ include: 2-(1-(*p*-tolyl)-1H-1,2,3-triazol-4-yl)pyridine (**pytri**), 2-(1-(*p*-tolyl)-1H-1,2,3-triazol-4-yl)quinoline (**quintri**), 1-(1-(*p*-tolyl)-1H-1,2,3-triazol-4-yl)isoquinoline (**iquintri**), 3,6-dimethyl-dipyrido[3,2-*f*:2',3'-*h*]-quinoxaline (**ddpq**), 3,6-dimethyldipyrido[3,2-*a*:2',3'-*c*]phenazine (**ddppz**), 3,6-dimethylbenzo[*i*]dipyrido[3,2-*a*:2',3'-*c*]phenazine (**dbdppz**), di(pyridin-3-yl)amine (**dpa**), 2,9-dibutyl-1,10-phenanthroline (**bphen**) and 1,10-phenanthroline-5,6-dione (**dmop**).

The optimized catalyst Cu(**batho**)(**XantPhos**)BF₄ was prepared using a reported procedure.⁴ The photophysical properties have been investigated by several groups. A summary is provided below:

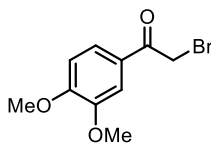
Abs max (nm)	Em max (nm)	Lifetime (μs)	ET (eV)	E* _{red} vs SCE	E* _{ox} vs SCE
(CH ₂ Cl ₂) ⁴	(CH ₂ Cl ₂) ⁴	(DME:H ₂ O)	(CH ₂ Cl ₂) ⁴	(MeCN) ⁵	(MeCN) ⁵
397	441	2.6	2.66	-1,37 V	+1,05 V

A5.3 Substrat synthesis

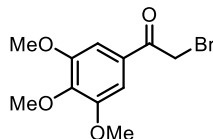




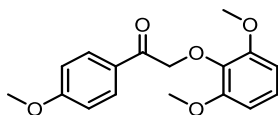
2-Bromo-1-(4-methoxyphenyl)ethan-1-one (2aS): To a solution of 1-(4-methoxyphenyl)ethan-1-one (1.50 g, 9.99 mmol) in EtOAc (30 mL, 333 mM) is added CuBr₂ (3.35 g, 15.0 mmol). The reaction mixture was stirred overnight at 90°C. The reaction was then allowed to cool to room temperature and filtered through a filter paper. The filtrate was added to a separatory funnel along with water (30 mL). It was then extracted three times with EtOAc (3 X 30 mL) and the combined organic phases were dried with Na₂SO₄ (2 g) and concentrated *in vacuo*. The product was then purified by column chromatography with Hexanes/EtOAc (8 : 2) to give a pink solid (1.48 g, 65%). Spectral data were in accordance with previous report.⁶ **¹H NMR (400 MHz, CDCl₃):** δ 8.00 (dt, 2H), 6.98 (dt, 2H), 4.43 (s, 2H), 3.91 (s, 3H).



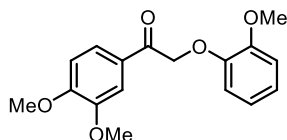
2-Bromo-1-(3,4-dimethoxyphenyl)ethan-1-one (1aS): To a solution of 1-(3,4-dimethoxyphenyl)ethan-1-one (1.80 g, 9.99 mmol) in EtOAc (30 mL, 333 mM) is added CuBr₂ (3.35 g, 15.0 mmol). The reaction mixture was stirred overnight at 90°C. The reaction was then allowed to cool to room temperature and filtered through a filter paper. The filtrate was added to a separatory funnel along with water (30 mL). It was then extracted three times with EtOAc (3 X 30 mL) and the combined organic phases were dried with Na₂SO₄ (2 g) and concentrated *in vacuo*. The product was then purified by flash chromatography (Hexanes : EtOAc ; 8 : 2) to give a slightly yellow solid (1.33 g, 51%). Spectral data were in accordance with previous report.⁶ **¹H NMR (400 MHz, CDCl₃):** δ 7.65 (dd, *J* = 8.4, 2.1 Hz, 1H), 7.58 (d, *J* = 2.1 Hz, 1H), 6.94 (d, *J* = 8.4 Hz, 1H), 4.44 (s, 2H), 4.00 (s, 3H), 3.98 (s, 3H).



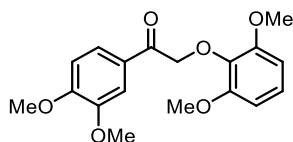
2-Bromo-1-(3,4,5-trimethoxyphenyl)ethan-1-one (10aS): To a solution of 1-(3,4,5-trimethoxyphenyl)ethan-1-one (2.10 g, 9.99 mmol) in EtOAc (30 mL, 333 mM) is added CuBr_2 (3.35 g, 15.0 mmol). The reaction mixture was stirred overnight at 90°C . The reaction was then allowed to cool to room temperature and filtered through a filter paper. The filtrate was added to a separatory funnel along with water (30 mL). It was then extracted three times with EtOAc (3 X 30 mL) and the combined organic phase was dried with Na_2SO_4 (2 g) and concentrated *in vacuo*. The product was then purified by flash chromatograph (Hexanes : EtOAc ; 8 : 2) to give a yellow solid (2.17 g, 75%). Spectral data were in accordance with previous report.⁶ **^1H NMR (400 MHz, CDCl_3):** δ 8.00 (m, 2H), 6.98 (m, 2H), 4.43 (s, 2H), 3.91 (s, 3H).



2-(2,6-Dimethoxyphenoxy)-1-(4-methoxyphenyl)ethan-1-one (2): To a solution of 2,6-dimethoxyphenol (443 mg, 2.87 mmol) in acetone (6.31 mL, 446 mM) is added cesium carbonate (917 mg, 2.82 mmol). The solution was stirred for 15 minutes before 2-bromo-1-(4-methoxyphenyl)ethan-1-one (6.45 g, 2.82 mmol) was added. The solution was then stirred overnight at room temperature. The solvent was evaporated under vacuum. The reaction vessel was then washed with water (30 mL) and EtOAc (30 mL), both of which were added to a separatory funnel. The aqueous phase was extracted three times with EtOAc (3 X 30 mL) and the combined organic phase was dried with Na_2SO_4 (2 g) and concentrated *in vacuo*. The product was then purified by flash chromatography (Hexanes : EtOAc ; 7 : 3) to give a white solid (800 mg, 94%). Spectral data were in accordance with previous report.⁷ **^1H NMR (500 MHz, CDCl_3):** δ 8.10 – 8.04 (m, 2H), 7.04 – 6.94 (m, 1H), 6.98 – 6.91 (m, 2H), 6.58 (d, $J = 8.4$ Hz, 2H), 5.13 (s, 2H), 3.87 (s, 3H), 3.81 (s, 6H).

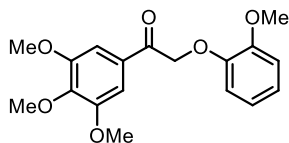


1-(3,4-Dimethoxyphenyl)-2-(2-methoxyphenoxy)ethan-1-one (1): To a solution of 2-methoxyphenol (605 μ L, 5.39 mmol) in acetone (11.5 mL, 446 mM) is added cesium carbonate (1.67 g, 5.13 mmol). The solution was stirred for 15 minutes before 2-bromo-1-(3,4-dimethoxyphenyl)ethan-1-one (1.33 g, 5.13 mmol) was added. The solution was then stirred overnight at room temperature. The solvent was evaporated under vacuum. The reaction vessel was then washed with water (30 mL) and EtOAc (30 mL), both of which were added to a separatory funnel. The aqueous phase was extracted three times with EtOAc (3 X 30 mL) and the combined organic phase was dried with Na_2SO_4 (2 g) and concentrated *in vacuo*. The product was then purified by flash chromatograph (Hexanes : EtOAc ; 7 : 3) to give a slightly pink powder (1.27 g, 82%). Spectral data were in accordance with previous report.⁷ **$^1\text{H NMR}$ (400 MHz, CDCl_3)** δ 7.71 (dd, $J = 8.4, 2.0$ Hz, 1H), 7.63 (d, $J = 2.0$ Hz, 1H), 7.04 – 6.94 (m, 1H), 6.98 – 6.90 (m, 2H), 6.93 – 6.84 (m, 2H), 5.32 (s, 2H), 3.98 (s, 3H), 3.97 (s, 3H), 3.92 (s, 3H).

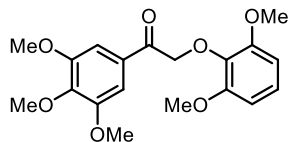


2-(2,6-Dimethoxyphenoxy)-1-(3,4-dimethoxyphenyl)ethan-1-one (6): To a solution of 2,6-dimethoxyphenol (315 mg, 2.05 mmol) in acetone (10 mL, 193 mM) is added cesium carbonate (673 mg, 2.06 mmol). The solution was stirred for 15 minutes before 2-bromo-1-(3,4-dimethoxyphenyl)ethan-1-one (500 mg, 1.93 mmol) was added. The solution was then stirred for 6h at room temperature. The solvent was evaporated under vacuum. The reaction vessel was then washed with water (30 mL) and EtOAc (30 mL), both of which were added to a separatory funnel. The aqueous phase was extracted three times with EtOAc (3 X 30 mL) and the combined organic phase was dried with Na_2SO_4 and concentrated *in vacuo*. The product was then purified by flash chromatography (Hexanes : EtOAc ; 7 : 3) to give a white solid (601 mg, 94%). Spectral data were in accordance with previous report.⁷ **$^1\text{H NMR}$ (500 MHz, CDCl_3)**: δ 7.73 (dd, $J = 8.4, 2.0$

Hz, 1H), 7.65 (d, $J = 2.0$ Hz, 1H), 7.01 (dd, $J = 8.4$ Hz, 1H), 6.90 (d, $J = 8.4$ Hz, 1H), 6.59 (d, $J = 8.4$ Hz, 2H), 5.15 (s, 2H), 3.95 (s, 4H), 3.95 (s, 3H), 3.82 (s, 6H).

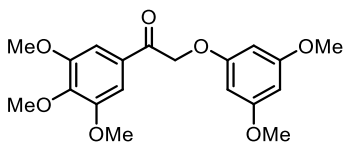


2-(2-methoxyphenoxy)-1-(3,4,5-trimethoxyphenyl)ethan-1-one (10): To a solution of 2-methoxyphenol (323 μ L, 2.94 mmol) in acetone (6.30 mL, 445 mM) is added cesium carbonate (913 mg, 2.80 mmol). The solution was stirred for 15 minutes before 2-bromo-1-(3,4,5-trimethoxyphenyl)ethan-1-one (810 mg, 2.80 mmol) was added. The solution was then stirred overnight at room temperature. The solvent was evaporated under vacuum. The reaction vessel was then washed with water (30 mL) and EtOAc (30 mL), both of which were added to a separatory funnel. The aqueous phase was extracted three times with EtOAc (3 X 30 mL) and the combined organic phase was dried with Na_2SO_4 (2 g) and concentrated *in vacuo*. The product was then purified by flash chromatograph (Hexanes : EtOAc ; 7 : 3) to give a white powder (570 mg, 61%). Spectral data were in accordance with previous report.⁸ $^1\text{H NMR}$ (400 MHz, CDCl_3) δ 7.37 (s, 2H), 7.05 – 6.86 (m, 4H), 5.29 (s, 2H), 3.95 (s, 3H), 3.94 (s, 6H), 3.91 (s, 3H).

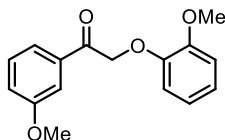


2-(2,6-Dimethoxyphenoxy)-1-(3,4,5-trimethoxyphenyl)ethan-1-one (9): To a solution of 2,6-dimethoxyphenol (560 mg, 3.63 mmol) in acetone (7.76 mL, 446 mM) is added cesium carbonate (1.13 g, 3.46 mmol). The solution was stirred for 15 minutes before 2-bromo-1-(3,4,5-trimethoxyphenyl)ethan-1-one (1.00 g, 3.46 mmol) was added. The solution was then stirred overnight at room temperature. The solvent was evaporated under vacuum. The reaction vessel was then washed with water (30 mL) and EtOAc (30 mL), both of which were added to a separatory funnel. The aqueous phase was extracted three times with EtOAc (3 X 30 mL) and the combined organic phase was dried with Na_2SO_4 (2 g) and concentrated *in vacuo*. The product was then purified by flash chromatograph (Hexanes : EtOAc ; 7 : 3) to give a white fluffy solid (1.07 g,

85%). Spectral data were in accordance with previous report.⁸ **¹H NMR (400 MHz, CDCl₃)** δ 7.41 (s, 2H), 7.06 (dd, *J* = 8.4 Hz, 1H), 6.63 (d, *J* = 8.4 Hz, 2H), 5.16 (s, 2H), 3.95 (bs, 9H) 3.85 (s, 6H).

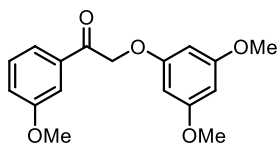


2-(3,5-Dimethoxyphenoxy)-1-(3,4,5-trimethoxyphenyl)ethan-1-one (12S): To a solution of 3,5-dimethoxyphenol (544 mg, 3.46 mmol) in acetone (7.76 mL, 446 mM) is added cesium carbonate (1.13 g, 3.46 mmol). The solution was stirred for 15 minutes before 2-bromo-1-(3,4,5-trimethoxyphenyl)ethan-1-one (1.00 g, 3.46 mmol) was added. The solution was then stirred overnight at room temperature. The solvent was evaporated under vacuum. The reaction vessel was then washed with water (30 mL) and EtOAc (30 mL), both of which were added to a separatory funnel. The aqueous phase was extracted three times with EtOAc (3 X 30 mL) and the combined organic phase was dried with Na₂SO₄ (2 g) and concentrated *in vacuo*. The product was then purified by flash chromatography (Hexanes : EtOAc ; 7 : 3) to give a slightly yellow solid (756 mg, 60%). Spectral data were in accordance with previous report.⁹ **¹H NMR (400 MHz, CDCl₃)**: δ 7.29 (s, 2H), 6.18 – 6.12 (m, 3H), 5.20 (s, 2H), 3.96 (s, 3H), 3.94 (s, 6H), 3.78 (s, 6H).

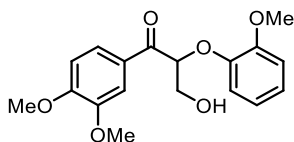


2-(2-Methoxyphenoxy)-1-(3-methoxyphenyl)ethan-1-one (4S): To a solution of 2-methoxyphenol (509 μL, 4.63 mmol) in acetone (9.70 mL, 446 mM) is added cesium carbonate (1.52 g, 4.67 mmol). The solution was stirred for 15 minutes before 2-bromo-1-(3-methoxyphenyl)ethan-1-one (1.00 g, 4.37 mmol) was added. The solution was then stirred for 3 h at room temperature. The solvent was evaporated under vacuum. The reaction vessel was then washed with water (30 mL) and EtOAc (30 mL), both of which were added to a separatory funnel. The aqueous phase was extracted three times with EtOAc (3 X 30 mL) and the combined organic phase was dried with Na₂SO₄ and concentrated *in vacuo*. The product was then purified by flash chromatography (Hexanes : EtOAc ; 7 : 3) to give a white solid (951 mg, 80%). **¹H NMR (400 MHz,**

CDCl₃) δ 7.64 – 7.55 (m, 2H), 7.42 (dd, J = 8.0 Hz, 1H), 7.18 (ddd, J = 8.3, 2.7, 1.0 Hz, 1H), 7.04 – 6.93 (m, 2H), 6.90 – 6.85 (m, 2H), 5.36 (s, 2H), 3.92 (s, 3H), 3.89 (s, 3H). **¹³C NMR (101 MHz, CDCl₃)** δ 194.35, 159.97, 149.83, 147.54, 135.93, 129.79, 122.51, 120.81, 120.54, 120.37, 114.95, 112.33, 112.23, 77.36, 77.04, 76.72, 72.18, 55.92, 55.50. **HRMS (ESI)** m/z calculated for C₁₆H₁₆O₄ [M+H]⁺ 273.1121; found 273.1128.

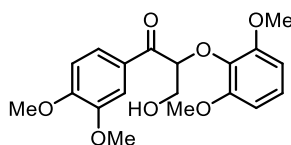


2-(3,5-Dimethoxyphenoxy)-1-(3-methoxyphenyl)ethan-1-one (5): To a solution of 3,5-dimethoxyphenol (808 mg, 5.24 mmol) in acetone (25 mL, 173 mM) is added cesium carbonate (1.85 g, 5.68 mmol). The solution was stirred for 15 minutes before 2-bromo-1-(3-methoxyphenyl)ethan-1-one (1 g, 4.37 mmol) was added. The solution was then stirred for 6h at room temperature. The solvent was evaporated under vacuum. The reaction vessel was then washed with water and EtOAc, both of which were added to a separatory funnel. The aqueous phase was extracted three times with EtOAc and the combined organic phases was dried with Na₂SO₄ and concentrated *in vacuo*. The product was then purified by flash chromatography (Hexanes : EtOAc ; 7 : 3) to give a off-white solid (1.10 g, 83%). Spectral data were in accordance with previous report.¹⁰ **¹H NMR (500 MHz, CDCl₃):** δ 7.56 (ddd, J = 7.6, 1.6, 0.9 Hz, 1H), 7.52 (dd, J = 2.7, 1.5 Hz, 1H), 7.40 (dd, J = 7.9 Hz, 1H), 7.16 (ddd, J = 8.3, 2.7, 0.9 Hz, 1H), 6.15 – 6.09 (m, 3H), 5.22 (s, 2H), 3.87 (s, 3H), 3.76 (s, 6H).

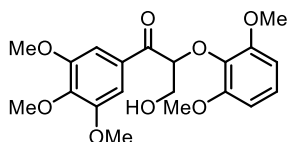


1-(3,4-Dimethoxyphenyl)-3-hydroxy-2-(2-methoxyphenoxy)propan-1-one (7): To a solution of 1-(3,4-dimethoxyphenyl)-2-(2-methoxyphenoxy)ethan-1-one (509 mg, 1.68 mmol) in EtOH : acetone (1 : 1, 8.42 mL, 200 mM) was added potassium carbonate (249 mg, 1.80 mmol). The solution was stirred for 15 minutes after which an aqueous formaldehyde solution was added (241 μ L of a 37% w.t. aqueous formaldehyde solution, 3.06 mmol). The resulting mixture was stirred at room temperature for 4 h. The solvents were evaporated under vacuum. The reaction

vessel was washed with water (30 mL) and EtOAc (30 mL) both of which were added to a separatory funnel. The aqueous phase was extracted three times with EtOAc (3 X 30 mL) and the combined organic phase was dried with Na₂SO₄ (2 g) and concentrated *in vacuo*. The product was then purified by flash chromatograph (Hexanes : EtOAc ; 5 : 5) to give a transparent oil (406 mg, 73%). Spectral data were in accordance with previous report.⁷ **¹H NMR (400 MHz, CDCl₃)** δ 7.78 (dd, *J* = 8.4, 2.0 Hz, 1H), 7.64 (d, *J* = 2.0 Hz, 1H), 7.07 – 6.99 (m, 1H), 6.99 – 6.85 (m, 4H), 6.89 – 6.79 (m, 1H), 5.43 (t, *J* = 5.3 Hz, 1H), 4.10 (d, *J* = 5.3 Hz, 2H), 3.98 (s, 3H), 3.95 (s, 3H), 3.89 (s, 3H).

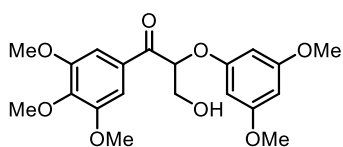


2-(2,6-Dimethoxyphenoxy)-1-(3,4-dimethoxyphenyl)-3-hydroxypropan-1-one (8): To a solution of 2-(2,6-dimethoxyphenoxy)-1-(3,4-dimethoxyphenyl)ethan-1-one (550 mg, 1.65 mmol) in EtOH : acetone (1 : 1, 16.5 mL, 100 mM) was added potassium carbonate (228 mg, 1.65 mmol). The solution was stirred for 15 minutes after which an aqueous formaldehyde solution was added (201 uL of a 37% w.t. aqueous formaldehyde solution, 2.48 mmol). The resulting mixture was stirred at room temperature for 2 h. The solvents were evaporated under vacuum. The reaction vessel was washed with water (30 mL) and EtOAc (30 mL) both of which were added to a separatory funnel. The aqueous phase was extracted three times with EtOAc (3 X 30 mL) and the combined organic phase was dried with Na₂SO₄ (2 g) and concentrated *in vacuo*. The product was then purified by flash chromatograph (Hexanes : EtOAc ; 5 : 5) to give a transparent oil (322 mg, 54%). Spectral data were in accordance with previous report.¹¹ **¹H NMR (500 MHz, CDCl₃)**: δ 7.73 (dd, *J* = 8.4, 2.0 Hz, 1H), 7.65 (d, *J* = 2.0 Hz, 1H), 7.01 (dd, *J* = 8.4 Hz, 1H), 6.90 (d, *J* = 8.4 Hz, 1H), 6.59 (d, *J* = 8.4 Hz, 2H), 5.15 (s, 2H), 3.95 (s, 3H), 3.95 (s, 3H), 3.82 (s, 6H).

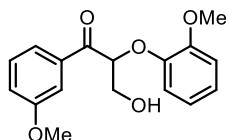


2-(2,6-Dimethoxyphenoxy)-3-hydroxy-1-(3,4,5-trimethoxyphenyl)propan-1-one (11): To a solution of 2-(2,6-dimethoxyphenoxy)-1-(3,4,5-trimethoxyphenyl)ethan-1-one (500 mg, 1.38

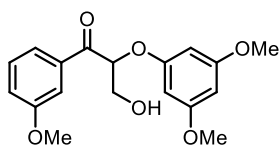
mmol) in EtOH : acetone (1 : 1, 6.90 mL, 200 mM) was added potassium carbonate (200 mg, 1.45 mmol). The solution was stirred for 15 minutes after which an aqueous formaldehyde solution was added (196 μ L of a 37% w.t. aqueous formaldehyde solution, 2.48 mmol). The resulting mixture was stirred at room temperature for 2 h. The solvents were evaporated under vacuum. The reaction vessel was washed with water (30 mL) and EtOAc (30 mL) both of which were added to a separatory funnel. The aqueous phase was extracted three times with EtOAc (3 X 30 mL) and the combined organic phase was dried with Na₂SO₄ (2 g) and concentrated *in vacuo*. The product was then purified by flash chromatograph (Hexanes : EtOAc ; 5 : 5) to give a transparent oil (361 mg, 67%). Spectral data were in accordance with previous report.¹¹ **¹H NMR (400 MHz, CDCl₃)** δ 7.41 (s, 2H), 7.07 (dd, *J* = 8.4 Hz, 1H), 6.62 (d, *J* = 8.4 Hz, 2H), 5.13 (dd, *J* = 7.3, 3.1 Hz, 1H), 4.05 (dd, *J* = 12.1, 7.3 Hz, 1H), 3.95 (s, 3H), 3.92 (s, 6H), 3.86 (dd, 1H), 3.78 (s, 6H).



2-(3,5-Dimethoxyphenoxy)-3-hydroxy-1-(3,4,5-trimethoxyphenyl)propan-1-one (12): To a solution of 2-(3,5-dimethoxyphenoxy)-1-(3,4,5-trimethoxyphenyl)ethan-1-one (500 mg, 1.38 mmol) in EtOH : acetone (1 : 1, 6.90 mL, 200 mM) was added potassium carbonate (200 mg, 1.45 mmol). The solution was stirred for 15 minutes after which an aqueous formaldehyde solution was added (196 μ L of a 37% w.t. aqueous formaldehyde solution, 2.48 mmol). The resulting mixture was stirred at room temperature for 2 h. The solvents were evaporated under vacuum. The reaction vessel was washed with water (30 mL) and EtOAc (30 mL) both of which were added to a separatory funnel. The aqueous phase was extracted three times with EtOAc (3 X 30 mL) and the combined organic phase was dried with Na₂SO₄ (2 g) and concentrated *in vacuo*. The product was then purified by flash chromatograph (Hexanes : EtOAc ; 5 : 5) to give a transparent oil (361 mg, 67%). **¹H NMR (400 MHz, CDCl₃)** δ 7.34 (s, 2H), 6.12 (s, 3H), 5.47 (dd, *J* = 6.1, 4.3 Hz, 1H), 4.23 – 4.08 (m, 2H), 3.95 (s, 3H), 3.89 (s, 6H), 3.75 (s, 6H). **¹³C NMR (126 MHz, CDCl₃)**: δ 195.34, 161.83, 159.24, 153.28, 143.61, 129.76, 106.53, 94.30, 94.13, 81.02, 63.42, 61.11, 56.41, 55.50. **HRMS (ESI)** *m/z* calculated for C₂₀H₂₄O₈ [M+Na]⁺ 415.1363; found 415.1369.

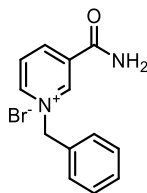


3-Hydroxy-2-(2-methoxyphenoxy)-1-(3-methoxyphenyl)propan-1-one (4): To a solution of 2-(2-methoxyphenoxy)-1-(3-methoxyphenyl)ethan-1-one (450 mg, 1.65 mmol) in EtOH : acetone (1 : 1, 16.5 mL, 100 mM) was added potassium carbonate (228 mg, 1.65 mmol). The solution was stirred for 15 minutes after which an aqueous formaldehyde solution was added (201 μ L of a 37% w.t. aqueous formaldehyde solution, 2.48 mmol). The resulting mixture was stirred at room temperature for 2 h. The solvents were evaporated under vacuum. The reaction vessel was washed with water (30 mL) and EtOAc (30 mL) both of which were added to a separatory funnel. The aqueous phase was extracted three times with EtOAc (3 X 30 mL) and the combined organic phase was dried with Na_2SO_4 (2 g) and concentrated *in vacuo*. The product was then purified by flash chromatograph (Hexanes : EtOAc ; 5 : 5) to give a transparent oil (213 mg, 43%). Spectral data were in accordance with previous report.¹² **$^1\text{H NMR}$ (400 MHz, CDCl_3):** δ 7.63 (ddd, $J = 7.7, 1.6, 0.9$ Hz, 1H), 7.57 (dd, $J = 2.7, 1.6$ Hz, 1H), 7.38 (dd, $J = 8.0$ Hz, 1H), 7.14 (ddd, $J = 8.3, 2.7, 0.9$ Hz, 1H), 7.02 (ddd, $J = 8.1, 7.3, 1.6$ Hz, 1H), 6.92 (ddd, $J = 8.2, 3.8, 1.6$ Hz, 2H), 6.84 (ddd, $J = 8.0, 7.4, 1.5$ Hz, 1H), 5.43 (dd, $J = 6.3, 4.0$ Hz, 1H), 4.09 – 4.02 (m, 2H), 3.85 (s, 3H), 3.85 (s, 3H).

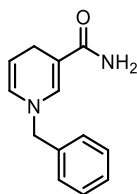


2-(3,5-Dimethoxyphenoxy)-3-hydroxy-1-(3-methoxyphenyl)propan-1-one (5): To a solution of 2-(3,5-dimethoxyphenoxy)-1-(3-methoxyphenyl)ethan-1-one (500 mg, 1.65 mmol) in EtOH : acetone (1 : 1, 16.5 mL, 100 mM) was added potassium carbonate (228 mg, 1.65 mmol). The solution was stirred for 15 minutes after which an aqueous formaldehyde solution was added (201 μ L of a 37% w.t. aqueous formaldehyde solution, 2.48 mmol). The resulting mixture was stirred at room temperature for 2 h. The solvents were evaporated under vacuum. The reaction vessel was washed with water (30 mL) and EtOAc (30 mL) both of which were added to a separatory funnel. The aqueous phase was extracted three times with EtOAc (3 X 30 mL) and the combined organic phase was dried with Na_2SO_4 (2 g) and concentrated *in vacuo*. The product was

then purified by flash chromatograph (Hexanes : EtOAc ; 5 : 5) to give a transparent oil (315 mg, 57%). **¹H NMR (500 MHz, CDCl₃):** δ 7.62 (ddd, *J* = 7.7, 1.6, 0.9 Hz, 1H), 7.53 (dd, *J* = 2.7, 1.6 Hz, 1H), 7.38 (dd, *J* = 8.0 Hz, 1H), 7.15 (ddd, *J* = 8.2, 2.7, 0.9 Hz, 1H), 6.11 – 6.05 (m, 3H), 5.54 (dd, *J* = 6.1, 3.9 Hz, 1H), 4.15 (dd, *J* = 12.1, 3.9 Hz, 1H), 4.07 (dd, *J* = 12.1, 6.1 Hz, 1H), 3.83 (s, 3H), 3.71 (s, 6H). **¹³C NMR (126 MHz, CDCl₃):** δ 196.2, 161.7, 160.1, 159.2, 136.0, 130.0, 121.2, 120.9, 112.9, 94.3, 94.2, 80.9, 63.4, 55.6, 55.5; **HRMS (ESI)** *m/z* calculated for C₁₈H₂₀O₆ [M+Na]⁺ 355.1152; found 355.1146.



1-Benzyl-3-carbamoylpyridin-1-ium bromide (NABn): To a solution of nicotinamide (2.00 g, 16.4 mmol) in acetonitrile (49.6 mL, 0.33 M) was added benzyl chloride (3.20 mL, 16.4 mmol). The solution was then refluxed for 4 h and allowed to cool to room temperature Diethyl ether (50 mL) was added to further precipitate the final product. The precipitate was recovered by filtration and washed with diethyl ether (3 × 10 mL) to afford a white powder (4.56 g, 95%). Spectral data were in accordance with previous report.¹³ **¹H NMR (400 MHz, D₂O):** δ 9.29 (s, 1H), 9.00 (dt, *J* = 6.2, 1.4 Hz, 1H), 8.84 (dt, *J* = 8.1, 1.5 Hz, 1H), 8.12 (dd, *J* = 8.2, 6.2 Hz, 1H), 7.49 – 7.40 (m, 5H), 5.83 (s, 2H).



1-Benzyl-1,4-dihydropyridine-3-carboxamide (NaBnH): To a solution of 1-benzyl-3-carbamoylpyridin-1-ium bromide (2.93 g, 10 mmol) in water (60 mL) was added sodium bicarbonate (4.20 g, 50 mmol) and sodium hydrosulfite (8.71 g, 50 mmol). The reaction mixture was stirred at room temperature for 3 h in the dark. The precipitate was filtered, washed with cold water (3 × 10 mL) and dried under vacuum to afford a bright yellow powder (1.65, 77%).¹³

¹H NMR (400 MHz, CDCl₃): δ 7.45 – 7.16 (m, 6H), 5.77 (dq, *J* = 8.1, 1.7 Hz, 1H), 5.21 (s, 2H), 4.78 (dt, *J* = 8.1, 3.4 Hz, 1H), 4.32 (s, 2H), 3.20 (dd, *J* = 3.5, 1.7 Hz, 2H).

A5.4 Photochemical decomposition of lignin models

General procedure for the photochemical decomposition of lignin models

Photochemistry: All the photochemical reactions were performed in 1-dram vials that were placed in the center of an aluminum cylinder the interior of which was lined with a light-emitting diode (LED) strip connected to a power source. The reactions media were thoroughly purged under a nitrogen stream prior to irradiation. LED strips were purchased from Creative Lightings (<https://www.creativelightings.com/>).

Representative Procedure of the *in-situ* optimization: To a 4 mL vial equipped with a cross-shaped stir bar was added [Cu(MeCN)₄]BF₄ (5 mol%) and a diphosphine (5 mol%). The vial was closed and N₂ degassed dichloromethane (1.60 mL, 50 mM) was added. The solution was allowed to stir for 1h before a diimine (5 mol%) was added. The solution was allowed to stir again for 1 h at which point 1-(3,4-dimethoxyphenyl)-2-(2-methoxyphenoxy)ethan-1-one (24.2 mg, 80.0 μmol), Hantzsch Ester (30.4 mg, 120 μmol) and diphenyl phosphoric acid (1.00 mg, 5 mol%) were added. The solution was then degassed using N₂ for 5 minutes. Additional N₂ degassed dichloromethane was added to compensate for evaporated solvent during degassing. The vial was then stirred under blue LED irradiation for 24 h. The solution was filtered through celite into a 10 mL volumetric flask containing 15.0 mg of 1,3,5-trimethoxybenzene (internal standard) and the volume was completed using EtOAc. The resulting solution was analysed by an Agilent 6890N-5973N GC-MS. Using the calibration curve below, the 1-(3,4-dimethoxyphenyl)ethan-1-one yield was determined.

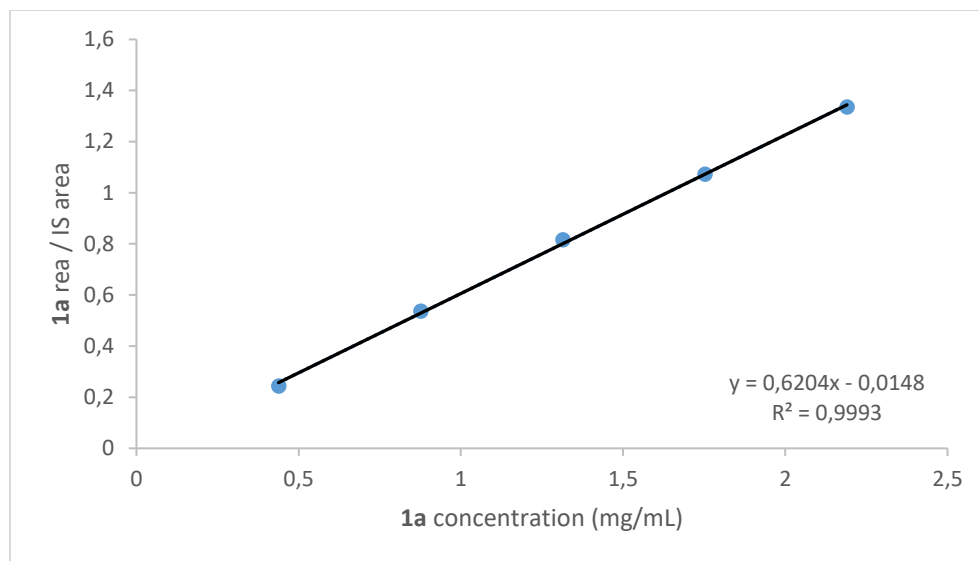


Figure A5 - 1 Calibration curve of 1-(3,4-dimethoxyphenyl)ethan-1-one

Table A5 - 1 Data used to build the 1-(3,4-dimethoxyphenyl)ethan-1-one calibration curve

	IS added (mg)	1-(3,4-dimethoxyphenyl)ethan-1-one concentration (mg/mL)	1-(3,4-dimethoxyphenyl)ethan-1-one area/IS area
Standard Solution 1	15.0	0.438	0.2438062
Standard Solution 2		0.876	0.53662017
Standard Solution 3		1.314	0.81504239
Standard Solution 4		1.752	1.071823
Standard Solution 5		2.19	1.33494341

Representative Procedure for isolated yield reactions (scope): To a 4 mL vial equipped with a cross-shaped stir bar was added Cu(bathocup)(Xantphos)BF₄ (1.70 mg, 1.65 μmol), NaBnH (7.1 mg, 33 μmol), 1-(3,4-dimethoxyphenyl)ethan-1-one (50 mg, 165 μmol), NaHCO₃ (16.6 mg, 198 μmol), and Na₂S₂O₄ (40.6 mg, 198 μmol). The vial was closed and N₂ degassed water (830 μL) and THF (2.48 mL) were added. The resulting solution was further degassed with N₂ for 5 minutes. The vial was then stirred under blue LED irradiation for 24 h. The solution was transferred to a separatory funnel and the vial was washed with EtOAc (3 x 2 mL). Water (30 mL) was added and extracted with EtOAc (3 x 30 mL). The combined organic phase was dried with Na₂SO₄ (2 g) and concentrated *in vacuo*. The desired products were purified by flash chromatography.

Tabular Data from Screening

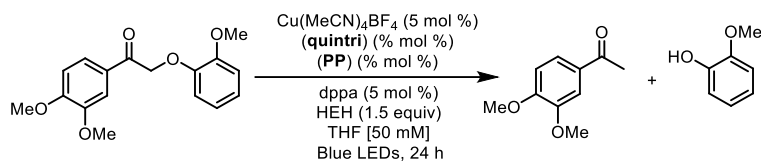


Table A5 - 2 Evaluation of Cu(quintri)(PP)BF₄-Based Photocatalysts in a Model Lignin Decomposition Process.

	PP	τ (ns)	E _T (eV)	% XX ^a
1	NXantPhos	19	2.49	90
2	PhanePhos	1948	2.25	97
3	XantPhos	1133	2.21	99
4	DPEPhos	14300	2.17	0
5	dppf	1.5	2.17	0
6	dppn	1.43	2.15	0
7	BINAP	2188	1.94	65
8	SEGPhos	340	1.92	12
9	none	90	1.65	0

^a Yield of the acetophenone by GC-MS analysis

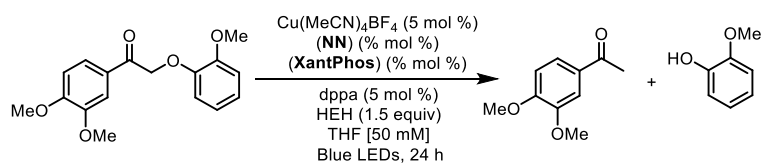


Table A5 - 3 Evaluation of Cu(NN)(XantPhos)BF₄-Based Photocatalysts in a Model Lignin Decomposition Process. IN-SITU ONLY 5 mol %

	NN	τ (ns)	E _T (eV)	In situ% XX ^a
1	phen	391	2.27	0
2	dmp	1133	2.21	99

3	tmp	1119	2.07	78
4	bphen	1798	2.61	99
5	dmbp	72	1.95	0
6	dtbbp	143	1.99	77
7	batho	3.2	2.50	0
8	bathocup	4	2.66	99
9	dq	393	1.89	0
10	pytri	752	2.26	0
11	quintri	3.6	2.59	99
12	iquintri	3.8	2.69	14
13	dpq	3	2.21	48
14	dppz	71	1.95	50
15	bdppz	75	2.19	45
16	dpa	3	2.88	0
17	dmop	4	2.55	22

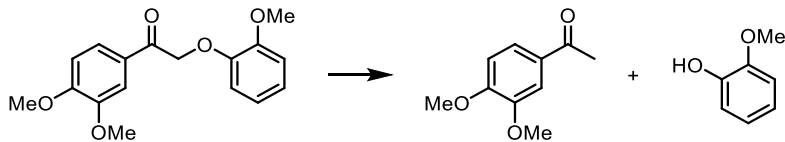
^a Yield of the acetophenone by GC-MS analysis

Decomposition of Lignin Models



2-(2,6-Dimethoxyphenoxy)-1-(4-methoxyphenyl)ethan-1-one: According to the general procedure, 1-(4-methoxyphenyl)ethan-1-one (150 mg, 495 μ mol) was converted to 1-(4-methoxyphenyl)ethan-1-one (52.4 mg 69%) and 2,6-dimethoxyphenol (51.4 mg, 69%). Spectral data were in accordance with previous report¹⁴; **1-(4-methoxyphenyl)ethan-1-one** : ¹H NMR (400

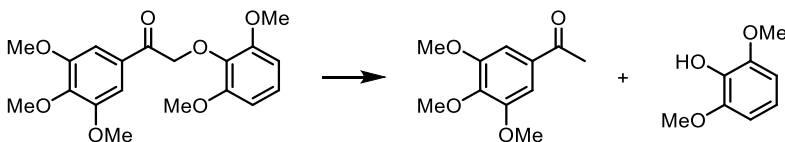
MHz, CDCl₃): δ 7.96 (m, 2H), 6.96 (m, 2H), 3.89 (s, 3H), 2.58 (s, 3H); **2,6-dimethoxyphenol** : **¹H NMR (400 MHz, CDCl₃):** δ 6.83 (dd, J = 8.7, 7.9 Hz, 1H), 6.62 (d, J = 8.3 Hz, 2H), 5.54 (s, 1H), 3.92 (s, 6H).



1-(3,4-Dimethoxyphenyl)-2-(2-methoxyphenoxy)ethan-1-one: According to the general procedure, 1-(3,4-dimethoxyphenyl)-2-(2-methoxyphenoxy)ethan-1-one (150 mg, 495 μ mol) was converted to 1-(3,4-dimethoxyphenyl)ethan-1-one (66.0 mg 74%) and 2-methoxyphenol (41.4 mg, 67%). Spectral data were in accordance with previous report¹⁴; **3-Methoxyacetophenone** : **¹H NMR (400 MHz, CDCl₃):** δ 7.58 (dd, J = 8.4, 2.0, 1H), 7.53 (d, J = 2.0 Hz, 1H), 6.89 (d, J = 8.4 Hz, 1H), 3.95 (s, 3H), 3.94 (s, 3H), 2.57 (s, 3H); **2-Methoxyphenol** : **¹H NMR (400 MHz, CDCl₃):** δ 7.09 – 7.01 (m, 1H), 7.01 – 6.90 (m, 3H), 5.80 (s, 1H), 3.92 (s, 3H).

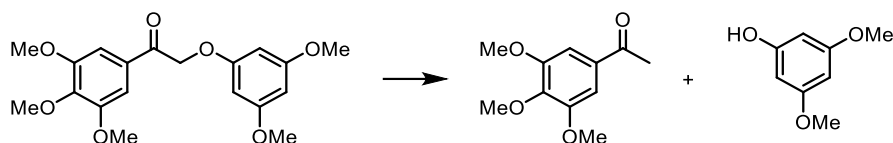


2-(2,6-dimethoxyphenoxy)-1-(3,4-dimethoxyphenyl)ethan-1-one: According to the general procedure, 1-(3,4-dimethoxyphenyl)ethan-1-one (164.4 mg, 495 μ mol) was converted to 1-(3,4-dimethoxyphenyl)ethan-1-one (66.9 mg 75%) and 2,6-dimethoxyphenol (54.9 mg, 72%). Spectral data were in accordance with previous report¹⁴; **1-(3,4-Dimethoxyphenyl)ethan-1-one** : **¹H NMR (400 MHz, CDCl₃):** δ 7.58 (dd, J = 8.4, 2.0, 1H), 7.53 (d, J = 2.0 Hz, 1H), 6.89 (d, J = 8.4 Hz, 1H), 3.95 (s, 3H), 3.94 (s, 3H), 2.57 (s, 3H); **2,6-Dimethoxyphenol** : **¹H NMR (400 MHz, CDCl₃):** δ 6.83 (dd, J = 8.7, 7.9 Hz, 1H), 6.62 (d, J = 8.3 Hz, 2H), 5.54 (s, 1H), 3.92 (s, 6H).

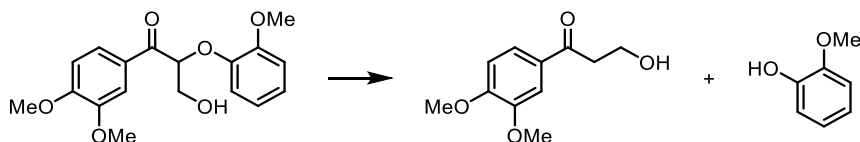


2-(2,6-dimethoxyphenoxy)-1-(3,4,5-trimethoxyphenyl)ethan-1-one: According to the general procedure, 2-(2,6-dimethoxyphenoxy)-1-(3,4,5-trimethoxyphenyl)ethan-1-one (179.4 mg, 495

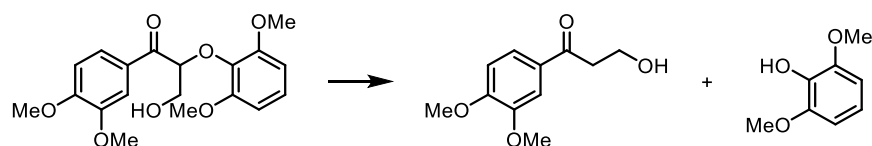
μmol) was converted to 1-(3,4,5-trimethoxyphenyl)ethan-1-one (91.6 mg 88%) and 2,6-dimethoxyphenol (52.7 mg, 69%). Spectral data were in accordance with previous report¹⁴; **2-(2,6-Dimethoxyphenoxy)-1-(3,4,5-trimethoxyphenyl)ethan-1-one** : $^1\text{H NMR}$ (400 MHz, CDCl_3): δ 7.23 (s, 2H), 3.93 (s, 6H), 3.93 (s, 3H), 2.60 (s, 3H), 2.18 (s, 1H); **2,6-dimethoxyphenol**: $^1\text{H NMR}$ (400 MHz, CDCl_3): δ 6.83 (dd, $J = 8.7, 7.9$ Hz, 1H), 6.62 (d, $J = 8.3$ Hz, 2H), 5.54 (s, 1H), 3.92 (s, 6H).



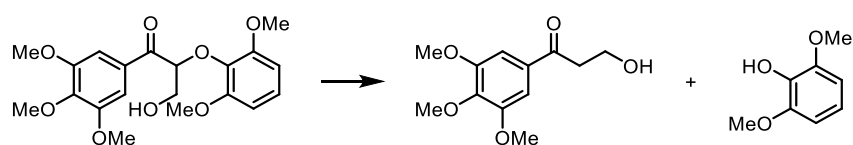
2-(3,5-dimethoxyphenoxy)-1-(3,4,5-trimethoxyphenyl)ethan-1-one: According to the general procedure, 2-(3,5-dimethoxyphenoxy)-1-(3,4,5-trimethoxyphenyl)ethan-1-one (179.4 mg, 495 μmol) was converted to 1-(3,4,5-trimethoxyphenyl)ethan-1-one (59.3 mg 57%) and 3,5-dimethoxyphenol (56.5 mg, 74%). Spectral data were in accordance with previous report¹⁴; **2-(2,6-Dimethoxyphenoxy)-1-(3,4,5-trimethoxyphenyl)ethan-1-one** : $^1\text{H NMR}$ (400 MHz, CDCl_3): δ 7.23 (s, 2H), 3.93 (s, 6H), 3.93 (s, 3H), 2.60 (s, 3H), 2.18 (s, 1H); **3,5-Dimethoxyphenol** : $^1\text{H NMR}$ (400 MHz, CDCl_3): δ 6.14 – 6.04 (m, 3H), 4.94 (s, 1H), 3.78 (s, 6H).



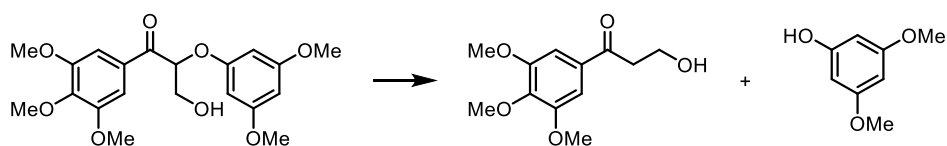
1-(3,4-dimethoxyphenyl)-3-hydroxy-2-(2-methoxyphenoxy)propan-1-one: According to the general procedure, 1-(3,4-dimethoxyphenyl)-3-hydroxy-2-(2-methoxyphenoxy)propan-1-one (164.4 mg, 495 μmol) was converted to 1-(3,4-dimethoxyphenyl)-3-hydroxypropan-1-one (55.2 mg 53%) and 2-methoxyphenol (36.9 mg, 60%). Spectral data were in accordance with previous report¹⁴; **1-(3,4-dimethoxyphenyl)-3-hydroxypropan-1-one** : $^1\text{H NMR}$ (400 MHz, CDCl_3): δ 7.59 (dd, $J = 8.4, 2.0$ Hz, 1H), 7.53 (d, $J = 2.0$ Hz, 1H), 6.90 (d, $J = 8.4$ Hz, 1H), 4.03 (t, $J = 5.4$ Hz, 2H), 3.95 (s, 3H), 3.94 (s, 3H), 3.20 (t, $J = 5.4$ Hz, 2H), 2.76 (s, 1H); **2-Methoxyphenol** : $^1\text{H NMR}$ (400 MHz, CDCl_3): δ 7.09 – 7.01 (m, 1H), 7.01 – 6.90 (m, 3H), 5.80 (s, 1H), 3.92 (s, 3H).



2-(2,6-Dimethoxyphenoxy)-1-(3,4-dimethoxyphenyl)-3-hydroxypropan-1-one: According to the general procedure, 2-(2,6-dimethoxyphenoxy)-1-(3,4-dimethoxyphenyl)-3-hydroxypropan-1-one (179.4 mg, 495 μmol) was converted to 1-(3,4-dimethoxyphenyl)-3-hydroxypropan-1-one (83.2 mg 80%) and 2,6-dimethoxyphenol (65.6 mg, 86%). Spectral data were in accordance with previous report¹⁴; **1-(3,4-Dimethoxyphenyl)-3-hydroxypropan-1-one** : $^1\text{H NMR}$ (400 MHz, CDCl_3): δ 7.59 (dd, $J = 8.4, 2.0$ Hz, 1H), 7.53 (d, $J = 2.0$ Hz, 1H), 6.90 (d, $J = 8.4$ Hz, 1H), 4.03 (t, $J = 5.4$ Hz, 2H), 3.95 (s, 3H), 3.94 (s, 3H), 3.20 (t, $J = 5.4$ Hz, 2H), 2.76 (s, 1H); **2,6-Dimethoxyphenol** : $^1\text{H NMR}$ (400 MHz, CDCl_3): δ 6.83 (dd, $J = 8.7, 7.9$ Hz, 1H), 6.62 (d, $J = 8.3$ Hz, 2H), 5.54 (s, 1H), 3.92 (s, 6H).

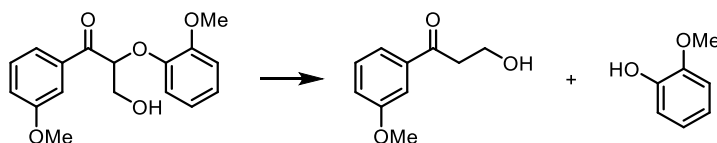


2-(2,6-Dimethoxyphenoxy)-3-hydroxy-1-(3,4,5-trimethoxyphenyl)propan-1-one: According to the general procedure, 2-(2,6-dimethoxyphenoxy)-3-hydroxy-1-(3,4,5-trimethoxyphenyl)propan-1-one (194.1 mg, 495 μmol) was converted to 3-hydroxy-1-(3,4,5-trimethoxyphenyl)propan-1-one (64.2 mg 53%) and 2,6-dimethoxyphenol (52.7 mg, 69%). Spectral data were in accordance with previous report¹⁴; **3-Hydroxy-1-(3,4,5-trimethoxyphenyl)propan-1-one** : $^1\text{H NMR}$ (400 MHz, CDCl_3): δ 7.22 (s, 2H), 4.02 (t, $J = 5.4$ Hz, 2H), 3.92 (s, 3H), 3.91 (s, 6H), 3.20 (t, $J = 5.5$ Hz, 2H), 2.78 (s, 1H); **2,6-Dimethoxyphenol** : $^1\text{H NMR}$ (400 MHz, CDCl_3): δ 6.83 (dd, $J = 8.7, 7.9$ Hz, 1H), 6.62 (d, $J = 8.3$ Hz, 2H), 5.54 (s, 1H), 3.92 (s, 6H).

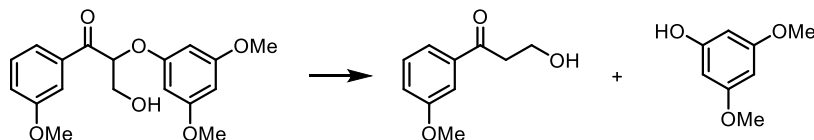


2-(3,5-Dimethoxyphenoxy)-3-hydroxy-1-(3,4,5-trimethoxyphenyl)propan-1-one: According to the general procedure, 2-(3,5-dimethoxyphenoxy)-3-hydroxy-1-(3,4,5-trimethoxyphenyl)propan-1-one (194.1 mg, 495 μmol) was converted to 3-hydroxy-1-(3,4,5-

trimethoxyphenyl)propan-1-one (63.0 mg 53%) and 3,5-dimethoxyphenol (57.2 mg, 75%). Spectral data were in accordance with previous report¹⁴; **3-Hydroxy-1-(3,4,5-trimethoxyphenyl)propan-1-one** : ¹H NMR (400 MHz, CDCl₃): δ 7.22 (s, 2H), 4.02 (t, *J* = 5.4 Hz, 2H), 3.92 (s, 3H), 3.91 (s, 6H), 3.20 (t, *J* = 5.5 Hz, 2H), 2.78 (s, 1H); **3,5-Dimethoxyphenol** : ¹H NMR (400 MHz, CDCl₃): δ 6.14 – 6.04 (m, 3H), 4.94 (s, 1H), 3.78 (s, 6H).



3-Hydroxy-2-(2-methoxyphenoxy)-1-(3-methoxyphenyl)propan-1-one: According to the general procedure, 3-hydroxy-2-(2-methoxyphenoxy)-1-(3-methoxyphenyl)propan-1-one (150 mg, 495 μmol) was converted to 3-hydroxy-1-(3-methoxyphenyl)propan-1-one (66.0 mg 74%) and 2-methoxyphenol (yield not determined). Spectral data were in accordance with previous report¹⁵; **3-Hydroxy-1-(3-methoxyphenyl)propan-1-one** : ¹H NMR (500 MHz, CDCl₃): δ 7.54 (ddd, *J* = 7.7, 1.3 Hz, 1H), 7.49 (dd, *J* = 2.7, 1.5 Hz, 1H), 7.38 (dd, *J* = 7.9 Hz, 1H), 7.13 (ddd, *J* = 8.2, 2.7, 1.0 Hz, 1H), 4.03 (t, *J* = 5.3 Hz, 2H), 3.86 (s, 3H), 3.22 (t, *J* = 5.3 Hz, 2H); **2-Methoxyphenol** : ¹H NMR (400 MHz, CDCl₃): δ 7.09 – 7.01 (m, 1H), 7.01 – 6.90 (m, 3H), 5.80 (s, 1H), 3.92 (s, 3H).



2-(3,5-Dimethoxyphenoxy)-3-hydroxy-1-(3-methoxyphenyl)propan-1-one: According to the general procedure, 2-(3,5-dimethoxyphenoxy)-3-hydroxy-1-(3-methoxyphenyl)propan-1-one (164.4 mg, 495 μmol) was converted to 3-hydroxy-1-(3-methoxyphenyl)propan-1-one (59.8 mg 67%) and 3,5-dimethoxyphenol (47.3 mg, 62%). Spectral data were in accordance with previous report¹⁵; **3-Hydroxy-1-(3-methoxyphenyl)propan-1-one** : ¹H NMR (500 MHz, CDCl₃): δ 7.95 (d, *J* = 8.6 Hz, 2H), 6.95 (d, *J* = 8.5 Hz, 2H), 4.08 – 4.02 (m, 2H), 3.88 (s, 3H), 3.19 (t, *J* = 5.3 Hz, 2H), 2.79 (s, 1H); **3,5-Dimethoxyphenol** : ¹H NMR (400 MHz, CDCl₃): δ 6.14 – 6.04 (m, 3H), 4.94 (s, 1H), 3.78 (s, 6H).

Reaction Scale-up using Flow Chemistry

Representative procedure for the degradation of 1 using the continuous flow setup:

1-(3,4-Dimethoxyphenyl)-2-(2-methoxyphenoxy)ethan-1-one (1.0 g, 3.31 mmol, 1 eq.), Cu(bathocup)(Xantphos)BF₄ (34 mg, 33.1 μmol, 1 mol %), and NABnH (142 mg, 0.62 mmol, 20 mol %) were dissolved in dimethoxyethane [66 mL, 25 mM]. NaHCO₃ (333 mg, 3.97 mmol, 1.2 eq.), and Na₂S₂O₄ (691 mg, 3.97 mmol, 1.2 eq.) were dissolved in H₂O [66 mL, 25 mM]. Both solutions were sparged with N₂ for 15 minutes. With an Asia Syringe Pump, the solutions were mixed by a T-mixer, and pumped through a 13.6 mL PFA-coiled reactor. The coil was irradiated with 450 nm LED and two 450 nm Kessil Lamps, and the flow rate was calculated for a 3-hour irradiation. The reaction mixture was then transferred to a separatory funnel. Water was added and extracted with EtOAc three times. The combined organic phase was dried with Na₂SO₄ and concentrated *in vacuo*. The desired products were purified by flash chromatography to give 2-methoxyphenol (270 mg, 71%) and 1-(3,4-dimethoxyphenyl)ethan-1-one (417 mg, 70%) as pure products. **3-Methoxyacetophenone** : ¹H NMR (400 MHz, CDCl₃): δ 7.58 (dd, *J* = 8.4, 2.0, 1H), 7.53 (d, *J* = 2.0 Hz, 1H), 6.89 (d, *J* = 8.4 Hz, 1H), 3.95 (s, 3H), 3.94 (s, 3H), 2.57 (s, 3H); **1-(3,4-Dimethoxyphenyl)ethan-1-one** : ¹H NMR (400 MHz, CDCl₃): δ 7.58 (dd, *J* = 8.4, 2.0, 1H), 7.53 (d, *J* = 2.0 Hz, 1H), 6.89 (d, *J* = 8.4 Hz, 1H), 3.95 (s, 3H), 3.94 (s, 3H), 2.57 (s, 3H);

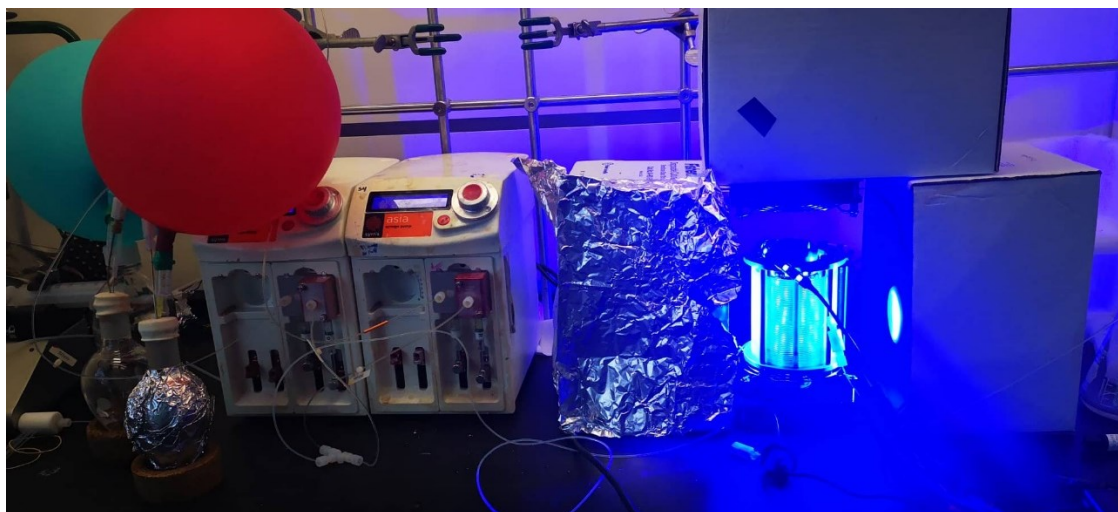


Figure A5 - 2 Continuous flow reactor set-up used for the scale-up reactions.

Synthesis and Degradation of the model polymer

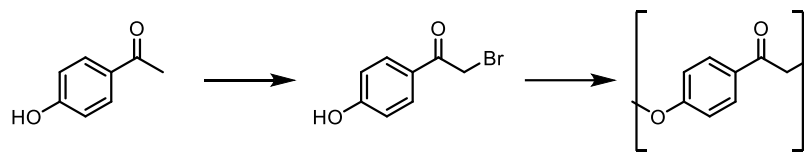
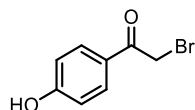
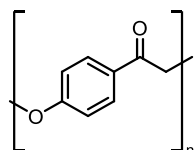


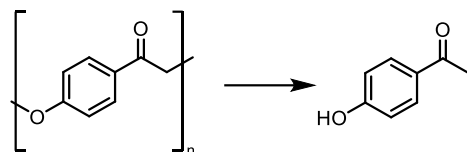
Figure A5 - 3 Synthesis of the model polymer



2-B -1-(4-hydroxyphenyl)ethan-1-one (13S): To a solution of 1-(4-hydroxyphenyl)ethan-1-one (1 g, 7.34 mmol) in EtOAc (40 mL, 134 mM) and CHCl_3 (15 mL, 134 mM) is added CuBr_2 (3.28 g, 14.7 mmol). The reaction mixture was stirred 2h30 at 80°C . The reaction was then allowed to cool to room temperature and filtered through a filter paper. The filtrate was added to a separatory funnel along with water (30 mL). It was then extracted three times with EtOAc (3 X 30 mL) and the combined organic phases were dried with Na_2SO_4 (2 g) and concentrated *in vacuo*. The product was then purified by flash chromatography (Hexanes : EtOAc ; 8 : 2) to give a white solid (1.58 g, 82%). Spectral data were in accordance with previous report¹⁶. **$^1\text{H NMR}$ (500 MHz, CDCl_3):** δ 7.98 – 7.91 (m, 2H), 6.94 – 6.86 (m, 2H), 4.39 (s, 2H).



Model polymer (13): To a solution of 2-bromo-1-(4-hydroxyphenyl)ethan-1-one (400 mg, 1.86 mmol) in DMF (5 mL, 372 mM) is added Cs_2CO_3 (1.21 g, 3.72 mmol). The reaction mixture was stirred for 24h at room temperature and 20 mL of H_2O was added. The orange precipitate was then filtered and washed with 5 mL of DMF and 5 mL of H_2O . The solid was then lyophilized to remove traces of solvent to give the pure polymer as an orange solid (345 mg, 69%). Characterisation of the polymer was done by HSQC.



Procedure for the degradation of the model polymer: To a 20 mL vial equipped with a cross-shaped stir bar was added Cu(**bathocup**)(Xantphos)BF₄ (1.9 mg, 1.84 μmol), NABnH (7.9 mg, 37 μmol), the polymer (25 mg), NaHCO₃ (18.5 mg, 220 μmol), and Na₂S₂O₄ (38.8 mg, 220 μmol). The vial was closed and N₂ degassed water (4 mL) and DME (4 mL) were added. The resulting solution was further degassed with N₂ for 5 minutes. The vial was then stirred under blue KESSIL® Lamp irradiation for 72 h. The solution was transferred to a separatory funnel and the vial was washed with EtOAc (3 x 2 mL). Water (30 mL) was added and extracted with EtOAc (3 x 30 mL). The combined organic phase was dried with Na₂SO₄ (2 g) and concentrated *in vacuo*. Purification by flash chromatography (80:20 Hexanes:EtOAc) gave the pure product **13a** as a white solid (15.1 mg, 60%). Spectral data were in accordance with previous report. ¹H NMR (500 MHz, CDCl₃): δ 7.95 – 7.88 (m, 2H), 6.96 – 6.89 (m, 2H), 2.58 (s, 3H), 2.20 (s, 1H).

A5.5 Stern-Volmer Experiments

Quenching experiments were performed by examining the effect on the excited state lifetime of the copper complexes through the addition of each component of the reaction. Lifetime measurements were done with an Edinburgh Instruments FLS-920 fluorimeter with an EPL 405 laser (exciting at 405 nm). To ensure complete solubility and homogeneous conditions, a 1:1 mix of DME:H₂O was used. Solutions were purged with N₂ for 5 min prior to measurement.

Table A5 - 4 Excited State Lifetime Quenching with NABnH

[NABnH] (mM)	Excited State Lifetime (ns)
0	2551
0.1	2144
0.3	1850
0.6	1234

0.9	1086
1.2	614

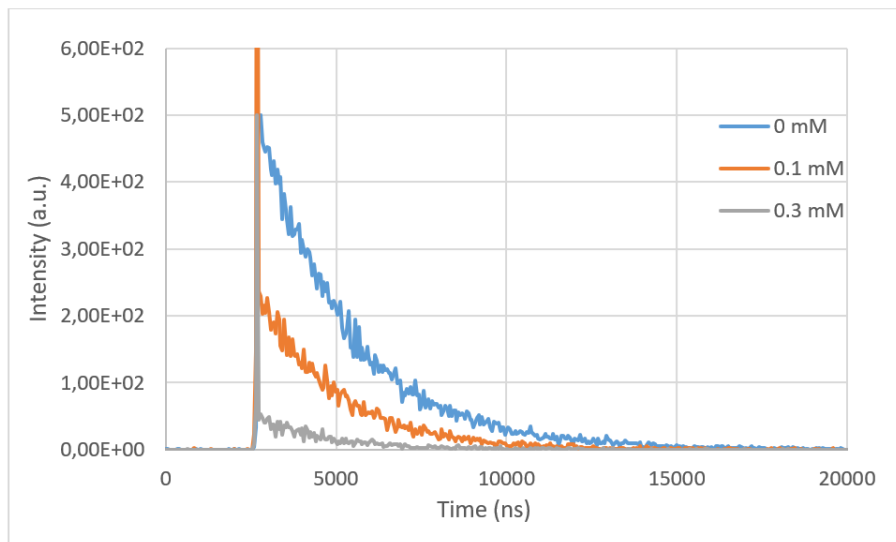


Figure A5 - 4 Life-time spectra of Cu(**bathocup**)(**Xantphos**)BF₄ with various concentrations of NABnH, excited at 405 nm, recorded at ambient temperature in 1:1 DME:H₂O (1.10⁻⁴M).

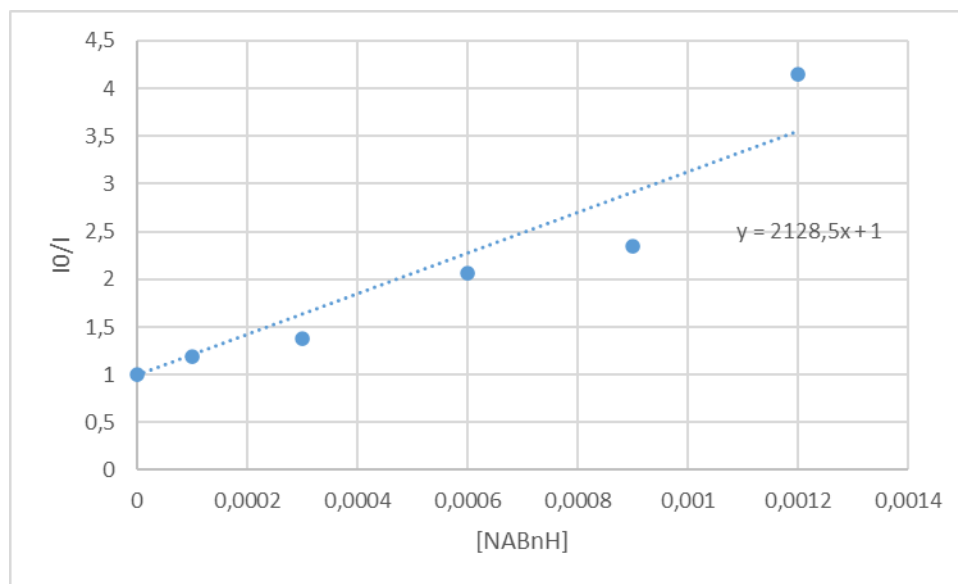


Figure A5 - 5 Stern-Volmer plot of Cu(**bathocup**)(**Xantphos**)BF₄ with NABnH

Table A5 - 5 Excited State Lifetime Quenching with 1-(3,4-dimethoxyphenyl)-2-(2-methoxyphenoxy)ethan-1-one (**1**)

[1] (mM)	Excited State Lifetime (ns)
0	2551
0,3	2475
0,6	2478
1,2	2524
2,4	2486
4,8	2501

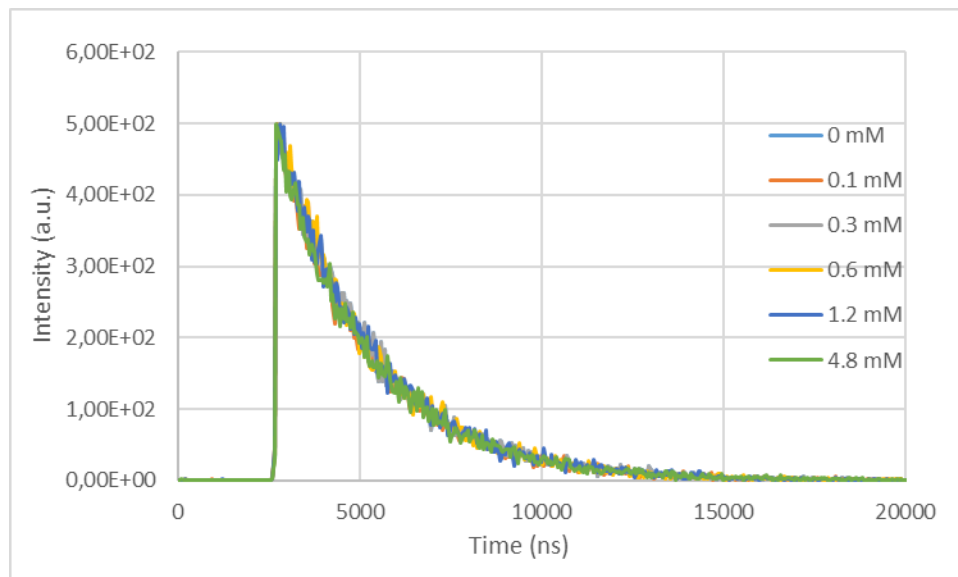


Figure A5 - 6 Life-time spectra of Cu(**bathocup**)(**Xantphos**)BF₄ with various concentrations of **1**, excited at 405 nm, recorded at ambient temperature in 1:1 DME:H₂O (1.10⁻⁴M).

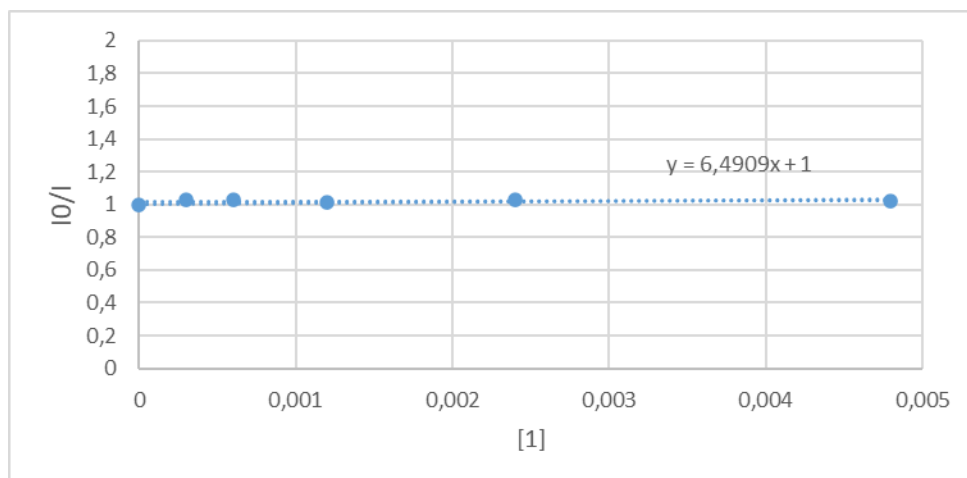


Figure A5 - 7 Stern-Volmer plot of Cu(Bathocup)(Xantphos)BF₄ with **1**

Table A5 - 6 Excited State Lifetime Quenching with NaHCO₃ and Na₂S₂O₄

[NaHCO₃]/ [Na₂S₂O₄] (mM)	Excited State Lifetime (ns)
0	2551
0,6	2431,93
1,2	2411,69
12	2442,23

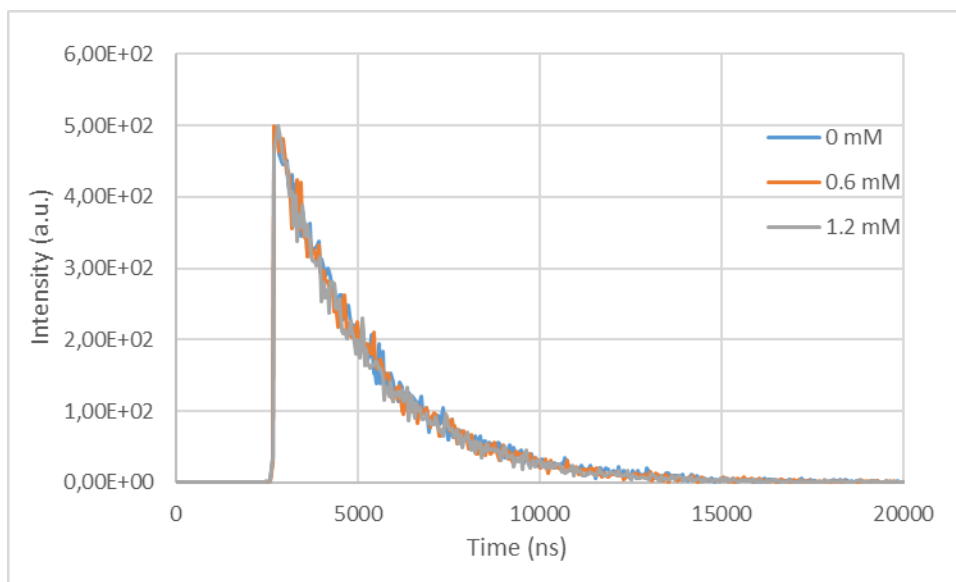


Figure A5 - 8 Life-time spectra of Cu(**bathocup**)(**Xantphos**)BF₄ with various concentrations of NaHCO₃ and Na₂S₂O₄, excited at 405 nm, recorded at ambient temperature in 1:1 DME:H₂O (1.10⁻⁴M).

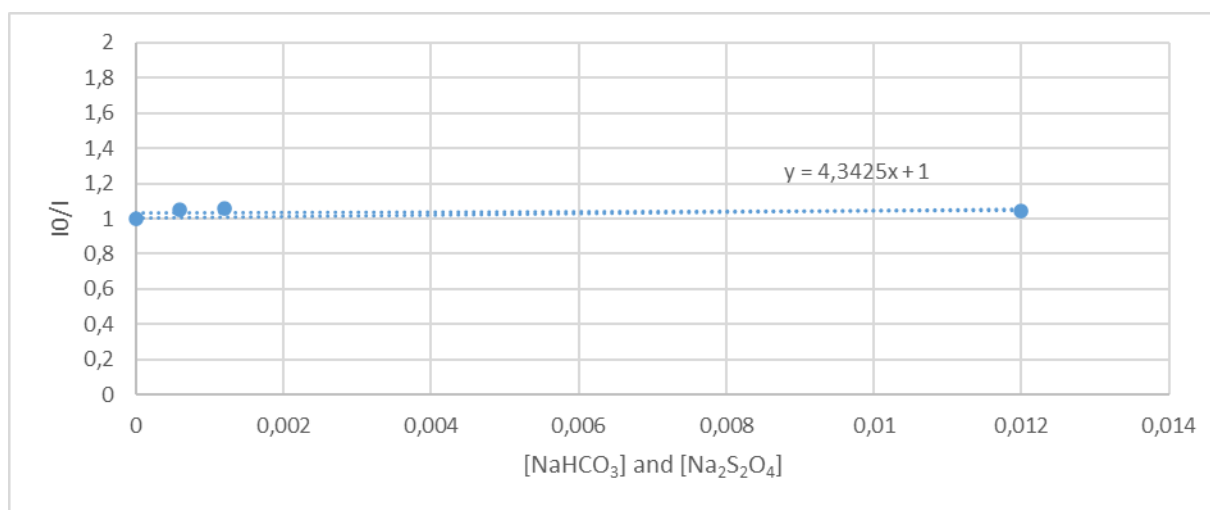


Figure A5 - 9 Stern-Volmer plot of Cu(**bathocup**)(**Xantphos**)BF₄ with NaHCO₃ and Na₂S₂O₄

Table A5 - 7 Bimolecular quenching constant k_q

Quench	k_q (M ⁻¹ · s ⁻¹)
NABnH	8,34E+09
1	2,54E+06

A5.6 Deuteration Experiments

Deuteration experiment was carried out in a solvent mixture of 3:1 THF:D₂O.

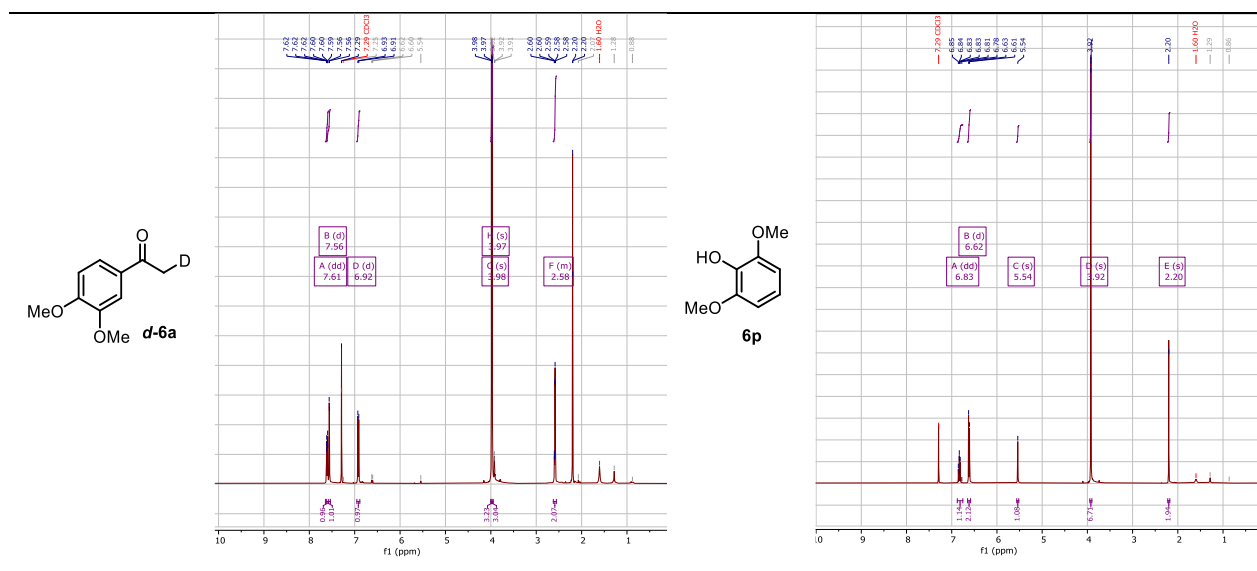
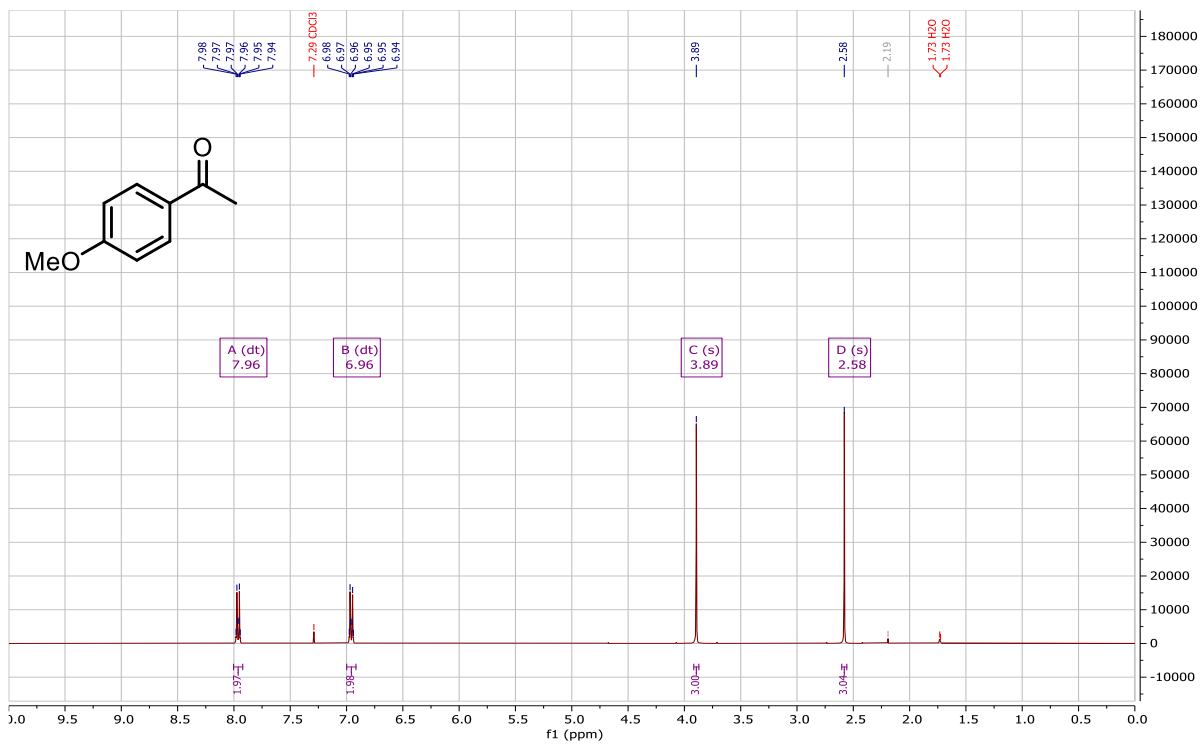


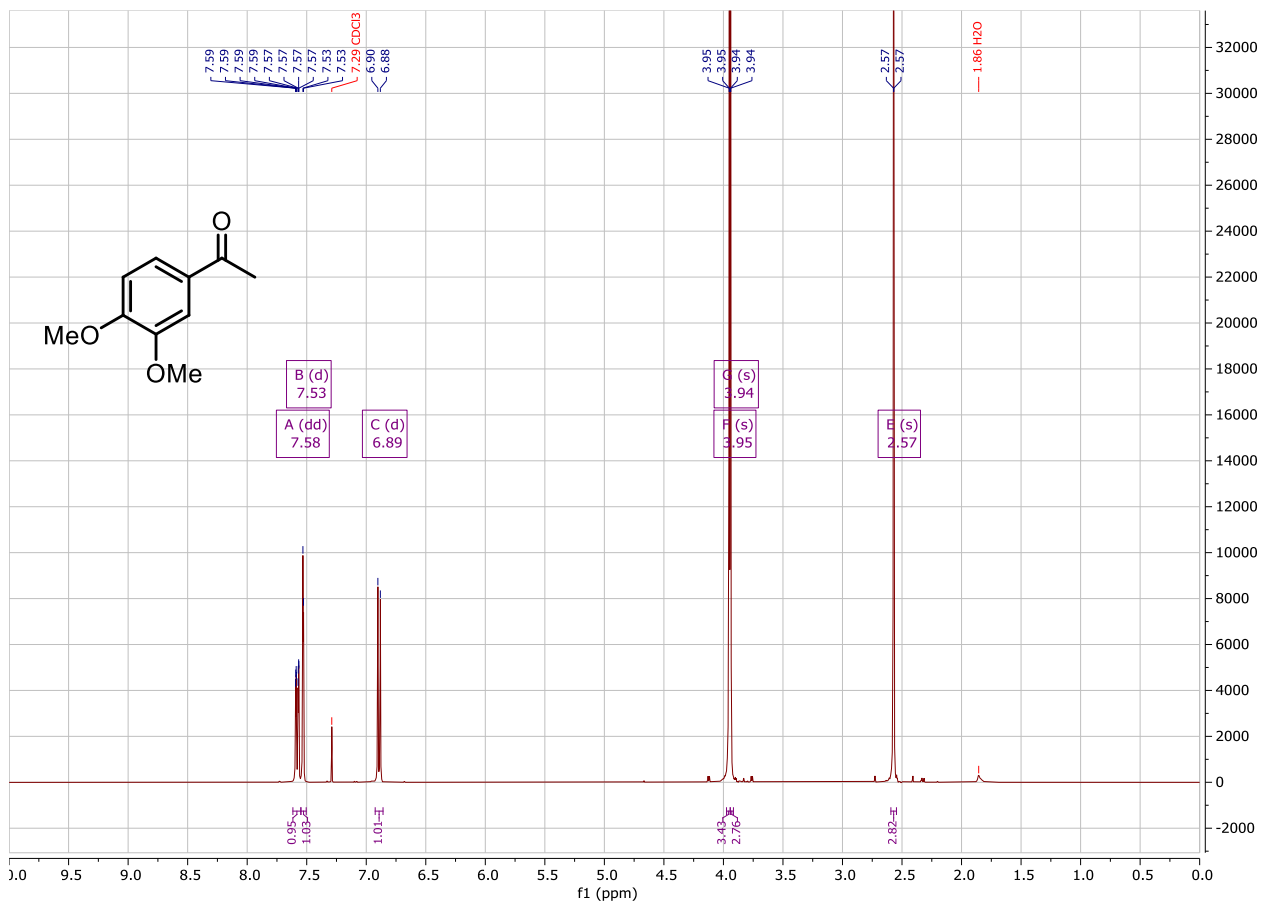
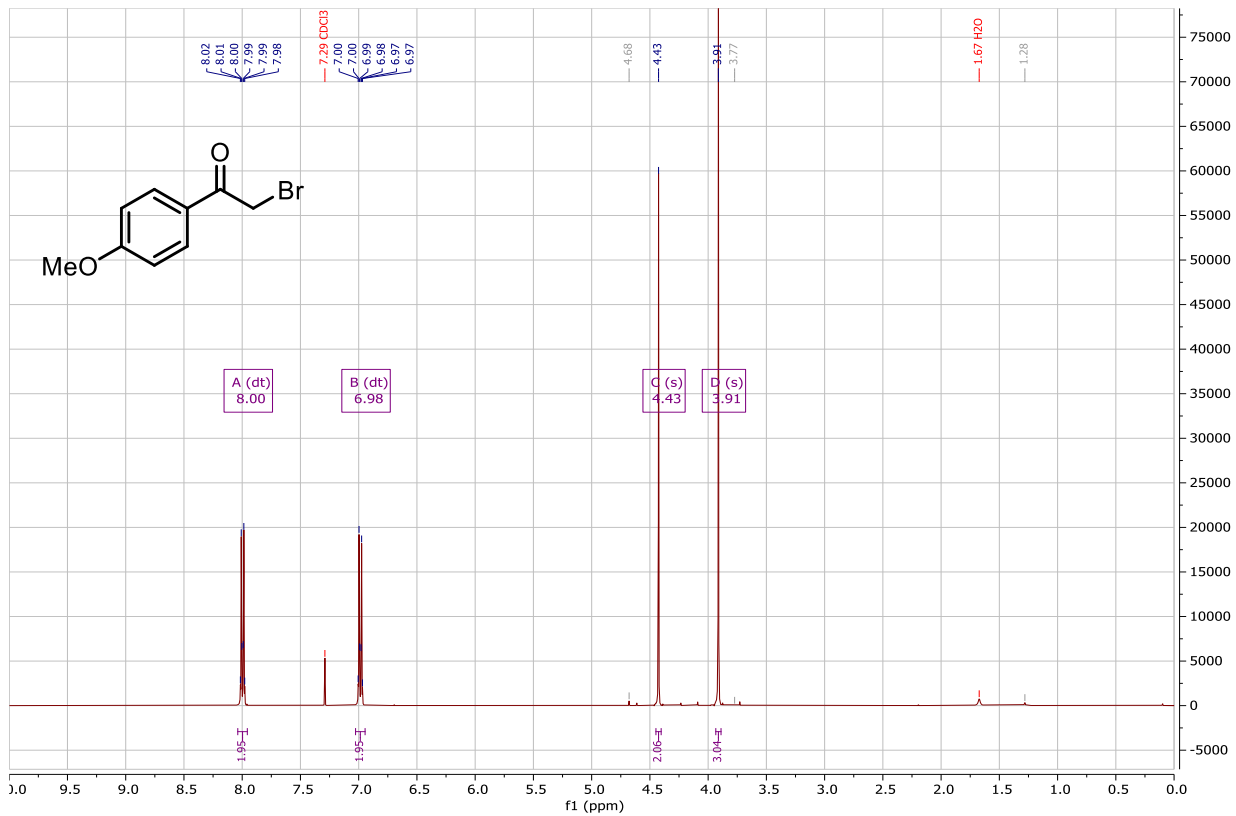
Figure A5 - 10 NMR Spectra for the deuteration experiment

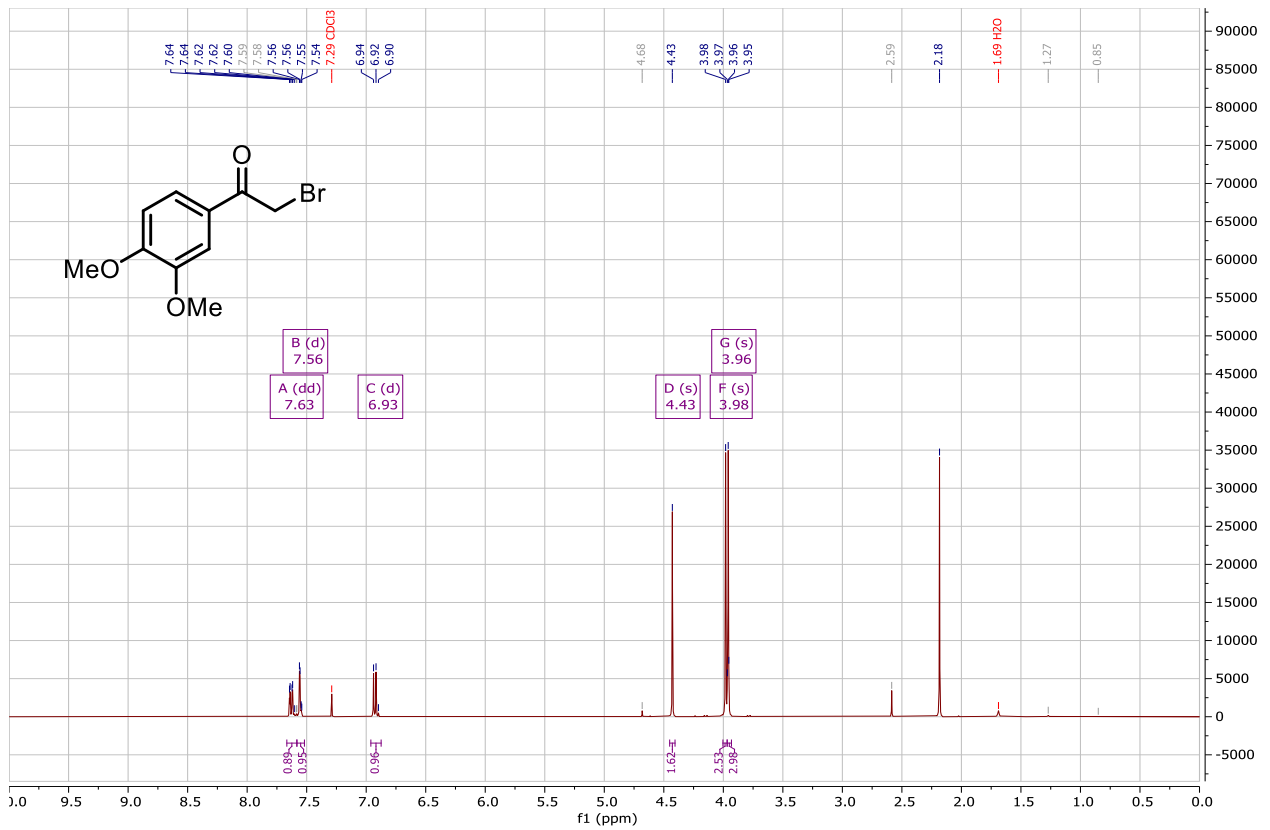
A5.7 NMR and Mass Spectra

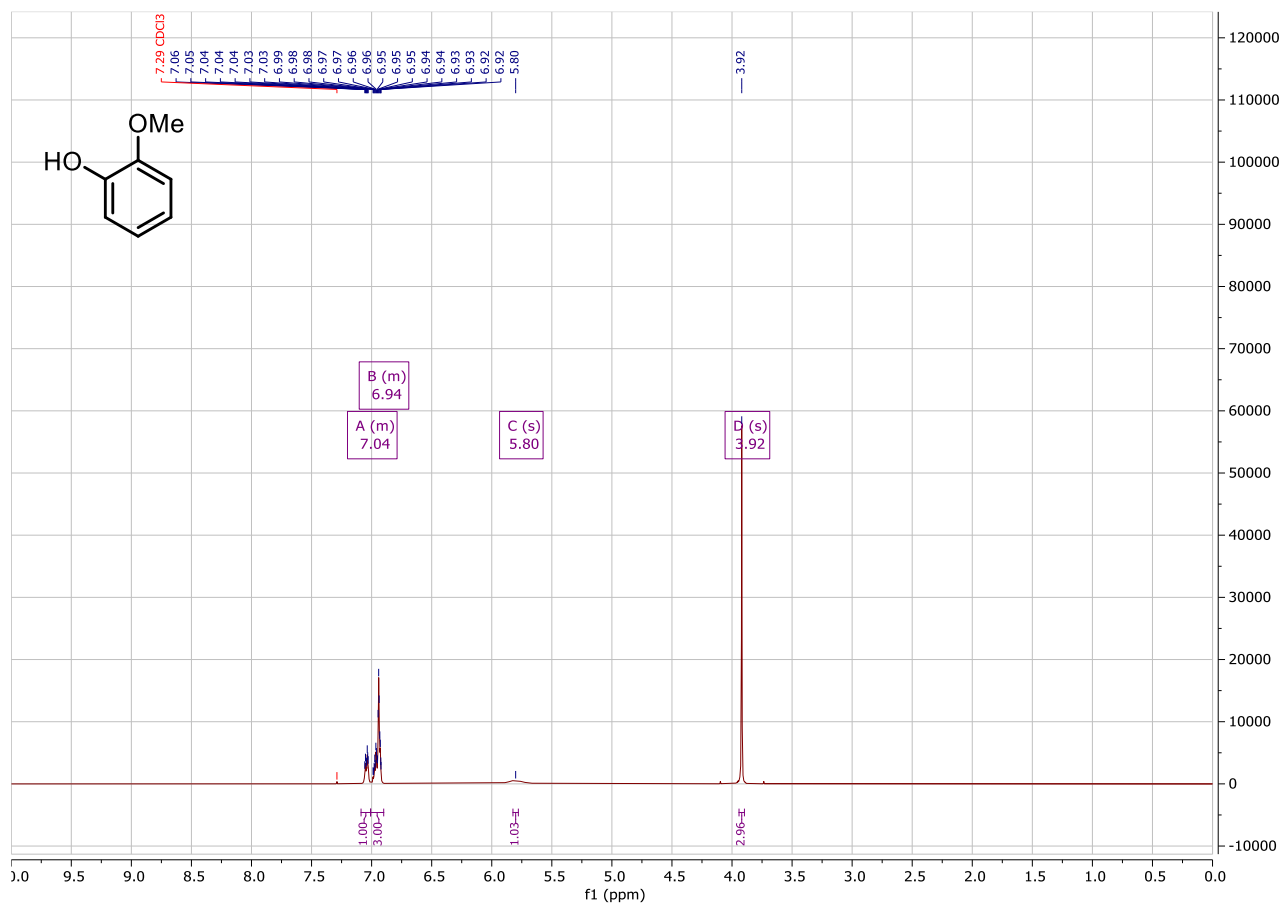
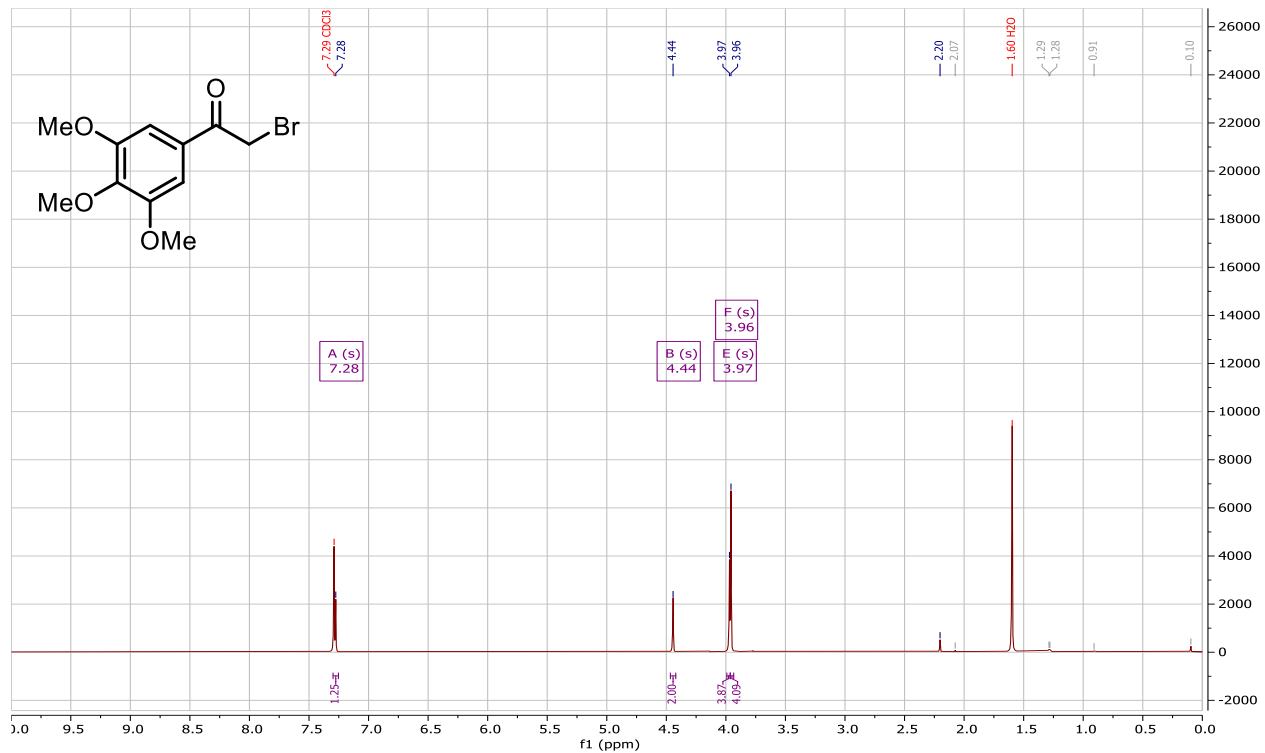
Lignin Models

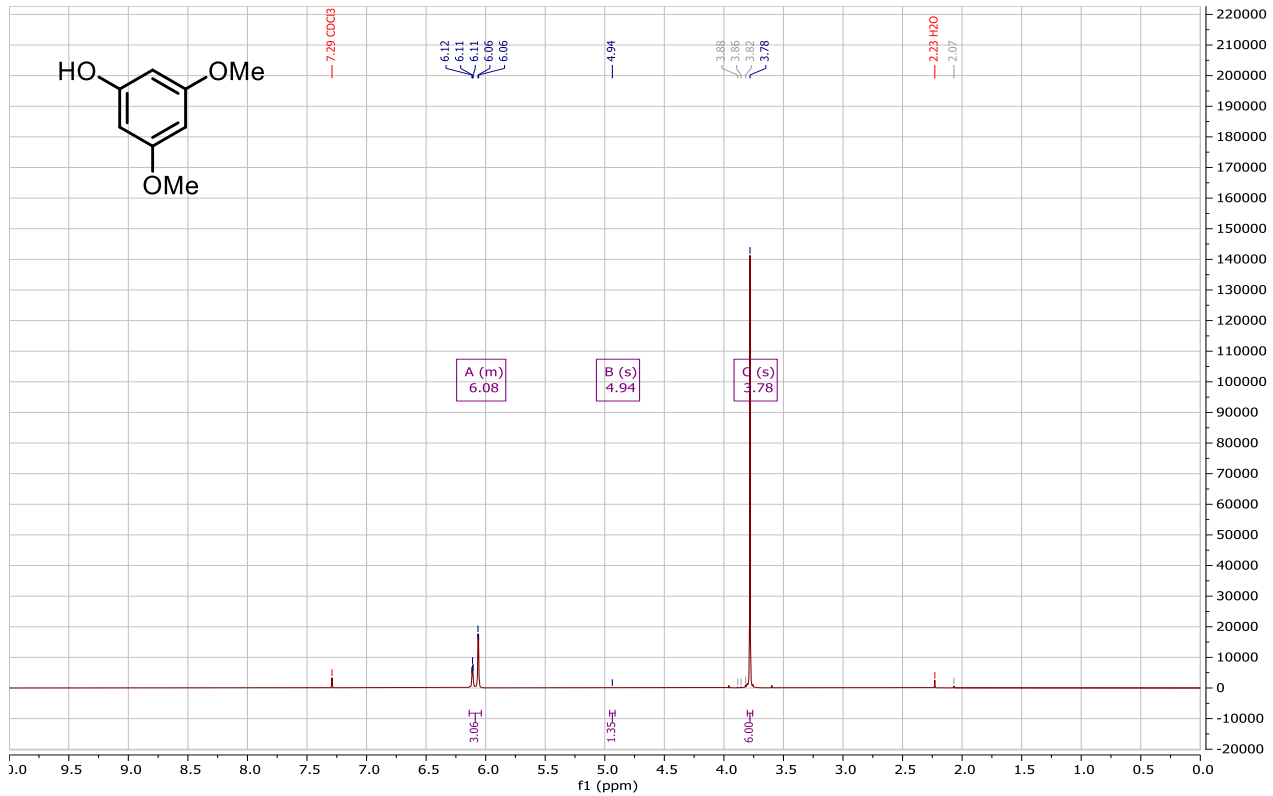
For previously reported compounds only the ¹H NMR is shown. For new compounds both the ¹H and ¹³C NMR spectra are provided:

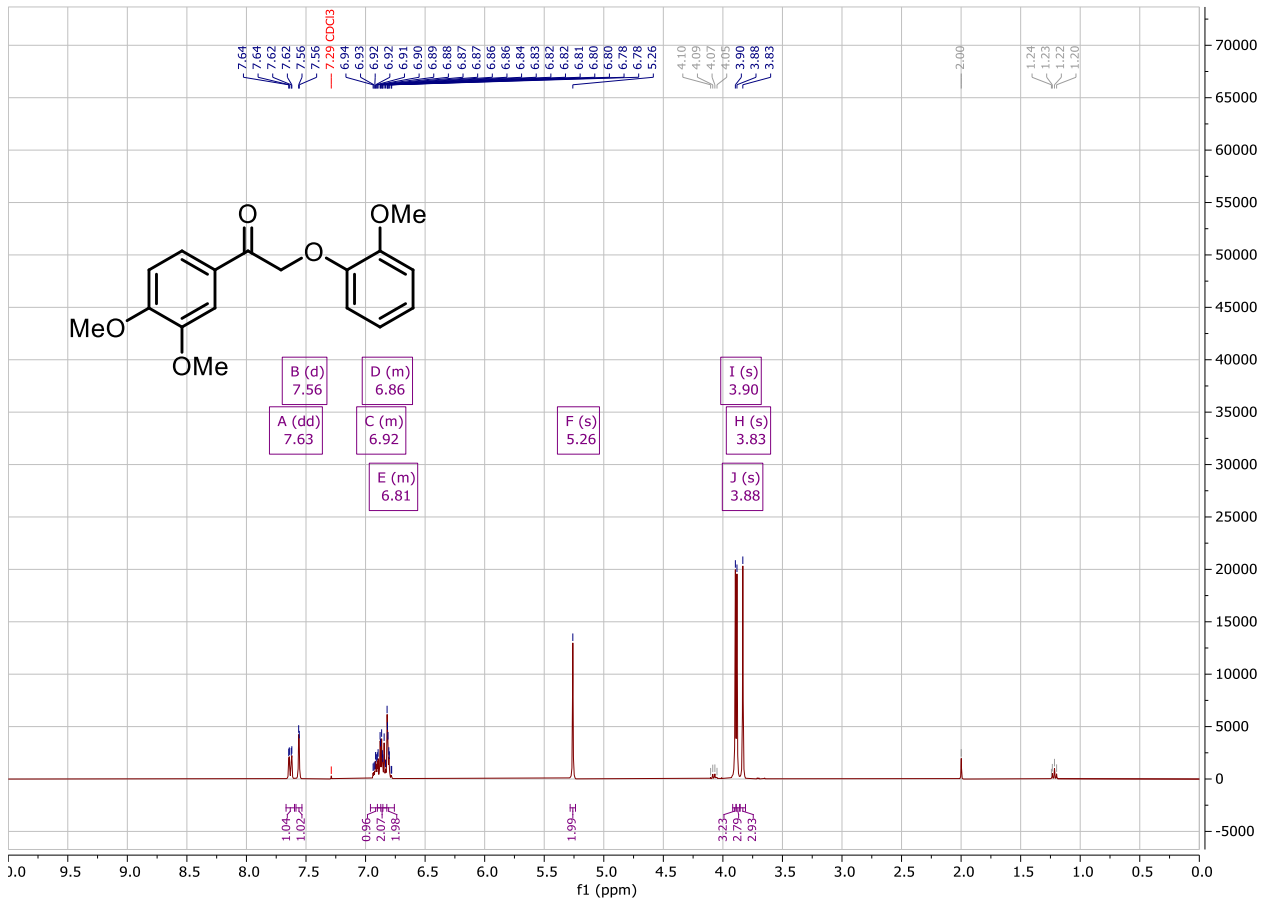
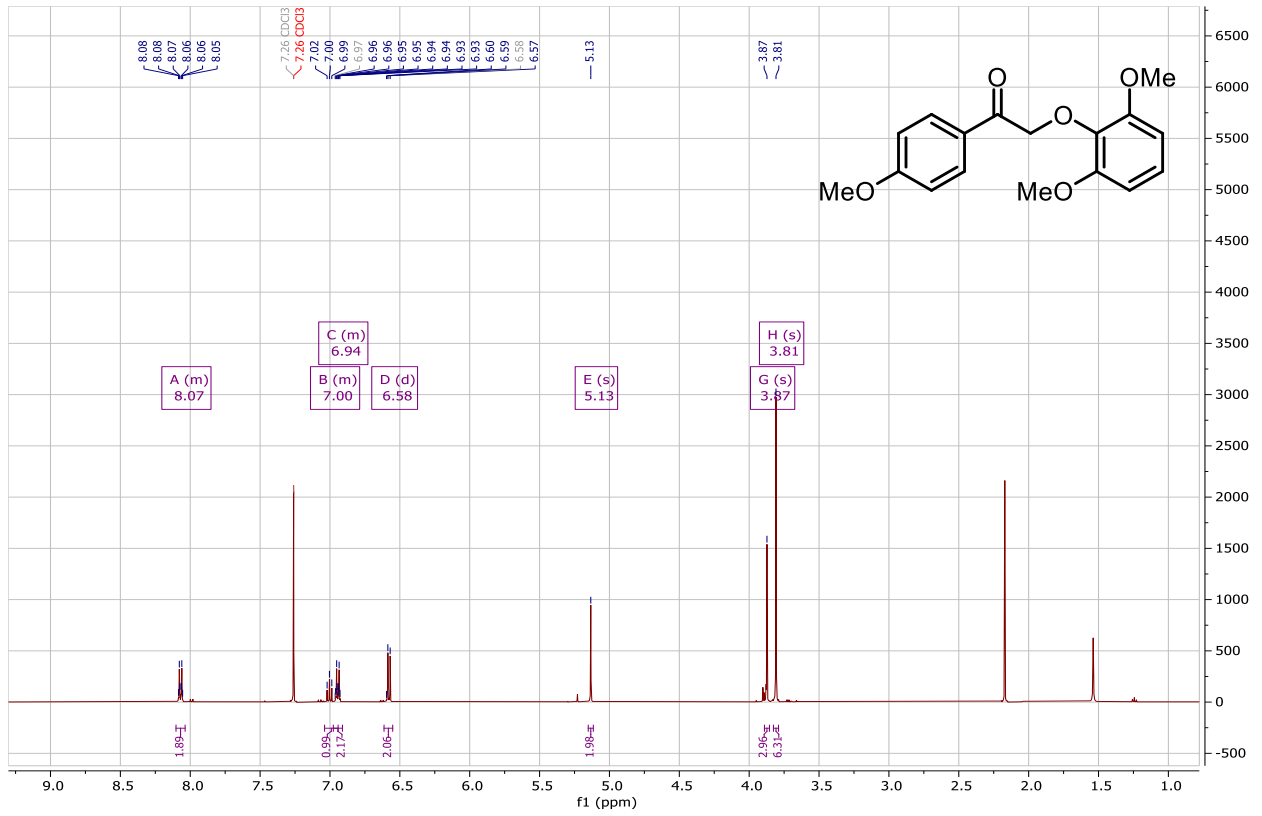


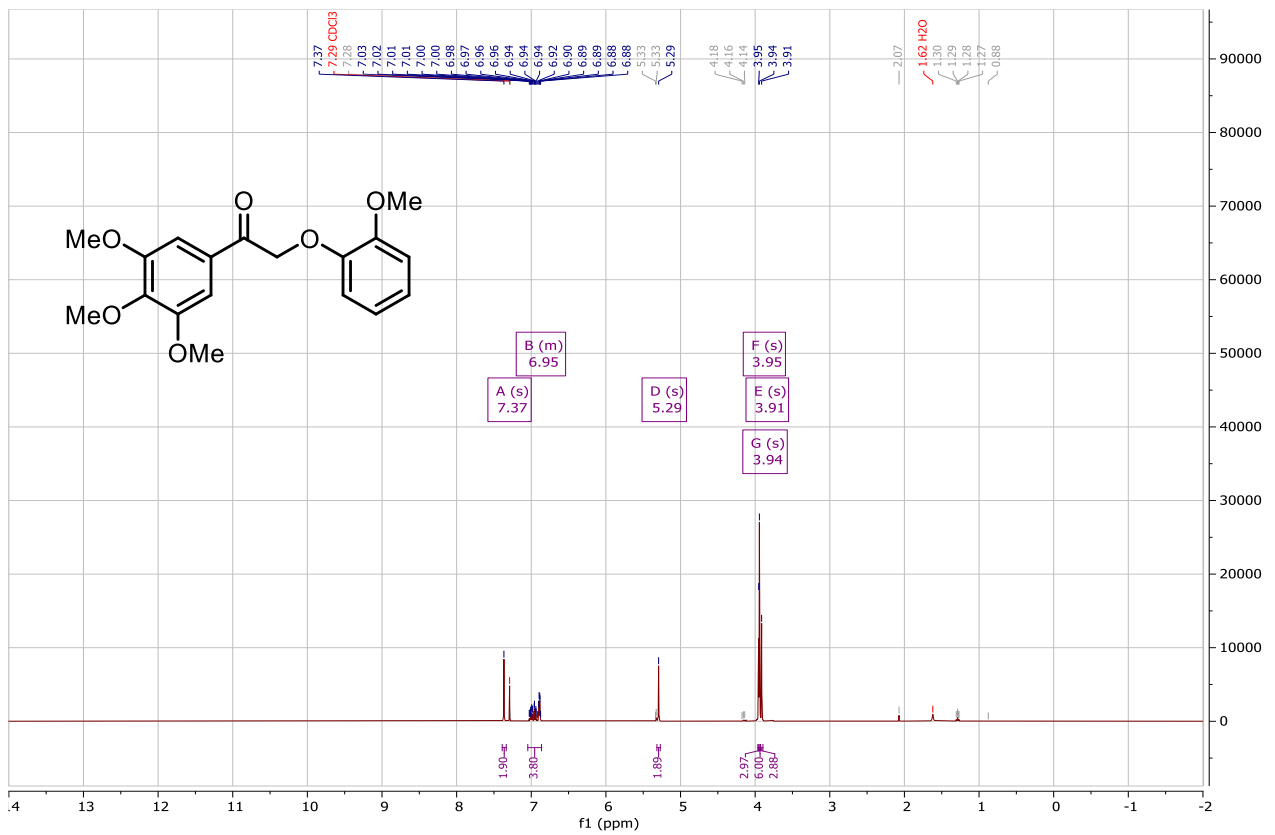
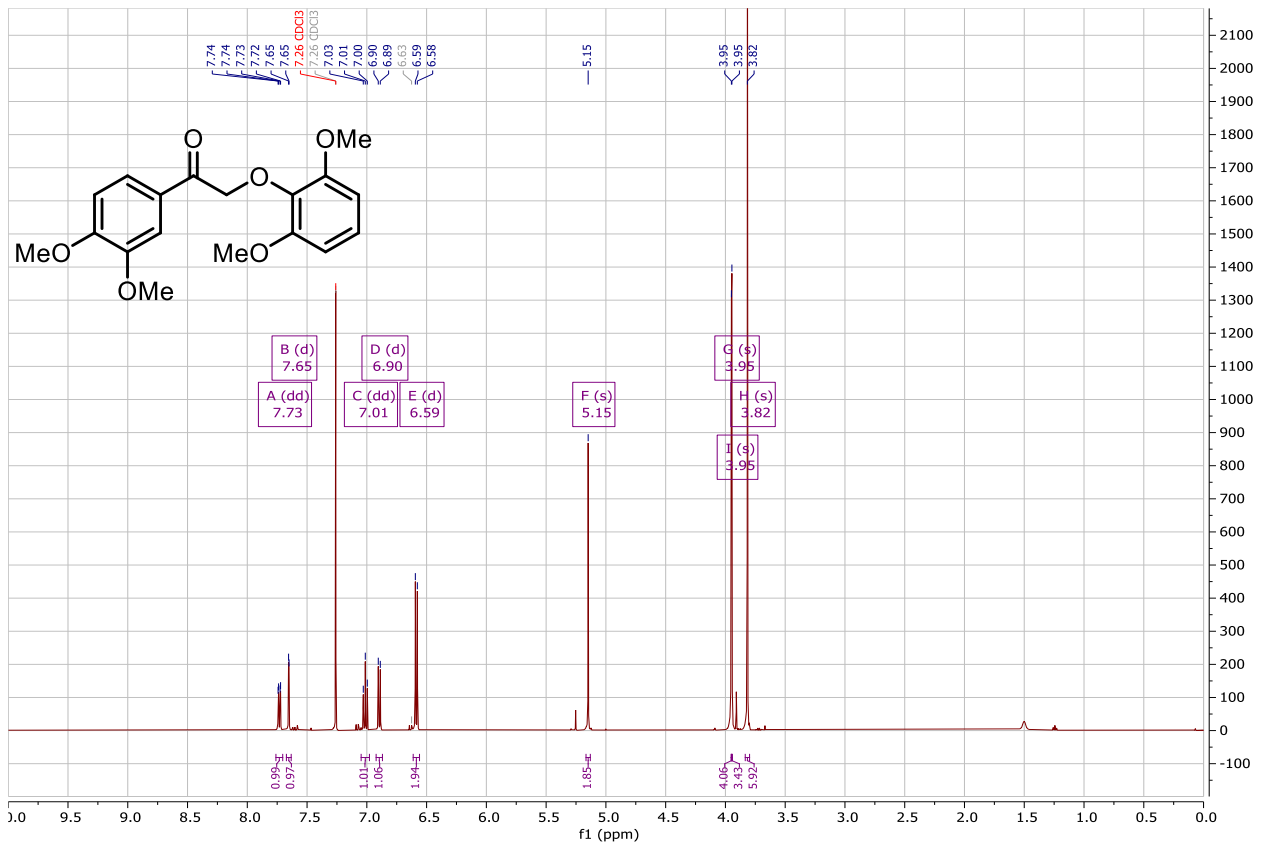


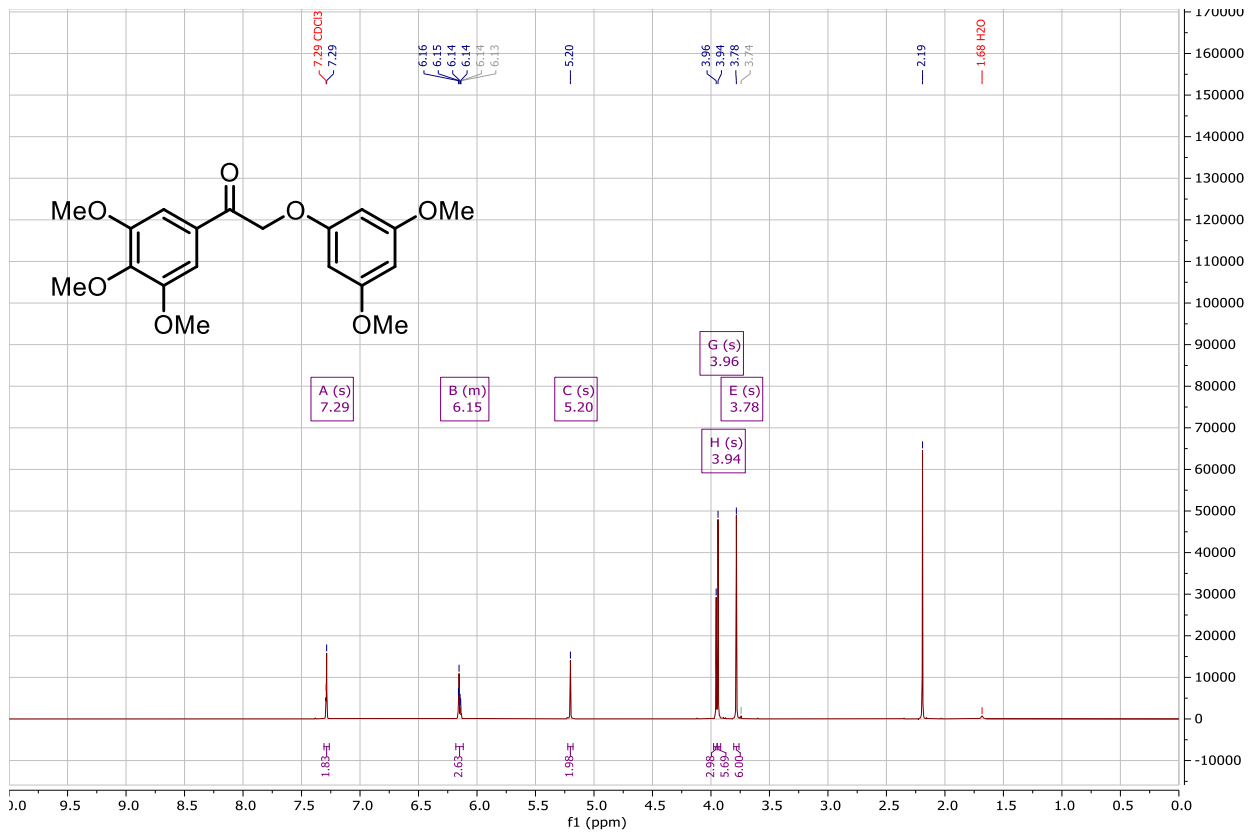
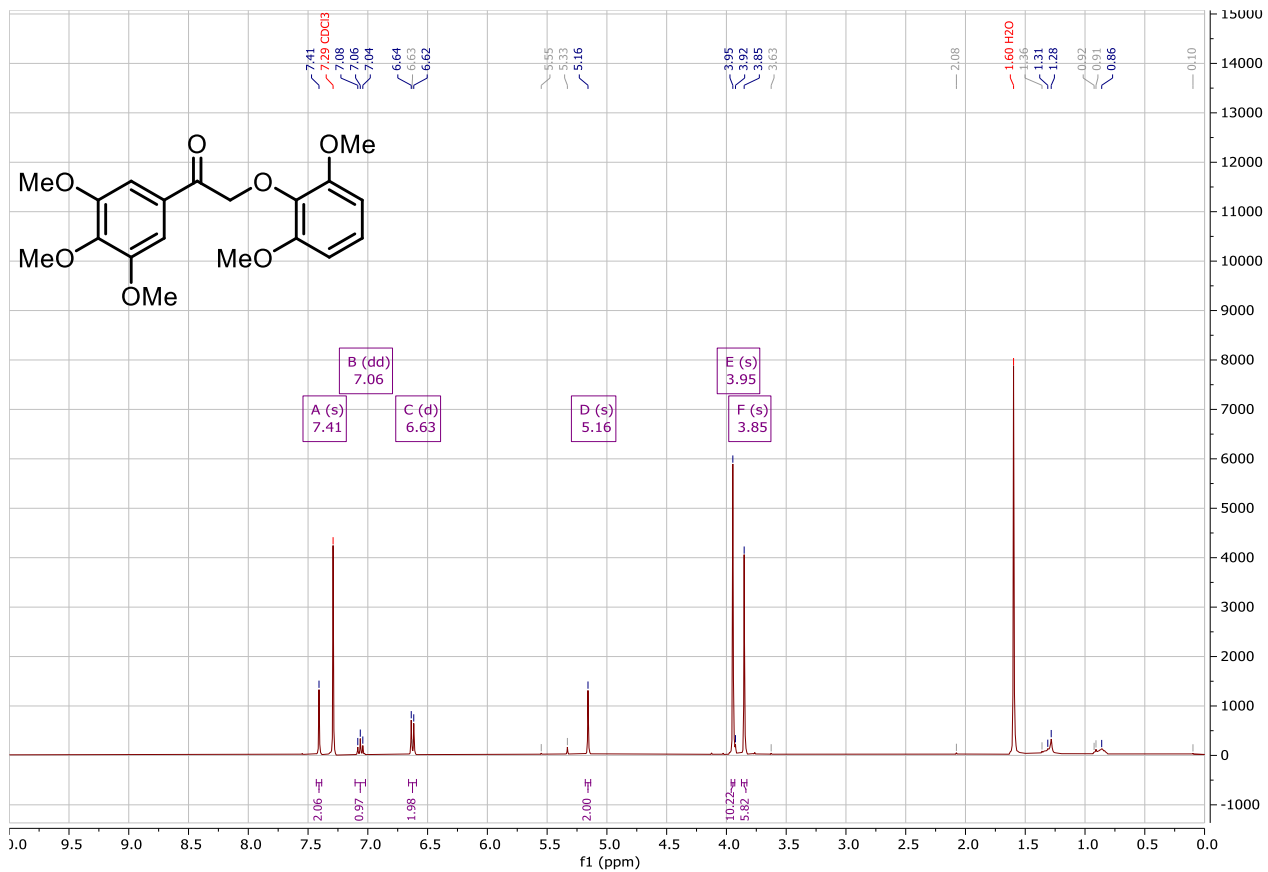


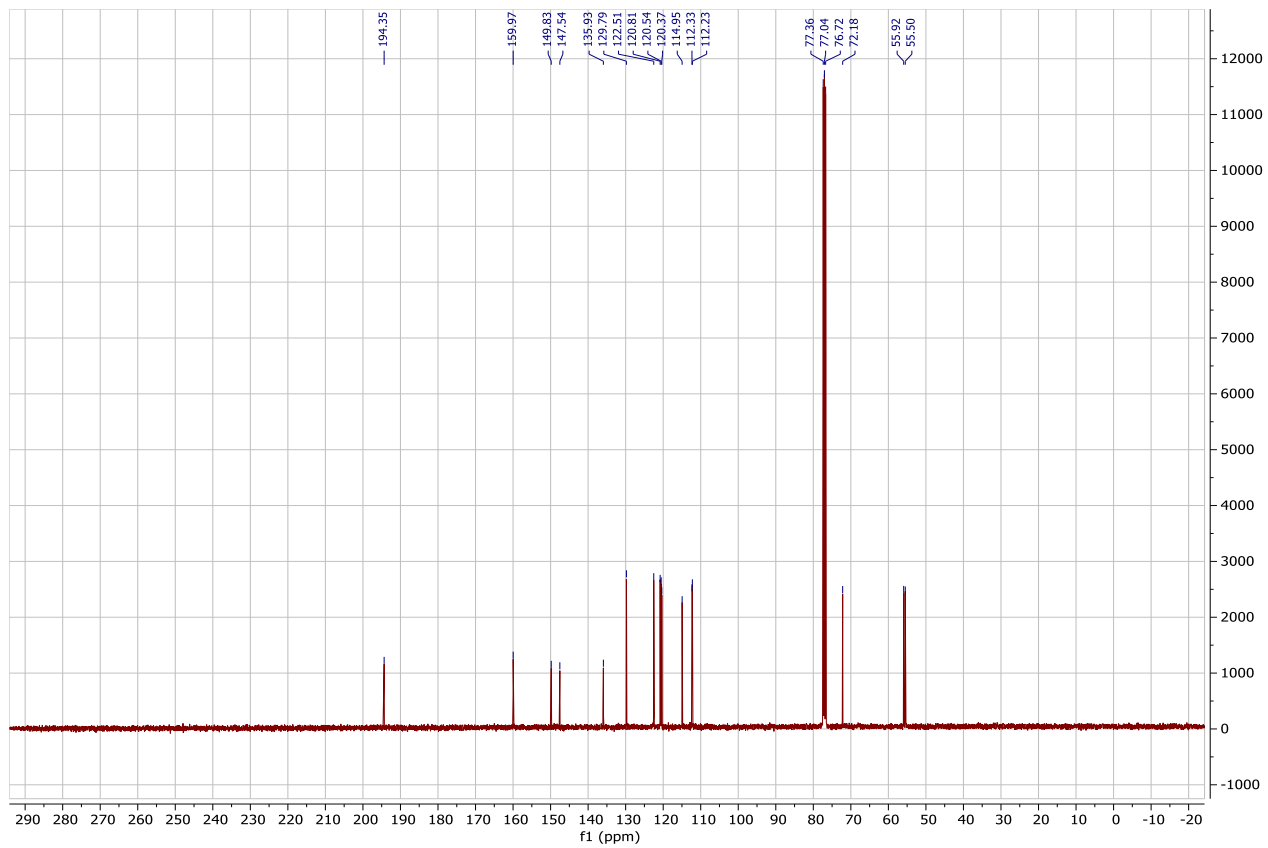
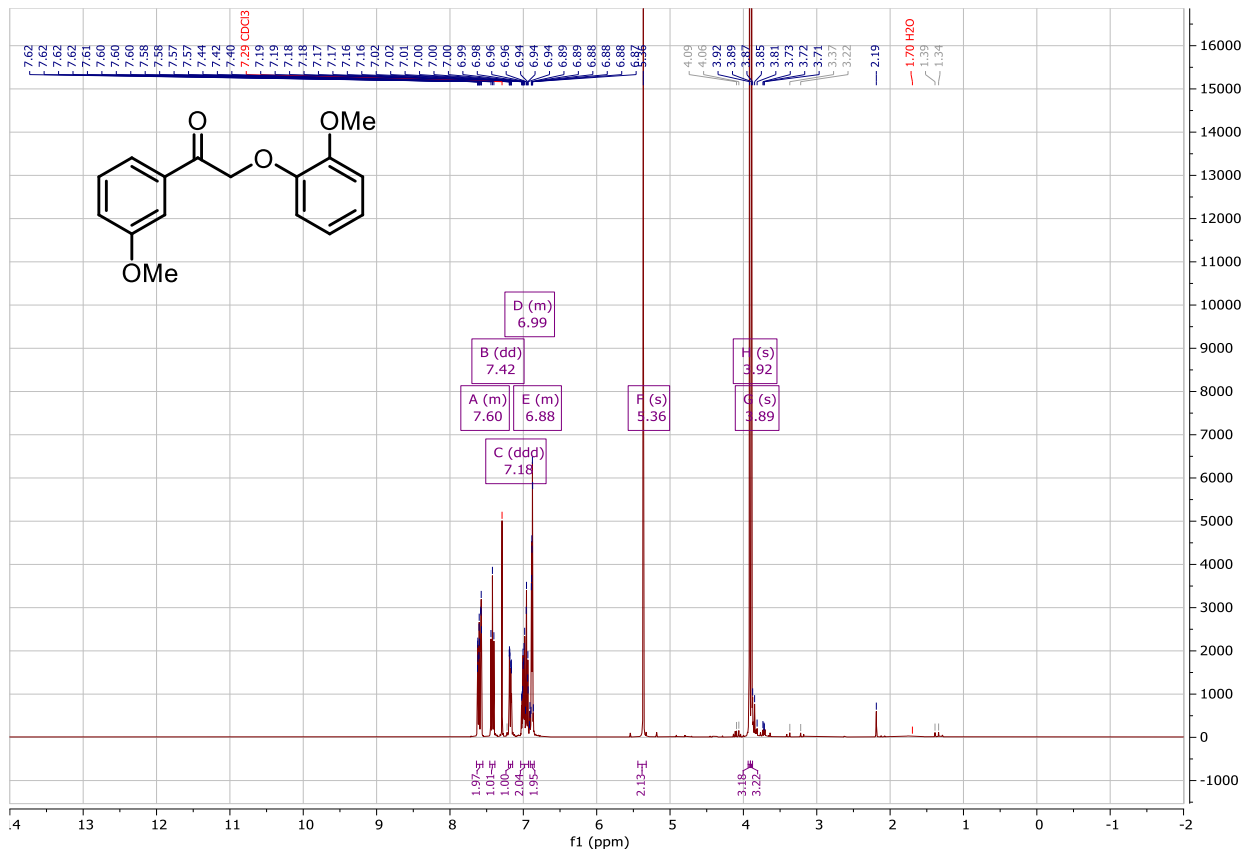


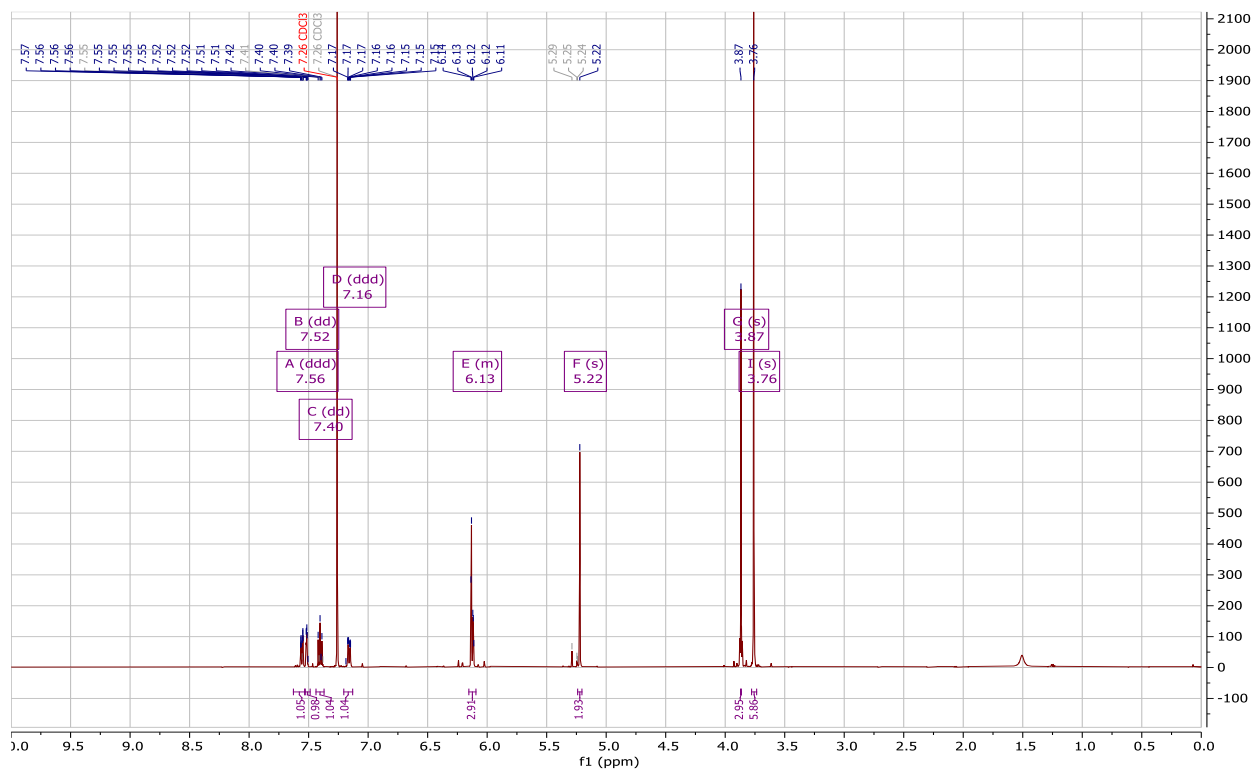
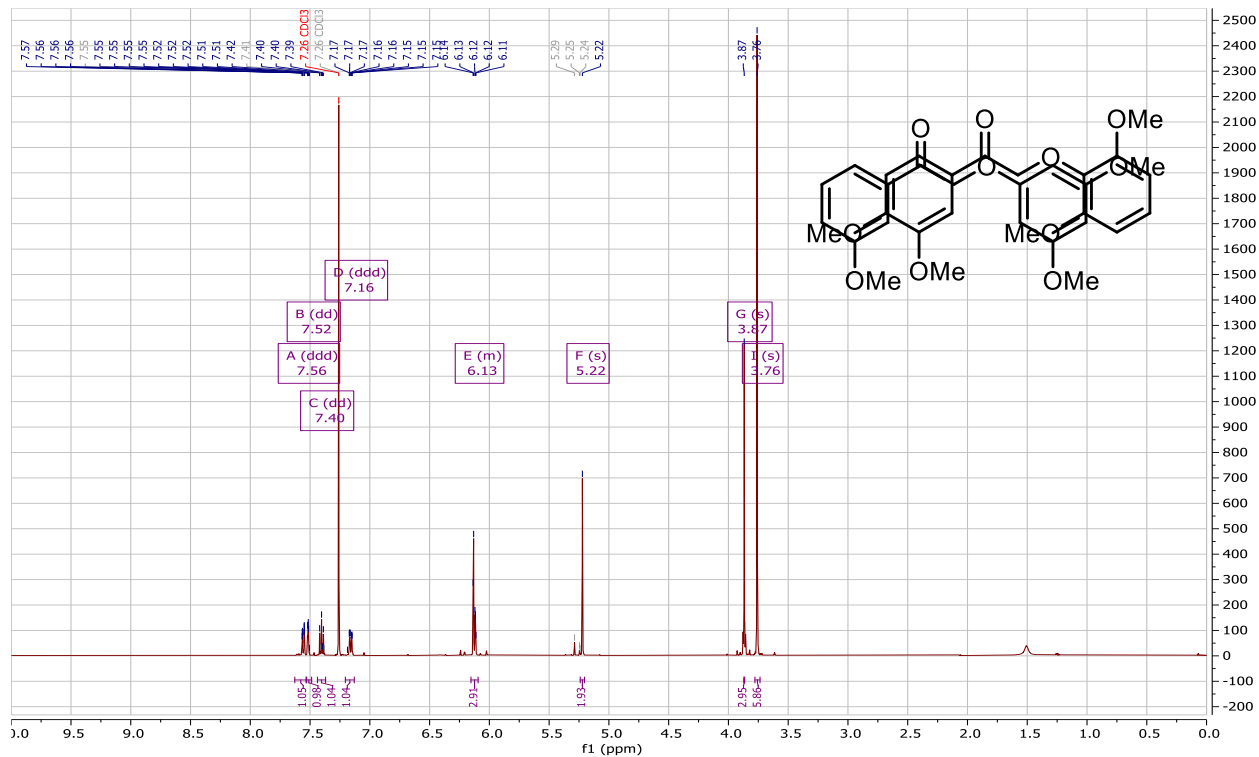


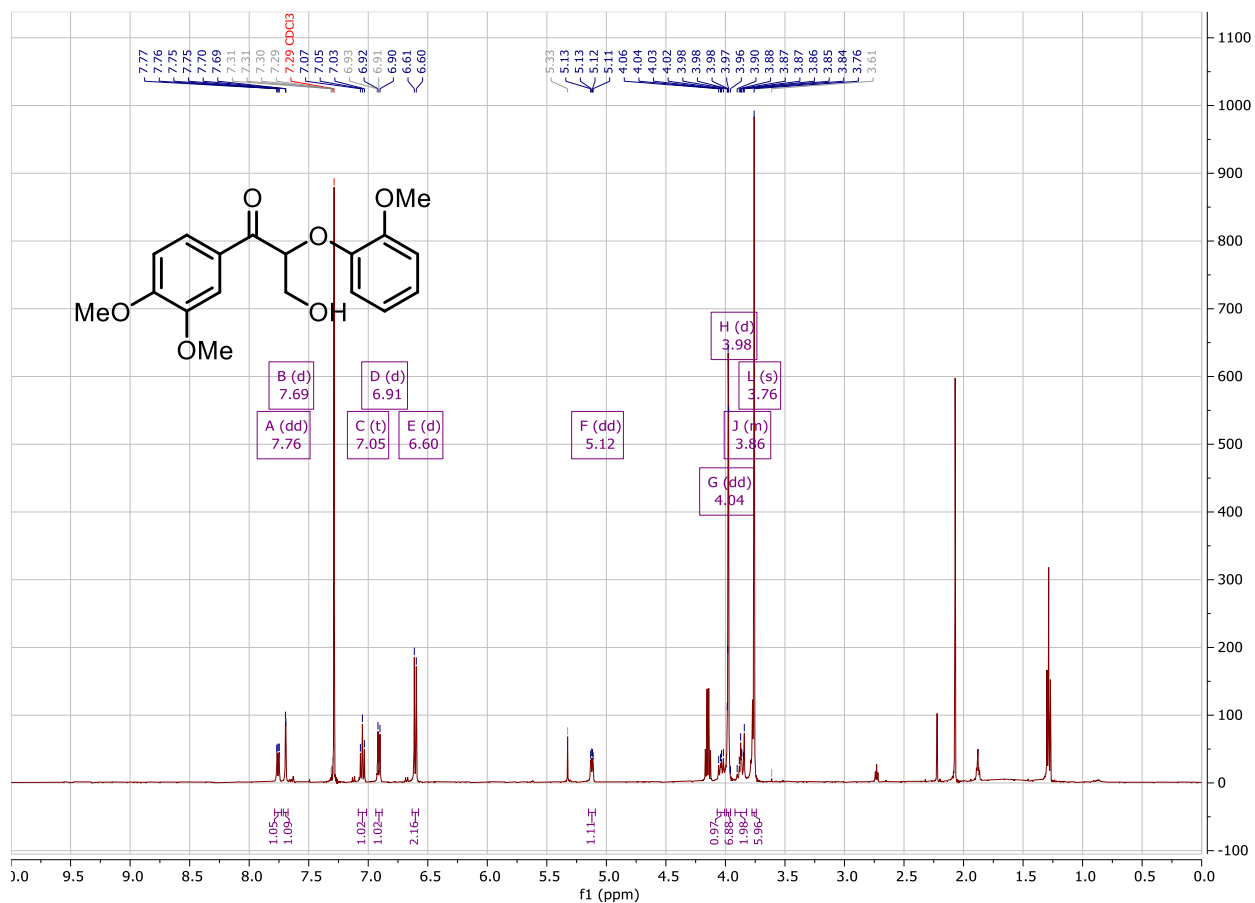
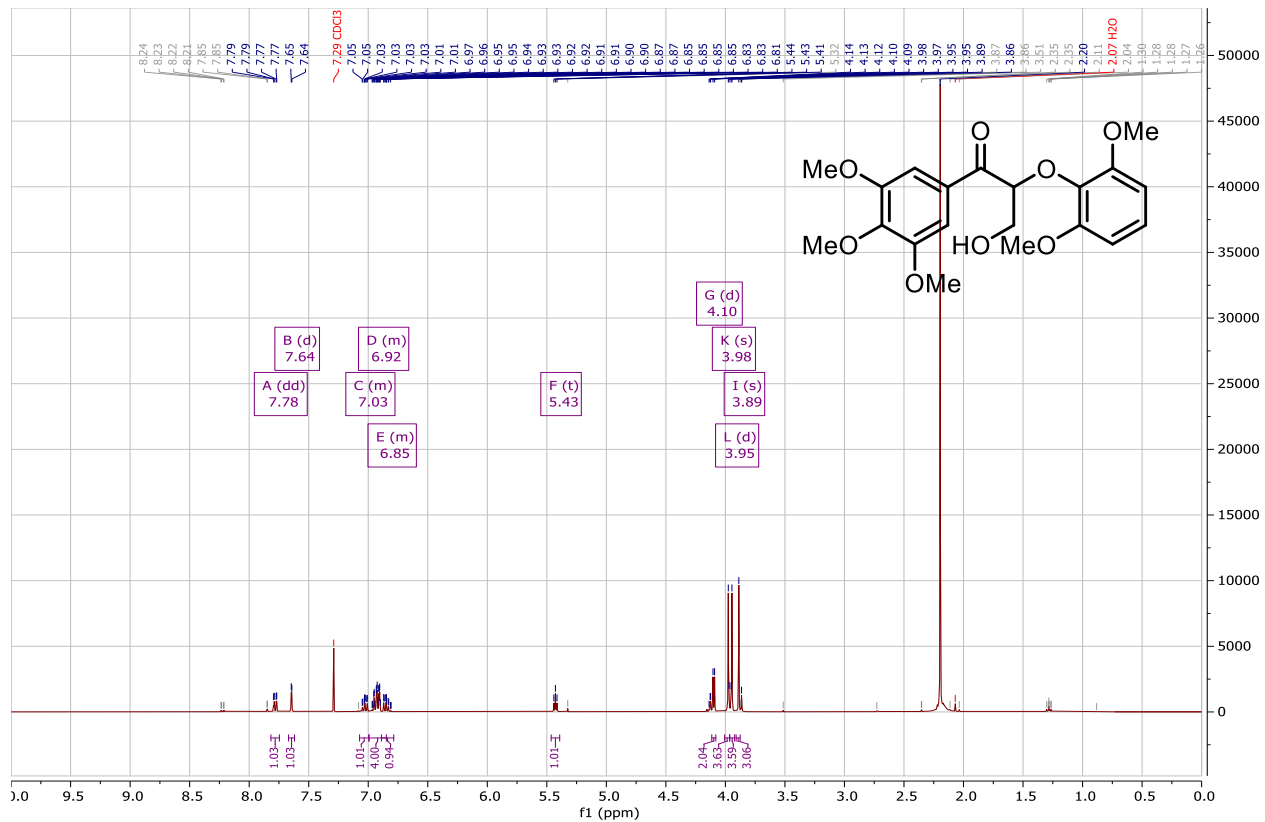


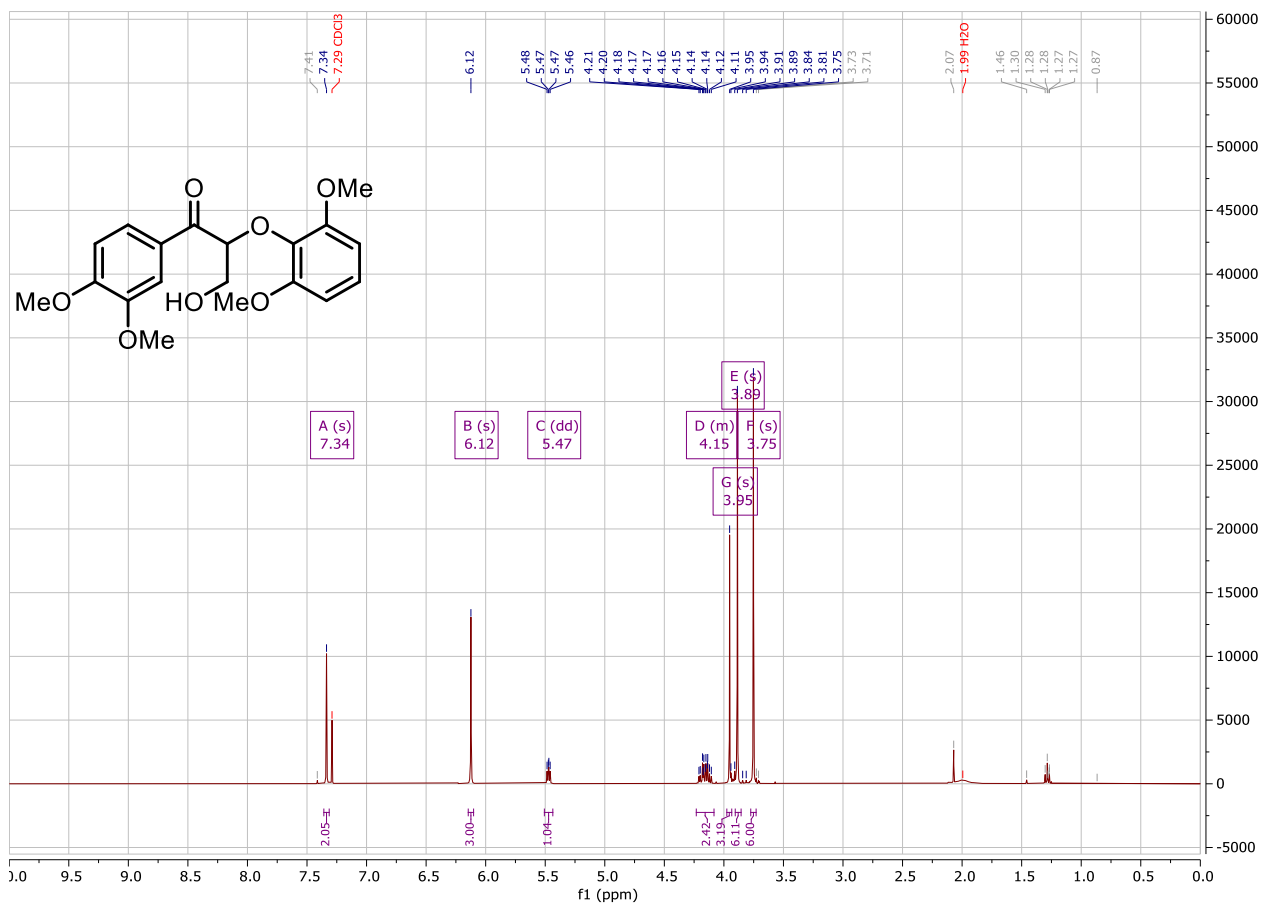
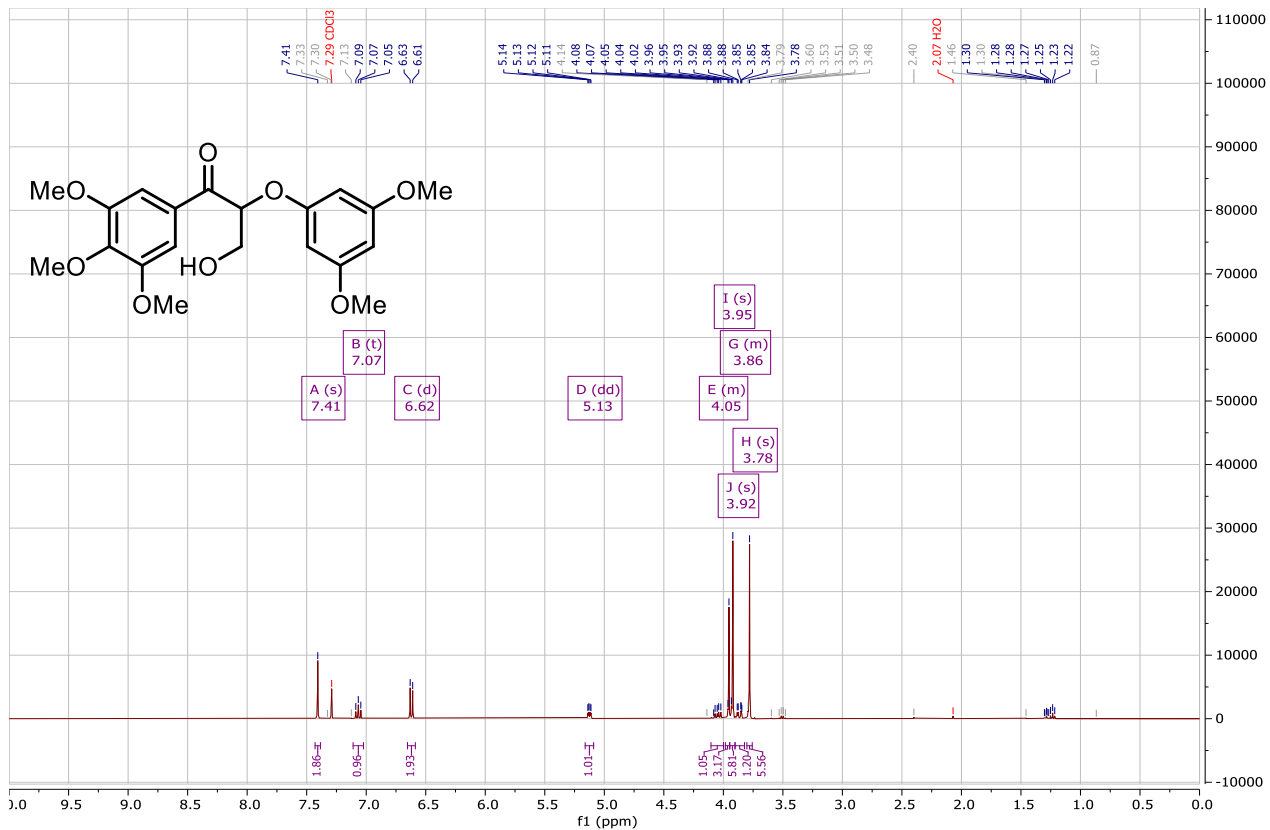


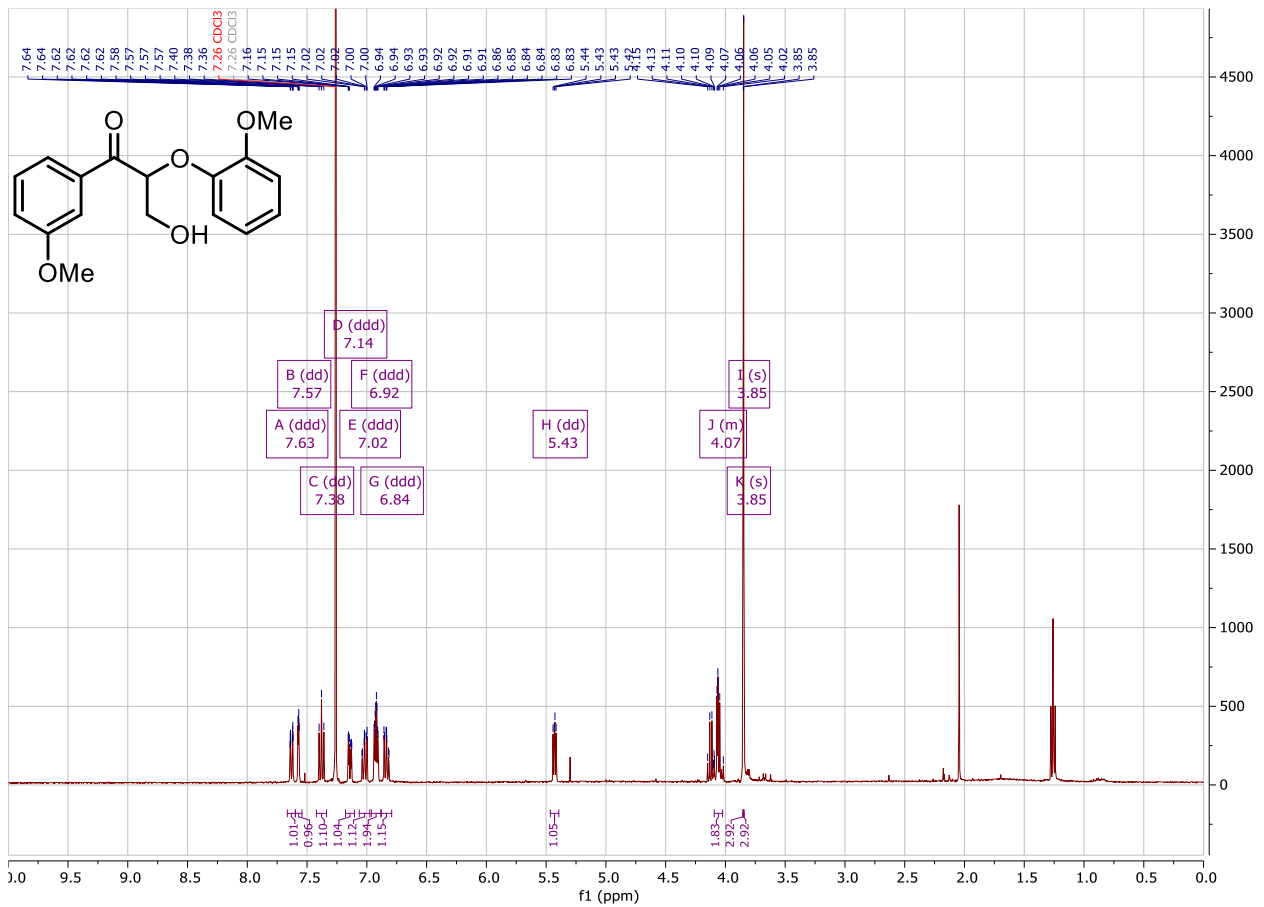
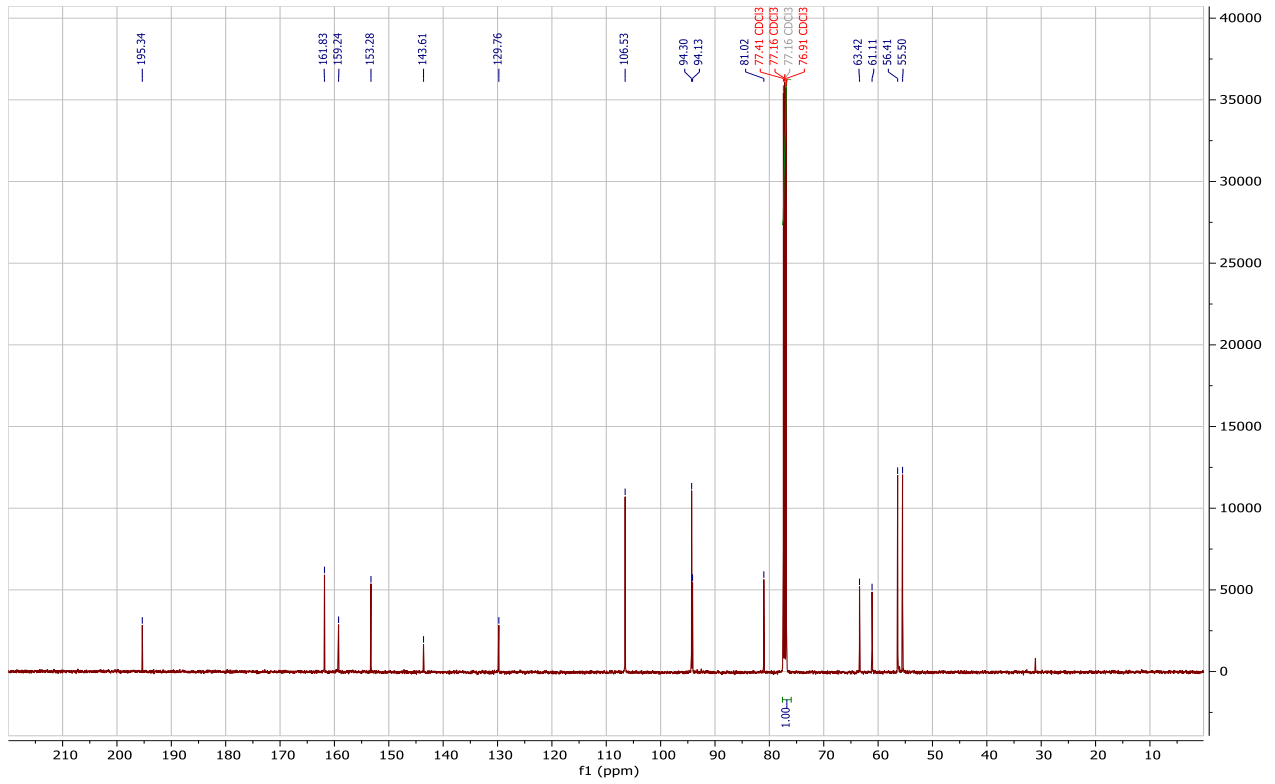


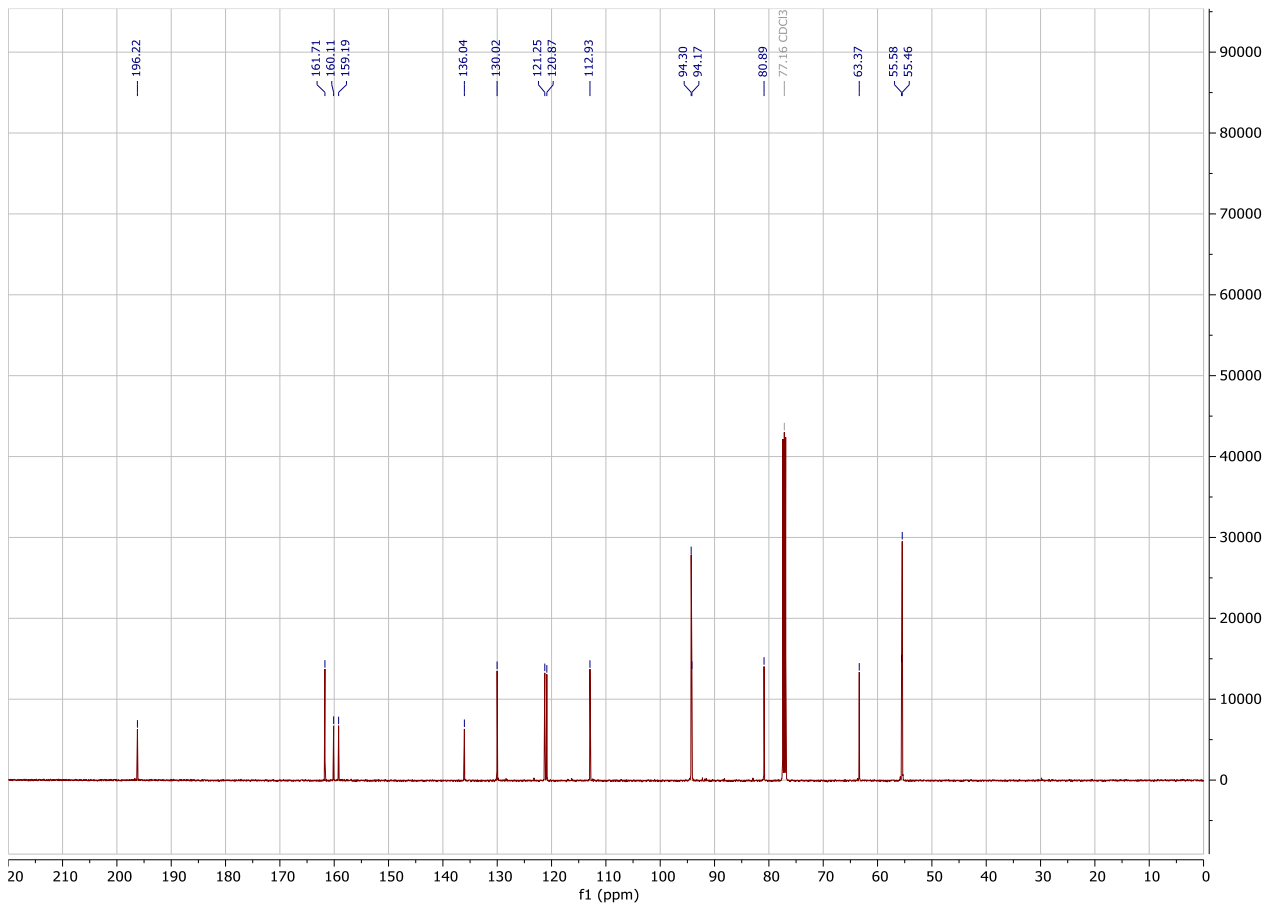
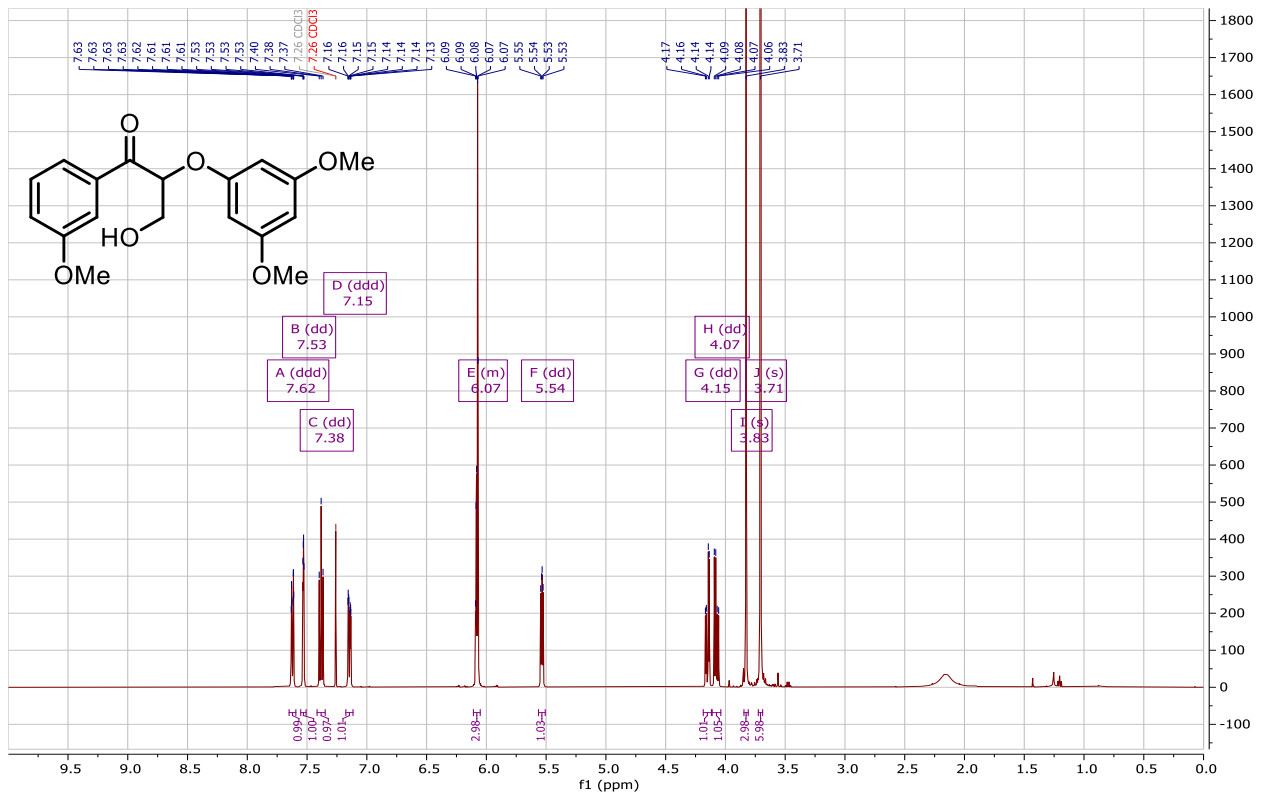


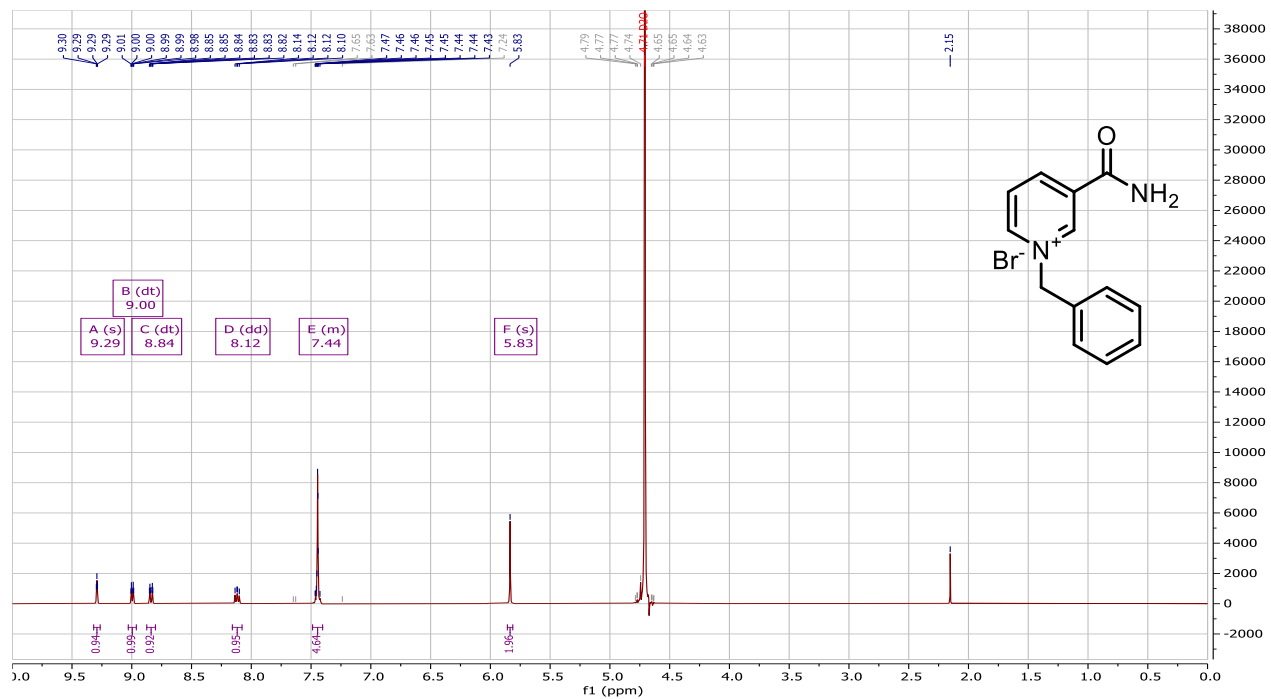


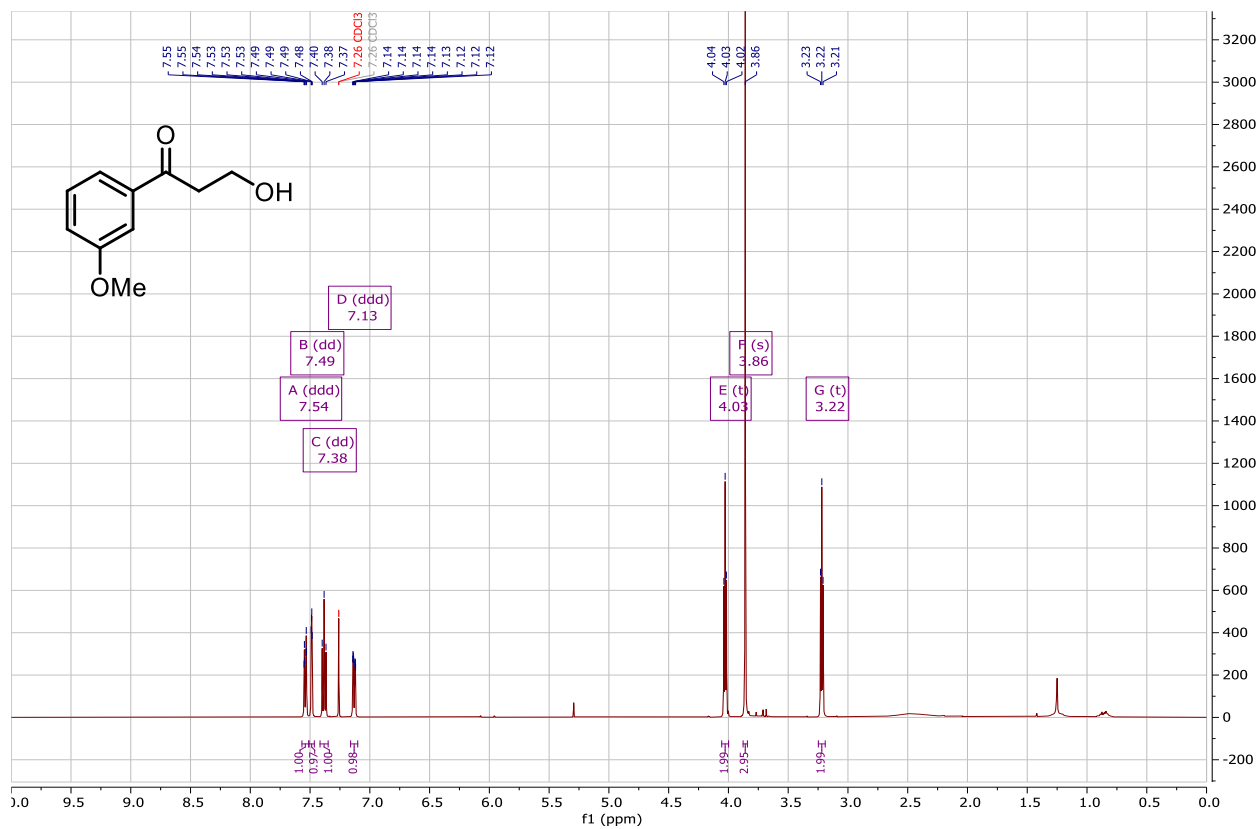
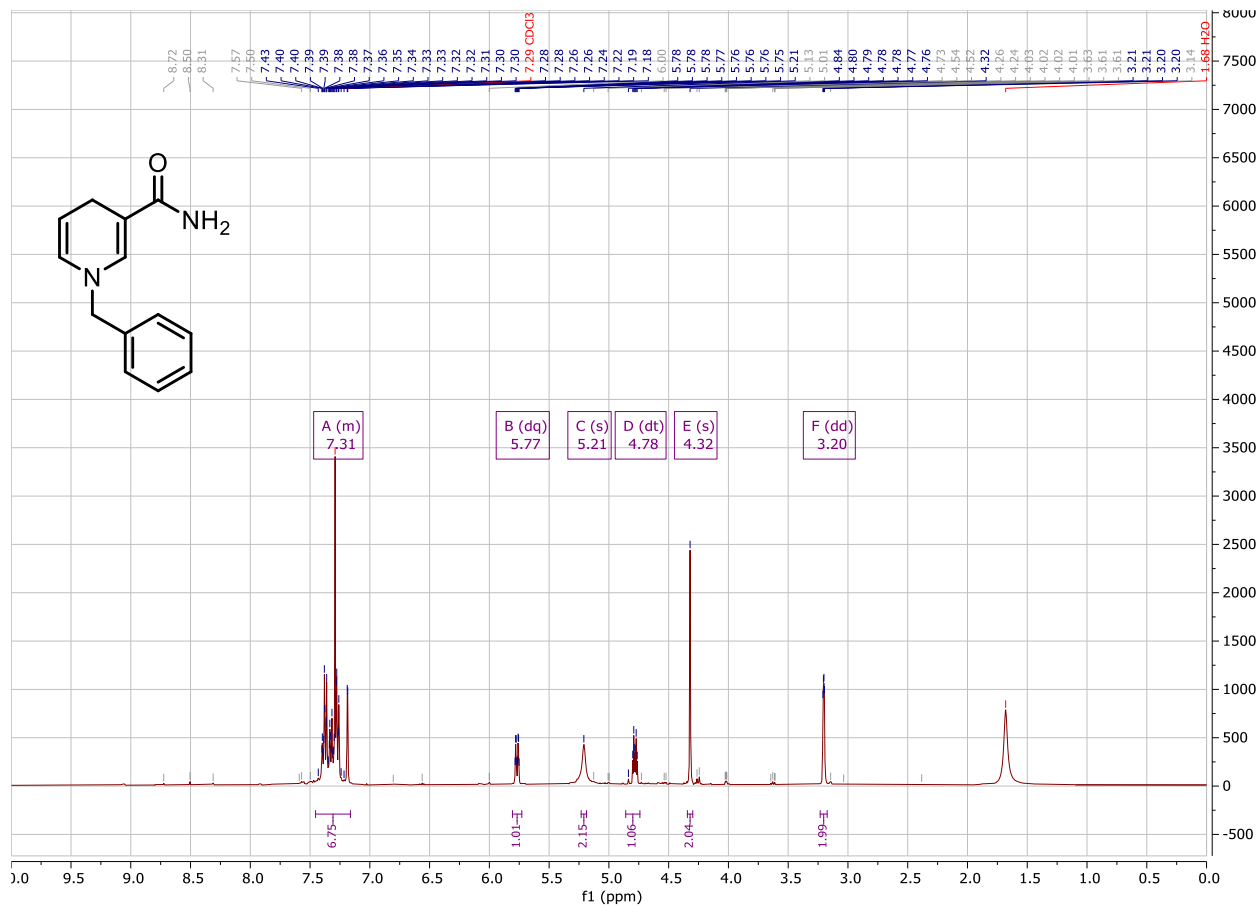


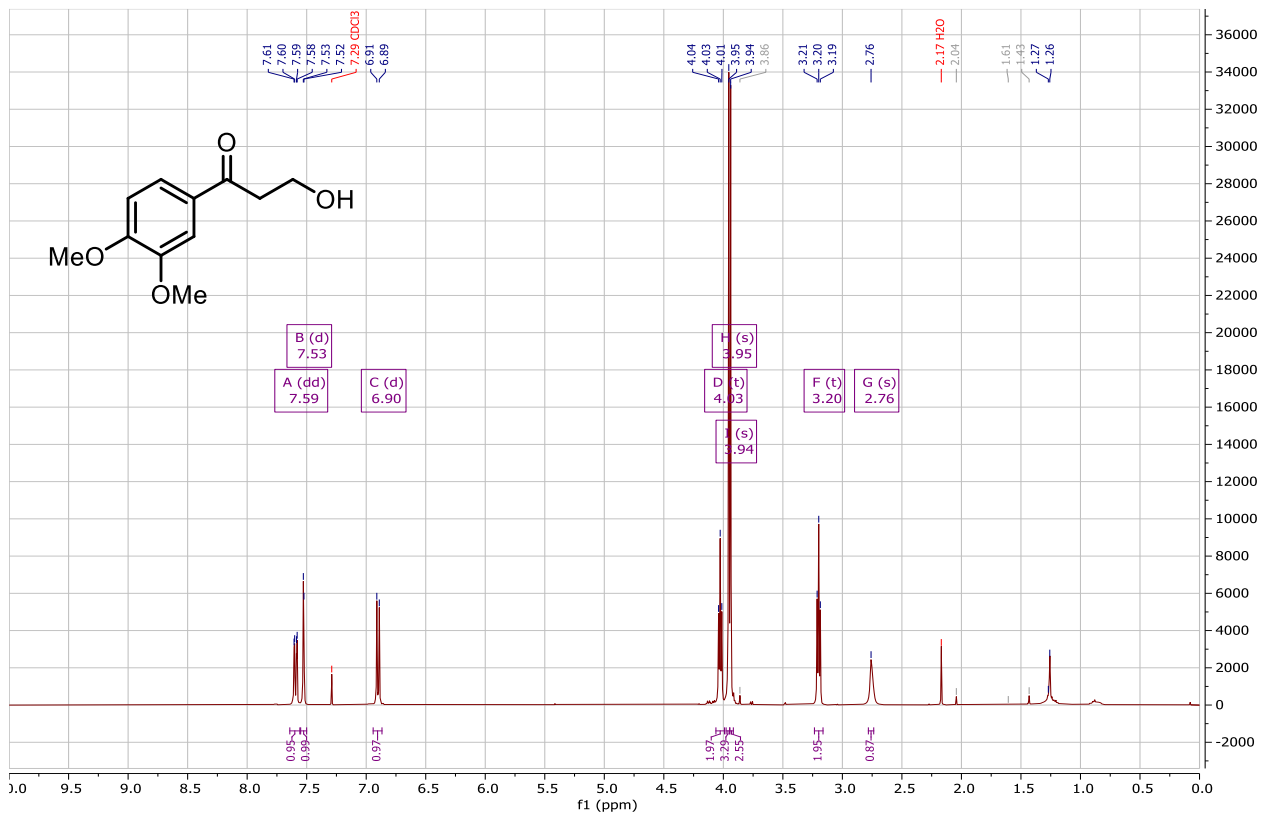
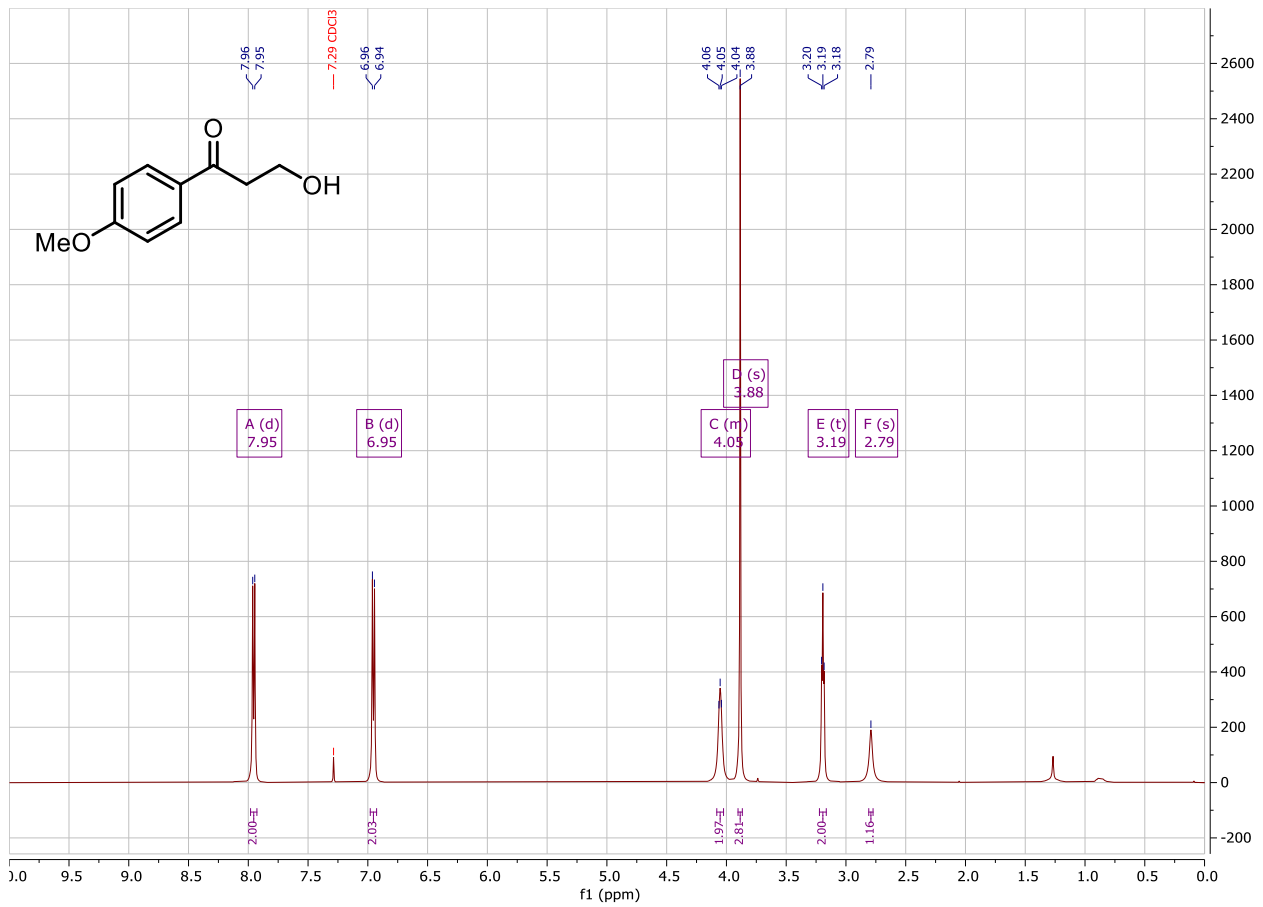


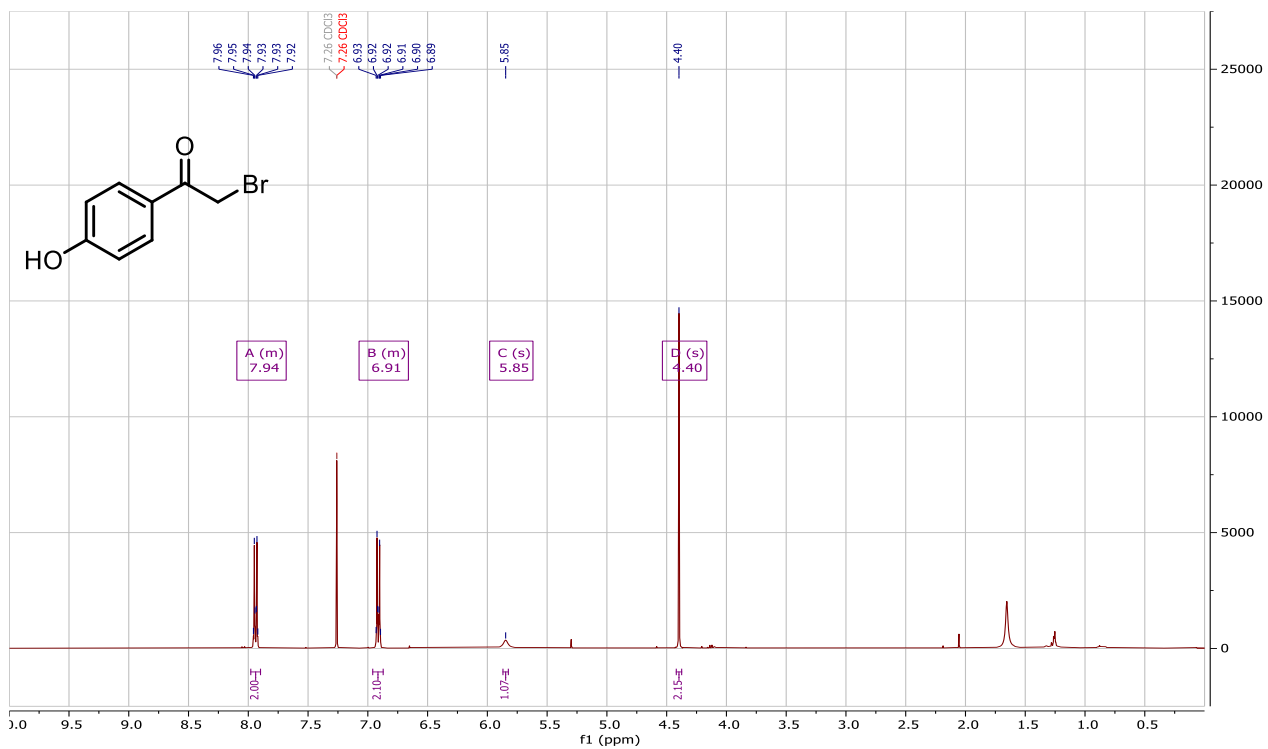
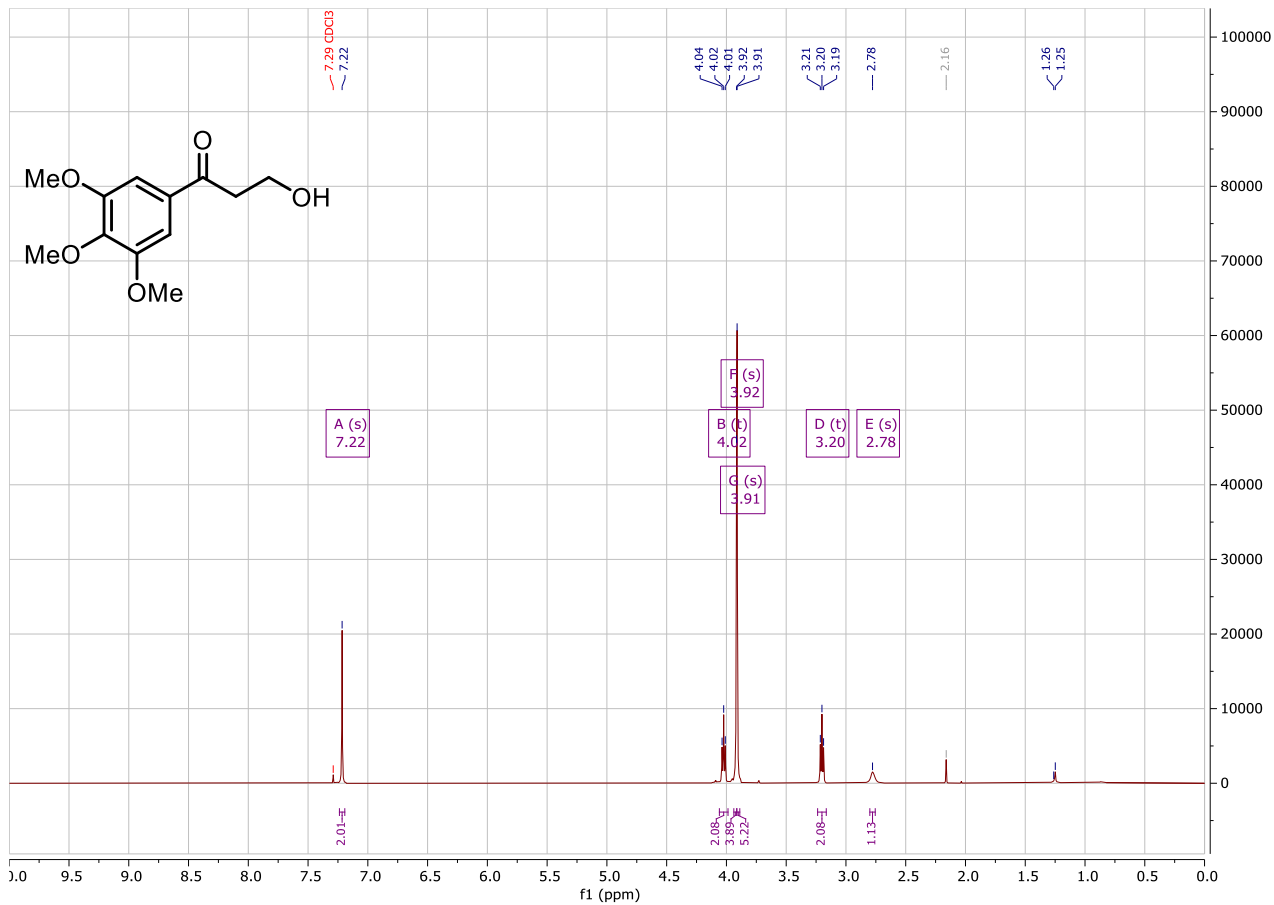


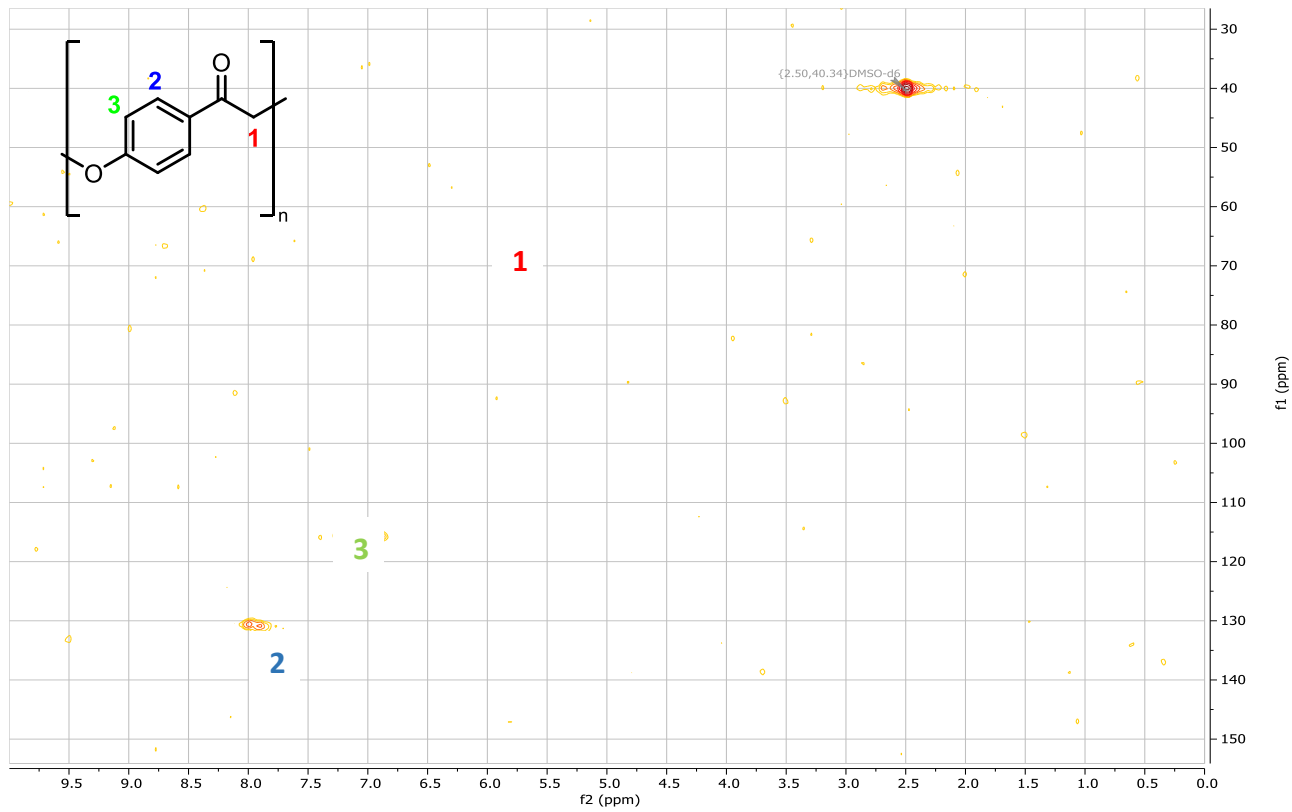












A5.8 References

1. Minozzi, C.; Caron, A.; Grenier-Petel, J.-C.; Santandrea, J.; Collins, S. K., *Angew. Chem., Int. Ed.* **2018**, *57* (19), 5477-5481.
2. Sosoe, J.; Cruché, C.; Morin, É.; Collins, S. K., *Can. J. Chem.* **2020**, *98* (9), 461-465.
3. Caron, A.; Morin, É.; Collins, S. K., *ACS Catal.* **2019**, *9* (10), 9458-9464.
4. Cruché, C.; Neiderer, W.; Collins, S. K., *ACS Catal.* **2021**, *11* (14), 8829-8836.
5. Zheng, L.; Jiang, Q.; Bao, H.; Zhou, B.; Luo, S.-P.; Jin, H.; Wu, H.; Liu, Y., *Org. Lett.* **2020**, *22* (22), 8888-8893.
6. Zuleta, E. C.; Bozell, J. J., *Tetrahedron* **2021**, *100*, 132475.
7. Guo, T.; Liu, T.; He, J.; Zhang, Y., *European J. Org. Chem.* **2022**, *2022* (2), e202101152.
8. Biannic, B.; Bozell, J. J., *Org. Lett.* **2013**, *15* (11), 2730-2733.
9. Arias, L.; Vara, Y.; Cossío, F. P., *J. Org. Chem.* **2012**, *77* (1), 266-275.
10. Lee, J. H.; Kim, M.; Kim, I., *J. Org. Chem.* **2014**, *79* (13), 6153-6163.
11. Hofmann, L. E.; Hofmann, D.; Prusko, L.; Altmann, L.-M.; Heinrich, M. R., *Adv. Synth. Catal.* **2020**, *362* (7), 1485-1489.
12. Dias, K. d. A.; Pereira Junior, M. V. P.; Andrade, L. H., *Green Chem.* **2021**, *23* (6), 2308-2316.
13. Tan, Z.; Han, Y.; Fu, Y.; Zhang, X.; Xu, M.; Na, Q.; Zhuang, W.; Qu, X.; Ying, H.; Zhu, C., *Adv. Synth. Catal.* **2022**, *364* (1), 103-113.
14. Bosque, I.; Magallanes, G.; Rigoulet, M.; Kärkäs, M. D.; Stephenson, C. R. J., *ACS Cent. Sci.* **2017**, *3* (6), 621-628.
15. Yun, J.-J.; Liu, X.-Y.; Deng, W.; Chu, X.-Q.; Shen, Z.-L.; Loh, T.-P., *J. Org. Chem.* **2018**, *83* (18), 10898-10907.
16. Damodar, K.; Shin, S.; Jeon, S. H.; Lee, J. T., *Tetrahedron Lett.* **2021**, *85*, 153482.

Annexe 6 – Supporting information of Chapter 7

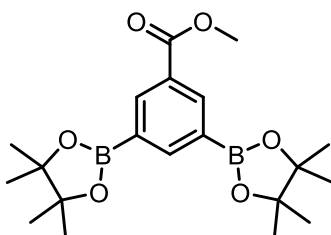
A6.1 General

All reactions that were carried out under anhydrous conditions were performed under an inert argon or nitrogen atmosphere in glassware that had previously been dried overnight at 120 °C or had been flame dried and cooled under a stream of argon or nitrogen. All chemical products were obtained from Sigma-Aldrich Chemical Company, Oakwood Chemical or Alfa Aesar and were reagent quality. Technical solvents were obtained from VWR International Co. Anhydrous solvents (CH₂Cl₂, Et₂O, THF, DMF, toluene, and n-hexane) were dried and deoxygenated using a GlassContour system (Irvine, CA). Isolated yields reflect the mass obtained following flash column silica gel chromatography. Organic compounds were purified using silica gel obtained from Silicycle Chemical division (40-63 nm; 230-240 mesh). Analytical thin-layer chromatography (TLC) was performed on glass-backed silica gel 60 coated with a fluorescence indicator (Silicycle Chemical division, 0.25 mm, F254.). Visualization of TLC plate was performed by UV (254 nm), KMnO₄ or p-anisaldehyde stains. All mixed solvent eluents are reported as v/v solutions. Concentration refers to removal of volatiles at low pressure on a rotary evaporator. All reported compounds were homogeneous by thin layer chromatography (TLC) and by ¹H NMR. NMR spectra were taken in deuterated CDCl₃ using Bruker AV-400 and AV-500 instruments unless otherwise noted. Signals due to the solvent served as the internal standard (CHCl₃: δ 7.27 for ¹H, δ 77.0 for ¹³C). The acquisition parameters are shown on all spectra. The ¹H NMR chemical shifts and coupling constants were determined assuming first-order behavior. Multiplicity is indicated by one or more of the following: s (singlet), d (doublet), t (triplet), q (quartet), m (multiplet), br (broad); the list of couplings constants (J) corresponds to the order of the multiplicity assignment. High resolution mass spectroscopy (HRMS) was done by the Centre régional de spectrométrie de masse at the Département de Chimie, Université de Montréal from an Agilent LC-MSD TOF system using ESI mode of ionization unless otherwise noted. X-ray structures were obtained from a shock-cooled single crystal at 150 K on a Bruker Venture Metaljet k-geometry diffractometer with

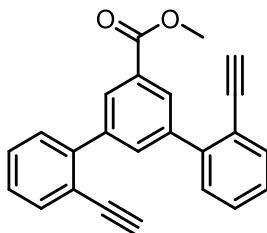
a Metal Jet using a Helios MX Mirror Optics as monochromator and a Bruker CMOS Photon III detector. The diffractometer was equipped with an Oxford Cryostream 700 low temperature device and used $\text{GaK}\alpha$ radiation ($\lambda = 1.34139 \text{ \AA}$). Computational studies were done with a commercial computer equipped with 24 processor and 32 GB of RAM.

A6.2 Synthesis

Multi-Step Synthesis:

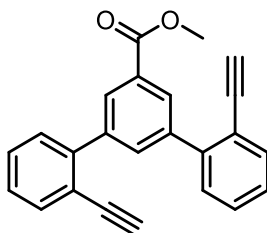


Methyl 3,5-bis(4,4,5,5-tetramethyl-1,3,2-dioxaborolan-2-yl)benzoate: In an open sealed tube was added methyl 3,5-dibromobenzoate (1.0 g, 3.4 mmol, 1 eq.), bis(pinacolato)diboron (1.99 g, 7.82 mmol, 2.3 eq.), and KOAc (2.0 g, 20.4 mmol, 6 eq.). Dry 1,4-dioxane (15 mL, [227 mM]) was added, and the mixture was purged with N_2 for 10 min. Under N_2 atmosphere, $\text{Pd}(\text{dppf})\text{Cl}_2 \cdot \text{CH}_2\text{Cl}_2$ (124 mg, 0.170 mmol, 0.05 eq.) was added. The reaction vial was sealed with a Teflon cap and the mixture was then heated to $90 \text{ }^\circ\text{C}$ for 16 h. The reaction mixture was cooled to room temperature, filtered through a thin pad of Celite (eluting with 50 mL EtOAc), and concentrated. Purification by column chromatography (4 to 12% AcOEt in Hexanes) afforded the desired product as a white solid (1.21 g, 92%). $^1\text{H NMR}$ (500 MHz, CDCl_3): δ 8.55 (d, $J = 1.3 \text{ Hz}$, 2H), 8.45 – 8.41 (m, 1H), 3.91 (s, 3H), 1.35 (s, 24H); $^{13}\text{C NMR}$ (101 MHz, CDCl_3): δ 167.3, 145.6, 138.7, 129.1, 84.2, 77.4, 52.1, 25.0; **HRMS (ESI):** m/z calculated for $\text{C}_{20}\text{H}_{30}[^{11}\text{B}]_2\text{O}_6$ $[\text{M}+\text{H}]^+$, 389.2301; found: 389.2304.

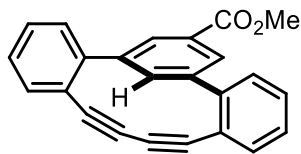


Methyl 2,2''-diethynyl-[1,1':3,1''-terphenyl]-5'-carboxylate: In a sealed tube vessel was added methyl 3,5-bis(4,4,5,5-tetramethyl-1,3,2-dioxaborolan-2-yl)benzoate (500 mg, 1.3 mmol, 1 eq.) and tripotassium phosphate (1.78 g, 7.7 mmol, 6 eq.). Toluene (26 mL [47 mM]) and H₂O (2.6 mL [47 mM]) were added, and the mixture was purged with N₂ for 10 min. Under N₂ atmosphere was added (2-bromophenylethynyl)trimethylsilane (631 μL, 3.0 mmol, 2.3 eq.), followed by SPhos (69.3 mg, 0.17 mmol, 0.13 eq.) and palladium acetate (18.8 mg, 0.084 mmol, 0.065 eq.). The vessel was sealed with a Teflon cap and the reaction mixture was then heated to 90 °C for 5 h. The reaction mixture was cooled to room temperature, filtered through a thin pad of Celite (eluting with 50 mL EtOAc), and concentrated. The crude mixture was diluted in AcOEt, washed with 10 mL of a saturated solution of K₂CO₃ and saturated brine, dried over Na₂SO₄, and concentrated *in vacuo*. The resulting solid was diluted in 5 mL of THF, and TBAF (6 mL, 1M in THF, 12 eq.) was added. The solution was stirred for 5 h. Then, 20 mL of water were added, and the mixture was extracted with 3 x 10 mL of AcOEt. The combined organics were dried with MgSO₄ and then concentrated under reduced pressure. Purification by column chromatography (10% AcOEt in Hexanes) afforded the desired product as a brown solid (308 mg, 71 %). **¹H NMR (400 MHz, CDCl₃):** δ 8.31 (d, *J* = 1.8 Hz, 2H), 7.99 (dd, *J* = 1.8, 1.8 Hz, 1H), 7.68 – 7.61 (m, 2H), 7.50 – 7.40 (m, 4H), 7.40 – 7.30 (m, 2H), 3.95 (s, 3H), 3.09 (s, 2H); **¹³C NMR (101 MHz, CDCl₃):** δ 167.1, 143.4, 140.4, 134.7, 134.1, 130.0, 129.7, 129.7, 129.3, 127.7, 120.7, 83.0, 80.9, 52.4; **HRMS (ESI):** *m/z* calculated for C₂₄H₁₆O₂ [M+H]⁺, 337.1223; found: 337.1210.

Synthesis of 3,5-TPDY : One-Pot Synthesis:

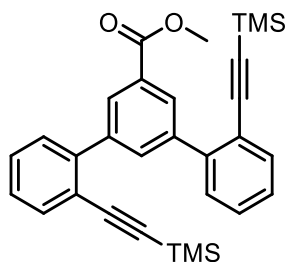


Methyl 2,2''-diethynyl-[1,1':3',1''-terphenyl]-5'-carboxylate : In a sealed tube vessel was added XPhos-Pd G3 (8.46 mg, 10 μ mol, 0.02 eq.), XPhos (9.53 mg, 20 μ mol, 0.04 eq.), tetrahydroxydiboron (269 mg, 3 mmol, 6 eq.), and KOAc (294 mg, 3 mmol, 6 eq.). The vessel was sealed and the atmosphere was flushed with N₂. Degassed EtOH (5 mL, [0.1M]) was added via syringe followed by the addition of the dibromoarene (147mg, 0.5 mmol, 1 eq.). The reaction mixture was then heated to 80 °C for 1.5 h. Then a needle outlet attached to a manifold under argon was inserted into the septum and degassed aqueous K₂CO₃ (6 eq., 1.8M, 1.67 mL, 3 mmol) and (2-bromophenylethynyl)trimethylsilane (257 mg, 1 mmol, 2 eq.) were added via syringe. The manifold needle was removed, and the reaction mixture was again heated to 80 °C for 15 h. The reaction mixture was cooled to room temperature, filtered through a thin pad of Celite (eluting with 50 mL EtOAc), and concentrated. The crude solid diluted with 20 mL of water, and the mixture was extracted with EtOAc (3 \times 10 mL), and the combined organics were dried with MgSO₄ and then concentrated under reduced pressure. The resulting solid was diluted in 5 mL of THF, and TBAF (6 mL, 1M in THF, 12 eq.) was added. The solution was stirred for 5 h. Then, 20 mL of water was added, and the mixture was extracted with 3 \times 10 mL of AcOEt. The combined organics were dried with MgSO₄ and then concentrated under reduced pressure. Purification by column chromatography (10% AcOEt in Hexanes) afforded the desired product as a brown solid (132 mg, 55%).



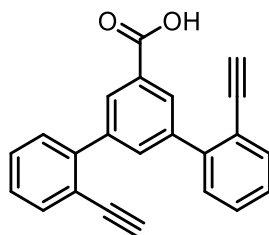
3,5-TPDY: To a solution of copper acetate (432 mg, 2.38 mmol, 4 eq.) in Et₂O:Pyridine 1:1 [3 mM] was slowly added over a period of 3 h a solution of methyl 2,2''-diethynyl-[1,1':3',1''-terphenyl]-5'-carboxylate (200 mg, 0.60 mmol, 1 eq.) in 20 mL of Et₂O:Pyridine 1:3. The solution was then stirred for an additional 2 h or until full consumption of the starting material observed by TLC. The solvent was removed, and the solution was diluted in CH₂Cl₂. The organic phase was then washed with 1M HCl twice, a saturated solution of NH₄OH four times and saturated brine. The organic phase was then dried over Na₂SO₄, and concentrated *in vacuo*, to give the pure product as an off-white solid (190 mg, 96%). Alternatively, the product can be purified by flash column chromatography (0→1% AcOEt in Hexanes). **¹H NMR (400 MHz, CDCl₃):** δ 8.55 (dd, *J* = 1.8, 1.8 Hz, 1H), 8.02 (d, *J* = 1.8 Hz, 2H), 7.62 (dd, *J* = 7.8, 1.3 Hz, 2H), 7.51 – 7.43 (m, 2H), 7.40 – 7.31 (m, 2H), 7.31 – 7.26 (m, 2H), 3.94 (s, 3H); **¹³C NMR (101 MHz, CDCl₃):** δ 166.9, 147.9, 142.1, 140.4, 131.5, 130.5, 130.1, 129.9, 128.1, 127.7, 121.9, 107.6, 87.0, 52.4; **HRMS (ESI):** *m/z* calculated for C₂₄H₁₄O₂ [M+H]⁺, 335.1067; found: 335.1069.

Synthesis of 3,5-TPDY-PEG-NH₃Cl

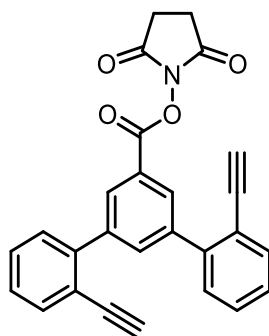


Methyl 2,2''-bis((trimethylsilyl)ethynyl)-[1,1':3',1''-terphenyl]-5'-carboxylate: In a sealed tube was added methyl 3,5-bis(4,4,5,5-tetramethyl-1,3,2-dioxaborolan-2-yl)benzoate (500 mg, 1.3 mmol, 1 eq.) and tripotassium phosphate (1.78 g, 7.7 mmol, 6 eq.). Toluene (26 mL [47 mM]) and H₂O (2.6 mL [47 mM]) were added, and the mixture was purged with N₂ for 10 min. Under N₂ atmosphere was added (2-bromophenylethynyl)trimethylsilane (631 μL, 3.0 mmol, 2.3 eq.),

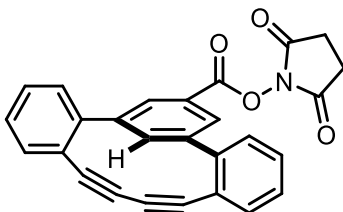
followed by SPhos (69.3 mg, 0.17 mmol, 0.13 eq.) and palladium acetate (18.8 mg, 0.084 mmol, 0.065 eq.). The vessel was sealed with a Teflon cap and the reaction mixture was then heated to 90 °C for 5 h. The reaction mixture was cooled to room temperature, filtered through a thin pad of Celite (eluting with 50 mL EtOAc), and concentrated. The crude mixture was diluted in AcOEt, washed with 10 mL of a saturated solution of K₂CO₃ and saturated brine, dried over Na₂SO₄, and concentrated *in vacuo*. Purification by flash column chromatography (0→2% AcOEt in Hexanes) afforded the pure product as a orange sticky solid (450 mg, 73 %). **¹H NMR (400 MHz, CDCl₃):** δ 8.35 (d, *J* = 1.8 Hz, 2H), 8.11 (dd, *J* = 1.8, 1.8 Hz, 1H), 7.60 (dd, *J* = 7.7, 1.4 Hz, 2H), 7.47 (dd, *J* = 7.8, 1.4 Hz, 2H), 7.40 (ddd, *J* = 7.6, 7.6, 1.4 Hz, 2H), 7.31 (ddd, *J* = 7.5, 7.6 1.4, Hz, 2H), 3.94 (s, 3H), 0.04 (s, 18H); **¹³C NMR (101 MHz, CDCl₃):** δ 167.2, 143.0, 140.2, 135.0, 133.7, 129.7, 129.7, 129.5, 129.0, 127.5, 121.6, 104.4, 98.2, 52.2, -0.3; **HRMS (ESI):** m/z calculated for C₃₀H₃₂O₂Si₂ [M+H]⁺, 481.2014; found: 481.2007.



2,2''-Diethynyl-[1,1':3',1''-terphenyl]-5'-carboxylic acid : 2,2''-Diethynyl-[1,1':3',1''-terphenyl]-5'-carboxylate (140 mg, 0.42 mmol, 1 eq.) was dissolved in THF:H₂O 12:1 (4.4 mL, [96 mM]). Sodium methoxide (25% wt in MeOH, 2 mL, 18 eq.) was slowly added and the mixture was stirred at room temperature overnight. The solution was quenched with 1M HCl, and extracted three times with CH₂Cl₂. The organic phases were combined, washed with saturated brine, dried over Na₂SO₄, and concentrated *in vacuo*. Purification by flash column chromatography (20→60% AcOEt in Hexanes) afforded the pure product as a orange powder (121 mg, 90%). **NMR (400 MHz, CDCl₃):** δ 8.43 – 8.38 (m, 2H), 8.07 – 8.02 (m, 1H), 7.69 – 7.62 (m, 2H), 7.50 – 7.42 (m, 4H), 7.41 – 7.31 (m, 2H), 3.11 (s, 2H); **¹³C NMR (101 MHz, CDCl₃):** δ 143.2, 140.5, 135.5, 134.1, 130.3, 129.7, 129.3, 127.7, 120.7, 82.9, 81.0; **HRMS (ESI):** m/z calculated for C₂₃H₁₄O₂ [M+H]⁺, 323.1067; found: 323.1061.

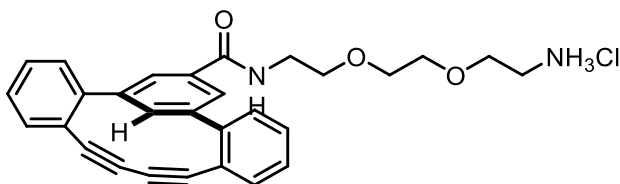


2,5-Dioxopyrrolidin-1-yl 2,2''-diethynyl-[1,1':3',1''-terphenyl]-5'-carboxylate: 2,2''-Diethynyl-[1,1':3',1''-terphenyl]-5'-carboxylic acid (150 mg, 0.47 mmol, 1 eq.) and N-hydroxysuccinimide (64 mg, 0.56 mmol, 1.2 eq.) were dissolved in dry CH₂Cl₂ (7.5 mL, [62 mM]). N-(3-Dimethylaminopropyl)-N'-ethylcarbodiimide hydrochloride (107 mg, 0.56 mmol, 1.2 eq.) was added and the mixture was stirred at room temperature overnight. The mixture was then diluted with 30 mL of CH₂Cl₂ and washed twice with 10 mL of water. The organic phase was dried over MgSO₄ and concentrated *in vacuo*. Purification by flash column chromatography (20→40% AcOEt in Hexanes) afforded the pure product as a off-white powder (142 mg, 73 %). **¹H NMR (400 MHz, CDCl₃):** δ 8.41 (d, *J* = 1.7 Hz, 2H), 8.09 (dd, *J* = 1.7, 1.7 Hz, 1H), 7.68 – 7.61 (m, 2H), 7.49 – 7.41 (m, 4H), 7.36 (ddd, *J* = 7.6, 5.2, 3.7 Hz, 2H), 3.13 (s, 2H), 2.91 (br, 4H); **¹³C NMR (101 MHz, CDCl₃):** δ 169.3, 162.0, 142.7, 140.9, 136.7, 134.1, 130.5, 129.6, 129.4, 128.0, 125.0, 120.8, 82.7, 81.3, 25.8; **HRMS (ESI):** *m/z* calculated for C₂₇H₁₇NO₄ [M+NH₄]⁺, 437.1496; found: 437.1507.



3,5-TPDY-OSucc: To a solution of copper acetate (482 mg, 2.65 mmol, 5.2 eq.) in Et₂O:Pyridine 1:1 [3 mM] was slowly added over a period of 3 h a solution of 2,5-dioxopyrrolidin-1-yl 2,2''-diethynyl-[1,1':3',1''-terphenyl]-5'-carboxylate (214 mg, 0.51 mmol, 1 eq.) in 20 mL of Et₂O:Pyridine 1:3. The solution was then stirred for an additional 2 h or until full consumption of the starting material observed by TLC. The solvent was removed, and the solution was diluted in

CH₂Cl₂. The organic phase was then washed with 1M HCl twice and saturated brine. The organic phase was then dried over Na₂SO₄ and concentrated *in vacuo*. Purification by flash column chromatography (20→60% AcOEt in Hexanes) afforded the pure product as an off-white powder (170 mg, 80 %). **¹H NMR (400 MHz, CDCl₃):** δ 8.63 (dd, *J* = 1.7, 1.7 Hz, 1H), 8.10 (d, *J* = 1.8 Hz, 2H), 7.62 (dd, *J* = 7.4, 1.1 Hz, 2H), 7.52 – 7.44 (m, 2H), 7.37 (dd, *J* = 7.6, 1.3 Hz, 2H), 7.31 – 7.20 (m, 2H), 2.92 (s, 4H); **¹³C NMR (101 MHz, CDCl₃):** δ 169.3, 161.8, 147.2, 144.0, 141.0, 132.2, 130.4, 130.2, 128.4, 127.7, 124.9, 121.9, 107.2, 87.0, 25.8; **HRMS (ESI):** *m/z* calculated for C₂₇H₁₅NO₄ [M+NH₄]⁺, 435.1339; found: 435.1334.



3,5-TPDY-PEG-NH₃Cl: 3,5-TPDY-OSucc (60 mg, 0.144 mmol, 1 eq.) and tert-butyl (2-(2-(2-aminoethoxy)ethoxy)ethyl)carbamate (65 mg, 0.262 mmol, 1.8 eq.) were dissolved in CH₂Cl₂ (2 mL, [72 mM]) and the reaction was stirred at room temperature for 5 h. The solvent was then concentrated *in vacuo* and purification by flash column chromatography (50→100% AcOEt in Hexanes) afforded 3,5-TPDY-PEG-NHBoc. The product was then directly dissolved in 1 mL of HCl 4M in dioxane. The reaction was stirred until disappearance of the starting material and then 7 mL of hexanes were added. The precipitate was filtered and rinsed with hexanes, affording the desired product as an off-white solid (22 mg, 34 %). **¹H NMR (400 MHz, DMSO-d₆):** δ 8.82 (dd, *J* = 5.6, 5.6 Hz, 1H), 8.40 (dd, *J* = 1.7, 1.7 Hz, 1H), 7.97 (br, 3H), 7.84 (d, *J* = 1.8 Hz, 2H), 7.76 (dd, *J* = 7.8, 1.3 Hz, 2H), 7.66 – 7.58 (m, 2H), 7.47 (ddd, *J* = 7.6, 7.6, 1.3 Hz, 2H), 7.39 (dd, *J* = 7.7, 1.4 Hz, 2H), 3.65 – 3.52 (m, 9H), 3.50 – 3.40 (m, 2H), 2.99 – 2.87 (m, 2H); **¹³C NMR (101 MHz, DMSO-d₆):** δ 165.8, 147.6, 139.5, 139.3, 134.1, 130.8, 130.6, 129.2, 128.4, 127.5, 120.4, 107.9, 86.2, 69.7, 69.5, 68.9, 66.6.

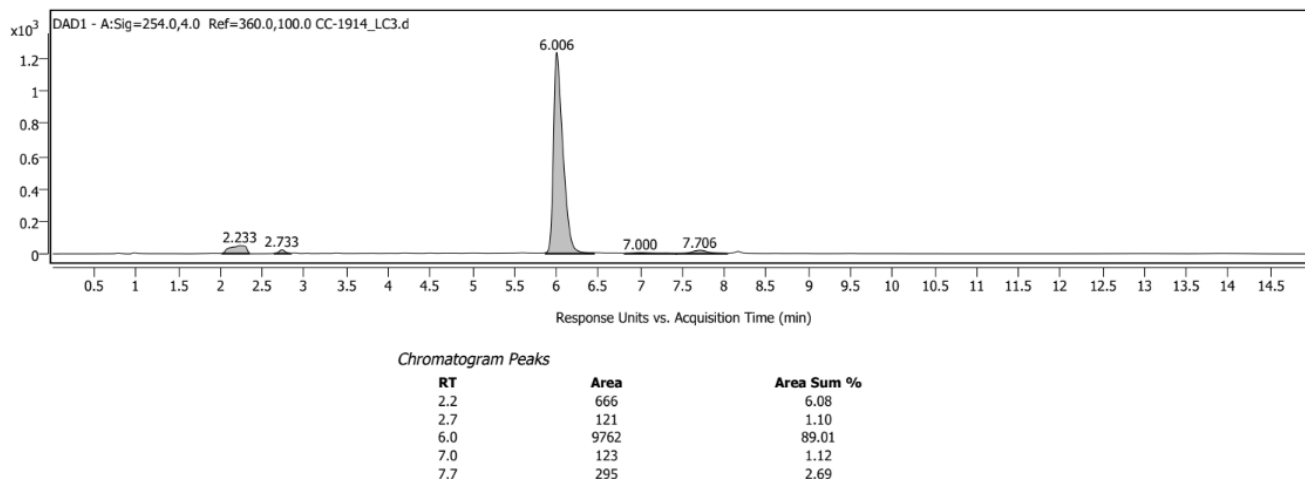
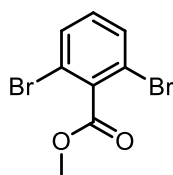
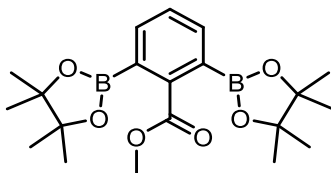


Figure A6 - 1 HPLC chromatogram of **3,5-TPDY-PEG-NH₃Cl**.

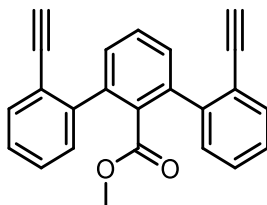
Synthesis of 2,6-TPDY



Methyl 2,6-dibromobenzoate: To a solution of 2,6-dibromobenzoic acid (1.0 g, 3.57 mmol, 1 eq.) in dry DMF (4 mL, [900 mM]) was added potassium carbonate (988 mg, 7.15 mmol, 42 eq.) and iodomethane (890 μ L, 14.3 mmol, 4 eq.) and the reaction mixture was stirred at room temperature for 16 h. The mixture was then diluted in EtOAc (30 mL) and washed 3 times with 10 mL of a 8:2 H₂O:LiCl sat. solution. The organic phase was then washed with brine, dried over Na₂SO₄, and concentrated *in vacuo* to afford the pure product as a brown solid (901 mg, 86 %). Spectral data were in accordance with previous reports.¹ ¹H NMR (400 MHz, CDCl₃): δ 7.53 (d, *J* = 8.1 Hz, 2H), 7.14 (dd, *J* = 8.1, 8.1 Hz, 1H), 3.98 (s, 3H).¹

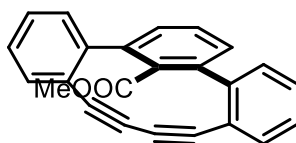


Methyl 2,6-bis(4,4,5,5-tetramethyl-1,3,2-dioxaborolan-2-yl)benzoate: In a sealed tube was added methyl 2,6-dibromobenzoate (500 mg, 1.7 mmol, 1 eq.), bis(pinacolato)diboron (1.30 g, 5.10 mmol, 3 eq.), and KOAc (1.0 g, 10.2 mmol, 6 eq.). Dry 1,4-dioxane (8 mL, [204 mM]) was added and the mixture was purged with N₂ for 10 min. Under N₂ atmosphere, Pd(dppf)Cl₂ · CH₂Cl₂ (91.6 mg, 0.125 mmol, 0.07 eq.) was added. The reaction vessel was then sealed with a Teflon cap and the mixture was then heated to 90 °C for 16 h. The reaction mixture was cooled to room temperature, filtered through a thin pad of Celite (eluting with 50 mL EtOAc), and concentrated. Purification by column chromatography (4 to 12% AcOEt in Hexanes) afforded the desired product as a white solid (360 mg, 55 %). ¹H NMR (400 MHz, CDCl₃): δ 7.69 (d, *J* = 7.4 Hz, 2H), 7.41 (dd, *J* = 7.4, 7.4 Hz, 1H), 3.88 (s, 3H), 1.34 (s, 24H); ¹³C NMR (101 MHz, CDCl₃): δ 170.7, 141.8, 135.5, 129.1, 84.1, 52.1, 24.9; HRMS (ESI): *m/z* calculated for C₂₀H₃₀[⁹B]₂O₆ [M+H]⁺, 387.2374; found: 387.2378.



Methyl 2,2''-diethynyl-[1,1':3',1''-terphenyl]-2'-carboxylate: In a sealed tube was added methyl 2,6-bis(4,4,5,5-tetramethyl-1,3,2-dioxaborolan-2-yl)benzoate (200 mg, 0.52 mmol, 1 eq.) and tripotassium phosphate (712 mg, 3.1 mmol, 6 eq.). Toluene (10 mL [47 mM]) and H₂O (1 mL [47 mM]) were added, and the mixture was purged with N₂ for 10 min. Under N₂ atmosphere was added (2-bromophenylethynyl)trimethylsilane (252 μL, 1.2 mmol, 2.3 eq.), followed by SPhos (27.7 mg, 0.068 mmol, 0.13 eq.) and palladium acetate (7.5 mg, 0.034 mmol, 0.065 eq.). The reaction vessel was sealed with a Teflon cap and the mixture was then heated to 90 °C for 5 h. The reaction mixture was cooled to room temperature, filtered through a thin pad of Celite

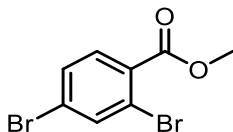
(eluting with 50 mL EtOAc), and concentrated. The crude mixture was diluted in AcOEt, washed with 10 mL of a saturated solution of K_2CO_3 and saturated brine, dried over Na_2SO_4 , and concentrated *in vacuo*. The mixture was then diluted in 2 mL of THF and 2 mL of MeOH, and cesium fluoride (1.27 g, 8.25 mmol, 16 eq.) was added. The reaction was stirred at room temperature for 4 hours. The mixture was diluted in AcOEt (30 mL) and washed two times with a saturated solution of NH_4Cl . The organic phase was washed with saturated brine, dried over Na_2SO_4 , and concentrated *in vacuo*. Purification by flash column chromatography (0→2% AcOEt in Hexanes) afforded the pure product as a yellowish powder (110 mg, 63%). **1H NMR (400 MHz, $CDCl_3$):** δ 7.61 (dd, $J = 7.5, 1.6$ Hz, 2H), 7.58 – 7.44 (m, 3H), 7.42 – 7.26 (m, 6H), 3.27 (s, 3H), 3.00 (s, 2H); **^{13}C NMR (101 MHz, $CDCl_3$):** δ 168.6, 143.9, 139.7, 133.1, 133.0, 130.1, 129.3, 128.8, 128.5, 127.4, 121.4, 82.4, 80.7, 51.6; **HRMS (ESI):** m/z calculated for $C_{24}H_{16}O_2$ $[M+H]^+$, 337.1223; found: 337.1225.



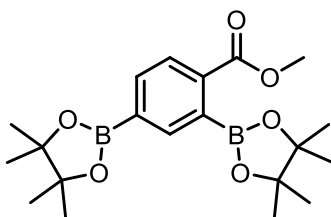
2,6-TPDY-Methyl ester: To a solution of copper acetate (189 mg, 1.04 mmol, 5 eq.) in Et_2O :Pyridine 1:1 [3 mM] was slowly added over a period of 3 h a solution of methyl 2,2''-diethynyl-[1,1':3',1''-terphenyl]-2'-carboxylate (70 mg, 0,20 mmol, 1 eq.) in 20 mL of Et_2O :Pyridine 1:3. The solution was then stirred for an additional 2 h. The solution was concentrated and diluted in CH_2Cl_2 . The organic phase was then washed with 1M HCl three times (or until the solution turned from blue to yellow) and saturated brine. The organic phase was then dried over Na_2SO_4 and concentrated *in vacuo*. Purification by flash column chromatography (0→1% AcOEt in Hexanes) afforded the desired product as a white powder that quickly turned to a dark oil (45.7 mg, 66 %). **1H NMR (400 MHz, $CDCl_3$):** δ 7.56 (dd, $J = 7.6, 7.6$ Hz, 1H), 7.50 (dd, $J = 7.7, 1.4$ Hz, 2H), 7.47 – 7.41 (m, 2H), 7.32 – 7.27 (m, 2H), 7.18 (dd, $J = 9.0, 7.2$ Hz, 4H), 3.37 (s, 3H); **^{13}C NMR (101 MHz, $CDCl_3$):** δ 165.8, 151.7, 144.0, 135.0, 131.9, 130.8, 129.5, 127.9, 127.3, 126.6, 123.0, 106.1, 85.9, 51.6; **HRMS (ESI):** m/z calculated for $C_{24}H_{14}O_2$ $[M+H]^+$, 335.1067; found:

335.1063. Note: The product quickly degrades in solid form but is stable for few days in diluted solution.

Synthesis of 2,4-TPDY

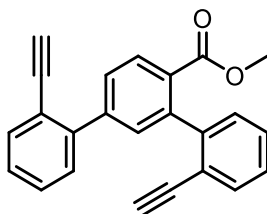


Methyl 2,4-dibromobenzoate: To a solution of 2,4-dibromobenzoic acid (1.0 g, 3.57 mmol, 1 eq.) in dry DMF (4 mL, [900 mM]) was added potassium carbonate (988 mg, 7.15 mmol, 42 eq.) and iodomethane (890 μ L, 14.3 mmol, 4 eq.), and the reaction mixture was stirred at room temperature for 16h. The mixture was then diluted in EtOAc (30 mL) and washed 3 times with 10 mL of a 8:2 H₂O:LiCl sat. solution. The organic phase was then washed with brine, dried over Na₂SO₄, and concentrated *in vacuo* to afford the pure product as a brown solid (930 mg, 89 %). Spectral data were in accordance with previous reports.² **¹H NMR (400 MHz, CDCl₃):** δ 7.85 (d, *J* = 1.9 Hz, 1H), 7.69 (d, *J* = 8.3 Hz, 1H), 7.51 (dd, *J* = 8.4, 1.9 Hz, 1H), 3.93 (s, 3H).



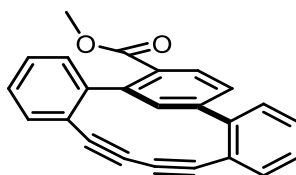
Methyl 2,4-bis(4,4,5,5-tetramethyl-1,3,2-dioxaborolan-2-yl)benzoate: In a sealed tube was added methyl 2,4-dibromobenzoate (400 mg, 1.36 mmol, 1 eq.), bis(Pinacolato)diboron (795 mg, 3.13 mmol, 2.3 eq.), and KOAc (800 mg, 8.16 mmol, 6 eq.). Dry 1,4-dioxane (6.7 mL, [204 mM]) was added and the mixture was purged with N₂ for 10 min. Under N₂ atmosphere, Pd(dppf)Cl₂ · CH₂Cl₂ (73.3 mg, 0.100 mmol, 0.07 eq.) was added. The vessel was then sealed with a Teflon cap and the reaction mixture was then heated to 90 °C for 16 h. The reaction mixture was cooled to room temperature, filtered through a thin pad of Celite (eluting with 50 mL EtOAc), and

concentrated. Purification by column chromatography (4 to 12% AcOEt in Hexanes) afforded the desired product as a white solid (440 mg, 83 %). **¹H NMR (400 MHz, CDCl₃):** δ 7.95 – 7.88 (m, 2H), 7.84 (dd, *J* = 7.8, 1.2 Hz, 1H), 3.91 (s, 3H), 1.42 (s, 12H), 1.34 (s, 12H); **¹³C NMR (101 MHz, CDCl₃):** δ 168.7, 138.5, 135.8, 135.5, 134.8, 128.7, 127.9, 84.2, 84.2, 52.5, 25.1, 25.0; **HRMS (ESI):** *m/z* calculated for C₂₀H₃₀[⁹B]₂O₆ [M+H]⁺, 387.2387; found: 387.2374.



Methyl 2,2''-diethynyl-[1,1':3',1''-terphenyl]-4'-carboxylate: In a sealed tube was added methyl 2,4-bis(4,4,5,5-tetramethyl-1,3,2-dioxaborolan-2-yl)benzoate (374 mg, 0.964 mmol, 1 eq.) and tripotassium phosphate (1.33 g, 5.78 mmol, 6 eq.). Toluene (20 mL [44 mM]) and H₂O (2 mL [44 mM]) were added, and the mixture was purged with N₂ for 10 min. Under N₂ atmosphere was added (2-bromophenylethynyl)trimethylsilane (511 μL, 2.40 mmol, 2.3 eq.), followed by SPhos (51.8 mg, 0.126 mmol, 0.13 eq.) and palladium acetate (14.1 mg, 0.063 mmol, 0.065 eq.). The vessel was then sealed with a Teflon cap and the reaction mixture was then heated to 90 °C for 5 h. The reaction mixture was cooled to room temperature, filtered through a thin pad of Celite (eluting with 50 mL EtOAc), and concentrated. The crude mixture was diluted in AcOEt, washed with 10 mL of a saturated solution of K₂CO₃ and saturated brine, dried over Na₂SO₄, and concentrated *in vacuo*. The mixture was then diluted in 2 mL of THF and 2 mL of MeOH, and cesium fluoride (1.17 g, 7.71 mmol, 8 eq.) was added. The reaction was stirred at room temperature for 16 hours. The mixture was diluted in AcOEt (30 mL) and washed two times with a saturated solution of NH₄Cl. The organic phase was washed with saturated brine, dried over Na₂SO₄, and concentrated *in vacuo*. Purification by flash column chromatography (0→2% AcOEt in Hexanes) afforded the pure product as an off-white powder (191 mg, 59 %). **¹H NMR (400 MHz, CDCl₃):** δ 8.05 (d, *J* = 8.1 Hz, 1H), 7.70 (dd, *J* = 8.1, 1.9 Hz, 1H), 7.63 (dd, *J* = 7.5, 1.2 Hz, 1H), 7.57 (dd, *J* = 8.4, 1.7 Hz, 2H), 7.45 – 7.37 (m, 3H), 7.37 – 7.29 (m, 3H), 3.68 (s, 3H), 3.09 (s, 1H), 2.94 (s,

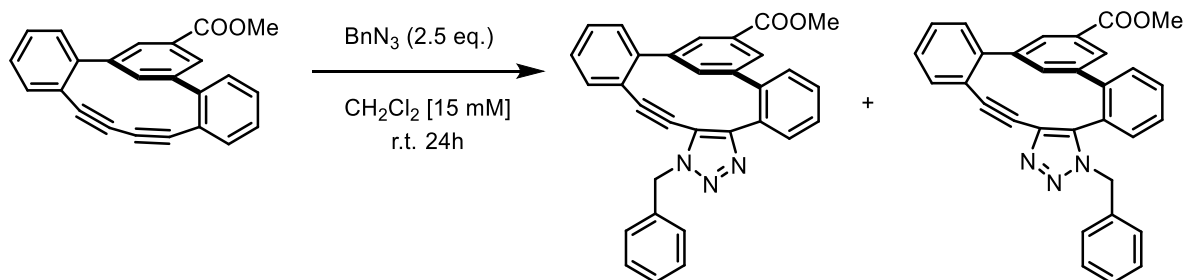
1H); ¹³C NMR (101 MHz, CDCl₃): δ 167.9, 144.9, 143.5, 143.1, 141.3, 134.1, 132.6, 132.4, 130.0, 129.6, 129.6, 129.2, 128.9, 128.8, 128.5, 127.8, 127.2, 121.3, 120.6, 82.9, 82.5, 80.9, 80.3, 52.2; HRMS (ESI): m/z calculated for C₂₄H₁₆O₂ [M+H]⁺, 337.1223; found: 337.1214.



2,4-TPDY-Methyl ester: To a solution of copper acetate (189 mg, 1.04 mmol, 5 eq.) in Et₂O:Pyridine 1:1 [3 mM] was slowly added over a period of 3 h a solution of methyl 2,2''-diethynyl-[1,1':3',1''-terphenyl]-4'-carboxylate (70 mg, 0,20 mmol, 1 eq.) in 20 mL of Et₂O:Pyridine 1:3. The solution was then stirred for an additional 2 h. The solution was concentrated, and diluted in CH₂Cl₂. The organic phase was then washed with 1M HCl three times (or until the solution turned from blue to yellow), and saturated brine. The organic phase was then dried over Na₂SO₄, and concentrated in vacuo. Purification by flash column chromatography (0→1% AcOEt in Hexanes) afforded the desired product as a white powder that quickly turned to a dark oil (48.6 mg, 70%). ¹H NMR (400 MHz, CDCl₃): δ 8.10 (d, J = 1.8 Hz, 1H), 7.83 (d, J = 8.0 Hz, 1H), 7.63 – 7.58 (m, 1H), 7.48 – 7.43 (m, 1H), 7.39 – 7.29 (m, 6H), 7.27 – 7.25 (m, 1H), 3.56 (s, 3H); ¹³C NMR (101 MHz, CDCl₃): δ 169.3, 148.1, 147.3, 143.0, 139.3, 139.3, 132.2, 130.6, 130.2, 130.0, 129.8, 129.0, 128.9, 128.2, 127.9, 127.5, 127.5, 122.3, 122.1, 108.1, 107.4, 88.2, 86.9, 52.1; HRMS (ESI): m/z calculated for C₂₄H₁₄O₂ [M+H]⁺, 335.1067; found: 335.1079. Note: The product quickly degrades in solid form but is stable for few days in diluted solution.

A6.3 Clicks reactions

General Procedure



To a solution of 3,5-TPDY (50 mg, 0.15 mmol, 1 eq.) in CH₂Cl₂ [15 mM] was added benzyl azide (50 mg, 0.37 mmol, 2.5 eq.) and the reaction was stirred at room temperature for 24 h. The solution was then concentrated in vacuo. Purification by flash column chromatography (1→2% AcOEt in Hexanes) afforded the desired regioisomers as off-white solids (66 mg, 94%, 7:3).

Kinetic Measurements

The second order rate constants were measured using ¹H NMR spectroscopy in CDCl₃ at 25 °C using 1,3,5-trimethoxybenzene as an internal standard. A solution of the diyne [20 mM] and 1,3,5-trimethoxybenzene [7mM] in 4 mL of CDCl₃ was prepared. In an NMR tube was added 0.5 mL of the solution. The tube was used to calibrate the NMR instrument and as a t=0 reference. Then, 0.25 mL (2.5 eq.) of a solution of benzylazide [8 mM] in CDCl₃ was added and the NMR tube was vigorously shaken and put into an NMR spectrometer immediately. Measurements were taken every 5 min until 50% conversion was achieved. The experiment was repeated three times. The rate constants were estimated using the equation:

$$k = \frac{1}{t(a-b)} \times \ln \frac{b(a-x)}{a(b-x)}$$

k is the rate constant in M⁻¹ × s⁻¹

t is the reaction time in seconds

a is the initial concentration of benzyl azide in mol/L

b is the initial concentration of the alkyne in mol/L

x is the sum of the concentrations of the regioisomer in mol/L

k is the slope of the graphic plot of $\frac{1}{(a-b)} \times \ln \frac{b(a-x)}{a(b-x)}$ versus the reaction time

3,5-TPDY

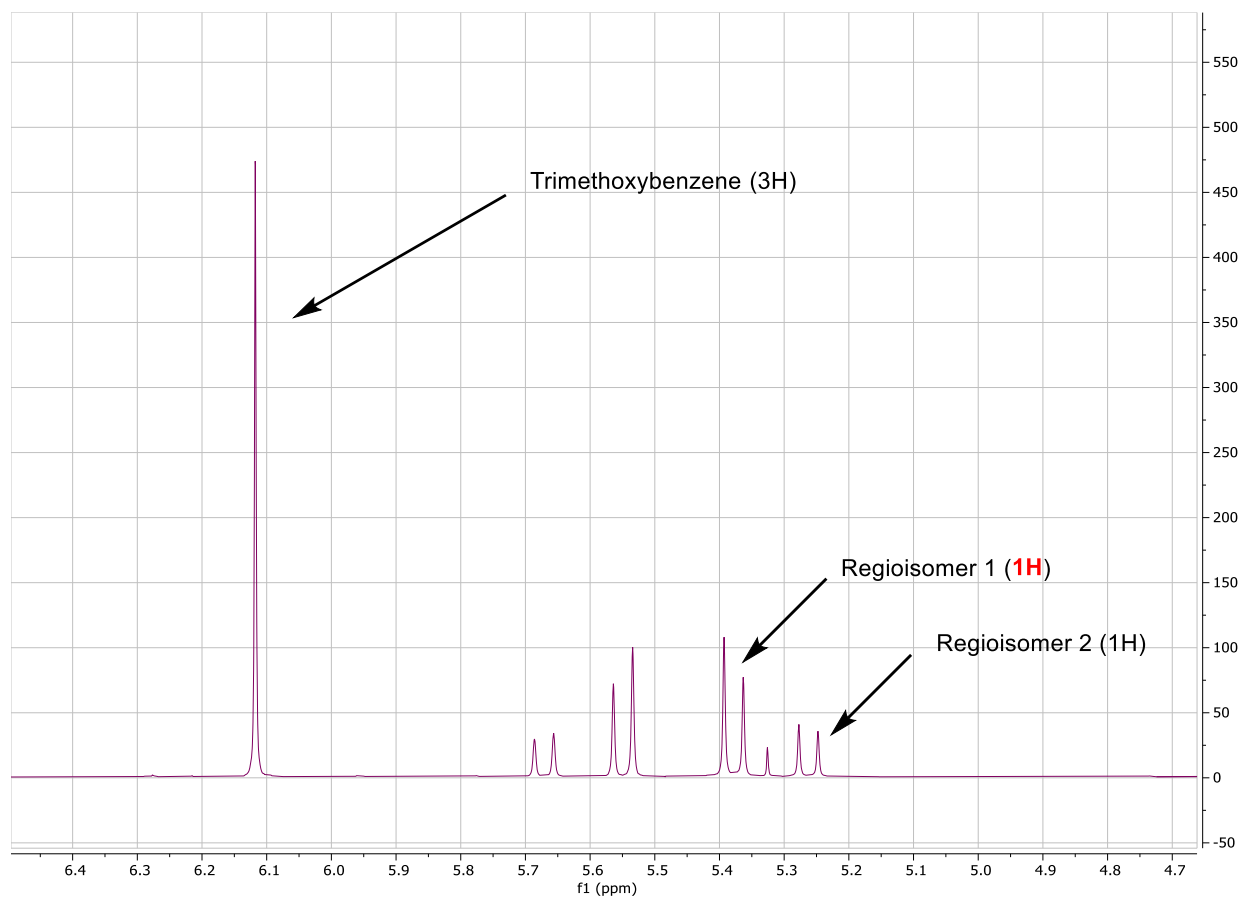
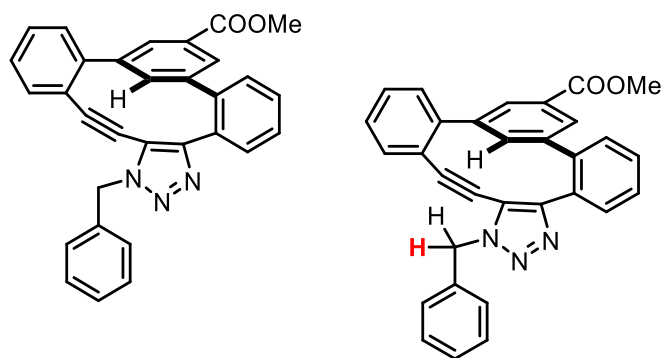
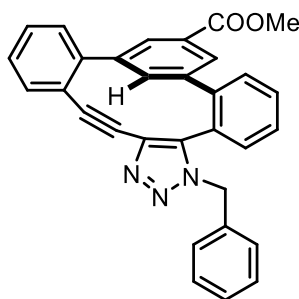


Figure A6 - 2 ¹H NMR peaks of the 3,5-triazole products and the internal standard



Regioisomer 1: $^1\text{H NMR}$ (400 MHz, CDCl_3): δ 8.35 (dd, $J = 1.7, 1.7$ Hz, 1H), 7.98 – 7.91 (m, 2H), 7.76 (dd, $J = 7.8, 1.4$ Hz, 1H), 7.71 (d, $J = 7.6$ Hz, 1H), 7.56 – 7.35 (m, 5H), 7.35 – 7.28 (m, 4H), 7.28 – 7.22 (m, 2H), 5.53 (d, $J = 14.9$ Hz, 1H), 5.36 (d, $J = 14.8$ Hz, 1H), 3.90 (s, 3H); $^{13}\text{C NMR}$ (176 MHz, CDCl_3): δ 166.9, 149.4, 145.3, 141.9, 140.6, 140.0, 138.1, 134.7, 133.1, 131.4, 130.5, 129.9, 129.8, 129.7, 128.9, 128.8, 128.5, 128.5, 128.3, 128.2, 128.1, 128.1, 127.0, 122.3, 118.8, 103.3, 83.6, 53.1, 52.3; **HRMS (ESI):** m/z calculated for $\text{C}_{31}\text{H}_{21}\text{N}_3\text{O}_2$ $[\text{M}+\text{H}]^+$, 468.1707; found: 468.1708.



Regioisomer 2: $^1\text{H NMR}$ (400 MHz, CDCl_3): δ 8.15 (dd, $J = 1.8, 1.8$ Hz, 1H), 7.87 (dd, $J = 1.7, 1.7$ Hz, 1H), 7.60 (dd, $J = 7.7, 1.3$ Hz, 1H), 7.57 – 7.52 (m, 1H), 7.51 – 7.40 (m, 3H), 7.38 – 7.28 (m, 3H), 7.25 – 7.20 (m, 3H), 6.96 (dd, $J = 1.7, 1.7$ Hz, 1H), 6.68 – 6.63 (m, 2H), 5.64 (d, $J = 14.8$ Hz, 1H), 5.23 (d, $J = 14.8$ Hz, 1H), 3.91 (s, 3H); $^{13}\text{C NMR}$ (101 MHz, CDCl_3): δ 166.7, 145.0, 142.9, 141.5, 138.4, 138.3, 138.0, 134.2, 131.5, 130.3, 130.3, 129.9, 129.8, 129.6, 128.9, 128.5, 128.4, 128.1, 127.6, 126.9, 123.0, 96.4, 88.2, 53.5, 52.2; **HRMS (ESI):** m/z calculated for $\text{C}_{31}\text{H}_{21}\text{N}_3\text{O}_2$ $[\text{M}+\text{H}]^+$, 468.1707; found: 468.1708.

Note: Regioisomers configurations were confirmed by X-ray crystallography of the regioisomer 2.

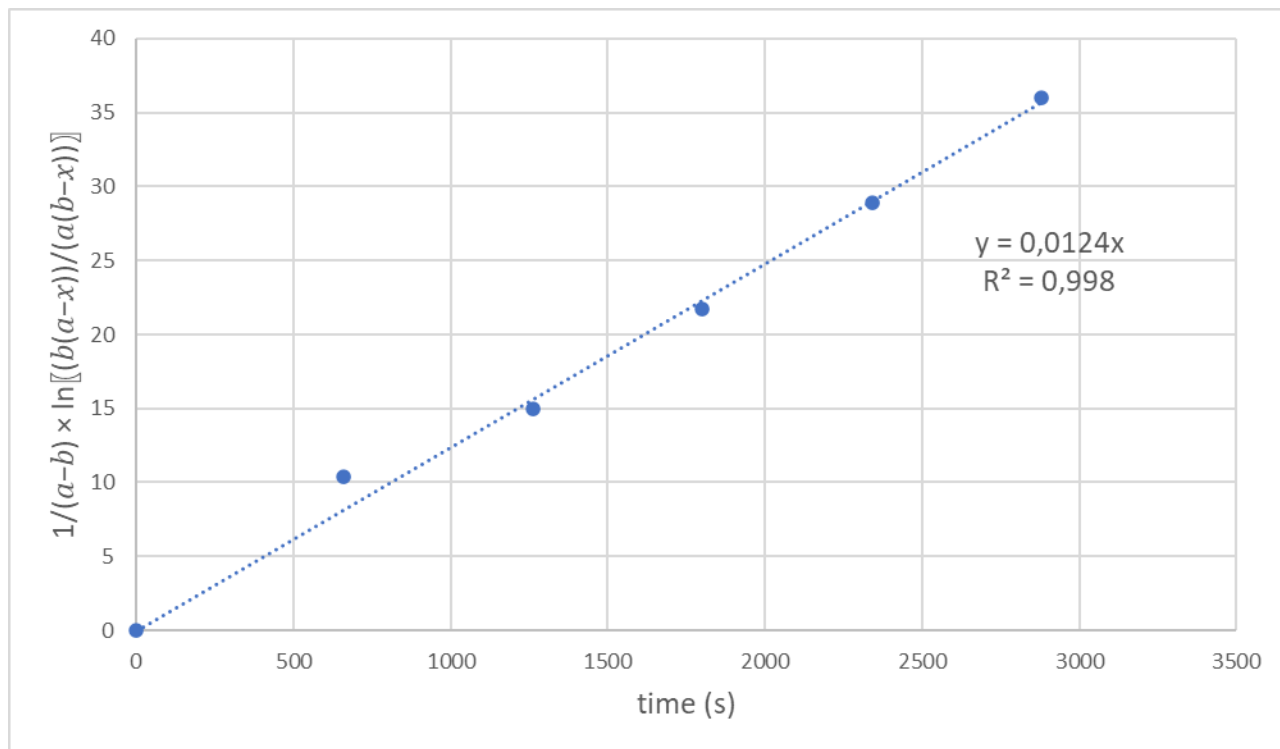


Figure A6 - 3 Plot of $\frac{1}{(a-b)} \times \ln \frac{b(a-x)}{a(b-x)}$ versus the reaction time for 3,5-TPDY Run 1

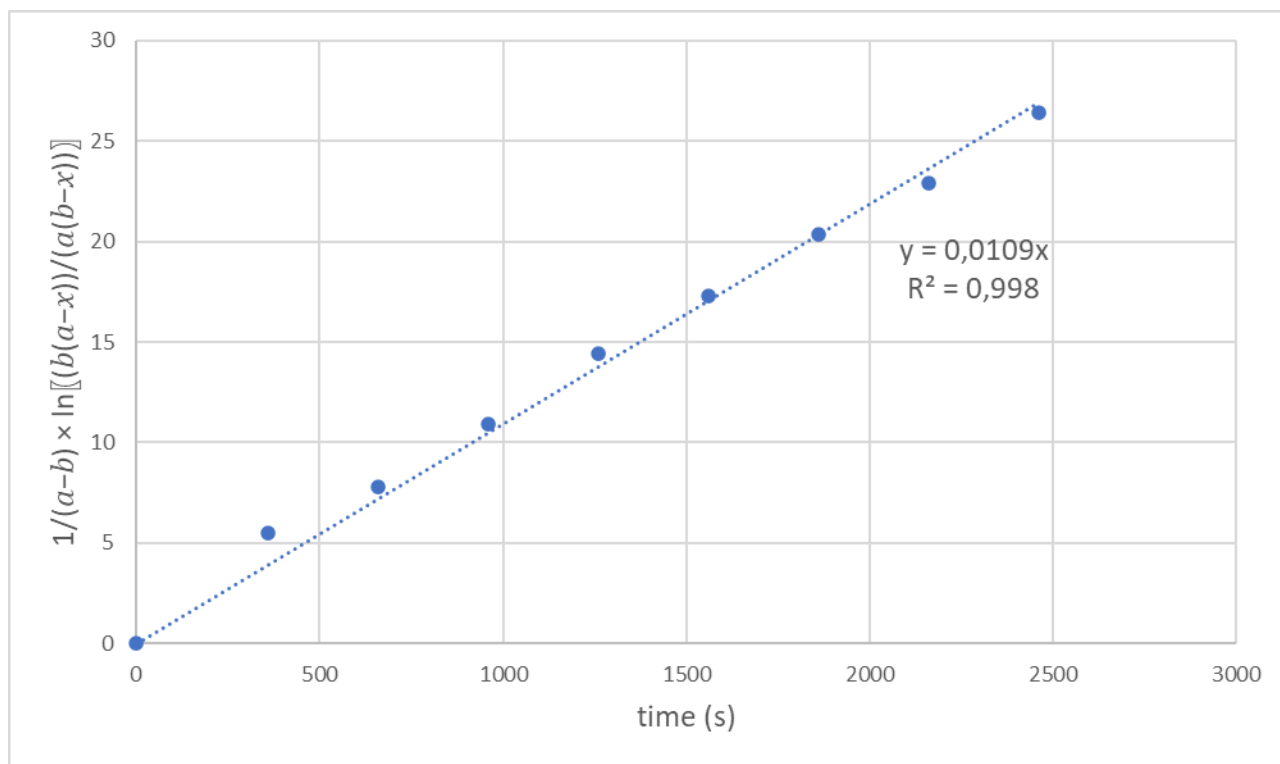


Figure A6 - 4 Plot of $\frac{1}{(a-b)} \times \ln \frac{b(a-x)}{a(b-x)}$ versus the reaction time for 3,5-TPDY Run 2

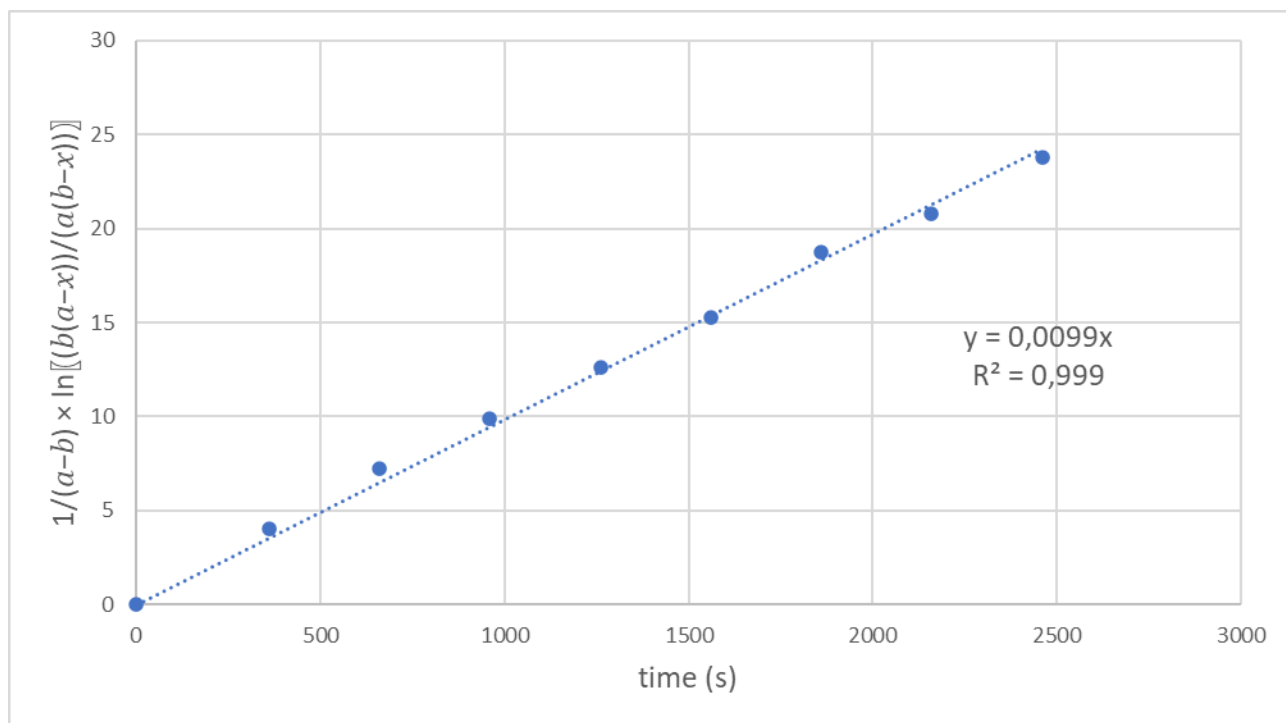
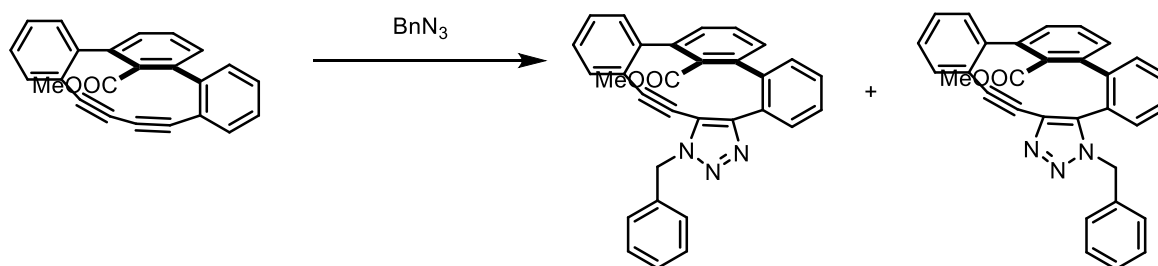


Figure A6 - 5 Plot of $\frac{1}{(a-b)} \times \ln \frac{b(a-x)}{a(b-x)}$ versus the reaction time for 3,5-TPDY Run 3

Average rate constant: $k = 11 \pm 1 \cdot 10^{-3} \text{ M}^{-1}\cdot\text{s}^{-1}$

2,6-TPDY



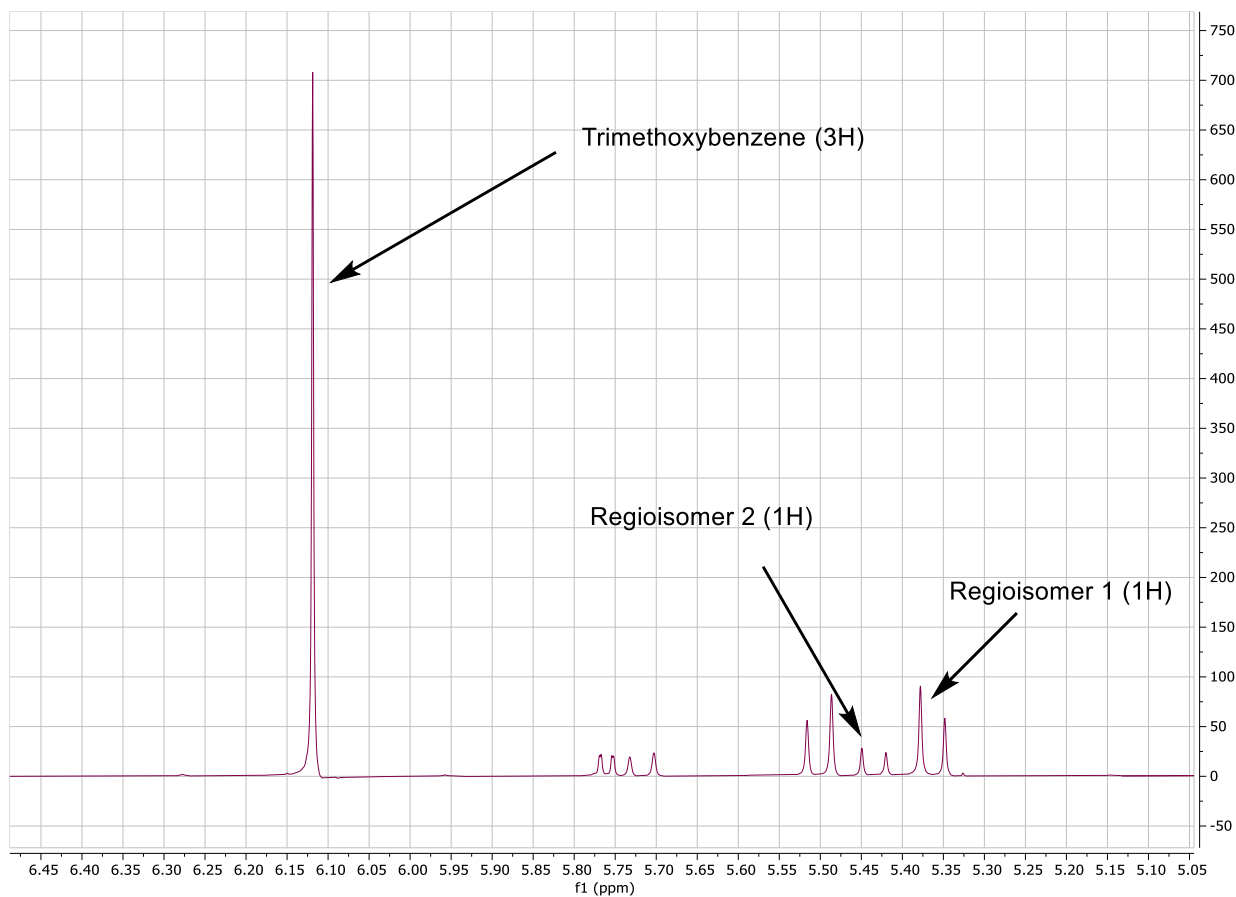
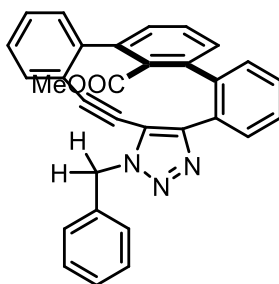
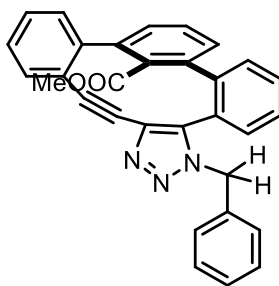


Figure A6 - 6 ^1H NMR peaks of the 2,6-triazole products and the internal standard



Regioisomer 1: ^1H NMR (400 MHz, CDCl_3): δ 7.92 (dd, $J = 7.9, 1.4$ Hz, 1H), 7.75 (d, $J = 7.6$ Hz, 1H), 7.58 – 7.46 (m, 2H), 7.44 – 7.34 (m, 4H), 7.34 – 7.29 (m, 3H), 7.25 – 7.19 (m, 4H), 7.16 (dd, $J = 7.6, 1.2$ Hz, 1H), 5.50 (d, $J = 14.9$ Hz, 1H), 5.36 (d, $J = 14.9$ Hz, 1H), 3.21 (s, 3H); ^{13}C NMR (101 MHz, CDCl_3): δ 168.0, 149.2, 146.8, 141.3, 140.9, 139.5, 137.5, 134.8, 132.2, 131.8, 130.0, 129.6, 129.0, 129.0, 128.8, 128.4, 128.2, 128.2, 128.1, 127.9, 127.8, 127.4, 126.2, 123.1, 118.6, 100.7, 83.3, 52.9, 51.7; HRMS (ESI): m/z calculated for $\text{C}_{31}\text{H}_{21}\text{N}_3\text{O}_2$ $[\text{M}+\text{H}]^+$, 468.1707; found: 468.1715.



Regioisomer 2: $^1\text{H NMR}$ (400 MHz, CDCl_3): δ 7.64 (dd, $J = 7.7, 1.3$ Hz, 1H), 7.57 (dd, $J = 7.6, 1.5$ Hz, 1H), 7.51 (ddd, $J = 7.5, 7.5, 1.4$ Hz, 1H), 7.45 (ddd, $J = 7.5, 7.5, 1.4$ Hz, 1H), 7.41 – 7.26 (m, 7H), 7.26 – 7.19 (m, 2H), 7.15 (dd, $J = 7.5, 1.3$ Hz, 1H), 7.08 (dd, $J = 7.5, 7.5$ Hz, 1H), 6.81 (dd, $J = 7.2, 1.8$ Hz, 2H), 5.77 – 5.67 (m, 2H), 5.43 (d, $J = 14.7$ Hz, 1H), 3.14 (s, 3H); $^{13}\text{C NMR}$ (101 MHz, CDCl_3): δ 167.9, 146.7, 141.3, 141.3, 139.1, 138.2, 137.1, 134.7, 130.7, 130.1, 129.6, 129.3, 129.2, 129.1, 128.8, 128.6, 128.5, 128.3, 128.2, 128.1, 127.8, 127.8, 126.7, 126.0, 123.9, 93.7, 87.8, 53.5, 51.7; **HRMS (ESI):** m/z calculated for $\text{C}_{31}\text{H}_{21}\text{N}_3\text{O}_2$ $[\text{M}+\text{H}]^+$, 468.1707; found: 468.1718.

Note: Regioisomers configurations were confirmed by Xray crystallography of the regioisomer 2

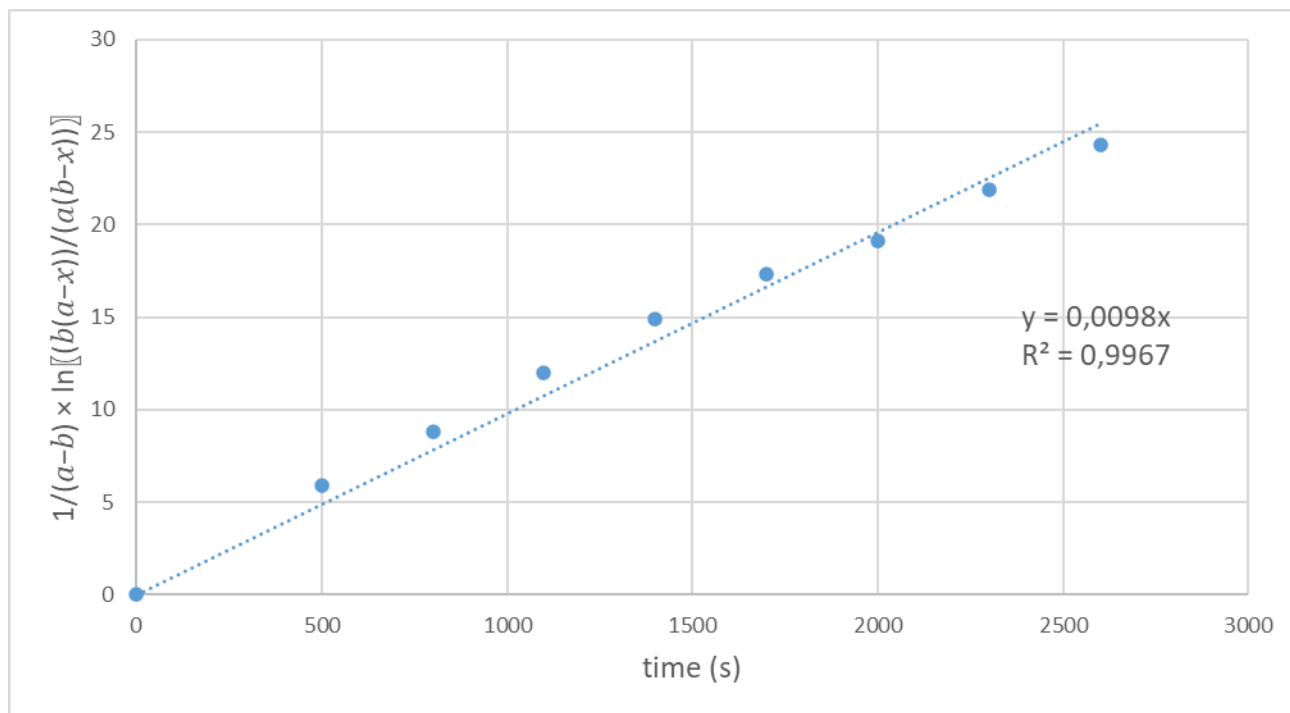


Figure A6 - 7 Plot of $\frac{1}{(a-b)} \times \ln\left[\frac{b(a-x)}{a(b-x)}\right]$ versus the reaction time for 2,6-TPDY Run 1

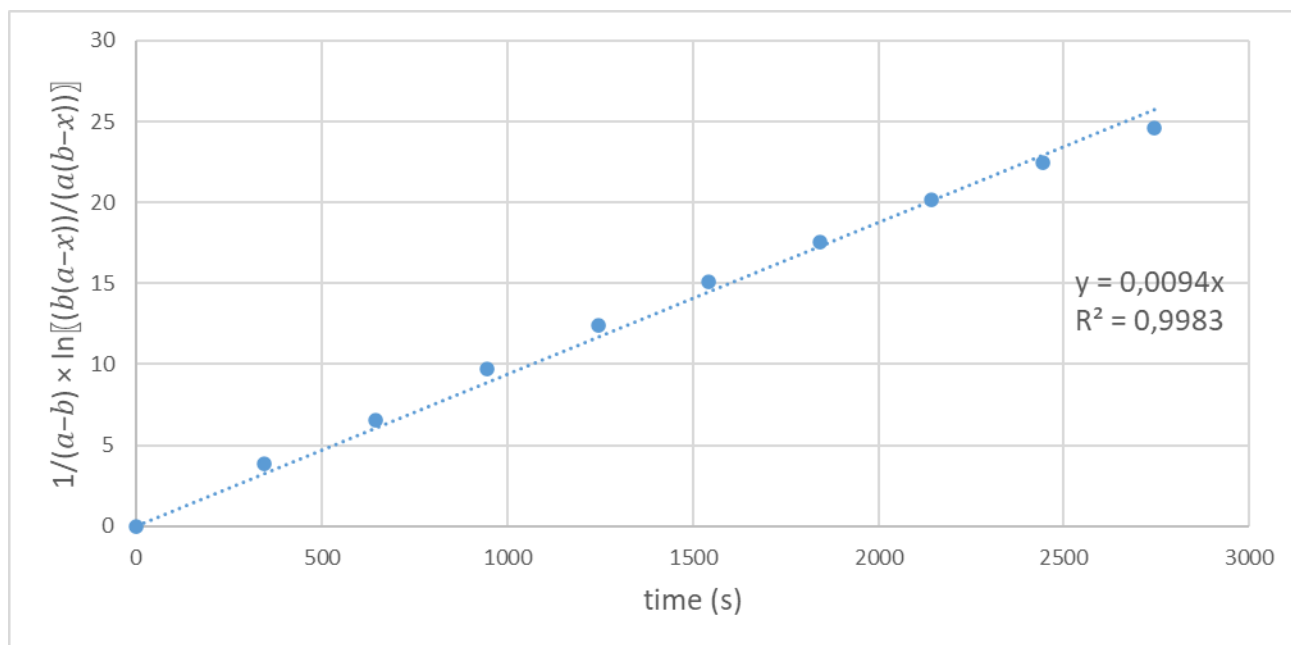


Figure A6 - 8 Plot of $\frac{1}{(a-b)} \times \ln\left[\frac{b(a-x)}{a(b-x)}\right]$ versus the reaction time for 2,6-TPDY Run 2

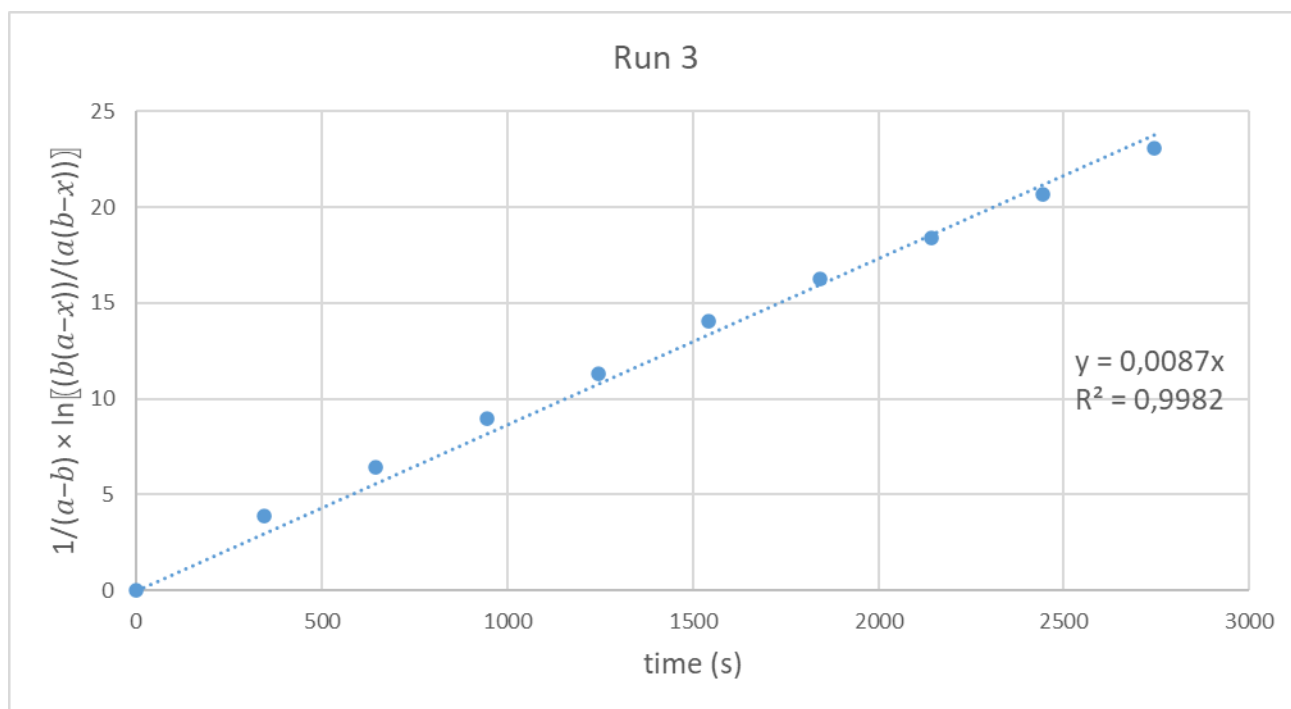


Figure A6 - 9 Plot of $\frac{1}{(a-b)} \times \ln\left[\frac{b(a-x)}{a(b-x)}\right]$ versus the reaction time for 2,6-TPDY Run 3

Average rate constant : $k = 9.3 \pm 0.5 \cdot 10^{-3} \text{ M}^{-1} \cdot \text{s}^{-1}$

2,4-TPDY

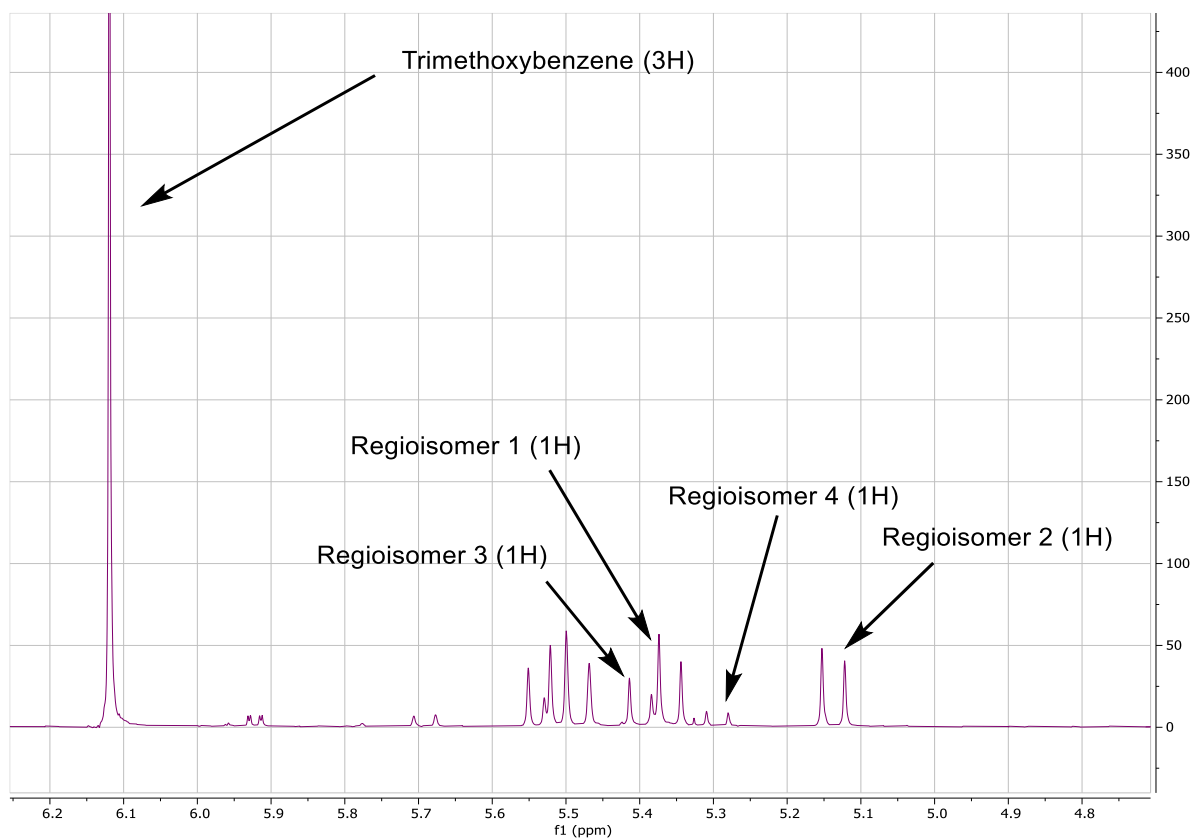
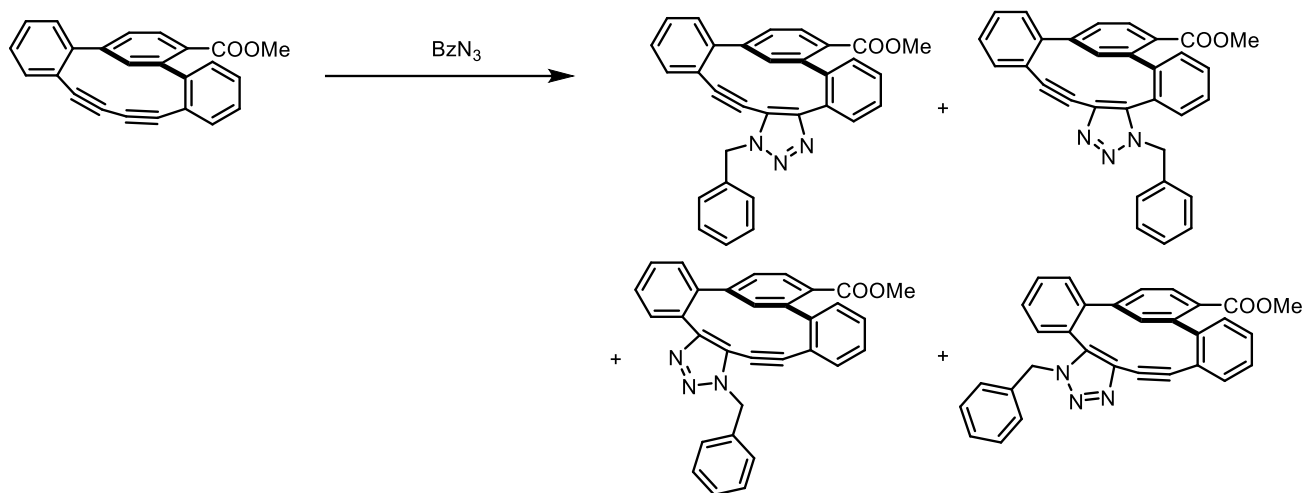


Figure A6 - ^{10}H NMR peaks of the 2,4-triazole products and the internal standard

Note : Due to the complexity of the mixture and the difficulty of separation, exact configuration of each regioisomer was not determined. Full spectra are reported in the NMR Spectra section.

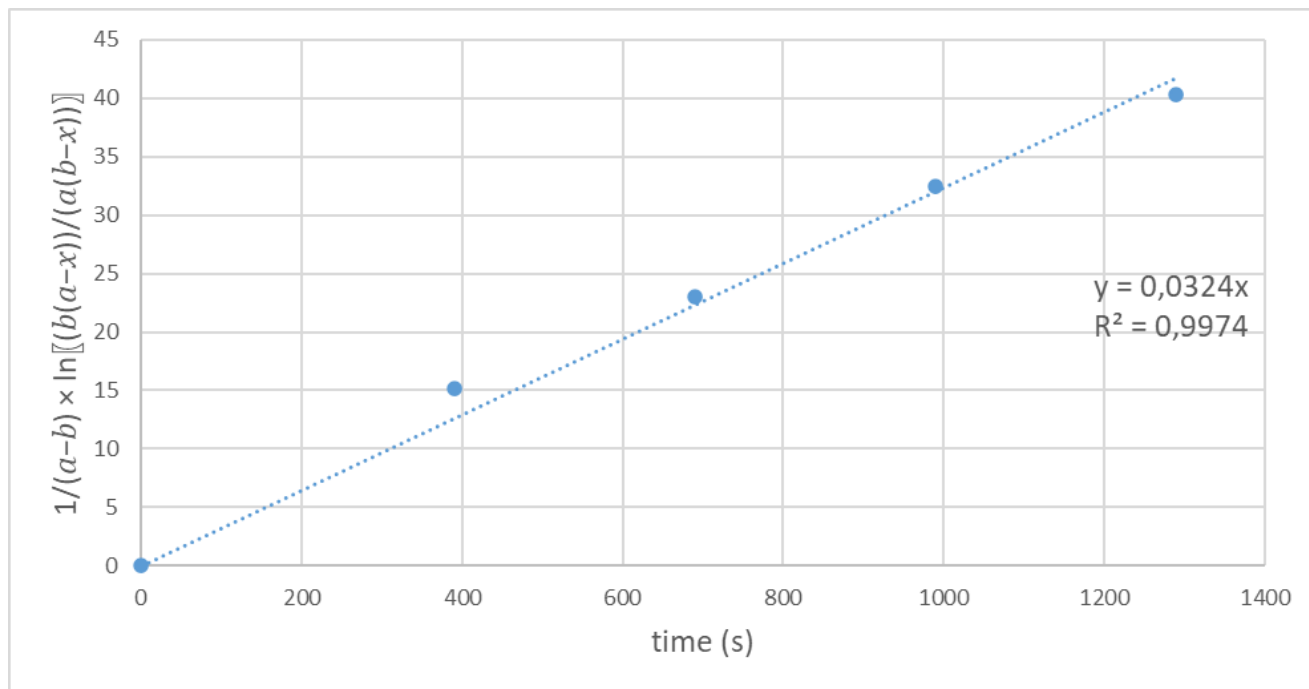


Figure A6 - 11 Plot of $\frac{1}{(a-b)} \times \ln\left[\frac{b(a-x)}{a(b-x)}\right]$ versus the reaction time for 2,4-TPDY Run 1

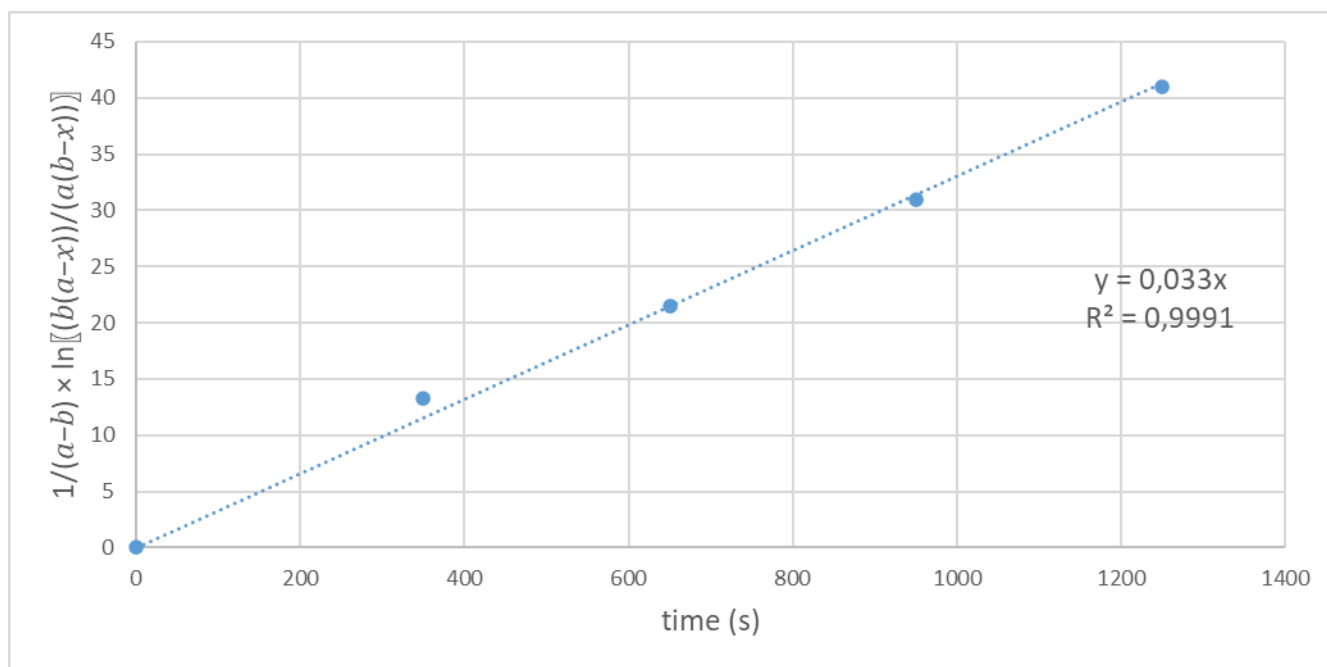


Figure A6 - 12 Plot of $\frac{1}{(a-b)} \times \ln\left[\frac{b(a-x)}{a(b-x)}\right]$ versus the reaction time for 2,4-TPDY Run 2

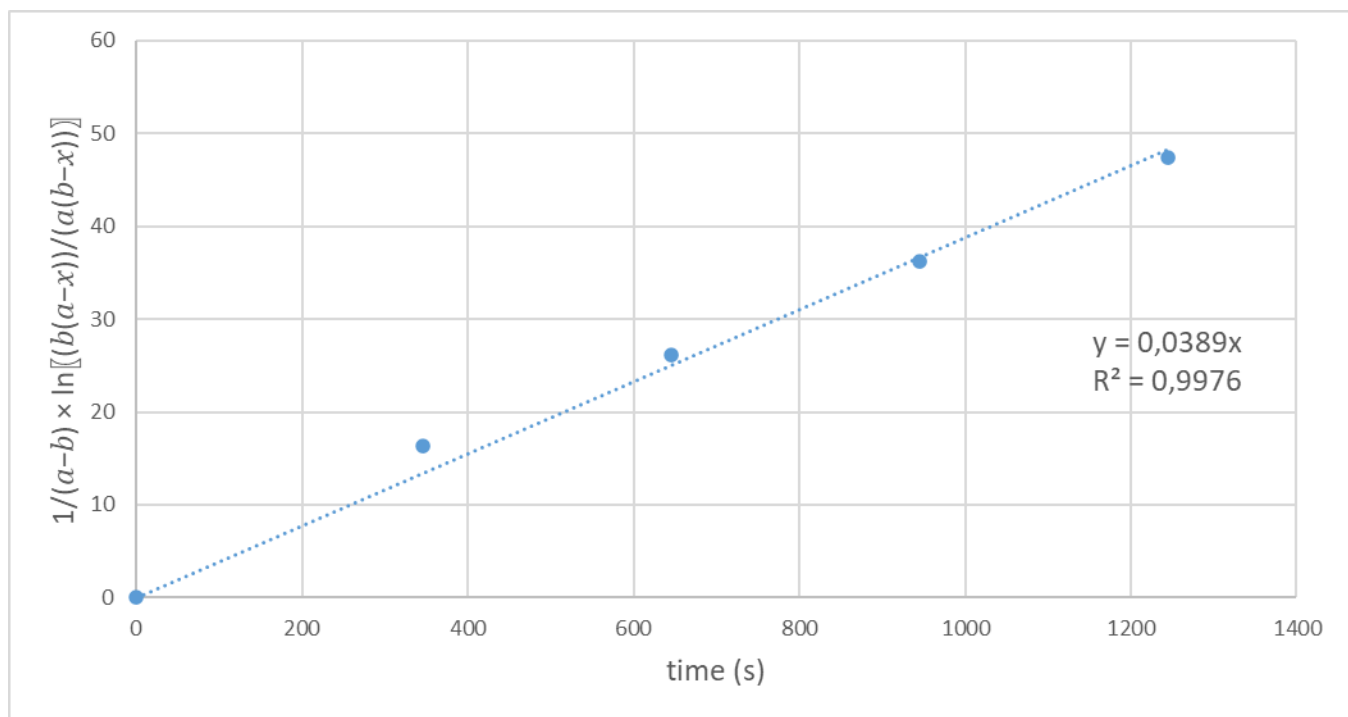
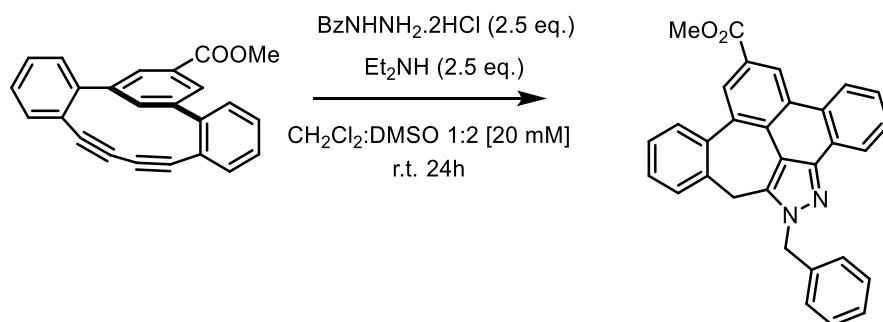


Figure A6 - 13 Plot of $\frac{1}{(a-b)} \times \ln \frac{b(a-x)}{a(b-x)}$ versus the reaction time for 2,4-TPDY Run 3

Average rate constant: $k = 34 \pm 4 \cdot 10^{-3} \text{ M}^{-1}\cdot\text{s}^{-1}$

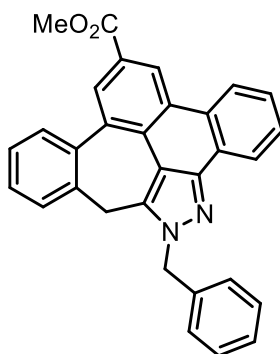
Strain Promoted Diyne Hydrazine Hydroamination

General procedure



To a solution of 3,5-TPDY (30 mg, 0.09 mmol, 1 eq.) in CH_2Cl_2 :DMSO 1:1 [30mM] was added benzyl hydrazine dihydrochloride (44 mg, 0.23 mmol, 2.5 eq.) and diethylamine (46.4 μmol , 5 eq.)

and the reaction was stirred at room temperature for 24 h. The solution was then diluted in CH₂Cl₂ and washed three times with brine. The organic phase was then concentrated *in vacuo*. Purification by flash column chromatography (4% to 20% AcOEt in Hexanes) afforded the desired product as a pale-yellow solid (16.7 mg, 41%).



Methyl 1-benzyl-1,14-dihydro-1,2-diazabenzophenanthrene-8-carboxylate : ¹H NMR (400 MHz, CDCl₃): δ 9.26 (d, *J* = 1.5 Hz, 1H), 8.69 – 8.50 (m, 3H), 7.70 – 7.59 (m, 2H), 7.52 (dd, *J* = 7.6, 1.6 Hz, 1H), 7.37 – 7.28 (m, 5H), 7.23 (dd, *J* = 7.8, 1.8 Hz, 2H), 7.08 (dd, *J* = 7.3, 1.7 Hz, 1H), 5.77 (s, 2H), 4.13 (s, 2H), 4.06 (s, 3H); ¹³C NMR (101 MHz, CDCl₃): δ 167.7, 145.2, 139.1, 138.6, 136.7, 136.6, 135.4, 133.9, 131.0, 130.1, 129.7, 129.2, 129.0, 128.7, 128.5, 128.2, 128.0, 127.8, 127.6, 126.9, 126.3, 126.1, 124.5, 124.4, 123.2, 115.4, 54.3, 52.5, 33.4; HRMS (ESI): *m/z* calculated for C₃₁H₂₂N₂O₂ [M+H]⁺, 455.1754; found: 455.1754.

A6.4 Computational studies

General considerations

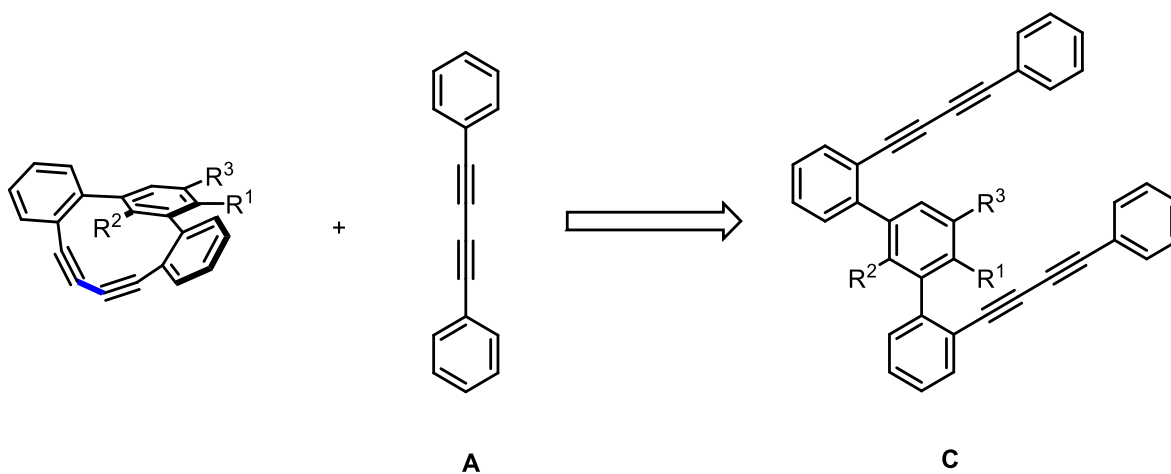
Conformational searches and pre-optimisations were performed with HyperChem 8.³ DFT calculations were performed by using the Gaussian 16 A.03 software package.⁴ Geometry optimizations of molecules were performed with the B3LYP⁵-D3⁶ density functional method and 6-31+G(d,p) basis set using SMD⁷ solvent model for dichloromethane. Frequency calculations were carried out for all structures to confirm them as either a minimum or a transition state (TS). Wavefunction stability calculations were carried out for all structures to confirm the stability of

the wavefunction with respect to RDFT to UDFT (i.e.: restricted to unrestricted DFT) and real to complex wavefunction perturbations. NBO deletion analysis were done using the NBO7 software.⁸⁻⁹ Three-dimensional structures were produced with GaussView6. Orbitals representations were done using Chemcraft 1.8.¹⁰ Cartesian coordinates for all structures are available at the end of the Supporting Information.

Ring Strain Energy (RSE)

Ring-Strain Energies were estimated using the homodesmotic reaction shown below. Geometry optimizations of molecules were performed, and the strain energies were calculated according to the equation:

$$RSE = (H_{TPDY} + H_A) - H_C$$



2,4-TPDY $R^1 = \text{CO}_2\text{Me}$, $R^2 = R^3 = \text{H}$

2,6-TPDY $R^1 = R^3 = \text{H}$, $R^2 = \text{CO}_2\text{Me}$

3,5-TPDY $R^1 = R^2 = \text{H}$, $R^3 = \text{CO}_2\text{Me}$

RSE = 23.4 kcal/mol

RSE = 23.3 kcal/mol

RSE = 21.8 kcal/mol

A6.5 Bioligation experiments

MTG expression and purification

mTG expression and purification and activity assay were performed as previously reported.¹¹ Activity greater than 20 U/mg of purified mTG was assessed, and purity was determined over 85% on 15% reducing SDS-PAGE.

hFc expression and purification

E. coli Shuffle T7 express transformed with pET-22b hFc and SOX plasmid were propagated overnight at 37 °C, 230 rpm in a 20 mL LB preculture with ampicillin (100 µg/mL) and chloramphenicol (50 µg/mL). A culture of LB media (500 mL) containing ampicillin and chloramphenicol was inoculated with an initial OD₆₀₀ of 0.1 and propagated at 37 °C, 230 rpm. When OD₆₀₀ reached 0.7-1.0, protein expression was induced by addition of 1 mM IPTG and the culture was incubated overnight at 22 °C, 230 rpm. Cells were pelleted at 5 500 ×g for 10 min and resuspended in 30 mL of IMAC-A buffer (50 mM Tris-HCl pH 8, 600 mM NaCl, 20 mM imidazole). The cell suspension was lysed using 3 cycles of 30 s sonication with 30 s rest on ice between cycles. The lysate was centrifuged at 50 000 ×g and filtered through 0.22 micron and applied to a 1 mL HisTrap Ni-NTA column (Cytiva) at a flow rate of 1 mL/min pre-equilibrated with IMAC-A buffer. After flow-through elution, the column was washed with 5 CV of 5% IMAC-B buffer (50 mM Tris-HCl pH 8, 600 mM NaCl, 500 mM imidazole), followed by protein elution through 10 CV of 100% IMAC-B buffer. Fractions (1 mL) were pooled according to the A₂₈₀ peak and dialyzed overnight against PBS buffer pH 7.2 (137 mM NaCl, 2.7 mM KCl, 9.2 mM Na₂HPO₄, 1.8 mM KH₂PO₄) at 4 °C. Protein was concentrated to 5 mg/mL using a 15 mL Amicon (Millipore Sigma, MWCO 10 kDa), supplemented with 10% glycerol and stored at -72 °C. Protein concentration was measured at 280 nm using a theoretical extinction coefficient of 71680 M⁻¹cm⁻¹ and a molecular weight of 54 kDa. Protein purity greater than 85% and proper folding of hFc was assessed on a 15% non-reducing SDS-PAGE gel.

GB1 expression and purification

E. coli BL21 (DE3) transformed with the pET-15b Gb1 I6Q variant were propagated overnight at 37°C, 230 rpm in a 20 mL LB preculture with ampicillin (100 µg/mL). The culture of LB media (500 mL) with ampicillin was inoculated at an initial OD₆₀₀ of 0.1 and propagated at 37°C, 230 rpm. When the OD₆₀₀ reached 0.7-1.0, protein expression was carried out by adding 1 mM IPTG and the culture was incubated overnight at 22°C, 230 rpm. Cells were pelleted at 5,500 ×g for 10 min and resuspended in 30 mL IMAC-A buffer. The cell suspension was lysed by 3 cycles of 30 s sonication with 30 s rest on ice between cycles. The lysate was centrifuged at 50,000 ×g, filtered through 0.22 micron and applied to a 1 mL HisTrap Ni-NTA column (Cytiva) at a flow rate of 1 mL/min, pre-equilibrated with IMAC-A buffer. After flow-through elution, the column was washed with 5 CV of 5% IMAC-B buffer followed by protein elution through 10 CV of 100% IMAC-B buffer. Fractions (1 mL) were pooled according to the A280 peak, and buffer exchanged with a 5 mL HiTrap desalting column (Cytiva) to PBS buffer pH 7.2 at 4 °C. Protein was concentrated to 5 mg/mL using a 15 mL Amicon (MWCO 3 kDa, Millipore Sigma), supplemented with 10% glycerol and stored at -72 °C. Protein concentration was measured at 280 nm using a theoretical extinction coefficient of 9970 M⁻¹cm⁻¹ and a molecular weight of 8475 Da. Protein purity greater than 85% was assessed on a 10% reducing tricine gel.

SDS-PAGE analysis of conjugation reaction to proteins

Proteins (hFc or Gb1, 50 µM) were incubated in presence of 3,5-TPDY-PEG-NH₃Cl (1 mM), sulfo-Cy5 azide (2 mM, Lumiprobe) and mTG (5 µM) in PBS buffer pH 7.2, 15% (v/v) DMSO at room temperature. Control reactions were run in the absence of mTG to evaluate background fluorescence on gels and in presence N-(1R,8S,9s)-Bicyclo[6.1.0]non-4-yn-9-ylmethyloxycarbonyl-1,8-diamino-3,6-dioxaoctane (BCN-amine, 1 mM, VWR) as a reference for mTG conjugation. Reactions were stopped by adding of 4% (v/v) formic acid and aliquots (10 µL) were resolved on 16,5% reducing tricine gels (Gb1) or 15% non-reducing tris-glycine SDS-PAGE gel (hFc). Fluorescence was revealed with an iBright FL1500 imaging system (ThermoFischer) using the Cy5 filter (Ex 608-632 nm, Em 675-720 nm) with an exposure time of 500 ms prior to Coomassie staining. Fluorescence intensity was quantified using ImageJ software.

Figures for additional MTG-mediated conjugation of B domain of protein G (Gb1).

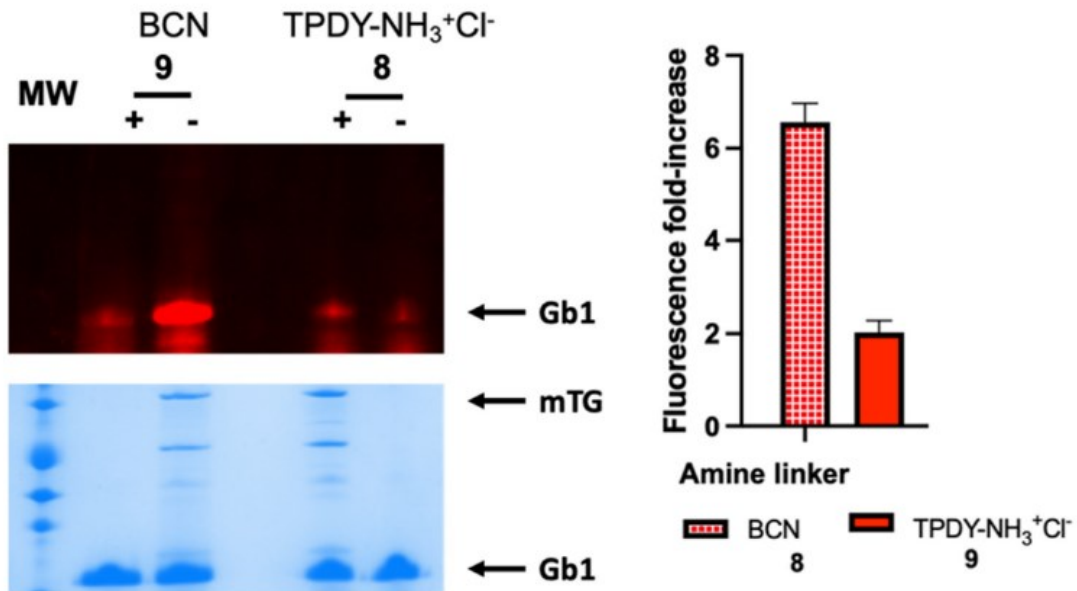
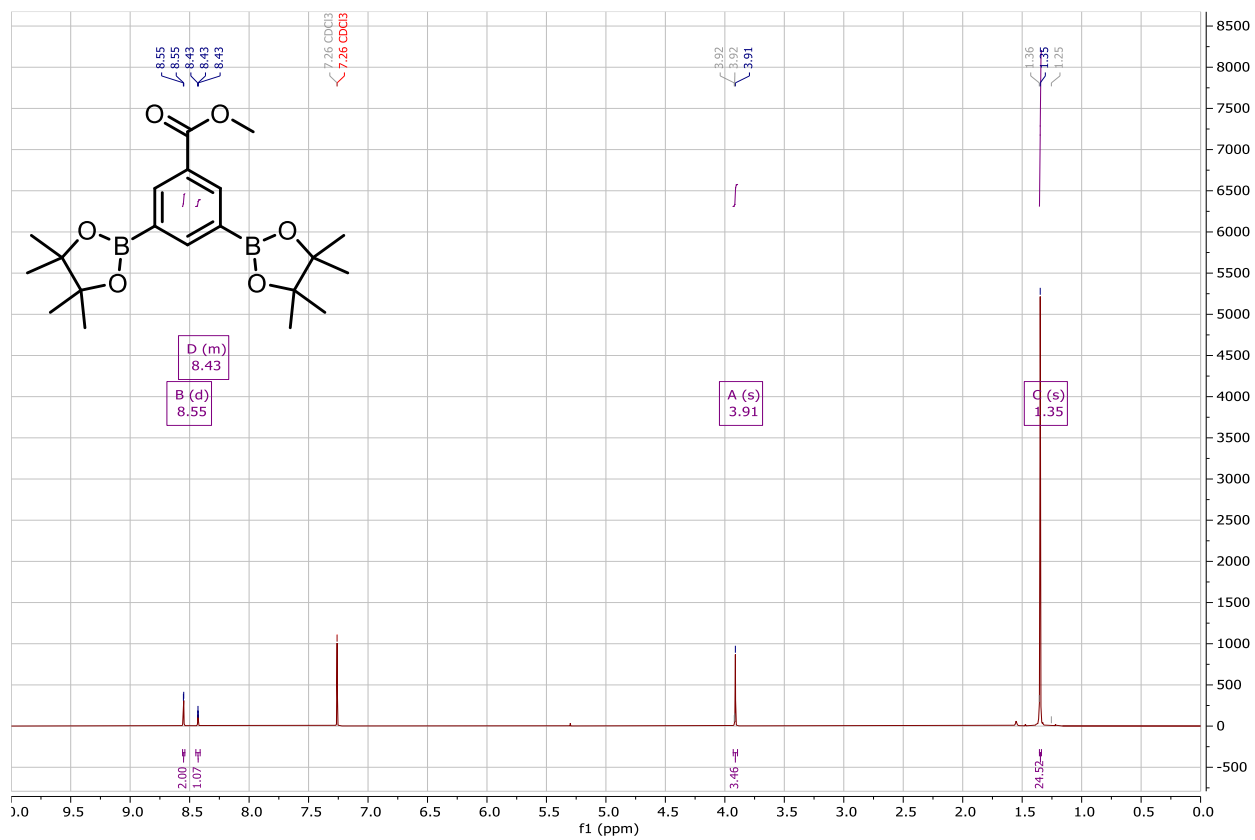
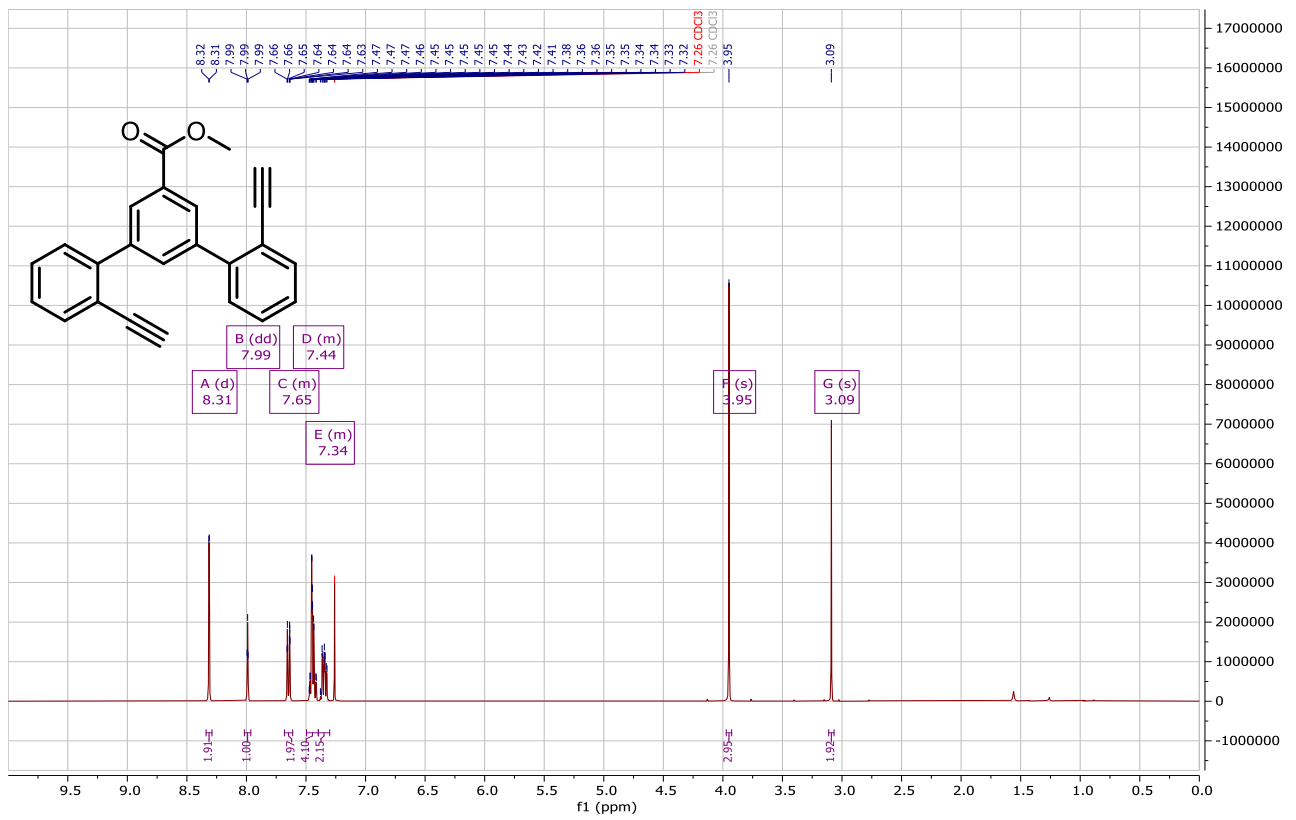
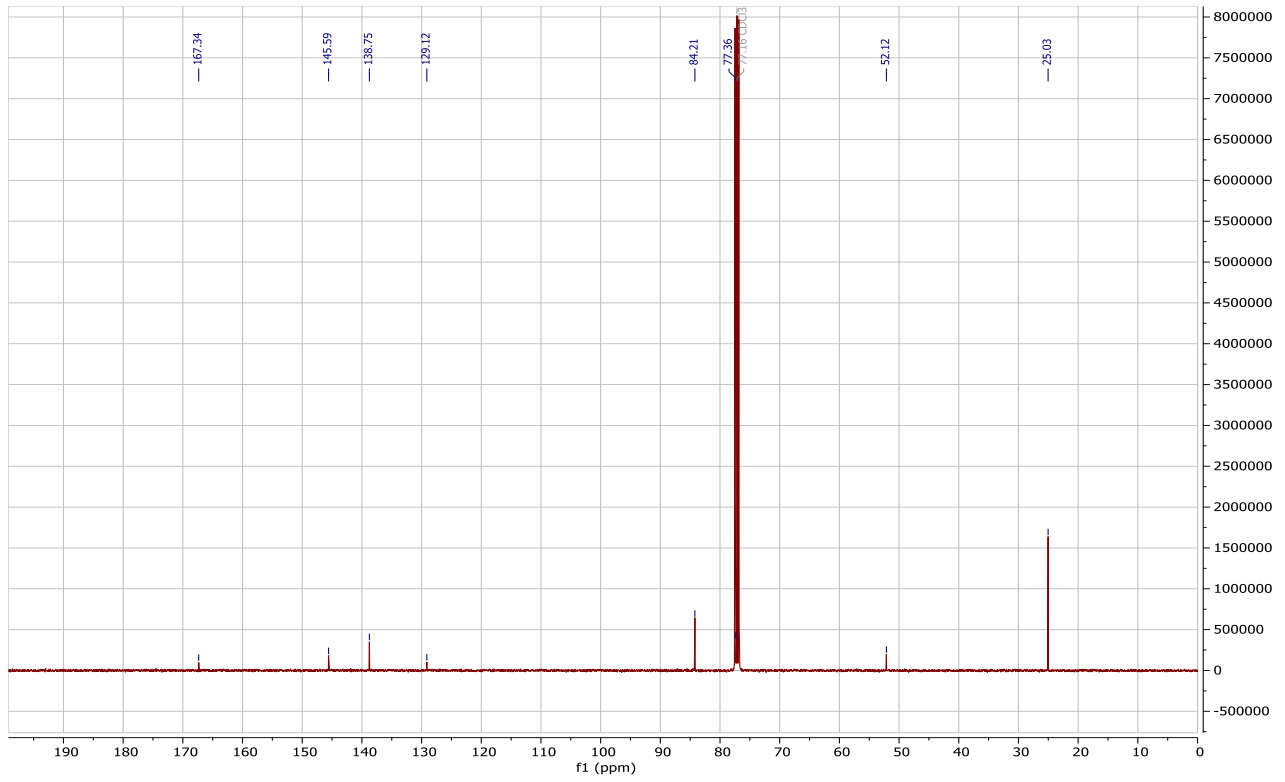
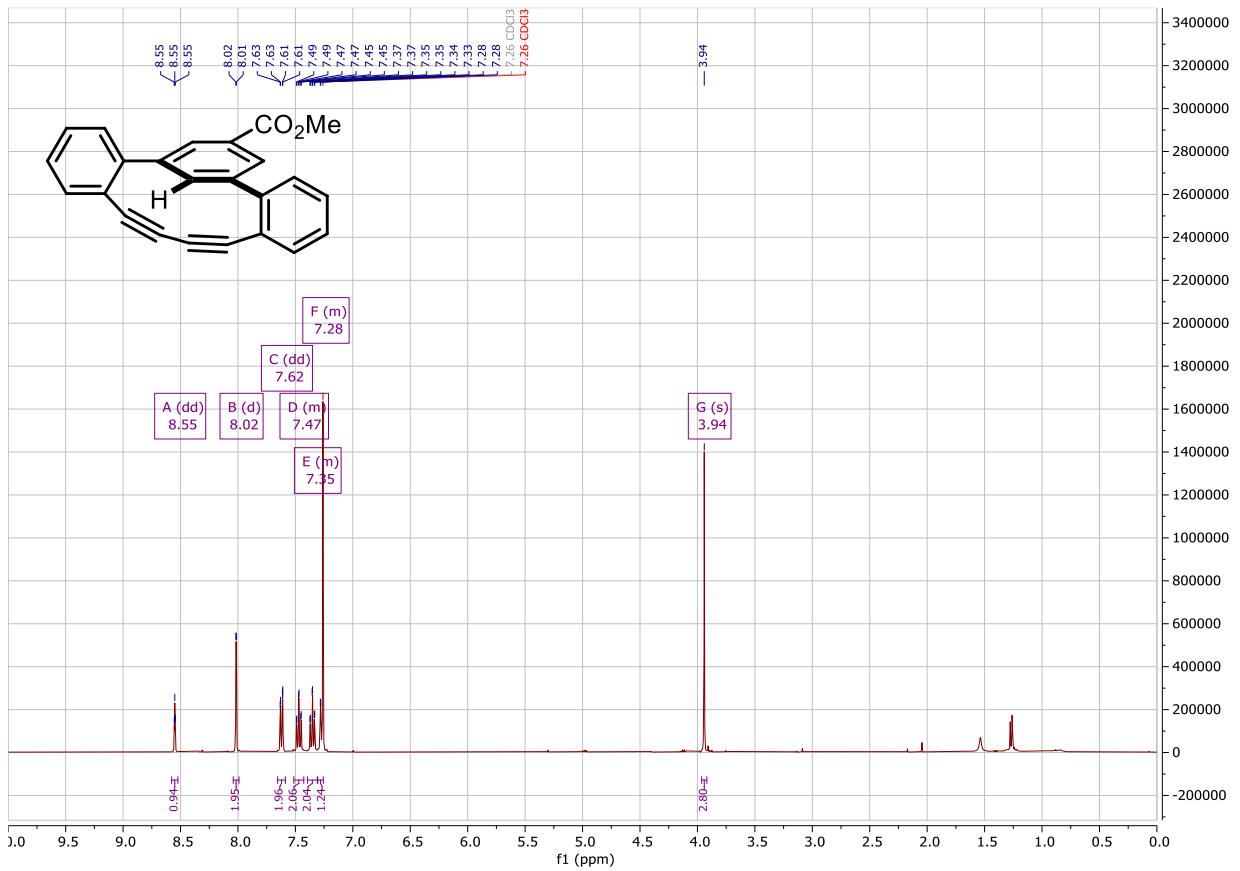
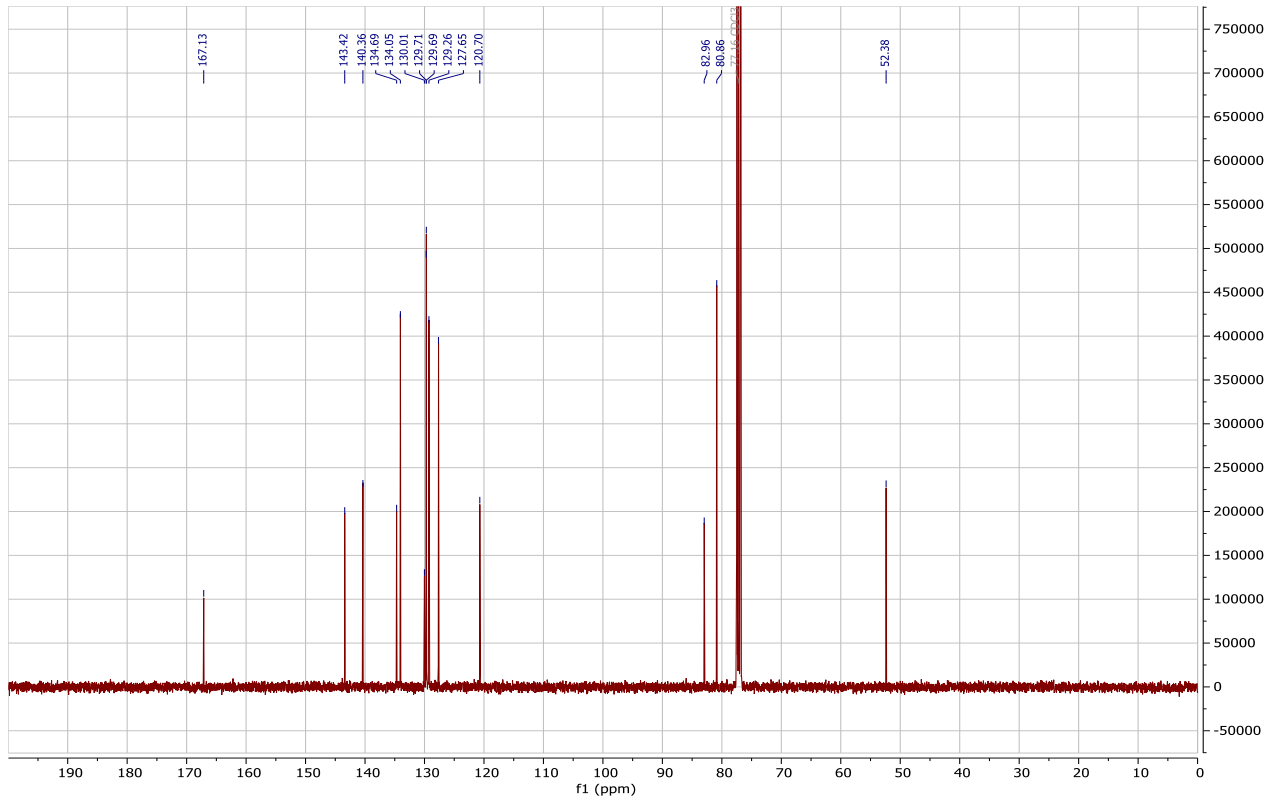


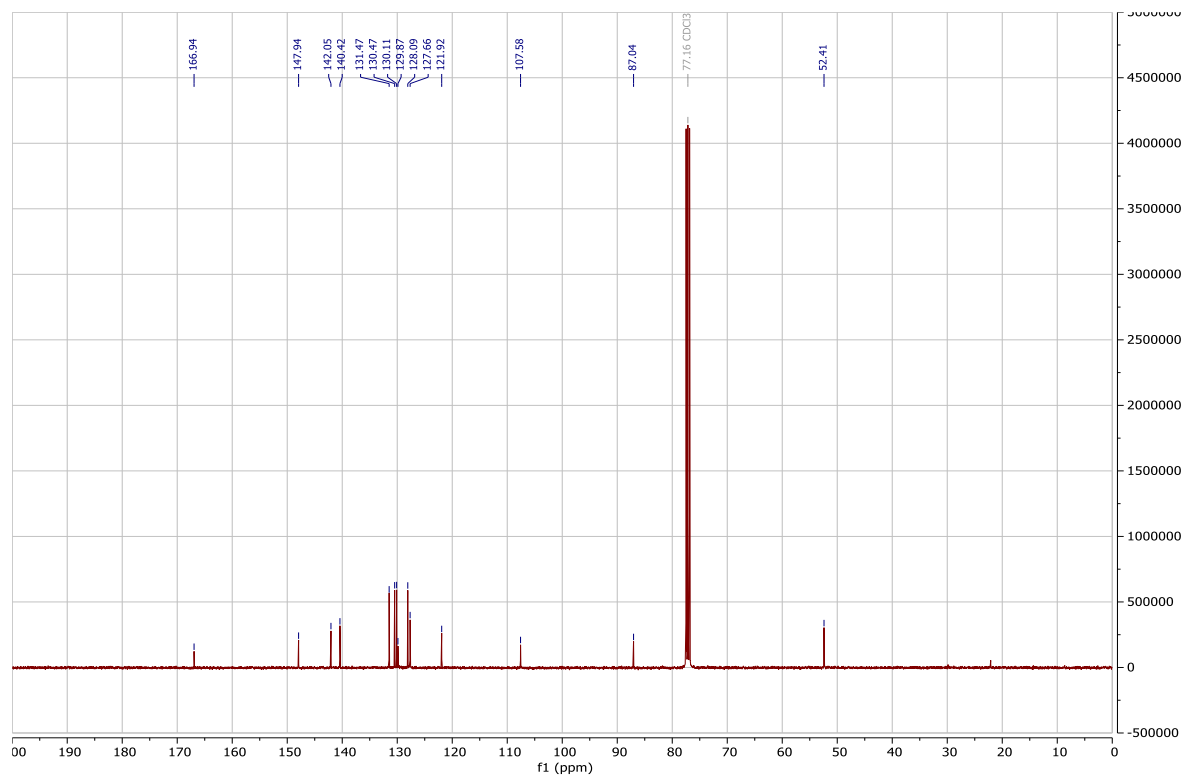
Figure A6 - 14 MTG-mediated conjugation of B domain of protein G (Gb1). Upper gel image: Fluorescence of sulfo-Cy-5 (500 ms exposure) Lower gel image: Coomassie stained to confirm equal loading of the protein. MW: molecular weight marker. The presence/absence (+ or -) of mTG is indicated. The bar graph represents fluorescence-fold increase relative to background (no mTG) for each reaction.

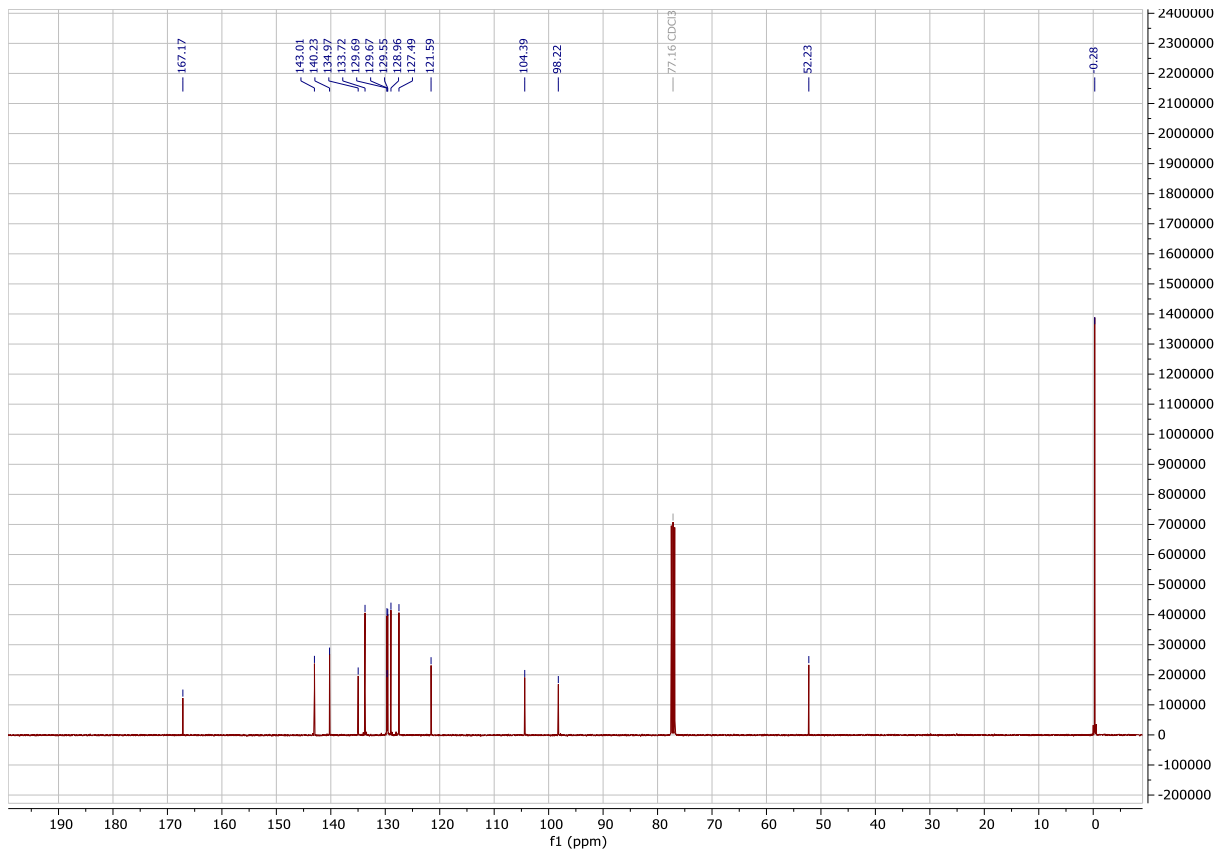
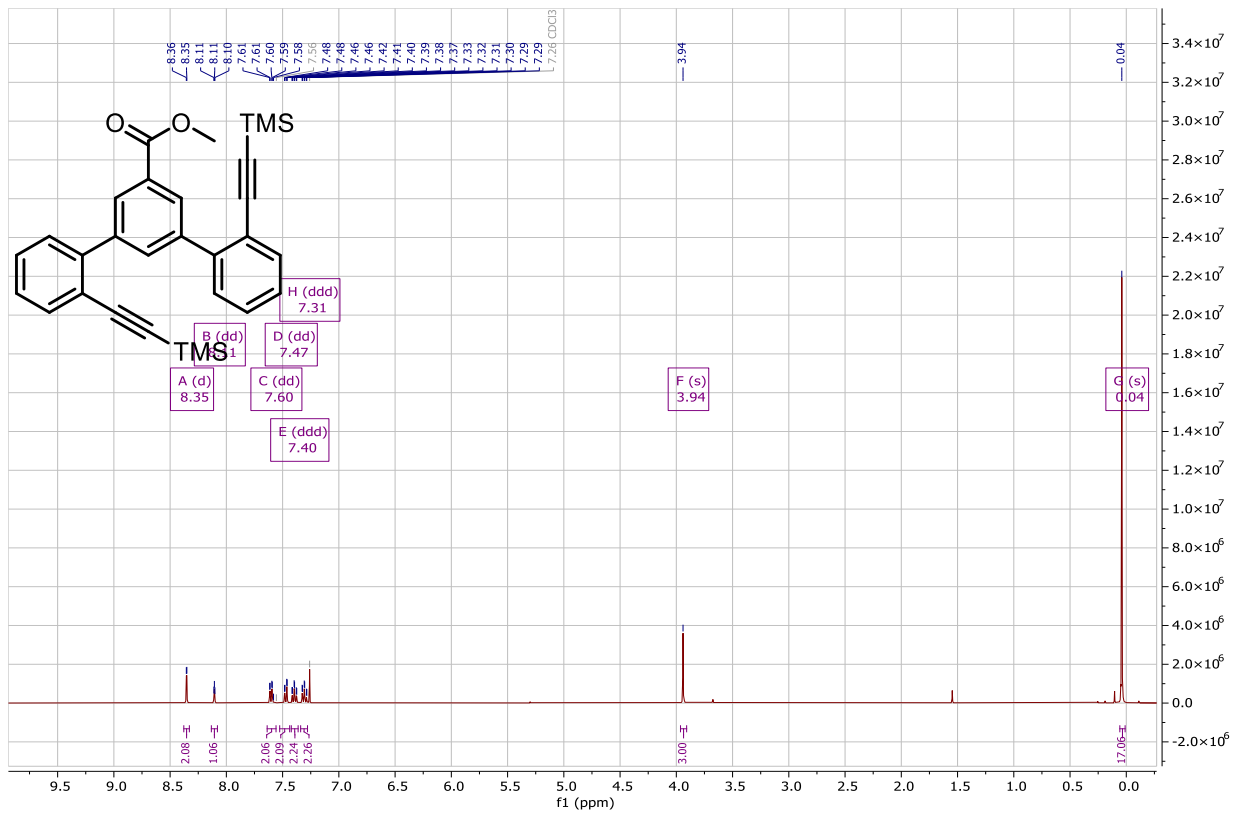
A6.6 NMR and Mass Spectra

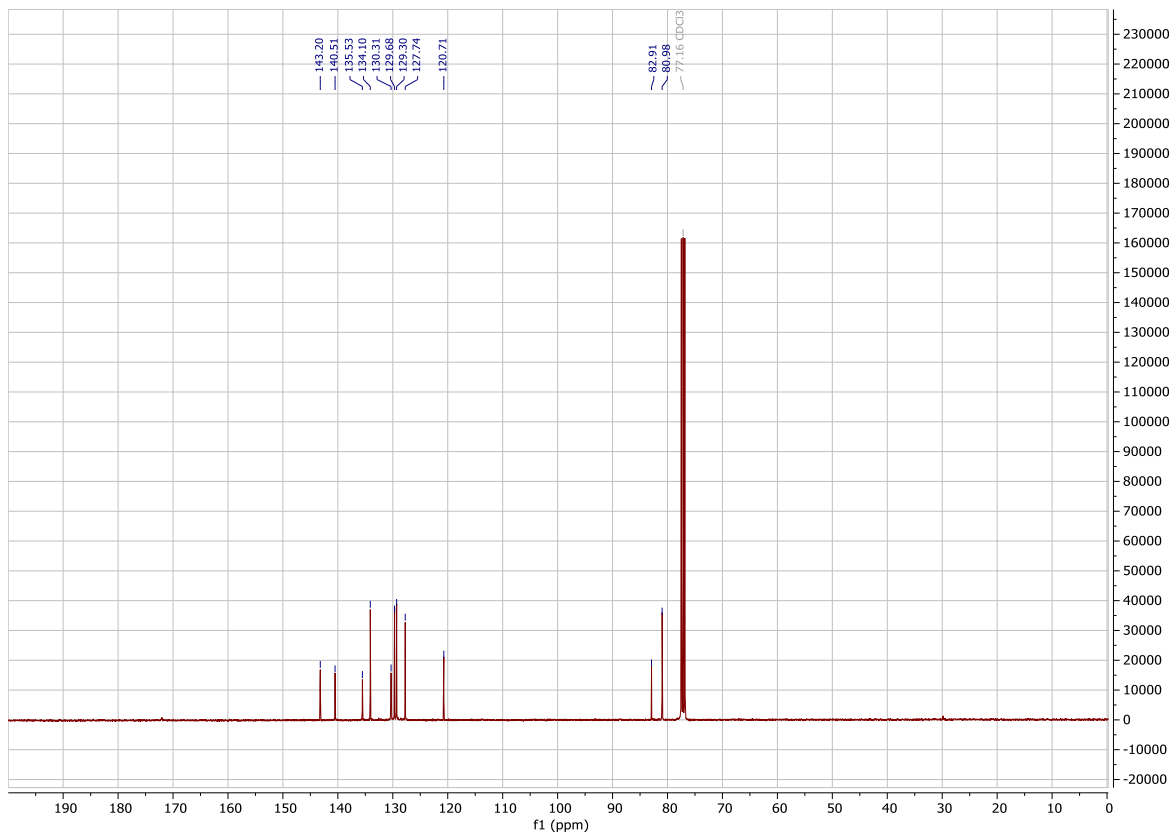
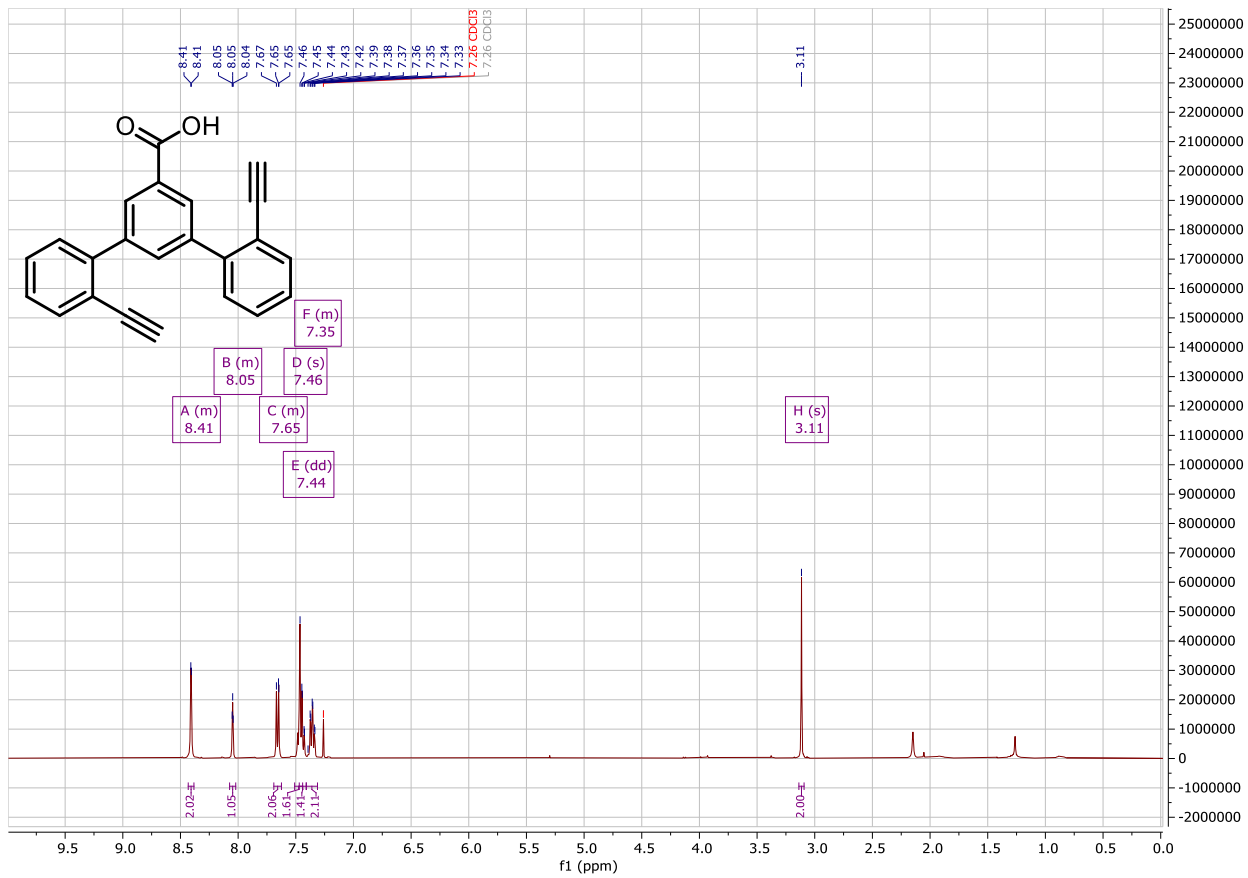


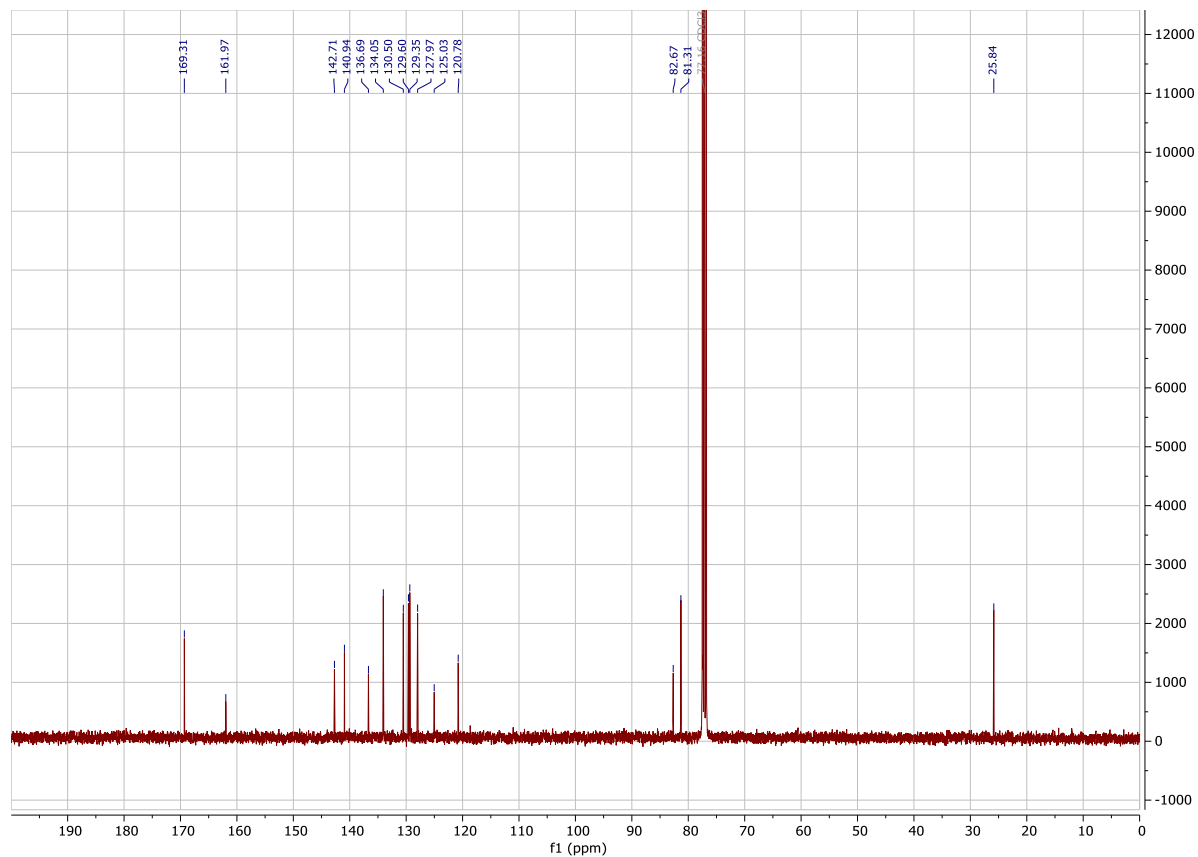
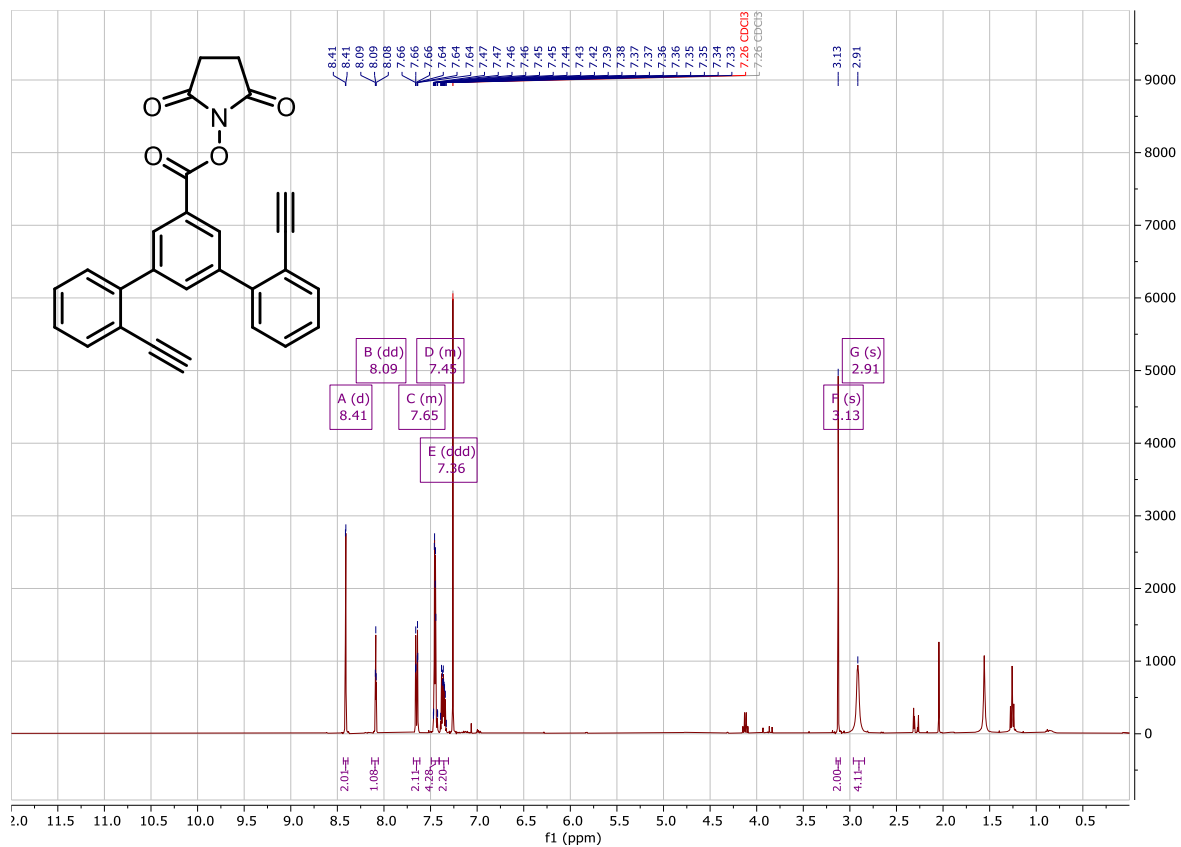


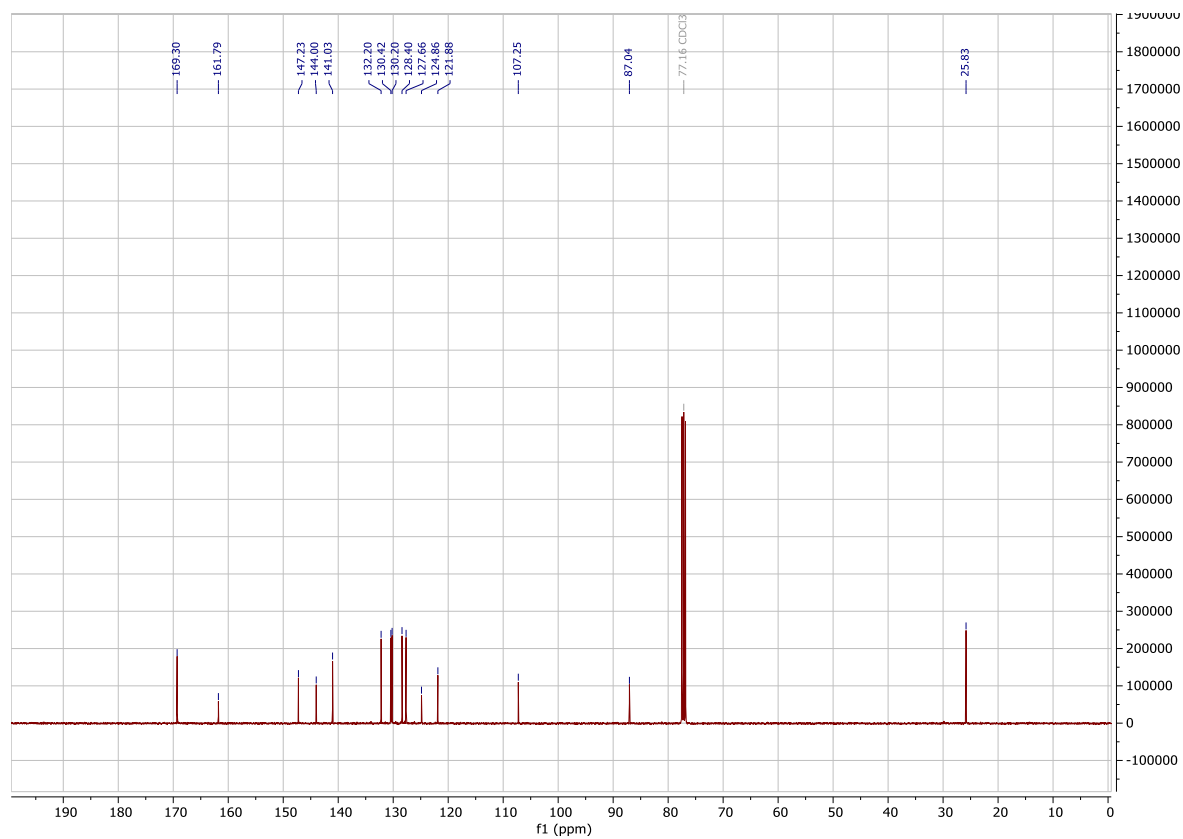
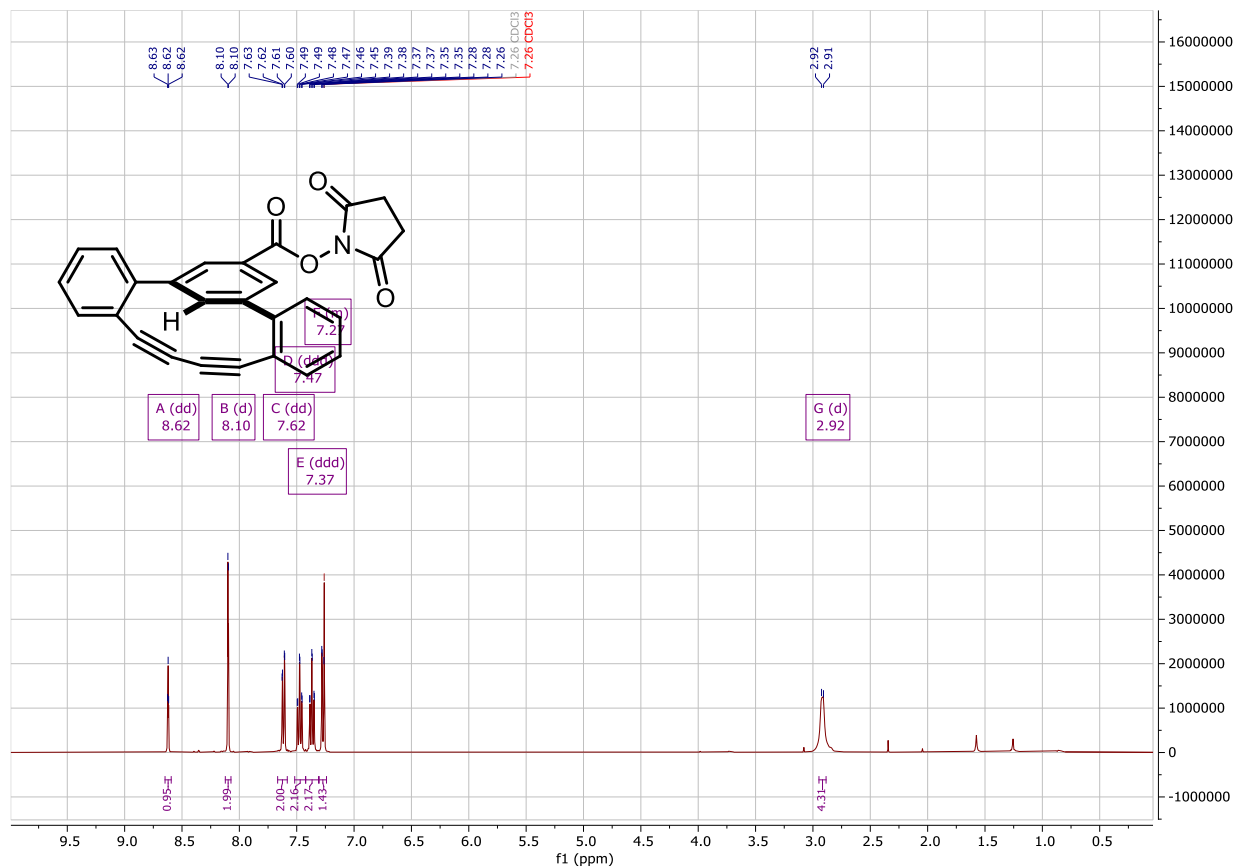


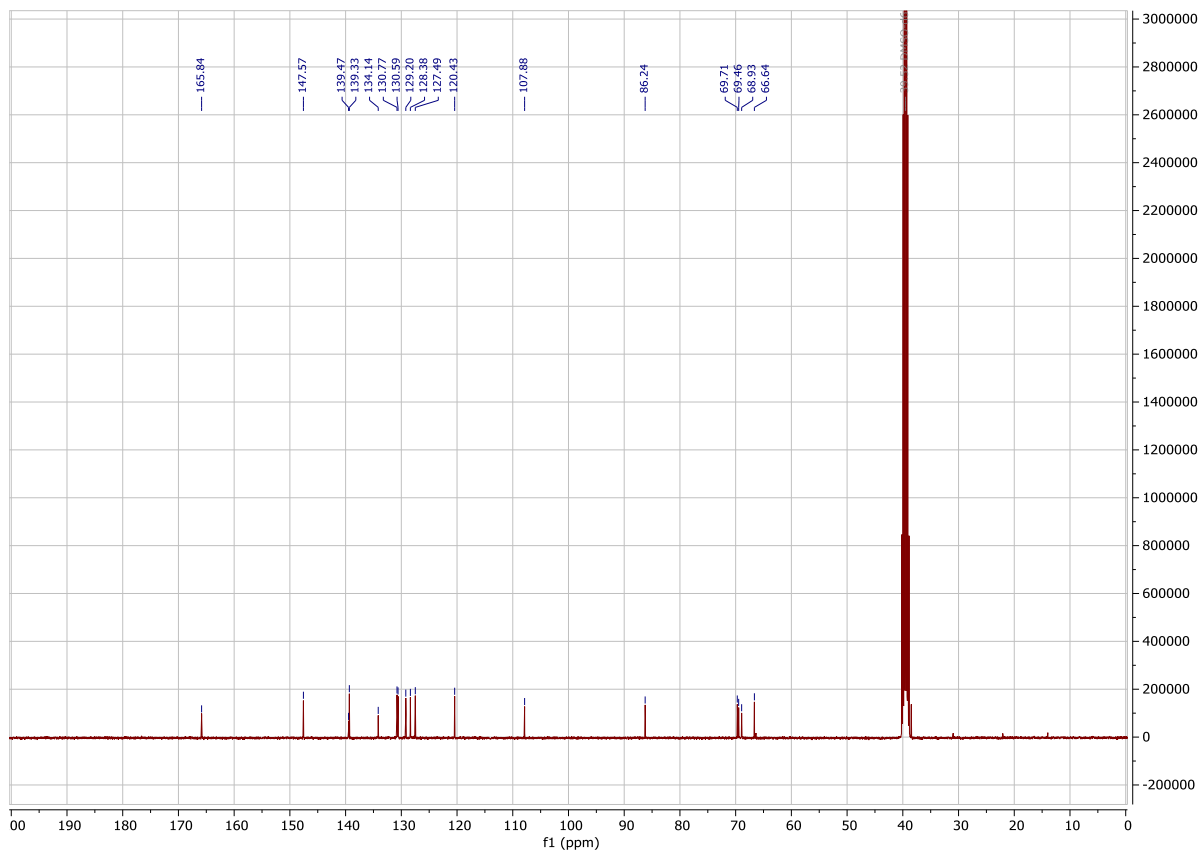
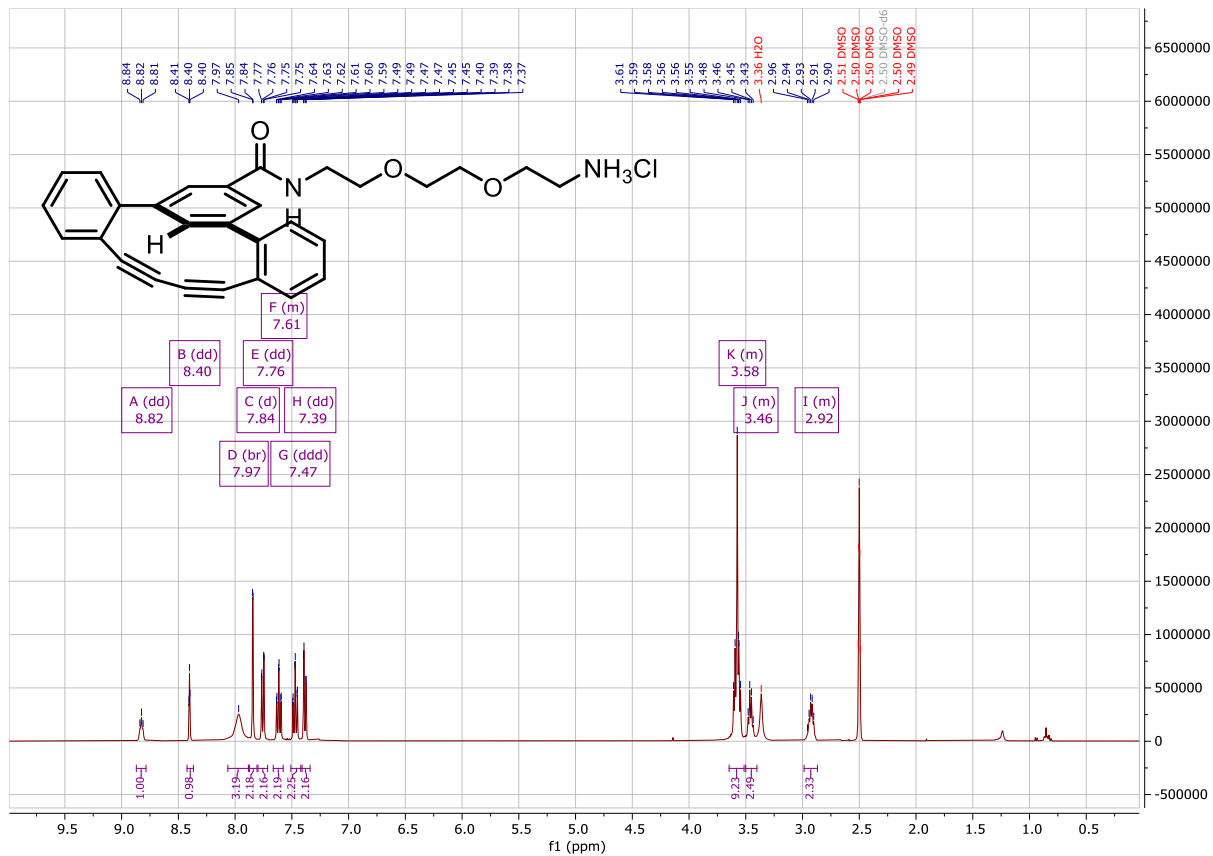


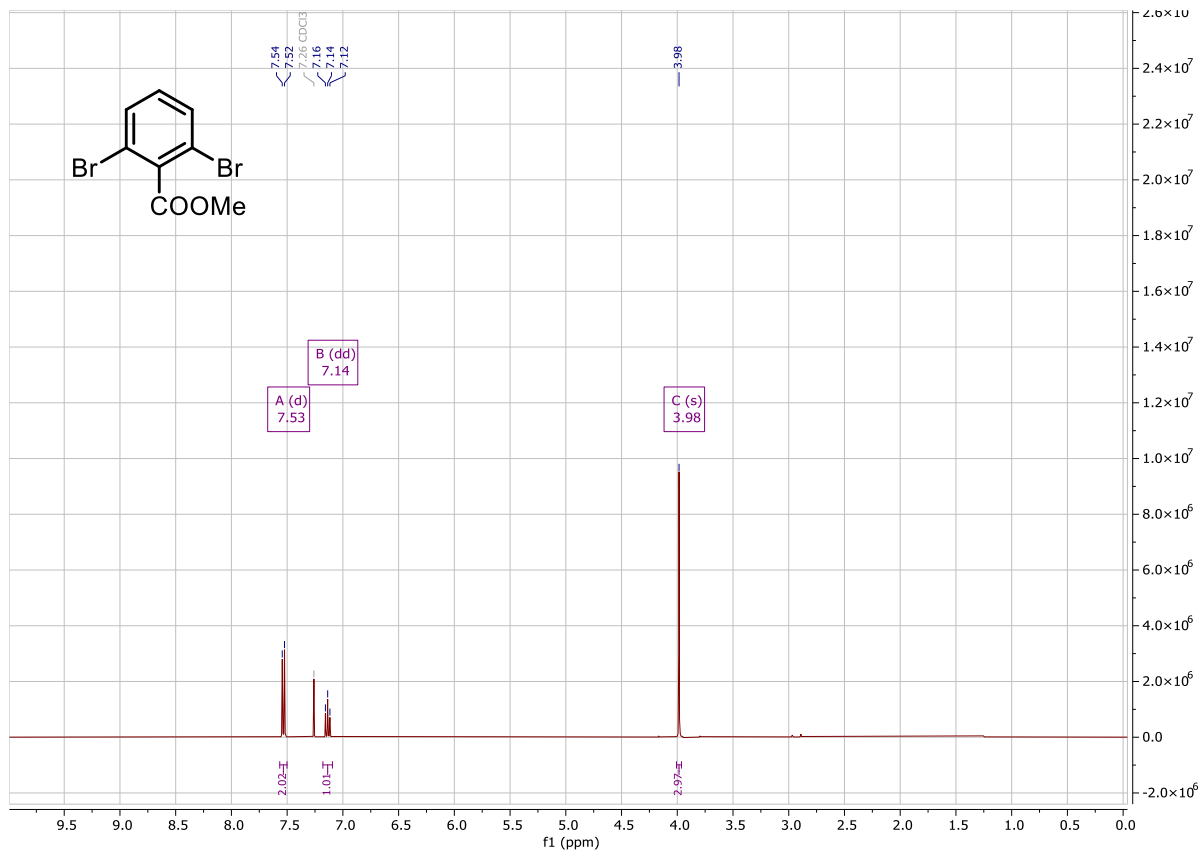


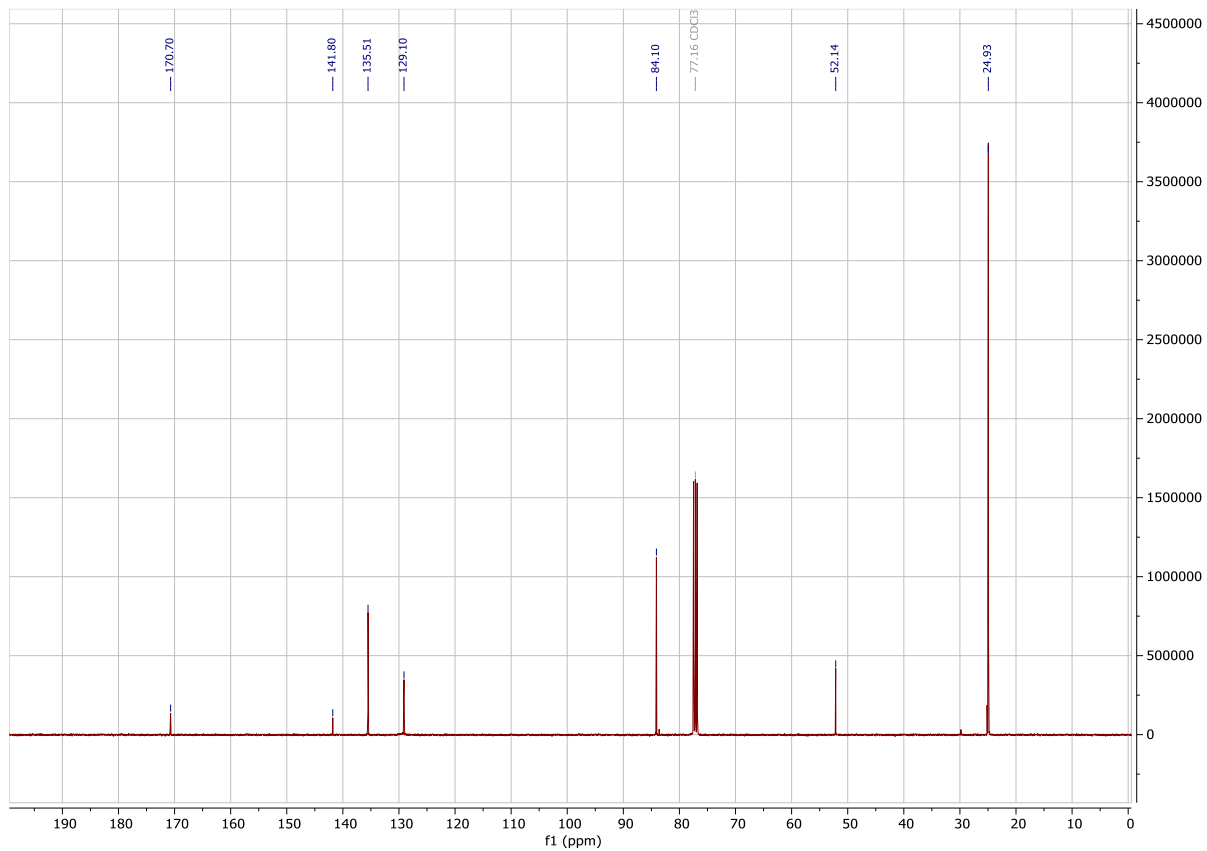
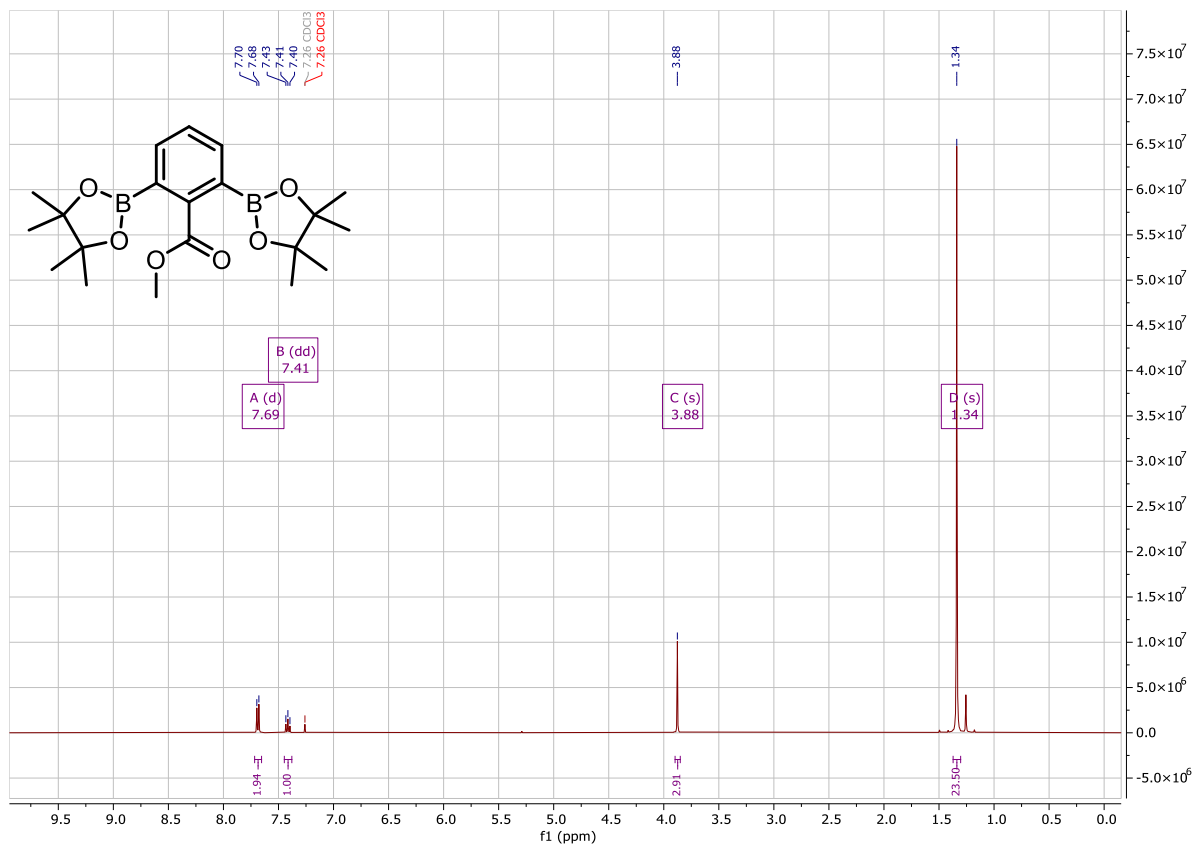


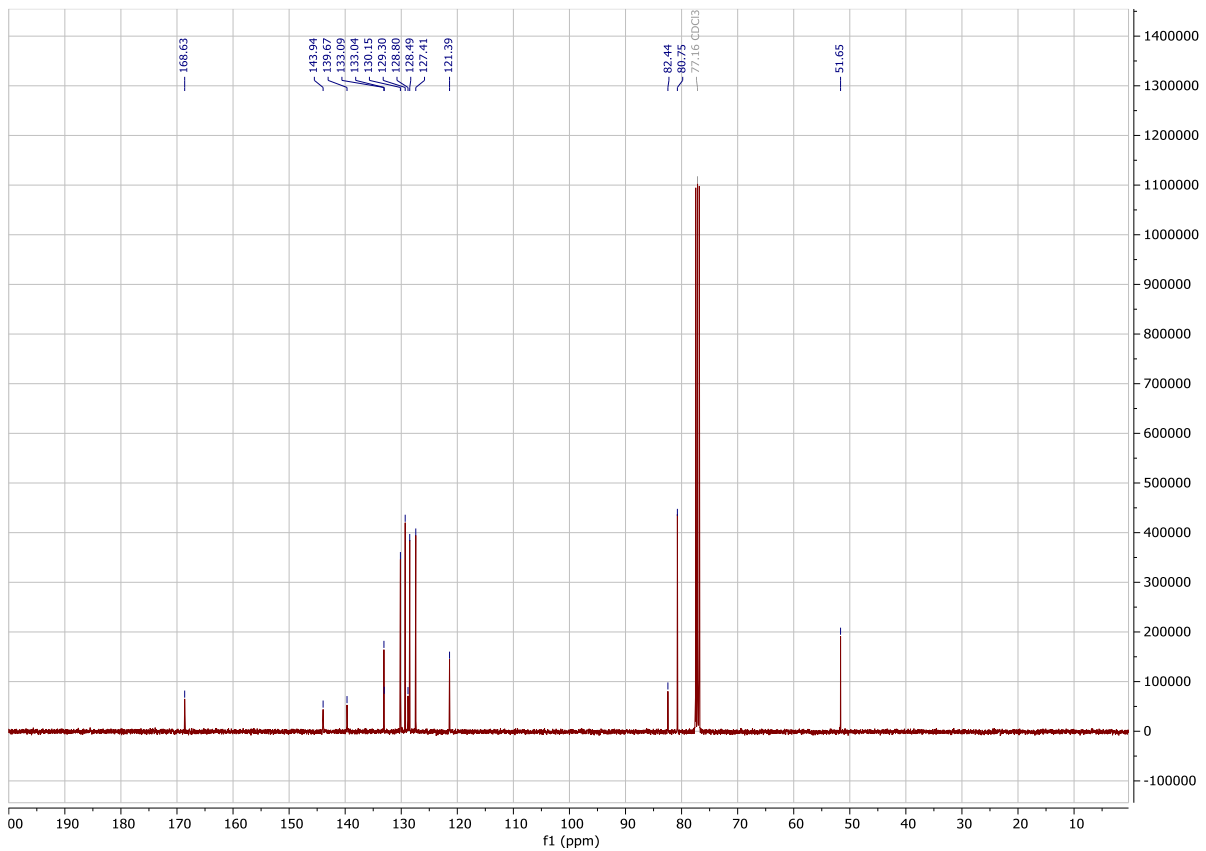
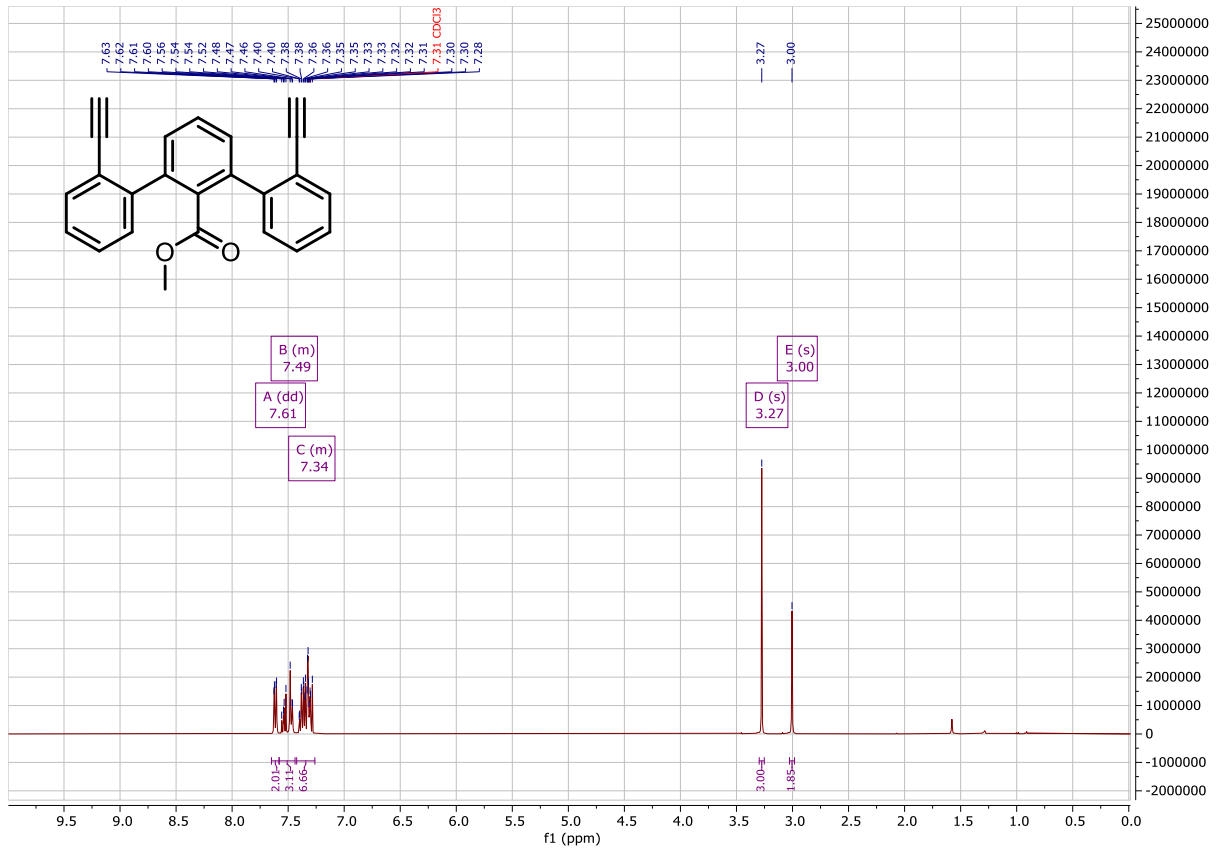


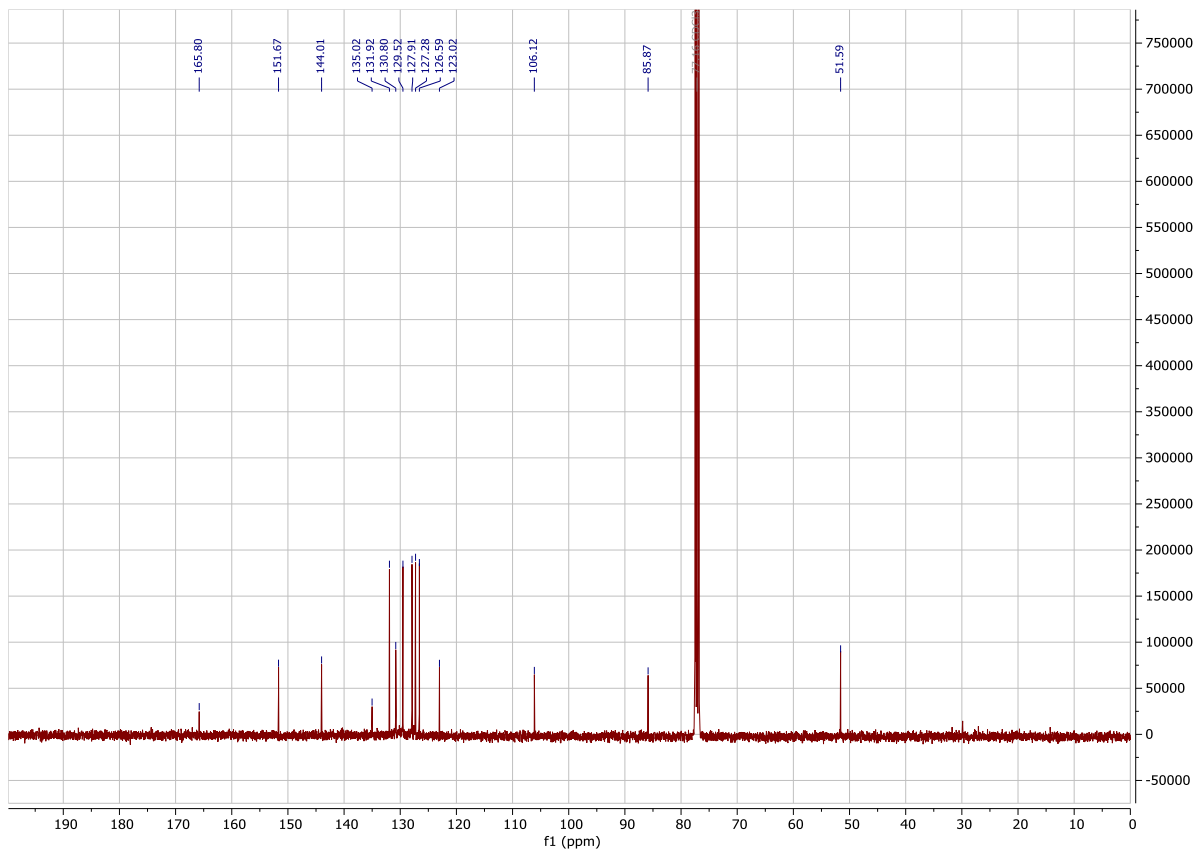
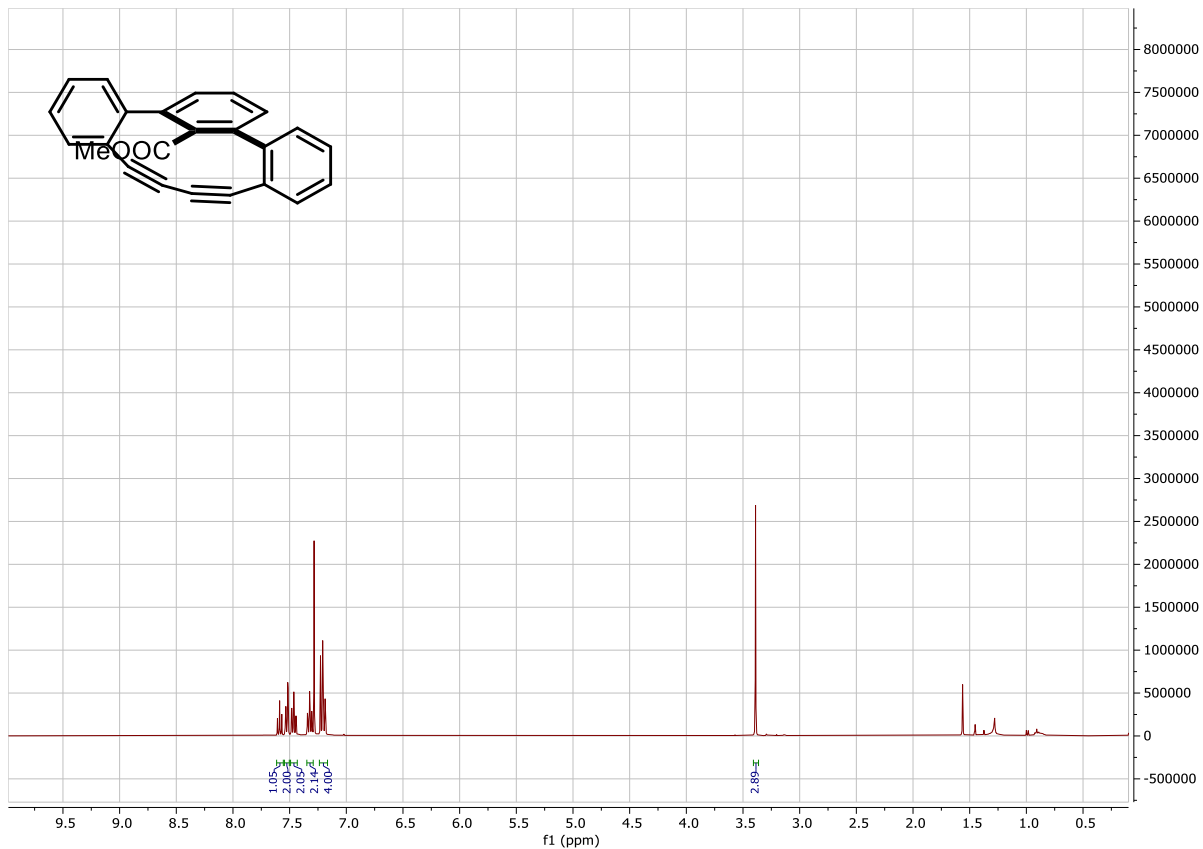


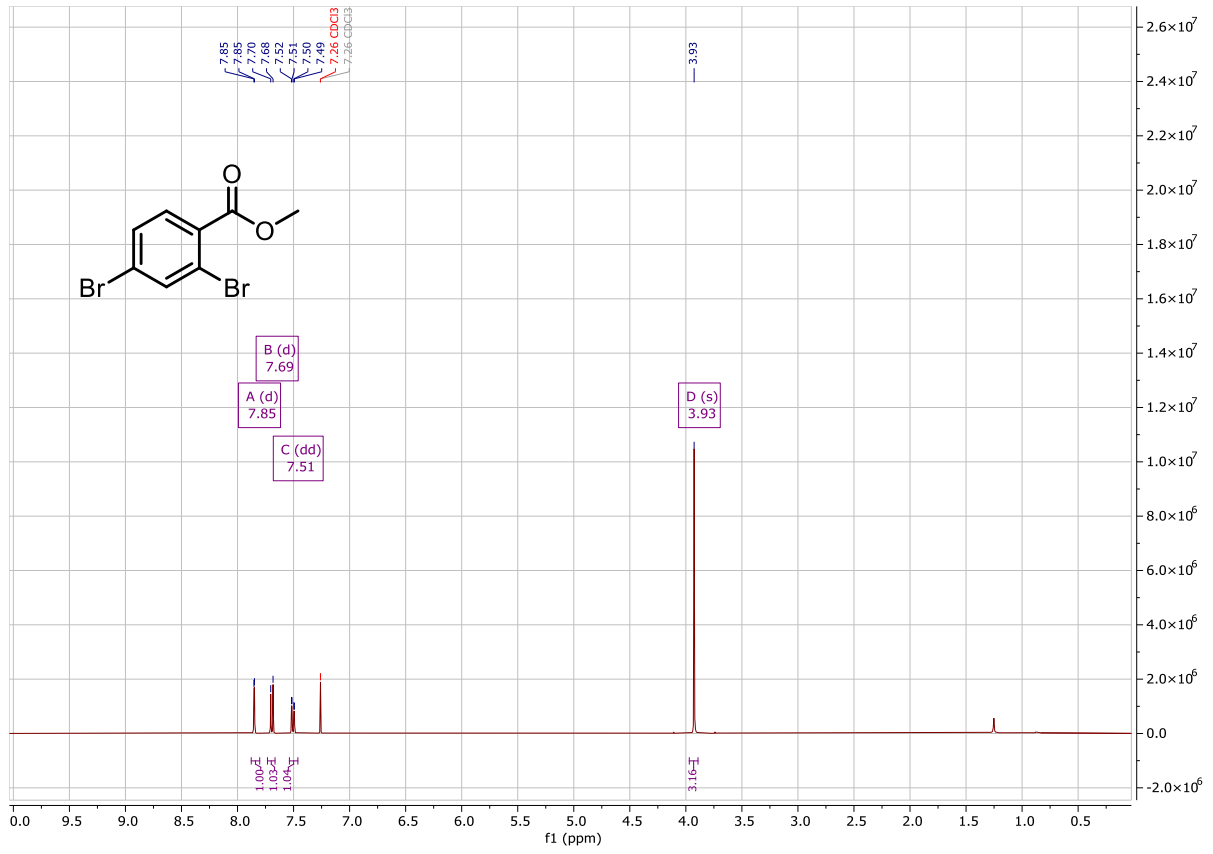


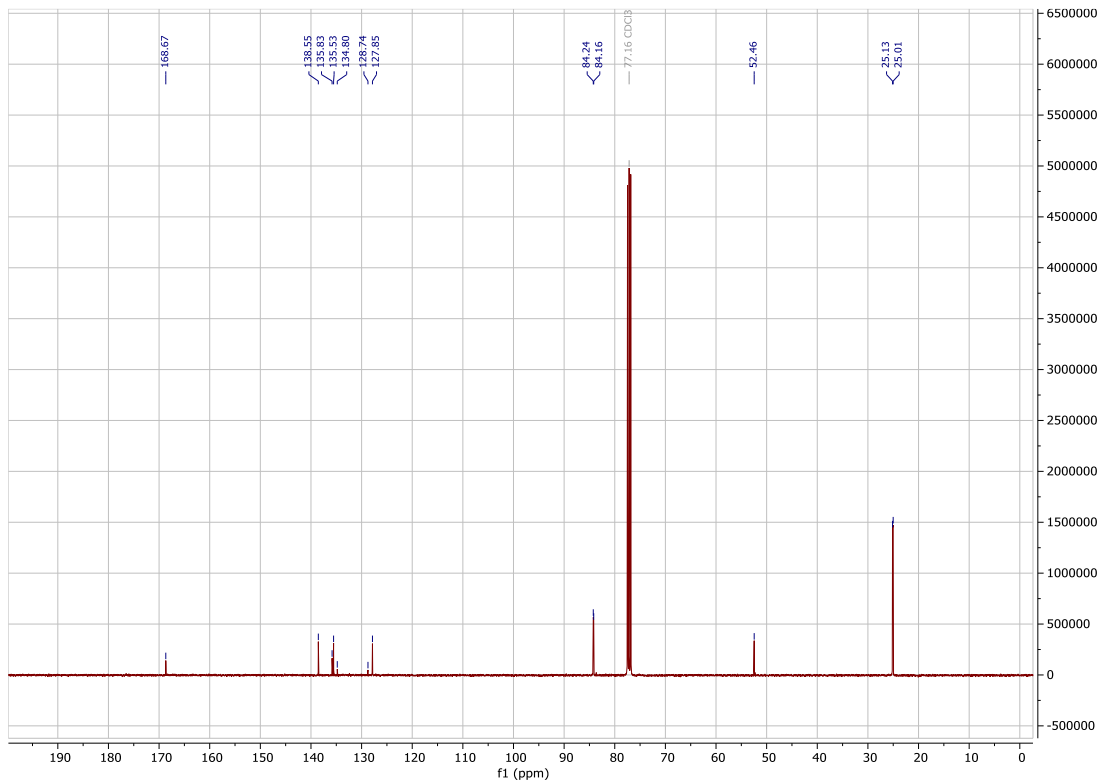
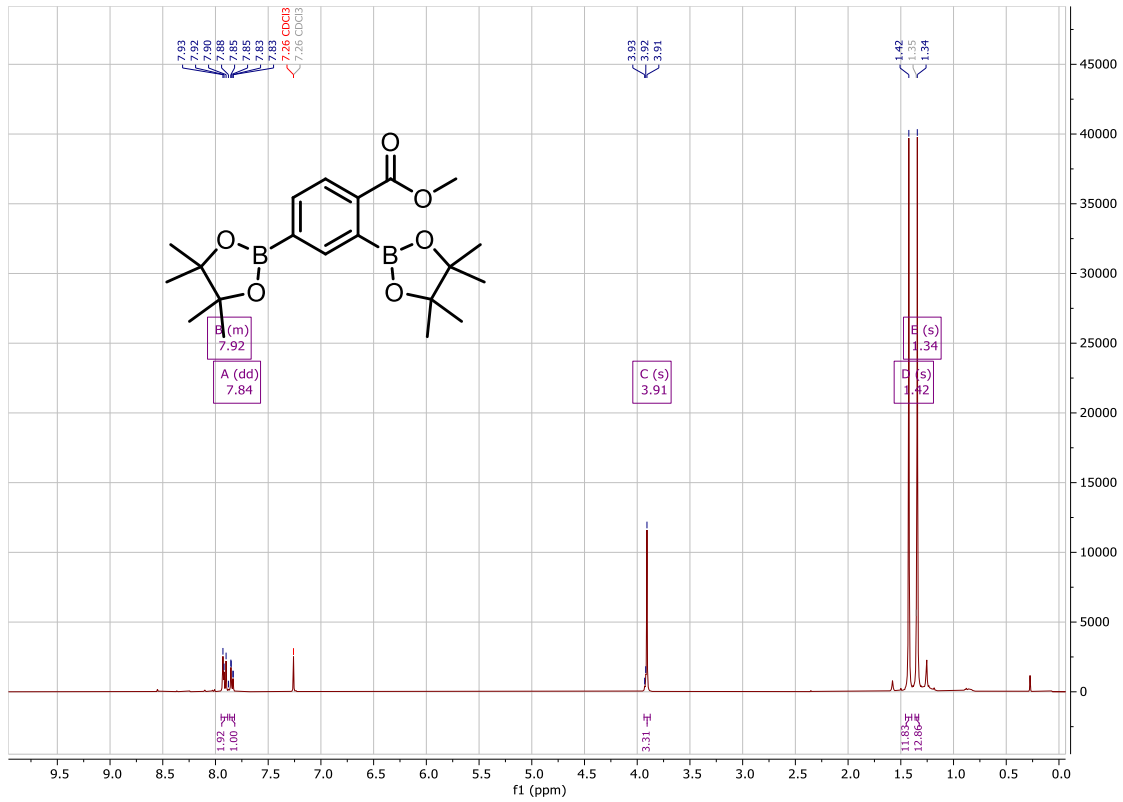


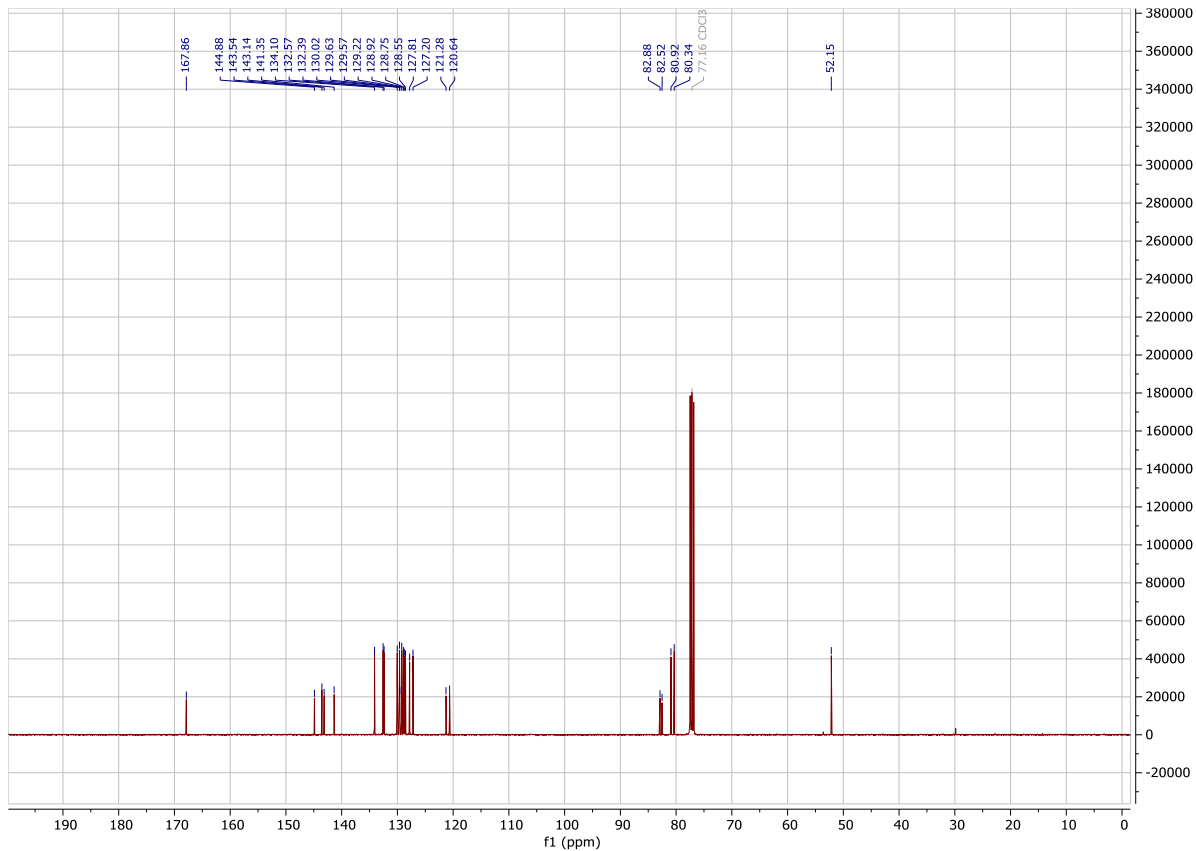
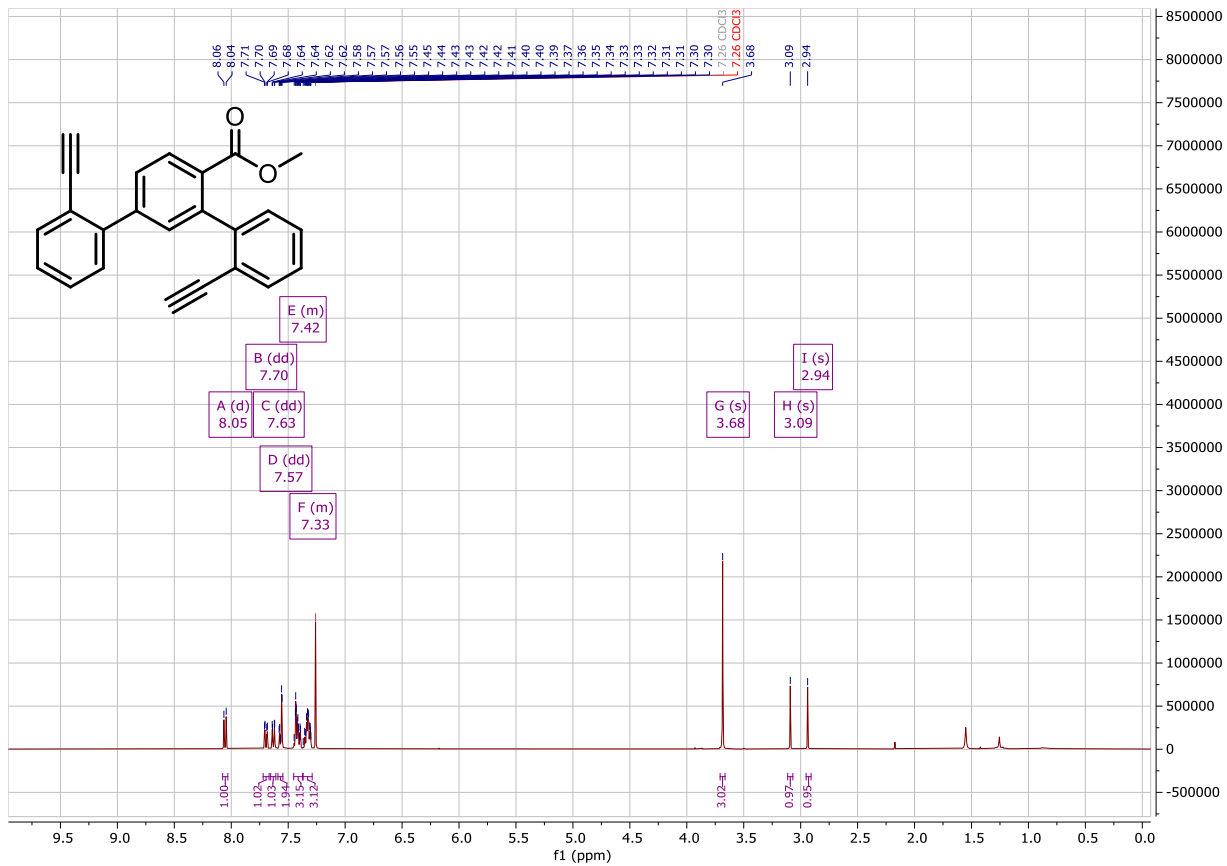


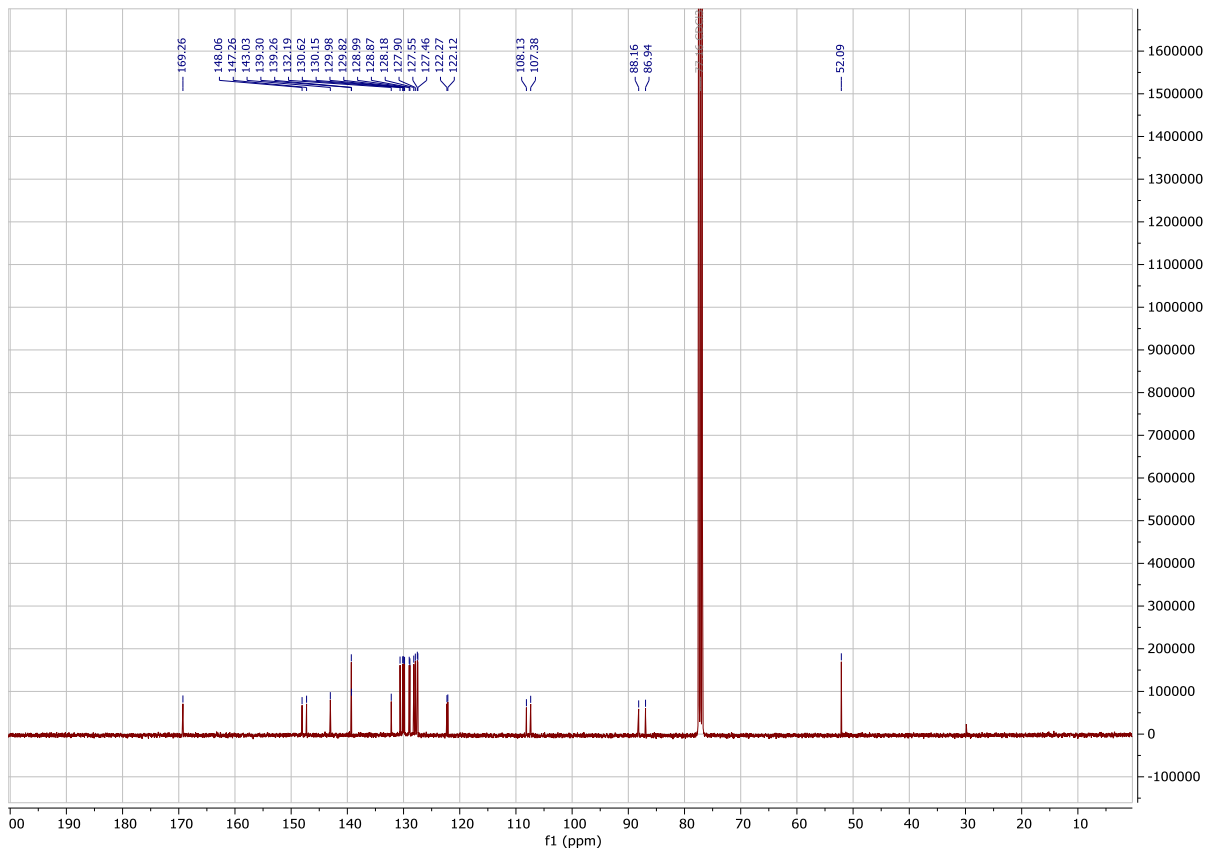
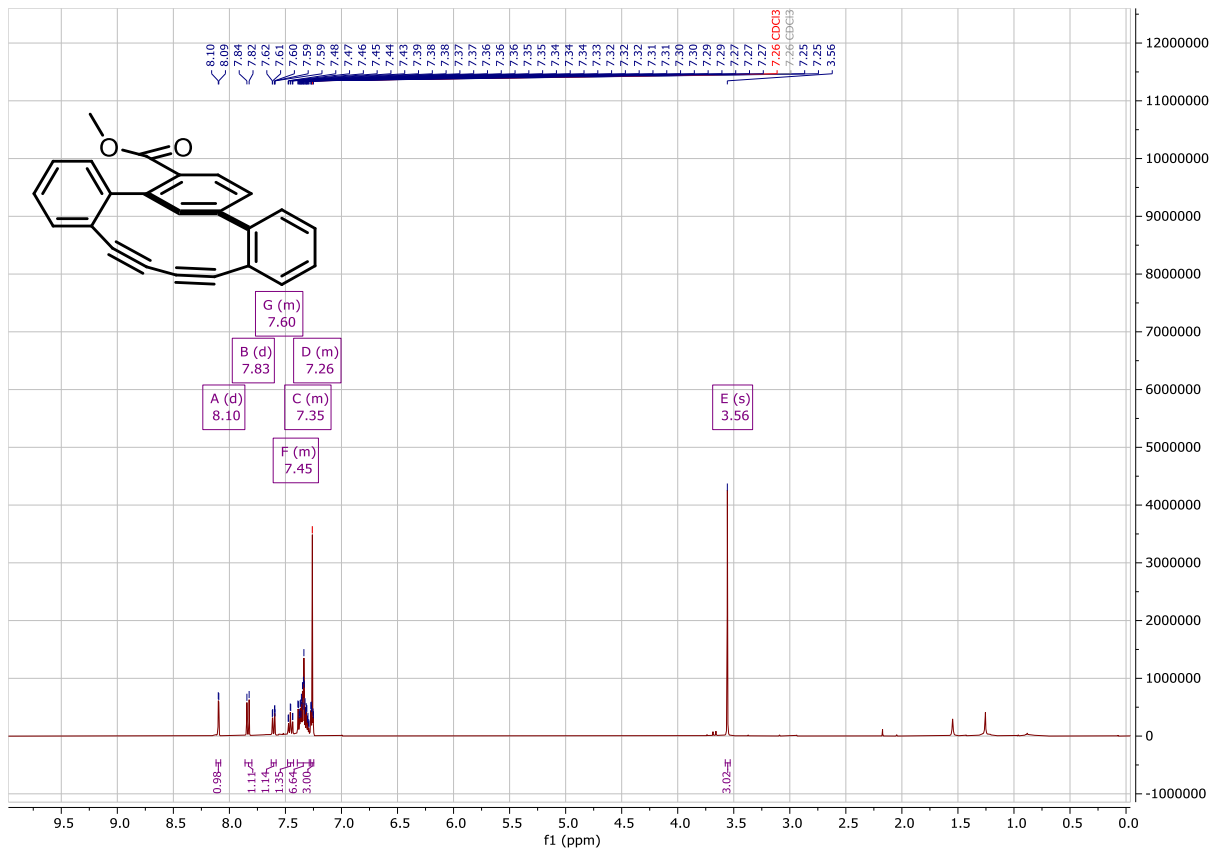


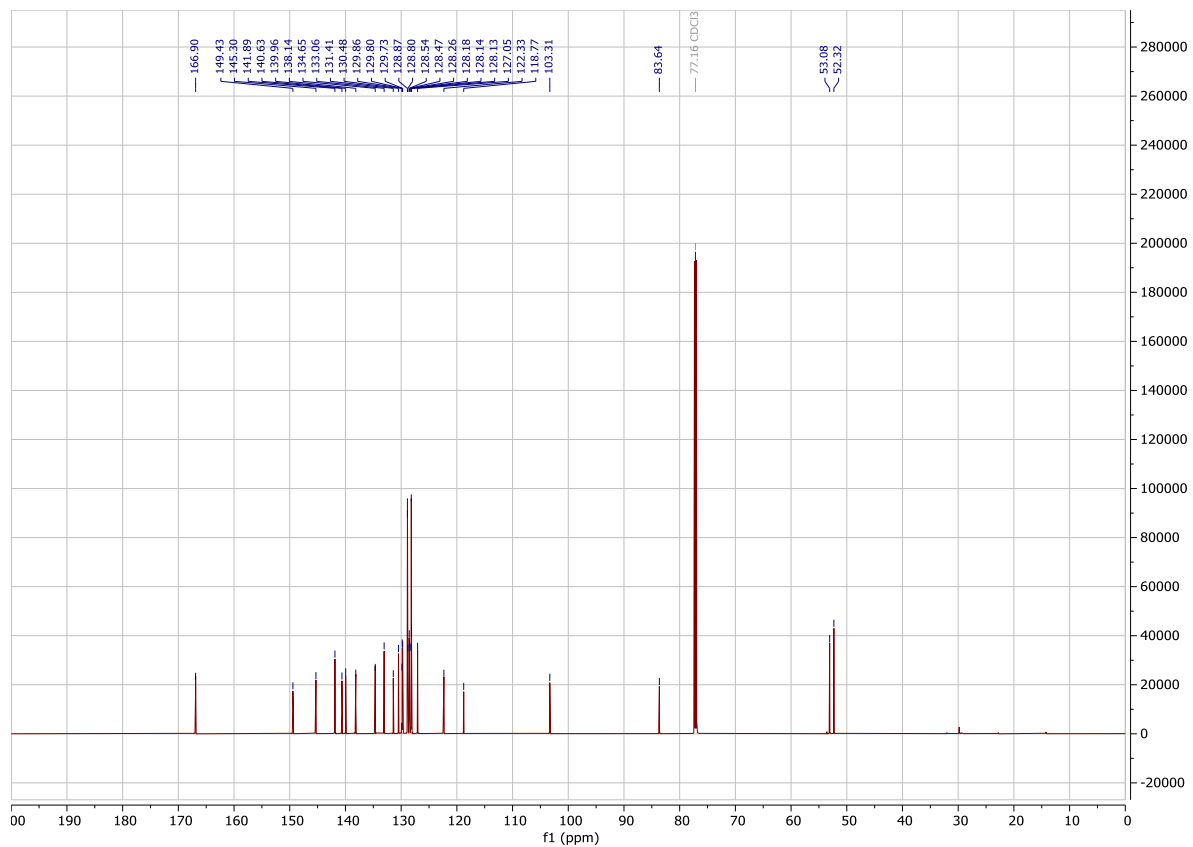
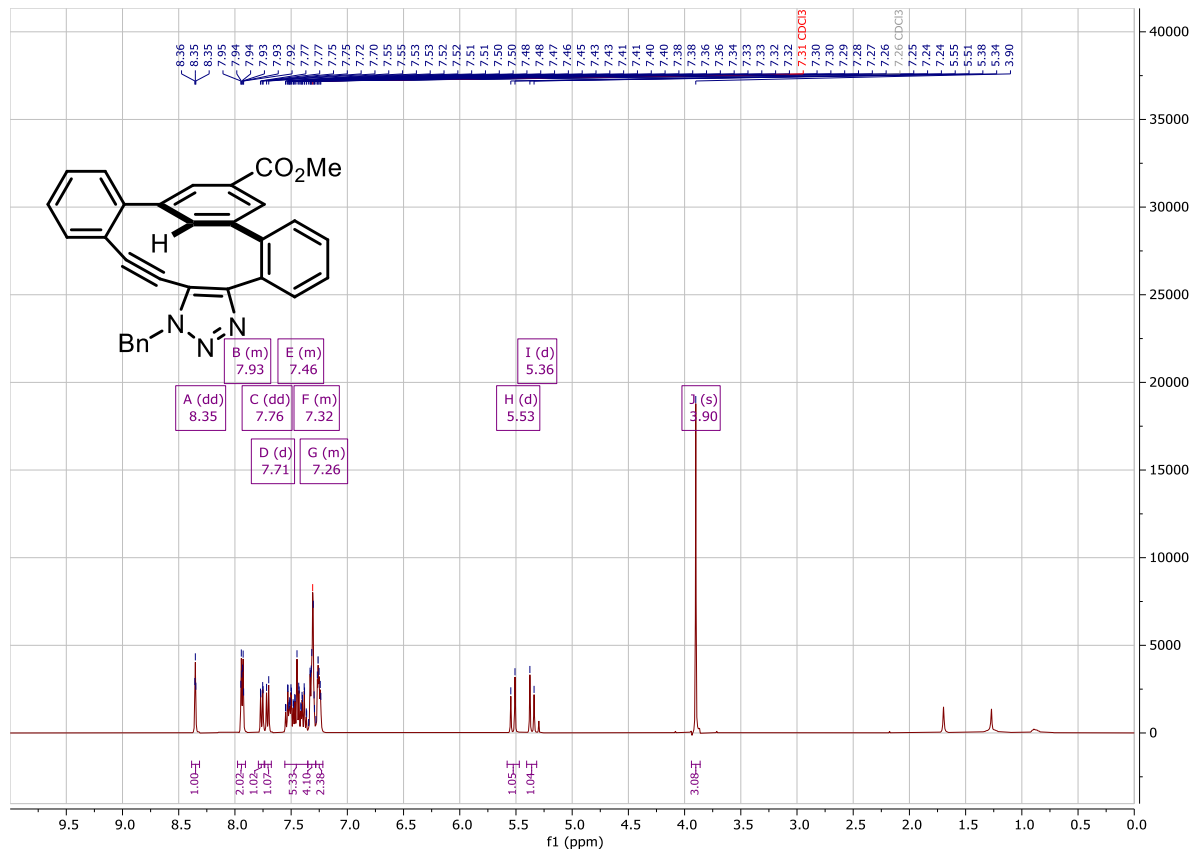


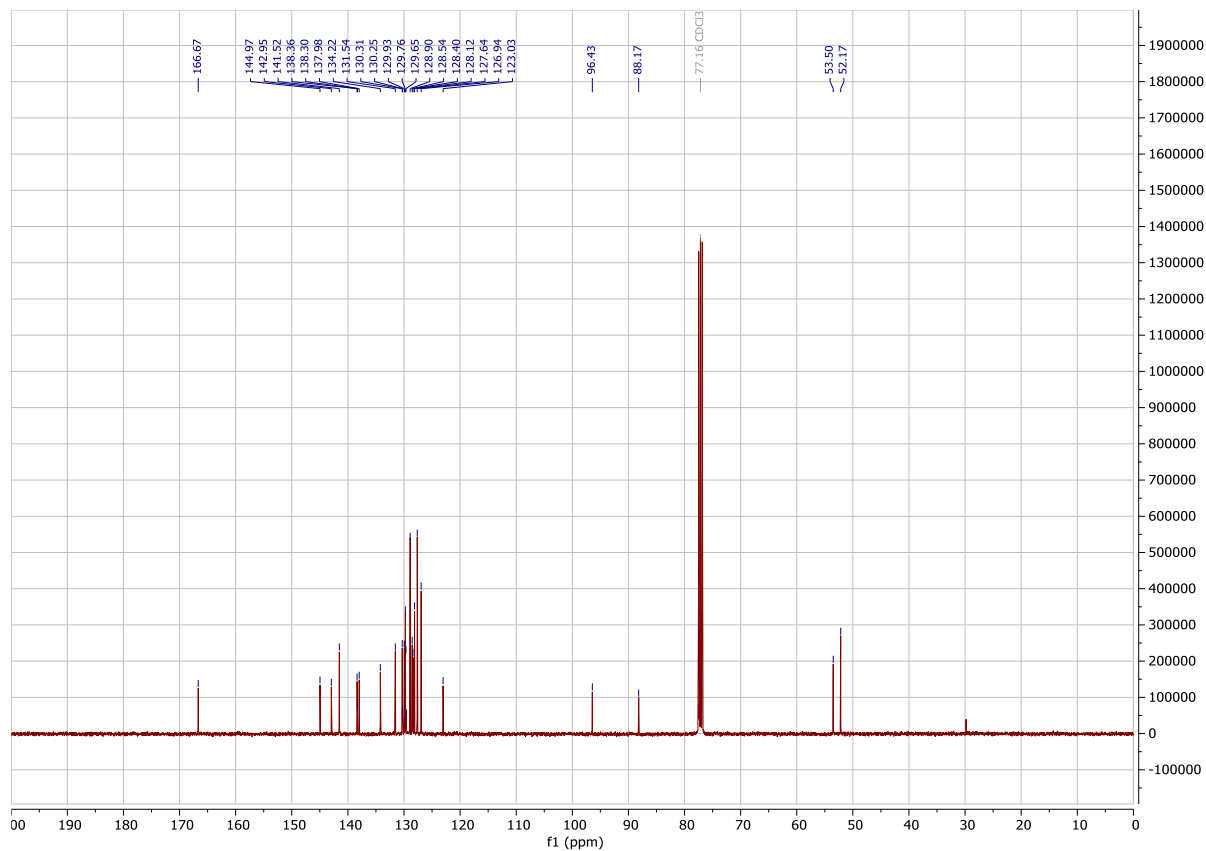
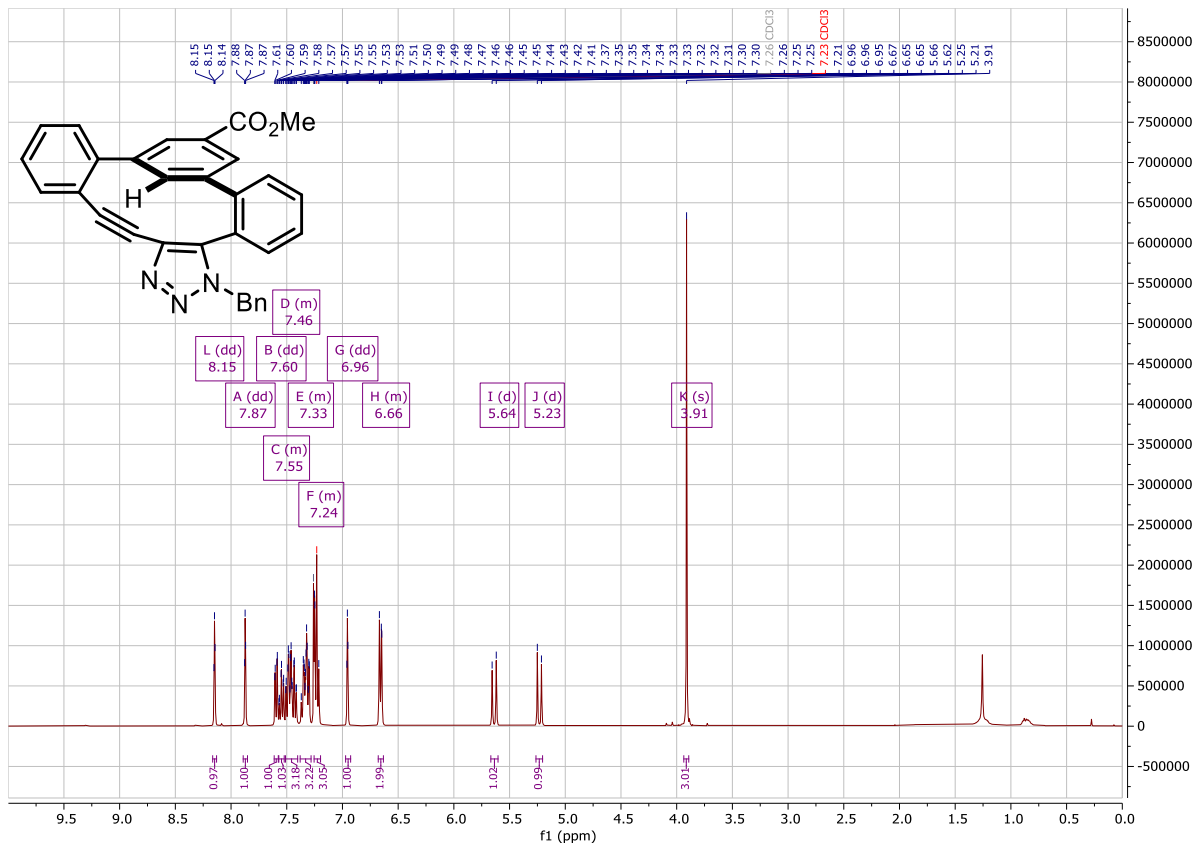


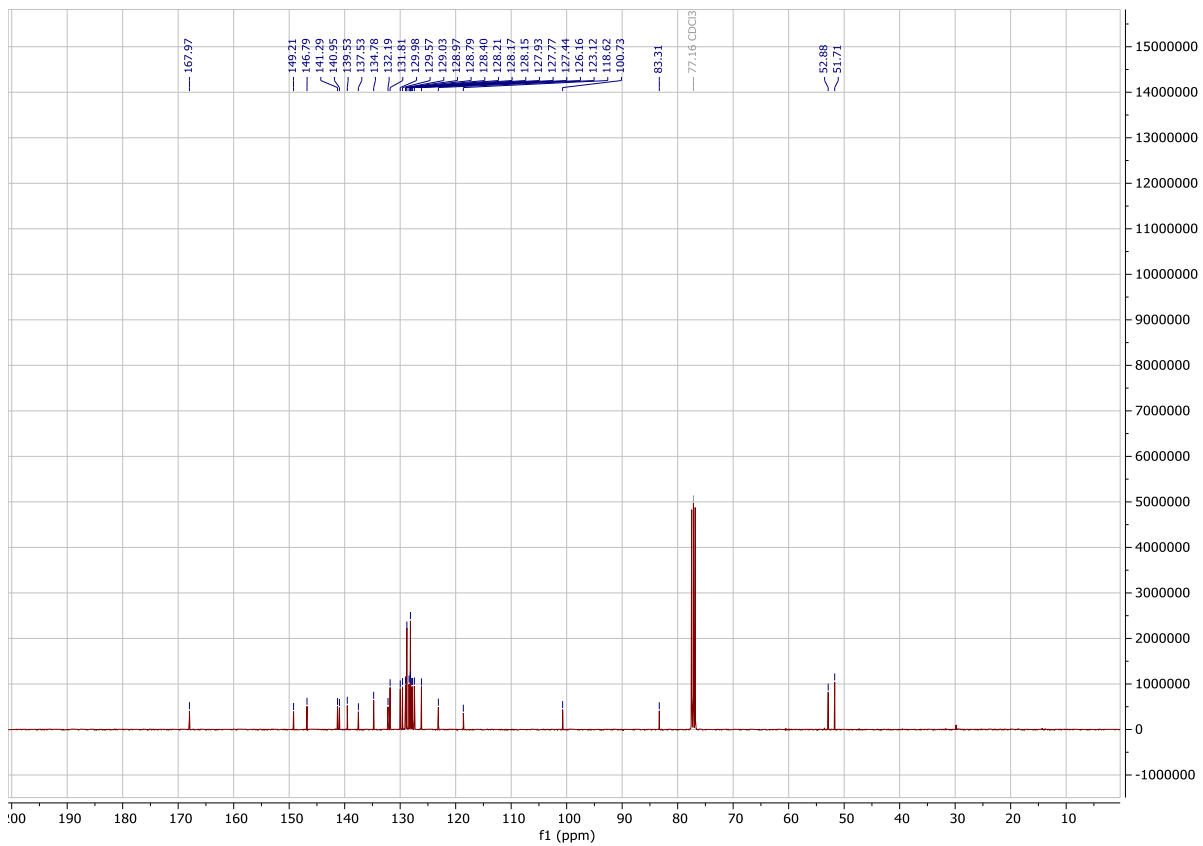
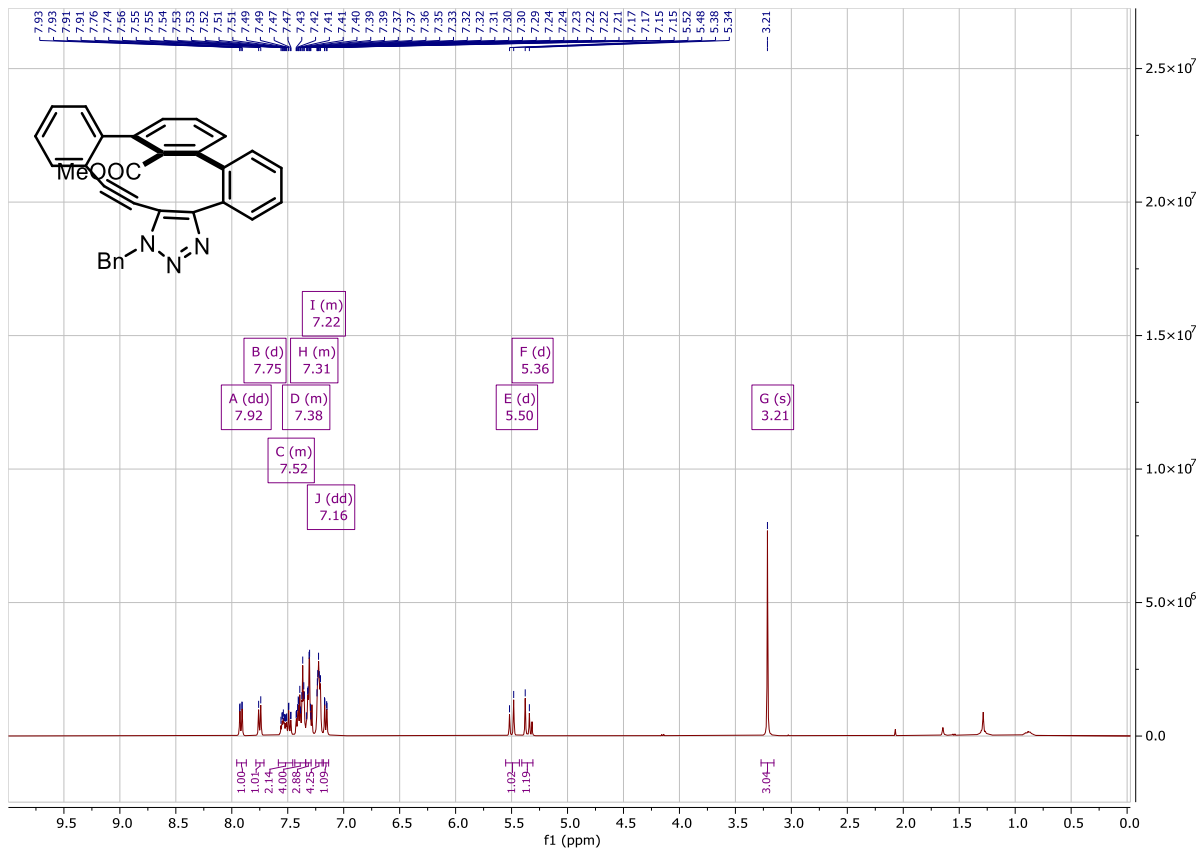


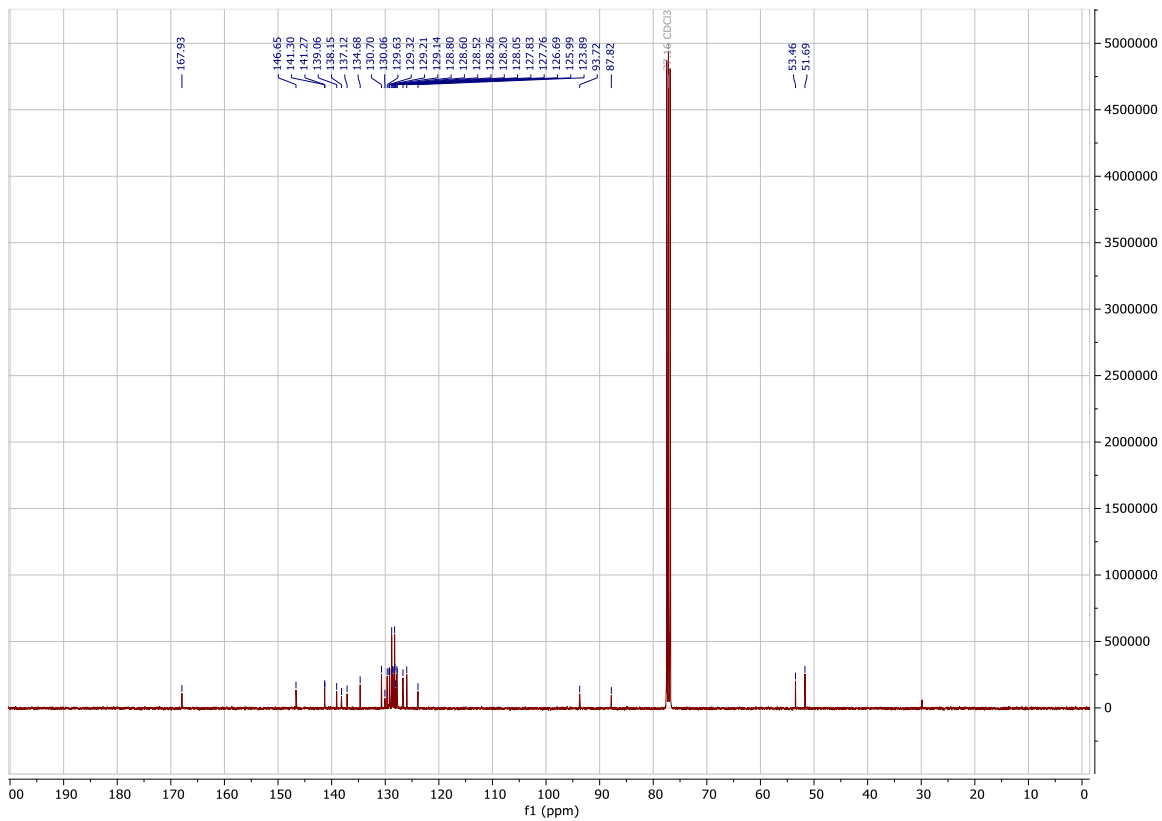
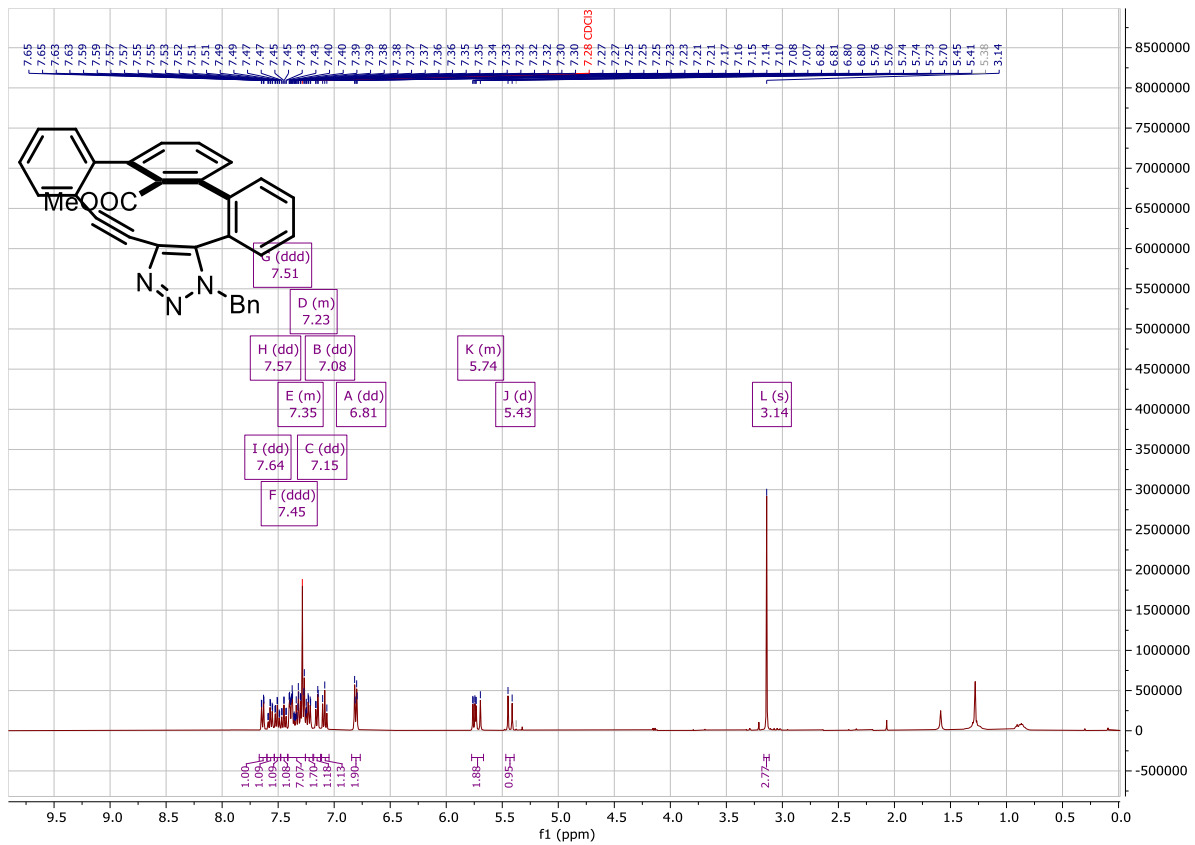




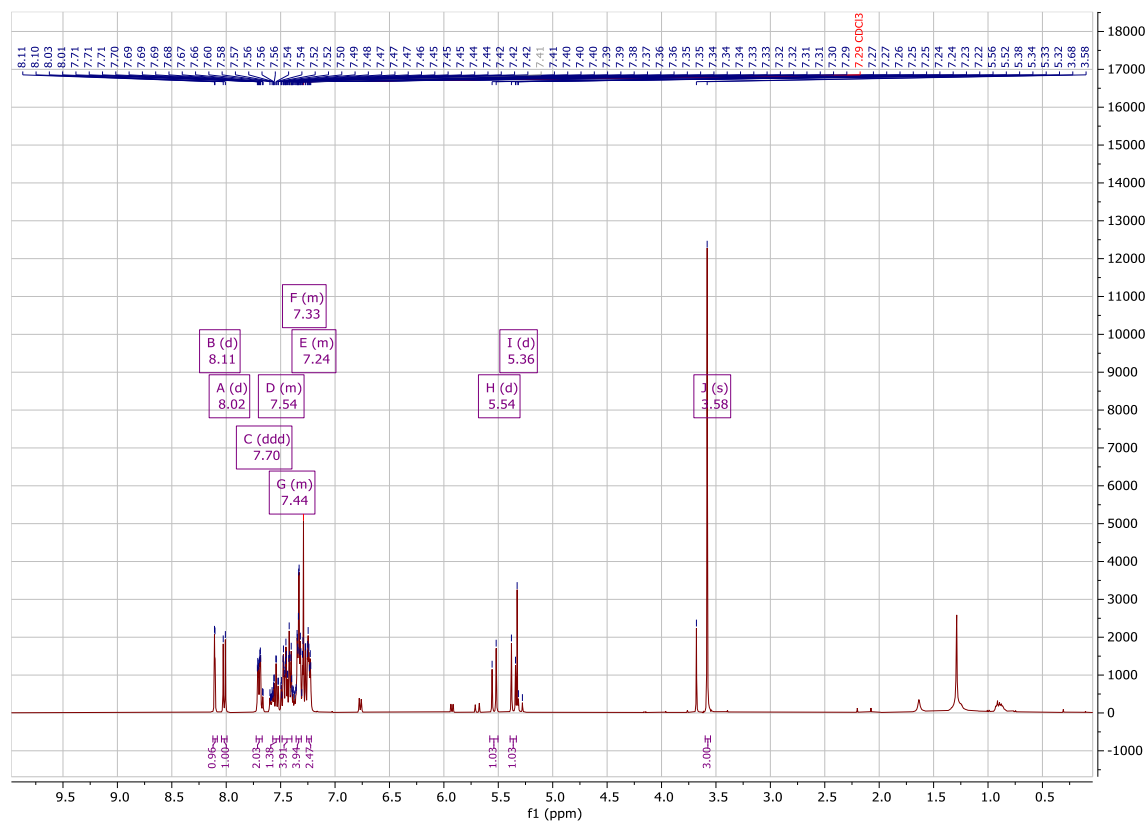
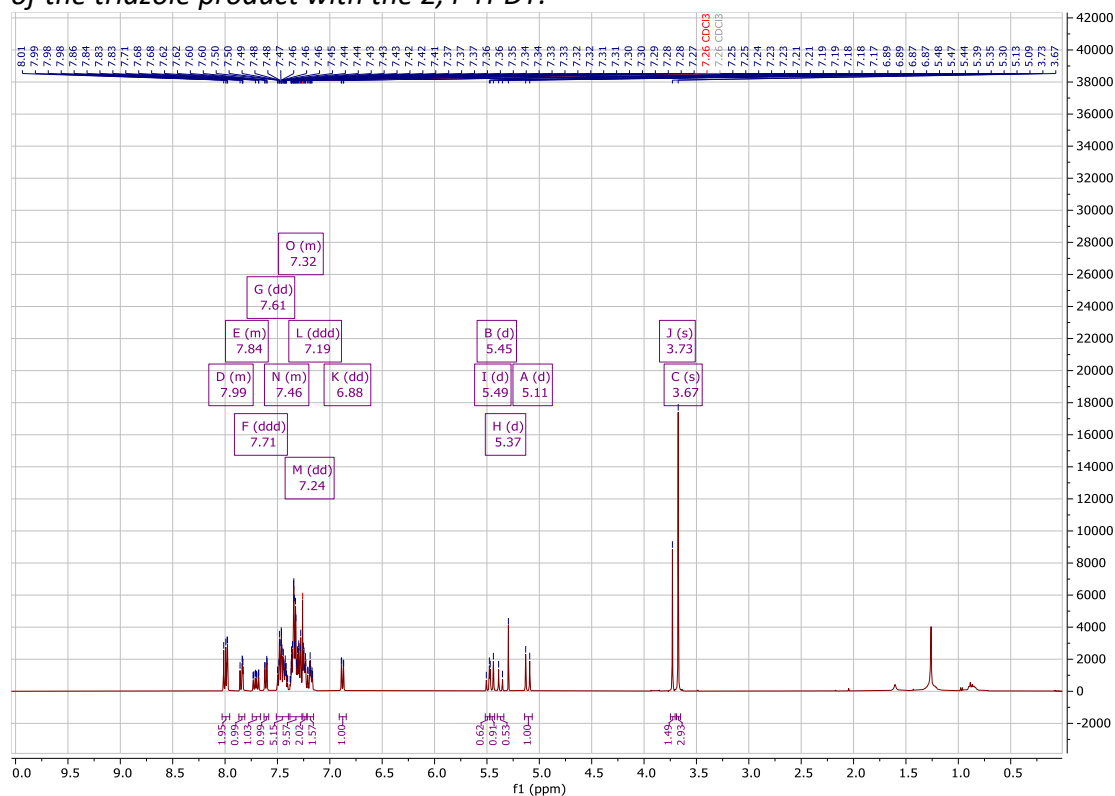


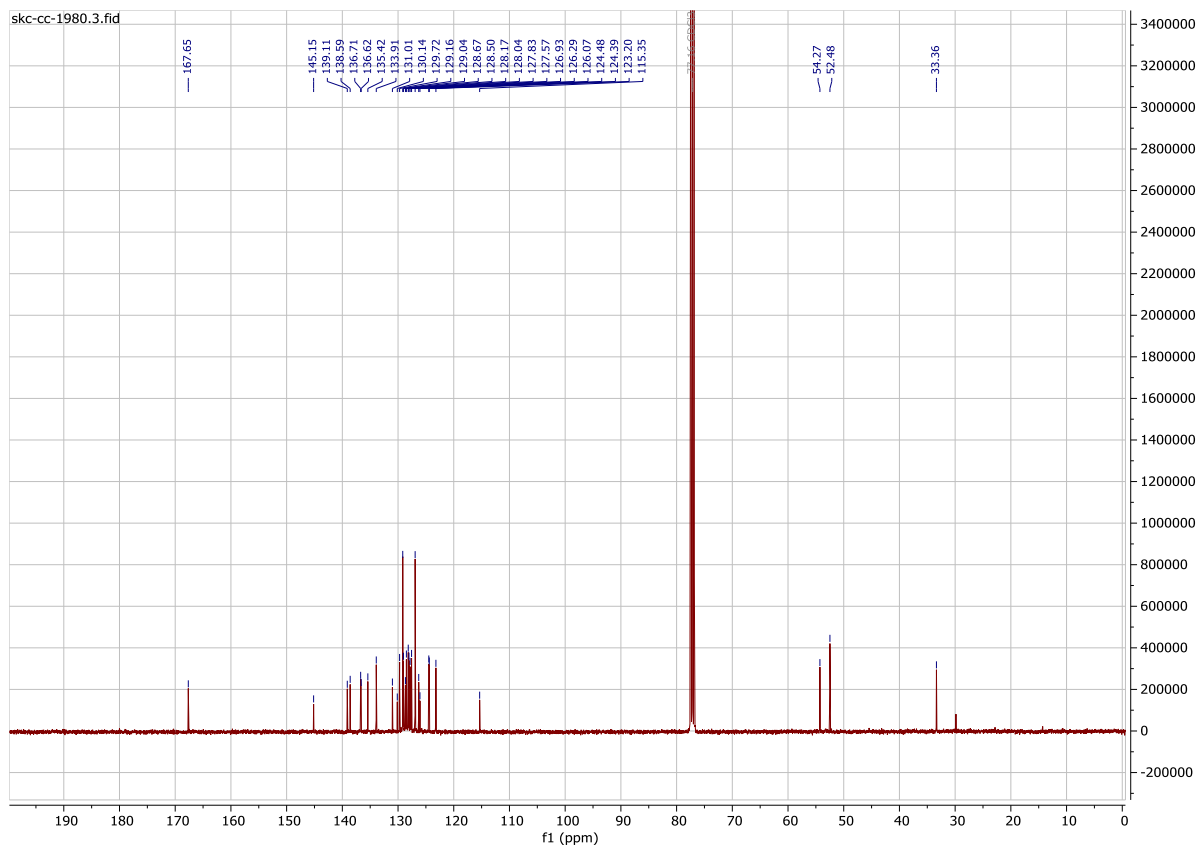
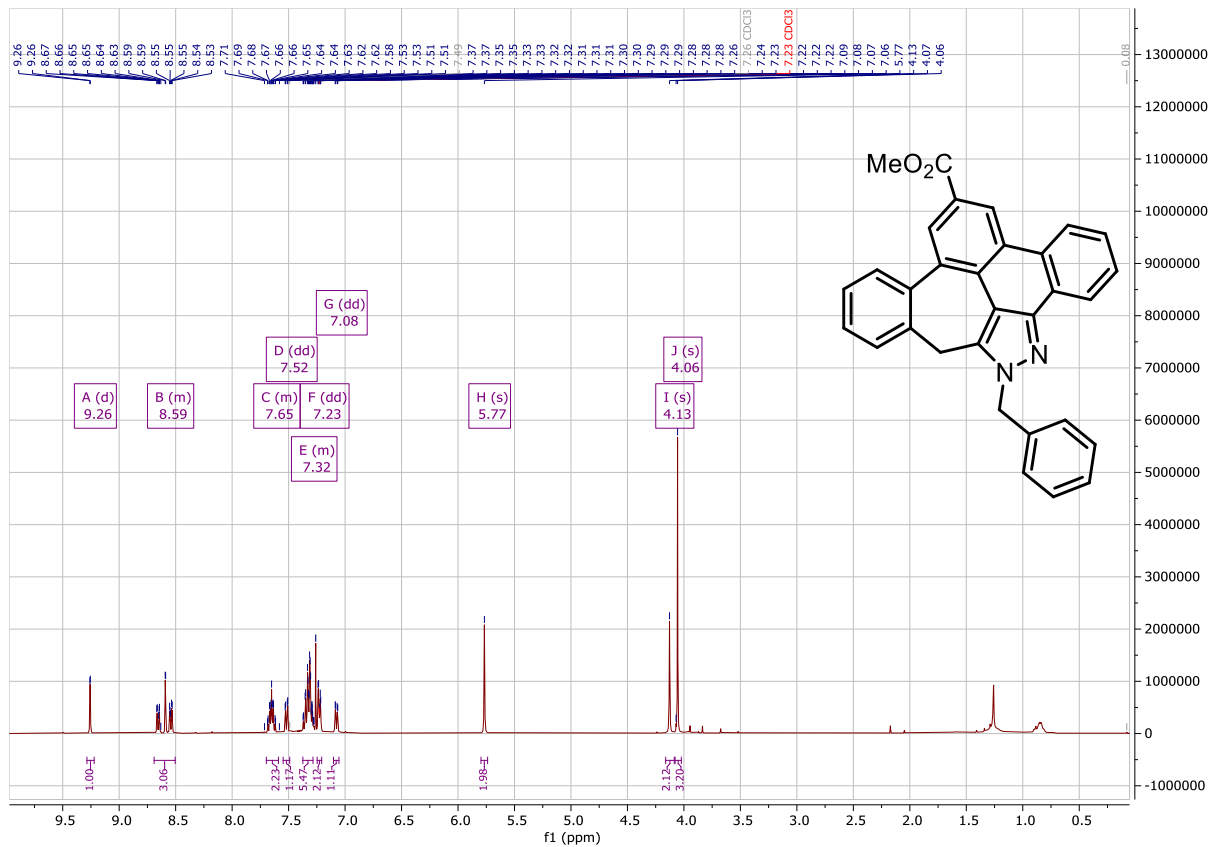






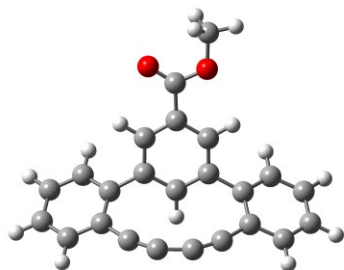
Note : The two following NMR spectra represent two mixtures containing each two regioisomers of the triazole product with the 2,4-TPDY.





A6.7 Computational Structures

3,5-TPDY



Number of imaginary frequencies: 0

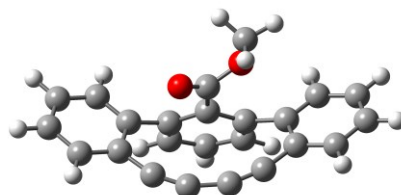
E = -1073.452807

H (298K) = -1073.127581

G (298K) = -1073.198268

Symbol	X	Y	Z
O	0.5123230	4.2936100	-0.4710090
O	-1.7049080	3.8714530	-0.4449780
C	-1.1499300	-0.1637210	0.3847040
C	-2.3510210	-1.0561010	0.4497340
C	-2.4651680	-2.2522400	-0.3280400
C	-1.3435290	-2.6587690	-1.1035110
C	-0.2122200	-2.7909490	-1.5539760
C	1.1376170	-2.5876950	-1.5623690
C	2.1842960	-2.1268710	-1.1236520
C	3.1453240	-1.4047210	-0.3623920
C	2.6923880	-0.2933220	0.4174760
C	1.2804670	0.2033630	0.3694840
C	0.1645940	-0.6318040	0.5645910
H	0.3221770	-1.6641610	0.8517030

2,6-TPDY



Number of imaginary frequencies : 0

E = -1073.441499

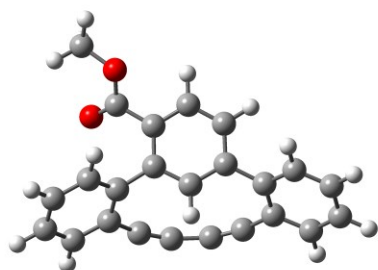
H (298K) = -1073.117169

G (298K) = -1073.187292

Symbol	X	Y	Z
C	4.8446340	0.4425250	0.6983280
C	5.0990610	-0.4572790	-0.3414750
C	3.5562830	0.9530270	0.8867660
C	2.4969260	0.5692780	0.0600140
C	2.7641500	-0.3402480	-1.0090620
C	4.0650470	-0.8430930	-1.1934060
H	4.2522950	-1.5329520	-2.0103960
H	5.6467560	0.7486960	1.3636080
H	6.0989070	-0.8537000	-0.4910600
H	3.3633610	1.6498100	1.6972180
C	1.6703840	-0.7182070	-1.8396810
C	0.5395300	-0.8706480	-2.2861420
C	-0.8235700	-0.8677860	-2.2937150
C	-1.9442530	-0.7208010	-1.8216260

C	1.0569950	1.5566120	0.0813080	C	-2.9861430	-0.4191310	-0.9000690
H	1.8943190	2.2270800	-0.0785650	C	-2.6399970	0.3955090	0.2220410
C	-0.2455580	2.0565830	-0.0346490	C	-4.2866630	-0.9364030	-1.0176130
C	-1.3425680	1.1951410	0.0943760	C	-5.2432220	-0.6707570	-0.0366580
H	-2.3459440	1.5761650	-0.0547030	C	-4.9084900	0.1187560	1.0664260
C	-0.4141840	3.5073110	-0.3370410	C	-3.6198580	0.6543700	1.1830730
C	-1.9584610	5.2642010	-0.7387330	H	-4.5344550	-1.5523380	-1.8765010
H	-1.5540140	5.9000270	0.0531430	H	-6.2442080	-1.0804390	-0.1339140
H	-3.0436430	5.3553590	-0.7847560	H	-5.6478390	0.3255340	1.8347240
H	-1.5104750	5.5382940	-1.6973460	H	-3.3692610	1.2802860	2.0347790
C	-3.4496340	-0.6785020	1.2341380	C	-1.3127180	1.0972640	0.2754560
H	-3.3792360	0.2246220	1.8333250	C	-1.3474510	2.4790790	0.0290100
C	-4.6212570	-1.4398270	1.2700770	C	-0.0549440	0.4706250	0.4634750
H	-5.4494780	-1.1222150	1.8967820	C	1.1417300	1.1956790	0.2136260
C	-4.7247290	-2.6049420	0.5041680	C	-0.1733230	3.2182810	-0.0929970
H	-5.6341620	-3.1978640	0.5259920	C	1.0605850	2.5702810	-0.0439930
C	-3.6528600	-3.0075690	-0.2896220	H	-0.2201530	4.2866700	-0.2823320
H	-3.7208920	-3.9090380	-0.8904760	H	1.9735280	3.1241480	-0.2402080
C	3.6399210	0.3956700	1.1869460	H	-2.3099420	2.9650340	-0.0974980
H	3.3128970	1.2398260	1.7869500	C	-0.0120400	-0.9419660	0.9603940
C	4.9848570	0.0158150	1.2062380	O	-0.9019220	-1.7661150	0.8374230
H	5.6901160	0.5671430	1.8212200	O	1.1249410	-1.1974170	1.6356140
C	5.4186950	-1.0691030	0.4383990	C	1.3019620	-2.5501810	2.1073650
H	6.4632300	-1.3656140	0.4472470	H	0.5206400	-2.8108950	2.8261560
C	4.5039200	-1.7741170	-0.3408370	H	2.2811470	-2.5607080	2.5863440
H	4.8280580	-2.6167870	-0.9435190	H	1.2793620	-3.2499410	1.2675580

2,4-TPDY



Number of imaginary frequencies : 0

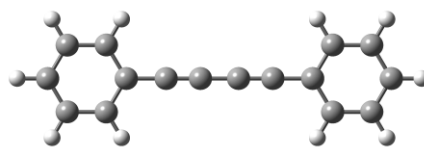
E = -1073.446071

H (298K) = -1073.121132

G (298K) = -1073.191448

Symbol	X	Y	Z
C	5.3037520	1.1179850	1.0761400
C	5.8634400	0.0464240	0.3734060
C	3.9227010	1.3306520	1.0468960
C	3.0641600	0.4819490	0.3347670
C	3.6455100	-0.6132240	-0.3802970
C	5.0391310	-0.8122400	-0.3507340
H	5.4621860	-1.6452280	-0.9034270
H	5.9389350	1.7881760	1.6479200
H	6.9362550	-0.1206700	0.3898440
H	3.4964930	2.1654510	1.5955890
C	2.7769080	-1.4912960	-1.0869820
C	1.7916270	-2.1009240	-1.4846590
C	0.4819480	-2.4824180	-1.4423880
C	-0.6493880	-2.4881400	-0.9724080
C	-1.7761140	-2.2009840	-0.1512040
C	-1.7993630	-0.9492490	0.5371660

1,4-diphenylbuta-1,3-diyne



Number of imaginary frequencies : 0

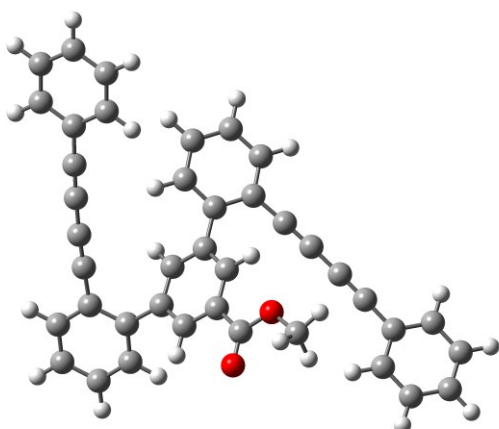
E = -615.697518

H (298K) = -615.481286

G (298K) = -615.538150

Symbol	X	Y	Z
C	-6.1356350	0.0001710	0.0001680
C	-5.4349140	-1.2118460	0.0041110
C	-4.0407390	-1.2187300	0.0040430
C	-3.3269430	-0.0000910	-0.0000280
C	-4.0405110	1.2186810	-0.0039970
C	-5.4346880	1.2120570	-0.0038750
C	-1.9037920	-0.0002260	-0.0001410
C	-0.6805300	-0.0002980	-0.0002220
C	0.6805300	-0.0000520	-0.0002990
C	1.9037920	0.0001650	-0.0003760
C	3.3269430	0.0000900	-0.0001410
C	4.0405640	-1.2186530	-0.0040500
C	5.4347390	-1.2119710	-0.0038220
C	6.1356350	-0.0000550	0.0002740
C	5.4348620	1.2119320	0.0041630
C	4.0406870	1.2187580	0.0039890

C	-2.8160170	-3.1297960	0.0428960	H	-7.2218410	0.0002720	0.0002440
C	-3.8623480	-2.8480060	0.9186340	H	-5.9758780	-2.1536950	0.0072370
C	-3.8779250	-1.6358100	1.6159800	H	-3.4946960	-2.1569280	0.0070720
C	-2.8582230	-0.7017370	1.4189080	H	-3.4942940	2.1567780	-0.0071090
H	-2.7873350	-4.0713670	-0.4964390	H	-5.9754760	2.1540080	-0.0069290
H	-4.6574770	-3.5735960	1.0617080	H	3.4943860	-2.1567720	-0.0072040
H	-4.6839170	-1.4142690	2.3093950	H	5.9755680	-2.1538990	-0.0068330
H	-2.8840530	0.2430570	1.9550010	H	7.2218410	-0.0001110	0.0004340
C	-0.7593750	0.1058480	0.3086470	H	5.9757860	2.1538050	0.0073310
C	-1.1244930	1.3969340	-0.1381640	H	3.4946050	2.1569340	0.0069750
C	0.6011420	-0.1518800	0.5418650				
C	1.6031120	0.7955050	0.2658110				
C	-0.1409560	2.3814120	-0.3119680				
C	1.2068040	2.0816060	-0.1372040				
H	-0.4337820	3.3715190	-0.6449830				
H	1.9572150	2.8364780	-0.3505270				
H	0.8866050	-1.1229620	0.9287140				
C	-2.5252810	1.7194250	-0.5503050				
O	-3.2464110	0.9850110	-1.2042920				
O	-2.8948460	2.9512290	-0.1498420				
C	-4.2028180	3.3973590	-0.5799560				
H	-4.2560810	3.4210580	-1.6715880				
H	-4.3142920	4.4011510	-0.1701780				
H	-4.9783040	2.7349100	-0.1870240				
3,5-TPDY _{acyclic}				2,4-TPDY _{acyclic}			



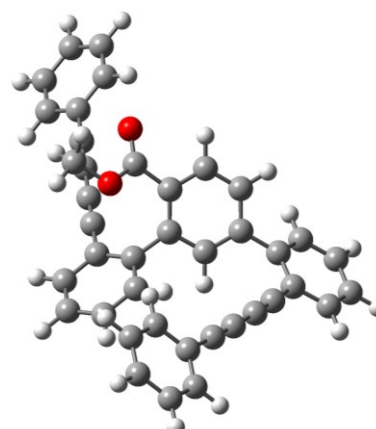
Number of imaginary frequencies : 0

E = -1689.187743

H (298K) = -1688.643633

G (298K) = -1688.755083

Symbol	X	Y	Z
C	-1.1531230	1.1074900	1.2766330
C	0.7793170	1.1214720	-0.7266560
C	-0.7211710	-0.1004140	0.7162520
C	-0.5989430	2.3208220	0.8487530
C	0.3835620	2.3387850	-0.1490600
C	0.2421000	-0.1028520	-0.3022950
H	1.5010120	1.1271120	-1.5358480
H	-1.1316780	-1.0340260	1.0774290
H	-0.9310380	3.2450150	1.3091590
C	0.7161690	-1.3706300	-0.9207210
C	1.7063950	-3.7461830	-2.0968130
C	-0.1801860	-2.3802740	-1.3743210
C	2.0937560	-1.5844040	-1.0799580
C	2.5899030	-2.7543180	-1.6574340
C	0.3337920	-3.5594390	-1.9575240



Number of imaginary frequencies : 0

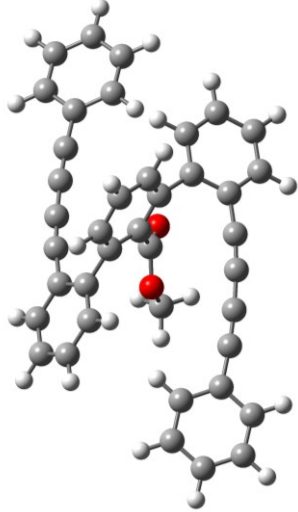
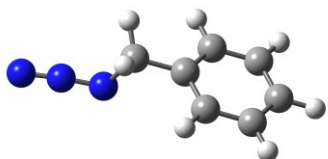
E = -1689.183332

H (298K) = -1688.639660

G (298K) = -1688.752254

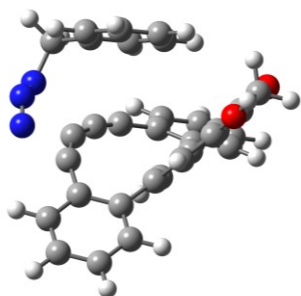
Symbol	X	Y	Z
C	1.3112580	-3.1424750	-2.3460710
C	-0.0480510	-2.8946270	-2.1679520
C	2.2542000	-2.3315980	-1.7064590
C	1.8307490	-1.2795370	-0.8909120
C	0.4705030	-1.0188100	-0.6835200
C	-0.4852410	-1.8374720	-1.3421390
H	-0.7889440	-3.5119040	-2.6665030
H	1.6317180	-3.9614930	-2.9831170
H	3.3164810	-2.5141320	-1.8400800
H	2.5661520	-0.6544400	-0.3949580
C	-1.8797580	-1.6113190	-1.1818650
C	-3.0785260	-1.4231020	-1.0312610
C	3.9267240	2.1140330	-0.0606920
C	3.1239710	3.0319210	-0.1523900
C	4.7668650	1.0482860	0.0269800
C	5.4870070	0.0618760	0.0959190
C	-4.4080310	-1.2076610	-0.8418980

H	2.0843300	-4.6596030	-2.5462440	C	-5.6017020	-1.0098910	-0.6631280
H	2.7867660	-0.8274570	-0.7267380	C	-6.9881960	-0.7755610	-0.4451720
H	3.6626520	-2.8915120	-1.7570450	C	-7.9517120	-1.3081960	-1.3295560
H	-0.3608830	-4.3181830	-2.3041150	C	-9.3081830	-1.0736290	-1.1085710
C	0.9698220	3.6313880	-0.5958350	C	-9.7235790	-0.3099770	-0.0112170
C	2.0126620	6.1251950	-1.4338930	C	-8.7737940	0.2210920	0.8696500
C	0.1245590	4.7119050	-0.8886570	C	-7.4144010	-0.0063180	0.6599300
C	2.3758640	3.8220620	-0.7211410	H	-6.6754350	0.4028740	1.3417340
C	2.8767140	5.0732210	-1.1434730	H	-7.6266860	-1.8995800	-2.1799350
C	0.6314980	5.9446680	-1.3035770	H	-10.0424150	-1.4870350	-1.7940100
H	2.4143110	7.0804260	-1.7584100	H	-10.7814910	-0.1298490	0.1567680
H	-0.9493210	4.5743280	-0.8042550	H	-9.0926920	0.8133990	1.7224700
H	3.9506430	5.2056570	-1.2303650	C	0.0817570	0.1464880	0.1647930
H	-0.0506900	6.7587300	-1.5302880	C	-0.7360320	0.0743950	1.3177610
C	3.2979590	2.7868390	-0.4010960	C	-1.0669340	1.2536130	2.0020030
C	4.0796300	1.8847470	-0.1351670	C	0.5587290	1.4031720	-0.2333650
C	4.8979560	0.8348630	0.1434530	C	0.2640060	2.5788220	0.4724610
C	5.5991790	-0.1386310	0.3821770	C	-0.5734910	2.4887790	1.5961460
C	-1.5900900	-2.2171810	-1.2758400	H	-1.7006310	1.1844040	2.8798660
C	-2.7969860	-2.0575700	-1.1600990	H	-0.8184410	3.3807870	2.1643250
C	-4.1273580	-1.8427900	-0.9777460	C	0.8008610	3.8948930	0.0364230
C	-5.3160060	-1.6274120	-0.7851300	C	-0.0633190	4.9957250	-0.0632880
C	-6.6901230	-1.3538010	-0.5379690	C	0.3961460	6.2511740	-0.4648440
C	-9.3980320	-0.8041480	-0.0355020	C	1.7480760	6.4351270	-0.7738790
C	-7.0619390	-0.1971660	0.1828960	C	2.6309740	5.3635010	-0.6754810
C	-7.6941110	-2.2305480	-1.0037260	C	2.1782890	4.0882940	-0.2714570
C	-9.0367100	-1.9520440	-0.7507630	H	-1.1168560	4.8565960	0.1602340
C	-8.4078260	0.0700620	0.4287820	H	-0.3009310	7.0804380	-0.5416460
H	-10.4453860	-0.5917260	0.1586670	H	2.1129300	7.4083190	-1.0883580
H	-6.2915810	0.4788160	0.5407880	H	3.6841110	5.4980320	-0.9016770
H	-7.4114030	-3.1199300	-1.5582980	C	6.2916080	-1.1089760	0.1697100
H	-9.8025520	-2.6318690	-1.1128650	C	7.6111760	-1.1079930	-0.3326500
H	-8.6846700	0.9619300	0.9835550	C	8.3856150	-2.2652860	-0.2624330
C	6.3803270	-1.2956290	0.6561890	C	7.8618510	-3.4331090	0.3048930
C	7.9054100	-3.5921440	1.1908580	C	6.5547370	-3.4407130	0.8065090

C	7.7665540	-1.3090540	0.3886080	C	5.7703070	-2.2900750	0.7433220
C	5.7686810	-2.4486200	1.1969470	H	4.7566210	-2.2929040	1.1315060
C	6.5313530	-3.5855380	1.4594460	H	9.3996970	-2.2561400	-0.6513590
C	8.5181870	-2.4524990	0.6563960	H	8.0143070	-0.2014550	-0.7731630
H	8.4953870	-4.4802890	1.3979480	H	6.1455110	-4.3447220	1.2481410
H	8.2390990	-0.4242720	-0.0264510	H	8.4690920	-4.3321980	0.3561080
H	4.7032140	-2.4402540	1.4043000	H	1.1587130	1.4621620	-1.1343730
H	6.0528740	-4.4677120	1.8749030	C	-1.2804050	-1.1906470	1.8982150
H	9.5841200	-2.4543720	0.4477300	O	-2.3054540	-1.2454220	2.5614550
C	-2.2116170	1.1480980	2.3266170	O	-0.5062710	-2.2591060	1.6544400
O	-2.6159470	2.1732080	2.8565050	C	-1.0042970	-3.5358070	2.1116970
O	-2.6947660	-0.0712000	2.6245120	H	-1.0828780	-3.5469840	3.2019380
C	-3.7492570	-0.1253220	3.6112510	H	-0.2706430	-4.2675440	1.7736040
H	-4.6158050	0.4488120	3.2731030	H	-1.9820450	-3.7408920	1.6680510
H	-3.3964430	0.2673740	4.5684960				
H	-4.0044540	-1.1811110	3.7015220				
2,6-TPDY _{acyclic}				Benzyl azide			
							
Number of imaginary frequencies : 0				Number of imaginary frequencies : 0			
E = -1689.178538				E = -435.192211			
H (298K) = -1688.635605				H (298K) = -435.050854			
G (298K) = -1688.747085				G (298K) = -435.095931			
Symbol	X	Y	Z	Symbol	X	Y	Z
N	-1.8999510	0.0004240	-0.4884950	N	-1.8999510	0.0004240	-0.4884950
N	-3.1166350	-0.0000340	-0.3058280	N	-3.1166350	-0.0000340	-0.3058280
N	-4.2592970	-0.0004320	-0.2475310	N	-4.2592970	-0.0004320	-0.2475310

C	-2.7428770	-4.2925530	0.0183740	C	-1.0701330	0.0003690	0.7636310
C	-1.3792580	-4.1610730	0.2725370	H	-1.3216110	-0.8903780	1.3503930
C	-3.3946300	-3.3518630	-0.7862470	H	-1.3213860	0.8912400	1.3503100
C	-2.6799800	-2.2815370	-1.3306640	C	0.3884340	0.0001500	0.3867460
C	-1.3140090	-2.1184530	-1.0761590	C	3.0986000	-0.0002650	-0.3538250
C	-0.6512470	-3.0811590	-0.2672580	C	1.0734510	1.2089560	0.1997720
H	-0.8616120	-4.8892000	0.8892600	C	1.0731330	-1.2088690	0.1999680
H	-3.2934030	-5.1261480	0.4441230	C	2.4217550	-1.2107260	-0.1683150
H	-4.4575450	-3.4475240	-0.9883820	C	2.4220810	1.2104000	-0.1684840
H	-3.1899780	-1.5461480	-1.9458270	H	0.5485530	2.1500750	0.3443620
C	0.7373000	-2.9347970	0.0029200	H	0.5479830	-2.1498270	0.3446910
C	1.9155170	-2.6707240	0.1947470	H	2.9429120	-2.1538020	-0.3078330
C	-1.8777510	2.7387180	0.1386290	H	2.9434840	2.1533210	-0.3081360
C	-0.6985940	3.0183870	-0.0239320	H	4.1473160	-0.0004310	-0.6377700
C	-3.1537320	2.3094600	0.3277600				
C	-4.2713640	1.8436050	0.4980060				
C	3.2004340	-2.2789250	0.4031440				
C	4.3343850	-1.8564830	0.5796070				
C	5.6214740	-1.2819430	0.7729100				
C	6.7453610	-2.0874680	1.0545600				
C	7.9960570	-1.4991800	1.2408980				
C	8.1445380	-0.1101230	1.1496980				
C	7.0330580	0.6947940	0.8709910				
C	5.7773910	0.1197440	0.6834960				
H	4.9115920	0.7391700	0.4710610				
H	6.6269470	-3.1642780	1.1247030				
H	8.8564260	-2.1255410	1.4582730				
H	9.1208810	0.3429010	1.2959440				
H	7.1444450	1.7731240	0.8018280				
C	-0.5786230	-0.9788970	-1.7048450				
C	-0.4935790	-0.9706950	-3.1047990				
C	0.2123790	0.0274540	-3.7730370				
C	0.0544370	0.0514660	-0.9699760				
C	0.7672940	1.0692750	-1.6455680				
C	0.8398260	1.0370720	-3.0459420				

H	0.2739220	0.0185250	-4.8572770	
H	1.3775170	1.8260550	-3.5625940	
C	1.4332370	2.2182540	-0.9593240	
C	2.8125460	2.3995920	-1.1137730	
C	3.4692400	3.4928620	-0.5430680	
C	2.7456970	4.4413830	0.1870330	
C	1.3699650	4.2900070	0.3458660	
C	0.7000450	3.1852440	-0.2180740	
H	3.3777210	1.6620980	-1.6758350	
H	4.5427060	3.6012550	-0.6686010	
H	3.2500740	5.2942560	0.6313180	
H	0.7976120	5.0211170	0.9082890	
C	-5.5268350	1.2015450	0.6873180	
C	-6.6866230	1.9388210	1.0070690	
C	-7.9026420	1.2809350	1.1910690	
C	-7.9808990	-0.1106650	1.0599550	
C	-6.8335290	-0.8482450	0.7427930	
C	-5.6121670	-0.2032640	0.5568140	
H	-4.7197930	-0.7710190	0.3120220	
H	-8.7910520	1.8552510	1.4374400	
H	-6.6233050	3.0178040	1.1083520	
H	-6.8901120	-1.9282950	0.6411520	
H	-8.9305480	-0.6176780	1.2045510	
H	-0.9712320	-1.7688260	-3.6647240	
C	0.0062120	0.0789660	0.5294120	
O	0.9418100	0.3957020	1.2439210	
O	-1.1993590	-0.2718940	1.0013300	
C	-1.3513090	-0.2938420	2.4355300	
H	-1.1625040	0.6982820	2.8536680	
H	-0.6634570	-1.0193410	2.8782730	
H	-2.3853960	-0.5904820	2.6101600	
3,5-TS				3,5-Triazole-Reg1



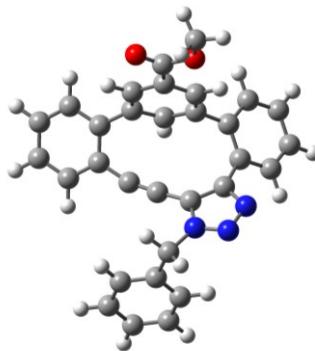
Number of imaginary frequencies : 1

E = -1508.637418

H (298K) = -1508.170384

G (298K) = -1508.262080

Symbol	X	Y	Z
O	-1.8006900	-4.0750000	0.0650890
O	0.3430950	-4.1673920	0.7639630
C	0.3881460	-0.1552520	1.8359030
C	1.6590590	0.4747880	2.3079100
C	2.3260820	1.4864130	1.5555200
C	1.7690450	1.9510070	0.3138340
C	0.8175370	2.2630730	-0.4406550
C	-0.5332220	2.4201220	-0.6056330
C	-1.7502930	2.3797950	-0.4921710
C	-3.0473580	2.0029050	-0.0338350
C	-3.1532670	0.8510850	0.8078370
C	-1.9549210	0.0236970	1.1411560
C	-0.7897790	0.5893940	1.6881250
H	-0.7881550	1.6348630	1.9744330
C	-1.9476300	-1.3372620	0.8171540
H	-2.8244100	-1.7979570	0.3752350
C	-0.7920630	-2.1078350	1.0024010
C	0.3764950	-1.5148780	1.4969430
H	1.2849020	-2.0988800	1.5874930
C	-0.8255660	-3.5313590	0.5648890
C	0.4089820	-5.5433540	0.3288730



Number of imaginary frequencies : 0

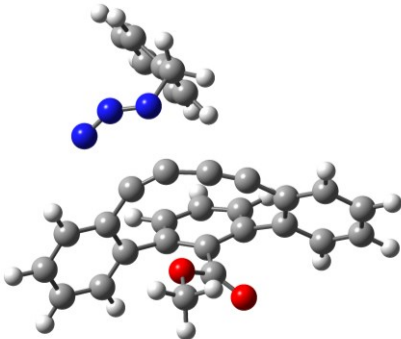
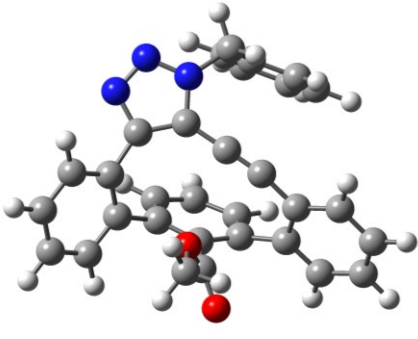
E = -1508.768932

H (298K) = -1508.296967

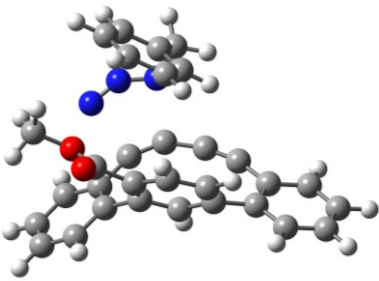
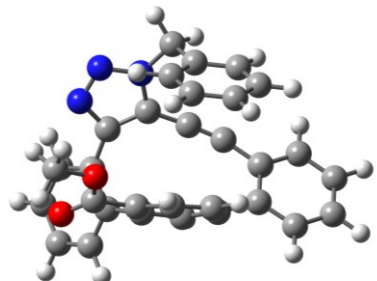
G (298K) = -1508.387814

Symbol	X	Y	Z
O	4.6847980	1.8634390	2.2116120
O	4.8826670	-0.3832330	2.1187560
C	2.0348540	-0.7188970	-0.8865880
C	1.5971560	-2.0289150	-1.4569110
C	0.4060650	-2.6799180	-1.0518870
C	-0.4801410	-2.2546660	0.0632440
C	-1.1546010	-1.0686270	0.4042460
C	-1.1625460	0.2417260	-0.1095990
C	-1.0661200	1.3789650	-0.5336450
C	-0.5984560	2.6494640	-0.9943850
C	0.8112780	2.8377880	-1.1372560
C	1.7148850	1.7019930	-0.8104350
C	1.4628590	0.4496770	-1.3897090
H	0.7509210	0.3739600	-2.2038860
C	2.6790690	1.7923160	0.1962390
H	2.8972840	2.7459910	0.6653620
C	3.3324970	0.6356350	0.6526340
C	2.9836540	-0.6230960	0.1382200
H	3.4421050	-1.5205950	0.5372790
C	4.3530260	0.7902830	1.7278860

H	-0.3132050	-6.1527310	0.8786710	C	5.8819400	-0.3227430	3.1615110
H	1.4264830	-5.8667400	0.5489630	H	6.7366440	0.2758630	2.8357550
H	0.2089260	-5.6149250	-0.7434330	H	6.1829230	-1.3564310	3.3320560
C	2.2507630	0.0221150	3.4950840	H	5.4561320	0.1067220	4.0720650
H	1.7498140	-0.7577190	4.0618760	C	2.3888130	-2.6115160	-2.4590450
C	3.4522830	0.5594820	3.9636740	H	3.3015550	-2.1043110	-2.7588680
H	3.8807630	0.1966840	4.8934320	C	2.0277560	-3.8127460	-3.0703120
C	4.0976280	1.5599470	3.2302600	H	2.6589190	-4.2397510	-3.8443910
H	5.0342390	1.9817550	3.5830980	C	0.8492370	-4.4533040	-2.6806120
C	3.5452310	2.0077650	2.0322800	H	0.5470710	-5.3855080	-3.1490810
H	4.0558470	2.7632300	1.4442150	C	0.0560570	-3.8918460	-1.6815470
C	-4.4256490	0.4658190	1.2475120	H	-0.8550080	-4.3951850	-1.3743940
H	-4.5168540	-0.4101700	1.8834820	C	1.2845050	4.0962180	-1.5193190
C	-5.5687180	1.1898620	0.8942390	H	2.3552070	4.2471750	-1.6232110
H	-6.5410470	0.8724100	1.2595380	C	0.4002530	5.1489460	-1.7784330
C	-5.4582110	2.3174400	0.0749880	H	0.7898480	6.1159550	-2.0829560
H	-6.3433340	2.8815890	-0.2037380	C	-0.9790100	4.9572350	-1.6502220
C	-4.2057820	2.7180820	-0.3890200	H	-1.6657690	5.7735920	-1.8528790
H	-4.1103920	3.5863810	-1.0336790	C	-1.4770240	3.7147680	-1.2563190
N	1.7075040	2.4382420	-2.4551630	H	-2.5452960	3.5601740	-1.1403440
N	2.8507510	2.0951950	-2.0708270	N	-1.8853540	-1.4055320	1.5134140
N	3.5034350	1.9100860	-1.1238170	N	-1.6992400	-2.6897370	1.8376070
C	1.0672190	1.6627320	-3.5531930	N	-0.8602240	-3.2027100	0.9738050
H	0.0837840	2.1211470	-3.6671990	C	-2.7978990	-0.5563560	2.2847610
H	1.6341630	1.8431680	-4.4725540	H	-2.2608550	0.3558340	2.5555690
C	0.9510090	0.1850210	-3.2476940	H	-3.0125210	-1.1161460	3.1983050
C	0.7672330	-2.5426670	-2.5932350	C	-4.0689210	-0.2305350	1.5248270
C	-0.2541490	-0.3536160	-2.7760310	C	-6.4366490	0.3790830	0.1453850
C	2.0639840	-0.6577570	-3.3913130	C	-4.8326010	-1.2532200	0.9441980
C	1.9746910	-2.0134300	-3.0622580	C	-4.4972630	1.0968320	1.4081070
C	-0.3479910	-1.7107690	-2.4560530	C	-5.6796200	1.4014210	0.7250380
H	-1.1166030	0.2935590	-2.6471800	C	-6.0090910	-0.9497220	0.2552050
H	3.0029280	-0.2516710	-3.7599470	H	-4.5020520	-2.2855850	1.0258830
H	2.8448620	-2.6545330	-3.1731310	H	-3.9007940	1.8937770	1.8447420
H	-1.2851820	-2.1140950	-2.0857440	H	-6.0020450	2.4354340	0.6394170

H	0.6966670	-3.5950700	-2.3325470	H	-6.5923140	-1.7487620	-0.1939680
				H	-7.3517310	0.6145420	-0.3908570
2,6-TS				2,6-Triazole-Reg1			
							
Number of imaginary frequencies : 1				Number of imaginary frequencies : 0			
E = -1508.625219				E = -1508.761088			
H (298K) = -1508.158741				H (298K) = -1508.289864			
G (298K) = -1508.251390				G (298K) = -1508.379648			
Symbol	X	Y	Z	Symbol	X	Y	Z
C	0.7068380	-4.9292540	1.1760130	C	-5.1167100	-0.5540760	0.8365210
C	1.5765770	-4.8721480	0.0840990	C	-5.0752650	-1.5384750	-0.1542550
C	0.0289520	-3.7757440	1.5856780	C	-3.9233950	-0.0520260	1.3593070
C	0.1849660	-2.5646730	0.9062450	C	-2.6817590	-0.5168690	0.9074770
C	1.0713330	-2.5059170	-0.2086090	C	-2.6340320	-1.5079230	-0.1012780
C	1.7645480	-3.6675780	-0.5941960	C	-3.8446720	-2.0102900	-0.6118470
H	2.4461780	-3.6169240	-1.4364370	H	-3.8116680	-2.7719190	-1.3846800
H	0.5595860	-5.8619310	1.7128960	H	-6.0688760	-0.1792420	1.2009360
H	2.1133940	-5.7602510	-0.2366260	H	-5.9950770	-1.9373570	-0.5721320
H	-0.6381450	-3.8140490	2.4423560	H	-3.9464290	0.7141070	2.1294270
C	1.2004120	-1.2790570	-0.9475230	C	-1.3790360	-2.1009720	-0.6236750
C	0.7312450	-0.2034270	-1.3882750	C	-0.1751670	-1.5689450	-1.1189620
C	-0.3060890	0.6827780	-1.4915370	C	0.3524170	-0.2710650	-1.2648740
C	-1.3343720	1.3372220	-1.3788270	C	0.8359140	0.8458220	-1.2989320
C	-2.5638060	1.8417740	-0.8571170	C	1.3167140	2.1504700	-0.9585680
C	-2.9518240	1.4279660	0.4549920	C	1.1035340	2.6110420	0.3777630
C	-3.3878880	2.7216070	-1.5816880	C	2.0132100	2.9606860	-1.8714460

C	-4.5782770	3.1935310	-1.0291140	C	2.5014330	4.2059890	-1.4741920
C	-4.9525680	2.8011070	0.2598490	C	2.3053850	4.6504570	-0.1625770
C	-4.1379720	1.9325090	0.9934880	C	1.6137450	3.8530500	0.7560300
H	-5.2084980	3.8683130	-1.6008710	H	3.0363690	4.8268340	-2.1866990
H	-5.8776210	3.1678330	0.6951790	H	2.6866430	5.6194160	0.1462770
H	-4.4327010	1.6264370	1.9930980	H	1.4550480	4.2018680	1.7721110
C	-2.0269250	0.5728840	1.2621650	C	0.3982570	1.6756490	1.3018240
C	-1.4128960	1.1519900	2.3771660	C	1.1308200	0.9400550	2.2374040
C	-1.6135240	-0.7149150	0.8349850	C	-0.9215010	1.2803310	0.9952780
C	-0.4818920	-1.3235320	1.4203820	C	-1.4207320	0.0554260	1.4661470
C	-0.3762070	0.4924390	3.0406600	C	0.5813410	-0.2066770	2.8194030
C	0.1075650	-0.7135840	2.5408840	C	-0.6637510	-0.6714660	2.3980900
H	0.0896430	0.9465240	3.9101170	H	1.1566050	-0.7758500	3.5433940
H	0.9665970	-1.1886410	3.0044640	H	-1.0509020	-1.6144930	2.7721270
H	-1.7219620	2.1429030	2.6960230	H	2.1570680	1.2234680	2.4514580
C	-2.4525190	-1.4077570	-0.1963060	C	-1.7508630	2.1821400	0.1269260
O	-3.6706800	-1.3123410	-0.2338530	O	-1.9522900	3.3552090	0.4012970
O	-1.7533420	-2.1652790	-1.0479390	O	-2.2561200	1.5781130	-0.9537630
C	-2.5087540	-2.9018870	-2.0338340	C	-3.1494760	2.3619200	-1.7767030
H	-3.2060820	-3.5881080	-1.5461900	H	-4.0181730	2.6788770	-1.1935370
H	-1.7652530	-3.4554200	-2.6073080	H	-3.4542310	1.6953740	-2.5832310
H	-3.0580400	-2.2135030	-2.6814470	H	-2.6302110	3.2366480	-2.1763520
H	-3.0824820	3.0307250	-2.5766280	H	2.1717340	2.6038310	-2.8844350
N	3.3727210	-1.1371800	-1.5606220	N	-1.2819050	-3.4615430	-0.7121100
N	3.2759210	-0.0690080	-2.0144440	N	-0.1121590	-3.7994020	-1.1961950
N	2.4539300	0.8074300	-2.3705470	N	0.5653630	-2.6739420	-1.4490580
C	2.7239670	2.2242730	-2.0135640	C	1.9765940	-2.7159000	-1.8497500
C	3.1588800	2.4017060	-0.5766910	C	2.8853580	-2.3351910	-0.6950170
H	1.7744570	2.7267210	-2.2114550	H	2.1107790	-2.0395500	-2.6966730
H	3.4684440	2.6225410	-2.7106940	H	2.1558300	-3.7393820	-2.1861720
C	2.2118460	2.4250050	0.4579460	C	3.7425580	-1.2337310	-0.7972180
C	2.6218810	2.5279750	1.7892040	C	4.5568730	-0.8678550	0.2797770
C	4.9338610	2.5846600	1.0751890	C	3.6588180	-2.7029280	1.5769710
C	4.5216950	2.4798370	-0.2573220	C	2.8486500	-3.0685210	0.4998340
H	5.2615370	2.4579940	-1.0539640	H	2.1754890	-3.9173430	0.5895580

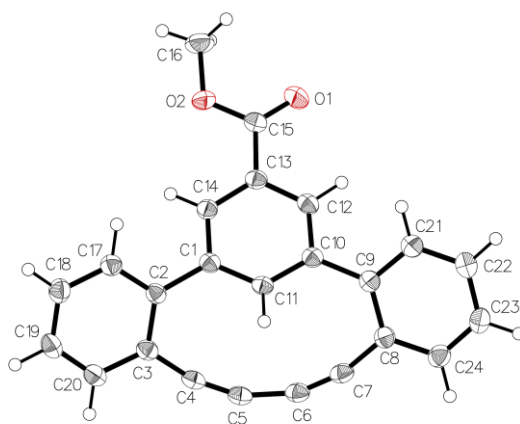
H	1.1547140	2.3520570	0.2201730	H	3.7618720	-0.6509160	-1.7140360
C	3.9837890	2.6089990	2.1011780	C	4.5151010	-1.6004940	1.4694560
H	1.8784780	2.5401270	2.5808360	H	5.2127800	-0.0062990	0.1912220
H	4.3019930	2.6893450	3.1369610	H	5.1414210	-1.3131760	2.3094730
H	5.9928750	2.6468100	1.3100260	H	3.6199580	-3.2750480	2.4997670
2,4-TS				2,4-Triazole-Reg1			
							
Number of imaginary frequencies : 1				Number of imaginary frequencies : 0			
E = -1508.632719				E = -1508.767143			
H (298K) = -1508.165939				H (298K) = -1508.295513			
G (298K) = -1508.257846				G (298K) = -1508.385084			
Symbol	X	Y	Z	Symbol	X	Y	Z
C	6.0858680	-0.9196850	0.4212340	C	4.7838430	-2.9722500	0.9119100
C	6.2499660	0.1399580	-0.4762640	C	4.9643030	-2.8098510	-0.4649190
C	4.8021380	-1.3582380	0.7592030	C	3.5953600	-2.5528910	1.5206740
C	3.6595570	-0.7683540	0.2038600	C	2.5707400	-1.9766220	0.7668020
C	3.8334670	0.3179160	-0.7113360	C	2.7624930	-1.7991880	-0.6389290
C	5.1310170	0.7569890	-1.0340770	C	3.9607300	-2.2227230	-1.2373260
C	2.6695440	0.9246050	-1.2701090	H	4.1003810	-2.0796820	-2.3043830
C	1.5071780	1.1135820	-1.6014300	H	5.5654890	-3.4265860	1.5137880
C	0.1706100	0.9811320	-1.8727150	H	5.8861120	-3.1357330	-0.9374300
C	-0.8069420	0.2089310	-2.0153980	H	3.4556060	-2.6817730	2.5901430
C	-1.4357510	-1.0820220	-1.9685260	C	0.7347800	-0.4984560	-1.6774090
C	-1.0709730	-2.0142960	-0.9562580	C	-0.4331120	0.2655210	-1.8695820
C	-2.4298670	-1.4351590	-2.9024340	C	-1.7926180	0.0422900	-1.6025040
C	-3.0428630	-2.6852830	-2.8590220	C	-2.5371780	-1.1306580	-1.0876580
C	-2.6863990	-3.6016890	-1.8642380				

C	-1.7139190	-3.2585410	-0.9227920	C	-2.2601100	-1.7364500	0.1591710
C	-0.0421820	-1.7025600	0.0843470	C	-3.6105300	-1.6122220	-1.8575030
C	-0.3624760	-1.6289630	1.4592590	C	-4.3817690	-2.6901260	-1.4234860
C	1.2929550	-1.5204240	-0.2941800	C	-4.0861760	-3.3062840	-0.2039220
C	2.2979310	-1.2010550	0.6337010	C	-3.0310070	-2.8295910	0.5752660
C	0.6583730	-1.4428980	2.4017350	H	-5.2033750	-3.0492250	-2.0365030
C	1.9707350	-1.2136740	1.9989330	H	-4.6766910	-4.1497690	0.1424130
C	-1.7573730	-1.6560180	1.9923820	H	-2.8087470	-3.2937610	1.5318360
O	-2.0663070	-2.1335510	3.0754010	C	-1.1122060	-1.2733610	0.9992420
O	-2.6293250	-1.0401150	1.1823840	C	-1.1214170	-0.1058710	1.7943420
C	-4.0073090	-1.0081350	1.6091350	C	0.0901170	-1.9628680	0.8437450
N	-2.5042550	1.6555220	-2.3276620	C	1.2989240	-1.4735150	1.3544000
N	-1.8625860	2.6024090	-2.1119510	C	0.0659840	0.3162060	2.4145980
N	-0.6887390	3.0197290	-1.9625560	C	1.2704900	-0.3491720	2.1887720
C	-0.4142480	3.8893400	-0.7822540	H	0.0543410	1.2072120	3.0318370
C	-0.8724150	3.2713800	0.5201250	H	2.1948350	0.0522860	2.5927840
C	-2.2190930	3.3543320	0.9066110	H	0.1080700	-2.8271100	0.1879440
C	0.0242340	2.5555280	1.3251840	C	-2.3699290	0.6953040	1.9513670
C	-0.4157200	1.9365610	2.4982210	O	-3.5033690	0.2476840	1.8859460
C	-1.7606480	2.0149530	2.8721740	O	-2.1079080	1.9983300	2.1769880
C	-2.6627970	2.7256270	2.0733950	C	-3.2562430	2.8590810	2.3490110
H	6.9532940	-1.4058230	0.8581070	H	-3.8764510	2.8464220	1.4490560
H	7.2450310	0.4860200	-0.7398580	H	-2.8466860	3.8555110	2.5158010
H	4.6799100	-2.1808320	1.4580830	H	-3.8486970	2.5394790	3.2105190
H	5.2480280	1.5859920	-1.7252120	C	0.7954760	2.3741430	-2.5887170
H	-2.7178370	-0.7119030	-3.6580510	C	1.4918540	2.7372980	-1.2898530
H	-3.8018810	-2.9394670	-3.5931420	C	2.8314650	2.3905620	-1.0814070
H	-3.1638000	-4.5761870	-1.8182630	C	3.4662320	2.7111190	0.1233820
H	-1.4430050	-3.9644530	-0.1424390	C	2.7610140	3.3757950	1.1307860
H	1.5454080	-1.5945840	-1.3456780	C	1.4187650	3.7186400	0.9290660
H	0.3991720	-1.4100350	3.4547990	H	3.3756260	1.8574850	-1.8564950
H	2.7313420	-0.9879640	2.7401000	H	4.5049810	2.4317780	0.2762290
H	-4.4039930	-2.0245670	1.6826050	H	3.2502530	3.6181390	2.0701550
H	-4.5333010	-0.4485930	0.8359040	H	-3.8288200	-1.1356010	-2.8084630
H	-4.0986880	-0.5057690	2.5752370	C	1.7308350	-1.1310920	-1.3746050

H	-0.8857140	4.8618070	-0.9584610	N	-2.4656050	1.1791760	-1.9461120
H	0.6677650	4.0286830	-0.7996610	N	-0.3930660	1.5516290	-2.3389040
H	-2.9228000	3.9078960	0.2892820	N	-1.6200920	2.0852420	-2.3761260
H	1.0648210	2.4707170	1.0254440	H	1.4625860	1.8181070	-3.2507630
H	0.2883250	1.3809170	3.1092030	H	0.4359660	3.2599620	-3.1170690
H	-2.1040090	1.5206780	3.7767430	C	0.7878400	3.4022850	-0.2755890
H	-3.7095390	2.7901260	2.3573630	H	-0.2586340	3.6561980	-0.4233790
				H	0.8616880	4.2259040	1.7117330

A6.8 X-ray Crystallography

3,5-TPDY



The data for **3,5-TPDY** crystallised from DCM/Et₂O, were collected from a shock-cooled single crystal at 150 K on a Bruker Venture Metaljet k-geometry diffractometer with a Metal Jet using Helios MX Mirror Optics as monochromator and a Bruker CMOS Photon III detector. The diffractometer was equipped with an Oxford Cryostream 700 low temperature device and used Ga K_{α} radiation ($\lambda = 1.34139 \text{ \AA}$). All data were integrated with *SAINT* (2020) and a multi-scan absorption correction using *SADABS* 2016/2 was applied.¹² The structure was solved by dual methods with *XT* and refined by full-matrix least-squares methods against F^2 using *XL*.¹³⁻¹⁴ Structure solution and refinement cycles were performed within the graphical user interface of *OLEX2*. All non-hydrogen atoms were refined with anisotropic displacement parameters. The hydrogen atoms were located from difference Fourier map and refined isotropically.¹⁵ This report and the CIF file were generated using *FinalCif*.¹⁶

Table A6 - 1 Crystal data and structure refinement for 3,5-TPDY

Empirical formula	C ₂₄ H ₁₄ O ₂
Formula weight	334.35
Temperature [K]	150
Crystal system	monoclinic
Space group (number)	<i>P</i> 2 ₁ / <i>c</i> (14)
<i>a</i> [Å]	3.8764(2)
<i>b</i> [Å]	38.1644(16)
<i>c</i> [Å]	10.9214(6)
α [°]	90
β [°]	99.461(2)
γ [°]	90
Volume [Å ³]	1593.74(14)
<i>Z</i>	4
ρ _{calc} [gcm ⁻³]	1.393
μ [mm ⁻¹]	0.443
<i>F</i> (000)	696
Crystal size [mm ³]	0.02×0.02×0.3
Crystal colour	clear light colourless
Crystal shape	Needle
Radiation	Ga K _α (λ=1.34139 Å)
2θ range [°]	4.03 to 113.91 (0.80 Å)
Index ranges	-4 ≤ <i>h</i> ≤ 4 -45 ≤ <i>k</i> ≤ 47 -13 ≤ <i>l</i> ≤ 13
Reflections collected	14884
Independent reflections	3171 <i>R</i> _{int} = 0.0525 <i>R</i> _{sigma} = 0.0457
Completeness to θ = 53.594°	100.0 %
Data / Restraints / Parameters	3171 / 0 / 292
Goodness-of-fit on <i>F</i> ²	1.054
Final <i>R</i> indexes [<i>I</i> ≥ 2σ(<i>I</i>)]	<i>R</i> ₁ = 0.0452 <i>wR</i> ₂ = 0.1017
Final <i>R</i> indexes [all data]	<i>R</i> ₁ = 0.0737 <i>wR</i> ₂ = 0.1134
Largest peak/hole [eÅ ⁻³]	0.25/-0.18
Extinction coefficient	0.0034(5)

Table A6 - 2 Atomic coordinates and U_{eq} [\AA^2] for 3,5-TPDY

Atom	x	y	z	U_{eq}
O1	-0.0166(4)	0.72812(3)	0.62060(13)	0.0414(4)
O2	0.1030(4)	0.69897(3)	0.80075(11)	0.0342(4)
C1	0.4569(5)	0.61153(4)	0.63393(16)	0.0239(4)
C2	0.5315(5)	0.57862(4)	0.70878(16)	0.0242(4)
C3	0.4162(5)	0.54509(4)	0.66197(17)	0.0262(4)
C4	0.2508(5)	0.54262(4)	0.53539(18)	0.0278(4)
C5	0.1553(5)	0.54790(4)	0.42597(18)	0.0279(4)
C6	0.1468(5)	0.56668(5)	0.31805(17)	0.0287(4)
C7	0.2256(5)	0.59050(5)	0.25602(17)	0.0282(4)
C8	0.3617(5)	0.62283(5)	0.21693(16)	0.0261(4)
C9	0.4584(5)	0.64908(5)	0.30824(16)	0.0253(4)
C10	0.4211(5)	0.64508(4)	0.44125(16)	0.0244(4)
C11	0.5165(5)	0.61480(4)	0.51158(16)	0.0225(4)
H11	0.630(5)	0.5956(5)	0.4759(16)	0.022(5)
C12	0.2838(5)	0.67308(5)	0.49973(17)	0.0257(4)
H12	0.215(5)	0.6949(5)	0.4551(17)	0.031(5)
C13	0.2381(5)	0.67109(4)	0.62301(17)	0.0253(4)
C14	0.3186(5)	0.64009(5)	0.68907(17)	0.0252(4)
H14	0.276(5)	0.6377(4)	0.7740(17)	0.019(4)
C15	0.0928(5)	0.70227(5)	0.67809(17)	0.0283(4)
C16	-0.0152(7)	0.72892(6)	0.8629(2)	0.0415(6)
H16A	0.113(7)	0.7501(7)	0.842(2)	0.059(7)
H16B	0.055(7)	0.7247(6)	0.951(3)	0.066(8)
H16C	-0.263(9)	0.7338(7)	0.835(2)	0.071(9)
C17	0.6996(5)	0.58073(5)	0.83099(17)	0.0279(4)
H17	0.778(5)	0.6047(5)	0.8661(17)	0.031(5)
C18	0.7591(6)	0.55124(5)	0.90602(19)	0.0323(5)
H18	0.873(5)	0.5536(5)	0.9929(19)	0.033(5)
C19	0.6471(5)	0.51871(5)	0.85939(19)	0.0321(5)
H19	0.679(6)	0.4976(6)	0.9111(19)	0.041(6)
C20	0.4750(5)	0.51561(5)	0.73876(18)	0.0302(5)
H20	0.391(5)	0.4928(5)	0.7053(17)	0.026(5)
C21	0.5814(5)	0.68089(5)	0.26850(18)	0.0289(4)
H21	0.646(5)	0.6993(5)	0.3325(18)	0.034(5)
C22	0.6182(5)	0.68662(5)	0.14621(18)	0.0326(5)
H22	0.712(6)	0.7098(5)	0.1210(18)	0.036(5)
C23	0.5305(6)	0.66033(5)	0.05875(18)	0.0337(5)
H23	0.562(5)	0.6647(5)	-0.0282(19)	0.032(5)
C24	0.4019(5)	0.62883(5)	0.09401(18)	0.0312(5)
H24	0.338(6)	0.6100(5)	0.0298(19)	0.041(6)

U_{eq} is defined as 1/3 of the trace of the orthogonalized U_{ij} tensor.

Table A6 - 3 Bond lengths and angles for 3,5-TPDY

Atom-Atom	Length [Å]	Atom-Atom-Atom	Angle [°]
O1-C15	1.208(2)	C21-C9-C10	118.91(16)
O2-C15	1.340(2)	C11-C10-C9	123.94(16)
O2-C16	1.442(2)	C12-C10-C9	118.26(16)
C1-C2	1.501(2)	C12-C10-C11	117.81(16)
C1-C11	1.398(2)	C1-C11-C10	121.75(16)
C1-C14	1.394(2)	C1-C11-H11	118.3(10)
C2-C3	1.422(2)	C10-C11-H11	120.0(10)
C2-C17	1.388(3)	C10-C12-H12	121.2(11)
C3-C4	1.428(3)	C13-C12-C10	121.43(17)
C3-C20	1.400(3)	C13-C12-H12	117.4(11)
C4-C5	1.208(3)	C12-C13-C14	119.65(17)
C5-C6	1.375(3)	C12-C13-C15	117.78(16)
C6-C7	1.203(3)	C14-C13-C15	122.54(16)
C7-C8	1.434(3)	C1-C14-H14	118.4(10)
C8-C9	1.419(2)	C13-C14-C1	120.60(17)
C8-C24	1.396(3)	C13-C14-H14	121.0(10)
C9-C10	1.491(2)	O1-C15-O2	123.14(17)
C9-C21	1.399(3)	O1-C15-C13	124.60(17)
C10-C11	1.403(2)	O2-C15-C13	112.25(15)
C10-C12	1.394(2)	O2-C16-H16A	109.2(15)
C11-H11	0.970(18)	O2-C16-H16B	106.0(16)
C12-H12	0.98(2)	O2-C16-H16C	112.2(16)
C12-C13	1.389(3)	H16A-C16-H16B	107(2)
C13-C14	1.394(2)	H16A-C16-H16C	106(2)
C13-C15	1.486(2)	H16B-C16-H16C	116(2)
C14-H14	0.972(18)	C2-C17-H17	118.5(11)
C16-H16A	0.99(3)	C2-C17-C18	121.78(18)
C16-H16B	0.97(3)	C18-C17-H17	119.7(11)
C16-H16C	0.98(3)	C17-C18-H18	120.1(11)
C17-H17	1.02(2)	C19-C18-C17	119.86(19)
C17-C18	1.389(3)	C19-C18-H18	120.0(11)
C18-H18	0.98(2)	C18-C19-H19	121.5(12)
C18-C19	1.384(3)	C20-C19-C18	120.08(18)
C19-H19	0.98(2)	C20-C19-H19	118.3(12)
C19-C20	1.380(3)	C3-C20-H20	118.7(11)
C20-H20	0.978(19)	C19-C20-C3	120.56(18)
C21-H21	0.99(2)	C19-C20-H20	120.8(11)
C21-C22	1.384(3)	C9-C21-H21	117.1(11)

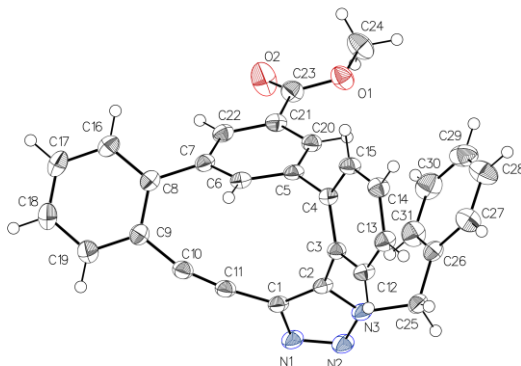
C22–H22	1.01(2)	C22–C21–C9	122.07(18)
C22–C23	1.388(3)	C22–C21–H21	120.9(11)
C23–H23	0.99(2)	C21–C22–H22	120.0(11)
C23–C24	1.380(3)	C21–C22–C23	119.83(18)
C24–H24	1.01(2)	C23–C22–H22	120.2(11)
		C22–C23–H23	118.9(11)
Atom–Atom–Atom	Angle [°]	C24–C23–C22	119.75(18)
C15–O2–C16	115.89(16)	C24–C23–H23	121.3(11)
C11–C1–C2	123.21(16)	C8–C24–H24	120.0(12)
C14–C1–C2	118.18(16)	C23–C24–C8	120.91(18)
C14–C1–C11	118.60(16)	C23–C24–H24	119.1(12)
C3–C2–C1	122.43(16)		
C17–C2–C1	119.55(16)		
C17–C2–C3	117.89(16)		
C2–C3–C4	118.15(16)		
C20–C3–C2	119.82(17)		
C20–C3–C4	122.00(17)		
C5–C4–C3	164.18(19)		
C4–C5–C6	153.46(19)		
C7–C6–C5	154.71(19)		
C6–C7–C8	163.29(19)		
C9–C8–C7	117.73(16)		
C24–C8–C7	122.14(17)		
C24–C8–C9	120.13(17)		
C8–C9–C10	123.76(16)		
C21–C9–C8	117.28(17)		

Table A6 - 4 Torsion angles for 3,5-TPDY

Atom–Atom–Atom–Atom	Torsion Angle [°]	Atom–Atom–Atom–Atom	Torsion Angle [°]
C1–C2–C3–C4	5.6(3)	C11–C1–C2–C3	–48.8(3)
C1–C2–C3–C20	–176.09(17)	C11–C1–C2–C17	135.40(19)
C1–C2–C17–C18	176.77(17)	C11–C1–C14–C13	0.7(3)
C2–C1–C11–C10	175.43(17)	C11–C10–C12–C13	–0.8(3)
C2–C1–C14–C13	–178.76(17)	C12–C10–C11–C1	4.0(3)
C2–C3–C4–C5	23.0(8)	C12–C13–C14–C1	2.4(3)
C2–C3–C20–C19	–0.6(3)	C12–C13–C15–O1	6.7(3)
C2–C17–C18–C19	–0.5(3)	C12–C13–C15–O2	–171.90(16)
C3–C2–C17–C18	0.7(3)	C14–C1–C2–C3	130.66(19)
C3–C4–C5–C6	–0.3(11)	C14–C1–C2–C17	–45.2(2)

C4-C3-C20-C19	177.61(18)	C14-C1-C11-C10	-4.0(3)
C4-C5-C6-C7	0.4(8)	C14-C13-C15-O1	-171.34(19)
C5-C6-C7-C8	-10.9(11)	C14-C13-C15-O2	10.0(3)
C6-C7-C8-C9	-14.9(8)	C15-C13-C14-C1	-179.54(17)
C6-C7-C8-C24	164.8(6)	C16-O2-C15-O1	-2.0(3)
C7-C8-C9-C10	-1.0(3)	C16-O2-C15-C13	176.67(18)
C7-C8-C9-C21	-178.21(17)	C17-C2-C3-C4	-178.47(17)
C7-C8-C24-C23	179.38(19)	C17-C2-C3-C20	-0.2(3)
C8-C9-C10-C11	44.6(3)	C17-C18-C19-C20	-0.3(3)
C8-C9-C10-C12	-135.56(19)	C18-C19-C20-C3	0.9(3)
C8-C9-C21-C22	-1.8(3)	C20-C3-C4-C5	-155.2(7)
C9-C8-C24-C23	-0.9(3)	C21-C9-C10-C11	-138.25(19)
C9-C10-C11-C1	-176.08(17)	C21-C9-C10-C12	41.6(3)
C9-C10-C12-C13	179.29(17)	C21-C22-C23-C24	1.0(3)
C9-C21-C22-C23	0.2(3)	C22-C23-C24-C8	-0.7(3)
C10-C9-C21-C22	-179.13(18)	C24-C8-C9-C10	179.32(18)
C10-C12-C13-C14	-2.4(3)	C24-C8-C9-C21	2.1(3)
C10-C12-C13-C15	179.52(17)		

3,5-Triazole-Reg2



The data for 3,5-Triazole-Reg2, crystallised from DCM/Et₂O, were collected from a shock-cooled single crystal at 150 K on a Bruker Venture Metaljet k-geometry diffractometer with a Metal Jet using Helios MX Mirror Optics as monochromator and a Bruker CMOS Photon III detector. The diffractometer was equipped with an Oxford Cryostream 700 low temperature device and used Ga K_{α} radiation ($\lambda = 1.34139 \text{ \AA}$). All data were integrated with *SAINT* (2020) and a multi-scan absorption correction using *SADABS* 2016/2 was applied.^{12, 17} The structure was solved by dual methods with *XT* and refined by full-matrix least-squares methods against F^2 using *XL*.¹³⁻¹⁴ Structure solution and refinement cycles were performed within the graphical user interface of *OLEX2*. All non-hydrogen atoms were refined with anisotropic displacement parameters. The hydrogen atoms were located from difference Fourier map and refined isotropically.¹⁵ This report and the CIF file were generated using *FinalCif*.¹⁶

Table A6 - 5 Crystal data and structure refinement for 3,5-Triazole-Reg2

Empirical formula	C ₃₁ H ₂₁ N ₃ O ₂
Formula weight	467.51
Temperature [K]	150
Crystal system	triclinic
Space group (number)	$P\bar{1}$ (2)
a [Å]	9.1237(13)
b [Å]	10.4155(15)
c [Å]	12.6877(19)
α [°]	100.575(6)
β [°]	91.287(6)

γ [°]	93.604(6)
Volume [Å ³]	1182.2(3)
Z	2
ρ_{calc} [gcm ⁻³]	1.313
μ [mm ⁻¹]	0.423
F(000)	488
Crystal size [mm ³]	0.11×0.15×0.16
Crystal colour	clear light colourless
Crystal shape	Block
Radiation	Ga K α (λ =1.34139 Å)
2 θ range [°]	6.17 to 114.03 (0.80 Å)
Index ranges	-11 ≤ h ≤ 11 -12 ≤ k ≤ 12 -15 ≤ l ≤ 15
Reflections collected	45392
Independent reflections	4777 $R_{\text{int}} = 0.0292$ $R_{\text{sigma}} = 0.0169$
Completeness to $\theta = 53.594^\circ$	99.1 %
Data / Restraints / Parameters	4777 / 0 / 327
Goodness-of-fit on F^2	1.032
Final R indexes [$I \geq 2\sigma(I)$]	$R_1 = 0.0350$ $wR_2 = 0.0907$
Final R indexes [all data]	$R_1 = 0.0385$ $wR_2 = 0.0930$
Largest peak/hole [eÅ ⁻³]	0.25/-0.18
Extinction coefficient	0.0117(12)

Table A6 - 6 Atomic coordinates and U_{eq} [Å²] for 3,5-Triazole-Reg2

Atom	x	y	z	U_{eq}
O1	0.15694(10)	0.53286(8)	0.95431(6)	0.0365(2)
C1	0.48365(11)	0.11700(10)	0.60471(9)	0.0260(2)
N1	0.62407(10)	0.11664(9)	0.64530(8)	0.0318(2)
O2	0.24689(14)	0.68273(9)	0.86332(8)	0.0591(3)
N2	0.62080(10)	0.05520(10)	0.72614(8)	0.0319(2)
C2	0.38860(11)	0.05039(10)	0.66364(8)	0.0235(2)
N3	0.48000(9)	0.01395(9)	0.73754(7)	0.0259(2)
C3	0.22969(11)	0.00773(10)	0.66190(8)	0.0228(2)

C4	0.11832(11)	0.09576(10)	0.68387(8)	0.0227(2)
C5	0.14799(10)	0.23858(10)	0.68437(8)	0.0232(2)
C6	0.16732(11)	0.27584(10)	0.58577(9)	0.0245(2)
H6	0.153167	0.211467	0.522211	0.029
C7	0.20701(11)	0.40531(10)	0.57716(9)	0.0255(2)
C8	0.25406(12)	0.43658(10)	0.47281(9)	0.0269(2)
C9	0.36228(12)	0.36261(10)	0.41537(9)	0.0276(2)
C10	0.42259(12)	0.26020(11)	0.46197(9)	0.0281(2)
C11	0.45392(11)	0.18791(10)	0.52139(9)	0.0273(2)
C12	0.19244(12)	-0.12662(10)	0.64908(9)	0.0269(2)
H12	0.266148	-0.186636	0.631066	0.032
C13	0.04983(12)	-0.17377(10)	0.66220(9)	0.0285(2)
H13	0.026376	-0.265338	0.653680	0.034
C14	-0.05859(11)	-0.08663(11)	0.68784(9)	0.0288(2)
H14	-0.155940	-0.118192	0.698903	0.035
C15	-0.02423(11)	0.04678(10)	0.69724(9)	0.0272(2)
H15	-0.099397	0.105802	0.713096	0.033
C16	0.20093(13)	0.54102(11)	0.43259(9)	0.0317(3)
H16	0.128221	0.590631	0.470283	0.038
C17	0.25266(15)	0.57380(11)	0.33813(10)	0.0371(3)
H17	0.215664	0.645538	0.311760	0.045
C18	0.35832(15)	0.50162(12)	0.28249(10)	0.0377(3)
H18	0.394084	0.524466	0.218175	0.045
C19	0.41235(13)	0.39599(12)	0.32016(9)	0.0333(3)
H19	0.483718	0.346281	0.280904	0.040
C20	0.15774(11)	0.33393(10)	0.77723(9)	0.0255(2)
H20	0.143731	0.310201	0.845294	0.031
C21	0.18837(11)	0.46514(10)	0.76933(9)	0.0271(2)
C22	0.21486(11)	0.49996(10)	0.66995(9)	0.0271(2)
H22	0.238401	0.589031	0.665874	0.033
C23	0.20122(13)	0.57203(11)	0.86499(10)	0.0328(3)
C24	0.16333(16)	0.63285(14)	1.04978(10)	0.0440(3)
H24A	0.098735	0.701572	1.039519	0.066
H24B	0.264491	0.670770	1.063779	0.066
H24C	0.131113	0.594138	1.110899	0.066
C25	0.44281(12)	-0.04244(11)	0.83198(9)	0.0280(2)
H25A	0.533745	-0.066436	0.865436	0.034
H25B	0.378098	-0.123238	0.809482	0.034
C26	0.36589(12)	0.05306(11)	0.91354(9)	0.0279(2)
C27	0.24242(13)	0.01146(13)	0.96249(10)	0.0374(3)
H27	0.203640	-0.076779	0.943186	0.045
C28	0.17464(15)	0.09837(15)	1.03997(11)	0.0464(3)
H28	0.090309	0.068927	1.073697	0.056
C29	0.22922(15)	0.22682(14)	1.06797(11)	0.0458(3)

H29	0.182487	0.286088	1.120540	0.055
C30	0.35220(17)	0.26875(13)	1.01914(11)	0.0469(3)
H30	0.390438	0.357165	1.038322	0.056
C31	0.42023(15)	0.18247(12)	0.94222(11)	0.0400(3)
H31	0.504758	0.212224	0.908874	0.048

U_{eq} is defined as 1/3 of the trace of the orthogonalized U_{ij} tensor.

Table A6 - 7 Anisotropic displacement parameters (\AA^2) for 3,5-Triazole-Reg2. The anisotropic displacement factor exponent takes the form: $-2\pi^2 [h^2(a^*)^2U_{11} + k^2(b^*)^2U_{22} + \dots + 2hka^*b^*U_{12}]$

Atom	U_{11}	U_{22}	U_{33}	U_{23}	U_{13}	U_{12}
O1	0.0447(5)	0.0311(4)	0.0306(4)	-0.0013(3)	0.0073(4)	-0.0026(4)
C1	0.0197(5)	0.0239(5)	0.0353(6)	0.0066(4)	0.0035(4)	0.0049(4)
N1	0.0203(4)	0.0329(5)	0.0454(6)	0.0145(4)	0.0028(4)	0.0047(4)
O2	0.0997(9)	0.0281(5)	0.0439(5)	-0.0028(4)	0.0162(5)	-0.0166(5)
N2	0.0189(4)	0.0346(5)	0.0451(6)	0.0144(4)	0.0010(4)	0.0031(4)
C2	0.0201(5)	0.0210(5)	0.0297(5)	0.0042(4)	0.0014(4)	0.0056(4)
N3	0.0181(4)	0.0268(4)	0.0343(5)	0.0088(4)	0.0010(3)	0.0038(3)
C3	0.0196(5)	0.0233(5)	0.0257(5)	0.0049(4)	0.0013(4)	0.0023(4)
C4	0.0208(5)	0.0229(5)	0.0242(5)	0.0034(4)	0.0005(4)	0.0028(4)
C5	0.0155(4)	0.0227(5)	0.0318(5)	0.0050(4)	0.0017(4)	0.0040(4)
C6	0.0202(5)	0.0236(5)	0.0293(5)	0.0026(4)	-0.0002(4)	0.0044(4)
C7	0.0212(5)	0.0254(5)	0.0309(5)	0.0068(4)	0.0000(4)	0.0048(4)
C8	0.0270(5)	0.0237(5)	0.0296(5)	0.0050(4)	-0.0030(4)	-0.0001(4)
C9	0.0282(5)	0.0251(5)	0.0294(5)	0.0059(4)	-0.0016(4)	0.0000(4)
C10	0.0243(5)	0.0286(5)	0.0318(6)	0.0058(4)	0.0055(4)	0.0035(4)
C11	0.0212(5)	0.0269(5)	0.0346(6)	0.0064(4)	0.0061(4)	0.0040(4)
C12	0.0244(5)	0.0234(5)	0.0331(6)	0.0040(4)	0.0012(4)	0.0055(4)
C13	0.0278(5)	0.0216(5)	0.0354(6)	0.0048(4)	-0.0009(4)	-0.0012(4)
C14	0.0203(5)	0.0294(6)	0.0362(6)	0.0061(5)	0.0009(4)	-0.0021(4)
C15	0.0198(5)	0.0272(5)	0.0348(6)	0.0050(4)	0.0027(4)	0.0040(4)
C16	0.0352(6)	0.0251(5)	0.0347(6)	0.0054(5)	-0.0035(5)	0.0038(4)
C17	0.0490(7)	0.0272(6)	0.0366(6)	0.0113(5)	-0.0081(5)	0.0013(5)
C18	0.0496(7)	0.0348(6)	0.0302(6)	0.0116(5)	0.0001(5)	-0.0026(5)
C19	0.0363(6)	0.0326(6)	0.0312(6)	0.0066(5)	0.0026(5)	0.0003(5)

C20	0.0213(5)	0.0258(5)	0.0297(5)	0.0051(4)	0.0032(4)	0.0036(4)
C21	0.0245(5)	0.0241(5)	0.0319(6)	0.0021(4)	0.0028(4)	0.0030(4)
C22	0.0252(5)	0.0210(5)	0.0355(6)	0.0056(4)	0.0018(4)	0.0036(4)
C23	0.0351(6)	0.0268(6)	0.0352(6)	0.0025(5)	0.0044(5)	0.0003(5)
C24	0.0483(8)	0.0443(7)	0.0330(7)	-0.0073(5)	0.0060(5)	-0.0061(6)
C25	0.0255(5)	0.0275(5)	0.0332(6)	0.0107(4)	-0.0007(4)	0.0039(4)
C26	0.0254(5)	0.0295(5)	0.0293(5)	0.0072(4)	-0.0048(4)	0.0030(4)
C27	0.0317(6)	0.0392(7)	0.0383(6)	0.0013(5)	0.0017(5)	-0.0038(5)
C28	0.0331(6)	0.0602(9)	0.0409(7)	-0.0033(6)	0.0047(5)	0.0001(6)
C29	0.0462(8)	0.0492(8)	0.0379(7)	-0.0064(6)	-0.0050(6)	0.0167(6)
C30	0.0603(9)	0.0311(6)	0.0460(8)	-0.0003(5)	-0.0040(6)	0.0025(6)
C31	0.0429(7)	0.0332(6)	0.0425(7)	0.0057(5)	0.0013(5)	-0.0036(5)

[1]

Table A6 - 8 Bond lengths and angles for 3,5-Triazole-Reg2

Atom-Atom	Length [Å]	Atom-Atom-Atom	Angle [°]
O1-C23	1.3355(14)	C23-O1-C24	115.71(9)
O1-C24	1.4428(14)	N1-C1-C2	108.75(9)
C1-N1	1.3705(14)	N1-C1-C11	120.46(9)
C1-C2	1.3915(15)	C2-C1-C11	130.57(10)
C1-C11	1.4268(15)	N2-N1-C1	108.79(9)
N1-N2	1.3047(14)	N1-N2-N3	107.77(8)
O2-C23	1.2051(15)	C1-C2-C3	138.21(10)
N2-N3	1.3482(12)	N3-C2-C1	103.20(9)
C2-N3	1.3616(13)	N3-C2-C3	118.50(9)
C2-C3	1.4880(14)	N2-N3-C2	111.48(9)
N3-C25	1.4654(14)	N2-N3-C25	118.77(9)
C3-C4	1.4096(14)	C2-N3-C25	128.99(9)
C3-C12	1.3979(15)	C4-C3-C2	123.24(9)
C4-C5	1.4939(14)	C12-C3-C2	117.38(9)
C4-C15	1.3924(14)	C12-C3-C4	119.01(9)

C5-C6	1.3879(15)	C3-C4-C5	121.21(9)
C5-C20	1.3918(15)	C15-C4-C3	119.05(9)
C6-H6	0.9500	C15-C4-C5	119.56(9)
C6-C7	1.3986(15)	C6-C5-C4	117.05(9)
C7-C8	1.4864(15)	C6-C5-C20	119.26(9)
C7-C22	1.3873(15)	C20-C5-C4	123.70(9)
C8-C9	1.4218(15)	C5-C6-H6	119.0
C8-C16	1.3920(15)	C5-C6-C7	121.98(10)
C9-C10	1.4425(15)	C7-C6-H6	119.0
C9-C19	1.3956(16)	C6-C7-C8	120.06(9)
C10-C11	1.2011(16)	C22-C7-C6	118.21(10)
C12-H12	0.9500	C22-C7-C8	121.43(10)
C12-C13	1.3862(15)	C9-C8-C7	119.20(9)
C13-H13	0.9500	C16-C8-C7	121.72(10)
C13-C14	1.3882(15)	C16-C8-C9	118.98(10)
C14-H14	0.9500	C8-C9-C10	118.03(10)
C14-C15	1.3877(15)	C19-C9-C8	119.40(10)
C15-H15	0.9500	C19-C9-C10	122.46(10)
C16-H16	0.9500	C11-C10-C9	164.25(11)
C16-C17	1.3896(17)	C10-C11-C1	171.22(11)
C17-H17	0.9500	C3-C12-H12	119.4
C17-C18	1.3856(19)	C13-C12-C3	121.14(9)
C18-H18	0.9500	C13-C12-H12	119.4
C18-C19	1.3901(17)	C12-C13-H13	120.1
C19-H19	0.9500	C12-C13-C14	119.72(10)
C20-H20	0.9500	C14-C13-H13	120.1
C20-C21	1.3997(15)	C13-C14-H14	120.1
C21-C22	1.3965(16)	C15-C14-C13	119.75(10)
C21-C23	1.4858(16)	C15-C14-H14	120.1
C22-H22	0.9500	C4-C15-H15	119.4
C24-H24A	0.9800	C14-C15-C4	121.25(9)

C24-H24B	0.9800	C14-C15-H15	119.4
C24-H24C	0.9800	C8-C16-H16	119.5
C25-H25A	0.9900	C17-C16-C8	120.99(11)
C25-H25B	0.9900	C17-C16-H16	119.5
C25-C26	1.5151(15)	C16-C17-H17	120.1
C26-C27	1.3825(16)	C18-C17-C16	119.84(11)
C26-C31	1.3867(17)	C18-C17-H17	120.1
C27-H27	0.9500	C17-C18-H18	119.8
C27-C28	1.3925(18)	C17-C18-C19	120.44(11)
C28-H28	0.9500	C19-C18-H18	119.8
C28-C29	1.378(2)	C9-C19-H19	119.8
C29-H29	0.9500	C18-C19-C9	120.33(11)
C29-C30	1.379(2)	C18-C19-H19	119.8
C30-H30	0.9500	C5-C20-H20	120.3
C30-C31	1.3859(19)	C5-C20-C21	119.34(10)
C31-H31	0.9500	C21-C20-H20	120.3
		C20-C21-C23	122.31(10)
		C22-C21-C20	120.56(10)
		C22-C21-C23	117.07(10)
		C7-C22-C21	120.42(10)
		C7-C22-H22	119.8
		C21-C22-H22	119.8
		O1-C23-C21	112.91(10)
		O2-C23-O1	122.93(11)
		O2-C23-C21	124.16(11)
		O1-C24-H24A	109.5
		O1-C24-H24B	109.5
		O1-C24-H24C	109.5
		H24A-C24-H24B	109.5
		H24A-C24-H24C	109.5
		H24B-C24-H24C	109.5

		N3–C25–H25A	109.4
		N3–C25–H25B	109.4
		N3–C25–C26	111.37(9)
		H25A–C25–H25B	108.0
		C26–C25–H25A	109.4
		C26–C25–H25B	109.4
		C27–C26–C25	120.36(10)
		C27–C26–C31	119.02(11)
		C31–C26–C25	120.60(10)
		C26–C27–H27	119.9
		C26–C27–C28	120.28(12)
		C28–C27–H27	119.9
		C27–C28–H28	119.8
		C29–C28–C27	120.36(13)
		C29–C28–H28	119.8
		C28–C29–H29	120.2
		C28–C29–C30	119.53(12)
		C30–C29–H29	120.2
		C29–C30–H30	119.9
		C29–C30–C31	120.29(13)
		C31–C30–H30	119.9
		C26–C31–H31	119.7
		C30–C31–C26	120.52(12)
		C30–C31–H31	119.7

[2]

Table A6 - 9 Torsion angles for 3,5-Triazole-Reg2

Atom–Atom–Atom– Atom	Torsion Angle [°]	Atom–Atom–Atom– Atom	Torsion Angle [°]
-------------------------	----------------------	-------------------------	----------------------

C1-N1-N2-N3	0.88(12)	C11-C1-C2-C3	9.6(2)
C1-C2-N3-N2	0.36(11)	C12-C3-C4-C5	-172.05(10)
C1-C2-N3-C25	170.10(10)	C12-C3-C4-C15	3.03(15)
C1-C2-C3-C4	-67.96(17)	C12-C13-C14-C15	1.76(17)
C1-C2-C3-C12	119.09(14)	C13-C14-C15-C4	-1.51(17)
N1-C1-C2-N3	0.18(11)	C15-C4-C5-C6	-102.93(11)
N1-C1-C2-C3	-175.92(11)	C15-C4-C5-C20	77.42(13)
N1-N2-N3-C2	-0.79(12)	C16-C8-C9-C10	176.11(10)
N1-N2-N3-C25	-171.71(9)	C16-C8-C9-C19	-0.17(16)
N2-N3-C25-C26	104.40(11)	C16-C17-C18-C19	0.41(19)
C2-C1-N1-N2	-0.67(12)	C17-C18-C19-C9	-0.94(18)
C2-N3-C25-C26	-64.71(14)	C19-C9-C10-C11	168.0(4)
C2-C3-C4-C5	15.10(15)	C20-C5-C6-C7	4.78(15)
C2-C3-C4-C15	-169.82(10)	C20-C21-C22-C7	1.86(16)
C2-C3-C12-C13	170.45(10)	C20-C21-C23-O1	-10.47(16)
N3-C2-C3-C4	116.36(11)	C20-C21-C23-O2	169.37(12)
N3-C2-C3-C12	-56.59(13)	C22-C7-C8-C9	124.37(11)
N3-C25-C26-C27	135.15(11)	C22-C7-C8-C16	-52.04(15)
N3-C25-C26-C31	-46.48(14)	C22-C21-C23-O1	172.36(10)
C3-C2-N3-N2	177.41(9)	C22-C21-C23-O2	-7.80(18)
C3-C2-N3-C25	-12.85(16)	C23-C21-C22-C7	179.08(10)
C3-C4-C5-C6	72.12(13)	C24-O1-C23-O2	1.56(18)
C3-C4-C5-C20	-107.53(12)	C24-O1-C23-C21	-178.59(10)
C3-C4-C15-C14	-0.91(16)	C25-C26-C27-C28	177.92(11)
C3-C12-C13-C14	0.42(17)	C25-C26-C31-C30	-178.10(11)
C4-C3-C12-C13	-2.82(16)	C26-C27-C28-C29	0.5(2)
C4-C5-C6-C7	-174.88(9)	C27-C26-C31-C30	0.28(19)
C4-C5-C20-C21	178.96(9)	C27-C28-C29-C30	-0.4(2)

C5–C4–C15–C14	174.25(10)	C28–C29–C30–C31	0.2(2)
C5–C6–C7–C8	168.36(9)	C29–C30–C31–C26	-0.1(2)
C5–C6–C7–C22	-5.46(15)	C31–C26–C27–C28	-0.47(18)
C5–C20–C21–C22	-2.58(15)		
C5–C20–C21–C23	-179.65(10)		
C6–C5–C20–C21	-0.69(15)		
C6–C7–C8–C9	-49.24(14)		
C6–C7–C8–C16	134.35(11)		
C6–C7–C22–C21	2.08(15)		
C7–C8–C9–C10	-0.41(15)		
C7–C8–C9–C19	-176.68(10)		
C7–C8–C16–C17	176.08(10)		
C8–C7–C22–C21	-171.65(10)		
C8–C9–C10–C11	-8.1(5)		
C8–C9–C19–C18	0.81(17)		
C8–C16–C17–C18	0.23(18)		
C9–C8–C16–C17	-0.35(16)		
C10–C9–C19–C18	-175.30(11)		
C11–C1–N1–N2	174.51(10)		
C11–C1–C2–N3	-174.35(11)		

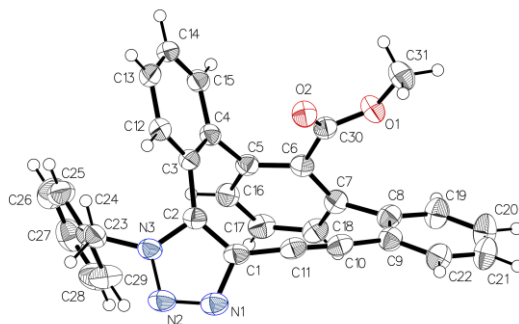
Table A6 - 10 Hydrogen bonds for 3,5-Triazole-Reg2

D–H···A [Å]	d(D–H) [Å]	d(H···A) [Å]	d(D···A) [Å]	<(DHA) [°]
C25–H25B···O2 ^{#1}	0.99	2.49	3.3696(15)	147.2

Symmetry transformations used to generate equivalent atoms:

#1: +X, -1+Y, +Z;

2,6-Triazole-Reg2



The data for 2,6-Triazole-Reg2, crystallised in DCM/Et₂O, were collected from a shock-cooled single crystal at 150 K on a Bruker Venture Metaljet k-geometry diffractometer with a Metal Jet using Helios MX Mirror Optics as monochromator and a Bruker CMOS Photon III detector. The diffractometer was equipped with an Oxford Cryostream 700 low temperature device and used Ga K_{α} radiation ($\lambda = 1.34139 \text{ \AA}$). All data were integrated with *SAINT* (2020) and a multi-scan absorption correction using *SADABS* 2016/2 was applied.^{12, 17} The structure was solved by dual methods with *XT* and refined by full-matrix least-squares methods against F^2 using *XL*.¹³⁻¹⁴ Structure solution and refinement cycles were performed within the graphical user interface of *OLEX2*. All non-hydrogen atoms were refined with anisotropic displacement parameters. The hydrogen atoms were located from difference Fourier map and refined isotropically.¹⁵ This report and the CIF file were generated using *FinalCif*.¹⁶

Table A6 - 11 Crystal data and structure refinement for 2,6-Triazole-Reg2

Empirical formula	C ₃₁ H ₂₁ N ₃ O ₂
Formula weight	467.51
Temperature [K]	150
Crystal system	monoclinic
Space group (number)	$P2_1/c$ (14)
a [Å]	12.4818(4)
b [Å]	19.2648(6)
c [Å]	9.9306(3)
α [°]	90
β [°]	98.037(2)
γ [°]	90

Volume [Å ³]	2364.45(13)
Z	4
ρ_{calc} [gcm ⁻³]	1.313
μ [mm ⁻¹]	0.423
F(000)	976
Crystal size [mm ³]	0.06×0.13×0.17
Crystal colour	clear light colourless
Crystal shape	block
Radiation	Ga K α (λ =1.34139 Å)
2 θ range [°]	6.22 to 111.88 (0.81 Å)
Index ranges	-14 ≤ h ≤ 15 -23 ≤ k ≤ 23 -12 ≤ l ≤ 12
Reflections collected	23285
Independent reflections	4593 $R_{\text{int}} = 0.0502$ $R_{\text{sigma}} = 0.0460$
Completeness to $\theta = 53.594^\circ$	99.7 %
Data / Restraints / Parameters	4593 / 0 / 327
Goodness-of-fit on F^2	1.028
Final R indexes [I ≥ 2 σ (I)]	$R_1 = 0.0420$ $wR_2 = 0.0922$
Final R indexes [all data]	$R_1 = 0.0746$ $wR_2 = 0.1045$
Largest peak/hole [eÅ ⁻³]	0.17/-0.16
Extinction coefficient	0.0028(3)

Table A6 - 12 Atomic coordinates and U_{eq} [Å²] for 2,6-Triazole-Reg2

Atom	x	y	z	U_{eq}
O1	0.91400(9)	0.40967(6)	0.16294(12)	0.0421(3)
C1	0.74906(13)	0.58744(9)	0.47619(15)	0.0342(4)
N1	0.70352(12)	0.61257(8)	0.58453(14)	0.0400(4)
O2	0.91226(9)	0.52466(6)	0.19309(12)	0.0408(3)
C2	0.70778(13)	0.62443(8)	0.36035(16)	0.0322(4)
N2	0.63528(12)	0.66224(8)	0.54146(13)	0.0405(4)
N3	0.63776(11)	0.66989(7)	0.40669(13)	0.0352(3)
C3	0.72532(12)	0.62757(8)	0.21549(15)	0.0308(4)
C4	0.70066(12)	0.57228(8)	0.12479(15)	0.0312(4)
C5	0.67247(13)	0.50307(8)	0.17697(15)	0.0317(4)
C6	0.75467(13)	0.45611(8)	0.22244(15)	0.0319(4)

C7	0.73202(13)	0.39674(9)	0.29527(16)	0.0347(4)
C8	0.82001(13)	0.35971(9)	0.38417(17)	0.0373(4)
C9	0.88271(13)	0.39834(9)	0.48842(17)	0.0375(4)
C10	0.85724(14)	0.47096(10)	0.50063(16)	0.0373(4)
C11	0.81632(14)	0.52743(10)	0.49236(16)	0.0361(4)
C12	0.76405(12)	0.68942(9)	0.16799(16)	0.0338(4)
H12	0.782858	0.725718	0.228437	0.041
C13	0.77495(13)	0.69766(9)	0.03181(16)	0.0368(4)
H13	0.802488	0.738817	0.001691	0.044
C14	0.74478(13)	0.64457(9)	-0.05869(16)	0.0367(4)
H14	0.748540	0.650677	-0.150815	0.044
C15	0.70895(13)	0.58226(9)	-0.01233(16)	0.0348(4)
H15	0.690047	0.546384	-0.073721	0.042
C16	0.56595(13)	0.48598(9)	0.18857(16)	0.0358(4)
H16	0.510393	0.516373	0.156133	0.043
C17	0.54222(14)	0.42406(9)	0.24806(17)	0.0409(4)
H17	0.470561	0.411475	0.250315	0.049
C18	0.62492(14)	0.38080(9)	0.30421(17)	0.0389(4)
H18	0.608521	0.340467	0.348574	0.047
C19	0.83822(15)	0.28940(9)	0.37516(19)	0.0474(5)
H19	0.797690	0.263695	0.306880	0.057
C20	0.91602(16)	0.25645(11)	0.4664(2)	0.0560(5)
H20	0.927840	0.209034	0.458764	0.067
C21	0.97574(15)	0.29412(10)	0.5682(2)	0.0522(5)
H21	1.027011	0.271679	0.630171	0.063
C22	0.96060(14)	0.36478(10)	0.57967(18)	0.0428(4)
H22	1.002235	0.389826	0.648016	0.051
C23	0.55813(14)	0.71510(9)	0.32878(17)	0.0399(4)
H23A	0.591801	0.739187	0.259849	0.048
H23B	0.534126	0.749688	0.388947	0.048
C24	0.46168(14)	0.67504(9)	0.26131(16)	0.0367(4)
C25	0.42238(17)	0.68610(10)	0.12640(18)	0.0495(5)
H25	0.457551	0.717227	0.075950	0.059
C26	0.33137(19)	0.65157(11)	0.0649(2)	0.0611(6)
H26	0.305096	0.660096	-0.025867	0.073
C27	0.28009(16)	0.60498(11)	0.1374(2)	0.0555(5)
H27	0.218641	0.581974	0.096131	0.067
C28	0.31870(16)	0.59220(12)	0.2698(2)	0.0595(6)
H28	0.284199	0.559978	0.318643	0.071
C29	0.40919(16)	0.62697(11)	0.33205(19)	0.0539(5)
H29	0.435066	0.617888	0.422749	0.065
C30	0.86792(13)	0.46934(9)	0.19403(16)	0.0336(4)
C31	1.02632(14)	0.41376(11)	0.1443(2)	0.0516(5)
H31A	1.032539	0.438143	0.061450	0.077
H31B	1.055098	0.367755	0.139488	0.077
H31C	1.066119	0.438103	0.219582	0.077

U_{eq} is defined as 1/3 of the trace of the orthogonalized U_{ij} tensor.

Table A6 - 13 Anisotropic displacement parameters (\AA^2) for 2,6-Triazole-Reg2. The anisotropic displacement factor exponent takes the form: $-2\pi^2 [h^2(a^*)^2U_{11} + k^2(b^*)^2U_{22} + \dots + 2hka^*b^*U_{12}]$

Atom	U_{11}	U_{22}	U_{33}	U_{23}	U_{13}	U_{12}
O1	0.0351(7)	0.0385(7)	0.0540(8)	-0.0064(6)	0.0104(6)	0.0027(5)
C1	0.0403(10)	0.0356(10)	0.0271(8)	-0.0031(7)	0.0065(7)	-0.0056(8)
N1	0.0496(9)	0.0389(9)	0.0327(8)	-0.0045(7)	0.0093(7)	-0.0068(7)
O2	0.0360(7)	0.0376(7)	0.0491(7)	0.0006(6)	0.0068(5)	-0.0035(6)
C2	0.0359(9)	0.0298(9)	0.0315(9)	-0.0042(7)	0.0070(7)	-0.0050(7)
N2	0.0512(9)	0.0405(9)	0.0316(8)	-0.0056(7)	0.0122(7)	-0.0051(8)
N3	0.0422(8)	0.0346(8)	0.0299(7)	-0.0047(6)	0.0088(6)	-0.0004(7)
C3	0.0300(8)	0.0338(10)	0.0288(8)	0.0005(7)	0.0047(7)	0.0029(7)
C4	0.0281(8)	0.0353(10)	0.0301(8)	-0.0003(7)	0.0039(7)	0.0035(7)
C5	0.0364(9)	0.0329(10)	0.0251(8)	-0.0043(7)	0.0021(7)	-0.0011(7)
C6	0.0341(9)	0.0330(10)	0.0281(8)	-0.0052(7)	0.0024(7)	-0.0030(7)
C7	0.0373(9)	0.0322(10)	0.0338(9)	-0.0033(7)	0.0017(7)	-0.0027(8)
C8	0.0369(9)	0.0362(10)	0.0386(9)	0.0040(8)	0.0049(8)	-0.0036(8)
C9	0.0363(9)	0.0369(11)	0.0393(9)	0.0027(8)	0.0054(8)	-0.0025(8)
C10	0.0396(10)	0.0426(12)	0.0289(9)	0.0015(8)	0.0025(7)	-0.0067(9)
C11	0.0416(10)	0.0392(11)	0.0269(9)	-0.0003(8)	0.0030(7)	-0.0075(9)
C12	0.0342(9)	0.0339(10)	0.0336(9)	0.0000(8)	0.0055(7)	0.0023(7)
C13	0.0372(9)	0.0364(10)	0.0375(9)	0.0075(8)	0.0082(7)	0.0042(8)
C14	0.0370(9)	0.0450(11)	0.0289(9)	0.0059(8)	0.0076(7)	0.0074(8)
C15	0.0332(9)	0.0409(11)	0.0297(9)	-0.0035(8)	0.0019(7)	0.0046(8)
C16	0.0306(9)	0.0419(11)	0.0342(9)	-0.0004(8)	0.0015(7)	0.0007(8)
C17	0.0324(9)	0.0505(12)	0.0393(10)	0.0012(9)	0.0037(8)	-0.0082(8)
C18	0.0414(10)	0.0365(10)	0.0383(9)	0.0015(8)	0.0034(8)	-0.0069(8)
C19	0.0493(11)	0.0372(11)	0.0521(11)	-0.0015(9)	-0.0054(9)	-0.0009(9)
C20	0.0566(13)	0.0367(11)	0.0698(14)	0.0017(10)	-0.0081(11)	0.0067(10)
C21	0.0465(11)	0.0474(13)	0.0585(12)	0.0068(10)	-0.0076(9)	0.0052(9)
C22	0.0398(10)	0.0431(12)	0.0437(10)	0.0012(9)	-0.0007(8)	-0.0025(8)
C23	0.0454(10)	0.0343(10)	0.0425(10)	-0.0020(8)	0.0145(8)	0.0045(8)
C24	0.0399(10)	0.0365(10)	0.0356(9)	-0.0034(8)	0.0118(8)	0.0057(8)
C25	0.0693(13)	0.0428(12)	0.0373(10)	0.0003(9)	0.0112(9)	0.0007(10)
C26	0.0796(16)	0.0563(14)	0.0424(11)	-0.0062(10)	-0.0092(11)	0.0050(12)

C27	0.0496(12)	0.0532(13)	0.0612(13)	-0.0172(11)	-0.0007(10)	0.0052(10)
C28	0.0521(12)	0.0714(15)	0.0580(13)	-0.0052(11)	0.0178(10)	-0.0179(11)
C29	0.0560(12)	0.0691(14)	0.0379(10)	0.0014(10)	0.0111(9)	-0.0127(11)
C30	0.0352(9)	0.0359(10)	0.0289(8)	-0.0013(8)	0.0018(7)	0.0002(8)
C31	0.0368(10)	0.0545(13)	0.0654(13)	-0.0045(10)	0.0142(9)	0.0050(9)

Table A6 - 14 Bond lengths and angles for 2,6-Triazole-Reg2

Atom-Atom	Length [Å]	Atom-Atom-Atom	Angle [°]	Atom-Atom-Atom	Angle [°]
O1-C30	1.341(2)	C30-O1-C31	116.04(14)	C20-C21-C22	120.92(18)
O1-C31	1.442(2)	N1-C1-C2	108.76(15)	C22-C21-H21	119.5
C1-N1	1.373(2)	N1-C1-C11	119.98(14)	C9-C22-H22	120.2
C1-C2	1.390(2)	C2-C1-C11	130.84(14)	C21-C22-C9	119.68(17)
C1-C11	1.425(2)	N2-N1-C1	108.82(13)	C21-C22-H22	120.2
N1-N2	1.312(2)	C1-C2-C3	137.25(15)	N3-C23-H23A	109.2
O2-C30	1.2016(19)	N3-C2-C1	103.37(13)	N3-C23-H23B	109.2
C2-N3	1.362(2)	N3-C2-C3	119.29(14)	N3-C23-C24	111.89(14)
C2-C3	1.486(2)	N1-N2-N3	107.38(13)	H23A-C23-H23B	107.9
N2-N3	1.3511(18)	C2-N3-C23	128.77(13)	C24-C23-H23A	109.2
N3-C23	1.459(2)	N2-N3-C2	111.67(13)	C24-C23-H23B	109.2
C3-C4	1.401(2)	N2-N3-C23	118.82(13)	C25-C24-C23	120.48(16)
C3-C12	1.393(2)	C4-C3-C2	122.85(14)	C25-C24-C29	117.94(17)
C4-C5	1.490(2)	C12-C3-C2	117.88(14)	C29-C24-C23	121.58(16)
C4-C15	1.393(2)	C12-C3-C4	119.22(14)	C24-C25-H25	119.5
C5-C6	1.395(2)	C3-C4-C5	119.87(13)	C24-C25-C26	120.93(18)
C5-C16	1.390(2)	C15-C4-C3	118.93(15)	C26-C25-H25	119.5
C6-C7	1.403(2)	C15-C4-C5	121.11(14)	C25-C26-H26	120.0
C6-C30	1.501(2)	C6-C5-C4	119.61(14)	C27-C26-C25	120.04(19)
C7-C8	1.491(2)	C16-C5-C4	121.05(15)	C27-C26-H26	120.0
C7-C18	1.386(2)	C16-C5-C6	119.23(15)	C26-C27-H27	120.0
C8-C9	1.418(2)	C5-C6-C7	120.23(15)	C28-C27-C26	120.0(2)
C8-C19	1.379(2)	C5-C6-C30	119.89(14)	C28-C27-H27	120.0
C9-C10	1.444(3)	C7-C6-C30	119.87(14)	C27-C28-H28	119.9
C9-C22	1.392(2)	C6-C7-C8	120.69(14)	C27-C28-C29	120.2(2)
C10-C11	1.200(2)	C18-C7-C6	118.63(15)	C29-C28-H28	119.9
C12-H12	0.9300	C18-C7-C8	119.55(15)	C24-C29-C28	120.87(18)
C12-C13	1.387(2)	C9-C8-C7	117.83(15)	C24-C29-H29	119.6
C13-H13	0.9300	C19-C8-C7	123.10(15)	C28-C29-H29	119.6
C13-C14	1.379(2)	C19-C8-C9	118.93(16)	O1-C30-C6	110.08(14)
C14-H14	0.9300	C8-C9-C10	117.66(15)	O2-C30-O1	123.08(15)

C14–C15	1.382(2)	C22–C9–C8	119.70(16)	O2–C30–C6	126.79(15)
C15–H15	0.9300	C22–C9–C10	122.50(16)	O1–C31–H31A	109.5
C16–H16	0.9300	C11–C10–C9	165.86(18)	O1–C31–H31B	109.5
C16–C17	1.382(2)	C10–C11–C1	169.15(18)	O1–C31–H31C	109.5
C17–H17	0.9300	C3–C12–H12	119.5	H31A–C31–H31B	109.5
C17–C18	1.382(2)	C13–C12–C3	120.94(15)	H31A–C31–H31C	109.5
C18–H18	0.9300	C13–C12–H12	119.5	H31B–C31–H31C	109.5
C19–H19	0.9300	C12–C13–H13	120.1		
C19–C20	1.386(2)	C14–C13–C12	119.71(16)		
C20–H20	0.9300	C14–C13–H13	120.1		
C20–C21	1.376(3)	C13–C14–H14	120.0		
C21–H21	0.9300	C13–C14–C15	119.91(15)		
C21–C22	1.381(3)	C15–C14–H14	120.0		
C22–H22	0.9300	C4–C15–H15	119.4		
C23–H23A	0.9700	C14–C15–C4	121.14(15)		
C23–H23B	0.9700	C14–C15–H15	119.4		
C23–C24	1.506(2)	C5–C16–H16	119.8		
C24–C25	1.377(2)	C17–C16–C5	120.31(16)		
C24–C29	1.382(2)	C17–C16–H16	119.8		
C25–H25	0.9300	C16–C17–H17	120.0		
C25–C26	1.383(3)	C16–C17–C18	120.04(16)		
C26–H26	0.9300	C18–C17–H17	120.0		
C26–C27	1.365(3)	C7–C18–H18	119.6		
C27–H27	0.9300	C17–C18–C7	120.87(16)		
C27–C28	1.358(3)	C17–C18–H18	119.6		
C28–H28	0.9300	C8–C19–H19	119.5		
C28–C29	1.383(3)	C8–C19–C20	120.97(18)		
C29–H29	0.9300	C20–C19–H19	119.5		
C31–H31A	0.9600	C19–C20–H20	120.1		
C31–H31B	0.9600	C21–C20–C19	119.79(19)		
C31–H31C	0.9600	C21–C20–H20	120.1		
		C20–C21–H21	119.5		

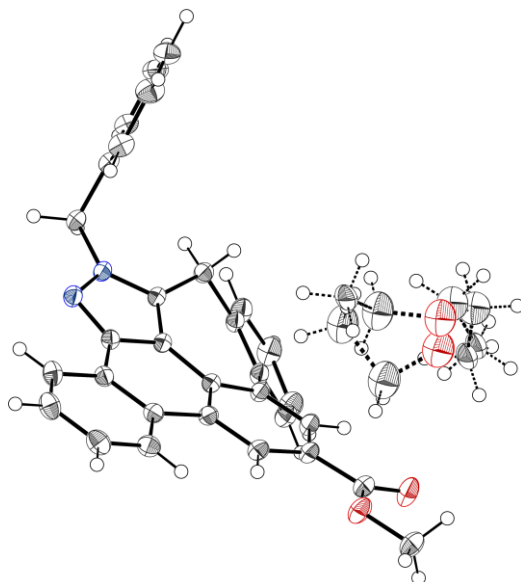
Table A6 - 15 Torsion angles for 2,6-Triazole-Reg2

Atom–Atom–Atom–Atom	Torsion Angle [°]	Atom–Atom–Atom–Atom	Torsion Angle [°]
C1–N1–N2–N3	-0.85(18)	C8–C9–C22–C21	-0.3(3)
C1–C2–N3–N2	0.14(17)	C8–C19–C20–C21	0.4(3)
C1–C2–N3–C23	-169.71(15)	C9–C8–C19–C20	0.3(3)
C1–C2–C3–C4	65.8(3)	C9–C10–C11–C1	23.7(14)
C1–C2–C3–C12	-116.7(2)	C10–C9–C22–C21	175.35(17)

N1-C1-C2-N3	-0.65(17)	C11-C1-N1-N2	-172.40(14)
N1-C1-C2-C3	175.68(17)	C11-C1-C2-N3	171.74(17)
N1-C1-C11-C10	88.0(9)	C11-C1-C2-C3	-11.9(3)
N1-N2-N3-C2	0.45(18)	C12-C3-C4-C5	172.34(14)
N1-N2-N3-C23	171.43(14)	C12-C3-C4-C15	-4.1(2)
C2-C1-N1-N2	0.96(19)	C12-C13-C14-C15	-3.2(2)
C2-C1-C11-C10	-83.7(9)	C13-C14-C15-C4	1.2(2)
C2-N3-C23-C24	73.8(2)	C15-C4-C5-C6	89.91(19)
C2-C3-C4-C5	-10.2(2)	C15-C4-C5-C16	-93.89(19)
C2-C3-C4-C15	173.31(14)	C16-C5-C6-C7	-8.5(2)
C2-C3-C12-C13	-175.36(14)	C16-C5-C6-C30	171.88(14)
N2-N3-C23-C24	-95.47(17)	C16-C17-C18-C7	-3.6(3)
N3-C2-C3-C4	-118.26(17)	C18-C7-C8-C9	-111.17(18)
N3-C2-C3-C12	59.2(2)	C18-C7-C8-C19	64.5(2)
N3-C23-C24-C25	-132.71(16)	C19-C8-C9-C10	-176.20(16)
N3-C23-C24-C29	48.0(2)	C19-C8-C9-C22	-0.3(2)
C3-C2-N3-N2	-177.01(13)	C19-C20-C21-C22	-1.1(3)
C3-C2-N3-C23	13.1(2)	C20-C21-C22-C9	1.0(3)
C3-C4-C5-C6	-86.45(19)	C22-C9-C10-C11	-162.4(6)
C3-C4-C5-C16	89.74(19)	C23-C24-C25-C26	-177.47(17)
C3-C4-C15-C14	2.5(2)	C23-C24-C29-C28	177.96(18)
C3-C12-C13-C14	1.5(2)	C24-C25-C26-C27	-1.0(3)
C4-C3-C12-C13	2.2(2)	C25-C24-C29-C28	-1.3(3)
C4-C5-C6-C7	167.80(14)	C25-C26-C27-C28	-0.4(3)
C4-C5-C6-C30	-11.9(2)	C26-C27-C28-C29	0.9(3)
C4-C5-C16-C17	-174.35(15)	C27-C28-C29-C24	0.0(3)
C5-C4-C15-C14	-173.94(15)	C29-C24-C25-C26	1.8(3)
C5-C6-C7-C8	-158.77(15)	C30-C6-C7-C8	20.9(2)
C5-C6-C7-C18	9.0(2)	C30-C6-C7-C18	-171.36(15)
C5-C6-C30-O1	-140.73(15)	C31-O1-C30-O2	7.6(2)
C5-C6-C30-O2	36.6(2)	C31-O1-C30-C6	-175.00(14)
C5-C16-C17-C18	4.2(3)		
C6-C5-C16-C17	1.9(2)		
C6-C7-C8-C9	56.5(2)		
C6-C7-C8-C19	-127.85(18)		
C6-C7-C18-C17	-2.9(2)		
C7-C6-C30-O1	39.61(19)		
C7-C6-C30-O2	-143.06(17)		
C7-C8-C9-C10	-0.3(2)		
C7-C8-C9-C22	175.52(15)		

C7-C8-C19-C20	-175.36(17)
C8-C7-C18-C17	164.95(16)
C8-C9-C10-C11	13.3(8)
C8-C9-C22-C21	-0.3(3)

3,5-Pyrazole



The data for 3,5-Pyrazole, crystallised from DCM/Et₂O, were collected from a shock-cooled single crystal at 150 K on a Bruker Venture Metaljet k-geometry diffractometer with a Metal Jet using a Helios MX Mirror Optics as monochromator and a Bruker CMOS Photon III detector. The diffractometer was equipped with an Oxford Cryostream 700 low temperature device and used Ga K_{α} radiation ($\lambda = 1.34139 \text{ \AA}$). All data were integrated with *SAINT* (2020) and a multi-scan absorption correction using *SADABS* 2016/2 was applied.^{12, 17} The structure was solved by dual methods with *XT* and refined by full-matrix least-squares methods against F^2 using *XL*.¹³⁻¹⁴ Calculation (structure solution and refinement cycles) were performed within the graphical user interface of *OLEX2*.¹⁵ All non-hydrogen atoms were refined with anisotropic displacement parameters. The hydrogen atoms were refined isotropically on calculated positions using a riding model with their U_{iso} values constrained to 1.5 times the U_{eq} of their pivot atoms for terminal sp^3 carbon atoms and 1.2 times for all other carbon atoms. Disordered parts of the solvent molecule were refined using restraints and constraints applied on distances and thermal atomic displacement parameters. This report and the CIF file were generated using *FinalCif*.¹⁶

Table A6 - 16 Crystal data and structure refinement for 3,5-Pyrazole

--	--

Empirical formula	C ₆₆ H ₅₄ N ₄ O ₅
Formula weight	983.13
Temperature [K]	150
Crystal system	triclinic
Space group (number)	$P\bar{1}$ (2)
<i>a</i> [Å]	11.0004(3)
<i>b</i> [Å]	11.5318(3)
<i>c</i> [Å]	11.5660(3)
α [°]	72.131(1)
β [°]	64.840(1)
γ [°]	69.268(1)
Volume [Å ³]	1220.64(6)
<i>Z</i>	1
ρ_{calc} [gcm ⁻³]	1.337
μ [mm ⁻¹]	0.427
<i>F</i> (000)	518
Crystal size [mm ³]	0.18×0.2×0.25
Crystal colour	clear light colourless
Crystal shape	Block
Radiation	Ga <i>K</i> _α (λ=1.34139 Å)
2θ range [°]	7.48 to 146.82 (0.70 Å)
Index ranges	-15 ≤ <i>h</i> ≤ 15 -16 ≤ <i>k</i> ≤ 16 -15 ≤ <i>l</i> ≤ 16
Reflections collected	51630
Independent reflections	7403 <i>R</i> _{int} = 0.0279 <i>R</i> _{sigma} = 0.0269
Completeness to θ = 53.594°	98.8 %
Data / Restraints / Parameters	7403 / 130 / 395
Goodness-of-fit on <i>F</i> ²	1.061
Final <i>R</i> indexes [<i>I</i> ≥ 2σ(<i>I</i>)]	<i>R</i> ₁ = 0.0562 w <i>R</i> ₂ = 0.1502
Final <i>R</i> indexes [all data]	<i>R</i> ₁ = 0.0573 w <i>R</i> ₂ = 0.1514
Largest peak/hole [eÅ ⁻³]	0.56/-0.48

Table A6 - 17 Atomic coordinates and *U*_{eq} [Å²] for 3,5-Pyrazole

Atom	<i>x</i>	<i>y</i>	<i>z</i>	<i>U</i> _{eq}
------	----------	----------	----------	------------------------

O1	-0.17710(8)	1.03996(7)	0.21542(9)	0.03471(19)
O2	0.00436(8)	1.12481(7)	0.10280(8)	0.03051(17)
N1	0.46143(8)	0.36299(7)	0.26134(8)	0.02120(16)
N2	0.56051(8)	0.42152(8)	0.16933(8)	0.02212(16)
C1	0.33027(9)	0.43762(8)	0.28329(9)	0.01996(17)
C2	0.20383(10)	0.40911(9)	0.39275(9)	0.02379(18)
H2A	0.180928	0.454647	0.462327	0.029
H2B	0.224272	0.317616	0.428934	0.029
C3	0.07899(9)	0.44577(9)	0.35293(9)	0.02207(17)
C4	0.00358(11)	0.35584(9)	0.39487(11)	0.0276(2)
H4	0.033300	0.277029	0.445581	0.033
C5	-0.11295(12)	0.37772(10)	0.36502(12)	0.0320(2)
H5	-0.162995	0.315389	0.396007	0.038
C6	-0.15564(11)	0.49204(11)	0.28917(12)	0.0310(2)
H6	-0.233629	0.507817	0.265514	0.037
C7	-0.08312(10)	0.58292(10)	0.24835(10)	0.02616(19)
H7	-0.112927	0.660665	0.196269	0.031
C8	0.03306(9)	0.56462(9)	0.28099(9)	0.02154(17)
C9	0.09448(9)	0.67511(8)	0.23386(9)	0.02062(17)
C10	0.23970(9)	0.66624(8)	0.18040(8)	0.01932(16)
C11	0.34221(9)	0.55063(8)	0.19725(8)	0.01918(16)
C12	0.48622(9)	0.53673(9)	0.13201(9)	0.02006(17)
C13	0.53956(9)	0.64223(9)	0.04527(9)	0.02076(17)
C14	0.68290(10)	0.63105(10)	-0.02036(10)	0.02622(19)
H14	0.747286	0.550893	-0.013124	0.031
C15	0.73070(11)	0.73588(11)	-0.09529(11)	0.0301(2)
H15	0.827619	0.728203	-0.139021	0.036
C16	0.63513(12)	0.85350(11)	-0.10622(10)	0.0296(2)
H16	0.667589	0.925924	-0.157194	0.036
C17	0.49381(11)	0.86520(10)	-0.04345(10)	0.02531(19)
H17	0.430618	0.945602	-0.053453	0.030
C18	0.44144(10)	0.76059(9)	0.03501(9)	0.02058(17)
C19	0.29022(9)	0.77408(8)	0.10520(9)	0.02020(17)
C20	0.19391(10)	0.89218(9)	0.09886(9)	0.02273(18)
H20	0.225683	0.965298	0.049535	0.027
C21	0.05236(10)	0.90312(9)	0.16414(9)	0.02298(18)
C22	0.00365(10)	0.79536(9)	0.22887(10)	0.02332(18)
H22	-0.093658	0.804219	0.270457	0.028
C23	-0.05254(10)	1.02721(9)	0.16462(10)	0.02459(19)
C24	-0.09425(12)	1.24720(10)	0.09949(12)	0.0324(2)
H24A	-0.044053	1.312799	0.052721	0.049
H24B	-0.154305	1.250679	0.055005	0.049
H24C	-0.151273	1.261132	0.188517	0.049
C25	0.50350(10)	0.23470(9)	0.32895(9)	0.02324(18)

H25A	0.603044	0.197672	0.282375	0.028
H25B	0.449277	0.182797	0.327658	0.028
C26	0.48156(10)	0.23034(9)	0.46833(9)	0.02235(18)
C27	0.53000(12)	0.30996(10)	0.49853(11)	0.0292(2)
H27	0.575106	0.369127	0.431282	0.035
C28	0.51249(14)	0.30299(12)	0.62662(12)	0.0356(2)
H28	0.546549	0.356798	0.646418	0.043
C29	0.44532(13)	0.21759(12)	0.72586(11)	0.0350(2)
H29	0.433766	0.212869	0.813246	0.042
C30	0.39526(12)	0.13935(11)	0.69701(11)	0.0305(2)
H30	0.348526	0.081497	0.764707	0.037
C31	0.41358(11)	0.14566(9)	0.56850(10)	0.02547(19)
H31	0.379392	0.091700	0.549066	0.031
C1A	0.2288(7)	1.0066(12)	0.4448(10)	0.0376(13)
H1AA	0.308238	0.941293	0.403372	0.056
H1AB	0.230868	1.088555	0.386291	0.056
H1AC	0.233997	1.010224	0.526107	0.056
C2A	0.0952(4)	0.9756(4)	0.4735(5)	0.0583(9)
H2AA	0.090593	0.970721	0.391541	0.070
H2AB	0.093726	0.892286	0.531543	0.070
O1A	-0.0214(3)	1.0682(3)	0.5333(4)	0.0539(7)
C3A	-0.1411(4)	1.0247(4)	0.6044(4)	0.0477(7)
H3AA	-0.212568	1.087745	0.657236	0.057
H3AB	-0.118561	0.945518	0.664934	0.057
C4A	-0.2007(7)	1.0006(9)	0.5216(5)	0.0394(12)
H4AA	-0.283937	0.970418	0.577436	0.059
H4AB	-0.225672	1.078945	0.462863	0.059
H4AC	-0.131558	0.936555	0.470570	0.059
C1B	0.1531(16)	0.9416(16)	0.409(2)	0.0583(9)
H1BA	0.222781	0.896374	0.339461	0.087
H1BB	0.197463	0.985056	0.434549	0.087
H1BC	0.111811	0.881418	0.484375	0.087
C2B	0.0375(13)	1.0398(13)	0.3606(10)	0.0596(13)
H2BA	0.073437	1.105157	0.286943	0.072
H2BB	-0.013404	1.000080	0.337461	0.072
O1B	-0.0423(10)	1.0864(9)	0.4772(10)	0.0548(9)
C3B	-0.0937(17)	0.9962(13)	0.5857(11)	0.0487(11)
H3BA	-0.125220	1.024138	0.669036	0.058
H3BB	-0.025603	0.912541	0.586692	0.058
C4B	-0.216(3)	0.998(5)	0.552(3)	0.0394(12)
H4BA	-0.267139	0.938912	0.618824	0.059
H4BB	-0.278038	1.083407	0.548643	0.059
H4BC	-0.179741	0.973289	0.467391	0.059

U_{eq} is defined as 1/3 of the trace of the orthogonalized U_{ij} tensor.

Table A6 - 18 Bond lengths and angles for 3,5-Pyrazole

Atom-Atom	Length [Å]	Atom-Atom-Atom	Angle [°]	Atom-Atom-Atom	Angle [°]
O1-C23	1.2125(13)	C23-O2-C24	114.87(8)	C31-C26-C27	119.04(9)
O2-C23	1.3394(12)	N2-N1-C25	119.71(7)	C26-C27-H27	119.9
O2-C24	1.4452(12)	C1-N1-N2	113.33(8)	C28-C27-C26	120.27(10)
N1-N2	1.3674(11)	C1-N1-C25	126.88(8)	C28-C27-H27	119.9
N1-C1	1.3529(11)	C12-N2-N1	103.54(7)	C27-C28-H28	119.9
N1-C25	1.4586(12)	N1-C1-C2	125.56(8)	C27-C28-C29	120.27(10)
N2-C12	1.3412(12)	N1-C1-C11	106.01(8)	C29-C28-H28	119.9
C1-C2	1.4888(12)	C11-C1-C2	127.72(8)	C28-C29-H29	120.1
C1-C11	1.3857(12)	C1-C2-H2A	109.0	C30-C29-C28	119.86(10)
C2-H2A	0.9900	C1-C2-H2B	109.0	C30-C29-H29	120.1
C2-H2B	0.9900	C1-C2-C3	113.12(8)	C29-C30-H30	120.0
C2-C3	1.5113(13)	H2A-C2-H2B	107.8	C29-C30-C31	119.93(10)
C3-C4	1.3990(13)	C3-C2-H2A	109.0	C31-C30-H30	120.0
C3-C8	1.4119(13)	C3-C2-H2B	109.0	C26-C31-C30	120.62(9)
C4-H4	0.9500	C4-C3-C2	116.58(8)	C26-C31-H31	119.7
C4-C5	1.3856(16)	C4-C3-C8	119.24(9)	C30-C31-H31	119.7
C5-H5	0.9500	C8-C3-C2	124.15(8)	H1AA-C1A-H1AB	109.5
C5-C6	1.3893(16)	C3-C4-H4	118.9	H1AA-C1A-H1AC	109.5
C6-H6	0.9500	C5-C4-C3	122.29(10)	H1AB-C1A-H1AC	109.5
C6-C7	1.3877(14)	C5-C4-H4	118.9	C2A-C1A-H1AA	109.5
C7-H7	0.9500	C4-C5-H5	120.4	C2A-C1A-H1AB	109.5
C7-C8	1.4110(13)	C4-C5-C6	119.12(10)	C2A-C1A-H1AC	109.5
C8-C9	1.4991(13)	C6-C5-H5	120.4	C1A-C2A-H2AA	109.5
C9-C10	1.4241(12)	C5-C6-H6	120.4	C1A-C2A-H2AB	109.5
C9-C22	1.3941(12)	C7-C6-C5	119.28(10)	H2AA-C2A-H2AB	108.1
C10-C11	1.4318(12)	C7-C6-H6	120.4	O1A-C2A-C1A	110.8(5)
C10-C19	1.4235(12)	C6-C7-H7	118.6	O1A-C2A-H2AA	109.5
C11-C12	1.4080(12)	C6-C7-C8	122.71(9)	O1A-C2A-H2AB	109.5
C12-C13	1.4445(13)	C8-C7-H7	118.6	C3A-O1A-C2A	113.2(3)
C13-C14	1.4063(13)	C3-C8-C9	127.28(8)	O1A-C3A-H3AA	108.8
C13-C18	1.4172(13)	C7-C8-C3	117.24(9)	O1A-C3A-H3AB	108.8
C14-H14	0.9500	C7-C8-C9	115.48(8)	O1A-C3A-C4A	113.8(4)
C14-C15	1.3815(14)	C10-C9-C8	124.52(8)	H3AA-C3A-H3AB	107.7
C15-H15	0.9500	C22-C9-C8	117.49(8)	C4A-C3A-H3AA	108.8
C15-C16	1.3997(16)	C22-C9-C10	117.60(8)	C4A-C3A-H3AB	108.8
C16-H16	0.9500	C9-C10-C11	122.83(8)	C3A-C4A-H4AA	109.5
C16-C17	1.3834(14)	C19-C10-C9	120.73(8)	C3A-C4A-H4AB	109.5

C17-H17	0.9500	C19-C10-C11	116.44(8)	C3A-C4A-H4AC	109.5
C17-C18	1.4094(13)	C1-C11-C10	131.17(8)	H4AA-C4A-H4AB	109.5
C18-C19	1.4821(13)	C1-C11-C12	105.10(8)	H4AA-C4A-H4AC	109.5
C19-C20	1.4021(13)	C12-C11-C10	123.40(8)	H4AB-C4A-H4AC	109.5
C20-H20	0.9500	N2-C12-C11	111.93(8)	H1BA-C1B-H1BB	109.5
C20-C21	1.3893(13)	N2-C12-C13	126.95(8)	H1BA-C1B-H1BC	109.5
C21-C22	1.3969(13)	C11-C12-C13	120.89(8)	H1BB-C1B-H1BC	109.5
C21-C23	1.4865(13)	C14-C13-C12	122.01(9)	C2B-C1B-H1BA	109.5
C22-H22	0.9500	C14-C13-C18	120.82(9)	C2B-C1B-H1BB	109.5
C24-H24A	0.9800	C18-C13-C12	117.06(8)	C2B-C1B-H1BC	109.5
C24-H24B	0.9800	C13-C14-H14	119.8	C1B-C2B-H2BA	112.5
C24-H24C	0.9800	C15-C14-C13	120.43(10)	C1B-C2B-H2BB	112.5
C25-H25A	0.9900	C15-C14-H14	119.8	H2BA-C2B-H2BB	110.1
C25-H25B	0.9900	C14-C15-H15	120.3	O1B-C2B-C1B	96.0(9)
C25-C26	1.5125(13)	C14-C15-C16	119.45(9)	O1B-C2B-H2BA	112.5
C26-C27	1.3966(14)	C16-C15-H15	120.3	O1B-C2B-H2BB	112.5
C26-C31	1.3933(13)	C15-C16-H16	119.7	C2B-O1B-C3B	114.7(5)
C27-H27	0.9500	C17-C16-C15	120.57(9)	O1B-C3B-H3BA	112.4
C27-C28	1.3906(16)	C17-C16-H16	119.7	O1B-C3B-H3BB	112.4
C28-H28	0.9500	C16-C17-H17	119.2	O1B-C3B-C4B	96.5(10)
C28-C29	1.3906(18)	C16-C17-C18	121.52(10)	H3BA-C3B-H3BB	110.0
C29-H29	0.9500	C18-C17-H17	119.2	C4B-C3B-H3BA	112.4
C29-C30	1.3861(17)	C13-C18-C19	121.39(8)	C4B-C3B-H3BB	112.4
C30-H30	0.9500	C17-C18-C13	117.21(8)	C3B-C4B-H4BA	109.5
C30-C31	1.3944(14)	C17-C18-C19	121.40(9)	C3B-C4B-H4BB	109.5
C31-H31	0.9500	C10-C19-C18	120.27(8)	C3B-C4B-H4BC	109.5
C1A-H1AA	0.9800	C20-C19-C10	118.53(8)	H4BA-C4B-H4BB	109.5
C1A-H1AB	0.9800	C20-C19-C18	121.20(8)	H4BA-C4B-H4BC	109.5
C1A-H1AC	0.9800	C19-C20-H20	119.7	H4BB-C4B-H4BC	109.5
C1A-C2A	1.511(4)	C21-C20-C19	120.52(9)		
C2A-H2AA	0.9900	C21-C20-H20	119.7		
C2A-H2AB	0.9900	C20-C21-C22	120.24(9)		
C2A-O1A	1.412(3)	C20-C21-C23	122.14(9)		
O1A-C3A	1.399(3)	C22-C21-C23	117.58(8)		
C3A-H3AA	0.9900	C9-C22-C21	121.54(9)		
C3A-H3AB	0.9900	C9-C22-H22	119.2		
C3A-C4A	1.501(4)	C21-C22-H22	119.2		
C4A-H4AA	0.9800	O1-C23-O2	122.90(9)		
C4A-H4AB	0.9800	O1-C23-C21	123.98(9)		
C4A-H4AC	0.9800	O2-C23-C21	113.12(8)		

C1B-H1BA	0.9800	O2-C24-H24A	109.5
C1B-H1BB	0.9800	O2-C24-H24B	109.5
C1B-H1BC	0.9800	O2-C24-H24C	109.5
C1B-C2B	1.553(5)	H24A-C24-H24B	109.5
C2B-H2BA	0.9900	H24A-C24-H24C	109.5
C2B-H2BB	0.9900	H24B-C24-H24C	109.5
C2B-O1B	1.408(4)	N1-C25-H25A	109.2
O1B-C3B	1.410(4)	N1-C25-H25B	109.2
C3B-H3BA	0.9900	N1-C25-C26	112.23(7)
C3B-H3BB	0.9900	H25A-C25-H25B	107.9
C3B-C4B	1.540(5)	C26-C25-H25A	109.2
C4B-H4BA	0.9800	C26-C25-H25B	109.2
C4B-H4BB	0.9800	C27-C26-C25	120.70(9)
C4B-H4BC	0.9800	C31-C26-C25	120.25(9)

Table A6 - 19 Torsion angles for 3,5-Pyrazole

Atom-Atom-Atom-Atom	Torsion Angle [°]	Atom-Atom-Atom-Atom	Torsion Angle [°]
N1-N2-C12-C11	-1.11(10)	C11-C10-C19-C20	-172.47(8)
N1-N2-C12-C13	173.43(9)	C11-C12-C13-C14	179.56(9)
N1-C1-C2-C3	-140.05(9)	C11-C12-C13-C18	3.48(13)
N1-C1-C11-C10	-176.50(9)	C12-C13-C14-C15	-175.36(9)
N1-C1-C11-C12	-2.96(10)	C12-C13-C18-C17	176.29(8)
N1-C25-C26-C27	-49.50(12)	C12-C13-C18-C19	-2.94(13)
N1-C25-C26-C31	131.10(9)	C13-C14-C15-C16	-0.46(16)
N2-N1-C1-C2	-168.46(9)	C13-C18-C19-C10	-2.87(13)
N2-N1-C1-C11	2.51(11)	C13-C18-C19-C20	177.46(8)
N2-N1-C25-C26	107.33(9)	C14-C13-C18-C17	0.15(14)
N2-C12-C13-C14	5.46(15)	C14-C13-C18-C19	-179.08(8)
N2-C12-C13-C18	-170.63(9)	C14-C15-C16-C17	-0.41(17)
C1-N1-N2-C12	-0.89(10)	C15-C16-C17-C18	1.18(16)
C1-N1-C25-C26	-69.21(12)	C16-C17-C18-C13	-1.03(14)
C1-C2-C3-C4	132.85(9)	C16-C17-C18-C19	178.20(9)
C1-C2-C3-C8	-49.26(13)	C17-C18-C19-C10	177.93(8)
C1-C11-C12-N2	2.61(10)	C17-C18-C19-C20	-1.74(14)
C1-C11-C12-C13	-172.31(8)	C18-C13-C14-C15	0.58(15)
C2-C1-C11-C10	-5.78(16)	C18-C19-C20-C21	179.34(8)
C2-C1-C11-C12	167.76(9)	C19-C10-C11-C1	164.98(9)
C2-C3-C4-C5	179.97(10)	C19-C10-C11-C12	-7.55(13)

C2-C3-C8-C7	178.26(9)	C19-C20-C21-C22	-4.82(15)
C2-C3-C8-C9	-1.37(15)	C19-C20-C21-C23	177.25(9)
C3-C4-C5-C6	1.00(17)	C20-C21-C22-C9	2.21(15)
C3-C8-C9-C10	40.93(14)	C20-C21-C23-O1	176.50(10)
C3-C8-C9-C22	-146.45(10)	C20-C21-C23-O2	-3.49(14)
C4-C3-C8-C7	-3.90(14)	C22-C9-C10-C11	170.07(8)
C4-C3-C8-C9	176.46(9)	C22-C9-C10-C19	-10.57(13)
C4-C5-C6-C7	-1.88(18)	C22-C21-C23-O1	-1.48(16)
C5-C6-C7-C8	-0.21(17)	C22-C21-C23-O2	178.53(9)
C6-C7-C8-C3	3.12(15)	C23-C21-C22-C9	-179.77(9)
C6-C7-C8-C9	-177.21(10)	C24-O2-C23-O1	-0.80(15)
C7-C8-C9-C10	-138.71(9)	C24-O2-C23-C21	179.19(9)
C7-C8-C9-C22	33.91(12)	C25-N1-N2-C12	-177.88(8)
C8-C3-C4-C5	1.98(16)	C25-N1-C1-C2	8.26(15)
C8-C9-C10-C11	-17.32(14)	C25-N1-C1-C11	179.24(8)
C8-C9-C10-C19	162.03(9)	C25-C26-C27-C28	-178.34(10)
C8-C9-C22-C21	-167.74(9)	C25-C26-C31-C30	178.77(9)
C9-C10-C11-C1	-15.64(15)	C26-C27-C28-C29	-0.66(18)
C9-C10-C11-C12	171.83(9)	C27-C26-C31-C30	-0.65(15)
C9-C10-C19-C18	-171.54(8)	C27-C28-C29-C30	-0.19(19)
C9-C10-C19-C20	8.14(13)	C28-C29-C30-C31	0.62(18)
C10-C9-C22-C21	5.40(14)	C29-C30-C31-C26	-0.20(16)
C10-C11-C12-N2	176.79(8)	C31-C26-C27-C28	1.08(16)
C10-C11-C12-C13	1.87(14)	C1A-C2A-O1A-C3A	-157.7(6)
C10-C19-C20-C21	-0.33(14)	C2A-O1A-C3A-C4A	-69.6(7)
C11-C1-C2-C3	50.93(13)	C1B-C2B-O1B-C3B	-61.4(14)
C11-C10-C19-C18	7.86(13)	C2B-O1B-C3B-C4B	-79(2)

[3]

Thermal atomic displacement ellipsoid plot for SKC-BD-62 / SHAW40(1) with the atomic numbering scheme. Ellipsoids are drawn at the 50% probability level and hydrogen atoms are shown as sphere of arbitrary size. Disordered Et₂O solvent molecule is omitted.

A6.9 References

- Shigeno, M.; Hanasaka, K.; Tohara, I.; Izumi, K.; Yamakoshi, H.; Kwon, E.; Nozawa-Kumada, K.; Kondo, Y., *Org. Lett.* **2022**, 24 (3), 809-814.
- Yang, C.; Lin, K.; Huang, L.; Pan, W.-d.; Liu, S., *Beilstein J. Org. Chem.* **2016**, 12, 2490-2494.

3. HyperChem(TM) Professional 8.0, H., Inc., 1115 NW 4th Street, Gainesville, Florida 32601, USA.
4. Frisch, M. J.; Trucks, G. W.; Schlegel, H. B.; Scuseria, G. E.; Robb, M. A.; Cheeseman, J. R.; Scalmani, G.; Barone, V.; Petersson, G. A.; Nakatsuji, H.; Li, X.; Caricato, M.; Marenich, A. V.; Bloino, J.; Janesko, B. G.; Gomperts, R.; Mennucci, B.; Hratchian, H. P.; Ortiz, J. V.; Izmaylov, A. F.; Sonnenberg, J. L.; Williams; Ding, F.; Lipparini, F.; Egidi, F.; Goings, J.; Peng, B.; Petrone, A.; Henderson, T.; Ranasinghe, D.; Zakrzewski, V. G.; Gao, J.; Rega, N.; Zheng, G.; Liang, W.; Hada, M.; Ehara, M.; Toyota, K.; Fukuda, R.; Hasegawa, J.; Ishida, M.; Nakajima, T.; Honda, Y.; Kitao, O.; Nakai, H.; Vreven, T.; Throssell, K.; Montgomery Jr., J. A.; Peralta, J. E.; Ogliaro, F.; Bearpark, M. J.; Heyd, J. J.; Brothers, E. N.; Kudin, K. N.; Staroverov, V. N.; Keith, T. A.; Kobayashi, R.; Normand, J.; Raghavachari, K.; Rendell, A. P.; Burant, J. C.; Iyengar, S. S.; Tomasi, J.; Cossi, M.; Millam, J. M.; Klene, M.; Adamo, C.; Cammi, R.; Ochterski, J. W.; Martin, R. L.; Morokuma, K.; Farkas, O.; Foresman, J. B.; Fox, D. J. *Gaussian 16 Rev. A.03*, Wallingford, CT, **2016**.
5. Becke, A. D., *J. Chem. Phys.* **1993**, *98* (7), 5648-5652.
6. Grimme, S.; Antony, J.; Ehrlich, S.; Krieg, H., *J. Chem. Phys.* **2010**, *132* (15).
7. Marenich, A. V.; Cramer, C. J.; Truhlar, D. G., *J. Phys. Chem. B* **2009**, *113* (18), 6378-6396.
8. NBO 7.0. E. D. Glendening, J., K. Badenhoop, A. E. Reed, J. E. Carpenter, J. A. Bohmann, C. M. Morales, P. Karafiloglou, C. R. Landis, and F. Weinhold, Theoretical Chemistry Institute, University of Wisconsin, Madison **2018**.
9. Glendening, E. D.; Landis, C. R.; Weinhold, F., *J. Comput. Chem.* **2019**, *40* (25), 2234-2241.
10. Chemcraft - graphical software for visualization of quantum chemistry computations. Version 1.8, build 654. <https://www.chemcraftprog.com>.
11. Deweid, L.; Hadjabdelhafid-Parisien, A.; Lafontaine, K.; Rochet, L. N. C.; Kolmar, H.; Pelletier, J. N., Chapter Five - Glutamine-walking: Creating reactive substrates for transglutaminase-mediated protein labeling. In *Methods Enzymol.*, Tawfik, D. S., Ed. Academic Press: 2020; Vol. 644, pp 121-148.
12. Krause, L.; Herbst-Irmer, R.; Sheldrick, G. M.; Stalke, D., *J. Appl. Crystallogr.* **2015**, *48* (1), 3-10.
13. Sheldrick, G., *Acta Crystallographica Section A* **2015**, *71* (1), 3-8.

14. Sheldrick, G., *Acta Crystallographica Section C* **2015**, 71 (1), 3-8.
15. Dolomanov, O. V.; Bourhis, L. J.; Gildea, R. J.; Howard, J. A. K.; Puschmann, H., *J. Appl. Crystallogr.* **2009**, 42 (2), 339-341.
16. D. Kratzert, F., V84, <https://www.xs3.uni-freiburg.de/research/finalcif>.
17. Bruker, S., (2020), Bruker AXS Inc., Madison, Wisconsin, USA.